SCHOLARLY PUBLICATIONS

A CURRENT AWARENESS BULLETIN
OF RESEARCH OUTPUT

@DTU

(15th Edition)

MARCH 2014

BY: CENTRAL LIBRARY

DELHI TECHNOLOGICAL UNIVERSITY
(FORMERLY *DELHI COLLEGE OF ENGINEERING)*
GOVT. OF N.C.T. OF DELHI
SHAHBAD DAULATPUR, MAIN BAWANA ROAD
DELHI 110042

PREFACE

This is the Fifteenth Issue of Current Awareness Bulletin started by Delhi Technological University, Central Library. The aim of the bulletin is to compile, preserve and disseminate information published by the faculty, students and alumni for mutual benefits. The bulletin also aims to propagate the intellectual contribution of Delhi Technological University (DTU) as a whole to the academia.

The bulletin contains information resources available in the internet in the form of articles, reports, presentations published in international journals, websites, etc. by the faculty and students of DTU. The publications of faculty and student which are not covered in this bulletin may be because of the reason that the full text either was not accessible or could not be searched by the search engine used by the library for this purpose.

The learned faculty and students are requested to provide their uncovered publications to the library either through email or in CD, etc to make the bulletin more comprehensive.

This issue contains the information published during March 2014. The arrangement of the contents is alphabetical. The full text of the article which is either subscribed by the university or available in the web is provided in this bulletin.

Central Library

CONTENTS

1. A Comprehensive Study of Modern Flow Control Methods and Their Applications, ***Shaktiman Singh, *Tanmay Goel, *Ritesh Singh, *Saurabh Kumar*** and ***Raj Kumar Singh***, Department of Mechanical Engineering

2. A Quality Model for E-Learning as a Service in Cloud Computing Framework, Dr Rajni Jindal and ***@Alka Singhal***, Research Scholar, CSE Dept

3. A review of Pulse current gas tungsten arc welding for different alloys, ****P. K. Baghela***, Department of Mechanical Engineering

4. A Review on Properties of phase change material for solar thermal storage system ****Kaushalendra Kumar Dubey*** and ****Radheshyam Mishra,*** Department of Mechanical Engineering

5. A Thermodynamic Analysis of a Hydrogen Enriched Compressed Natural Gas Fuelled HCCI Engine, ****Devendra Kumar Gupta, *Rohit Goyal, *Rajesh Kumar*** and ****Md Nadim Shams***, Department of Mechanical Engineering

6. Application of Selective Inventory Control Techniques for Cutting Tool Inventory Modeling and Inventory Reduction-A Case Study, ****A K Madan*** and ****Ranganath M S***, Department of Mechanical Engineering

7. Biosensors for pathogen detection: A smart approach towards clinical diagnosis RENU SINGH, MAUMITA DAS MUKHERJEE, GAJJALA SUMANA, RAJINDER K. GUPTA, SEEMA SOOD and ***B. D. MALHOTRA,*** Department of Biotechnology

8. Building Automation Control System for Smart Grid ****Md. Tausif Ahmad, *Priyanka Chaudhary,*** and ****Narendra Kumar,*** Department of Electrical Engineering

9. Comprehensive Study on Various Types of Particle Image Velocimetry with Explicit Instrumentation, ***Vishvendra Singh Tomar, *Sahib Chawla, *Vipul Sangwan, *Raj Kumar Singh,*** Department of Mechanical Engineering and ***Arun Dhyani***, Department of Electronics and Communication Engineering

10. Design, Analytical Analysis, Instrumentation and Cost Estimation of Sub-Sonic Open Circuit Wind Tunnel Model, ***Vishvendra Singh Tomar, *Vipul Sangwan, *Raj Kumar Singh, IB*** and ***Sahib Chawla***, Department of Mechanical Engineering

11. Economic Load Dispatch Problem and Mat lab Programming of Different Methods Rahul Dogra, ***Nikita Gupta,*** and ***Harsha Saroa***, Department of Power Systems

12. Energetic and Exergetic Based Comparison Multiple Evaporators with Compound Compression and Flash Intercooler with Individual or Multiple Throttle Valves Kapil Chopra, V. Sahni, and ***R. S Mishra***, Department of Mechanical Engineering

13. ETHICAL VALUES AND ECONOMIC VALUES, ***Priyanka Chaudhary*** and ***$Manish Sharma***, Delhi School of Management

14. Experimental Studies for Accessing the Influence of Micro-Dimple Area Density on Tribological Performance of Mating Contacts, ***R. C. Singh***, R. K. Pandey, and ***S. Maji***, Department of Mechanical Engineering,

15. Extreme Weather Events and Climate Change Impact on Construction Small Medium Enterprises (SME's): Imbibing Indigenous Responses for Sustainability of SME's, ***Shubham Gandhi, *Anik Gupta*** and ***Sanchit Sethi***, Department of Environmental Engineering

16. First and Second Law Analysis of a Solar Operated Ejector Absorption Refrigeration System, ***Rohit Goyal, *D.K. Gupta, *Rajesh Kumar,*** and ***Md. Nadim Shams***, Department of Mechanical Engineering

17. Generalized neural network and wavelet transform based approachfor fault location estimation of a transmission lineMajid Jamila, Abul Kalama, A.Q. Ansaria, ***M. Rizwan***, Department of Electrical Engineering

18. Hardware Implementation of Prototype Model of Two Port Network, ***Harsha Saroa*** and ***Nikita Gupta***, Department of Power Systems

19. Irriversibility Analysis of Multi-Evaporators Vapour Compression Refrigeration ystems Using New and Refrigerants: R134a, R290, R600, R600a, R1234yf, R502, R404a and R152a and R12, R502, ***R. S. Mishra***, Department of Mechanical Engineering

20. Lasing potentialities and White Light Generation Capabilities of Dy3þ doped Oxy-fluoroborate Glasses, Sk. Mahamuda, K. Swapna, P. Packiyaraj, ***A. Srinivasa Rao***, and G. Vijaya Prakash, Department of Applied Physics

21. Limnological Studies Related to Physico-Chemical Characteristics of Water in Anasagar Lake, Ajmer, Rajasthan, ***Abhas Jain*** and ***S. K. Singh***, Department of Environmental Engineering

22. Multiple Criteria Decision Making Techniques in Manufacturing Industries-A Review Study with the Application of Fuzzy, ***A K Madan*** and ***Ranganath M S***, Department of Mechanical Engineerng

23. Nanostructured nickel oxide film for application to fish freshness biosensor, Surendra K. Yadav, Jay Singh, Ved V. Agrawal and ***B. D. Malhotra***, Department of Biotechnology

24. NATURAL CONVECTION GREENHOUSE DRYING OF VERMICELLI: AN EXPERIMENTAL STUDY, ***$Punit Kumar***, M.Tech. Student, Mechanical Engineering Department

25. Non-parametric Clustering and Topic Modeling via Small Variance Asymptotics with Local Search: A Thesis Presented in Partial Fulllment of the Requirements for the Degree Master of Science in the Graduate School of The Ohio State University By ***£Siddharth Singh***, B.E, Graduate Program in Department of Computer Science & Engineering

26. Optimization of Process Parameters in Turning Operation of Aluminium (6061) with Cemented Carbide Inserts Using Taguchi Method and ****Anova Ranganath M S, *Vipin,*** and ****R. S. Mishra***, Department of Mechanical Engineering

27. OTRA based Voltage mode third order Quadrature Oscillator ****Rajeshwari Pandey *Neeta Pandey, *K.GuruMurthy,*** and Rashika Anurag, Department of Electronics and Communication Engineering

28. Phase transformation and two-mode phonon behavior of (1-x) [Ba Zr0.025Ti0.975O3] – (x) [BiFeO3] solid solutions, ****Priyanka A. Jha***, ****A.K. Jha***, , Pardeep K. Jha, R. K. Kotnala and R.K. Dwivedi, Department of Applied Physics

29. Potential Application of Particle Image Velocimetry To Sub-Sonic Open Circuit Wind Tunnel, ****Vishvendra Singh Tomar, *Sahib Chawla, *Shanu Sinha, *Raj Kumar Singh***, Department of Mechanical Engineering, and ****Arun Dhyani***, Department of Electronics and Communication Engineering

30. Security Requirements Engineering: Analysis and Prioritization ****A. Daya Gupta, *B. Shruti Jaiswal*** and ****C. Anupriya Tewari,*** Computer Engineering Department

31. Selection of Candidate by Political Parties Using Fuzzy Logic, Kiran Pal and ****Surendra Tyagi***, Department of Computer Science

32. SOME SANDWICH RESULTS ASSOCIATED WITH A GENERALIZED LINEAR OPERATOR ROMAI J., v.9, no.2(2013), 107–118, ****S. Sivaprasad Kumar,*** and ****Virendra Kumar***, Department of Applied Mathematics

33. Sort Range Optical Wireless Communication, ***Sanjeev Mishra***, Department of Technical Instructor

34. Study of 4 Wheel Steering Systems to Reduce Turning Radius and Increase Stability ***Arun Singh, *Abhishek Kumar, *Rajiv Chaudhary,*** and ***R. C. Singh,*** Department of Mechanical Engineering,

35. Synthesis and antimicrobial activity of some new 1,2,4-trazine and benzimidazole derivatives, Abha Bishnoi, Suruchi Singh, Anil K Tiwari, ***Archna Rani, *Sapna Jain,*** Department of Applied Chemistry and C K M Tripathi

36. Theoretical Investigation and Flow Simulation of a Sub-Sonic Open Circuit Wind Tunnel Model, ***Vishvendra Singh Tomar, *Vasu Kumar, *Raj Kumar Singh,*** and ***Sahib Chawla***, Department of Mechanical Engineering

37. Thermal analysis of a Claude system for Liquefaction of Various Gases, ***Devender Kumar***, and ***R. S. Mishra***, Department of Mechanical Engineering

38. Thermodynamic Analysis of a Absorption Refrigeration Cycle Using Flat Plate Collector, ***Rohit Goyal, *D K Gupta, *Rajesh Kumar*** and ***Md. Nadim Shams***, Department of Mechanical Engineering

***Faculty @Research Scholar $PG Scholar #Alumni**
£Undergraduate Student ~ Ex Faculty <Ex Research Scholar

ISBN 978-93-5156-328-0
International Conference of Advance Research and Innovation (ICARI-2014)

A Comprehensive Study of Modern Flow Control Methods and Their Applications

Shaktiman Singh *, Tanmay Goel, Ritesh Singh, Saurabh Kumar, Raj Kumar Singh
Department of Mechanical Engineering, Delhi Technological University, New Delhi, India

Article Info

Article history:
Received 29December 2013
Received in revised form
10 January 2014
Accepted 20 January 2014
Available online 1 February 2014

Keywords

Turbulence
Drag
Separation
Control
Flow
Methods

Abstract

Flow control is a rapidly developing technological area which is relevant to several engineering sectors with goals such as the reduction of drag and the reduction in flow-induced vibrations. It involves aero-acoustics, fluid instabilities and closed-loop control of unstable fluid systems. Development of control strategies involves simulation followed by laboratory testing of control models. To design a fluid flow system, a thorough understanding of the available flow control technologies is crucial. In this paper we will go through the developments in the flow control technology over last few decades and then study some modern techniques which will give us a whole new viewpoint on the science of flow control.

1. Introduction

Flow Control techniques have been used for many years to control the fluid flow, and some employ diverse concepts to serve this purpose in past decades. Flow control comprises of passive or active devices to effect a beneficial change in wall-bounded or free-shear flows. Whether the task is to delay or advance transition, to suppress or enhance turbulence or to prevent/provoke separation, useful end results include drag reduction, lift enhancement, mixing augmentation and flow-induced noise suppression. This area of Fluid Mechanics has always interested the researchers because of its wide range of potential benefits for the military as well as civilian sectors. Prompted by the fresh advances in chaos control, micro fabrication and neural networks, reactive control of turbulent flows is now in the realm of the possibility for future practical devices.

The objective of flow control problems may at times be interconnected, leading to potential conflicts as the attainment of one particular goal may undesirably affect another goal. For example, consider an aircraft wing for which the performance is measured by the improvement in lift-to-drag ratio. Promoting transition will lead to a turbulent boundary layer that is more resistant to separation and increased liftcan be obtained at higher angle of incidence. The viscous or skin-friction drag for a laminar boundary layer can be an order of magnitude smaller than for a turbulent boundary layer. However, a laminar boundary layer is more prone to separation resulting in a loss in lift and an increase in form drag. The design trade-offs of a particular method of control must carefully be evaluated and compromises are often necessary to reach a particular design goal.

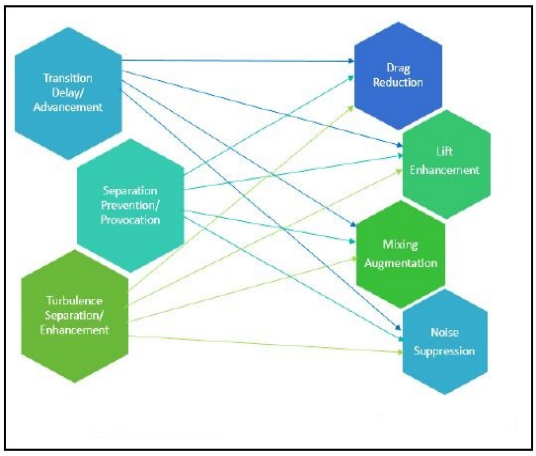

Fig: 1. Engineering Objectives and Corresponding Flow Changes

Corresponding Author,
E-mail address: meshaktiman@gmail.com
All rights reserved: http://www.ijari.org

Flow control is rapidly developing as a key technological area relevant to several engineering sectors with goals such as the reduction of drag and the reduction in flow-induced vibrations. It involves aero-acoustics, fluid instabilities and closed-loop control of unstable fluid systems. Development of control strategies involves simulation followed by laboratory testing of control models.

2. Historical Developments in Flow Control Technology

Flow control methods are being used since very early times. The development of this technology to what it is today spans over five major eras. The empirical era (prior to 1900); the scientific era (1900-1940); the World War II era (1940-1970); the energy crisis era (1970-1990) and the 1990s and beyond. The art of flow control probably has its roots in prehistoric times when streamlined spears, sickle-shaped boomerangs, and fin-stabilized arrows evolved empirically by archaic Homo sapiens. Relatively soon after the dawn of civilization and the establishment of an agriculture way of life 8,000 years ago, complex systems of irrigation were built along inhabited river valleys to control the water flow, thus freeing man from the vagaries of the weather. For centuries, farmers knew the value of windbreaks to keep top soil in place and to protect fragile crops.

The science of flow control originated with Prandtl (1904), who, in a mere 8-page manuscript, introduced the boundary layer theory, explained the physics of the separation phenomena and described several experiments in which a boundary layer was controlled. Thus, the birth of the scientific method to control a flow field. Slowly but surely, the choice of flow control devices is no longer a trial and error feat, but physical reasoning and even first principles are more often than not used for rational design of such artefacts.

Stimulated by the Second World War and the subsequent cold war, that trend accelerated significantly during the third era (1940-1970). Military needs of the superpowers dictated the development of fast, highly maneuverable, efficient aircraft, missiles, ships, submarines and torpedoes, and flow control played a major role in achieving these goals. Natural laminar flow, laminar flow control and polymer drag-reduction are notable achievements during this era. Partial summaries of flow control research during this period are contained within the books edited by Lachmann (1961) and Wells (1969).

The energy crises exemplified by the 1973 Arab oil embargo brought about a noticeable shift of interest from the military sector to the civilian one. During the period 1970-1990, government agencies and private corporations around the world but particularly in the industrialized countries invested valuable resources searching for methods to conserve energy, and hence drag reduction for civilian air, sea and land vehicles, for pipelines and for other industrial devices was emphasized. The availability of fast, inexpensive computers made it possible to simulate numerically complex flow situations that have not been approachable analytically. Some control strategies, for example transition-delaying compliant coatings (Gad-el-Hak, 1996), were rationally optimized using computational fluid dynamics. Large-eddy breakup devices (LEBUs) and rib lets are examples of control methods developed during this period to reduce skin-friction drag in turbulent boundary layers. Good sources of information on these and other devices introduced during the fourth era are the books edited by Hough (1980), Bushnell and Hefner (1990), and Barnwell and Hussaini (1992). Numerous meetings devoted to flow control, particularly drag reduction, were held during this period. Plentiful fuel supplies during the 1990s and the typical short memory of the long gas lines during 1973 have, unfortunately, somewhat dulled the urgency and enthusiasm for energy conservation research as well as practice. For the 1990s and beyond, more complex reactive control devices, geared specifically towards manipulating the omnipresent coherent structures in transitional and turbulent shear flows (Cantwell, 1981; Robinson, 1991), are pursued by several researchers. Theoretical advances in chaos control and developments of micro electro mechanical systems (MEMS) and neural networks should help such efforts. Papers specifically addressing reactive control strategies include those by Wilkinson (1990), Moin and Bewley (1994), and Gad-el-Hak (1994).

3. Active Flow Control

Active flow-control (AFC) is a fast growing multi-disciplinary science and technology aimed at altering a natural flow state or development path into a more desired state (or path).

Active control schemes can be divided into predetermined or interactive methods. A predetermined method of control involves the introduction of steady or unsteady energy inputs without consideration for the state of the flow field. E.g. jet vectoring using piezoelectric actuators (Smithand Glezer, 1997).In interactive methods of flow control, the power input to the actuator (controller) is continuously adjusted based on some

form of measurement element (sensor). The control loop for interactive control can be either a feed forward (open) or feedback (closed) loop.

Active flow control has received increasing attention in the last decade, where n knowledge from fluid mechanics is combined with control theory to affect the properties of flow systems. A common goal is to stabilize a flow subject to linear instability, like for instances the Tollmien-Schlichting waves on an aeroplane wing (see e.g. Hogberg & Henningson (2002), or force the flow back to a laminar regime, like for instance in a turbulent channel flow (see e.g. Hogberg et al. (2003); Kim (2003)).

3.1 Contribution of Reynold's & Navier-stokes to A.F.C. & Rise of "Closure Problem"

Reynolds (1883) discovered the phenomenon of transition in pipe flows. He differentiated between quiescent (laminar) flow and sinuous (turbulent) flow separating the instantaneous velocity vector into steady and random components. Turbulence due to its non-deterministic nature was described in statistical terms that decomposed the velocity and the pressure into mean and fluctuating components. This decomposition created a new set of equations unsolvable by Reynolds Time averaging equations (Reynolds, 1894), this problem also being referred as closure problem. Currently Reynolds averaged Navier-Stokes (RANS) methods are practically used in industrial applications since they are capable of postdicting the type of flows about which there is a substantial amount of information, rather than predicting the behavior of an entirely novel flow.

3.2 Prandtl's Contribution to A.F.C. & The Separation Concept

The most important advance leading to the AFC concept was Prandtl's boundary-layer theory which separated the flow field into a thin layer of rotational fluid adjacent to a solid surface, surrounded by a large body of irrotational flow that can be considered to be in viscid explaining the flow around streamlined bodies and also the frictional losses and the convective heat transfer occurring between the surface and the adjacent fluid.

3.3 The concept of a "Super Layer"

The use of Reynolds-averaged equations was practically limited to homogeneous and isotropic only. Corrsin and Kistler (1955) recognized this shortcoming and introduced the concept of a "super layer", which represents a thin, highly contorted boundary separating the turbulent from the irrotational zones. Vorticity is imparted to their rotational fluid along this boundary through the action of viscosity. By assuming that the super layer is continuous without islands of turbulent fluid being present in the irrotational zone, Corrsin and Kistler were able to measure the duration T of the large eddies at the outer edge of the boundary layer, determining that TU8 /d ˜ 2.5. This was probably the first measurement delineating the average size of a large eddy propagating at the outer edge of the boundary layer and indicating that turbulence is not as random as it was previously believed to be.

3.4 Coherent structures in Turbulence

Large coherent structures in turbulent shear flows were discovered. And the most important discovery in this was made by Brown and Roshko (1971, 1974) in a two-dimensional mixing layer. Their Schlieren photograph showed that the turbulent mixing layer is dominated by large-scale eddies, which transport within them much smaller and approximately homogeneous turbulent eddies. The mixing-layer spreading rate could clearly be related to the growth of the large eddies, which engulf irrotational fluid from the surrounding streams.

3.5 The concept of "Triple Decomposition"

The triple decomposition (Reynolds and Hussain, 1972) recognizes that the unsteady motion may be decomposed into large, coherent, deterministic structures that are predictable and smaller ones that presently cannot be predicted and are described by statistical methods and therefore presumed to be random.

3.6 Interrelation of Flow control Goals

One important issue is interrelation of flow control goals, showed by (Gad-el-Hak, 1998). Let us consider an external wall bounded flow, such as that developing on the exterior surface of an aircraft or a submarine. This kind of flow can be manipulated to achieve transition delay, separation postponement; lift increase, skin friction and pressure drag reduction, turbulence augmentation, heat transfer enhancement, or noise suppression. These objectives are not necessarily mutually exclusive.

To focus the discussion further, think of the flow developing on a lifting surface such as an aircraft wing. If the boundary layer becomes turbulent, its resistance to separation is enhanced and more lift could be obtained at increased incidence. On the other hand, the skin-friction drags for a laminar boundary layer can be as much as an order of magnitude less than that for a turbulent one. If transition is delayed &

so on. The ultimate goal of all this is to improve the airfoil's performance by increasing the lift-to-drag ratio.

All of the above points to potential conflicts as one try to achieve a particular control goal only to adversely affect another goal. A skilled engineer has to make continuous compromises to achieve a particular design goal.

4. Recent Innovations in Actuator Technology

One of the greatest challenges in making active flow control technology practical is the development of robust actuators. Desired characteristics of actuators include low power consumption, fast response, reliability, and low cost. Three different actuator concepts are highlighted below to give a brief overview of the variety of actuators that can be used in flow control

4.1 Synthetic jet Actuator

A recent breakthrough in actuator concepts is the synthetic jet actuator developed at Georgia Institute of Technology. This class of actuators uses an oscillatory surface within a cavity to generate a jet from the flow that is being controlled without the need for mass injection (Smith and Glezer, 1998). Flow enters and exits the cavity through an orifice. On the intake stroke, fluid is drawn into the cavity from the area surrounding the orifice. As this fluid is driven out of the cavity, a shear layer is formed between the expelled fluid and the surrounding fluid. This layer of vorticity rolls up to form a vortex ring. By the time the diaphragm begins to move away from the orifice to pull fluid back into the cavity, the vortex ring has moved far enough away that it is virtually unaffected. Thus a train of vortex rings is created by the actuator. These are compact and requiring no flow plumbing. A variety of flow control results have been achieved using the synthetic jet actuator including thrust-vectoring, mixing enhancement, separation control and virtual surface shaping.

4.2 The second-generation Cavity Noise Suppression Actuator

A promising actuator concept was developed by Cattafestaet al. (1999) for cavity noise suppression. This actuator was an improved design over the first generation piezoelectric flaps developed by Cattafesta et al. (1997). The first generation piezo flap sex hibited a tendency to fail mechanically before reaching their respective electrical limitations. The second-generation actuator is used to construct an active, segmented flap at the upstream separation edge of the cavity and is called a monolithic, piezoelectric flap actuator. The separation edge is an appropriate choice for active control devices because it is the location of maximum receptivity

4.3 Lorentz Force Actuator

The third actuator concept highlighted here is a Lorentz-force actuator. Experiments performed by Nosenchuck and Brown (1992), Nosenchuck et al. (1995), and Nosenchuck (1996)using a specific electromagnetic forcing have indicated that viscous drag can be reduced by as much as 90%. Flush-mounted Lorentz force actuators are used to induce a current-density field ,j, and a magnetic field, B, in the vicinity of the wall to provide a three-dimensional body force L=j x B. The actuator is comprised of a pair of subsurface permanent magnets and two surface-mounted. The arrangement creates a three dimensional Lorentz force above the actuator. The curl of the Lorentz force represents a source of Vorticity.

5. Turbulence Control

The flow in which the various quantities of flow show a random variation with space and time coordinates is called turbulent flow. Due to loss of mechanical energy (as a result of eddying motions) a lot of heat is dissipated. The effects of turbulence is predicted by turbulence modeling. The aim of turbulence control is to identify turbulence cycles and improving the turbulent models.

Turbulence in its own way is necessary in some areas as well as poses a threat of energy losses. While in the case of aircrafts and ships, it has adverse effects on their progression as it generates friction drag due to air or water and increasing fluid noise, it is advantageous and necessary as it accelerates mixing, combustion and heat transfer.

The turbulence control methods are necessary for research purposes as it has the potential of reducing drag during water transportation, pipeline oil and air transportation.

Turbulence can be controlled both by active and passive methods. Turbulence can be reduced by Feed forward (Reactive) as well as Predetermined methods. Feedback control has a great advantage that it can control the flow at each time. Turbulent drag can also be reduced by using in-plane wall motion.

As far as the present scenario is concerned, research in the field of turbulence control is being extensively carried out due to the development of hardware for control, CFD and modern control theory.

6. Flow Separation Control

Flow separation occurs when the boundary layer travels far enough against an opposing pressure gradient that the speed of the boundary layer relative to the object falls almost to zero. The fluid flow becomes detached from the surface of the object, and instead takes the forms of eddies and vortices, leading to Flow Separation. To improve the performance of natural or man-made flow systems, it may be beneficial to delay or advance this detachment process. In aerodynamics, flow separation can often result in increased drag, particularly pressure drag which is caused by the pressure differential between the front and rear surfaces of the object as it travels through the fluid. And therefore, Separation delay is one of the key aspects of flow control. Much effort and research has gone into the design of aerodynamic and hydrodynamic surfaces which defer flow separation and keep the local flow attached for as long as possible. Examples of this include the fur on a tennis ball, dimples on a golf ball, turbulatorson a glider, which induce an early transition to turbulent flow regime; vortex generators on light aircraft, for controlling the separation pattern.

6.1 Phenomenon of Flow Separation

Fluid particles in a boundary layer are slowed down by wall friction. If the flow is sufficiently retarded, for example, owing to the presence of an adverse pressure gradient, the momentum of those particles will be reduced by both the wall shear and the pressure gradient. In terms of energy principles, the kinetic energy gained at the expense of potential gradient in the favourable-pressure-gradient region is depleted by viscous effects within the boundary layer. In the adverse-pressure-gradient region, the remaining kinetic energy is converted to potential energy but is too small to surmount the pressure hill, and the motion of near-wall fluid particles is eventually arrested. At some point, the viscous layer breaks away from the bounding surface. The surface streamline nearest to the wall leaves the body at this point, and the boundary layer is said to separate (Maskell, 1955).

Usually Flow Separation implies a loss of lift, an increase of drag, diminished pressure recovery etc. Therefore, a considerable amount of research has been devoted to the control of flow separation and many

possibilities to achieve separation control have been investigated. Among the most popular are shaping as a passive means and suction, blowing and wall movement as active control methods. While passive means naturally do not produce any running costs, achievable improvements are modest and performance under off-design conditions is mostly poor. Active control methods may be adjusted to actual operating conditions, but require additional power, i.e. running costs.

The performance and stability of an airplane is often degraded by flow separation. In recent years, control devices involving zero-net-mass-flux oscillatory jets or synthetic jets have shown good feasibility for industrial applications and effectiveness in controlling flow separation (Glezer & Amitay 2002; Rumsey et al. 2004; Wygnanski2004). The application of synthetic jets to flow separation control is based on their ability to stabilize the boundary layer by adding/removing momentum to/from the boundary layer with the formation of vortical structures. The verticalstructures in turn promote boundary layer mixing and hence momentum exchange between the outer and inner parts of the boundary layer.

6.2 Inspiration from Nature

Inspired from the natural properties of birds' feathers, i.e. porosity, anisotropy and compliance, an original model for a hairy layer was proposed and tested by Julien Favier et al. (J. Fluid Mech. (2009) A model of hairy medium was developed using a homogenized approach, and the fluid flow around a circular cylinder partially coated with hair was analysed by means of numerical simulations. It was found numerically that such a coating was capable of increasing global aerodynamics performances of an immersed body, by adapting to the separated flow.

The effects of the control were found to be of order one, and appear on the mean pressure and velocity fields. The topology of the flow was changed in the vicinity of the wall but also further downstream, thus modifying the vortex shedding process, and positively affecting the pressure distribution, to reduce lift fluctuations and drag.

The flow dynamics is dominated by the shear layer instability, and the pressure is found to play a coupling role between separation and re-attachment, potentially leading to global instability. The large dimensionality of the discretized flow system is a challenge for control design.

6.3 Introduction of Vortices

In the technical report by Ola Logdberg in 2008, turbulent boundary layer separation control by means of longitudinal vortices was studied. In an experiment stream wise vortices were introduced in turbulent boundary layers to transport higher momentum fluid towards the wall. This enabled the boundary layer to stay attached at larger pressure gradients.

6.4 Change in Synthetic Jet Design

The performance and stability of an airplane is often degraded by flow separation. In recent years, control devices involving zero-net-mass-flux oscillatory jets or synthetic jets have shown good feasibility for industrial applications and effectiveness in controlling flow separation (Glezer&Amitay 2002; Rumsey et al. 2004; Wygnanski2004). The application of synthetic jets to flow separation control is based on their ability to stabilize the boundary layer by adding/removing momentum to/from the boundary layer with the formation of vortical structures. The vorticalstructures in turn promote boundary layer mixing and hence momentum exchange between the outer and inner parts of the boundary layer. The control performance of the synthetic jets greatly relies on parameters such as the amplitude, frequency, and location of the actuation, and numerical simulations are especially suitable for an extensive parametric study to optimize the control parameters.

In 2007, the experimental founding that the synthetic jets which are produced through a slot across the entire span on suction surface at 12% chord location, effectively delays the onset of flow separation and causes a significant increase in the lift coefficient[1] [2], was confirmed[4] using Large Eddy Simulation Techniques. It was found that in the case of 20. angle of attack where flow separates near the leading edge, LES provides comparable results to experimental data when grid resolution is sufficient to predict the separated shear layer. The synthetic-jet actuation at 12% chord location is found marginally effective in controlling leading edge separation.

6.5 Local Surface Modulation

It has been shown in the literature[21] that blowing or suction over the air foil surface is an economical process to prevent flow separation by energizing the boundary layer (in the case of blowing) or pulling the separated flow towards the airfoil due to pressure differential (in the case of suction). Furthermore, it has been shown that a process of periodic blowing is even more efficient than steady blowing. Therefore, if both the blowing and suction process are repeated alternatively and periodically, the process is expected to be even more efficient. This can be achieved by a periodic modulation of the local airfoil surface, which helps in re-attaching the flow.

7. Drag Reduction

Drag is a force which acts on a solid object in the direction of the relative fluid flow velocity, it depends on velocity. Drag forces always decrease fluid velocity relative to the solid object in the fluid's path. Drag can be reduced by drag reducing agents, micro bubble, surfactant solutions, electromagnetic flow, and feedback control.

Drag reducing agents are polymers used as additives in pipelines to reduce turbulence in a pipe. In petroleum pipelines, they increase the pipeline capacity by reducing turbulence and therefore allowing the oil to flow more efficiently. They are used in very small amount in the pipelines. In pipelines oil pushes up against the inside wall of the pipe, the pipe pushes the oil back down causing a swirling of turbulence to occur, then the polymer is added, it interacts with the oil and the wall to help reduce the contact of the oil with the wall. Temperature, diameter of pipe, roughness inside the pipe effect the working of reducing agent. At higher temperature, the drag reducing agent is easier to degrade. At a low temperature the drag reducing agent will tend to cluster together. This problem can be solved by adding another chemical, such as aluminium to help lower the drag reducing agent's attraction to one another. With decrease in pipe diameter, the drag reduction is increased. The rougher the inside, the higher the percent drag reduction occurring.

Microbubbles are used for reducing the skin friction when small gas bubbles are injected into he flow from an upstream position. Gas is injected into liquid turbulent boundary layer to form bubbles which reduces skin friction drag locally by as much as 80 %. The bubble sizes in a micro bubble cloud are subject to any of three competing mechanisms: the initial formation at the wall; bubble splitting by turbulence action and bubble coalescence upon collision. The most significant characteristic of the bubble sizes (500 – 1200 μm) is their diameter in comparison to the boundary layer scales.

7.1 Anionic Surfactants

Anionic surfactants reduce drag in the aqueous solution. Alkali metal and ammonium soaps are used to reduce drag upto 30 % for 0.2% sodium oleatesolutions. Addition use of an electrolyte (eg.KCl) increases the drag reduction as KCl helps in the enhancement of the association of the soap molecules and that the soap micelles, which were initially spherical in the aqueous solution, were rearranged under the influence of the electrolyte into cylindrical shapes, which forms a network of interlaced rod-like elements. The concentration of soap is 0.1 %, which is considerably higher than the polymer concentration.

7.2 Cationic Surfactants

Cetryltrimethyl ammonium bromide (CTAB) is the cationic surfactant which also reduces drag. CTAB naphthol mixture is used to reduce turbulent friction, because the mixture shows shear-thinning characteristics. Similar to anionic surfactant solutions, the drag reducing ability of the CTAB-naphthol solution terminated at some upper Reynolds number corresponding a critical shear stress where there was a scission of the micelles. One marked advantage of cationic surfactants over the anionic ones is that these complex soaps do not precipitate in the presence of calcium ion.

Drag reduction in turbulent pipe flow with feedback control is applied partially to the wall. In this the control input is applied only partially over a limited length in the stream wise direction, but not on the entire wall surface. The upstream control effect remains over a distance of about 11–14 times the pipe radius downstream of the point where the control is terminated. Active feedback control system generally consists of three functional hardware components, i.e., sensors, controllers and actuators, and an additional software component, i.e., a control algorithm which determines the action of actuators depending upon the sensor output. In parallel with intensive R&D studies of hardware components, the control algorithm has been develop and assessed by using direct numerical simulation of controlled turbulent flow field. Following results were obtained by simulation with the control on partial surface.

1. Average drag reduction is proportional to the area of control.
2. The local skin friction coefficient exhibits a complex stream wise variation despite the simple relation for the average drag reduction rate.
3. The flow recovers to the uncontrolled state about 11R–14R downstream of the controlled region.
4. The rapid recovery of the skin friction is observed right downstream of the controlled region.

7.3 Electro-Magneto-Hydro-Dynamic

(EMHD) Flow Control is used for reducing the intensity of the turbulence fluctuations which reduce frictional drag and heat transfer of turbulent boundary layer. In this the electromagnetically generated force field, or Lorentz field is generated by arrays of magnets and electrodes, called actuators, placed justbeneath or on a wall. Traditionally two types of actuator design have been used. One type generates a Lorentz field which is mostly parallel to the wall in the stream wise direction and the other generates a Lorentz field which is mostly normal to the wall. Although actuators which generate forces normal to the wall show promise of successfully controlling turbulent fluctuations.

8. Modern Methods of Flow Control

The manipulation in path of flow of the fluid for reduction in drag, increase in lift, increment in heat transfer can be done by techniques and methods that fall under the field of flow control. A few of the latest flow control technologies are discussed below.

8.1 A magneto rheological fluid (MR fluid) is a smart fluid. It is a type of smart fluid in a carrier fluid, usually a type of oil. When subjected to a magnetic field, the fluid greatly increases its apparent viscosity, to the point of becoming a viscoelastic solid. Magneto Rheological Fluids (MRFs), i.e. suspensions of ferri- or ferromagnetic particles in a water or an oil-based carrier fluid, stabilized by a surfactant or polymer, are deemed suitable for fluid flow control in oil and gas recovery operations. Porsche has introduced magneto rheological engine mounts in the 2010 Porsche GT3 and GT2.

8.2 In High Altitude Long Endurance (HALE) Aircrafts there is a necessity of high fuel storage. But due to vortex shredding, the wings of theaircraft cannot be made thick enough for carrying the extra load. So for this purpose, vortex entrapping is done to avoid vortex shredding and hence preventing reduction in lift. One way of doing this is to design a cavity on the surface of the airfoil around the point of separation which prevents the flow speed in the region around the mouth of the cavity to not drop to zero.

8.3 Plasma Actuators fall under the category of active flow control and is a type of actuator. These are used for flow control techniques due to their properties like induced body force by strong electric field. These can behave as vortex generators by inducing a local flow perturbation. Plasma actuators can be used for flight control by mounting actuators on the air foil to control the flight altitude and flight trajectory.

8.4 MEMS (Micro Electro MechanicalSystems)are one of the major advances in flow control is the emergence of Micro Electro Mechanical Systems (MEMS) technology, which employs the methods developed for the fabrication of silicon chips to construct very small-scale mechanical devices. The significance of micro machine technology is that it makes it possible to provide mechanical parts of micron size, batch fabricated in large quantities, and integrateablewith electronics. Miniaturized actuators also simplify the integration of

the control system with the overall structure or subsystem.

MEMS fabrication processes provide not only miniaturization, but also modular integration of sensors, actuators, and electronics and the affordability enabled by batch processing. However, micro devices for active flow control do not obviate the role of meso devices in flow control technologies.

9. Conclusion

In this paper we looked upon the developments in the Flow control technology in an organized and concise fashion. We studied about its historical advancement over five eras and its modern application in Turbulence Control, Separation Control and Drag Reduction. In the end we saw some examples of modern technologies like MR Fluid and MEMS which gave us a whole new outlook on how the science of flow control has changed over time.

References

[1] J. L. Gilarranz, L. W. Traub, & O. K. Rediniotis, "A new class of synthetic jet actuators - part II: application to flow separation control", Journal of Fluids Engineering 127, 377–387, 2005

[2] A. Glezer, & M. Amitay, "Synthetic jets, Annual Review of Fluid Mechanics", 34, 503–529, 2002

[3] T. R. Bewley, "Flow control: new challenges for a new renaissance", Progr Aero Sci 2001; 37:21–58

[4] D. You, P. Moin, "Study of flow separation over an airfoil with synthetic jet control using large-eddy simulation", Center for Turbulence Research Annual Research Briefs, 2007

[5] L. N. III Cattafesta, S. Garg, M. Choudhari, "Active Control of Flow-Induced Cavity Resonance," AIAA Paper 97-1804, 4th AIAA Shear Flow Control Conference, Snowmass, CO, June, 1997

[6] M. Gad-el-Hak, "Introduction to flow control" In: Gad-el-Hak M, Pollard A, Bonnet J, editors. Flow control: fundamentals and practices. Berlin: Springer; 1998.p. 199–273, 1998

[7] M. Amitay, A. Glezer, "Aerodynamic Flow Control of a Thick Airfoil using Synthetic Jet Actuators," ASME, FEDSM99-6922, (1999)

[8] C.-M. Ho, Y.-C. Tai, "Review: MEMS and Its Applications for Flow Control," ASME Journal of Fluid Engineering, 118, pp. 437-447, 1996

[9] B. G. Newman, "The deflection of plane jets by adjacent boundaries—Coanda effect", In: Lachman GV, editor. Boundary layer and flow control. Oxford: Pergamon Press; 1961

[10] R. Rathnasingham, Breuer K. S. System identification and control of a turbulent boundary layer. Phys Fluids 1997; 9(7):1867(9)

[11] S. S. Sritharan, "Optimal control of viscous flows Philadelphia", PA: SIAM, 1998.

[12] J. Lumley, P. Blossey, "Control of turbulence", Annu Rev Fluid Mech 1998; 30:311}27

[13] P. Perrier, "Multiscale Active Flow Control," in Flow Control: Fundamentals and Practices, eds. M. Gad-el-Hak, A. Pollard, and J.-P. Bonnet, pp. 275–334, Springer–Verlag, Berlin, 1998

[14] A. Seifert, O. Stalnov, D. Sperber, G. Arwatz, V. Palei, S. David, I. Dayan, I. Fono, "Large Trucks Drag Reduction Using Active Flow Control" 46th AIAA Aerospace Sciences Meeting and Exhibit7 - 10 January 2008, Reno, Nevada

[15] R. D. Wagner, D. W. Bartlett, D. V. Maddalon, "Laminar Flow Control is Maturing", Aerospace America 26, January, pp. 20-24, 1988

[16] M. C. M. Wright, P. A. Nelson, "Wind tunnel experiments on the optimization of distributed suction for laminar flow control", Proceedings of the Institution of Mechanical Engineers Part G: Journal of Aerospace Engineering, G215(6), 343-54, 2001

[17] S. M. Kellogg, "Immersed boundary methods with applications to flow control. Master's thesis", Rice University, Mechanical Engineering and Materials Science, 2000

[18] R. D. Joslin, "Using DNS for active flow control", AIAA Paper 2001-2544, 2001

[19] M. Amitay, V. Kibens, D. E. Parekh, A. Glezer, "Flow Reattachment Dynamics over a Thick Airfoil Controlled by Synthetic Jet Actuators", AIAA Paper No. 99-1001, 37thAIAA Aerospace Sciences Meeting, Reno, NV, January, 1999

[20] M. Gad-el-Hak, A. Pollard, J. Bonnet editors, "Flow control: fundamentals and practices" Berlin: Springer; 1998

[21] D. Greenblatt, I. J. Wygnanski, "The Control of Flow Separation by Periodic Excitation", Progress in Aerospace Sciences, 36 (2000), 487-545

[22] A. Seifert, T. Bachar, D. Koss, M. Shepshelovich and I. Wygnanski, "Oscillatory Blowing: ATool to Delay Boundary Layer Separation", AIAA Journal, 31(11), November 1993

The International Journal of Soft Computing and Software Engineering [JSCSE], Vol. 3, No. 3, Special Issue:
The Proceeding of International Conference on Soft Computing and Software Engineering 2013 [SCSE'13],
San Francisco, CA, U.S.A., March 1-2, 2013
Doi: 10.7321/jscse.v3.n3.123 e-ISSN: 2251-7545

A Quality Model for E-Learning as a Service in Cloud Computing Framework

Dr Rajni Jindal
Professor, Department of IT
Indira Gandhi Institute of Technology,
New Delhi, INDIA
rajnijindal@dce.ac.in

Alka Singhal
Research Scholar, CSE Dept
Delhi Technological University
New Delhi, INDIA
alkasinghal83@gmail.com

***Abstract* — Absence of proper metrics to evaluate cloud services holds back the customers to decide whether to shift their E-learning services on clouds or not. Therefore there is a requirement for a reliable Quality of Service Model which will act as a base to a well defined Service Level Agreement between Cloud providers and consumers. The Quality of Service model will be based on various functional and non functional requirements. This paper will provide a set of Cloud metrics like Availability, Elasticity etc which will help the cloud provider to create Cloud computing a mature and stable framework for E-learning system which will be adopted by the consumers at any level with reliability. The paper proposes a Quality of Service model for Cloud computing based E-learning system where construction and maintenance of the e-learning system is done by the cloud service providers and further these services are used by the E-learning provider by paying in cost per unit.**

Keywords— Framework, Quality of Service, Cloud Computing, Service layers, E-learning system

I. INTRODUCTION

A. Traditional E-learning Model

E-learning has emerged as a new paradigm of learning in the modern world. It economizes the cost of infrastructure and facilitates online learning. It also provides reusability of learning material and facilitates time and space independence. There can be lots of ways to use E-learning in education, example: continuous education, company training or community colleges etc but the underlying architecture is common. Traditional E-learning system is composed of following elements as shown in Fig1:

Content experts are responsible for the production of authorized learning material. Material can be lecture notes, video courses etc.

Learning Content Manager is responsible for management of the system. He is responsible for the management of the repository, registration of students, allocation of courses, conducting exams etc.

Repository consists of the content management. It is the metadata about the content. It involves proper indexing of the data. It involves authorization and authentication at the time of access etc.

Distribution Environment is the environment used for delivery of content. It includes high speed networks and setup for networking (switches, routers etc).

Finally, **Learner** is the one using the system to gain knowledge. He registers in the course and pay for the usage and content [1].

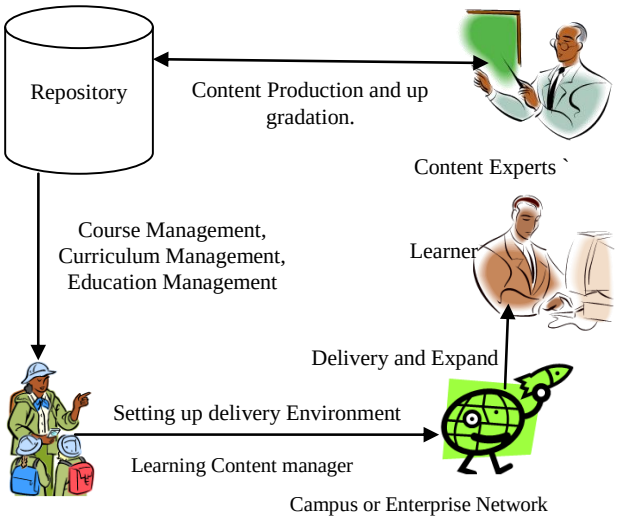

FIG1. TRADITIONAL E-LEARNING MODEL [2]

There were many challenges in front of traditional E-learning system which hampers its development and universal acceptance. The major challenge was the requirement of proper infrastructure and change management. Generally E-contents are videos, seminars which are bulky and require high speed networks for delivery. E-learning can be only successful if there is a proper infrastructure used for it. As infrastructural investment is more than the capital gained through the system, providers avoid switching their system to an online one. Other challenge is change management which depicts the required enhancement, up-gradation of content, updating all elements of E learning system like students, examinations etc. In E-learning system, there is a

The International Journal of Soft Computing and Software Engineering [JSCSE], Vol. 3, No. 3, Special Issue:
The Proceeding of International Conference on Soft Computing and Software Engineering 2013 [SCSE'13],
San Francisco, CA, U.S.A., March 1-2, 2013
Doi: 10.7321/jscse.v3.n3.123 e-ISSN: 2251-7545

requirement of an efficient application which enable regular change management.

Both of these problems can be solved by cloud computing. Cloud computing offers a dynamic provision of virtualized resources and payment on basis of the use of the resources. Cloud computing prevents the E-learning service provider to invest in initial hardware like servers, virtualization etc. In e-learning cloud computing business model, cloud provider is responsible for building and maintaining e-learning cloud, providing technical support to it. Cloud users pay to cloud provider for services from e-learning cloud and services accessed on- demand [2].

II. EVOLUTION OF CLOUD COMPUTING

Cloud computing is considered to be the fifth era of computing paradigms. Although there are many upcoming computing technologies which are still in development phase like HPC (High Performance Computing), Pervasive Computing, Service Oriented Computing etc but still cloud computing is considered as fifth era of Computing [3]. The reason is versatility of services which targets a broad area of users of various fields. It can be a scientist to a business man doing his deals. All the former computing paradigms target only specific users like HPC was made for the scientists or the people who require high computational powers [4][5].Pervasive Computing was for the people who require adaptability of their application. As their environment regularly changes due to their mobility, they require intelligent software which can provide a flexible mode of computation. And similarly, Service oriented computing targets the web service providers and consumers and doesn't care about computational power and flexibility. Cloud computing not only helps to increase the computational power by providing them infrastructural support but also provide flexible computing with on demand self service.

Cloud computing has many advantages as [5]:

(1) demand Self service

(2) Flexibility

(3) Availability

(4) Robustness

(5) Scalability

(6) Resource Sharing

Cloud computing provides 24X7 service to the customers. Whenever there is a need for the customer of any service (such as Software, Platform, Hardware etc), all what he needs is an internet connection and subscription to the provider. He can access the service without any manual intervention of the provider. Cloud computing services are flexible and they are not location dependent.

A. Cloud Computing Service Layer Model

The Cloud computing provides services at various levels and it can be viewed as layered structure as shown in Fig2. Various layers in Cloud computing service layer architecture are [6]:

Hardware Layer: It is the layer which provides actual hardware resources to the cloud infrastructure. As it is composed of different types of servers like rack servers, blade servers, it is also called server layer. It is basically the heart of the cloud and composed of data centre. It helps virtualization layer to implement redundancy and fault tolerance.

Virtualization Layer: This layer is basically a separator between request of service and actual underlying hardware. It helps in attaining hardware independence and also helps in managing multiple OS to provide efficient and reliable performance. It provides dynamic mapping of resources and service. It can be further viewed in three small layers Core Layer, Aggregation Layer and Access layer. Core Layer helps in traffic management, Aggregation helps in load balancing and Access layer manages multiple servers and interconnect them using switches.

Infrastructure as Service Layer: Infrastructure is to connect resources to business. It offers users to build their Virtual machines as service. They can create machine, configure them according to their requirement. They are billed according to their consumption of VM. This prevents them for spending in setting up data centers including physical server, networking devices.

Platform as Service Layer: It is not VM sufficient to build and run an application. One requires suitable operating system, programming languages. This layer provides user a complete setup to create and run programs. There is no need to manage operating system, but one just has to create programs in a given customized environment.

Software as Service Layer: This layer eliminates the requirement of developing of application. It provides complete application to work on. User uses these application and pay according to the usage of the software.

Client layer: It is User Interface on the client/user machine, which helps him to use the underlying services.

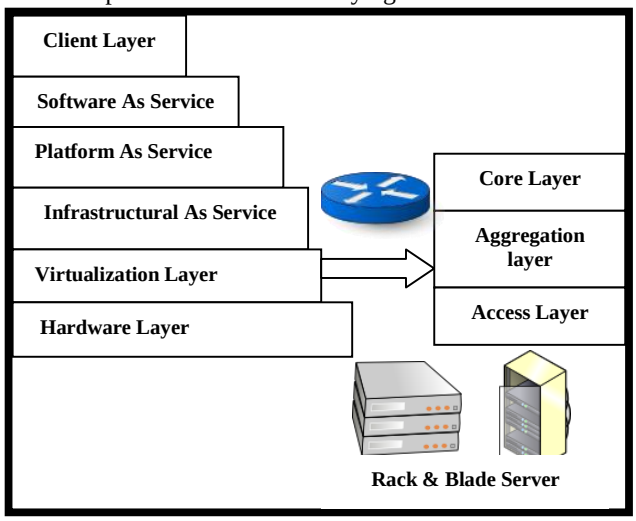

FIG2. CLOUD COMPUTING SERVICE MODEL

The International Journal of Soft Computing and Software Engineering [JSCSE], Vol. 3, No. 3, Special Issue:
The Proceeding of International Conference on Soft Computing and Software Engineering 2013 [SCSE'13],
San Francisco, CA, U.S.A., March 1-2, 2013
Doi: 10.7321/jscse.v3.n3.123 e-ISSN: 2251-7545

B. Cloud Computing Deployment

There are following cloud computing deployment model [7]:

Private cloud: It is a proprietary architecture subscribed by an organization, which provides hosted services to the users within the organization. This is protected by the firewall to form a barrier against outside the world to access hosted services from the private cloud. A private cloud infrastructure is operated solely within a single organization, and managed by the organization or a third party regardless whether it is located premise or off premise.

Public cloud: It is not proprietary of any organization; the services provided in these clouds can be accessed by any organization. The public cloud is used by the general public cloud consumers and the cloud service provider has the full ownership of the public cloud with its own policy, value, profit, costing, and charging model.

Hybrid cloud: In Hybrid cloud, the services are offered to the limited and well defined number of parties. The cloud infrastructure is a combination of two or more clouds (private, community, or public) that remain unique entities but are bound together by standardized or proprietary technology that enables data and application portability (e.g., cloud bursting for load-balancing between clouds).

Community cloud: Several organizations jointly construct and share the same cloud infrastructure as well as policies, requirements, values, and concerns. The cloud community forms into a degree of economic scalability and democratic equilibrium. The cloud infrastructure could be hosted by a third-party vendor or within one of the organizations in the community.

III. E-LEARNING ON CLOUDS

As earlier explained the major challenges to adopt E-learning as a business model are infrastructure and change management.
Both of these problems can be solved by cloud computing as it offers a dynamic provision of virtualized resources and payment on the basis of the use of the resources. Cloud computing prevents the E-learning service provider to invest in initial hardware like servers, virtualization etc. In e-learning cloud computing business model, cloud provider is responsible for building and maintaining e-learning cloud, providing technical support to it. Cloud users pay to cloud provider for services from e-learning cloud and services accessed on- demand [9].
Cloud computing provides various layers of services which can be utilized by the E-learning providers. Therefore there can be various architectures for E-learning on clouds as shown in Fig4. It can be Infrastructural as Service (IaaS) and Platform as Service (PaaS), where one will utilize just the basic infrastructure or platform provided by the cloud. Rest the software, application setup is consumer's overhead. In this case the second challenge of change management is still in the part of consumer. Here consumer has to develop the software for the whole system.

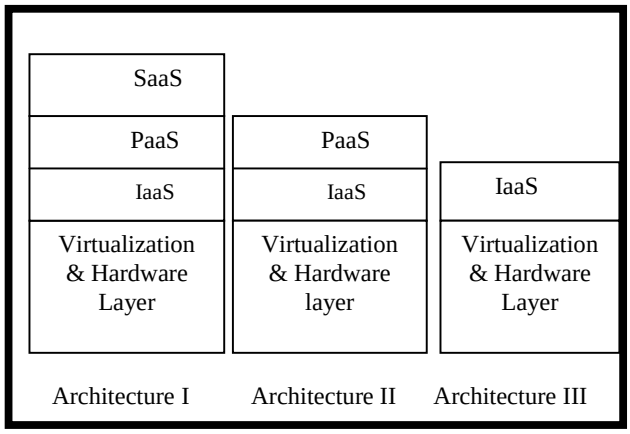

FIG3.VARIOUS CLOUD SERVICE ARCHITECTURE OF e-LEARNING

Second option is to utilize Software as Service (SaaS) where cloud provider will provide the whole application to maintain E learning system as shown in Fig 4. At the lowest level, the institutions which will provide the e-learning service produce courses, content management and its up-gradation and maintenance. E-learning Cloud provides suitable resources for storage and computation. Then the service layers in cloud computing, namely, SaaS (Software as a Service), PaaS (Platform as a Service), IaaS (Infrastructure as a Service) provides services to cloud users (Institutions) for Education management, Course management etc. On the other hand it provides environment for delivery to the learner. Learner can be at any remote place. Cloud services help in efficient delivery. Learner pays to the Institution for courses undertaken and in response cloud users (Institutions) pay Cloud providers for their services. Such services are provided by SCORM cloud.

SCORM (Sharable content object reference Model) provides set of technical standards for E-learning software and SCORM cloud provides an API to develop ones E-learning system in a standardized form with full maintenance provided by them [11].

IV. QUALITY OF SERVICE IN E-LEARNING BASED ON CLOUDS

Though there are lots of advantages of adopting cloud services for E-learning, absence of proper metrics to evaluate cloud services holds back the customers to decide whether to shift their E-learning services on clouds or not. Therefore there is a requirement for a reliable Quality of Service Model which will act as a base to a well defined Service Level Agreement between Cloud providers and consumers. The Quality of Service model will be based on various functional and non functional requirements. It will make Cloud computing a mature, stable and computable framework for E-learning system which will be adopted by the consumers at

The International Journal of Soft Computing and Software Engineering [JSCSE], Vol. 3, No. 3, Special Issue:
The Proceeding of International Conference on Soft Computing and Software Engineering 2013 [SCSE'13],
San Francisco, CA, U.S.A., March 1-2, 2013
Doi: 10.7321/jscse.v3.n3.123 e-ISSN: 2251-7545

any level with reliability. Key process areas responsible to make a quality cloud suitable for E-learning system are:

A) Availability

B) Response Time

of first response of service. Response time reflects the fastness of the service. Less is the time, better is the service. Average Response time can also be calculated by

Response Time (RT) =Time taken by the service to give first response on the request of service

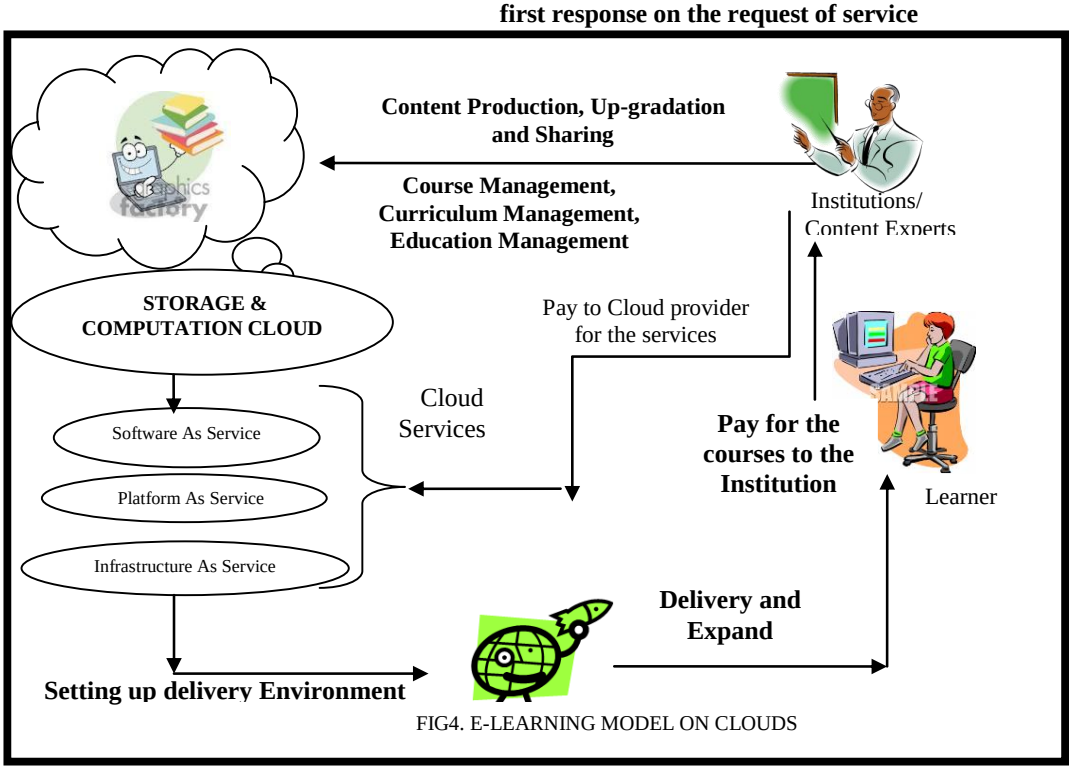

FIG4. E-LEARNING MODEL ON CLOUDS

C) Change management

D) Elasticity

E) Reliability

Availability: Availability is expressed as the percentage of time the application can be accessed by the user. If cloud technology is used for E-learning systems, it should provide 24x7 (100%) availability to the customers (students). Availability lacks when service cannot be invoked due to some service failure at the provider side. Availability is an important quality metric as it is the most important factor which motivated the switching from traditional learning to E-learning.

Availability can be calculated by

$$\mathbf{Av} = \frac{\textbf{Number of times service was able to invoke}}{\textbf{Number of times service was called}}$$

Value ranges from 0…1

Average Response time: Response Time can be expressed as time elapsed between time of requesting service and time

Average response time = RT_n/n

Change management (Agility): Change management can be viewed as the efforts required for changing the software with respect to customers requirement. E-learning system is a system which requires regular updation with time.

It requires regular amendment in curriculum; syllabus, policies etc and all these are reflected in the software. The Cloud SaaS used for E-Learning should be easily modifiable according to time.

Modifiability of the application can be measured by cohesiveness and degree of coupling between different modules of the code. More is the cohesiveness; difficult is to modify the code.

Elasticity: Elasticity is the criterion which depicts the capability of software to keep its performance consistent with increase or decrease in demand. In case of E-learning system it is basically the number of users which can increase as well as decrease with time. Software should be adaptable to scale its resources according to the requirement.

$$\mathbf{Elasticity} = \frac{\textbf{Number of resources getting utilized for ith of n service}}{\textbf{Number of resources available for ith of n service}}$$

The International Journal of Soft Computing and Software Engineering [JSCSE], Vol. 3, No. 3, Special Issue:
The Proceeding of International Conference on Soft Computing and Software Engineering 2013 [SCSE'13],
San Francisco, CA, U.S.A., March 1-2, 2013
Doi: 10.7321/jscse.v3.n3.123 e-ISSN: 2251-7545

Elasticity also depends on number of services (n) running at a given point of time. If users of one service reduce in number then its allocated resources can be given to other service whose users are greater than expected.

Reliability: Reliability can be expressed as the chances of failure free operation of the application for a specified time in a given environment. It depends on occurrence of failures and fault recovery. It is measured in terms of
Number of failures (n) per execution time and

$$\textbf{Fault tolerance} = \frac{\textbf{Number of failures recovered}}{\textbf{Number of failures occurs}}$$

V.FUTURE WORK AND CONCLUSION

With above mentioned Quality criteria, there are some more criteria which should also be addressed like Accountability, Cost model. Accountability is responsible for creating trust between provider and user. It plays vital role in Security issues and data ownership. It ensures user that his data will not be shared with any unauthorized user. Costing Model is also required for a proper E-learning system. There can be two ways of costing (CAPEX and OPEX). Cloud based application generally follows OPEX model. But then also a proper costing model is yet to be made for an E-learning system cloud based on usage of infrastructure and services.

This paper proposes a quality of service model of Cloud Computing based E-learning. It comprise of a framework where construction and maintenance of e-learning system is done by the cloud services providers and further these services are used by the e-learning provider by paying in cost per unit. Here E-learning provider is not concerned about the infrastructural and maintenance expenses but focuses on the content quality and management .Whereas, the Cloud providers have already established infrastructure, so they can utilize it for providing E-learning services without any additional investment in compare if it is done by Institution itself. This paper provides a basic Quality model for E-learning Cloud to measure basic quality metrics for an E-learning Cloud. It extracts five basic quality attributes which will help cloud provider to create efficient, flexible cloud for E-learning system.

REFERENCES

[1] Xiaofei Liu, Abdulmotaleb El Saddik, Nicolas D. Georganas, "An implementable architecture of an E-learning system", presented at CCECE 2003, Montreal, May 2003

[2] Rajni Jindal, Alka Singhal "Social Networking based E-Learning System on Clouds" International Journal of Computer Applications, March 2012, pp.45-48

[3] Laisheng,Wang Zhengxia, "Cloud Computing: a New Business Paradigm for E-learning", presented at Third International Conference on Measuring Technology and Mechatronics Automation 2010

[3] Sameer Rajan, Apurva Jairath, "Cloud Computing: The Fifth generation of Computing", presented at International Conference on Communication Systems and Network Technologies, 2010

[4] Shuai Zhang, Shufen Zhang, Xuebin Chen, Xiuzhen Huo, "The Comparison Between Cloud Computing and Grid Computing", presented at International Conference on Computer Application and System Modeling (ICCASM 2010)

[5] Naidila Sadashiv,S. M Dilip Kumar, "Cluster, Grid and Cloud Computing: A Detailed Comparison", presented at the sixth International Conference on Computer Science & Education (ICCSE 2011) August 3-5, 2011

[6] Tharam Dillon, Chen Wu and Elizabeth Chang," Cloud Computing: Issues and Challenges" presented at 24th IEEE International Conference on Advanced Information Networking and Applications, 2010

[7] Junjie Peng, Xuejun Zhang, Zhou Lei, Bofeng Zhang, Wu Zhang, Qing Li, "Comparison of Several Cloud Computing Platforms",2009 IEEE.

[8] Lijun Mei,W.K. Chan†,T.H. Tse, "A Tale of Clouds: Paradigm Comparisons and Some Thoughts on Research Issues", presented at IEEE Asia-Pacific Services Computing Conference 2008

[9] Laisheng,Wang Zhengxia, "Cloud Computing: a New Business Paradigm for E-learning", Third International Conference on Measuring Technology and Mechatronics Automation 2011

[10] Mohssen M. Alabbadi, "Cloud Computing for Education and Learning: Education and Learning as a Service (ELaaS)", presented at 14th International Conference on Interactive Collaborative Learning (ICL2011)

[11] Shared Content Object Reference Model (SCORM), http://scorm.com/scorm-explained

Volume 1 (2013) 86-89 ISSN 2347 - 3258
International Journal of Advance Research and Innovation

A review of Pulse current gas tungsten arc welding for different alloys

P. K. Baghela
Department of Mechanical Engineering, Delhi Technological University, Delhi, India

Article Info

Article history:
Received 1 July 2013
Received in revised form
15 July 2013
Accepted 22 July 2013
Available online 1 August 2013

Keywords

Abstract

Pulse current gas tungsten arc welding is an important joining technique for different metals like Aluminium, Magnesium, Steel, Titanium and their alloys. With increasing application of these metals and alloys in aerospace, aircraft, automotive, electronics and other industries PTIGW is the best technique evolved so far. In this document an attempt has been made to critically review this welding technique from different perspective for different metals and alloys. Some important PTIGW processing parameters and their effect on weld quality are discussed. The microstructure and metallurgical defects encountered during welding process such as porosity, cracking, oxide inclusions and loss of alloying elements are described. Mechanical properties of welds such as hardness, tensile and fatigue strength, and other important structural properties are discussed. The aim of the report is to review the recent progress in PTIGW of different metals and alloys and to provide the basis for follow-on research.

1. Introduction

Reduction of mass is a prime concern for many industries involved in making household appliances and transportation. Therefore the selection of metals and its alloys on the basis of properties suited to different industries has become significant. Hence the focus on lightweight materials like aluminium and magnesium and other corrosion resistant materials like steel and titanium has become predominant [1]. Aluminium based alloys have been widely used in automobile structures due to their unique property such as high strength to weight ratio. Although large scale production of these metals will not be feasible in near future, there is no doubt that the use of these metals and alloys based material will be increasing steadily. Metals and its alloys can be joined by most fusion and solid state welding processes, as well as by brazing and soldering. Fusion welding is commonly done by GMAW (Gas Metal Arc Welding), GTAW (Gas Tungsten Arc Welding) and resistance spot and seam welding. Plasma and Electron Beam Welding are used in special applications. SMAW (Shielded Metal Arc Welding) and oxy-fuel gas welding may be used for applications where high strength and quality are not much of the interest. Two welding process mostly used for Al, steel, Mg and titanium are GMAW, and GTAW. GTAW was the first arc welding process applied to aluminium [2]. It produces very attractive welds, with good profile and bright appearance. GTAW welding, often requiring hand fed filler rod to build up the weld deposit. In GTAW welding technique the tungsten electrode is used to strike arc and melt the base metal where welding is to be done.

Corresponding Author,
E-mail address:mech.dtu@gmail.com
All rights reserved: http://www.ijari.org

2. Pulse TIG Welding

This is modified version of TIG welding in which the welding current (DC) is supplied in form of pulses. The pulsed current alternates between a low or background level and peak level. The duration and amplitude of both peak and background currents can be varied independently to suit the job. The melting takes place during peak current period, and the weld pool solidifies between pulses as the heat is dissipated in the job during the background current period [3]. This current pulsing leads to intermittent melting along the joint seam, giving a series of discrete melt spots, which overlap each other [4]

3. Advantages of the Pulse TIG welding

- It tolerates variation in the fit-up or clamping.
- It permits welding of sheets down to 1 mm with ease, which is normally difficult by standard TIG process.

- It minimizes distortions owing to controlled heat input.
- It makes positional welding easy.
- It requires less operator skill as compared to the normal TIG process.
- It shows marked improvement in weld quality.
- The strong electromagnetic forces developed by the high pulse of current agitate the weld puddle and therefore eliminate weld porosity and thorough root fusion[5].

4. Pulse TIG welding on Aluminium Alloys

Senthil Kumar et.al [6] studied the influence on the tensile properties of AA 6061 aluminium alloy and found out that factorial experimentation technique is more convenient to predict the effect of pulsed current welding parameters on tensile properties of AA 6061 welded aluminium alloy joints. Investigation shows that peak current and pulse frequency are directly proportional to the tensile properties of the welded joints. Study also revealed that base current and pulse on time is having inversely proportional relationship with the tensile strength.

Sanjeev Kumar [7] explored the possibility of welding higher thickness aluminium plates of 6mm. Experimental investigation revealed that tensile strength of the joint has been found to be comparable with DC current, when prepared at some gas flow rate i.e. 7 litre/min. It was also found that tensile strength is optimum at pulse current of 250 Amp and gas flow rate of 15 litre/min and base current 200 Amp.s. It has also been observed that shear strength varies with change of pulse current. Microstuctural studies of weld deposit shows two distinct zones, co-axial dendrites adjacent to fusion line and the fine equiaxed grain in the region of weld center.

Kumar and Sundarrajan [8] attempted to optimize the pulsed TIG welding process parameters of AA 5456 Aluminium alloys welds for increasing the mechanical properties. Experiments were conducted to find out influence of pulsed welding parameters such as peak current, base current, welding speed and frequency on mechanical properties such as ultimate tensile strength, yield strength, percent elongation and hardness of AA 5456 Aluminium alloy weldments. Experimental results showed that there is 10-15% improvement in mechanical properties after planishing. Metallographic analysis further revealed the fine grain structure at the weld centre, which resulted in higher mechanical properties.

Karunakara and Balasubramanian [9] studied the effect of pulsed current on temperature distribution, weld bead profiles and characteristics of gas tungsten arc welded aluminium alloy joints and found out that pulsed current welding technique records lower peak temperatures and lower magnitude of residual stresses compared with constant current welding, which is highly preferable for thin sheet welding. Results further revealed that joint produced by gas tungsten arc welded aluminium alloy exhibits superior tensile properties compared with constant current welding technique. Research further pointed out that the formation of finer grains caused by pulsed current is the main reason for enhanced tensile and hardness properties of the joints.

Laiping et.al [10] developed the model of welding pool surface reflectance of aluminium alloy. Study showed that during welding, surface height of welding pool plays an important role in precise control of welding process. Surface reflectance model of welding pool was built after the analysis of arc intensity, filter system, shape and reflectance characteristics of welding pool and camera parameters which was based on predictions of weld pool characteristics.

5. Pulse TIG welding on Steel alloys

Lothongkum et.al [11] studied the effect of PTIGW parameters on the delta-ferrite content, shape factor and bead quality in the orbital welding of AISI 316L stainless steel plate. The experimental results clearly revealed that increasing welding speed will increase the pulse current. Further they also observed that while increasing the nitrogen content in argon gas decreases the pulse currents, and due to this the solubility of nitrogen in the weld decreases. Researchers found out that from the 6 to 12 h welding positions the pulse currents decrease to be a minimum at 9 h welding position and increase again at 12 h welding position. Delta-ferrite content also observed in the weld ranges from 6 to 10 % by volume.

Lothongkum, Chaumbai and Bhandhubanyong [12] explored the possibility of PTIGW of 304L austenitic stainless steel in flat, vertical and overhead positions. Researchers sucessfully identified the PTIGW parameters at three different positions with nitrogen content of 0-3% (v/v) in the argon which is used as a shielding gas and same nitrogen content in argon was also enough to control the delta-ferrite content which is often accepted in range of 3-12% (v/v). The welding speed in those positions was found to be 3.4 mm/s at 55% on-time with fixed pulse and base currents.

Madadi et.al [13] explored the deposition process of stellite 6 on plain carbon steel plate using PTIGW cladding process and experimental facts revealed that

the central composite rotatable design technique with five-level, full-factor full-factorial design matrix and mathematical models was used to predict hardness and dilution of satellite 6 on carbon steel with high accuracy. Results also indicated that the parameters chosen were significant in clad dilution. Further, welding current found out to be effective parameter which influences heat input and melting and dilution.

6. Pulse TIG welding on Titanium alloys

Balasubramanian et.al [14] attempted to develop mathematical models to predict grain size and hardness of PTIG welded Ti-6Al-4V alloy and found out that procedure is limited to the range of factors considered for investigation. The model developed can also be effectively used to predict the hardness and grain size of titanium alloy within the range of parameters.

Some researchers [15] performed the experimental study to understand the effect of process parameters of PTIG welded titanium alloy and results reveals that four important process parameters of PTIGW were used to optimize the three quality characteristics of tensile properties. Further, the experimental investigation showed that pulse frequency is having greater effect on the multiple quality characteristics of the tensile properties.

Some researchers [16] studied the effect of PTIG on corrosion rate of titanium alloy. It was observed that effect of pulse frequency and peak current had two regions with initially decreasing the corrosion rate and then increasing the corrosion rate irrespective of changes in the base current and pulse on time. Further investigations revealed that the grain refinement has taken place which resulted in increase in corrosion resistance. Study also revealed the parameters which mostly influence the corrosion properties of titanium alloy were peak current and pulse frequency.

Some researchers [17] studied the effect of microstructure on the impact strength of PTIG welded α-β titanium alloy. It have been found that Impact toughness of the joints is having inversely proportional relationship to grain size. Further study revealed the parameters which mostly influence the grain size effect on impact strength are peak current and pulse frequency.

Some investigators [18] studied the effect of PTIGW parameters on Ti-6AI-4V titanium alloy and it was observed that effect of pulsing frequency and peak current had two regions with initially increasing the tensile properties irrespective of changes in base current and pulse-on-time. It has been observed that the main reason of increased tensile property at weld fusion zone is due to grain refinement. Further the value of optimum frequency at which tensile properties are maximum has also been determined.

7. Pulse TIG welding on Magnesium alloys

Roze et.al [19] developed the empirical relationship to predict tensile strength of PTIG welded AZ61A magnesium alloy by incorporating process parameters such as pulse current, base current, pulse frequency and pulse on time. Different statistical tools such as design of experiments, analysis of variance, and regression analysis were used to develop the relationships. Further the effect of pulse current on AZ61A magnesium alloy was studied and experimental results revealed that effect of peak current and pulsing frequency initially increasing the tensile properties and then decreasing the tensile properties irrespective of changes in base current and pulse on time. Study also revealed that pulse current was more sensitive than the other parameters such as pulsed on time, pulse frequency and base current.

Padmanaban et.al [20] compared the fatigue crack growth behaviour of AZ31B magnesium alloy welded by three techniques i.e PTIGW, Friction stir welding (FSW), Laser beam welding (LBW). It was found that laser beam welded joints offered better resistance against the fatigue cracks as compared to FS and PTIG welded joints. Fine grains were observed in weld region and higher hardness was observed in fusion zone. It was also observed that precipitates and favourable residual stress field of the weld region are the main reasons for superior fatigue performance of laser beam welded joints of AZ31B magnesium alloy.

8. Conclusion

PTIG welding is probably an important joining technique for different metals and alloys and can promote their wider uses in aerospace, aircraft, automotive, electronics and other industries. This review explores the effect of some influencial parameters of PTIGW process which effects tensile strength and bead geometry of the joint being fabricated by this process. In the future scientific investigation is still needed to understand and overcome these basic weldability problems like distortion and warpage of metals and alloys.

References

[1] K. Elangovan, V. Balasubramanian, " Influences of tool pin profile and tool shoulder diameter on FSP zone formation in AA6061 aluminium Alloy", J Materials & Design 28(2): 362−373, 2008

[2] T. S. Kumar, V. Balasubramanian, M. Y. Sanavullah, "Influences of pulsed current tungsten inert gas welding parameters on tensile properties of AA6061 aluminium alloy", J Materials & Design 28(2): 2080-2092, 2007

[3] W. Lucas, "Alternating current MIG welding. Welding Inst", Conference. Advance in welding processes, pp 117-121, 1975

[4] T. N. Ngugen, M. A. Wahid, "The Effect of residual stresses on fatigue of butt Joints. J welding" 75(2):55-61, 1996

[5] K. J. Schroeder, "Structural adhesives for aluminium vehicles. Conference Developments in Aluminium use for vehicle Design, 26-29 Feb 1996, Detroit MI, U.S.A

[6] Senthil Kumar T, V. Balasubramanian, M. Y. Sanavullah, "Influences of pulsed current tungsten inert gas welding parameters", J of Materials & Design 26(2): 2045-2092, 2007

[7] S. Kumar, "Experimental investigation on PTIG welding of Aluminium plate", J of Advanced Engineering and Technology 23(3): 2374-2398, 2009

[8] A. Kumar, S. Sundarrajan, "Optimization of pulsed TIG welding process parameters on mechanical properties of AA 5456 Aluminium alloy weldments. J Material & Design 30:1288-1297, 2009

[9] N. Karunakaran, V Balasubramanian, "Effect of pulsed current on temperature distribution, weld bead profiles and characteristics of gas tungsten arc welded aluminium alloy joints", J Trans.Nonferrous Met. Soc.China 21:278-286, 2011

[10] Li Laiping, C Shanben, L Tao, "The modelling of welding pool surface reflectance of aluminium alloy pulse GTAW", J Material Science & Engineering 394:320-326, 2005

[11] G. Lonthongkum, E. Viyanit, Bhandhubanyong, "Study on the effects of pulsed TIG welding parameters on delta-ferrite content, shape factor and bead quality of AISI 316L SS plate", J Materials Processing Technology 110:233-238 2001

[12] G. Lothongkum, P. Chaumbai, Bhandhubanyong, "TIG pulse welding of 304L austenitic stainless steel in flat, vertical and overhead positions", J Materials processing Technology 90:410-414, 1999

[13] F. Maddai, F. Ashrafizadeh, M. Shamanian, "Optimization of pulsed TIG cladding process of stelite alloy on carbon steel using RSM", J Alloys and Compounds 510:71-77, 2012

[14] M. Balasubramanian, V. Jayabalan, V. Balasubramanian, "Developing mathematical models to predict grain size and hardness of PTIG welded titanium alloy", J Materials Processing Technology 196:222-229, 2008

[15] M. Balasubramanian, V. Jayabalan, V. Balasubramanian, "Process Parameter Optimization of the Pulsed Current Argon Tungsten Arc Welding of Titanium Alloy J Mater",, Sci. Technol.24 (3):423, 2008

[16] M. Balasubramanian, V. Jayabalan, V. Balasubramanian, "Effect of pulsed gas tungsten arc welding on corrosion behavior of Ti–6Al–4V titanium alloy", J Materials and Design 29:1359–1363, 2007

[17] M. Balasubramanian, V. Jayabalan, V. Balasubramanian, "Effect of microstructure on impact toughness of pulsed current GTA welded α–β titanium alloy", J Materials Letters 62; 1102–1106, 2007

[18] M. Balasubramanian, V. Jayabalan, V. Balasubramanian, "Effect of current pulsing on tensile properties of titanium alloy," J Materials and Design 29:1459–1466, 2008

[19] R. A. Razal, K. Manisekar, Balasubramanian, Rajakumar S, "Prediction and optimization of pulsed current tungsten inert gas welding parameters to attain maximum tensile strength in AZ61 A magnesium alloy", J Materials and design 37:334-348, 2012

[20] G. Padmanaban, V. Balasubramanian, G. M. Reddy, "Fatigue crack growth behaviour of pulsed current gas tungsten arc, friction stir, and laser beam welded AZ31B magnesium alloy joints", J Materials Processing Technology 211:1224-1233, 2011

ISBN 978-93-5156-328-0
International Conference of Advance Research and Innovation (ICARI-2014)

A Review on Properties of phase change material for solar thermal storage system

Kaushalendra Kumar Dubey*, Radheshyam Mishra
Department of Mechanical Engineering, Delhi Technological University, New Delhi, India

Article Info

Article history:
Received 29 December 2013
Received in revised form
10 January 2014
Accepted 20 January 2014
Available online 1 February 2014

Keywords

TSED,
Micro/Macro-encapsulation,
Phase Change Slurry

Abstract

Thermal energy could have several geneses but storage of solar thermal energy is one of the principal areas of investigation. The various conventional and unconventional materials are investigated for their capability to store thermal energy. These thermal energy storage devices (TESD) are selected on the basis of some essential properties like, thermal, physical, chemical properties and economic aspects. Melting point, heat of fusion, density, heat capacity, thermal conductivity, compatibility with container and cost of production are the chief parameters for selection of phase change material. Phase change materials (PCMs) have the capability of storing heat (latent heat storage units) and phase transition point to the environment of the operating temperature. This research paper focus on assessment of PCMs properties and economic aspect for rural and industrial applications. The design and development of thermal storage system depend on fundamentals of thermodynamic or heat transfer analysis

Nomenclature

Cp=Specific Heat (J/Kg ^{0}C)
C_{lp}= Specific Heat between Tm and T_2 (J/kg K)
Csp= Specific Heat between T_1 and Tm (J/kg K)
Δh_m = Heat of fusion per unit mass (J.kg)
k= Thermal Conductivity (W/m^{0}C)
m=Mass of heat storage medium (kg)
ρ = Density of PCM medium ($kg \cdot m^{-3}$)
Q= Quantity of heat stored (J).
T_1= Initial Temperature (^{0}C)
Tm= Melting Temperature (^{0}C)
T_2= Final Temperature (^{0}C)
X_m=Fraction Melted
$X\tau$ = Fraction rejected
$\Delta h\tau$ = Endothermic heat of rejection.
VHC = Volumetric heat capacity($\cdot m^{-3} \cdot K^{-1}$)
TESD-Thermal Energy storage devices
PCM-Phase change material.
PCS-Phase change slurry.
TES-Thermal Energy storage
LHS-Latent heat storage
CG-Commercial grade
AG-Analytical grade
EGDS-Ethylene glycol distearate
BTU-British-thermal-unit
DSC-Differential scanning calorimeteic
TGA-Thermal gravimetric analysis

Corresponding Author,
E-mail address: kaushalendra@gmail.com
All rights reserved: http://www.ijari.org

1. Introduction

The different forms of energy that can be stored include mechanical, electrical, and thermal energy. Mechanical energy storage systems include gravitational energy storage or Pumped Hydro Power Storage, Compressed Air Energy Storage and Flywheels, these technologies can be used for large-scale utility energy storage. Apart from these systems, Thermal energy can be stored as a change in internal energy of a material as sensible heat, latent heat, and thermo-chemical heat. In case of sensible heat storage (SHS) system, energy is stored or extracted by heating of cooling a solid or a liquid which does not change its phase during charging and discharging process. Water, heat transfer oils, and certain molten salts have

been used in liquid type SHS systems where as rocks, pebbles and refractories used in solid type SHS systems. The latent heat storage system using Phase Change Materials (PCM) is an effective way of storing thermal energy (solar energy, off-peak electricity, and industrial waste heat) and has the advantages of high storage density and the isothermal nature of the storage process. In latent heat storage system, heat is stored in a material when it melts and extracted from the material when it freezes by the phase change of used materials (S.P Shukhatme,).1940s Dr. Telkes found idea about some chemicals based energy storage system, which posses the heat during phase change and define the new area of research as a Latent Heat Storage materials or phase change materials, but did not receive much attention, however until the energy crisis of the late 1970s and early 1980s.The first PCM application described for heating and cooling in buildings by Telkes in 1975 and by Lane in 1983 (Kaygusuz, 1999; Sari et al. 2000)

1.1 Thermal Energy Storage (TES)

The need of thermal energy storage may often be linked to the following cases-

• There is a mismatch between thermal energy supply and energy demand,
• When intermittent energy sources are utilized, and
• For compensation of the solar fluctuation in solar heating systems.

Water appears to be the best SHS liquid because it is inexpensive and has high specific heat. However above 1000c, oils, molten salts and liquid metals, etc are used. For air heating applications rock bed type storage materials are used. In the application of load levelling, heat is usually stored in a refractory bricks storage heater, these units capable of providing space heating during the day from the stored heat during the night (Prabhu et al,2012).

2) Latent Heat Storage (LHS)-

If the material changes its phase at a certain temperature while heating the substance then heat is stored in the phase change. Reversing, heat is dissipated when at the phase change temperature it is cooled back. The heat storage capacity of the phase change materials is equal to the phase change enthalpy at the phase change temperature + sensible heat stored over the whole temperature range of the storage (Sharma, S.D et al, 2005, Buddhi.D.et al, 2007).

There are three main physical ways for thermal energy storage: sensible heat, phase change reactions and thermo chemical reactions. Storage based on

1.2Physical principles of thermal energy storage

When a thermal storage need occurs, there are three main physical principles to provide a thermal energy function:

1) Sensible Heat Storage (SHS)-

The thermal energy stored by raising the temperature of a solid or liquid material. The amount of heat stored depends on the specific heat of material, change in temperature and amount of storage material (Sharma, S.D et al,2005).

$$Q = \int_{T1}^{T2} m\,Cp\,dT \qquad (1)$$

$$= mCp\,(T_2\text{-}T_1) \qquad (2)$$

2) Latent Heat Storage (LHS)-

If the material changes its phase at a certain temperature while heating the substance then heat is stored in the phase change. Reversing, heat is dissipated when at the phase change temperature it is cooled back. The heat storage capacity of the phase change materials is equal to the phase change enthalpy at the phase change temperature + sensible heat stored over the whole temperature range of the storage (Sharma, S.D et al,2005, Buddhi.D.et al,2007)

1.2 Physical principles

chemical reactions has much higher thermal capacity than sensible heat but are not yet widely commercially viable. Large volume sensible heat systems are promising technologies with low heat losses and attractive prices

$$Q = \int_{T1}^{Tm} mCp\,dT + mX_m\Delta h_m + \int_{Tm}^{T2} Cp dT \qquad (3)$$

$$= m\,[Csp\,(Tm - T_1) + X_m\Delta h_m + Clp\,(T_2 - T_m)] \quad (4)$$

This method of heat energy storage provides much higher energy storage density with a smaller temperature swing. However, practical difficulties usually arise in applying the latent heat method due to the low thermal conductivity, density change, and stability of properties under extended cycling and sometimes phase segregation and sub cooling of the phase change materials (Prabhu et al 2012)

3) Thermochemical energy storage-

The sorption or thermo chemical reactions provide thermal storage capacity. The basic principle is: AB + heat ⇔ A+B; using heat a compound AB is broken into components A and B which can be stored

separately bringing A and B together AB is formed and heat is released. The storage capacity is the heat of reaction or free energy of the reaction (Sharma, S.D et al, 2005)

$Q = X\tau m\Delta h\tau$ (5)

2. Characteristics and classification of PCM

Phase change materials (PCMs) have the capability of storing heat (latent heat storage units) and phase transition point to the environment of the operating temperature. The purpose for which they are designed is to prevent heat loss by absorption or release thereof. A PCM classification based on their composition is detailed in fig-1.

PCMs are categorized as Organic, Inorganic and Eutectic materials source

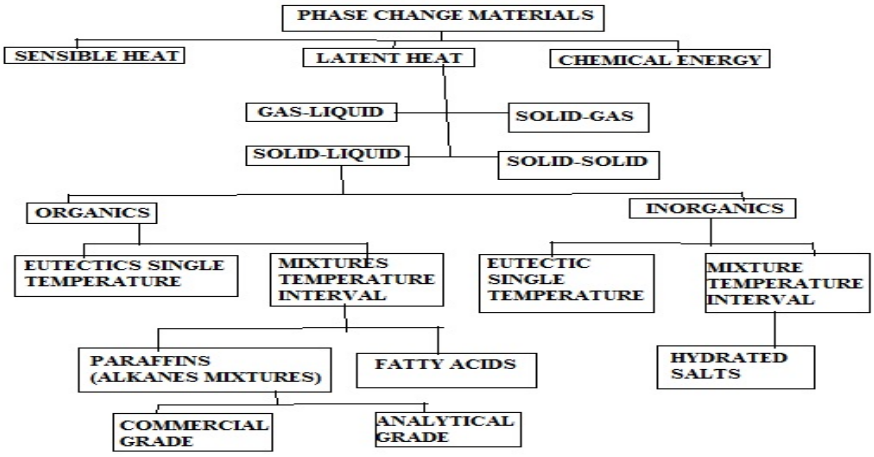

Fig: 1. Classification of phase change material (D.Juárez et al, 2013)

2.1 Organic PCMs-(Paraffin (C_nH_{2n+2}) and fatty acids ($CH_3(CH_2)_{2n}COOH$))

Organic materials are further described as paraffin and non-paraffins. Organic materials include congruent melting, self-nucleation and usually non-corrosiveness to the container material (A.Sharma et al,2009). Commonly used organic PCMs for heating and cooling in buildings falling in the range of 20–320C with their melting point and latent heat of fusion are listed in Table 1.

2.1.1 Advantages

1. Freeze without much supercooling.
2. Ability to melt congruently.
3. Self nucleating properties.
4. Compatibility with conventional material of construction.
5. No segregation.
6. Chemically stable.
7. High heat of fusion.
8. Safe and non-reactive.
9. Recyclable

2.1.2 Disadvantages

1. Low thermal conductivity in their solid state. High heat transfer rates are required during the freezing cycle**.**
2. Volumetric latent heat storage capacity is low**.**
3. Flammable. This can be easily alleviated by a proper container**.**
4. To obtain reliable phase change points, most manufacturers use technical grade paraffins which are essentially paraffin mixture(s) and are completely refined of oil, resulting in high costs

2.2 Inorganic PCMs (Salt hydrates (M_nH_2O))

Inorganic materials are further classified as salt hydrate and metallics. Inorganic compounds have a high latent heat per unit mass and volumes are low in cost in comparison to organic compounds and are non-flammable (Prabhu et al 2012). However they suffer from decomposition and supercooling which further can affect their phase change properties listed in Table 1

2.2.1 Advantages

1. High volumetric latent heat storage capacity**.**
2. Availability and low cost**.**
3. Sharp melting point**.**
4. High thermal conductivity**.**
5. High heat of fusion**.**
6. Non-flammable

2.2.2 Disadvantages

1. Change of volume is very high**.**
2. Super cooling is major problem in solid–liquid transition**.**
3. Nucleating agents are needed and they often become inoperative after repeated cycling

Table: 1. Thermo physical properties of selected organic/Inorganic PCMs
(Source-http://www.nrel.gov/csp/troughnet/pdfs/tamme_phase_change_storage_systems.pdf-)

Material	Organic PCM	Melting point ^{o}C	Heat of fusion kJ·kg^{-1}	Heat of fusion MJ·m^{-3}	c_p solid kJ·kg^{-1}·K^{-1}	c_p liquid kJ·kg^{-1}·K^{-1}	ρ solid kg·m^{-3}	ρ liquid kg·m^{-3}	k solid W·m^{-1}·K^{-1}	VHC solid kJ·m^{-3}·K^{-1}	VHC liquid kJ·m^{-3}·K^{-1}	Cost USD·kg^{-1}
Water	No	0	333.6	319.8	2.05	4.186	917	1,000	1.6-2.22	1,880	4,186	0.00312
Sodium sulphate (Na2SO4·10H2O)	No	32.4	252	NA	NA	NA	NA	NA	NA	NA	NA	0.05
NaCl·Na2SO4·10H2O	No	18	286	NA	NA	NA	NA	NA	NA	NA	NA	0.05
Lauric acid	Yes	44.2	211.6	197.7	1.76	2.27	1,007	862	NA	1,772	1,957	1.6
TME(63% w/w)+ H2O(37% w/w)	Yes	29.8	218.0	240.9	2.75	3.58	1,120	1,090	NA	3,080	3,902	NA
Mn(NO3)2·6H2O+MnCl2·4H2O (4% w/w)	No	15–25	125.9	221.8	2.34	2.78	1,795	1,728	NA	4,200	4,804	NA
Na2SiO3·5H2O	No	72.20	267.0	364.5	3.83	4.57	1,450	1,280	0.103−0.128	5,554	5,850	8.0
Aluminium	No	660.32	396.9	1,007.2	0.8969	NA	2,700	2,375	237	2,422	NA	2.04626
Copper	No	1,084.62	208.7	1,769.5	0.3846	NA	8,940	8,020	40	3,438	NA	6.81256
Gold	No	1,064.18	63.72	1,166.3	0.129	NA	19,300	17,310	318	2,491	NA	34,297.8
Iron	No	1,538	247.3	1,836.6	0.4495	NA	7,874	6,980	80.4	3,539	NA	0.3248
Lead	No	327.46	23.02	253.2	0.1286	NA	11,340	10,660	35.3	1,459	NA	2.1151
Lithium	No	180.54	432.2	226.0	3.5816	NA	534	512	84.8	1,913	NA	62.2164
Silver	No	961.78	104.6	1,035.8	0.235	NA	10,490	9,320	429	2,465	NA	492.524
Titanium	No	1,668	295.6	1,273.5	0.5235	NA	4,506	4,110	21.9	2,359	NA	8.0469
Zinc	No	419.53	112.0	767.5	0.3896	NA	7,140	6,570	116	2,782	NA	2.15735
NaNO3	No	310	174	NA	NA	NA	NA	NA	NA	NA	NA	NA
NaNO2	No	282	212	NA	NA	NA	NA	NA	NA	NA	NA	NA
NaOH	No	318	158	NA	NA	NA	NA	NA	NA	NA	NA	NA
KNO3	No	337	116	NA	NA	NA	NA	NA	NA	NA	NA	NA
KOH	No	360	167	NA	NA	NA	NA	NA	NA	NA	NA	NA
NaOH/ Na2CO3 (7.2%)	No	283	340	NA	NA	NA	NA	NA	NA	NA	NA	NA
NaCl(26.8%)/NaOH	No	370	370	NA	NA	NA	NA	NA	NA	NA	NA	NA
NaCl/KCL(32.4 %)/LiCl(32.8%)	No	346	281	NA	NA	NA	NA	NA	NA	NA	NA	NA
NaCl(5.7%)/ NaNO3 (85.5%)/Na2SO4	No	287	176	NA	NA	NA	NA	NA	NA	NA	NA	NA
NaCl/ NaNO3 (5.0%)	No	284	171	NA	NA	NA	NA	NA	NA	NA	NA	NA
NaCl(5.0%)/ NaNO3	No	282	212	NA	NA	NA	NA	NA	NA	NA	NA	NA
NaCl(42.5%)/KCl(20.5)/MgCl2	No	385-393	410	NA	NA	NA	NA	NA	NA	NA	NA	NA
KNO3(10%)/NaNO3	No	290	170	NA	NA	NA	NA	NA	NA	NA	NA	NA

2.3Eutectics (Organic-organic, organic-inorganic, inorganic-inorganic compounds)

An eutectic is a minimum-melting composition of two or more components, each of which melts and freeze congruently forming a mixture of the component crystals during crystallization (Sharma, S.D et al,2005). Commonly used Organic–Organic, Organic–Inorganic and Inorganic– Inorganic eutectics PCMs used for building applications are listed in Table-2.

Table: 2. Inorganic eutectics PCM

PCM Compound	Melting temperature (C)	Heat of fusion (kJ/kg)	References
66.6% CaCl2 .6H2O+33.3% Mgcl2 .6H2O	25	127	[9]
48% CaCl2+4.3% NaCl+0.4% KCl+47.3% H2O	26.8	188	[10]
47% Ca(NO3)2 . 4H2O+53% Mg(NO3)2 .6H2O	30	136	[10]
60% Na(CH3COO) .3H2O+40% CO(NH2)2	30	200.8	[11]

2.3.1 Advantages

1. Eutectics have sharp melting point similar to pure substance
2. Volumetric storage density is slightly above organic compounds

2.3.2 Disadvantages

Only limited data is available on thermo-physical properties as the use of these materials are very new to thermal storage application. For latent heat storage commercial grade (CG) PCMs are preferred due to their large scale availability and low cost. The thermo physical properties/behaviour of CG materials in general was found to be very much different than those quoted in the literature for analytical grade (AG) materials therefore, it becomes important to verify the melting temperature, latent heat of fusion and specific heat of CG latent heat storage materials . (D.Juárez et al,2013) A list of commercial PCMs, which can be used in the buildings for thermal storage (available in the International market) is given in Table-3.

Table: 3. Commercially available PCMs in world wide

PCMs Name	Type of product	Melting temperature (C)	Heat of fusion (kJ/kg)	References
RT20	PARAFFIN	22	172	[12]
RT25	PARAFFIN	26	232	[12]
RT26	PARAFFIN	25	131	[12]
RT27	PARAFFIN	28	179	[12]
RT32	PARAFFIN	31	130	[12]
CLIMSEL C 23	SALT HYDRATE	23	148	[13]
CLIMSEL C 24	SALT HYDRATE	24	216	[13]
CLIMSEL C 32	SALT HYDRATE	32	212	[13]
STL 27	SALT HYDRATE	27	213	[16]
S 27	SALT HYDRATE	27	207	[14]
TH 29	SALT HYDRATE	29	188	[15]

The another category of PCMs based on the size of the capsules (Microtek Laboratories,2010), may be the following:

• Micro PCMs
• Macro PCMs

Microencapsulation defined as the process of surrounding or wrapping one substance to another substance at very limited scale, producing capsules ranging from less than one micron to several hundred microns in size. The microcapsules may be spherical, with a continuous wall surrounding the core, while others are asymmetrical and with varying shapes, with a number of droplets of core material incorporated throughout the microcapsule. Microencapsulation provide a solution to the increasing consumer demand for improved energy efficiency and thermal

regulation. The PCM substance is typically a paraffin or fatty ester acid that absorbs and releases heat in order to maintain a defined temperature. Regardless of the state (liquid or solid) of the PCM, the capsule remains in the solid state, because it is a very stable and inert polymer. It allows the PCMs to be incorporated into construction materials, such as concrete, easily and economically. Micro-encapsulated PCMs also provide a portable heat storage system. By coating a microscopic sized PCM with a protective coating, the particles can be suspended within a continuous phase such as water. This system can be considered a phase change slurry (PCS) (Buddhi.D.et al, 2007).

Typical features are:

- Any colour
- Temperatures available: adjustable ranges on request.
- Form: Dry or wet filter cake. The filter can be diluted further to suit its application.
- Average particle size: microns.
- Stability at elevated temperatures

Macro PCMs are spherical capsules of a larger size (3-5 mm) containing high concentrations of phase change materials. These materials were originally developed for use in cooling vests and clothing. They regulate body temperature of individuals working in hot environments, such as soldiers in missions in the desert. The macro PCM absorbs heat excess and allows the user for a longer time in a more comfortable temperature. The particles are typically charged into the vests, on the inside, which is in contact with the skin. However, most applications are emerging (Buddhi.D.et al, 2007).

Typical features are:

- Any colour.
- Temperatures available: adjustable ranges on request.
- Form: spherical solid balls.
- Average particle size: mm.

Molecular-encapsulation is another technology, developed by Dupont de Nemours that allows a very high concentration of PCM within a polymer compound. It allows storage capacity up to 515 kJ/m2 for a 5 mm board (103 MJ/m3). Molecular-encapsulation allows drilling and cutting through the material without any PCM leakage (Buddhi.D.et al, 2007).

The state of the art is more developed during low and medium temperature than in high temperature. There is ample scope for the R & D in terms of PCM screening (selection), micro/macro encapsulation, the development of new materials and storage systems. Fallahi and Fang prepared micro PCMs based upon different types of paraffins and analyze their thermal behaviour. Hadam discusses the transfer of heat during the melting of a phase-change material, determining the spread and inclination of the solid-liquid interface at the time. Alkan studied the preparation, characterization and thermal properties of a microencapsulated PMC for thermal energy storage. Alvarado and Bukovec come equally to performance micro PCMs analysis with differential scanning calorimetric (DSC) and thermal gravimetric analysis (TGA) techniques. Huang studied the improvements made by a 3D model analysis with phase change materials and compare the results with those provided by previous 2D model. Finally, in a longer term, research in nano fluids and nano-PCM can be a significant advance through the application of PCM-based technologies

3. Properties of PCMs

Selection criteria of PCMs for particular applications follows some important points from properties of PCMs (A.Sharma et al, 2009).

- The operating temperature of the heating or cooling should be matched to the transition temperature of the PCM.
- High thermal conductivity would assist the charging and discharging of the energy storage.
- Phase stability during freezing melting would help towards setting heat storage and high density is desirable to allow a smaller size of storage container.
- Small volume changes on phase transformation and small vapour pressure at operating temperature to reduce the containment problem.
- Supercooling has been a troublesome aspect of PCM development, particularly for salt hydrates. Supercooling of more than a few degree will interfere with proper heat extraction from the store, and 5-10^{0}C supercooling can prevent it entirely.
- PCM can suffer from degradation by loss of water of hydration, chemical decomposition or incompatibility with materials of construction.
- Low cost and large-scale availability of the phase change material is also very important.

Some crucial PCM properties listed in table-4

Thermal properties	Physical properties	Chemical properties	Kinetic properties	Economic factors
Phase change temperature suitable to the desired operating range.	High density	Long-Term Chemical stability	High nucleation rate to avoid supercooling of the liquid phase	Abundant
High latent heat per unit mass. High specific heat. and High thermal conductivity in both solid and liquid phases	Low density variation during phase change	No degradation after a large number of freeze/melt cycle, Complete reversible freeze/melt cycle	High rate of crystal growth, so that the system can meet demands of heat recovery from the storage system	Available in large quantities
Small volume changes on phase transformation and small vapor pressure at operating temperatures to reduce the containment problem	Little or no supercooling during freezing	Compatibility with container materials.		Inexpensive
Congruent melting		Non-corrosiveness, non-toxic, non-flammable and non-explosive materials.		

The comparison between latent and sensible heat storage shows that using latent heat storage, storage densities typically 5 to 10 times higher can be reached. PCM storage volume is two times smaller than that of water (Garg et al., 1985; Hasnain, 1998). Latent heat storage can be used in a wide temperature range. A large number of PCMs are known to melt with a heat of fusion in any required range. The PCM to be used in the design of thermal storage systems should accomplish desirable thermophysical, kinetics and chemical properties (Hale et al., 1971; Garg et al., 1985; Buddhi et al., 1994).Thermal stability of fatty acid type novel PCM Ethylene Glycol Distearate (EGDS). During heat treatment EGDS kept with calcium oxalate under atmosphere air condition at temperature range of 30^0C to 800^0C for heating rate 10^0C/min. Heat storage capacity increase with higher density. EGDS has the advantages of higher energy storage capacity over the paraffin's PCMs.The recorded value of EGDS is 0.9729 kg/m^3 where as paraffin's PCMs density lies between 0.7-0.9 kg/m^3 (Alkan et al, 2008). Low heat transfer coefficient helps longer solidification time and provide thermal stability for design of thermal energy storage system. Higher Stefan number shows the charging and discharging rate of mass flow, and estimated in size of spherical capsule type PCMs (Felix & Solanki ,2009).

4. Working of PCM in solar heat storage.

PCM's are chemical substances that undergo a solid-liquid transition at temperatures within the desired range for heating purposes. During the transition process, the material absorbs energy as it goes from a solid to a liquid and releases energy as it goes back to a solid. As on date , Glauber's salt (sodium sulfate decahydrate) is being sold commercially. Glauber's salt changes phases at 90°F and has a 108-BTU-per-pound "latent heat" (amount of heat absorbed or released during phase change). Because of its high latent heat, Glauber's salt requires less storage volume than either rock or water; that could mean lower storage facility cost and more usable space within the home to offset the material's relatively high cost (Prabhu et al, 2012).

5. Major Application area of PCM.

The application of PCMs in building can have two different goals. First, using natural heat that is solar energy for heating or night cold for cooling. Second, using manmade heat or cold sources. In any case, storage of heat or cold is necessary to match availability and demand with respect to time and also with respect to power (D. Buddhi et al 2007). Basically three different ways to use PCMs for heating and cooling of buildings are:

1. PCMs in building walls.
2. PCMs in other building components other than walls; and,
3. PCMs in heat and cold storage units.

The first two are passive systems, where the heat or cold stored is automatically released when indoor or outdoor temperature rises or falls beyond the melting point. The third one is active system, where the stored heat or cold is in containment thermally separated from the building by insulation. Therefore, the heat or cold is used only on demand not automatically. Depending on where and how the PCM is integrated, PCMs with different melting points are applied. Currently, there is a lack of commercial PCMs in the lower temperature range that is between 5 and 25^0C. Especially between 15 and 20^0C available products show too low enthalpies. Most important PCMs are in the range of 22–25^0C, as almost everybody agrees that this is the range for building passive heating and cooling (Mehling H et al,2002). Various possible latent heat thermal energy storage (LHTES) devices studied for space heating and cooling are as follows.

1) PCM trombe wall.
2) PCM wallboards.
3) PCM shutter.
4) PCM building blocks.
5) Air based heating system.
6) Floor heating.
7) Ceiling heating.

Other storage systems have been developed by many researchers; **Kaygusuz and Ayhan** investigated the performance of the combined solar heat pump system with energy storage in encapsulated phase change material packing for residential heating. The concept of free cooling was developed for air conditioning applications, where coolness was collected and stored from ambient air during night, and relived to the indoor ambient during the hottest hours of the day . **Vakilatojjar and Saman** worked on the analysis and modeling of phase change storage system for air conditioning applications. Another application of PCMs in buildings is thermoelectric refrigeration**. Omer et al. and Riffat et al**. integrated a phase change material in the thermal diode to improve effectiveness of the heat sink. **John et al**. designed a novel ventilation night time cooling system (a novel combination of PCM and heat pipes) as an alternative to air conditioning. The system offers substantial benefits in terms of reducing or eliminating the need for air conditioning and thereby significantly reducing CO2 emissions and saving energy in buildings. Apart from storage systems PCM plays important role in medical applications: transportation of blood, operating tables, hot-cold therapies (Kenisarin.M et al 2007,Omar A,2008).Telecom shelters in tropical regions. They protect the high-value equipment in the shelter by keeping the indoor air temperature below the maximum permissible by absorbing heat generated by power-hungry equipment such as a Base Station Subsystem. In case of a power failure to conventional cooling systems, PCMs minimize use of diesel generators, and this can translate into enormous savings across thousands of telecom sites in tropics (Kenisarin.M et al 2007, Omar A,2008)

6. Conclusion

This review paper is focused on assessment of properties of various PCMs. A PCM with an easily adjustable melting point would be a necessity as the melting point is the most important criterion for selecting a PCM for passive solar applications. This paper presents the current research in the particular field of space heating and cooling application for buildings. The use of encapsulated materials with phase change (PCM) is an efficient method for the thermal effects of regulation in heating and cooling systems. The micro PCM can be considered ideal for incorporation as an additive to thermoplastic materials due to its size. The emerging application of Molecular-encapsulation allows drilling and cutting through the material without any PCM leakage

References

[1] S. P. Sukhatme, “Solar energy – principles of thermal collection and storage”.
[2] K. Kaygusuz, “The viability of thermal energy storage”, *Energy Sources* 21: 745–755.1999
[3] A. Sari, K. Kaygusuz, “Energy and exergy calculations of latent heat storage systems”, Energy Sources 22: 117-126.2000
[4] S. D. Sharma, Sagara. Kazunobu, “Latent Heat Storage Material and System-A Review,Int.Journal of Green Energy-2”,1- 56,2005
[5] Vineet Veer Tyagi, D. Buddhi, “PCM thermal storage in building-A state of art. Renewable and sustainable Energy Reviews”, 11, 1146-1166, 2007
[6] P. A. Prabhu, N. N. Shinde, P. S. Patil, “Review of Phase Change Materials for Thermal Energy Storage Application”, Int Journal of Engineering and application, 2(3),871-875,2012

[7] D. Juárez (1), R. Balart, S. Ferrándiz, M. A. Peydró, “Classification of phase change materials and his behaviour in SEBS/PCM blends”, Proceedings of the 5th Manufacturing Engineering Society International Conference – Zaragoza – June 2013
[8] Atul Sharma, V. V. Tyagi, C. R. Chen, D. Buddhi, “Review on thermal storage with phase change materials and applications”, Renewable and Sustainable Energy Reviews 13,318-345,2009
[9] J Heckenkamp, Baumann H. Latent, “warme speicher Sonderdruck aus Nachrichten 1997; 11:1075–81
[10] A. Abhat, “Low temperature latent heat thermal energy storage: heat storage materials. Sol Energy ;30:313–32.1983
[11] Li JH, Zhang GE, Wang JY. “Investigation of a eutectic mixture of sodium acetate trihydrate and urea as latent heat storage”, Sol Energy; 47(6):443–5.1991
[12] www.rubitherm.de.
[13] www.climator.com.
[14] www.cristopia.com.
[15] www.teappcm.com.
[16] Kakiuchi H. Mitsubishi Chemical Corporation, Private Communication, 2002.
[17] Microtek Laboratories, I., "Phase Change Materials", Microtek Laboratories, Inc., (2010).
[18] E. Fallahi, M. Barmar, M. H. Kish, "Preparation of Phase-change Material Microcapsules with Paraffin or Camel Fat Cores: Application to Fabrics", Iranian Polymer Journal, 19:(4), 277-286 (2010)
[19] G. Y. Fang, Li, H., Liu, X., Wu, S. M., "Experimental Investigation of Performances of Microcapsule Phase Change Material for Thermal Energy Storage", Chemical Engineering & Technology, 33: (2), 227-230 (2010)
[20] Y. T. Fang, Kuang, S. Y., Gao, X. N., Z. G. Zhang, "Preparation of nanoencapsulated phase change material as latent functionally thermal fluid", Journal of Physics D-Applied Physics, 42:(3), (2009)
[21] M. A. Hamdan, I. Al-Hinti, "Analysis of heat transfer during the melting of a phase-change material", Applied Thermal Engineering, 24:(13), 1935-1944 (2004)
[22] C. Alkan, A. Sari, A. Karaipekli, O. Uzun, "Preparation, characterization, and thermal properties of microencapsulated phase change material for thermal energy storage", Solar Energy Materials and Solar Cells, 93: (1), 143-147 (2009).
[23] J. L. Alvarado, C. Marsh, C. Sohn, Vilceus, M., Hock, V., G. Phetteplace, T. Newell, "Characterization of supercooling suppression of microencapsulated phase change material by using DSC", Journal of Thermal Analysis and Calorimetry, 86:(2), 505-509 (2006)
[24] N. Bukovec, P. Bukovec, V. Arbanas, "TG AND DSC INVESTIGATION OF CACL2.6H2O, A PHASE-CHANGE MATERIAL FOR ENERGY-STORAGE", Thermochimica Acta, 148: (281-288, 1989
[25] M. J. Huang, P. C. Eames, B. Norton, "Comparison of predictions made using a new 3D phase change material thermal control model with experimental measurements and predictions made using a validated 2D model", Heat Transfer Engineering, 28:(1), 31-37 (2007)
[26] D. Buddhi, R. L. Sawhney, “Proceeding of thermal energy storage and energy conversion”, School of energy and environmental studies. Devi Ahilya University, Indore, India. February 24–25, 1994
[27] H. P. Garg, S. C. Mullick, Bhargava, A. K. Solar Thermal Energy Storage. Dordrecht, Holland: D. Reidel Publishing Co.1985
[28] S. Hasnain, “Review on sustainable thermal energy storage technologies, part I: heat storage materials and techniques. *Energy Conservation and Management* 39: 1127–1138, (1998)
[29] D. V. Hale, M. J. Hoover, M. J. O’Neill, “Phase Change Materials Hand Book, Report no. HREC-5183-2LMSC-HREC D225138. NASA”. Marshal Space Flight Center, Alabama, (1971)
[30] A. Felix Regin, S. C. Solanki, J, S. Saini, “An analysis of a packed bed latent heat thermal energy storage system using PCM capsules”, Numerical Investigation. Renewable Energy, Elsevier, 34; 1765-1773,2009
[31] Cemil Alkan, Kemal Kaya, Ahmet Suri.Preparation and thermal properties of ethylene glycol distearate as a novel phase change materials for energy storage. Material Letters, Elsevier; 62: 1122-1125.2008
[32] H. Mehling S. Hiebier L F. Cabeza “News on the application of PCMs for heating and cooling of buildings” Advanced thermal energy storage through phase change materials and chemical reactions feasibility studies and demonstration project, third workshop, IEA, ECES IA Annex 17, 1–2 October, Tokyo, Japan,2002
[33] V. Kaygusuz, T. Ayhan, “Experimental and theoretical investigation of combined solar heat pump system for residential heating, Energy Convers Manage; 40: 1377–96, 1999
[34] S M Vakilatojjar, W. Saman, “Domestic heating and cooling with thermal storage”, In: Proceedings of the Terrastock, Stuttgart, Germany, p. 382–6.2000

[35] F. Bruno, W. Saman, “Testing of a PCM energy storage system for space heating. In: Proceedings of the world renewable energy congress WII”, Cologne, Germany, 2002

[36] S. M. Vakilatojjar, W. Saman, “Analysis and modeling of a phase change storage system for air conditioning applications”, Appl Therm Eng :249–63.2001

[37] S. A. Omer, S. B. Riffat, Ma X., “Experimental investigation of a thermoelectric refrigeration system employing a phase change material integrated with thermal diode (thermosyphons)”, Appl Therm Eng ;21:1265–71.2001

[38] S. B. Riffat, S. A. Omer, X. Ma, “A novel thermoelectric refrigeration system employing heat pipes and a phasechange material”, an experimental investigation. Renewable Energy; 23: 313–23.2001

[39] T. John, E. David, R. David, “A novel ventilation system for reducing air conditioning in buildings: testing and theoretical modeling”, Appl Therm Eng ; 20: 1019–37.2000

[40] M. Kenisarin, K. Mahkamov, "Solar energy storage using phase change materials". Renewable and Sustainable Energy Reviews **11** (9): 1913–1965, 2007

[41] A Omer, "Renewable building energy systems and passive human comfort solutions". Renewable and Sustainable Energy Reviews **12** (6): 1562–1587, 2008

[42] http://www.nrel.gov/csp/troughnet/pdfs/tamme_phase_change_storage_systems.pdf.

International Journal of Applied Engineering Research.
ISSN 0973-4562, Volume 8, Number 17 (2013) pp. 2051-2056
© Research India Publications
http://www.ripublication.com/ijaer.htm

A Thermodynamic Analysis of a Hydrogen Enriched Compressed Natural Gas Fuelled HCCI Engine

Devendra Kumar Gupta[1], Rohit Goyal[*2], Rajesh Kumar[3], Md Nadim Shams[4]

[1,2,3,4] *Department of Mechanical Engineering, Delhi Technological University (Government of NCT of Delhi), Bawana Road, Delhi-110042, India.*

Abstract

A second-law based exergetic study is undertaken for a parametric examination of CNG fuelled HCCI engine. The effects of change in hydrogen enrichment on the engine performance are investigated through energy and exergy efficiencies. The major findings derived from the present analysis is the reduction in combustion and heat transfer irreversibilities in HCCI engine from 55% to 43.4% with 100% hydrogen addition accompanied by simultaneous increase in power output from 31.4% to 38.4%.

Keywords: Energy, exergy, entropy, gases, heat transfer, thermodynamic analysis, HCCI engine.

1. Introduction

Recently, environmental protection and energy conservation have been increasingly concerned worldwide, more and more attention in the auto industry has been shifted to the use of alternative fuels. Natural gas is regarded as one of the most promising alternative fuels and probably one of the cleanest fuels for combustion. The combustion of natural gas produces less emission than that of gasoline and diesel fuels. But natural gas has the penalty of very low-flame speed and narrowest lean flammability limits which lead to an incomplete combustion, high compression ratio and large cycle-by-cycle variation at lean mixture combustion [Das, A., Wasten, H.C., 1997]. Hydrogen addition thought to be an ideal approach to compensate such problems since hydrogen has very high flame speed and low ignition energy along with the wider lean flammability limits. Adding a small amount of hydrogen into natural gas can improve the combustion characteristics and reduce exhaust emissions [Akansu, S.O. et al., 2004].

Many investigators observed the effect of the addition of hydrogen into natural gas on the performances and emissions of conventional SI and CI engines in the past

several years. However, it is apparent that little information is available on the second law analysis including the effect of hydrogen addition. [Rakopoulos, C.D., et al., 2008] investigated the effect of mixing hydrogen into natural gas for direct injection diesel engine combustion from the second law perspective. Their results showed that second law efficiency increases and irreversibility generation decreases with increasing engine load. [Ozcan, H., 2010] examined the hydrogen enrichment effects on the second law analysis of lean burn natural gas engine by using a two zone quasi-dimensional thermodynamic cycle model. He suggested that when adding 30% hydrogen in volume into CNG, lean mixture combustion and ignition timing optimizations could significantly decrease the combustion irreversibilities, and obtain relatively higher second law efficiency.

This paper reports a comprehensive second-law (exergy) analysis of hydrogen enriched natural gas powered HCCI engine using entropy generation model to simulate the combustion process and perform exergy analysis of the sub processes associated with combustion.

2. System Description

To facilitate the second law analyses of CNG-H_2 fuelled HCCI combustion engine, its schematic diagram is shown in Fig. 1. The ambient air enters the turbocharger which delivers air to the heat exchanger which reduces the compressed air temperature. Next CNG which is stored at a high pressure is injected into the fuel mixer at a turbocharger delivery pressure and temperature mixes with the compressed air. The hydrogen which is stored in another cylinder is also injected to the fuel mixer, mixes with the compressed air. The mixing process in the fuel mixture produced a homogeneous mixture of CNG and air, which then enters HCCI engine. An engine compression ratio (16:1) is assumed to ensure auto-ignition of the CNG-air charge where a chemical reaction in the freshly burned zone occurs under constant volume conditions, resulting in a pressure rise in the combustion products which are in a state of chemical equilibrium. The freshly burned products expand to equilibrate the cylinder pressure and hence develop power, and thereafter mix with the previously burned gases to form a homogeneous charge. The cylinder exhaust gases enter the turbine to generate power for the turbocharger. Finally, the engine details are given in Table 1

Table 1: HCCI engine specifications.

Displacement	**0.612 L**
Bore	82.6 mm
Stroke	114 mm
Engine speed	800 r.p.m
Turbocharger efficiency	80%
Type of loading	Non varying load
Nature of combustion in HCCI engine	Bulk auto ignition process controlled by chemical kinetics
Mean inlet air temperature (T_0) (K)	300

Inlet pressure (p_0) (kPa)	101.3
Air inlet temperature (Fuel mixer)	93^0C
Cooling water inlet and exit temperatures	25^0C and 35^0C
HCCI engine compression ratio	16:1
Engine volumetric efficiency	100%
Chemical exergy of hydrogen	113500 KJ/Kg
LHV of hydrogen	120000 KJ/Kg
Chemical exergy of CNG	51780 KJ/Kg
LHV of CNG	50000 KJ/Kg

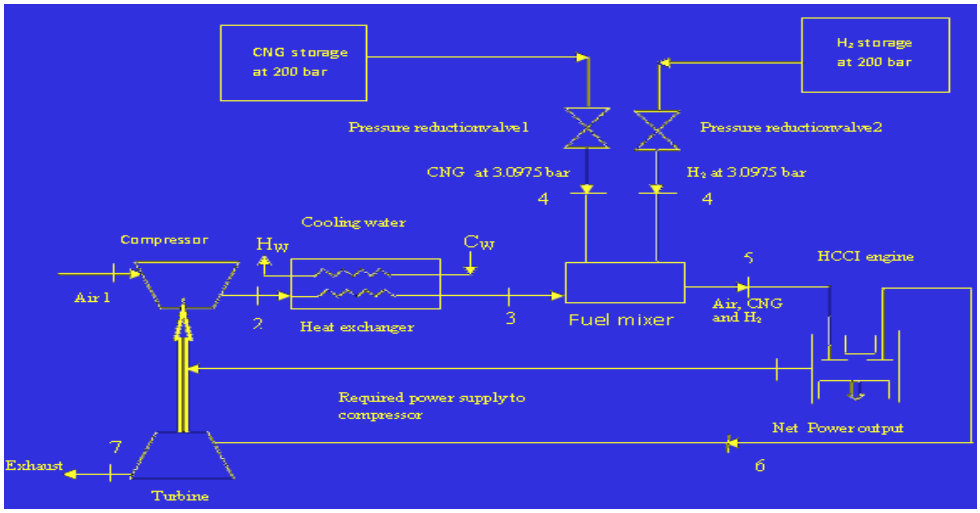

Figure 1: Schematic of a CNG H2 fuelled HCCI engine.

3. Analysis

For the transient operation of an open system (engine cylinder, exhaust manifold, turbocharger etc.) experiencing mass exchange with the surroundings, the following equations holds for the energy and entropy balances:

$$\frac{dE_{cv}}{dt} = \dot{Q}_{cv} - \dot{W}_{cv} + \sum_i \dot{m}_i \left(h_i + \frac{V_i^2}{2} + gz_i\right) - \sum_e \dot{m}_e \left(h_e + \frac{V_e^2}{2} + gz_e\right) \quad (1)$$

$$\frac{dS_{cv}}{dt} = \sum_i \frac{\dot{Q}_i}{T_i} + \sum_i \dot{m}_i s_i - \sum_e \dot{m}_e s_e + \dot{S}_{gen} \quad (2)$$

The rate of lost available work $\dot{I}$ in a process is characterized by entropy generation $\dot{S}_{gen}$ in the process. For continuous process performed by a system, it can be written as

$$\dot{I} = T_0 \dot{S}_{gen} \quad (3)$$

3.1 Performance parameters

The overall performance of CNG fuelled HCCI engine can be estimated based on first and second laws of thermodynamics.

3.1.1 Energy efficiency (η_I)

The first law (energy) efficiency is the fuel utilization efficiency which is defined as the ratio of specific brake thermal power output to the rate of energy input and is given by

$$\eta_I = \frac{\dot{W}_{BT}+\dot{W}_T-\dot{W}_{TC}}{\dot{m}_f \times LHV \times \eta_{cc}} \quad (4)$$

3.1.2 Exergy efficiency (η_{II})

The second law (exergy) efficiency is defined as the ratio of amount of exergy supplied in the product to the amount of exergy associated with the fuel. By definition, it is then given by the following expression

$$\eta_{II} = \frac{\dot{W}_{BT}+\dot{W}_T-\dot{W}_{TC}}{\dot{m}_f \times E_{fuel}} \quad (5)$$

Where E_{fuel} is exergy of fuel in kJ/kg.

4. Results and Discussion

The effects of change in percentage of hydrogen in CNG have been observed on both combustion irreversibility and exergy lost via heat transfer during combustion separately.

The percentage of hydrogen varies continuously from 20% to 100% as shown in Fig 2. As can be seen, the first law efficiency is increasing with the increasing percentage of hydrogen and it is maximum with 100% hydrogen. It is observed that for lower percentages of hydrogen second law efficiency is considerably lower than the first law efficiency for the same power output of HCNG fuelled HCCI engine.

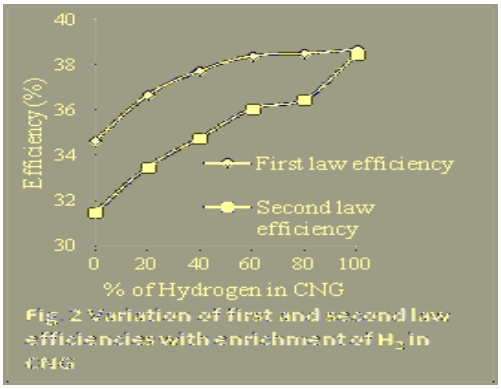

Fig. 2 Variation of first and second law efficiencies with enrichment of H_2 in CNG

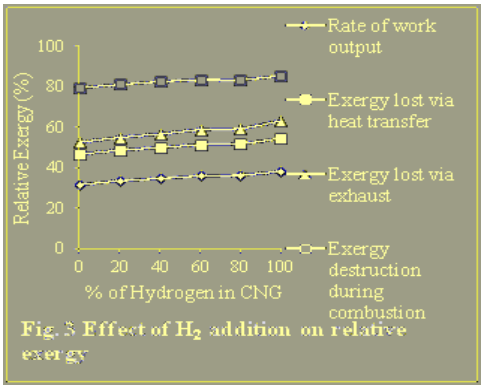

Fig. 3 Effect of H_2 addition on relative exergy

Fig. 3 shows the exergy destroyed during the combustion and heat transfer processes as a function of percentage of hydrogen addition. The exergy destroyed due to combustion decreases and exergy lost via heat transfer increases with the increase in percentage of hydrogen addition due to the simplest molecular structure of hydrogen

and its high auto-ignition temperature respectively. The rate of work produced also increases in hydrogen addition which is due to the fact that the energy content (LHV) of hydrogen is much higher than the energy content of CNG The amount of increase in heat released during combustion of HCNG mixture dominates over the amount of decrease in density of charge (HCNG), therefore, the rate of work output increases. The amount of energy lost via exhaust also increases considerably with the increase in percentage of hydrogen addition due to the high auto-ignition temperature of hydrogen than CNG.

5. Conclusion

This paper has presented a second-law based exergetic study for a parametric examination of CNG fuelled HCCI engine. The effects of hydrogen enrichment on the engine performance are investigated through energy and exergy efficiencies. The major findings derived from the present analysis is the reduction in combustion and heat transfer irreversibilities in HCCI engine from 55% to 43.4% with 100% hydrogen addition accompanied by simultaneous increase in power output from 31.4% to 38.4%.

References

[1] S O Akansu, A Dulger, N Kahraman and T N Veziroglu (2004), Internal combustion engines fueled by natural gas-hydrogen mixtures, International Journal of Hydrogen Energy **29**, pp. 1527-1539.

[2] A Das and H C Wasten (1997), Development of a natural gas spark ignition engine for optimum performance, Proc. Instn. Mech. Engrs., Part D, Journal of Automobile Engineering **211** (D5), pp. 361-378.

[3] H Ozcan (2010), Hydrogen enrichment effects on the second law analysis of a lean burn natural gas engine, International Journal of Hydrogen Energy **35**, pp. 1443-1452.

[4] C D Rakopoulos, M A Scott, D C Kyritsis and E G Giakoumis (2008), Availability analysis of hydrogen/natural gas blends combustion in internal combustion engines, Energy **33**, pp. 248-255.

ISBN 978-93-5156-328-0
International Conference of Advance Research and Innovation (ICARI-2014)

Application of Selective Inventory Control Techniques for Cutting Tool Inventory Modeling and Inventory Reduction-A Case Study

A K Madan *, Ranganath M S
Department of Mechanical Engineering, Delhi Technological University, New Delhi, India

Article Info

Article history:
Received 29December 2013
Received in revised form
10 January 2014
Accepted 20 January 2014
Available online 1 February 2014

Keywords

ABC
VED
JIT
Selective inventory control
Inventory reduction

Abstract

The study shows the need of inventory control and inventory reduction in the industries. It shows the importance and need of Zero inventory (JIT system) in the industries. In this work ABC and VED selective inventory control techniques are applied for cutting tool inventory modeling in an industry. It was suggested that the conventional inventory model formulated as per their convenience is not very effective. A 2-D matrix of the ABC-VED analysis has been constructed for inventory modeling to achieve high efficiency. For Inventory reduction Ageing analysis, Analysis of Scrap and Lead Time analysis was carried out on the cutting tools. The results showed that there are a number of items present as scrap and a lot of items are just being accumulated and are not in use. It was suggested that to sell off the scraps and extra unused items in order to reduce the inventory holding costs and empty the space which have been un-necessarily being occupied. Feasibility of JIT system was carried out for the cutting tools and it was found that it cannot be applied to the plant. The reasons for the same were stated. The research helped the company to understand their current inventory model and the failures of the model. The study helped them to examine their inventory more effectively and hence later it helped them to reduce the inventory which added increased productivity, business growth and reduce the losses.

1. Introduction

The purpose of the project is to create a definite structure of cutting tool inventory modeling and quantity for the cutting tools in the company. An ideal model for the cutting tools such as hobs, cutters, broaches was determined by using the selective inventory control techniques along with it, the quantity of the tools that must be available at a time are also determined. The purpose is also to reduce the inventory of the cutting tools both non-moving and moving. This will directly lead to reduction of inventory cost and shelf space in the organization. In the process, the actual and promised lead time of the vendors were compared, which was used for checking the feasibility of the current system with theapplication of JIT in the plant.The projectcovers all the Hobs, Cutters and Broaches that have been used in the company in the last 1 year time but the ones before that have not been included. Also due to lesser inventory the tools such as milling cutters and drills have not been added. Other than cutting tools, a major part of the inventory is covered by items such as Jigs and Fixtures, but my project is restricted to cutting tools only.The project covers the financial and operational aspect of inventory modeling. The consumption of cutting tools depends on the demand of the different types of Gears, thus there is no particular fast and slow moving inventory in the company for a consistent period. Thus we are not considering the materials aspect or modeling.The study is restricted to cutting tools.It does not consider the other tools such as fixtures and drills.We are not taking milling cutters and drills into account.We have assumed that the lead time and the cost of tools are

Corresponding Author,
E-mail address:ashokmadan79@gmail.com
All rights reserved: http://www.ijari.org

constant.We also assume that every Hob can be re-sharpened 30 times which is not always true.In ABC analysis instead of considering the exact holding cost, we will consider the purchase cost of the tool. In lead time comparison, we will only take a sample of tools and not all the tools.

2. Literature Review

The variety of research in the field of inventory theory is very huge. In this a brief literature survey is given which gives reviews on various reports of inventory control practice in the form of case studies published in academic journals. In the following paragraphs, a view about application of selective inventory control techniques for inventory management has been discussed. During the last decades, a number of inventory control case studies have appear in the academic literature, reporting applications mostly in the electronics, chemical, and automotive industries. One of the earliest such publications is by Gelders and van Looy (1978) (4), who present various inventory policies both for slow-moving and fast-moving items in a petrochemical plant with around 22,500 SKUs. Vereecke and Verstraeten (1994) (5), described an algorithm for the implementation of a computerized inventory management system for spare parts in a large chemical plant, located in Belgium. The spare parts inventory contains about 34,000 different types of items, 90% of which have demand frequency lower than 4 times a year. Prakash, Ganesh, and Rajendran (1994) (6) used the AHP to evaluate the criticality of spares. Their approach was to categorize the parts using a variety of partitioning techniques that complemented the use of good forecasting procedures including ABC analysis, FSN analysis and VED analysis. Anwaruddin T., Abdul Q.L., & Ghulam Y.S, (2000) (7), presented ABC Analysis to control the inventory costs associated with spare parts store of a service industry and suggested about the past inventory problems are due to the congestion of spare parts and use of inappropriate computer package. Ghobbar and Friend (2003) (8) dealt with techniques applicable to predicting spare parts demand for airline fleets. They tested 13 forecasting methods and devise d a predictive error-forecasting model which compared and evaluated forecasting methods based on their factor levels. Caglar, Li, and Simchi -Levi (2004) (9) studied a spares inventory problem faced by a manufacturer of electronic machines with expensive parts that were located at various customer locations. Assuming that parts failed infrequently according to a Poisson process, he formulated a model to minimize the system-wide inventory cost subjected to a response time constraint at each field depot. R Gupta, K K Gupta, B R Jain and R K Garg (2007) (10), applied ABC and VED analysis for inventory control in medical stores. An ABC-VED matrix was constructed for economic analysis of drug expenditure of priced vocabulary of medical stores (PVMS) section 01 for the year 2003 of a 190 bedded service hospital was done. By this they were able to control and reduce the inventory to a large extent which ultimately increased their profits.

3. Selective Inventory Control

Expansion of industries has been the major goal of the industries. Companies are trying to expand their production, sales etc. in order to stand in the global market. The expansion has resulted into the expansion of various activities of the industry. This in-turn increases the number of items to be purchased and hence, their upkeep has also increased significantly. Purchase and control of the items before their use, irrespective of their usage value, price or procurement problems, is therefore uneconomical. Industries store a number of different types of items. The stored items can be classified as follows:

1. Items needed for production which directly enters the finished product which is marketed to the customers.
2. Maintenance spares needed for keeping production machines in running order.
3. Supplies needed for operations such as lubrication oils, cotton waste, etc.
4. Office equipment to carry the company's transactions smoothly.
5. Furniture, fans, lights, etc. to keep workplace in order.

The criteria for inventory and stock control for various classified items are bound to be different. Various researches done in this field has revealed that various objective functions are needed to keep inventories of all these varieties of items. For this purpose selective treatment has to be given to these items and hence **"Selective Inventory Control techniques"** were used to classify inventories of these items.These Inventory Control methods are based on the principles that it is impossible to manage and control every item in inventory holdings in the same way and skill so as to meet the two broad objectives of inventory control i.e. to reduce investment in inventories, and to avoid stock outs and shortages. Selective inventory control management therefore concentrates on those items where it is justified either

due to essentially or amount of money involved. Selective control means variations in the method of control from inventory class to class based on its classification. The criterion used for the purpose is annual usage value criticality, lead time, consumption rate, procurement difficulties, etc. Selective inventory control has been divided into 9 categories. The table below shows the various categories along with their respective criteria (1).

4. Case Study on Cutting Tool Inventory Modeling and Inventory Reduction

A case study has been illustrated which was carried out in **"Action Construction Equipments (ACE) Limited".** In this case study **"ABC and VED"** techniques of selective inventory control are applied in the industry for **"Cutting Tool Inventory Modeling and Inventory Reduction".**

Cutting Tool Inventory at ACE Limited

The cutting tools in ACE Limited are mainly of 4 types namely Hobs, Gear Shaper Cutters, Shaving Cutters and Broaches.

Table: 1. Selective Inventory Control Categories and Criteria

S No.	Category	Criteria	Application
1.	ABC Analysis	Annual usage value (consumption rate*Price Rs/piece)	For materials which go into Production
2.	HML (High, Medium, Low) Analysis	Unit Price	To keep in check high cost items
3.	VED (Vital, Essential, Desirable) Analysis	Criticality or loss of production	For controlling maintenance of spare and manufacturing equipments.
4.	SDE (Scarce, Difficult, Easy) Analysis	Procurement difficulties: geography, reliability, etc. Source of Procurement	To keep vigil on availability, should be kept in stock keeping in mind difficulty of procurement and may follow forward buying
5.	GOLF (Govt., Ordinary, Local, Foreign) Analysis	➢ Govt.-lead time more for retrieval, advance payment ➢ Foreign-procedure long, through bank, port, permission, duty, etc.	Government supplies need patience to get material, canalizing agency can be used, foreign procurement lead time factor counts
6.	SOS (Seasonal, Off-Season) Analysis	Soya bean, farm produce, high off season price, low in harvest season	Should buy in harvest season to get price advantage and good quality supply
7.	FSN (Fast, Slow and Non-moving) Analysis	Issues from stores give idea. Dispose off non-moving inventory	Fast moving items should be kept in high levels
8.	XYZ Analysis (use for 2-D study)	Closing stock value of inventory at the time of physical stock verification	A category status, e.g. A category in X: Watch C category in X: Reduce stocks
9.	MUSIC-3D (Multi-Unit, Selective, Inventory, Control) Analysis	The control criteria of 3- dimensions are finance operations and materials	Can be used for all varieties of materials. It is a combination of all the above analysis.

Hobs: These are the most important cutting tools used. It is used to cut teeth's in a gear by a process called Hobbing.

ISBN 978-93-5156-328-0

Gear Shaper Cutter: As the name suggests, these are used in the shaping process of gears.

Shaving Cutter: This is used in Gear shaving, which is a finishing process.

Broaches: This is another kind of cutting tool used for material removal.

There are mainly two kinds of stores in ACE Limited

- **Main Store**- In the main store, the new and unused cutting tools are kept. For the purpose of usage, the tool crib issues tools from main stores when required.
- **Tool Crib**- It is the WIP store in which semi used, broken or scraped tools are present. When not on the machine, a cutting tool is deposited in the tool crib.

Present Inventory Model

ACE Limited follows a very basic inventory model. According to the present model, the number of Hobs present in the main store depends on the number of settings in which the hob is used. If the Hob is used in a single setting, a quantity of 2 hobs is kept in use at the tool crib and 2 more hobs are available in the main store. It varies in a similar way with the increase in number of settings.

Whenever there is a decrease in the level of hobs in the tool crib due to consumption or breakages and one of the available hobs in the main store has to be issued, the hob is reordered. Thus ACE Limited follows a fixed order type of inventory model. Thus the re order point for them is 1 tool per setting in the main store.

For Gear Shaper Cutter, 2 cutters are available in the main store and the cutters available in tool crib vary from 2-5 according to the usage.

For Shaving cutter and Broach, there are usually 1 tool each, present in tool crib and main store.

ABC at ACE Limited

Source of data- purchase orders since May 2009

Assumptions

- Holding cost is directly proportional to the cost of inventory
- The cost used is the net price, which includes discount as well as taxes and duties.
- Since these tools have been purchased buy different vendors in different times, we are taking the current price of the tools.

Limitations

- Data taken is for last 10 months only
- Exact holding cost is unknown

The following is the list of the tools categorized into A, B and C. There has been done a separate ABC analysis for all the different types of cutting tools. After every type of tool, the recommendations are given.

ABC Analysis for Hobs

Recommendations for Hobs

A. There are 11 hobs lying in this category, since the cost of these hobs are higher than the others, their holding costs will be much higher if we keep them in store for a longer time. Thus it is recommended

ISBN 978-93-5156-328-0

that these hobs are not kept in the store for long, therefore should be ordered in small quantities.

B. There are 33 hobs in this category. They are priced in between A and C. Their holding cost will be lesser than A but still be on a moderate side. Thus these hobs should be ordered to requirement and the quantity in store should be between 1 and 2.

C. There are 42 hobs in this section. They are the least expensive hobs and thus have minimum holding cost. The company can afford to order larger quantities of these tools.

Conclusion

The hobs have a lot of variation in the cost. Thus the ones in category A should be in least quantity and the ones in C can be kept in higher quantities if demanded.

ABC Analysis for Gear Shaper Cutters

A

S No.	ED No.	Teeth	Net price
1	5102	20	41975.00
2	7013AA	20	36455.97
3	7712	19	29371.50
4	5326/5334	21	29001.28

B

S No.	ED No.	Teeth	Net price
1	2014	27	250[illegible]
2	2015	33	250[illegible]
3	6102	18	249[illegible]
4	5301	16	22[illegible]
5	5335	28	221[illegible]
6	7007/7005	28	221[illegible]
7	7013	20	201[illegible]
8	5327	16	186[illegible]
9	2046	17	184[illegible]

C

S No.	ED No.	Teeth	Net price
1	5319	42	176[illegible]
2	5311	42	176[illegible]
3	5319	13	160[illegible]
4	5327	28	147[illegible]
5	5334	28	147[illegible]
6	5335	28	147[illegible]
7	6108	16	139[illegible]
8	2014/2015	36	128[illegible]
9	6102	10	114[illegible]
10	2009	42	107[illegible]
11	7027	42	99[illegible]
12	2035	18	85[illegible]
13	2035	34	85[illegible]
14	7026	39	78[illegible]

Recommendations for Gear Shaper Cutters

A. There are 4 cutters in this category, out of which 7013AA was a specially ordered tool, thus is not regularly ordered. For the other 3 cutters, the order level and the quantity in store is recommended to be not more than 1.

B. There are 9 cutters in this section. The holding cost is moderate and thus the order quantity and stock can vary between 1 and 2.

C. There are 14 cutters in this category. The holding cost is low. So the order quantity can be high. But Gear Shaper Cutters have very long life, thus we can keep a lesser quantity of these tools.

Recommendations for Shaving Cutters after ABC Analysis

A. There are 8 cutters in the category. They are high priced, thus have high holding cost. They also take a lot of shelf space due to their size. Thus it is better to keep a lesser quantity of such tools. One at a time is recommended

B. There are 18 items in this list. The holding cost is again on a higher side so it is better to keep a quantity of 1 at time.

C. There are 26 items in the list. Though the prices are comparatively lower, they are still on a higher side, thus the quantity of 1 is preferred.

Recommendations for Broaches

A. There are 2 broaches in the category. They are priced near to Rs. 1 lacs thus have extremely high holding cost. Thus the broaches should be made available on demand and only unit quantities should be there in the stores.

B. There 5 broaches in the list which are also fairly priced and have a high holding cost, thus it is recommended to be kept in unit quantities too.

C. These too are highly priced except the ones in the bottom. Thus leaving the bottom ones, the others should be kept in least quantities

VED at ACE Limited

Source of data -Issue list from SAP.

Assumptions

- The tool issued was used or is in use.
- Due to variability in life of tools, we consider issue as the representation of criticality.

Limitations

- Data taken is for last 1 year and 3 months only
- Some tools used for trial purposes were neglected

The following is the list of the tools categorized into V, E and D. There has been done a separate VED

ISBN 978-93-5156-328-0

analysis for all the different types of cutting tools. After every type of tool, the recommendations are given.

VED Analysis for Hobs

V Used More Than 4 Times

E Used 2 to 3 Times

D Used Just Once**.**

Recommendations for Hobs

V- There are 11 items in the list. Here hobs like 7453 and 7018 have been in use regularly. So it is better to follow the existing model for them. But for the items with around 4 units of consumption, only 1 hob can be present in the main store.

E- There are 17 items in the list. They are moderately used items thus are not very critical. Therefore 1 unit quantity in the main stores and 2 units at setting may be enough.

D- There are 38 items in the list. These are rarely used items. Single units of these in both tool crib and main store would be enough

VED Analysis for Gear Shaper Cutters

V is More Than 3 Units

E is 2 Units

D is 1 Unit

VITAL

S No.	ED No.	TEETH	ISSUES
1	5353		3
2	7007		4
3	5319	13	3
4	5335	28	3
5	7013	20	3
6	5301	16	3

ESSENTIAL

S No.	ED No.	TEETH	ISSUES
1	2003	31	2
2	7027	42	2
3	5334	78	2
4	7026		2
5	5316		2
6	2015	33	2

DESIRABLE

S No.	ED No.	TEETH	ISSUES
1	5302	62	1
2	7716	78	1
3	2006	26	1
4	2004	26	1
5	5334	78	1
6	5311	42	1
7	2009		1
8	5326	21	1
9	2017	53	1
10	2014	27	1
11	2016	51	1
12	5301	14	1
13	7004	78	1
14	5112	20	1

Recommendations for Gear Shaper Cutters

V- If we look at the vital items we observe that in the time period of more than one year, only a maximum of 4 cutters of a particular components are used, which is not a very large quantity. We also know that cutters have longer life so we can still afford to reduce the amount of hobs present in main store to 1. We continue to use larger quantities at tool crib because these tools can be re coated and re used.

E- The desirable items are also very less frequently issued thus it is enough to keep unit stock in the main store and keeping the tool crib inventory as the existing one.

D- The quantity is too less thus unit stock at main store and tool crib will do.

VED Analysis for Shaving Cutters

V is 3 Units

E is 2 Units

Recommendations for Shaving Cutters

V- There is only 1 cutter which was issued thrice in the last year. Thus we can afford to keep this cutter in a quantity of 2 in the tool crib and in unit quantity in the main store.

E- There are 2 items in the list. But we can afford to keep them in unit quantities

D- It is preferable to keep them in unit quantity both in main store and in tool crib.

VED Analysis for Broaches

V is3 Units

E is 2 Units

D is 1 Unit

Recommendations for Broaches

V- No item could qualify as vital

E- There are 5 items which partially qualify as essentials but even these are used only in quantity of 2. Thus it is not very important have them in excessive stock. Unit quantities will be enough.

D- There are 14 desirable items which have only been used once. No special care is needed for such items and unit quantities of all will be sufficient.

D Matrix Model

Till now we looked at the financial and operational aspect individually. Now we will try to merge both the aspects by forming a 2-2 matrix between holding cost and criticality of the tools.

Source of data - From the data of ABC and VED analysis

Limitations

- Data is for a limited period
- We are only including the tools present in both the analysis.

PRICE

1 **High Price and Low Usage**	**2** **High Price and High Usage**
3 **Low Price and Low Usage**	**4** **Low Price and High Usage**

USAGE

Recommendations for each Matrix

1. For high priced and low usage tools, we must keep as less quantities as possible because they will be used less frequently and will cost higher to the company. For such tools even JIT can be used if possible. Unit quantities of such items are ideal.
2. For high priced and high usage items, there has to be a standard that has to be followed. Here we cannot afford to keep the quantity less and if we exceed the quantity the cost increases. Thus we must have a fixed re-order point for such items. We must keep some buffer for such items
3. Low priced and low usage items should also be kept in lesser quantities. Since the usage is low, higher quantities will only add to the holding cost.
4. These are the most important items in the company. Special care should be taken for such item. It is recommended to keep proper buffer for such items as the holding cost will also be minimum.

Phase -2 Inventory Reductions

5.4.1 Introduction

Inventory reduction is one of the most important functions of the company. It is essential so that the company does not incur losses and the extra shelf space occupied by the un-used inventory can be eliminated. The space thus obtained can be used for other purposes. Proper inventory modeling leads to inventory reduction. A proper inventory model shows what all parts should be present in the inventory and in what quantity, hence by analyzing the results of inventory modeling inventory reduction can be achieved.

In this work inventory reduction has been done in three ways. They are:

- Ageing Analysis
- Analysis of Scrap
- Lead Time Analysis

Ageing Analysis

Ageing analysis is basically an inventory reduction tool in which the inventory is segregated according to the duration of time since the material is kept in stores without being used. The analysis is mainly done for the reduction of stationary inventory. The inventory which has been kept since a long duration of time is either obsolete or is a very rarely used item. If the inventory is obsolete it either has to be modified and used or must be re-sold. For the rarely used items it is recommended that the no extra stock of those must be present in the store.

In the following analysis we have observed the items which have not been in use since the beginning of year 2009. Following are the different cutting tools that are not used in the inventory. The quantity given is the sum total of those in the tool crib as well as in the main store.

Source of data- Tool crib and Main store Inventory.

Conclusion

The obsolete items mentioned above are in fact blocked money and the company has been bearing the holding cost of such items. Also, they are consuming a lot of shelf space in the stores which actually can be utilized for better purposes. Thus the above materials should either be modified or used or should be sold.

Analysis of Scrap

Scrap is referred to as the material which has been 100% consumed or is broken or chipped off in

such a way that it cannot be used further. Such materials are of no use to the company. They can neither be modified nor be re used. Thus the only option remains is to sell off such inventory, so as to increase the shelf space in the stores.

Following are the quantities of each type of scrap in the tool crib.

Source of Data - Count of the scraps in shelves in the tool crib.

S No.	Cutting Tool	Qty.
1	Hobs	144
2	Gear Shaper Cutter	28
3	Shaving Cutter	20
4	Broach	6

Lead Time Analysis

Lead time is the time taken in procurement of a material. It is the time between the ordering of that material to the time it is retrieved. Lead time is a very important factor in cutting tool inventory because the production of gears depends on the availability of cutting tools. If the cutting tools are not available in the stores when required, it will stop the production and will cause monetary as well as goodwill loss to the company.

Following is the variability of the lead times of various tools and vendors.

Source of data- Record of purchase orders of 2010.

Assumption- It is assumed that the promised lead time of the vendors is 8 weeks.

Limitation- Only a sample of 25 orders was taken and of a limited period of time.

Feasibility of JIT

JIT is the Japanese tool in which the raw material reaches the machine only when it is required. There is no extra inventory present in the stores. For such a system to be implemented, discipline from Vendor's end id a must. JIT has been beneficial to various industries as it has helped them in reduction of inventory, cost and increase production.

Here we are going to check the feasibility of application of JIT for cutting tools in the plant. Looking at the lead time, and the consumption pattern of the tools, JIT does not seem feasible in the following plant due to the following reason:

- Lead time of the vendors are variable, whereas in JIT the material must reach the plant exactly on the time it is required.
- Cutting tools are made to order products. There is no ready- made one present with the vendor, thus ordering requires perfect planning.
- The production is dependent on the daily demands of the heavy vehicles division of the company.
- Life and consumption pattern of tools vary significantly.
- There are problems such as breakages of tools which are sometimes not iin human control. Thus a buffer stock of some tools is mandatory.

5. Conclusion

Globalization and industrialization has led to great advancements in the industries. Inventory which was a necessity for the industries has now being considered as one of the waste.

The study shows that in order to survive in this growing environment industry has to seek for measures for inventory elimination or inventory reduction. This has enabled the managers to design an appropriate inventory management or inventory modeling system which would keep track of the entire inventory and hence help in reducing them.

Zero inventories have been achieved by the use of JIT manufacturing system which was first introduces by the Japanese. But still the industries are not able to adapt to JIT because of its competiveness. The industries are still using the older forms which incur huge amounts of money in the inventory.

The overall study reveals the need of inventory modeling and inventory reduction in the industries. It gives the various inventory modeling and inventory control methods that can be used for managing the inventory. The literature review gives the effectiveness of the selective inventory control methods and shows their reliability for the same purpose.

The study also reveals that the company was not operating with maximum efficiency. In order to increase their efficiency it was suggested to them to use the inventory control techniques.

Then a case study was carried out in the industry in which cutting tool inventory modeling and inventory reduction was achieved by using ABC and VED analysis. By combining the two techniques a 2-D matrix was formed and cutting tool inventory modeling was done. The results of the analysis have been shown earlier. The use of this technique was found very effective and efficient. The results thus

obtained were satisfactory and helped the industry to improve their present inventory model to a large extent. After that Ageing analysis, Analysis of Scrap and Lead Time analysis was done on the cutting tools which helped in reducing the inventory of the industry.

The results of the study were very helpful for the industry. They were able to monitor their inventory and measures were taken to rectify the flaws and reducing the inventory. Inventory reduction helped them in getting the space that was getting wasted by unused inventory and also capital which was wasted to maintain the inventory also reduced and added to the growth of the business. Feasibility of JIT in the plant for cutting tool of the industry was also done. But it was found that this was not possible due to the following reasons:

- Lead time of the vendors are variable, whereas in JIT the material must reach the plant exactly on the time it is required.
- The production is dependent on the daily demands of the heavy vehicles division of the company.
- There are problems such as breakages of tools which are sometimes not in human control. Thus a buffer stock of some tools is mandatory.

References

[1] Materials Management by: A.K. Chitale and R.C. Gupta
[2] Materials Management and Materials Handling by: S.C. Sharma
[3] Philip Slater, "Five Myths of Inventory Reduction", Business Focus
[4] L. F. Gelders, P. M. Van Looy, "An inventory policy for slow and fast movers in a petrochemical plant: a case study", Journal of the Operational Research Society 29 (9), 1978, 867–874
[5] A. Vereecke, P. Verstraeten, "An inventory management model for an inventory consisting of lumpy items, slow movers and fast movers", International Journal of Production Economics 35 (1-3), 379–389, 1994
[6] G. P. Prakash, L. S. Ganesh, C. Rajendran, Criticality analysis of spare parts using the analytic hierarchy process. International Journal of Production Economics, 35(1–3), 293–297, 1994
[7] T. Anwaruddin, Q. L. Abdul, Y. S. Ghulam, "ABC Analysis saa Inventory Control Technique", Quaid-E-Awam University, Research Journal of Engineering, Science & Technology, volume 1, no. 1 January-June, 2000
[8] A. A. Ghobbar, C. H. Friend, "Evaluation of forecasting methods for intermittent parts demand in the field of aviation: A predictive model", Computers and Operations Research, 30(14), 2097–2114, 2003
[9] D. Caglar, C. L. Li, D. Simchi-Levi, "Two-echelon spare parts inventory system subject to a service constraint", IIE Transactions (Institute of Industrial Engineers), 36(7), 655–666, 2004
[10] R. Gupta, K. K. Gupta, B. R. Jain, R. K. Garg, "ABC and VED Analysis in Medical Stores Inventory Control", MJAFI, 63(4), 2007
[11] www.ace-cranes.com
[12] www.inventorymanagement.com
[13] www.materialsmanagement.info/inventory/**abc**.htm
[14] www.inventorysolutions.org/def_**jit**.htm

Accepted Manuscript

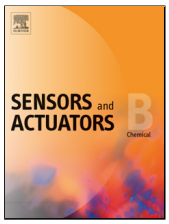

Title: Biosensors for pathogen detection: A smart approach towards clinical diagnosis

Author: Renu Singh Maumita Das Mukherjee Gajjala Sumana Rajinder K. Gupta Seema Sood B.D. Malhotra

PII: S0925-4005(14)00262-7
DOI: http://dx.doi.org/doi:10.1016/j.snb.2014.03.005
Reference: SNB 16645

To appear in: *Sensors and Actuators B*

Received date: 17-7-2013
Revised date: 10-2-2014
Accepted date: 2-3-2014

Please cite this article as: R. Singh, M.D. Mukherjee, G. Sumana, R.K. Gupta, S. Sood, B.D. Malhotra, Biosensors for pathogen detection: A smart approach towards clinical diagnosis, *Sensors and Actuators B: Chemical* (2014), http://dx.doi.org/10.1016/j.snb.2014.03.005

This is a PDF file of an unedited manuscript that has been accepted for publication. As a service to our customers we are providing this early version of the manuscript. The manuscript will undergo copyediting, typesetting, and review of the resulting proof before it is published in its final form. Please note that during the production process errors may be discovered which could affect the content, and all legal disclaimers that apply to the journal pertain.

ACCEPTED MANUSCRIPT

Biosensors for pathogen detection: A smart approach towards clinical diagnosis

RENU SINGH[a,b], MAUMITA DAS MUKHERJEE[d], GAJJALA SUMANA[a], RAJINDER K. GUPTA[b], SEEMA SOOD[e] and B. D. MALHOTRA[c*]

[a]Department of Science & Technology Centre on Biomolecular Electronics, Biomedical Instrumentation Section, National Physical Laboratory (Council of Scientific & Industrial Research), Dr. K.S. Krishnan Marg, New Delhi-110012, India
[b]School of Biotechnology, Guru Gobind Singh Indraprastha University, Sector -16 C, Dwarka, Delhi 110075, India,
[c]Department of Biotechnology, Delhi Technological University, Shahbad Daulatpur, Main Bawana Road, Delhi-110042, India
[d]Amity Institute of Applied Sciences, Amity University, Sector 125, Noida, U.P, India
[e]Department of Microbiology, All India Institute of Medical Sciences, New Delhi 110002, India

Keywords: Nucleic Acid Sensor; Human Pathogen; Diseases; Bacteria, virus, Electrochemical

*Corresponding author: Tel.: +91 11 27294668 (O), email: bansi.malhotra@gmail.com.

Accepted Manuscript

ACCEPTED MANUSCRIPT

ABSTRACT

The present review concerns the recent developments of nucleic acid biosensors for detection of the human pathogens as infectious diseases management at an early stage is currently of prime interest so as to circumvent the delay in diagnosis, side effects of drugs and unnecessary health hazards. The advantages of biosensors over existing detection methodologies and the role of various immobilization matrices used for fabrication of nucleic acid sensors are discussed. Besides this, efforts have been made to discuss the various techniques used for biosensor construction, the analytical performance of these biodevices for the bacterial and viral pathogens for their applications to medical diagnosis.

Accepted Manuscript

ACCEPTED MANUSCRIPT

1. Introduction

Recent years have seen continued growth of the interdisciplinary field of biosensors due to an increased interest between basic and applied sciences researchers for development of novel electronic devices that can be utilized for a variety of applications including human health care and environmental monitoring [1]. A biosensor is an integrated miniaturized analytical device that integrates biological sensing elements like enzymes [2], antibodies [3], nucleic acids [4], cells etc. with transducer equipped with an electronic amplifier [5]. Biosensors offer interesting features such as real-time, on-site, simultaneous detection of multiple pathogenic agents utilizing selectivity of the biomolecules and the processing power of modern nano-electronics [6,7]. They are known to provide fast and accurate results arising due to interaction of an analyte with a given biomolecule and have been found to have applications in various fields including clinical diagnostics [8], environmental monitoring [9], bioprocess monitoring [10], food, water [11] and agricultural product processing [12], etc. According to IUPAC, a biosensor is a self-contained integral device which is capable of providing specific quantitative or semi-quantitative analytical information using a biological element.

There is an increased interest towards the development of nucleic acid biosensors for clinical monitoring [13]. Voltammetry of nucleic acids after the discovery of anodic peak specific for guanine is an important milestone for monitoring of double-stranded and denatured single-stranded DNA. Monitoring change in the DNA redox properties (oxidation of guanine) provides a unique opportunity to detect the hybridization process [14]. Through, the electrochemical detection using guanine oxidation is known to cause irreversible damage to DNA; however, redox indicator-based indirect electrochemistry has been shown to be an important alternative for development of nucleic acid hybridization biosensors. The

ACCEPTED MANUSCRIPT

electrochemical DNA biosensors with redox indicators like methylene blue (MB) [15-16], daunomycin [17], metal complexes such as ruthenium (Ru) complex [18], cobalt complex [19] etc have been found to be advantageous due to re-usability of the electrode. Besides this, electrochemical biosensors do not require additional labeling step and can be easily integrated with electronics for fabrication of miniaturized devices for diagnosis of infectious diseases and the detection of pathogenic biological species of environmental and clinical interest. Thus, DNA hybridization biosensor technology is at the vanguard of clinical diagnosis which commonly relies on measuring techniques like electrochemical [20], optical [21] and mass-sensitive [22] to recognize the complementary target DNA strand.

For the fabrication of a high performance biosensor, the role of an immobilization matrix is very crucial. Among the various matrices, nanomaterials are being explored due to their exceptional optical and electrical properties owing to electron and phonon confinement, high surface-to-volume ratio, modified surface work function, high surface reaction activity, high catalytic efficiency and strong adsorption ability. In particular, nanomaterials with engineered morphology, size, functionality, adsorption capability and high biomolecule loading capacity have been found to provide enhanced electron transport between a biomolecule and the electrode. The microenvironment provided by a nanomaterial may help a biomolecule to retain its conformation with maximum biological activity, resulting in enhanced signal transduction and biosensor stability. These unique properties of nanomaterials can perhaps be utilized for interfacing biological recognition events with electronic signal transduction and for designing a new generation of bioelectronics devices that may exhibit novel functions.

Infectious diseases, especially those resulting from life-threatening pathogens, have significantly increased over the past few decades, and deaths may occur primarily because of

Accepted Manuscript

ACCEPTED MANUSCRIPT

delay in diagnosis, side effects of drugs and commodities necessary for rapid detection, prevention or cure [23]. Pathogens are microbes that are capable of causing illness, remain the world's greatest killer of children and young adults, accounting approximately 13 million deaths a year. Pathogen detection is currently of utmost importance, due to health and safety concern. The most common pathogens are bacteria, viruses, fungi and parasites (SI). The increased viral outbreaks e.g., H1N1 flu, H5N1 flu, and SARS etc., recently boost the alarm and raised significant worries as the viruses could rapidly spread and turn into a pandemic. In spite of developments in the diagnostic fields for pathogen detection, there is an urgent need for availability of rapid, portable and accurate diagnostic technique that can be used to control the epidemics and may perhaps have a significant impact on clinical management. This manuscript deals with the recent development of electrochemical, optical biosensing techniques based on nucleic acids for pathogens detection that have implications towards the clinical management of bacterial and viral infections.

2. Conventional techniques for detection of pathogens

The traditional methods for pathogen detection include microscopy, culture and serology. Microscopy is simple, easy to use and a versatile technique. Culture is the gold standard for diagnosis of many microorganisms, e.g., *Mycobacterium tuberculosis* and serology forms the mainstay of diagnosis in some of the diseases, e.g., syphilis. The traditional methods of detection are inexpensive but protracted methods. Microscopy has limited sensitivity in many settings and the interpretation may be subjective. On the other hand, culture runs the risk of contamination with commensal flora and the possibility of reduced viability during transportation. In addition, choice of culture media and interpretation of culture results requires technical skill. The main

Accepted Manuscript

ACCEPTED MANUSCRIPT

disadvantage of serology is the requirement of convalescent sera and the occurance of false-positive results due to cross-reaction with other organisms. The last two decades have seen a switch to molecular methods that offer a growth independent strategy. It is particularly sited for unculturable organisms, e.g., *Treponema pallidum*; difficult to grow organisms, e.g., HIV, HBV, *Bordetella pertussis;* slow growing organsism, e.g., *Mycobacterium tuberculosis*; and dangerous to culture organsisms, e.g., *Coxiella burnetti*. Molecular methods include the non-amplification methods, e.g., hybridization using probes as well as amplification based methods. The nucleic acid amplification techniques (NAATs) have taken an irreversible position in diagnostics. These include polymerase chain reaction-PCR, transcription based amplification (target amplification), ligase chain reaction-LCR (probe amplification), branch DNA technology (signal amplification) and loop-mediated isothermal amplification-LAMP (isothermal amplification). These methods are known to be sensitive and yield both qualitative and quantitative information of the tested microorganisms. However, these techniques are expensive and require long assay time.

Among nucleic acid amplification tests, PCR which is most commonly used, can detect a single copy of a target DNA sequence, and thus, can be used to detect a single pathogenic bacterium. It is promising because it detects the organism by amplifying the target rather than the signal, and is therefore less prone to producing false-positives. Thus, PCR detection of pathogens has distinct advantages over culture and other standard as it offers the advantages of specificity, sensitivity, rapidity, accuracy and capacity to detect small amounts of target nucleic acid in a sample [36-41].

ACCEPTED MANUSCRIPT

3. Electrochemical biosensors

A biosensor is a bioanalytical device incorporating a molecular recognition entity associated with or integrated with a physicochemical transducer [5] (Fig. 2). It consists of two main components: a bioreceptor or biorecognition element, which recognizes the target analyte and a transducer, for converting the recognition event into a measurable electrical signal. A bioreceptor can be a nucleic acid (DNA, PNA, RNA and aptamer etc.) (Supplementary Fig. 1, 2, 3, 4), enzyme, antibody, cell and microorganism etc [42-45] and the transduction may be electrochemical, optical and piezoelectric. The immobilization of a nucleic acid molecule onto a matrix (Fig. 3) requires complete retention of their biological recognition properties in the active state (Fig. 4a). The desired probes are attached at one terminus onto the surface (Fig. 4b). This allows for the highest degree of thermodynamic freedom, that significantly speeds up the hybridization rate. Binding should not occur at the nucleotide bases, since these sites are the target capture sites.

The bioreceptor recognizes the target analyte and the corresponding biological response in turn are converted into equivalent electrical signals by the transducer. The amplifier in the biosensor responds to the small input signal from the transducer and delivers a large output signal that contains the essential features of an input signal. The amplified signal is then processed by the signal processor wherein it can be stored, displayed and analyzed. Biosensors can be classified as point-of-care devices which can bring the capability of analyzing clinical samples at home or at the doctor's office. In order to develop appropriate biosensor technologies, specific markers need to be identified to ensure specificity of the given devices. Biosensors provide advanced platforms for biomarker analysis with the advantages of being easy to use, are inexpensive, rapid and robust and offer multi-analyte testing capability. Biosensors have been

Accepted Manuscript

ACCEPTED MANUSCRIPT

widely applied to a variety of analytical problems in medicine, the environment, food, process industries, security and defense [46-47].

Biosensors have broadly been classified into two categories depending on the biorecognition element (bioreceptor) and the method of detection i.e. transducers (Fig. 1b). The biorecognition elements, mainly used in nucleic acid sensors, can be further divided as (i) *DNA*, (ii) *RNA*, (iii) *PNA* and (iv) *Aptamer* [48-49]. Biorecognition elements DNA/RNA/PNA/aptamers nucleic acid fragments rely on either complementary base-pairing between the sensor's nucleic acid sequence and the analyte of interest, or generating nucleic acid structures [50] (Fig. 5).

On the basis of transducing element, biosensors can be categorized as electrochemical, optical, piezoelectric, and thermal sensors. Among the various biosensors, electrochemical biosensors have gained considerable interest as bioanalytical devices and have played an important role in the detection of desired pathogens [51]. They allow high sensitivity, lower detection limits, automation, reduced costs of testing, and development of disposable devices and methodologies capable of working with very small sample volumes. Further, unlike spectroscopy-based techniques, electrochemical sensors are not affected by sample turbidity, quenching, or interference from absorbing and fluorescing compounds, and they require relatively simple instrumentation that is low-power and can be easily miniaturized. Use of electrochemical techniques, over optical and other transduction techniques, exhibits excellent sensitivity and a large linear detection range in a wide range of solvents, electrolytes, temperatures, etc.

ACCEPTED MANUSCRIPT

3.1. Electrochemical nucleic acid sensors for pathogen detection

Majority of the biosensors used for detection of pathogens are electrochemical in nature. The advantages of electrochemical biosensors include high sensitivity, suitability for microfabrication, and simple instrumentation. Electrochemical detection is commonly employed as a means of investigating the recognition between DNA–DNA, DNA-PNA, DNA-RNA and DNA-aptamers for nucleic acid pathogen detection [52-54]. The electrochemical sensors are based on measurement of changes in current, potential and impedance induced to biochemical reactions. Electrochemical transducers have been considered as a simple and sensitive method of DNA hybridization detection using affinity of single-stranded DNA for complementary strands for both indirect and direct measurement methods [55-58]. Indirect approaches are based on detection of an electroactive label that may intercalate or associate with a double-stranded DNA. On the other hand, direct methods are label-free and rely mostly on the intrinsic electroactivity of nucleobases. Use of electrochemical impedance spectroscopy [EIS, 59-60] by monitoring both resistance and reactance in a biosensor is becoming more common. Considering the suitability and ease of handling and easy detection, researchers are focusing on electrochemical biosensors for pathogen detection.

3.1.1. Electrochemical nucleic acid sensors for bacterial pathogens detection

Researchers are continuously evaluating several new engineered materials for the fabrication of bioelectrode for bacrterial pathogen detection [61-62]. Among them, the thin films of polymers like polyaniline (PANI), nanostructured metal oxides like ZrO_2, self assembled monolayers (SAM) of silanes, carbon nanostructures like carbon nanotubes, fullerene etc. are some of the widely used materials in present age. Since the biotin-strept(avidin) system has high binding capacity for nucleic acids immobilization due to the high affinity constant (Ka = 10^{15} M^{-}

ACCEPTED MANUSCRIPT

[1]) between avidin and biotin, it is also widely used to immobilize nucleic acids on solid support interface to construct biosensors for bacterial detection. Arora et al. have made a significant contribution for the development of voltammetric biosensors utilizing avidin-modified polyaniline (PANI) electrochemically deposited onto a platinum (Pt) disk electrode for direct detection of *E. coli* by immobilizing a 5′-biotin-labeled *E. coli* probe, in the presence of methylene blue as a DNA hybridization indicator (Fig. 6). Depending on the target sample and the sonication time, this biotin immobilized avidin PANI bioelectrode can be utilized to electrochemically detect a complementary target probe (0.009 ng/μL), *E. coli* genomic DNA (0.01 ng/μL) and 11 *E. coli* cells/mL in 60s to 14 min without using PCR and can be used 5-7 times at temperatures of 30-45°C. [63]. Shiraishi et al. have observed that the incorporation of fullerene into this polymeric structure dramatically improves the surface coverage of the immobilized probe specific to *E. coli* extracted from 16S rDNA [64]. SAM is considered an ideal method to immobilize the nucleic acid in the construction of biosensors for bacterial detection which provides a convenient and flexible route to generate ultrathin and ordered biological monomolecular films on a variety of substrates by organic molecules (both aliphatic and aromatic) containing free anchor groups such as thiols, disulphides, amines, silanes, or acids. Loaiza et al have worked on a new approach of the fabrication of SAM of 3,3'-dithiodipropionic acid di(N-succinimidyl ester) (DTSP), which usually used as a spacer, onto gold (Au) disk and immobilized 25-base single-stranded probe specific to *E. coli* lac Z gene. [65]. Pandey et.al have utilized the SAM platform for the detection of *E. coli* using 1-fluoro-2-nitro-4-azidobenzene modified octadecanethiol SAM and have observed that the fabricated sensor exhibits high sensitivity (0.5×10^{-18} M) and linearity as 0.5×10^{-18}–1×10^{-6} M [68]. However, the SAM immobilization method still suffers from some drawbacks, such as electric field induced and

ACCEPTED MANUSCRIPT

thermal desorption of monolayer and nonspecific adsorption due to high surface energy. Solanki et al. have exploited sol–gel derived Nano zirconia (ZrO_2) platform for the detection of *E. coli*. They have immobilized 17-base single stranded (ss) DNA identified from the 16s rRNA coding region of *E. coli*, and utilized this bioelectrode for sensing of *E. coli*. This sensor has shown high selectivity and sensitivity towards hybridization with detection limits of 10^{-6}-10^{6} pM of complementary DNA which may be due to the nanostructured ZrO_2 which provided more surface area [66]. Wu et al. have fabricated a simple signal-off DNA sensor that employs an Exonuclease III -aided target recycling strategy for sequence specific DNA detection with excellent discrimination ability for single-nucleotide polymorphisms. A redox mediator, $Ru(NH_3)_6^{3+}$ (RuHex) is electrostatically adsorbed onto signaling probe and provides detection limit as low as 20 fM. [67]. An electrochemical genosensor based on 1-fluoro-2-nitro-4-azidobenzene modified octadecanethiol SAM fabricated for *E. coli* detection by Pandey et al. have revealed that the fabricated sensor exhibits high sensitivity (0.5×10^{-18} M) and linearity as 0.5×10^{-18}–1×10^{-6} M [68]. Majid et al. have exploited o-nitro phenol, released from o-nitrophenyl--D-galactopyranose as catalyzed by -galactosidase, a tetramer of *E. coli,* for the detection of *E. coli* contamination in foodstuffs, using a boron doped diamond electrode poised at 0.93 V, without any surface modification. The enzyme is effectively induced by isopropyl--D-thiogalacto-pyranoside with the maximum enzyme activity observed with sodium dodecyl sulfate at 50°C. A biphasic calibration plot is observed as 4×10^{4} to 2×10^{5} cells/mL and 2×10^{5} to 6×10^{6} cells/mL for the first and second region, respectively. The detection limit is 4×10^{4} cells/mL with a total analysis time of 1.5 h [69]. The electrochemical impedance studies (EIS) for the monitoring of DNA hybridization has also attracted much attention. This interesting technique allows analysis of interfacial changes originating from biorecognition events at electrode

ACCEPTED MANUSCRIPT

surfaces. Besides this, it offers several advantages such as simplicity, label-free detection, low cost, easy operation and can be miniaturized. Wang et al. have demonstrated a novel biosensor based on ssDNA probe functionalized aluminum anodized oxide (AAO) nanopore membranes for *E. coli* O157:H7 DNA detection via impedimmetry. An original and dynamic polymerase-extending DNA hybridization procedure has also been proposed, wherein hybridization occurs in the presence of Taq DNA polymerase and deoxynucleotide triphosphates under controlled reaction temperature [70]. Pandey et al. have reported micro dendritic structural cystine (Cys) modified DNA electrode for detection of *E. coli* and exhibits linear response in the concentration range of 10^{-6} to 10^{-14} M with response time of 30 min [71]. In spite of its convenience, this method has however found limited applications due to low stability and the random orientation of the bio-recognition elements immobilizing on electrodes, resulted in the decrease of the binding. In spite of these intersting developments, these biosensing devices suffer from some drawbacks such as EIS signals resulting from nucleic acid-based impedimetric biosensors are remarkably affected by repulsions between the negatively charged phosphate backbone and redox anions such as $[Fe(CN)_6]^{3-/4-}$ that make the quantitation of DNA hybridization reactions rather difficult.

The detection of life threatening, food borne bacterial pathogens, biosensor has been considered as an important tool and presently holds great promise for the diagnosis of diseases. Hence, the researchers are using conducting polymers as a platform due to their unique properties. Food-borne bacterial pathogen *Salmonella Enteritidis* has been detected electrochemically by Zhang et al. who fabricated streptavidin modified nanoporous silicon based biosensor for the detection of biotin modified DNA. The observed results show that the DNA probe is specific to the target DNA, and the porous silicon-based biosensor provides more active

Accepted Manuscript

ACCEPTED MANUSCRIPT

surface area and higher sensitivity (1 ng/mL) than the planar silicon based biosensor [72]. Though the biotin-strept(avidin) system is an effective method to immobilize the bio-recognition elements on the surface of solid supports, this method has disadvantages such as the high cost of the reagents involved and the need for a suitable linker layer attach to the electrode. Nandakumar et al have detected *Salmonella typhimurium* using EIS concentrations in the order of 500 CFU/ml which is lower than infectious pathogen levels [73]. The efforts should be directed for delineating the mechanism of the surface modified semiconductor electrode, especially modified with DNA sequences. At the same time, decreasing the random error during sensor fabrication to confirm the stability of the signal is a key issue.

Foodborne pathogen *Bacillus cereus* group has been detected using a conducting polymer as a platform via cyclic voltammetry by Velusamy et al [74]. The fabricated sensor shows 10^3 CFU/ml detection limit, allowing rapid detection of this bacterial pathogen [75]. This group has electrochemically polymerized a conducting pyrrole with $MgCl_2$ as a doping electrolyte for the specific detection of *B. cereus.* This DNA hybridization biosensor has been found to have improved selectivity, sensitivity and reproducibility of hybridization events. This method does not require special chemical modification of the DNA and hence can be easily used. The major limitation relates to the physical adsorption of DNA which is weaker than the covalent binding resulting in lower sensitivity [76] An emerging food borne pathogen *Aeromonas hydrophila* has been detected via chronocoulometry and square wave voltammetry (SWV) by Tichoniuk et al. using SAM of thiolated (th) DNA [77].

Sheng et al. have reported PANI based ultrasensitive biosensor for detection of the amplified target syphilis DNA. The current response of PANI is linearly related to target DNA

ACCEPTED MANUSCRIPT

concentration between 1.0 pM and 1.0 nM with a correlation coefficient of 0.998. The detection limit is determined to be as 0.5 pM with the signal-to-noise ratio of 3 [78].

Wang et al. have utilized reduced graphene oxide platform for the fabrication of a highly sensitive and selective nucleic acid sensor for the detection of methicillin-resistant *S. aureus* and observed that the sensor can be used to detect upto 100 fM of target concentration [79]. Castro et al. have developed an electrochemical method, different from the real time-PCR approach, for semi-quantitative evaluation of *L. pneumophila*. A PCR assay targeting the 16S-rRNA gene of *L. pneumophila* giving rise to a 95-mer amplicon has been established. Amplicons have been hybridized with a biotin-labeled reporter sequence and then to a thiolated stem-loop structure immobilized onto gold electrodes as a reporter molecule with 1-naphthyl phosphate as a substrate. After 40 cycles of PCR amplification, this methodology has limit of detection (LOD) of 10 genomes, allowing reliable detection of 10^2 genomes of *L. pneumophila* as well as distinguishing 10^3 and 10^4 genomes of the pathogen [80]. Damrow et al. have developed anthrax DNA biosensor for detection of *Bacillus anthracis* using the principle of DNA displacement via amperommetry. They have used "Signal On" transduction method that leads to larger current when hybridization occurs between test sample and the captured probe [81] (Supplementary Fig. 5).

For the detection of life threatening, food borne bacterial pathogens, biosensor has been considered as an important tool and presently holds the great promise for the diagnosis of diseases. The researchers have been focusing on conducting polymers as a platform due its unique properties. Prabhakar et al. have reported fabrication of conducting polymer based DNA and PNA based hybridization biosensor for detection of *M. tuberculosis.* The authors have also investigated the effect of various redox indicators on the hybridization events. Compared to Ru

ACCEPTED MANUSCRIPT

complex, MB has been found to have better redox behaviour to capture DNA hybridization. PNA immobilized polypyrrole (PPY) polyvinylsulphonate electrode can be used to detect complementary sequence in heat-shocked genomic DNA and in serum samples, containing genomic *M. tuberculosis* DNA up to 2.5 pg/µl within about 60 s at 30^{o} C and can be used 8-9 times [82]. The specific interaction between guanines and MB is confirmed by a linear relationship between the number of guanine bases in the oligonucleotide used to modify the electrode and the amount of charge passed. In another approach, the same group has utilized twenty-base long NH_2-modified DNA and PNA probes specific to *M. tuberculosis*, covalently immobilized onto PANI/Au electrode to detect nucleic acid hybridization. They have shown that PNA-PANI/Au electrode exhibits improved specificity (1000 times) and detection limit of 0.125 $\times$ 10^{-18} M as compared to that of DNA-PANI/Au electrode (2.5 $\times$ 10^{-18} M) [83]. Covalent binding of DNA onto electrode allows enough freedom of motion of the immobilized DNA molecule and enables the control of orientation and hybridization capacity. Though the conducting polymer based sensors exhibit good characteristics. However, there is a greater scope to improve the characteristics of nucleic acid based DNA biosesnors for *M. tuberculosis* detection based on nano-structured metal oxides, quantum dots, carbon nanotubes (CNT), graphene etc. In view of the recent revelations and potential applications of CNT-DNA nanobiohybrid, the core-shell structural biowire comprising of CNT and DNA has been fabricated via electrophoretic deposition technique by Das et al. (Supplementary Fig. 6). They have postulated the wrapping mechanism in the light of co-ordination chemistry and have revealed that the peripheral wrapping of DNA along the length of CNT in nanoscale may act as a single nanowire enhancing the electron transport capability. These Mg^{2+} ions assisted core (CNT)–shell (DNA) complexes have implications towards the fabrication of novel nano-biochips

ACCEPTED MANUSCRIPT

and ultrasensitive biomolecular electronic systems that are likely to revolutionize the emerging field of genotronics [84].

The nanostructured metal oxides and their composites are of utmost research interest. In recent years emphasis have been given to the synthesis of nanostructured metal oxides and carbon nanostructures composite to enhance the surface coverage, electrical and mechanical propertiies which can be used in fields like medical diagnosis. Considering the synergy between biocompatible ZrO_2 and electrochemically superior CNT, ZrO_2 grafted CNTs (crystallite size of ZrO_2 ~28.63 nm), obtained via isothermal hydrolysis of zirconium oxychloride in presence of CNT, have been electrophoretically deposited indium tin oxide (ITO) and used for the immobilization of ssDNA specific to *M. Tuberculosis* [85] (Supplementary Fig. 7) by Das et al. EIS studies indicate ~3.5 fold enhancement in charge transfer behaviour of NanoZrO_2-CNT/ITO electrode compared to that of NanoZrO_2/ITO electrode and bioelectrode is able to detect 1×10^{-8} mM of target DNA concentration.

Sexually transmitted diseases (STD) currently represent a major public health problem in the world and the advent of human immunodeficiency virus infection during the last decade has highlighted the importance of its rapid, easy, cost-effective way of detection. Singh et al. have fabricated STD (Gonorrhoea) sensor based on nucleic acid probe (from *Opa*, a multi-copy gene of *N. gonorrhoeae*) functionalized using avidin–biotin as cross-linking agent onto PANI matrix. This DNA functionalized electrode can be used to specifically detect upto 0.5×10^{-15} M of complementary target within 60 s of hybridization time at 25° C by DPV using MB [86]. In order to amplify the detection signal and achieve lower detection limits, the main interaction signal may be enhanced by the incorporation of multi walled (MW) CNT that provide conducting channels facilitating faster charge transfer via electrons from one polymer chain to the other and

ACCEPTED MANUSCRIPT

finally to the electrode surface. Singh et al. incorporated MWCNT into the PANI matrix and utilized as a platform for the immobilization of 5′amino-labeled probe specific to *N. gonorrhoeae*. The DPV studies have revealed that this sensor can selectively detect complementary DNA concentration upto to a lower detection limit of 1.2×10^{-17} M [87].

Singh et al have recently utilized chitosan (CH)–iron oxide (Fe_3O_4) nanobiocomposite for the detection of *N. gonorrhoeae* (Supplementary Fig. 8). It has been found that the presence of

Fe_3O_4 nanoparticles (~18 nm) increases the electro-active surface area of the nanobiocomposite

that provides desirable environment for loading of DNA with better conformation leading to increased electron transfer kinetics between the medium and electrode. This STD biosensor has been found to have a detection limit (1×10^{-15} M) and a wide dynamic range (from 1×10^{-16} M to1×10^{-6} M) using the complementary target DNA. In addition, the sensing system has been utilized to accurately discriminate complementary sequence from mis-match sequences [88]. Another species of *Neisseria* has been detected through biosensor by Patel et al. They have fabricated an electrochemical biosensor by immobilizing thiolated ssDNA onto Au coated glass electrode and have shown that it can detect the complementary DNA in the range of 7–42 ng/µl revealing sensitivity as 115.8 µA/ng [89]. This sensor can be used to detect genomic DNA and PCR amplicon upto 10–60 ng/µl revealing sensitivities as 0.0115 µA/ngcm^{-2} and 0.0056µA/ngcm^{-2}, respectively [90] (Table 1).

3.1.2. Electrochemical nucleic acid sensors for viral pathogens detection

ACCEPTED MANUSCRIPT

Rapid identification of viruses has important implications for medical healthcare. The presently available methods of detection are mainly based on rapid immunoassay techniques that require trained manpower and are time consuming and expensive. However a biosensor facilitates a doctor to identify the specific virus quickly and prescribe an appropriate course of treatment. Viruses can be advantageously used for the development of a real-time sensor to rapidly and selectively detect target in a variety of harsh conditions, such as under acidic or basic pH ranges.

Hepatitis B is an infectious illness of the liver caused by the hepatitis B virus (HBV) that affects hominoidea, including humans. Originally known as "serum hepatitis", the disease has caused epidemics in parts of Asia and Africa, and it is endemic in China. About a third of the world population has been infected at one point in their lives including 350 million who are chronic carriers. Hence it is important to diagnose HBV in its early stages. In this context, Ariksoysal et al. have developed a novel assay for voltammetric detection of DNA sequences related to the hepatitis B virus (HBV) genotype on the development of lamuvidine resistance by monitoring the oxidation signal of guanine (G). Under optimum conditions, biosensor can be used to detect 457 fmol/mL of target DNA [91]. Kara et al. have developed direct label free electrochemical genosensor with an aim to optimize the effect of probe sequence relative position in an amplicon related to HBV. Hybridization occurs after surface coverage with denatured amplicons followed by identification by using the differences between the responses of G oxidation signals [92]. Li et al. have utilized a novel hybridization indicator, bis(benzimidazole)cadmium(II) dinitrate [$Cd(bzim)_2(NO_3)_2$], to develop an electrochemical DNA biosensor for detection of a short DNA sequence related to the HBV with the detection range 1.49×10^{-7} M to 1.06×10^{-6} M and detection limit of 8.4×10^{-8} M. The novelty of this sensor

ACCEPTED MANUSCRIPT

lies in the selection of the redox indicator but this DNA biosensor suffers from the narrow detection range [93]. Li et al. have used [Cu(dmp)(H_2O)Cl_2] (dmp = 2,9-dimethyl-1,10-phenanthroline) as a redox indicator to improve the detection limit (7.0×10^{-8} M) for the HBV detection. [94]. Ding et al. have exploited 2,9-dimethyl-1,10-phenantroline cobalt [Co(dmp)(H_2O)$(NO_3)_2$] as redox indicator and studied its interaction with DNA. Under the optimum conditions, the electrical signal exhibits a linear relationship with the concentration of target DNA ranging from 3.96×10^{-7} to 1.32×10^{-6} M, and the detection limit is 1.94×10^{-8} M [95]. Niu et al. have detected HBV virus following the same DNA hybridization principle but with different redox indicator such as rutin–Cu complex. It has been revealed that the target DNA for coliform virus gene can be quantified and ranges from 1.62×10^{-8} mol L^{-1} to 8.10×10^{-7} mol L^{-1} with a good linearity and a detection limit of 2.3×10^{-9} mol L^{-1} [96]. Zhang et al. have utilized the complex diaquabis[N-(2-pyridinylmethyl) benzamide-k^2 N,O]-cadmium(II) dinitrate {[$CdL_2(H_2O)_2$]$(NO_3)_2$, wherein L=N-(2-pyridinylmethyl) benzamide}, as a electroactive indicator for voltammetric detection of HBV. They have observed that the target HBV DNA can selectively detect HBV from 1.01×10^{-8} to 1.62×10^{-6} mol L^{-1} with good linearity with detection limit of 7.19×10^{-9} mol L^{-1} [97].

Hepatitis C is an infectious disease affecting primarily the liver, caused by the hepatitis C virus (HCV). The infection is often asymptomatic, but chronic infection can lead to scarring of the liver and ultimately to cirrhosis, which is generally apparent after many years. In some cases, those with cirrhosis will go on to develop liver failure, liver cancer or life-threatening esophageal and gastric varices. Riccardi et al. have demonstrated an electrochemical transduction scheme for the detection of HCV. However, this sensor takes much longer time (10 min) for the

Accepted Manuscript

ACCEPTED MANUSCRIPT

hybridization to occur [98]. Azar et al. have detected the HCV virus using DPV monitoring of G signal revealing 6.5 nM detection limit [99].

Liu et al. have developed a new electrochemical approach for qualitative and quantitative detection of HCV based on the site-specific DNA cleavage of BamHI endonuclease. The difference in the peak currents varies linearly with the concentration of target DNA ranging from 0.1 to 2.5 μM. [100]. Hejazi et al. have developed Au electrode modified with a SAM composed of PNA probe and 6-mercaptohexanol (MCH) for detection of short sequences of HCV and found the detection limit as 5.7×10^{-11} M [101].

Human immunodeficiency virus (HIV) is known to be an important virus that is known to affect humans. HIV is a lentivirus that causes the acquired immunodeficiency syndrome which is a condition in humans in which progressive failure of the immune system allows life-threatening opportunistic infections and cancers to thrive. The early detection of HIV is very important to manage the disease and prevent the spreading of the disease effectively. In this context, nanomaterials and their composites have been found to provide interesting platform for the fabrication of nucleic acid based biosensors for HIV detection. An ultra-trace voltammetric method has been developed by Wang et al. for the detection of HIV-1. CNT loaded with silver nanoparticles, placed on a gold microelectrode, have been used as a matrix for immobilization of 21-mer ssDNA. The detection range varies from 1.0 to 100 pM with the detection limit of 0.5 pM [102]. Haseen et al have fabricated streptavidin modified magnetic nanoparticles based DNA

ACCEPTED MANUSCRIPT

biosensor for detection of HBV. A layer of functionalized nanoparticles is directly immobilized onto bare Au electrode using a magnet. Non-faradic impedance spectroscopy technique can be used to detect 50 pmol of HBV DNA and 160 pmol of HIV DNA on sample of 20μL [103]. Tran et al. have fabricated CH/Fe_3O_4 nanobiocomposite-based platform for electrochemical HIV-1 detection. Suitable microenvironment provided by Fe_3O_4 nanoparticles contributes to higher electron transfer and enhanced sensitivity. This electrode has a low detection limit (50 pM), acceptable stability and good reproducibility [104]. MWCNT have been used as a platform by Tam et al. for the detection of another pathogenic virus known as influenza virus. The results show that the DNA sensor can detect as low as 0.5 nM of the target DNA samples.This method has a longer response time of ~4 min [105]. Chen et al. have demonstrated an ultrasensitive electrochemical biosensor for the detection of influenza A virus based on glucose oxidase (GOx)-catalyzed deposition of copper hexacyanoferrate (CuHCF) nanoparticles. The detection limit of 1.0 fM has been assigned to the high sensitivity of DPV technique, high catalytic activity of GOx, and the cumulative nature of the formation of the CuHCF nanoparticles catalyzed by GOx attached to the hybridized DNA. This sensor has linearity of 1.0 fM to 10 pM and a detection limit of 1.0 fM [106]. Fan et al. have developed a facile ethanolamine/glucose mixed solution route for the controllable synthesis of cadmium selenide (CdSe) hollow nanostructures and consequently used it for the fabrication of electrochemical DNA sensor for Avian Influenza Virus (AIV) [107]. AIV can be detected using MWCNT–cobalt phthalocyanine (CoPc) nanocomposite and poly (amidoamine) (PAMAM) dendrimer as a platform onto glassy carbon electrode (GCE). This nucleic acid sensor is based on oxidation signals of guanine without any external labels and can be used to detect from 0.01 to 500 ng/ml with a detection limit of 1.0 pg/ml [108].

Accepted Manuscript

ACCEPTED MANUSCRIPT

Zari et al. have fabricated thssDNA immobilized screen printed electrode (SPE) for the detection of short DNA fragments specific to the human papilloma virus (HPV) followed by hybridization. They have utilized guanine oxidation signal to detect the hybridization phenomena by treating DNA with 0.5 M chloridric acid and the acid-released purine bases can be detected using SWV. Under optimal conditions, this sensor has a good calibration range of target DNA sequence with detection limit of 2 $pgml^{-1}$, but suffers from its reusability. As guanine oxidation is monitored, the electrode can be used only once [109]. Civit et al. reported in 2010, a proof-of-concept of an electrochemical genosensor array for the simultaneous detection of two HPV types, HPV16E7p and HPV45E6 sequences. The detection limit obtained is in the pM range that is sufficient for majority of real RNA/DNA samples obtained from PCR amplification [110]. Zhang et al. have developed a sensitive label-free bio-barcode assay for quantitative detection, based on the redox activity of G and adenine (A) nucleobases, of two nucleic acid targets Human T-lymphotropic virus (HTLV-I and HTLV-II) simultaneously This DNA biosensor based on two-component oligonucleotide-modified Au nanoparticles (NPs) and two-component oligonucleotide-modified magnetic beads (MBs). On release of the adsorbed thiolated barcode DNA strands (poly A and poly G) from the AuNPs surface with dithiothreitol and acidic dipurinization, the electrochemical measurements can be directly performed. It has been observed that the sensor can detect target sequences in the range from 4.4×10^{-11} to 2.0×10^{-9} M, and the detection limit is estimated 1.71×10^{-12} M for T_1-DNA and 1.55×10^{-12} M for T_2-DNA [111] (Table 2).

4. Optical nucleic acid sensors for bacterial and viral pathogens detection

Accepted Manuscript

ACCEPTED MANUSCRIPT

Optical transducers are particularly attractive for application to direct (label-free) detection of bacteria [112]. Among these, surface plasmon resonance (SPR) sensors based on reflectance spectroscopy are in the advent of current science. In SPR measurements resonance angle is very sensitive to the change in refractive index and hence it can be exploited for sensor application. The SPR shift in millidegrees, due to the change in refractive index, is used as the response to quantify the binding of the macromolecules at the sensor surface. These types of sensors can be used to detect minute changes in the refractive index where biomolecules bind with the receptors immobilized on the optical transducer surface.

Prabhakar et al. have reported cysteine modified NH_2-end PNA and 5'-thiol end labeled DNA based for detection of *Mycobacterium tuberculosis* using SPR technique (Fig. 7). The PNA/Au bioelectrode shows improved detection limit (1.0 ng ml^{-1}) over the DNA-Au bioelectrode (3.0 ng ml^{-1}). The values of the association (*k*a) and dissociation rate constant (*k*d) for the complementary sequence in case of the PNA/Au bioelectrode have been estimated to be as 8.5×10^4 m^{-1} s^{-1} and 3.6×10^{-3} s^{-1}, respectively [113]. Cheong et al. have reported a microfluidic chip using the longitudinal resonance of Au nanorods that transforms near infrared energy into thermal energy. The resulting heat causes pathogen lysis. Consequently, the DNA can be extracted out of the cell body and transferred to the PCR system. Two different Au rods AR 3 and AR 15 exhibits efficient lysis of *E. coli* cells and quick pathogen detection by real-time PCR using SYBR Green I without any optical hindrance (Ct values, 21.60 and 22.07 respectively). When a different Taq polymerase is used without hot start, they have obtained better Ct values (17.31 and 18.67 for AR 3 and 15 respectively) with the Au nanorods, suggesting that Au nanorods are also compatible with different Taq polymerases. This has led to successful demonstration of a one step real-time PCR system for pathogen detection without

ACCEPTED MANUSCRIPT

removal or changing of reagents [114]. Bai et al have demonstrated an SPR biosensor using biotinylated aptamers immobilized on the gold surface coated with streptavidin via streptavidin-biotin binding. They observed an increase in the refraction index when immobilized aptamers captured AIV H5N1 in a sample solution and it was linearly related (R2 = 0.99) to the concentration of AIV in the range of 0.128 to 1.28 HAU. Negligible signal (<4% of H5N1) has been observed from six non-target AIV subtypes. The AIV H5N1 in poultry swab samples with concentrations of 0.128 to 12.8 HAU could be detected using this aptasensor in 1.5 h [115].

Drinking water is usually contaminated with pathogens and their toxins; hence biosensors aimed at detecting these pathogens would be highly expedient. Baeumner et al., have developed a highly sensitive and specific RNA biosensor for the rapid detection of viable *E. coli* as an indicator organism in water that can detect as few as 40 viable *E. coli* in water [116]. The same group has developed quantitative and highly sensitive, yet simple and rapid, biosensor system for the detection of nucleic acid sequences [117]. Wang et al have proposed a method that allows for the simultaneous, real-time discrimination of *S. aureus, P. aeruginosa, C. tetani* and *C. perfringens* in mixed bacterial infections. Moreover, this method has a specificity equivalent to bacterial culture based methods and allows for the semi-quantitative assessment of multiple bacteria, which is helpful for the clinical diagnosis and follow-up treatment [118]**.** Zuo et al used a simple strategy to integrate the aptamer-functionalized GO biosensor in the microfluidic biochip through the novel use of the porous chromatography paper as a simple 3D storage substrate for the aptamer-functionalized GO nano-biosensor in microwells. This approach detects pathogen microorganisms directly, without cumbersome sample preparation procedures, making it feasible for field detection [119] (Table 3).

ACCEPTED MANUSCRIPT

5. Other nucleic acid sensors for Bacterial and Viral Pathogens Detection

Many other techniques have been reported for pathogen detection. In this context, Chua et al. have fabricated the glass fibre-based lateral flow DNA biosensor that uses capture reagents coupled to carrier beads and detector reagent bioconjugated to AuNps, for the detection of foodborne pathogen, *Vibrio cholerae*. The DNA biosensor contains a test line that captures the target PCR amplicons, an internal amplification control (IC) line which captures IC amplicons and a control line that acts as membrane control to validate the functionality of this device. The test line captured biotin labelled DNA, while the IC line captures digoxigenin labelled DNA. The detector reagent recognizes the fluorescein haptens of the amplified DNA and produces visual red lines. This DNA biosensor has LOD of 5 ng of target DNA. A clinical evaluation was carried out with 174 strains of *V. cholerae* and non *V. cholerae* bacteria and the DNA biosensor recorded 100% for both sensitivity and specificity. It is thus a viable alternative to agarose gel analysis and is easy-to-use, disposable [120]. Hao et al. have developed a quartz crystal microbalance (QCM) biosensor to detect *B. anthracis* based on the recognition of its specific DNA sequences, i.e., the 168 bp fragment of the Ba813 gene in chromosomes and the 340 bp fragment of the pag gene in plasmid pXO1 via thssDNA immobilization onto Au QCM electrode to hybridize with the target ssDNA sequence obtained by asymmetric PCR (Fig. 8). To amplify the signal, a thiol-DNA fragment complementary to the other end of the target DNA was functionalized with AuNPs. The LOD reached 3.5×10^2 CFU/ml of *B. anthracis* vegetative cells just after asymmetric PCR amplification, but without culture enrichment [121]. Shen et al have increased the binding of bacteria to their carbohydrate receptor through bacterial surface binding lectins that significantly enhanced specificity and sensitivity of QCM biosensors [122]. Fletcher et al. have demonstrated a modular biosensor that can rapidly identify sequences associated with the

ACCEPTED MANUSCRIPT

Dengue virus genome. Disruption of the aptamer releases the restriction endonuclease EcoRI from aptamer-mediated inhibition. Active EcoRI can rapidly cleave multiple signalling molecules to generate a detectable signal [123]. Zhang et al. have presented an innovative silicon nanowire (SiNW) based sensor for highly sensitive and rapid detection of RT-PCR product of Dengue serotype 2 (DEN-2). A specific PNA is covalently attached onto the SiNW surface. A complementary fragment of DEN-2 (69 bp) is obtained through one-step RT-PCR amplification, and is applied to the PNA-functionalized SiNW. The hybridization event can be verified by measuring the resistance change of the SiNW before and after binding of the RT-PCR product of DEN-2 to the PNA sequence. It has been found that the SiNW sensor can detect below 10 fM concentrations of the amplicons within 30 min [124]. Lin et al. have demonstrated functionalized poly-crystalline silicon nanowire field-effect transistor (FET) based sensor for detection of high pathogenic strain virus (H5 and H7) DNA of AIV. Specific electric changes are observed for AI virus DNA sensing when nanowire surface of poly-SiNW FET is modified with complementary captured DNA probe and target DNA (H5) at fM to pM range could be distinguished [125]. Wu et al. have developed a circulating-flow system for real-time detection of *E. coli* O157:H7 gene eaeA. Synthetic oligonucleotide targets (30 and 104-mer) and PCR-amplified DNA fragments from the *E. coli* O157:H7 eaeA gene (104 bp) has been used for immobilization and hybridization. The addition of 12-dT to the probes as a spacer, significantly enhanced ($P < 0.05$) 1.4- and 2-fold hybridization efficiency when the probes hybridized with 30- and 104-mer targets, respectively [126]. Liu et al. have demonstrated the feasibility of detecting 250 zM *E. coli* O157:H7 *eae*A target DNA by using a magnetic bead-based DNA detection assay with designed labeling strategy within 40–60 min [127]. Schrumpf et al. have developed a new method for the detection of nucleic acid hybridization, based on a simple latex agglutination test

ACCEPTED MANUSCRIPT

that can be evaluated by the unaided eye. In artificially contaminated chicken samples, 3 colony-forming units (cfu)/25 g can be detected in one of three replicates, and 30 cfu/25 g were detected in both of two replicates when samples for PCR are taken directly from primary enrichment [128].

A microfluidic biosensor [129] comprises of a network of microchannels fabricated in polydimethylsiloxane (PDMS) substrate and super paramagnetic beads are incorporated into the system as a mobile solid support and can be operated under continuous solution flow of up to 80 μL min^{-1}. This assay reduced time upto only 15 min including sample incubation time [130-132].

Roh et al have developed RNA biosensor for HCV NS3 protein detection. They have previously shown that quantum dots-conjugated RNA oligonucleotide can recognize the HCV NS3 protein specifically and sensitively. At a concentration of 0.01 μg·mL−1, 7,8,4′-trihydroxyisoflavone and 6,7,4′-trihydroxyisoflavone showed more than a 30% inhibition activity of a nanoparticle-based RNA oligonucleotide biochip system [133].

A subtype of influenza virus H1N1, has been reported by Kao et al. They have fabricated a silicon based microfluidic device for H1N1 2009 strain vs. the seasonal influenza A strain (Fig. 9). The proposed system includes two functional modules: a multiplexed PCR module for amplification of nucleic acid target and a multiplexed SiNW module for sequence determination. The PCR module consists of a microfluidic PCR chamber and an electrical controller to perform a multiplexed protocol that can simultaneously detect enriched specific segment of both H1N1 and FluA strains, with 10^4–10^5 amplification efficiency. The system has a sensitivity of 20–30 fg/μl for H1N1 and seasonal FluA nucleic acids in a 10 μl sample [134] (Table 4).

6. Challenges and future prospects

Accepted Manuscript

ACCEPTED MANUSCRIPT

The management of pathogen detection using a simple, rapid and cost-effective method presents a major challenge to the biological safety of the world. The field of pathogen detection is nascent and therefore, faces a dynamic set of challenges as the field evolves. One of the major challenges in pathogen detection using electrochemical nucleic acid sensor design is to immobilize biomolecules onto an electrode substrate for effective signal transduction. Detecting pathogens using biosensors is a relatively new concept and many of the techniques discussed, are still in their infancy. Existing pathogen detection methods are time consuming and expensive, and consequently, demand for accurate pathogenic biosensors by rapid detection systems is increasing. The electrochemical techniques will probably become more popular as microelectronics and microfluidics also progress. Some techniques are restricted due to unsuitability in-field and requirement of highly trained personnel. Many of these methods currently have limitations involving sensor surface formation, reproducibility, renewability and necessary sample preparation. The immense efforts are needed to develop this comprehensive library of core techniques into practical diagnostic applications. The general basis of methods to detect binding pathogenic analytes to specific bioreceptors are available but require refinement and in some cases further miniaturization. With the increasing use of novel nanomaterials, like nano-structured metal oxides, CNTs, grapheme, quantum dots, nano-structured conducting polymers etc., the problem of immobilization of biomolecules to obtain proper signal transduction has been minimized to a greater extent.

The commercial biosensors for pathogen detection are tips of the iceberg compared to the vast literature on academic research. The intrinsic disadvantages (slow response, low sensitivity, and poor selectivity) using bacteria and virus as the biosensing element limit the widespread interest of biosensors for pathogen detection on the market. Fortunately, with the amalgamation

Accepted Manuscript

ACCEPTED MANUSCRIPT

of biotechnology, nano-technology, physics, chemistry, electronics, bioengineering and novel immobilization strategy in the past years, biosensors for pathogen detection are becoming more powerful in the field of analytical chemistry.

The new bioreceptor designs are being evolved to increase both the sensitivity, selectivity and signal amplification of pathogenic sensors. The sensors will become smaller and portable and the resulting costs will reduce, as fewer or new materials are utilized. This will hopefully lead to the production of sensitive, cheap, reliable and rapid detection systems for use in the clinical environment for diagnosis of pathogenic infections. A fruitful fusion between biological sciences and other disciplines will help to realize the full potential of this technology in the future.

7. Conclusions

In summary, recent developments in nucleic acid biosensors for pathogen detection have been reviewed. The conventional pathogen detection methods are sensitive but still lag behind the analytical methods due to long response time and decreasing in the response time is a needle in a haystack problem. Electrochemical techniques offer a sensitive approach for direct or multi step measurement for pathogen detection. These methods provide the possibility of simultaneous measurement of various analyte in short time. Besides this, recent developments in nanotechnology and materials science can be advantageously used to obtain engineered and customerized nanomaterials that could provide novel platforms for immobilization of biorecognition component that may lead to the development of useful and reliable biosensor devices. And the use of microarray for simultaneous measurement with integrated microfluidic system, molecularly imprinted may provide solution for reliable pathogen detection and in

Accepted Manuscript

ACCEPTED MANUSCRIPT

fabrication of smart low cost point-of-care devices. Efforts should be directed towards the synthesis of novel nanomaterials for the fabrication of electrochemical and other biosensors on a large scale so as to benefit the mankind. With exposure of the commercial market the applications of the biosensor technology can be greatly enhanced and with time, miniaturized biosensor for pathogen detection may become available that could be used near a patient's bedside, a doctor's clinic or even home use.

Acknowledgements

Renu Singh is thankful to Council of Scientific and Industrial Research (CSIR), India for the award of Senior Research Fellowship. We acknowledge the financial support received from Department of Science & Technology (DST) [DST/TSG/ME/2008/18 and GAP-070932], in-house project (OLP-070632D) and Department of Biotechnology, Govt. of India (DBT/GAP070832).

Accepted Manuscript

ACCEPTED MANUSCRIPT

References

1. A.K. Wanekaya, W. Chen, A. Mulchandani, Recent biosensing developments in environmental security, J. Environ. Monit. 10 (2008) 703–712.
2. M.I. Prodromidis, M.I. Karayannis, Enzyme Based Amperometric Biosensors for Food Analysis, Electroanalysis 14 (2002) 241-261.
3. P.J. Conroy, S. Hearty, P. Leonard, R.J. O'Kennedy, Antibody production, design and use for biosensor-based applications, Semin Cell Dev Biol. 1 (2009) 10-26.
4. R. Singh, C. Dhand, G. Sumana, R. Verma, S. Sood, R.K. Gupta, B.D. Malhotra, Polyaniline/carbon nanotubes platform for sexually transmitted disease detection, J Mol Recognit. 23 (2010) 472-479.
5. B.D. Malhotra, A. Chaubey, S.P. Singh, Prospects of conducting polymers in biosensors. Anal Chim Acta. 18 (2006) 59-74.
6. J.J. Gooding, Biosensor technology for detecting biological warfare agents: Recent progress and future trends, Analytica Chimica Acta 559 (2006) 137–151.
7. R. Syam, K.J. Davis, M.D. Pratheesh, B. S. Joseph, Biosensors: A novel approach for pathogen detection, ISSN 7 (2012) 0973-6980.
8. M.S. Belluzo, M.E. Ribone, C.M. Lagier, Assembling Amperometric Biosensors for Clinical Diagnostics, Sensors 8 (2008) 1366-1399.
9. S. Rodriguez-Mozaza, M.J. L´opez de Aldaa, M.P. Marcob, D. Barcel´oa, Biosensors for environmental monitoring A global perspective Talanta 65 (2005) 291-297.
10. A. Mulchandani, A.S. Bassi, Principles and applications of biosensors for bioprocess monitoring and control. Crit Rev Biotechnol. 15 (1995) 105-24.
11. P. Leonard, St. Hearty, J. Brennan, L. Dunne, J. Quinn, T. Chakraborty, R. O'Kennedy, Advances in biosensors for detection of pathogens in food and water, Enzyme and Microbial Technology 32 (2003) 3–13.
12. Li. Suiqiong, A. Simonian, B.A. Chin, Sensors for Agriculture and the Food Industry, The Electrochemical Society Interface Winter (2010).

ACCEPTED MANUSCRIPT

13. G. Leegsma-Vogt, M.M. Rhemrev-Boom, R.G. Tiessen, K. Venema, J. Korf, M. Jeffrey, W.G. Halliday, K.C. Taylor, The potential of biosensor technology in clinical monitoring and experimental research, Biomed Mater Eng. 14 (2004) 455-64.
14. S. Cagnin, M. Caraballo, C. Guiducci, P. Martini, M. Ross, M. SantaAna, D. Danley, T. West, G. Lanfranchi, Overview of Electrochemical DNA Biosensors: New Approaches to Detect the Expression of Life, Sensors 9 (2009) 3122-3148.
15. R. Singh, R. Verma, G. Sumana, A.K. Srivastava, S. Sood, R.K. Gupta, B.D. Malhotra, Nanobiocomposite Platform based on Polyaniline-Iron oxide–Carbon nanotubes for Bacterial Detection, Bioelectrochemistry 86 (2012a) 30-37.
16. R. Singh, Z. Matharu, A.K. Srivastava, S. Sood, R.K. Gupta, B.D. Malhotra, Nanostructured platform for the detection of Neisseria gonorrhoeae using electrochemical impedance spectroscopy and differential pulse voltammetry, Microchimica acta 177 (2012b) 201-210.
17. P.N. Chandra, H.B. Noha, M.S. Wonb, Y.B. Shim, Bioelectrochemistry Fundamentals, Experimental Techniques and Applications, Biosens. Bioelectron. 26 (2011) 4442-4449.
18. S.B. Pieper, S.P. Mestas, K.L. Lear, Z. Zhong, K.F. Reardon, Phosphorescence characteristics of ruthenium complex as an optical transducer for biosensors, Appl Phys Lett. 92 (2008) 081915.
19. Guangjiu, Li., Liu, N., Liu, S., Zhang, S., Electrochemical biosensor based on the interaction between copper (II) complex with 4, 5-diazafluorene-9-one and bromine ligands and deoxyribonucleic acid, Electrochim Acta 53 (2008) 2870-2876.
20. D. Grieshaber, R. MacKenzie, J. V¨or¨os, E. Reimhu, Electrochemical Biosensors - Sensor Principles and Architectures, Sensors 8 (2008) 1400-1458.
21. H. Fan, P. Ju, S. Ai, Controllable synthesis of CdSe nanostructures with tunable morphology and their application in DNA biosensor of Avian Influenza, Sens Actuators B 149 (2010) 98–104.
22. G. García-Martinez, E.A. Bustabad, H. Perrot, C. Gabrielli, B. Bucur, M. Lazerges, D. Rose, Development of a mass sensitive quartz crystal microbalance (QCM)-based DNA biosensor using a 50 MHz electronic oscillator circuit. Sensors 11 (2011) 7656-64.

ACCEPTED MANUSCRIPT

23. P. Tallury, A. Malhotra, L. M Byrne, S. Santra, Nanobioimaging and sensing of infectious diseases, Advanced Drug Delivery Reviews 62 (2010) 424–437.

24. L. Su, W. Jia, C. Hou, Y. Lei, Microbial biosensors: A review, Biosens Bioelectron. 26 (2011) 1788‑1799.

25. A.M. AbdEl-Malek, S.F.H. Ali, R.H. Moemen, A. Mohamed, K.I. Elsayh, Occurrence of Listeria species in meat, chicken products and human stools in Assiut city, Egypt with PCR use for rapid identification of Listerias monocytogenes, Vet World. 3 (2010) 353-359.

26. E. De Boer, R.R. Beumer, Methodology for detection and typing of foodborne microorganisms, Int. J. Food Microbiol. 50 (1999) 119-130.

27. Anon (1999) Directorate-General.

28. K. Silbernagel, R. Jechorek, W.M. Barbour, P. Mrozinski, W. Alejo, V. Aleo, V. Andeloro, F. Beacorn, J. Benzinger, S. Bogar, C. Brayman, J. Broom, M. Carson, C. Carver, C. Cheng, B. Centrella, J. Clayborn, C. Collins, C. Deibel, M. Divine, S.J. Eliasberg, D. Farmer, S. Frye, T. Gatesy, E. Goodstein, C. Halker, G.V. Hall, P. Hanson, G. Hartman, K. Heddaeus, J. Hembree, J. Hutchins, P. Istafanos, J. Jenkins, K. Kerdahi, S. Kremer, A. Lal, S. Leighton, D. Lester, J.H. Lewis, J. Lin, J. Martin, M. Maselli, P. McCarthy, B. McGovern, M. Mills, F. Mohnke, B. Moon, D. Moss, M. Plaza, S. Robeson, H. Romero, D. Rubalcaba, M. Schultz, J. Seehusen, C. Shaw, K. Siem, E. Sloan, J. Stanerson, N. Stepanova, K. Van, K. Enkenvoort, M. Vialpando, W. Warren, K. Watts, K. Wilson, T. Woodruff, Evaluation of the BAX System for detection of *Listeria monocytogenes*, J. AOAC Int. 87 (2004) 395-410.

29. M.W. Sanderson, G.M. Gay, D.D. Hancock, C.C. Gay, L.K. Fox, T.E. Bess, Sensitivity of bacteriologic culture for detection of *Escherichia coli* O157:H7 in bovine feces J. Clin. Microbiol. 33 (1995) 2616-2619.

30. H. Takahashi, B. Kimura, Y. Tanaka, J. Shinozaki, T. Suda, T. Fujii, Real-time PCR and enrichment culture for sensitive detection and enumeration of *Escherichia coli*, J. Microbiol. Methods 79 (2009) 124e127.

ACCEPTED MANUSCRIPT

31. S.D. Saroj, R. Shashidhar, M. Karani, J.R. Bandekar, Distribution of *Salmonella* pathogenicity island (SPI)-8 and SPI-10 among different serotypes of *Salmonella,* J MED Microbiol. 57 (2008) 424-427.
32. B.P. Upadhyay, F. Utrarachkij, J. Thongshoob, Y. Mahakunkijcharoen, N. Wongchinda, USDA, Hudson Foods Recalls Beef Burgers Nationwide for *E.coli* O157:H7.
33. M. Magliulo, P. Simoni, M. Guardigli, E. Michelini, M. Luciani, R. Lelli, A rapid multiplexed chemiluminescent immunoassay for the detection of *Escherichia coli* O157: H7, *Yersinia enterocolitica*, *Salmonella typhimurium*, and *Listeria monocytogenes* pathogen bacteria, J Agric Food Chem. 55 (2007) 4933-9.
34. R.P. Jechorek, R.L. Johnson, Evaluation of the VIDAS staph enterotoxin II (SET 2) immunoassay method for the detection of staphylococcal enterotoxins in selected foods: collaborative study, Journal of AOAC International 91 (2008) 164-73.
35. I. Hochel, J. Skvor, Characterization of rabbit antibodies for immunochemical detection of Yersinia enterocolitica, Folia Microbiol (Praha). 52 (2007) 511-8.
36. G. Panicker, M.L. Myers, A.K. Bej. Rapid detection of Vibrio vulnificus in shellfish and Gulf of Mexico water by real-time PCR, Appl Environ Microbiol. 70 (2004) 498-507.
37. S.W. Polson, J.L. Higgins, C.M. Woodley, PCR-based assay for the detection of four coral pathogens, Proc. of the 11th International Coral Reef Symposium, Ft. Lauderdale, Florida, 8 (2008).
38. M. Palka-Santini, B.E. Cleven, L. Eichinger, M. Krönke, O. Krut, Large scale multiplex PCR improves pathogen detection by DNA microarrays, BMC Microbiology 9 (2009).
39. R. Wang, C. Xue, M. Gao, H. Qi, C. Zhang, Biosensors for environmental monitoring A global perspective, Microchim Acta 172 (2011) 291–297.
40. A.M. Caliendo, Multiplex PCR and Emerging Technologies for the Detection of Respiratory Pathogens, Clin Infect Dis. 52 (2011) S326-S330.
41. L.D. Tran, B.H. Nguyen, N.V. Hieu, H.V. Tran, H.L. Nguyen, P.X. Nguyen, Electrochemical detection of short HIV sequences on chitosan/Fe_3O_4 nanoparticle based screen printed electrodes, Mater Sci Eng C 31 (2011) 477-485.
42. J. Wang, PNA Biosensors for Nucleic Acid Detection, Current Issues Molec. Biol. 2 (1999) 117-122.

ACCEPTED MANUSCRIPT

43. J. Wang, DNA biosensors based on Peptide Nucleic Acid (PNA) recognition layers. A review, Biosens Bioelectron. 13 (1998) 757–762.

44. K. Kerman, M. Kobayashi, and Eiichi Tamiya, Recent trends in electrochemical DNA biosensor technology Measurement Science and Technology 15 (2004) R1–R1.

45. R. E. Wang, Y. Zhang, J. Cai, W. Cai, T. Gao, Aptamer-Based Fluorescent Biosensors, Curr Med Chem. 27 (2011) 4175–4184.

46. M.I. Pividori, S. Alegret, Electrochemical biosensors for food safety, Contributions to Science, 2 (2010) 1575-6343.

47. K. Arora, S. Chand, B.D. Malhotra, Recent developments in bio-molecular electronics technique for food pathogens, Analytica Chimica Acta 568 (2006) 259–274.

48. S. Song, L. Wang, J. Li, J. Zhao, C. Fan, Aptamer-based biosensors,Trends in Analytical Chemistry, 27 (2008).

49. K.M. Song, S. Lee, C. Ban, Aptamers and Their Biological Applications, Sensors 12 (2012) 612-631.

50. A. Sassolas, B.D. Leca-Bouvier, L.J. Blum, DNA Biosensors and Microarrays, Chem. Rev. 108 (2008) 109-139.

51. M. Nayak, A. Kotian, S. Marathe, D. Chakravortty, Detection of microorganisms using biosensors−A smarter way towards detection techniques, Biosens Bioelectron. 25 (2009) 661‑667.

52. T.G. Drummond, M.G. hill, J.K. barton, Electrochemical DNA sensors, Nature biotechnology 21 (2003) 1192 -1199.

Accepted Manuscript

ACCEPTED MANUSCRIPT

53. E.A. Mothershed, A.M. Whitney, Nucleic acid-based methods for the detection of bacterial pathogens: Present and future considerations for the clinical laboratory, Clinica Chimica Acta 363 (2006) 206 – 220.

54. S. Girousi, S. Karastogianni, C. Serpi, Innovative Configurations of Electrochemical DNA Biosensors (A Review), Sensing in Electroanalysis 6 (2011) 65-87.

55. M. Mascini, F. Lucarelli, I. Paichetti, G. Marrazza, Y. Zhou, S. Xu, Electrochemical application of DNA biosensors, International Conference on Sensor Technology 4414 (2001), 0277-786.

56. J.J. Gooding, Electrochemical DNA Hybridization Biosensors, Electroanalysis 14 (2002) 1149–1156.

57. F. Lucarelli, S. Tombelli, M. Minunni, G. Marrazza, M. Mascini, Electrochemical and piezoelectric DNA biosensors for hybridisation detection, analytica chimica acta 609 (2008) 139–159.

58. P. He, Y. Xu, Y. Fang, A Review: Electrochemical DNA Biosensors for Sequence Recognition, Analytical Letters 38 (2005) 2597–2623.

59. Y. Wang, Z. Ye, Y. Ying, New Trends in Impedimetric Biosensors for the Detection of Foodborne Pathogenic Bacteria, Sensors 12 (2012) 3449-3471.

60. L. Yang, R. Bashir, Electrical/electrochemical impedance for rapid detection of foodborne pathogenic bacteria, Biotechnology Advances 26 (2008) 135–150.

61. D.H. Yu, B. Blankert, J.C. Vire, J.M. Kauffmann, Biosensors in drug discovery and drug analysis. Anal. Lett. 38 (2005) 1687-1701.

62. J.C. Liao, M. Mastali, Y. Li, V. Gau, M.A. Suchard, J. Babbitt, J. Gornbein, E.M. Landaw, E.R. McCabe, B.M. Churchill, D.A Haake, Development of an Advanced

Accepted Manuscript

ACCEPTED MANUSCRIPT

Electrochemical DNA Biosensor for Bacterial Pathogen Detection, J Mol Diagn. 9 (2007) 158-68.

63. K. Arora, N. Prabhakar, S. Chand, B.D. Malhotra, *Escherichia coli* Genosensor Based on Polyaniline, Anal. Chem. 79 (2007) 6152-6158.
64. H. Shiraishi, T. Itoh, H. Hayashi, K. Takagi, M. Sakane, T. Mori, J. Wang, Electrochemical detection of *E. coli* 16S rDNA sequence using air-plasma-activated fullerene-impregnated screen printed electrodes, Bioelectrochemistry 70 (2007) 481-487.
65. Ó.A. Loaiza, S. Campuzano, M. Pedrero, J.M. Pingarrón, DNA sensor based on an Escherichia coli lac Z gene probe immobilization at self-assembled monolayers-modified gold electrodes, Talanta 73 (2007) 838-844.
66. P.R. Solanki, A. Kaushik, P.M. Chavhan, S.N. Maheshwari, B.D. Malhotra, Nanostructured zirconium oxide based genosensor for *Escherichia coli* detection, Electrochem Commun. 11 (2009) 2272-2277.
67. D. Wu, B.C. Yin, B.C. Ye, A label-free electrochemical DNA sensor based on exonuclease III-aided target recycling strategy for sequence-specific detection of femtomolar DNA, Biosens Bioelectron. 28 (2011) 232-238.
68. C.M. Pandey, R. Singh, G. Sumana, M.K. Pandey, B.D. Malhotra, Electrochemical Genosensor Based on Modified Octadecanethiol Self-Assembled Monolayer for *Escherichia coli* Detection, Sens Actuators B 151 (2011a) 333-340.
69. E. Majid, K.B. Male, J.H.T. Luong, Boron Doped Diamond Biosensor for Detection of *Escherichia coli*, J. Agric. Food Chem. 56 (2008) 7691-7695.
70. L. Wang, Q. Liu, Z. Hu, Y. Zhang, C. Wu, M. Yang, P. Wang, A novel electrochemical biosensor based on dynamic polymerase-extending hybridization for *E. coli* O157:H7 DNA detection, Talanta 78 (2009) 647-652.
71. C.M. Pandey, G. Sumana, B.D. Malhotra, Microstructured Cystine Dendrites based Impedimetric Sensor for Nucleic Acid Detection, Biomacromolecules 8 (2011b) 2925-32.
72. D. Zhang, E.C. Alocilja, Characterization of Nanoporous Silicon-Based DNA Biosensor for the Detection of Salmonella Enteritidis, IEEE Sensors Journal 8 (2008).

ACCEPTED MANUSCRIPT

73. V. Nandakumar, J.T. La Belle, J. Reed, M. Shah, D. Cochran, L. Joshi, T.L. Alford, A methodology for rapid detection of *Salmonella typhimurium* using label-free electrochemical impedance spectroscopy, Biosens Bioelectron. 24 (2008) 1039‑1042.

74. V. Velusamy, K. Arshak, O. Korostynska, K. Oliwa, C. Adley, An overview of foodborne pathogen detection: In the perspective of biosensors, Biotechnology Advances 28 (2010) 232–254.

75. V. Velusamy, K. Arshak, O. Korostynska, K. Oliw, C. Adley, Design of a real time biorecognition system to detect foodborne pathogens-DNA Biosensor SAS–IEEE Sensors Applications Symposium New Orleans, LA, USA , (2009) 17-19.

76. V. Velusamy, K. Arshak, C. Yang, L. Yu, O. Korostynska, K. Oliwa-Stasiak, C. Adley, IEEE Sensors Applications Symposium, SAS 5439420 (2010) 135-138.

77. M. Tichoniuk, D. Gwiazdowska, M. Ligaj, M. Filipiak, Electrochemical detection of foodborne pathogen Aeromonas hydrophila by DNA hybridization biosensor, Biosens Bioelectron. 26 (2010) 1618-1623.

78. Q. Sheng, J. Wang, J. Zheng, Z. Xu, H. Zhang, Ultrasensitive electrical biosensing of syphilis DNA using target-guided formation of polyaniline based on enzyme-catalyzed polymerization, Biosens Bioelectron. 25 (2010) 2071-2077.

79. Z. Wang, J. Zhang, P. Chen, X. Zhou, Y. Yang, S. Wu, L. Niu, Y. Han, L. Wang, P. Chen, F. Boey, Q. Zhang, B. Liedberg, H. Zhang, Label-free, electrochemical detection of methicillin-resistant staphylococcus aureus DNA with reduced graphene oxide-modified electrodes, Biosens Bioelectron. 26 (2011) 3881–3886.

80. R. Miranda-Castro, N. de-los-Santos-Álvarez, M.J. Lobo-Casta˜ nón, A.J. Miranda-Ordieres, P. Tu˜ nón-Blanco, PCR-coupled electrochemical sensing of Legionella pneumophila, Biosens Bioelectron. 24 (2009) 2390-2396.

81. T. Damrow, B. Hagemeyer, H. Ismail, R. Oldham, Electronic Anthrax DNA Biosensor Review, (2009).

Accepted Manuscript

ACCEPTED MANUSCRIPT

82. N. Prabhakar, H. Singh, B.D. Malhotra, Nucleic acid immobilized polypyrrole-polyvinylsulphonate film for Mycobacterium tuberculosis detection, Electrochem Commun. 10 (2008a) 821-826.

83. N. Prabhakar, K. Arora, H. Singh, B.D. Malhotra, Polyaniline Based Nucleic Acid Sensor, J. Phys. Chem. B 112 (2008b) 4808-4816.

84. M. Das, C. Dhand, G. Sumana, A.K. Srivastava, R. Nagarajan, B.D. Malhotra, Electrophoretically fabricated core-shell CNT-DNA biowires for biosensing, J. Mater. Chem. 22 (2012) 2727-2732.

85. M. Das, C. Dhand, G. Sumana, A.K. Srivastava, N. Vijayan, R. Nagarajan, B.D. Malhotra, Zirconia grafted carbon nanotubes based biosensor for *M. Tuberculosis* detection, Appl Phys Lett. 99 (2011) 143702-3.

86. R. Singh, R. Prasad, G. Sumana, K. Arora, S. Sood, R.K. Gupta, B.D. Malhotra, STD Sensor Based on Nucleic Acid Functionalized Nanostructured Polyaniline, Biosens Bioelectron. 24 (2009) 2232-2238.

87. R. Singh, C. Dhand, G. Sumana, R. Verma, S. Sood, R.K. Gupta, B.D. Malhotra, Polyaniline/carbon nanotubes platform for sexually transmitted disease detection, J. Mol. Recognit. 23 (2010) 472–479.

88. R. Singh, R. Verma, A. Kaushik, G. Sumana, S. Sood, R.K. Gupta, B.D. Malhotra, Chitosan-Iron Oxide Nano-composite Platform for Mismatch-Discriminating DNA Hybridization for detection of *Neisseria gonorrhoeae* causing Sexually Transmitted Disease, Biosens Bioelectron. 26 (2011) 2967-2974.

89. M.K. Patel, P.K. Solanki, A. Kumar, S. Khare, S. Gupta, B.D. Malhotra, Electrochemical DNA sensor for *Neisseria meningitidis* detection, Biosens Bioelectron. 25 (2010) 2586-2591.

90. M.K. Patel, P.K. Solanki, S. Seth, S. Gupta, S. Khare, A. Kumar, B.D. Malhotra, CtrA gene based electrochemical DNA sensor for detection of meningitis, Electrochem Commun. 11 (2009) 969-973.

91. D.O. Ariksoysal, H. Karadeniz, A. Erdem, A. Sengonul, A.A. Sayiner, M. Ozsoz, Label-Free Electrochemical Hybridization Genosensor for the Detection of Hepatitis B

Accepted Manuscript

ACCEPTED MANUSCRIPT

Virus Genotype on the Development of Lamivudine Resistance, Anal. Chem. 77 (2005) 4908-4917.

92. P. Kara, S. Cavdar, B. Meric, S. Erensoy, M. Ozsoz, Electrochemical probe DNA design in PCR amplicon sequence for the optimum detection of microbiological diseases, Bioelectrochem. 71 (2007) 204-210.
93. X.M. Li, H.Q. Ju, Li.P. Du, S.S. Zhang, A nucleic acid biosensor for the detection of a short sequence related to the hepatitis B virus using bis benzimidazole cadmium II dinitrate as an electrochemical indicator, J. Inorg. Chem. 101 (2007a) 1165-1171.
94. X.M. Li, H.Q. Ju, C.F. Ding, S.S. Zhang, Nucleic acid biosensor for detection of hepatitis B virus using 2,9-dimethyl-1,10-phenanthroline copper complex as electrochemical indicator, Anal. Chim. Acta 582 (2007b) 158-163.
95. C. Ding, F. Zhao, M. Zhang, S. Zhang, Hybridization biosensor using 2,9-dimethyl-1,10-phenantroline cobalt as electrochemical indicator for detection of hepatitis B virus DNA, Bioelectrochem. 72 (2008) 28-33.
96. S.Y. Niu, M.L. Wu, L.Z. Hu, Z.H. Mei, S.H. Liu, Nucleic acid biosensor for DNA hybridization detection using rutin–Cu as an electrochemical indicator, Electrochim. Acta 54 (2009) 1564-1569.
97. S. Zhang, Q. Tan, F. Li, X. Zhang, Hybridization biosensor using diaquabis[N- 2-pyridinylmethyl benzamide-k2 N,O]-cadmium II dinitrate as a new electroactive indicator for detection of human hepatitis B virus DNA, Sens Actuators B 124 (2007) 290-296.
98. C.S. Riccardi, J. Kowalik, M. Josowicz, H.Yamanaka, B. Mizaikoff, C. Kranz, Label-free DNA detection of hepatitis C virus HCV-1 , ECS 210th Meeting 2091 (2006).
99. M.H. Pournaghi-Azar, F. Ahour, M.S. Hejazi, Differential Pulse Voltammetric Detection of Hepatitis C Virus 1a Oligonucleotide Chain by a Label-Free Electrochemical DNA Hybridization Biosensor Using Consensus Sequence of Hepatitis C Virus 1a Probe on the Pencil Graphite Electrode, Electroanalysis 21 (2009) 1822-1828.
100. S. Liu, Y. Hu, J. Jin, H. Zhang, C. Cai, Electrochemical detection of hepatitis C virus based on site-specific DNA cleavage of BamHI endonuclease, Chem. Commun. (2009) 1635–1637.

Accepted Manuscript

ACCEPTED MANUSCRIPT

101. M.S. Hejazi, M.H. Pournaghi-Azar, F. Ahour, Electrochemical detection of short sequences of hepatitis C 3a virus using a peptide nucleic acid-assembled gold electrode, Anal Biochem. 399 (2010) 118-124.

102. R. Wang, C. Xue, M. Gao, H. Qi, C. Zhang, Ultratrace voltammetric method for the detection of DNA sequence related to human immunodeficiency virus type 1, Microchim Acta 172 (2011) 291–297.

103. W.M. Hassen, C. Chaix, A. Abdelghani, F. Bessueille, D. Leonard, N. Jaffrezic-Renault, An impedimetric DNA sensor based on functionalized magnetic nanoparticles for HIV and HBV detection, Sens Actuators B 134 (2008) 755-760.

104. L.D. Tran, B.H. Nguyen, N.V. Hieu, H.V. Tran, H.L. Nguyen, P.X Nguyen, Electrochemical detection of short HIV sequences on chitosan/Fe_3O_4 nanoparticle based screen printed electrodes, Materials Science and Engineering C 31 (2011) 477–485.

105. P.D. Tam, N.V. Hieu, N.D. Chien, A.T. Le, A.T. Tuan, DNA sensor development based on multi-wall carbon nanotubes for label-free influenza virus type A detection, J of Immunol Methods 350 (2009) 118-124.

106. X. Chen, H. Xie, Z.Y. Seow, Z. Gao, An ultrasensitive DNA biosensor based on enzyme-catalyzed deposition of cupric hexacyanoferrate nanoparticles, Biosens. Bioelectron. 25 (2010) 1420-1426.

107. H. Fan, P. Ju, S. Ai, Controllable synthesis of CdSe nanostructures with tunable morphology and their application in DNA biosensor of Avian Influenza Virus, Sensors and Actuators B 149 (2010) 98–104.

108. X. Zhu, S. Ai, Q. Chen, H. Yin, J. Xu, Label-free electrochemical detection of Avian Influenza Virus genotype utilizing multi-walled carbon nanotubes–cobalt phthalocyanine–PAMAM nanocomposite modified glassy carbon electrode, Electrochem Commun.11 (2009) 1543-1546.

109. N. Zari, A. Amine, M.M. Ennaji, Label-Free DNA Biosensor for Electrochemical Detection of Short DNA Sequences Related to Human Papilloma Virus, Anal. Lett. 42 (2009) 519-535.

110. L. Civit, A. Fragoso, C.K. O'Sullivan, Electrochemical biosensor for the multiplexed detection of human papillomavirus genes, Biosens. Bioelectron. 26 (2010) 1684-1687.

Accepted Manuscript

ACCEPTED MANUSCRIPT

111. X. Zhang, H. Su, S. Bi, S. Li, S. Zhang, DNA-based amplified electrical bio-barcode assay for one-pot detection of two target DNAs, Biosens Bioelectron. 24 (2009) 2730-2734.

112. H.I. Peng, B.L. Miller, Recent advancements in optical DNA biosensors: Exploiting the plasmonic effects of metal nanoparticles Analyst 136 (2011) 436–447.

113. N. Prabhakar, K. Arora, S.K. Arya, P.R. Solanki, M. Iwamoto, H. Singh, B.D. Malhotra, Nucleic acid sensor for *M. tuberculosis* detection based on surface Plasmon resonance, Analyst 133 (2008c) 1587-1592.

114. K.H. Cheong, D.K. Yi, J.G. Lee, J.M. Park, M.J. Kim, J.B. Edel, C. Koa, Gold nanoparticles for one step DNA extraction and real-time PCR of pathogens in a single chamber, Lab Chip 8 (2008) 810-813.

115. H. Bai, R. Wang, B. Hargis, H. Lu, Y. Li, A SPR Aptasensor for Detection of Avian Influenza Virus H5N1, Sensors 12 (2012) 12506-12518.

116. A.J. Baeumner, R.N. Cohen, V.M., Junhong Min, RNA biosensor for the rapid detection of viable *Escherichia coli* in drinking water, Biosens Bioelectron 18 (2003) 405-413.

117. A.J. Baeumner, C.J., Ching Y.W., Andrew Price, A generic sandwich-type biosensor with nanomolar detection limits, Anal Bioanal Chem 378 (2004) 1587–1593.

118. J. Wang, Y. Luo, B. Zhang, M. Chen, J. Huang, K. Zhang, W. Gao, W. Fu, T. Jiang, P. Liao, Rapid label-free identification of mixed bacterial infections by surface plasmon resonance, Journal of Translational Medicine (85) 2011.

119. P. Zuo, X. Li, D. Dominguez, B.C. Ye, A PDMS/paper/glass hybrid microfluidic biochip integrated with aptamer-functionalized graphene oxide nano-biosensors for one-step multiplexed pathogen detection, Lab Chip 13 (2013) 13, 3921-3828.

120. A.L. Chua, C.Y. Yean, M. Ravichandran, B.H. Lim, P. Lalitha, A rapid DNA biosensor for the molecular diagnosis of infectious disease, Biosensors and Bioelectronics, Biosens Bioelectron. 26 (2011) 3825-3831.

121. R.Z. Hao, H.B. Song, G.M. Zuo, R.F. Yang, H.P. Wei, D.B. Wang, Z.Q. Cui, Z.P. Zhang, Z.X. Cheng, X.A. Zhang, DNA probe functionalized QCM biosensor based on

Accepted Manuscript

ACCEPTED MANUSCRIPT

gold nanoparticle amplification for Bacillus anthracis detection, Biosens Bioelectron. 26 (2011) 3398-3404.

122. Z. Shen, M. Huang, C. Xiao, Y. Zhang, X. Zeng, P.G. Wang, Non-labeled QCM Biosensor for Bacterial Detection using Carbohydrate and Lectin Recognitions Anal Chem.79 (2007) 2312–2319.

123. S.J. Fletcher, L.W. Phillips, A.S. Milligan, S.J. Rodd, Toward specific detection of Dengue virus serotypes using a novel modular biosensor, Biosens Bioelectron. 26 (2010) 1696-1700.

124. G.J. Zhang, L. Zhang, M.J. Huang, Z.H.H. Luo, G.K.I. Tay, E.J.A. Lim, T.G. Kang, Y. Chen, Silicon nanowire biosensor for highly sensitive and rapid detection of Dengue virus, Sens Actuators B 146 (2010) 138-144.

125. C.H. Lin, C.H. Hung, C.Y. Hsiao, H.C. Lin, F.H. Ko, Y.S. Yang, Poly-silicon nanowire field-effect transistor for ultrasensitive and label-free detection of pathogenic avian influenza, Biosens Bioelectron. 24 (2009) 3019-3024.

126. V.C.H. Wu, S.H. Chen, C.S. Lin, Real-time detection of *Escherichia coli* O157:H7 sequences using a circulating-flow system of quartz crystal microbalance, Biosensors and Bioelectronics 22 (2007) 2967–2975.

127. Y.J. Liu, D.J. Yao, H.Y. Chang, C.M. Liu, C. Chen, Magnetic bead-based DNA detection with multi-layers quantum dots labeling for rapid detection of *Escherichia coli* O157:H7, Biosens Bioelectron. 24 (2008) 558-565.

128. S.V. Schrumpf, R. Buresch, M. Schinkinger, A simple nucleic acid hybridization/latex agglutination assay for the rapid detection of polymerase chain reaction amplicons, J. Microbiol. Methods 68 (2007) 568-576.

129. S.W. Dutse, N.A. Yusof, Microfluidics-Based Lab-on-Chip Systems in DNA-Based Biosensing: An Overview, Sensors 11 (2011) 5754-5768.

130. N.V. Zaytseva, V.N. Goral, R.A. Montagna, A.J. Baeumner, Development of a microfluidic biosensor module for pathogen detection, Lab Chip 5 (2005) 805–811.

131. C. Lui, N.C. Cady, C.A. Batt, Nucleic Acid-based Detection of Bacterial Pathogens Using Integrated Microfluidic Platform Systems, Sensors 9 (2009) 3713-3744.

Accepted Manuscript

ACCEPTED MANUSCRIPT

132. J. Mairhofer, K. Roppert, P. Ertl, Microfluidic Systems for Pathogen Sensing: A Review, Sensors 9 (2009) 4804-4823.

133. C. Roh, Facile Inhibitor Screening of Hepatitis C Virus NS3 Protein Using Nanoparticle-Based RNA, Biosensors 2 (2012) 427-432.

134. L.T.H. Kao, L. Shankar, T.G. Kang, G. Zhanga, G.K.I. Tay, S.R.M. Rafei, C.W.H. Lee, Multiplexed detection and differentiation of the DNA strains for influenza A H1N1 2009 using a silicon-based microfluidic system, Biosens Bioelectron. 26 (2011) 2006-2011.

Accepted Manuscript

ACCEPTED MANUSCRIPT

Biographies

Dr. Renu Singh received her Ph.D. degree (2013) from Guru Gobind Singh Indraprastha University, New Delhi, India in biotechnology. She is currently employed as Research Scientist in Ulsan National Institute of Science and Technology (UNIST), South Korea and working on the topic carbon-nanotubes based airborne virus detection sensor system for swine influenza virus H1N1 detection and removal of proteins, antibodies and biofilms using carbon dioxide aerosols. She has research experience of 7 years in the area of development of biosensors based on nanomaterials, nanobiocomposites, and conducting polymers for health care.

.

Dr. Maumita Das Mukherjee received her Ph.D. degree (2012) from University of Delhi, Delhi in Chemistry. She is currently working as Assistant Professor in Amity Institute of Applied Sciences, Amity University, Noida, Uttar Pradesh, India. She has research Experience of 8 years in the area of development of biosensors based on nanomaterials, nanobiocomposites, conducting polymers for health care and glass and glass-ceramic materials.

Dr. G. Sumana received her Ph.D. (1998) from Jiwji University in chemistry. She is currently working as scientist in biomolecular electronics and conducting polymer research group, National Physical Laboratory, New Delhi. She has a research experience of 10 years in controlled drug delivery, liquid crystal polymers, polymer dispersed liquid crystals and biosensors.

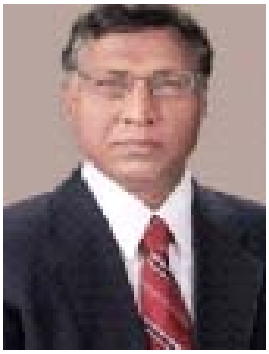

Prof. Rajinder K. Gupta received his Ph.D. degree Org.Chem. from Delhi University in Organic Chemistry of Natural Products. He earned his second PhD in Microbiology/Biotechnology from University of Idaho, USA. He has over 99 research publications to his credit and has more than three decades of experience in academia, and industry (pharmaceutical, agrochemical, polymer and commercial test house. He is now Professor and Dean, School of Biotechnology, Guru govind singh Indraprastha University, New Delhi, India. His current areas of research include identification of bioactive agent from actinomycetes & plants, biotransformations, and production of nanomaterials using microorganisms (nanobiotechnology).

Accepted Manuscript

ACCEPTED MANUSCRIPT

Dr. Seema Sood received her MBBS from M.B.B.S. from Lady Hardinge Medical College, New Delhi in 1987 and her MD (Microbiology) from Lady Hardinge Medical College, New Delhi. She is currently employed as Assistant Professor in the Department of Microbiology, AIIMS, New Delhi. She is currently working towards introducing novel technologies for the diagnosis of Infectious Diseases, with her focus being Sexually Transmitted Diseases.

Dr. B.D.Malhotra received his Ph.D. degree in physics from University of Delhi, Delhi, India in 1980. He has published 212 papers, has obtained 9 patents, has edited/co-edited books on biosensors and polymer electronics, and is currently the Scientist G and Head of the Biomolecular Electronics & Conducting Polymer Research Group at the National Physical Laboratory, India. He has research experience of about 25 years in the field of biomolecular electronics and has guided 17 PhD students till date. His current research activities including biosensors, conducting polymers, Langmuir–Blodgett films, self-assembled monolayers nanomaterials and nano bioelectronics, etc.

Accepted Manuscript

ACCEPTED MANUSCRIPT

Figure Captions:

Fig. 1: (a) Different existing conventional methods employed for human pathogen detection **(b)** Classification of biosensors.

Fig. 2: Biosensors act to convert biological information to an electrical signal through a molecular recognition reaction on a physical transducer.

Fig. 3: Schematic showing the immobilization of DNA onto solid support via different immobilization methods

Fig. 4: (a) Schematic showing working principle of a nucleic acid sensor **(b)** Illustration of good vs. bad orientation of probes.

Fig. 5: Schematic exhibits the interaction of different nucleic acid based analytes with the immobilized probe.

Fig. 6: MB interaction in the DNA hybridization event

Fig. 7: (a) Principle of Surface Plasmon Resonance measurement and **(b)** Schematic of change in resonance angle due to binding of target DNA with ssDNA via hybridization **(c)** Real-time detection of four bacteria by SPR biosensor (Wang et al., 2011)

Fig. 8: (a) Schematic of QCM setup **(b)** Frequency change vs. time curve when the mannose-QCM electrode was exposed to different concentrations of *E. coli* W1485 (Shen et al., 2007).

Fig. 9: (a) Schematic of a microfluidic module **(b)** Results of the differential measurement from the SiNW biosensor (Kao et al., 2011)

ACCEPTED MANUSCRIPT

Table Captions:

Table 1: Electrochemical nucleic acid sensors for bacterial pathogen detection

Table 2: Electrochemical nucleic acid sensors for viral pathogen detection

Table 3: Optical nucleic acid sensors biosensors for bacterial and viral pathogens detection

Table 4: Other nucleic acid sensors biosensors for bacterial and viral pathogens detection

Fig.1

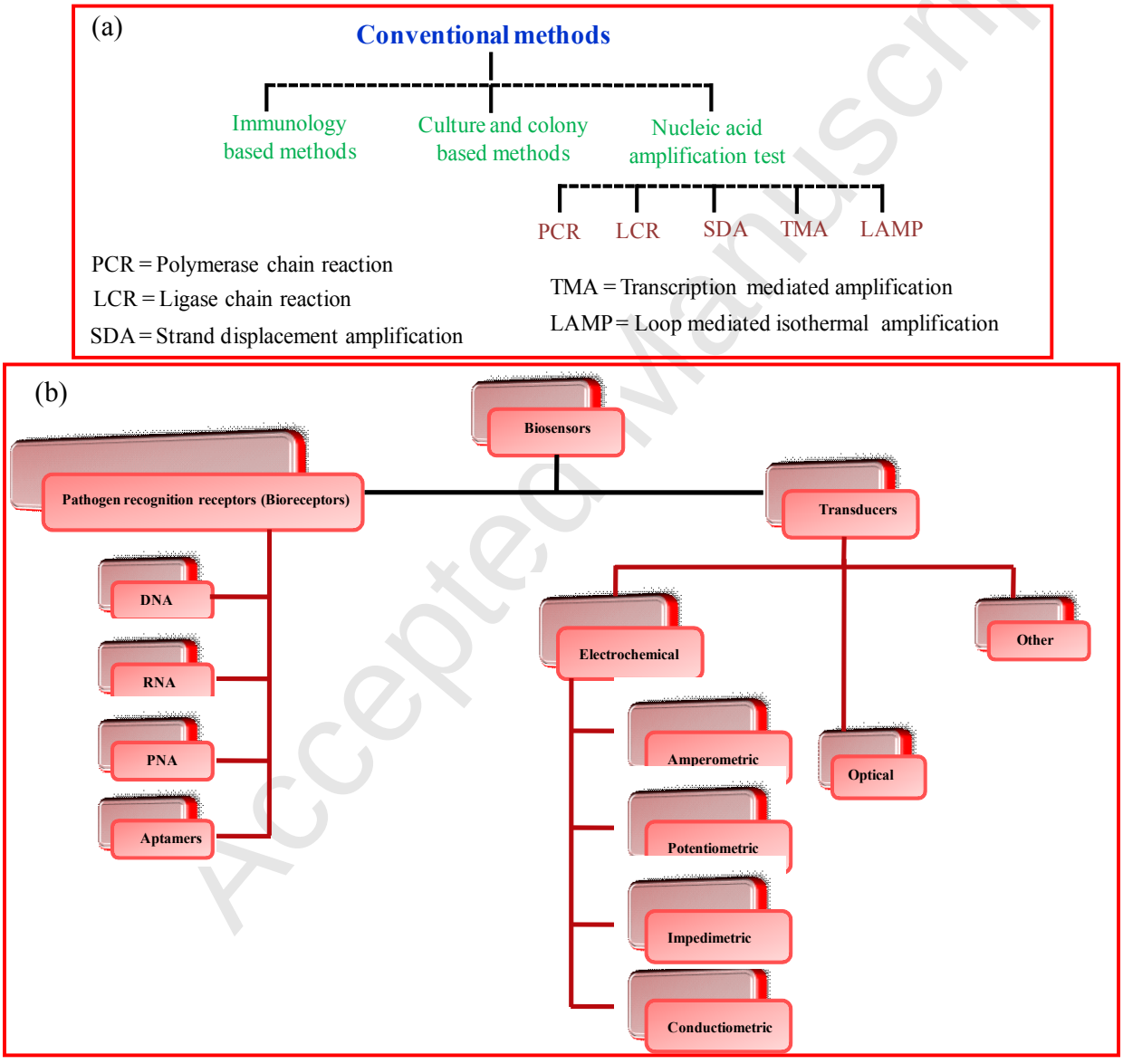

ACCEPTED MANUSCRIPT

Fig. 2

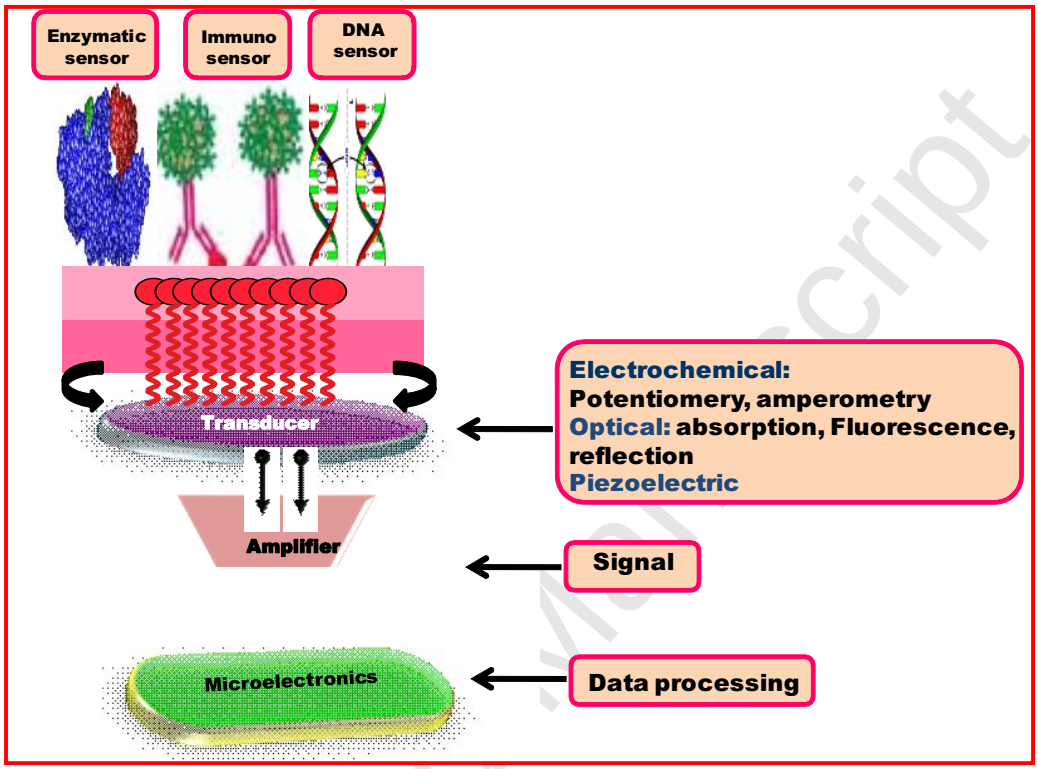

Accepted Manuscript

ACCEPTED MANUSCRIPT

Fig. 3

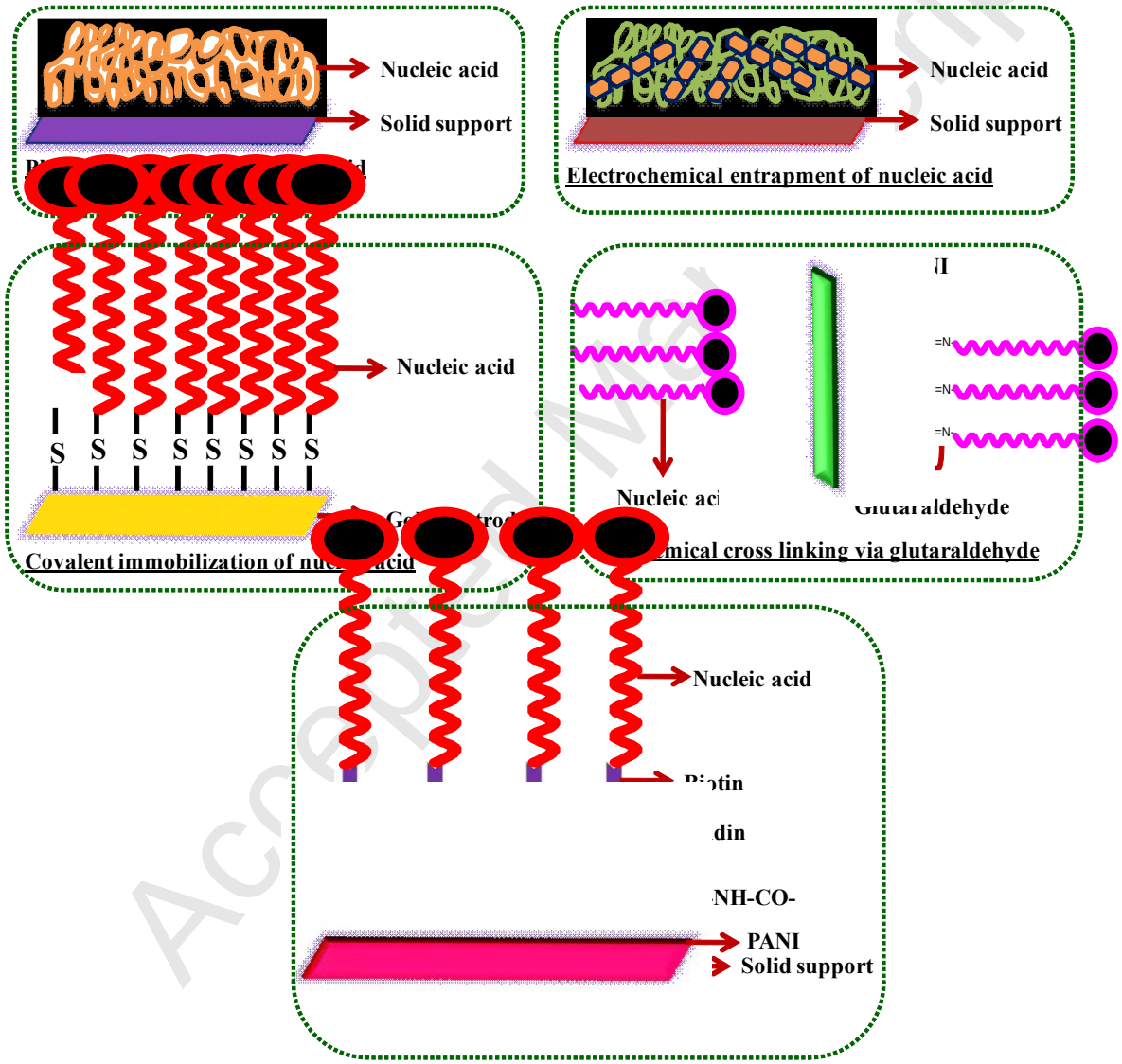

ACCEPTED MANUSCRIPT

Fig. 4

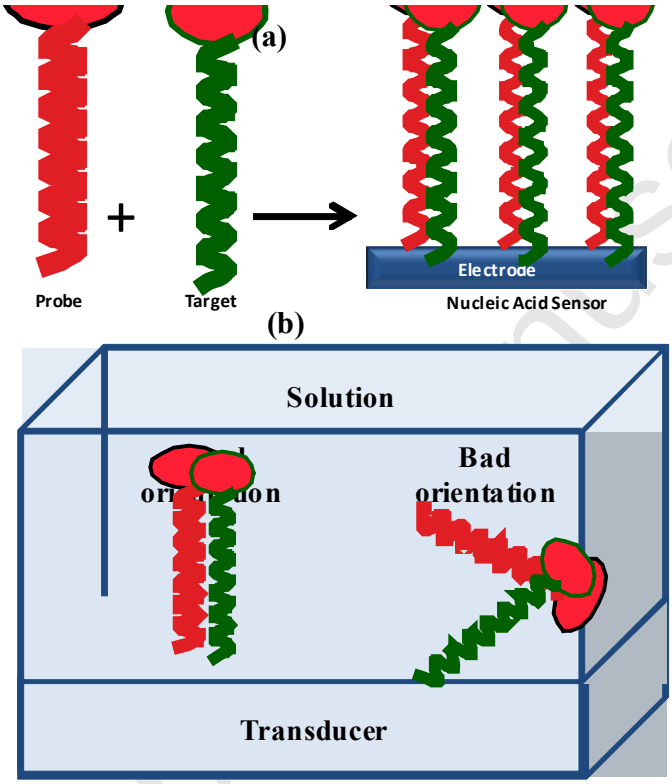

ACCEPTED MANUSCRIPT

Fig. 5

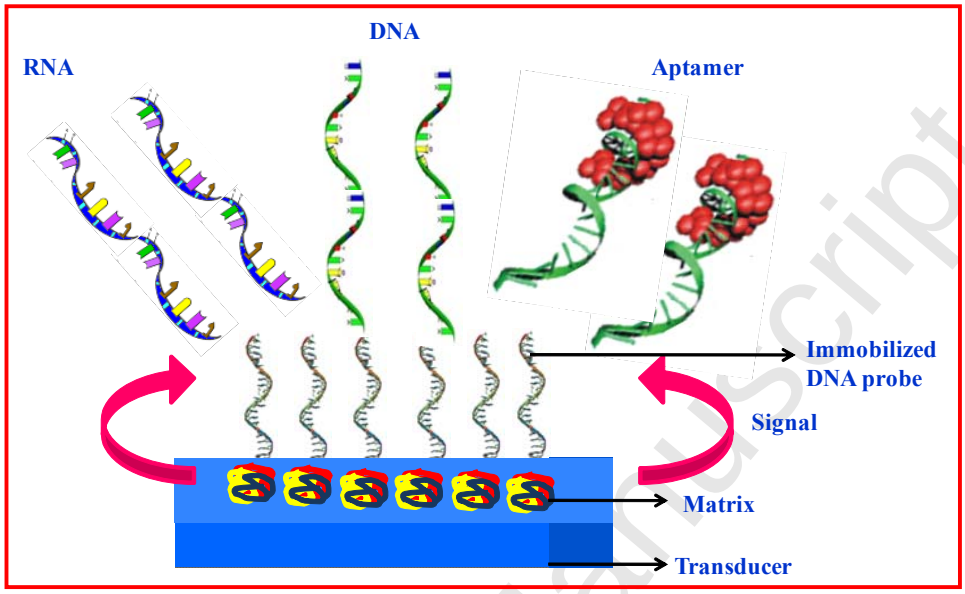

Accepted Manuscript

ACCEPTED MANUSCRIPT

Fig. 6

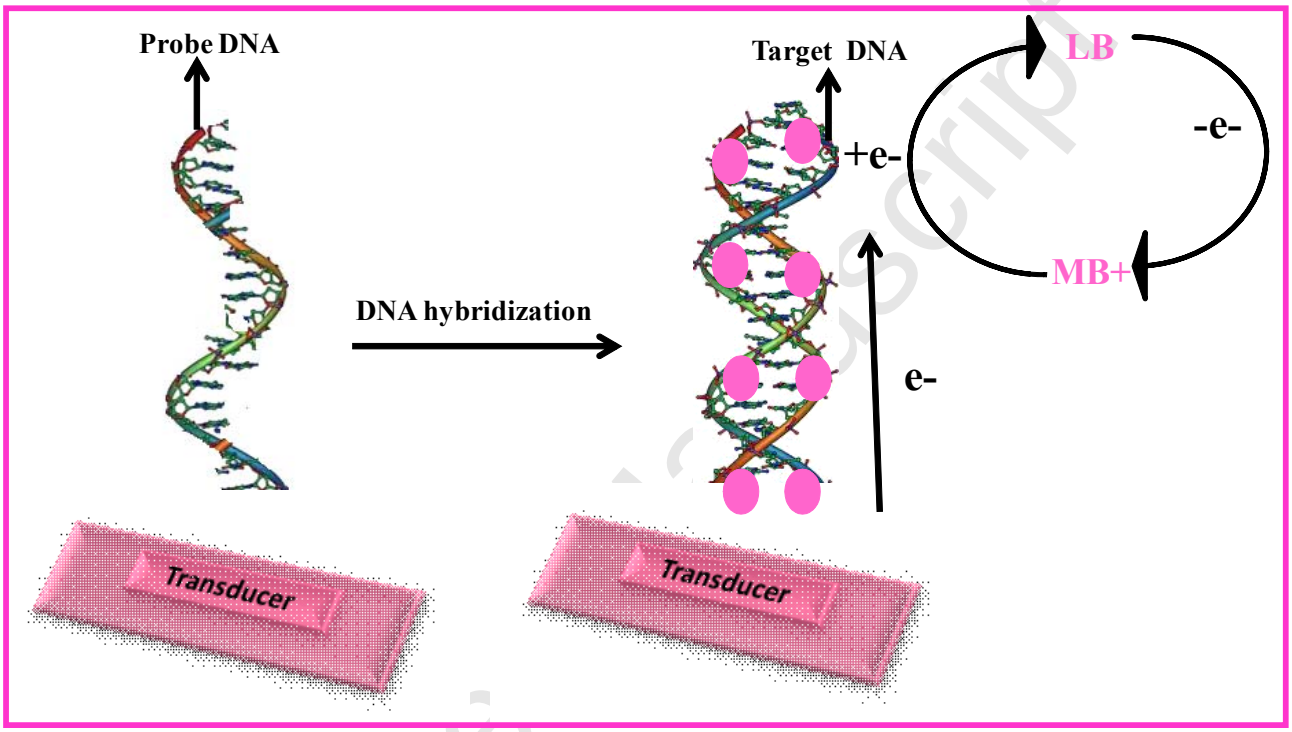

Accepted Manuscript

ACCEPTED MANUSCRIPT

Fig. 7

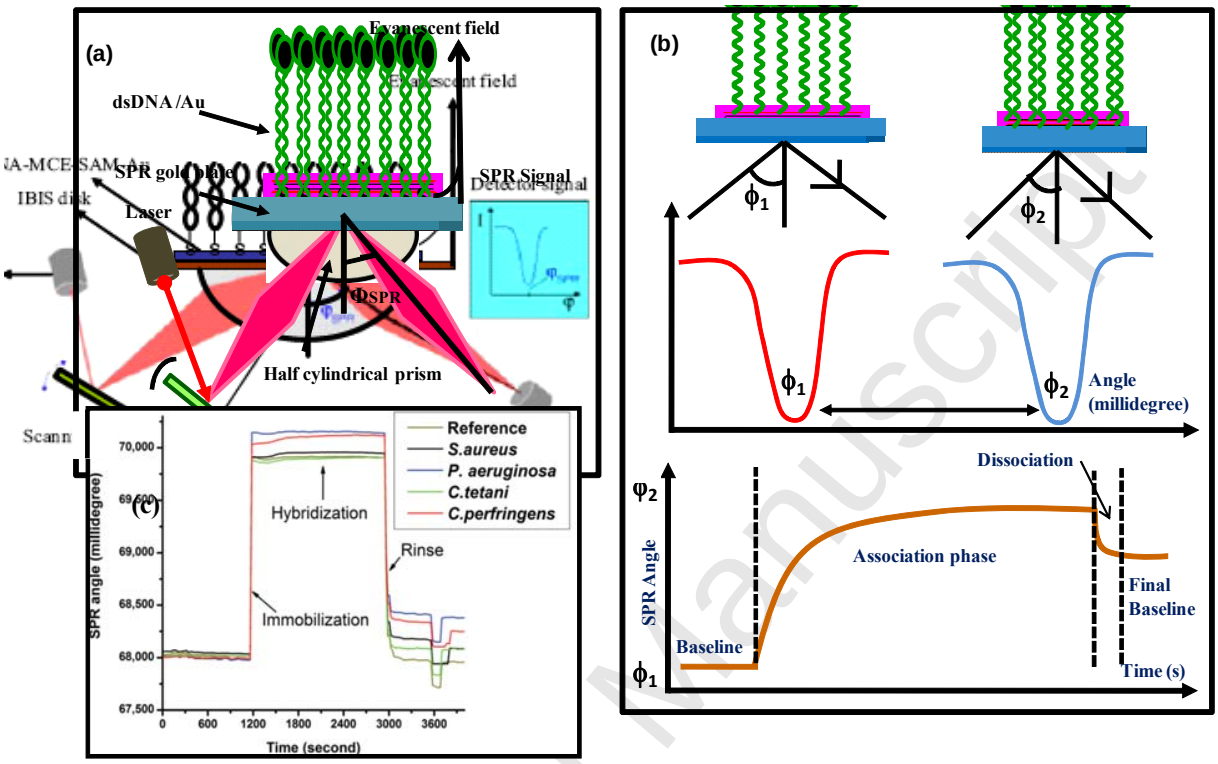

Accepted Manuscript

ACCEPTED MANUSCRIPT

Fig. 8

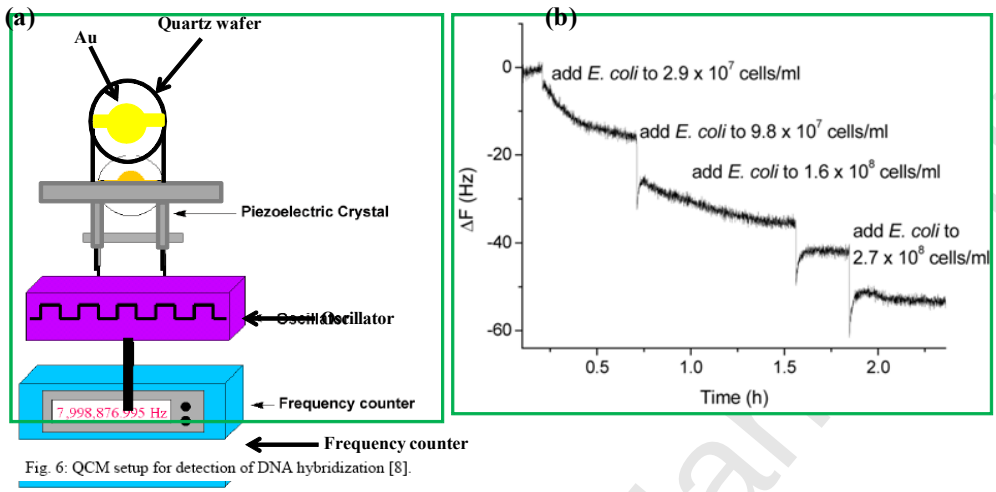

Fig. 6: QCM setup for detection of DNA hybridization [8].

Accepted Manuscript

ACCEPTED MANUSCRIPT

Fig. 9

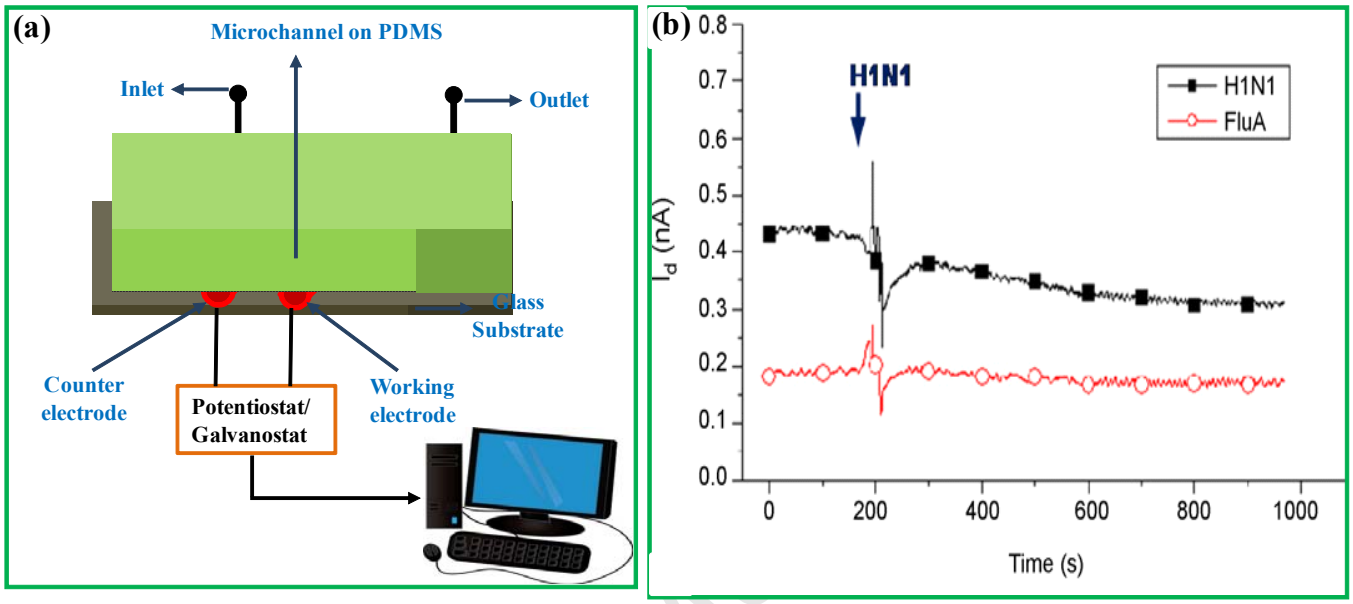

Accepted Manuscript

ACCEPTED MANUSCRIPT

Matrix	Microorganism Detected	Method of immobilization	Measurement conditions	Redox indicator	Detection limit	Detection Range	Correlation coefficient	Detection time	Reusability	Technique used	[Reference] (Year)
PANI electrochemically deposited onto a Pt disk electrode	*E. coli*	Avidin-biotin coupling	20 μM MB pretreatment in phosphate buffer, 0.05 M, pH 7.0, at 0.1 V pulse height of 50 mV, and pulse width of 70 ms for 10 s , 30-45 °C	MB	Artificial DNA-(0.009 ng/μL), *E. coli* genomic DNA-(0.01 ng/μL) and *E. coli* cells-11 cells/mL	0.0064-2.3 ng/μL	-	8-14 min, 60-360 s, 60 s	5-7 times	DPV	[63] (2007)
Fullerene into poly(methylmethacrylate)	*E. coli*	Physical adsorption	0.02 M Tris–HCl buffer, pH 7.0, Room temperature (RT)	$(Co(phen)_3^{3+})$	-	-	-	-	-	DPV	[64] (2007)
DTSP-SAM	*E. coli*	Covalent binding	−0.50 to+0.10V with amplitude of 30mV and a step potential of 5mV at 100 Hz,50mM Tris–HCl, 20mM NaCl, pH 7.2, 25±0.5◦C	MB	45nM	3.1–50.0 ng	0.999	-	10 times	SWV	[65] (2007)
Sol–gel derived Nano ZrO2	*E. coli*.	Electrostatic interaction	PBS, 50 mM, pH 7.0 and 0.7% NaCl, 20 μM MB	MB	10^{-6} pM	10^{-6} 6–10^{6} pM	0.993	-	-	DPV	[66] (2009)
Au electrode	Sequence-specific DNA	Au-SH bond	10 mM Tris‑HCl, 5 _M RuHex, pH 7.0, 22‑25 ◦C	$Ru(NH_3)_6^{3+}$	20 fM	20 fM to 50 pM	0.8974	-	-	SWV	[67] (2011)
1-fluoro-	*E. coli*	Covalent	PBS 0.05 M, pH	MB	0.5×10^{-18} M	0.5×10^{-18}-	0.99	60 s	10 time	DPV	[68] (2011a)

Accepted Manuscript

ACCEPTED MANUSCRIPT

Table 1

Table 2

Matrix	Method of immobilization	Measurement conditions	Micro organism Detected	Redox Indicator	Detection limit	Detection Range	correlation coefficient	Detection Time	Technique used	[Reference] (Year)
Pencil graphite electrode (PGE)	Physical adsorption	+0.75 and 1.40 V in ABS with 20 mmol/L NaCl, 25 ±0.5 °C	Hepatitis B virus	-	457 fmol/mL	-	-	15 min	DPV	[91] (2005)
Amino linked inosine modified capture probes immobilized onto PGE	Electrostatic interaction, Covalent binding	2×SSC buffer with amplitude of 10 mVat 20 mV/s scan rate, 25 °C	Hepatitis B virus	-	-	-	-	-	DPV	[92] (2007)
GCE	Covalent binding	CV--0.40 V to -1.20 V, 60 mV s^{-1} DPV, -1.20 V to -0.40 V; pulse pH 50 mV for 60 ms, step height 2 mV, and step time	Hepatitis B virus	bis(benzimidazole) cadmium(II) dinitrate [$Cd(bzim)_2(NO_3)_2$]	8.4×10^{-8} M	1.49×10^{-7} M to 1.06×10^{-6} M	0.9973	15 min	CV, DPV	[93] (2007a)

Accepted Manuscript

ACCEPTED MANUSCRIPT

		0.1 s, 40 °C								
GCE	Covalent binding	0.2M BR buffer, pH 7.0, 0.1mM $[Cu(dmp)(H_2O)Cl_2]$ at $60mVs^{-1}$, 25 °C	Hepatitis B virus	$[Cu(dmp)(H_2O)Cl_2]$ (dmp = 2,9-dimethyl-1,10-phenanthroline)	7.0×10^{-8} M.	8.82×10^{-8} to 8.82×10^{-7} M	0.9937	-	DPV	[94] (2007b)
GCE	Covalent binding	CV,-0.20 V to -0.40 V, $0.10Vs^{-1}$ DPV, -0.20 V to 0.40 V, amplitude 0.05 V, 25 °C	Hepatitis B virus	2,9-dimethyl-1,10-phenantroline cobalt $[Co(dmp)(H_2O)(NO_3)_2]$	1.94×10^{-8} M	3.96×10^{-7} to 1.32×10^{-6} M	0.9951	-	CV, DPV	[95] (2008)
GCE	Covalent binding	0.2 mol L^{-1} B-R buffer solution, pH 4.0; potential scan from 0.2V to −0.4V at the scan rate of $0.1Vs^{-1}$	Hepatitis B virus	rutin–Cu complex	2.3×10^{-9} mol L^{-1}	$1.62\times10-8$ mol L^{-1} to $8.10\times10-7$ mol L^{-1}	0.9989	5 min	DPV	[96] (2009)
GCE	Covalent binding	50 mmol L^{-1} PBS, pH 7.4 ; 0.2 mol L^{-1} NaAc-HAc media, pH 7.02, $[CdL_2]^{2+}$, −0.4 to −1.1V	Hepatitis B virus	diaquabis[N-(2-pyridinyl methyl) benzamide-k^2 N,O]-cadmium(II) dinitrate $\{[CdL_2(H_2O)_2](NO_3)_2$, wherein	7.19×10^{-9} mol L^{-1}	1.01×10^{-8} to 1.62×10^{-6} mol L^{-1}	0.9962	-	DPV	[97] (2007)

Accepted Manuscript

ACCEPTED MANUSCRIPT

				L=N-(2-pyridinyl methyl) benzamide }						
PPy film deposited at microelectrodes	Electrostatic interaction	0.1 mol L^{-1} Tris-HCl buffer pH 7.2	Hepatitis C virus	[Cu(dmp)(H_2O)Cl_2] (dmp = 2,9-dimethyl-1,10-phenanthroline)	1.0 x 10^{-15} mol L^{-1}	-	-	10 min	CV	[98] (2006)
20-mer DNA containing 2 guanine and 11 cytosine bases as probe onto PGE	Covalent binding	20 mM Tris-HCl buffer, pH 7.00; potential 0.50 to 1.2 Vat a pulse amplitude of 25 mV	Hepatitis C virus	2,9-dimethyl-1,10-phenantroline cobalt [Co(dmp)(H_2O)(NO_3)$_2$]	6.5 nM	0.05 - 0.75 µM	0.999	15 min	DPV	[99] (2009)
Thionine-labeled probe DNA self-assembled onto Au electrode	Au-SH Bond	0.1M acetate buffer, pH 5 at 50 mV s^{-1}	Hepatitis C virus	Thionine	0.1 µM	0.1 to 2.5 µM	0.999	-	CV	[100] (2009)
PNA SAM and 6-MCH onto Au	Covalent binding	20 mM Tris–HCl buffer, pH 7.0, 20 mM NaCl and potential	Hepatitis C virus	MB	5.7× 10-11 M	1–50 nM	0.999	2 min	DPV	[101] (2010)

ACCEPTED MANUSCRIPT

electrode		0.10 to -0.50 V at a pulse amplitude of 25 mV, 85–90 °C								
CNT loaded with silver nanoparticles	Au-SH Bond	0.10 M PBS, pH 7.4, pulse amplitude, 20 mV; pulse width, 60 ms; scan rate, 20 mV. s^{-1}, RT	HIV-1	-	0.5 pM	1.0×10^{-12} to 1.0×10^{-10} M	0.9956	60 min	DPV	[102] (2011)
Streptavidin modified magnetic nanoparticles onto Au electrode	Streptavidin- biotin coupling	PBS buffer pH 7; frequency range between 100mHz and 100 kHz under a potential value of −300mV, RT	HIV	$[Fe(CN)_6]^{4-/3-}$	50 pmol of HBV DNA and 160 pmol of HIV DNA	2.53 nmol/mL to 50.6 nmol/mL.	-	-	EIS	[103] (2008)
CH/Fe_3O_4 nanobiocomposite onto SPE	Covalent binding	CV: scan rate: 50 mV/s; potential range: −0.5 V−+0.2 V vs. SCE. SWV: frequency: 12.5 Hz; start potential: −0.6 V; end potential: +0.4 V; step:	HIV-1	MB	50 pM	50 to 300 pM	-	-	EIS, SWV	[104] (2011)

ACCEPTED MANUSCRIPT

		8 mV; amplitude: 25 mV EIS: frequency range from 200 kHz to 10 mHz using 5 mV								
MWCNT onto SiO_2 grown Si wafer	Covalent binding	PBS, pH 7.5	HIV	-	0.5 nM	1 and 10 nM	-	4 min	EIS	[105] (2009)
CuHCF nanoparticles onto Au electrode	Avidin-biotin coupling	Potential, 4mV-1.0 V; step potential, 4mV; amplitude, 50mV; pulse, 0.05 s; and pulse period, 0.2 s; electrolyte solution, 0.10M KNO3, RT	HIV	-	1.0 fM	1.0 fM to 10pM	0.98	2 h	DPV	[106] (2010)
CdSe hollow nanostructures onto GCE	Physical adsorption	B-R buffer, pH 7.0, containing 2.0×10^{-5} mol L^{-1} MB with 0.02 mol L^{-1} NaCl, Scan rate 50 mV/s, 40°C	AIV	MB	1.0×10^{-12} mol L^{-1}	-	-	60 min	DPV	[107] (2010)
(MWNTs–CoPc)	Covalent binding	TBS (20 mM Tris–HCl buffer	AIV	-	1.0 pg/ml	0.01 to 500	0.998	20 min	DPV	[108] (2009)

ACCEPTED MANUSCRIPT

s–CoPc) and PAMAM		buffer solution, pH 7.0, 20 mM NaCl +0.30 to +1.20 V pulse amplitude 0.1 V, pulse width 0.05 s, and pulse period 0.2 s				500 ng/ml				
ThssDNA immobilized SPE Au electrode	Au-SH Bond	0.25M Acetate buffer pH5.8 , potential 0.6V, frequency 25 Hz, amplitude 40mV, and step potential 5mV, RT	Human papilloma virus (HPV)	-	2 $pgml^{-1}$	0.5–5 $ng.ml^{-1}$	0.998	5 min	SWV	[109] (2009)
ThssDNA immobilized SPE Au electrode	Au-SH Bond	PBS pH 7.4, 2 steps at 0V for 1ms and −0.2V for 0.5 s, RT	HPV	TMB	10 nM	0.1-50nM	0.999	1 h	Steps and sweeps technique	[110] (2010)
AuNPs and two-component oligonucleotide-modified MBs	Covalent binding		HTLV-I, HTLV-II	-	1.71×10^{-12} M for T_1-DNA and 1.55×10^{-12} M for T_2-	4.4×10^{-11} to 2.0×10^{-9} M	0.9955 and 0.9975	-	DPV	[111] (2009)

Accepted Manuscript

ACCEPTED MANUSCRIPT

					DNA					

Table 3

Matrix	Microorganism Detected	Method of immobilization	Measurement conditions	Type of biosensor	Detection limit	Detection Range	Detection time	correlation coefficient	Reusability	Technique used	[Reference] (Year)
PNA/Au bioelectrode DNA-Au bioelectrode	*Mycobacterium tuberculosis*	Au-SH Bond	800 s (association phase or nucleic acid hybridization), 25◦C.	PNA, DNA biosensor	1.0 ng ml^{-1}, 3.0 ng ml^{-1}	5-50 ng mL^{-1}	600 s	-	8-9 times	SPR	[113] (2008c)
Au nanoparticle	*E. coli*	-	PBS buffer	Optothermal biosensor	10000 cells μl^{-1}	-	30 s	-	-	Real-time PCR	[114] (2008)
Au surface	AIV H5N1	Avidin-biotin coupling	PBS buffer	Aptasensor	0.128 HAU	0.128 to 1.28 HAU	1.5 h	0.99	5-7 times	SPR	[115] (2012)

Accepted Manuscript

ACCEPTED MANUSCRIPT

Biotinylated aptamers immobilized on the gold surface	*E. coli*	Physical adsorption	Wavelength 560 nm, potassium phosphate buffer, pH 7.5, RT	RNA biosensor	5 fmol per sample , 40 E. coli cfu/ml	5 fmol to 5 pmol, 0 and 1 000 000 cfu/ml	15-20 min	0.9631	-	Reflectometery	[116] (2003)
Liposomes entrapping sulforhodamine B coated with streptavidin, and polyethersulfone membranes with anti-fluorescein antibodies	*E. coli, C. parvum* and *B. anthracis*	Avidin-biotin coupling	Wavelength 560 nm, Tris buffer, 42^{o}C	RNA, DNA biosensor	50 fmol, 10 fmol, 10 fmol	0.1 - 1000 00 fmol,	20-30 min	-	-	Fluorescence	[117] (2004)
SPR Au chip	*Pseudomonas aeruginosa*, *Staphylococcus aureus*	Au-SH bonding	System buffer, ±0.1°C at 25~60°C	SPR based DNA sensor	0.03 nM, 0.02 nM, 0.01 nM	0.1 nM to 100 nM	15 min	> 0.99	>100 times	SPR	[118] (2011)

ACCEPTED MANUSCRIPT

	aureus, Clostridium tetani and Clostridium perfringens				nM, 0.02 nM						
A PDMS /paper/ glass hybrid microfluidic biochip	*Lactobacillus acidophilus*, *Staphylococcus aureus* and *Salmonella enterica.*	Covalent binding	Fluorescence intensities, Cy3 optical filters (Ex = 550 nm; Em = 570 nm). 37^{o} C	Aptamer Microfluidic sensor	11.0 cfu $mL^{-1,}$ 61 cfu $mL^{-1,}$, 800 cfu $mL^{-1,}$	9.4–150.0 cfu $mL^{-1,}$ 10^{4}–10^{6} cfu mL^{-1}, 42.2–675.0 cfu mL^{-1}	-	99.7, 99.5, 99.3	-	Fluorescence	[119] (2013)

Accepted Manuscript

ACCEPTED MANUSCRIPT

Table 4

Matrix	Microorganism Detected	Method of immobilization	Measurement conditions	Type of biosensor	Detection limit	Detection Range	Detection Time	Technique used	[Reference] (Year)
AuNps	*Vibrio cholerae*	Covalent binding	50µl 10mM PBS, pH 7.4 with 0.5% Tween-20, 24 ◦C.	Disposable lateral flow-based DNA biosensor	5 ng	1 to 100 ng	10 min	Glass fibre membrane carrier bead system	[120] (2011)
AuNPs coated QCM electrode	*B. anthracis*	Au-SH Bond	0.3M NaCl, 10mM PB with pH 7.4, 200µl/min of buffer, 30 ◦C	DNA biosensor	3.5×10^2 CFU/ml	3.5×10^2 to 3.5×10^7 CFU/ml	30 min	QCM	[121] (2011)
Au-Mannose SAM	*E. coli*	Au-SH Bond	M in 1.0 mL of PBS buffer (pH 7.2) with 1 mM Mn2+ and 1 mM Ca2+	Cell based biosensor	few hundred bacterial cells	7.5 102 to 7.5 107 cells/mL	-	QCM	[122] (2007)
Dengue serotype target-induced	Dengue virus genome	-	Buffered solution containing the aptamer/EcoRI complex and MBL, 30 ◦C.	Novel modular biosensor	6 pmol	-	20 min	Fluorescence	[123] (2010)

Accepted Manuscript

ACCEPTED MANUSCRIPT

d biosensor assay									
SiNW	Dengue serotype 2	Covalent binding	10 µm PNA in citrate buffer (15mM sodium citrate, 150mMNaCl,pH7.4), RT	PNA biosensor	10 fM	100 fM to 1 fM	30 min	Electrical detection	[124] (2010)
Poly-SiNW-FET	AIV	Cross linking	Bias voltage (VG from 5.0 to 9.0V with a step of 1.0 V) while sweeping the VD from 0 to 3.0V in PBS (10mM, pH 7.0), RT	FET DNA Biosensor	1 fM	100 pM-100fM	3 min	Electrical detection	[125] (2009)
Au QCM electrode	*E. coli*	Au-SH Bond	0.1 Hz, sampling period: 1 s, frequency range: 2–16 MHz, temperature range: 4–60 ◦C and voltage: 110V, 50–60 Hz	DNA biosensor	0.5 µM	0-1 µM	30 min	circulating-flow QCM	[126] (2007)
Magnetic bead with multi-layers quantum dots labeling	*E. coli*	-	20mM Tris–HCl, pH 7.5, 1.0M LiCl, 2mM EDTA, RT	Fluorescence based assay	250 zM	500zM-250zM	40–60 min	QCM	[127] (2008)

ACCEPTED MANUSCRIPT

Polystyrene beads with PCR DNA product	*Salmonella spp*	-	10 mM Tris–HCl, pH 8	Multiplex assays	3 cfu/25 g, 30 cfu/25 g	-	7 min		[128] (2007)
PDMS-superparamagnetic beads	*Bacillus anthracis*, *Cryptosporidium parvum, E. coli, Dengue viru*	Avidin-biotin coupling	540/25 nm band pass exciter; 620/60 nm band pass emitter), and 100 W mercury illumination sourc, 10 mM Tris-HCl, 1 mM EDTA, 2 M NaCl, pH 7.5, RT	Microfluidic RNA biosensor	-	-	-	Fluorescence	[130] (2005)
Carboxyl-terminated QDs605	HCV	Covalent binding	Phosphate buffer pH 7.2, RT	Inhibitor screening on a biochip	0.01 $\mu g \cdot mL^{-1}$	0.1 $\mu g \cdot mL^{-1}$ - 0.5 $\mu g \cdot mL^{-1}$	-	Emission wavelength as the optical imaging probe	[133] (2012)
SiNW based microfluidic	Influenza virus H1N1	-	-	DNA based microfluidic system	20–30 fg/µl	50 pg - 2µg	15-20 min	Electrical detection	[134] (2011)

ISBN 978-93-5156-328-0
International Conference of Advance Research and Innovation (ICARI-2014)

Building Automation Control System for Smart Grid

Md. Tausif Ahmad *, Priyanka Chaudhary, Narendra Kumar
Department of Electrical Engineering, Delhi Technological University, Delhi, India

Article Info

Article history:
Received 2 January 2014
Received in revised form
10 January 2014
Accepted 20 January 2014
Available online 1 February 2014

Keywords

Building Automation Control System (BACS)
Optimal Scheduling,
Smart Grid,
Smart Homes,
Home Area Network (HAN),
Real Time pricing

Abstract

An advanced control method of Building Automation Control System (BACS), as part of home automation to interface with smart grid system. An optimization technique, Dynamic Programming, is employed to solve the scheduling of building appliances. The cost savings achieved by interrupting the cycle of building appliances has been explored within the optimisation suite. The BACS automation controller is using price signals made available by smart meters to shift and interrupt building appliances in order to maximize the benefits for theresidential consumers. Described optimization can be used in home automation for cost savings while allowing users different levels of control on the smart appliances. A case study carried out with Volt/Var optimization techniques, Binary Integer Programming and Dynamic Programming shows substantial cost savings under real time pricing.

1. Introduction

The world has a huge appetite for electric energy, consuming thousands of billions of kilowatt hours (kwh) annually, as more countries become industrialized, electric consumption has increased and is expected to grow to33.300 billionKwh by 2030.

To achieved energy target 20% energy from renewable sources 20% increase in efficiency and 20% reducing gas emission. In order to achieve these targets new polices and technologies such as Smart Grid are essential.

With the development of smart Grid technologies, both residential and commercial consumer will save their cost of energy also the losses during transmission to distribution as a result energy will also be saved. In this context, the suppliers will offer real time pricing(RTP) to its customers because it includes (a) more competitive market during peak usage hours.(b)customers have choice of resources available.(c)optimize the use of renewable energy sources.(d)reduces the frequency and magnitude of energy scarcity events.(e)customers provide valuable reliability services to the local area.

In this paper a review of different optimization process has been studied that schedules the operation of appliances loads is proposed. Building Automation Control System (BACS) module employed to provide real time pricing (RTP) tariff to consumers through smart meter. The BACS employs cost optimization to maximize the savings on consumed energy by shifting domestic loads as well as energy resources.

Corresponding Author,
E-mail address: mtahmad16@gmail.com
All rights reserved: http://www.ijari.org

2. Background

An extensive study of the potential benefits volt/var optimization (VVO), that is operating capacitor banks and voltage regulation in a co-ordinate manner to provide optimal voltage and reactive power usage to their distribution feeders. This reduces the cost of energy as a raw material, reducing overall production costs.

The cost savings achieved by interrupting the cycle of smart appliances has been explored within the optimization suite. The home automation controller is using price signals made available by smart meters to shift and interrupt smart appliances in order to maximize the benefits for the residential consumers. The owners were offered day-ahead variable electricity tariffs as an incentive to shift different loads. The system can automatically schedule appliances to operate in periods with low energy prices. Results from the trial are expected from the end of 2012.

By optimizing the schedule of appliances the use of price- based incentives promote renewable source of energy such as wind or solar. RTP tariffs have been

used to simulate BACS which shifts the controllable residential loads to low price periods. The optimal schedule results from dynamic programming. Review of this study confirms that using BACS can reduce the household electricity bill and also the peak –to-average ratio in load profile.

3. Implementation

3.1 Function of BACS

The present work is aimed at study & development of an energy management system (EMS) suitable for underdeveloped countries. Studies involve designing of a BACS module by using optimization method of dynamic programming which will accounting the energy and metering, managing the load in the premises, Sending reports to distribution control system i.e. smart grid, Display of required information to the user. It will perform energy accounting, and control the load by making communication with smart grid. Practical study can be done on a simulated network. BACS may be tested on this prototype. The home area network (HAN) can be drawn for a typical house and load study under various conditions can be made by a computer. Dynamic programming makes the direct search feasible because instead of searching among the set of all admissible controls that cause admissible trajectories, we consider only those controls that satisfy an additional necessary condition—the principle of optimality.

3.2 Building Automated Control System (BACS) Block Diagram

Proposed building automated control system (BACS) is shown in block diagram below.

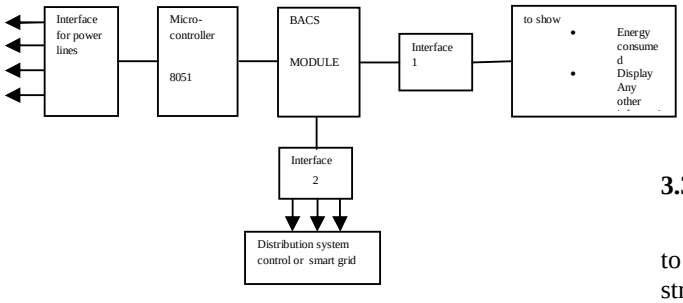

Fig: 1. BACS Block Diagram

BACS block diagram consists of three interface unit namely interface unit 1 which is placed between BACS module and display to show energy consume as well as any other information. Interface unit 2 to make output communication channel of BACS compatible to smart grid if required. Interface unit 3 connected with the power lines and residential load which are placed in Home Area Network (HAN). The energy accounting and load control as par user demand achieved by microcontroller. BACS module is used to access all the electrical appliances such as lightning load, heaters, air-conditioner, motors etc. installed within the house.

It will perform energy accounting, and control the load by making communication with smart grid. Practical study can be done on a simulated network. BACS may be tested on this prototype. The home area network (HAN) can be drawn for a typical house and load study under various conditions can be made by a computer.

- Development of hardware and software for BACS for domestic or industrial consumers [or Low-Tension or High-Tension consumers].
- Particulars or Technical details of interface on input and output side of BACS
- Choice of communication channel from BACS to smart grid on the basis of
  - Reliability
  - Cost considerations and
  - Installations

Common type of communication lines are normally power line wiring, Telephone wiring, Ethernet or Wi-Fi. However telephone lines are not present in all the premises and may not be suitable under such conditions.

Benefits

Application of BACS in smart grid will:

- Improve the efficiency of electrical distribution system
- Control the energy consumption of consumers

Create awareness to users to minimize their demand during peak hours thereby reducing the overall peak demand

Help the Government in forming an energy policy to increase the operational efficiency.

3.3 Cost Function

With the implementation of BACS it is possible to offer innovative tariffs such as RTP tariff structures. RTP tariffs can be transmitted to customers in a time range between seconds to days ahead. In this study the RTP tariff used is based on the RTP scheme implemented by Ameren Illinois Power Co. for residential customers[]. The price of electricity varies hourly and the customers are notified of the hourly prices on a day ahead basis. It is assumed that the tariff is broadcast to customers with the help of the

BACS and from the smart grid. Based on the RTP tariff, a price vector [] is considered.

4. Conclusions

In this paper a method of controlling smart domestic appliances is presented. The controller takes advantage of new technologies such as smart metering and home automation together with services such as RTP tariff to minimize the cost of running smart appliances. The method employs optimization with a cost function as objective. The smart appliance features such as smart timing and cycle interruption are implemented in the optimization. The optimization problem is solved using dynamic programming. That using BACS our optimization, the building appliances can be controlled in order to minimize the operation cost. As the user allows more time for the automatic operation of appliances, it can be observed that the cost savings start saturating. Increasing the interruption duration of smart appliances cycles has a small influence on the cost savings with the RTP tariff employed in this study. It can be concluded that a more granular RTP tariff (e.g. half hourly) that includes more price peaks has to be used to utilize the full potential of the smart appliances interruption feature.

References

[1] European Regulators Group for Electricity & Gas, "Final Guidelines of Good Practice on Regulatory Aspects of Smart Metering for Electricity and Gas", Feb. 2011. http://www.energy-regulators.eu-/portal/page/portal/EER_HOME/EER_CONSULT/CLOSED%20PUBLIC%20CONSULTATIONS/CUSTOMERS/Smart%20metering/CD/E10-RMF-29-05_GGP_SM_8-Feb-2011.pdf

[2] EU WG3 on Demand and Metering from ETP Smart Grids, "Energy Retailers' Perspective on Deployment of Smart Grids in Europe", 2010. http://www.smartgridsflanders.be/sites/default/files/nieuws/-ETPSmartGrids_EnergyRetailers_ White Paper_Final_v1.0.pdf

[3] C. W. Gellings, "The Smart Grid: Enabling Energy Efficiency and Demand Response", the Fairmont Press, 2009, p. 148

[4] EU Smart-A Report, "Smart Domestic Appliances Supporting the System Integration", Nov. 2009, www.smart-a.org/SmartA_Pro-ject_Final_ Brochure_ 2009.pdf

[5] K. Kok, S. Karnouskos, J. Ringelstein, A. Dimeas, A. Weidlich, C. Warmer, S. Drenkard, N. Hatziargyriou, V. Lioliou, "Field- Testing Smart Houses for a Smart Grid", Proceedings of the 21st International Conference on Electricity Distribution CIRED, Frankfurt, 2011, http://www.smarthouse-smartgrid.eu/fileadmin /templateSHS- G/docs/publications/CIRED_Field Testing.pdf

[6] P. Finn, C. Fitzpatrick, D. Connolly, M. Leahy, L. Relihan, "Facilitation of renewable electricity using price based appliance control in Ireland's electricity market", Energy, 36 (5), May 2011, http://www.sciencedirect.com/science/article/pii/S0360544211001162

[7] A.-H. Mohsenian-Rad, A. Leon-Garcia, "Optimal Residential Load Control with Price Prediction in Real-Time Electricity Pricing Environments," Smart Grid, IEEE Transactions on, 1(2), pp.120133, Sept. 2010, http://ieeexplore.ieee.org/stamp/stamp.jsp?tp=&arnumber=5540263&isnumber=5552162

[8] EU Smart-A D2.3 Report, Synergy Potential of Smart Appliances, Nov. 2008, http://www.smart-a.org/WP2_D_2_3_Synergy_P-otential_of_ Smart_Appliances.pdf

[9] Bliek, F.; Albert van den Noort, Roosien B., Kamphuis R., Johan de Wit, Power Matching City, a living lab smart grid demonstration, Oct. 2010, http://static.progressivemediagroup.com/

[10] Real-time pricing for residential customers, Ameren Illinois Power Co., Mar. 2010, https://www2.ameren.com/RetailE-nergy/ realtimeprices.aspx

[11] Iman Mansouri, Marcus Newborough, Douglas Probert, "Energy consumption in UK households: Impact of domestic electrical appliances", Applied Energy, 54(3), Domestic Demand- Side Management, July 1996, Pages 211-285, ISSN 0306-26190306-261, http://www.sciencedirect .com / science /article/pii/030626 1996000013

[12] I. Richardson, M. Thomson, D. Infield, "A high-resolution domestic building occupancy model for energy demand simulations. Energy and Buildings", 40 (8), pp.1560-1566, 2008, http://hdl.handle.net/2134/3112

[13] S. Nisor, J. Wu, M. Sooriyabandara, "Cost optimization of smart appliances", IEEE, PES, conference 2011

ISBN 978-93-5156-328-0
International Conference of Advance Research and Innovation (ICARI-2014)

Comprehensive Study on Various Types of Particle Image Velocimetry with Explicit Instrumentation

Vishvendra Singh Tomar [a,*], Sahib Chawla [a], Vipul Sangwan [a], Raj Kumar Singh [a], Arun Dhyani [b]

[a] Department of Mechanical Engineering, Delhi Technological University, New Delhi, India
[b] Department of Electronics and Communication Engineering , Delhi Technological University, New Delhi, India

Article Info

Article history:
Received 29December 2013
Received in revised form
10 January 2014
Accepted 20 January 2014
Available online 1 February 2014

Keywords

Digital Particle Image Velocimetry
Cross-Correlation
Optical Measurements
FPGA
Ultrasonic Waves

Abstract

This paper reviews the recent advancements in Particle Image Velocimetry (PIV) along with the specific Instrumentation required. The conventional PIV systems often faced with various problems like longer time lag between pulses, object's shadow problem, opacity of the Test section, PIV errors, restricted Velocity range etc. To curb down these, various PIV systems have been proposed and still PIV is in development phase. Some of the recent developments discussed in this paper include Double-Wavelength Digital PIV, Ultrasonic or Echo PIV and PIV with three color pulsed lamps. To validate these systems, an efficient design and architecture for Real Time PIV based on FPGA technology has been discussed.

1. Introduction

Particle Image Velocimetry (PIV) has been a subject of exhaustive research and development since last three decades due to its ability to provide simultaneous data of the velocity distribution instead of a single point data, when compared with other measuring techniques. It is a whole field, non-intrusive instantaneous flow field measurement technique based on the direct determination of the two fundamental dimensions of the velocity: displacement and time.

In 1991, C. E. Willert set up a new PIV system in which, he substituted the analog camera with a CCD camera, enhancing the accuracy level of measurements. The new PIV system was termed as Digital Particle Image Velocimetry (DPIV). The basic principle of the PIV (Fig. 1.) is that a laser light sheet is used to illuminate the flow field which is seeded with small particles to visualize a flow to be measured. A double pulse YAG laser and a double shutter camera are synchronized to record two particle images with very short time separation. The observed tracer patterns at two subsequent instances are considered as the input and output of the system, and the velocity field is inferred from the analysis of the input and output signals. Cross-correlation algorithm is used to get the displacement of same particles in two images and the velocity of any point in the flow field is analyzed by the time interval between two images and movement of particles. Time interval of the two images should be as short as possible to improve the superior limit of measurable Velocimetry of DPIV system [1, 2].

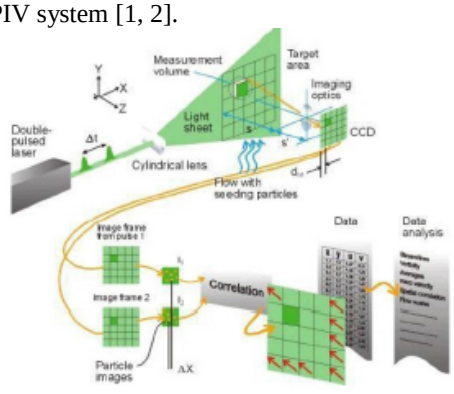

Fig: 1. Experimental Set-Up of DPIV

Corresponding Author,
E-mail address:vst.dtu@gmail.com
All rights reserved: http://www.ijari.org

The notable features of PIV includes: (a) Non-intrusive velocity measurement, (b) Indirect velocity measurement by measuring the velocity of tracer particles within the flow, (c) Whole field technique-allowing to record images of large parts of flow fields in a variety of applications in gaseous and liquid media, (d) Velocity lag between seeding particles and fluid flow, (e) Illumination-Using a high power light source for illumination of the tiny tracer particles in order to well expose the photographic film or the video sensor by scattered light, (f) Duration of illumination pulse-short enough to "freeze" the motion of the particles in order to avoid image blurring, (g) Time delay between illumination pulses-long enough to determine the displacement between the images and short enough to avoid particles with an out-of-plane velocity component leaving the light sheet between subsequent illuminations, (h) Distribution of tracer particles in the flow, (i) Density of tracer particle images, (j) Number of illuminations per recording, (k) Number of components of the velocity vector, (l) Extension of the observation volume, (m) Temporal resolution, (n) Spatial resolution and (o) Repeatability of evaluation. Therefore the PIV system must be designed and calibrated keeping in view the above mentioned features [3, 4].

2. Double-Wavelength PIV

These days, 'Frame Straddling' is the most extensively used technique for velocity measurement in DPIV, especially at high speeds. In Frame straddling (Fig. 2.), the first laser pulse is produced at the end of first exposure period of camera and the second one is produced at the beginning of the second exposure period by controlling time sequence between the pulsed laser and the special high speed cameras. These cameras can hold two images recorded in rapid succession by transferring the first image recorded by each pixel to on-chip storage well and then recording a second image which is quite expensive. Another restriction to its use is due to its limitation imposed by the frame rate of the cameras and laser pulses controlling.

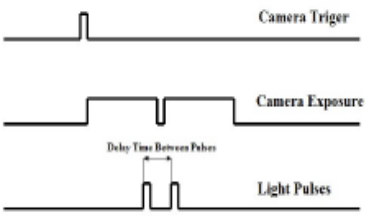

Fig: 2. Basic idea behind Frame-Straddling.

To enhance the superior limit of measurable Velocimetry of DPIV system, DPIV is supplemented with Double-Wavelength system (Fig. 3.). The basic idea behind this is, the light with different wavelengths propagates independently and thus, the two laser pulses can be separated by themselves which allows the use of several laser pulses with different wavelengths to illuminate flow field at different moments. Particle images are captured by different CCDs, each being sensitive to one certain wavelength. In this, the time interval between different particle images in multi-wavelength DPIV just depends on the pulse interval time of different wavelengths, and is independent of the frame rate of the camera leading to a shorter time interval [2-5].

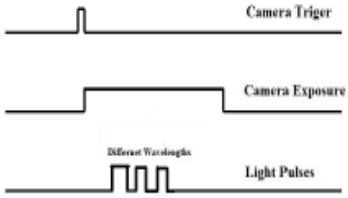

Fig: 3. Basic Idea behind Mullti-Wavelength DPIV.

Chunxiao et al [5] used two different wavelengths 650 nm and 532 nm pulsed lasers for experimental set up behaving as Double-Wavelength DPIV system (Fig. 4.).

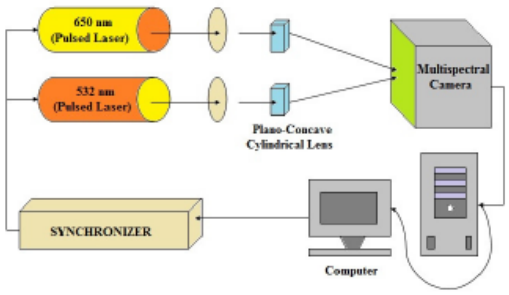

Fig: 4. Experimental Set-Up of Double-Wavelength DPIV.

It consisted of a color camera (RGB CCD), a synchronizer and a computer with frame grabber. A synchronize controls time sequence of the camera exposure and laser pulses. The computer sends a start signal to the synchronizer through the image grabber then synchronizer controls the camera to open the shutter which controls the lasers to generate laser pulses at different moments in one exposure time to illumine the flow field. Light entering the camera through the lens and is separated by a diachronic

prism. For selective selection of wavebands, optional narrowband filters were placed in front of the CCD arrays. The red CCD is only sensitive to 650nm light and the green one is only sensitive to 532nm light. Pixel data from each of the CCD arrays was digitized and processed by the Digital Signal Processing module separately. The cross-correlation method was incorporated to statistically determine the most probable displacement of a group of particles in a sampled area.

3. Ultrasonic or Echo PIV

An Ultrasound based Particle Image Velocimetry (Echo PIV) technique for opaque flow analysis consists of identifying and tracking a flow tracer (ultrasound contrast Micro-bubbles) within a flow field, and computing local velocity vectors. In Echo PIV, ultrasound imaging is achieved by sweeping a focused ultrasonic beam generated by ultrasound transducer through the desired field of view of the fluid. The Micro-Bubbles of gas seeded into the fluid flow scatter the ultrasonic beam and due to the huge acoustic impedance mismatch on the interface of bubble and fluid, the bubbles scatter strongly and shine acoustically in ultrasound field. This results in a clear brightness mode image of the particle positions with excellent signal to noise ratio. Following this, two sequential images are then subjected to image processing and data manipulation (Fig. 5.).

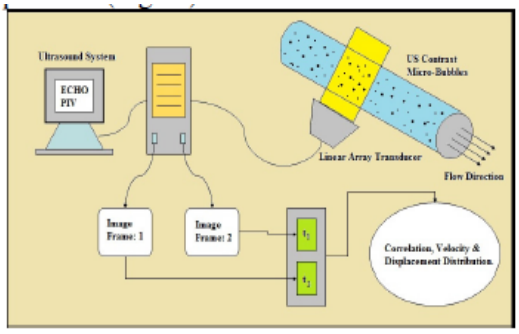

Fig: 5. Experimental Set-Up of Ultrasonic or Echo DPIV.

Using a Cross-Correlation algorithm between the two images, the displacement of the particles, velocity vector field can be evaluated depending on the time difference between the two images. Velocity fields from various flow patterns ranging from rotating flow, transient jet vortex to the flow around carotid plaques can be obtained with good spatial accuracy and dynamic velocity range using Echo PIV. One of the limitation faced by Echo PIV is, the ultrasound contrast micro-bubbles seeded in fluids usually decay with time because their instability in fluids and effect of ultrasonic force. But still, for opaque flow measurement this technique is one of the best, providing a very high degree of precision and accuracy. Moreover, controlled time-sensitive micro-bubble concentration can be varied, depending on the level of measurement required [6, 7].

4. PIV System Based on Three COLOUR Pulsed Lamps

The classical PIV with Laser [8] as illumination source is faced with so many challenges like expensive cost of experimental set-up (mainly due to Laser), its limits on the velocity range that can be measured simultaneously with adequate accuracy and the difficulty in using relatively thick light sheets. As a substitute of it, a simple PIV acquisition system with three colored halogen lamps as pulsed-light sources can be employed. The basic principle behind this is to us three light pulses which provides images of slow particles being well separated, in the long time interval, and images of fast particles being well resolved and maintained on the same image in the short time interval. This gives notably different populations of moving particles depending on their velocity. With such high velocity gradients, the classical correlation analysis can be applied to the whole field by widening the interrogation cell and reducing the velocity field resolution, or more complex evolutions of the correlation technique need to be used. The three flashes provide for two different time intervals between pulses which help in resolving of the low velocities with the same spatial resolution as for the high velocities. Among three lamps, there can be three time intervals available as: Δt_{RG},Δt_{RB} andΔt_{GB} = Δt_{RB} -Δt_{RG}. Hence, now three different velocities can be correlated, which is very helpful for in-cell validation of measurements (Fig. 6.).

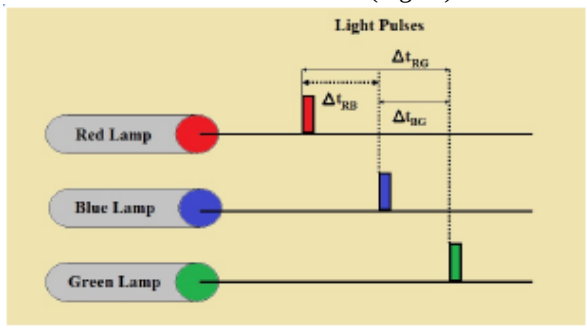

Fig: 6. Three time intervals generated by three lamps.

In the presence of large turbulent structures, the velocity component normal to the light sheet can be significant and the number of particles that remain in

the measurement sheet for several elementary measurement times depends on the thickness of the sheet. Due to the mono illumination source, part of the flow around an obstacle may be placed in a shadow region where the measurement is not possible. Using three colored lamps, problems due to shadows can be tackled.

5. PIV Based on FPGA

The PIV algorithms require the region captured on video frames to be divided into small rectangles called interrogation windows. During processing one velocity vector is associated to each rectangle. Subsequently, a uniform grid of results is provided as a practical set of data for post-computations. A smaller piece of one image, called particle image pattern A (PIPA), is extracted from one of those images and the second image is named AREAB. PIPA is compared to all possible sample-shift patterns of AREAB through a correlation formula (RAB) that is computed for each sample-shift [9].

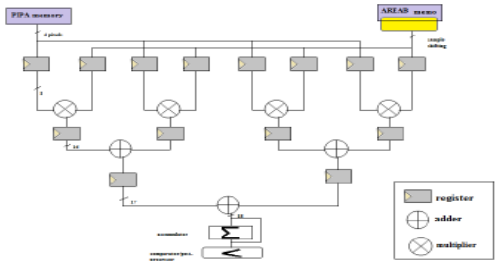

Fig: 7. Fundamental Processor (FP).

Thus, the sample-shift patterns of AREAB are sized like PIPA. Therefore, the peak position of the correlation map is used to search the displacement of particles between both images in the interrogation window. By assuming n = k. We also can define the side size of AREAB as m, with m >n. The architecture implemented in this work is shown in Fig. 7. and named as fundamental processor (FP). The number of multipliers per FP is set by FPGA resources characteristics. Each FP module has a post-processing unit that computes the position of the correlation maximum and may retain useful local data of the RAB map for the sub-pixel computation of the peak position. The critical FSM is named as process controller (PC).

6. Conclusions

The various types of PIV have been conferred, having certain advantages over conventional PIV. The problems like longer time lag between pulses, object's shadow problem, opacity of the Test section, PIV errors, restricted Velocity range etc are sorted out using explicit optical and electronics instrumentation as in Double-Wavelength PIV, Echo PIV and PIV system based on three color pulsed lamps. PIV, one of the best non-intrusive techniques, has got so much potential to generate more accurate and precise results. Further, the instrumentation described above provides it too much flexibility. PIV based on FPGA is described at last.

References

[1] "Particle image Velocimetry: a review", Fluid Loading and Instrumentation Centre, Heriot-Watt University, Edinburgh, Scotland

[2] Wei-Hsin Tien, Patrick Kartes, Toru Yamasaki. "A color-coded back-lighted defocusing digital particle image velocimetry system".ExpFluids, 2008, 44:1015–1026

[3] Wei Run-jie, SHEN Gong-xin. "The research of DPIV system and its application", Experiments and Measurements in Fluid Mechanics, Jun.2003, 17(2): 88-92

[4] R. J. Adrian. "Twenty Years of Particle Image Velocimetry", 12th International Symposium on Applications of Laser Techniques to Fluid Mechanics, Lisbon, July 2004:12-15

[5] "Double-wavelength Digital Particle Image Velocimetry", ChunxiaoTang, Enbang Li, School of Information and Communication Engineering, Tianjin Polytechnic University, Tianjin, China. 978-14577-0860-2/11, ©2011 IEEE

[6] H. B. Kim, J. R. Hertzberg, R. Shandas, "Development and validation of echo PIV," Experiments in Fluids, 36, pp. 455-462, 2004

[7] H. R. Zheng, L. L. Liu, L. Williams, J. R. Hertzberg, C. Lanning, R. Shandas, "Real time multicomponent echo particle image Velocimetry technique for opaque flow imaging," Applied Physics Letters, 88, 2006

[8] Sergio De Ponte, Stefano Malavasi, GianlucaGalzerano, CesareSvelto, Novel Particle Image Velocimetry System Based on Three-Color Pulsed Lamps and Image Processing IEEE Transactions On Instrumentation And Measurement, 53(1), February 2004 175

[9] José M. Iriarte Muñoz, DamiánDellavale, Maximiliano O. Sonnaillon, Fabián J. Bonetto, Real-Time Particle Image Velocimetry Based On Fpga Technology, 978-1-42443846-4/09, ©2009 IEEE

ISBN 978-93-5156-328-0
International Conference of Advance Research and Innovation (ICARI-2014)

Design, Analytical Analysis, Instrumentation and Cost Estimation of Sub-Sonic Open Circuit Wind Tunnel Model

Vishvendra Singh Tomar *,Vipul Sangwan, Raj Kumar Singh, Sahib Chawla
Department of Mechanical Engineering, Delhi Technological University, New Delhi, India

Article Info

Article history:
Received 29December 2013
Received in revised form
10 January 2014
Accepted 20 January 2014
Available online 1 February 2014

Keywords

Abstract

The Wind Tunnel is well known for its enormous amount of potential in Civil, Environmental, Automobile and Aeronautical applications. In today's world, Everyone's main focus is to save time, material and money which have compelled us to opt for the experimental testing on scale models, before the final product is to be shaped. The Wind Tunnel is one such platform, which provides us the appropriate desired environment conditions around the model scaled to the compatible dimensions. Therefore, to develop the favorable conditions, the design of the tunnel plays the foremost role in its proper functioning. In this paper, knowing the intricacy of the tunnel's requirements, A Sub-Sonic Open Circuit Wind Tunnel (SOWT) Model is developed having a Mach Number (M) of 0.15. The guiding dimensions taken for the Test Chamber are: Length (LT) = 45cm, Height (HT) = 18cm and Width (WT) = 24cm with maximum operating speed to be 50m/s. Using these, the secondary design parameters were estimated and the design is finalized. Moreover, the instrumentation of the Tunnel including Data Acquisition Systems (DAQs) is reviewed and the estimation of the cost for its fabrication is calculated.

1. Introduction

Today, the wind tunnel is an indispensable part of development of modern aircraft, automobile etc as no one would contemplate committing an advanced design without first measuring its stability, lift and drag properties. The utility of the wind tunnel is obvious, but it was not the first aerodynamic test device. The quest to measure drag and various aspects of aviation theory started with the very first advancement in aviation with the introduction to whirling arm. The whirling arm apparatus (4 feet long) was developed by Benjamin Robins (17071751), a brilliant English mathematician. It spun by a falling weight acting on a pulley and spindle arrangement having velocities of only a few feet per second at the arm tip (top speeds ranging from 3 to 6 m/s). The large amount of turbulence posed serious problems in front of experimenters like indetermination of the true relative velocity between the model and air. Also, it was difficult to mount the instruments and measure the small forces exerted on the model when it was spinning at high speeds. Francis Herbert Wenham (1824–1908), a council member of the Aeronautical Society of Great Britain, addressed the issue by inventing, designing and operating the first enclosed wind tunnel in 1871. After some of the experimental studies, it was found that lift-to-drag ratios were very high as such wings could support substantial loads, making powered flight which seemed much more attainable than previously thought possible. Further research work revealed the effect of what is now known as aspect ratio: long, narrow wings, like those on modern gliders, provided much more lift than stubby wings with the same areas [1-3].

Corresponding Author,
E-mail address:vst.dtu@gmail.com
All rights reserved: http://www.ijari.org

Nomenclature

a_N Coefficient of cubic fitting polynomial at narrow section

b_N Coefficient of cubic fitting polynomial at narrow section

c_N Coefficient of cubic fitting polynomial at narrow section

d_N Coefficient of cubic fitting polynomial at narrow section

a_W Coefficient of cubic fitting polynomial at wider section

b_W Coefficient of cubic fitting polynomial at wider section

c_W Coefficient of cubic fitting polynomial at wider section

d_W Coefficient of cubic fitting polynomial at wider section

l_D Diffuser Non-Dimensional Length

l_S Settling Chamber Non Dimensional Length

x_Nx- Coordinate at narrow section

y_Ny- Coordinate at narrow section

x_M x- Coordinate at midpoint of curve

y_My- Coordinate at midpoint of curve

xWx- Coordinate at wider section

y_Wy- Coordinate at wider section

θ Opening angle of Diffuser

α Contraction angle of Contraction cone

β Contraction angle of Contraction cone

ρ Density of fluid surrounding the airfoil

A_1 Projected area of the body on the top plane

A_2 Projected area of the body on the front plane

A_T Cross-Sectional Area of the Test Chamber

CCWT Closed Circuit Wind Tunnel

C_DCoefficient of Drag

C_LCoefficient of Lift

DAQ Data Acquisition System

F_D Force generated by Drag

F_L Force generated by Lift

H_T Test Chamber Height

i Angle of attack

L_C Contraction Cone Length

L_D Diffuser Length

L_S Settling Chamber Length

L_T Test Chamber Length

L_{WT} Wind Tunnel Length

LSWT Low Speed Wind Tunnel

M Mach Number

N Contraction ratio

OCWT Open Circuit Wind Tunnel

SOWT Sub-Sonic Open Circuit Wind Tunnel

SSWT Sub-Sonic Wind Tunnel

V_T Maximum Operating Velocity

W_T Test Chamber Width

Wilbur Wright (1867-1912) and Orville Wright (1871-1948) built their first flying machine in August 1899 and then their first unpowered manned glider in 1900. However, the glider was generating far less lift and more drag than they expected. They developed a simple experiment using natural winds to compare the relative lifting forces of flat and cambered surfaces. Then they built an aerodynamic balance that showed unambiguously, which test airfoil (among the two being tested) can develop more lift. Thus for the first time "Wind Tunnel without Walls" was subjected to test. It confirmed the accepted aerodynamic design tables that they were using, were seriously in error. This helped them in rectification of the wing area, airfoil curvature. During the experimental work, they reached at conclusion that without synthesizing a well equipped wind tunnel they could not continue their work anymore as such they developed the wind tunnel in its true sense and helped themselves to trigger the flight! [1, 4]

Wind tunnels are designed for a specific purpose and speed range. Therefore, there are different types of wind tunnels and several different ways to classify wind tunnels. On the basis of Speed Regime developed in the test section relative to the speed of sound (Mach Number 'M'), Wind Tunnels are classified as subsonic (M < 0.8), transonic (0.8 < M< 1.2), supersonic (1.2 < M <5.0), hypersonic (M >

5.0). On the basis of Tunnel Geometry, Wind tunnels are classified as Closed Circuit Wind tunnel (CCWT) and Open Circuit Wind Tunnel (OCWT) (Fig. 1.). A wind tunnel that is closed and re-circulates the air through the test section is called a Closed Circuit Wind Tunnel. A wind tunnel that is open on both ends and draws air from the atmosphere into the test section is called an Open Circuit Wind Tunnel [5, 6].

The OCWTs Models are used to investigate the different automotive designs by testing on scale models of cars, trucks etc. Airflow over a vehicle determines the drag forces, which in turn affects the vehicle's performance and efficiency. The three basic forces are lift, drag, and side force as measured in an axis system referenced to the direction of the vehicle. The concept of Lift and Drag can be understood with the help of airfoil. The airfoil long in the direction perpendicular to the plane of the drawing and the flow can be considered as two dimensional. The airfoil is tilted with respect to the (undisturbed) flow direction, defined by the angle of attack (AOA). The force experienced by airfoil is FR. Decomposing the force

ISBN 978-93-5156-328-0

FR into components FL and FD {Given by (1) and (2)} perpendicular and parallel to the flow direction. FL is termed as lift force and FD is termed as drag force, the resistance to be balanced by the propulsion force generated by the engines (Fig. 2.).

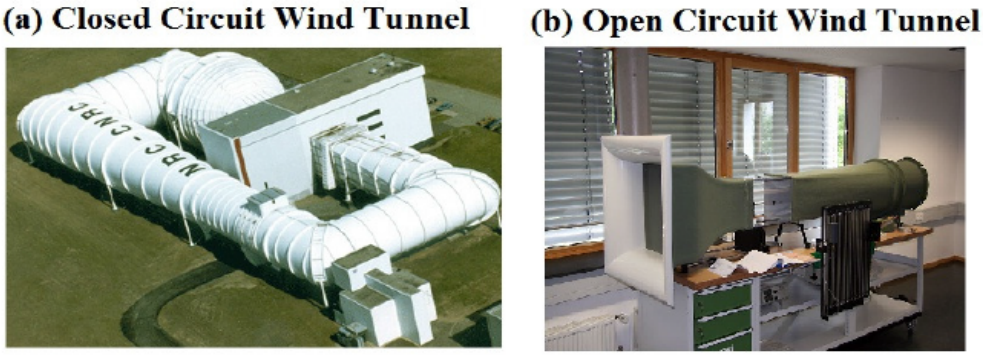

Fig: 1. Classification of Wind Tunnels on the basis of Tunnel Geometry as (a) Closed Circuit Wind Tunnel and (b) Open Circuit Wind Tunnel.

The expressions for Lift and Drag Forces are as follows:

$$F_L = 0.5\, C_L\, \rho\, A_1\, u^2 \quad \ldots.(1)$$
$$F_D = 0.5\, C_D\, \rho\, A_2\, u^2 \quad \ldots.(2)$$

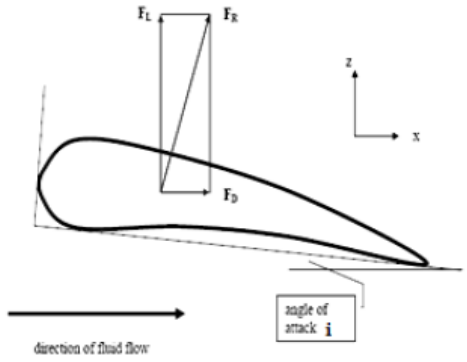

Fig: 2. Lift and Drag Forces on Airfoil subjected to fluid flow

The designer of an airplane tries to maximize CL and to minimize C_D. C_L and C_D are dependent on the angle of attack. Usually the C_L drops sharply and C_D increases strongly at i = 15° (approx.) [7].

Wind tunnels have been used widely to simulate airflow about complete aircraft, specific aircraft components, and to conduct fundamental research concerning flow phenomena related to flight for over a century. Wind tunnels are made in different shapes and sizes, from just 30 cm long to large enough to contain a passenger airplane. The various sorts of Wind Tunnels find potential applications in estimation of pollution dispersion level near the building, investigation of wind-driven rain and building envelop, various aspects of wind loading on roofs and wind effects on towers and bridges. In Wind Engineering, wind tunnel tests are used to measure the velocity around, and forces or pressures upon structures. Very tall buildings, buildings with unusual or complicated shapes (such as a tall building with a parabolic or a hyperbolic shape), cable suspension bridges or cable stayed bridges are analyzed in specialized atmospheric boundary layer wind tunnels. The basic idea behind all wind tunnels is universal. Depending upon the situations like thermal and hydraulic testing, it generates uniform air flows with low turbulence intensity. The aerodynamic principles of the wind tunnel work equally on watercraft, except the water is more viscous and so sets greater forces on the object being tested. External flow tunnels are used to study the external flow through the chassis climatic tunnels and used to evaluate the performance of door systems, braking systems etc. under various climatic conditions. Aero-acoustic tunnels are used in the studies of noise generated by flow and its suppression. Wind tunnel tests are also performed to measuring the air movement of the fans, Turbine Blades, Propellers etc at a specific pressure exactly [3, 8-12].

A lot of research work have been accomplished to optimize the Wind Tunnel Design and still to make it better at various levels depending upon the situations research work is still in progress. Peter et al. in their work, focused on the wind tunnel test section flow quality and its application to a numerical CCWT by studying the effects of various variables for its evaluation [8]. Diana et al. evaluated the design criteria that supported the choice of the original solution for potential application of a new large wind tunnel in Civil, Environmental and Aeronautical aspects and discussed the feasibility of a plant on the basis of experimental analysis on a 1:9 scale model [13]. Lohan [14] focused on the design and

application of LSWTs having well-defined, controllable, uniform flow of air for experimental and design validation purposes. Senol and Cinar with the help of Flow Simulation Fluent 6.0 program corrected the earlier developed design of a suction-type SOWT by simulating it in computer environment [15]. Eckert et al. discussed some Aerodynamic design guidelines and computer program for estimation of SSWT performance [16]. The enormous amount of research work and experiments undertaken in wind tunnels and their importance for human life motivated the high demands that are posed on optimum design level for Wind Tunnels against the minimum cost with optimum output. This paper deals with the Sub-Sonic Open Circuit Wind Tunnel (SOWT) with negligible effect of compressibility. Following the previous research works and significant guidelines related to design consideration, the design for SOWT Model is developed. The Mach Number of 0.15 allows it to use for aerodynamics tests and performance of some scale models having speeds around 150 km/hr.

2. Design of Sub-Sonic Open Circuit Wind Tunnel Model

The Wind tunnels cannot be perfect simulations of environmental conditions, but up to some extent they can be treated as ideal to surrounding conditions. The degree to which they are flawed is measured with the help of Reynolds Number. The SSWTs are designed to provide a well-defined, controllable, uniform flow of air for experimental and design validation purposes. These tunnels when applied as open circuit cannot be used where a very high accuracy level and precise results are required due to their inability to control air flow up to a large extent. However, with proper designs and controlled instrumentation, these tunnels can be made to produce accurate results within close limit to practical value. The major advantage associated with this tunnel is its Set-Up and Maintenance Cost, which is very small as compared to CCWT. The leading manufacturer of automobiles use the OCWTs for the Drag and performance estimation of the vehicles as with current technology &designs, these tunnels are giving results quite close to practical values under proper calibrations.

The OCWT (Fig. 3.) consists of five basic parts, which are (From front to back) the Settling Chamber, the Contraction Cone, the Test Section, the Diffuser and the Drive Section. The Settling Chamber is at the very front of the wind tunnel and is made up of screens and honeycomb-shaped mesh, which straighten out the air and reduce turbulence. The Contraction Cone forces a large volume of air through a small opening in order to increase the wind velocity in the tunnel, as there is gradual decrease in area. The Test Section is the place where a model is mounted on sensors. The Diffuser is at the end of the Test Section and keeps the air running smoothly as it goes toward the back. It also increases in volume in order to slow the air down as it exits the tunnel. The Drive Section is at the very back of the wind tunnel, and it is where the fan is housed and draws air into the wind tunnel by blowing air out of it and hence reduces turbulence along with greater control of the airflow through the tunnel. The decisive characteristic of wind tunnels lies in the flow quality inside the test chamber and the overall performances.

Three main criteria that are commonly used to define them are: maximum achievable speed, flow uniformity and turbulence level. Hence in general, the design aim of a wind tunnel is to get a controlled flow in the test chamber, achieving the necessary flow performance and quality parameters. The main specifications for a wind tunnel are the dimensions of the test section and the desired maximum operating speed. Also, it is crucial to avoid flow separation close to the walls of the contraction zone. In the subsequent sections, the design of each of the component of the Wind Tunnel is developed one by one, from the design of the Test Chamber to the Diffuser.

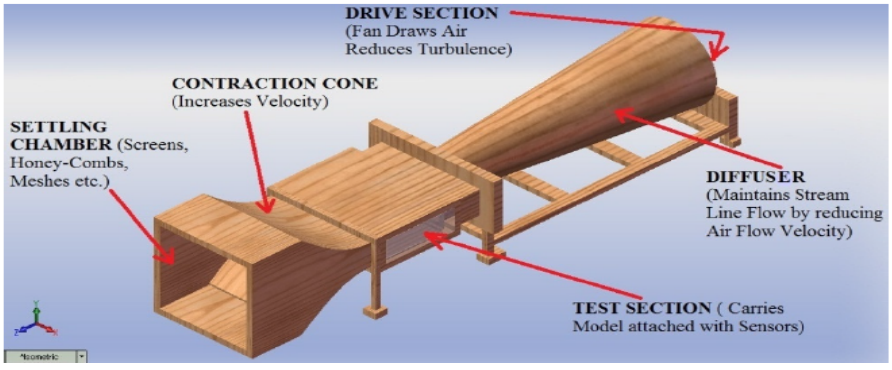

Fig: 3. Isometric View of Sub-Sonic Open Circuit Wind Tunnel Model developed Solid-Works

2.1 Test Chamber (T.C.)

The test chamber (Fig. 4.) is the most delicate part of the tunnel and is also called as "The Heart of the Wind Tunnel" as it is the region for experimental study, carrying the scale model, sensors etc along with the controlled flow. Its size must be defined according to the wind tunnel main specifications, which also include the operating speed and desired flow quality. Its size and operating speed determine the maximum size of the models and the maximum achievable Reynolds number.

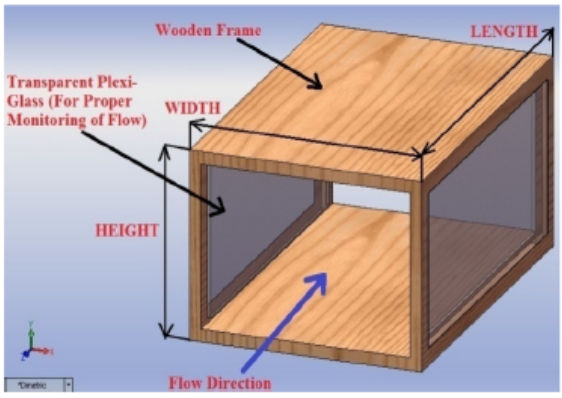

Fig: 4. Dimetric View of The Test Chamber developed using Solid-Works.

In most of the cases, its cross-section is square in shape and its area should be decided according to the scale model which is going to be tested. The equivalent frontal area of the model should not be higher than 10% of the test chamber cross-sectional area. The width to height ratio adopted for 3-D Tests is 4:3. The Test Section Assembly is composed of the Test Section (Plexiglas) to avoid pressure loss and the Test Section Base (wooden stand and sensor mounts) [14-19].

2.2 Contraction Cone (C.C.)

The Contraction Cone is the most important part in the design of a Wind Tunnel as it has the highest impact on the Test Chamber flow quality. It accelerates the flow from the Settling Chamber to the Test Chamber as such also known as 'Nozzle'. It also helps in reduction of flow turbulence and non-uniformities in the test chamber. The flow acceleration and non-uniformity attenuations mainly depend on the ratio of cross-section area of inlet to that of exit, termed as contraction ratio (N). Theoretically, the value of N should be as large as possible but it has an upper limit as it strongly influences the overall wind tunnel dimensions and hence its cost. For the Wind Tunnels used in civil or industrial applications, a contractions ratio between 4.0 and 6.0 may be sufficient reducing the flow turbulence and non-uniformities levels to the order of 2.0%, which is acceptable for many applications. Further with just one screen placed in the settling chamber it reduces to 0.5%. Even this is a very reasonable value for some aeronautical purposes.

$$\text{N (Contraction Ratio)} = \frac{\text{Area at entry of C.C.}}{\text{Area at exit of C.C.}} \quad \ldots (3)$$

The second characteristic of the contraction Cone is its shape, taking into account that the contraction is rather smooth. For this 1-D (One-Dimensional) approach to the flow analysis is applied to determine the pressure gradient along it. The important point of consideration is the pressure distribution on the contraction walls, as if it has some regions with adverse pressure gradient, it may produce local boundary layer separation which can increase the turbulence level considerably, resulting in poor flow quality in the test chamber. The solution to this is to make the ratio of the radius of curvature to the flow width about the same at each end. But at the upstream end the radius s of curvature cannot be too large as it leads to slow acceleration and therefore increased rate of growth of boundary-layer thickness which causes centrifugal instability in the tunnels having laminar flow. The contraction semi-angles: $\alpha/2$ and $\beta/2$ are taken to be e in the order of 12º, this causes the contraction cone e to possess a reasonable length and a good fluid dynamic behavior. Bradshaw et al. recommended two segments of third degree polynomial curves for deciding the exact curve (Fig. 55.) for the Contraction Cone [14-20]. The polynomials are:

$$y = a_W + b_W x + c_W x^2 + d_W x^3 \quad \ldots.(4)$$
$$y = a_N + b_N x + c_N x^2 + d_N x^3 \quad \ldots.(5)$$

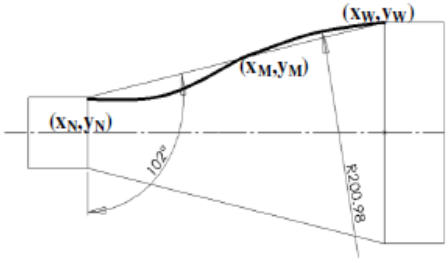

Fig: 5. Fitting Polynomial for the Contraction n Cone Curve developed using Solid-Works.

The Contraction Cone developed using the above curve (Fig. 6.) doesn't allow boundary layer to separate and keep boundary layer thickness within certain limit. It provides the favorable flow to the Test Chamber.

ISBN 978-93-5156-328-0

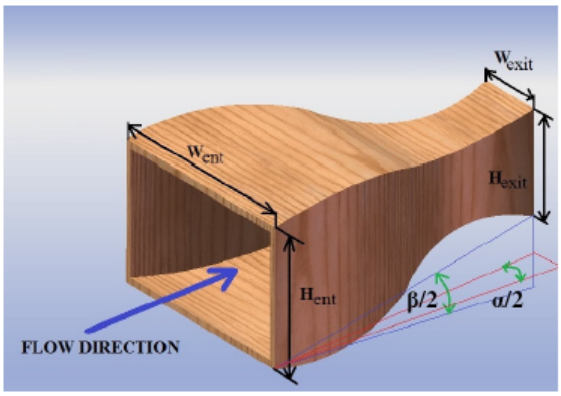

Fig: 6. Isometric View of The Contraction Co one developed using Solid-Works.

2.3 Settling Chamber

The Settling Chamber (Fig. 77.) is the very first region designed to provide controlled high quality flow to the Contraction Cone by attenuating the various flow components responsible for turbulence. To develop high quality flow some devices like screens and honeycombs etc are installed to increase the flow uniformity and to reduce the turbulence level at the entrance of the contraction cone. They produce a relatively high total pressure loss. Honeycomb b is very efficient at reducing the lateral turbulence e, as the flow pass through long and narrow pipes. But the problem with Honeycombs is, it introduces axial turbulence of the size equal to its diameter r which restrains the thickness of the honeycomb b. To tackle this problem, Screens are introduced as they reduce longitudinal turbulence very efficiently. In this case, the problem is that in th he Contraction Cone the lateral turbulence is less attenuated than the longitudinal one. Hence, to obtain better flow characteristics, a combination o of Honeycombs and Screens is used. This configuration requires the honeycomb to be located upstream of 1 or 2 screens [14-21].

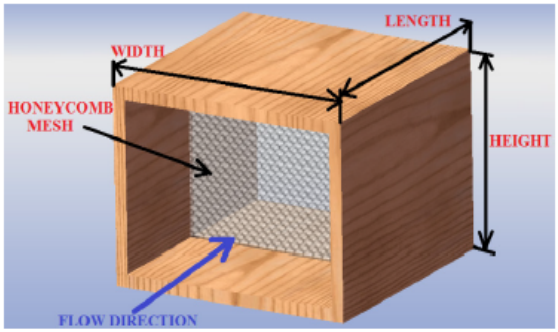

Fig: 7. Isometric View of The Settling Chamber developed using Solid-Works.

2.4 Diffusers

The Diffuser (Fig. 8.) plays an important role in controlling the flow quality inside the Test Chamber by avoiding the flow detachment as in case of flow detachment; the pressure pulsation is transmitted upstream into the test chamber, resulting in pressure and velocity non-uniformities. To avoid flow detachment, the maximum semi-opening angle in the diffuser has to be smaller than 3.5° [14-21].

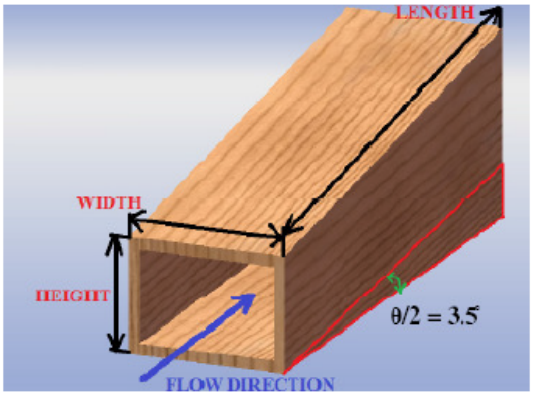

Fig: 8. Dimetric View of The Diffuser developed using Solid-Works.

3. Analysis of Sub-Sonic Open Circuit Wind Tunnel Model

The Primary Design Parameters for the overall design of the Wind Tunnel include Test chamber dimensions i.e. Width (W_T), Height (H_T) and length (L_T). With the help of these parameters cross-sectional area of the Test Chamber can be calculated as $A_T = W_T.H_T$. The hydraulic diameter is given by the relation [14-21].

$$D_T = \frac{2\,W_T\,H_T}{(W_T + H_T)} \qquad \ldots(6)$$

The Contraction ratio (N) is taken 5 for the Wind Tunnel with Mach number (M=0.15), having Maximum operating speed (VT) to be 50 m/s. These Design variables can be summarized in the Table. 1. The dimensions for the Test Section are W_T = 24cm, H_T = 18cm, L_T = 45cm and the V_T is taken to be 50m/s which gives us the Mach Number (M) to be 0.15. So, The Designing of all other parts is done based on these dimensions with N = 5. The semi angle in the Contraction Cone (α/2) is taken as 12° and the semi angle in the Diffuser (θ/2) is taken as 3.5°. The non-dimensional lengths for the Settling Chamber (l_S) and Diffuser (l_D), for Sub-Sonic Open Circuit Flow,

ISBN 978-93-5156-328-0

are taken as 0.5 and 3.2 respectively. The calculated parameters are displayed in Table.2. And the final design for this analytical analysis is represented by (Fig. 9). The total length of the SOWT is:

$L_{WT} = L_S + L_C + L_T + L_D$ ….(7)

$L_{WT} = 26.83 + 45 + 69.78 + 76.80 = 218$cm

Hence, L_{WT} is equal to 218cm.

Table: 1. The primary and secondary design parameters required for designing of SOWT Model.

PRIMARY DESIGN PARAMETERS	SECONDARY DESIGN PARAMETERS
Test Chamber Width (W_T)	Semi Angle In Contraction Cone ($\alpha/2$)
Test Chamber Height (H_T)	Semi Angle in Diffuser ($\theta/2$)
Test Chamber Length (H_T)	Settling Chamber Non Dimensional Length (l_S)
Contraction Ratio (N)	Diffuser Non Dimensional Length (l_D)
Maximum Operating Speed (V_T)	Settling Chamber Length (L_S)
Mach Number (M)	Contraction Cone Length (L_C)
	Diffuser Length (L_D)

Table: 2. Secondary design Parameters of SOWT Model.

Secondary Parameters	Expressions	Values
Cross-Sectional Area of the Test Chamber (A_T)	$A_T = W_T H_T$	432 cm^2
Hydraulic Diameter of the Test Chamber (D_T)	$D_T = \frac{2W_T H_T}{W_T + H_T}$	20.57 cm
Length of The Contraction Cone (L_C)	$L_C = \frac{(\sqrt{N} - 1) W_T}{2\tan(\alpha/2)}$	69.78 cm
Length of The Settling Chamber (L_S)	$L_S = \sqrt{N}\, W_T l_S$	26.83 cm
Length of The Diffuser (L_D)	$L_D = W_T l_D$	76.80 cm

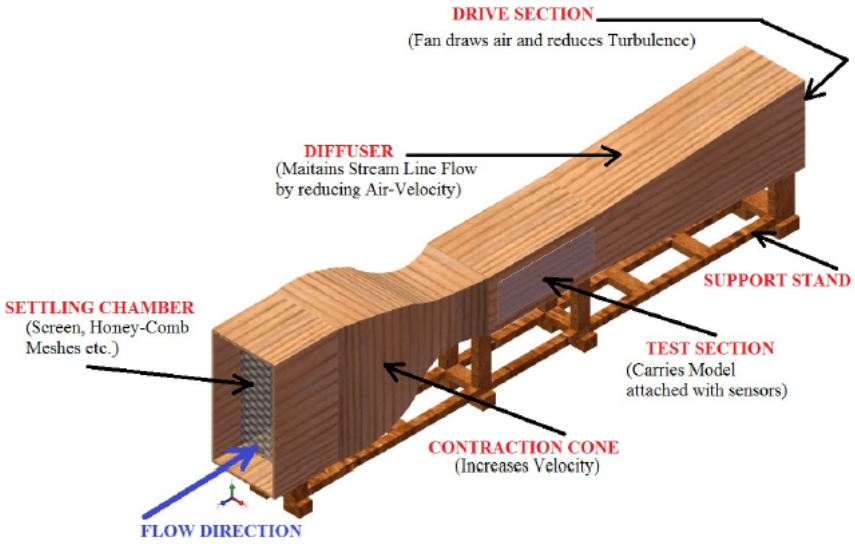

Fig: 9. Isometric View of the complete model of SOWT developed using Solid-Works

4. Instrumentation of Sub-Sonic Open Circuit Wind Tunnel Model

The instrumentation of wind tunnel emphasizes on the various instruments and Data Acquisition Systems (DAQs) required by a tunnel for its proper

functioning, Pressure and Flow measuring ability, Flow Visualization and Image Acquisition. In the instrumentation of the tunnel, Standard data acquisition (DAQ), Motion Control, and Image Capture hardware play a very crucial role. Data acquisition is the process of sampling signals that measure real world physical conditions and converting the resulting samples into digital numeric values that can be manipulated by a computer. Data acquisition systems convert analog waveforms into digital values for processing. The various components of data acquisition systems are Sensors (convert physical parameters to electrical signals), Signal conditioning circuitry (convert sensor signals into a form that can be converted to digital values) and Analog-to-Digital converters (convert conditioned sensor signals to digital values). Further, various operations can be integrated to the system including Flow Visualization with Image Acquisition, Multipoint differential pressure scanning, Hot Wire Anemometry, Force and Moment measurement using internal balances, Roll, Pitch and Yaw angle measurements, and Noise and Temperature measurements. For Pressure and Flow Measurements, measuring devices coupled with DAQs like Lab VIEW and pressure scanners etc. can be used. Similarly for Force and Moment Measurements, Six-component Strain Gauge Balances can be applied. And for Flow Visualization and Image Acquisition, light sheets using Argon-ion lasers with CCD cameras and recording system can be used to capture and analyze the exact trajectory of flow particles, even sometimes incorporating IMAQ hardware and software (IMAQ vision). With such a proper design and proper instrumentation, a wind tunnel can be used for Full-model tests with sting support mechanism, Half-model testing with external balance, Two-dimensional model testing, Ground effect simulation with moving belt, Gust and cross wind simulation, Aero-acoustic testing etc. For a Wind Tunnel with M < 0.3, the instrumentation required is not so much complex but still it requires attention for getting accurate and precise results [22-26].

5. Cost Evaluation

The cost of fabricating the Wind Tunnel designed above depends majorly on the cost of Plexiglas Sheets required for the Test Chamber, the Plywood required for the other sections and the Driving Fan. The various auxiliary components like Screens, Honey-comb Mesh etc cannot be neglected for its proper functioning but can be replaced by other temporary substitutes possible like thin wire sheets otherwise they add to the final cost. A rough estimate of some of the major components required is described in the Table. 3. (Taken on the September, 2013 New Delhi, India Market prices). Also the tertiary components required during the tunnel fabrication includes adhesive rubber, gasket stripping, springs, soldering materials, egg crate mesh board, electrical wiring materials, saws, drill, screws, wood screws, nuts, bolts, washers, lock washers, screwdrivers, related materials, wood glue etc which occupies 30% of the total cost of fabrication.

Table: 3. Cost estimation of Major Components required for the fabrication of SOWT Model (Taken on September, 2013, New Delhi, India)

MATERIALs	QUANTITY	COST
Plexiglass sheet, 2' x 4'	1	Rs. 1000
Plywood board, 4' x 8'	1	Rs. 1750
Plywood board, 17" x 17"	1	Rs. 325
Fan with blade diameter of 14 in. and entire-fan diameter no greater than 17 in.	1	Rs. 2000
Oakboards2'x4' (plywood boards)	4	Rs. 800
Cut of wire sheet, enough to cover a 17" x 17" area	-	Rs. 600
TOTAL		Rs. 6475

6. Conclusion

The design of Low Cost SOWT model has been generated. The main considerations like Boundary Layer Separation, Controlled Air Flow Quality, Turbulence Intensity, Stream Line Flow, Cost-Effectiveness, Design Ease and Mach Number (M = 0.15) etc were taken into the account and accordingly the model is designed. The primary design parameters of the Test Chamber were taken as the baseline and following the design guidelines, the secondary design parameters for approximately 220 cm tunnel were calculated. The Contraction Cone and the Test Chamber section were given special attention as they have direct influence on the scale model testing and the data generated. A brief insight is given to the instrumentation segment of the tunnel, especially to the various measurements and DAQs that are still playing their part in research and development concerning the various wind tunnel applications.

References

[1] M. G. Dodson, "An Historical and Applied Aerodynamic Study of the Wright Brothers", Wind Tunnel Test Program and Application to Successful Manned Flight, US Naval Academy Technical Report, USNA-334, 2005

[2] Whirling Arms and the First Wind Tunnels, Wind Tunnels of NASA by Donald D. Baals and William R. Corliss, (Searched on Sept 1, 2013) http://www.grc.nasa.gov/WWW/k12/WindTunnel/ history.html

[3] History, Origins of Wind Tunnel, NASA Aeronautics and Space Administration, http://en.wikipedia.org/wiki/Wind_tunnel (Searched on Sept 1, 2013).

[4] Wright Brothers, National Memorial, Wind Tunnel Tests 1901, (Searched on Sept 1, 2013) http://www.cr.nps.gov/history/online_books/hh/34/ hh34i.htm.

[5] Types of Wind Tunnels, "NASA Aeronautics and Space Administration", (Searched on Sept 1, 2013)http://www.grc.nasa.gov/WWW/k12/airplane /tuntype.html

[6] Science Buddies: How to Build a Subsonic Wind Tunnel (Searched on Sept 1, 2013) http://www.sciencebuddies.org/sciencefairprojects/wind-tunnel-toc.shtml

[7] A Textbook of Fluid Mechanics and Hydraulic Machines, Dr. R. K. Bansal, Laxmi Publications Pvt. Ltd., New Delhi, Forces on Submerged Bodies, Page No. 657-659.

[8] Peter Moonen, Bert Blocken, Jan Carmelieta, Indicators for the evaluation of wind tunnel test section flow quality and application to a numerical closed-circuit wind tunnel, Journal of Wind Engineering and Industrial Aerodynamics 95 (2007) 1289–1314

[9] AlyMousaad, Alberto Zasso and FerruccioResta (2011), On the dynamics of a very slender building under winds: reponse reduction using MR dampers with lever mechanism, The Structural Design of Tall and Special Buildings.

[10] Windless Wind Tunnels for High Altitude Tests, Popular Mechanics, February 1952, Page No-105.

[11] J. E. Cermak, "Wind tunnel for the study of turbulence in the atmospheric surface layer", Final Report Air Force Cambridge Center, Air Research and Development Command, Bedford, MA (Contract AF 19(604)-1706), 1958, 36 pages.

[12] R. E. Whitbread, "The measurement of non-steady wind forces on small-scale building models", in: Proceedings of the fourth International Conference on Wind Effects on Buildings and Structures, Heathrow, England, 1975, pages-567– 574

[13] G. Diana, S. De Ponte, M. Falco, A. Zasso, "A new large wind tunnel for civil-environmental and aeronautical applications", Journal of Wind Engineering and Industrial Aerodynamics 74-76 (1998) 553-565

[14] John Lohan, PhD, "Article on Design and Applications of Low Speed Wind Tunnels", Galway-Mayo Institute of Technology (GMIT), Dublin Road, Galway, Ireland

[15] Serhat Senol, Ali Cinar, "Design and Flow Simulation of an Open Circuit Wind Tunnel", EnginSoft International Conference 2009 1st-2nd Oct. 2009

[16] W. T. Eckert, K. W. Mort, J. Jope, Aerodynamic design guidelines and computer program for estimation of subsonic wind tunnel performance, NASA technical note / D-8243, NASA Washington, 1976

[17] E. C. A Maskell, "Theory of the blockage effects on bluff bodies and stalled wings in a closed wind tunnel", R. & M. 3400, November, 1963

[18] The Royal Aeronautical Society, "Wind tunnels and wind tunnel test techniques", Royal Aeronautical Society London, 1992

[19] R. D. Mehta, P. Bradshaw, "Design Rules for Small Low-Speed Wind Tunnels", Aero. Journal, (Royal Aeronautical Society), (1979), 73, 443

[20] G. G. Borger, "The optimization of wind tunnel contractions for the subsonic range", NASA Technical Translation / F-16899, NASA Washington, 1976

[21] J. Scheiman, "Considerations for the installation of honeycomb and screens to reduce wind-tunnel turbulence", NASA Technical Memorandum / 81868, NASA Washington, 1981

[22] S. M. Gorlin, I. I. Slezinger, "Wind tunnels and their instrumentation", Israel Program for Scientific Translations Jerusalem, 1966

[23] Data Acquisition, (Searched on Sept 15, 2013) http://en.wikipedia.org/wiki/Data_acquisition

[24] Kamal Poddar, Sanjay Gupta, "Instrumentation for National Wind Tunnel Facility", IIT Kanpur

[25] J. B. Barlow, W. H. Rae, A. Pope, "Low-speed wind tunnel testing", John Wiley & Sons New York, 1999

[26] Sub-Sonic Wind Tunnels and Instrumentation, www.aerolab.com, 301-776-6585 Laurel, Maryland, USA

ISBN 978-93-5156-328-0
International Conference of Advance Research and Innovation (ICARI-2014)

Economic Load Dispatch Problem and Mat lab Programming of Different Methods

Rahul Dogra [a,*], Nikita Gupta [b], Harsha Saroa [b]
[a] Siemens Limited India, India
[b] Department of Power Systems, Delhi Technological University, Delhi, India

Article Info

Article history:
Received 29 December 2013
Received in revised form
10 January 2014
Accepted 20 January 2014
Available online 1 February 2014

Keywords
Economic Load Dispatch
Fuel Cost
Lambda Iteration Crankshaft

Abstract

Economic Load Dispatch (ELD) is one of an important optimization tasks and operational decision which provides an economic condition for power systems. This paper presents overview of economic load dispatch problems and solution methodologies. MATLAB programming of different methods used for solving economic load dispatch problem was done and results are given in tabular form. Lambda iteration method is implemented for three cases of

- Without generation limits and losses
- With generation limits and without losses and
- With generation limits and losses. Newton's and the dynamic programming methods were put into action for coding.

1. Introduction

The efficient and optimum economic operation of electric power systems has always occupied an important position in electric power industry. In recent decades, it is becoming very important for utilities to run their power systems with minimum cost while satisfying their customer demand all the time and trying to make profit. With limited availability of generating units and the large increase in power demand, fuel cost and supply limitation, the committed units should serve the expected load demand with the changes in fuel cost and the uncertainties in the load demand forecast in all the different time intervals in an optimal manner[1],[2],[3]&[4].

The basic objective of ELD of electric power generation is to schedule the committed generating unit outputs, so as to meet the load demand at minimum operating cost while satisfying all unit and system equality and inequality constraints. The ELD problem has been tackled by many researchers in the past. ELD problem involves different problems. The first is Unit Commitment or pre-dispatch problem where in it is required to select optimally out of the available generating sources to operate to meet the expected load and provide a specified margin of operating reserve over a specified period of time. The second aspect of ELD is on-line economic dispatch where in it is required to distribute the load among the generating units actually parallel with the system in such a manner as to minimize the total cost of supplying power. In case of ELD, The generations are not fixed but they are allowed to take values again within certain limits so as to meet a particular load demand with minimum fuel consumption [5], [6].

Corresponding Author,
E-mail address: guptanikita08@gmail.com
All rights reserved: http://www.ijari.org

2. Problem Formulation

The ELD problem is defined as to minimize the total operating cost of a power system while meeting the total load plus transmission losses within generator limits. Mathematically the problem is defined as (including losses) by equation (1) given as [1]

Minimize:

$$F_i(P_i) = \sum_{i=1}^{n_g} (\gamma_i P_i^2 + \beta_i P_i + \alpha_i) \quad (1)$$

Subject to (1) the energy balance equation

$$\sum_{i=1}^{n_g} P_i = P_D + P_L \quad (2)$$

(2) the inequality constraints

$$P_{i(min)} \leq P_i \leq P_{i(max)} \quad (3)$$

Where α_i,β_i, γ_i are cost coefficients , P_D is load demand, P_i is real power generation, P_L is power transmission loss and n_g is number of generation busses.

One of the most important, simple but approximate method of expressing transmission loss as function of generator powers is through B-coefficients. This method uses the fact that under normal operating condition, the transmission loss is quadratic in the injected bus real power. The general form of the loss formula using B-coefficient is given by eqn(4)

$$P_L = \sum_{i=1}^{n_g}\sum_{j=1}^{n_g} P_i B_{ij} P_j \quad \text{MW} \qquad (4)$$

Where P_i, P_j are real power injection at the i^{th}, j^{th} buses and B_{ij} are loss coefficients which are constant under certain assumed conditions [8], [9], & [11]. The above loss formula is known as the George's formula. Another more accurate form of transmission loss expression, frequently known as the Kron'lossf ormula is eqn (5)

$$P_L = \sum_{i=1}^{n_g}\sum_{j=1}^{n_g} P_i B_{ij} P_j + \sum_{i=1}^{n_g} B_{0i} P_i + B_{00} \quad \text{MW} \qquad (5)$$

where, B_{00}, B_{i0}, and B_{ij} are the loss coefficient which are constant under certain assumed conditions. The above constrained optimization problem is converted into an unconstrained optimization problem. Lagrange multiplier method is used in which a function minimized (or maximized) is subjected to side conditions in the form of equality constraints. Using Lagrange multipliers, an augmented function is defined by eqn (6)

$$L(P_i, \lambda) = F(P_i) + \lambda(P_D - P_L - \sum_{i=1}^{n_g} P_i) \qquad (6)$$

Where, λ is the Lagrangian multiplier. Necessary conditions for the optimization problem are

$$\frac{\partial L(P_i,\lambda)}{\partial P_{i'}} = \frac{\partial F(P_i)}{\partial P_i} + \lambda\left(\frac{\partial P_L}{\partial P_i} - 1\right) = 0, \ (i = 1, 2 \ldots n_g) \qquad (7)$$

Rearranging the above equation

$$\frac{\partial F(P_i)}{\partial P} = \lambda_i\left(1 - \frac{\partial P_L}{\partial P_i}\right), \ (i=1, 2, 3 \ldots n_g) \qquad (8)$$

Where, $\frac{\partial F(P_i)}{\partial P_i}$: Incremental cost of the i^{th} generator (Rs/MW h) Equation (9) is known as the exact coordination equation and

$$\frac{\partial L(P_i,\lambda)}{\partial \lambda} = P_D + P_L - \sum_{i=1}^{n_g} P_i = 0 \qquad (9)$$

By differentiating the transmission loss eqn (5) with respect to P_i, the incremental transmission loss can be obtained as

$$\frac{\partial P_L}{\partial P_i} = \sum_{j=1}^{n_g} 2 B_{ij} P_j \qquad (10)$$

and by differentiating the cost function of Eqn (1) with respect to P_i , the incremental cost can be obtained as

$$\frac{\partial F(P_i)}{\partial P_i} = 2\gamma_i P_i + \beta_i, \ (i=1, 2, 3 \ldots\ldots\ldots n_g) \qquad (11)$$

to find the solution $2\gamma_i P_i + \beta_i = \lambda(1 - 2\sum_{i=1}^{n_g} B_{ij} P_j)$

$(i=1, 2, 3 \ldots\ldots\ldots n_g)$ (12)

Rearranging the eqn(12) to get P_i, i.e.

$$2\gamma_i P_i + \beta_i = \lambda(1 - 2b_{ij} P_i - \sum_{i=1}^{n_g} 2 B_{ij} P_j)$$

$(i=1, 2, 3 \ldots\ldots\ldots n_g)$

$$2(\gamma_i + \lambda b_{ij}) P_i + 2\sum_{j=1}^{n_g} B_{ij} P_j = (\lambda - \beta_i)$$

$(i=1, 2, 3 \ldots\ldots\ldots n_g)$ (13)

The above linear eqn(13) can be solved to obtain the value of P_i if λ is known.

3. Lambda Iteration Method

The solution to this problem can be approached by considering a graphical technique for solving the problem and then extending this into the area of computer algorithms. The lambda-iteration procedure converges very rapidly for this particular type of optimization problem. The actual computational procedure is slightly more complex [1], [12].

We use following MATLAB code formulated for no losses and no generation losses as:

```
for i=1:3
n(i)=(f(i,2)/(2*f(i,3)));
p(i)=(1/(2*f(i,3)));
end
m=sum(n);
q=sum(p);
lambda = ((Demand+m)/q);
disp(lambda)
for i=1:3
P(i)=((lambda-f(i,2))/(2*f(i,3)));
end
P
for i=1:3
   totalcost=(f(i,1)+(f(i,2)*P)+(f(i,3)*P*P));
end
```

For inclusion of losses:

```
Ploss = 0.00003*P
(1,1)^2+0.00009*P(1,2)^2+0.00012*P(1,3)^2
for j=1:4
for i=1:3
n(i)=f(i,2)/(2*f(i,3));
w(i)=(1-(2*PL(1,i)*P(1,i)))/(2*f(i,3));
end
m=sum(n);
q=sum(w);
lambda=(PD+Ploss+m)/q
for i=1:3
P(i)=(lambda*(1-2*PL(1,i)*P(1,i))-f(i,2))/(2*f(i,3));
end
j=j+1;
end
    disp(P)
```

4. Newton's Method

The economic dispatch can also be solved by observing that the aim is to always drive

$$\nabla L_x = 0 \quad (14)$$

Since this is a vector function, the problem can be formulated as one of finding the correction that exactly drives the gradient to zero (i.e., to a vector, all of whose elements are zero). Newton's method can be used to find this. Newton's method for a function of more than one variable is developed as follows [1], [13]&[14].

Suppose for the function **g(x)** to be driven to zero. The function **g** is a vector and the unknowns, **x,** are also vectors. Then, to use Newton's method eqn(15):

$$g(x+\Delta x) = g(x) + [g'(x)]\Delta x = 0 \quad (15)$$

If the function is defined as:

$$g(x) = \begin{bmatrix} g_1(x_1, x_2, x_3) \\ g_2(x_1, x_2, x_3) \\ g_3(x_1, x_2, x_3) \end{bmatrix}$$

then

$$g'(x) = \begin{bmatrix} \frac{\partial g_1}{\partial x_1} & \frac{\partial g_1}{\partial x_2} & \frac{\partial g_1}{\partial x_3} \\ \frac{\partial g_2}{\partial x_1} & \frac{\partial g_2}{\partial x_2} & \frac{\partial g_2}{\partial x_3} \\ \frac{\partial g_3}{\partial x_1} & \frac{\partial g_3}{\partial x_2} & \frac{\partial g_3}{\partial x_3} \end{bmatrix}$$

Which is the familiar Jacobian matrix. The adjustment at each step is then $\Delta x = -[g'(x)]^{-1} g(x)$

Now, if the g function is the gradient vector ∇L_x , then $\Delta x = -inv\left[\frac{\partial}{\partial x}\nabla L_x\right] . \Delta L$

For economic dispatch problem this takes the form eqn(16):

$$L = \sum_{i=1}^{N} F_i(P_i) + \lambda(P_{load} - \sum_{i=1}^{N} P_i) \quad (16)$$

and ∇L is as it was defined before. The Jacobian matrix now becomes one made up of second derivatives and is called the Hessian matrix:

$$\left[\frac{\partial}{\partial x}\nabla L_x\right] = \begin{bmatrix} \frac{d^2L}{dx_1^2} & \frac{d^2L}{dx_1 dx_2} \cdots \\ \frac{d^2L}{dx_2 dx_1} & \cdots \\ \vdots & \vdots \\ \frac{d^2L}{d\lambda dx_1} & \cdots \end{bmatrix}$$

Generally, Newton's method will solve for the correction that is much closer to the minimum generation cost in one step than would the gradient method.

We use following MATLAB code formulated as:

```
Alpha=X;
Beta =Y;
Gamma =Z;
Lambda=input ('Enter the value of lambda :');
P_load=A
P_sum=sum(P_initial(1)+P_initial(2)+P_initial(3))
%.....Formation of Hessian Matrix.....
for i=1:3
   L(i)=beta(i)+2*gamma(i)*P_initial(i);
end
dellambda=[L(1)-Lambda;L(2)-Lambda;L(3)-
Lambda;P_load-P_sum]
G=2*gamma;
H= [G(1) 0 0 -1;0 G(2) 0 -1;0 0 G(3) -1;-1 -1 -1 0]
M= inv(H)
delp_Power=-(M*dellambda)
Lambda_optimal=delp_Power(4)

P_optimal=(P_initial')+delp_Power;
```

5. Dynamic Programming Method

The application of digital methods to solve a wide variety of control and dynamics optimization problems in the late 1950s led Dr. Richard Bellman and his associates to the development of dynamic programming. These techniques are useful in solving a variety of problems and can greatly reduce the computational effort in finding optimal trajectories or control policies. The theoretical mathematical background, based on the calculus of variations, is somewhat difficult. The applications are not, however, since they depend on a willingness to express the particular optimization problem in terms appropriate for a dynamic-programming (DP) formulation [1].

In the scheduling of power generation systems, DP techniques have been developed for the economic dispatch of thermal systems, the solution of hydrothermal economic-scheduling problems and the practical solution of the unit commitment problem. If valve points are considered in the input-output curve, the possibility of non-convex curves must be accounted for if extreme accuracy is desired. If non-convex input-output curves are to be used, an equal incremental cost methodology cannot be used since there are multiple values of MW output for any given value of incremental cost.

Under such circumstances, there is a way to find an optimum dispatch which uses dynamic programming (DP). The dynamic programming solution to economic dispatch is done as an allocation problem. Using this approach, not just a single optimum set of generator MW outputs is calculated for a specific total load supplied-rather a set of outputs are generated, at discrete points, for an entire set of load values[16]. One problem that is common

to economic dispatch with dynamic programming is the poor control performance of the generators. When the economic dispatch is to be done with dynamic programming and the cost curves are non-convex, a difficult problem is encountered whenever a small increment in load results in a new dispatch that calls for one or more generators to drop their output a great deal and others to increase a large amount. The resulting dispatch may be at the most economic values as determined by the DP, but the control action is not acceptable and will probably violate the ramp rates for several of the units.

The only way to produce a dispatch that is acceptable to the control system, as well as being the optimum economically, is to add the ramp rate limits to the economic dispatch formulation itself. This requires a short-range load forecast to determine the most likely load and load-ramping requirements of the units. This problem can be stated as follows [17], [18].

Given a load to be supplied at time increments $t = 1 \ldots t_{max}$, with load levels of P_{load}^t and N generators on-line to supply the load:

$$\sum_{i=1}^{N} P_i^t = P_{load}^t \quad (17)$$

Each unit must obey a rate limit such that:

$$P_i^{t+1} = P_i^t + \Delta P_i$$

And $-\Delta P_i^{max} \leq \Delta P_i \leq \Delta P_i^{max}$

Then the units must be scheduled to minimize the cost to deliver power over the time period as:

$$F^{total} = \sum_{t=1}^{T_{max}} \sum_{i=1}^{N} F_i(P_i^t) \quad (18)$$

Subject to: $\sum_{i=1}^{N} P_i^t = P_{load}^t \quad for\ t = 1 \ldots\ldots t_{max}$ (19)

And $P_i^{t+1} = P_i^t + \Delta P_i$

With $-\Delta P_i^{max} \leq \Delta P_i \leq \Delta P_i^{max}$

This optimization problem can be solved with dynamic programming and the "control performance" of the dispatch will be considerably better than that using dynamic programming and no ramp limit constraints.

6. Result And Discussions

Lambda iteration method is implemented on 3 cases of without losses and generation limits, with losses and with generation limits. Newton's method was used and the dynamic programming method for 1 m/c, two m/c and 3 m/c was used. The programs were written on MATLAB 9 and implemented on Intel Core 2 Duo having 2.4 GHZ 3GB RAM.

6.1 Lambda Iteration method

MATLAB promming of three kind of economic dispatch problem was done namely without losses and generation limits, with generation limits and with losses. Problem taken from Wood and Wollenberg [1], p 36 given as,

The heat rates for three thermal plants in MBtu/h are given as: $H_1 = 510.0 + 7.2\ P_1 + 0.00142\ P_1^2$, $H_2 = 310.0 + 7.85 P_2 + 0.00194\ P_2^2$, $H_3 = 78.0 + 7.97\ P_3 + 0.00482\ P_3^2$. With the following fuel costs: Unit 1 = 1.1 Rs/MBtu, Unit 2 = 1.0 Rs/MBtu, Unit 3 = 1.0 Rs/MBtu and total load of 850MW.Results obtained are summarized in TABLEI.

In TABLE II, lambda iteration method is applied on economic load dispatch problem with generation limits whose problem considered is given by-

The fuel cost functions for 3 thermal plants in Rs/hr are, $C_1 = 500 + 5.3\ P_1 + 0.004\ P_1^2$, $C_2 = 400 + 5.5\ P_2 + 0.006\ P_2^2$, $C_3 = 200 + 5.8\ P_3 + 0.009\ P_3^2$, the total load $P_{D,}$ is 975 MW with the following generator limits (in MW): $200 \leq P_1 \leq 450$, $150 \leq P_2 \leq 350$, $100 \leq P_3 \leq 225$.

In TABLE III, lambda iteration method is applied on economic load dispatch problem with losses considered whose problem considered is same as problem one with the loss expression given by $P_L = 0.00003\ P_1^2 + 0.00009\ P_2^2 + 0.00012\ P_3^2$.

$\lambda_{initial}$	$P_{total_initial}$	delP	dellambda	$\lambda_{optimal}$	$P1_{optimal}$	$P2_{optimal}$	$P3_{optimal}$	Total Cost
2	-915.2778	1890.3	7.1632	9.4000	450	325	200	8236.3
7	404.1667	570.8333	2.1632	9.4000	450	325	200	8236.3
8	668.0556	306.944	1.1632	9.400	450	325	200	8233

Table: 1. Economic Load Dispatch result for Lambda Iteration Method

Parameter	Value
P_{loss}	15.600
Lambda	9.5279
$P1_{optimal}$	435.0215
$P2_{optimal}$	299.8997
$P3_{optimal}$	130.6788

P_{loss}	15.8211

Table: 2. Economic Load Dispatch result for Lambda Iteration Method

6.2 Newton's Method

MATLAB priming of Newton's method was done. Problem was taken as, The fuel cost functions for 3 thermal plants in Rs/hr are $C_1 = 561 + 7.92\ P_1 + 0.001562\ P_1^2$, $C_2 = 310 + 7.85\ P_2 + 0.001940 P_2^2$, $C_3 = 78 + 7.97\ P_3 + 0.00482\ P_3^2$ with total load varied.

$\lambda_{initial}$	P_{load}	$P1_{initial}$	$P2_{initial}$	$P3_{initial}$	P_{sum}	$\lambda_{optimal}$	$P1_{optimal}$	$P2_{optimal}$	$P3_{optimal}$
1	800	450	325	200	975	9.0749	369.68	315.69	114.61
0	800	300	200	300	800	9.0749	369.68	315.69	114.61
8	600	250	100	150	500	8.78	275.75	140.08	84.17
4	900	400	300	200	900	9.22	416.65	353.51	129.83
8	900	300	250	350	900	9.22	416.65	353.51	129.83

Table: 3. Economic Load Dispatch result for Newton Method

6.3 Dynamic Programming Method

MATLAB priming of dynamic programming method was done. Problem taken from Wood and Wollenberg [1], p 51 given as, There are three units in the system; all are on-line. Their input-output characteristics are neither smooth nor convex. Data are as follows.

Power Levels (MW) $P_1 = P_2 = P_3$	Costs (Rs/hour) F_1	Costs (Rs/hour) F_2	Costs (Rs/hour) F_3
0	∞	∞	∞
50	810	750	806
75	1355	1155	1108.5
100	1460	1360	1411
125	1772.5	1655	11704.5
150	2085	1950	1998
175	2427.5	∞	2358
200	2760	∞	∞
225	∞	∞	∞

In this problem, 10000 have been taken in place of infinity

Demand	Cost	P_1	P_2	P_3
300	4168	150	100	50
250	3558	150	50	50
200	2971	100	50	50
250	3558	150	50	50

Table: 4. Economic Load Dispatch result for Dynamic Programming Method

7. Conclusion

This paper gives overview of economic load dispatch problems and solution methodologies. Implementation is done using MATLAB programming and results are given in tabular form. Conventional method like lambda iteration method converges rapidly but complexities increases as system size increase also lambda method always requires that one be able to find the power output of a generator, given an incremental cost for that generator. In cases where cost function is much more complex, method like gradient and Newton can be used. If non convex input-output curves are to be used dynamic programming can be used to solve economic

dispatch problems. Hence different methods have different applications.

References

[1] J. Wood and B. F., "Wollenberg, *Power generation, operation and control"*, New York: John Wiley Inc., 1984.

[2] R. Balamurugan† and S. Subramanian, "An Improved Dynamic Programming Approach to Economic Power Dispatch with Generator Constraints and Transmission Losses", *Journal of Electrical Engineering & Technology, 3 (3), pp. 320~330, 2008*

[3] G. Sreenivasan, C. H. Saibabu, S. Sivanagaraju, "Solution of Dynamic Economic Load Dispatch (DELD) Problemwith Valve Point Loading Effects and Ramp Rate Limits Using PSOInternational", Journal of Electrical and Computer Engineering (IJECE), 1(1), September 2011

[4] H. H. Happ, "Optimal power dispatch – a comprehensive survey", IEEE Trans. Power Apparatus Syst. PAS-96 (3) (1977) 841–854.

[5] B.H. Chowdhury, S. Rahman, "A review of recent advances in economic dispatch", IEEE Trans. Power Syst. 5 (4) (1990) 1248–1259.

[6] W.G. Wood, "Spinning reserve constraints static and dynamic economic dispatch", IEEE Trans. Power Apparatus Syst. PAS-101 (2) (1982) 338–1338.

[7] C.B. Somuah, N. Khunaizi, "Application of linear programming redispatch technique to dynamic generation allocation", IEEE Trans. Power Syst. 5 (1) (1990) 20–26.

[8] X.S. Han, H.B. Gooi, "Effective economic dispatch model and algorithm", Elect. Power Energy Syst. 29 (2007) 113–120.

[9] T.E. Bechert, H.G. Kwatny, "On the optimal dynamic dispatch of real power", IEEE Trans. Power Apparatus Syst. PAS-91 (1972) 889–898. Flow Solution Using Lagrangian Multipliers and the Hessian Matrix." =E Transactions on Power Apparatus and Systems, PAS-93. pp 1292-1297, 1974

[10] H. H. Happ. "Optimal Power Dispatch," IEEE Transactions on Power Apparatus and Systems", PAS-93, pp 820-830, No. 3, May I June 1974.

[11] D. I. Sun, B. Ashley, B. Brewer, A. Hughes and W.F. Tinney, "Optimal Power Flow by Newton Approach," IEEE Transactions on Power Apparatus and Systems", PAS-103, pp 2864-2880, 1984.

[12] K.S. Hindi, M. R. Ab Ghani, "Multi-period economic dispatch for large scale power systems", Proc. IEE Pt. C 136 (3) (1989) 130–136.

[13] X. S. Han, H.B. Gooi, D. Kirschen, "Dynamic economic dispatch: feasible and optimal solutions", IEEE Trans. Power Syst. 16 (1) (2001) 22–28.

[14] D. Attaviriyanupap, H. Kita, E. Tanaka, J. Hasegawa, "A hybrid EP and SQP for dynamic economic dispatch with nonsmooth incremental fuel cost function", IEEE Trans. Power Syst. 17 (2) (2002) 411–416.

[15] M. Basu, "Particle swarm optimization based goal-attainment method fordynamic economic emission dispatch", Elect. Power Components Syst. 34 (2006) 1015–1025.

[16] M. Basu, "Dynamic economic emission dispatch using evolutionary programming and fuzzy satisfied method", Int. J. Emerging Elect. Power Syst. 8 (4) (2007) 1–15.

[17] M. Basu, "Dynamic economic emission dispatch using nondominted sorting genetic algprthim-II", Elect. Power Energy Syst. 30 (2008) 140–149

[18] P. Attaviriyanupap, H. Kita, E. Tanaka, J. Hasegawa, "A fuzzy-optimization approach to dynamic economic dispatch considering uncertainties", IEEE Trans. Power Syst. 19 (3) (2004) 1299–1307.

Volume 1 (2013) 73-81 ISSN 2347 - 3258
International Journal of Advance Research and Innovation

Energetic and Exergetic Based Comparison Multiple Evaporators with Compound Compression and Flash Intercooler with Individual or Multiple Throttle Valves

Kapil Chopra [a, *], V. Sahni [a], R. S Mishra [b]
[a] Department of Mechanical Engineering, Sant Longowal Institute of Engineering & Technology, Longowal, India
[b] Department of Mechanical Engineering, Delhi Technological University, Delhi , India

Article Info

Article history:
Received 1 July 2013
Received in revised form
15 July 2013
Accepted 22 July 2013
Available online 1 August 2013

Keywords

Exergetic efficiency,
Energetic efficiency,
Irreversibility rate,
Ecofriendly refrigerants

Abstract

The utility of second law analysis on vapour compression refrigeration systems is well defined because it gives the idea for improvements in efficiency due to modifications in existing design in terms of reducing exergy destructions in the components. Due to effect of global warming and ozone depletion the comparison and impact of environmental friendly refrigerants (R507a, R410a, R290, R600, R600a, R1234yf, R404a, R125, R717, R152a and R407C) on multiple evaporators at different temperature with compound compression and flash intercooler with individual and multiple throttle valves is important for calculating first law and second law performance on the basis of energetic and exergetic approach. Comparison was done for multiple evaporators with compound compression and flash intercooler with individual throttle valves (system-1) and multiple evaporators with compound compression and flash intercooler with multiple throttle valves (system-2) in terms of coefficient of performance, rational efficiency and total system defect. It was observed that for all considered refrigerants second law & first law efficiency of system-1 is lower than sytem-2 conversely system defect of system-1 is higher than system-2.In terms of energetic efficiency, rational efficiency and system defect for both systemsR407C shows minimum performance and performances of R600, R152a and R717 better with comparison of other selected refrigerants for system-1 and system-2. But R600 is highly inflammable and R717 is toxic in nature and restricted to limited applications, so R152a is suggested for both systems.

Nomenclature

COP coefficient of performance (non-dimensional)
ODP ozone depletion potential
GWP global warming potential
P power (kJ/s)
f flash intercooler
Q rate of heat transfer (kW)
W work rate (kW)
T temperature (K)
ΔT_{sc} degree of subcooling
sc subcooler
TV throttle valve
x dryness fraction(non-dimensional)
EP evaporator
Φ specific enthalpy (kJ/kg)
Ψ irreversibility rate(kW)
c compressor
X exergy rate of fluid (kW)
$\dot{m}$ mass flow rate (kg/s)
s specific entropy (kJ/kgK)
$\dot{E}P$ exergy rate of product (kW)

Subscript

e evaporator
c compressor
o dead state
f flash intercooler

Corresponding Author,
E-mail address: professor_rsmishra@yahoo.co.in
All rights reserved: http://www.ijari.org

r refrigerant, space to be cooled
tv throttle valve
sc subcooler
k kth component
gen generation
cond condenser

1. Introduction

Nowadays most of the energy utilize in cooling and air conditioning in industrial as well as for domestic applications. In addition with energy consumption, using of refrigerants in cooling and air conditioning having high GWP and ODP are responsible for global warming and ozone depletion. The primary requirements of ideal refrigerants is having good physical and chemical properties, due to good physical and chemical properties such as non-corrosiveness, non-toxicity, non- flammability, low boiling point, Chlorofluorocarbons (CFCs) have been used over the last many decades. But hydrochloro fluorocarbons (HCFCs) and Chlorofluorocarbons (CFCs) having large amount of chlorine content as well as high GWP and ODP, so after 90s refrigerants under these categories are almost prohibited [1].Most of the study has been carried out for the performance evaluation of vapour compression refrigeration system using energetic analysis. But with the help of first law analysis irreversibility destruction or losses in components of system unable to determined [2], so exergetic or second law analysis is the advanced approach for thermodynamic analysis which gives a additional practical view of the processes [3-5]. In addition to this second law analysis also provides new thought for development in the existing system [6].In this paper great emphasis put on saving of energy and using of eco friendly refrigerants due to increase of energy crises, global warming and depletion of ozone layer. In this investigation the work input required running the vapour compression refrigeration system reduced by using compound compression and work input further decrease by flash inter-cooling between two compressors using of eco-friendly refrigerants. The methods for finding the first law and second law efficiency of vapour compression and vapour absorption refrigeration systems are well defined in literature.COP of system can be enhanced either by decreasing the work of compressor by introduction of multi stages compressors or increasing the refrigeration effect. It is also possible to reduce the compressor work to considerable extent by compressing the refrigerant very close to the saturation line this can be achieved by compressing the refrigerants in more stages with intermediate intercooler. The refrigeration effect can be increase by maintaining the condition of refrigerants in more liquid stage at the entrance of evaporator which can be achieved by expanding the refrigerant very close to the liquid line. The expansion can be brought close to the liquid line by sub-cooling the refrigerant and removing the flashed vapours by incorporating the flash chamber in the working cycle. The evaporator size can be reduced because unwanted vapours formed are removed before the liquid refrigerant enters in the evaporator.

Xuan and Chen presented in this manuscript about the replacement of R502 by mixture of HFC-161.Through experimental study it was found that mixture of HFC-161 gives same and higher performance than R404A at lower and higher evaporative temperature respectively on the vapour compression refrigeration system designed for R404A.

Cabello et al. effect of condensing pressure, evaporating pressure and degree of superheating was experimentally investigated on single stage vapour compression refrigeration system using R22, R134a and R407C.It was observed that mass flow rate is greatly affected by change in suction conditions of compressor in results on refrigeration capacity because refrigeration capacity depended on mass flow rate through evaporator. It was also found that for higher compression ratio R22 gives lower COP than R407C.

Spatz and Motta, focused on replacement of R12 with R410a through experimental investigation of medium temperature vapour compression refrigeration cycles. In terms of thermodynamic analysis, comparison of heat transfer and pressure drop characteristics, R410a gives best performance among R12, R404a and R290a.

Han et al. under different working conditions experimental results revealed that there could be replacement of R407C in vapour compression refrigeration system having rotor compressor with mixture of R32/R125/R161 showing higher COP, less pressure ratio and slightly high discharge compressor temperature without any modification in the same system.

Most of the researchers did not gone through second law analysis in terms of system defect defined as irreversibility calculations in various components of multiple evaporators with compound compression and flash intercooler with individual and multiple throttle valves. Therefore objective of the present investigations to find out irreversibility occurred in the components of vapour compression refrigeration systems because second law analysis is very useful for finding the irreversibility in components as well as in whole system it is a powerful tool for designing

and analyzing of air conditioning and refrigeration systems.

2. Multiple evaporators at different temperatures with compound compression, flash intercooler and individual throttle valves (system-1)

Multiple evaporators at different temperatures with compound compression, flash intercooler and individual throttle valves (system-1) consists of compressors (C1, C2, C3) throttle valves (TV1, TV2, TV3), condenser and evaporators(EP1, EP2, EP3) as shown in Fig.1.

Exergy at any state is given as

$$X = (\Phi - \Phi_0) - T_0(s - s_0) \quad (1)$$

2.1 Energetic analysis

2.1.1 Mass flow analysis

$$\dot{m}_{c1} = \dot{m}_{e1} = \frac{\dot{Q}_{e1}}{(\Phi_1 - \Phi_{10})} \quad (2)$$

$$\dot{m}_{e2} = \frac{\dot{Q}_{e2}}{(\Phi_3 - \Phi_9)} \quad (3)$$

$$\dot{m}_{f1} = \frac{\dot{m}_{c1}(\Phi_2 - \Phi_3)}{(\Phi_3 - \Phi_9)} \quad (4)$$

$$\dot{m}_{c2} = \dot{m}_{c1} + \dot{m}_{e2} + \dot{m}_{f1} \quad (5)$$

$$\dot{m}_{e3} = \frac{\dot{Q}_{e3}}{(\Phi_5 - \Phi_8)} \quad (6)$$

$$\dot{m}_{f2} = \frac{\dot{m}_{c2}(\Phi_4 - \Phi_5)}{(\Phi_5 - \Phi_8)} \quad (7)$$

$$\dot{m}_{c3} = \dot{m}_{c2} + \dot{m}_{e3} + \dot{m}_{f2} \quad (8)$$

2.1.2 Power required running the compressors

$$P_{c1} = \frac{\dot{m}_{c1}(\Phi_2 - \Phi_1)}{60} \quad (9)$$

$$P_{c2} = \frac{\dot{m}_{c2}(\Phi_4 - \Phi_3)}{60} \quad (10)$$

$$P_{c3} = \frac{\dot{m}_{c3}(\Phi_6 - \Phi_5)}{60} \quad (11)$$

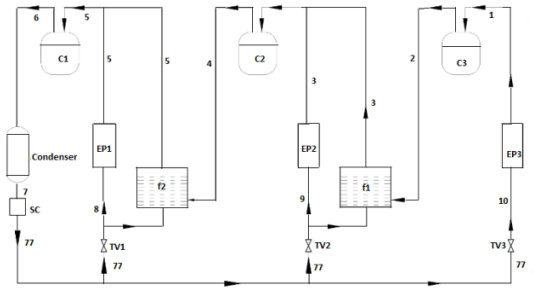

Fig: 1. Multiple evaporators with compound compression and flash intercooler with individual throttle valves

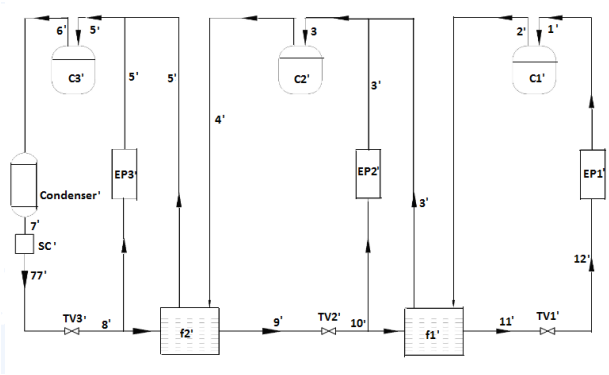

Fig: 2. Multiple evaporators with compound compression and flash intercooler with multiple throttle valves

2.1.3 Energetic performance

Energetic performance

$$= \frac{\dot{Q}_e}{P_c * 60} \quad (12)$$

2.2 Rate of exergy loss due to irreversibilties ($T_o\dot{S}_{gen}$) in various components of system-1

Compressors

$$(T_o\dot{S}_{gen})_{c1} = \dot{W}_{c1} + \dot{m}_{c1}(X_2 - X_1) \quad (13)$$

$$(T_o\dot{S}_{gen})_{c2} = \dot{W}_{c2} + \dot{m}_{c2}(X_4 - X_3) \quad (14)$$

$$(T_o\dot{S}_{gen})_{c3} = \dot{W}_{c3} + \dot{m}_{c3}(X_6 - X_5) \quad (15)$$

Total irreversibility due to compressors

$$\dot{\Psi}_c = (T_o\dot{S}_{gen})_{c1} + (T_o\dot{S}_{gen})_{c2} + (T_o\dot{S}_{gen})_{c3} \quad (16)$$

Evaporators

$$(T_o\dot{S}_{gen})_{e1} = \dot{m}_{e1}(X_1 - X_{10}) - \dot{Q}_{e1}\left(1 - \frac{T_0}{T_{r1}}\right) \quad (17)$$

$$(T_o\dot{S}_{gen})_{e2} = \dot{m}_{e2}(X_3 - X_9) - \dot{Q}_{e2}\left(1 - \frac{T_0}{T_{r2}}\right) \quad (18)$$

$$(T_o\dot{S}_{gen})_{e3} = \dot{m}_{e3}(X_5 - X_8) - \dot{Q}_{e3}\left(1 - \frac{T_0}{T_{r3}}\right) \quad (19)$$

Total irreversibility due to evaporators

$$\dot{\Psi}_e = (T_o\dot{S}_{gen})_{e1} + (T_o\dot{S}_{gen})_{e2} + (T_o\dot{S}_{gen})_{e3} \quad (20)$$

Condenser

$$\dot{\Psi}_{cond} = (T_o\dot{S}_{gen})_{cond} = \dot{m}_{c3}(X_6 - X_7) - \dot{Q}_e\left(1 - \frac{T_0}{T_r}\right) \quad (21)$$

Throttle Valves

$$(T_o\dot{S}_{gen})_{tv1} = \dot{m}_{e1}(X_{77} - X_{10}) \quad (22)$$

$$(T_o\dot{S}_{gen})_{tv2} = (\dot{m}_{e2} + \dot{m}_{f1})(X_{77} - X_9) \quad (23)$$

$$(T_o\dot{S}_{gen})_{tv3} = (\dot{m}_{e3} + \dot{m}_{f2})(X_{77} - X_8) \quad (24)$$

Total irreversibility due to throttle valves

$$\dot{\Psi}_{tv} = (T_o\dot{S}_{gen})_{tv1} + (T_o\dot{S}_{gen})_{tv2}(T_o\dot{S}_{gen})_{tv3} \quad (25)$$

Subcooler

$$\dot{\Psi}_{sc} = (T_o\dot{S}_{gen})_{sc} = \dot{m}_{c3}(X_7 - X_{77}) \quad (26)$$

Flash intercoolers

$$(T_o\dot{S}_{gen})_{f1} = \dot{m}_{f1}(X_9 - X_3) + \dot{m}_{c1}(X_2 - X_3) \quad (27)$$

$$(T_o\dot{S}_{gen})_{f2} = \dot{m}_{f2}(X_8 - X_5) + \dot{m}_{c1}(X_4 - X_5) \quad (28)$$

Total irreversibility due to flash intercoolers

$$\dot{\Psi}_f = (T_o\dot{S}_{gen})_{f1} + (T_o\dot{S}_{gen})_{f2} \quad (29)$$

Total irreversibility destruction in system-1

$$\sum \dot{\Psi}_k = \dot{\Psi}_e + \dot{\Psi}_c + \dot{\Psi}_{cond} + \dot{\Psi}_{tv} + \dot{\Psi}_{sc} + \dot{\Psi}_f \quad (30)$$

3. Multiple evaporators at different temperatures with compound compression, flash intercooler and multiple throttle valves (system-2)

The main components of Multiple evaporators at different temperatures with compound compression, flash intercooler and multiple throttle valves (system-2) are compressors ($C1', C2', C3'$) throttle valves ($TV1', TV2', TV3'$), condenser ($cond'$) and evaporators ($EP1', EP2', EP3'$) as shown in Fig. 2.

3.1 Energetic analysis

3.1.1 Mass flow analysis

$$\dot{m}_{c1'} = \dot{m}_{e1'} = \frac{\dot{Q}_{e1'}}{(\Phi_{1'} - \Phi_{12'})} \quad 2A$$

$$\dot{m}_{e2'} = \frac{\dot{Q}_{e2'}}{(\Phi_{3'} - \Phi_{10'})} + \dot{m}_{c1'}\left(\frac{x_{10'}}{1 - x_{10'}}\right) \quad 3A$$

$$\dot{m}_{f1'} = \frac{\dot{m}_{c1'}(\Phi_{2'} - \Phi_{3'})}{(\Phi_{3'} - \Phi_{10'})} \quad 4A$$

$$\dot{m}_{c2'} = \dot{m}_{c1'} + \dot{m}_{e2'} + \dot{m}_{f1'} \quad 5A$$

$$\dot{m}_{e3'} = \frac{\dot{Q}_{e3'}}{(\Phi_{5'} - \Phi_{8'})} + \dot{m}_{c2'}\left(\frac{x_{8'}}{1 - x_{8'}}\right) \quad 6A$$

$$\dot{m}_{f2'} = \frac{\dot{m}_{c2'}(\Phi_{4'} - \Phi_{5'})}{(\Phi_{5'} - \Phi_{8'})} \quad 7A$$

3.1.2 Power required for running the compressors

$$P_{c1'} = \frac{\dot{m}_{c1'}(\Phi_{2'} - \Phi_{1'})}{60} \quad 8A$$

$$P_{c2'} = \frac{\dot{m}_{c2'}(\Phi_{4'} - \Phi_{3'})}{60} \quad 9A$$

$$P_{c3'} = \frac{\dot{m}_{c3'}(\Phi_{6'} - \Phi_{5'})}{60} \quad 10A$$

3.1.3 Energetic performance

Energetic performance

$$= \frac{\dot{Q}_{e'}}{P_{c'} * 60} \quad 11A$$

3.2 Rate of exergy loss due to irreversibilties $(T_o\dot{S}_{gen})$ in various components of system-2

Compressors

$$(T_o\dot{S}_{gen})_{c1'} = \dot{W}_{c1'} + \dot{m}_{c1'}(X_{2'} - X_{1'}) \quad 12A$$

$$(T_o\dot{S}_{gen})_{c2'} = \dot{W}_{c2'} + \dot{m}_{c2'}(X_{4'} - X_{3'}) \quad 13A$$

$$(T_o\dot{S}_{gen})_{c3'} = \dot{W}_{c3'} + \dot{m}_{c3'}(X_{6'} - X_{5'}) \quad 14A$$

Total irreversibility due to compressors

$$\dot{\Psi}_{c'} = (T_o\dot{S}_{gen})_{c1'} + (T_o\dot{S}_{gen})_{c2'} + (T_o\dot{S}_{gen})_{c3'} \quad 15A$$

Evaporators

$$(T_o\dot{S}_{gen})_{e1'} = \dot{m}_{e1'}(X_{1'} - X_{12'}) - \dot{Q}_{e1'}\left(1 - \frac{T_0}{T_{r1'}}\right) \quad 16A$$

$$(T_o\dot{S}_{gen})_{e2'} = \dot{m}_{e2'}(X_{3'} - X_{10'}) - \dot{Q}_{e2'}\left(1 - \frac{T_0}{T_{r2'}}\right) \quad 17A$$

$$(T_o\dot{S}_{gen})_{e3'} = \dot{m}_{e3'}(X_{5'} - X_{8'}) - \dot{Q}_{e3'}\left(1 - \frac{T_0}{T_{r3'}}\right) \quad 18A$$

Total irreversibility due to evaporators

$$\dot{\Psi}_{c'} = (T_o\dot{S}_{gen})_{c1'} + (T_o\dot{S}_{gen})_{c2'} + (T_o\dot{S}_{gen})_{c3'} \quad 19A$$

Condenser

$$\dot{\Psi}_{cond'} = (T_o\dot{S}_{gen})_{cond'} = \dot{m}_{c3'}(X_{6'} - X_{7'}) - \dot{Q}_{e'}\left(1 - \frac{T_0}{T_{r'}}\right) \quad 20A$$

Throttle Valves

$$(T_o\dot{S}_{gen})_{tv1'} = \dot{m}_{e1'}(X_{11'} - X_{12'}) \quad (21A)$$

$$(T_o\dot{S}_{gen})_{tv2'} = \dot{m}_{c2'}(X_{9'} - X_{10'}) \quad (22A)$$

$$(T_o\dot{S}_{gen})_{tv3'} = \dot{m}_{c3'}(X_{77'} - X_{8'}) \quad (23A)$$

Total irreversibility due to throttle valves

$$\dot{\Psi}_{tv'} = (T_o\dot{S}_{gen})_{tv1'} + (T_o\dot{S}_{gen})_{tv2'} + (T_o\dot{S}_{gen})_{tv3'} \quad (24A)$$

Subcooler

$$\dot{\Psi}_{sc'} = (T_o\dot{S}_{gen})_{sc'} = \dot{m}_{c3'}(X_{7'} - X_{77'}) \quad (25A)$$

Flash intercoolers

$$(T_o\dot{S}_{gen})_{f1'} = \dot{m}_{f1'}(X_{10'} - X_{3'}) + \dot{m}_{c1'}(X_{2'} - X_{3'}) \quad (26A)$$

$$(T_o\dot{S}_{gen})_{f2'} = \dot{m}_{f2'}(X_{8'} - X_{5'}) + \dot{m}_{c2'}(X_{4'} - X_{5'}) \quad (27A)$$

Total irreversibility due to flash intercoolers

$$\dot{\Psi}_{f'} = (T_o\dot{S}_{gen})_{f1'} + (T_o\dot{S}_{gen})_{f2'} \quad (28A)$$

Total irreversibility destruction in system-1

$$\sum\dot{\Psi}_{k'} = \dot{\Psi}_{e'} + \dot{\Psi}_{c'} + \dot{\Psi}_{cond'} + \dot{\Psi}_{tv'} + \dot{\Psi}_{sc'} + \dot{\Psi}_{f'} \quad (29A)$$

4. Rational efficiency or exergetic efficiency

$$\text{Rational efficiency} = \frac{\text{Exergy of cooling load of evaporators}}{\text{Compressors work}} = \frac{\dot{E}P}{\dot{W}} \quad (31)$$

For System-1

Rational efficiency

$$= \frac{(\dot{Q}_{e1} + \dot{Q}_{e2} + \dot{Q}_{e3}) - T_o\left(\frac{\dot{Q}_{e1}}{T_{r1}} + \frac{\dot{Q}_{e2}}{T_{r2}} + \frac{\dot{Q}_{e3}}{T_{r3}}\right)}{P_c * 60} \quad (32)$$

For System-2

Rational efficiency

$$= \frac{(\dot{Q}_{e1'} + \dot{Q}_{e2'} + \dot{Q}_{e3'}) - T_o\left(\frac{\dot{Q}_{e1}}{T_{r1'}} + \frac{\dot{Q}_{e2}}{T_{r2'}} + \frac{\dot{Q}_{e3}}{T_{r3'}}\right)}{P_{c'} * 60} \quad (33)$$

5. Results and discussion

For carrying out the energetic and exergetic analysis a numerical model has been developed. Comparison of multiple evaporators at different temperatures with compound compression and flash intercooler with individual and multiple throttle valves and impact of chosen refrigerants on theses systems was made using Engineering Equation Solver software[7].In this investigation following assumptions were made:

1. Loads ($\dot{Q}_{e1}, \dot{Q}_{e2}$ and $\dot{Q}_{e3}$) on the evaporators EP1, EP2 and EP3 are 35KW, 70KW and 105KW respectively.
2. Dead state temperature (T_0): 298K
3. Difference between evaporator and space temperature (T_r-T_e):5K.
4. Adiabatic efficiency of compressor (η_c):76%.
5. Dead state enthalpy (Φ_0) and entropy (s_0) of the refrigerants have been calculated corresponding to the dead state temperature (T_0) of 298K.
6. Temperature of evaporators EP_1, EP2 and EP3 are 263K, 273K and 283K respectively.
7. Condenser temperature (T_c): 313K.
8. Degree of sub cooling (ΔT_{sc}): 10K.

Fig.3-5 presents the variation of EP1, EP2 and EP3 temperature of system-1 with coefficient of performance of multiple evaporators and compressors with individual expansion valves (System-1) respectively on the other hand Fig.6-8 shows the variation of EP1, EP2 and EP3 temperature of system-2 verses coefficient of performance of multiple evaporators and compressors with multiple expansion valves (System-2) respectively for selected refrigerants. Both systems (system-1& system-2) were analytically analyzed and observed that COP of system-2 is better than system-1for different refrigerants.

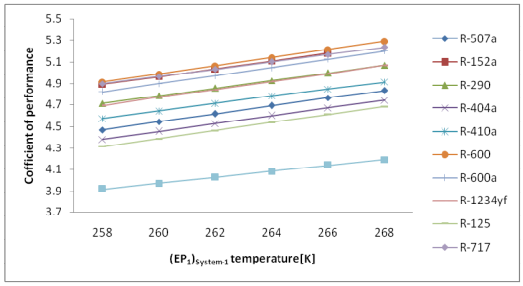

Fig.3: Evaporator-1 temperature of system-1 versus coefficient of performance

The maximum and minimum percentage difference of COP between system-2 and system-1 is 10.65% for R404a at 268K EP3 temperature and 1.70% for R717 at 268K EP1 temperature respectively.

The energetic efficiency of both system-1 and system-2 increase with increase in evaporator temperature for chosen refrigerants. It was also observed that R600, R717 and R152a show better energetic performance (COP) than other refrigerants for both systems and R407c shows lowest COP.

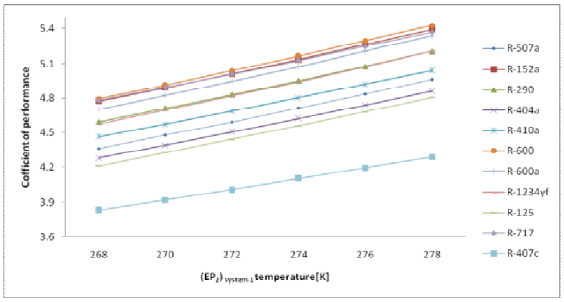

Fig: 4. Evaporator-2 temperature of system-1 versus coefficient of performance

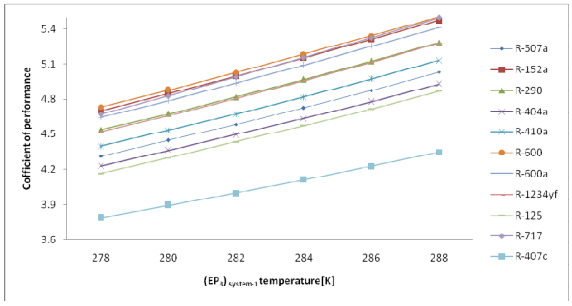

Fig: 5. Evaporator-3 temperature of system-1 versus coefficient of performance

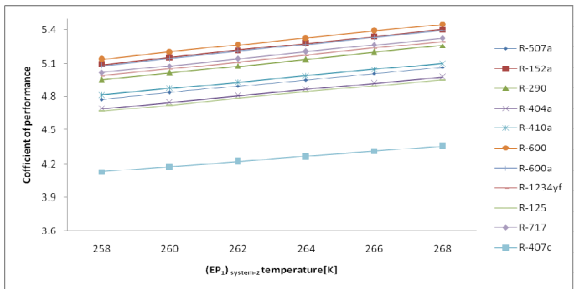

Fig: 6. Evaporator-1 temperature of system-2 versus coefficient of performance

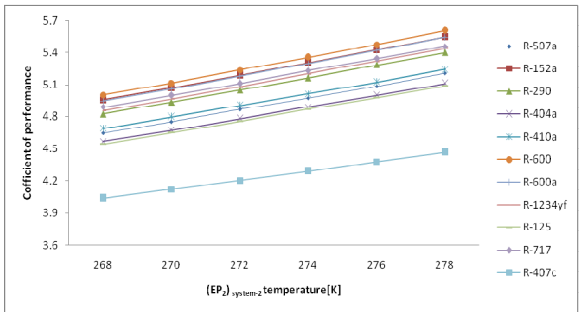

Fig: 7. Evaporator-2 temperature of system-2 versus coefficient of performance

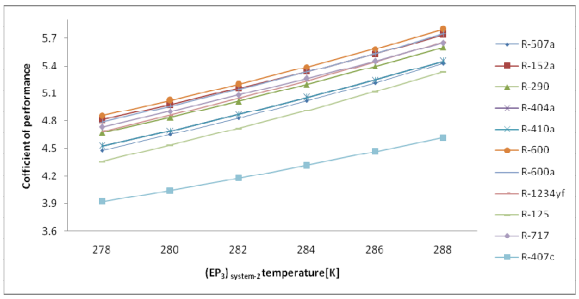

Fig: 8. Evaporator-3 temperature of system-2 versus coefficient of performance

Fig.9-11and Fig.11-14 presents impact of rational efficiency with change in temperature of EP1, EP2 and EP3 of system-1 and system-2 respectively and observed that that rational efficiency decrease with increase in evaporator temperature. As with Similar case of energetic performance R600 shows maximum and both R717 and R152a show second highest energetic performance than chosen refrigerants.

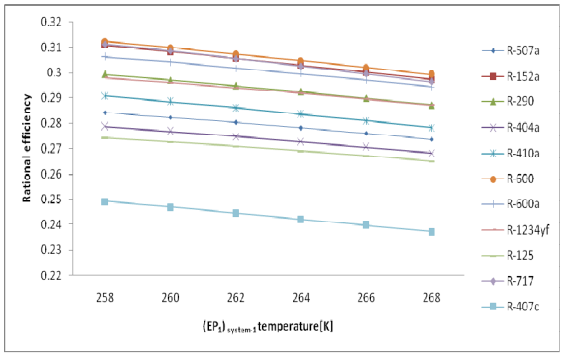

Fig: 9. Evaporator-1 temperature of system-1 versus rational efficiency

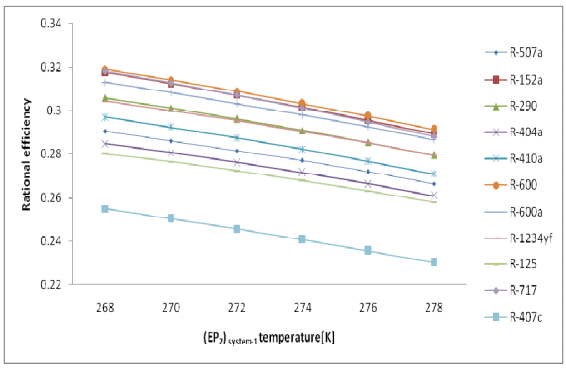

Fig: 10. Evaporator-2 temperature of system-1 versus rational efficiency

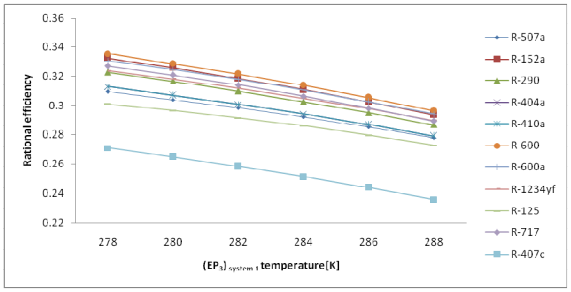

Fig: 11. Evaporator-3 temperature of system-1 versus rational efficiency

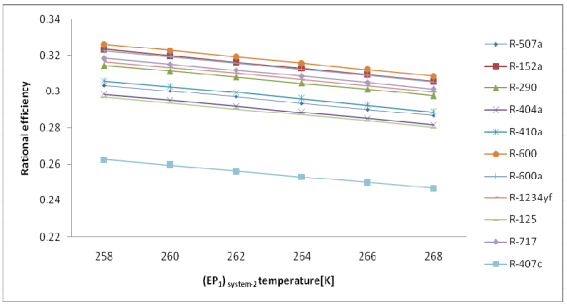

Fig: 12. Evaporator-1 temperature of system-2 versus rational efficiency

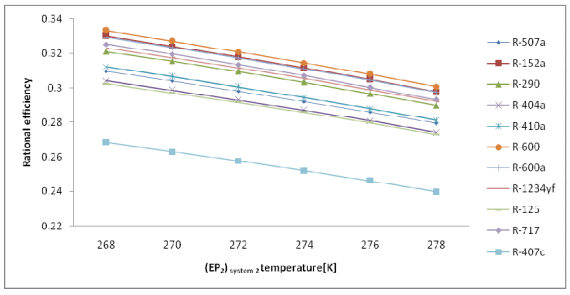

Fig: 13. Evaporator-2 temperature of system-2 versus rational efficiency

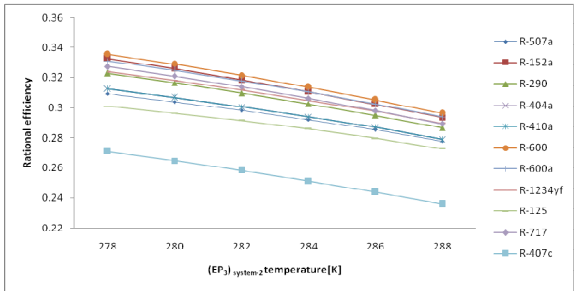

Fig: 14. Evaporator-3 temperature of system-2 versus rational efficiency

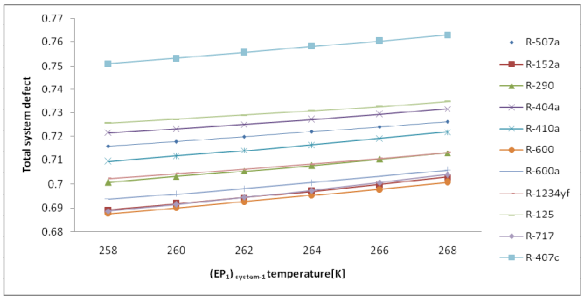

Fig: 15. Evaporator-1 temperature of system-1 versus total system defect

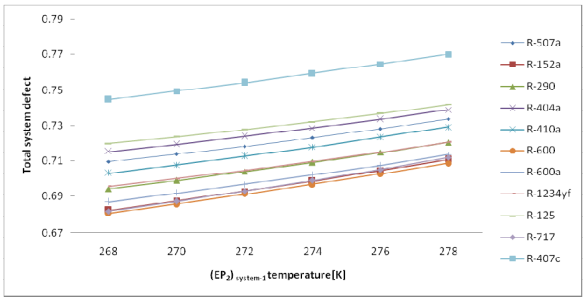

Fig: 16. Evaporator-2 temperature of system-1 versus total system defect

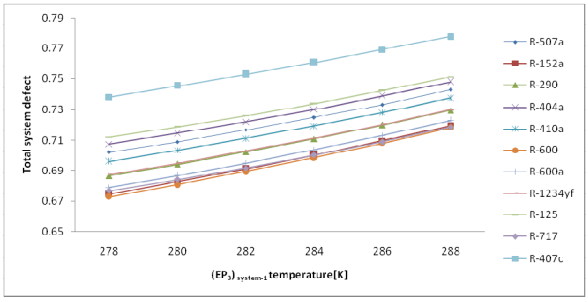

Fig: 17. Evaporator-3 temperature of system-1 versus total system defect

The irreversibility analysis of system-1 and system-2 is shown by Figs.15-17 and Figs.18-20 respectively. It was experienced that system defect of both system-1 and system-2 increase with increase in temperature of any evaporator.R407C shows maximum system defect but R600, R717 and R152a show minimum system defect compare with another selected refrigerants.

The impact of change in condenser temperature from 298K to 318K on energetic efficiency, exergetic efficiency and total system defect shown in Figs.21-26 for sytem-1 and system-2 using eco-friendly refrigerants. This analysis reveals that first law and second law efficiency decreases with increase in condenser temperature on the other hand exergy

destruction increase with increase in condenser temperature for system-1 & sytem-2

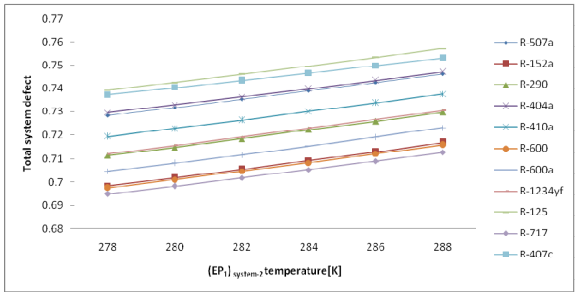

Fig: 18. Evaporator-1 temperature of system-2 versus total system defect

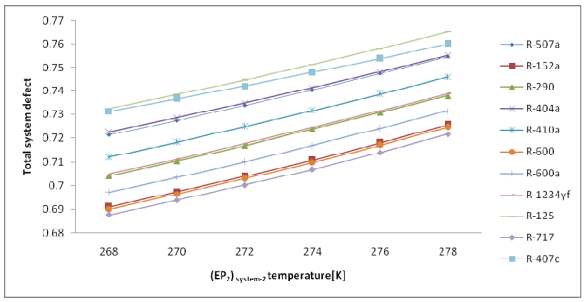

Fig: 19. Evaporator-2 temperature of system-2 versus total system defect

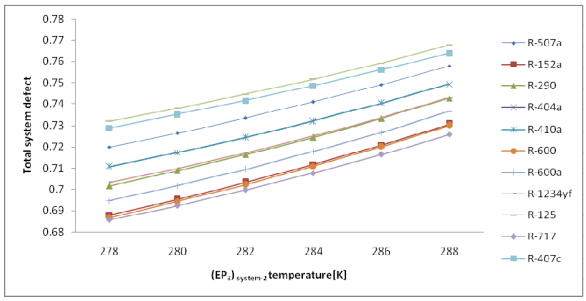

Fig: 20. Evaporator-3 temperature of system-2 versus total system defect

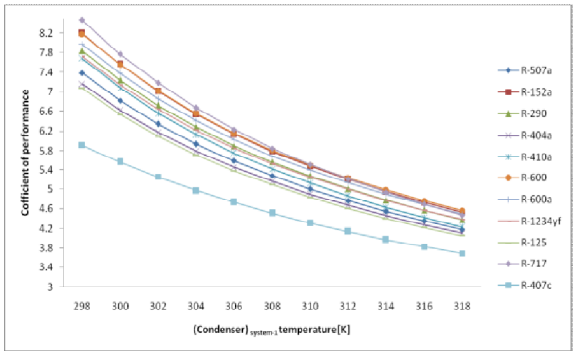

Fig: 21. Condenser temperature of system-1 versus coefficient of performance

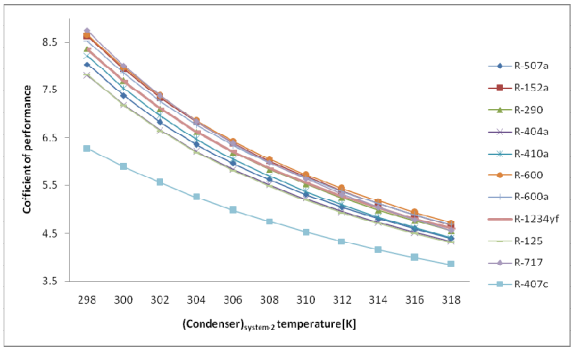

Fig: 22. Condenser temperature of system-2 versus coefficient of performance

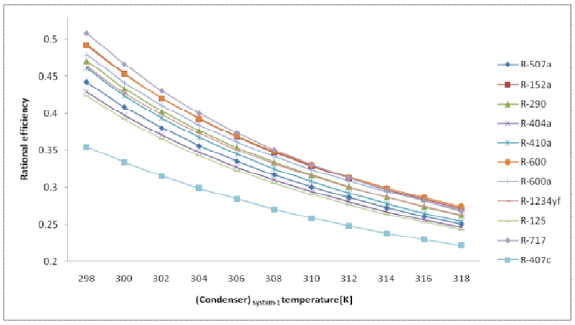

Fig: 23. Condenser temperature of system-1 versus rational efficiency

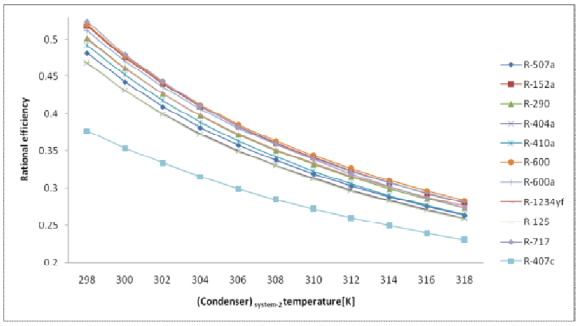

Fig: 24. Condenser temperature of system-2 versus rational efficiency

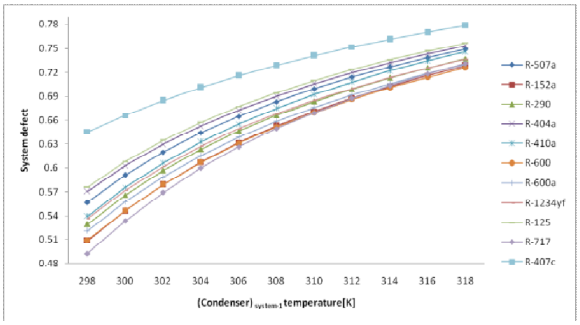

Fig: 25. Condenser temperature of system-1 versus system defect

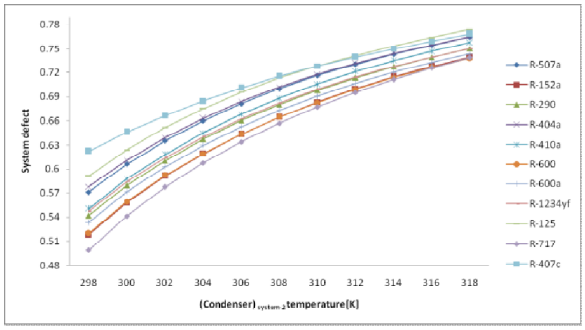

Fig: 26. Condenser temperature of system21 versus system defect

6. Conclusions

Analysis multiple evaporators at different temperature with compound compression and flash intercooler with individual throttle valves and multiple evaporators at different temperature with compound compression and flash intercooler with multiple throttle valves have been made in terms of energetic efficiency, exergetic efficiency and irreversibility destruction and from the current study following conclusions were made:

1. Energetic and exergetic performance of system-2 is higher than system-1 for selected temperature range of condenser and evaporators for chosen ecofriendly refrigerants.
2. System defect in sytem-2 is less as compare with system-1, so system-2 is better system than system-1 for selected refrigerants.
3. R407C shows minimum performance in terms of first law efficiency, second law efficiency and system defect for both systems
4. Performances of R600, R152a and R717 better with comparison of other selected refrigerants for system-1 and system-2. But R600 is highly inflammable and R717 is toxic and limited to industrial application, so R152a is recommended for both systems.

References

[1] C. Stanciu, A. Gheorghian, D. Stanciu, A. Dobrovicescu, “Exergy analysis and refrigerant effect on the operation and performance limits of a one stage vapour compression refrigeration system,Termotehnia”, 36-42, 2011

[2] V. Siva Reddy, N. L. Panwar, S. C. Kaushik, “Exergetic analysis of a vapour compression refrigeration system with R134a, R143a, R152a, R404A, R407C, R410A, R502 and R507A”, Clean Techn Environ Policy,14:47–53, 2011

[3] J. U. Ahamed , R. Saidur, H. H. Masjuki, “A review on exergy analysis of vapor compression refrigeration system”, Renewable and Sustainable Energy Reviews,15: 1593–1600, 2011

[4] D. Szargut, R. Petela, Egzergia (1965), WNT

[5] J. Szargut, D. Morris, F. Steward, “Exergy analysis of thermal, chemical and metallurgical processes”, New York: Hemisphere Publishing Corporation, 1998

[6] R. Saidur, H. H. Masjuki, M. Y. Jamaluddin, “An application of energy and exergy analysis in residential sector in Malaysia”, Energy Policy, 35: 1050–63, 2007

[7] Y. Xuan, G. Chen, “Experimental study on HFC-161 mixture as an alternative refrigerant to R502”, Int J Refrigeration, Article in Press

[8] R. Cabello a, E. Torrella b, J. Navarro-Esbr, “Experimental evaluation of a vapour compression plant performance using R134a, R407C and R22 as working fluids”, Int J Applied Thermal Engineering.2004; 24:1905-1917.

[9] Mark W. Spatz, Samuel F. Yana Motta, “An evaluation of options for replacing HCFC-22 in medium temperature refrigeration systems”, Int J Refrigeration.2004; 27:475-483

[10] X. H. Han, Q. Wang, Z. W. Zhu, G. M. Chen, “Cycle performance study on R32/R125/R161 as an alternative refrigerant to R407C”, Int J Applied Thermal Engineering.2007; 27:2559-2565.

[11] S. A. Klein, F. Alvarado, “Engineering Equation Solver”, 7.441. F Chart Software, Middleton, WI, 2005

ETHICAL VALUES AND ECONOMIC VALUES

Priyanka Chaudhary*

Manish Sharma**

ABSTRACT

Values, this word has two meanings which cannot be said as mutually exclusive. In ethics, "values" denote orientations standards and objectives which guide and drive people's actions. In the economy, "values" is related with money and denote the exchange, utility and capitalised value of goods. The value is measured against demand, usefulness and relative rarity. "Value" also denotes the financial earning power of companies (shareholder value). Understanding of the terms value and value creation differs greatly. Value is not inherent in a commodity, but is rather a relation between persons and expressed as a relation between things. Value is what a customer is willing to pay for a product or service. Philosophers often use value as an attributive or a predicative. Sociologists or anthropologists, on the other hand, usually use the concept of value as a substantive. Examples of this include economic value, protected value, existence or preservation value, moral values or self-oriented values, social values, capitalist values, liberal values, socialist values, green values and democratic values. Now a day, organisations try to create win-win situation in order to maximise all the types of "values". Value creation in contemporary industrial business is a complex and multi-faceted issue in which new aspects are emerging. It is crucial to create processes that contribute to achieve appropriate fit between the all types of values. There are organisations where ethical values are part of a positive strategy to achieve competitive advantage. Organizations need to be aware that ethical values and principles change over time and vary across contexts. The ethical aspects of business might form a new and critical source for value creation between companies acting in global business markets. This paper addresses the need for maintaining a balance between both the types and may help profit making businesses in doing the same.

*Assistant Professor, Delhi School of Management, Delhi Technological University, Bawana Road, Delhi, India

**Student, Delhi School of Management, Delhi Technological University, Bawana Road, Delhi, India

INTRODUCTION

Value is what is affirmed within objects by subjects. This includes three points: (1) it meets the needs of subjects; (2) it is what a subject willed or created; (3) it is what a subject appreciated or enjoyed. Value is not the same as object. Value is what a subject finds experiences and enjoys in an object: one finds, senses, knows, cognition, etc.; it is also what a subject needs, chooses, supposes, and expects. In most cases, it is taken as the purpose of an action: by will and feeling it is brought into being. At the end of the process one can experience, enjoy, savour, and thereby affirm it. Hence, value is not far from us; it is in our feelings, cognition, experiences and enjoyment. It is what we hold and confirm by use of our body and mind. It might be some utility, function or meaning that is to be found, experienced and enjoyed, but could not be reduced to only one of them; rather it is a general term for all of them.

Thus, value can be of many kinds in relation to a subject's needs, creations and enjoyment. However, though they can be distinguished in terms of their subject as individual or social, they are relative, and rely on wholeness, harmony and compatibility. A subject's activities are also many, such as economic, political, social, scientific, educational, literary, artistic and theoretical.

ETHICAL VALUES AND ECONOMIC VALUES

Ethical concerns are very important concerns in the area of organizational context both in the internal and external environment. Ethics are not a recent discovery. Over the centuries philosophers in their struggle with human behaviour have developed different approaches to ethics, each leading to different conclusion. Ethics are a combination of moral principles or set of values about what is right or wrong, true or false, fair or unfair, proper or improper what is right is ethical and what is wrong is unethical.

In the era of globalization and privation, with the entry of multinational and increasing foreign trade in 21st century people are losing their faith in government, law, ethics and society. On one hand business concerns are competing with immense competition in the market for their survival and for producing and delivering innovative products in the market and on the other hand they are violating the principles of proper and ethical conduct.

As might be suspected, early writings on ethics were centred not on economics or business, but personal beliefs and actions. It becomes readily apparent from early discussions of ethics that philosophers and writers viewed ethics as a matter of choice. Individuals must make choices in their lives. This is important to note—businesses don't make choices. Choices are

made and/or implemented by individuals within the economic enterprise. People in government make choices, people in educational institutions make choices, people in businesses make choices, everyone is forced to make choices, and even the choice not to choose is a decision.

Economic value is one of many possible ways to define and measure value. Although other types of value are often important, economic values are useful to consider when making economic choices – choices that involve tradeoffs in allocating resources.

Measures of economic value are based on what people want – their preferences. Economists generally assume that individuals, not the government, are the best judges of what they want. Thus, the theory of economic valuation is based on individual preferences and choices. People express their preferences through the choices and tradeoffs that they make, given certain constraints, such as those on income or available time.

If economist use 'values' and 'tastes' and 'preference' interchangeably (quotation from Arrow) and if at the same time they refer to 'value' and 'price' as if these two terms meant the same thing (as, for example, in the traditional reference to 'price theory' as the 'theory of value') then confusion immediately beckons. What is the connection between 'values' in the first sense and the 'values in the second?

Economics is often described as the 'theory of choice' or as having its subject-matter defined by choice. And although that description is neither entirely clear nor uncontested, it is clear that there is a close connection between economics under that choice-based description, and ethics. For ethics too is concerned with choice – with the evaluation of alternative actions. In what ways, we might ask, do the economic account and the ethical account of choice diverge – if indeed they do diverge? And what exactly is the relation between choices whether economic or ethical? Besides Malthus Ricardo, all classicists before and after him conceived value as closely connected to price. While in ordinary language, we often refer to the 'value' of a bundle of shares or a house or a painting, meaning the price it could obtain in prevailing markets. But real values only emerge in the process of exchange for determining the level of price a product should be charged. The term 'value' always precedes 'price' as price are determined by the value attached to any product. If we say that values precede prices, it does not imply that values are fully absorbed in prices nor does it imply that values have no connection with the prices. In fact the term 'values' refers both to the relative price of the good as well as to the underlying preferences on the basis of which those relative prices

emerge. Value is not a static term; it depends upon the preference attached to that product in comparison to others in the market.

In a market economy, dollars (or some other currency) are a universally accepted measure of economic value, because the number of dollars that a person is willing to pay for something tells how much of all other goods and services they are willing to give up to get that item. This is often referred to as "willingness to pay." {1}

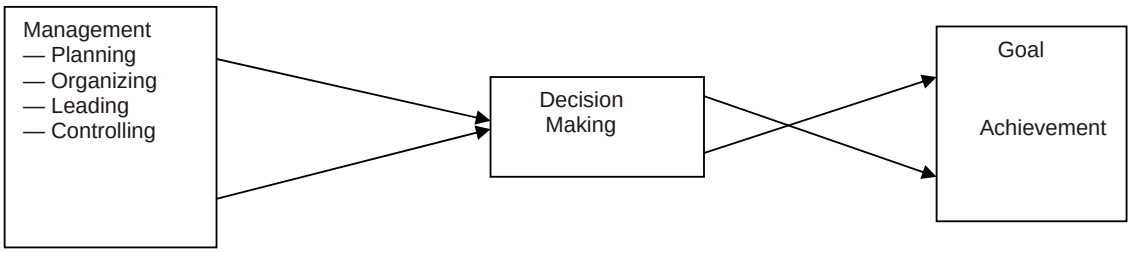

Ethics like economics, involves choice between alternatives. In the economics, the options are usually thought of as actions. In ethics, they are sometimes actions, sometimes beliefs, sometimes attitudes. The apparatus that guides such choices in economics is that of 'preference'. The apparatus that guides such choices in moral philosophy is 'values'. For economists, typically, 'values' just are preference. {5}

CODE OF ETHICS FOR ECONOMIST

The American Economic Association (AEA) and the International Economic Association, unlike most professional associations, do not have codes of ethics to guide their members in conducting their daily professional activities. Yet there is general agreement among most professionals that without codes of ethics, significant harm can be done both directly and indirectly. Moreover, in business settings, employees who lose the direct recognition and economic rewards they deserve may be less trusting of the system, less motivated to do their best, and less willing to work collaboratively, all of which are counterproductive. In academic settings, instructors may lose confidence in their abilities, students may quit doing their best and the acquisition or creation of economic knowledge may proceed at a much slower pace than otherwise would be the case.

Economists are presumed to have more knowledge and understanding of how individuals decide to allocate scarce resources and how the economy operates than the average individual on the street. A layperson may have difficulty evaluating the quality of statements made by economists. They assume (i) that economists possess the education, skills and information to

make such statements; (ii) that economists are truthful about what they know; and (iii) that economists are honest about the limitations and purposes to which their knowledge can be applied. These assumptions may be seen as part of an unwritten ethical contract that serves as a basis for the individual to accept the validity of what an economist says. Economists recently began arguing for a code of ethics. Enders and Hoover (2004) {6} recommend a code of ethics for economists because a sizeable majority of the editors they questioned attributed plagiarism and other unethical behaviour to poor training and mentoring. Margolis (2003) {7}suggests that economists might find an ethical code helpful to sustain 'motivation and adherence to noble practices even in the most difficult or tedious moments of collecting data, cleaning data sets, running regressions, writing up results, or responding to reviewers' (p. 12). De Martino (2005) {8}concludes that a code of ethics for economists would at the very least make these professionals more aware of issues and encourages them to reflect critically on the possible ethical repercussions of their work. {3}

The need for a code of ethics for economists

A number of factors contribute to the growing need for a code of ethics for economists:

● The composition of membership of the profession has changed dramatically since the establishment of the AEA in 1885.

● Interdisciplinary work has become more commonplace.

● The potential impact of policy recommendations is unknown.

● Funding agencies increasingly require applicants to provide assurances that they will do no harm.

A Framework for Ethics- business ethics

Ethics are a framework which is not confined to a single area; ethics can be seen in every part of an organization. Major branches of ethics include:

- Meta-ethics, about the theoretical meaning and reference of moral propositions and how their truth-values (if any) may be determined;
- Normative ethics, about the practical means of determining a moral course of action;
- Applied ethics, about how moral outcomes can be achieved in specific situations;
- Moral psychology, about how moral capacity or moral agency develops and what its nature is;
- Descriptive ethics, about what moral values people actually abide by.

Ethics are not confined to a single specific area rather it captures a huge area. There are multiple research topics that may be linked implicitly or explicitly to ethical concerns in

across organization, such as; business, economics, accounting, information technology, marketing, laws, government, social system, management.

This paper addresses the problem areas of how Ethics are related to various areas of an organisation or business and to evaluate ethical concerns across the various functions of an organization and how ethical concerns have changed their meaning in the era of 21st century.

Business ethics are present in every organization from top executives to bottom line employees, it is not just the matter of high officials of an organization neither it is only high level of return on investment or profit maximization rather it is dealing one's own business profitably in the era of social challenges, ethically at the same time.

Business ethics are the systematic handling of values in business and industry:

• Business ethics are the rules of business by which the propriety of business activity may be judged.

•Business ethics concentrate on moral standard as they apply to business policies, institutions and behaviour. It is a specialized study of moral right or wrong. It is a form of applied ethics.

Law + Knowledge = Ethics

• Business ethics are nothing but the application of ethics in business. It proves that business can be and have been ethical and still make profits. Today more and more interest is being given to the application of ethical practices in business dealings and the ethical implications of business.

The 3 C's of Business ethics:

1. Compliance: (The need for compliance of rules including):

- Laws
- principles of morality
- policy of the company

2. The Contribution (Business can make to the society):

- The core values
- Quality of products/services
- Employment
- Usefulness of activities to surrounding activities
- QWL

3. The Consequences of business activity:

- Toward environment inside and outside the organization
- Social responsibility toward shareholders, bankers, customers and employees of organization.
- Good public image, sound activity- good image.{2}

Ethical Problems while working in an Organization: while discussing about ethics in business activity, there are various problems where business man find dilemmas while making choices among alternatives and not getting a clear cut solution. There can be problems like choosing between alternatives that are equally justifiable, truth verses reality, individual verses community, and significant value conflict among different alternatives.

SIGNIFICANCE OF BUSINESS ETHICS

"Good business ethics promote good business"

This statement is supported by the research findings of some well known authorities like Raymond Baum hart, Brener and Molander, and Strom and Ruch. It was clear from their findings that only those businesses can develop on a long term bases which conducts activities on ethical grounds. Once 'Robert Day' has said that good ethics not only promotes professionalism in management but it purifies the inner mind of every business man. Another writer Thomas Donaldson (Ethics in business- a new look) has observed that-"there are some key reasons why business Ethics are vital and why ethics plays a key role in business."

1. Positive Consequences
2. Goodwill of the business and businessman
3. Self satisfaction
4. Encourage others
5. Success and development
6. New management

The ethical concern for a business organization could be to make organization profitable, generate employment opportunities, utilising the resources in an appropriate manner, providing quality products, protecting the environment, safeguarding the health of employees etc.

Global Ethics:

Is it possible to have a global ethics – where certain principles are accepted universally? Hans Kung argues strongly for this, summarized in the stirring slogans. There will be no survival

of our globe without world ethics. No peace among the nations without peace among the religions. No peace among the religions without dialogue and cooperation among the religions and civilizations. (Hans Kung 1991, xv) {9}

Globalization raises many issues of injustice and strife, from financial and labour markets to ecology and organized crime. Hence, such a global ethic is necessary if the global order is to be managed. Hence, argues Kung, there is a need to develop peace between religions. Such a peace would demand wide ranging dialogue between religions, cultures and civilizations. The West tends to assume that society is secular and religious in the minority. Globally, it is quite the opposite; a majority of the world's population is strongly committed to a religious faith. Kung argues that a global ethic is not a uniform system of ethics but rather 'a necessary minimum of shared ethical values' to which different regions, cultural groups, religions, nations and other interest groups can commit themselves. {4} Ethics is something the parameters of which can't be stated in some lines, it is something inherent in nature or experiences which you gain through your internal and external environment. What we call global ethics are basically the norms which are stated for maintaining peace within the countries.

REFRENCES:

1. Essentials, Section 1, Basic Concepts of Economic Value.
2. Paliwal, Manisha, " Business Ethics", New Delhi: New Age International (P) Limited, Publishers, 2006
3. Jan Peil and Irene van, " Handbook Of Economics and Ethics", The Netherlands, 2009
4. Simon Robinson, Ross Dixon, Christopher Preece and Krisen Moodley, " Engineering, Business and Professional Ethics" 2007
5. Geoffrey Brennan, "The Economics of Ethics and Ethics of Economics, Values Market and State" The Australian National University, Canberra, Australia
6. Enders, Walter and Gary A. Hoover (2004), "Whose line is it? Plagiarism in economics", *Journal of Economic Literature*, **42** (2), 487–93.
7. Margolis, Joshua D. (2003), 'Preparing for ethical challenges', *The Committee on the Status of Women in the*
8. *Economics Profession Newsletter*, (Winter), 12–14.
9. DeMartino, George (2005), 'A professional ethics code for economists', *Challenge*, **48** (4), 88–104.

10. Kung, H. (1991). *Global Responsibility: In Search of a New World Ethics*. London: SCM.

Volume 1 (2013) 1-12 ISSN 2347 - 3258
International Journal of Advance Research and Innovation

Experimental Studies for Accessing the Influence of Micro-Dimple Area Density on Tribological Performance of Mating Contacts

R. C. Singh [a,*], R. K. Pandey [b], S. Maji [a]
[a] Department of Mechanical Engineering, Delhi Technological University, New Delhi, India
[b] Department of Mechanical Engineering, I.I.T. Delhi, New Delhi, India

Article Info

Article history:
Received 1 July 2013
Received in revised form
15 July 2013
Accepted 22 July 2013
Available online 1 August 2013

Keywords
Micro-Circular Dimples,
Pin-On-Disc,
Mating Contact,
Spiral Array

Abstract

The present research has been done to investigate the influence of the relative motion of a plane surface with the other having micro-circular dimples throughout the contact. Using pin-on-disk setup, experiments have been carried out to study the influence of micro-dimple area density on friction and specific wear rate at the interface of two materials. Circular dimples are distributed in spiral array on the disk face. Based on the experiments, better tribological results have been achieved in the starved boundary lubrication mode.

1. Introduction

Existence of controlled dimple on mating surfaces reduces the friction and improves the tribological properties of the interface. Recently researchers [1-4] have provided more thrusts on improving the tribological issues using the surface engineering as a tool. Surface texture for friction reduction comprise of a flat surface interrupted by local micro-dimples. It has been established by researchers that shallow micro-dimpled surface generates innumerable tiny hydrodynamic bearings, which separate the mating surfaces. Moreover, micro-dimples act as oil reservoirs and wear debris/contaminants trapping pits, which greatly contribute in enhancing the tribological performances of contacts even during the existence of mixed/boundary lubrication. Effective lubrication at the interface is influenced by many parameters such as surface roughness, dimple depth, dimple area density, dimple shape, and lubricant properties in addition to operating parameters. Therefore, the objective of this paper is to explore the influence of dimple area density on the friction and wear behaviors of the contacts under various operating conditions.

Corresponding Author,
E-mail address: rcsingh68@hotmail.com
All rights reserved: http://www.ijari.org

2. Experimentation

2.1 Specimen of disc, pin and lubricating oil

Specimen of mild steel plate of 165 mm diameter and 8 mm thick has been taken as shown in Fig.1a for experimentation. Surface grinding and lapping fabrication processes has been performed on it to reach up to the level of surface roughness of 0.2 to 0.3 micrometer root mean square value and checked by surface roughness tester.

Cylindrical mild steel C-50 pin of diameter 12 mm has been taken for test on mild steel circular plate as dimensions shown in Fig.1b. The circular pin face has labeled and checked by rubbing on soft paper to remove debris and its flatness by ink impression on paper respectively the length of pin is about 30 mm, and diameter is 12 mm. The 26 mm length of pin is rigidly clamped and only 4 mm remains out in fixture for test on disc so that bending may be minimized and neglected during evaluation of tribological properties.

The lubricating oil (20W40) has been used which have the following characteristics measured in laboratory by true density meter, specific gravity meter and kinematic viscosity meter are 0.89036 g/cm3, 0.8912 and 120.79248 mm2/sec at 40°C and atmospheric pressure as per ASTM D-4052, D-287 and D-445 respectively.

Fig: 1a mild steel plate

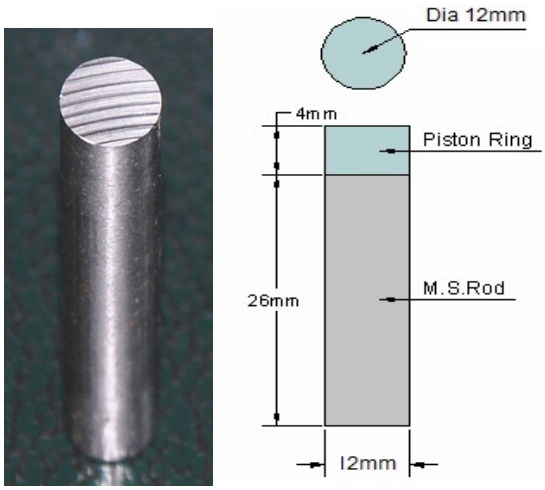

Fig. 1b Cylindrical mild steel C-50 pin

2.2 Specimen of wear test rig

The wear test rig as shown in Fig. 2a and the specification in Table 1 has a motor that rotates with different speed based on rheostat and the speed may be fixed as desired between the ranges 200 to 2000 rpm of speeds. A horizontal plate fixture is attached over which specimen of disc is bolted at four points. Speed detector and wear measurement probe is attached on it. Loading is done on pan that have horizontal platform supporting the direction of gravity. The applied direction of force is transmitted through wire and pulleys arrangements. Bell-crank mechanism with uni-leverage is used and force detector probe is used at the side to determine the sheer friction force. Following are specification of wear test rig.

Table: 1.

Details		**Description**	**Remarks**
Top specimen (mm)	Pin	Dia 3,4,6,8,10 & 12	Material; Ms
Bottom specification (mm)	Disc	Diameter 165	Material: Ms
		Thickness 8	
Speed (rpm)	Disc	Minimum 200	
		Maximum 2000	
Frictional force (N)	Between pin & disc	0 to 200	

2.3 Dimples calculations

The minimum diameter of pin is 3 mm as per specification of test rig so radial distance have been grouped in set of 3 mm ranging from radius 10-70 mm on disc. Again the middle of those three have been considered for calculating number of dimples required to be fabricated on disc. At considered radius having circumferential distance has been divided by required 1 mm, 2 mm, 3 mm and 4 mm pitches to know the number of dimples. So the four plates have been prepared of 420 microns for analysis of minimum coefficient of friction.

The dimples are prepared in such a way that the minimum diameter of pin was taken in consideration of 3mm. The radial distance has been taken in interval of one millimeter. The distribution of dimples along circumferential distance is taken according to the required pitch between two dimples.

For continuous three millimeter set of radial distance, the angle between two dimples is divided into three parts. The distribution of dimples starts from reference line for the first circumferential distance.

For the second circumferential distance in the same set of three radial distances, dimples starts from second angle. The third circumferential distance corresponding to third radial distance in the same set, dimple starts from third angle. In this way all the circumferential distance corresponding to set of three radial distances, dimples are formed.

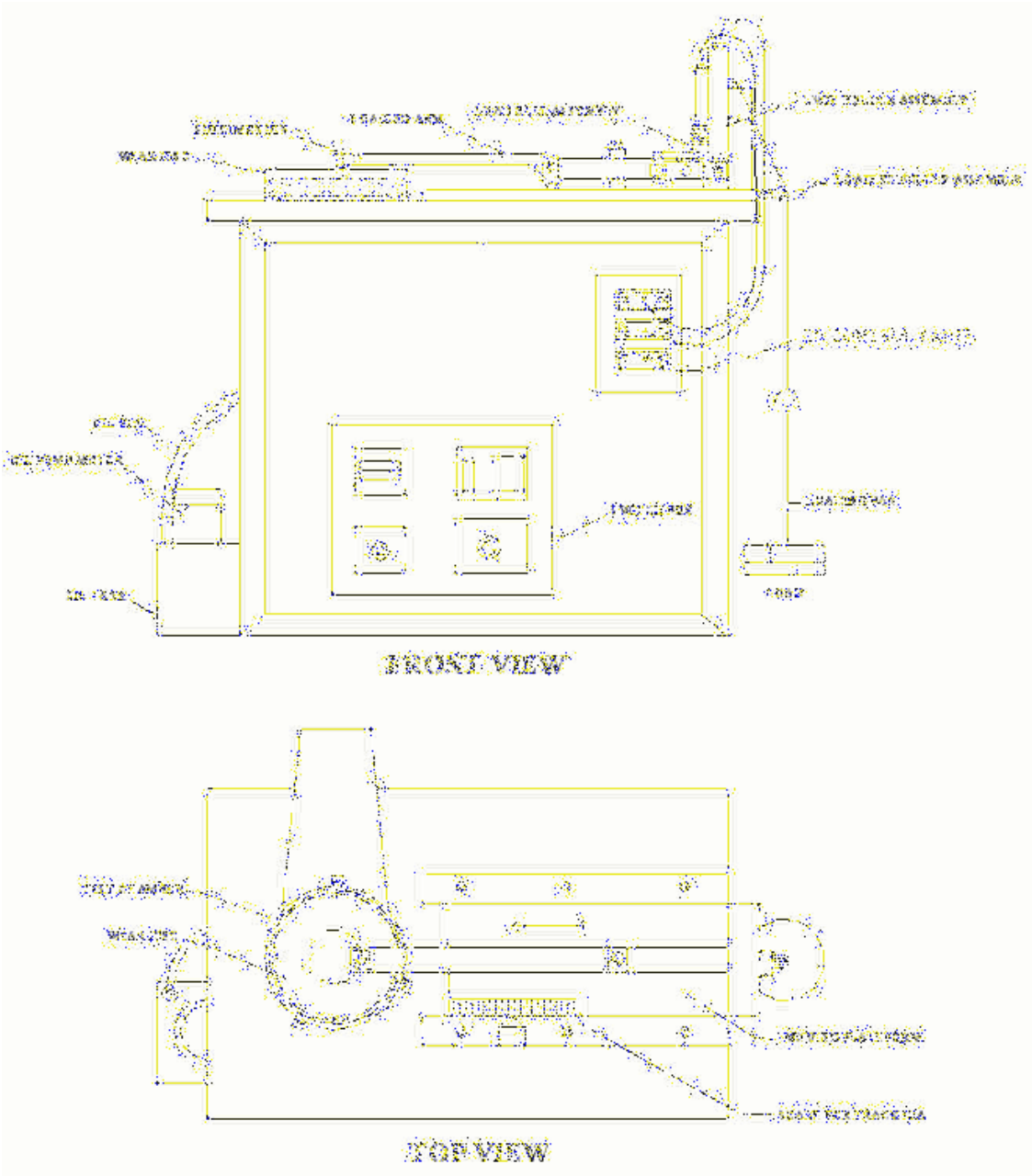

Fig: 2. Schematic diagram of pin on disk test rig

2.4 Specimen of disc with dimples

The dimples have been fabricated using chemical etching process for different disc with the different pitches. Drawings have been made by using Catia software as shown in Fig. 3 as follows:

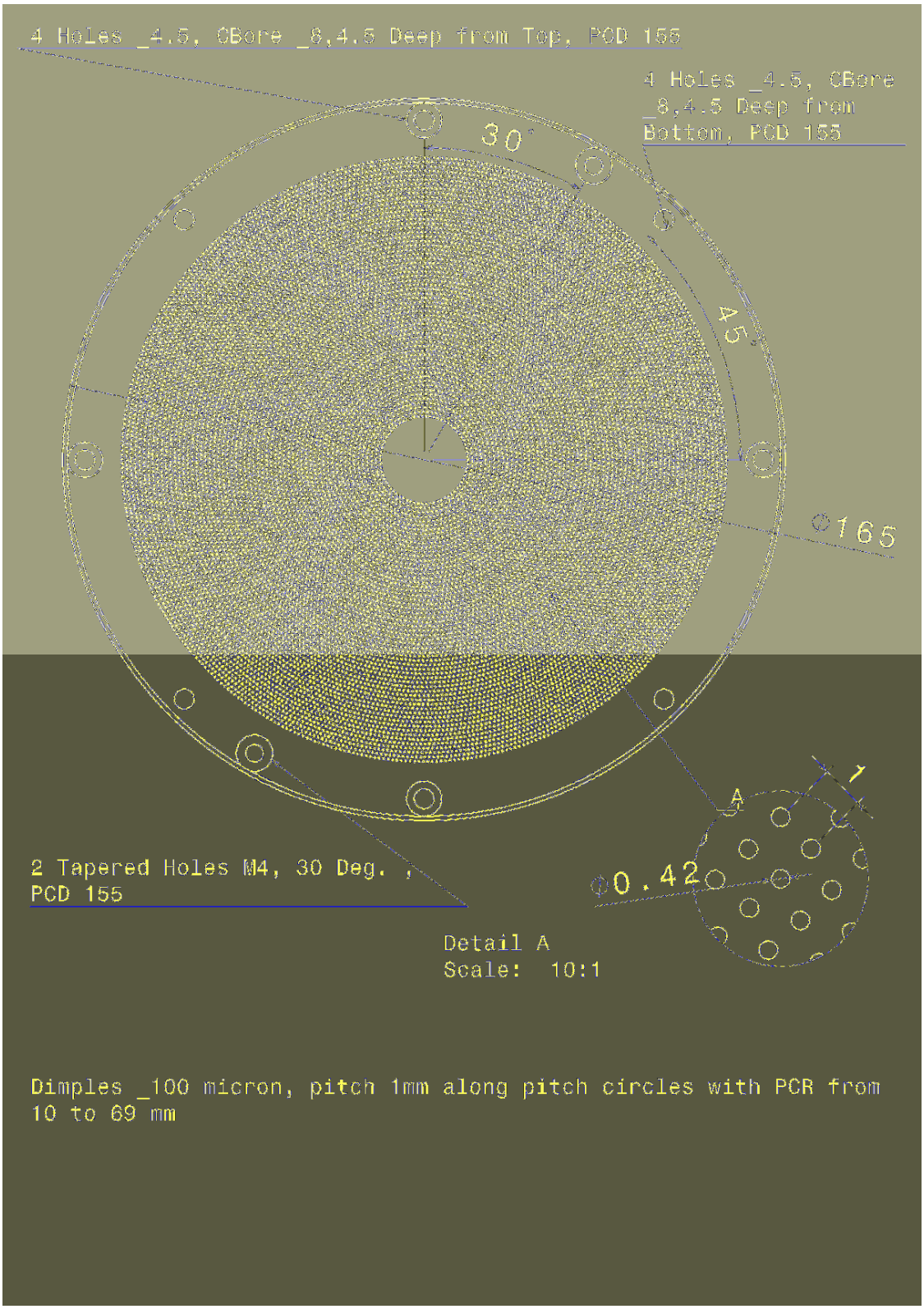

Fig. 3a Dimples of 420 micrometer diameter, pitch 1 mm along circumferential distance

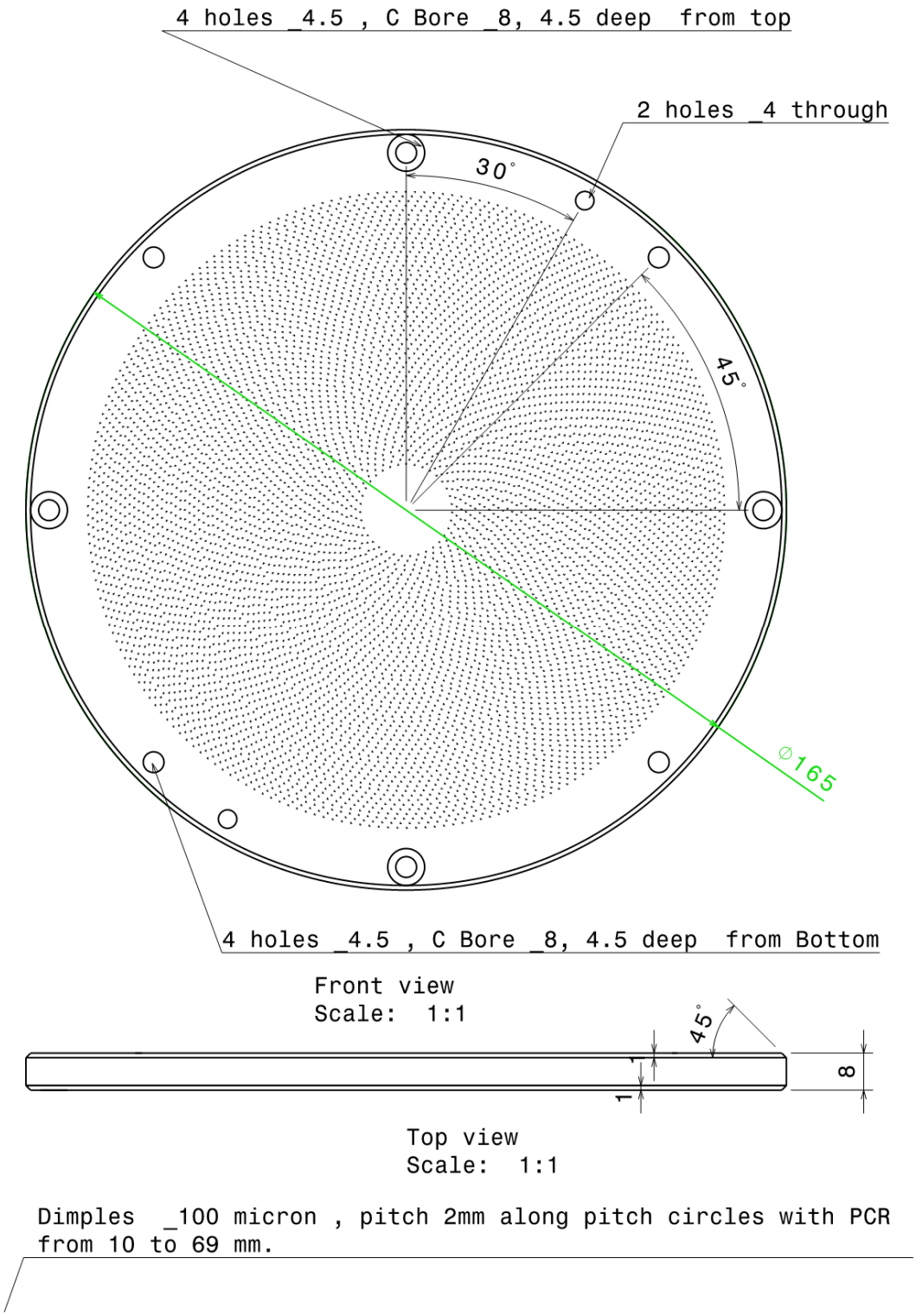

Fig: 3b. Orthographic drawing of test plate with dimples of 420 mm diameter and having pitch 2 mm

For determining of the friction and wear at the interface formed between the pin end and disk face and worn disc and pin figures have been shown in Fig. 4. Both disk and pin are made of mild steel (C-50). The end faces of mating bodies have been lapped to the roughness of RMS to around 0.2 μm. The face of disk is textured in the pattern as shown in Fig.1. Circular micro-dimples of diameter of 420 μm and depth of 200-250 μm are created by chemical etching process on mild steel disk. Tribological studies are conducted for the loads characterized by pressure varying in the range of 0.4- 1.4 MPa at sliding speeds 0.5-10 m/s (equivalent to 200 –2000 RPM).

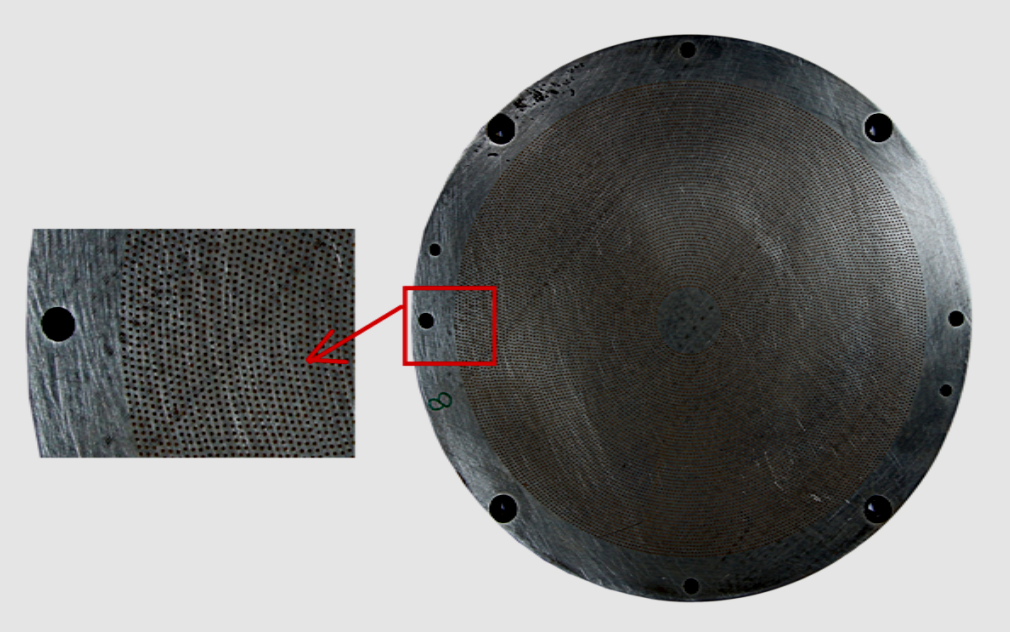

Fig: 4a. Disc with elaborated part

Fig: 4b. Disc with worn track

3. Results and Discussions

Typical trends of friction coefficient μ at different sliding speeds are plotted in Fig. 5 at load of 118 N for starved lubrication. Dimples on the contact surface of disk having pitch 1mm improves the tribological performance immensely in comparison to disks having pitches 2, 3, and 4 mm.

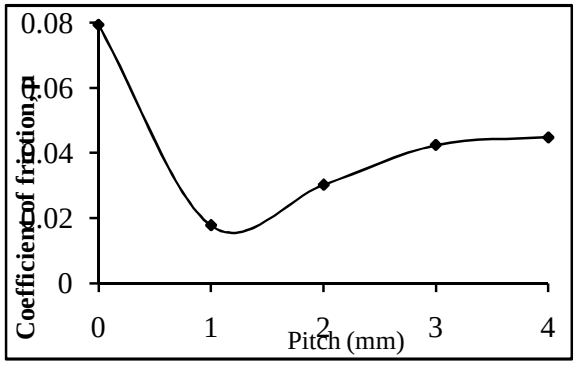

A plane and four dimpled disc having pitch 1 mm, 2 mm, 3 mm and 4 mm has been taken for determining of coefficient of friction between pin and disc. Experiments have been done by applying 118N (12 kg) load, 110 mm diameter of the disc, running at 500 rpm and pin has diameter 12 mm by applying lubricant having properties shown in table. Also the dry frictional coefficient between plain disc and pin is 0.233. The graph shown in figure, plane disc or zero dimples has maximum value of order 0.079. Where as dimpled have 0.0178, 0.072, 0.042 and 0.032 corresponding to disc having pitch 1 mm, 2 mm, 3 mm and 4 mm respectively. The plate having pitch 1 mm has minimum coefficient so considered for experiment.

The disc has been lubricated only once during starting of experiment. The experiment has conducted at different rpm by keeping the load of 12kgf constant for 2400 second at diameter 110 mm. The frictional force with respect to different rpm has been read to plot variation of coefficient of friction vs load as shown in fig. It has been observed that coefficient of friction initially decreases and after that it increases linearly with speed. There is no wear as shown by wear characteristics in fig. leaving last part where rapid grouth of wear take place.

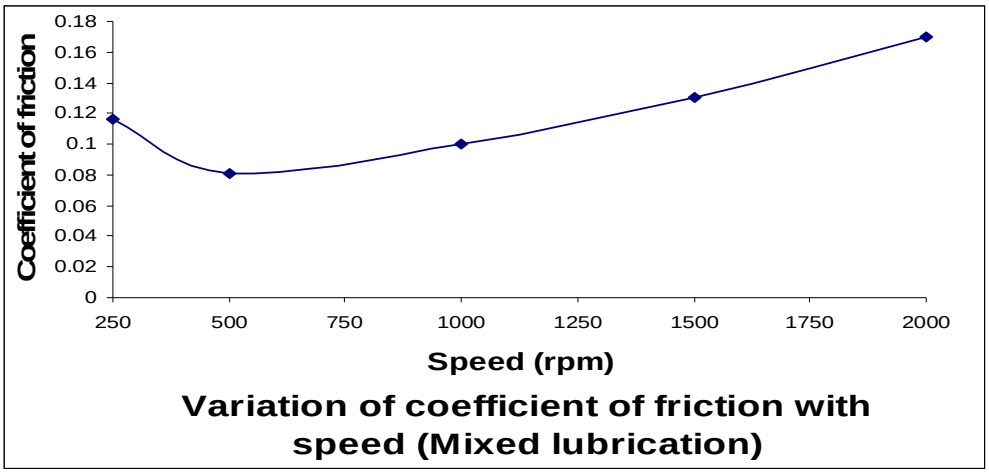

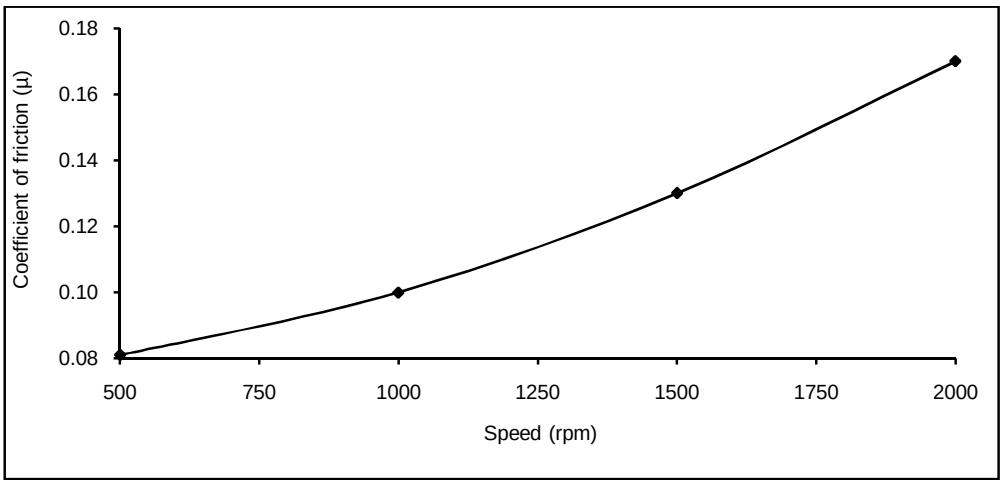

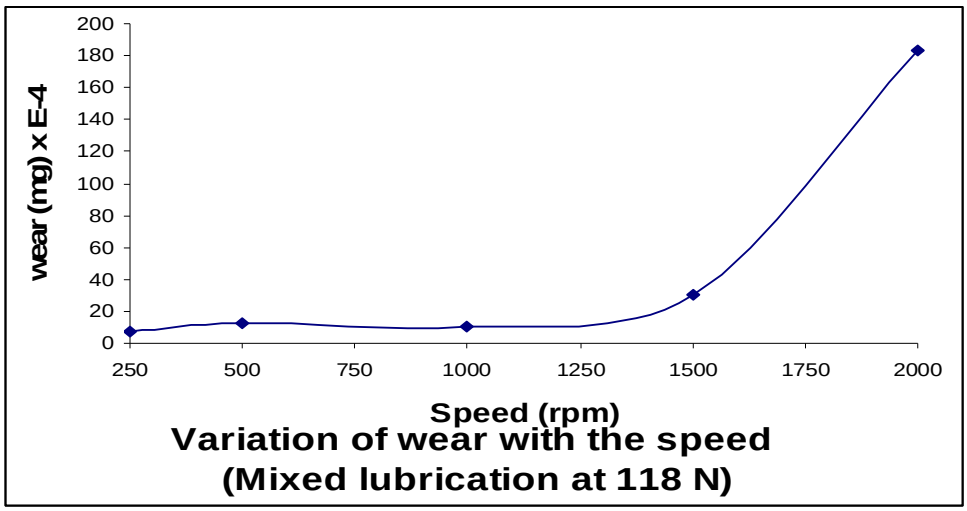

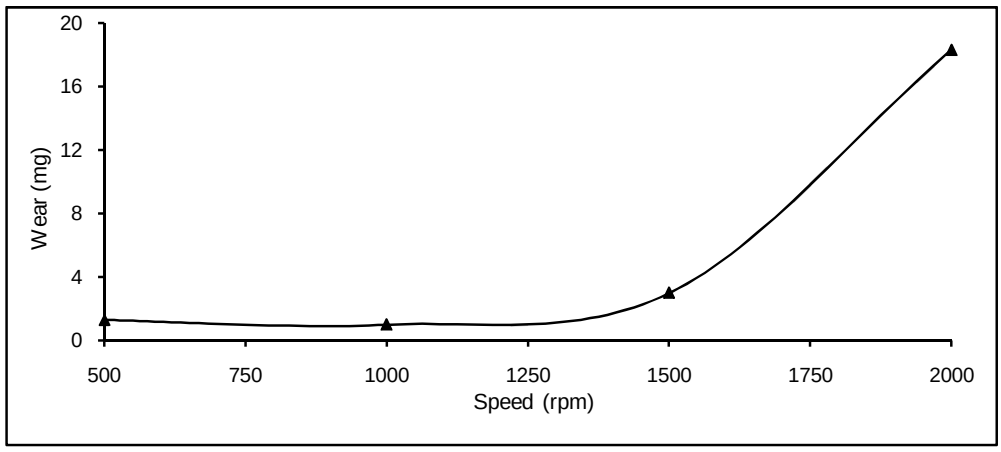

The variation coefficient of friction with respect to load is shown in fig for mixed lubrication. It decreases with load and at last it takes positive slop.

Whereas wearing of material shows that initially it increase and after that it reduces.

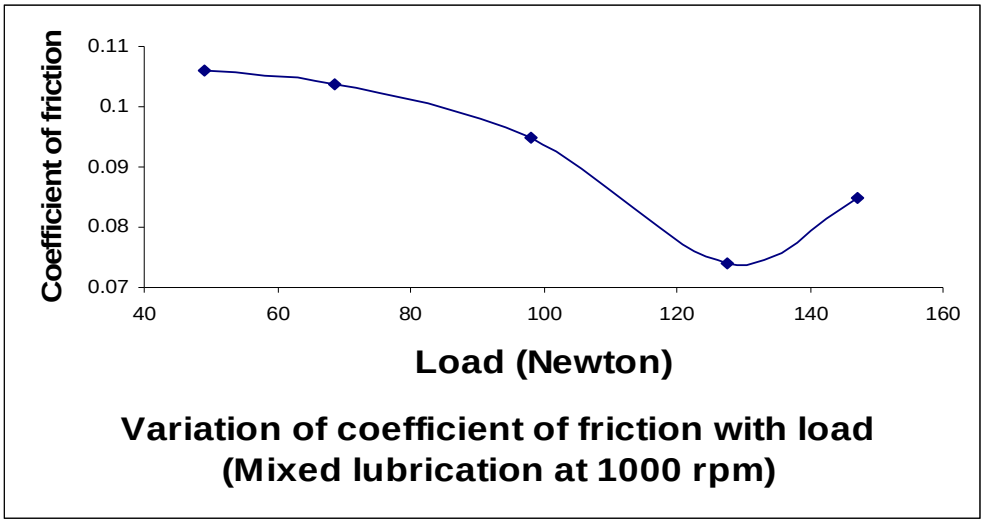

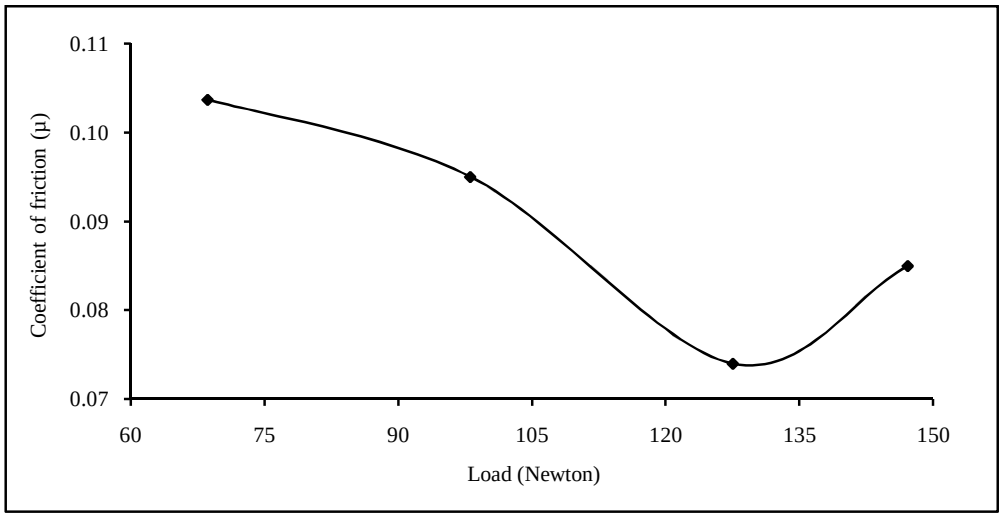
0.11
0.10
0.09
0.08
0.07
Coefficient of friction (μ)
60
75
90
105
120
135
150
Load (Newton)

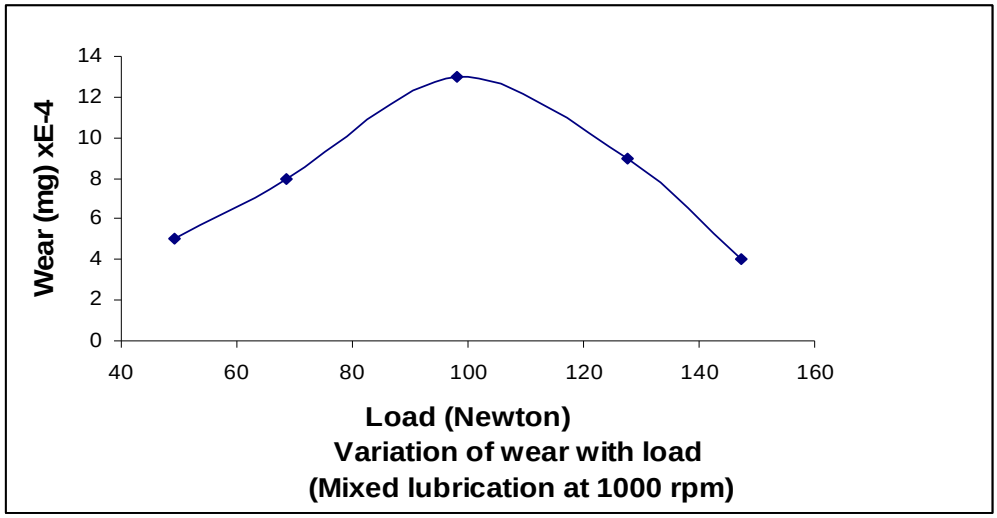
14
12
10
8
6
4
2
0
Wear (mg) xE-4
40
60
80
100
120
140
160
Load (Newton)
Variation of wear with load
(Mixed lubrication at 1000 rpm)

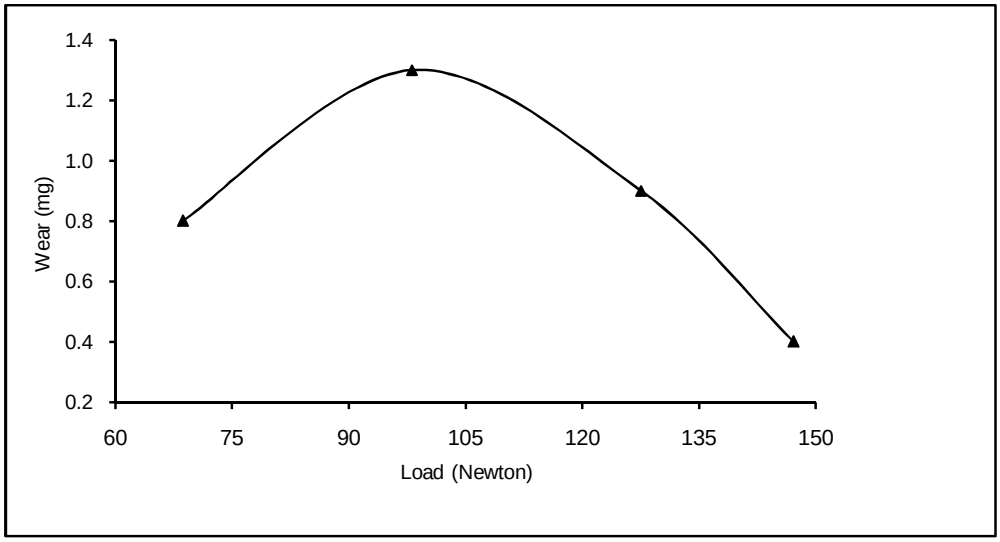
1.4
1.2
1.0
0.8
0.6
0.4
0.2
Wear (mg)
60
75
90
105
120
135
150
Load (Newton)

The experiment has been carried out with continuous flow of lubricating oil at the interface of pin and disc to form hydrodynamic lubrication. The load has been kept constant of 12kgf. And the speed has been varied. It has been observed that coefficient of friction continuously decreases with speed and after certain period it remains constant at minimum value nearly 0.03. The wear increases for very short period and after that it decreases continuously to become constant.

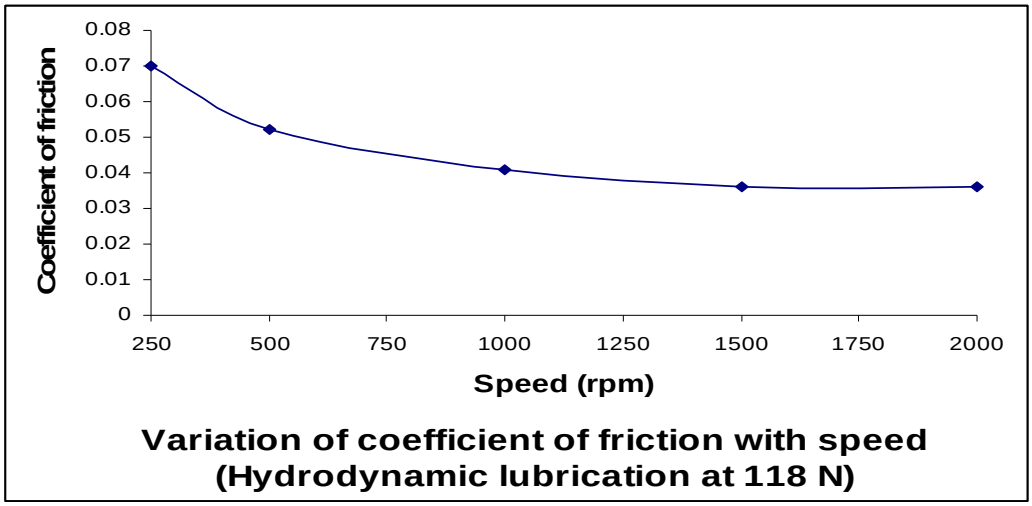

Variation of coefficient of friction with speed (Hydrodynamic lubrication at 118 N)

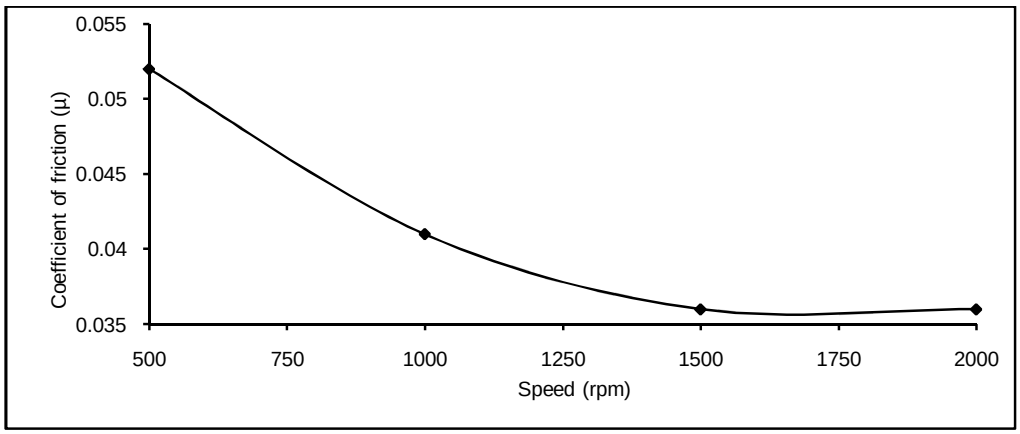

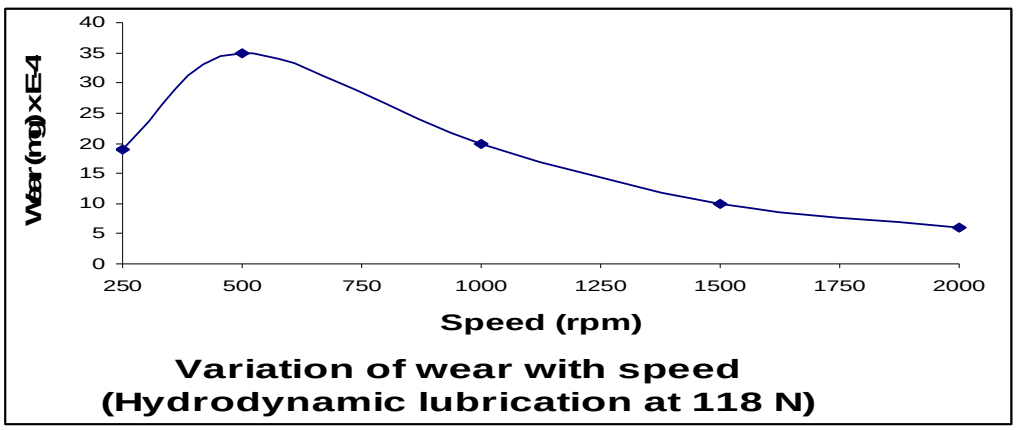

Variation of wear with speed (Hydrodynamic lubrication at 118 N)

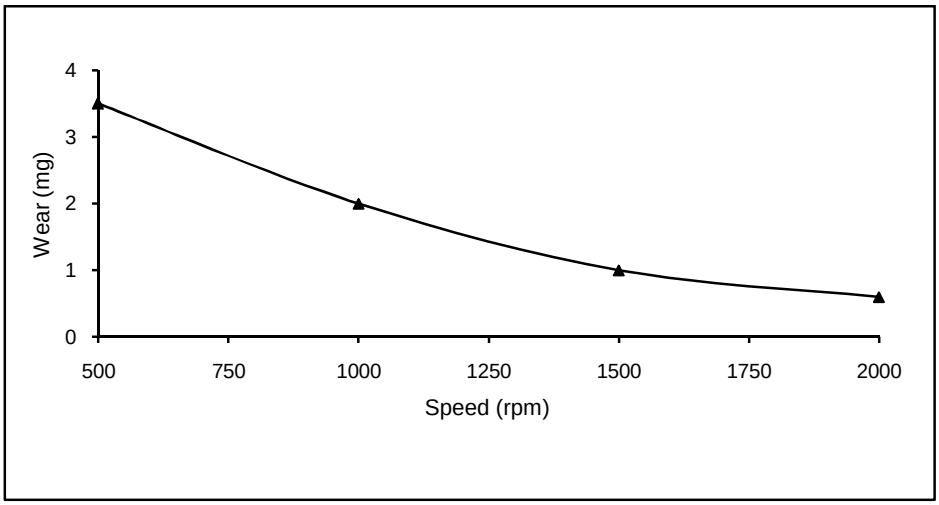

The experiment has been carried out by keeping the speed constant 1000 rpm at 110 mm diameter of disc and varying load. It has been observed that during hydrodynamic lubrication coefficient of friction initially at low load increases but after that continuously decreases if last part would be taken as straight. Wear characteristic follow the same variation of coefficient of friction with load as shown in fig.

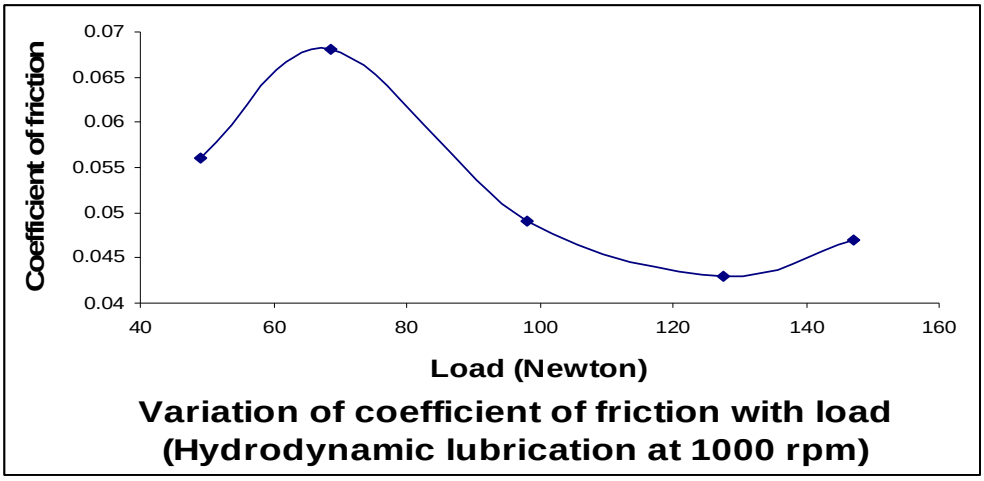

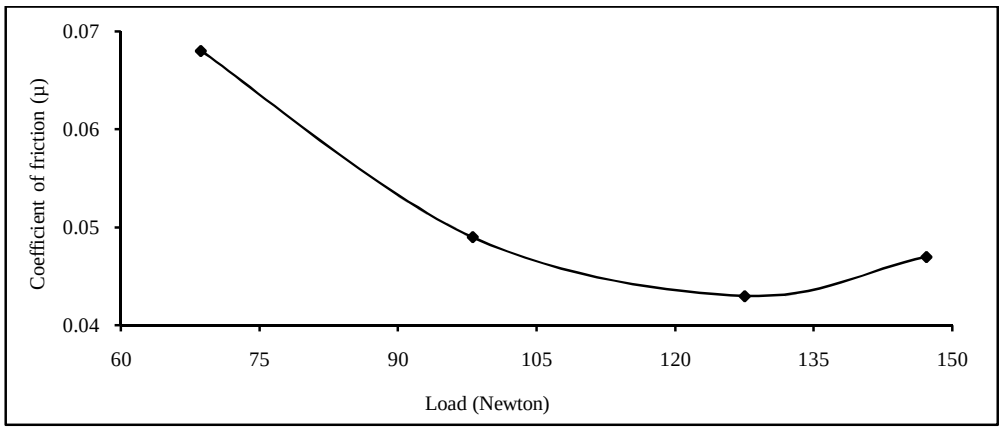

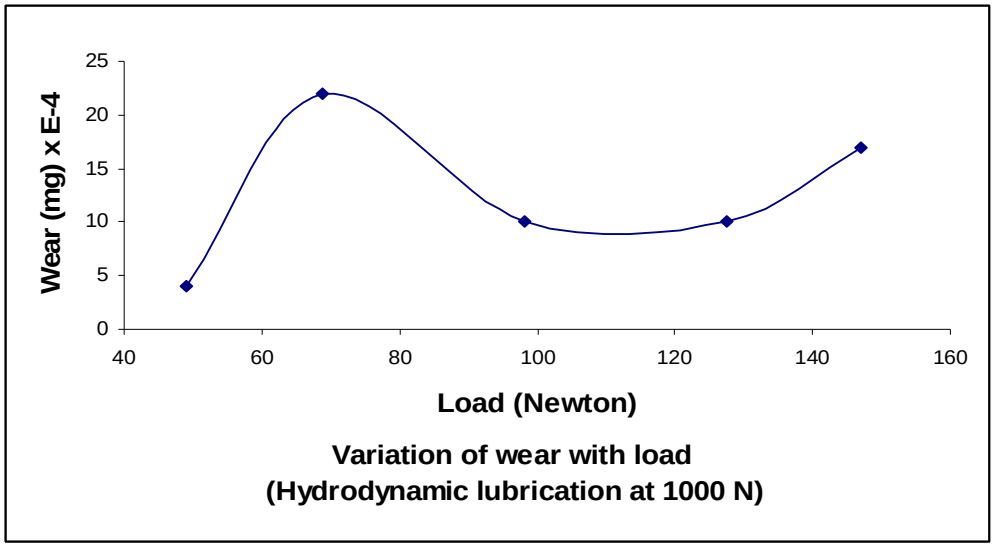

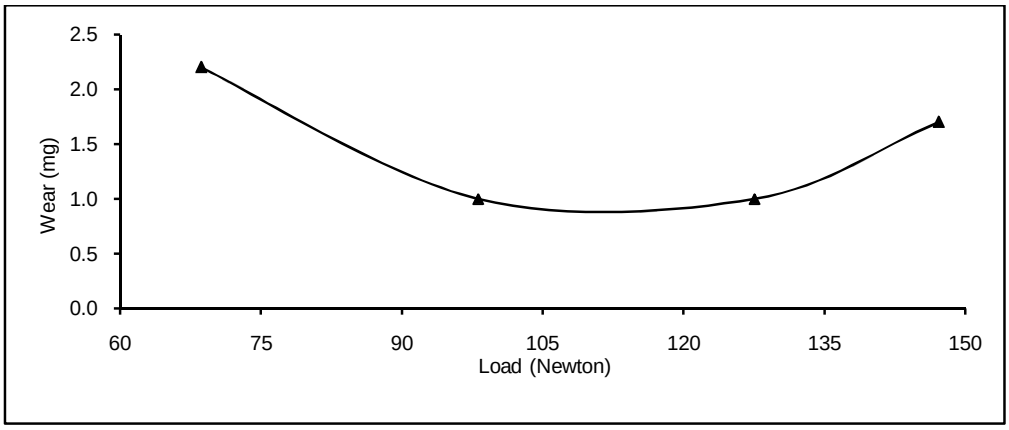

4. Summary

Based on the experiments reported in this paper, authors have observed that micro-dimple area density play great role in improving the coefficient of friction at interface in boundary/mixed lubricating conditions. The coefficient of friction first decreases then increases continuously with speed whereas wear remains constant. Whereas in hydrodynamic lubrication coefficient of friction continuously decreases with speed.

References

[1] D. F. Moore, "A History of Research on Surface Texture Effects," Wear, 13, 1969, 381-410
[2] U. Pettersson, S. Jacobson, "Influence of Surface Texture on Boundary Lubricated Sliding Contacts," Tribol. Int., 36, 2003, 857-864
[3] I. Etsion, "State of the Art in Laser Surface Texturing," ASME J. Tribology, 127, 2005, 248-253
[4] A. Erdemir, "Review of Engineered Tribological Interfaces for Improved Boundary Lubrication," Tribol. Int., 38, 2005, 249-256
[5] M. Fowell, at. al, "Entrainment and Inlet Suction: Two Mechanisms of Hydrodynamic Lubrication in Textured Bearings,"ASME Journal of Tibology,129(2), 2007,336-47.
[6] Y. Qiu, M. M. Khonsari, "Experimental Investiggation of Tribological Performance of Laser Textured Stainless Steel Rings," Tribology International, 2011

Earth Science & Climatic Change

Gandhi et al., J Earth Sci Clim Change 2013, 5:1
http://dx.doi.org/10.4172/2157-7617.1000173

Review Article Open Access

Extreme Weather Events and Climate Change Impact on Construction Small Medium Enterprises (SME's): Imbibing Indigenous Responses for Sustainability of SME's

Shubham Gandhi*, Anik Gupta and Sanchit Sethi

Department of Environmental Engineering, Delhi Technological University, Delhi, India

Abstract

Purpose: India has a rich tradition of cultural practices and a textual heritage that dates back to several hundreds of years. The intellectual achievements of Indian thought are found across several fields of study in ancient Indian texts ranging from the Vedas and the Upanishads to a whole range of scriptural, philosophical, scientific, technical and artistic sources, which advocates environmentalism. However as the globalization took roots in India in late 80's and to withstand the competition face from global markets Indian Small Medium Enterprises ignored the environmental safety and as results of this pollution is now crossing critical limits in metro cities. Delhi experienced a number of Extreme Weather Events (EWEs) during recent years and a significant number of businesses were affected including the construction sector, which is a major employment driver, being the second largest employer in the country, next only to agriculture. However, little research work has been undertaken on how construction industry is at the risk due to the EWEs. The paper profoundly aims at exploring various such EMEs and their impact on the construction businesses. And finally suggests the ways through which it could be tackled.

Research design/methodology/approach: A mix and match research design was adopted to elicit information from construction industry, involving a questionnaire survey and interviews to obtain responses from construction practitioners. Mean was used to establish the average scores for analysis and conclusion. Direct and Indirect impacts from extreme weather events on logistics, people premises, process, markets and finance are discussed in detail

Findings/conclusions: Direct and indirect impacts from climate change include damage to products and tools from higher temperatures and increased rainfall, with consequent delays and increased costs to projects. The predominance of outdoor workers in this sector leaves its employees at higher risk from increased direct-heat stress, mostly dehydration all leading to severe effect on people.

Keywords: Indigenous knowledge; India; Extreme weather events; SMEs; Sustainability; Construction industry

Introduction

A brief about knowledge traditions and practices of India

India has a rich tradition of cultural practices and a textual heritage that dates back to several hundreds of years. It had a magnificently advanced knowledge base, which gave birth to rich traditions and ingenious practices during the medieval era. The intellectual achievements of Indian thought are found across several fields of study in ancient Indian texts ranging from the Vedas and the Upanishads to a whole range of scriptural, philosophical, scientific, technical and artistic sources. In many parts of India, communities have inherited the rich tradition of love and reverence for nature through ages. Religious preaching, traditions and customs have played a big role in this regard: Indian religions have generally been the advocates of environmentalism. India has witnessed the great environmental movements in past.

The four Vedas - Rigveda, Samaveda, Yajurveda and Atharvaveda - are full of hymns dedicated to the supremacy of various natural entities. The Rigvedic hymns refer to many gods and goddesses identified with sun, moon, thunder, lightening, snow, rain, water, rivers, trees etc. They have been glorified and worshipped as givers of health, wealth and prosperity. *The rain –god Indra* has the largest number of hymns attached to him. *Sun worship* is of vital importance in Vedic worship; the sun was worshipped in the form of gods like Surya, Martanda, Usa, Pusan, Rudra, etc because solar energy is the ultimate source of energy that regulates the energy flow through the food-chain, drives various nutrient cycles and thus controls the entire ecosystem all over the earth, but it was probably well understood and realized by the ancient people as well. Holy book "*Guru Granth Sahib" states, 'Air is the guru (Teacher), water is the father, and earth is the great Mother of all.'*

A brief about flora and fauna wealth of India

Trees and plants were considered as animate beings and to harm them was regarded as a sacrilege. The Atharva-Veda glorifies the medicinal value of various herbs with mythical powers. Three major factors are responsible for the origin of the tree-cult in India:

Their wood leaves, fruits, etc. were useful to humans; it was believed that trees were possessed by spirits who guided humans in their distress; and humans developed respect for trees which often provided them with an alternative for medicinal plants.

The pipal (*Ficus religiosa*) tree (Figure 1), which is considered sacred among Indian masses, continuously releases oxygen in the atmosphere, and therefore, our ancestors must have put such knowledge into

***Corresponding author:** Shubham Gandhi, Department of Environmental Engineering, Delhi Technological University, Delhi-110042, Delhi, India, Tel. 011-27871018; E-mail: shubhamgandhi14@gmail.com

Received July 29, 2013; **Accepted** November 28, 2013; **Published** December 05, 2013

Citation: Gandhi S, Gupta A, Sethi S (2013) Extreme Weather Events and Climate Change Impact on Construction Small Medium Enterprises (SME's): Imbibing Indigenous Responses for Sustainability of SME's. J Earth Sci Clim Change 4: 173. doi:10.4172/2157-7617.1000173

Copyright: © 2013 Gandhi S, et al. This is an open-access article distributed under the terms of the Creative Commons Attribution License, which permits unrestricted use, distribution, and reproduction in any medium, provided the original author and source are credited.

Figure 1: The pipal (Ficus *religiosa*) tree.

spiritual form. Epics like *Meghaduta, Abhijnanasakuntalam,* etc. They provide colourful portrayal of trees, creepers, animals and birds conversing with people and sharing their joys and sorrows, which shows that people believed in harmony between man and nature. According to Kautilya (Figure 2), cutting trees or its branches is an offence and he prescribed various punishments for it. Watering the plants is considered as greatly rewarding in the *dharmaśāstra* texts.

Many gods and goddess have Bird as their vehicles or *vahana.* These include lion, tiger, elephant, bull, horse, peacock, swan, owl, vulture, ox, mouse, etc. The association of wild animals with peoples' religious beliefs played a significant role in their preservation since long period in India, until the colonial rule indulged in intensive hunting of wild animals.

The case of Sacred Grooves

A sacred groove (Figure 3) consists of a bunch of old trees, generally at the outskirts of a village, which were left, untouched when the original settlers cleared the forest to establish the village. Such groves were regarded as the abodes of gods and goddesses or spirits and hence protected with utmost care. The cutting of trees was prohibited in these areas and nobody dared to disobey the injunction, partly because of religious faith and partly due to the fear of facing the wrath of the gods, goddesses and spirits.

Conservation teachings in Jainism and Buddhism

Buddhism and Jainism, the two most popular heterodox sects of ancient times also advocated nature conservation. Buddhism believes in tolerance, love, compassion, forgiveness and non-violence to all. Jainism advocates complete non-violence or Ahimsa; it treats every creature on earth including the smallest insects or microbes as of equal importance and forbids their killing by all means. This perception went a long way towards preserving biodiversity.

Environmental movements in India-and tradition of resistance

The love for trees was so greatly infused in the minds and souls of the Bishnois (A farming community of Rajasthan and its adjoining states) that in Khejrali village of Rajasthan about 363 young and old men and women embraced the *khejri* trees (*Prosopiscineraria)* to protect them from being felled by the king's men. The local ruler had ordered the cutting of *khejri* trees to use them for his limekilns as fuel; the Bishnois hugged them and many were killed in the episode. Later, a temple was built in honour of the Bishnoi martyrs. One of the leading women of the movement was Amrita Devi Bishnoi. The repentant king later issued an edict protecting trees and animals in Bishnoi-controlled lands.

Chipko movement: The first movement against indiscriminate tree felling was started in India in 1730. It was fought against indiscriminate tree felling in Jodhpur, a city in Rajasthan province of India. Amrita Devi, a village woman, collected 362 other women from her village and marched to forest nearby. They declared that the forest trees could be cut down only over their dead bodies. "Chipko" means "hug". And each woman clung to a tree and stood motionless when timber contractors came. All the 362 women were axed to death by the tree fellers. This heart-rending incident compelled the then king of Jodhpur to ban tree felling in forest. The movement soon became famous all over the world. Environmentalists from France, Germany, Sweden, etc. came India to learn about unique Chipko movement. Then there was the *Baliyapal Movement*. This was against the taking over of the thickly populated village of Baliyapal village's fertile land for testing Missiles.

Later on some other persons have also been involved in this movement and have given it proper direction. Mr Sunderlal Bahuguna, a Gandhian activist and philosopher, whose appeal to Mrs Indira Gandhi, the then Prime Minister of India, resulted in the green-felling ban. Mr Bahuguna coined the Chipko slogan: *'ecology is permanent*

Figure 2: Chanakya is traditionally identified as Kautilya or Vishnu Gupta, who authored the ancient Indian political treatise called Arthaśāstra. As such, he is considered as the pioneer of the field of economics and political science in India, and his work is thought of as an important precursor to Classical Economics.

Figure 3: A sacred groove.

economy'. Mr Ghanasyam Raturi, the Chipko poet, whose songs echo throughout the Himalayas of Uttar Pradesh, wrote a poem describing the method of embracing the trees to save them from felling:

Embrace the trees and

Save them from being felled;

The property of our hills,

Save them from being looted.'

SME's in India and Effect of Globalization and Liberalization

Small and Medium Enterprises (SMEs) are considered as the backbone of economic growth in all countries because they account for 80 percent of global economic growth. In the newly developing or Newly Industrialized Countries (NICs), SMEs generally employ the largest percentage of the workforce and are responsible for income generation opportunities. The initiation of economic reforms through industrial and trade liberalization in 1991-1992 marked the beginning of a new era for industry in India. The measures included industrial de-licensing, the removal of threshold limits on the assets of large enterprises, the implementation of a liberal policy to facilitate Foreign Direct Investment (FDI), the expansion of the Open General License (OGL) list, reductions in customs duties and similar actions. Global competition confronts the majority of purely domestic SMEs, whose products and sales are extremely localized and/or segmented. Trade liberalization increases the capacity of well-established foreign manufacturers and retailers to penetrate both remote and underdeveloped markets. Against this development, local SMEs find it increasingly difficult to survive or even maintain their current business position in their respective markets. Most of the entrepreneurs think that Environmental regulations damages competitiveness and it is the reason that SMEs account for 70% of total industrial pollution.

Construction industry/construction sector SMEs

The construction industry is the second largest industry of the country after agriculture accounting for 11 percent of India's GDP. Indian construction industry employs 32 million people and its total market size is estimated at Rs. 2, 48,000 crores (35,640 million €) (Source: www.marketresearchindia.in). The activities of the construction industry include working on new structures as well as additions, alterations, and repairs to existing ones. SMEs account for a significant proportion of the construction sector.

Problems faced by Indian construction industry

- Construction industry suffers from capacity constraints.
- Lack of trained manpower and managerial skills with performance much below international level.
- Small and medium contractors do not have the wherewithal to upgrade their capability.
- Quality, safety, environment and social aspects are also not being addressed appropriately.

Also, Due to the nature of their operations, businesses operating in the construction sector have always been considered significantly vulnerable to weather extremes. Indeed, Mills [1] identified the construction sector as one of the most vulnerable to climate change and EWEs. Therefore there is a need to increase the understanding the risk associated with it. And thus greater research has to be undertaken on how construction SMEs responds to the risk of EWEs and build resilience.

EWE and construction industry

Basically, the climate of India is dominated by the summer monsoon (June to September). The entire year is, however, divided into four seasons: (i) Winter (December and January) (ii) Pre-monsoon or Hot Weather season (March - May) (iii) Southwest or Summer Monsoon season (June - September) (iv) Post monsoon season (October - November). Year to year deviations in the weather and occurrence of climatic anomalies / extremes in respect of these four seasons are:

- Cold wave, Fog, Snow storms
- Hailstorm, Thunderstorm and Dust storms
- Heat wave
- Floods, Heavy rain

These are all related to the meteorological factors. Whereas earthquakes, volcanoes and tsunamis are other geo physically triggered disasters and not discussed in the present research paper.

EWEs can have both direct and indirect effects on the construction sector and those associated with it.

Direct effects include disruption to site works as a consequence of the extreme weather event itself (e.g. the site might be flooded); indirect effects include disruption to site works as a consequence of the secondary effects of an extreme weather event (e.g. disruptions to deliveries and utility supplies through the supply chain) [2]. Many authors have found that: there is a lack of forward planning; lack of capital for recovery; ineffectual interactions with national agencies; infra-structure problems [3]; individual attitudes and organizational culture; access to expertise; perceived exposure to risk [4]; and the relatively low importance assigned to climate change and EWEs by the construction sector [5], all contribute to a general inertia amongst organizations to consider resilience to EWEs.

Research Methodology Adopted for Study

The methodology adopted in this research work is given below

- Study of literature related to impact of extreme weather events in construction business.
- Preparation of Questionnaire.
- Site visit to major construction project sites.
- Questionnaire survey and personnel interviews with in-charges and managers and collection of data from site.

Questionnaire design

The six identified impact areas and 29 factors formed a questionnaire used as survey tool. Respondents were asked to express the degree of impact EWE is likely to have on their businesses on a five-point Likert scale. After interviewing professionals and different academicians the questionnaire was finalized and was distributed among 60 clients. While interviewing the professionals they were asked to quote their responses based on their experiences in the past. No incentives to participation in the survey were offered. Questionnaires were posted in the months of January - February, 2013. Out of 60 questionnaires only 20 fully filled questionnaires were received i.e. a response rate of 30%. The mean score (out of 5) of each factor under a given parameter was calculated

indicating the relative importance of each factor. Significance of the score 1 - Very Low Impact, 2 - Low Impact, 3 - Moderate Impact, 4 - High Impact and 5 - Very High impact. A descriptive figure of research methodology has been depicted in the flow chart below (Figure 4).

Results and Discussion

The entire respondent said that they had been affected by extreme weather events in the last 2 years. By far the most common extreme weather event recalled by the sample was High Temperatures (4.517), Rainfall (4.312) and Drought/Water restrictions (4.116) followed by low temperature (3.47) and winds (2.34) which is not surprising given the fact that the India has been affected by a number of Extreme Weather Events (EWEs) in the recent past (Table 1). The 2003, 2012 heat waves, 2005 flood, and 2004, 2005 heavy winter, 2013 drought, 1988 hailstorm are some examples. Such weather extremes have lead to significant economic as well as societal costs.

Identified impact areas are mentioned below:

Logistics - for example vulnerability of supply chain, utilities and transport arrangements

Premises - for example impacts on maintenance, facilities management or building design and construction

People - for example implications for workforce or customers

Process - for example impacts on concreting works and other construction works.

Finance - for example implications for investment, insurance and stakeholder reputation

Markets - for example changing demand for goods and services

As shown, in Table 2, Industries were most likely to be affected by the severe weather causing implications in terms of logistics (4.843) and people (4.719), process (4.173). A smaller proportion also mentioned that the weather had affected premises (3.129), finance (2.207) and markets (1.302).

Most of the respondent mentioned impact on workers health/ Employee Productivity (4.452) with also staff/key personnel not being able to get access to work or, simply access to work (3.167). Problems caused by staff not getting into work were most pronounced in the times of Heat waves and cold waves, possibly due to a larger number of financially weaker labourers in this area who can't cope up with changing weather conditions

The fact that the customers could not get to the business because of extreme weather (2.389) and daily workers wage loss (2.868) was also mentioned by respondents (Table 3).

"Employees could not get to work." "Our staff had to clear the Water and Mud." "Our customers were not satisfied because project was late." "We were without staff for 2-3 days." "People were sent home because there was no electricity after the flooding."

When asked to specify the greatest proportion of businesses who said extreme weather had impacted logistics mentioned supply of resources affected (3.87) because of disruptions to either transport or access (3.465) also causing delayed and delayed/failed deliveries (3.111) (Table 4).

ICT related problems and somewhat impact on schedule control were also notable issues with 2.698 as the mean.

As shown in the Table 5, it is site logistics that suffered mostly due to extreme weather events with increased difficulty in material storage, processing and handling difficulty (4.342) followed by problems in coordination of material flows on the building site (3.878). When EWE is sudden rainfall, Loss of resources (like CCTV cameras) (2.749) and disposal of waste (3.217) is an also problem due to marshy surface. Most of the comments were (Table 5):

"Deliveries were held up - materials coming into the business and outgoing to customers. Staff also couldn't get into work."

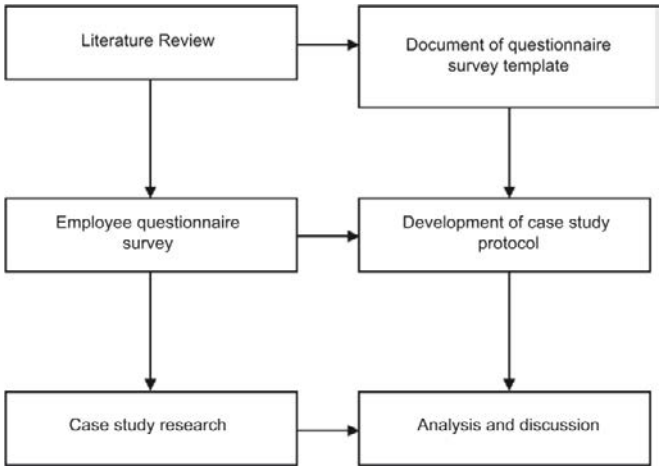

Figure 4: A descriptive figure of research methodology.

Dimensions	MEAN
Low Temperatures	3.472
Rain/ flooding	4.312
Winds	2.347
High Temperatures	4.517
Drought / Water restrictions	4.116
Snowfall	0

Source: Self Study through questionnaire

Table 1: EWEs which impacts most in Delhi-NCR region.

Dimensions	Mean
People	4.719
Logistics	4.843
Process	4.173
Premises	3.129
Markets	1.302
Finance	2.207

Source: Self Study through questionnaire

Table 2: Imapct of EWE on Construction Industry.

Dimensions	Mean
Impact on workers health/ Employee Productivity	4.452
Customers couldn't get to the business/site visits etc.	2.389
Access to work of key personnel	3.167
Daily workers wage loss (payee side)	2.868

Source: Self Study through questionnaire

Table 3: Impacts of Extreme Weather Events on "People".

Dimensions	Mean
Supply logistics	
Supply of resources affected	3.871
Delayed / failed deliveries	3.111
Transport disrupt/ access	3.465
Others like ICT related problems and Impact on schedule control	2.698

Source: Self Study through questionnaire

Table 4: Impact of EWEs on supply Logistics.

Dimensions	Mean
Site logistics	
Material storage, processing and handling difficulty	4.342
Coordination of material flow on construction site.	3.878
Loss of resources	2.749
Disposal of waste	3.217

Source: Self Study through questionnaire

Table 5: Impact of EWEs on Site Logistics.

"The fog affected everything. The roads were inaccessible this meant that deliveries inbound and outbound to customers was affected."

"We had trouble moving goods." "Production was slowed down because there were no staffs."

All the construction processes were significantly affected during extreme weather events except that of painting-flooring and tiling process (Table 6). Major problem is of mobility on premises (3.9854) during the rainfall and low temperatures at the time of dense fog. Structural damage (3.374) was also frequently occurring problem for businesses whose premises had been affected by extreme weather. Freezing and leaks (2.585), floodwater loggings (3.274) and even water scarcity (3.161) were also mentioned by respondents (Table 7).

In total, respondent stated that the market they operate in had been slightly affected by the impact of severe weather in the last 2 years. Some respondents also pointed out that extreme weather had affected their customers in some ways (2.341) and brought demand fluctuations (2.109) while there was very less impact on decrease in sales (1.676) (Table 8). Most of the respondents agreed with increase in marginal costs during EWEs (4.141) leading to income or revenue loss (3.983) (Table 9).

"We supply more sweaters, coolers, fans, etc. to site for our staff at the times of heat and cold waves."

"Demand increase as parts break more often."

"We still had to pay the staff even though they were not at work." "Our turnover and profitability dropped."

Following results were obtained on when respondents were asked about how much they are concerned about extreme weather events on their businesses (Figure 5).

Almost all respondents who were somewhat concerned about impact of EWEs were treating it same as traditional risks problems and taking simple steps like distributing sweaters and providing more facilities like liquid stamina drinks to the workers at the time of heat waves.

The respondents who marked "Very Concerned" have started incorporating new risk assessment methods including policy level changes and insurance related changes.

On asking about factors that enable them to initiate action on

Dimensions	Mean
Excavation-Foundation-Reinforcement placing	4.129
Shuttering/ framework	4.097
Concreting- Brickwork-Curing	4.129
Plastering (internal/external)	3.023
Plaster of Paris	2.112
Painting-Doors-windows-Flooring - Tiling	1.076

Source: Self Study through questionnaire

Table 6: Impacts of EWEs on processes at site.

Dimensions	Mean
Damages to land/ structural damages/	3.374
Mobility on premises	3.985
Floods water loggings	3.274
Water scarcity	3.161
If Other. Then please specify? Leaks / freezing	2.585

Source: Self Study through questionnaire

Table 7: Impacts of EWEs on premises.

Dimensions	Mean
Client's / vendor's affected	2.341
Demand fluctuations	2.109
Decrease in Sales	1.676

Source: Self Study through questionnaire

Table 8: Impacts of EWEs on Markets.

Dimensions	Mean
Increase in Marginal costs during EWEs	4.141
Income/ Revenue loss	3.983
Slow/ lost business	1.211

Source: Self Study through questionnaire

Table 9: Impacts of EWEs on Finance.

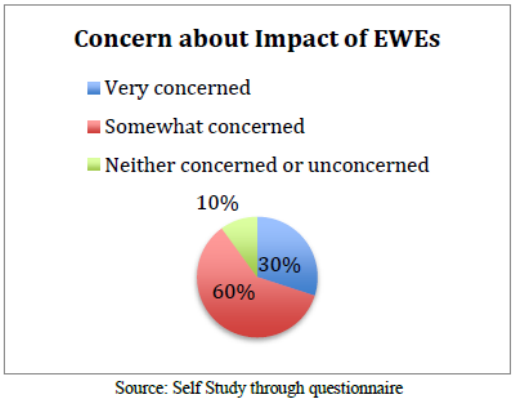

Source: Self Study through questionnaire

Figure 5: Impacts of EWEs.

Climate change and EWEs and build resilience most of them rated cost savings (3.376) as the important factor followed by improved competitiveness (3.376) and customer demands (3.423) (Table 10).

Conclusion

Construction SMEs do not see EWEs as out of the ordinary as weather has always affected the construction industry at the project level.

The severity of the events that the SMEs have experienced was not significant enough to cause a major disruption to the business. Therefore, SMEs may tend to consider EWEs more as an annoyance than a threat to the future of the company. Consequently, this might have directed them not to consider implementing coping strategies. *However, now the SMEs are more concerned about the risk of EWEs and have identified several coping strategies, as they have experienced significant impacts of EWEs recently.*

Also, where the SMEs developed new coping strategies, these were an extension of their existing approaches for risk management/transfer rather than radical approaches to minimize the impacts of future EWEs.

Recommendations

Community engagement

Local communities often have a fund of knowledge and expertise that is extremely valuable in project planning and implementation. Local people have specific interests in the impacts that the project might have on them. Local communities have a sense of self-identity that is an important aspect to be preserved. For these and many other reasons, it is important to ensure that local communities are intimately involved as stakeholders in project development when that project has a direct or indirect effect on them. An emphasis on traditional values can help to predict and mitigate the effects of cultures that have different value systems including the treatment of women, conflict resolution style, and acceptable norms of behaviour.

Include indigenous knowledge and peoples from the very beginning

While a project is still in the thinking stages, it is a wise decision to include the indigenous peoples and their knowledge to assist in determining the feasibility of the project. Bringing the indigenous peoples in after the decision has been made to carry out the project is not respectful of the integrity and autonomy of the indigenous peoples.

Build on the strengths of indigenous knowledge

Indigenous knowledge is intensely local and of long duration. It uses indirect indicators to predict events. These are complementary aspects to the strengths of the scientific basis of development projects. Traditional knowledge of the area can significantly reduce the effort to acquire this knowledge if it is included in the survey. The development of large scale detailed maps, catalogues, and even Geographical

Dimensions	Mean
Cost savings	4.137
Improved PR as a result	2.147
Improved competitiveness as a result	3.376
Customer demand	3.423

Source: Self Study through questionnaire

Table 10: Factors that enable construction industry to build resilience.

Name of species	Significance with respect to climate change
Ficus species	Flowering and generation of new leaves indicates near rainfall onset.
Butterfly	Appearance of many butterflies indicate early rainfall onset and also gives a prospect of good season
Corn field ant, *Fanghmir* (Lasius *alienus)*	When there are a number of ants moving along a path carrying their food items with them, a heavy rain is expected on the same day, or within one or two days.
Common Frog, *Uchang* (Rana *temporaria):*	If the frogs croak in a water body in the afternoon until sunset, rain will be coming soon, even during winter and spring season.
Sukarvar *ribadri,rahishanicharjaye,barsabinanajaya (proverb)*	It means that if clouds form on Friday and remain till Saturday then they will not go without rain, such indications predict rains.
Nada *tankan,baladbikavan. matbajetu,adhesaawan (proverb)*	It means that in mid monsoon if South east wind blow then farmer of marwar region cries because it indicates famine in the particular region
Height of bird's nest	Floods are predicted from the height of bird's nests near rivers.
Moths	Moths decreasing numbers can predict drought.
Position of the sun or the cry of a specific bird on trees near rivers	Indicators such as the position of the sun or the cry of a specific bird on trees near rivers help people to predict the onset of the rainy season.
Bamboo Partridge, *Vahlah* (Bambusicola *fytchii):*	If male bamboo partridges roar frequently during spring and summer in the morning after sunrise, rain is expected in the immediate future. Similarly, when it rains in the morning, the roaring of the bamboo partridge at this time indicates that the rain will soon stop for that day in that location.
Field cricket, *Perhpawng* (Gryllus *pensylvanicus);*	If a cricket brings new soil particles out of its hole during the dry season, it is thought that rain is coming soon (Figure 6). If the same activity occurs during the rainy season, a heavy rain is expected during the season.
Winged termite, *Phingphihlip* (Reticulitermes sp.)	When these insects come out of the soil in a group after a rainfall occurs, it is believed that rain will not come again for some time. (If there was no rain in the previous day or week but the insects are coming out of the soil, rain is expected to come soon.
Bird/Hen and cock, *Arpui/arpa* [(*Circus cyaneus*)]	If local domestic chickens search for food even during the rain, it is commonly thought that the rain will last for the whole day. But if the birds stop searching for food when it is raining and take shelter (in the morning or afternoon), the rain is expected to cease soon and to be minimal.
Location, pattern of clouds (blackish colour), Chhumdum:	When the clouds are thick and black in colour, and are arranged perpendicular to the orbit of the sun in the morning, it is said that rain is approaching.
A person having sciatica problem	Nowadays, a patient suffering from sciatica is said to be able to foretell weather phenomena according to their body temperature and the pain in the affected body part (One man, Mr. Ngawihkhonang (L) (1945- 2006) was known to forecast weather (humidity, temperature and rainfall) three or four days ahead, through the temperature of his body part (foot, leg, ear or forehead) affected by sciatica. The people of Ngailzawl village were dependent on his weather forecasting ability.

Bug species (brown in colour, medium side, living both at the edge of the river and in the forest according to the weather conditions), Tiauhmi(consumed as curry)	If this particular bug is found under a stone on the bank of the river after the monsoon season, it is said that the autumn season is over and winter is beginning. If this bug species is found in the forest during summer, it is expected that rainfall and flooding are about to begin.
Dried ripen chilli (*Solanum frutescence)* and dried tobacco leaves (Hmarcharep)	If dried chillies become moist except during the rainy season, it indicates high humidity and imminent rain.
Flowering pattern of peach species, *Theite par. (Prunus sp.):*	If peach or plum flowers grow from the basal region to the terminal of the tree in flowering season, it is predicted that there will be a good rain and higher crop production than in other years. This indicator has been accurate until today.
Soil moisture and ground water level	During the spring and summer seasons, the villagers might turn over any stone or border stone near a river or a hillside in an open space and or clearing within the tree canopy. If the soil under the rock or under the surface is moist it is thought that summer rain is approaching.
Water bubble formation, *Puakkau* (*Paihte dialect):*	If water bubbles forms at any place on the surface of a flowing or stagnant water body, particularly during a morning rain shower, it is thought that the rain will last for whole day. My experience confirmed that this indicator was applicable.
Cloud colour, time, direction and location of appearance in the sky:	If reddish colour cloud is seen at sunset one western horizon (Figure 6), rain is predicted to come within two to four days. If there is thick cloud toward the south or north, the rain will be more on that side within the region. If the sky is full of reddish coloured clouds appearing after a long rainfall, it is a sign that the rain will not come again in that particular season.
General Duration of hot days	If the first 10-15 of the month May-June are very hot a good rainfall is predicted.
Dragon fly swarm	If Dragon fly swarm in a large group over water surface a dry weather is predicted, if they swarm over open dry lands then early rainfall is predicted.
Centipedes	If centipedes emerge from their holes carrying their eggs in swarms an early rainfall is predicted.
Sun and Moon	Presence of visible spectrum with a greater diameter around the sun than around the moon indicates rainfall after a day or two.

Annexure: List of traditional indicators for climate change and use of traditional knowledge in daily life.

Information Systems of traditional information by some indigenous associations will vastly speed the process of transfer of information. Because these are being compiled by indigenous peoples for indigenous peoples, the means used to collect the information will have been done inside their own cultural system.

Time schedule of construction project

Develop a time schedule with culture and nature-based indicators of when tasks should be completed, or when certain milestones will be met. Indigenous peoples who live on the land are tied to the rhythm of the land, its seasons, and the movement of wildlife. For many people, hunt or gathering occurs at a particular time of year, or it does not happen. Failure to meet these cyclic imperatives can be dangerous for indigenous peoples. Plan the schedule for a project with indigenous peoples and their knowledge to develop a flexible schedule based on their seasonal and cultural requirements. This should be worked out in advance with the local people.

All parties can agree that at certain stages a milestone should be met. Problems usually arise when the agreed- on milestone is missed. Project work schedule are defined by time frames, but these are often not effective for indigenous peoples who have their own internal needs and schedules that are not easily adjusted. Instead of time scales, it is sometimes better to use indicators based on their traditions.

It has become abundantly clear to informed practitioners that including traditional knowledge (whether indigenous or not) is an important and helpful approach to modern project planning and implementation when traditional peoples are directly or indirectly affected.

Integrated strategy

Co-management agreements where traditional knowledge and technological knowledge are used together can significantly improve the management of resources.

The people best equipped to discover these subtle potential changes are often the holders of traditional knowledge of the area. When traditional knowledge is used in its original context, and in partnership with other knowledge systems, the combination is often a powerful tool.

Research Implications and Future Research Ahead

Mostly responses were obtained from SMEs in construction industry due to their easy approachability while MNCs in construction sectors were not considered. Hence research can be generalized for only SMEs and since research was done in Delhi, results may also vary for location-to-location and developing to developed nations.

Further work is necessary to refine the survey tool to ensure that it does contain all climate change issues and factors affecting construction business. Furthermore a much larger sample of clients is required to validate the relative importance of variables and to permit analysis on how the influence of factors may change over time and/or in relation to type of extreme weather events taking place.

Acknowledgments

We would like to express our special thanks and gratitude to Prof. P.B SHARMA, Hon'able Vice Chancellor Delhi Technological University, Delhi for his guidance and support. We would also like to thanks Shri PC Jain- Head, Bawana Chambers of Industries, Prof. S.K Singh, Head, Department of Environmental Engineering, DTU and Delhi Technological University-Management Research Group for their indispensible support to carry out this research work.

The Authors would like to pay highest regards to the various organizations that provided their genuine inputs to this research work and supported to the their best of capabilities.

References

1. Mills E (2003) Climate change, insurance and the buildings sector: technological synergisms between adaptation and mitigation. Building Res Informat 31: 257-77.
2. Metcalf G, Jenkinson K, Johnstone K (2009) A changing climate for business. UK Climate Impacts Programme, Oxford, UK.
3. Wackman D, Runyan RC (2006) Small business in the face of crisis: identifying barriers to recovery from a natural disaster. J Contingencies Crisis Manag 14: 12-26.
4. Yoshida K, Deyle RE (2005) Determinants of small business hazard mitigation. Nat Hazards Rev 6: 1-12.
5. Harty C, Goodier CI, Soetanto R, Austin S, Dainty ARJ, et al. (2007) The futures of construction: a critical review of construction future studies. Const Manage Econ 25: 477-493.

International Journal of Applied Engineering Research.
ISSN 0973-4562, Volume 8, Number 17 (2013) pp. 1963-1968
© Research India Publications
http://www.ripublication.com/ijaer.htm

First and Second Law Analysis of a Solar Operated Ejector Absorption Refrigeration System

Rohit Goyal*[1], D.K. Gupta[2], Rajesh Kumar[3], Md. Nadim Shams[4]

[1,2,3,4] *Department of Mechanical Engineering, Delhi Technological University (Government of NCT of Delhi), Bawana Road, Delhi-110042, India.*

Abstract

This analysis for the first and second law of a solar operated ejector absorption refrigeration system using duratherm 600 oil as the heat transfer fluid is performed. The proposed cycle is an integration of ejector in the absorption refrigeration cycles which could produce refrigeration output with independent of pressure of the condenser so amount of refrigerant vaporized increased. Both exergy destruction and losses in each component and hence in the overall system are determined. The effects of some influenced parameters like; generator temperature and the evaporator temperature have been observed on first and second law performance. Analysis clearly shows that performance evaluation based on first law analysis is inadequate and hence more meaningful evaluation must include second law analysis.

Keywords: Solar energy, absorption cycle, ejector, first law efficiency, second law efficiency.

1. Introduction

Solar energy is attractive as an energy source for cooling since it is inexhaustible and is most abundant in areas where the need for cooling is greatest. In order to utilize the solar energy for its potential in reducing fossil fuel consumption and alleviating environmental problem, more interests have been paid to the solar thermal-driven refrigeration technologies like ; solar absorption cooling, solar ejector cooling [1, 2].

Sun el al [3] describes a novel refrigeration cycle based on the combination of an absorption cycle with ejector refrigeration cycle and developed a computer simulation program used to determine the performance of the system and shows the advantages of absorption and ejector refrigeration systems and provides high COP for refrigeration and air-conditioning. Agrawal et al [4] proposed a new solar-driven triple-effect refrigeration cycle by using heliostat field .The proposed cycle is an integration of

ejector, absorption, and cascaded refrigeration cycles which could produce refrigeration output of different magnitude at different temperature simultaneously.

This analysis of a new solar operated ejector absorption refrigeration system, second law of thermodynamics along with the traditional first law approach is highly desirable in order to make the theoretical treatment of the proposed cycle in general and to identify and quantify the sources of losses for evaluating its true efficiency in particular. The effect of most influenced parameters has been observed on the first law and second law efficiency of the proposed cycle along with the exergy destruction in its various components.

2. Description of the Proposed Cycle

The proposed system consists of ejector absorption refrigeration cycle (EARC) with solar heat source as shown Figure 1. The concentrated rays which falls onto the receiver results in high temperature of the central receiver is used to heat the oil (Duratherm600). The oil is flowing through the pipes which transfer the thermal energy from central receiver to the generator (a-b) and extract heat at constant temperature to the steam jet absorption refrigeration cycle which uses this heat to raise the temperature of the $LiBrH_2O$ solution so that only water vapors comes out from the generator makes it weak and the water vapors coming out from generator passes through converging diverging supersonic nozzle of ejector (SJE). The mixed stream (4) is cooled in condenser (C). The saturated liquid (5) pressure and temperature is reduced as it passed through the throttle valve (TV1) and gives the refrigeration output in the evaporator (E). The liquid part (9) sent to the absorber (A) where it mixes with the $LiBrH_2O$ makes the solution rich. The rich solution is pumped to heat exchanger (HX) to take some heat from out coming weak solution from generator so the less heat is required to vaporize the water within the rich solution and increases efficiency of cycle. For the analysis, the specifications of the EARC and solar cycle are given in Table 1

Table 1: Main parameters considered for the analysis.

Environment Temperature(^{0}C)	27	Absorber temperature (^{0}C)	35
Hot oil outlet temperature (^{0}C)	220– 200	Nozzle efficiency (%)	85
Generator temperature(^{0}C)	180-200	Diffuser efficiency (%)	90
Solar radiation received per unit area(Wm^{-2})	800	Mixing chamber efficiency (%)	85
		First law efficiency of heliostat field	75
Apparent Sun temperature(K)	4500	(%)	90
Heliostat aperture area(m^2)	3000	First law efficiency of central	75
Evaporator temperature (^{0}C)	4 –11	receiver (%)	30
Condenser temperature (^{0}C)	35	Second law efficiency of heliostat	
Generator pressure (kPa)	190	field (%)	
		Second law efficiency of central	
		receiver (%)	

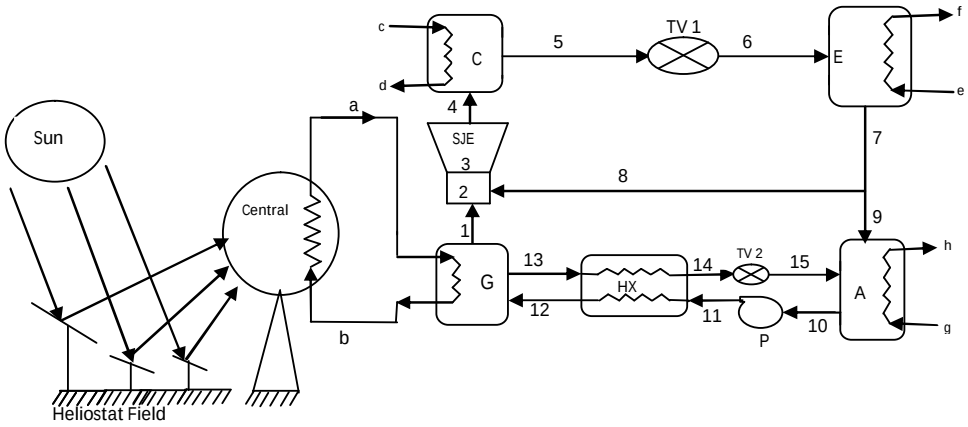

Figure 1: Schematic diagram of solar operated ejector absorption refrigeration system.

3. Thermodynamic Analysis

The basic principle of the ejector was introduced by Keenan et al. [5] based on gas dynamics and formulated by Huang et al. [6] and Ouzzane et al.[7]. The formulation and various equations to solve ejector are developed by Dai et al.[8]

In the absence of magnetic, surface tension effect, nuclear, electrical, and considering the system is at rest relative to the environment, the total exergy associated with the work obtainable by bringing a stream of matter from its initial state to a state that is in thermal and mechanical equilibrium with the environment. Mathematically,

$$\dot{E} = \dot{m}[(h - h_0) - T_0(s - s_0)] \tag{1}$$

According to the Bejan [9] entropy generation over a control volume is given by

$$\dot{S}_{gen} = \frac{dS}{dt} - \sum_{i=o}^{n} \frac{\dot{Q}_i}{T_i} - \sum_{in} \dot{m}\, s + \sum_{out} \dot{m}\, s \geq 0 \tag{2}$$

According to Gouy-Stodola theorem, the exergy destruction and entropy generation are related as

$$\dot{E}_D = T_0\, \dot{S}_{gen} \tag{3}$$

3.1 First Law Efficiency (η_I)

The first law efficiency can be defined as the ratio of the desired effect to the thermal energy of solar input $\dot{Q}_{solar}$.

$$\eta_I = \frac{\dot{Q}_E}{\dot{Q}_{Solar}} \tag{4}$$

3.2 Second Law Efficiency (η_{II})

Second law efficiency is defined as the ratio of exergy contained in the product to the exergy associated with the solar energy input and the second law efficiency of cycle may be reported as

$$\eta_{II} = \frac{\Delta \dot{E}_{E}}{\dot{E}_{Solar}} \tag{5}$$

Where, $\dot{E}_{Solar}$ is incoming exergy associate with solar radiation falling on heliostat, $\Delta\dot{E}_{E1}$ is the change in exergy at ejector evaporator of ERC.

4. Results and Discussion

A thermodynamic investigation has been persuaded to identify the effect of some influenced parameters on the performance of the solar operated ejector absorption refrigeration system. The parameters have been chosen in the typical range of its operation; generator temperature (180^0C-200^0C) and evaporator temperature (4^0C-11^0C).

The first law efficiency and energy distribution of solar heat source is obtained by energy balance approach or first law analysis of the cycle. The exergy destruction in each component of the cycle as a whole is non dimensional by expressing it as a percentage of the solar heat source exergy. Thermodynamic properties of LiBr/H_2O mixture for the operation of absorption refrigeration are taken from Chua et al. [10]. In order to clarify, the energy and exergy distribution of solar heat driven cycle is shown in Figs. 2 -3.

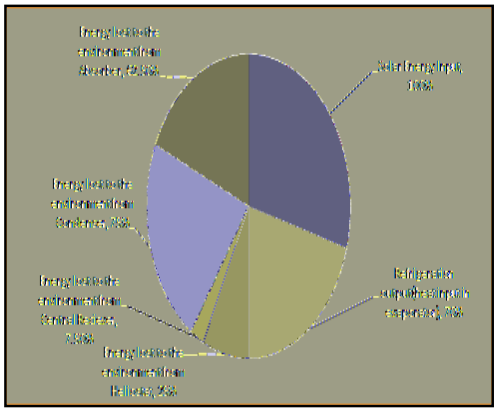

Figure 2 Energy lost from various components of the system

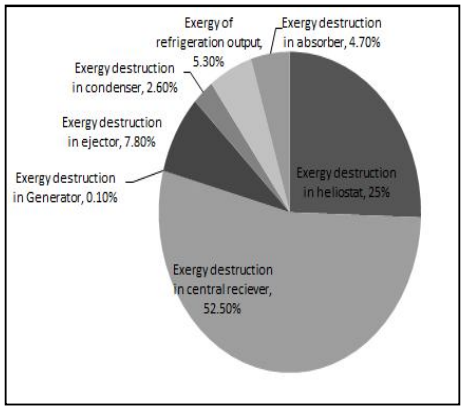

Figure 3. Exergy distructed from various components of the system

Fig. 2 indicates that out of 100% solar energy supplied to the system, around 70% is available as useful energy output (refrigeration capacity), 170% is lost to the environment via thermal energy exhaust from the system. Application of second law analysis to the proposed cycle leads to the exergy distribution in the system. It is found that around 5.3% of the total input exergy is available as an exergy output and 94.7% of the input (solar heat) exergy is destructed and lost due to irreversibilities occurred in various components of the proposed cycle and exergy carried away by the cooling water at absorber and condensers as shown in Fig.3.

Fig.4 shows the variation of the generator temperature on the first law and second law efficiency refrigeration cycle. It is observed that both first law and second law efficiencies are increase with generator temperature. This is due to the fact that the quantity of vaporized refrigerant will be improved with the increase in generator temperature.

The effect of change in evaporator temperature on first and second law efficiency of the system is shown in Fig.5 and it is found that first law efficiency increases significantly with the increase in ejector evaporator temperature while the second law efficiency of the system decreases due to higher losses.

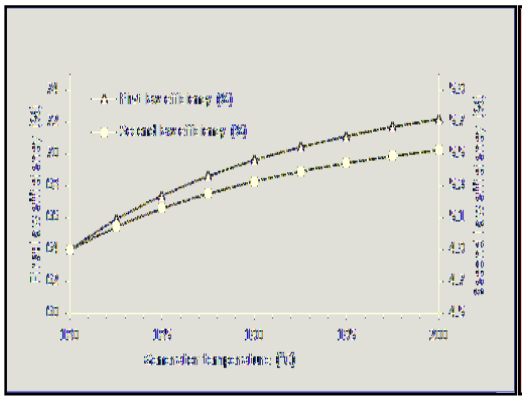

Figure 4. Variation of the generator temperature on the first law and second law efficiency

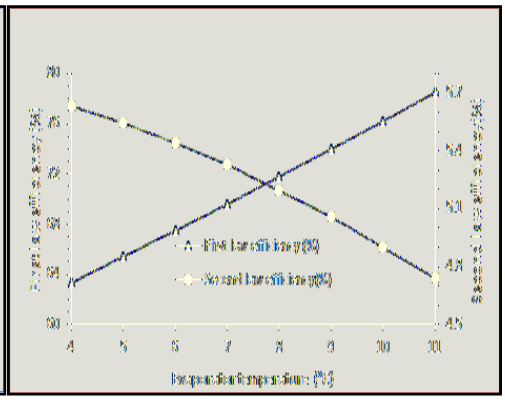

Figure 5. Variation of the Evaporator temperature on the first law and second law efficiency

5. Conclusion

The conclusions of the present analysis can be summarized as follows:

- Out of 100% energy (solar heat source) supplied to the system around 70% is produced as refrigeration capacity and 170% is lost to the environment.
- About 5.3% of the input exergy is available as exergetic refrigeration output and 94.7% is lost due to irreversibilities in the components and via thermal lost to the ambient.
- The largest contribution to cycle irreversibility comes from central receiver and heliostat field of 52.5% and 25%, respectively.

References

[1] Duffie JA, Beckman WA (1980). *Solar Engineering of Thermal Processes.* 2nd edition, John Wiley Publication, New York.

[2] Dincer I, Edin M, Ture IE (1996). Investigation of thermal performance of a solar powered absorption refrigeration system. *Energy Conversion & Management* .**37,** 51-58.

[3] Sun, Da-Wen, Eames, I. W., Aphornratana, S (1996).Evaluation of a novel combined ejector-absorption refrigeration cycle - I: computer *lnt J. Refrig.* **19**,3,172-180.

[4] Agrawal S K, Kumar R, Khaliq A (2013). First and Second Law investigations of a new solar assisted thermodynamic cycle for triple effect refrigeration. Int J. Energy Research.

[5] Keenan H, Neumann EP, Lustwerk F (1950). An investigation of ejector design by analysis and experiment. *J Appl Mech, Transactions of the ASME.* **72**, 299-309.

[6] Huang BJ, Chang JM, Wang CP, Petronko VA (1999). A 1-D analysis of ejector performance International *Journal of Refrigeration* **22**, 354-364.

[7] Ouzzane M, Aidoun Z (2003). Model development and numerical procedure for detailed ejector analysis and design. *Applied Thermal Engineering* .**23**, 2337-2351.

[8] Dai Y, Wang J, Gao L (2009). Exergy analysis, parametric analysis and optimization for a novel combined power and ejector refrigeration cycle. *Applied Thermal Engineering.* **29**. 1983-1990.

[9] Bejan A (2002). Fundamentals of exergy analysis, entropy generation minimization, and the generation of flow architecture. *International Journal of Energy Research.* **26**, 545-565

[10] Chua HT, Toh HK, Malek A, Ng KC, Srinivasan K (2000). Improved thermodynamic property fields of LiBr-H_2O solutions. *International Journal of Refrigeration.* **23**,412-429.

Applied Soft Computing xxx (2014) xxx–xxx

Contents lists available at ScienceDirect

Applied Soft Computing

journal homepage: www.elsevier.com/locate/asoc

Generalized neural network and wavelet transform based approach for fault location estimation of a transmission line

Majid Jamil [a], Abul Kalam [a,*], A.Q. Ansari [a], M. Rizwan [b]

[a] Department of Electrical Engineering, Jamia Millia Islamia, New Delhi 110025, India
[b] Department of Electrical Engineering, Delhi Technological University, Delhi 110042, India

ARTICLE INFO

Article history:
Received 18 April 2013
Received in revised form
25 November 2013
Accepted 20 February 2014
Available online xxx

Keywords:
Generalized neural network
Wavelet transform
Artificial neural network
Transmission line protection
Transient signals

ABSTRACT

To maintain the efficient and reliable operation of power systems, it is extremely important that the transmission line faults need to be detected and located in a reliable and accurate manner. A number of mathematical and intelligent techniques are available in the literature for estimating the fault location. However, the results are not satisfactory due to the wide variation in operating conditions such as system loading level, fault inception instance, fault resistance and dc offset and harmonics contents in the transient signal of the faulted transmission line. Keeping in view of aforesaid, a new approach based on generalized neural network (GNN) with wavelet transform is presented for fault location estimation. Wavelet transform is used to extract the features of faulty current signals in terms of standard deviation. Obtained features are used as an input to the GNN model for estimating the location of fault in a given transmission systems. Results obtained from GNN model are compared with ANN and well established mathematical models and found more accurate.

© 2014 Elsevier B.V. All rights reserved.

1. Introduction

Faults can occur in any component of power systems including generator, transformer, buses and transmission lines. As the transmission line is one of the main components of power systems, therefore the detection of faults on transmission lines is the primary concern of the power systems, necessitating high speed fault clearance and improved transient stability [1].

Transmission line fault detection techniques can be classified into two main categories: techniques based on the fundamental power frequency component, and techniques utilizing the higher frequency components of the fault signals. Further these two categories of fault location techniques can be divided into two subgroups: to use single ended information or to use information from both ends using current and voltage data of the faulted line [2–5]. A number of mathematical models are available in the literature for identifying the types and location of the fault of transmission systems [2–8]. In recent study, the sampled current values at the relaying point i.e. single ended data have been used for classification and location of faults [11–13,16]. This technique is more attractive than the technique based on two terminals. Two terminals technique has drawbacks like requirement of communication links and synchronized sampling equipment which not only increase the cost but also affect the accuracy [3]. Therefore techniques using single ended data are preferred.

In fact correct fault location of a transmission line depends upon many factors such as on the geometry/configuration and the line parameters of the transmission network (i.e. whether the line is transposed/un-transposed, charging capacitance and shunt reactance being present neglected or taken into consideration for the transmission line model). In addition to that the accuracy of fault location also depends upon the resistance of the faulted path, the fault inception angle, the system loading level and on the amplitude of the dc offset and harmonics content in the transient signal of the faulted transmission line. Besides that transmission line being geographically wide distributed systems and exposed to the environment there is uncertainty about the fault events and the line parameters. Therefore, in such situation, where there is ambiguity and uncertainty about the fault events and the line parameters, it is difficult to deal with the transmission lines protection problems through strict mathematical approaches (deterministic approaches) effectively, and hence these factors introduce the considerable amount of error for the fault location estimation of the transmission system using conventional mathematical (deterministic approach) model of the transmission system.

To overcome these problems several intelligent techniques including fuzzy logic, artificial neural networks, neuro-fuzzy and

* Corresponding author at: Department of Electrical Engineering, Jamia Millia Islamia, Jamia Nagar, New Delhi 110025, India. Tel.: +91 9958281028.
E-mail address: kalam.a@rediffmail.com (A. Kalam).

http://dx.doi.org/10.1016/j.asoc.2014.02.020
1568-4946/© 2014 Elsevier B.V. All rights reserved.

UNCORRECTED PROOF

Please cite this article in press as: M. Jamil, et al., Generalized neural network and wavelet transform based approach for fault location estimation of a transmission line, Appl. Soft Comput. J. (2014), http://dx.doi.org/10.1016/j.asoc.2014.02.020

combined wavelet-ANN have been developed and presented in the literature for fault identification and location of transmission system as discussed in [1] and [9–28]. Among aforesaid approaches it is seen that wavelet-ANN has been quite successful in identifying the types and location of fault. However, there are certain drawbacks of ANN like large training time, huge data requirement for training, unknown ANN structure, the relatively larger number of hidden nodes required, problem of local minima, etc. To overcome some of the problems of ANN and to improve it's training and testing performance, a new approach based on GNN in combination with wavelet transform is presented in this paper. The applications of GNN in the field of load forecasting, aircraft landing system, power system stabilizer, estimation of solar energy etc., are available in the literature [29–38]. However, the application of GNN with wavelet for the fault location estimation of transmission line is rarely available.

In the present work, single ended fault current signals are analyzed using wavelet transform. Obtained data is used as input parameters in GNN modeling for estimating the fault location of the three phase transmission system. The performance of the GNN model for the fault location estimation is evaluated on the basis of mean value of absolute relative error in percentage, considering the un-transposed transmission line model for the same network and parameters of power system as modeled in [6] and found to produce very accurate fault location result which is around 2.0%. While, the percentage error as reported in [6], which describes iterative method of fault location for the same power system network as considered in the proposed study is varies up to 4.81%. Whereas in [1] the percentage error is reported up to 6.5% using wavelet and fuzzy logic based technique for the fault location estimation of the transmission system.

Observations of all test results ascertain that the wavelet-GNN based model of fault location estimation performs excellent even at voltage zero crossing situation of fault inception angle and at different fault locations starting from relay end (sending end) to the end terminal of the transmission line for all kinds of phase to phase and phase to ground faults.

This paper is organized as follows: Wavelet transform used for pre-processing of fault current signals to obtain the features of fault current signals in terms of statistical feature i.e. standard deviation is presented in Section 2. Section 3 presents the generalized neural networks and fault location estimation based on GNN model. Section 4 describes the simulation studies. In Section 5 results are discussed. Section 6 presents conclusion followed by references.

2. Wavelet transform

The wavelet transform is a powerful tool for the analysis of transient phenomena because of its ability to extract time frequency information from the transient signal. Most of the transient signals based relay principle adopts the wavelet transform technology to construct the algorithms. Wavelet transform (WT) expands a signal into several scales belonging to different frequency regions by using translation (shift in time) and dilation (compression in time) of a fixed wavelet function known as mother wavelet. The discrete wavelet transform and multi resolution analysis provides a short window for high frequency components and long window for low frequency components and hence provides an excellent time frequency resolution [17].

Continuous wavelet transform (CWT) is defined as the sum over all time of the signal multiplied by scaled and shifted versions of the wavelet function $\psi(t)$. The CWT of a $x(t)$ signal is defined as

$$\mathrm{CWT}(x, a, b) = \int_{-\infty}^{\infty} x(t)\psi^{*}a,\ b(t)dt \quad (1)$$

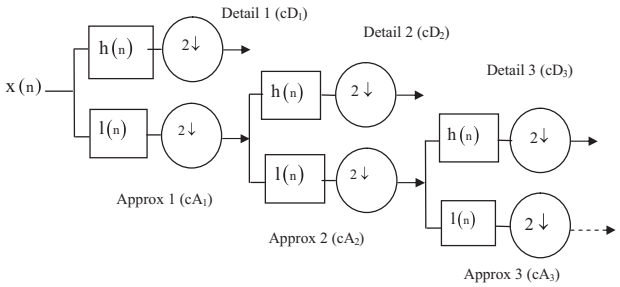

Fig. 1. Multi level wavelet decomposition scheme.

where $\psi_{a,b}(t) = |a|^{-1/2}\psi(t - b/a)$, the analyzing function $\psi(t)$ is known as the mother wavelet and $\psi_{a,b}(t)$ are its dilated and translated versions; the choice of a mother wavelet is flexible provided that it satisfies the following condition:

$$\int_{-\infty}^{\infty} \psi(t)dt = 0$$

This implies that a wavelet is compactly supported in both the time domain and frequency domain. The asterisk in (1) denotes a complex conjugate, $a, b \in \Re$, $a \neq 0$ ($\Re$ is a real continuous number system) are the scaling and shifting parameters respectively. $|a|^{-1/2}$ is the normalized value of $\psi_{a,b}(t)$ so that if $\psi(t)$ has a unit length, then its scaled version $\psi_{a,b}(t)$ also has a unit length.

Wavelet transform of sampled waveforms can be obtained by implementing the discrete wavelet transform which is given by:

$$\mathrm{DWT}(x,\ m,\ n) = a_o^{-m/2} \sum \left(x[k]\psi^{*} \left[\frac{k - n\, a_o^m b_o}{a_o^m} \right] \right)$$

where m, n and k are integer variables and it refers to a sample number in an input signal and a_o and b_o are the discrete steps of the scale and translation respectively.

2.1. Wavelet decomposition and multi resolution analysis

Multi-resolution analysis (MRA) is a time frequency analysis technique which has been found to be an effective signal processing tool in monitoring and analyzing power system disturbances including power quality assessment and system protection against faults [9]. It has also other desirable properties such as providing a substantial amount of data reduction and having a simple and fast algorithm. Therefore, DWT is most appropriate for fault detection and location problems in power systems. In this study phase A, phase B and phase C fault current signals, generated on a three phase transmission line considered as $x(n)$ in time domain is passed through high pass $h(n)$ and low pass filter $l(n)$. The outputs from both the filters are decimated by 2 to obtain the detail coefficient (cD_1) and the approximation coefficient (cA_1) which constitutes the level one decomposition of the original signal at stage first. The approximation coefficient (cA_1) is then sent to the second stage to repeat the procedure. Finally, the signal is decomposed up to the ninth levels. The details information and approximations at different levels are seen to provide useful clues regarding the faults locations on the transmission line [27]. A multi-level DWT decomposition scheme shown in Fig. 1 shows the essence of the procedure. The approximations and details at level-1, level-2 and level-3 have been represented using suffixes 1, 2 and 3 and so on.

2.2. Features extraction

In the present study wavelet transform is used to capture the useful fault signature of the faulty current signals of a given three

Please cite this article in press as: M. Jamil, et al., Generalized neural network and wavelet transform based approach for fault location estimation of a transmission line, Appl. Soft Comput. J. (2014), http://dx.doi.org/10.1016/j.asoc.2014.02.020

UNCORRECTED PROOF

Table 1
Details wavelet coefficients at different frequency range for 100 kHz sampling frequency.

Wavelet coefficients up to ninth-levels of wavelet decomposition	Frequency band (Hz)
cD_1	25,000–50,000
cD_2	12,500–25,000
cD_3	6250–12500
cD_4	3125–6250
cD_5	1562.5–3125
cD_6	781.25–1562.5
cD_7	390.62–781.25
cD_8	195.31–390.62
cD_9	97.66–195.31

phase transmission line in terms of statistical features like standard deviation to be used as input to the GNN model. Three phase fault current signals recorded at the relaying point sampled at the rate of 100 kHz frequency are pre-processed passing through the multi level wavelet filter bank, selecting Db4 as mother wavelet, for different fault operating condition using MATLAB software. Since the selected sampling frequency is 100 kHz at the base frequency of 50 Hz, therefore ninth level wavelet detail coefficient includes second and third harmonics (97.66–195.31 Hz) which are predominant in case of transmission line faults and is useful for the fault classification and fault location estimation of the transmission line. The details coefficient at different frequency range for 100 kHz sampling frequency is shown in Table 1. Feature vectors in terms of standard deviation are obtained using Eq. (2), considering the ninth level detail coefficient denoted as: $[\sigma_A cD_9; \sigma_B cD_9; \sigma_C cD_9]$ for three phase fault current signals [25].

$$\text{Standard deviation } \sigma_\chi cD_i = \left[\frac{1}{N-1}\sum_{j=1}^{N}(cD_{ij} - \mu_\chi cD_i)^2\right]^{1/2}$$
$$\text{Mean } \mu_\chi cD_i = \frac{1}{N}\sum_{j=1}^{N} cD_{ij} \quad (2)$$

where χ represents phase A, phase B and phase C, $i = 1, 2, \ldots, l$ is the wavelet decomposition level from level 1 to level l, N = number of samples of wavelet details coefficient.

If the wavelet coefficients are used as inputs to the GNN, it will results in rather large number of inputs (equals to the N number of samples) posing difficulty for training and testing of GNN in connection with accuracy and speed [14]. Therefore, in order to overcome this problem but retaining important features of the wavelet signals, features are obtained in terms of standard deviation using ninth level detail coefficient which are predominant in case of transmission line faults.

3. Generalized neural network (GNN)

The general structure of the common neuron is an aggregation function and its transformation through a filter. It is shown in the literature [29–38] that the ANNs can be universal function approximators for given input–output data. The common neuron structure as shown in Fig. 2 has summation as the aggregation function with sigmoidal, radial basis, tangent hyperbolic or linear limiters as the thresholding function. The aggregation operators used in the neurons are generally crisp. However, they overlook the fact that most of the processing in the neural networks is done with incomplete information at hand. Thus, a GNN model approach has been adopted that uses the fuzzy compensatory operators [37] that are partly sum and partly product to take into account the vagueness involved.

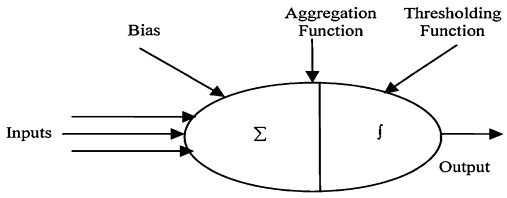

Fig. 2. Simple neuron model.

3.1. GNN model

Use of the sigmoidal thresholding function and ordinary summation or product as aggregation functions in the existing model fails to cope with the nonlinearities involved in real life problems. To deal with these, the proposed model has both sigmoidal and Gaussian functions with weight sharing. The GNN model has flexibility at both the aggregation and threshold function level to cope with the nonlinearity involved in the type of applications dealt with, as shown in Fig. 3. The neuron model described above is known as the summation type compensatory neuron model, since the outputs of the sigmoidal and Gaussian functions are summed up. Similarly, the product-type compensatory neuron models may also be developed. The neuron has both Σ and π aggregation functions. The Σ_1 aggregation function has been used with the sigmoidal characteristic function (f_1) while the π aggregation function has been used with the Gaussian function (f_2) as a characteristic function.

The output of the Σ_1 part with a sigmoidal characteristic function of the GNN is

$$o_\Sigma = f_1(s_net) = \frac{1}{1 + e^{-\lambda_s * s_net}} \quad (3)$$

where

$$s_net = \sum W_{\Sigma_i} X_i + X_{o\Sigma}$$

and λ_s is the gain scale factor of Σ_1

The output of the π part with Gaussian characteristics function of GNN is

$$o_\pi = e^{-\lambda_p * pi_net^2} \quad (4)$$

where

$$pi_net = \Pi W_{\Pi_i} X_i * X_{o\Pi}$$

and λ_p is the gain scale factor of π_1.

The final output of the neuron is a function of the two outputs and with the weights W and $(1 - W)$ respectively, and can be written in mathematical form as

$$o_{pk} = o_\pi * (1 - W) + o_\Sigma * W \quad (5)$$

The GNN model gives only one output. If a system requires more than one output, one GNN is used for each output.

The neuron model described above is known as the summation type compensatory neuron model, since the outputs of the

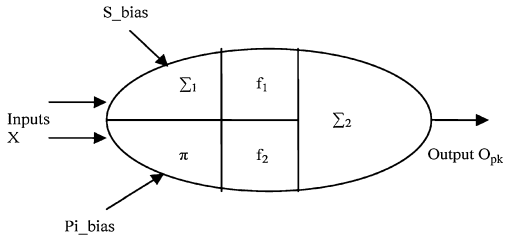

Fig. 3. GNN model.

Please cite this article in press as: M. Jamil, et al., Generalized neural network and wavelet transform based approach for fault location estimation of a transmission line, Appl. Soft Comput. J. (2014), http://dx.doi.org/10.1016/j.asoc.2014.02.020

sigmoidal and Gaussian functions are summed up. Similarly, the product-type compensatory neuron models may also be developed. It is found that in most of the applications, the summation-type compensatory neuron model works well and is the one used for the estimation of fault location of the transmission line.

3.2. Learning algorithm of a GNN model

The following steps are involved in the training of a GNN:

Step (1) Calculate the output of GNN as given in (3) and (4).
Step (2) After calculating the output of the GNN in the forward pass, as in the feed-forward neural network, it is compared with the desired output to find the error. Using a back-propagation algorithm, the GNN is trained to minimize the error. In this step, the output of the single flexible GNN is compared with the desired output to get the error for the i_{th} set of inputs.
(6)Error $E_i = (Y_i - O_i)$
Step (3) Then, the sum squared error for the convergence of all the patterns is
(7)$E_p = 0.5\sum E_i^2$
A multiplication factor of 0.5 has been taken to simplify the calculations.
Step (4) Reverse pass for modifying the connection strength.
(a) Weight associated with the Σ_1 and part Σ_2 of the GNN is(8)$W(k) = W(k-1) + \Delta W$where $\Delta W = \eta\delta_k(o_\Sigma - o_\pi)X_i + \alpha W(k-1)$and $\delta_k = \Sigma(Y_i - O_i)$
(b) Weights associated with the inputs of the Σ_1 part of the GNN are(9)$W_{\Sigma_i}(k) = W_{\Sigma_i}(k-1) + \Delta W_{\Sigma_i}$where $\Delta W_{\Sigma_i} = \eta\delta_{\Sigma i}X_i + \alpha W_{\Sigma i}(k-1)$and $\delta_{\Sigma j} = \sum\delta_k W(1 - O_\Sigma) * O_\Sigma$
(c) Weights associated with the input of the π – part of the GNN are(10)$W_{\Pi i(k)} = W_{\Pi i(k-1)+\Delta W_{\Pi i}}$where $\Delta W_{\Pi i}$
$= \eta\delta_{\Pi j}Xi + \alpha W_{\Pi i}(k-1)\delta_{\Pi j} = \sum\delta_k(1-W) * (-2 * pi_net) * O_\Pi$
α is the momentum factor for better convergence, and η is the learning rate. The range of these factors is from 0 to 1 and is determined by experience.

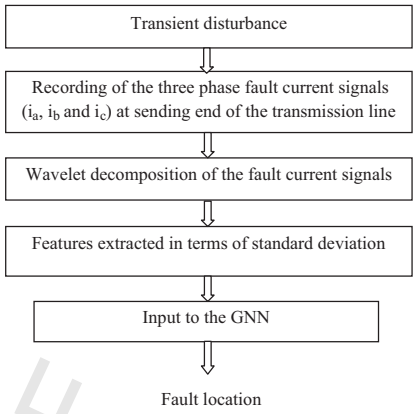

Fig. 4. Flow chart for fault location scheme.

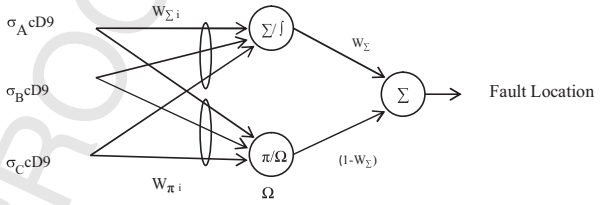

Fig. 5. Architecture of GNN model for the fault location estimation of transmission line.

3.3. Wavelet-GNN model based fault location estimation

The fault current signals of three phase transmission line are filtered through wavelet transform. Obtained data from wavelet is used as input to GNN model. The input data is extracted features of fault current signals whereas the output of the GNN model is location of fault.

The neural network toolbox of MATLAB software is used for estimating the fault location of the transmission line. The flow chart of the proposed method is presented in Fig. 4. Firstly, the fault current signal is obtained at the sampling frequency of 100 kHz for each

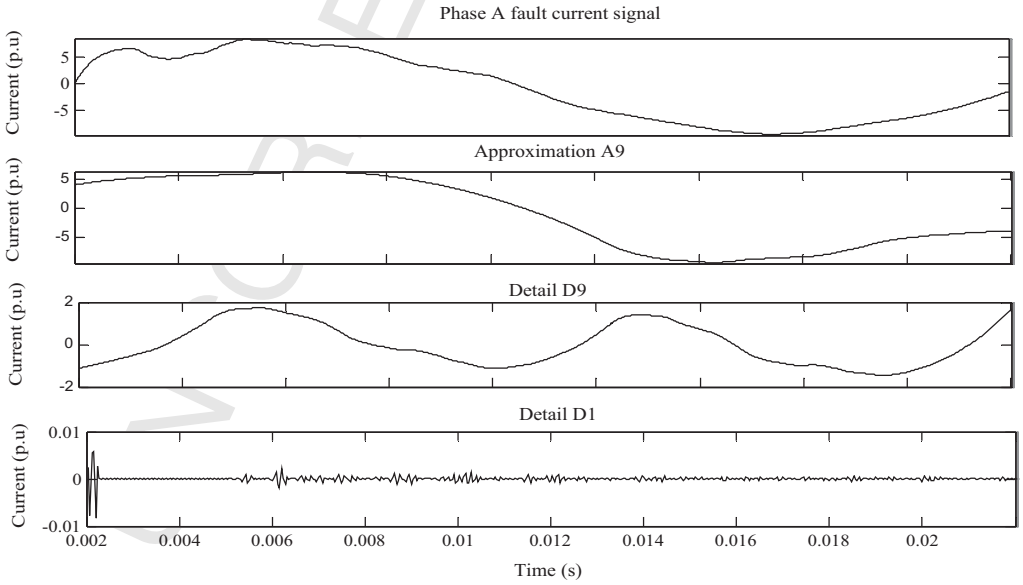

Fig. 6. Wavelet decomposition of phase A fault current signal for phase to ground (AG) fault due to the fault occurred at 240 km away from the relaying point operating at $R_f = 100\,\Omega$, FIA = 36° and $\delta = -15°$.

Please cite this article in press as: M. Jamil, et al., Generalized neural network and wavelet transform based approach for fault location estimation of a transmission line, Appl. Soft Comput. J. (2014), http://dx.doi.org/10.1016/j.asoc.2014.02.020

UNCORRECTED PROOF

case, created for different fault operating conditions. Thereafter the multi-resolution analysis (MRA) based on Discrete Wavelet Transform (DWT) is used to capture the transient characteristics of the fault current signal. The information captured during the ninth level frequency bands by the details wavelet coefficients in terms of standard deviation is fed as input to the GNN and target as the fault location of the transmission line. Since the input and output data are not of the same order of magnitude, therefore it is necessary to normalize the input and output data in the same order of magnitude. If actual data is directly used, this may cause a convergence problem during the learning process. To avoid such problem, the input and output data are scaled such that they remain within the range of (0.1–0.9). This process is known as normalization. Normalization has a major role in the training and testing of neural networks. The actual data is scaled using the following expression for the fault location estimation problem [37].

$$L_S = \frac{(Y_{\max} - Y_{\min})}{(L_{\max} - L_{\min})}(L - L_{\min}) + Y_{\min} \quad (11)$$

where L = the actual data; L_s = the scaled data which is used as input to the network; $L_{\max}$ = maximum value of particular data set; $L_{\min}$ = minimum value of particular data set; $Y_{\max}$ = upper limit (0.9) of normalization range; $Y_{\min}$ = lower limit (0.1) of normalization range.

The GNN model is developed for the fault location estimation of a given three phase transmission line as shown in Fig. 5. The neurons in the input layer receive three input signals representing the features of the three phase fault current signals in terms of standard deviation. The output layer, on the other hand consists of one output neuron representing fault location of the transmission line. The generalized neuron structure summation and product as aggregation functions have been incorporated and the aggregated outputs passed through a non-linear squashing/thresholding function. The Σ-part has the summation of weighted input with sigmoidal activation function f_1, while the π-part has the product of weighted input with Gaussian activation function f_2. The final output of the neuron is a function of the weighted outputs O_Σ and O_π.

The output of summation (Σ) part of the generalized neuron is

$$O_{\sum} = f_1\left(\sum W_{\sum i} X_i + X_o \sum\right) \quad (12)$$

The output of product (π) part of the generalized neuron is

$$O_\pi = f_2(\pi W_{\pi i} X_i + X_{o\pi}) \quad (13)$$

Finally, the outputs are summed up to get the neuron output. The output of the neuron can be mathematically written as

$$Oi = O_\Sigma * W_\Sigma + O_\pi * (1 - W_\Sigma) \quad (14)$$

4. Simulation studies

The proposed fault location estimation approach is extensively tested on a 500 kV, 50 Hz transmission line of 300 km length connected between two sources as shown in Fig. 10. The parameters of the system under consideration are as follows:

Sending and receiving end source voltage

E_s = 500 kV; E_R = 475 $\angle\delta$ kV; where $\angle\delta$ is the receiving end phase voltage angle.

Sending and receiving end positive and zero sequence source impedance

$$Z_{s1} = 17.177 + j37.9404\,\Omega; \quad Z_{s0} = 2.5904 + j12.2773\,\Omega;$$

$$Z_{R1} = 15.31 + j38.2704\,\Omega; \quad Z_{R0} = 0.7229 + j12.6073\,\Omega;$$

Transmission line parameters

$$Z_1 = 0.15483 + j0.3050\,\Omega/\text{km};$$

$$Z_0 = 0.37432 + j0.9429\,\Omega/\text{km};$$

$$C_1 = 1.2097E - 8F/\text{km};$$

$$C_0 = 7.4982E - 9F/\text{km}.$$

In simulation studies, a large numbers of test cases are generated for different values of fault resistance (R_f) varying from 10 Ω to 1000 Ω for ground faults and for phase faults from 1 Ω to 10 Ω, which cover most of the high resistance faults. The variation of distance from the relay point to the end terminal (receiving end) in steps of every 5 km is considered, and the receiving end phase voltage angle (δ) of −15°, 15°, 30° and 90°. For simulation, fault is created at different fault inception angles (FIA) of 36°, 54°, 90° and 180°, considering 0.02 s simulation time. The fault inception angle specially voltage zero crossing situation has also been widely investigated. The data considered in the analysis is less than one cycle. The fault current signals are obtained at 100 kHz sampling frequency at the relaying point in order to be used in feature extraction using multi-resolution analysis based on DWT. For each fault operating condition, simulation of the program generates 59 data files that is a matrix of the order of 59 × 3 = 177 data. Out of which 80% data randomly chosen are fed to train the GNN and remaining 20% for testing. To validate the proposed wavelet-GNN model, the fault location results are compared with the other intelligent model like wavelet-ANN (presented in Appendix I), and with the mathematical based method (measuring symmetrical components of voltage and current shown in Appendix II) of fault location estimation.

5. Results

To show the effectiveness of the proposed model, an extensive series of simulation studies have been carried out for a wide variation of fault operating conditions. Due to the paucity of space, as an application example, current waveform and wavelet decomposition of phase A fault current signal for one type of fault (phase A to ground fault i.e. AG fault) due to the fault occurred at 240 km away from the relaying point operating at R_f = 100 Ω, FIA = 36°, δ = −15° is illustrated in Fig. 6. The characteristics features of fault current signals (extracted transient characteristics features of phase A, phase B and phase C fault current signals in terms of standard deviation considering the ninth level wavelet detail coefficient) corresponds to the different fault points along the line are depicted in column fifth to seventh of Tables 2 and 3. It is clear from the Fig. 6, that the detail signal at level-1 shows the distinctive features of the transient signal for faulted phase A i.e. just after the occurrence of fault sharp spikes appear in the detail signal which signifies the occurrence of fault. It is observed from the Tables 2 and 3, that the value of features vector (standard deviation) of the faulted phase decreases as the fault distance increases from the relay point. These distinguishable characteristics feature of the fault signals are applied as an input to the neural network, which help to determine the fault locations estimation of the transmission line. The column number eight and nine of Tables 2 and 3 respectively provides the estimated fault locations, and the training and testing performance of fault locations result using Wavelet-GNN model due to the fault occurred at the various locations of the line starting from the relay end to the end terminal and it is found that the error varies from 0.15% to 2.05%. While using wavelet-ANN model it varies from 0.83% to 3.41% as depicted in column number eleven. Whereas in case of conventional symmetrical components based method of fault location as represented in column number four of Tables 2 and 3, it is found that the error varies from 4.05% to 10.75% which is considerably high. Graphically the comparisons of training and testing performance of fault locations result for the same are illustrated through

UNCORRECTED PROOF

Please cite this article in press as: M. Jamil, et al., Generalized neural network and wavelet transform based approach for fault location estimation of a transmission line, Appl. Soft Comput. J. (2014), http://dx.doi.org/10.1016/j.asoc.2014.02.020

Table 2
Training performance of AG fault operating at $R_f = 100\,\Omega$, FIA = 36° and $\delta = -15°$.

S. no.	Actual distance to fault from relaying point (km)	Fault location measuring zero sequence components of voltage and current		Normalized value of features vector in terms of standard deviation of phase A, phase B and phase C fault current signals						
		Computed distance (d) (km)	Absolute value of relative error in %	Applied as input to GNN					Applied as input to ANN	
				$\sigma_A D_9$	$\sigma_B D_9$	$\sigma_C D_9$	Estimated fault location (km)	Absolute value of relative error in %	Estimated fault location (km)	Absolute value of relative error in %
1	10	9.35	6.50	0.8740	0.8978	0.1234	9.82	1.80	9.75	2.50
2	50	46.16	7.68	0.6917	0.8543	0.2918	49.39	1.22	48.41	3.18
3	120	109.45	8.79	0.4582	0.6892	0.5133	118.21	1.49	116.39	3.01
4	155	140.73	9.21	0.3691	0.5930	0.5948	153.43	1.01	151.42	2.31
5	200	180.56	9.72	0.2719	0.4451	0.6986	204.02	2.01	195.74	2.13
6	225	202.43	10.03	0.2236	0.3504	0.7527	222.91	0.93	220.16	2.15
7	240	215.45	10.23	0.1960	0.2906	0.7837	237.10	1.21	233.02	2.91
8	275	246.21	10.47	0.1344	0.1580	0.8568	270.77	1.54	269.28	2.08
9	280	250.43	10.56	0.1258	0.1413	0.8676	278.01	0.71	275.38	1.65
10	285	254.71	10.63	0.1172	0.1256	0.8782	284.57	0.15	277.13	2.76
11	295	263.28	10.75	0.1000	0.1000	0.9000	289.31	1.93	287.83	2.43

Table 3
Testing performance for AG fault operating at $R_f = 100\,\Omega$, FIA = 36° and $\delta = -15°$.

S. no.	Actual distance to fault from relaying point (km)	Fault location measuring zero sequence components of voltage and current		Normalized value of features vector in terms of standard deviation of phase A, phase B and phase C fault current signals						
		Computed distance (d) (km)	Absolute value of relative error in %	Applied as input to GNN					Applied as input to ANN	
				$\sigma_A D_9$	$\sigma_B D_9$	$\sigma_C D_9$	Estimated fault location (km)	Absolute value of relative error in %	Estimated fault location (km)	Absolute value of relative error in %
1	35	32.46	7.26	0.7550	0.8764	0.2325	34.57	1.23	34.31	1.97
2	45	41.60	7.56	0.7122	0.8617	0.2725	44.60	0.89	43.81	2.64
3	60	55.28	7.87	0.6525	0.8383	0.3279	59.03	1.62	58.07	3.22
4	90	82.45	8.39	0.5476	0.7747	0.4274	89.06	1.04	89.12	0.98
5	100	91.43	8.57	0.5162	0.7483	0.4572	101.99	1.99	98.42	1.58
6	150	136.32	9.12	0.3810	0.6031	0.5842	152.49	1.66	153.50	2.33
7	160	145.18	9.26	0.3575	0.5821	0.6059	158.46	0.96	156.74	2.04
8	180	162.93	9.48	0.3132	0.5175	0.6529	181.89	1.05	178.15	1.03
9	220	198.05	9.98	0.2330	0.3702	0.7422	216.38	1.65	212.50	3.41
10	245	219.73	10.31	0.1870	0.2719	0.7942	243.41	0.65	242.97	0.83
11	260	233.10	10.35	0.1605	0.2143	0.8252	265.32	2.05	257.24	1.06

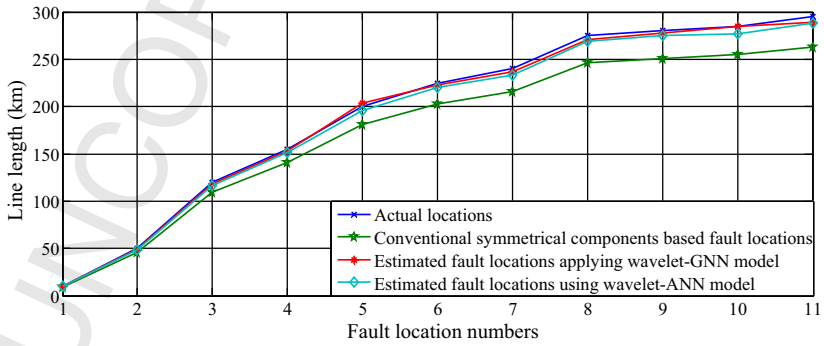

Fig. 7. Training output and performance comparison of wavelet-GNN model with ANN and conventional symmetrical method based fault location estimation for AG fault (phase A to ground fault) due to the fault occurred at the various locations of the line, operating at $R_f = 100\,\Omega$, FIA = 36° and $\delta = -15°$.

UNCORRECTED PROOF

Please cite this article in press as: M. Jamil, et al., Generalized neural network and wavelet transform based approach for fault location estimation of a transmission line, Appl. Soft Comput. J. (2014), http://dx.doi.org/10.1016/j.asoc.2014.02.020

Table 4
Fault location results measuring sequence components of voltage and current for AG fault, operating at $R_f = 100\,\Omega$, FIA = 36° and $\delta = -15°$.

Fault location points	Actual fault location from relaying point	Sending end zero sequence component voltage (at Bus1)		Zero sequence component voltage at fault point (at Bus3)		Sending end zero sequence current component		Zero sequence impedance between Bus1 to Bus3 (p.u)	Computed fault location distance (d) (km)	Absolute value of relative error in %
		Mag. (p.u)	Angle (degree)	Mag. (p.u)	Angle (degree)	Mag. (p.u)	Angle (degree)			
1	15	0.08926	−142.26	0.12164	−141.49	5.78	−22.78	0.0056	14	6.65
2	35	0.08077	−145.51	0.14899	−144.19	5.25	−25.17	0.01298	32.46	7.26
3	105	0.05749	−153.21	0.20197	−150.95	3.77	−30.53	0.03837	95.93	8.64
4	170	0.04114	−156.46	0.20774	−153.28	2.7	−32.55	0.06164	154.1	9.35
5	180	0.03894	−156.38	0.20538	−153.31	2.55	−32.64	0.06517	162.93	9.48
6	215	0.03117	−156.26	0.18969	−152.79	2.05	−32.48	0.07747	193.67	9.92

Table 5
Fault location results measuring sequence components of voltage and current for ABG fault, operating at $R_f = 1000\,\Omega$, FIA = 180° and $\delta = 30°$.

Fault location points	Actual fault location from relaying point	Sending end zero sequence component voltage (at Bus1)		Zero sequence component voltage at fault point (at Bus3)		Sending end zero sequence current component		Zero sequence impedance between Bus1 to Bus3 (p.u)	Computed fault location distance (d) (km)	Absolute value of relative error in %
		Mag. (p.u)	Angle (degree)	Mag. (p.u)	Angle (degree)	Mag. (p.u)	Angle (degree)			
1	30	0.00518	−160.8	0.00899	−159.81	0.30171	−52.39	0.01261	31.53	5.1
2	40	0.00521	−154.55	0.01019	−155.05	0.29071	−51.88	0.01715	42.87	7.16
3	55	0.0052	−148.29	0.01188	−149.95	0.27432	−51.07	0.02437	60.92	10.76
4	215	0.00493	−109.94	0.01612	−134.82	0.11668	−35.45	0.09595	239.87	11.57
5	225	0.00485	−108.4	0.0154	−134.85	0.10793	−34.05	0.09774	244.35	8.6
6	235	0.00473	−107.04	0.01447	−135.34	0.09921	−32.62	0.09822	245.56	4.49

UNCORRECTED PROOF

Please cite this article in press as: M. Jamil, et al., Generalized neural network and wavelet transform based approach for fault location estimation of a transmission line, Appl. Soft Comput. J. (2014), http://dx.doi.org/10.1016/j.asoc.2014.02.020

Table 6
Fault location results measuring sequence components of voltage and current for AB fault, operating at $R_f = 10\ \Omega$, FIA = 54° and $\delta = -15°$.

Fault location points	Actual fault location from relaying point	Sending end zero sequence component voltage (at Bus1)		Zero sequence component voltage at fault point (at Bus3)		Sending end zero sequence current component		Zero sequence impedance between Bus1 to Bus3 (p.u)	Computed fault location distance (d) (km)	Absolute value of relative error in %
		Mag. (p.u)	Angle (degree)	Mag. (p.u)	Angle (degree)	Mag. (p.u)	Angle (degree)			
1	170	4.75E−06	0	1.82E−05	0	0.00018	0	0.07537	188.43	10.84
2	180	4.63E−06	0	1.76E−05	0	0.00017	0	0.07731	193.27	7.37
3	210	4.21E−06	0	1.48E−05	0	0.00014	0	0.07775	194.37	7.44
4	215	4.02E−06	0	1.42E−05	0	0.00013	0	0.07842	196.04	8.82

Table 7
Fault location results measuring sequence components of voltage and current for ABC fault, operating at $R_f = 1\ \Omega$, FIA = 36° and $\delta = 15°$.

Fault location points	Actual fault location from relaying point	Sending end zero sequence component voltage (at Bus1)		Zero sequence component voltage at fault point (at Bus3)		Sending end zero sequence current component		Zero sequence impedance between Bus1 to Bus3 (p.u)	Computed fault location distance (d) (km)	Absolute value of relative error in %
		Mag. (p.u)	Angle (degree)	Mag. (p.u)	Angle (degree)	Mag. (p.u)	Angle (degree)			
1	175	7.64E−15	0	1.13E−14	0	4.51E−14	0	0.08025	200.62	14.64
2	225	7.51E−15	0	9.19E−16	0	8.54E−14	0	0.07722	193.04	14.20
3	230	4.63E−15	0	8.79E−15	0	5.18E−14	0	0.08029	200.73	12.73
4	270	2.39E−15	0	8.25E−15	0	5.80E−14	0	0.1012	252.99	6.30
5	275	2.11E−15	0	1.27E−14	0	9.28E−14	0	0.11398	284.95	3.62

UNCORRECTED PROOF

Please cite this article in press as: M. Jamil, et al., Generalized neural network and wavelet transform based approach for fault location estimation of a transmission line, Appl. Soft Comput. J. (2014), http://dx.doi.org/10.1016/j.asoc.2014.02.020

Table 8
Comparisons of performance of wavelet-GNN model with ANN and conventional symmetrical method of fault location at various fault operating conditions for LG, LLG, LL and LLL faults.

Type of faults	Actual distance to fault from relaying point	Fault resistance	Fault inception angle	Receiving end phase voltage angle (δ)	Conventional method based fault location		Normalized value of features vector in terms of standard deviation of phase A, phase B and phase C fault current signals							
					Using zero sequence components of voltage and current		Fault location estimation applying feature vectors as input to GNN						Fault location estimation applying feature vectors as input to ANN	
	(km)	(ohm)	(degree)	(degree)	Computed distance (d) (km)	% Error	$\sigma_A D_9$	$\sigma_B D_9$	$\sigma_C D_9$	Estimated fault distance (km)	% Error		Estimated fault distance (km)	% Error
LG (AG)	15	100	36	−15	14	6.65	0.8487	0.895	0.1465	15.29	1.93		15.33	2.20
	35	100	36	−15	32.46	7.26	0.7550	0.8764	0.2325	34.08	2.63		35.58	1.65
	105	100	36	−15	95.93	8.64	0.5012	0.7344	0.4718	106.74	1.66		105.62	0.59
	170	100	36	−15	154.1	9.35	0.3349	0.5524	0.6291	167.24	1.62		165.47	2.66
	180	100	36	−15	162.93	9.48	0.3132	0.5175	0.6529	181.67	0.93		182.09	1.16
	215	100	36	−15	193.67	9.92	0.2426	0.3895	0.7316	218.99	1.86		218.53	1.64
LLG (ABG)	30	1000	180	30	31.53	5.10	0.6296	0.5756	0.4344	29.42	1.93		30.96	3.20
	40	1000	180	30	42.87	7.16	0.5363	0.4796	0.4984	39.44	1.40		38.95	2.62
	55	1000	180	30	60.92	10.76	0.4100	0.3597	0.5936	53.87	2.05		56.54	2.80
	215	1000	180	30	239.87	11.57	0.1029	0.2607	0.6804	219.21	1.96		220.14	2.39
	225	1000	180	30	244.35	8.60	0.1028	0.3081	0.6163	222.45	1.13		230.85	2.60
	235	1000	180	30	245.56	4.49	0.1243	0.3642	0.5451	240.64	2.40		241.03	2.57
LL (AB)	170	10	54	−15	188.43	10.84	0.2741	0.2728	0.8821	168.22	1.05		174.73	2.78
	180	10	54	−15	193.27	7.37	0.2562	0.2548	0.8632	183.03	1.68		176.52	1.93
	210	10	54	−15	194.37	7.44	0.2078	0.2064	0.7415	214.07	1.94		204.21	2.76
	215	10	54	−15	196.04	8.82	0.2004	0.199	0.706	219.47	2.08		209.42	2.60
LLL (ABC)	175	1	36	15	200.62	14.64	0.2472	0.2455	0.2454	172.11	1.65		179.41	2.52
	225	1	36	15	193.04	14.20	0.1745	0.1734	0.1735	231.11	2.72		231.02	2.68
	230	1	36	15	200.73	12.73	0.1683	0.1673	0.1679	227.33	1.16		233.49	1.52
	270	1	36	15	252.99	6.30	0.1239	0.1234	0.1243	265.33	1.73		277.26	2.69
	275	1	36	15	284.95	3.62	0.119	0.1185	0.1197	269.55	1.98		270.45	1.65

UNCORRECTED PROOF

Please cite this article in press as: M. Jamil, et al., Generalized neural network and wavelet transform based approach for fault location estimation of a transmission line, Appl. Soft Comput. J. (2014), http://dx.doi.org/10.1016/j.asoc.2014.02.020

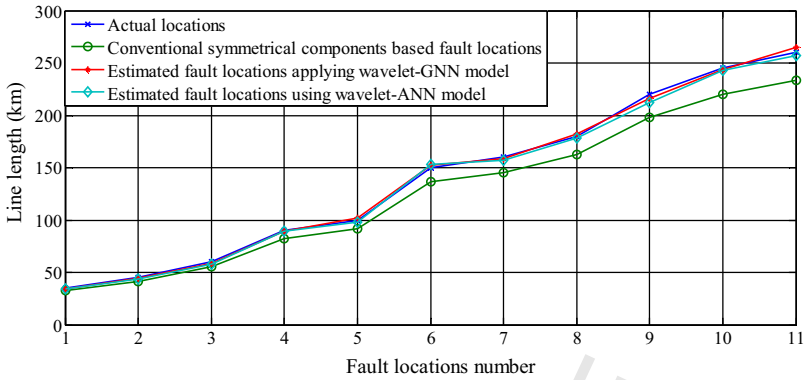

Fig. 8. Testing output and performance comparison of wavelet-GNN model with ANN and conventional symmetrical method based fault location estimation for AG fault (phase A to ground fault) due to the fault occurred at the various locations of the line, operating at $R_f = 100\,\Omega$, FIA = 36° and $\delta = -15°$.

Figs. 7 and 8. It is clearly seen from the graph that during training of wavelet-GNN model, both the actual and trained values are overlapping or very close to each other. This indicates that the network is trained successfully.

The task of estimation of fault locations is carried out for all kinds of phase and ground faults i.e. for line to ground (LG), double line to ground (LLG), line to line (LL) and double line to line (LLL) fault under different fault operating conditions as mentioned above. The performance of the models is evaluated on the basis of mean value of absolute relative error in percentage using the following formula

$$\text{Absolute relative error} = \frac{|\text{Actual fault location} - \text{Estimated fault location}|}{\text{Actual fault location}} \times 100$$

It is found that the mean value of absolute relative error using wavelet-GNN model is around 2%, while it is around 3% using wavelet-ANN model. Whereas in case of conventional symmetrical based fault location estimation method, it is in the range of 10%, considering the different fault operating conditions for all kinds of phase and ground faults. The comparative results of the wavelet-GNN based model of fault location estimation considering the same input parameters as in wavelet-ANN are depicted in Table 8. The comparison of fault locations using symmetrical components of voltage and current are also illustrated in Table 8, considering the same fault operating conditions as in GNN and ANN model. Observations of all test results ascertain that the wavelet-GNN based model of fault location estimation performs excellent even at voltage zero crossing situation of fault inception angle and at different fault locations starting from relay end (sending end) to the receiving end.

6. Conclusion

In the proposed study a GNN based fault location technique on three phase transmission line is presented. The fault current signals of the three phase transmission line are filtered through wavelet transform. The fault current signals are obtained at the sampling frequency of 100 kHz. MRA based on DWT is used to capture the transient characteristics of the fault current signals. The information captured during the ninth level frequency bands by the details wavelet coefficient in terms of standard deviation is fed as an input to the GNN and target as the fault location of the transmission line. The obtained results are compared with the conventional symmetrical components based method of fault location. To validate the proposed approach, it is applied to a large number of test cases generated for different fault operating conditions. The performance of the proposed wavelet-GNN model is also compared with ANN technique. It is found that the performance of the proposed GNN based model is better than the other method. As GNN requires less data to analyze. Therefore the time taken for identifying the location of the fault is quite less.

Acknowledgements

The authors would like to thanks to Prof. D.K. Chaturvedi, Department of Electrical Engineering, Dayalbagh Educational Institute (DEI), Deemed University, Agra (U.P.), India for giving us continuous support and suggestions in the development of GNN model for estimating the fault location of a given transmission systems.

Appendix I.

A multilayered feed forward neural network (FFNN) is chosen as shown in Fig. 9, for the fault location estimation of the transmission line considering the same input parameters and fault operating conditions as in wavelet-GNN based model of fault location estimation.

Appendix II.

In this study a faulted transmission line extending between two power systems as shown in Fig. 10, is considered to locate the fault distance '*d*' from the sending end of the transmission line to the

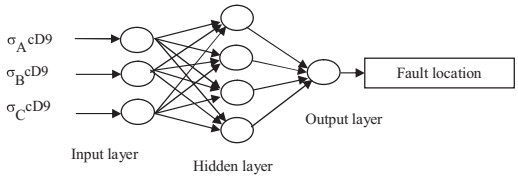

Fig. 9. Structure of Artificial neural network (ANN) for the fault location estimation.

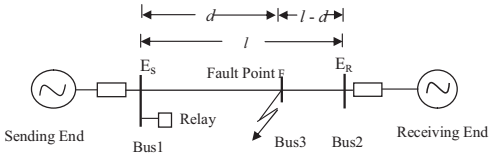

Fig. 10. Power system model.

Please cite this article in press as: M. Jamil, et al., Generalized neural network and wavelet transform based approach for fault location estimation of a transmission line, Appl. Soft Comput. J. (2014), http://dx.doi.org/10.1016/j.asoc.2014.02.020

UNCORRECTED PROOF

fault point, due to the fault occurred under various fault operating conditions by measuring the sequence components of voltage and current at Bus1 and Bus3 using Eqs. (15)–(17).

The computed fault locations 'd' in (km) for line to ground (LG), double line to ground (LLG), double line (LL), and double line to line LLL (symmetrical faults) faults are depicted in Tables 2–7 for different fault operating conditions.

$$Z_{13}^{0} = \frac{V_{sa}^{0}(F) - V_{3}^{0}(F)}{I_{13}^{0}} \tag{15}$$

$$Z_{13}^{1} = \frac{V_{sa}^{1}(F) - V_{3}^{1}(F)}{I_{13}^{1}} \tag{16}$$

$$Z_{13}^{2} = \frac{V_{sa}^{2}(F) - V_{3}^{2}(F)}{I_{13}^{2}} \tag{17}$$

where $V_{sa}{}^{0}(F) = 0 - Z_{13}{}^{0} I_{fa}{}^{0}$; $V_{sa}{}^{1}(F) = V_{sa}(F) - Z_{13}{}^{1} I_{fa}{}^{1}$; $V_{sa}{}^{2}(F) = 0 - Z_{13}{}^{2} I_{fa}{}^{2}$ and $Z_{13}^{0} = xZ^{0}$, $Z_{13}^{1} = xZ^{1}$, $Z_{13}^{2} = xZ^{2}$; $Z_{23}^{0} = (l-x)Z^{0}$, $Z_{23}^{1} = (l-x)Z^{1}$, $Z_{23}^{2} = (l-x)Z^{2}$; $V_{sa}{}^{0}(F)$, $V_{sa}{}^{1}(F)$ and $V_{sa}{}^{2}(F)$: zero, positive and negative components of sending end voltage; $V_{3}^{0}(F)$, $V_{3}^{0}(F)$ and $V_{3}^{0}(F)$: zero, positive and negative components of voltage at Bus3; $V_{sa}(0)$: pre-fault phase voltage at sending end; I_{fa}^{0}, I_{fa}^{1} and I_{fa}^{2}: zero, positive and negative components of current at fault point; Z_{13}^{0}, Z_{13}^{1} and Z_{13}^{2}: zero, positive and negative components of impedance between Bus1 and Bus3; Z_{23}^{0}, Z_{23}^{1} and Z_{23}^{2}: zero, positive and negative components of impedance between Bus2 and Bus3; l = total length of the transmission line in km; d = fault distance from relay to the fault point in km; Z^{0}, Z^{1} and Z^{2}: zero, positive and negative components of impedance of transmission line; base value selected for voltage (line to line) = 500 kV; Base value for power (VA 3 phase) = 100 MVA.

References

[1] M.J.B. Reddy, D.K. Mohanta, Performance evaluation of an adaptive network based fuzzy inference system approach for location of faults on transmission lines using Monte Carlo simulation, IEEE Trans. Fuzzy Syst. 16 (4) (2008) 909–917.
[2] T. Takagi, Y. Yamakoshi, M. Yamaura, R. Kondow, T. Matsushima, Development of a new type fault locator using the one terminal voltage and current data, IEEE Trans. Power Apparat. Syst. 101 (8) (1982) 2892–2898.
[3] H.-X. Ha, B.-H. Zhang, Z.-L. Lv, A novel principle of single ended fault location technique for EHV transmission lines, IEEE Trans. Power Deliv. 18 (4) (2003) 1147–1151.
[4] M.B. Djuric, Z.M. Radojevic, V.V. Terzija, Distance protection and fault location utilizing only phase current phasors, IEEE Trans. Power Deliv. 13 (4) (1998) 1020–1026.
[5] C. Wang, Q.-Q. Jia, X.-B. Li, C.-X. Dou, Fault location using synchronized sequence measurements, Int. J. Electr. Power Energ. Syst. 30 (2008) 134–139.
[6] S.M. Brahama, Iterative fault location scheme for a transmission line using synchronized phasor measurements, Int. J. Emerg. Electr. Power Syst. 8 (6) (2007) 1–14.
[7] Y. Liao, N. Kang, Fault location algorithms without utilizing line parameters based on the distributed parameter line model, IEEE Trans. Power Deliv. 24 (2) (2009) 579–584.
[8] C.E. de Morais Pereira, L.C. Zanetta, Fault location in transmission lines using one terminal postfault voltage data, IEEE Trans. Power Deliv. 19 (2) (2004) 570–574.
[9] S.R. Samantaray, P.K. Dash, G. Panda, Fault classification and location using HS-transform and radial basis function neural network, Electr. Power Syst. Res. 76 (2006) 897–905.
[10] J. Sadeh, H. Afradi, A new and accurate fault location algorithm for combined transmission lines using adaptive network based fuzzy inference system, Electr. Power Syst. Res. 79 (2009) 1538–1545.
[11] O.A.S. Youssef, Combined fuzzy logic wavelet based fault classification for power system relaying, IEEE Trans. Power Deliv. 19 (2) (2004) 582–589.
[12] D. Chanda, N.K. Kisore, A.K. Sinha, A wavelet multi resolution analysis for location of faults on transmission lines, Electr. Power Energ. Syst. 25 (2003) 59–69.
[13] A.H. Osman, O.P. Malik, Transmission line distance protection based on wavelet transform, IEEE Trans. Power Deliv. 19 (2) (2004) 59–69.
[14] P.S. Bhowmik, P. Purkait, K. Bhattacharya, A novel wavelet transform aided neural network based transmission line fault analysis method, Electric. Power Energ. Syst. 31 (2009) 213–219.
[15] J. Biswarup Das, V. Reddy, Fuzzy logic based fault classification scheme for digital distance protection, IEEE Trans. Power Deliv. 20 (2) (2005) 609–616.
[16] R.N. Mahanty, P.B. Dutta Gupta, A fuzzy logic based fault classification approach using current samples only, Electr. Power Syst. Res. 77 (2007) 501–507.
[17] S.R. Samantray, P.K. Dash, G. Panda, Distance relaying for transmission line using support vector machine and radial basis function neural network, Electric. Power Energ. Syst. 29 (2007) 551–556.
[18] H. Wang, W.W.L. Keerrthipala, Fuzzy neuro approach to fault classification for transmission line protection, IEEE Trans. Power Deliv. 13 (4) (1998) 1093–1102.
[19] C. Fan, K.K. Li, W.L. Chan, W. Yu, Study of protection scheme for transmission line based on wavelet transient energy, Electric. Power Energ. Syst. 28 (2006) 459–470.
[20] H. Osman, O.P. Malik, Protection of parallel transmission lines using wavelet transform, IEEE Trans. Power Deliv. 19 (1) (2004) 49–55.
[21] S. El Safty, A. El-Zonkoly, Applying wavelet entropy principle in fault classification, Electric. Power Energ. Syst. 31 (2009) 604–607.
[22] S. Ekici, S. Yildirim, M. Poyraz, Energy and entropy based feature extraction for locating fault on transmission lines by using neural network and wavelet packet decomposition, Exp. Syst. Appl. 34 (2008) 2937–2944.
[23] P. Chiradeja, A. Ngaopitakkul, Identification of fault types for single circuit transmission line using discrete wavelet transform and artificial neural networks, Proc. Int. Multi Conf. Eng. Comp. Sci. 2 (2009).
[24] N. Zhang, M. Kezunovic, Transmission line boundary protection using wavelet transform and neural network, IEEE Trans. Power Deliv. 22 (2) (2007) 859–869.
[25] B.K. Panigrahi, V.R. Pandi, Optimal feature selection for classification of power quality disturbances using wavelet packet based fuzzy k-nearest neighbour algorithm, IET Gener. Transm. Ditribut. 3 (2009) 296–306.
[26] A. Abdollahi, S. Seyedtabaii, Transmission line fault location estimation by Fourier and wavelet transforms using ANN, in: International Power Engineering and Optimization Conf., 2010, pp. 23–24.
[27] M. Jayabharata Reddy, D.K. Mohanta, A Wavelet fuzzy combined approach for classification and location of transmission line faults, Electric. Power Energ. Syst. 29 (2007) 669–678.
[28] M.P. Nikhli, A.A. Safavi, Path characteristic frequency based fault locating in radial distribution systems using wavelets and neural network, IEEE Trans. Power Deliv. 26 (2011) 752–781.
[29] D.K. Chaturvedi, S.A. Premdayal, A. Chandiok, Short-term load forecasting using soft computing techniques, Int. J. Commun. Netw. Syst. Sci. 3 (2010) 273–279.
[30] D.K. Chaturvedi, O.P. Malik, P.K. Kalra, Performance of a generalized neuron-based PSS in a multimachine power system, IEEE Trans. Energy Convers. 19 (3) (2004) 625–632.
[31] D.K. Chaturvedi, M. Mohan, P.K. Kalra, Improved generalized neuron model for short-term load forecasting, Soft Comput. 8 (2004) 370–379.
[32] D.K. Chaturvedi, R. Chauhan, P.K. Kalra, Applications of generalized neural networks in for aircraft landing control system, Soft Comput. 6 (2002) 441–448.
[33] D.K. Chaturvedi, P.S. Satsangi, P.K. Kalra, Fuzzified neural network approach for load forecasting, Eng. Intell. Syst. 1 (2001) 3–9.
[34] Manmohan, D.K. Chaturvedi, P.S. Satsangi, P.K. Kalra, Neuro fuzzy approach for development of new neuron model, Soft Comput. 8 (2003) 19–27.
[35] D.K. Chaturvedi, P.S. Satsangi, P.K. Kalra, Load frequency control: a generalized neural network approach, Int. J. Electr. Power Energy Syst. 21 (1999) 405–415.
[36] D.K. Chaturvedi, Soft Computing Techniques and its Applications in Electrical Engineering, Springer Verlag, Berlin, Heidelberg, Germany, 2008.
[37] D.K. Chaturvedi, Soft Computing Techniques and its Applications in Electrical Engineering, Springer Verlag, Berlin, Heidelberg, 2008.
[38] M. Rizwan, M. Jamil, D.P. Kothari, Generalized neural network approach for global solar energy estimation in India, IEEE Trans. Sust. Energ. 3 (3) (2012) 576–584.

UNCORRECTED PROOF

Please cite this article in press as: M. Jamil, et al., Generalized neural network and wavelet transform based approach for fault location estimation of a transmission line, Appl. Soft Comput. J. (2014), http://dx.doi.org/10.1016/j.asoc.2014.02.020

ISBN 978-93-5156-328-0
International Conference of Advance Research and Innovation (ICARI-2014)

Hardware Implementation of Prototype Model of Two Port Network

Harsha Saroa *, Nikita Gupta
Department of Power Systems, Delhi Technological University, Delhi, India

Article Info

Article history:
Received 29 December 2013
Received in revised form
10 January 2014
Accepted 20 January 2014
Available online 1 February 2014

Keywords

Two Port Network
T networks
π networks

Abstract

The study of two port networks is important in the field of electrical engineering. Keeping in mind the importance of two port network in the electrical engineering field authors have designed and developed 2-port network prototype. The networks involved in the prototype are 12 V AC and DC purely resistive T-network, π-network, Series T-network and Parallel T-network. The parameters of a 2-port network completely describe the behavior of the system in terms of the voltage and current that may be measured at each port. For making prototype more viable author(s) have provided both AC and DC supply. The results of impedance, admittance, transmission, inverse transmission, hybrid and inverse hybrid parameters of these networks are shown in the paper.

1. Introduction

The study of two port networks is important in the field of electrical engineering because most electric circuits and electronic modules have at least two ports, namely input and output terminal pairs. Two-port parameters describe a system in terms of the voltage and current that may be measured at each port. A pair of terminals through which a current may enter or leave a network is known as a port [1]. A port is an access to the network and consists of a pair of terminals; the current entering one terminal leaves through the other terminal so that the net current entering the port equals zero. We may apply an input signal in one port and obtain an output signal from the other port. The parameter of a two-port network completely describes its behavior in terms of the voltage and current at each port. Thus, knowing the parameters of a two port network permits us to describe its operation when it is connected into a larger network [1-6]. Two-port networks are also important in modeling electronic devices and system components.

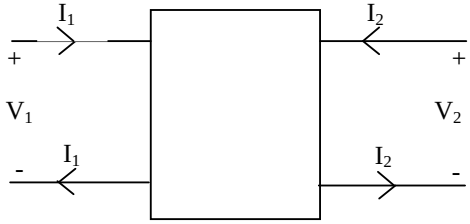

Fig: 1. A general two port network

Fig: 1. represents a two-port network. A four terminal network is called a two-port network when the current entering one terminal of a pair exits the other terminal in the pair. Here I1 is the current entering port 1, I2 is the current entering port 2, and V1 and V2 are voltages that exist at ports 1 and 2, respectively.

2. Types Of Two Port Parameters

A 2-port network has four variables: voltages V1 and V2 measured across each port and corresponding currents, I1 and I2. The 2-port network does not contain any internal independent sources, thus we can characterize the 2-ports by purely linear relations and that the port voltages and currents are dependent only upon one another. There are total six types of two port network parameters based on above mentioned four variables I1, I2, V1 and V2. The matrix equations of these parameters are as follows:

2.1 Z-parameter : The two port equations are as follows

$$V_1 = z_{11} I_1 + z_{12} I_2 \quad (1)$$

$$V_2 = z_{21} I_1 + z_{22} I_2 \quad (2)$$

Corresponding Author,
E-mail address: abc_harsha@yahoo.com
All rights reserved: http://www.ijari.org

From Equations (1) and (2) Z_{11}, Z_{12}, Z_{21} and Z_{22} are defined by equations 3

$$z_{11} = \left.\frac{V_1}{I_1}\right|_{I_2=0}, \quad z_{12} = \left.\frac{V_1}{I_2}\right|_{I_1=0}, \quad z_{21} = \left.\frac{V_2}{I_1}\right|_{I_2=0}, \quad z_{22} = \left.\frac{V_2}{I_2}\right|_{I_1=0} \tag{3}$$

2.2 Y parameters: The two port equations are as follows

$$I_1 = y_{11}V_1 + y_{12}V_2 \tag{4}$$

$$I_2 = y_{21}V_1 + y_{22}V_2 \tag{5}$$

From Equations (7) and (8) Y_{11}, Y_{12}, Y_{21} and Y_{22} are defined by equations 6

$$y_{11} = \left.\frac{I_1}{V_1}\right|_{V_2=0}, \quad y_{12} = \left.\frac{I_1}{V_2}\right|_{V_1=0}, \quad y_{21} = \left.\frac{I_2}{V_1}\right|_{V_2=0}, \quad y_{22} = \left.\frac{I_2}{V_2}\right|_{V_1=0} \tag{6}$$

2.3 Transmission parameters: The two port equations are as follows

$$V_1 = AV_2 - BI_2 \tag{7}$$

$$I_1 = CV_2 - DI_2 \tag{8}$$

From Equations (13) and (14) A, B, C and D are defined by equations 9

$$A = \left.\frac{V_1}{V_2}\right|_{I_2=0}, \quad B = \left.\frac{V_1}{-I_2}\right|_{V_2=0}, \quad C = \left.\frac{I_1}{V_2}\right|_{I_2=0}, \quad D = \left.\frac{I_1}{-I_2}\right|_{V_2=0} \tag{9}$$

2.4 Hybrid parameters : The two port equations are as follows

$$V_1 = h_{11}I_1 + h_{12}V_2 \tag{10}$$

$$I_2 = h_{21}I_1 + h_{22}V_2 \tag{11}$$

From Equations (19) and (20) h_{11}, h_{12}, h_{21} and h_{22} are defined by equations 12

$$h_{11} = \left.\frac{V_1}{I_1}\right|_{V_2=0}, \quad h_{21} = \left.\frac{I_2}{I_1}\right|_{V_2=0}, \quad h_{12} = \left.\frac{V_1}{V_2}\right|_{I_1=0}, \quad h_{22} = \left.\frac{I_2}{V_2}\right|_{I_1=0} \tag{12}$$

3. Development Of Prototype Hardware Model

Figure 2 shows the networks designed for the hardware prototype. Authors designed four basic networks which include π, T, Series-T, Parallel-T networks. These networks are devised using 120 Ω resistances which are embedded on the PCB. These networks are designed for single phase 12 V AC and 12 V DC supply. The voltmeter (0-15) V and ammeter (0-100) mA are mounted on the display panel of working board for measuring of voltage and current.

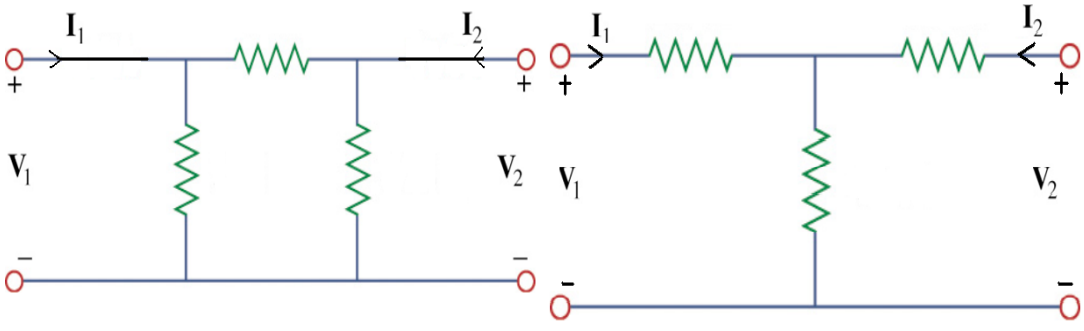

(**π**-network) (T-network)

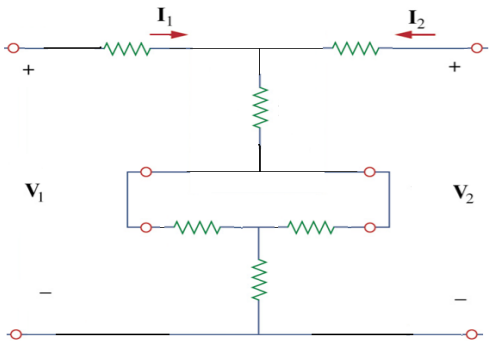

(Series connection of T-network)

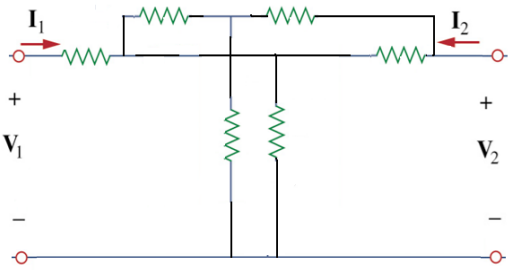

(Parallel connection of T-network)

Fig: 2. *Circuit diagram of different networks*

The hardware setup for testing the prototype model is shown in figure3. The supply, ammeter and voltmeter are put on the display board of the model to make it well equipped. Separate terminals are provided for each type of network on board with specified circuit diagram as shown in figure 3.

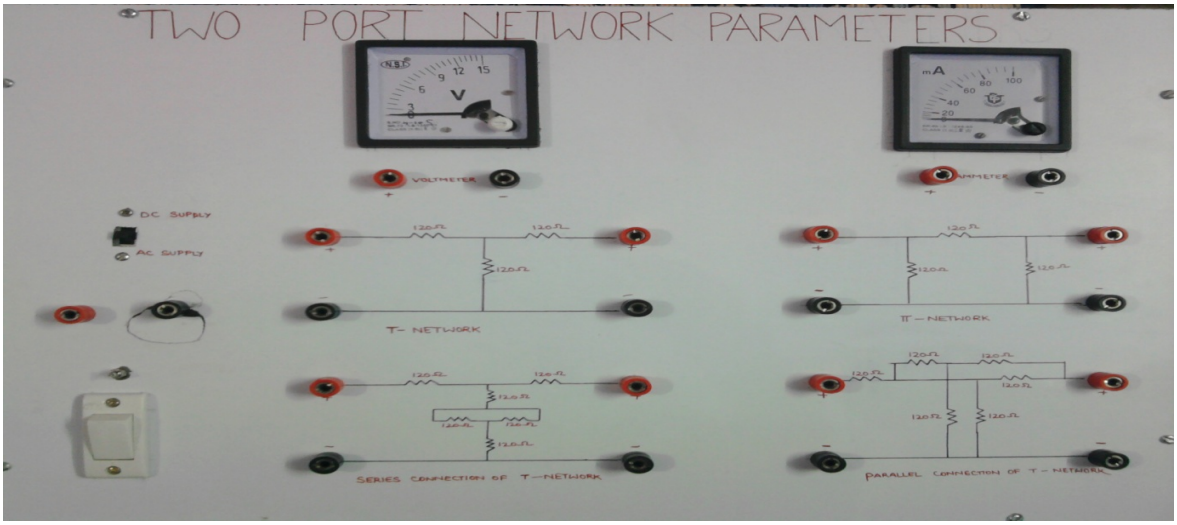

Fig: 3. Experimental setup of hardware prototype

4. Results And Discussions

The reading of ammeter and voltmeter are taken for various networks connected to AC and DC supply available on the display board. Tables I to IV show sthe readings of Z-parameters, Y-parameters, ABCD parameters and hybrid parameters respectively.

	Supply Type	Z_{11} (m Ω)	Z_{12} (m Ω)	Z_{21} (m Ω)	Z_{22} (m Ω)
π	AC	0.2	0.33	0.053	0.088
	DC	0.157	0.325	0.039	0.0813
T	AC	0.3	0.5	0.05	0.0571
	DC	0.233	0.4	0.055	0.0942
Parallel T	AC	0.206	0.375	0.056	0.0103
	DC	0.164	0.311	0.049	0.0933
Series T	AC	0.48	0.363	0.012	0.0909
	DC	0.35	0.291	0.01	0.0833

Table: 1. Readings obtained for Z-parameters

	Supply Type	Y_{11} (m mho)	Y_{12} (m mho)	Y_{21} (m mho)	Y_{22} (m mho)
π	AC	5	18.75	3	11.25
	DC	6.3	25.4	3.07	12.2
T	AC	3.33	20	2	12.3
	DC	4.28	18.18	2.5	16.5
Parallel T	AC	4.833	17.5	2.66	9.69
	DC	6.071	20.23	3.21	17.3
Series T	AC	2.083	8.33	2.75	11.4
	DC	2.857	10	3.42	12.6

Table: 2. Readings obtained for Y-parameters

	Supply Type	A	B (m Ω)	C (m mho)	D
π	AC	3.75	0.33	18.75	-1.66
	DC	4	0.325	25.4	-2.069
T	AC	6	0.5	20	-1.66
	DC	4.242	0.4	18.18	-1.71
Parallel T	AC	3.636	0.375	17.5	-1.812
	DC	3.333	0.311	20.23	-1.88
Series T	AC	4	0.363	8.33	-0.75
	DC	3.5	0.291	10	-0.833

TABLE: 3. Readings obtained for Transmission-parameters

	Supply Type	h_{11} (m Ω)	h_{12}	h_{21}	h_{22} (m mho)
π	AC	0.2	3.75	0.6	11.25
	DC	0.157	4	0.48	12.2
T	AC	0.3	6	0.6	12.3
	DC	0.233	4.242	0.58	16.5
Parallel T	AC	0.206	3.636	0.55	9.69
	DC	0.164	3.333	0.53	17.3
Series T	AC	0.48	4	1.32	11.4
	DC	0.35	3.5	1.2	12.6

Table: 4. Readings obtained for Hybrid-parameters

5. Conclusion

A prototype model of 12V, AC and DC two port networks has been designed and developed. For a given circuits the reading obtained in the prototype model is found to be within acceptable limits. Hence, developing the sets of parameters that are used to relate the output variables of voltage and current, typically designated as V2 and I2, respectively, to the input variables of voltage and current, typically designated as V1 and I1, respectively are able to accomplish the designing of hardware prototype.

References

[1] M. E. Van Valkenburg, "Network Analysis" Prentice-Hall, 1955. Englewood Cliffs, NJ

[2] J. M. Rabaey, "Digital Integrated Circuits—A Design Perspective", Saddle River, NJ, USA: Prentice-Hall, 2003.

[3] P. R. Gray and R. G. Mayer, "Analysis and Design of Analog Integrated Circuits", 3-rd ed. New York, Wiley, 1993.

[4] W. Prodanov, M. Valle, R. Buzas, and H. Pierscinski, "Behavioralmodels of basic mixed mode circuits: Practical issues and application," in *Proc. IEEE Eur. Conf. Circuit Theory Design*, May 2008, pp. 854–857.

[5] Grigorescu, "Computational method of the sensitivities for steady-state two-ports circuits using the relative values," WSEAS Trans.on Circuits and Systems, 5 (3), pp. 332-338, May 2006

[6] *Advanced Design System, User-Defined Models*, Agilent Technologies, Santa Clara, CA, USA, Sep. 2006, pp. 121–170.

Volume 1 (2013) 46-58 ISSN 2347 - 3258
International Journal of Advance Research and Innovation

Irriversibility Analysis of Multi-Evaporators Vapour Compression Refrigeration Systems Using New and Refrigerants: R134a, R290, R600, R600a, R1234yf, R502, R404a and R152a and R12, R502

R. S. Mishra
Department of Mechanical Engineering, Delhi Technological University, India

Article Info

Article history:
Received 1 July 2013
Received in revised form
15 July 2013
Accepted 22 July 2013
Available online 1 August 2013

Keywords

Vapour Compression Refrigeration Systems
First and second Law Analysis,
Irreversibility Analysis in VCR

Abstract

The methods for improving first law and second law efficiency have been considered in this paper. Detailed energy and exergy analysis of multi-evaporators at different temperatures with multiple compressors and multiple expansion valves in parallel and series with intercooler and flash chambers in the six type vapour compression refrigeration systems for finding irreversibilities in the systems have been done in terms of performance parameter for eco-friendly R134a, R290, R600, R600a, R1234yf, R1234ze, R404a and R152a and conventional R12, R502refrigerants. The numerical computations have been carried out for six systems. It was observed that first law and second law efficiency improved by 22%. It was also observed that performance of above six systems using R600 and R152a nearly matching same values under the accuracy of 5% can be used in the above system .But difficulties using R600, R290 and R600a have flammable problems therefore safety measures are required using these refrigerants, therefore R134a refrigerant is recommended for practical and commercial applications although it has slightly less thermal performance than R152a which is not widely used refrigerant for domestic and industrial applications.

Nomenclature

COP	coefficient of performance (non-dimensional)
VCR	vapour compression refrigeration
CFC	chlorofluorocarbon
HCFC	hydrochlorofluorocarbon
Q	rate of heat transfer (kW)
W	work rate (kW)
T	temperature (K)
δ	efficiency defect (non-dimensional)
ΔT_{sc}	degree of subcooling
EP	exergy rate of product (kW)
EV	Expansion Valve
EP	Evaporator

Subscript

e	evaporator
comp	compressor
h	specific enthalpy (kJ/kg)
P	pressure (kPa)
IR	irreversibility (kW)
E_x	exergy rate of fluid (kW)
m	mass flow rate (kg/s)
s	specific entropy (kJ/kgK)
EF	exergy rate of fuel (kW)
EL	exergy loss rate (kW)
η	efficiency (non-dimensional)
r	refrigerant, space to be cooled
ex	exergetic
ev	expansion valve
c	condenser
sc	subcooler
k	kth component

Corresponding Author,
E-mail address: professor_rsmishra@yahoo.co.in
All rights reserved: http://www.ijari.org

1. Introduction

It is well known the fact that after 90's CFC and HCFC refrigerants have been forbidden due to chlorine content and their high ozone depleting potential (ODP) and global warming potential (GWP).

Thus, HFC refrigerants are used nowadays, presenting a much lower GWP value, but still high with respect to non-fluorine refrigerants. Many research papers have been published on this subject, of replacing "old" refrigerants with "new" ones [1-6]. Lately, many papers focused on researches about finding better and better refrigerants or mixtures, considering different criteria, as for example: Relative COP, COP, EDR, exergetic efficiency, and exergy defect in compressor, condenser, expansion valve subcooler and evaporators. This paper presents a comparative analysis of eight refrigerants working in a multi-evaporators VCR system with subcooling and superheating. These eight refrigerants are:1,2-Difluoroethane (R152a), Propane (R290), Butane (R600),Isobutane (R600a),2,3,3,3-Tetrafluoropropene (R1234yf), a azeotropic blend (R404a), (R410a) and (R502). R404a is a near-azeotropic blend of R125 / R143a / R134a with mass percentages of 44% / 52% / 4%.R410a is an azeotropic blend of Difluoromethane R32 Pentafluorethane R125 with mass percentages of 50% / 50%. Blends do not necessarily remain at constant temperature during constant pressure evaporation or condensation. This paper mainly deals with a comparative analysis of the refrigerant impact on the performances of six types multi-evaporators multiple compression and multiple expansion valves in series and parallel with introducing intercoolers in the vapor compression refrigeration systems. The aim of this paper is to present and propose an analysis model for comparing the effects of multi-evaporators, Multiple expansion valves in series and parallel combination and multiple compressors VCR System for improving first law and second law efficiency with different eco-friendly refrigerants as compared with R12 and R502.

2. Literature Review

Refrigeration is a technology which absorbs heat at low temperature and provides temperature below the surrounding by rejecting heat to the surrounding at higher temperature. Simple vapour compression system which consists of four major components compressor, expansion valve, condenser and evaporator in which total cooling load is carried at one temperature by single evaporator but in many applications like large hotels, food storage and food processing plants, food items are stored in different compartment and at different temperatures. Therefore there is need of multi evaporator vapour compression refrigeration system. The systems under vapour compression technology consume huge amount of electricity, this problem can be solved by improving performance of system.

Performance of systems based on vapour compression refrigeration technology can be improved by following:

- The performance of refrigerator is evaluated in term of first law efficiency (COP) which is the ratio of refrigeration effect to the net work input given to the system.
- The COP of vapour compression refrigeration system can be improved either by increasing refrigeration effect or by reducing work input given to the system.
- It is well known that throttling process in vapour compression refrigeration (VCR) is an irreversible expansion process. Expansion process is one of the main factors responsible for exergy loss in cycle performance because of entering the portion of the refrigerant flashing to vapour in evaporator which will not only reduce the cooling capacity but also increase the size of evaporator. This problem can be eliminated by adopting multi-stage expansion with flash chamber where the flash vapours is removed after each stage of expansion as a consequence there will be increase in cooling capacity and reduce the size of the evaporator.
- Work input can also be reduced by replacing multi-stage compression or compound compression with single stage compression.
- Refrigeration effect can also be increased by passing the refrigerant through subcooler after condenser to evaporator.

Vapour compression refrigeration system based applications make use of refrigerants which are responsible for greenhouse gases, global warming and ozone layer depletion. Montreal protocol was signed on the issue of substances that are responsible for depleting Ozone layer and discovered how much consumption and production of ozone depletion substances took place during certain time period for both developed and developing countries. Another protocol named as Kyoto aimed to control emission of green house gases in 1997[1]. The relationship between ozone depletion potential and global warming potential is the major concern in the field of GRT (green refrigeration technology) so Kyoto proposed new refrigerants having lower value of ODP and GWP. Internationally a program being pursued to phase out refrigerants having high chlorine content for the sake of global environmental problems [2].Due to presence of high chlorine content, high global warming potential and ozone depletion potential after 90's CFC and HCFC refrigerants have been restricted. Thus, HFC refrigerants are used nowadays, showing

much lower global warming potential value, but still high with respect to non-fluorine refrigerants. Lots of research work has been done for replacing "old" refrigerants with "new" refrigerants [3-8]. Reddy et al. (2012) carried out numerical analysis of vapour compression refrigeration system using R134a, R143a, R152a, R404A, R410A, R502 and R507A for finding the effect of evaporator temperature, degree of sub cooling at condenser outlet, superheating of evaporator outlet, vapour liquid heat exchanger effectiveness and degree of condenser temperature on COP and exergetic efficiency. They concluded that evaporator and condenser temperature have significant effect on both COP and exergetic efficiency and also found that R134a gives the better performance while R407C has poor performance in all respect. Selladurai and Saravanakumar (2013) have designed domestic refrigerator which was used R134a as eco-friendly refrigerant and also compared the thermal performance of the system with using another eco-friendly refrigerant as hydrogen mixture (i.e. R290/R600a mixture) and found that R290/R600a hydrocarbon mixture gives better performance in terms of higher COP and exergetic efficiency than R134a. They also concluded that highest irreversibility obtained in the compressor compare to condenser, expansion valve and evaporator in the domestic refrigeration system. Nikolaidis and Probert (1998) analytically found the considerable effect on plant irreversibility by change in evaporator and condenser temperatures of two stage vapour compression refrigeration plant using R22 refrigerant. They concluded that there is need for optimizing condenser and evaporator conditions. Kumar et al. (1989) carried out energy and exergy analysis of vapour compression refrigeration system using of exergy-enthalpy diagram. They also used detailed first law analysis for calculating the coefficient of performance and second law analysis for evaluating irreversibility in terms of various losses occurred in different components of vapour compression cycle using R11 and R12 as refrigerants. Mastani Joybari et al. (2013) conducted experiments on a domestic refrigerator originally manufactured to use of 145g of R134a and also concluded exergetic defect occurred in compressor was highest as compare to other components and through their analysis it has been found that instead of 145g of R134a if 60g of R600a is used in the considered system gave same performance which ultimately result into economical advantages and reduce the risk of flammability of hydrocarbon refrigerants. Anand and Tyagi (2012) carried out detailed exergetic analysis of two ton capacity of window air conditioning test rig with R22 as working fluid and concluded that irreversibility in system components will be highest when the system is 100% charged and lowest when 25% charged and found irreversibility in compressor is highest among other system components. Arora and Kaushik (2008) studied numerical model of vapour compression refrigeration system with liquid vapour heat exchanger and carried out energy and exergy analysis on the VCR for the specific temperature range of evaporator and condenser. They concluded that R502 is the best refrigerant compare to R404A and R507A, compressor is the worst and liquid vapour heat exchanger is best component of the system. Ahamed et al. (2012) experimentally investigated thermal performance using hydrocarbons (isobutene and butane) refrigerant on domestic refrigerator by energy and exergy analysis and found that energy efficiency ratio of hydrocarbons is comparable with R134a. They concluded that exergy efficiency and sustainability index of hydrocarbons is much higher than R134a at evaporator temperature and found that compressors are showing highest system defect (69%) among components of that system. Stanciu et al. (2011) carried out numerical and graphical investigation on one stage vapour compression refrigeration system by using refrigerants (i.e R22, R134a, R717, R507a, and R404a) in terms of COP, compressor work, exergy efficiency and refrigeration effect. They also studied the effect of sub-cooling, superheating and compression ratio on the same system using considered refrigerants and presented system optimization when working with specific refrigerant. Ahamed et al. (2011) emphasized on use of hydrocarbons and mixture of hydrocarbons and R134a in vapour compression refrigeration system and found that compressor showed much higher exergy destruction as compared to other components of vapour compression refrigeration system and found that exergy destruction can be minimized by using of nanofluid and nanolubricants in compressor.

Bolaji et al. (2011) conduced experimentally comparative analysis of R32, R152a and R134a refrigerants in vapour compression refrigerator concluded that R32 is showing lowest thermal performance and also found that R134a and R152a showing nearly same thermal performance but best performance was obtained of same system using R152aas ecofriendly refrigerant. Yumrutas et al. (2002) carried out detailed exergy analysis and found the effect of condensing and evaporating temperature on vapour compression refrigeration cycle in terms of pressure losses, COP, second law efficiency and exergy losses. They conclude that the variation in condenser temperature have negligible effect on exergy losses of compressor and expansion valve, and also found that first law efficiency and exergy

efficiency increases and total exergy losses of system is decreasing with increasing evaporator and condenser temperatures. Padilla et al. (2010) carried out exergy analysis of domestic vapour compression refrigeration system using R12 and ecofriendly R413a refrigerant and found that better thermal performance of the system using R413a in terms of power consumption, irreversibility and exergy efficiency is better than R12, and recommended R12 can be replaced by R413a in domestic vapour compression refrigeration system. Getu and Bansal (2008) optimized design and operating parameters of cascade refrigeration system in terms of condensing temperature, sub cooling temperature, evaporating temperature ,superheating temperature and temperature difference using cascade heat exchanger R744-R717. They obtained optimum thermodynamic parameters of same system using regression analysis. Spatz and Motta (2004) carried out experimental investigation by using R410a for replacing R12 for medium temperature vapour compression refrigeration systems in terms of thermal performance. Detailed thermodynamic analysis is also carried out and comparison was made for heat transfer and pressure drop characteristics and it was found that R410a gives best thermal performance among R12, R404a and R290a. Mohanraj et al. (2009) through experimental investigation concluded the effect of different environmental temperatures on first law efficiency (COP) of domestic refrigeration system using mixture of R290 and R600a in the ratio of 45.2: 54.8 by weight and found 3.6% greater performance than R134a in the same system. They also found the discharge temperature of compressor with mixture of R290 and R600a is lower in the range of 8.5-13.4K than same compressor with R134a. Han et al. (2007) conducted experimental results under different working conditions revealed that there could be replacement of R407C in vapour compression refrigeration system having rotor compressor with mixture of R32/R125/R161 showing higher COP, less pressure ratio and slightly high discharge compressor temperature without any modification in the same system than R-12 which produced global warming and ozone depletion. Halimic et al. (2003) have compared thermal performance of vapour compression refrigeration system using ecofriendly refrigerants such as R401A, R290 and R134A with R12 and found that due to similar performance of R134a in comparison with R12, the eco friendly refrigerant R134A can be replaced R12 in the same system without any medication in the system components and also has zero ozone depletion. They also concluded that in reference to green house impact, R290 presented best results than R134a. Xuan and Chen (2004) conducted experimental study on vapour compression refrigeration system for replacement of R502 by mixture of HFC-161 and found that mixture of HFC-161 gives same and higher performance than R404A at lower and higher evaporative temperature respectively Cabello et al. (2007) had studied about the effect of operating parameters on COP, work input and cooling capacity of single-stage vapour compression refrigeration system. There is great influence on energetic parameters due change in suction pressure, condensing and evaporating temperatures.

Cabello et al. (2004) experimentally investigated the effect of condensing pressure, evaporating pressure and degree of superheating on single stage vapour compression refrigeration system using R22, R134a and R407C.It was observed that mass flow rate is greatly affected by change in suction conditions of compressor in results on refrigeration capacity because refrigeration capacity depended on mass flow rate through evaporator. It was also found that for higher compression ratio R22 gives lower COP than R407C.

Based on the literature it was observed that researchers have gone through detailed first law analysis in terms of coefficient of performance and second law analysis in term of exergetic efficiency of simple vapour compression refrigeration system with single evaporator. Researchers did not go through the irreversibility analysis or second law analysis of: simple VCR with flash intercooler, flash chamber, water intercooler, liquid sub cooler and stages in compression (double stage and triple stage) and ultiple evaporators systems with multi-stage expansion and compound compression in vapour compression refrigeration systems.

To improve thermal performance of vapour compression refrigeration systems (both single and multiple evaporator system) by improving:

1. First Law Efficiency
2. Second Law Efficiency
3. Reduction of System

Defect in components of system which results into reduction of work input and detailed analysis of vapour compression refrigeration systems using ecofriendly refrigerants.

Energy and Exergy analysis of Vapour compression Refrigeration systems

The multiple evaporators at the same temperature with single compressor and expansion valve vapour compression refrigerator with subcooler is shown in Fig. 1.According to first law of thermodynamics, the measure of performance of the refrigeration cycle is

the coefficient of performance (COP), which is defined as the net refrigeration effect produced per unit of work input. It is expressed as

$$\text{COP} = \frac{Q_e}{W_{comp}} \quad (1)$$

The concept of exergy was given by second law of thermodynamics, which always decreases due to thermodynamic irreversibility. Exergy is defined as the measure of usefulness, quality or potential of a stream to cause change and an effective measure of the potential of a substance to impact the environment [7]. Exergy balance for a control volume undergoing steady state process is expressed as [8].

$$IR_k = \sum (me_x)_{in} - \sum (me_x)_{out} + \left[\sum \left(Q\left(1-\frac{T_0}{T}\right)\right)_{in} - \sum \left(Q\left(1-\frac{T_0}{T}\right)\right)_{out}\right] \pm \sum W \quad (2)$$

Where IR_k indicates the rate of irreversibility occurring in the compressor, expansion valve, evaporators, condenser and sub-cooler

The first two terms on the right hand side represent exergy of streams entering and leaving the control volume. The third and fourth terms are the exergy associated with heat transfer Q from the source maintained at constant temperature T and is equal to work obtained by Carnot engine operating between T and T_o, and is therefore equal to maximum reversible work that can be obtained from heat energy Q. The last term is the mechanical work transfer to or from the control volume.

Irreversibility (IR) in the system components

Irreversibility in each component of the cycle is calculated as per Eqs. (3)– (9), specified below:

Evaporator-1

$$IR_{e1} = E_{x4} + Q_{e1}\left(1-\frac{T_0}{T_r}\right) - E_{x1} = m_{r1}(h_4 - T_0 s_4) + Q_{e1}\left(1-\frac{T_0}{T_r}\right) - m_{r1}(h_1 - T_0 s_1) \quad (3)$$

Evaporator-2

$$IR_{e2} = E_{x4} + Q_{e2}\left(1-\frac{T_0}{T_r}\right) - E_{x1} = m_{r2}(h_4 - T_0 s_4) + Q_{e2}\left(1-\frac{T_0}{T_r}\right) - m_{r2}(h_1 - T_0 s_1) \quad (4)$$

Evaporator-3

$$IR_{e3} = E_{x4} + Q_{e3}\left(1-\frac{T_0}{T_r}\right) - E_{x1} = m_{r3}(h_4 - T_0 s_4) + Q_{e3}\left(1-\frac{T_0}{T_r}\right) - m_{r3}(h_1 - T_0 s_1) \quad (5)$$

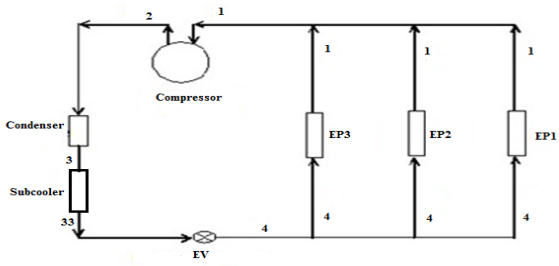

Fig.1: Schematic diagram of a multi-evaporators vapour compression refrigeration system.

For

Compressor

$$IR_{comp} = E_{x1} + W_{comp} - E_{x2} = m_r(T_o(s_2 - s_1)) \quad (6)$$

Condenser

$$IR_c = E_{x2} - E_{x3} = m_r(h_2 - T_o s_2) - m_r(h_3 - T_o s_3) \quad (7)$$

Expansion Valve

$$IR_{ev} = E_{x33} - E_{x4} = m_r(T_o(s_4 - s_{33})) \quad (8)$$

Subcooler

$$IR_{sc} = E_{x3} - E_{x33} = m_r(h_3 - T_o s_3) - m_r(h_{33} - T_o s_{33}) \quad (9)$$

The total irreversibility in the system is the sum of irreversibility in each components of the system and is given by

$$\sum IR_k = IR_{e1} + IR_{e2} + IR_{e3} + IR_{comp} + IR_c + IR_{ev} + IR_{sc} \quad (10)$$

Thermal exergy loss rate in a component is given by

$$EL_k = Q_k\left(1-\frac{T_0}{T_k}\right) \quad (11)$$

Where Q_k is the heat rejected by the kth component and T_k is the temperature at the boundary of the kth component. When considering thermal exergy loss rate, Eq. (2) can be rewritten as

$$IR_k + EL_k = \sum (me_x)_{in} - \sum (me_x)_{out} + Q1 - T0Tin \pm W \quad (12)$$

Thermal exergy loss rate is related to external irreversibility which takes place because of temperature difference between the control volume and the immediate surroundings. It depends upon how the boundary of the system is selected. If the system includes the immediate surroundings then the boundary of the thermal system is at the same temperature as the temperature of immediate surroundings and hence the value of thermal exergy loss turns out to be zero. However, temperature differential between system boundary and immediate surroundings exists if the system boundary does not include the immediate surroundings. In a vapour compression refrigeration system, condenser is the component where heat is rejected. However in the

present case, thermal exergy loss in condenser is neglected as the boundary of the condenser is assumed to be at the environment temperature. Second law performance of the system can be measured in terms of exergetic efficiency [9]. Exergetic efficiency is the ratio between exergy rate of product and fuel. If we consider a system at steady state where, in terms of exergy, the rates at which the fuel is supplied and the product is generated are EF and EP, respectively, and $\sum IR_k$ and $\sum EL_k$ represent rate of total irreversibility and total thermal exergy loss in a system, respectively, then exergy rate balance for the system is given by (13) and exergetic efficiency by (14).

$$EF = EP + \sum IR_k + \sum EL_k \quad (13)$$

and

$$\eta_{ex} = \frac{Exergy\ in\ product}{Exergy\ of\ fuel} = \frac{EP}{EF} = 1 - \frac{\sum IR_k + \sum EL_k}{EF} \quad (14)$$

For the vapour compression refrigeration system, product is the exergy of the heat abstracted in to the evaporators i.e. $Q_e = Q_{e1} + Q_{e2} + Q_{e3}$ from the space to be cooled at temperature T_r, i.e.

$$EP = Q_e \left|\left(1 - \frac{T_0}{T_r}\right)\right| \quad (15)$$

and exergy of fuel is actual compressor work input,W_c.Hence, exergetic efficiency is given by

$$\eta_{ex} = \frac{Q_e\left|\left(1-\frac{T_0}{T_r}\right)\right|}{W_{comp}} \quad (16)$$

Exergy destruction ratio (EDR) is the ratio of total exergy destruction in the system to exergy in the product [10] and it is given by Eq.(17). EDR is related to the exergetic efficiency by Eq. (18)

$$EDR = \frac{IR_{total}}{EP} = \frac{1}{\eta_{ex}} - 1 \quad (17)$$

$$\eta_{ex} = \frac{1}{1+EDR} \quad (18)$$

Efficiency defect is defined as the ratio between the exergy flow destroyed in each component and the exergy flow required to sustain the process [11] (i.e. the electrical power supplied to the compressor in the present case) and is given by

$$\delta_k = \frac{\sum IR_k + \sum EL_k}{W_{comp}} \quad (19)$$

where k stands for particular component. The efficiency defects of the components are linked to the exergetic efficiency of the whole system by means of the following relation:

$$\eta_{ex} = \left(1 - \sum_k \delta_k\right) \quad (20)$$

2. Models description of multiple evaporators and compressors with individual expansion valves (system-1) and multiple evaporators and compressors with multiple expansion valves (system-2) vapour compression refrigeration systems.

The multiple evaporators and compressors with individual expansion valves vapour compression refrigeration system (system-1) consists of compressors (C_1, C_2, C_3) throttle valves (TV_1, TV_2, TV_3), condenser and evaporators(EP_1, EP_2, EP_3) as shown in Fig.1(a).The pressure versus enthalpy chart for this system is shown in Fig.1(b). In this system all refrigerant coming out at point '77' from subcooler distributed by mass $\dot{m}_1$, $\dot{m}_2$, $\dot{m}_3$ to expansion valves TV_1, TV_2, and TV3 respectively. Both liquid and vapour formed by TV_1 ,TV_2 ,TV_3 represented by point '10', '9' and '8' take care the load of EP_1 ,EP_2 and EP_3 respectively. The low pressure vapours formed by EP_1 ,EP_2 and EP_3 supplied to the compressor C_1 ,C_2 and C_3 represented by point '1', '3' and '5' respectively. The high pressure vapours formed by compressor C_1 ,C_2 and C_3 respectively represented by points '2', '4' and '6' .then high pressure vapours coming out from compressor C_1 , C_1 ,C_1 collectively enter through condenser by point '7'. The main components of multiple evaporators and compressors with individual expansion valves vapour compression refrigeration system (system-2) are compressors (C_1, C_2, C_3) throttle valves (TV_1, TV_2, TV_3), condenser and evaporators(EP_1, EP_2, EP_3) as shown in Fig. 2(a)

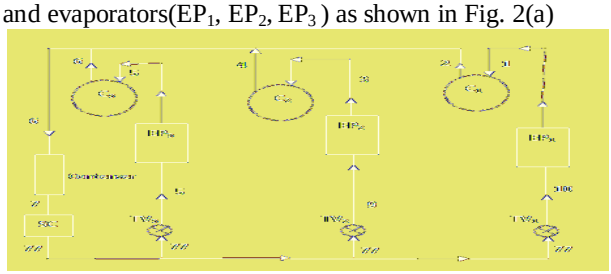

Fig: 2. a. Schematic diagram of multiple evaporators at different temperatures with individual compressors and I ndividual expansion valve.

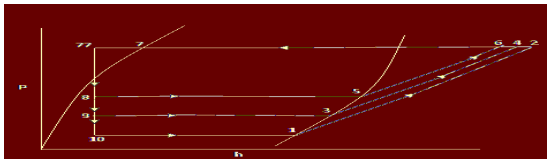

Fig: 2. b. Pressure enthalpy diagram of multiple evaporators at different temperatures with individual compressors and individual expansion valves

The corresponding pressure versus enthalpy chart for this system is shown in Fig. 2(b).In this system all the refrigerant from condenser at point 'g' followed by subcooler exit at point 'gg' flows through the throttle valve TV3 where its pressure is reduced from condenser pressure of the third evaporator. All the vapours formed after leaving the expansion valve TV3 at point 'h' plus enough liquid to take care of the load of evaporator EP3.The remaining refrigerant then enter at point 'i' through the expansion valve TV2 where its pressure is reduced from pressure of the third evaporator to pressure of the second evaporator.

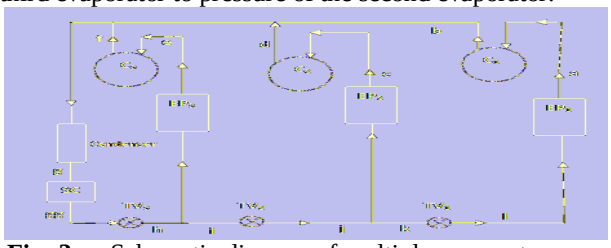

Fig: 3. a. Schematic diagram of multiple evaporators at different temperatures with individual compressors and multiple expansion valves

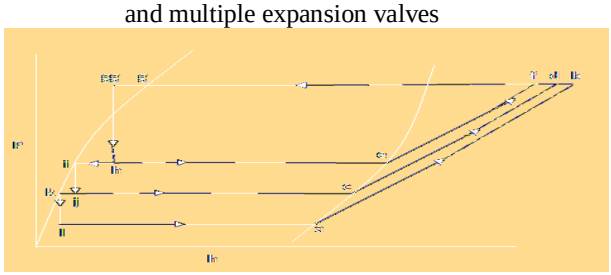

Fig: 3 b. Pressure enthalpy diagram of multiple evaporators at different temperatures with individual compressors and multiple expansion valves

3. First law analysis (COP & work input analysis) of multiple evaporators and compressors with individual or multiple expansion valves vapour compression refrigeration systems

Again all the vapour formed after leaving the expansion valve TV_2 at point 'j'plus enough liquid to take care of the load of evaporator EP_2 passes through this evaporator .The remaining liquid now enter at point 'k' through the expansion valve TV_1 and exit at point 'l'which supplied it to the first evaporator EP_1.The vapours formed by EP_1,EP_2 ,EP_3 supplied to compressors C_1, C_2 and C_3 shown by point 'a','c' and 'e' respectively. High pressure vapours formed by compressors C_1, C_2 and C_3 as shown by points 'b','d' and 'f' respectively supplied to the condenser.

The multiple evaporators and compressors with individual or multiple expansion valves vapour compression refrigeration system as shown in Fig.1 and Fig.2 respectively. From the energy analysis point of view first law of thermodynamics, evaluate the performance of the vapour compression systems as given below

System-1

$$COP1 = \frac{\dot{Q}_{e_1}}{\dot{W}_{comp_1}} \quad (1b)$$

Similarly for system-2

$$COP2 = \frac{\dot{Q}_{e_2}}{\dot{W}_{comp_2}} \quad (1c)$$

3.1 Second law analysis of multiple evaporators and compressors with individual or multiple expansion valves vapour compression refrigeration system

Second law of thermodynamics gives the concept of exergy, which always decreases due to thermodynamic irreversibility. Exergy is defined as the measure of usefulness, quality or potential of a stream to cause change and an effective measure of the potential of a substance to impact the environment [7]. Exergy balance for a control volume undergoing steady state process is expressed as [8].

$$\dot{E}D_k = \sum(\dot{m}e_x)_{in} - \sum(\dot{m}e_x)_{out} + \left[\sum\left(\dot{Q}\left(1 - TOTin - Q1 - TOTOut \pm W\right)\right)\right] \quad (2b)$$

Where $\dot{E}D_k$ represents the rate of irreversibility occurring in compressors, throttle valves, evaporators, condenser and subcooler. The first two terms on the right hand side represent exergy of streams entering and leaving the control volume. The third and fourth terms are the exergy associated with heat transfer $\dot{Q}$ from the source maintained at constant temperature T and is equal to work obtained by Carnot engine operating between T and T_o, and is therefore equal to maximum reversible work that can be obtained from heat energy $\dot{Q}$. The last term is the mechanical work transfer to or from the control volume. Exergy destruction (ED) in system-1can be find out in terms of irreversibilities. Exergy destruction in each component of the multiple evaporators and compressors with individual expansion valves vapour compression refrigeration system is evaluated as per Eqs. (3b)– (14b) given below:

Evaporators

(EP$_1$) System-1

$$\dot{E}D_{e1} = \dot{E}_{x10} + \dot{Q}_{e1}\left(1 - \frac{T_0}{T_{r1}}\right) - \dot{E}_{x1}$$

$$= \dot{m}_{e1}(\psi_{10} - T_0 s_{10}) + \dot{Q}_{e1}\left(1 - \frac{T_0}{T_{r1}}\right) - \dot{m}_{e1}(\psi_1 - T_0 s_1) \quad (3b)$$

(EP$_2$) System-1

$$\dot{E}D_{e2} = \dot{E}_{x9} + \dot{Q}_{e2}\left(1 - \frac{T_0}{T_{r2}}\right) - \dot{E}_{x3}$$

$$= \dot{m}_{e2}(\psi_9 - T_0 s_9) + \dot{Q}_{e2}\left(1 - \frac{T_0}{T_{r2}}\right) - \dot{m}_{e2}(\psi_3 - T_0 s_3) \quad (4b)$$

(EP$_3$) System-1

$$\dot{E}D_{e3} = \dot{E}_{x8} + \dot{Q}_{e3}\left(1 - \frac{T_0}{T_{r3}}\right) - \dot{E}_{x5}$$

$$= \dot{m}_{e3}(\psi_8 - T_0 s_8) + \dot{Q}_{e3}\left(1 - \frac{T_0}{T_{r3}}\right) - \dot{m}_{e3}(\psi_5 - T_0 s_5) \quad (5b)$$

Compressors

(C$_1$) System-1

$$\dot{E}D_{comp1} = \dot{E}_{x1} + \dot{W}_{comp1} - \dot{E}_{x2} = \dot{m}_{c1}(T_0(s_2 - s_1)) \quad (6b)$$

(C$_2$) System-1

$$\dot{E}D_{comp2} = \dot{E}_{x3} + \dot{W}_{comp2} - \dot{E}_{x4} = \dot{m}_{c2}(T_0(s_4 - s_3)) \quad (7b)$$

(C$_3$) System-1

$$\dot{E}D_{comp3} = \dot{E}_{x5} + \dot{W}_{comp3} - \dot{E}_{x6} = \dot{m}_{c3}(T_0(s_6 - s_5)) \quad (8b)$$

(Condenser) System-1

$$\dot{E}D_c = (\dot{E}_{x2} - \dot{E}_{x7}) + (\dot{E}_{x4} - \dot{E}_{x7}) + (\dot{E}_{x6} - \dot{E}_{x7}) \quad (9b)$$

Subcooler

(SC) System-1

$$\dot{E}D_{sc} = \dot{E}_{x7} - \dot{E}_{x77} = (\dot{m}_{c1} + \dot{m}_{c2} + \dot{m}_{c3})((\psi_7 - T_0 s_7) - (\psi_{77} - T_0 s_{77})) \quad (10b)$$

Throttle valves

(TV$_1$) System-1

$$\dot{E}D_{TV_1} = \dot{E}_{x77} - \dot{E}_{x10} = \dot{m}_{c1}(T_0(s_{10} - s_{77})) \quad (11b)$$

(TV-2) System-1

$$\dot{E}D_{TV_2} = \dot{E}_{x77} - \dot{E}_{x9} = \dot{m}_{c2}(T_0(s_9 - s_{77})) \quad (12b)$$

(TV-3)System-1

$$\dot{E}D_{TV_3} = \dot{E}_{x77} - \dot{E}_{x8} = \dot{m}_{c3}(T_0(s_8 - s_{77})) \quad (13b)$$

(Mass balance)System-1

$$\dot{m}_{e1} = \dot{m}_{c1}$$
$$\dot{m}_{e2} = \dot{m}_{c2}$$
$$\dot{m}_{e3} = \dot{m}_{c3}$$

The total irreversibility in the system is the sum of irreversibility in each components of the system and is given by

$$\sum \dot{E}D_k = \dot{E}D_{e1} + \dot{E}D_{e2} + \dot{E}D_{e3} + \dot{E}D_{comp1} + \dot{E}D_{comp2} + \dot{E}D_{comp3} + \dot{E}D_c + \dot{E}D_{sc} + \dot{E}D_{TV_1} + \dot{E}D_{TV_2} + \dot{E}D_{TV_3} \quad (14b)$$

For system 2, exergy destruction in each component of the multiple evaporators and compressors with multiple expansion valves vapour compression refrigeration system is evaluated as per Eqs. (15)– (26) given below:

Evaporators

$(EP1)_{System\text{-}2}$

$$\dot{E}D_{e1} = \dot{E}_{xl} + \dot{Q}_{e1}\left(1 - \frac{T_0}{T_{r1}}\right) - \dot{E}_{xa}$$

$$= \dot{m}_{e1}(\psi_l - T_0 s_l) + \dot{Q}_{e1}\left(1 - \frac{T_0}{T_{r1}}\right) - \dot{m}_{e1}(\psi_a - T_0 s_a) \quad (15)$$

$(EP2)_{System\text{-}2}$

$$\dot{E}D_{e2} = \dot{E}_{xj} + \dot{Q}_{e2}\left(1 - \frac{T_0}{T_{r2}}\right) - \dot{E}_{xc}$$

$$= \dot{m}_{e2}(\psi_j - T_0 s_j) + \dot{Q}_{e2}\left(1 - \frac{T_0}{T_{r2}}\right) - \dot{m}_{e2}(\psi_c - T_0 s_c) \quad (16)$$

$(EP3)_{System\text{-}2}$

$$\dot{E}D_{e3} = \dot{E}_{xh} + \dot{Q}_{e3}\left(1 - \frac{T_0}{T_{r3}}\right) - \dot{E}_{xe}$$

$$= \dot{m}_{e3}(\psi_h - T_0 s_h) + \dot{Q}_{e3}\left(1 - \frac{T_0}{T_{r3}}\right) - \dot{m}_{e3}(\psi_e - T_0 s_e) \quad (17)$$

Compressors

$(C\text{-}1)_{System\text{-}2}$

$$\dot{E}D_{comp1} = \dot{E}_{xa} + \dot{W}_{comp1} - \dot{E}_{xb} = \dot{m}_{c1}(T_0(s_b - s_a)) \quad (18)$$

$(C\text{-}2)_{System\text{-}2}$

$$\dot{E}D_{comp2} = \dot{E}_{xc} + \dot{W}_{comp2} - \dot{E}_{xd} = \dot{m}_{c2}(T_0(s_d - s_c)) \quad (19)$$

$(C\text{-}3)_{System\text{-}2}$

$$\dot{E}D_{comp3} = \dot{E}_{xe} + \dot{W}_{comp3} - \dot{E}_{xf} = \dot{m}_{c3}(T_0(s_f - s_e)) \quad (20)$$

$Condenser)_{System\text{-}2}$

$$\dot{E}D_{cond} = (\dot{E}_{xb} - \dot{E}_{xg}) + (\dot{E}_{xd} - \dot{E}_{xg}) + (\dot{E}_{xf} - \dot{E}_{xg})$$

$$= \dot{m}_{c1}\left((\psi_b - T_0 s_b) - (\psi_g - T_0 s_g)\right) + \dot{m}_{c2}\left((\psi_d - T_0 s_d) - (\psi_g - T_0 s_g)\right)$$

$$+\dot{m}_{c3}\left((\psi_f - T_0 s_f) - (\psi_g - T_0 s_g)\right) \quad (21)$$

$(SC)_{System\text{-}2}$

$$\dot{E}D_{sc} = \dot{E}_{xg} - \dot{E}_{xgg} = (\dot{m}_{c1} + \dot{m}_{c2} + \dot{m}_{c3})\left((\psi_g - T_0 s_g) - (\psi_{gg} - T_0 s_{gg})\right) \quad (22)$$

Throttle valves

$(TV\text{-}1)_{System\text{-}2}$

$$\dot{E}D_{TV_1} = \dot{E}_{xk} - \dot{E}_{xl} = \dot{m}_{c1}(T_0(s_l - s_k)) \quad (23)$$

$(TV\text{-}2)_{System\text{-}2}$

$$\dot{E}D_{TV_2} = \dot{E}_{xi} - \dot{E}_{xj} = (\dot{m}_{c1} + \dot{m}_{c2})(T_0(s_j - s_i)) \quad (24)$$

$(TV\text{-}3)_{System\text{-}2}$

$$\dot{E}D_{TV_3} = \dot{E}_{xgg} - \dot{E}_{xh} = (\dot{m}_{c1} + \dot{m}_{c2} + \dot{m}_{c3})(T_0(s_h - s_{gg})) \quad (25)$$

$(Mass\ balance)_{System\text{-}2}$

$$\dot{m}_{c1} = \dot{m}_{e1}$$

$$\dot{m}_{c2} = \dot{m}_{e2} = \dot{m}_2 + \dot{m}_{e1}\left(\frac{\varphi_j}{1-\varphi_j}\right)$$

$$\dot{m}_2 = \left(\frac{\dot{Q}_{e2}}{\psi_c - \psi_j}\right)$$

$$\dot{m}_{c3} = \dot{m}_{e3} = \dot{m}_3 + (\dot{m}_{e1} + \dot{m}_{e2})\left(\frac{\varphi_h}{1-\varphi_h}\right)$$

$$\dot{m}_3 = \left(\frac{\dot{Q}_{e3}}{\psi_e - \psi_h}\right)$$

The total irreversibility in the system is the sum of irreversibility in each components of the system and is given by

$$\sum \dot{E}D_k = \dot{E}D_{e1} + \dot{E}D_{e2} + \dot{E}D_{e3} + \dot{E}D_{comp1} + \dot{E}D_{comp2} + \dot{E}D_{comp3} + \dot{E}D_c + \dot{E}D_{sc} + \dot{E}D_{TV_1} + \dot{E}D_{TV_2} + \dot{E}D_{TV_3} \quad (26)$$

For the multi evaporators vapour compression refrigeration system, product is the exergy of the heat abstracted in to the evaporators i.e.$Q_e = Q_{e1} + Q_{e2} + Q_{e3}$ from the space to be cooled at temperature T_r, and exergy of fuel is actual compressor work input

$$\dot{E}P = \dot{Q}_{e1}\left|\left(1-\frac{T_0}{T_{r1}}\right)\right| + \dot{Q}_{e2}\left|\left(1-\frac{T_0}{T_{r2}}\right)\right| + \dot{Q}_{e3}\left|\left(1-\frac{T_0}{T_{r3}}\right)\right| \quad (27a)$$

Hence, exergetic efficiency is given by

$$\eta_{ex} = \frac{\dot{Q}_{e1}\left|\left(1-\frac{T_0}{T_{r1}}\right)\right| + \dot{Q}_{e2}\left|\left(1-\frac{T_0}{T_{r2}}\right)\right| + \dot{Q}_{e3}\left|\left(1-\frac{T_0}{T_{r3}}\right)\right|}{(\dot{W}_{comp1} + \dot{W}_{comp2} + \dot{W}_{comp3})} \quad (27b)$$

Result and Discussion

A computational model is developed for carrying out the energy and exergy analysis of the system using EES software [12].The result evaluated on the basis of following assumed data shown Figs.2 are furnished below:

Degree of sub cooling of liquid refrigerant in subcooler (ΔT_{sc}): 5K., Isentropic efficiency of compressor (η_{comp}): 75%. , Difference between evaporator and space temperature (T_r-T_e):5K., Temperature of evaporators EP_1, EP2 and EP3 are 263K ,273K and 283K respectively, Condenser temperature (T_c): 313K, Dead state temperature (T_0): 298K, Dead state enthalpy (ψ_0) and entropy (s_0) of the refrigerants have been calculated corresponding to the dead state temperature (T_0) of 298K., Loads on the evaporators EP1, EP2 and EP3 are 35KW, 70KW and 105KW respectively., Evaporators' temperature is 273K., Condenser temperature (T_c): 313K (the condenser temperature is based on climatic conditions persisting in summer in tropical countries).., Reference enthalpy (h_0) and entropy (s_0) of the working fluids have been computed corresponding to the dead state temperature (T_0) of 298K.. Loads on the evaporators EP1, EP2 and EP3 are 35KW, 70KW and 105KW respectively.

Table-1: presents the variation of coefficient of performance for all six systems for different ecofriendly refrigerants and Bar charts are shown in Table1. It was observed that COP of R12 in all six cases are higher but due to consideration of global warming and ozone depletion one can consider ecofriendly refrigerants for reducing global warming and ozone depletion. The cop of 600 is although is better than R152a but the refrigerants R290, R600 and R600a are flammable properties. Therefore by consideration of safety measures R152a gives better first law performance than R404a ,R134a and R410a. With increase in evaporators' temperature, the pressure ratio across the compressor reduces causing compressor work to reduce and cooling capacity increases because of increase in specific refrigerating effect. The combined effect of these two factors is to increase the overall COP. It was observed that COP of system using R600 and R152a nearly matching same values Both R-600 and R-152a show better COP than R-502, R-290, R-404a, R-410a, R-600a and R-1234yf at 313K condenser temperature. Although R600,R600a and R290 have flammable properties

cannot use directly due to safety measures, the system will be modified by taking into the considerations safety measures and precautions must be taken when using these refrigerants and also they are responsible for global warming. The maximum difference observed between COPs of R-152a and R-404a is 22.57% at 313K condenser temperature. Table-2 show the effect of ecofriendly refrigerants on exergetic efficiency at 313K condenser temperature. The increase and decrease of the exergetic efficiency, with increase in evaporators temperature, are based on two parameters. First parameter is exergy of cooling effect, i.e., Q_e $|1-T_o / T_r|$with rise in evaporators temperature Q_e, increases however the term Q_e $|1-T_o / T_r|$ reduces since T_r approaches T_0, and second being the compressor work which decreases with increase in evaporators temperature. Both Q_e and W_c have positive effect on increase of exergetic efficiency whereas the decreasing value of term $|1-T_o / T_r|$ has a negative effect on increase of exergetic efficiency. The combined effect of these factors is to increase the exergetic efficiency till the optimum evaporators' temperature is achieved, i.e. the evaporators' temperature at which maximum exergetic efficiency is achieved. Beyond optimum evaporators' temperature, the overall effect of these factors is to reduce the exergetic efficiency. Both R600 and R152a have higher exergetic efficiency than R502, R290, R404a, R410a, R600a and R1234yf. Exergetic efficiency of R152a is 15–22% higher than R404A and R600 is 12–20% higher than R404aA at 313K condenser temperature. This also confirms that with increase in condenser temperature the difference among the exergetic efficiency of R152a, R600 and its alternate refrigerants increases. It is observed from Table.2 - Table.3, that variation of EDR and exergetic efficiency are almost reverse because that exergetic efficiency is inversely proportional to EDR. The EDR initially decreases and then increases with the increase in evaporators' temperature. The exergetic efficiency is inversely proportional to EDR. For a fixed condenser temperature, the increase in dead state temperature causes the irreversibility (due to finite temperature difference) to decrease and hence EDR decreases and exergetic efficiency increases. Table3: presents that R-404a shows maximum EDR among all the refrigerants corresponding to the range of dead state temperatures considered. Both R-152a and R-600 show the identical trends .The exergetic efficiency for R-600 is 0.4-0.5% higher than that of R-152a. It was observed that the effect of degree of subcooling on COP, exergetic efficiency and EDR. It is evident that subcooling increases refrigeration capacity whereas there is no change in compressor work, hence COP increases. It apparent that increase in COP decreases EDR and increases exergetic efficiency. The increase in COP is nearly 5.6%/K of sub cooling in case of R-404a.However, the corresponding increase in COP in R-152a and R-600 is less. The rate of increase of exergetic efficiency is approximately 0.4%/K for R404a.The total increase in exergetic efficiency for 10K of subcooling is 3.97% for R404a and 2.5% for R152a and R-600 at 313K condenser temperature. Hence it is easy to understand why EDR increases and exergetic efficiency decreases. It is observed that COP and exergetic efficiency are almost same for considered eco-friendly refrigerants as compared with R-12 refrigerant, both COP and EDR will decrease with increase in condenser temperature. EDR increase with increase in condenser temperature rational efficiency with increase in condenser temperature at 273K temperature of all evaporators with 5K degree of subcooling.

Refrigerants	COP(Coefficient of Performance)					
Previously used	System1	System2	System3	System4	System5	System6
R12	3.117	3.397	4.078	5.243	6.745	5.205
R502	2.819	3.189	3.838	5.033	6.39	4.994
Suggested new ecofriendly refrigerants	System1	System2	System3	System4	System5	System6
R152a	3.173	3.425	4.122	5.276	6.822	5.246
R290	2.983	3.308	3.97	5.145	6.582	5.105
R404a	2.649	3.072	3.685	4.893	6.145	4.835
R410a	2.856	3.192	3.842	4.983	6.386	4.959
R600	3.186	3.473	4.145	5.334	6.862	5.294

R600a	3.061	3.392	4.055	5.277	6.743	5.237
R1234yf	2.887	3.284	3.933	5.18	6.569	5.141
R1234ze	3.02	3.373	4.036	5.267	6.763	5.14
R134a	3.034	3.354	4.031	5.227	6.689	5.188

Table: 1. Variation of First law efficiency (COP) of multiple evaporators vapour compression refrigeration systems using eco-friendly refrigerants

Refrigerants	Second Law efficiency (Exergetic Efficiency)					
Previously used	System1	System2	System3	System4	System5	System6
R12	0.187	0.2913	0.3496	0.3146	0.4047	0.3123
R502	0.1691	0.2734	0.329	0.302	0.3834	0.2996
Suggested new ecofriendly refrigerants	System1	System2	System3	System4	System5	System6
R152a	0.1904	0.2937	0.3534	0.3166	0.4093	0.3147
R290	0.179	0.2836	0.3404	0.3087	0.3949	0.3063
R404a	0.1589	0.2634	0.3159	0.2936	0.3687	0.2901
R410a	0.1714	0.2737	0.3294	0.2989	0.3831	0.2975
R600	0.1911	0.2978	0.3554	0.3201	0.4117	0.3177
R600a	0.1837	0.2908	0.3477	0.3166	0.4046	0.3142
R1234yf	0.1732	0.2816	0.3372	0.3108	0.3942	0.3085
R1234ze	0.1812	0.2892	0.346	0.316	0.3958	0.3095
R134a	0.182	0.2876	0.3456	0.3136	0.4013	0.3113

Table: 2. Variation of Second law efficiency of multiple evaporators vapour compression refrigeration systems using eco-friendly refrigerants

Refrigerant	EDR					
Previously used	System1	System2	System3	System4	System5	System6
R12	4.253	2.02	1.86	2.255	1.47	2.2
R502	5.262	2.192	2.039	2.412	1.608	2.335
Suggested new ecoecofriendlyrefrigerants	System1	System2	System3	System4	System5	System6
R152a	4.045	2.003	1.829	2.229	1.442	2.173
R290	4.695	2.092	1.938	2.326	1.532	2.263
R404a	5.829	2.282	2.165	2.504	1.711	2.424
R410a	5.027	2.207	2.035	2.431	1.607	2.349
R600	4.051	1.953	1.814	2.2	1.429	2.147
R600a	4.426	2.011	1.876	2.247	1.472	2.182
R1234yf	4.952	2.088	1.965	2.313	1.537	2.242
R1234ze	4.586	2.024	1.89	2.256	2.902	2.565
R134a	4.504	2.049	1.894	2.274	1.491	2.211

Table: 3. Variation of Exergy Destruction Ratio (EDR) of multiple evaporators vapour compression refrigeration systems using eco-friendly refrigerants

4. Conclusions

In this paper, first law and second law analysis of six multi-evaporators multiple compressor and multiple expansion valves in series and parallel combinations of vapour compression refrigeration systems using ecofriendly refrigerants (R410a, R290, R600, R600a, R1234yf, R502, R404a and R152a) have been presented. The conclusions of the present analysis are summarized below:

1. COP and exergetic efficiency for R152a and R600 are matching the same values. are better than that for R404A at 313K condenser temperature and showing 12–23% higher value of COP and exergetic efficiency in comparison to R404a.
2. For practical applications R-134a is recommended because it is easily available in the market has second law efficiency slightly lesser than R-152a which was not applicable for commercial applications.
3. The worst component from the viewpoint of irreversibility is expansion valve followed by condenser, compressor and evaporators, respectively. The most efficient component found to be subcooler. The R-152a has least efficiency defects for 313K condenser temperature.
4. The increase in dead state temperature has a positive effect on exergetic efficiency and EDR, i.e. EDR decreases and exergetic efficiency increases with increase in dead state temperature. Both R-152a and R-600 show the identical trends for exergetic efficiency are nearly overlapping. The exergetic efficiency for R-600 is 0.4-0.5% higher than that of R-152a for the practical range of dead state temperature considered.

References

[1] M. Padilla, R. Revellin, J. Bonjour, “Exergy analysis of R413A as replacement of R12 in a domestic refrigeration system”, Energy Conversion and Management 51, 2195–2201, 2010

[2] H. O. Spauschus, “HFC 134a as a substitute refrigerant for CFC 12”, Int J Refrig 11: 389–92, 1988

[3] J. U. Ahamed, R. Saidur, H. H. Masjuki, “A review on exergy analysis of vapor compression refrigeration system”, Renewable and Sustainable Energy Reviews 15, 1593–1600, 2011

[4] R. Llopis, E. Torrella, R. Cabello, D. Sánchez, “Performance evaluation of R404A and R507A refrigerant mixtures in an experimental double-stage vapour compression plant”, Applied Energy 87, 1546–1553, 2010

[5] A. Arora, S. C. Kaushik, “Theoretical analysis of a vapour compression refrigeration system with R502, R404A and R507A”, International Journal of Refrigeration 31, 998 – 1005, 2008

[6] V. Havelsky, “Investigation of refrigerating system with R12 refrigerant replacements”, Appl Therm Eng; 20: 133–40 2000

[7] I. Dincer, “Refrigeration Systems and Applications”, Wiley, UK, p. 26. 2003

[8] S. F. Lee, S. A. Sherif, “Second law analysis of various double effect lithium bromide/water absorption chillers”, ASHRAE Transactions AT-01-9-5, 664–673, 2001

[9] S. A. Said, B. Ismail, “Exergetic assessment of the coolants HCFC123, HFC134a, CFC11 and CFC12”, Energy 19 (11), 1181–1186, 1994

[10] T. J. Kotas, “The Exergy Method of Thermal Plant Analysis.Butterworths”, London, pp. 73–74, 1985

[11] S. A. Klein, F. Alvarado, “Engineering Equation Solver”, Version 7.441. F Chart Software, Middleton, WI, 2005

Author's Accepted Manuscript

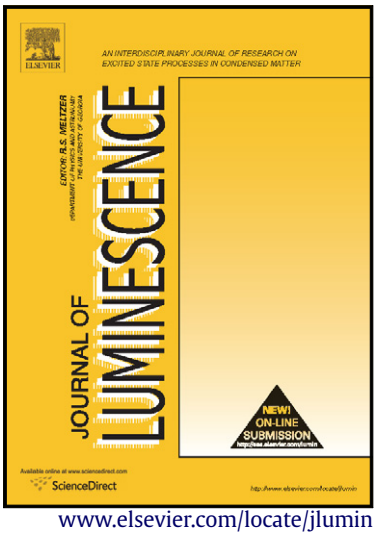

www.elsevier.com/locate/jlumin

Lasing potentialities and White Light Generation Capabilities of Dy^{3+} doped Oxy-fluoroborate Glasses

Sk. Mahamuda, K. Swapna, P. Packiyaraj, A. Srinivasa Rao, G. Vijaya Prakash

PII: S0022-2313(14)00156-2
DOI: http://dx.doi.org/10.1016/j.jlumin.2014.03.009
Reference: LUMIN12578

To appear in: *Journal of Luminescence*

Received date: 25 December 2013
Revised date: 17 February 2014
Accepted date: 3 March 2014

Cite this article as: Sk. Mahamuda, K. Swapna, P. Packiyaraj, A. Srinivasa Rao, G. Vijaya Prakash, Lasing potentialities and White Light Generation Capabilities of Dy^{3+} doped Oxy-fluoroborate Glasses, *Journal of Luminescence,* http://dx.doi.org/10.1016/j.jlumin.2014.03.009

This is a PDF file of an unedited manuscript that has been accepted for publication. As a service to our customers we are providing this early version of the manuscript. The manuscript will undergo copyediting, typesetting, and review of the resulting galley proof before it is published in its final citable form. Please note that during the production process errors may be discovered which could affect the content, and all legal disclaimers that apply to the journal pertain.

ACCEPTED MANUSCRIPT

Lasing potentialities and White Light Generation Capabilities of Dy^{3+} doped Oxy-fluoroborate Glasses

Sk.Mahamuda[1], K.Swapna[1], P.Packiyaraj[3], A.Srinivasa Rao*[1, 2] and G.Vijaya Prakash[3]

[1]Department of Physics, K L University, Green Fields, Vaddeswaram, Guntur (Dt.)- 522 502, A P, India
[2]Department of Applied Physics, Delhi Technological University, New Delhi-110 042, India
[3]Nanophotonics Laboratory, Department of Physics, Indian Institute of Technology Delhi, New Delhi-110016, India.
Electronic E-mail: drsrallam@gmail.com, Tel: +91 85860 39007

Abstract

Oxy-fluoroborate (OFB) glasses doped with different concentrations of Dy^{3+} ions were synthesized by using melt quenching technique and characterized by using optical absorption, photoluminescence and decay analysis to understand the lasing potentialities and their utility for white light emitting diodes (LEDs). The XRD spectrum recorded for undoped OFB glass confirms the amorphous nature of the prepared glasses. Judd-Ofelt theory has been applied to the recorded absorption spectra to measure the radiative properties such as transition probability (A_R), radiative lifetimes (τ_R), branching ratios (β_R) and spectroscopic quality factor (χ) for the prominent fluorescent levels. The emission spectra recorded for these glasses gives four emission transitions $^4F_{9/2}\rightarrow{}^6H_{15/2}$, $^6H_{13/2}$, $^6H_{11/2}$ and $^6H_{9/2}$ for which effective band widths ($\Delta\lambda_p$), experimental branching ratios (β_{exp}) and stimulated emission cross-sections (σ_{se}) are evaluated. To know the potentialities of these glasses as lasers, quantum efficiency (η) of these glasses are measured by recording the decay curves for the prominent emission levels $^4F_{9/2}\rightarrow{}^6H_{15/2}$ and $^4F_{9/2}\rightarrow{}^6H_{13/2}$. Among the observed emission transitions, a transition at 575nm ($^4F_{9/2}\rightarrow{}^6H_{13/2}$) indicates the lasing potentialities. The CIE chromaticity co-ordinates and the con-focal photoluminescence images of these glasses further suggests the near white light generation capabilities in principle.

Accepted manuscript

ACCEPTED MANUSCRIPT

Key words: *Dysprosium, Glasses, J-O parameters, CIE co-ordinates, Con-focal images***.**

1. Introduction

In recent years considerable research work has been carried out at different laboratories on the spectroscopic characteristic of rare earth ions in both crystalline and non-crystalline materials [1-3]. When compared to crystalline materials, glasses are favorable hosts for rare earth ions due to their broad inhomogeneous band width, possibility of tuning the wavelength, large doping capability and easy to mould and shape in large size as well. Quite recently rare earth doped glasses have attracted much attention because of their wide range applications in the areas such as optical fibers, solid state lasers, solar energy concentrators, optical detectors, optical data storage devices and undersea optical communications [4-6]. The design and development of a glassy system for the above said applications require a thorough analysis of the optical properties of RE doped glasses through absorption and fluorescence spectral studies. These properties mainly depend on the nature and local environment situated around the doped rare earth ion in the glass and also on the phonon energies of the host glass. Many glassy materials such as phosphate, fluorides, borates and telluride's have been investigated widely through absorption and emission spectral studies with an aim to know their suitability for the above said applications.

On the other hand, near white light emitting diodes (LEDs), the next generation Solid State Lightening (SSL) technology, has been the focus of current research in lightening industries as well as researchers because of their high efficiency, less energy consumption, longer lifetime when compared with the conventional light sources like incandescent lamps and fluorescent lamps. SSL technology, now a day emerging as a highly competent and viable alternative for the

Accepted manuscript

ACCEPTED MANUSCRIPT

presently existing technology in the back drop of the increasing demand for energy and environmental friendliness. White light LEDs are in general realized as a combination of single phase crystalline phosphors and UV/blue InGaN type LEDs [7, 8]. Recently rare-earth doped vitreous systems are considered as an alternative source for crystalline phosphors, due their obvious fabrication and integration advantages [9, 10]. The rare-earth ion doped white light emitting glasses are superior than white light emitting phosphor's because of their homogeneous light emitting capacity, simple manufacturing process, low production cost and better thermal stability. One of the ways to combine the luminescent glass with semiconductor chip is to mould the glass into a lens and replace the normal plastic lens in the current LEDs. Moreover, glass lens integrated with semiconductor chip (LED's) can also acts as a protecting layer for LED chips, and such system does not require any extra encapsulation. White light emitting glass was first developed by Zhang et al. in 1991 [11] and it receives increasing interest in recent years [12-14] because of their wide range applications in diversified fields such as LCD displays, color displays, traffic signals, automotive displays and cellular phone illumination and so on.

Among the conventional glass formers, boric acid (B_2O_3) is one of the best glass former known when compared with several other conventional glass formers and can form glass alone with good transparency, thermal stability and good rare-earth ion solubility [15]. However a glassy system with B_2O_3 alone possesses high phonon energies (~1300 cm^{-1}) and cannot suppress non-radiative decay process and hence rare earth ion emissions are strongly reduced. For the above mentioned applications the non radiative processes produced by multi phonon relaxation should be as low as possible. Addition of fluoride compounds such as BaF_2 and CaF_2 to borate glass can reduce phonon energies, because the maximum phonon energies of the additives are ~ 340 cm^{-1}, which are less than the phonon energies of the oxides (B-O ~ 1300 cm^{-1}) [16].

Accepted manuscript

ACCEPTED MANUSCRIPT

Moreover addition of fluoride compounds helps to remove OH group from borate glass by reacting with OH group and can reduce phonon energy of the borate glass to (200-400cm^{-1}) [17]. In recent years, glasses containing ZnO have attracted the scientific community because of its optical, electrical and magnetic properties in combination with its non-toxicity, non-hygroscopic nature. Its direct wide band gap, large exciting binding energy and intrinsic emitting property makes them as promising devices for the development of optoelectronic devices, solar energy converters, ultraviolet emitting lasers and gas sensors [18]. Presence of Al_2O_3 in a glass can increase mechanical strength and thermal stability of the glass. Hence, in the present work, we took B_2O_3, BaF_2, CaF_2, ZnO and Al_2O_3 as chemical constituents to prepare a good optical glass.

Among RE ions, Dy^{3+} ($4f^9$) ion is one of the best suitable candidate for the preparation of visible lasers and phosphor materials as it is capable of emitting several interesting visible wavelengths between its f-f transitions, depending on the host. The visible fluorescence of Dy^{3+} ion contains two intense bands one in blue (~ 470-500nm) and the other one in yellow (~570-600nm) regions, which are due to the transitions $^4F_{9/2} \rightarrow {}^6H_{15/2}$ and $^4F_{9/2} \rightarrow {}^6H_{13/2}$ respectively. The latter one is hypersensitive and whose intensity strongly depends on the host matrix. Optimization of local field environment around Dy^{3+} ions in a material is an important task to obtain white light emission with a suitable yellow to blue (Y/B) intensity ratio. The variation of Y/B ratio of Dy^{3+} ions to emit near white light emission can be achieved by varying the composition of host glass or by changing the concentration of the Dy^{3+} ions in the host glass. Further, the fluorescence at 1.32μm originating from $^4F_{11/2} \rightarrow {}^6H_{9/2}$ level of Dy^{3+} ion is suitable for fiber amplification in optical transmission systems [19]. The Dy^{3+} ions doped glasses and crystals can also give intense emissions in the yellow-orange (570-590 nm) and in the NIR (1.35 and 3.0

Accepted manuscript

ACCEPTED MANUSCRIPT

nm) regions, which have potential laser applications [20-22]. In the present work, Oxy-fluoroborate glasses were prepared with Dy^{3+} ions at different concentration to study the optical and fluorescent properties to identify the better glass for solid state laser devices and also for n-UV based white LEDs.

2. Experimental

The glass samples used for the present work were prepared by conventional melt quenching method with the following compositions. 15 ZnO – (10-x) Al_2O_3 – 10 BaF_2 – 10 CaF_2 – 60 B_2O_3 – x Dy_2O_3 where x = 0.1, 0.5, 1.0, 1.5, 2.0 and 2.5 mol%. These glasses can be designated as OFBDy0.1, OFBDy0.5, OFBDy1.0, OFBDy1.5, OFBDy2.0 and OFBDy2.5 depending on the Dy^{3+} ion concentration from 0.1 to 2.5 mol% respectively. About 8g of the batches of composition were taken and grounded thoroughly in an agate mortar to obtain homogenous mixture. The homogeneous mixture was then taken into an alumina crucible and heated at 1200^{o}C in an electrical furnace for 40-60 min until the homogeneous melt was obtained. This melt was then poured quickly on a pre-heated brass mould and presses quickly with another brass mould to obtain circular shaped glass samples with uniform thickness. The glass samples thus prepared were annealed at 400°C in order to make them free from thermal strains. The densities were measured by using Archimedes's method with water as an immersion liquid. The XRD measurement were taken using XPERT-PRO diffractometer with CuKa radiation (k=1.54°A) in the 2θ angle range 5° - 70° with step size 0.02° s^{-1}. The refractive indices of these glasses are measured with Brewster's angle method using He-Ne laser (650 nm line). The optical absorption spectra of the samples were recorded in the spectral wavelength range 300-1800 nm with a spectral resolution of 0.1nm using JASCO model V-670 UV-vis-NIR spectrometer. The emission and excitation spectra for all the prepared glasses were recorded at room temperature

Accepted manuscript

ACCEPTED MANUSCRIPT

using RF-5301 PC Spectrofluorophotometer. The time-resolved photoluminescence (PL) measurements were carried out using home-built setups with 410 nm (CW laser) laser as the excitation source. The emission from sample was coupled into a monochromator (Acton SP2300) coupled to CCD (charge coupled detector) through the appropriate lenses and filters. For time-resolved photoluminescence, a frequency generator (5 Hz), lock-in amplifier, digital storage oscilloscope and a monochromator (Acton SP2300) coupled to a photomultiplier tube (PMT) were employed. The PL images were carried out by a modified laser scanning con-focal microscope (Olympus, BX51) equipped with XY-piezo stage and excited with same 410 nm CW laser.

3. Results and discussion

3.1 XRD spectral analysis

In order to verify the glassy nature of the prepared glasses, XRD pattern has been recorded for an undoped OFB glass and is shown in Fig. 1. The featureless XRD observed for an undoped OFB glass confirms the characteristic of an amorphous material. Hence the prepared OFB glasses have amorphous nature.

3.2 Physical properties

From the practically measured values of density and refractive index, various other physical properties were calculated by using the expressions that are available in literature [23] and are tabulated in Table 1. From the Table 1, it was observed that with the increase of Dy^{3+} ion concentration, the average molecular weight, mean atomic volume, molar refraction, field strength and optical basicity values are increasing, where as the other physical properties such as optical dielectric constant, dielectric constant, reflection losses, polaron radius, inter atomic distance and molecular electronic polarizability are decreasing. The optical basicity values in

Accepted manuscript

OFB glasses indicate the ability of a glass to donate negative charges to the probe ion. A low field strength value obtained for the present glass indicates the high solubility of rare earth ions in these glasses. Molecular electronic polarizability is related to many macro and microscopic physical and chemical properties such as optical UV absorption, ionic refraction, dielectric properties and chemical stability. The relatively lower values of molecular electronic polarizability observed for the present glasses makes them more stable.

3.3 Absorption spectral analysis

The absorption spectrum of 1mol% Dy^{3+} doped OFB glass in UV-vis and NIR regions is shown in Fig. 2 in the region 300 -1800nm along with the assignment of transitions from $^6H_{15/2}$ ground state. The spectra consists of 13 transitions originating from the $^6H_{15/2}$ ground state of Dy^{3+} ions to different excited states such as $^6H_{11/2}$, $^6F_{11/2}$+$^6H_{9/2}$, $^6F_{9/2}$+$^6H_{7/2}$, $^6F_{7/2}$, $^6F_{5/2}$, $^6F_{3/2}$, $^4F_{9/2}$, $^4I_{15/2}$, $^4G_{11/2}$, $^4F_{7/2}$ + $^4I_{13/2}$, $^6P_{5/2}$ + $^4M_{19/2}$ + $^4(P,D)_{3/2}$, $^6P_{7/2}$, $^4M_{17/2}$ + $^6P_{3/2}$. The energy levels identification and their assignments are made from those reported by Carnall et.al [24]. The transition $^6F_{5/2}$→$^6F_{11/2}$ is located at 7892 cm^{-1} is a hypersensitive transition satisfies the selection rule $|\Delta S| = 0, |\Delta L| \leq 2, |\Delta J| \leq 2$ [25]. From Fig. 2 it is observed that the intense transitions are lying between $^6H_{15/2}$ ground state and ^6H and ^6F terms in the near infrared region because they are spin allowed transitions ($|\Delta S| = 0$). The transitions within the ^6H term are allowed by the selection rule of the orbital angular momentum ($\Delta L = 0$) and hence they are intense. The observed band positions (cm^{-1}), nephelauxetic ratio (β) and bonding parameters(δ) are presented in Table 2. The necessary mathematical expressions for the evaluation of nephelauxetic ratio and bonding parameter are collected from literature [26].

Depending on the field environmental, the bonding parameter (δ) may be positive or negative indicating covalent or ionic bonding. From Table 2 it is observed that the bonding parameter (δ)

Accepted manuscript

for all the OFB glasses is negative i.e, the prepared glasses are ionic nature and such ionic nature decreases gradually with increase in Dy^{3+} ion concentration. The observed transition intensities for Dy^{3+} doped OFB glasses are determined in terms of oscillator strengths using the following expression [27].

$$f_{exp} = 4.318 \times 10^{-9} \int \varepsilon(\vartheta) d\vartheta \quad (1)$$

Where $\varepsilon(\vartheta)$ is the molar extinction coefficient at a wave number ϑ cm^{-1}. The experimental oscillator (f_{exp}) strengths can be calculated by measuring the integrated areas of the observed absorption bands. The J-O theory has been applied to the experimentally evaluated oscillator strengths to find the J-O intensity parameters (Ω_2, Ω_4 and Ω_6) by least square fit analysis. The necessary equations for least square fit analysis were collected from the literature [28, 29]. The experimental and calculated oscillator strengths are given in Table 3. The small rms (δ_{rms}) deviation observed between the experimental and calculated oscillator strengths indicate the validity of J-O theory and the degree of fitness between the two oscillator strengths.

The J-O intensity parameters and Spectroscopic quality factor ($\chi = \frac{\Omega_4}{\Omega_6}$) for the titled glasses are presented in Table 4 along with the reported J-O parameters for other glasses [30-39]. The J-O intensity parameter are important to study the local structure and bonding nature of RE ions which indicates the covalence of metal ligand bond and also on the asymmetry of ion sites in the neighborhood of RE ion. The bulk properties such as viscosity and rigidity can be known through the magnitudes of Ω_4 and Ω_6 parameters measured using the J-O theory. From Table 4, it is observed that Ω_2 is higher than Ω_4 and Ω_6 and follows the trend $\Omega_2 > \Omega_6 > \Omega_4$. The J-O intensity parameter Ω_2 increases from glass OFBDy0.1 to OFBDy1.0 and then decreases from OFBDy1.5 to OFBDy2.5. In the present work the Ω_2 increases with the increase of intensity of

Accepted manuscript

hypersensitive transitions and vice versa. The intensity of hypersensitive transition is maximum for OFBDy1.0 glass (1 mol% of Dy^{3+}) and minimum for OFBDy2.5 glass (2.5 mol% of Dy^{3+}) which indicates the higher symmetry of crystal field at the rare earth site for OFBDy1.0 glass and lower symmetry of crystal field at the rare earth ion site for OFBDy2.5 glass. From Table 4 it is observed that the spectroscopic quality factor is highest for OFBDy1.0 glass than other glasses. Hence OFBDy1.0 glass is suitable for lasing emission because the larger spectroscopic quality factor predicts the higher stimulated emission cross-section.

3.4 Analysis of emission spectra and evaluation of radiative properties

To study the emission spectra of Dy^{3+} doped OFB glasses, it is essential to identify the excitation wavelengths of Dy^{3+} ions. Hence, an excitation spectrum of OFBDy1.0 glass has been recorded from 300-440nm fixing the emission wavelength at 483nm and is shown in Fig. 3. The excitation spectra recorded show five excitation bands at wavelengths approximately 325, 350, 365, 387 and 426nm related to the transitions $^6H_{15/2}\rightarrow{}^4M_{17/2}$, $^6P_{7/2}$, $^6P_{5/2}$, $^4I_{13/2}$ and $^4G_{11/2}$ respectively. It is well known that emission spectra can give intense emissions if the wavelength used for excitation is very intense. Though the excitation band related to the magnetic dipole transition ($^6H_{15/2}\rightarrow{}^6P_{7/2}$) is found to be more intense at 387nm than other transitions, the emission spectra in the present work were recorded at 410 nm using CW laser source. A laser source can excite the atoms to desired level much effectively than the conventional excitation sources. As we don't have a laser source at 387nm, we have used the nearest wavelength CW laser source (410nm) for excitation. Fig. 4 shows the room temperature emission spectra of Dy^{3+} doped OFB glasses with different concentrations. The emission spectra exhibit four emission bands at 486, 576, 664 and 757nm corresponding to $^4F_{9/2}\rightarrow{}^6H_{15/2}$, $^6H_{13/2}$, $^6H_{11/2}$ and $^6H_{9/2}$ transitions

Accepted manuscript

ACCEPTED MANUSCRIPT

respectively. Among the four transitions, two transitions corresponding to $^4F_{9/2} \rightarrow {}^6H_{15/2}$ and $^4F_{9/2} \rightarrow {}^6H_{13/2}$ observed in blue and yellow regions respectively are more intense than the remaining two transitions. Among these two transitions, $^4F_{9/2} \rightarrow {}^6H_{13/2}$ transition is more intense (yellow region) than the other transition $^4F_{9/2} \rightarrow {}^6H_{15/2}$ (blue region). The transition $^4F_{9/2} \rightarrow {}^6H_{13/2}$ observed in yellow region of the visible spectra can be influenced strongly by the environment around Dy^{3+} ions as it is hypersensitive in nature. When the Dy^{3+} ions are excited with 410nm CW laser to the $^4G_{11/2}$, the energy levels lying above 21,000 cm^{-1} have small energy gaps in between them. Therefore the $^4F_{9/2}$ state is quickly populated by non-radiative relaxation. Hence blue, yellow, red and near-IR luminescence originating from the $^4F_{9/2}$ state is observed. The partial energy level diagram shown in Fig. 5 clearly explains the emission process observed in OFBDy1.0 glass. Due to sufficient energy gap ~ 8000 cm^{-1} between $^4F_{9/2}$ and the next lower level of $^6F_{5/2}$, a pure radiative relaxation rate occurs in $^4F_{9/2}$ level.

The radiative properties like luminescence branching ratio (β_R), radiative transition probability (A_R), total transition probability (A_T) and radiative lifetime (τ_R) have been estimated by considering refractive index and J-O parameters for the excited states of Dy^{3+} ions using the relevant equations available in our previous paper [40] and are given in Table 5. A glassy material under investigation can act as a good laser host if its stimulated emission of cross-section is large. The stimulated emission cross-section for transition from an initial manifold to final manifold is expressed as [41]

$$\sigma_{se} = \frac{\lambda_p^4}{8\pi c n^2 \Delta\tilde{\nu}_{eff}} A_R$$

ACCEPTED MANUSCRIPT

Here λ_P is the emission peak wavelength, $\Delta\lambda_{eff}$ is the effective line-width of the transition. Emission peak wavelength (λ_P), effective band widths($\Delta\lambda_P$), measured and experimental branching ratios (β_R & β_{exp}) and stimulated emission cross-sections (σ_{se}), gain band width(σ_{se} x $\Delta\lambda_p$) and optical gain (σ_{se} x τ_R) for transitions $^4F_{9/2}\rightarrow{}^6H_{15/2,}$ $^4F_{9/2}\rightarrow{}^6H_{13/2}$ and $^4F_{9/2}\rightarrow{}^6H_{11/2}$ are presented in Table 6. The potentiality of laser emission can be decided by the luminescence branching ratio if its value $\beta_R \geq 0.5$. From Table 6 it is observed that, for the transition $^4F_{9/2}\rightarrow{}^6H_{13/2}$ the luminescence branching ratio (β_R) values for all the glasses are higher than 0.5 and is maximum for OFBDy1.0 glass. These values are in good agreement with the reported values [31, 42]. From Table 6, it is observed that among all the emission transitions, an intense yellow emission transition $^4F_{9/2}\rightarrow{}^6H_{13/2}$ observed at 576nm gives highest stimulated emission cross-section in all the glasses. From Table 6, it is observed that $^4F_{9/2}\rightarrow{}^6H_{13/2}$ transition related to OFBDy1.0 glass (1mol% of Dy^{3+}) is very encouraging for lasing action since this transition has highest stimulated emission cross-section and branching ratio values among the prepared OFB glasses. This result is in consistence with the measured spectroscopic quality factor also. Fig. 6(a) & 6(b) shows the decay profiles of the intense emission transitions $^4F_{9/2}\rightarrow{}^6H_{15/2,}$ $^4F_{9/2}\rightarrow{}^6H_{13/2}$ of Dy^{3+} ions in OFB glasses respectively excited at 410nm using CW laser. The decay profiles observed for both the emission transitions for all the glasses are single exponential in nature as shown in Fig. 6(a) & 6(b). The experimental lifetimes (τ_{exp}) of $^4F_{9/2}$ excited state are evaluated by taking the first e -folding times of the decay curves of Dy^{3+} ions in OFB glasses and are tabulated in Table 7. From Table 7, it can be observed that the experimental lifetimes of $^4F_{9/2}$ level decreases in both the transitions with increase in the Dy^{3+} ions concentration in OFB

Accepted manuscript

glasses. The radiative lifetimes (τ_R) measured from J-O theory are also given in Table 7 for both the transitions for all glasses. It can be observed that for both the transitions in all these glasses measured lifetimes are less than the radiative lifetimes. Due to multi phonon relaxation process, the small inconsistency occurred between the experimental and radiative lifetimes. In such cases the experimental life times (τ_{exp}) of an emitting state is associated with radiative lifetimes (τ_R) and non radiative decay rates (W_{NR}) as

$$\frac{1}{\tau_{exp}} = \frac{1}{\tau_R} + W_{NR}$$

The non radiative decay rates evaluated by using the above equation are also given in Table 7. In the present Dy^{3+} doped OFB glasses the decrease in experimental lifetimes may be due to energy transfer between the Dy^{3+} ions at higher concentrations. The quantum efficiency (η %), another parameter used to know the efficiency of a material for lasing action is measured by taking the ratio between The ratio between experimental(τ_{exp}) and radiative lifetimes (τ_R). Such quantum efficiency (η %) values measured for all the OFB glasses are given in Table 7. The quantum efficiency values are increasing up to 1 mol% of the Dy^{3+} ions in OFB glasses for both transitions and then decreasing beyond 1 mol% Dy^{3+}. Among all the glasses studied here, OFBDy1.0 glass (1 mol% of Dy^{3+} doped OFB glass) possesses highest quantum efficiency values for both transitions. Among the two emission transitions, the transition $^4F_{9/2} \rightarrow {}^6H_{13/2}$ in yellow region (576 nm) for OFBDy1.0 glass (1 mol% of Dy^{3+} doped OFB glass) possesses highest quantum efficiency. Hence OFBDy1.0 glass is quite suitable for lasing emission in yellow region with 576 nm when excited at 410 nm. If a glassy material possess highest values of gain band width (σ_{se} x $\Delta\lambda_p$) and optical gain (σ_{se} x τ_R) then it acts as a good optical fiber. From Table 6, it is observed that OFBDy1.0 glass is having highest values of gain band width (σ_{se} x

Accepted manuscript

ACCEPTED MANUSCRIPT

$\Delta\lambda_p$) and optical gain (σ_{se} x τ_R among all the glasses. Hence OFBDy1.0 glass is also suitable for fibers of optical amplification.

3.5 CIE chromaticity co-ordinates

To investigate the white light emission of OFB glasses, an excitation spectrum was recorded fixing the blue emission at 483 nm. The excitation spectrum exhibits five excitation bands ranging from UV (300 nm) to Blue (440 nm). The five excitation bands observed for this glass gives the flexibility of excitation from UV to Blue light to use these glasses as glass phosphors. Moreover the excitation wavelengths found for OFB glasses matches well with the commercial UV and Blue LEDs (λ_{ex} = 300-440nm). Table 8 gives the color co-ordinates evaluated for all the OFB glasses excited at different wavelengths. From Table 8, it can also be observed that the CIE co-ordinates are invariant almost with the increase in Dy^{3+} concentration. Fig. 7 shows the CIE chromaticity co-ordinates of Dy^{3+} ions in OFB glasses excited at 410 nm (CW laser) along with con-focal photoluminescence images of Dy^{3+} ions in OFB glasses. From the emission details observed from all the UV to blue excitations, the resultant CIE co-ordinates falls in near white light region, due to appropriate combination of prominent yellow and blue color emissions (Y/B rations, Table 8). Among all the glasses, the color co-ordinates possessed by OFBDy1.0 glass (x=0.338, y=0.335) are very close to the perfect white light CIE co-ordinates (x=0.33, y=0.33). Hence it can be concluded that among all the OFB glasses, OFBDy1.0 with 1 mol% of Dy^{3+} concentration is more suitable for white light emission when excited at 410nm. This result is inconsistent with the con-focal photoluminescence image given by OFBDy1.0 glass having more intense white light than the other glasses.

4 Conclusions

Accepted manuscript

ACCEPTED MANUSCRIPT

The lasing potentialities and near white light emission capacity of Oxy-fluoroborate glasses doped with different concentrations of dysprosium have been investigated through absorption, emission, lifetime and con-focal photoluminescence measurements. From the absorption spectra the radiative properties such as transition probability, branching ratios and radiative lifetimes are evaluated using the J-O theory for the prominent fluorescent levels. The intensity of hypersensitive transition is maximum for OFBDy1.0 glass (1 mol% of Dy^{3+}) and minimum for OFBDy2.5 glass (2.5 mol% of Dy^{3+}) indicating the higher and lower symmetry of crystal field at the rare earth site for OFBDy1.0 and OFBDy2.5 glasses respectively. The spectroscopic quality factor which predicts the higher stimulated emission cross-section is found to be maximum for OFBDy1.0 glass than the other glasses. The emission spectra recorded for all the OFB glasses when excited at 410nm CW laser gives four emission transitions corresponding to the transitions $^4F_{9/2}\rightarrow{}^6H_{15/2}$, $^6H_{13/2}$, $^6H_{11/2}$ and $^6H_{9/2}$. The experimental branching ratios and stimulated emission cross-sections measured for all the emission peaks were found to be maximum for OFBDy1.0 glass with 1 mol% of Dy^{3+} ions. The decay profiles measured for two intense emission transitions ($^4F_{9/2}\rightarrow{}^6H_{15/2}$ and $^4F_{9/2}\rightarrow{}^6H_{13/2}$) are coupled with their corresponding radiative lifetimes to calculate quantum efficiency of the prepared glasses. From the measured spectroscopic quality factor, stimulated emission cross-section and quantum efficiency, it was concluded that OFBDy1.0 glass with 1 mol% of Dy^{3+} ions is quite suitable for lasing emission in yellow region (576nm) when excited at 410nm.The CIE chromaticity co-ordinates were evaluated for all the emission spectra under the excitation of different n-UV wavelengths confirm the possibility of generating near white light from these OFB glasses. Among all the glasses, the color co-ordinates possessed by OFBDy1.0 glass when excited at 410nm using CW laser are very close to

Accepted manuscript

ACCEPTED MANUSCRIPT

the near white light coordinates. Hence it is concluded that OFBDy1.0 glass with 1 mol% of Dy^{3+} concentration is more suitable for near white light generation in principle when excited at 410nm. This result is also inconsistent with the con-focal photoluminescence image given by OFBDy1.0 glass showing more intense white light emission than the other glasses.

Acknowledgements

Two of the authors, Mahamuda Shaik (File No: SR/WOS-A/PS-53/2011) and Swapna Koneru (File No: SR/WOS-A/PS-35/2011) are very much thankful to Department of Science and Technology (DST), Government of India, New Delhi, for awarding them with a Women Scientist's scheme under DST-WOS (A) programme. This work is also partly supported by High-impact Research initiative of IIT Delhi, UK-India Education Research Initiative (UKIERI) and Department of Science and Technology (DST, Govt. of India).

Accepted manuscript

ACCEPTED MANUSCRIPT

References

[1] A. A. Kaminskii, Laser Crystals, Springer, Berlin, 1990.

[2] R. C. Powel, Physics of Solid State Laser Materials, Springer, Berlin, 1998.

[3] D. C. Brown, High Peak Power Nd Glass Laser System, Springer, Berlin, 1992.

[4] A. Agarwal, I. Pal, S. Sanghi, M. P. Agarwal, Opt. Mater. 32 (2009) 339-344.

[5] T. Suhasini, J. Suresh Kumar, T. Sasikala, Kiwan Jang, Ho Sueb Lee, M. Jayasimhadri, Jung Hyun Jeong, Soung Soo Yi, L. Rama Moorthy, Opt. Mater. 31 (2009) 1167-1172.

[6] M. A. K. Elafayumi, M. Farouk, M. G. Brik, M. M. Elokr, J. Alloys Compd. 492 (2010) 712-716.

[7] S. K. Jong, T. I. Kwon, S. J. Yong, E. J. Pyung, C. C.J in, L. P. Hong, Solid State Commun.135 (2005) 21-24.

[8] X. X. Wang, J. Wang, J. X. Shi, Q. Su, M. I. Cong, Mater. Res. Bull. 42 (2007) 1669-1673.

[9] S. Liu, G. Zhao, X. Lin, H. Ying, J. Liu, J. Wang, G. Han, J. Solid State Chem. 181 (2008) 2725-2730.

[10] S. Liu, G. Zhao, H. Ying, J. Wang, G. Han, Opt. Mater. 31 (2008) 47-50.

[11] J. C. Zhang, C. Parent, G. le Flem, P. Hagenmullar, J. Solid State Chem. 93 (1991) 17-29.

[12] H. T. Amorim, M. V. D. Vermelho, A.S. Gouveianeto, F.C. Cassanjes, S. J. L. Ribeiro, Y. Messaddeq, J. Solid State Chem. 171 (2003) 278-281.

[13] C. Liu, J. Heo, Material Lett. 61 (2007) 3751-3754.

[14] M. Jayasimhadri, Kiwan Jang, Ho Sueb Lee, Baojiu Chen, Soung-Soo Yi, Jung-Hung Jeong. J. App. Phys. 106 (2009) 013105(1-4).

[15] N. Soga, K. Hauro, M. Yoshimoto, H. Yamamoto, J. Appl. Phys. 63 (1988) 4451-4454.

Accepted manuscript

ACCEPTED MANUSCRIPT

[16] S. A. Pollack, C. B. Chang, J. App. Phys. 64 (1988) 2885-2893.

[17] G. Wang, S. Dai, J. Zhang, S. Xu, L.Hu, Z. Jing, J. Lumin. 113 (2005) 27-32.

[18] K. Annapurana, M. Das, M. Kundu, R. N. Dwivedhi, S. Buddhudu, J. Molecular structure 741 (2005) 53-60.

[19] Y. B. Shin, J. Heo, J. Non-Cryst. Solids 253 (1999) 23-29.

[20] V. K. Rai, S. B. Rai, D. K. Rai, Opt. Commun. 257 (2006) 112-119.

[21] A. A. Kaminskii, Crystalline Lasers: Physical Processes and Operating Schemes CRC, Boca Raton, FL, 1996, Chapter 4, p.304.

[22] A. A. Kaminskii, U. Hommerich, D. temple, J. T. Seo, K. Ueda, S. Bagayev, A. Pavlyuk, Jpn. J. Appl. Phys. Part 2. 39 (2000) L208-L211.

[23] A.S. Rao, Y.N. Ahammed, R.R. Reddy, T.V.R. Rao, Opt. Mater. 10 (1998) 245-252.

[24] W. T. Carnall, P.R. Fields, K. Rajnak, J. Chem. Phys. 49 (1968) 4424-4442.

[25] A. Thulasiramudu, S. Buddhudu, Spectrochim. Acta Part A 67 (2007) 802-807.

[26] R. T. Karunakaran, K. Marimuthu, S. Surendra Babu, S. Armugam, J. Lumin. 130 (2010) 1067-1072.

[27] W. T. Carnall, K. A. Gschneidner, L. Eyring (Eds.), Hand book of Physics and Chemistry of Rare-Earths, Vol.3, North Holland, Amsterdam, 1987, Chapter 24, p.171-208.

[28] B. R. Judd, Phys. Rev. 127 (1962) 750-761.

[29] G. S. Ofelt, J. Chem. Phys. 37 (1962) 511-520.

[30] M. V. Vijay Kumar, B. C. Jamaliah, K. Rama Gopal, R. R. Reddy, J. Lumin. 132 (2012) 86-90.

[31] B. C. Jamaliah, L.Rama Moorthy, Hyo Jin Seo, J. Non-Cryst. Solids 358 (2012) 204-209.

Accepted manuscript

ACCEPTED MANUSCRIPT

[32] C. Venkateswarlu, M. Seshadri, Y. C. Ratnakaram, Opt. Mat. 33 (2011) 799-806.

[33] S. A. Saleem, B. C. Jamaliah, M. Jayasimhadri, A.Srinivasa Rao, Kiwan Jang, L.Rama Moorthy, J. Quantitative Spectroscopy and Radiative Transfer. 112 (2011) 78-84.

[34] M. Seshadri, K. Venkata Rao, J. Lakshmana Rao, K.S.R Koteswara Rao, Y. C. Ratnakaram, J. Lumin 130 (2010) 536-543.

[35] J. Suresh Kumar, K. Pavani, A. Mohan Babu, Neeraj Kumar Giri, S. B. Rai, L.Rama Moorthy, J. Lumin. 130 (2010) 1916-1923.

[36] D. V. R. Murthy, B. C. Jamaliah, A. Mohan Babu, T. Sasikala and L.Rama Moorthy, Opt. Mater. 32 (2010) 1112-1116.

[37] R. T. Karunakaram, K. Marimuthu, S. Surendra Babu, S. Armugam, Physica B 404 (2009) 3995-4000.

[38] Y.C. Ratnakaram, D. Tirupathi Naidu, A. Vijaya Kumar, J. L. Rao, Opt. Mat. 27 (2004) 409-417.

[39] Yong Beon Shin, Jong Heo, J. Non-Crys. Solids 253 (1999) 23-29.

[40] Sk. Mahamuda, K. Swapna, A. Srinivasa Rao, M. Jayasimhadri, T. Sasikala, K. Pavani, L. Rama Moorthy, J. Phys. Chem. Solids. 74 (2013) 1308-1315.

[41] F. Krupke, IEEE J. Quant. Electron 10 (1974) 450-457.

[42] K. Maheswaran, K. Marimuthu, J. Alloys Compd. 509 (2011) 7427-7433.

Accepted manuscript

ACCEPTED MANUSCRIPT

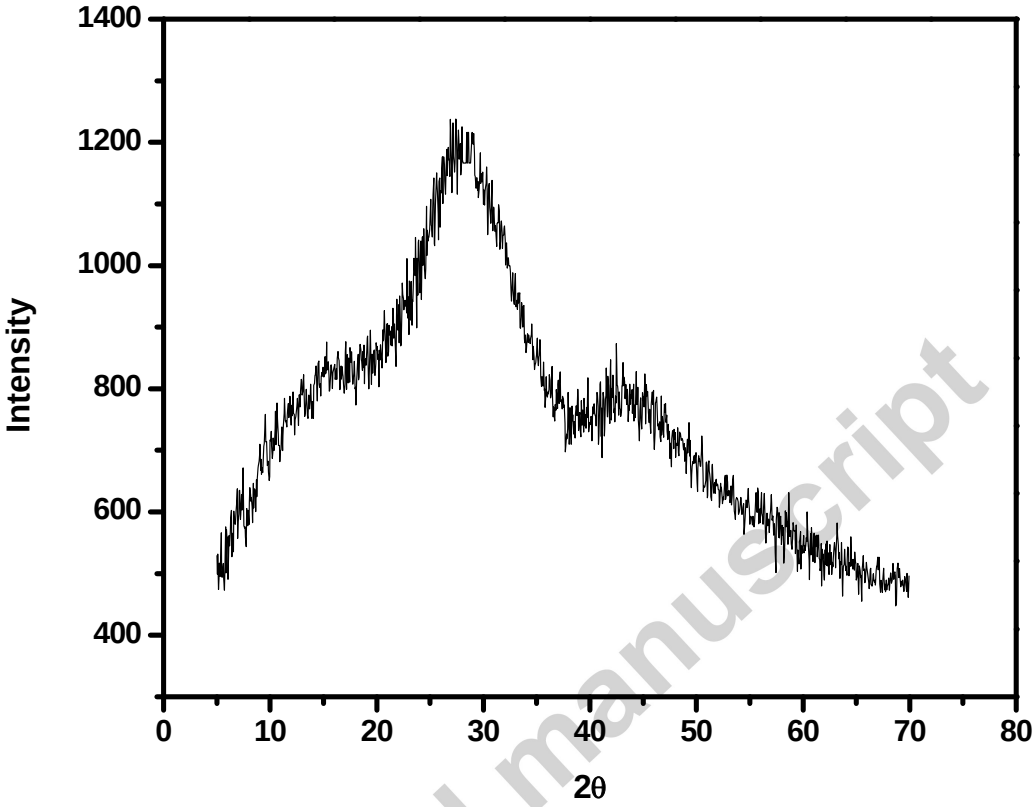

Fig.1. XRD spectrum of an undoped OFB Glass

Accepted manuscript

ACCEPTED MANUSCRIPT

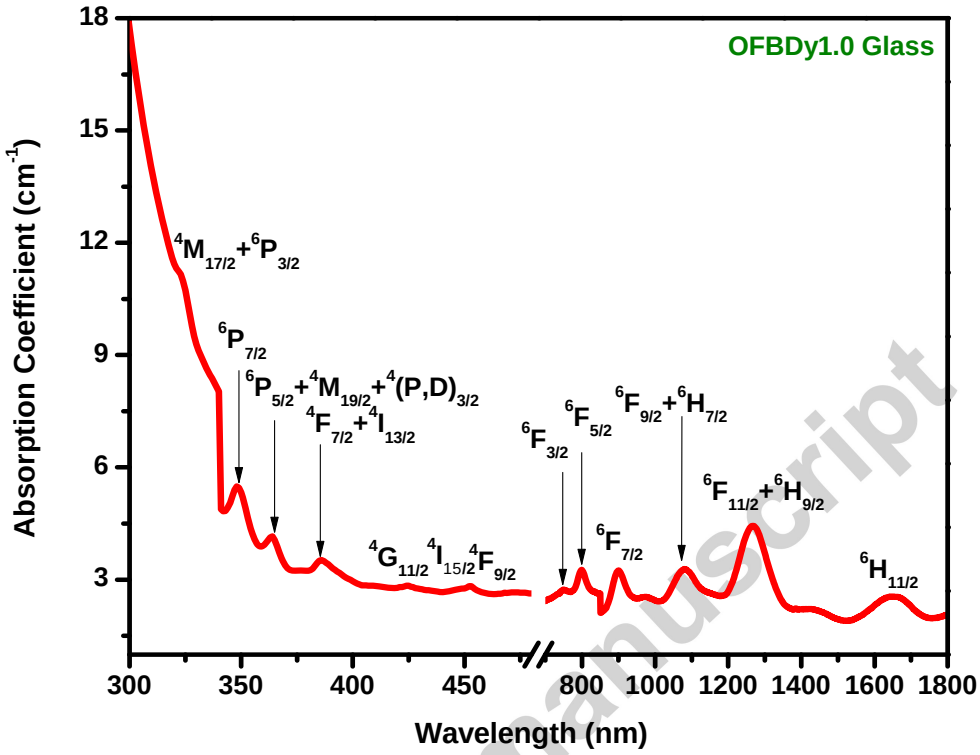

Fig. 2. UV-vis-NIR Absorption spectrum of 1.0 mol% of Dy^{3+} ions in OFB glass (OFBDy1.0).

Accepted manuscript

ACCEPTED MANUSCRIPT

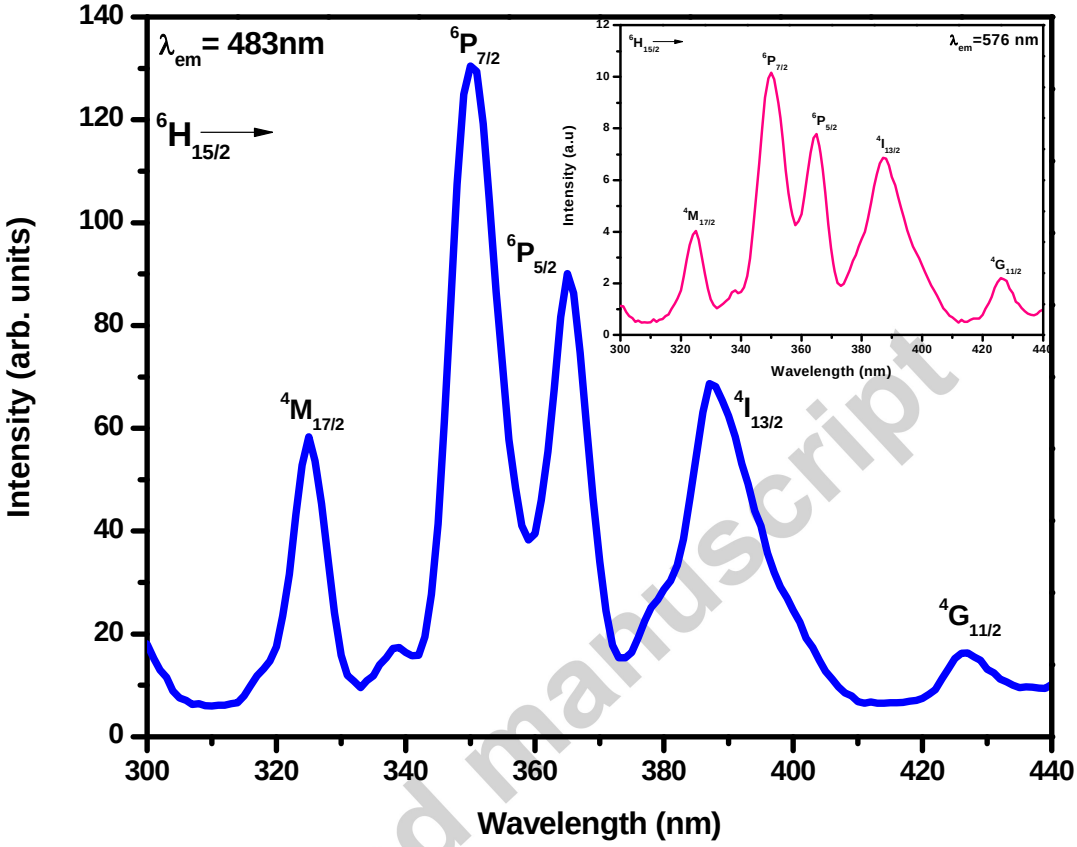

Fig. 3. Excitation spectrum of 1.0 mol % of Dy^{3+} ions in OFB glass (OFBDy1.0). Inset is the excitation spectrum of the same glass at an emission wavelength 576 nm.

Accepted manuscript

ACCEPTED MANUSCRIPT

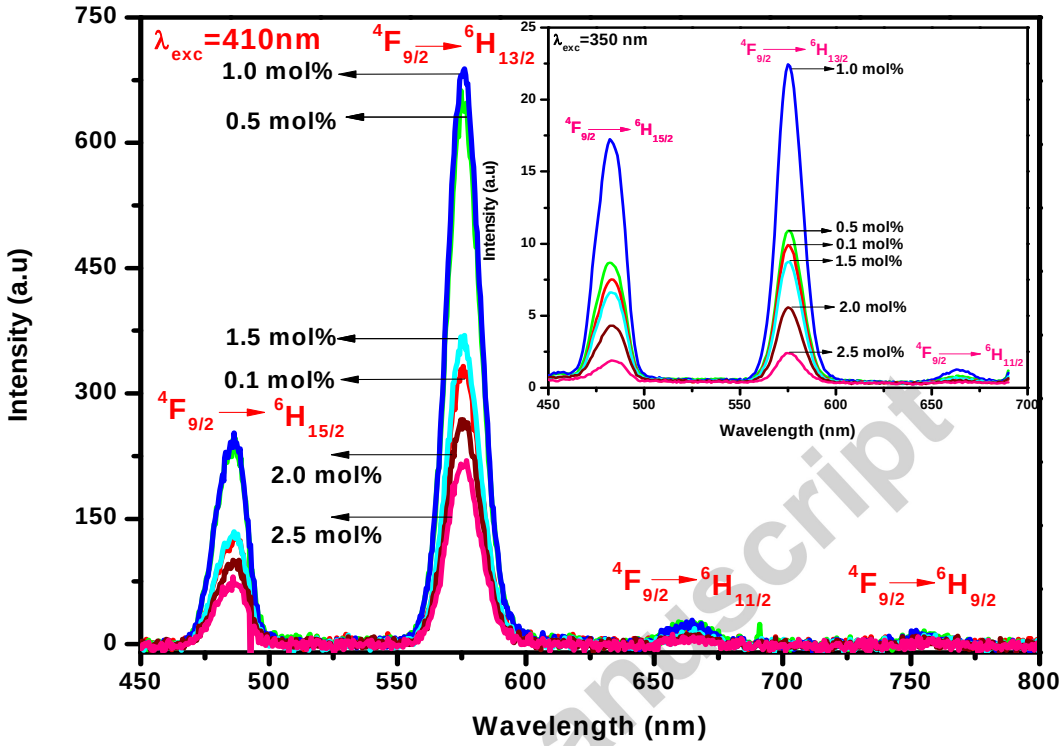

Fig. 4. Fluorescence spectra of Dy^{3+} ions in OFB glasses at 410 nm excitation wavelength (CW Laser). Inset is shows the fluorescence spectra of Dy^{3+} ions in OFB glasses at an excitation wavelength 350 nm.

Accepted manuscript

ACCEPTED MANUSCRIPT

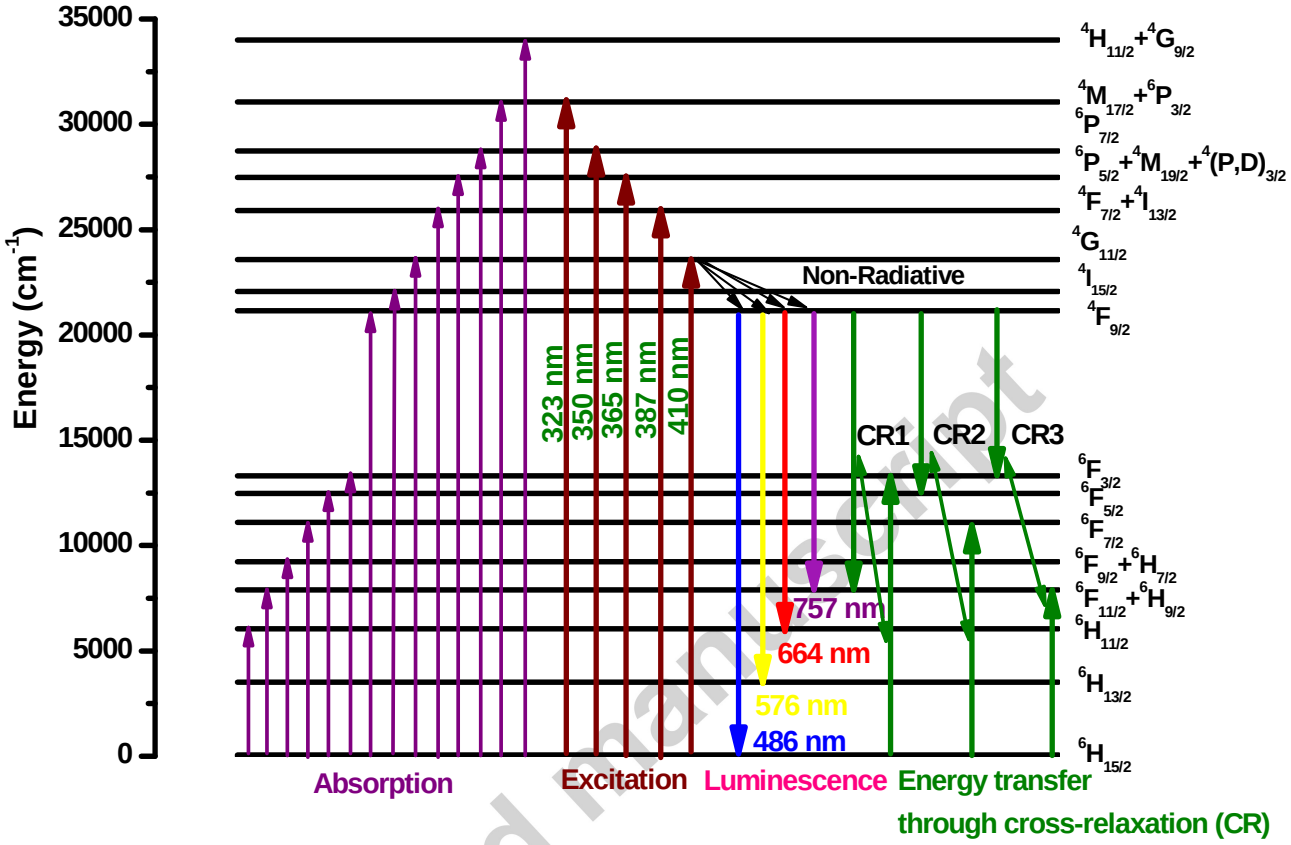

Fig. 5. Partial energy level diagram of 1 mol% of Dy^{3+} ions in OFB glass (OFBDy1.0) with absorption, excitation, luminescence and cross-relaxation channels

Accepted manuscript

ACCEPTED MANUSCRIPT

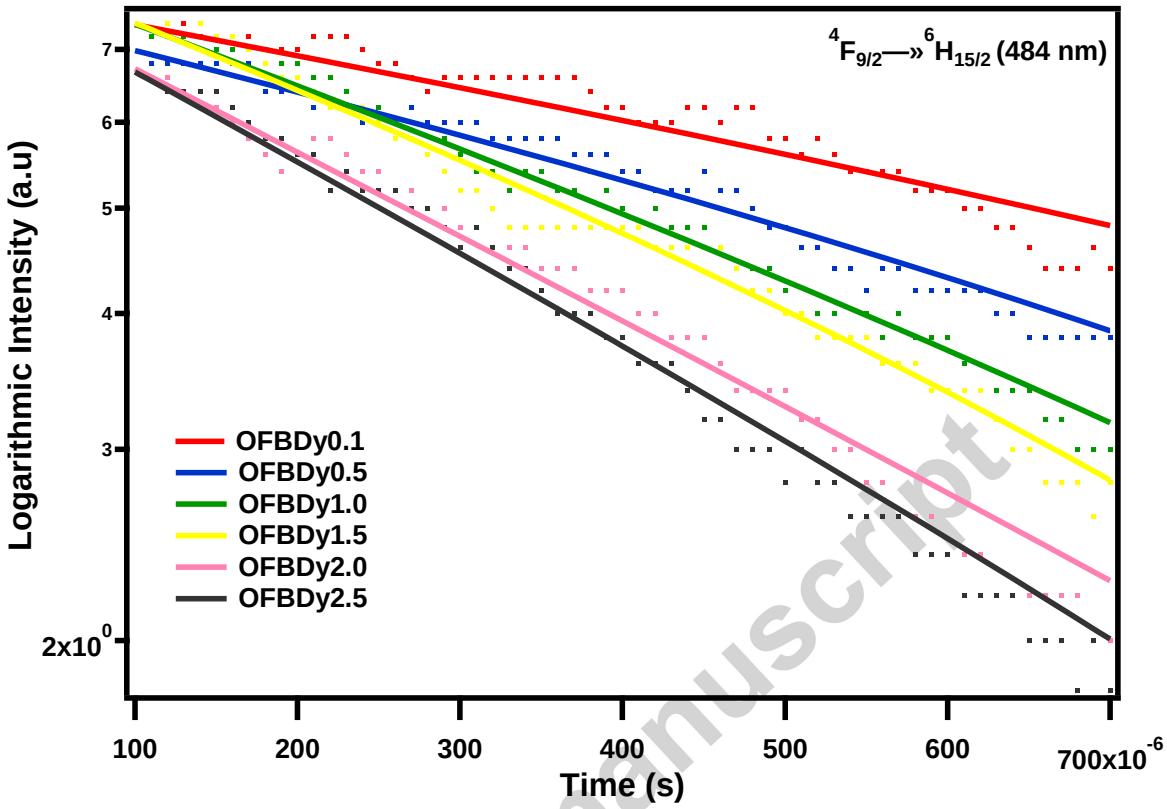

Fig. 6(a): The decay curves for $^4F_{9/2} \rightarrow {}^6H_{15/2}$ (484 nm) emission of Dy^{3+} ions in OFB glasses when excited at 410 nm.

Accepted manuscript

ACCEPTED MANUSCRIPT

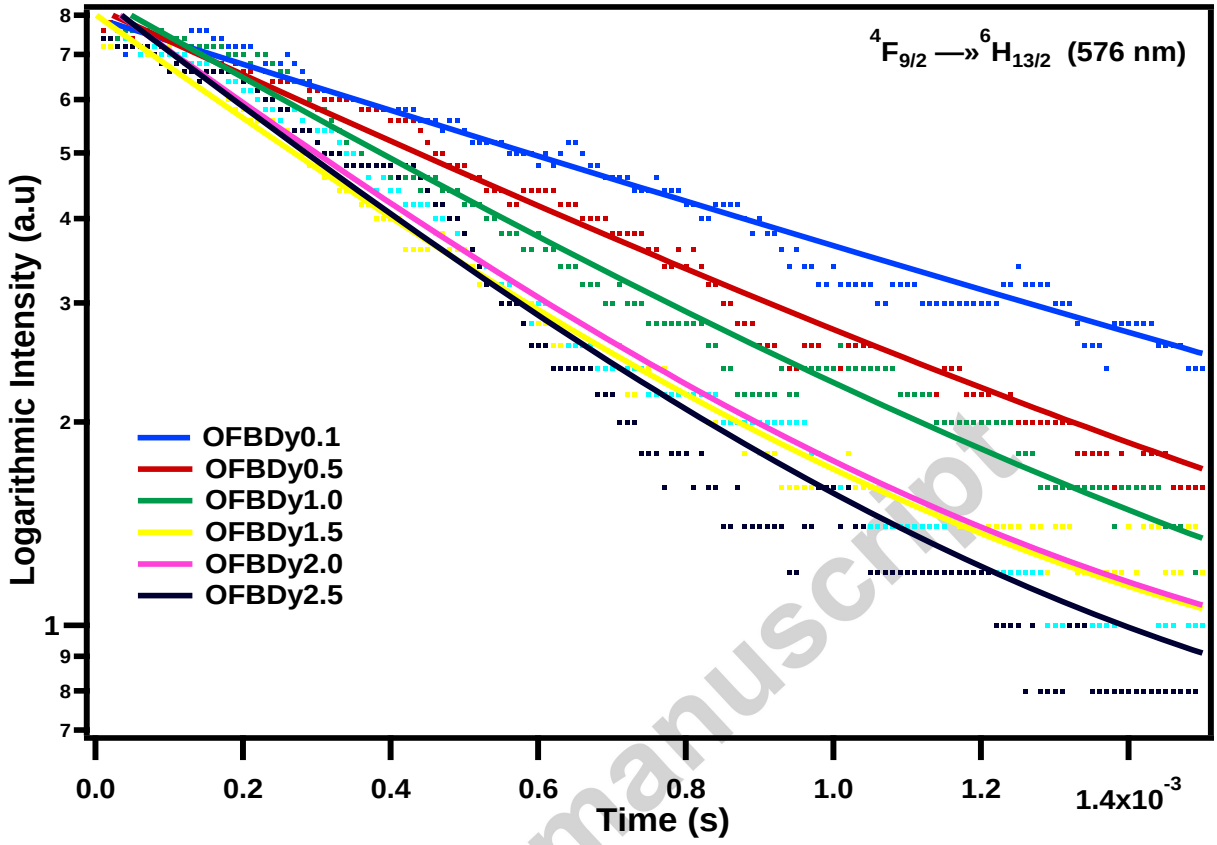

Fig. 6(b): The decay curves for $^4F_{9/2} \rightarrow {}^6H_{13/2}$ (576) nm emission of Dy^{3+} ions in OFB glasses when excited at 410 nm.

Accepted manuscript

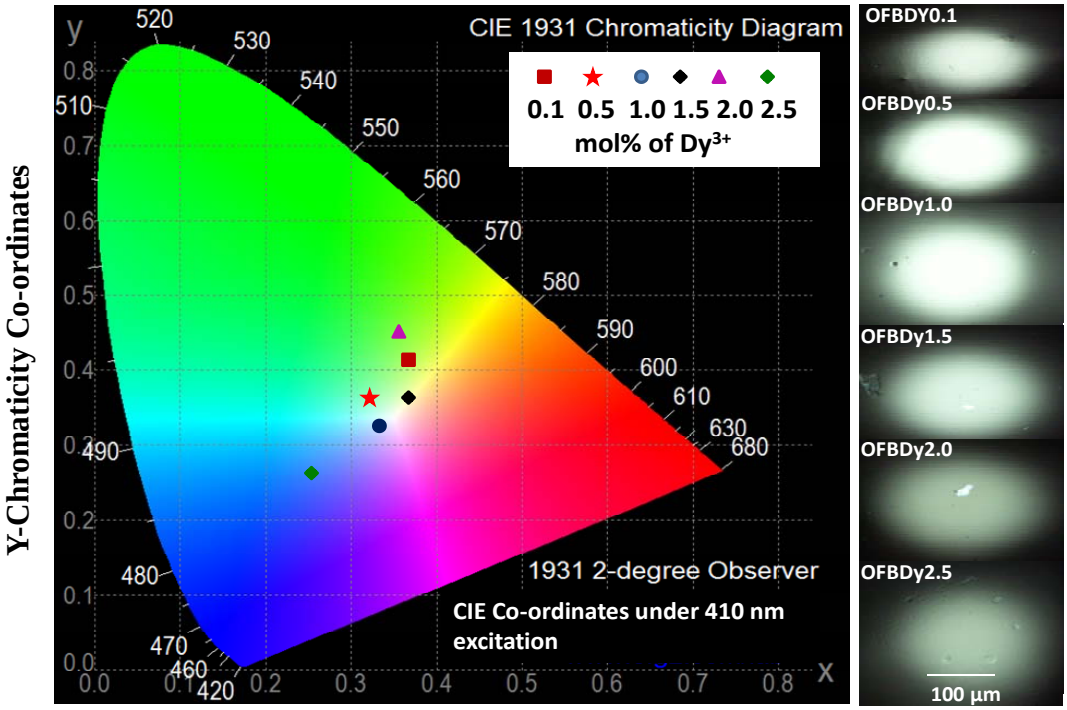

Fig. 7. CIE chromaticity coordinates of Dy^{3+} ions in OFB glasses and their confocal photoluminescence images at 410 nm CW laser excitation.

Accepted M

ACCEPTED MANUSCRIPT

High Lights

1. Dy^{3+} doped OFB glasses have been synthesized using melt quenching technique.
2. Radiative properties for the prepared glasses have been calculated using J-O theory.
3. Branching ratio's and emission cross-sections are evaluated for laser transitions.
4. CIE colour co-ordinates were evaluated using emission spectra.
5. OFBDy1.0 glass was found to be the best for laser action and white light generation.

Table 1

Various physical properties of Dy^{3+} ions in OFB glasses

S.No	Physical Property	OFBDy0.1	OFBDy0.5	OFBDy1.0	OFBDy1.5	OFBDy2.0	OFBDy2.5
1.	Refractive index (n_d)	1.6090	1.6070	1.6050	1.6030	1.6010	1.5990
2.	Density, d (gm/cm^3)	3.3796	3.3950	3.4142	3.4334	3.4526	3.4718
3.	Average molecular weight, $\bar{M}$(g)	84.690	85.774	87.129	88.484	89.839	91.195
4.	Dy^{3+} ion concentration, N(10^{22} ions/cm^3)	0.2403	1.1917	2.3597	3.505	4.6285	5.7314
5.	Mean atomic volume (g/cm^3/atom)	6.0382	6.0879	6.1493	6.2100	6.2700	6.3294
6.	Dielectric constant (ϵ)	2.5888	2.5824	2.5760	2.5696	2.5632	2.5568
7.	Optical dielectric constant ($\epsilon - 1$)	1.5888	1.5824	1.5760	1.5696	1.5632	1.5568
8.	Reflection losses (R %)	0.0544	0.0542	0.0539	0.0536	0.0533	0.0531
9.	Molar refraction (R_m)(cm^{-3})	8.6765	8.7246	8.7892	8.8522	8.9138	8.9740
10.	Polaron radius (r_p) (Å)	3.0586	1.7945	1.4294	1.2529	1.1421	1.0637
11.	Inter-atomic distance (r_i) (Å)	7.5894	4.4528	3.5468	3.1089	2.8340	2.6393
12.	Molecular electronic polarizability α ($10^{-23}cm^3$)	3.4416	0.6921	0.3486	0.2340	0.1767	0.1423
13.	Field strength ,F ($10^{15}cm^{-2}$)	3.2066	9.3154	14.682	19.109	22.996	26.514
14.	Optical basicity ,(Λ_{th})	0.4866	0.5352	0.5368	0.5383	0.5399	0.5415

ACCEPTED MANUSCRIPT

Table 2

Observed band positions (cm^{-1}), nephelauxetic ratios (β) and bonding parameters (δ) for Dy^{3+} ions in OFB glasses

Transition	OFBDy0.1	OFBDy0.5	OFBDy1.0	OFBDy1.5	OFBDy2.0	OFBDy2.5
$^6H_{11/2}$	6146	6049	6056	5988	6002	5977
$^6F_{11/2}+{}^6H_{9/2}$	7880	7880	7892	7905	7905	7892
$^6F_{9/2}+{}^6H_{7/2}$	9363	9216	9233	9363	9199	9225
$^6F_{7/2}$	11049	11098	11098	11123	11123	11135
$^6F_{5/2}$	12515	12515	12484	12515	12515	12547
$^6F_{3/2}$	13386	13315	13315	13351	13351	13333
$^4F_{9/2}$	21186	21097	21141	21097	21141	21186
$^4I_{15/2}$	22123	22123	22075	22123	22123	22123
$^4G_{11/2}$	23696	23696	23584	23529	23584	23529
$^4F_{7/2}+{}^4I_{13/2}$	25974	25906	25906	25906	25974	25906
$^6P_{5/2}+{}^4M_{19/2}+{}^4(P,D)_{3/2}$	27548	27548	27472	27472	27472	27472
$^6P_{7/2}$	-	28735	28735	28653	28653	28653
$^4M_{17/2}+{}^6P_{3/2}$	-	30959	31055	30864	30959	30959
$^4H_{11/2}+{}^4G_{9/2}$	-	-	-	34013	34013	34013
β	1.0142	1.0098	1.0097	1.0086	1.0079	1.0076

Accepted manuscript

δ	-1.40	-0.9781	-0.9610	-0.8622	-0.7879	-0.7622

Table 3

Experimental (f_{exp} x 10^{-6}), calculated (f_{cal} x 10^{-6}) oscillator strengths and r.m.s deviation for Dy^{3+} ions in OFB glasses

Transitions from	**OFBDy0.1**		**OFBDy0.5**		**OFBDy1.0**		**OFBDy1.5**		**OFBDy2.0**		**OFBDy2.5**	
$^6H_{15/2}\rightarrow$	**f_{exp}**	**f_{cal}**	**f_{exp}**	**f_{cal}**	**f_{exp}**	**f_{cal}**	**f_{exp}**	**f_{cal}**	**f_{exp}**	**f_{cal}**	**f_{exp}**	**f_{cal}**
$^6H_{11/2}$	4.608	3.898	5.050	4.709	6.503	6.077	4.834	4.768	3.910	4.088	2.842	3.081
$^6F_{11/2}+{}^6H_{9/2}$	9.230	9.407	10.08	10.17	15.31	15.43	11.28	11.30	10.23	10.18	8.968	8.905
$^6F_{9/2}+{}^6H_{7/2}$	5.217	4.409	6.114	4.356	8.282	6.671	6.897	5.054	5.995	4.254	4.409	3.079
$^6F_{7/2}$	5.138	6.704	6.149	7.865	8.273	10.38	6.707	8.313	5.857	6.946	4.499	4.882
$^6F_{5/2}$	3.133	3.101	4.027	3.918	5.598	4.785	4.667	3.933	3.926	3.276	2.160	2.271
$^6F_{3/2}$	0.548	0.586	0.733	0.736	1.108	0.902	0.704	0.741	0.667	0.617	0.324	0.426
$^4F_{9/2}$	0.322	0.517	0.600	0.608	0.837	0.796	0.569	0.637	0.421	0.533	0.241	0.374
$^4I_{15/2}$	1.059	1.303	1.983	1.631	2.741	2.052	1.889	1.648	1.510	1.403	0.932	1.045
$^4G_{11/2}$	0.354	0.257	0.459	0.177	0.696	0.391	0.422	0.268	0.339	0.230	0.222	0.179
$^4F_{7/2}+{}^4I_{13/2}$	1.174	1.258	1.824	1.150	2.920	1.932	1.703	1.425	1.086	1.214	0.669	0.910
$^6P_{5/2}+{}^4M_{19/2}+{}^4(P,D)_{3/2}$	1.332	1.534	2.014	1.869	2.760	2.365	1.938	1.916	1.240	1.599	0.816	1.114
$^6P_{7/2}$	-	-	5.240	7.009	14.86	16.09	8.895	10.97	7.030	9.345	5.093	7.190
$^4M_{17/2}+{}^6P_{3/2}$	-	-	1.606	1.650	2.338	2.043	1.727	1.653	1.183	1.391	0.776	0.984

Accepted manuscript

$^4H_{11/2}+{}^4G_{9/2}$	-	-	-	-	-	-	0.364	0.221	0.294	0.193	0.191	0.158
δ_{rms} (x10^{-6})	±0.588		±0.844		±0.931		±0.888		±0.857		±0.688	

Table 4

Judd-Ofelt Parameters (Ω_λ x10^{-20}cm^2) and Spectroscopic quality factor ($\chi = \frac{\Omega_4}{\Omega_6}$) for the $^4F_{3/2}$ level of Dy^{3+} ions in OFB glasses

Glass System	Ω_2	Ω_4	Ω_6	χ	Trend	References
OFBDy0.1	16.3±0.01	6.99±0.01	7.28±0.01	0.95	$\Omega_2 > \Omega_6 > \Omega_4$	present work
OFBDy0.5	19.9±0.01	4.52±0.02	9.21±0.01	0.49	$\Omega_2 > \Omega_6 > \Omega_4$	present work
OFBDy1.0	27.9±0.12	10.9±0.01	11.2±0.01	0.97	$\Omega_2 > \Omega_6 > \Omega_4$	present work
OFBDy1.5	20.5±0.01	7.22±0.01	9.24±0.01	0.78	$\Omega_2 > \Omega_6 > \Omega_4$	present work
OFBDy2.0	19.1±0.09	6.18±0.01	7.73±0.01	0.79	$\Omega_2 > \Omega_6 > \Omega_4$	present work
OFBDy2.5	17.9±0.01	4.78±0.01	5.36±0.01	0.89	$\Omega_2 > \Omega_6 > \Omega_4$	present work
Dy: NaLTB	9.86	3.39	2.41	1.40	$\Omega_2 > \Omega_4 > \Omega_6$	[16]
PYBDy10	7.75	2.31	2.70	0.85	$\Omega_2 > \Omega_6 > \Omega_4$	[58]
L4BTAFDy	18.31	4.29	2.04	2.10	$\Omega_2 > \Omega_4 > \Omega_6$	[59]
Li – Na	18.13	4.79	4.48	1.06	$\Omega_2 > \Omega_4 > \Omega_6$	[60]

Accepted manuscript

Li – K	15.46	4.75	3.45	1.37	$\Omega_2 > \Omega_4 > \Omega_6$	[61]
Li	12.60	7.06	2.52	2.80	$\Omega_2 > \Omega_4 > \Omega_6$	[61]
CFBDy10	5.98	2.33	2.33	1.00	$\Omega_2 > \Omega_4 = \Omega_6$	[62]
SrTP	7.78	3.37	0.88	3.82	$\Omega_2 > \Omega_4 > \Omega_6$	[63]
D0LBE	5.319	0.54	1.54	0.35	$\Omega_2 > \Omega_6 > \Omega_4$	[63]
D1LBE	6.45	2.02	3.87	0.52	$\Omega_2 > \Omega_6 > \Omega_4$	[64]
LSG	19.08	1.88	6.04	0.31	$\Omega_2 > \Omega_6 > \Omega_4$	[65]
SPG	20.87	0.56	2.82	0.19	$\Omega_2 > \Omega_6 > \Omega_4$	[65]
$Ge_{25}Ga_{10}S_{65}$	13.1	12.5	11.6	1.07	$\Omega_2 > \Omega_6 > \Omega_4$	[66]

Table 5

Transition probabilities (A_R) (s^{-1}), luminescence branching ratios (β_R) and total transition probability (A_T) (s^{-1}) for the observed emission transitions for Dy^{3+} ions in OFB glasses

Transition	A_R	β_R	A_T
OFBDy0.1			
$^4F_{9/2} \rightarrow {}^6H_{11/2}$	223.33	0.677	3297.34
$^4F_{9/2} \rightarrow {}^6H_{13/2}$	2045.24	0.6203	
$^4F_{9/2} \rightarrow {}^6H_{15/2}$	658.35	0.1997	
OFBDy0.5			
$^4F_{9/2} \rightarrow {}^6H_{11/2}$	257.67	0.0681	3782.51
$^4F_{9/2} \rightarrow {}^6H_{13/2}$	2380.39	0.6293	
$^4F_{9/2} \rightarrow {}^6H_{15/2}$	768.25	0.2031	
OFBDy1.0			
$^4F_{9/2} \rightarrow {}^6H_{11/2}$	360.21	0.0689	5226.15
$^4F_{9/2} \rightarrow {}^6H_{13/2}$	3322.83	0.6358	
$^4F_{9/2} \rightarrow {}^6H_{15/2}$	1008.32	0.2329	
OFBDy1.5			

ted manuscript

$^4F_{9/2}\rightarrow{}^6H_{11/2}$	268.15	0.0676	3969.42
$^4F_{9/2}\rightarrow{}^6H_{13/2}$	2484.66	0.6260	
$^4F_{9/2}\rightarrow{}^6H_{15/2}$	798.69	0.2012	
OFBDy2.0			
$^4F_{9/2}\rightarrow{}^6H_{11/2}$	246.60	0.0699	3526.79
$^4F_{9/2}\rightarrow{}^6H_{13/2}$	2228.61	0.6319	
$^4F_{9/2}\rightarrow{}^6H_{15/2}$	671.44	0.1904	
OFBDy2.5			
$^4F_{9/2}\rightarrow{}^6H_{11/2}$	224.55	0.0762	2945.57
$^4F_{9/2}\rightarrow{}^6H_{13/2}$	1915.44	0.6503	
$^4F_{9/2}\rightarrow{}^6H_{15/2}$	472.34	0.1604	

Table 6

Emission peak wavelength (λ_p)(nm), effective band widths ($\Delta\lambda_p$)(nm), measured and experimental branching ratios (β_R & β_{exp}), stimulated emission cross-sections (σ_{se})(cm^2), gain band width ($\sigma_{se} \times \Delta\lambda_p$) ($cm^3$) and optical gain ($\sigma_{se} \times \tau_R$) ($cm^2$ s) for the emission transitions of Dy^{3+} ions in OFB glasses.

Spectral parameters	OFBDy0.1	OFBDy0.5	OFBDy1.0	OFBDy1.5	OFBDy2.0	OFBDy2.5
$^4F_{9/2} \rightarrow {}^6H_{15/2}$ (Blue) $\lambda_p = 486\ nm$						
$\Delta\lambda_p$	15.2	12.0	10.9	13.0	13.0	14.1
β_R	0.199	0.203	0.232	0.209	0.190	0.160
β_{exp}	0.532	0.545	0.586	0.541	0.538	0.517
σ_{se} (x 10^{-22})	12.3	18.3	26.5	17.5	14.8	9.61
$\sigma_{se} \times \Delta\lambda_p$ (x 10^{-28})	18.7	21.8	28.7	22.8	19.2	13.6
$\sigma_{se} \times \tau_R$ (x 10^{-25})	3.72	4.83	6.16	4.40	4.18	3.26
$^4F_{9/2} \rightarrow {}^6H_{13/2}$ (Yellow) $\lambda_p = 576\ nm$						
$\Delta\lambda_p$	14.1	13.0	12.0	13.0	14.1	15.2
β_R	0.620	0.629	0.635	0.626	0.631	0.650
β_{exp}	0.411	0.454	0.463	0.417	0.393	0.426

σ_{se} (x 10^{-22})	81.7	103.0	158.3	108.5	89.9	71.9
$\sigma_{se} \times \Delta\lambda_p$ (x 10^{-28})	115.2	135.4	189.7	141.2	127.0	109.1
$\sigma_{se} \times \tau_R$ (x 10^{-25})	24.8	27.3	36.8	27.2	25.4	24.4
$^4F_{9/2} \rightarrow {}^6H_{11/2}$ (Red) λ_p = 664 nm						
$\Delta\lambda_p$	21.7	17.4	13.0	15.2	19.6	21.7
β_R	0.067	0.068	0.068	0.067	0.069	0.076
β_{exp}	0.041	0.045	0.046	0.041	0.039	0.042
σ_{se} (x 10^{-22})	10.2	14.8	27.7	17.7	12.7	10.4
$\sigma_{se} \times \Delta\lambda_p$ (x 10^{-28})	22.3	25.7	36.1	26.9	24.8	22.7
$\sigma_{se} \times \tau_R$ (x 10^{-25})	3.10	3.91	6.45	4.44	3.59	3.53
$^4F_{9/2} \rightarrow {}^6H_{9/2}$ (IR) λ_p = 787 nm						
$\Delta\lambda_p$	15.2	13.0	8.69	10.9	15.2	19.6
β_R	0.051	0.047	0.046	0.047	0.050	0.056
β_{exp}	0.034	0.035	0.039	0.031	0.033	0.032
σ_{se} (x 10^{-22})	18.7	23.1	44.5	29.6	19.9	14.5
$\sigma_{se} \times \Delta\lambda_p$ (x 10^{-28})	28.5	30.1	38.7	32.2	30.3	28.3
$\sigma_{se} \times \tau_R$ (x 10^{-25})	5.68	6.09	10.4	7.44	5.64	4.90

Table 7: comparison of experimental branching ratios (β_{exp}) and stimulated emission cross-sections (σ_{se}) (x 10^{-22}) (cm^2) for Dy^{3+} doped OFB glasses at two different excitation wavelengths 410 and 350 nm.

Spectral parameters	OFBDy0.1		OFBDy0.5		OFBDy1.0		OFBDy1.5		OFBDy2.0		OFBDy2.5	
	λ_{exc}											
	410 nm	350 nm	410 nm	350 nm	410 nm	350 nm	410 nm	350 nm	410 nm	350 nm	410 nm	350 nm
$^4F_{9/2} \rightarrow {}^6H_{15/2}$ (Blue) λp=486nm												
β_{exp}	0.53	0.41	0.54	0.44	0.58	0.48	0.54	0.45	0.53	0.43	0.51	0.42
σ_{se} (x 10^{-22})	12.3	10.5	18.3	12.3	26.5	18.0	17.5	12.9	14.8	9.87	9.61	6.96
$^4F_{9/2} \rightarrow {}^6H_{13/2}$ (Yellow) λp=576nm												
β_{exp}	0.41	0.38	0.454	0.41	0.463	0.42	0.417	0.39	0.39	0.30	0.426	0.40
σ_{se} (x 10^{-22})	81.7	71.8	103.0	94.2	158.3	151.0	108.5	98.9	89.9	79.0	71.9	68.1
$^4F_{9/2} \rightarrow {}^6H_{11/2}$ (Red) λp=664nm												
β_{exp}	0.067	0.036	0.068	0.049	0.068	0.055	0.067	0.067	0.069	0.067	0.076	0.069
σ_{se} (x 10^{-22})	10.2	11.3	14.8	13.1	27.7	20.2	17.7	13.7	12.7	11.6	10.4	7.46

Accepted manuscript

ACCEPTED MANUSCRIPT

Table 8

Experimental (τ_{exp}) (μs)**,** radiative (τ_R) (μs) lifetimes, quantum efficiencies (η) and non-radiative decay rates (W_{NR}) for Dy^{3+} ions in OFB glasses

Name of the Sample	$^4F_{9/2} \rightarrow {}^6H_{15/2}$				$^4F_{9/2} \rightarrow {}^6H_{13/2}$			
	τ_{exp}	τ_R	η (%)	W_{NR}	τ_{exp}	τ_R	η (%)	W_{NR}
OFBDy0.1	172	303	56	2514	174	303	57	2447
OFBDy0.5	155	264	58	2664	158	264	59	2541
OFBDy1.0	132	191	69	2340	134	191	70	2227
OFBDy1.5	103	251	41	5725	105	251	41	5540
OFBDy2.0	87	283	30	7961	89	283	31	7702
OFBDy2.5	63	339	18	12923	66	339	19	12202

Table 9

The CIE color co-ordinates (CIE) and Yellow-Blue ($^4F_{9/2} \rightarrow {}^6H_{13/2}$ /$^4F_{9/2} \rightarrow {}^6H_{15/2}$ **,** Y/B) ratios for Dy^{3+} ions in OFB glasses at different wavelengths

Name of the Sample	CIE Co-ordinates				
	λ_{exc} =325 nm	λ_{exc} =350 nm	λ_{exc} =365 nm	λ_{exc} =387 nm	λ_{exc} =410 nm
OFBDy0.1	(0.298, 0.339)	(0.322,0.366)	(0.294,0.319)	(0.308,0.334)	(0.370, 0.396)
OFBDy0.5	(0.321, 0.356)	(0.339,0.384)	(0.316,0.360)	(0.332,0.376)	(0.340, 0.357)
OFBDy1.0	(0.326,0.342)	(0.330,0.375)	(0.301,0.343)	(0.324,0.367)	(0.338, 0.335)

Accepted manuscript

ACCEPTED MANUSCRIPT

OFBDy1.5	(0.325,0.355)	(0.325,0.355)	(0.319,0.340)	(0.332,0.375)	(0.370, 0.361)
OFBDy2.0	(0.314,0.350)	(0.426,0.483)	(0.243,0.323)	(0.276,0.321)	(0.425, 0.450)
OFBDy2.5	(0.337,0.371)	(0.346,0.383)	(0.310,0.352)	(0.342,0.377)	(0.436, 0.464)

Y/B Ratios

OFBDy0.1	1.13	1.19	1.08	1.18	2.45
OFBDy0.5	1.26	1.26	1.18	1.24	2.55
OFBDy1.0	1.20	1.27	1.19	1.24	2.56
OFBDy1.5	1.17	1.24	1.15	1.21	2.56
OFBDy2.0	1.16	1.27	1.11	1.19	2.50
OFBDy2.5	1.19	1.31	1.21	1.28	2.46

Accepted manuscript

ACCEPTED MANUSCRIPT

Table 10:

Comparison of Y/B ratios of OFBDy1.0 glass at different n-UV excitation wavelengths with other reported glasses

Name of the glass matrix	Y/B Ratio	Reference
OFBDy1.0 (λ_{exc} =325 nm)	1.20	Present system
OFBDy1.0 (λ_{exc} =350 nm)	1.27	Present system
OFBDy1.0 (λ_{exc} =365 nm)	1.19	Present system
OFBDy1.0 (λ_{exc} =387 nm)	1.24	Present system
OFBDy1.0 (λ_{exc} =410 nm)	2.56	Present system
LTTDy10	1.02	[44]
ZnAlBiB:Dy	1.18	[45]
ZnAlBiB:Dy	1.19	[46]
PTBDy10	1.085	[58]
L3BTAFDy	2.49	[59]
MgTP	1.20	[63]
B1TD	3.325	[68]
GC Glass	1.05	[69]
NAPDy1	2.90	[70]
PbFPDy10	0.63	[71]
Dy3+:NaCaPO4	0.75	[72]
Silicate	2.03	[73]
SLBiBDy10	0.97	[74]
PKAlCaFDy10	0.68	[75]

Accepted manuscript

Volume 1 (2013) 65-72 ISSN 2347 - 3258
International Journal of Advance Research and Innovation

Limnological Studies Related to Physico-Chemical Characteristics of Water in Anasagar Lake, Ajmer, Rajasthan

Abhas Jain *, S. K. Singh
Department of Environmental Engineering, Delhi Technological University, New Delhi, India

Article Info

Article history:
Received 1 July 2013
Received in revised form
15 July 2013
Accepted 22 July 2013
Available online 1 August 2013

Keywords

Physio-chemical parameters
Limnology
Anasagar Lake
Eutrophication

Abstract

The study deals with the seasonal limnological investigation related to physico-chemical characteristics of water of the Anasagar Lake in Ajmer (Rajasthan). The limnological parameters were tested following standard methods at three sampling sites/stations in the lake. The physico-chemical parameters (temperature, turbidity, pH, DO, BOD, COD, free CO_2, total alkalinity, conductivity, TSS, TDS, Chloride, Ammonia, Nitrate, Phosphate, etc.) showed distinct temporal or seasonal variation in the lake. Higher nutrient content (nitrate, phosphate) was present in the lake. This finding also signifies eutrophication/higher trophic level. Water transparency, dissolved oxygen, BOD, total alkalinity, conductivity, $CaCO_3$ hardness, TSS, nitrate and phosphate was correlated with various physico-chemical parameters in the lake. The physico-chemical characteristics of water of the lake revealed the poor water quality in Anasagar Lake.

1. Introduction

Water is one of the most important compounds that profoundly influence life. The quality of water is usually described according to its physical, chemical and biological characteristics. Rapid industrialization and indiscriminate use of chemical fertilizers and pesticides in agriculture are causing heavy and varied pollution in aquatic environment leading to deterioration of water quality and depletion of aquatic biota. Due to use of contaminated water, human population suffers.

Lake and their surrounding are unique assets and valuable ecosystems of society and nature. These are resources of social, cultural, and aesthetic value. Maintaining lake water quality helps maintaining healthy surroundings. But, an excessive introduction of nutrients by humans has led to severe eutrophication of certain freshwater systems worldwide. Anasagar Lake is one of them.

There has been a large fluctuation in the water quality of the Anasagar Lake. The lake has significant environmental problems. Around 30% of the city's population resides in the catchment area of the lake. The agricultural run-off and the municipal waste are washed of in the lake. Although, heavy rains in the last two-three years have improved some water quality parameters, but the lake water quality is still unfit for general water uses. Undesirable values of total dissolved solids, chloride, fluoride, BOD, total coliform organism's etc. makes the water unfit for drinking and other household uses.

Corresponding Author,
E-mail address: abhasjain01@gmail.com
All rights reserved: http://www.ijari.org

2. Study Area

Anasagar Lake was made in the 12th century by building a dam across the river Luni and was named after the ruler Anaji Chauhan who constructed the lake during 1135-1150 AD. Later, Mughal Emperor Jehangir contributed the Daulatbagh gardens and Shah Jehan built the Baradari. It is situated at the centre of the Ajmer city (74^0 38' - 74^0 42' and 26^0 25' - 26^0 29' N). Lake has a capacity of 4.75 million cubic metre upto a maximum depth of 4.4 m. It has a catchment area of 56 sq. kms.

Among the existing lakes in Ajmer, Anasagar Lake is the biggest one with the maximum catchment area. Foy Sagar is another major lake of the city. There are more than a dozen small ponds in the Ajmer city.

Table: 1. Geographical features of Anasagar Lake

Characteristics	Description
Geographical Location	74^0 38' - 74^0 42' and 26^0 25' - 26^0 29' N
Location in Ajmer	North West in Ajmer
Catchment Area	56 sq. km (gross), 20 sq. km (intercepted by foysagar), 5 sq. km (built up area)
Nature of catchment area	Steep to gentle slope with low vegetal cover
Storage capacity	4.75 million cubic meter (for max depth of 4.4 m
Circumference	4.81 km (Nov, 06), 7.3 km (maximum water level)
Depth	Maximum 4.4 m
Overflow arrangement	Four overflow gates of size 4' X 6'

3. Methodology

Three representative stations, (station - I, II and III) located in different stretches of the water area were selected for collection of water samples, considering the disturbance aspect on the water body such that the samples may provide reasonably representative status of water quality. The station were Centre of Electric tower (AW 1S), Floating Fountain (AW 2S) and Baradari (near boat house) (AW 3S). All the samples were collected at a fixed time, from 9 a.m. to 2 p.m. on a specified date during October- 2012 to August- 2013.

The methods of instrumentation and procedures for the analysis of the water samples were carried out elsewhere following the standard methods mentioned in the APHA, 21st Edition, 2005.

The testing of the chemical parameters in Anasagar Lake is carried out in a laboratory which is under National Lake Conservation Program (NLCP) (under Ministry of Environment and Forest (MoEF)). Permission for using the data has been obtained from Executive Engineer, UIT, Ajmer (Rajasthan).

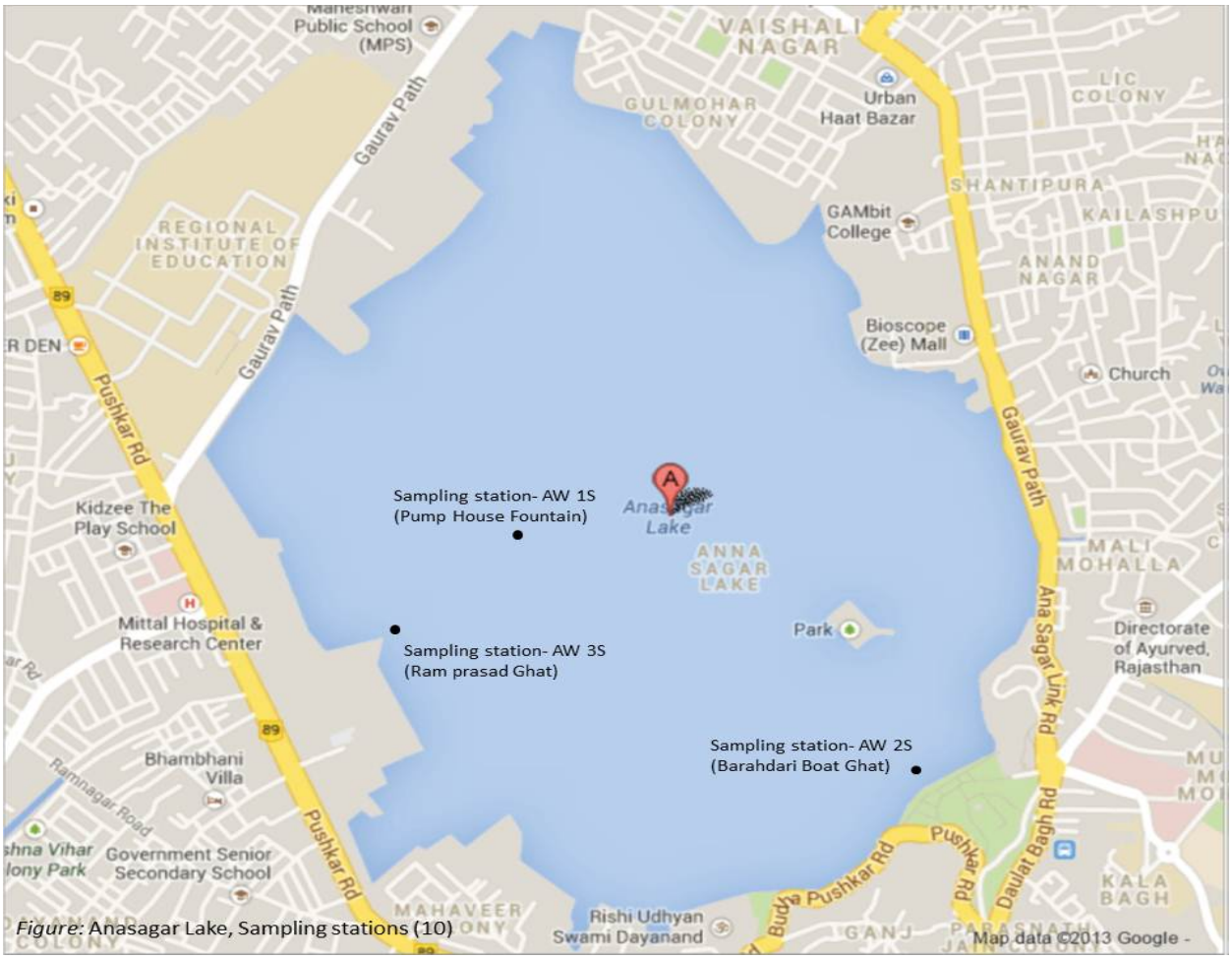

Figure: Anasagar Lake, Sampling stations (10)

4. Observations

There is a mutual agreement between Government of Rajasthan and MoEF for rejuvenating the lake's health. The samples from the lake are tested every month. Various parameters mentioned in the Table 2, Table 3 and Table 4 are obtained from the office under NLCP.

Temperature: Seasonal change was observed in the lake temperature. Minimum and maximum temperature recorded was 18.2^0 C and 29^0 C.

pH: Maximum and minimum values of 8.9 and 7.3 were recorded in the lake water. pH values are in accordance with earlier work by Wetzel (et al 1975) who reported that the value of pH ranges from 8 to 9 in Indian waters.

Turbidity: When water is cloudy, sunlight will warm it more efficiently because suspended particles absorb the sunlight, warming the water. This can lead to problems associated with increased water temperature

Dissolved Oxygen: DO level in the lake reached to almost negligible some years back in 2007-2008. Situation is now under control as the outflow channel gates' level has been increased and the area under lake has now increased, hence improving the dissolved oxygen in the lake (9).

Nitrates: Minimum and maximum values of Nitrates were 10.1 mg/L and 17.8 mg/L.

Electrical conductivity: In Anasagar, the value varied between the range 2140 to 3500 µmho/cm indicating high salt content.

Salinity: The water of Anasagar Lake is slightly saline as the average values were found to be above 1000 ppm throughout the monitoring period. Range of values observed was 1400-1700 ppm.

Chloride: Observed values were in the range 430-590 mg/l with an average of 510 mg/l.

5. Results And Discussions

The major problem of the lake relates to the advanced level of eutrophication due to heavy nutrient and pollution loading. Three four years back one of the problems was insufficient water in the lake. Scanty rainfall in the area was an obvious reason. But in the last two years, heavy rains over the city have improved overall quality of the lake water. But the quality of the lake water is still the same because of the simultaneous increase in pollutants inflow. The pollution loads of the lake originate from various point and non-point source and include nutrients and fecal coliform from sewage. Also, lechate from the waste adds to the bad health of the lake.

atmospheric oxygen by wind action and partly due to mechanical agitation (for example fountains

There was a seasonal Temperature change with maximum and minimum of 18.2^0 C and 29^0 C. The temperature has greater role in the dynamic of aquatic ecosystem. Temperature dictates the behavioral characteristics of organisms, solubility of gases and salts in water bodies. The bacterial action in a lake, which is responsible for the decomposition of organic matter for nutrient cycle, is directed by the temperature of the water. The hydrogen ion concentration of a body is generally controlled by the concentration of CO_2, which in turn is controlled by the photosynthetic activity of the producers (Hutchinson, 1857). High pH in the lake will have serious problems as high pH promotes cyanobacteria to form blooms. Anasagar Lake's pH has been recorded above the neutral scale and the values range was 7.3-9. The free CO_2 concentration in Anasagar Lake was found to be almost negligible. Low level of free CO_2 might be either due to its consumption in carbon assimilation or its complete conversion into carbonic acid and ultimately into stable carbonates and bicarbonates.

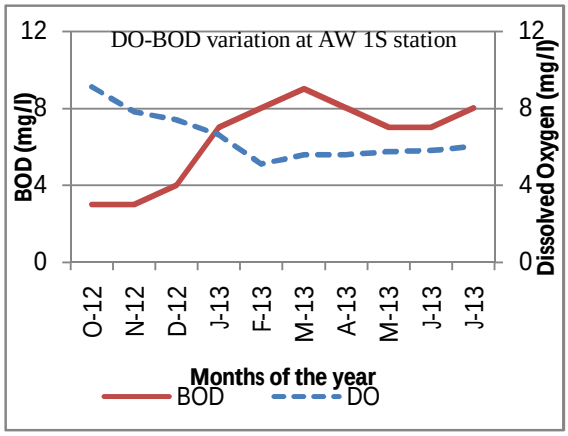

Fig: 1. Graph showing DO-BOD variation at the station AW 1S

The DO, an important physico-chemical parameter of water quality, has special significance for aquatic organisms in natural waters (7). The DO content in the Anasagar Lake's surface layers varies between 5.3 mg/l and 10 mg/l and the nature of variation at different sites is almost similar to that of variation of temperature (between 18.2^0 C and 29^0 C) and pH (between 7.3 and 9). The DO content in the surface layer is found to be higher with respect to higher water temperature, which has also been observed by several authors (8). The high amount of oxygen in the surface layers is due to the diffusion of and mechanical aerators placed in the lake) (9). Low DO in lakes is due to the presence of inorganic

reductants such as, H_2S, ammonia, nitrates, ferrous ions and other oxidisable substances.

The BOD, a widely accepted parameter in determining water quality, varies between 3 mg/l and 10 mg/l, which on an average is 6.5 mg/l, whereas the COD varies from 10 mg/l to 41 mg/l, with an average of around 25.5 mg/l. As calculated in the Table 5, the ratio of BOD to COD is very low (0.2 to 0.4), implying the presence of large portion of undegraded organic matter of refractory origin arising from allochthonous and autochthonous sources in the medium.

Phillipose (1960) was able to categorise lakes in to three categories based on the alkalinity values. According to his criteria, water with alkalinity range 4-50 mg/l are believed to be nutrient poor, 50-100 mg/l indicates moderate nutrient concentration and those having 100-600 mg/l concentrations are nutrient rich. As per his categorization, Anasagar Lake has high dissolved solids content with values ranging from 1400-1600 mg/l.

Nitrate ions (NO_3^-) found in water samples result from a variety of natural and manmade sources. Nitrates are an important source of nitrogen necessary for plants and animals to synthesize amino acids and proteins enter the lake ecosystem through run-off and decomposition of organic matter. In Anasasgar Lake the Nitrate level was 11 mg/l to 19 mg/l. The higher inflow of water and consequent land drainage cause high value of Nitrate. Nitrate level in freshwater is usually found in the range of 0.1 to 4 mg/L. Unpolluted waters generally have nitrate levels below 1 mg/L. The effluent of some sewage treatment plants may have levels in excess of 20mg/L. The city's municipal waste is released directly into the lake.

Nitrate ions (NO_3^-) found in water samples result from a variety of natural and manmade sources. Nitrates are an important source of nitrogen necessary for plants and animals to synthesize amino acids and proteins enter the lake ecosystem through run-off and decomposition of organic matter. In Anasasgar Lake the Nitrate level was 11 mg/l to 19 mg/l. The higher inflow of water and consequent land drainage cause high value of Nitrate. Nitrate level in freshwater is usually found in the range of 0.1 to 4 mg/L. Unpolluted waters generally have nitrate levels below 1 mg/L. The effluent of some sewage treatment plants may have levels in excess of 20mg/L. The city's municipal waste is released directly into the lake.

Low Conductivity (0 to 200 µmho/cm) is an indicator of pristine or background conditions. Mid-range conductivity (200 to 1000 µmho/cm) is the normal background for most major freshwater lakes. Conductivity outside this range could indicate that the water is not suitable for certain species of fish or bugs. High conductivity (1000 to 10,000 µmho/cm) is an indicator of saline conditions. Waters that have been heavily impacted by industry can fall into this range (13). The increase of E. C. in Anasagar Lake is an indication of the enrichment of the ions in water bodies which is may be due to natural sources or by the anthropogenic sources.

It was noticed that the concentration of Cl^- was high in the water of the lake. This could be attributed to evaporation from surface water leaving the relative high content of chloride (13). Chloride contamination in Lake Water is considerably harmful for humans to drink and irrigation at high levels, because it is made of chlorine chemically combined with heavy metals. The National River Water Quality (NRWQ) standard ranges from 45 to 155 mg/l. As observed, the chloride content is very high in Lake, indicates that Lake Anasagar water is not at all suitable for drinking and other aquatic organisms. Also, the chloride and EC relationship indicates that electrical conductivity is sharply increased with increasing chloride concentration in water.

Table: 2. BOD and COD ratio at the AW 1S station of Anasagar Lake

	BOD (mg/l)	**COD (mg/l)**	**BOD/COD**
Oct-12	4	15	0.27
Nov-12	3	11	0.27
Dec-12	3	10	0.30
Jan-13	9	29	0.31
Feb-13	8	32	0.25
Mar-13	7	33	0.21
Apr-13	9	28	0.32
May-13	7	28	0.25
Jun-13	7	26	0.27
July-13	7	21	0.33
Aug-13	10	41	0.24

6. Conclusions

The pH of the lake water is slightly high then the limits mentioned in the CPCB guidelines for the water use. DO of the lake water satisfy the bathing water quality criteria (for example Class B as per the CPCB and IS 2296, 1963) but the level of the BOD and coliform count are well above the permissible limits for human use. Thus, the water becomes unsuitable even for outdoor bathing. Samples collected adjacent to the lake bank show higher concentrations in the water quality parameters, as compared to the mid-

reach samples, implying the entry of the non-point sources and extreme thrust on the water body due to the anthropogenic activities. The water of Anasagar is not fit for 1-4 guidelines mentioned in CPCB. The quality of water in the lake has improved considerably over the last 5-6 years but it continues to be unfit for day-to-day human consumption.

	Temp	pH	Condu-ctivity	TSS	TDS	Total Solids	Chloride	DO	BOD	COD	Flouride	Nitrate	P	Phosphate	Total Coliforms	Fecal coliforms
	^{O}C	-	µmho/cm	mg/l	mg/l	mg/l	mg/l	mg/l	mg/l	mg/l	mg/l	mg/l	mg/l	mg/l	MPN/100 ml	MPN/100 ml
Oct-12	28	7.6	3040	42	1405	1447	490	10.7	3	14	0.1	11.12	0.68	0.28	5850	1100
Nov-12	24	7.8	2911	38	1446	1484	451	7.8	3	15	0.2	12.41	0.23	0.48	4990	1132
Dec-12	18	8.8	2631	16	1473	1489	457	7.4	4	17	1.0	14.43	0.35	1.05	3590	1200
Jan-13	21	8.9	2161	15	1513	1528	482	6.6	7	23	1.1	17.05	0.07	0.21	28301	2301
Feb-13	23	8.7	2241	21	1530	1551	503	5.1	8	28	1.2	17.33	0.12	0.55	11021	3012
Mar-13	27	8.6	2334	28	1540	1568	594	5.6	6	27	1.2	17.66	0.19	0.32	12110	4000
Apr-13	29	8.8	2616	16	1603	1619	498	5.6	10	31	1.1	11.13	1.07	1.74	24380	4032
May-13	34	8.6	2815	39	1707	1746	545	5.7	5	27	1.4	16.98	0.14	0.32	28443	4032
Jun-13	36	8.6	2715	29	1601	1630	531	5.8	7	29	1.4	17.1	0.21	0.41	30152	3800
Jul-13	28	8.5	2210	21	1445	1466	514	6	9	36	1.3	18.09	0.29	0.49	34127	3305
Aug-13	25	8.9	2350	21	1458	1479	433	8.9	8	32	1.1	14.64	0.09	0.12	34295	8083

Table 3: Physio-chemical parameters in Anasagar Lake, **Station- AW 1S**, October-2012 to August- 2013

	Temp	pH	Condu-ctivity	TSS	TDS	Total Solids	Chloride	DO	BOD	COD	Flouride	Nitrate	P	Phosphate	Total Coliforms	Fecal coliforms
	^{O}C	-	µmho/cm	mg/l	mg/l	mg/l	mg/l	mg/l	mg/l	mg/l	mg/l	mg/l	mg/l	mg/l	MPN/100 ml	MPN/100 ml
Oct-12	29	7.4	2400	26	1603	1629	452	7.1	4	15	0.1	13.22	0.26	0.24	14990	1500
Nov-12	23	7.5	2510	20	1500	1520	466	10.7	3	11	0.2	10.12	0.24	0.52	11260	1500
Dec-12	18	8.7	2752	15	1541	1556	471	8	3	10	1.7	11.09	0.31	0.08	11260	1500
Jan-13	20	8.8	2140	20	1498	1518	492	6.1	9	29	1.1	17.8	0.08	0.24	16556	2500
Feb-13	23	8.8	2218	22	1501	1523	501	5.3	8	32	1.2	15.54	0.1	0.36	17002	3510
Mar-13	27	8.7	2317	23	1504	1527	506	5.9	7	33	1.3	16.45	0.2	0.41	16060	5882
Apr-13	29	8.8	3055	14	1490	1504	488	5.6	9	28	1.1	13.35	0.92	1.72	28587	4032
May-13	34	8.5	2870	26	1684	1710	535	6.1	7	28	1.4	17.33	0.08	0.17	20218	3305
Jun-13	35	8.6	2510	18	1512	1530	521	5.5	7	26	1.4	17.41	0.22	0.34	18992	3102
Jul-13	28	8.6	2182	9	1478	1487	543	4.6	7	21	1.3	17.68	0.58	1.07	12151	4031
Aug-13	25	8.9	2598	24	1612	1636	429	7.7	10	41	1.1	14.9	0.18	0.3	40012	3305

Table 4: Physio-chemical parameters in Anasagar Lake, Station- **AW 2S,** October-2012 to August- 2013

	Temp	pH	Condu-ctivity	Turbidity	TSS	TDS	Chloride	DO	BOD	COD	Flouride	Nitrate	P	Phosphate	Free CO2	Total Coliforms	Fecal coliforms
	^{O}C	-	µmho/cm	NTU	mg/l	mg/l	mg/l	mg/l	mg/l	mg/l	mg/l	mg/l	mg/l	mg/l	mg/l	MPN/100 ml	MPN/100 ml
Oct-12	29	7.2	2910	7.8	9	1409	411	4.8	4	15	0.1	13.2	0.07	0.14	NIL	38834	7722
Nov-12	23	7.4	2700	6.1	11	1450	420	8.1	5	20	0.17	13.3	0.12	0.12	NIL	3590	1002
Dec-12	19	8.7	2650	3.9	10	1485	434	7.4	3	14	1.22	11.2	0.13	0.14	NIL	2062	734
Jan-13	21	8.8	2160	1.6	22	1512	506	4.2	9	29	1.11	17.9	0.75	0.80	NIL	28434	2305
Feb-13	25	8.5	2220	1.9	26	1520	530	5.1	6	24	1.12	15.2	0.18	0.50	NIL	10223	3055
Mar-13	27	8.6	2334	4.9	28	1540	594	5.6	6	21	1.17	17.7	0.19	0.32	NIL	7142	4000
Apr-13	28	8.7	2892	2.8	16	1578	498	5.6	8	26	1.05	10.7	0.91	0.80	NIL	34464	3305
May-13	35	8.5	2880	2.7	15	1732	563	6	4	19	1.39	16.8	0.12	0.36	NIL	20309	3305
Jun-13	35	8.6	2440	3.7	20	1604	560	5.4	6	21	1.25	14.6	0.16	0.37	NIL	24056	3500
Jul-13	27	8.9	2220	4.7	28	1513	552	4.3	7	25	1.27	15.5	0.15	0.38	NIL	28438	4032
Aug-13	25	8.7	2565	9.4	21	1590	433	5.1	11	29	1.13	15.4	0.12	0.10	NIL	34464	12124

Table: 5. Physio-chemical parameters in Anasagar Lake, **Station- AW 3S**, October-2012 to August- 2013

References

[1] Water Research Center, Stream Water Quality Importance of Temperature, by: Mr. Brian Oram, PG. http://www.water-research.net/Watershed/ temperature.htm

[2] Environment Canada: http://www.ec.gc.ca/eaudouce-freshwater/default.asp?lang=en&n=61A967F4-1

[3] Mohamed A.F. Toufeek and Mostafa A. Korium, 2009, Physicochemical Characteristics of Water Quality in Lake Nasser Water, Global Journal of Environmental Research 3 (3): 141-148, ISSN 1990-925X.

[4] Wetzel. 'The Oxygen Content in Freshwater' Limnology, M. Brown, 1983, p 172.

[5] APHA, AWWA, and WPCF, Standard Methods for the Examination of Water and Wastewater, 17th edition, American Public Health Association, Washington DC, U.S.A, 2000

[6] Wetzel, R.G., Limnology, W. B. Saunders Co., Philadelphia, USA, 74,1975

[7] A. Mazumdar, N. R. Samal, "Physico-chemical Characteristics of Water in a Shallow Lake", Rabindra Sarobar, Kolkata, 88, Sep 2007

[8] A L Ramanathan, R Ramesh, "Recent Trends in Hydro geochemistry", Capital Publishing Company, New Delhi, 2003, p 37, 2003

[9] A. L. Downing, Z. Turesdate. 'Some Factors Affecting Rate of Solution of Oxygen in Water', J App. Chem., 5, 1995, p 570

[10] https://maps.google.co.in/maps?hl=en&tab=wl , Map of Ajmer (Rajasthan), India- 305001.

[11] Rafiullah M. Khan, Milind J. Jadhav, I. R. Ustad, "Physicochemical analysis of triveni lake water of Amravati district in (MS) India", Bioscience Discovery, 3(1):64-66, Jan. ISSN: 2229-3469 (Print), 2012

[12] NEERI, A laboratory manual on water analysis, 1987

[13] A. Patra, K. B. Santra, C. K. Manna, Limnological Studies Related to Physico-Chemical Characteristics of Water of Santragachi and Joypur Jheel, W.B., India, Our Nature 8:185-203, 2010

[14] R. Purohit, S. P. Singh, Seasonal Variation in Physio-chemical Limnology of Shalow zones of Nainital Lake, Western Himalaya, Proc, Indian natn, Sci. Acad., B47, No. 2 pp 194-203, 1981.

[15] S. Jain, G. Sharma, "Effects of Pesticides on hormone and enzyme systems of aqua population: a view over Anasagar lake, Ajmer", IOSR Journal of Environmental Science, Toxicology and Food Technology (IOSR-JESTFT) ISSN: 2319-2402, ISBN: 2319-2399, 1 (5) (Nov. - Dec.), PP 24-28, 2012

[16] Patil Shilpa G., Chonde Sonal Goroba, "Study of physicochemical and biological characteristics of lakes from Shivaji University Campus", Kolhapur, Maharashtra, Pelagia Research Library, Advances in Applied Science Research, 2 (6):505-519, 2011

[17] R. Jacklin Jemi, G.S. Regini Balasingh, "Studies on physico-chemical characteristics of freshwater temple ponds in Kanyakumari district", South Tamilnadu

[18] Pond and lake Management, Otterbine Barebo, Inc

[19] Rajasthan Travel Guide, http://www.indianholiday.com/tourist-attractions/rajasthan/ajmer.

[20] P. Mathur, S. Patan, "Assessment of Physico-chemical properties of Anasagar lake of Ajmer (India)", Journal of Environmental Research And Development 4(3), Jan-Mar 2010

ISBN 978-93-5156-328-0
International Conference of Advance Research and Innovation (ICARI-2014)

Multiple Criteria Decision Making Techniques in Manufacturing Industries-A Review Study with the Application of Fuzzy

A K Madan *, Ranganath M S
Department of Mechanical Engineerng, Delhi Technological University, Delhi, India

Article Info

Article history:
Received 29December 2013
Received in revised form
10 January 2014
Accepted 20 January 2014
Available online 1 February 2014

Keywords
Fuzzy Logic
AHP
TOPSIS
Fuzzy MCDM

Abstract

Manufacturing industries are facing stiff market competition, work pressures and a very competitive environment. This has forced them to be alert and take the desired decisions in order to achieve their goals. In this paper, a review study has been made on MCDM techniques in Manufacturing Industries. We found that the managers and engineers of the industries face a number of problems and situations in which decision making is very difficult and the margin of safety is very less. Any wrong decision would lead to losses. These situations are mainly of multiple criteria decision making, in which decision has to be taken by analyzing various criteria's and them select the best alternatives among various alternatives present to him. These situations become more tough and complex when the data available for the analysis is not precise. The data is in imprecise form and vague. This requires use of Fuzzy Logic techniques to deal with these types of data. In order to overcome both the problems, the paper proposes Fuzzy MCDM techniques which can deal with these situations.

1. Introduction

Globalization has made a significant effect in the current market scenario. It has resulted in immense competition in the market among the manufacturing industries. Companies are forced to be very careful in decision making due to limited resources, stiff competition, etc. factors that affect the working of the organization in an efficient and effective manner. Any waste of resources such as money, time, workforce, etc., due to inappropriate decisions, directly increases the costs of companies, which, in turn, affects the customers. The manufacturing industries are presently being affected by the structural changes caused due to the internal and external factors of an enterprise. The market conditions are becoming more dynamic, more global, and more customers driven. The manufacturing performance is no longer driven by the product price; instead other competitive factors such as flexibility, quality, delivery, and customer service have become equally important. The demand of the customer for tailored product has resulted in a shorter product life, reduced batch quantities and increased product varieties. Manufacturing firms need to give prominence to issues such as reduction of manufacturing lead time and flexibility to adapt to changes in the market. The improvement in productivity and reduction of costs of goods and services has become the key for maintaining the market share.

Real world engineering is full of chaotic disturbances, randomness and complex non-linear dynamics. Conventional methods such as trial and error are often used to solve complex optimization problems. This approach relies on the use of the analyst's qualitative knowledge to explore the design space. Expensive advanced computational analyses (such as finite element) are also used to understand the behavior of complex engineering problems. These are often invoked repeatedly during the search process making the optimization and concept exploration time consuming. This traditional search method often results in sub-optimal solutions due to inherent limitations in incomplete knowledge representation and the fact that elaborate exploration of the design space is inhibited. Competitive market conditions have forced the manufacturing industries to make carefuldecisions. Any waste of resources such as

Corresponding Author,
E-mail address: ashokmadan79@gmail.com
All rights reserved: http://www.ijari.org

money, time, workforce, etc., due to inappropriate decisions, directly increases the costs of companies, which, in turn, is reflected to the customer.

There is a tendency to accept local optimal solutions considered to be sufficiently good for the chosen objective due to the following reasons: subjective judgment, similarity to historical result or simply constraint on time to deliver workable solutions. Multiple global optimal solutions are desirable for these classes of problems to give alternative solutions in the presence of increasing dynamic and ill-defined problem space.

In the current competitive business scenario, one of the key requirements on global as well as local firms is to provide their markets with products and services at lower costs, at a higher quality, with a shorter product development cycle, and with a shorter delivery time. In order to achieve these objectives, several important and critical decisions have to be taken at a tactical as well as a strategic level. Economic justification methods, such as return on investment, or analytic justification methods, such as linear programming, are frequently employed before making decisions involving significant investment decisions. It is important to note that irrespective of the kind of evaluation – economic or analytic – the information available for making the decision is generally vague and uncertain. It is very difficult to obtain exact data on attributes like investment cost, expenses, project lifetime, depreciation, etc. for making these decisions. Hence, these evaluation methods tend to be less effective in delivering required information in such an imprecise, or fuzzy, decision environment.

To tackle the problem mentioned above, fuzzy set theory can play a significant role. The approximate reasoning of fuzzy set theory can properly represent linguistic terms [1]. To deal quantitatively with imprecision and uncertainty, all of the assessment data can be specified as triangular fuzzy numbers [2, 3]. Subsequently, a fuzzy multi-criteria decision-making (MCDM) method can be applied to integrate various linguistic assessments and weights in order to determine the best selection. In contrast to traditional approaches, which tend to adopt only one specific evaluation technique, an integrative approach is proposed, combining strategic, economic, and analytic justification approaches.

2. Decision Making

A decision is a choice made from two or more alternatives. Decision-making is the process of sufficiently reducing uncertainty and doubt about alternatives to allow a reason able choice to be made among them. Researchers have studied different decision-making problems by using different decision-making methods such as the analytic hierarchy process (AHP), fuzzy multiple-attribute decision making model, linear and 0 – 1 integer programming models, genetic algorithms (GA), etc.

The analysis of the way the people makes decisions (prescriptive theories) or the way people ought to make decisions (normative theories) is perhaps as old as the recorded history of mankind. The development of the development of the perfect decision making method for rational real life decision making still remains an elusive goal. The contradiction between the extensiveness of the study on this subject and the elusiveness of the final goal of the real life applicability of the findings constitutes in a way the ultimate decision making paradox.

Decision making is one of the main abilities of human being that differs them from other creatures. Now, decision making and analysis is an important part of management sciences, and it is perhaps as old as history of mankind. In many real-world problems, the decision maker likes to pursue more than one target or consider more than one factor or measure. Such a desire transforms the decision making problem to a multi-objective decision making (MODM) problem or a multi-attribute decision making (MADM) problem. These groups of problems all come together in one category, named multi-criteria decision making (MCDM) problems.

Multi-Criteria Decision Making (MCDM) is one of the most well-known branches of decision making. MCDM is divided into multi-objective decision making (MODM) and multi-attribute decision making (MADM). However, very often the terms MADM and MCDM are used to mean the same class of models (i.e. MCDM).

MODM studies decision problems in which the decision space is continuous. An example is mathematical programming problems with multiple objective functions. MCDM/MADM concentrates on the problems with discrete decision spaces. In these problems, the set of decision alternatives have been predetermined.

Alternatives are the different choices of action available to the decision maker. The set of alternatives are assumed to be finite ranging from several to hundreds. They are supposed to screened, prioritized and eventually ranked according to the weights obtained.

Multiple attributes are the main constituent of the MCDM problems. The attributed can also be referred as goals or decision criteria. Attributes represent the different dimensions from which the alternatives can be viewed.

A Decision making problem can be defined as the process of finding the best alternative from all of the feasible alternatives available for the decision maker (DM). This means that the DM encounters a number of MCDM problems. In these kinds of problems the multiplicity of criteria for judging the alternatives is found to be pervasive.

3. Need of Fuzzy MCDM in Manufacturing Industries

Manufacturing organizations are very challenging as they involve in number of multiple activities. In order to achieve best results all the multiple activities must be properly planned, designed, coordinated and executed through a collective effort. The managers of the company may be an expert in their respective areas, all the persons has to work collectively in order to achieve the desired goals. Hence only an efficient and productive organization can survive in today's competitive environment. We all know that a manufacturing industry faces a number of day to day challenges. In order to sustain decision making is an important aspect of the industry.

Managers confront with a number of problems which involves decision making in multiple criteria situations i.e the manager has to decide among a set of alternatives present in front of him. They may occur with fuzzy nature i.e the data available to the manager is not precise and exact. Hence these types of problems require special attention because decision making is very important. A bad decision can result into heavy loses to the industry and this in turn will affect the customers also. In order to deal with these types of situations Fuzzy MCDM techniques have been proposed which take into account both the fuzzy nature of the problem and the multiple criteria confronted by the managers. Use of these techniques help in reaching to a best optimal solution which takes into account all the alternatives present in front of him.

Some of the areas which require Fuzzy MCDM techniques in the manufacturing industry are:

Selection of best Supply Chain

- Vendor Selection
- 3PL selection
- Machine Tool selection
- Plant/Site Selection for a new plant, etc.

Fuzzy MCDM methods help the decision makers to take best decisions. They are like an aid in the decision making in fuzzy and multiple criteria environment. An appropriate decision taken results into best results in the field and hence will add to the profits of the organization.

Fuzzy MCDM technique has been discussed in details later.

The main steps of multiple criteria decision making are as follows:

a) Establishing system evaluation criteria that relate system capabilities to goals.
b) Developing alternative systems for attaining the goals (generating alternatives).
c) Evaluating alternatives in terms of criteria (the values of the criterion functions)
d) Applying a normative multi-criteria analysis method.
e) Accepting one alternative as ‘‘optimal’’ (preferred).
f) If the final solution is not accepted, gather new information and go into the next iteration of multi-criteria optimization.

Steps (a) and (e) are performed at the upper level, where decision makers have the central role, and the other steps are mostly engineering tasks. For step (d), a decision maker should express his/her preferences in terms of the relative importance of criteria, and one approach is to introduce criteria weights. These weights in MCDM do not have a clear economic significance, but their use provides the opportunity to model the actual aspect s o f decision making (the preference structure). Various MCDM techniques have been discussed below.

4. Classification of MCDM Methods

Multiple criteria decision-making (MCDM) [35] is one of the most well-known branches of decision-making. It refers to making decisions in the presence of multiple, usually conflicting, objectives. The basic idea behind MCDM is the construction of a decision tree using a selection of criteria relevant to a particular decision and the weighting scoring of the criteria and the alternatives for each different criterion.

Various MCDM methods are:

1. Weighted Sum Model (WSM)
2. Weighted Product Model (WPM)
3. Analytic Hierarchy Process (AHP)
4. Revised AHP Method
5. ELECTRE Method
6. TOPSIS Method

5. Analytic Hierarchy Process AHP

The analytic hierarchy process (AHP) was developed by Thomas L. Saaty (36). The AHP is designed to solve complex problems involving multiple criteria. An advantage of the AHP is that it is

designed to handle situations in which the subjective judgments of individuals constitute an important part of the decision process.

Basically the AHP is a method which involves various processes. They are as follows:

1. Breaking down a complex, unstructured situation into its component parts.
2. Arranging the parts, or variables into a hierarchic order.
3. Assigning numerical values to subjective judgments on the relative importance of each variable and
4. Synthesizing the judgments to determine which variables have the highest priority and should be acted upon to influence the outcome of the situation.

5.1 Advantages of AHP

AHP provides a single easily understood, flexible model for a wide range of unstructured problems.

- It enables people to refine their definition of a problem and to improve their judgment and understanding through repetition.
- It does not insist on consensus but synthesizes a representative outcome from diverse judgments.
- It takes into consideration the relative priorities of factors in a system and enables people to select the best alternative based on their goal.
- It leads to an overall estimate of the desirability of each alternative.
- It integrates deductive and system approaches in solving complex problems.
- It can deal with the interdependence of the elements in a system and does not insist on linear thinking.
- It reflects the natural tendency of the mind to sort elements of a system into different levels and to group like elements in each level.
- It provides a scale for measuring intangibles and a method for establishing priorities.
- It tracks the logical consistency of judgments used in determining priorities.

5.2 Disadvantages of AHP

- Linear hierarchy structure
- Static decision evaluation
- Independence assumption among criteria
- Simple matrix algorithm to find maximum eigen-value
- No feedback mechanism

6. Fuzzy AHP

Analytic hierarchy process (AHP) has been widely used as a useful multiple criteria decision making (MCDM) tool or a weight estimation technique in many areas such as selection, evaluation, planning and development, decision making, forecasting, and many more. The traditional AHP requires exact judgments. However, due to the complexity and uncertainty involved in real world decision problems, a decision maker (DM) may sometimes feel more confident to provide fuzzy judgments than exact comparisons.

7. Fuzzy TOPSIS

TOPSIS is called technique for order preference by similarity to ideal solution. It is very effective in multi-criteria decision making (MCDM). It was developed by Yoon and Hwang in 1980 [58] as an alternative to other MCDM methods. The basic concept of this method is that the alternative should have the shortest distance from the ideal solution and farthest distance from the negative-ideal solution in some geometrical case. Positive ideal solution is a solution that maximizes the benefit criteria and minimizes cost criteria, whereas the negative ideal solution maximizes the cost criteria and minimizes the benefit criteria

The TOPSIS method assumes that each criterion has a tendency of monotonically increasing and decreasing utility. Therefore, it is to define the ideal and negative-ideal solutions. The Euclidean distance approach was proposed to evaluate the relative closeness of the alternatives to the ideal solution. Thus, the preference order of the alternatives can be derived by a series of comparisons of these relative distances.

In the classical TOPSIS method, the weights of the criteria and the ratings of alternatives are known precisely and crisp values are used in the evaluation process. However, under many conditions crisp data are inadequate to model real-life decision problems. Therefore, the fuzzy TOPSIS method is proposed where the weights of criteria and ratings of alter natives are evaluated by linguistic variables represented by fuzzy numbers to deal with the deficiency in the traditional TOPSIS. There are necessary steps in utilizing TOPSIS involving numerical measures of the relative importance of various criteria and the performance of each alternative with respect to these criteria. However, exact numerical data are inadequate to model real life situations since human judgments are often vague under many conditions. This method has been successfully used in land use planning project, venture

evaluation of project, the evaluation of hospital performance, optimal material selection, Etc., it makes the evaluation decision more scientific, accurate and operable.

8. Literature Review

De Grann (1980) first adopted triangular fuzzy numbers in the traditional AHP. Then in 1983, Van Laarhoven and Pedrycz [37] extended and modified the fuzzy AHP approach of De Grann (1980) by using extended theory and approximation theory. Buckley in 1985 addressed the concept of consistency into fuzzy AHP model.

A number of methods have been developed to handle fuzzy comparison matrices. Some of them are given below:

- Logarithmic least squares method (LLSM) [38], to obtain triangular fuzzy weights from a triangular fuzzy comparison matrix.
- Geometric mean method to calculate fuzzy weights [39].
- Extent analysis method by Chang [40], which derives crisp weights for fuzzy comparison matrices.
- Fuzzy preference programming method (PPM), by Mikhailov [41].
- Lambda-Max method, which is the direct fuzzification of the well-known kmax method by Csutora and Buckley [42].

Among the above approaches, the extent analysis method has been employed in quite a number of applications due to its computational simplicity. However, such a method is found unable to derive the true weights from a fuzzy or crisp comparison matrix. The weights determined by the extent analysis method do not represent the relative importance of decision criteria or alternatives at all. Therefore, it should not be used as a method for estimating priorities from a fuzzy pair wise comparison matrix

Many fuzzy AHP methods have been proposed by various authors. These methods are systematic and useful approaches to the alternative selection and gives justification to the problem by using the concepts of fuzzy set theory and hierarchical structure analysis. Decision makers have experienced that it is more confident and easy to give interval judgments than fixed value judgments. This is due to the fuzzy nature of the comparison process.

The earliest work in fuzzy AHP was by Van Laarhoven and Pedrycz (1983) [37], which compared fuzzy ratios described by triangular membership functions.

Stam et al. (1996) [43] explore, how recently developed artificial intelligence techniques can be used to determine or approximate the preference ratings in AHP. They concluded that the feed-forward neural network formulation appears to be a powerful tool for analyzing discrete alternative multi-criteria decision problems with imprecise or fuzzy ratio-scale preference judgments. Chang (1996) [44] introduces a new approach for handling fuzzy AHP, with the use of triangular fuzzy numbers for pairwise comparison scale of fuzzy AHP, and the use of the extent analysis method for the synthetic extent values of the pairwise comparisons.

Cheng (1997) [45] proposes an algorithm for evaluating naval tactical missile systems by the fuzzy AHP based on grade value of membership function.

Weck et al. (1997) [46] gave a method to evaluate different production cycle alternatives adding the mathematics of fuzzy logic to the classical AHP. Any production cycle evaluated in this manner yields a fuzzy set. The outcome of the analysis can finally be defuzzified by forming the surface centre of gravity of any fuzzy set, and the alternative production cycles investigated can be ranked in order in terms of the main objective set.

Kahraman et al. (1998) [47] employed a fuzzy objective and subjective method obtaining the weights from AHP and make a fuzzy weighted evaluation. Deng (1999) [48] presents a fuzzy approach for tackling qualitative multi-criteria analysis problems in a simple and straight forward manner. Lee et al. (1999) [49] review the basic ideas behind the AHP. Based on these ideas, they introduce the concept of comparison interval and propose a methodology based on stochastic optimization to achieve global consistency and to accommodate the fuzzy nature of the comparison process. Cheng et al. (1999) [50] propose a new method for evaluating weapon systems by analytical hierarchy process based on linguistic variable weight. Zhu et al. (1999) [51] make a discussion on extent analysis method and applications of fuzzy AHP.

Chan et al. (2000a) [52] presented a technology selection algorithm to quantify both tangible and intangible benefits in fuzzy environment. They describe an application of the theory of fuzzy sets to hierarchical structural analysis and economic evaluations. By aggregating the hierarchy, the preferential weight of each alternative technology is found, which is called fuzzy appropriate index. The fuzzy appropriate indices of different technologies are then ranked and preferential ranking orders of technologies are found. From the economic evaluation perspective, a fuzzy cash flow analysis is employed. Chan et al. (2000b) [53] report an integrated approach

for the automatic design of FMS, which uses simulation and multi-criteria decision-making techniques. The design process consists of the construction and testing of alternative designs using simulation methods. The selection of the most suitable design (based on AHP) is employed to analyze the output from the FMS simulation models. Leung and Cao (2000) [54] propose a fuzzy consistency definition with consideration of a tolerance deviation. Essentially, the fuzzy ratios of relative importance, allowing certain tolerance deviation, are formulated as constraints on the membership values of the local priorities. The fuzzy local and global weights are determined via the extension principle. The alternatives are ranked on the basis of the global weights by application of maximum–minimum set ranking method.

Kuo et al. (2002) [55] develop a decision support system for locating a new convenience store. The first component of the proposed system is the hierarchical structure development for fuzzy analytic process.

In the year 2003, CengizKahraman et al. (2003) [56], employed fuzzy AHP technique for comparison of catering service companies. He carried out the process on certain main and sub attributes which were proposed by experts that are required in a catering firm. He then proposed the best firm out of the three firms presented and also concluded that fuzzy AHP can be effectively applied in the given field.

A brief literature review about the fuzzy TOPSIS technique has been discussed below.

Jahanshaloo et al. [59] developed an algorithmic method to extend TOPSIS for decision making problems with interval data. Yang and Hung [60] utilized TOPSIS for solving a plant layout design problem. In particular, Wang and Lee [61] proposed two operator Up and Lo to find positive-ideal and negative-ideal solutions and used these operators to solve fuzzy multiple-criteria group decision making problem.

Chen and Tsao [62] extended the concept of TOPSIS to develop a method for solving MADM problems with interval-valued fuzzy data and compared the results using different distance measures, including Hamming distance, Euclidean distance and their normalized forms.

9. Conclusion & Future Scope

Globalization has made a global impact on the current market scenario. It has resulted in immense competition in the market among the manufacturing industries. In this competitive environment everyone is trying to compete in the market. In order to achieve the desired goals industries have to make a lot of major changes that would help in increasing their productivity, reducing lead times, improving quality, etc. This requires the managers and the engineers to take appropriate decisions very rapidly that would help in growth of the industry. Any waste of resources such as money, time, workforce, etc., due to inappropriate decisions, directly increases the costs of companies, which, in turn, affects the customers.

In many real-time problems in the industries, managers and engineers are faced with situations where multiple criteria has to be taken into account while selecting the best alternative or solution to that situation among various alternatives available to him. The situations can be the following have been listed earlier in the work.

In these cases careful decision has to be taken by doing various analyses in order to select the best alternative or solution that would not harm the industry and would lead to industrial growth. So these types of problems are known as Multi-Criteria Decision Making (MCDM) problems and hence require the use of MCDM techniques (AHP, WSM, ELECTRE, TOPSIS, etc.) to find their solutions.

Not all of the decision data can be precisely assessed. When information is easily measurable or accessible, the information should be coded in crisp (real) numbers. For those data that cannot be precisely obtained or is too costly to assess, fuzzy numbers are used to denote them. Fuzzy set theory makes it possible to incorporate un-quantifiable information, incomplete information, non-obtainable information, and partially ignorant facts into the decision model.

The above discussion depicts the need of both MCDM and Fuzzy methodology. In this work a systematic and an integrated approach has been proposed and discussed incorporating both the techniques and are called Fuzzy MCDM techniques. The advantages of this new approach over the existing ones are as follows:

- Conventional approaches, both deterministic and stochastic, tend to be less effective in conveying the imprecision or vagueness of the linguistic assessment.
- By using the concepts of fuzzy numbers and linguistic variables, the objective and subjective factors are evaluated in such a manner that the viewpoints of an entire decision-making body can be expressed with minimal constraints.
- The proposed approach allows multiple criteria decision making problems to take data in the form of linguistic terms, fuzzy numbers, and/or crisp numbers. This facilitates more realistic decision models compared to those generated using existing methods to be created.

- Triangular fuzzy numbers are mathematically easy to implement in comparison to trapezoidal fuzzy numbers and the mathematical computations are reduced. The easy-to-use and easy-to-understand characteristics of this new approach provide a valuable evaluation tool for management and system analysts.

Some research areas that require special attention in the future have been identified. In a decision process, conflict, uncertainty, fuzziness, imprecision, and randomness simultaneously exist.

- Due to its complex nature, research on searching and solving multiple criteria decision-making problems is suggested.
- Since the proposed methodology is generic enough for other decision-making processes, applications of the proposed methodology to other business or engineering problems are encouraged.
- Ranking approaches are very important to solve fuzzy or imprecise attributes and constraints. It is worth noting that even though most of the existing ranking methods are not perfect, they have shown the process of human efforts to find ways of solving problems. There are always some benefits produced by each method. Recognizing and continuing the effort in improving these methods is necessary.
- Flawless ranking methods may possibly be obtained by combining some of the good points of each of these methods into one algorithm. In this connection, searching for better ranking methods is urgently needed to solve fuzzy or imprecise constraints and other problems.

References

[1] L. A. Zadeh, "The concepts of linguistic variable and its application to approximate reasoning", InfSci 8(1):199–249, 1975

[2] G. S. Liang, M. J. Wang, "A fuzzy multi-criteria decision making method for facility site selection. Int J Prod Res 29(11):2313–2330, 1991

[3] T. R. Prabhu, K. Vizayakumar "Fuzzy hierarchical decision making method (FHDM): A methodology for technology choice", Int J ComputApplTechnol 9(5):322–329, 1996

[4] Z. C. Lin, C. B. Yang, "Evaluation of machine selection by the AHP method. Journal of Materials Processing Technology", 57, 253–258, 1994

[5] M. T. Tabucanon, D. N. Batanov, D. K. Verma, "Intelligent Decision Support System (DSS) for the selection process of alternative machines for Flexible Manufacturing Systems (FMS)", Computers in Industry, 25, 131–143, 1994

[6] A. Atmani, R. S. Lashkari, "A model of machine tool selection and operation allocation in flexible manufacturing systems", International Journal of Production Research, 36, 1339–1349,

[7] Devedzic Goran B., Pap Endre, "Multicriteria-multistages linguistic evaluation and ranking of machine tools", Fuzzy Sets and Systems 102, 451-61

[8] T. Y. Wang, C. F. Shaw, Y. L. Chen, "Machine selection in flexible manufacturing cell: A fuzzy multiple attribute decision making approach", International Journal of Production Research, 38, 2079–2097, 2000

[9] M. C. Arslan, B. Catay, E. Budak, "A decision support system for machine tool selection", Journal of Manufacturing Technology Management, 15, 101–109, 2004

[10] M. Yurdakul, "AHP as a strategic decision-making tool to justify machine tool selection", Journal of Materials Processing Technology, 146, 365–376, 2004

[11] C. Chung, Q. Peng. "The selection of tools and machines on web-based manufacturing environments", International Journal of Machine Tools & Manufacture 44 317–326, 2004

[12] M. Yurdakul, "AHP as a strategic decision-making tool to justify machine tool selection", Journal of Materials Processing Technology 146 365–376, 2006

[13] H. Chtourou, W. Masmoudi, A. Maalej, "An expert system for manufacturing systems machine selection", Expert Systems with Applications 28 (2005) 461–467, 2005

[14] Z. Ayag, R. G. Ozdemir, "A fuzzy AHP approach to evaluating machine tool alternatives", Journal of Intelligent Manufacturing, 17, 179–190, 2006

[15] Z. Ayag, "A hybrid approach to machine tool selection through AHP and simulation", International Journal of Production Research, 45(9), 2029–2050, 2007

[16] E. Çimren, B. Çatay, E Budak, "Development of a machine tool selection system using AHP", Int. J Adv Manuf. Technology 35:363 – 376 DOI 10.1007/s00170-006-0714-0, 2007

[17] O. Duran J. Aguilo, "Computer-aided machine-tool selection based on a Fuzzy-AHP approach", Expert Systems with Applications 34 (2008) 1787–1794, 2008

[18] Z. Ayag, R. G. Ozdemir, "An intelligent approach to machine tool selection through fuzzy

analytic network process", J IntellManuf DOI 10.1007/s10845-009-0269-7, 2006
[19] M. Alberti, J. Ciurana, C. A. Rodríguez, "Özel T, "Design of a decision support system for machine tool selection based on machine characteristics and performance tests", J IntellManuf DOI 10.1007/s10845-009-0286-6, 2009
[20] M. Yurdakul, Y. Tansel, "Analysis of the benefit generated by using fuzzy numbers in a TOPSIS model developed for machine tool selection problems", Journal of materials processing technology 2 0 9 (2009) 310–317, 2009
[21] K. P. Jarboe, "Location decisions of high-technology firms: a case study", Technovation, 4, pp. 117–129, 1986
[22] G. A. Spohrer, T. R. Kmak, "Qualitative analysis used in evaluating alternative plant location scenarios" Industrial Engineering, pp. 52–56, 1984
[23] J. A. Tompkis, J. A. White, Facilities Planning, John Wiley, 1984
[24] M. D. Dahlberg, J. H. May, "Linear programming for siting of energy facilities. Journal of Energy Engineering, pp. 5–14, 1980
[25] K. Yoon, C. L. Hwang, "Manufacturing plant location analysis by multiple attribute decision making: single-plant strategy", International Journal of Production Research, 23, pp. 345–359, 1985
[26] L. A. Zadeh, "The concept of a linguistic variable and its application to approximate reasoning, Part 1, 2 and 3", Information Science, 8, pp. 199–249, pp. 301–357 1975; 9, 43–80, 1976
[27] G. S. Liang, M. -J. J Wang, "A fuzzy multi-criteria decision making method for facility site selection", International Journal of Production Research, 29, pp. 2313–2330, 1991
[28] J. Yang, H. Lee, "An AHP decision model for facility location selection", Facilities 15(9/10)· pp. 241–254 © MCB University Press · ISSN 0263-2772
[29] T.-C. Chu, "Selecting Plant Location via a Fuzzy TOPSIS Approach", Int J Adv ManufTechnol 20:859–864, 2002
[30] K. F. Au, W. K. Wong, X. H. Zeng, "Decision model for country site selection of overseas clothing plants", Int J Adv ManufTechnol DOI 10.1007/s00170-004-2505-9, 2005
[31] D. Yong, "Plant location selection based on fuzzy TOPSIS", Int J Adv ManufTechnol 28: 839–844 DOI 10.1007/s00170-004-2436-5, 2006
[32] C. H. Chen, W. Y. Yu, "Using a strategic approach t o analysis the location selection for high-tech fir ms in Taiwan", Management Research News 31(4), pp. 228-244. 0140-9174 DOI 10.1108/01409170810851311, 2008
[33] Z. R. Farahani, M. SteadieSeifi, N. Asgari "Multiple criteria facility location problems: A survey. Applied Mathematical Modelling 34, 1689–1709, 2010
[34] L. Zadeh, "Fuzzy sets", Information Control 8, 338–353, 1965
[35] Book title: - "Multi-Criteria Decision Making Methods: a Comparative Study". By: Evangelos Triantaphyllou
[36] T. L. Satty, "The Analytical Hierarchy Process"
[37] P. J. M. Van Laarhoven, W. Pedrycz, "A fuzzy extension of Saaty's priority theory. Fuzzy Sets and Systems", 11,229–241, 1983
[38] M. Weck, F. Klocke, H. Schell, E. R. uenauver, "Evaluating alternative production cycles using the extended fuzzy AHP method", European Journal of Operational Research 100 (2), 351–366, 1997
[39] U. Cebeci, C. Kahraman, "Measuring customer satisfaction of catering service companies using fuzzy AHP: The case of Turkey", Proceedings of International Conference on Fuzzy Systems and Soft Computational Intelligence in Management and Industrial Engineering, Istanbul, 29–31May, pp. 315–325
[40] D.-Y. Chang, "Extent Analysis and Synthetic Decision", Optimization Techniques and Applications, 1, World Scientific, Singapore, p. 352, 1992
[41] P. Tsvetinov, L. Mikhailov, "Reasoning under Uncertainty during Pre-negotiations Using a Fuzzy AHP", Available at http://www.expertguide.qut.com/guide/expert-details.jsp, 2004
[42] J. J. Buckley, "Fuzzy Analytical hierarchical analysis", Fuzzy Sets and Systems 17, 233–247, 1985
[43] A. Stam, S. Minghe, M. Haines, "Artificial neural network representations for hierarchical preference structures", Computers and Operations Research 23 (12), 1191–1201, 1996
[44] D.-Y. Chang, "Applications of the extent analysis method on fuzzy AHP", European Journal of Operational Research 95, 649–655, 1996
[45] C.-H. Cheng, "Evaluating naval tactical missile systems by fuzzy AHP based on the grade value of membership function", European Journal of Operational Research 96 (2), 343–350
[46] M. Weck, F. Klocke, H. Schell, E. R. uenauver, "Evaluating alternative production cycles using the extended fuzzy AHP method", European Journal of Operational Research 100 (2), 351–366, 1997

[47] C. Kahraman, Z. Ulukan, E. Tolga, "A fuzzy weighted evaluation method using objective and subjective measures", In: Proceedings of the International ICSC Symposium on Engineering of Intelligent Systems (EIS'98), 1, University Laguna Tenerife, Spain, pp. 57–63, 1998
[48] H. Deng, "Multicriteria analysis with fuzzy pair wise comparison" International Journal of Approximate Reasoning21 (3), 215–231, 1999
[49] M. Lee, H. Pham, X. Zhang, "A methodology for priority setting with application to software development process", European Journal of Operation al Research 118,375–389, 1999
[50] C.-H. Cheng, K.-L. Yang, C.-L. Hwang, "Evaluating attack helicopters by AHP based on linguistic variable weight", European Journal of Operation al Research 116 (2), 423–435, 1999
[51] K.-J. Zhu, Y. Jing, D.-Y. Chang, "A discussion of extent analysis method and applications of fuzzy AHP", European Journal of Operational Research 116,450–456, 1999
[52] F. T. S. Chan, M. H. Chan, N. K. H. Tang, "Evaluation methodologies for technology selection", Journal of Materials Processing Technology 107, 330–337, 2000a
[53] F. T. S. Chan, B. Jiang, N. K. H. Tang, "The development of intelligent decision support tools to aid the design of flexible manufacturing systems", International Journal of Production Economics 65 (1), 73–84, 2000b
[54] L. C. Leung, D. Cao, "On consistency and ranking of alternatives in fuzzy AHP", European Journal of Operational Research 124, 102–113, 2000
[55] R. J. Kuo, S. C. Chi, S. S. Kao, "A decision support system for selecting convenience store location through integration of fuzzy AHP and artificial neural network", Computers in Industry 47 (2), 199–214, 2002
[56] Cengiz Kahraman, Ufuk Cebeci, Da Ruan, "Multi-attribute comparison of catering service companiesusing fuzzy AHP: The case of Turkey", Int. J. Production Economics 87 171–184, 2003
[57] Da-Yong Chang "Applications of the extent analysis method on fuzzy AHP", European Journal of Operational Research 95, 649-655, 1996
[58] C. L. Hwang, K. Yoon, "Multiple attributes decision making methods and applications" Springer, Berlin, 1980
[59] G. R. Jahanshahloo, F. Hosseinzadeh, M. Lotfi, Izadikhah, "An algorithmic method to extend TOPSIS for decision-making problems with interval data", Applied Mathematics and Computation, 2005
[60] T. Yang, C. C. Hung, "Multi-attribute decision making methods for plant layout design problem", Robotics Comput Intregrated Manufacturing 23, 126-137, 2007
[61] Y. J. Wang, H. S. Lee, "Generalizing TOPSIS for fuzzy multiple-criteria group decision-making", Comput. Math, Appl. 53, 1762-1772, 2007
[62] T. Y. Chen, C. Y. Tsao, "The interval-valued fuzzy TOPSIS method and experimental analysis", Fuzzy Sets and Systems159, 1410-1428, 2008
[63] C. T. Chen, "Extensions of the TOPSIS for group decision-making under fuzzy environment", Fuzzy Sets and Systems 114, 1-9, 2000
[64] C. T. Chen, "Extensions of the TOPSIS for group decision-making under fuzzy environment", Fuzzy Sets and Systems 114, 1-9, 2006

EPAPS Document No.: To be filled in by AIP staff]: [to be filled in by AIP staff]

All Authors: Surendra K. Yadav, Jay Singh, Ved V. Agrawal and B. D. Malhotra

Title: Nanostructured nickel oxide film for application to fish freshness biosensor

Description: Fig [S1] Scheme

Fig [S2] Hall–Williamson plot

Fig [S3] FTIR

Fig [S4] SEM

Fig [S5] Contac angle measurement

Fig [S6] EIS

Fig [S7] Scan rate

Fig [S8] Response time

Fig [S9] Shelf-life

Fig [S10] Real sample analysis

Table I

Total No. of Files: 1

File Names: README.TXT, and supplementary file

File Types: Doc

Special Instructions: None

Contact Information: Prof. B.D. Malhotra,
Department of Biotechnology, Delhi Technological University, Shahbad Daulatpur, Delhi 110042, India.
Email: bansi.malhotra@gmail.com, Tel.: +91-11-27294668
Fax: 91-11-27871023

Supplementary File

Fig [S1] Schematic representation of xanthine biosensor and mechanism of electron exchange between xanthine oxidase and electrode surface.

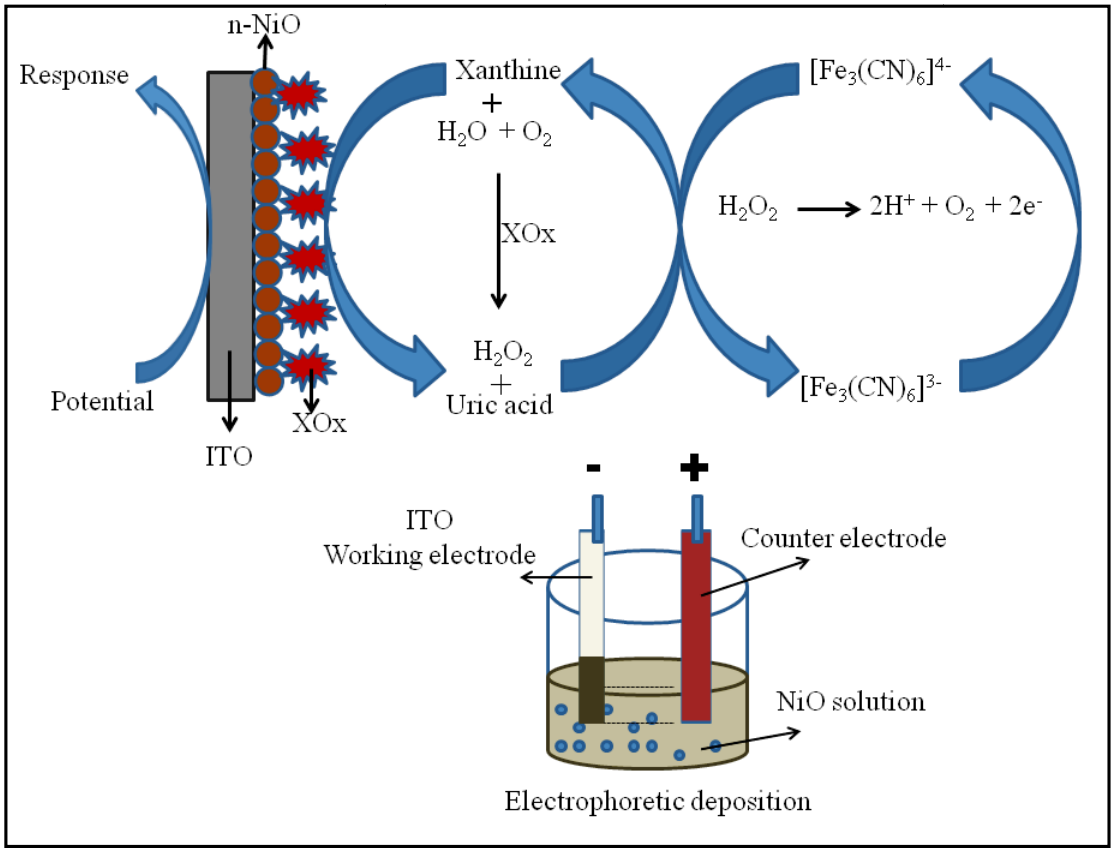

Fig [S2] Hall–Williamson plot of the n-NiO nanoparticles.

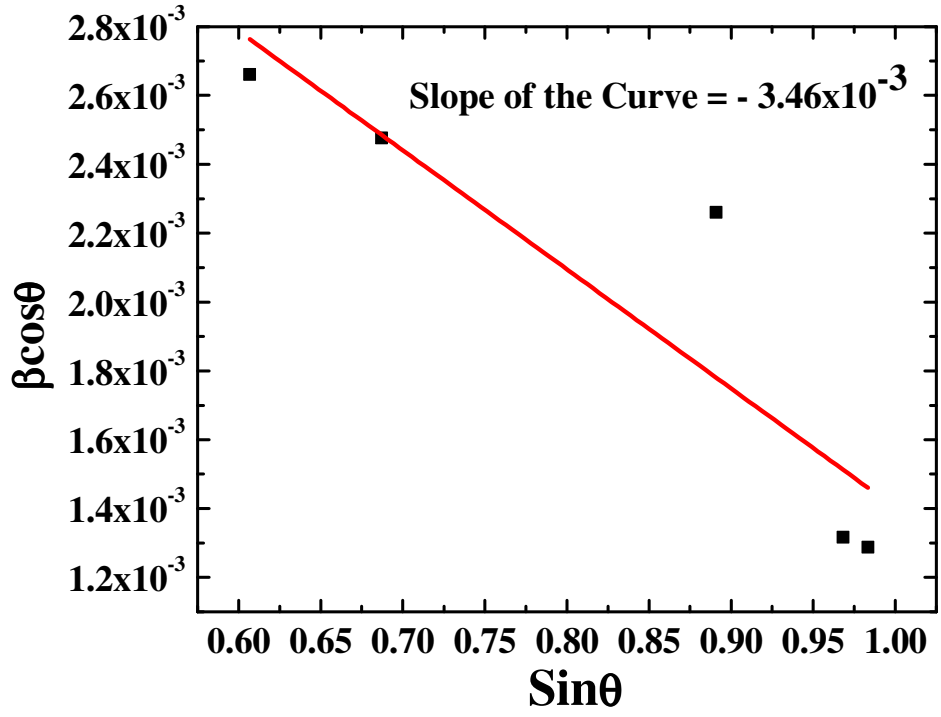

Fig [S3] Fourier Transform Infrared spectra of (a) n-NiO/ITO electrode and (b) XOx/n-NiO/ITO bioelectrode.

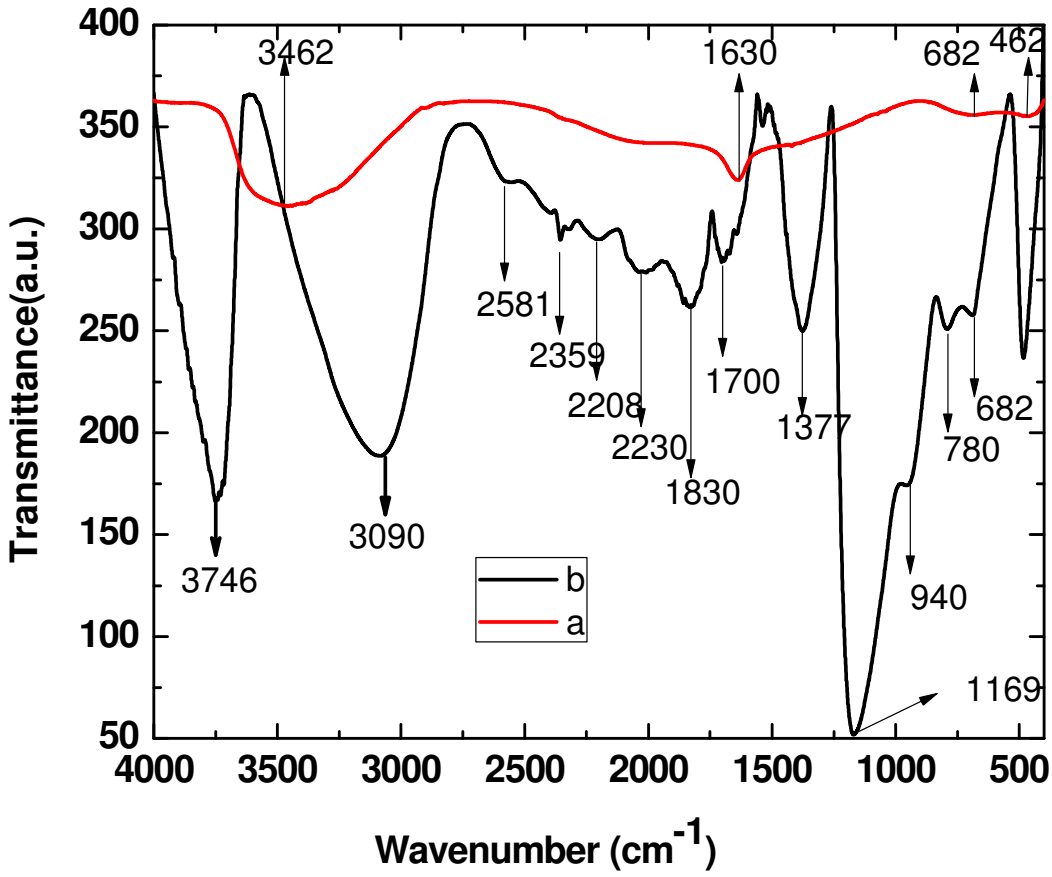

Fig [S4] Scanning electron microscopic images of n-NiO nanoparticle (a & b) and XOx/n-NiO/ITO (c & d) bioelectrode at different magnification.

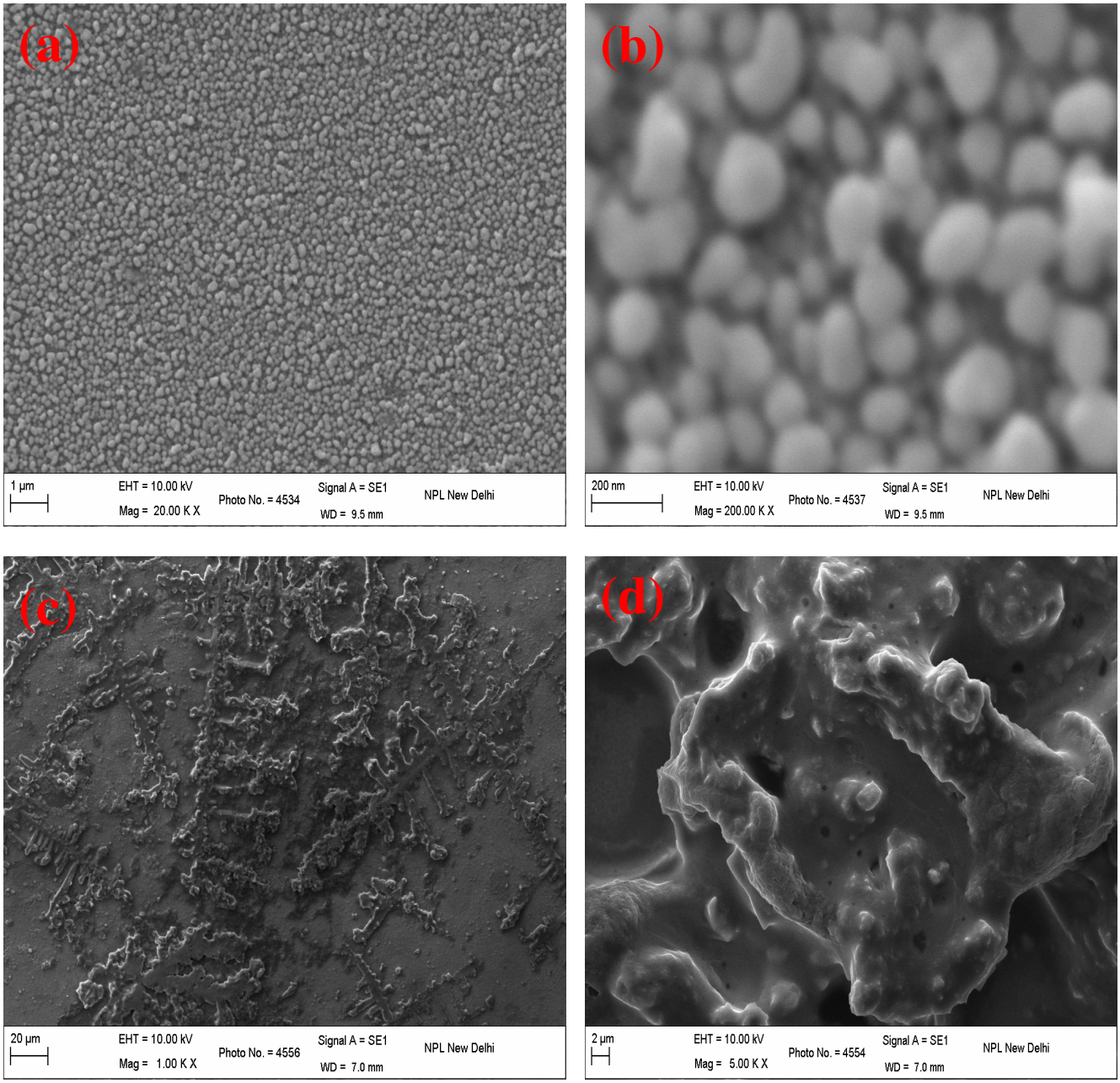

Fig [S5] Contact Angle measurement of ITO electrode (i), n-NiO nanoparticle (ii) and XOx/n-NiO/ITO bioelectrodes (iii)

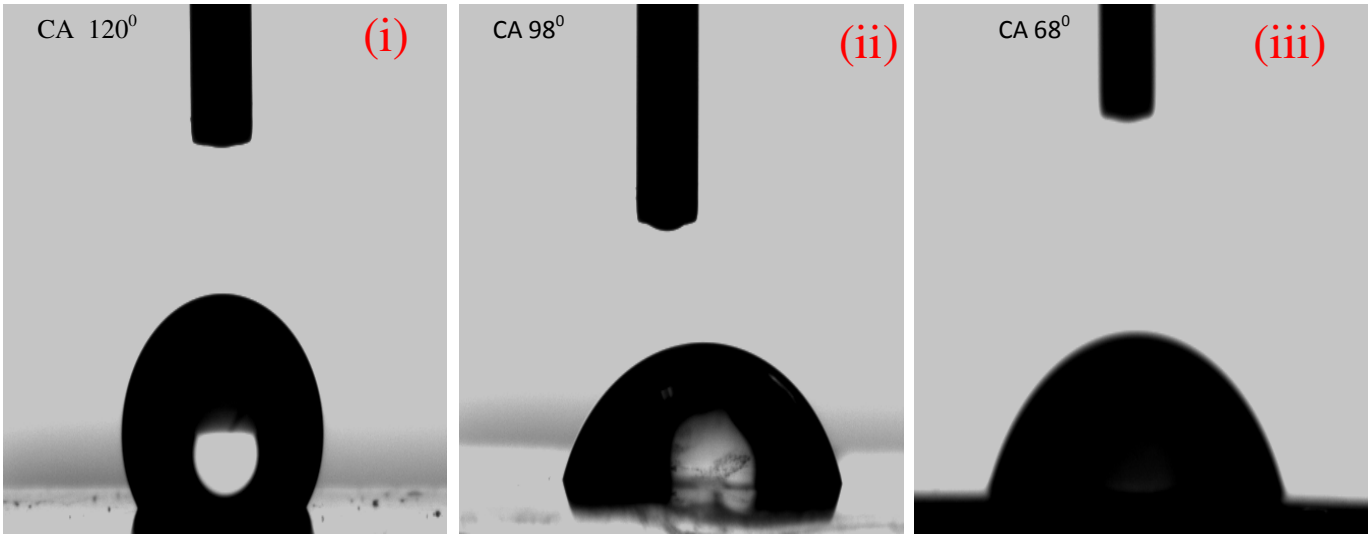

Fig [S6] The Nyquist plot of the electrochemical impedance spectra of (a) ITO, (b) n-NiO/ITO electrode (c) XOx/n-NiO/ITO bioelectrode having phosphate buffer (50mM, pH 7.0, 0.9% NaCl) containing 5mM $[Fe(CN)_6]^{3-/4-}$.

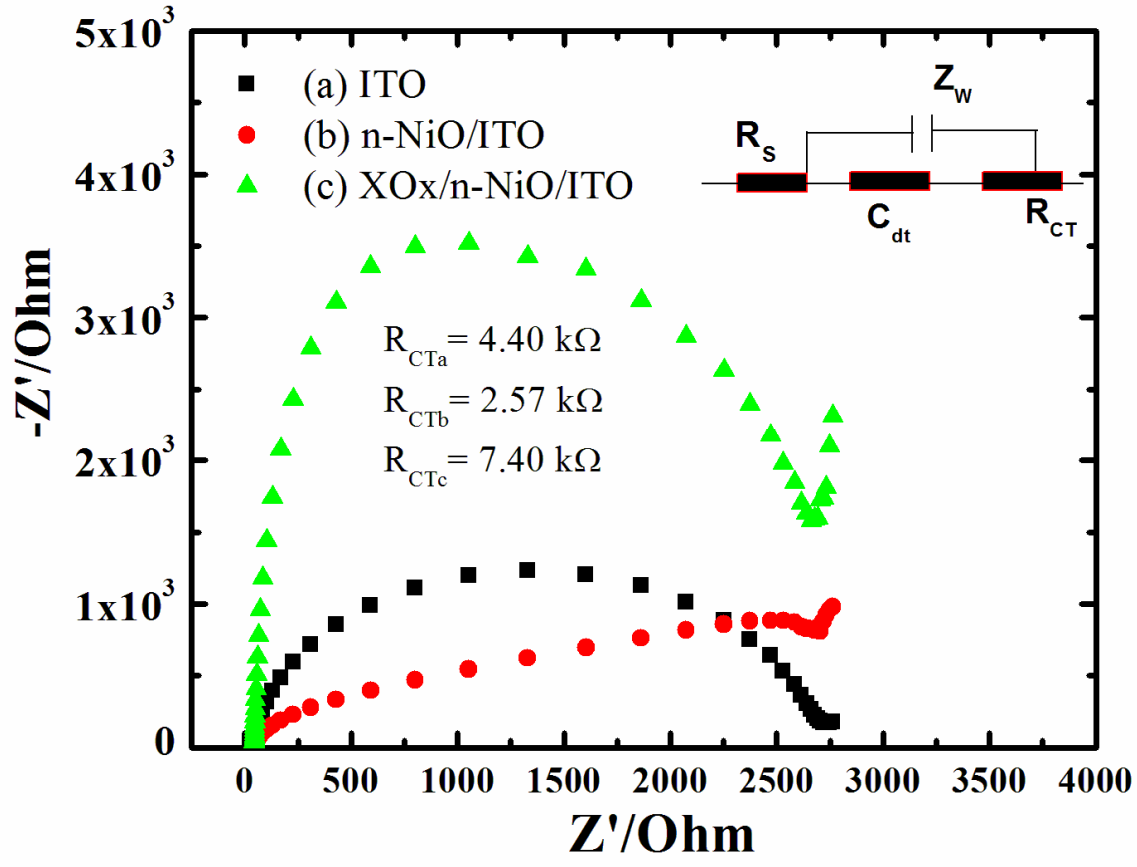

Fig [S7] Electrochemical response curve potential V/S current as a function of scan rate inset current vs (scan rate)$^{1/2}$.

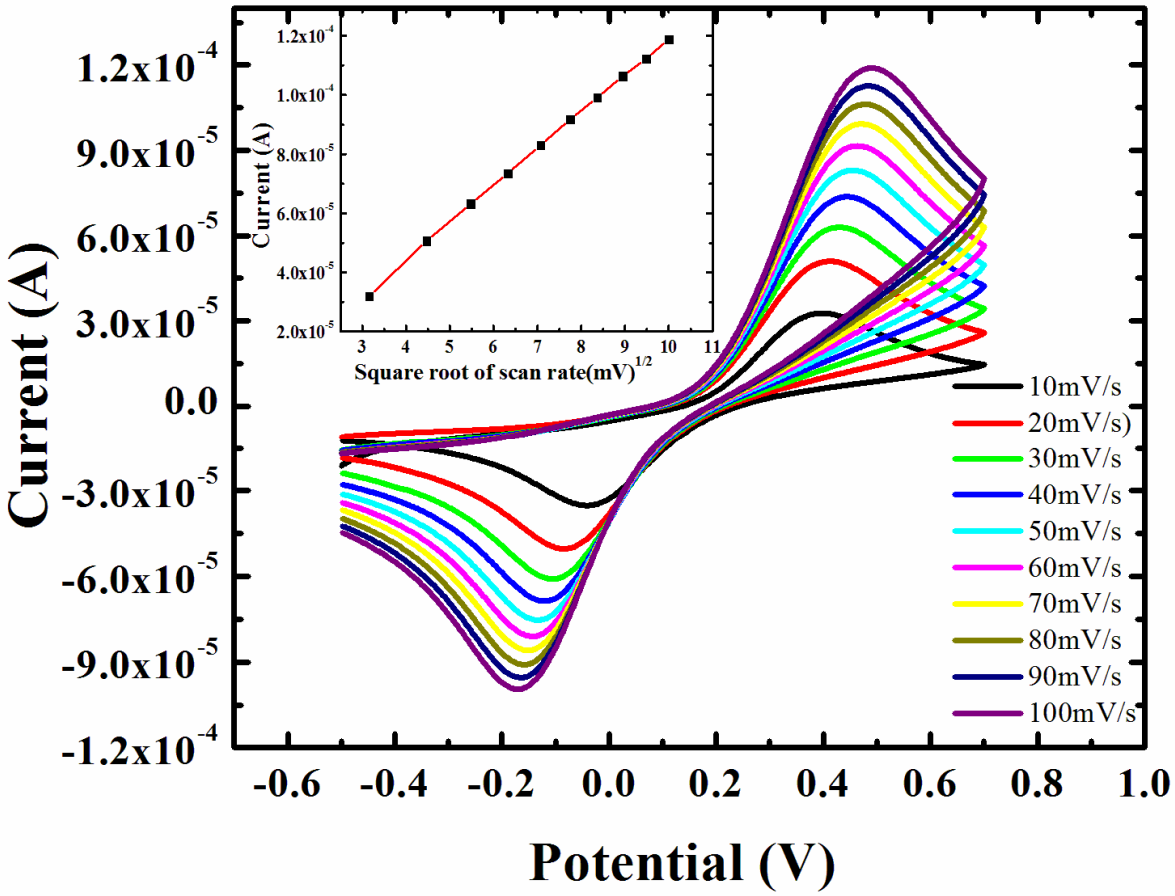

Fig [S8] Electro chemical response time on XOx/n-NiO/ITO bioelectrode from 5 to 40 seconds of incubation period.

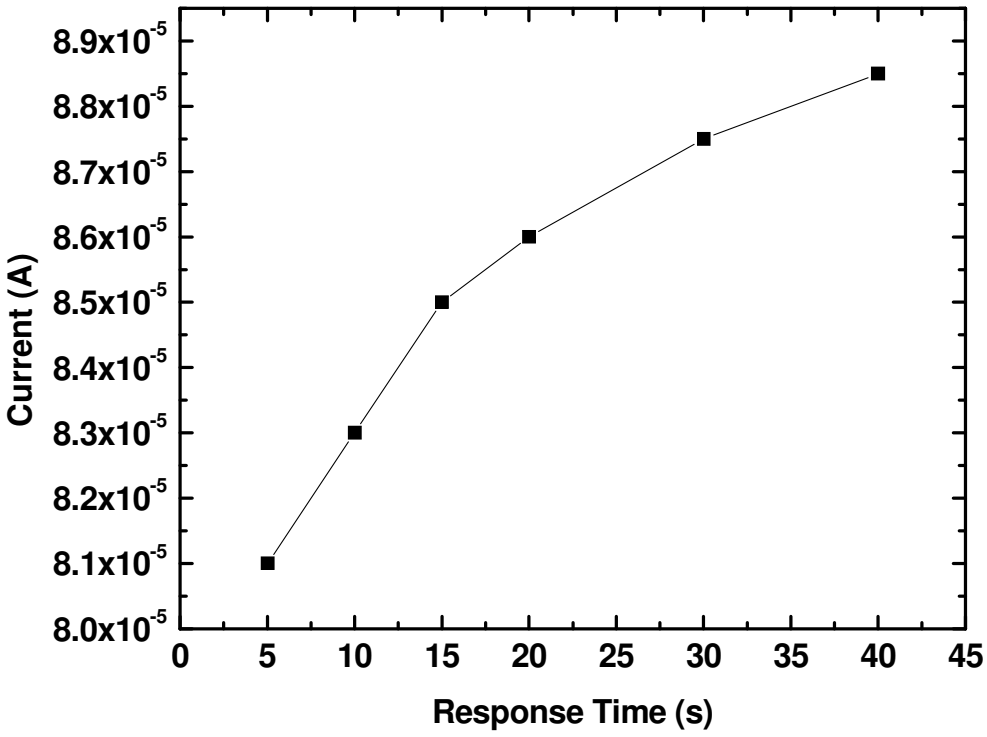

Fig [S9] Self life curve for XO_x/n-NiO/ITO bioelectrode as a function of time.

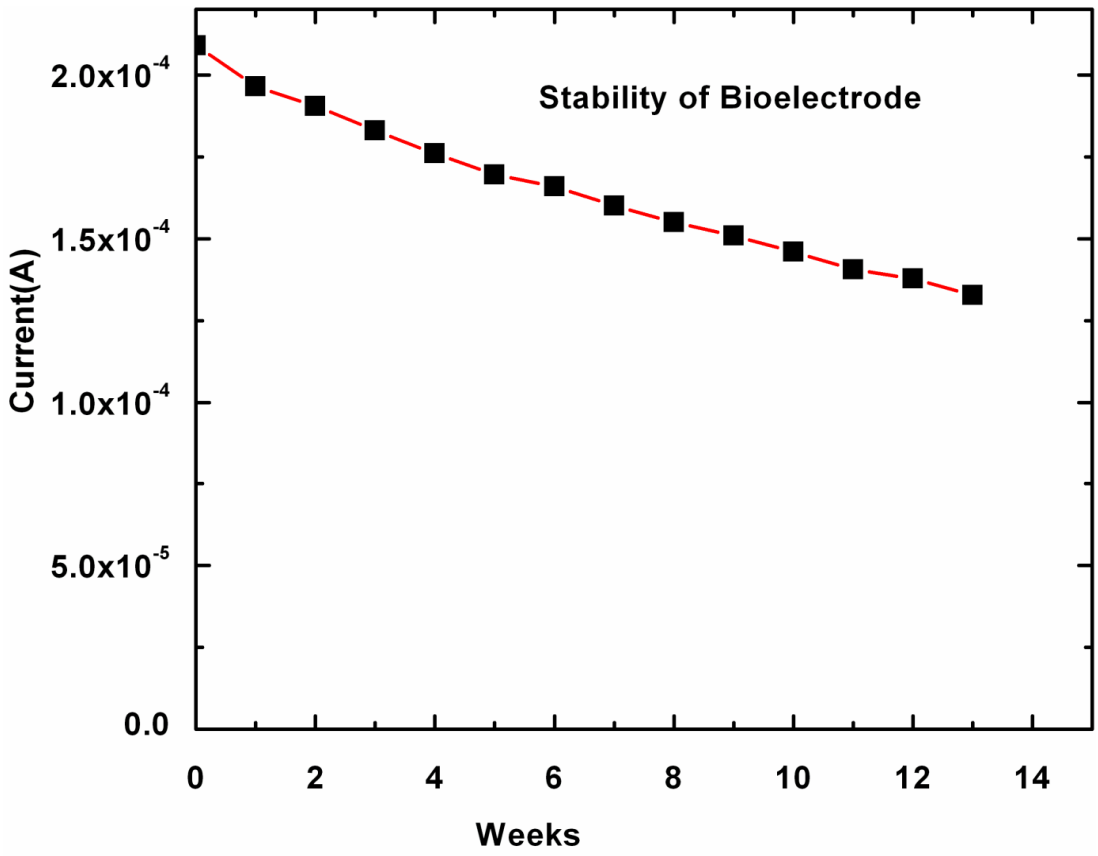

Fig [S10] Linearity curve for real sample (fish) analysis for xanthine estimation.

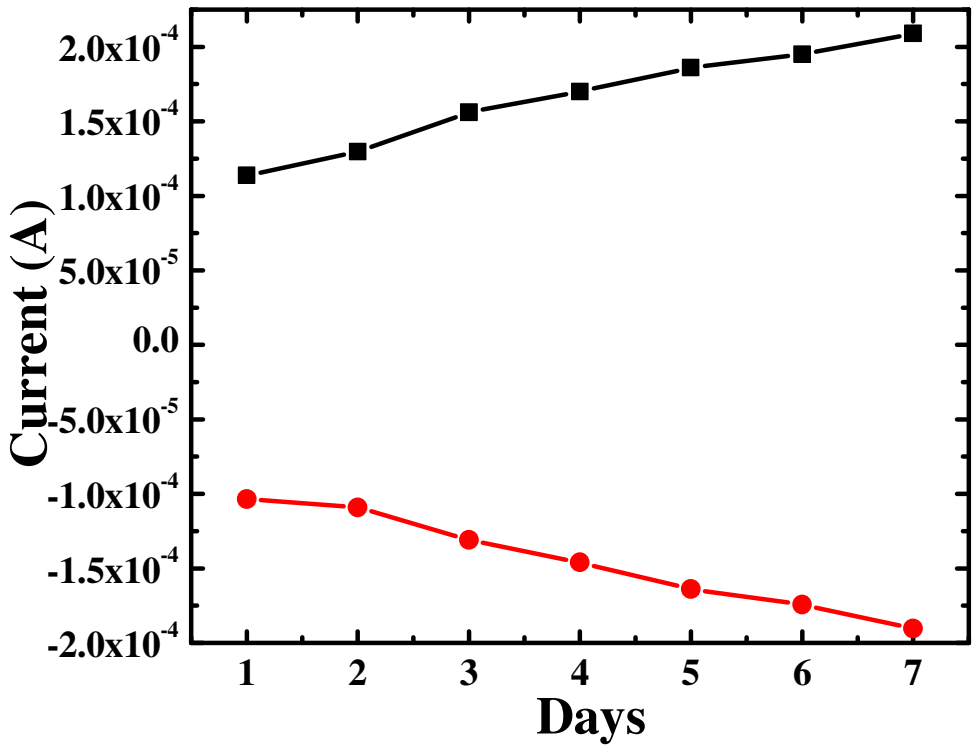

Table I. Characteristics of the xanthine oxidase based biosensor including those reported in literature.

Material	**Detection limit (µM)**	**Linearity (µM)**	**Sensitivity (µA/µM-cm^2)**	**Response time(s)**	**Storage Time(days)**	**(%) Loss**	**Ref.**
Graphite	1.5	1.5-70	0.39	60	------	------	1
Graphite rod	0.1	0.1-0.6	------	35	15	------	2
Polypyrrole	1	1-20	------	------	------	------	3
Zinc oxide-PPY	0.8	0.8–40	------	5	100	40	4
Nafion	0.5	2-185	------	30	10	------	5
DW-CNT	2	2–50	------	150	--------	------	6
Au-polypyrrole	0.4	0.4 - 100	------	------	100	40	7
Modified graphite	4.5	0-40	0.210	120	500 h	35	8
(c-MWCNT)(PANI)	0.6	0.6–58	------	------	100	50	9
MWCNT	------	1 - 100	------	150	------	------	10
CNT glassy carbon	0.1	0.2 - 10	------	------	15	-----	11
Glassy carbon paste	5.3	20-80	------	------	------	------	12
ZnO/Ch/MWCNT/PANI	0.1	0.1–100	------	4	30	30	13
n-NiO Nanoparticle	2.9	10-200	0.6214	15	100	30	Present Work.

References

1. T. Dodevska, E. Horozova, N. Dimcheva, Cent. Eur. J. Chem. **8**, 19 (2010).
2. R. Devi, J. Narang, S. Yadav, and C. S. Pundir, J. Anal Chem. **67**, 273(2012).
3. Y. Liu, L. Nie, W. Tao, S. Yao, Electroanalysis, **16**, 1271(2004).
4. R. Devi, M. Thakur, C.S. Pundir, Biosens. Bioelectron. **26**, 3420 (2011).
5. H. S. Nakatani, L. V. d.santos, C. P. Pelegrine, S. T.M. Gomes, M. Matsushita, N. E. de Souza, J. V. Visentainer , Am. J. Biochem. Biotech.**1**, 85(2005).
6. U. anik, S. Çevik, Microchim Acta, **166**, 209 (2009).
7. R. Devi, S. Yadav, C.S. Pundir, Coll. and Sur. A: Physicochem. Eng. Asp. **394**, 38(2012).
8. N. Dimcheva, E. Horozova, Z. Jordanova, Z. Naturforsch. **57**c, 883 (2002).
9. R. Devi, S. Yadav, C.S. Pundir, Biochem. Eng. J. **58**, 148 (2011).
10. U. anik, M. Cubukcu, Turk J Chem. **32**, 711(2008).
11. Y. Gao, C. Shen, J. Di, Y. Tu, Mat. Sci. and Eng. **C 29**, 2213 (2009).

12. U. A. Kirgoz, S. Timur, J. Wang, A. Telefoncu, Electrochem. Comm. **6**, 913(2004).
13. R. Devi, S. Yadav, C.S. Pundir, Analyst. 137, 754 (2012)

Vol.2 Issue.3,
March 2014.
Pgs: 64-80

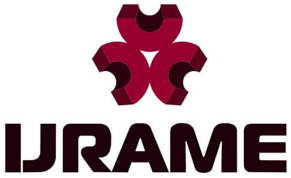

ISSN (ONLINE): 2321-3051

INTERNATIONAL JOURNAL OF RESEARCH IN AERONAUTICAL AND MECHANICAL ENGINEERING

NATURAL CONVECTION GREENHOUSE DRYING OF VERMICELLI: AN EXPERIMENTAL STUDY

Punit Kumar[1]

[1] *M.Tech. Student, Mechanical Engineering Department, Guru Jambheshwar University of Science &Technology, Hisar-125001, Haryana, India, E-mail: punit_hsr@yahoo.in*

Correspondence: Punit Kumar, Mechanical Engineering Department, Guru Jambheshwar University of Science &Technology, Hisar-125001, Haryana, India, Mobile No. +918396844895, E-mail: punit_hsr@yahoo.in

Abstract

In this research paper, investigated the behaviour of heat and mass transfer phenomenon during greenhouse vermicelli drying under natural convection mode by comparison in roof type even span greenhouse and slant height greenhouse. Various experiments were performed in the month of September 2013 at Guru Jambheshwar University of Science and Technology Hisar (29°5'5" N 75°45'55" E). Experimental data obtained for natural convection greenhouse drying of vermicelli were used to determine the constants in the Nusselt number expression by using the simple linear regression analysis and the values of convective heat transfer coefficients were evaluated. The values of experimental constants *C* and *n* were determined as 0.59 to 1.53 and 0.04 to 0.17 respectively. The values of convective heat transfer coefficients were observed to vary from 0.49 W/m^2 °C to 1.34 W/m^2 °C respectively.

Keywords: Vermicelli, Vermicelli drying, Convective heat transfer coefficient, Natural convection greenhouse.

1. Introduction

The sun is the main source of energy producer of our solar system. A small fraction of the energy produced in the sun hits the earth and makes life possible on our planet. Solar radiation drives all natural cycles and processes such as rain, wind, photosynthesis, ocean activities and many other which are important for life. The radiation intensity of 6000°C solar surface correspondence to 70,000 to 80,000 KW/m².Earth receives a very small portion of this energy. The solar radiation intensity outside the atmosphere is in average 1360W/m² (solar constant) [1].

Vermicelli is a popular and one of traditional Indian item which is prepared on the occasion of any festival. It is generally prepared at household level by extruding the dough with a cylindrical hand extruder whose diameter generally varies from 1.25 mm to 3 mm. Various companies involved in the manufacturing of vermicelli in India are: Bambino Agro Industries Ltd., MTR Foods Pvt. Ltd., Fryums, Maggie (Nestle group), Victoria Foods Pvt. Ltd. (Rajdhani Group) etc. [2, 3].

Drying reduces the moisture content of a product by which its shelf life can be increased. In the drying process, the product is spread in a thin layer on the earth surface and exposed directly to the solar radiation. The product drying rate depends on various parameters like solar radiation, wind velocity, relative humidity, air and earth temperature, type of product, initial moisture content, product absorptivity, and mass of product per unit exposed area [4].

In the most of developing countries, people have been drying food products for decades by placing on ground surface in open air. Generally, open sun dried products do not have the international quality standards and it cannot be sold in the international market. Open sun drying has many disadvantages. The alternative means for drying of some of the agricultural and food products in developing countries may be provided by well-designed solar dryers. The acquisition and operational costs of dryers available in the market significantly increase the costs of the dried products. Therefore, in the present work greenhouse type dryer is to be used to dry vermicelli. Greenhouse solar dryers improve the dry products value and their marketability [5].

The presence of moisture contents in vermicelli is one of the major reasons for its spoilage during storage period [6]. This problem can be overcome up to certain extent by minimizing the moisture contents by using greenhouse dryer under natural convection condition. Kumar et al [7] determined of convective heat transfer coefficients of papad under open sun drying and indoor forced convection drying modes. The values of convective heat transfer coefficients under open sun drying and forced convection modes were found to be 3.54W/m² °C and 1.56 W/m² °C respectively. Jain and Tiwari [16] evaluated the convective heat transfer coefficient for cabbage and peas in open sun drying and greenhouse. The values of convective heat transfer coefficient under natural convection for cabbage or peas ranged 25 to 10 W/m² °C and 17 to 8 W/m² °C for open sun drying and greenhouse drying respectively. Sehdev et al [17] determined the convective heat transfer coefficient of vermicelli under indoor forced convection drying mode. The convective heat transfer coefficient values for vermicelli were found to vary from 0.98 to 1.10 W/m² °C. Sehdev et al [18] determine the convective heat transfer coefficients of vermicelli for different thicknesses under open sun drying mode. The average values of convective heat transfer coefficients were found to be 5.61 W/m² °C and 4.13 W/m² °C for vermicelli of diameters 2 mm and 1.25 mm respectively.

2. Drying Processes

Drying is the process of moisture removal from a product. Open sun drying is one of the most primitive methods of vermicelli drying and it is still practiced in India despite many disadvantages associated with it. Most of the modern drying technologies available are expensive as compared to sun drying. It is a simple and low cost method. Solar energy is renewable and zero pollutant source of energy. Vermicelli drying involves a heat and mass transfer phenomenon in which heat energy supplied to the vermicelli surface is utilized in two ways: to increase the vermicelli surface temperature in the form of sensible heat and to vaporize the moisture present in vermicelli through provision of the latent heat of vaporization [7]. The removal of moisture from the interior of the vermicelli takes place due to induced vapour pressure difference between the vermicelli and surrounding medium. The rate of drying depends on a number of external parameters (solar radiation, ambient temperature, wind velocity, and relative humidity) and internal parameters (initial moisture content) [9]. In natural convection greenhouse drying process free convection will take place. The circulation of air is caused due to the difference in temperature of the surface and atmospheric air [5].

3. Materials and Methods

3.1 Experimental set-up and instrumentation

A roof type even span greenhouse of 120×80 cm² effective floor area was fabricated of PVC pipe and a UV film covering of 0.02mm (200 microns). The central height and the walls heights were maintained as 60 cm and 40 cm respectively with an air vent of area an air vent of area 422.24 cm^2 [9,10].

A rectangular shaped wire mesh tray of dimension 160×10 cm² was used to accommodate the vermicellies. An electronic weighing balance (capacity 6 kg; Scaletech, model TJ-6000) having a least count of 0.1g was used to measure the mass of moisture evaporated. An eight channel digital temperature indicator (0-199.9 °C, least count of 0.1 °C) with a calibrated thermocouple was used to measure the greenhouse temperature and ambient

temperature. A digital hygrometer (model Lutron HT-305) was used to measure the relative humidity and temperature of exit air.

A photograph of the experimental setup for greenhouse drying in the forced mode is shown in Fig. 1 and its schematic view is shown in Fig. 2.

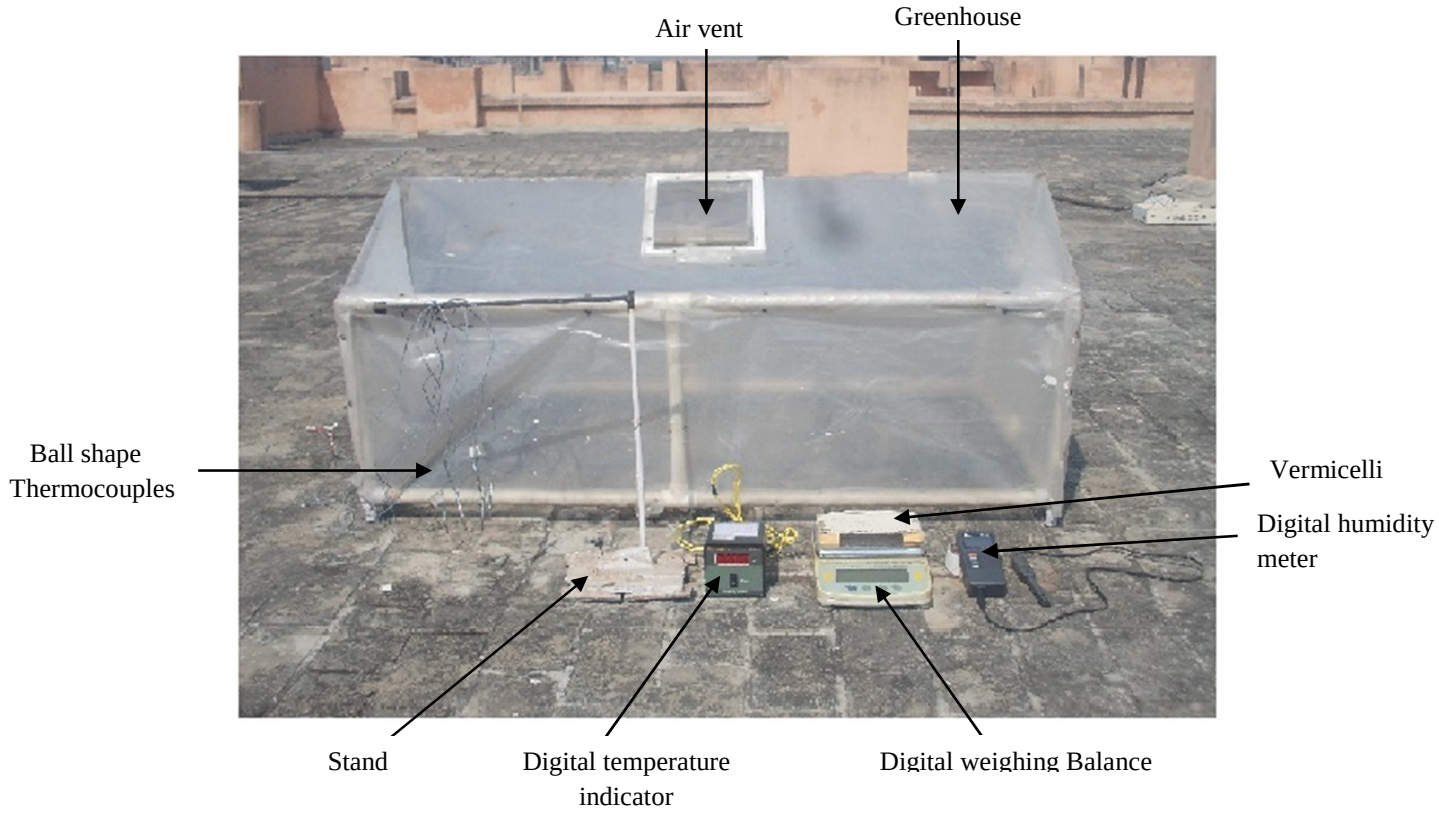

Figure 1: Experimental set-up of Evan Span Greenhouse vermicelli drying under Natural Convection mode.

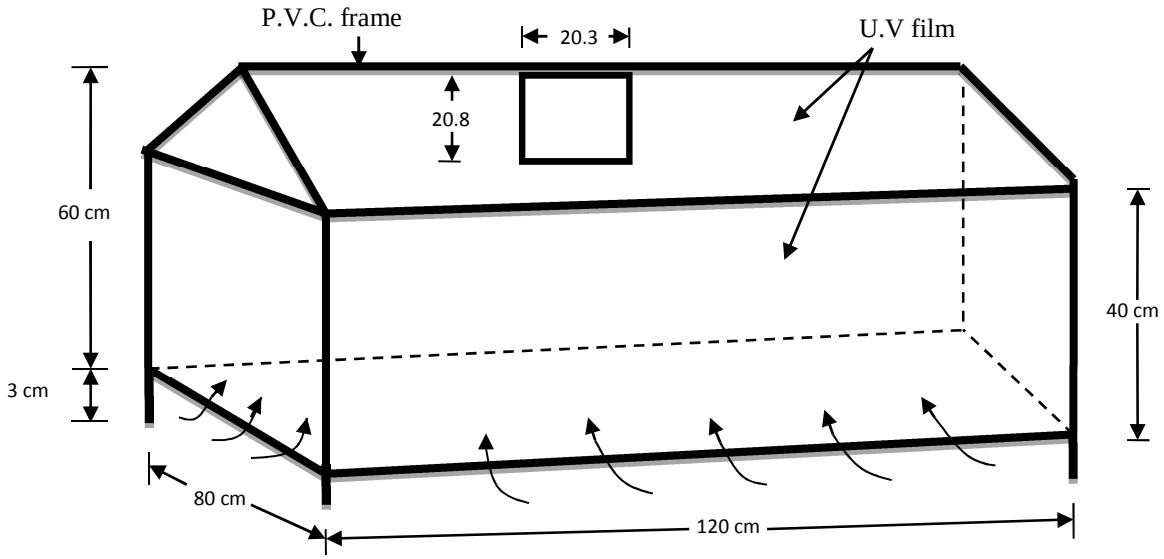

Figure 2: Schematic view of Evan Span Greenhouse vermicelli drying under Natural Convection mode**.**

3.2 Sample preparation and experimental observations

Vermicelli has been freshly prepared by taking semolina flour mixed with 30% of water content per kg of vermicelli weight. The flour was purchased locally, and that fraction of flour which passes through a 40-mesh sieve (610 microns) was used for making vermicelli. Dough has been made and rolled in circular shape and extruded in cylindrical extruder. The bottom of extruder is attached with steel die plates of 57 mm diameter having holes of 1.25mm, 2 mm and 3 mm diameters respectively. The freshly prepared vermicelli of 15.4 gram of 1.25 mm, 28.8 gram of 2 mm and 34.9 gram of 3 mm thickness respectively were used for each run of the greenhouse drying mode.

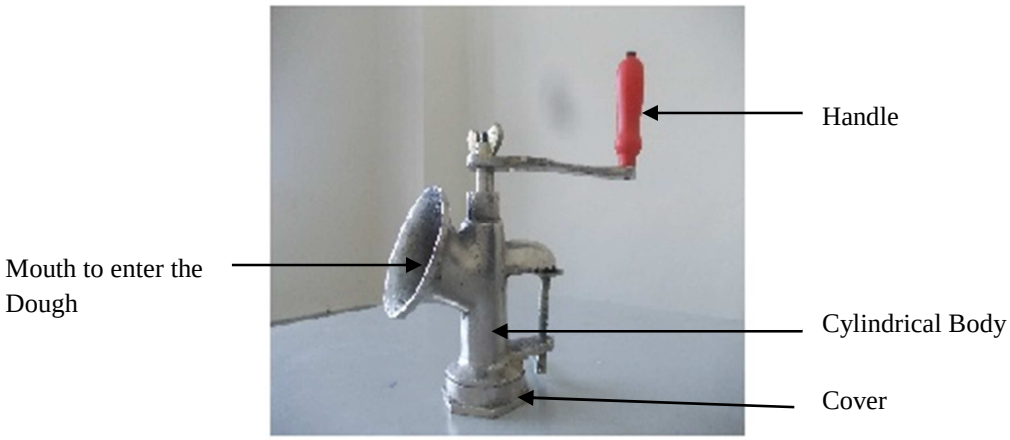

Figure 3: A photograph of cylindrical hand extruder.

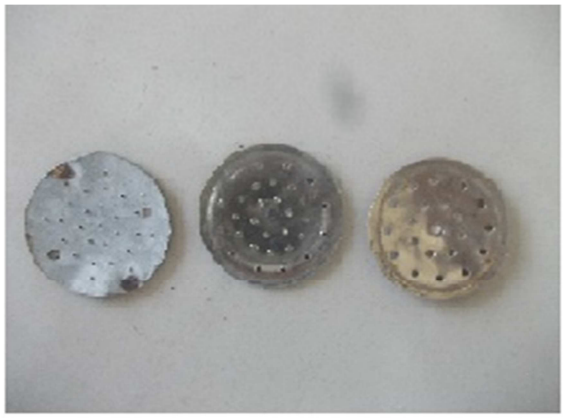

Figure 4: A photograph of steel die plates of 1.25 mm, 2mm and 3 mm holes.

Experiments have been conducted in the months of August and September 2013 in the climatic conditions of Guru Jambheshwar University of Science and Technology, Hisar (29°5’5” N 75°45’55” E). The orientation of the greenhouse during the experimentation was kept east-west because sunlight availability is more in comparison to north-south. Experimental setup was located on the open floor of a three-floor building to have a good exposure to the solar radiation. Each observation have been recorded at every 10 min time intervals. The vermicelli samples were kept on the weighing balance using the wire mesh tray. The whole unit has been kept in greenhouse with negligible wind velocity. The difference in weight directly gave the quantity of water evaporated during that time interval. To get accurate results, the above mentioned experimentation procedure was repeated three times for each freshly prepared similar vermicelli sample of same size (i.e., 1.25 mm, 2 mm

and 3 mm thickness) on consecutive days at the same timing. The initial mass of vermicelli sample for each run of drying was kept constant (i.e., 15.4 g, 28.8 gm and 34.9 gm).

3.3 Thermal modelling

The convective heat transfer coefficient in greenhouse drying under natural convection can be calculated as [8, 15]:

$$Nu = \frac{h_c X}{K_v} = C(Gr\,\mathrm{Pr})^n$$

or

$$h_c = \frac{K_v}{X} C(Gr\,\mathrm{Pr})^n \tag{1}$$

The rate of heat utilized to evaporate moisture is given [14] as

$$Q_e = 0.016 h_c \left[P(T_v) - \gamma P(T_e)\right] \tag{2}$$

on substituting h_c from Eq. (1), Eq. (2) becomes

$$Q_e = 0.016 \frac{K_v}{X} C(Gr\,\mathrm{Pr})^n \left[P(T_v) - \gamma P(T_e)\right] \tag{3}$$

The moisture evaporated is determined by dividing Eq. (3) by the latent heat of vaporization (λ) and multiplying by the area of vermicelli drying tray (A_t) and time interval (t).

$$m_{ev} = \frac{Q_e}{\lambda} t A_t = 0.016 \frac{K_v}{X\lambda} C(Gr\,\mathrm{Pr})^n \left[P(T_v) - \gamma P(T_e)\right] t\, A_t \tag{4}$$

Let

$$0.016 \frac{K_v}{X\lambda} \left[P(T_v) - \gamma P(T_e)\right] t\, A_t = Z \tag{5}$$

$$\frac{m_{ev}}{Z} = C(Gr\,\mathrm{Pr})^n \tag{6}$$

Taking logarithm of both sides of Equation (6),

$$\ln\left[\frac{m_{ev}}{Z}\right] = \ln(C) + n \ln(Gr\,\mathrm{Pr}) \tag{7}$$

This is in the form of liner equation,

$$Y = mX_o + C_o \tag{8}$$

Where

$$Y = \ln\left[\frac{m_{ev}}{z}\right],$$

$m = n$,

$X = \ln(Gr\,\mathrm{Pr})$,

$C_o = \ln C$

Thus, $C = e^{C_0}$

Values of *m* and C_o in Eq. (7) are obtained by using the simple linear regression method by using the following formulae

$$m = \frac{N\sum X_o Y - \sum X_o \sum Y}{N\sum {X_o}^2 - \left(\sum X_o\right)^2} \tag{9}$$

and

$$C_o = \frac{\sum {X_o}^2 \sum Y - \sum X_o \sum X_o Y}{N\sum {X_o}^2 - \left(\sum X_o\right)^2} \tag{10}$$

Then the constant '*C*' and exponent '*n*' can be obtained from the above equations. The values of these constant were considered further to determine the convective heat transfer coefficient. After knowing the convective heat transfer coefficient (h_c), the evaporative heat transfer coefficient (h_c) can also be calculated from Eq. (11) as follows [16]:

$$h_c = 0.016\ h_c \left[\frac{P(Tv) - \gamma P(T_e)}{Tp - T_e}\right] \tag{11}$$

3.4 The physical properties of humid air

The physical properties of humid air, i.e., specific heat (C_v), thermal conductivity (K_v), density (μ_v), viscosity (μ_v), and partial vapour pressure, P(T) have been determined by using following expressions:

$$C_v = 999.2 + 0.1434T_i + 1.101\times10^{-4}{T_i}^2 - 6.7581\times10^{-8}{T_i}^3 \tag{12}$$

$$K_v = 0.0244 + 0.7673\times10^{-4}T_i \tag{13}$$

$$\rho_v = \frac{353.44}{T_i + 273.15} \tag{14}$$

$$\mu_v = 1.718\times10^{-5} + 4.620\times10^{-8}T_i \tag{15}$$

$$P(T) = \exp\left[25.317 - \frac{5144}{(T + 273.15)}\right] \tag{16}$$

Where $T_i = \frac{\bar{T}_v + \bar{T}_e}{2}$

4. Result and Discussion

The experimental data obtained for vermicelli drying under natural convection greenhouse mode are given in Tables 1 (a) to 1(f).

Table 1(a): Observations for natural convection Slant Height Greenhouse drying of vermicelli sample for diameter = 1.25 mm (31-08- 2013)

Sr. No.	Time	Wt. of Vermicelli (gm)	Time differ.	T_v (°C)	γ (%)	T_e (°C)	Tg (°C)	T_a (°C)	hc	C	n
1	11:15	15.2	0	40.1	35.2	41	42.6000	40.2	-	1.53	0.04
2	11:25	14.3	10	43.9	29.7	44.9	44.1000	39.4	0.49		
3	11:35	14.0	20	40.75	32.5	40.5	40.6500	38.5	0.58		
4	11:45	13.6	30	46.6	29.3	44.7	43.8500	40.1	0.55		
5	11:55	13.3	40	46.5	24.4	47.9	42.3000	39.5	0.56		
6	12:05	13.1	50	45.65	26.6	45.8	42.9000	38.6	0.55		
7	12:15	12.9	60	44.65	31	42.5	42.1000	38.8	0.55		
8	12:25	12.5	70	48.95	25.6	46.9	44.3000	40.2	0.57		
9	12:35	12.3	80	47.6	22.4	49.3	43.0000	40.5	0.57		
10	12:45	11.9	90	49.55	23.5	49.2	45.1000	42.9	0.57		
11	12:55	11.6	100	51.6	22.2	50.7	46.5500	42.6	0.57		
12	1:05	11.4	110	44.3	24.7	46.7	41.9000	38.1	0.55		
13	1:15	11.1	120	47.85	20	51	43.3000	39	0.57		
14	1:25	10.9	130	44.85	29	43.1	41.6500	39.7	0.55		
15	1:35	10.8	140	42.05	30	41.6	41.0000	38.1	0.53		

Table 1(b): Observations for natural convection Slant Height Greenhouse drying of vermicelli sample for diameter = 2 mm (07-09- 2013)

Sr. No.	Time	Wt. of Vermicelli (gm)	Time differ.	T_v (°C)	γ (%)	T_e (°C)	Tg (°C)	T_a (°C)	hc	C	n
1	11:15	19.9	0	40.1	32	39.8	41.3500	35.5	-	1.47	0.05
2	11:25	18.9	10	40.6	28.5	41.9	40.7000	37.2	0.51		
3	11:35	18.4	20	41.9	28.2	42.8	41.1500	37	0.56		
4	11:45	17.9	30	43.05	25.3	44.8	41.9500	38	0.57		
5	11:55	17.4	40	44	23.3	47.8	43.0500	37.7	0.57		
6	12:05	17.0	50	44.35	23.3	46.4	42.4500	38.5	0.59		
7	12:15	16.7	60	46.55	21	48.1	43.7000	38	0.61		
8	12:25	16.5	70	47.1	20.6	49.2	43.6500	38.6	0.61		
9	12:35	16.3	80	44.2	26	43.1	42.3000	37.1	0.59		
10	12:45	16.1	90	44.55	25.9	44.2	42.9500	38.8	0.58		
11	12:55	15.9	100	43.45	26.5	42.8	42.0500	37.3	0.58		
12	1:05	15.4	110	48.7	19.3	50.5	45.4000	40.3	0.61		
13	1:15	15.2	120	46.7	20.7	48.7	43.7500	38.3	0.61		
14	1:25	15.0	130	49.15	17.2	25.5	45.7500	40	0.61		
15	1:35	14.9	140	44.15	25.7	43.2	43.4500	38.3	0.56		
16	1:45	14.7	150	46.75	22.6	46.6	45.3500	39.6	0.61		
17	1:55	14.5	160	45.6	24.5	44.5	44.7500	39	0.57		
18	2:05	14.3	170	44.55	23.3	45.5	43.8500	38.7	0.56		
19	2:15	14.2	180	44.6	22	46.5	44.2500	38.3	0.54		

Table 1(c): Observations for natural convection Slant Height Greenhouse drying of vermicelli sample for diameter = 3 mm (15-09- 2013)

Sr. No.	Time	Wt. of Vermicelli (gm)	Time differ.	T_v (°C)	γ (%)	T_e (°C)	Tg (°C)	T_a (°C)	hc	C	n
1	11:15	35.0	0	42.35	27.1	46.8	44.2500	41.9	-	1.37	0.06
2	11:25	34.0	10	44.95	22.5	50.9	47.1000	42.3	0.63		
3	11:35	33.1	20	44.85	26.5	46.5	45.3500	43.7	0.58		
4	11:45	32.3	30	46.6	25.4	47.8	46.1000	43.6	0.58		
5	11:55	31.6	40	47.5	21.8	51.6	47.7000	44.7	0.55		
6	12:05	30.9	50	49.45	20.9	51.7	48.9500	45.2	0.58		
7	12:15	30.3	60	49.95	20.8	53.6	48.2000	46	0.63		
8	12:25	29.7	70	49.9	19.7	52.8	48.2000	45.1	0.63		
9	12:35	29.1	80	50.85	21.9	51.3	48.3000	44.3	0.64		
10	12:45	28.6	90	52.65	18.2	55.6	48.8500	43.4	0.66		
11	12:55	28.1	100	52.4	15.3	56.6	50.1000	44.7	0.64		
12	1:05	27.7	110	49.85	20.3	51.4	50.1000	45.5	0.59		
13	1:15	27.3	120	53.05	14.9	55.9	50.5000	44.2	0.65		
14	1:25	26.9	130	52.65	16.3	53.9	48.8000	43.4	0.66		
15	1:35	26.6	140	53.15	13.9	56.1	50.4500	44.4	0.65		
16	1:45	26.3	150	51.1	19.1	49.6	49.6500	44.6	0.62		
17	1:55	26.0	160	54	13.2	56.1	50.7000	45.8	0.66		
18	2:05	25.8	170	51.55	15.3	53.3	50.6000	44.9	0.61		
19	2:15	25.6	180	51.65	14.6	54.2	52.3500	45.1	0.59		
20	2:25	25.4	190	52.15	13.4	57.2	51.3500	44.6	0.60		
21	2:35	25.3	200	52.55	13	55.8	51.1000	44.7	0.62		

Table 1(d): Observations for natural convection Evan Span Greenhouse drying of vermicelli sample for diameter = 1.25 mm (01-09- 2013)

Sr. No.	Time	Wt. of Vermicelli (gm)	Time differ.	T_v (°C)	γ (%)	T_e (°C)	Tg (°C)	T_a (°C)	hc	C	n
1	11:15	15.3	0	37.9	38.5	38.6	40.0000	37.4	-	1.19	0.09
2	11:25	14.1	10	39.15	36.8	38.7	39.4500	36.3	0.66		
3	11:35	13.6	20	41.0	31.9	41.4	41.6500	38.3	0.71		
4	11:45	13.3	30	40.8	32	41.4	41.1500	37.9	0.68		
5	11:55	13.1	40	41.1	31.8	41.7	41.5500	37.2	0.69		
6	12:05	12.9	50	40.95	32.9	41	42.0500	38.2	0.75		
7	12:15	12.7	60	41.35	33.1	41.1	42.2500	39	0.74		
8	12:25	12.4	70	42.35	30.5	42.6	43.5500	40.5	0.76		
9	12:35	12.1	80	40.8	33.8	40.3	41.8500	38.3	0.75		
10	12:45	11.9	90	38.6	35	39.1	39.7500	37.1	0.75		
11	12:55	11.5	100	43.05	30.3	43.1	43.7000	39.5	0.72		
12	1:05	11.3	110	40.1	31.3	41.3	41.4500	37.4	0.76		
13	1:15	11.1	120	39.9	34.5	39.7	44.5000	37.5	0.85		
14	1:25	11.0	130	44.05	29.2	43.9	44.5000	40.7	0.69		
15	1:35	10.9	140	43.2	28	44.3	44.0500	39.4	0.74		

Table 1(e): Observations for natural convection Evan Span Greenhouse drying of vermicelli sample for diameter = 2 mm (08-09- 2013)

Sr. No.	Time	Wt. of Vermicelli (gm)	Time differ.	T_v (°C)	γ (%)	T_e (°C)	Tg (°C)	T_a (°C)	hc	C	n
1	11:15	28.7	0	35.85	33.3	37.8	39.7000	36.9	-	0.71	0.15
2	11:25	27.6	10	38.95	31.6	41.2	42.1500	38	1.09		
3	11:35	26.9	20	36.4	31.2	38.8	38.9500	35.3	1.05		
4	11:45	26.2	30	38.5	33	37.7	40.6500	37.5	1.02		
5	11:55	25.6	40	38.65	30	39.6	41.0500	38.5	1.04		
6	12:05	25.0	50	42.6	24.6	44.9	44.9000	39	1.04		
7	12:15	24.5	60	38.8	29.6	38.7	40.6500	37.9	0.99		
8	12:25	24.1	70	38.65	30.3	38.4	39.8500	36.8	0.94		
9	12:35	23.6	80	41.85	23.8	43	43.5500	39.7	0.99		
10	12:45	23.1	90	44.4	22	44.8	45.6000	41.3	0.94		
11	12:55	22.7	100	44.4	21.6	45.4	45.7500	41.1	0.96		
12	1:05	22.3	110	42.85	22.7	43.7	44.0000	39.4	0.93		
13	1:15	21.9	120	46.95	18.5	48.4	47.1000	42.5	0.69		
14	1:25	21.6	130	46.05	17.1	49.8	46.4500	44.3	0.79		
15	1:35	21.3	140	46.95	18.6	48.3	44.9000	41.9	1.02		
16	1:45	21.0	150	42.75	20.9	44.7	45.6500	39.6	1.07		
17	1:55	20.8	160	48.85	16.3	50.6	46.8000	44.4	1.02		
18	2:05	20.7	170	48.35	16.5	50.4	47.8500	43.1	0.83		
19	2:15	20.5	180	49	15.6	51.6	47.5000	42	0.97		

Table 1(f): Observations for natural convection Evan Span Greenhouse drying of vermicelli sample for diameter = 3 mm (24-09- 2013)

Sr. No.	Time	Wt. of Vermicelli (gm)	Time differ.	T_v (°C)	γ (%)	T_e (°C)	Tg (°C)	T_a (°C)	hc	C	n
1	11:15	34.1	0	38	41.5	41.3	40.8000	37.1	-	1.40	0.10
2	11:25	33.2	10	38.55	41	41.6	41.3000	39.8	1.09		
3	11:35	32.4	20	39.1	37.8	42.3	41.6500	39.4	1.08		
4	11:45	31.7	30	39.55	41	41.7	40.6500	39	0.99		
5	11:55	31.1	40	38.95	41.8	41	39.3000	37.4	0.89		
6	12:05	30.5	50	39.75	39.9	40	40.2500	38.7	0.92		
7	12:15	30.0	60	39.8	38.6	40.9	40.1500	37.9	0.89		
8	12:25	29.5	70	40.8	32.8	44	41.9500	41.5	1.00		
9	12:35	29.0	80	41.45	33.4	42.9	41.6000	39.2	0.82		
10	12:45	28.6	90	39.7	37.3	40.9	39.9000	38.7	0.84		
11	12:55	28.2	100	40.05	37.8	41.2	39.8000	39	0.86		
12	1:05	27.8	110	40.05	39.5	40.5	39.5000	38.4	0.93		
13	1:15	27.5	120	43.95	30	46.2	42.3000	41.2	1.04		
14	1:25	27.2	130	41.55	32.3	43	41.1000	40	0.91		
15	1:35	27.0	140	45.2	27.4	47.8	43.5500	41.2	1.04		
16	1:45	26.8	150	43.35	29	46.3	42.9500	41.8	0.9		
17	1:55	26.6	160	46.75	24.1	50.5	45.4000	43.7	1.03		

18	2:05	26.4	170	44	29.8	45	42.9500	41.1	0.99		
19	2:15	26.2	180	47.35	26.4	47.9	45.0000	42.3	1.08		
20	2:25	26.1	190	45.75	27.8	46.9	44.1500	40.5	1.04		
21	2:35	26.0	200	45	28.6	45.9	44.0000	40.8	0.99		

The data given in Tables 1(a) to 1(f) were used to determine the values of constant *C* and exponent *n* in the Nusselt number expression by simple linear regression analysis. Then the values of the constant *C* and exponent *n* were used further for determining the values of the convective heat transfer coefficient. The values of constants (*C* and *n*), convective heat transfer coefficients (h_c), for vermicelli drying under natural convection greenhouse mode are summarized in Table 2(a) to 2(f).

Table 2(a): Values of *C*, *n* and h_c under natural convection Even Span greenhouse drying vermicelli samples for 1.25 mm diameter

Diameter of vermicelli (mm)	C	N	h_c ($W/m^2\,^oC$)	$h_{c,\,avg.}$ ($W/m^2\,^oC$)
1.25	1.19	0.09	0.66 - 0.85	0.76
	0.91	0.11	0.52 - 0.81	0.67
	0.86	0.12	0.54 - 0.8	0.68

Table 2(b): Values of *C*, *n* and h_c under natural convection Slant Height greenhouse drying vermicelli samples for 1.25 mm diameter

Diameter of vermicelli (mm)	C	N	h_c ($W/m^2\,^oC$)	$h_{c,\,avg.}$ ($W/m^2\,^oC$)
1.25	1.53	0.04	0.49 - 0.58	0.54
	1.33	0.08	0.63 - 0.79	0.71
	1.17	0.07	0.56 -0.64	0.60

Table 2(c): Values of *C*, *n* and h_c under natural convection Even Span greenhouse drying vermicelli samples for 2 mm diameter

Diameter of vermicelli (mm)	C	N	h_c ($W/m^2\,^oC$)	$h_{c,\,avg.}$ ($W/m^2\,^oC$)
2	0.71	0.15	0.69 - 1.09	0.90
	0.68	0.17	0.66 - 1.34	1.00
	0.59	0.17	0.69 - 1.27	1.08

Table 2(d): Values of *C*, *n* and h_c under natural convection Slant Height greenhouse drying vermicelli samples for 2 mm diameter

Diameter of vermicelli (mm)	C	N	h_c (W/m^2 ^{o}C)	$h_{c, avg.}$ (W/m^2 ^{o}C)
2	1.47	0.05	0.51 - 0.61	0.60
	1.15	0.12	0.72 - 1.21	1.07
	0.69	0.15	0.57 -1.09	0.90

Table 2(e): Values of *C*, *n* and h_c under natural convection Even Span greenhouse drying vermicelli samples for 3 mm diameter

Diameter of vermicelli (mm)	C	n	h_c (W/m^2 ^{o}C)	$h_{c, avg.}$ (W/m^2 ^{o}C)
3	0.61	0.17	0.88 - 1.29	1.09
	1.40	0.10	0.82 - 1.09	1.05
	0.87	0.17	1.08 - 1.9	1.50

Table 2(f): Values of *C*, *n* and h_c under natural convection Slant Height greenhouse drying vermicelli samples for 3 mm diameter

Diameter of vermicelli (mm)	C	n	h_c (W/m^2 ^{o}C)	$h_{c, avg.}$ (W/m^2 ^{o}C)
3	1.37	0.06	0.55 - 0.66	0.61
	1.10	0.09	0.61 – 0.78	0.70
	1.16	0.12	0.72 -1.14	0.93

It is observed from Table 2(a) to 2(f) that the values of constant *C* and exponent *n* vary from 0.59 to 1.53 and 0.04 to 0.17 respectively. The convective heat transfer coefficients were observed to vary from 0.49 W/m^2 °C to 1.34 W/m^2 °C respectively. It is observed that different values of convective heat transfer coefficients were obtained for similar vermicelli sample dried on consecutive days. This variation may be due to change in operating conditions on each day.

The variation in convective heat transfer coefficients with drying time is illustrated in Figs. 4.1 to 4.6 respectively:

Vol.2 Issue.3,
March 2014.
Pgs: 64-80

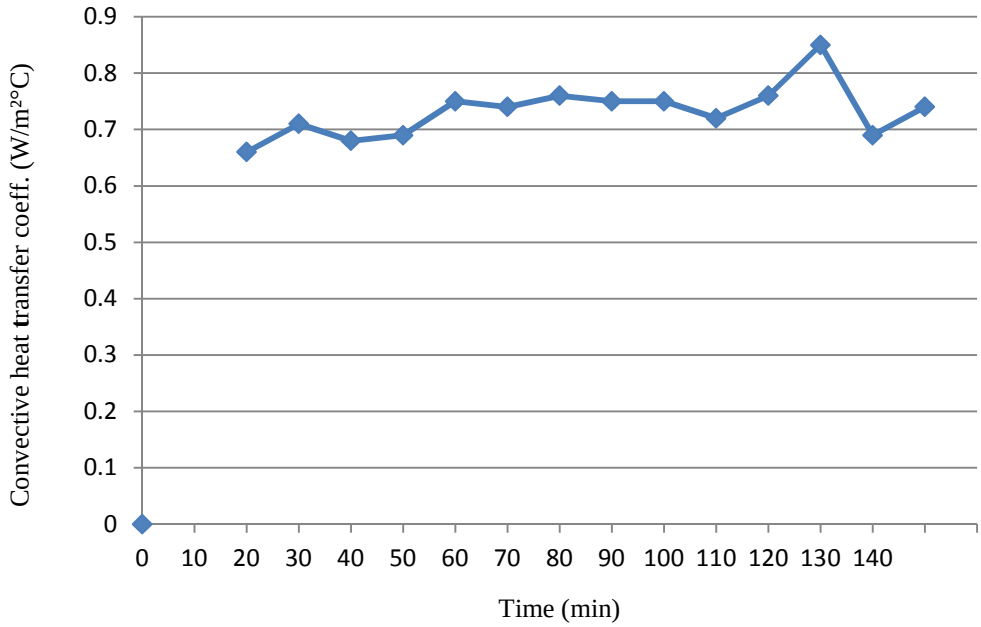

Figure 4.1: Heat Transfer Coefficient (h_c) vs Thickness vermicelli (mm) samples for 1.25 mm diameter drying in Even Span greenhouse

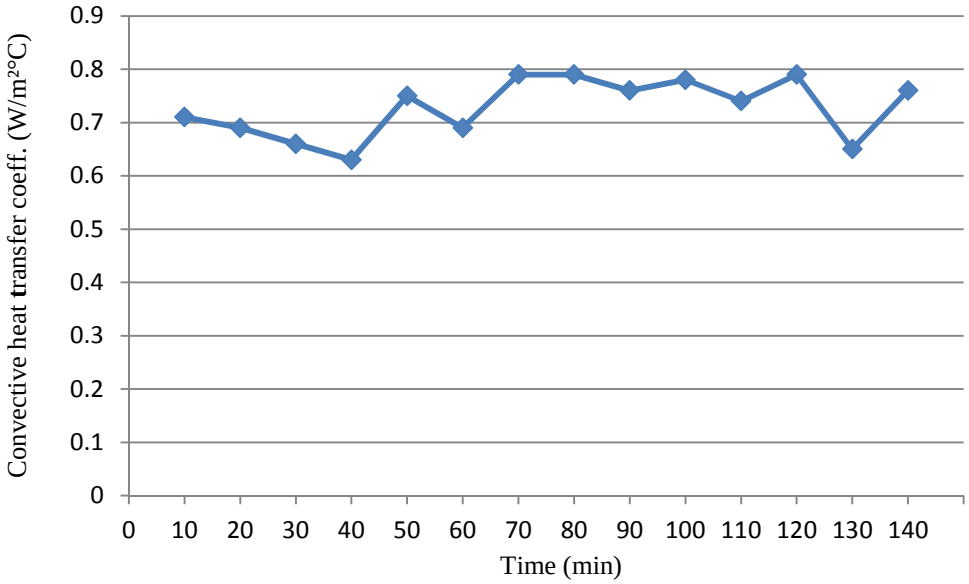

Figure 4.2: Heat Transfer Coefficient (h_c) vs Thickness vermicelli (mm) samples for 1.25 mm diameter drying in Slant Height greenhouse

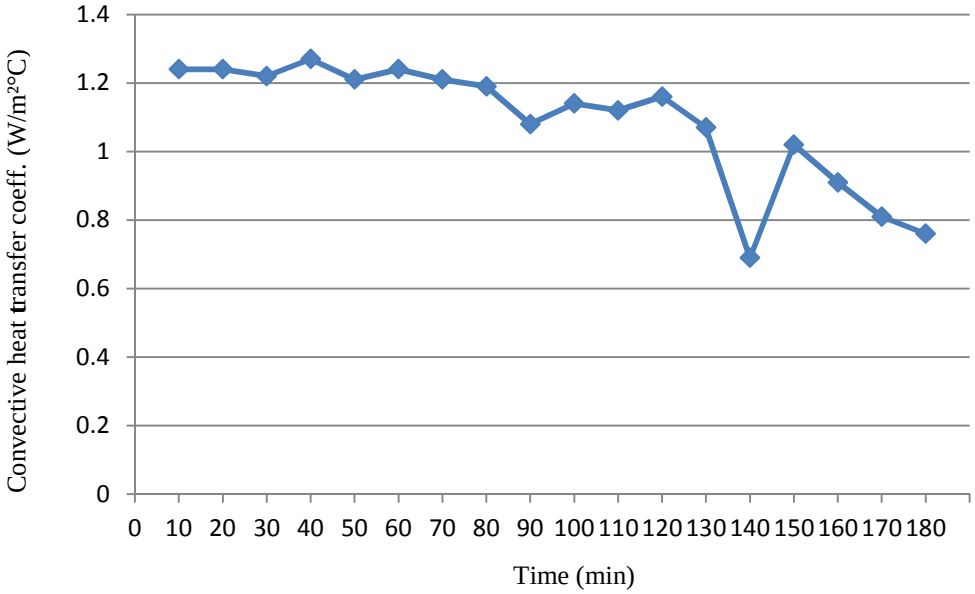

Figure 4.3: Heat Transfer Coefficient (h_c) vs Thickness vermicelli (mm) samples for 2 mm diameter drying in Even Span greenhouse

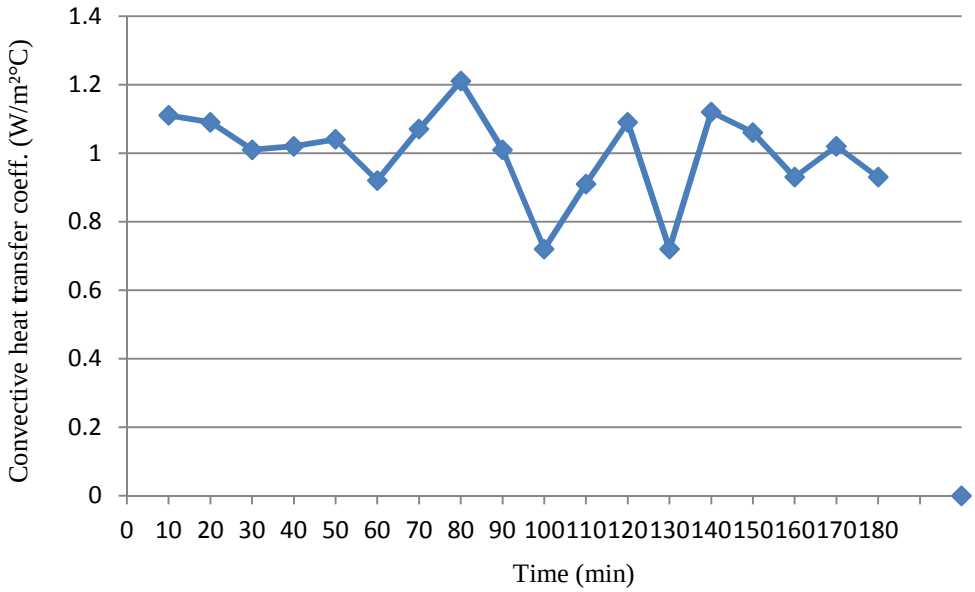

Figure 4.4: Heat Transfer Coefficient (h_c) vs Thickness vermicelli (mm) samples for 2 mm diameter drying in Slant Height greenhouse

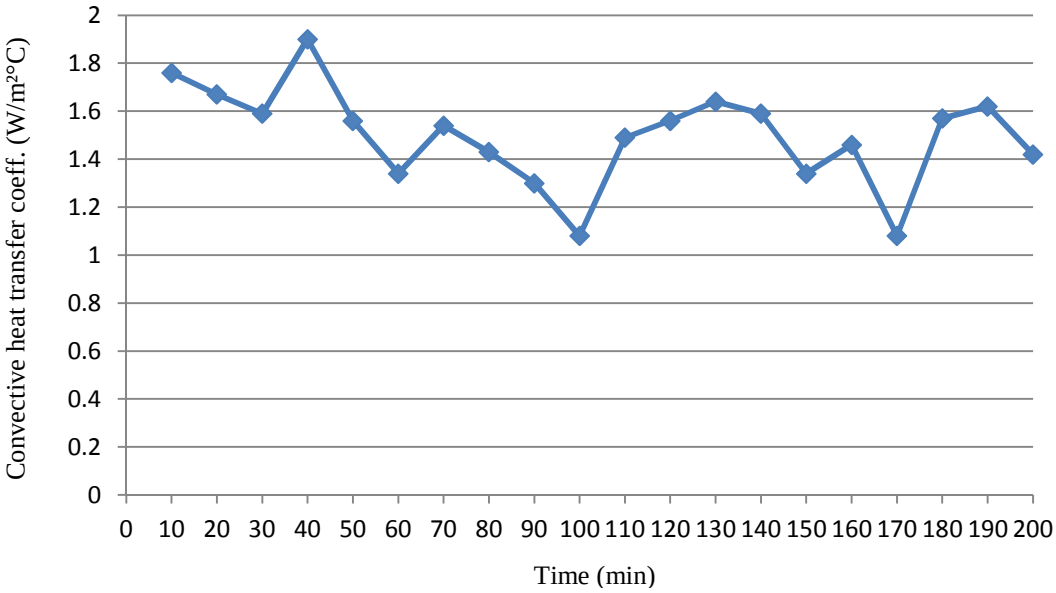

Figure 4.5: Heat Transfer Coefficient (h_c) vs Thickness vermicelli (mm) samples for 3mm diameter drying in Even Span greenhouse

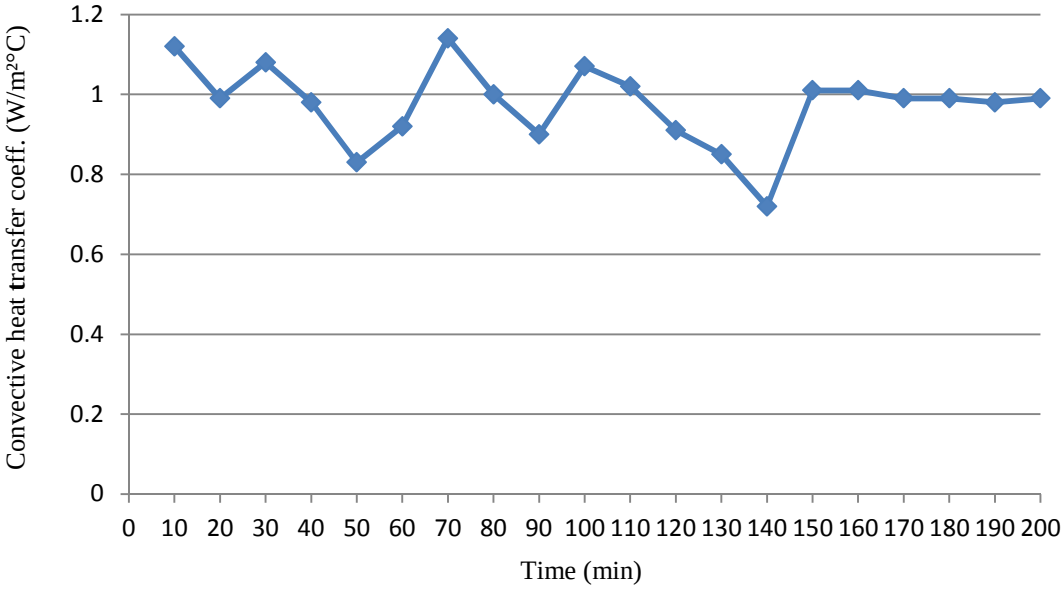

Figure 4.6: Heat Transfer Coefficient (h_c) vs Thickness vermicelli (mm) samples for 3 mm diameter drying in Slant Height greenhouse

Nomenclature

A_t	Area of rectangular wire mesh tray, m^2
C	Experimental constant
C_v	Specific heat of humid air, J/kg °C
g	Acceleration due to gravity, m/s^2
Gr	Grashof number $= \beta g X^3 \rho_v^2 \Delta T / \mu_v^2$
h_c	Convective heat transfer coefficient, W/m^2 °C
$h_{c,av}$	Average convective heat transfer coefficient, W/m^2 °C
K_v	Thermal conductivity of humid air, W/m °C
m_{ev}	Moisture evaporated, kg
n	Experimental constant
Nu	Nusselt number $= h_c X / K_v$
Pr	Prandtl number $= \mu_v C_v / K_v$
$P(T)$	Partial vapor pressure at temperature T, N/m^2
Q_e	Rate of heat utilized to evaporate moisture, J/m^2 s
t	Time, s
Ta	Ambient temperature, °C
Tg	Greenhouse temperature, °C
T_v	Vermicelli surface temperature, °C
T_e	Temperature just above vermicelli surface, °C
$\overline{T}_v$	Average vermicelli surface temperature, °C
$\overline{T}_e$	Average temperature of humid air, °C
T_i	Average of vermicelli surface and humid air temperature, °C
ΔT	Effective temperature difference, °C
X	Characteristic dimension, m

Greek Symbols

β	Coefficient of volumetric expansion, 1/ °C
γ	Relative humidity, %
$\bar{\gamma}$	Average relative humidity, %
λ	Latent heat of vaporization, J/kg
μ_v	Dynamic viscosity of humid air, N s/m²
ρ_v	Density of humid air, kg/m^3

5. Conclusion

The convective heat transfer coefficients for vermicelli under natural convection greenhouse drying mode were evaluated by using the values of the constants (*C* and *n*) in the Nusselt number expression obtained for vermicelli based on experimental data by using simple linear regression analysis. The values of the constant *C* and exponent *n* were found to be 0.59 to 1.53 and 0.04 to 0.17 respectively. The values of convective heat transfer coefficients were observed to vary from 0.51 W/m^2 ^{o}C to 1.50 W/m^2 ^{o}C respectively. The values of h_c average have been observed to vary from 0.54 W/m^2 °C to 1.50 W/m^2 °C.

References

1 Werner W. and Buchinger J. (2002) "Handbook of Solar Drying", AEE INTEC, *Institute for Sustainable Technologies*, Austria.

2 http://www.rajdhanigroup.com/vermicelli.html"Rajdhanigroup vermicelli"/pdf, Retrieved on 12/12/2014.

3 Sehrawat (2012) "Thesis on An Experimental study on open sun drying of vermicelli".

4 Jain, D., and Tiwari, G.N., (2003),"Thermal aspects of open sun drying of various crops", *Journal of Food Technology*, Vol.28, No.1, pp. 37-54.

5 Kumar S. (2012) "Thesis on Convective Heat transfer coefficient of papad during greenhouse drying".

6 http:// www.inseda.org/ (2009), "A manual on rural solar food processing technologies"/pdf, Retrieved on 13/02/2014.

7 Kumar, M., Khatak**,** P.**,** Kumar, R., and Parksh, O. (2011), "The effect of open sun and indoor forced convection on heat transfer coefficient for drying of papad", *Journal of Energy in Southern Africa*, Vol.22, No.2, pp.40-46.

8 Tiwari, G. N. and Jain, D. (2003), "Thermal aspect of open sun drying of various crops", *Journal of Food Technology*, Vol.28, pp. 37-54.

9 John W. Bartok, Jr. (2000), "Greenhouses for Homeowners and Gardeners", *NRAES-137 Published by NRAES*.

10 Dr. Giacomelli G (2012), "Your First Greenhouse: What You Need to Know", *NRAES-137, ISBN: 0-935817-51-4*, E-mail: NRAES@cornell.edu, http://www.nraes.org/.

11 Tiwari G.N., (2006), "Handbook of Solar Energy", New Delhi, Narosa: ISBN 81-719-450-5.

12 Akpinar, E.K. (2004),"Experimental investigation of convective heat transfer coefficient of various agricultural products under open sun drying", *International Journal of Green Energy*, Vol. 1, No. 4, pp. 429-440.

13. Malik, M.A.S.; Tiwari, G.N.; Kumar, A.; and Sodha, M.S. (1982). *Solar distillation*. Pergamon Press, Oxford.

14. Kumar, M.; Kasana, K.S.; Kumar, S.; and Prakash, O. (2011). Experimental investigation on convective heat transfer coefficient for khoa drying. *International Journal of Current Research*, 3(8), 88-93.

15. Kumar, M.; Prakash, O.; and Kasana, K.S. (2011). Experimental investigation on natural convective heating of milk. *Journal of Food Process Engineering*, 35(5), 715-726.

16 Jain, D., and Tiwari, G. N., (2004), "Effect of greenhouse on crop drying under natural and forced convection I: Evaluation of convective mass transfer coefficient", *Energy Conversion and Management*, Vol. 45, pp. 765-783.

17 Sehdev et al (2012), "Convective heat transfer coefficient for indoor forced convection drying of vermicelli". *IOSR Journal of Engineering*, Vol. 2(6) pp: 1282-1290.

18 Sehdev et al (2012), "An Experimental Study on Open Sun Drying of Vermicelli", *International Journal of Advances in Engineering Sciences*, Vol.2, Issue 3.

19 Kumar, R., Kumar, M., Rathi, C., (2013), "Convective heat transfer coefficient for indoor forced convection drying of corn kernels", *International Journal of Mechanical Engineering and Robotics Research, ISSN 2278 – 0149*,Vol. 2, No. 4.

A Brief Author Biography

Punit Kumar received his Bachelor's degree in Mechanical Engineering from Guru Jambheshwar University of Science & Technology, Hisar, Haryana (India). He is currently doing Master's degree in Mechanical Engineering from Guru Jambheshwar University of Science & Technology, Hisar, Haryana (India).

Non-parametric Clustering and Topic Modeling via Small Variance Asymptotics with Local Search

A Thesis

Presented in Partial Fulfillment of the Requirements for the Degree Master of Science in the Graduate School of The Ohio State University

By

Siddharth Singh, B.E

Graduate Program in Department of Computer Science & Engineering

The Ohio State University

2013

Master's Examination Committee:

Brian Kulis, Advisor

Eric Fosler-Lussier

© Copyright by

Siddharth Singh

2013

Abstract

Clustering of data has been a very well studied topic in the Machine Learning community, with various different methods trying to solve the same problem of grouping similar objects together. Traditional approaches have been algorithmically simpler and easier to implement with reasonable results. More recently, algorithms derived from asymptotics on Bayesian Non-parametric Infinite Mixture Models have appeared as an alternate. These algorithms in general have pointed at a very clear relation between probabilistic methods like Expectation Maximization, and hard assignment based algorithms like K-Means. They provide both the flexibility of a Bayesian Non-parametric model and scalability of hard clustering algorithms like K-Means. Aysmptotics on further complex mixture models have been used to derive algorithms that resemble hierarchical clustering and hard Topic Modeling.

Although these new algorithms are highly scalable and they open a new dimension in modeling data based on different similarity measures, they still suffer from problems traditionally seen in any optimization based method, like that of local optima. Also, being non-parametric in nature, parameters like number of clusters are not fixed upfront in these algorithms. This leads to a new problem of choosing the right set of initial values for the parameters existing in the model. This work primarily addresses the issues of local optima and how to reject sub-optimal solutions and get *better* solutions, and also the initialization of the values of parameters present in the model.

We achieve this by adding certain new steps to the existing algorithm, and at last we quantitatively verify the improvements.

Our focus would be mostly on the K-Means like algorithm derived from asymptotics on the Dirichlet Process Mixture Model of infinite Gaussians, and its extension to hierarchies via the Hierarchical Dirchlet Process. We will also focus on a similar mixture model more generalized by replacing Gaussians with the Exponential family of distributions. The algorithm derived from its hierarchical version resembles hard Topic Modeling in a special case, which is one of our main areas of focus.

All of the code related to this work has been compiled into a software which can be used to perform scalable Non-parametric hard clustering via DP-Means and hard Topic Modeling over sparse documents. The code and executables for the software are free to download and use.

Acknowledgments

First and foremost I would like to thank my Adviser, Dr. Brian Kulis, for all of his guidance and support during the entire course of this Thesis. Without him this piece of work was unthinkable. I could not have imagined a better adviser and mentor for my Master's studies.

Besides my adviser, I would like to thank my Thesis committee member, Dr. Eric Fosler-Lussier for taking time out of his schedule and all the encouragement and guidance. I also thank Ke Jiang for his insightful opinions on some really crucial ideas that I stumbled upon.

Lastly, and importantly, I thank my family for always supporting me in all of my pursuits.

Vita

2006-2010 ..... B.E. Computer Engineering,
Delhi College of Engineering

2011-present ..... Graduate Student,
The Ohio State University

Publications

Research Publications

Dasgupta, U.; Singh, S.; Jewalikar, V "Sunspot Number Calculation Using Clustering". *NCVPRIPG*, 2011.

Jewalikar, V.; Singh, S. "Automated Sunspot Extraction, Analysis and Classification". *IVPCV*, 2010.

Table of Contents

Page

Abstract ii

Acknowledgments iv

Vita v

List of Tables viii

List of Figures ix

1. Introduction 1

    1.1 Motivation and Background 4
    1.2 Sparse Documents and the Bag-of-Words Model 6
    1.3 Contributions 8

2. Background on Clustering and Expectation-Maximization 9

    2.1 K-Means and Expectation-Maximization 10
    2.2 Challenges in K-Means 11
    2.3 Topic Modeling 13
        2.3.1 Latent Dirichlet Allocation 14
        2.3.2 Topic Modeling through Clustering 16

3. Background on Algorithms via Small Variance Asymptotics 18

    3.1 Dirichlet Process Mixture Models 19
        3.1.1 DP-Means 21
    3.2 Hierarchical Dirichlet Process Mixture Model and Hard HDP . . . 23
    3.3 Extension to the Exponential Family 26

4. Parameter Selection 29

4.1 Parameters in DP-Means 30
4.2 Simple Heuristics 31
4.3 Initialization Strategies using Parametric methods 32

5. Local Search 34

5.1 Local Optima and Singleton Clusters in DP-Means & Hard HDP . 35
5.2 Local Search and Merge move 38

6. Experimental Results 41

6.1 DP-Means 42
6.1.1 Clustering with new Parameters 48
6.1.2 Clustering with Local Search and new Parameters 48
6.2 Hard Exponential HDP with KL-Divergence 55
6.2.1 Topic Modeling on Sparse Documents 55
6.2.2 Topic Modeling with Local Search 56

7. Conclusion and Future Work 58

Appendices 60

A. Software for running DP-Means and Topic Modeling 60

Bibliography 61

List of Tables

Table **Page**

1.1 A Data-set of three documents 7

1.2 A Vocabulary over the Data-set in Table 1.1 7

1.3 A Data-set of three documents in BOW Model 7

3.1 The DP-Means algorithm [4] 21

3.2 The Hard-HDP algorithm [4] 24

4.1 Parameter Initialization in DP-Means 33

6.1 DP-Means Clustering on KOS 45

6.2 DP-Means Clustering on NIPS 45

6.3 Average classification error after clustering over 4 different synthetic mixtures 54

6.4 Topics obtained from the NIPS data-set 55

6.5 Topics obtained from the NYTimes data-set 56

List of Figures

Figure **Page**

1.1 K-Means on data sampled from 3 Gaussians 2

1.2 Expectation-Maximization on data sampled from 3 Gaussians 3

2.1 Topic Modeling problem description [7] 14

2.2 Graphical Model describing LDA [7] 15

4.1 A Clustering of data showing the maximum distance of a point from its mean 31

5.1 A continuous function of degree four 35

5.2 The given set of inputs for Clustering 36

5.3 A possible state of Convergence for DP-Means 37

6.1 Synthetic data sampled from three Normal distributions 42

6.2 Final state of Clustering after running DP-Means for a fixed value of λ 43

6.3 Cost function for DP-Means over the synthetic data-set 44

6.4 Cost function for the KOS data-set during DP-Means 46

6.5 Cost function for the NIPS data-set during DP-Means 47

6.6 Averaged Cost functions in case of standard DP-Means (blue) and DP-Means with Local search (red) for the synthetic data 50

6.7 Best state of clustering at convergence on the synthetic data after using Local search 51

6.8 Averaged Cost functions of DP-Means with (red) and without (blue) Local search compared over the KOS data-set 52

6.9 Averaged Cost functions of DP-Means with (red) and without (blue) Local search compared over the NIPS data-set 53

6.10 Cost function comparison of Topic Modeling with and without Local search on the NYTimes data-set 57

Chapter 1: Introduction

Clustering of data has always been a problem of interest to Statisticians and Computer Scientists. It sees applications in various fields which employ statistical data analysis, like machine learning, information retrieval, pattern recognition and bio-informatics. At its root the problem is of grouping *similar* object based on a measure. At present, various algorithms differing in their complexity, ease of implementation and scalability, try to solve this same problem. Some of the simpler algorithms have been around for more than forty years now [1]. Out of those the most popular is unarguably the K-Means algorithm [2]. The algorithm is still very much popular owing to its simplicity and scalability, making it a widely acceptable method for cluster analysis. Inherently the problem of clustering is NP-hard but heuristics can be used to find solutions that are reasonable.

The notion of a cluster in a traditional clustering algorithm or mixture models can be defined as a group or subset of data objects within a data-set. Although different methods treat clusters differently, a common divide is between algorithms that assign objects hard and soft labels. These labels or cluster indicators denote the group that they belong to. The hard assignment allocates labels that can have only one value, and a single data point can belong to only one cluster. K-Means is an example of this category of algorithms. In contrast, the probabilistic methods like

Expectation-Maximization [6] allocates soft values to the cluster indicators, meaning that a single point will have a certain probability of belonging to every cluster.

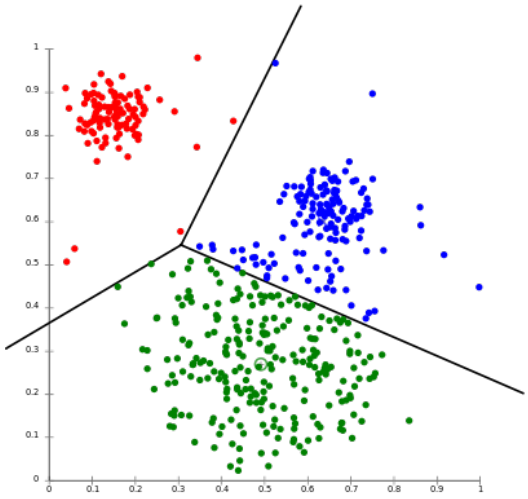

Figure 1.1: K-Means on data sampled from 3 Gaussians

In Figure 1.1 the data has been sampled from three different Gaussians and the result of the K-Means clearly shows that there is a distinct boundary between each cluster, and a single data point belongs only to one cluster with points of same color belonging to the one cluster.

Comparing it to Figure 1.2 which is the result of running Expectation-Maximization on the same data sampled from three different Gaussians, the parameters of the Gaussians have been estimated as shown by the circular boundaries. Although every point can be said to be closer to one of the Gaussian centers, there is a probability associating them with every other Gaussian center. This difference, and similarity to some

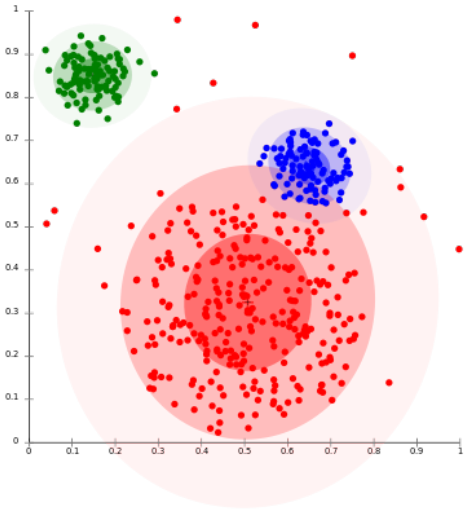

Figure 1.2: Expectation-Maximization on data sampled from 3 Gaussians

extent, is one of the key motivations behind this body of work, as it will become more evident in the following chapters of this thesis.

More recently, Non-parametric mixture models based in Bayesian Statistics have been suggested as alternate. These models provide added flexibility in the model by not fixing parameters like the number of clusters upfront. The Dirichlet Process Mixture [3] has been the most influential on this work since most of the algorithms derived have their roots in one way or the other in the DP Mixture Model. Although, these newer algorithms give a very flexible alternate, the flexibility comes at a cost of compromise in scalability. Bayesian algorithms suffer from slow inference methods making them impractical in a lot of scenarios. Previous works have tried to find relations between simple probabilistic and Bayesian Non-parametric methods, with hard assignment methods to exploit the good of both the worlds, namely flexibility

of being non-parametric and scalability of hard assignments. Our work explores this new breed of algorithms derived from doing Small Variance Asymptotics on existing mixture models. We try to address some of the problems arising in them like local optima, singleton clusters and initialization. Our work has been compiled into a software package which allows running these scalable algorithms over large and sparse data-sets.

1.1 Motivation and Background

The main motivation behind this work comes from asymptotics done over the Dirichlet Process Mixture Model of Infinite Gaussians, from which a hard clustering like non-parametric algorithm called DP-Means is derived [4]. Further extensions to a hierarchical setup and generalization over the exponential family [5], and their relation to Topic Models are the areas we explore in this work.

As pointed out earlier, the type of algorithms derived from the asymptotics over the Bayesian Infinite mixture models have both the flexibility in terms of complexity of the model as it grows, and at the same time the scalability and ease of implementation of a classical hard assignment based algorithm. Despite of this they suffer from problems like suboptimal solutions due to local optima during the optimization and creation of Singleton clusters. Moreover, since there are no exploit parameters, like the number of clusters, that directly control the output of the algorithm, these all methods in general suffer from a problem of initialization. The parameters present in these models are a part of the cost function but they lack the intuitive insight that a more direct parameter, like the number of clusters, provides into the final output of the algorithm.

To get to the background of this work, we go back to the original work [4] where the subtle relations between probabilistic mixture models and hard clustering algorithms were shown. The same relations were extended over Infinite Mixture of Gaussians, or the Dirichlet Process Mixture Model [3]. The result was a new K-Means like algorithm called DP-Means. This new algorithm was similar to the K-Means algorithm since it was built on a similar optimization of a monotonically decreasing objective function. The objective function differed from K-Means as the penalty parameter λ was added to the regular K-Means cost function. The K-Means objective functions looks like:

$$\min_{\{l_c\}_{c=1}^{k}} \sum_{c=1}^{k} \sum_{x \in l_c} \parallel x - \mu_c \parallel^2$$

Where, μ_c is the mean of cluster c, x is the observation, and l_c is the set of points belonging to cluster c.

Based on this cost function, the algorithm works in a way to optimize it and find a state of minima. Due to the nature of steps of this method, its easy to figure out that it suffers from the common issue of local optima seen in various optimization problems. To solve this problem we use Local search as an added step in the algorithm. This search method looks for better solution after every step of the algorithm and helps in getting out of the local optima. There is also a problem of creation of singleton clusters during one of the steps of the algorithm. The way this algorithm works it discourages merging of clusters and therefore any Singleton cluster created always retains its data point. The third and last main problem we address is that of finding a way to initialize the parameters of these algorithms. In DP-Means the parameter λ signifies a penalty that is added to the cost function whenever a new cluster is created. It lacks the intuition of a parameter like the number of clusters which the user of the algorithm can set based on the requirements. To make a good suggestion

for the value of this parameter to be set initially, we propose a new method based on the parametric version of the algorithm. We will discuss this further in Chapter 3. The next section now discusses briefly the type of data we use in our experiments.

1.2 Sparse Documents and the Bag-of-Words Model

Clustering and Statistical analysis of Sparse documents is a common problem in the Natural Language and Machine Learning communities. Most of the real-word data relating to large data-sets of documents is highly sparse. This sparsity in High-dimensional data brings with it additional problems, mostly relating to the scalability of any existing method, which needs to addressed separate from the main problem in hand. This sparsity arises mostly because of the way documents are represented mathematically as a series of vectors in a data-set. This representation of documents also know as the Bag of Words model, is quite popular in the areas of Natural Language and Computer Vision. Simply speaking, every document in this model is represented as a vector over the ordered vocabulary of the data-set, with each cell representing the word count corresponding to that index. In this way every document can be represented as a vector of same size, equal to the vocabulary. And the entire data-set of documents can now be mathematically represented as a matrix of size $N \times M$, where N is the number of documents in the data-set, and M is the dimension or the size of the vocabulary. The Bag of Words model doesn't take into account the sequence of words in the original documents in the data-set. It only considers the count of each word in a document as a relevant statistic. A few examples below will further illustrate how a document is represented in this model.

James has a brown dog.
The dog is under the table.
This table belongs to James. But not the brown table.

Table 1.1: A Data-set of three documents

james	brown	dog	under	table	belongs

Table 1.2: A Vocabulary over the Data-set in Table 1.1

Lets consider that our data-set comprises of these three documents as shown in Table 1.1.

Now, when we create the vocabulary associated with this entire data-set we order all of the words in a sequence and removing all of the stop words. The vocabulary is in Table 1.2.

And the documents can now be represented as a vector of counts of each word over the vocabulary. This is shown in Table 1.3 where each row represents a distinct document and each column is the count of a particular word from the vocabulary.

1	1	1	0	0	0
0	0	1	1	1	0
1	1	0	0	2	1

Table 1.3: A Data-set of three documents in BOW Model

This small example demonstrates how documents can be represented by a Bag of Words model, where each Bag represents all of the words occurring in a single document with their counts. Additionally, in case of sparse documents most of the cells of a vector representing a single document are filled with zeroes, so to avoid storing all the zeroes we use a slightly different notation. This notation only lists words with non-zero counts with their corresponding index in the vocabulary vector. The data that we experiment on is highly sparse and therefore we will be using this new modified form of the Bag-of-Words model as part of our experiment.

1.3 Contributions

This section will further summarize our contributions in this piece of work. We open with a discussion of the background related to our work, starting with the k-Means clustering method, and pointing at some of the weaknesses in the basic algorithm. We suggest some alternate approaches to clustering, namely non-parametric approaches that do not fix the number of clusters upfront. We build our work on the DP-Means algorithm [4] and the Hard-HDP algorithm [5].

Our contribution here addresses some of the key issues existing in these new breed of algorithms. We try to solve the problem of initialization of these algorithms by suggesting *good* values for the parameters. We then address the issue of local optima and how to *reject* sub-optimal solutions to get to a better state of clustering with a lower cost function value. We also address a key problem present in DP-Means like algorithms, namely that of creation of singleton clusters.

Chapter 2: Background on Clustering and Expectation-Maximization

Separating or Modeling mixtures has been a well studied problem by the Machine Learning community. A range of methods exist that try to model or separate data through different approaches. Some of the more successful methods are clustering based (K-Means), or probabilistic in nature (Expectation-Maximization), and lately more complex models appearing in a relatively newer area of Topic Modeling (Latent Dirichlet Allocation) have surfaced. All of these methods differ vastly in their approach to the same problem of grouping similar data-points together and bring forth the underlying structure present in the data. Through a different interpretation, they also try to optimize a mathematical function formulated differently for each problem, based on the requirements and the assumptions under a given model. In this chapter we will briefly go through all the popular existing methods used in separating a mixture of data-points. We will discuss how they differ from each other and what similarities exist in all of them. We will also argue that there is a deep underlying relation between probabilistic methods like Expectation-Maximization and hard assignment based clustering algorithms like K-Means, and which can be exploited to get to a *better* solution trying to solve the same inherent problem.

2.1 K-Means and Expectation-Maximization

This section talks about the relations between a probabilistic method Expectation Maximization [6], and a hard assignment based clustering, K-Means. We also discuss how both of these algorithms share a common theoretical ground that serves as the basis of modeling or clustering the data. We will discuss how K-Means is asymptotically related to the Expectation-Maximization [6] algorithm. Before that we discuss these two algorithms in their native forms and see how they both solve inherently a problem of grouping similar objects together via optimizing a function. We start with Expectation-Maximization and discuss its two steps and later we describe the K-Means algorithm and show how K-Means can be derived by doing asymptotics on the EM algorithm.

The Expectation-Maximization algorithm commonly used to model mixture of Gaussians is an iterative method used to estimate the parameters of a mixture models. It was first explained in 1977 by Dempster et al. [6]. The method essentially works on the principle of finding the maximum likelihood for the given set of parameters which are unobserved variables in the given model. It iterates between two steps called the Expectation step and the Maximization step. The Expectation step creates a function for the expectation of the log-likelihood of the model evaluated from the current parameters. The Maximization step actually computes the parameters that maximize the expected log-likelihood function from the E step. The algorithm runs till convergence and the final parameters are used to determine the distribution of all the latent variables in the model.

In case of fixed Gaussians with equal covariance equal to σI, the Expectation step can be shown to be:

$$\gamma(z_{ic}) = \frac{\pi \cdot exp((-\frac{1}{2\sigma} \parallel x_i - \mu_c \parallel_2^2)}{\sum_{j=1}^{k} \pi_j \cdot exp(-\frac{1}{2\sigma} \parallel x_i - \mu_j \parallel_2^2)}$$

where, $\gamma(z_i c)$ is the probability of assigning data-point i to cluster c, σ is the variance, x_i is a single observation, and μ_c is the mean of cluster c.

While doing asymptotics on this, as we see that $\sigma \to 0$ the value of the probability of assigning a data-point a certain cluster reaches zero, except for the one cluster which is closest. The M step in this case is not changed since the covariances are fixed and need not be recalculated.

Comparing this to the reassignment step of the K-Means algorithm where every point is shifted from its current mean or cluster to the closest mean, they both now assign a single point to a single cluster. We can therefore say that doing asymptotics over a probabilistic model like the Expectation-Maximization reduced it down to a hard assignment based algorithm like K-Means. Similar asymptotics done over more complex mixture models like the Dirichlet Process Mixture Model and such can lead to further interesting algorithms as we will see in the next section. Before we move on to the next section, we will take a diversion and discuss a relatively newer type of statistical modeling method called Topic Models and one of its popular implementation via the Latent Dirichlet Allocation [8].

2.2 Challenges in K-Means

K-Means algorithm is one of the most widely popular algorithm used for clustering or modeling data. Its popularity comes from the fact that in its basic form it is easy to implement and scales very well over large scale data. Although this version of the

K-Means still suffers from some problems like choice of the number of clusters K and converging at a local minima.

The K-Means algorithm starts with an assumption that the number of the clusters in the data are fixed and known. And therefore the fixed number of clusters are a part of the model and the algorithm. In situations where the number of clusters are unknown, the K-Means algorithm would not be the best way to model the data. This rigidity in terms of the number of mixing components is a weakness that the DP-Means algorithm [4] approaches in a different way. It starts out without fixing the number of clusters and growing the model in complexity as it progresses.

The other common problem seen in the basic versions of the K-Means and the DP-Means algorithm is that of local optima. Local optima is seen commonly in greedy search based algorithms over a discrete domain. Due to a local minima in case of K-Means [1] and DP-Means [4] where we are trying to minimize an objective function, it could be the case that the final state of convergence is not a good solution in terms of the objective value. In order to address this issue we can use an iterative method that searches for better solutions at every given state of clustering. In DP-Means this can be done simply, owing to the flexibility of the algorithm in terms of adjusting the number of clusters.

We will discuss in further details in the coming chapters how DP-Means is different when it doesn't fix the number of clusters upfront and how the problem of local minima is approached in such a setup.

2.3 Topic Modeling

Topic Modeling is a statistical model used to discover underlying *Topics* in a given set of documents (Figure 2.1). Some of the popular modeling methodologies consider it to be a probabilistic model with underlying distributions governing the makeup of the corpus. The goal of Topic Modeling [7] here is to infer these hidden variables which are part of these probability distributions. One of the most popular methods used for Topic Modeling is called Latent Dirichlet Allocation [8] and we will limit our discussion on Topic Models to LDA and its assumptions.

To begin with, we first argue that Topic Models are relevant to our work because inherently they are also trying to group up *similar* objects or words together and then group up those group of words together forming a topic. We will show that one of the algorithms derived through asymptotics on the Hierarchical Exponential Dirichlet Process Mixture Model resembles a hard Topic Modeling algorithm, differing from probabilistic methods similar to the way K-Means differs from EM, by having hard assignment of words or topics instead of probabilistic and soft assignments.

Going back to the subject of Topic Models [7] and LDA [8], we start with discussing some of the assumptions that the LDA makes about the structure of the data based on which its inference works. LDA being a probabilistic model makes some of these assumptions as follows. The idea of a *topic* stems from the fact that a *topic* is a distribution over the words in the vocabulary. As a next level, the *documents* are mixtures of these topics. And lastly every *word* is drawn from one of these *topics*. Also, the only observation is the corpus of documents, all of the other parameters are latent. The goal now is to infer these hidden variables and compute their distributions based on the observed documents. In the next section we will now discuss

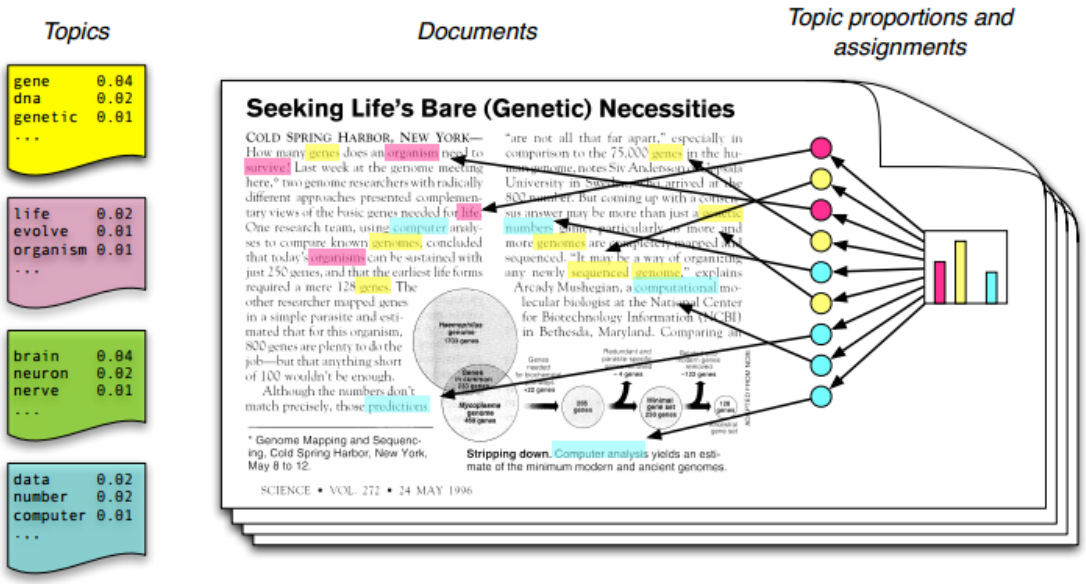

Figure 2.1: Topic Modeling problem description [7]

Latent Dirichlet Allocation in some details to understand how a probabilistic method approaches this problem as we will be comparing it with the new algorithm derived in chapter 3.

2.3.1 Latent Dirichlet Allocation

As described in the previous section the most popular method commonly used to model data-sets of documents is the LDA, or Latent Dirichlet Allocation [8]. In this section we will briefly go through the Graphical Model of the LDA and discuss what inference methods are typically used under it. The later sections will compare LDA with the new algorithm derived via asymptotics on the Exponential Hierarchical Dirchlet Process.

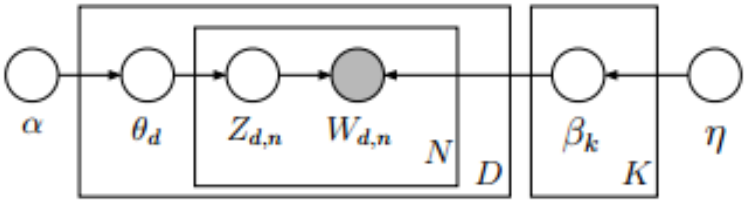

Figure 2.2: Graphical Model describing LDA [7]

The Plate Notation for the LDA is illustrated in Figure 2.2. The graphical model itself encodes all of the assumptions made, as described in the previous sections, while modeling the data. The graphical model here follows standard notations, with nodes being variables and edges showing dependencies. White nodes are unobserved while shaded nodes are observed, and plates represent repeating structures with variables. The variables, starting from left most, are - α, the proportion parameter for each topic; θ_d, the per document topic proportion; $z_{d,n}$, the per word topic proportion; $W_{d,n}$, observed word; N, number of words in the document; D, the number of documents in the corpus; β_k, the distribution of topics; K, the number of topics; η, parameter for the topic distribution. The topic proportions over documents, and the words over topic are the ones coming from the Dirichlet distribution, which in short is an exponential family distribution over the simplex. The dimension of the distribution for the topic proportions is equal to the number of topics K, and words over topic being equal to V which is the size of vocabulary or the dimension of the data in case of the hard assignment based algorithm.

The main reason why LDA works is that the word-probabilities are maximized when the words are divided into topics and in a mixture this is sufficient to search

for clusters of words that co-occur. The goal of this method is now to infer the parameters $z_{d,n}$, which is the per-word topic proportion, θ_d, the per-document topic proportion, and β_k, the per-document topic distribution. For Approximate Inference various different methods can be employed here, with one of the popular ones being the Collapsed Gibbs Sampling [9]. The posterior expectations then can be used to perform tasks like document classification, data exploration and representation etc. There are various extensions of LDA, e.g. a Dynamic Topic Model [7] that models topics that are evolving with time, or the Correlated Topic Model [7] which finds patterns in how topics co-occur in a give corpus.

To summarize in short, the goal of LDA is find out hidden structure in the data based on certain assumptions describing a thematic composition via the idea of *topics*. It works on all kind of text data, and any other data that can be transcribed into text e.g. computer vision data describing a scene based on certain features through BOW model [18]. Being probabilistic in nature, inherently inference in LDA is slow and difficult to scale-up over large and sparse data-sets. A hard-clustering based algorithm can be a possible solution and we will see more about it in the following chapter which talks about this new type of algorithms derived from asymptotics done over non-parametric mixture models which reduces them down to algorithmically simpler methods, similar to how Expectation-Maximization is related to the K-Means algorithm.

2.3.2 Topic Modeling through Clustering

As discusses earlier, Topic Modeling is a statistical method for discovering *topics* in the given data. The idea of topics is an abstract one and with the assumptions that

a Topic Model [6] makes, its is not entirely clear how a clustering based algorithm can attempt to model the data under similar constraints.

Looking at the output of the Topic Modeling, one can see that the organization of words into topics and then topics into documents has a certain hierarchy. Each word in a document can be said to belong to one or more than one topics, and then similarly each document can be said to have been made out of one or more than topics. Topic Modeling with LDA is a probabilistic method and therefore it assigns soft values for each of these relationships between a word and a topic, and a topic and a document. Intuitively, if a similar asymptotic applied to a setup like that of LDA it may give rise to a hard Topic Modeling algorithm, where a single word in a document will belong only to one topic. A hierarchical model with sharing of means at the global level (topics) and local clusters of words in a document, with the local clusters making global clusters, seems like a good choice to start with. We will see in further details how the Hierarchical Dirichlet Process over the exponential family generalizes [5] the idea of infinite mixture models, and then under a special case (for multinomials) the algorithm resembles Topic Modeling as shown in our experiments.

Chapter 3: Background on Algorithms via Small Variance Asymptotics

We discussed in Section 2.1 how a Probabilistic algorithm like the Expectation-Maximization is closely related to a hard-assignment based clustering method, K-Means; and also how they both try to solve the same problem of modeling mixture of gaussians. Extending the same argument of asymptotic similarity over further complex mixture models where the covariance of mixtures is fixed gives rise to a new method of deriving non-probabilistic algorithms from Bayesian or probabilistic methods, referred to as Small Variance Asymptotics. These new algorithms try to exploit the good of both the worlds by being flexible due to the non-parametric nature and scalable at the same time due to the hard-assignment nature. Previously, such Small Variance Asymptotics have been done on the Dirichlet Process Mixture of Gaussians, and its hierarchical version on the HDP [4]. An extension on the Dirichlet Process over the exponential family of Mixtures and then its hierarchical version has also been explored [5]. In this chapter we go through these asymptotics and the derivations of the algorithms that serve as the basis of this work in the following chapters.

3.1 Dirichlet Process Mixture Models

The Gaussian Mixture model is one of the simplest and most studied of all the mixture models. The GMM is based on the fact that the number of distributions are fixed and therefore makes it somewhat rigid in some sense. It doesn't allow the model to grow in complexity at any point since the total number of mixture components remain constant. In contrast, Non-parametric mixture models, or Infinite Mixture models do not make any such assumption. One such mixture model is the Dirichlet Process over a Mixture of Gaussians [3].

The Dirichlet Process is a Stochastic Process and a distribution over random distributions. It has two parameters H and α, standing for the base distribution and the concentration factor respectively. Considering it as a generative model a sample from the DP will output a random distribution from a value drawn from H. A much simpler description of the Dirichlet Process says that it is a generalized infinite dimensional Dirichlet distribution instead of K which is a parameter of the Dirichlet distribution governing the dimensions. This immense possibility of modeling any mixture over infinite components in the limit makes it a very solid Non-parametric mixture model. The Dirichlet Process was first described in 1973 by Thomas Ferguson. [10]

Now speaking of the mixture model over gaussians, as we fix the covariance of the distributions to σI we can describe the Bayesian model as:

$$
\begin{aligned}
&\mu_1, ..., \mu_k \sim G_0 \\
&\pi \sim Dir(k, \pi_0) \\
&z_1, ..., z_n \sim Discrete(\pi) \\
&x_1, ..., x_n \sim \mathcal{N}(\mu_z, \sigma I)
\end{aligned}
$$

Next, based on this description now asymptotics on the DP mixture model is done as described in details in [4]. G_0, which is the prior distribution over the means now becomes a zero-mean Gaussian with σI covariance. We will now skip forward to the final form of the Gibbs probabilities after simplifying. For more detailed derivations refer to the original work [4].

Therefore, the Probability of a point moving to an existing cluster is:

$$\frac{n_{-i,c} \cdot exp(-\frac{1}{2\sigma} \parallel x_i - \mu_c \parallel^2)}{exp(-\frac{\lambda}{2\sigma} - \frac{\|x_i\|^2}{2(\rho+\sigma)}) + \sum_{j=1}^{k} n_{-i,j} \cdot exp(-\frac{1}{2\sigma} \parallel x_i - \mu_j \parallel^2)}$$

and the Probability of a point creating its own cluster is:

$$\frac{exp(-\frac{\lambda}{2\sigma} - \frac{\|x_i\|^2}{2(\rho+\sigma)})}{exp(-\frac{\lambda}{2\sigma} - \frac{\|x_i\|^2}{2(\rho+\sigma)}) + \sum_{j=1}^{k} n_{-i,j} \cdot exp(-\frac{1}{2\sigma} \parallel x_i - \mu_j \parallel^2)}$$

where, $n_{-i,c}$ is the number of points in cluster c without the point in consideration, σ is the coefficient of the covariance matrix of the normal distribution $\mathcal{N}$ from which the data is coming, ρ is the coefficient of the covariance matrix of the origin centered prior normal distribution G_0 from which the μ_i are coming, x_i are the observation, and μ_c are the means of cluster c.

Considering the asymptotic behavior now, it can be seen that as $\sigma \to 0$ with a fixed covariance σ, the λ term remains the dominating term in the numerator and all of these probabilities become binary. In limit, the smallest value of the squared Euclidean norm between a data-point x_i a mean μ_k dominate the denominator, with only the smallest value receiving a non-zero probability. This now looks exactly like the assignment step of the K-Means algorithm, where a point is reassigned to the closest mean. And we create a new cluster when the squared Euclidean norm is greater than *lambda*. Given this asymptotic detail, a new algorithm can be now described. It is now a Hard-assignment based K-Means like algorithm where a point

can join an existing mean or create its own cluster based on whether or not the closest mean has a squared Euclidean norm within a certain value. The next section discusses this new algorithm as described first in [4].

3.1.1 DP-Means

The result of Small Variance Asymptotics on the Dirichlet Process Mixture now is a K-Means like algorithm, called DP-Means [4]. The steps of the algorithm are given in Table 3.1. It accepts as input the data in a sequence with *lambda* the cluster penalty parameter. The algorithm starts out with a single mean and splitting out data-points based on certain conditions.

Input: $x_1, ..., x_n$: input data, λ: cluster penalty parameter
Output: Clustering $l_1, ..., l_k$ and number of clusters k

1. Init. $k = 1$, $l_1 = \{x_1, ..., x_n\}$ and μ_1 the global
2. Init. cluster indicators $z_i = 1$ for all $i = 1, ..., n$

Repeat 3-5 until convergence

3. For each point x_i:
   - Compute $d_{ic} = \| x_i - \mu_c \|^2$ for c = 1 ,..., k
     - If $min_c d_{ic} > \lambda$, set $k = k + 1$, $z_i = k$, and $\mu_k = x$
     - Otherwise set $z_i = argmin_c d_{ic}$.
4. Generate clusters $l_1, ..., l_k$ based on $z_1, ..., z_k$
5. Compute means of the clusters, $\mu_j = \frac{1}{|l_j|} \sum_{x \in l_j} x$

Table 3.1: The DP-Means algorithm [4]

The first step inside the iterative part of the algorithm calculates the Square Euclidean norm of every point and every mean (single mean in the first iteration). If

the closest mean has a value of its norm with the point greater than λ then a new cluster is started and that point is assigned to it. Otherwise, the point is reassigned to the closest mean. After every step the means are updated and the algorithm runs until convergence.

Since, this is a K-Means like algorithm there should be a similar objective function or cost function associated with it which we are trying to minimize. The objective is nothing but the K-Means objective with a penalty term added to it as shown below.

$$\min_{\{l_c\}_{c=1}^{k}} \sum_{c=1}^{k} \sum_{x \in l_c} \| x - \mu_c \|^2 + \lambda k$$

where, μ_c is the mean of cluster c.

It can be proved that this is a monotonically decreasing function by a simple argument that none of the steps increase in the value of this function at any point. When a point is reassigned because the distance between the point and the mean was less than λ, the function will not increase. And when we create a new cluster because the closest mean was at a distance greater than λ we can pay a penalty of λ which gets added to the cost function in the second term. The algorithm will converge locally is also guaranteed since the cost function is not increasing and there are only a finite possible arrangements for the clustering.

With this we now move on to further complex mixture models and see the result of asymptotics over them and what different scalable algorithms can be derived which can be used for tasks such as Clustering, Hierarchical Clustering etc.

3.2 Hierarchical Dirichlet Process Mixture Model and Hard HDP

Extending the notion of asymptotics now over a hierarchical process like the Hierarchical Dirichlet Process will lead us to a different algorithm. Comparing it with the Dirichlet Process, the most significant change in the model is that G_0 is now not used as a base measure and instead we replace it with a Dirichlet process with its base measure being a prior over the means. The resulting process is now hierarchical in nature and can be used to model multiple datasets with the datasets being clustered internally and at a higher level with a sharing of the means. The Hierarchical Dirichlet Process and its sampling algorithm is discussed in detail in Teh et. al. [11].

The basic idea in this Hierarchical version is that we will have a set of data-sets. These Data-sets will independently and locally cluster the data-points, and also some of the means of these clusters will be shared across the data-set. Therefore, each data-point will be associated to a local cluster and each local cluster will be associated with a global mean giving rise to a hierarchy. This kind of a setup now starts to resemble a hard assignment based Topic Modeling algorithm where the global means represent Topics, and local means are clusters of words inside a document all belonging to the same topic or global mean. We will next describe the Hard HDP algorithm derived from asymptotics over the Hierarchical Dirichlet Process. Take note that all of these mixture models are built over the Gaussian distribution.

Starting with DP-Means and how the one parameter added in its cost function makes it a converging Optimization problem, adding a new parameter on top of the existing λ makes it hierarchical in nature. The two parameters now are representing the local threshold for local clusters within a data-set, and a global threshold for the

global clusters shared across the data-sets. Table 3.2 shows the Hard-HDP algorithm and its steps in details.

Input: $\{x_{ij}\}$: input data, λ_l, λ_g: local and global cluster penalty parameters
Output: Clustering $l_1, ..., l_g$ and number of clusters k_j for every data set j

1. Init. $g = 1$, $k_j = 1$ for all j and μ_1 to be the global mean
2. Init. local cluster indicators $z_{ij} = 1$ for all i and j
3. Init. global cluster associations $v_{j1} = 1$ for all j

Repeat 5-7 until convergence

5. For each point x_{ij}:
   - Compute $d_{ijp} = \parallel x_i - \mu_p \parallel^2$ for $p = 1, ..., g$
   - For all p such that $v_{jc} \neq p$ for all $c = 1, ..., k_j$, set $d_{ijp} = d_{ijp} + \lambda_l$
   - If $min_p d_{ijp} > \lambda_l + \lambda_g$
     - Set $k_j = k_j + 1$, $z_i j = k$, $g = g + 1$, $\mu_g = x_{ij}$, and $v_{jk_j} = g$
   - Else, let $\hat{p} = argmin_p d_{ijp}$
     - If $v_{jc} = \hat{p}$ for some c, set $z_{ij} = c$ and $v_{jc} = \hat{p}$
     - Else, set $k_j = k_j + 1$, $z_{ij} = k_j$, and $v_{jk_j} = \hat{p}$
6. For all local clusters:
   - Let $S_{jc} = \{x_{ij} | z_{ij} = c\}$ and $\bar{\mu}_{jc} = \frac{1}{|S_{jc}|} \sum_{x \in S_{jc}} x$
   - Compute $\bar{d}_{jcp} = \sum_{x \in S_{jc}} \parallel x - \mu_p \parallel^2$ for $p = 1, ..., g$
   - If $min_p \bar{d}_{jcp} > \lambda_g + \sum_{x \in S_{jc}} \parallel x - \bar{\mu}_{jc} \parallel^2$
     - set $g = g + 1$, $v_{jc} = argmin_p \bar{d}_{icp}$, $\mu_g = \bar{\mu}_{jc}$
     - else set $v_{jc} = argmin_p \bar{d}_{icp}$
7. For each global cluster, $p = 1, ..., g$ update the means

Table 3.2: The Hard-HDP algorithm [4]

The algorithm starts by taking as input the data-sets, e.g. a corpus of documents, along with the penalty parameters λ_l the local penalty parameter governing the creation of local clusters in a single data-set, and λ_g the global penalty parameter thresholding the creation of global clusters that are shared across the data-sets. Like

DP-Means [4], Hard-HDP also starts with all of the points in a data-set and all of the local clusters in all of the data-sets belonging to one single local and global mean respectively.

The algorithm now can be described in two separate steps. Step one deals with individual points inside a data-set. The distance between every point in a data-set is calculated from every global mean, adding a local penalty for points and their global clusters. If the distance between the closest mean is more than $\lambda_l + \lambda_g$ a new local mean and a new global mean is created with the single point being the local mean and the global mean. If the distance is less than $\lambda_l + \lambda_g$, the point is reassigned to the closest local mean. Step two of the algorithm deals with the local clusters inside individual data-sets. The distance of all points inside a local cluster is calculated from a global mean, and if the minimum sum total of these distances is greater than the sum of λ_g and the distance of every point in the cluster to its local mean, then a new local and global cluster is created with every point in the old local cluster now belonging to the new local cluster and the new global cluster having only this new local cluster. The means and indicator variables are all updated in each iteration. This is repeated till convergence.

The cost function for Hard-HDP is similar to that of DP-Means, the only difference being the addition of a new penalty term. The following section discusses the cost function for Hard-HDP. Both the penalty terms are now part of this objective function with the local parameter added to the cost function on creation of every new local cluster, and the global parameter added on creation of every new global cluster.

$$\min_{\{l_p\}_{p=1}^{g}} \sum_{p=1}^{g} \sum_{x_{ij} \in l_p} \parallel x_{ij} - \mu_p \parallel_2^2 + \lambda_l k + \lambda_g g$$

where, μ_p is the mean of the global cluster p.

With this we finish our discussion of Small Variance Asymptotics over the Dirichlet Process Mixture Model and its extension over Hierarchies. The distance measure in both of these methods was the Squared Euclidean Norm. It is interesting to note that with various different distance measures, the algorithm might behave in an interestingly different way. We will now explore further extensions of these asymptotics over more generalized Mixtures, like the Infinite mixture of Exponentials.

3.3 Extension to the Exponential Family

In the previous sections asymptotics done over the Dirichlet Process mixture of Gaussians was shown and a resulting algorithm DP-Means was therefore described. This chapter now deals with an extension of the same stochastic process over the Exponential family of Mixtures, further generalizing the model over many probability distributions.

The Exponential family of distributions have a generalized form that resembles [5]:

$$p(x|\theta) = exp((x, \theta) - \psi(\theta) - h(x))$$

Where $\psi(\theta) = log \int exp((x, \theta) - h(x))dx$ is the log-partition function. For simplicity an assumption is made that x is a minimal sufficient statistic for θ which is the natural parameter of the exponential family of distributions. The log-partition function is also used to calculate the the mean and covariance of $p(x|\theta)$. The mean is computed to be $\nabla\psi(\theta)$ and the covariance $\nabla^2\psi(\theta)$. For more details on how the collapsed gibbs sampler [9] performs inference on the Dirichlet Process Mixture model over the exponential family, refer to [5].

We will skip the asymptotics of the Exponential Dirichlet Process mixture model and would talk about the cost function and how it affects creation of local and global means. We would also discuss how the algorithm derived from asymptotics is different from the algorithm derived from the Gaussian version.

The Objective of this algorithm looks similar to that of DP-Means [4]. The major difference being the equared euclidean distance being replaced by the Bregman-Divergence between a point and a mean.

$$\min_{\{l_c\}_{c=1}^{k}} \sum_{c=1}^{k} \sum_{x \in l_c} D_\phi(x, \mu_c) + \lambda k$$

where, c is the cluster, k is the total number of clusters, x is the observation, μ_c is the mean of cluster c, D_ϕ is the Bregman-Divergence, and λ is the cluster penalty term.

The asymptotics over the Dirichlet Process Mixture of exponentials can be further extended to a hierarchical setup and the resulting algorithm will resemble the Hard-HDP algorithm [5], with the only change being that the distance calculation in Hard-HDP being replace by Bregman-Divergence instead of the squared euclidean distance. And the following objective appears for the Hard Exponential HDP with the same change of the distance measure between a point and a mean being replaced by Bregman-Divergence over the squared euclidean:

$$\min_{\{l_c\}_{c=1}^{k}} \sum_{c=1}^{k} \sum_{x \in l_c} D_\phi(x_{ij}, \mu_c) + \lambda_{bottom} t + \lambda_{top} k$$

where, c is the global cluster, t is the total number of local clusters, k is the total number of global clusters, x_{ij} is the observation i from document j, μ_c is the mean of the global cluster c, D_ϕ is the Bregman-divergence, and λ is the cluster penalty term.

Now that we have this Hard Exponential HDP algorithm, we can plug in any distribution in the exponential family of distributions, put the correct Bregman Divergence measure and arrive at a different algorithm altogether. In [5] one such experiment was run over the multinomial distribution, which serves as the basis for Topic Modeling in LDA [8]. The corresponding Bregman-Divergence to the multinomial is the KL-Divergence [12]. By just plugging in KL-Divergence instead of squared euclidean in Hard-HDP [5], we get a hard assignment based Topic Modeling algorithm. This new algorithm has both the flexibility of a non-parametric hierarchical model and the scalability of a hard-assignment based approach which reduces overheads in computation significantly. We will test this algorithm in our results section over data-sets of sparse documents and also suggest an improvement into it in one of the later chapters.

Chapter 4: Parameter Selection

Now that we have described the algorithms in detail, we can start exploring some of the problems that surround them. In this chapter we will discuss how to initialize these new algorithms, DP-Means and exponential Hard-HDP, with *good* parameter values. The K-Means algorithm has only one parameter K, the number of clusters in the data. In contrast, DP-Means does not fix the number of clusters in the data at any point. It grows in complexity, or number of clusters, as it progresses. The only parameter it has is the penalty parameter λ. Due to this nature of an non-intuitive parameter, it is difficult for the user to decide a value for λ that would give roughly K clusters. The original algorithms in their native forms do not have any methods described to initialize the parameters. They use the farthest-first heuristic both in [4] and [5]. We will discuss how the farthest-first heuristic works and what other simple heuristics can be used for initializing the parameter values. We will then propose a new method that can be used to initialize the parameters given the number of clusters that are *roughly* needed at the end of the clustering. We will later quantitatively verify this new method.

4.1 Parameters in DP-Means

The DP-Means algorithm (figure 3.3) described in [4] takes one parameter as a part of its input. This is the penalty parameter λ. It appears in the DP-Means cost function as an added term in the K-Means objective. The way the algorithm proceeds, for every point the distance (squared euclidean) to the closest mean is calculated and compared with this parameter λ. A split of the data-point from the original cluster is made a new mean is created if the value of the distance from the closest mean is greater than λ. Otherwise, the point is just reassigned to the closest mean. Now, quantitatively speaking, this λ is also the farthest a point can be in a cluster as illustrated in figure 4.1. In the given figure the points with same color represent one cluster, $\lambda_1, \lambda_2 and \lambda_3$ are three of the candidates for the largest distance of a point from its mean.

So, for a given set of points if we know the largest distance, λ' of a point from its mean at convergence of DP-Means, we can say that:

$$\lambda \geq \lambda'$$
$$\lambda = \lambda' + \epsilon, \text{ where } \epsilon \geq 0$$

Our new method will use this fact that the value of λ can be estimated given a possible state at convergence. The next section discusses the parameters in Hard Exponential HDP and proposes a similar method of parameter estimation.

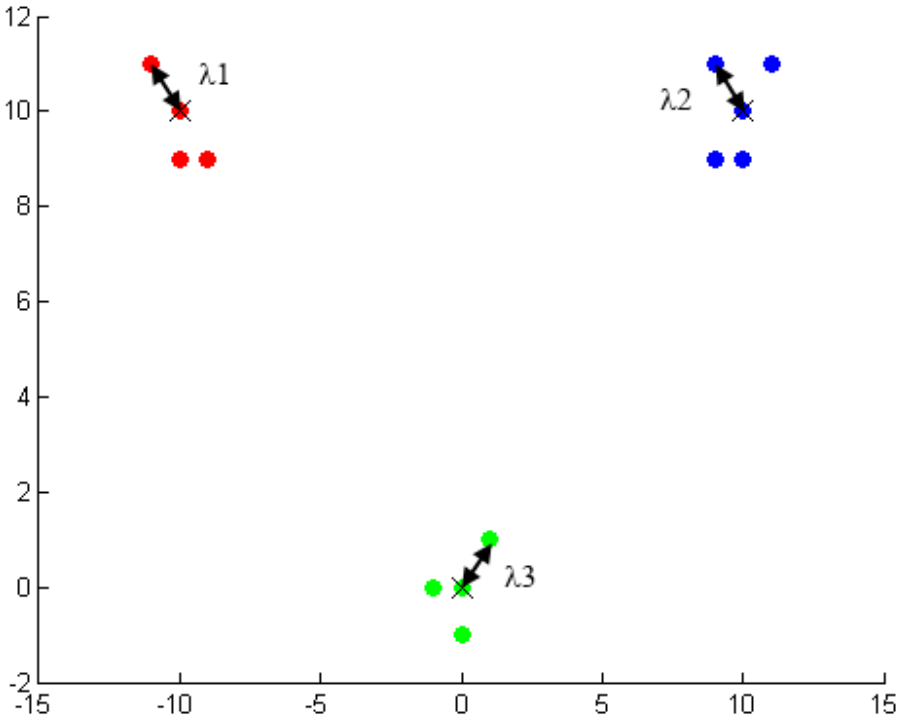

Figure 4.1: A Clustering of data showing the maximum distance of a point from its mean

4.2 Simple Heuristics

In the original work on DP-Means [4] and Hard Exponential HDP [5], the authors used a heuristic called farthest-first to initialize the parameters. Given a rough number of clusters needed at convergence, it started by finding out the K farthest points in the data-set and then returning the value of distance of the Kth farthest point. The way this heuristic works is by initializing a set with the global mean of the data, and then adding the farthest point to T. The distance to T being the smallest distance in all points in T. Then this is repeated K times and the value of the distance

after last round is returned as a possible value of λ. Essentially this method finds out the K points which are farthest from every other point.

As it can be seen that the main problem with this method is that it is not good when the data is scattered or when there are outliers in the data-set. The value of λ would be typically much higher than the desired value. To suggest a better method we would resort to parametric methods. It would be a much costlier method overall, but the values of the parameters would be better for clustering in a non-parametric fashion, as we will see in the subsequent section.

4.3 Initialization Strategies using Parametric methods

This section discusses how a new method for initialization of these parameters based on parametric methods can be used to get a good estimate of the number of clusters at convergence. As pointed out in the previous section the original heuristic can be weakened in case of sparsity or outliers in the data. We propose a new method of parameter selection via K-Means like parametric techniques.

To begin with, we are given a set of data-points and a value for roughly the number of clusters that are desired. We start with K-Means clustering on these set of points and observe the state at convergence. We calculate a relevant statistics like the largest distance between a point and its mean for the entire data-set. Going back to Section 4.1, we now know the value of λ' for our data, and we now have to estimate a value for λ. Since the random sequence of points in K-Means changes the final convergence state, we run the K-Means algorithm multiple times on the same data-set in different random sequences, and note the λ' for all of the non-repeating states at convergence. At last we take an average of these λ's and arrive at a measure for the value of λ.

The steps of this method are given as:

1. **Input:** $x_1, x_2, ...x_n$: the input data; K: the number of clusters desired
2. Run K-Means on the given data with K as the number of Clusters
3. Gather distance statistics from the final state of convergence
4. Calculate λ'
5. Repeat 2-4 until enough non-repeating λ' collected
6. Average the collected λ's
7. **Output:** Estimate on λ for DP-Means

Table 4.1: Parameter Initialization in DP-Means

This same method can be extended over the Hard Exponential HDP method to obtain estimates on just λ_g or both λ_l and λ_g. We will quantitatively verify this new method in a later chapter of this work. The next chapter now discusses some of the other issues relevant to the DP-Means and the Hard Exponential HDP algorithms.

Chapter 5: Local Search

Optimization is commonly seen in various different problems generally in the area of machine learning. Loosely defined, it is a problem to find the best solution from all possible solutions. A lot of the problems in machine learning when broken down take the form of a mathematical function (discrete or continuous) and the problem becomes of finding an optima. A subset of these problems do not particularly need the best possible solution or the global optima. But the rest of the problems in that set are looking for a better solution or the best possible solution. This is when the problem of Local optima comes into effect. A problem like K-Means or DP-Means which is NP-Hard inherently need not reach the global optima in all cases. The final solution will vary with change in configuration of the data.

So far we have seen the descriptions of the DP-Means and Hard Exponential HDP algorithms, but the problem of Local optima has not been separately addressed. In the following sections we will first define and describe Local optima as it occurs in DP-Means and Hard Exponential HDP and then will propose novel methods that will try to solve this problem of Local optima. Also, a problem inherent to the DP-Means algorithm is that of singleton clusters. Recall the way new clusters are formed in DP-Means [4] whenever the thresholding distance is larger than λ. Due to this unique way of creating clusters and the way the algorithm and the objective function

behaves, whenever a singleton cluster is created it will never merge with any other cluster. So, the point will always be associated with that cluster only since the closest distance between a point and a mean will be always zero. This problem also appears to be in the same domain of local optima and we will investigate further on it in the following sections.

5.1 Local Optima and Singleton Clusters in DP-Means & Hard HDP

Going back to the discussion on local optima and how to overcome it, we start by first describing the general problem briefly. As stated in the previous section, any suboptimal solution to an optimization problem is caused due to the problem of local optima. As you can see that a continuous function illustrated in figure 5.1 has a global minima (trough on the left) and a local minima (on the right). When we optimize a continuous function, and are stuck at a local optima simple calculus methods can be applied to test for global optima. But, the domain we consider is typically discrete and we need search methods to solve the problem in that case.

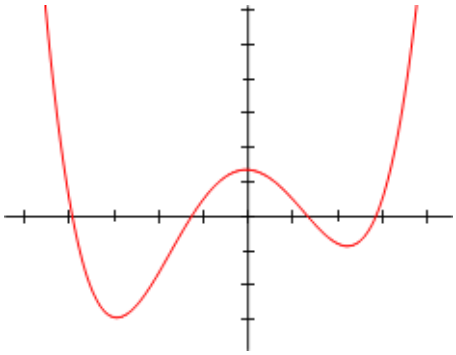

Figure 5.1: A continuous function of degree four

DP-Means, just like the K-Means algorithm operates on a discrete domain. The random sequence of data in which individual points are processed largely affect the final state of convergence. Every time when the algorithm converges it is not a guarantee that the solution is optimal. The figures below (figure 5.2-3) illustrate some of the possible situations that may arise when DP-Means is run on synthetic data. In figure 5.3 as it can be noticed that a total of four clusters (four different colors) have been formed while the data seems to have been sampled from three distributions.

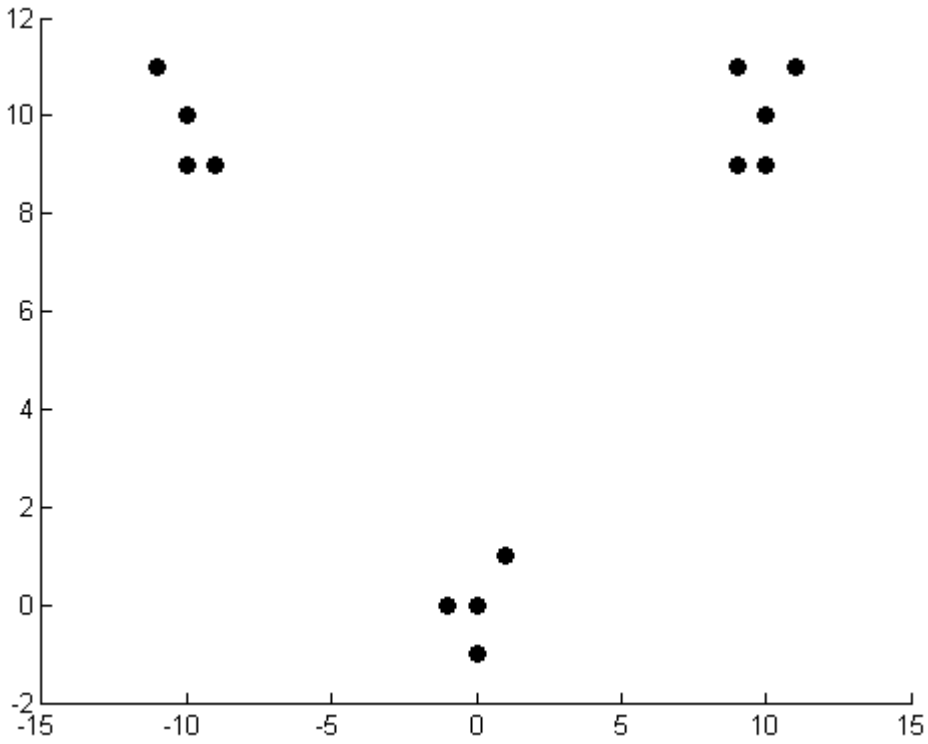

Figure 5.2: The given set of inputs for Clustering

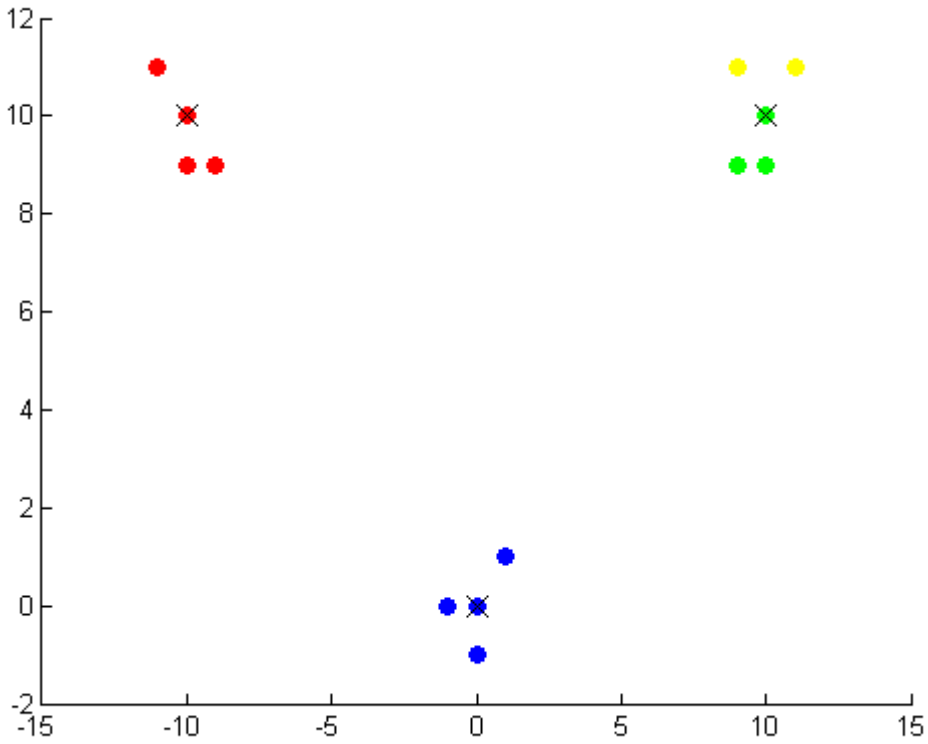

Figure 5.3: A possible state of Convergence for DP-Means

Due to the randomness of processing of data-points in a sequence, every time a different final state might be the solution for the same set of data-points. Each of these final states will differ in their final objective values. We need to choose the one which has the minimum value of cost function at convergence. A simple but naive way to do so is to run the algorithm multiple times, every time in a different random sequence and present the solution with the minimum cost function value as the optimal solution. This method may work but it will be very costly to run this algorithm multiple times, possibly infinite times until the global optima is found. A

better way is to find the global optima after each step and change the value of the cost function with the state of the clustering outside the usual steps in DP-Means. We propose one such method via Local Search and Merge move in the next section.

5.2 Local Search and Merge move

The DP-Means algorithm is highly flexible in nature owing to its Non-parametric roots. At the same time is scalable because of hard assignments of points and therefore less overhead in terms of data being processed. As discussed in the sections above, the DP-Means algorithm just like the K-Means algorithm suffers from the problem of Local Optima mainly due to the random nature of processing the data-points. To solve this problem we will exploit this flexibility of the DP-Means algorithm to create or merge clusters as the algorithm progresses. So far, the only step in the algorithm that changes the number of clusters is the step when a new cluster is created. We will add a new step to this algorithm where we search for *better* solutions at the given state of clustering and follow the next iterations of the algorithm with this new and *better* solution.

We call this new step Local Search and Merge Move for DP-Means:

1. **Input:** $\mu_1, ..., \mu_k$: the set of means; C: value of the Cost function
2. For every mean μ_i, for all $i < K$
   (a) Virtual Merge μ_i with μ_k for all $k > i$
   (b) Compute the objective C' for the new state
   (c) If for any i and k the new cost $C' < C$
      i. Then, Merge μ_i with μ_k and get to a new optimal state

ii. Else, Check for next possible combination

3. **Output:** A new state of Clustering with a new Objective $C' < C$

This step is inserted in the DP-Means algorithm [4] right before Step 3 where the means and the cluster indicators are updated.

With this type of combinatorial search we can guarantee that if there exists a more optimal solution at any instance as the DP-Means progresses, it will always find it and switch to this new optimal state of clustering. This is possible mainly due to the flexibility of the DP-Means algorithm which allows it to grow or shrink in complexity with the number of the clusters. We will verify this new local search method quantitatively in the results section later. We will also point out that local search and merge move also decreases the number of singleton clusters formed.

A similar local search and merge method can be extended over the Hard Exponential HDP or the Topic Modeling algorithm, where there are both a global and local mean associated with every point and every local cluster respectively. The following steps can be taken to perform a similar combinatorial search over the domain of all possible merges over local and global means:

1. **Input**: $\mu_1, ...\mu_G$: the global means; C: the global cost function value

2. For every pair of global mean, μ_g for all $g < G$:

   (a) Calculate the new objective C' after a virtual merge of the two global means

   (b) If, $C' < C$: Then, Merge the pair of Global means and create a new and more optimal state at the global level

3. **Output**: An optimal state at the global level $C' < C$

Here, D is the total number of documents, G is the total number of global means, k_j is the total number of local clusters in document j.

With this we end our chapter on local search and merge move. The following chapter will now verify the DP-Means algorithms, with local search and merge, and new parameter selection method, and the Hard Exponential HDP algorithm that resembles Topic Modeling, with local search and merge, over different data-sets.

Chapter 6: Experimental Results

We will conclude this work by demonstrating the working of DP-Means algorithm, followed by the Hard Exponential HDP for Multinomials which resembles a hard-assignment based Topic Modeling. We will then highlight the utility of the new methods proposed in this Thesis for Parameter Selection and also the addition of the new step to these algorithms to solve the problem of local optima.

We will use both synthetic and real data. The synthetic data is sampled from three two-dimensional Gaussians and is used only for demonstrating correctness. The data-set we use is from the UCI Machine Learning Repository [17]. We use their Sparse Document Data-set for document clustering and topic modeling, called the Bag of Words Data Set. We will be using the NIPS, KOS and the NYTimes data-sets for our experiments. The NIPS data-set has 1500 documents over a vocabulary of size 12419 and about 2 Million total words. The KOS data-set has 3430 documents over a vocabulary of size 6906 and a total of 500,000 words. The NYTimes data-set is the largest with 300,000 documents over a vocabulary of 102,660 with a total of 100 Million words approximately. All of the words are stored in a sparse format in these data-sets and in the Bag of Words model. The following sections now describe our experiments in details.

Our synthetic data (Figure 6.1) has just fifteen data-points, with five each sampled from three different Gaussians centered at $(0, 0)$, $(10, 10)$, and $(-10, 10)$.

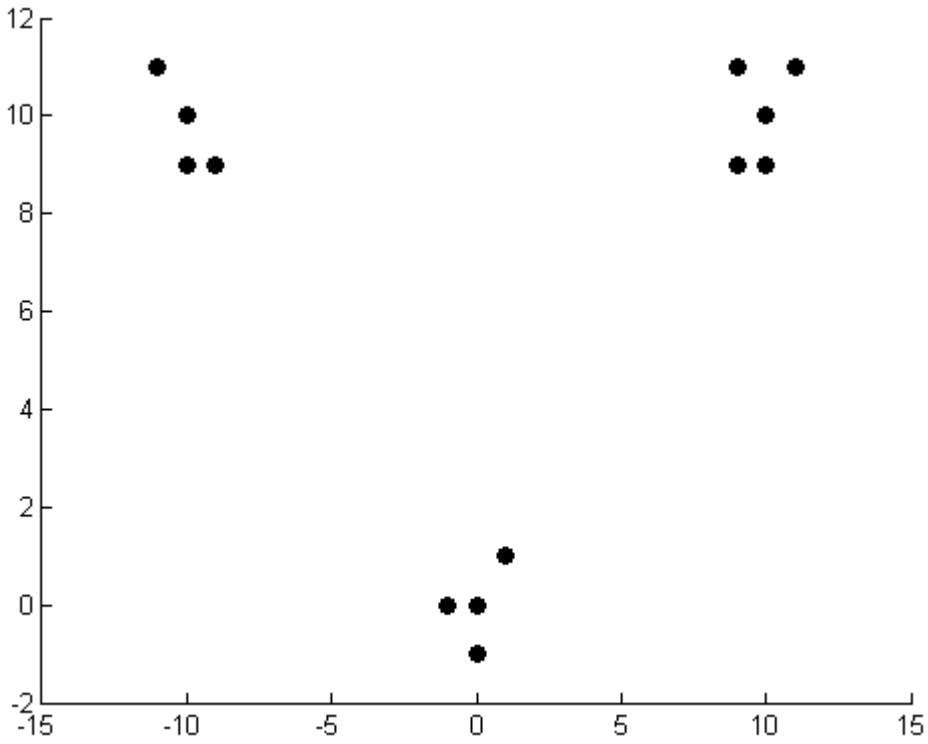

Figure 6.1: Synthetic data sampled from three Normal distributions

6.1 DP-Means

This section will start out with showing some of the results of running the stock DP-Means over synthetic and real data. We ran the algorithm on the synthetic data for verifying correctness and making the clustering interpretable. We used the first

500 documents from both the KOS data-set and the NIPS data-set for clustering with DP-Means.

Following are the results of basic DP-Means clustering on the synthetic data:

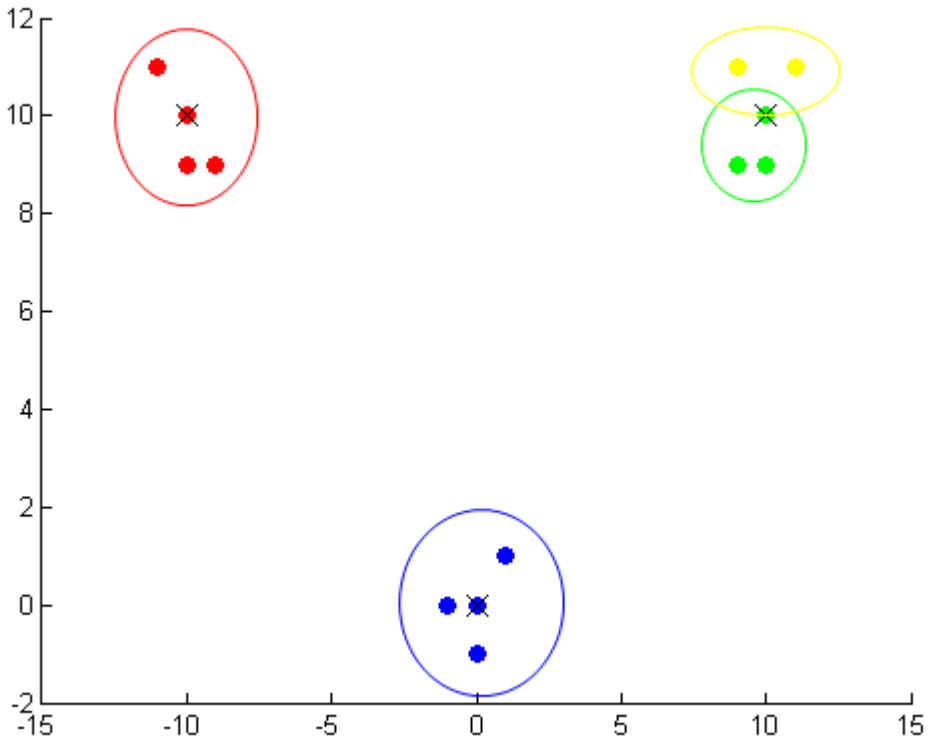

Figure 6.2: Final state of Clustering after running DP-Means for a fixed value of λ

The total number of clusters formed are four in this case. The value of λ was not chosen using the suggested method in chapter 4. It was an arbitrary value which gave about three clusters. As we pointed our earlier, we can further improve this clustering by using local search as it will be shown in the next section. The algorithm converged in three iterations as shown in the graph in Figure 6.3. The plot shows the

best cost function values out of ten total runs with a random sequence of ordering of the data-points in each of them.

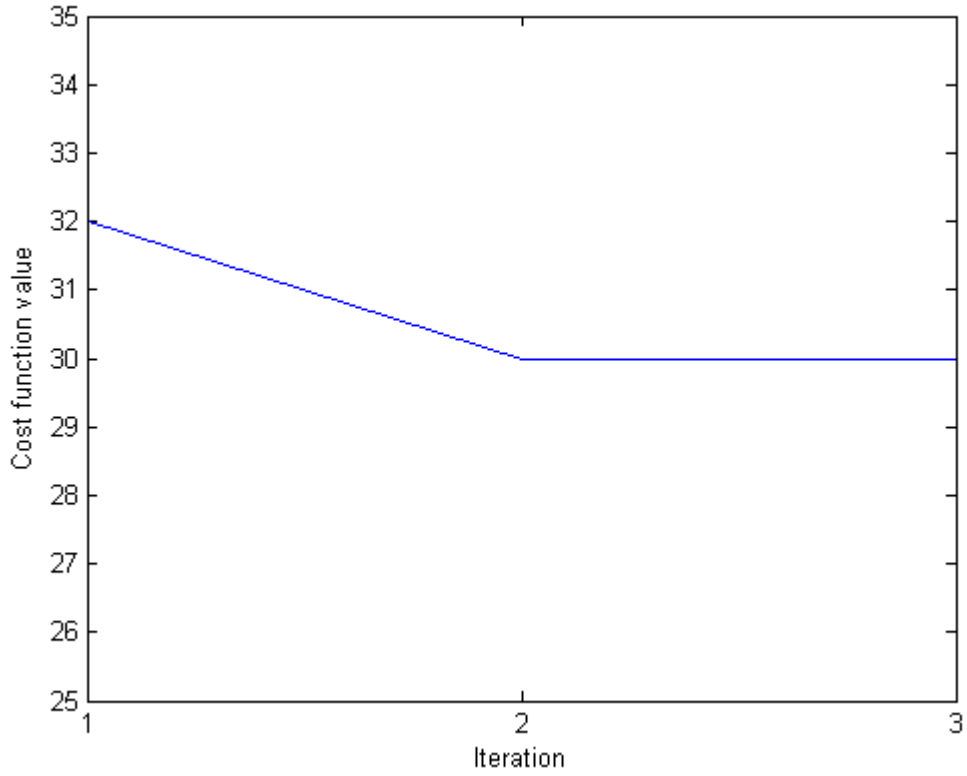

Figure 6.3: Cost function for DP-Means over the synthetic data-set

Cluster # 1
bush, carter, attack, president
bush, campaign, kind, necessarily
thoughts, bush
Cluster # 2
cheney, commission, change
cheney, dump, kerry

Table 6.1: DP-Means Clustering on KOS

Cluster # 1
model, algorithm, network, function, structure, system, sonn, number, mdl, node
point, algorithm, network, layer, learning, local, matrices, unit, matrix, set
mean, field, mfa, spin, temperature, annealing, graph, solution, problem, network
Cluster # 2
character, field, system, recognition, scan, input, net, window, digit, approach
character, field, system, window, net, center, input, saccade, distance, set
Cluster # 3
road, network, unit, weight, autonomous, hidden, range, neural, navigation, alvinn
network, road, training, alvinn, image, direction, steering, driving, lane, vehicle

Table 6.2: DP-Means Clustering on NIPS

When we ran the DP-Means on the sparse document data-sets following results were obtained. The rows in the Tables 6.1 and 6.2 represent a single document with words from left to right appearing in the order of their occurrence in the document. The Figures 6.4 and 6.5 illustrate the cost function as it changes with iterations and finally converges. The value of the cost functions here are also the best out of ten random runs. The λ was again chosen arbitrarily and not with our method.

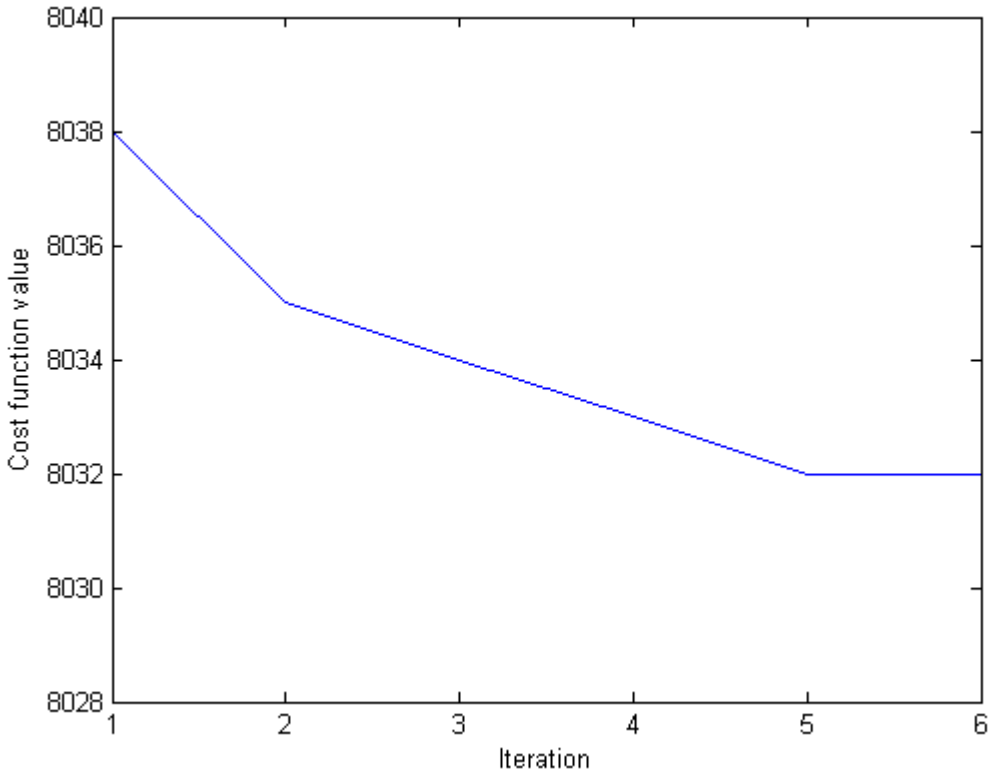

Figure 6.4: Cost function for the KOS data-set during DP-Means

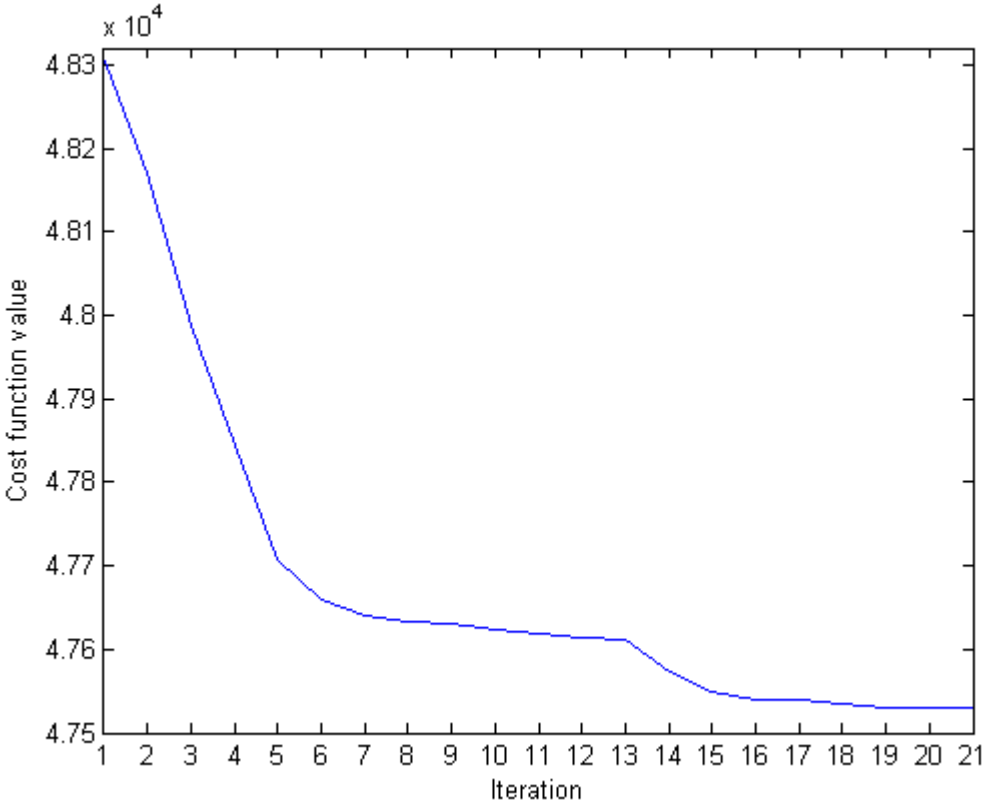

Figure 6.5: Cost function for the NIPS data-set during DP-Means

6.1.1 Clustering with new Parameters

To use the parametric method for parameter estimation we first run K-Means on the data and obtain the value of λ' as described in Chapter 4. We then average out the non-repeating λ's and that serves as a lower bound for our estimate of λ. For these experiments, we start with a value $1.1 \times \lambda'$. The number of clusters we obtained after running DP-Means from the λ' obtained over the synthetic data we got 4 clusters as the output, while we wanted it to be 3. For the NIPS data-set, we got 16 clusters instead of 25, and for the KOS data-set we got 22 clusters instead of 35. This shows that although the number of clusters are way off the mark, this method serves as a good heuristic for obtaining clusters within a certain limit of the desired number of clusters.

We ran further tests on a mixture of known number of Gaussians and ran the DP-Means algorithm with our new parameter estimation technique. Because the data was sampled from a known number of Gaussians and the parameters of those Gaussians were known upfront, we tested the accuracy based on correct classification of the data-points. Every point that was not a part of its own cluster was labeled as incorrect classification. We then averaged this classification accuracy over a total of ten random runs. The results of these experiments are discussed in the next section.

6.1.2 Clustering with Local Search and new Parameters

We now run the DP-Means with the new step of local search and Merge move added to it. For our first set of experiments we chose an arbitrary value of λ for each of the data-set and demonstrate that the clustering converges with a cost function of

lesser value when the merge move is on. We averaged the cost values over a total of ten random runs. The averaged cost values are shown below:

The following results compare the averaged cost functions of two different runs, one with the merge move on and one without it. We first experiment with synthetic data and show how it always converges to the global optima and forms three clusters (Figure 6.7). The corresponding cost functions are shown in Figure 6.6. Similar experiments when run on the KOS and the NIPS data-set give expected result. The differences in the cost function values can be noted in the graphs in Figure 6.8 and 6.9. We also note a slight fall in the number of singleton clusters. In the KOS data-set it was about 12% and in the case of NIPS data-set it was about 16%.

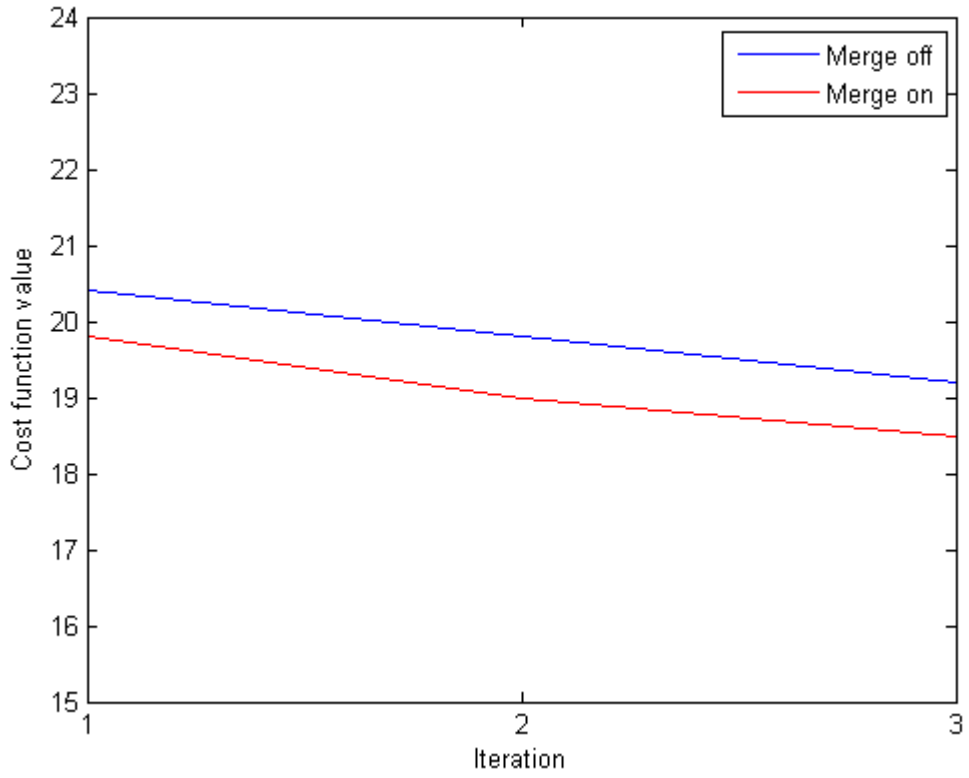

Figure 6.6: Averaged Cost functions in case of standard DP-Means (blue) and DP-Means with Local search (red) for the synthetic data

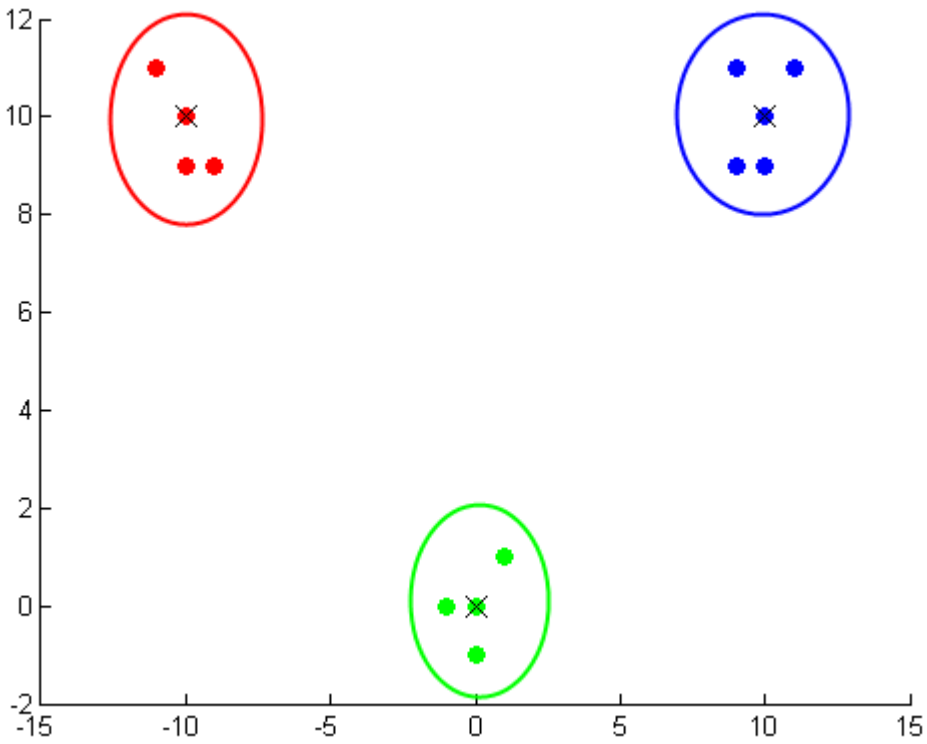

Figure 6.7: Best state of clustering at convergence on the synthetic data after using Local search

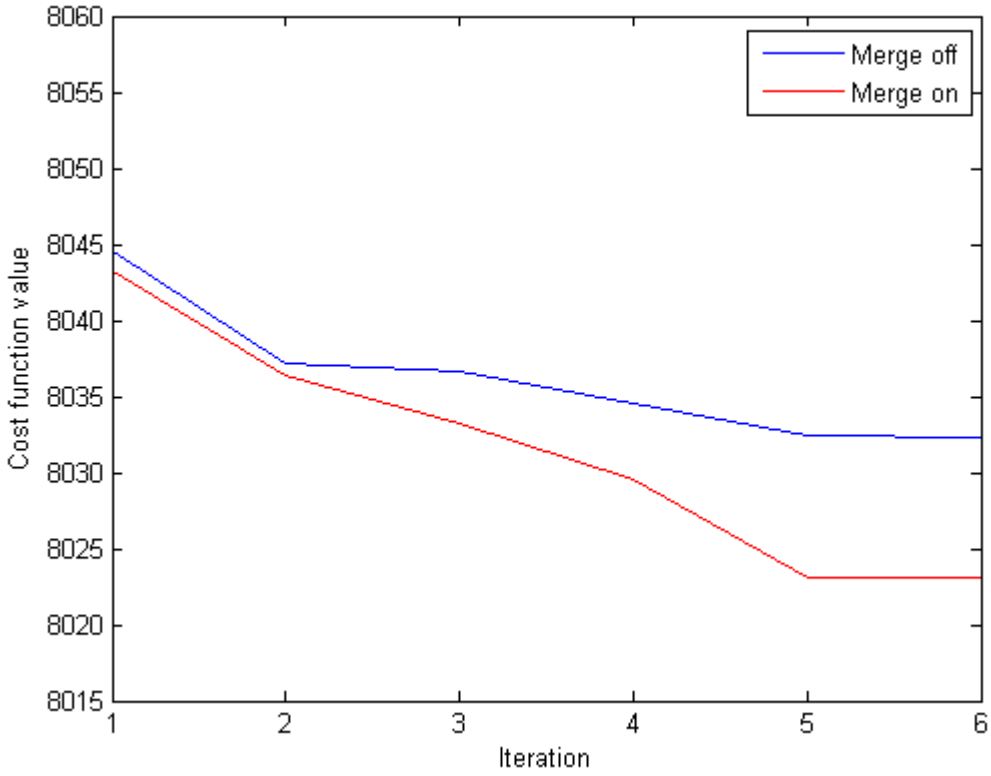

Figure 6.8: Averaged Cost functions of DP-Means with (red) and without (blue) Local search compared over the KOS data-set

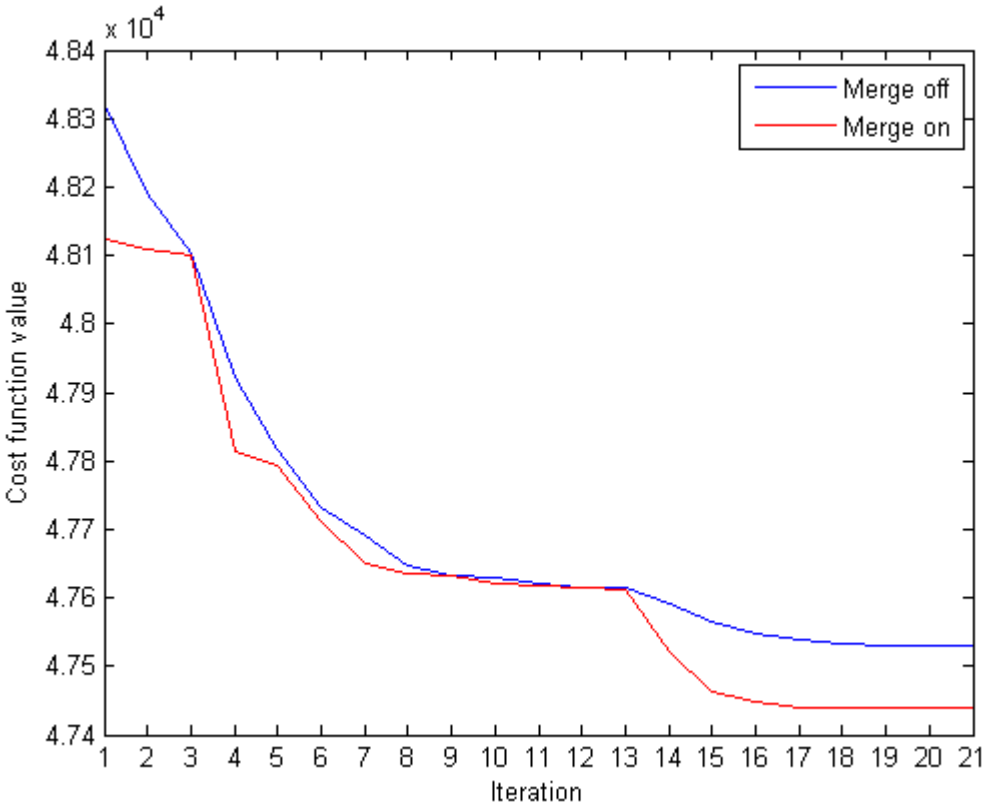

Figure 6.9: Averaged Cost functions of DP-Means with (red) and without (blue) Local search compared over the NIPS data-set

We then tested our new parameter selection method combined with the search and merge move. We used another set of synthetic data for this. We created 4 different data-sets with sampling from 3, 4, 5 and 10 different Gaussians. The total number of data points in each of these mixtures were 15, 20, 25, 100 respectively. This experiment was run in order to verify the parameter selection method together with the merge move, and whether or not the algorithm actually converges to a better solution. We clustered these mixtures over ten different random runs and averaged the classification error. The result of the final classification and the percentage errors are given in the following table:

Number of Clusters	Merge off	Merge on
3	14%	7.3%
4	22.1%	13.5%
5	24.4%	18.2%
10	35.2%	27.2%

Table 6.3: Average classification error after clustering over 4 different synthetic mixtures

6.2 Hard Exponential HDP with KL-Divergence

As discussed earlier in Chapter 3, when we run the Hard Exponential HDP over the Multinomial distribution we just have to change the distance measure from Squared Euclidean in Hard-HDP [4] to the corresponding Bregman Divergence for the multinomial distribution, which is the Discrete KL-Divergence. We run this algorithm only on the real data and show the Topics inferred by the algorithm.

6.2.1 Topic Modeling on Sparse Documents

The following topics were obtained on running the Hard Exponential HDP on the NIPS and the NYTimes data-set. We show the top 10 word occurring in some of the topics as a result in the following tables (6.3 and 6.4).

Topic # 1: algorithm, network, function, learning, model, data, input, set, unit, system
Topic # 2: learning, actor, university, generalization, critic, examples, ing, difference, full, computation
Topic # 3: unit, structure, zero, eigenvalues, free, ackley, rank, code, tion, eigenvalue
Topic # 4: learning, weight, net, mean, line, find, adopt, positive, trained, form
Topic # 5: prior, segmentation, parameter, scales, technique, bayesian, similar, malik, model, log

Table 6.4: Topics obtained from the NIPS data-set

Topic # 1: com, site, web, sites, www, need, business, choosing, put, card
Topic # 2: boeing, problem, control, planes, army, system, pilot, flight, order, plane
Topic # 3: game, team, season, playoff, yard, quarterback, coach, nfl, dolphin, games
Topic # 4: campaign, right, algore, president, georgebush, question, need, newhampshire, bush, america
Topic # 5: play, film, friend, music, movie, broadway, billclinton, actor, woman, family

Table 6.5: Topics obtained from the NYTimes data-set

6.2.2 Topic Modeling with Local Search

We now run the Topic Modeling algorithm on the NYTimes dataset, with the Local Search enabled over the Global means and obtain the following cost function values (Figure 6.10). The composition of topics does not change enough to be noticed since we only take note of the top n words in each topic.

To summarize these experiments, we say that we have demonstrated a local search method addresses the issue of local optima in a non-parametric DP-Means algorithm. We have also suggested an initialization method based on a parametric version. We have demonstrated that the objective function has improved due to Local search and Merge move, but there is still no verification of the quality of the clustering and it remains an important thing to discuss and accomplish in the future.

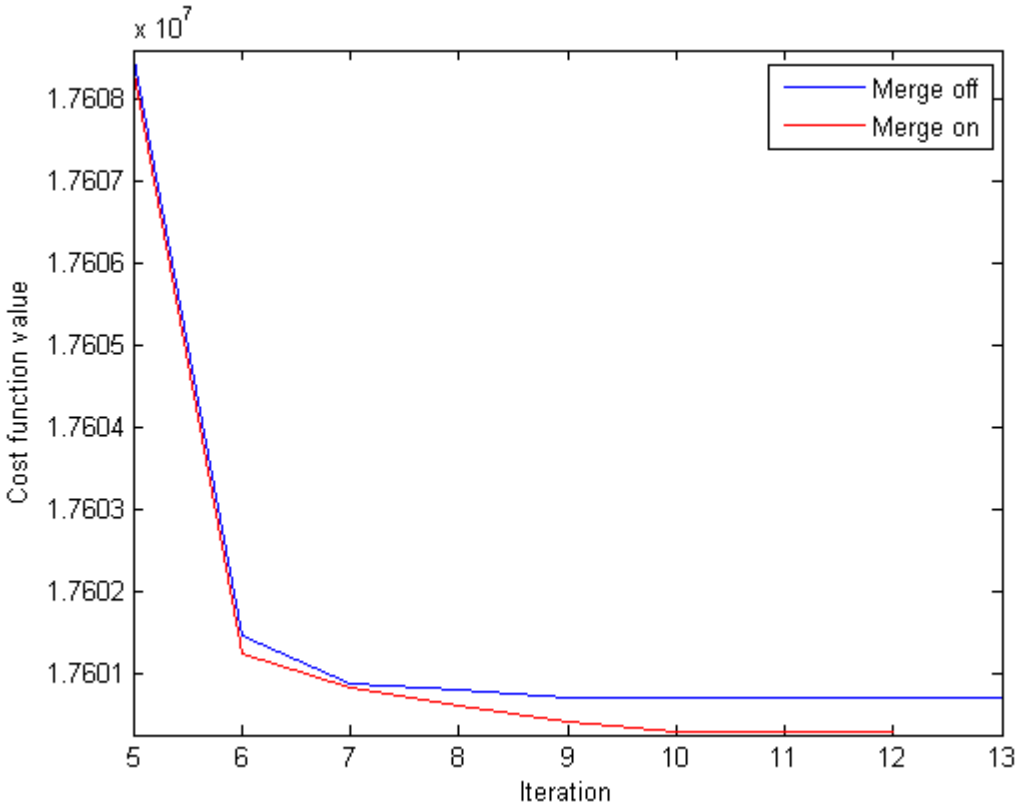

Figure 6.10: Cost function comparison of Topic Modeling with and without Local search on the NYTimes data-set

Chapter 7: Conclusion and Future Work

As a concluding remark, we would like to re-emphasize the utility of these new breed of algorithms derived from Asymptotics over various Non-parametric processes. These algorithms present an entirely new approach towards tasks like Clustering and Topic Modeling being inherently more flexible than their traditional counterparts due to their Non-parametric roots. But, being a problem in optimization they still suffer from issues like Local optima. The other problem that is faced while running these algorithms is that of initialization.

In this work, we explored the DP-Means algorithm and its Hierarchical counterpart, both of which were derived from the Dirichlet Process and the Hierarchical Dirichlet Process over a mixture of Gaussians. And the Exponential version of the Dirichlet Process and then its Hierarchical extension. We also saw how a Topic Modeling algorithm can be derived by just replacing the distance measure in the Exponential version of the Hierarchical DP by the corresponding Bregman Divergence of the Multinomial distribution.

We addressed the issues of Local optima and Initialization by providing additional steps that can be added to the algorithms to make them find *better* solutions, and reject sub-optimal solutions by the means of Combinatorial Local Search and a Merge

move. The initialization of parameters being the other challenging problem was addressed in the DP-Means algorithm by using a Parametric method based technique that provides a heuristic for getting *roughly* a desired number of clusters.

We will continue to focus on some of the open problems at this point. We wish to optimize the slow Combinatorial Search in a way that it becomes more a part of the algorithm rather than a separate step altogether. We will also try to further improve the heuristics for initialization parameters. Comparing the Hard Topic Modeling method with various state of the art Topic Models is also a goal that we have for the near future. Using it for some discrete data task like Scene classification is also something that we might touch upon. We wish that with the Local search and the initialization methods added to this algorithm, it would find more use in the Applied Machine Learning community.

Appendix A: Software for running DP-Means and Topic Modeling

The software that was built as a part of this project is free to download and use for non-commercial purposes. It provides features to run a scalable implementation of the DP-Means and the Hard Topic Modeling algorithms as described in the text. It also has several features that handle Sparse or Dense data, do Local Search and Merge, Paremeter Estimation etc. The software with a detailed specification will be available on the author's website at: *www.cse.ohio-state.edu/~singsidd*.

Bibliography

[1] J. MacQueen *Some methods for classification and analysis of multivariate observations.* Proc. Fifth Berkeley Symp. on Math. Statist. and Prob., Vol. 1, Univ. of Calif. Press, 1967

[2] Lloyd S. P. *Least square quantization in PCM.* IEEE Transactions on Information Theory, 1982

[3] Hjort N., Holmes C., Mueller P., and Walker S. *Bayesian Non-parametrics: Principles and Practice.* Cambridge University Press, Cambridge, UK, 2010

[4] B. Kulis, and M.I. Jordan *Revisiting K-Means: New Algorithms via Bayesian Non-parametrics.* Proc. ICML, 2012

[5] K. Jiang, B. Kulis, and M.I. Jordan *Small-Variance Asymptotics for Exponential Family Dirichlet Process Mixture Models.* Proc. NIPS, page 3167-3175, 2012

[6] Dempster A.P., Laird N.M., Rubin D.B. *Maximum Likelihood from Incomplete Data via the EM Algorithm.* Journal of the Royal Statistical Society, Series B 39, 1977

[7] D. Blei *Probabilistic Topic Models.* ICML Tutorial, 2012

[8] D.M. Blei, A.Y. Ng, and M.I. Jordan *Latent Dirichlet Allocation.* Journal of Machine Learning Research - JMLR , vol. 3, pp. 993-1022, 2003

[9] T. Grifths and M. Steyvers *A probabilistic approach to semantic representation* . 2002

[10] Ferguson, T. *Bayesian analysis of some nonparametric problems.* Annals of Statistics 1 (2): 209230, 1973

[11] Y.W. Teh, M.I. Jordan, M.J. Beal,and D.M. Blei *Hierarchical Dirichlet Process.* JASA, 101(476): 1566-1581, 2006

[12] A. Banerjee, S. Merugu, I.S. Dhillon, and J. Ghosh *Clustering with Bregman Divergences.* JMLR, 6:1705-1749, 2005

[13] R.M. Neal *Markov Chain Sampling methods for Dirichlet Process mixture models.* JCGS, 9:249-265, 2000

[14] I.S. Dhillon, Y. Guan, and J. Kogan *Iterative clustering of High dimensional text data augmented by Local Search.* In Proc. IEEE ICDM, pages 131-138, 2002

[15] A. Frank and A. Asuncion. *UCI Machine Learning Repository.* 2010

[16] C.D. Manning, P. Raghavan, and H. Schutze *Introduction to Information Retrieval.* Cambridge University Press, 2008

[17] Bache, K. and Lichman, M. *UCI Machine Learning Repository* . University of California, Irvine, School of Information and Computer Sciences, 2013

[18] Fei-Fei, L. and Perona, P. *A Bayesian hierarchical model for learning natural scene categories.* In Proc. CVPR, 2005

Volume 1 (2013) 13-21 ISSN 2347 - 3258
International Journal of Advance Research and Innovation

Optimization of Process Parameters in Turning Operation of Aluminium (6061) with Cemented Carbide Inserts Using Taguchi Method and Anova

Ranganath M S, Vipin, R. S. Mishra
Department of Mechanical Engineering, Delhi Technological University, New Delhi, India

Article Info

Article history:
Received 1 July 2013
Received in revised form
15 July 2013
Accepted 22 July 2013
Available online 1 August 2013

Keywords
Aluminium (6061),
ANOVA,
Surface Roughness,
Taguchi Method,
Turning

Abstract

This paper investigates the parameters affecting the roughness of surfaces produced during the turning process for the material Aluminium 6061. The surface roughness is considered as quality characteristic while the process parameters considered are speed, feed and depth of cut .Design of experiments were conducted for the analysis of the influence of the turning parameters on the surface roughness by using Taguchi design.. The results of the machining experiments for Aluminium 6061were used to characterize the main factors affecting surface roughness by the Analysis of Variance (ANOVA) method.. The feed and speed are identified as the most influential process parameters on surface roughness.

1. Introduction

Surface roughness is mainly a result of process parameters such as tool geometry (i.e. nose radius, edge geometry, rake angle, etc). and cutting conditions (feed rate, cutting speed, depth of cut, etc).Surface roughness is harder to attain and track than physical dimensions are, because relatively many factors affect surface roughness. Some of these factors can be controlled and some cannot. Controllable process parameters include feed, cutting speed, tool geometry, and tool setup. Other factors, such as tool, work piece and machine vibration, tool wear and degradation, and work piece and tool material variability cannot be controlled as easily. The important cutting parameters discussed here are cutting speed, feed and depth of cut. It is found in most of the cases surface roughness decreases with increase in cutting speed and decrease in feed and depth of cut. Since these cutting parameters will decide about the type of chips which we expect at the time of machining of a single constant material thus we have to analyze them for no such built-up edge chips formation. The Taguchi method is statistical tool, adopted experimentally to investigate influence of surface roughness by cutting parameters such as speed, feed and depth of cut. Many researchers developed many mathematical models to optimize the cutting parameters to get lowest surface roughness by turning process. The variation in the material hardness, alloying elements present in the work piece material and other factors affecting surface finish. Proper selection of cutting parameters and tool can produce longer tool life and lower surface roughness. Hence, design of experiments by Taguchi method on cutting parameters was adopted to study the surface roughness

Corresponding Author,
E-mail address: ranganathdce@gmail.com
All rights reserved: http://www.ijari.org

2. Taguchi Method

Taguchi's parametric design is the effective tool for robust design it offers a simple and systematic qualitative optimal design to a relatively low cost. The Taguchi method of off-line (Engineering) quality control encompasses all stages of product/process development. However the key element for achieving high quality at low cost is Design of Experiments (DOE). In this paper Taguchi's (DOE) approach is used to analyze the effect of process parameters like cutting speed, feed, and depth of cut on Surface Roughness of Aluminium 6061 work material while machining with cemented carbide insert type tool and

to obtain an optimal setting of these parameters that may result in good surface finish.

Steps of Taguchi method are as follows:

1. Identification of main function, side effects and failure mode.
2. Identification of noise factor, testing condition and quality characteristics.
3. Identification of the main function to be optimized.
4. Identification the control factor and their levels.
5. Selection of orthogonal array and matrix experiment.
6. Conducting the matrix experiment.
7. Analysing the data, prediction of the optimum level and performance.
8. Performing the verification experiment and planning the future action.

3. ANOVA (Analysis Of Variance)

Since there are a large number of variables controlling the process, some mathematical models are required to represent the process. However, these models are to be developed using only the significant parameters influencing the process rather than including all the parameters. In order to achieve this, statistical analysis of the experimental results will have to be processed using the analysis of variance ANOVA is a computational technique that enables the estimation of the relative contributions of each of the control factors to the overall measured response. ANOVA can be useful for determining influence of any given input parameter from a series of experimental results by design of experiments for machining process and it can be used to interpret experimental data. Analysis of variance (ANOVA) is a collection of statistical models, and their associated procedures, in which the observed variance in a particular variable is partitioned into components attributable to different sources of variation. In its simplest form, ANOVA provides a statistical test of whether or not the means of several groups are all equal, and therefore generalizes *t*-test to more than two groups. ANOVA is used in the analysis of comparative experiments, those in which only the difference in outcomes is of interest. The statistical significance of the experiment is determined by a ratio of two variances. This ratio is independent of several possible alterations to the experimental observations: Adding a constant to all observations does not alter significance. Multiplying all observations by a constant does not alter significance. So ANOVA statistical significance results are independent of constant bias and scaling errors as well as the units used in expressing observations.

4. Experiment Set Up

CNC Lathe

The CNC Lathe consists of the machine unit with a three jaw independent chuck, a computer numerically controlled tool slide, which cud move accordingly to two axis horizontal and vertical X and Z axis. X axis represents the vertical movement which gives the depth of cut where as Z axis represents the location of the cutting tool. Thus after deciding the machining zero at a certain point the command is given in the form of a part program. The machine is also provided with a automatic lubrication motor for its slides.

Cutting Tool Material

The cutting tool which provided with the CNC lathe Trainer was a 30 mm square tool with 60 mm length having the same tool angles as for a normal turning tool. The tool used was cemented carbide insert type. The geometry of tool is: Rake angle 6^0(+ve), 5^0 (+ve) clearance angle, 60^0 (+ve) major cutting edge angle, 60^0 (+ve) included angle and 0^0 cutting edge inclination angle. All the three elements-tungsten, molybdenum and cobalt help in achieving high hot hardness; the first two do so by forming complex carbides and the cobalt forms an alloy by going into solid solution in the ferrite matrix and thus raising the recrystallisation temperature. Vanadium in high speed steels increases the wear resistance of tool at all operating temperatures. Vanadium also helps to inhibit grain growth at the high temperatures required in heat treatment.

Work piece material

CNC Lathe made LMW was available for turning only Non-ferrous materials. The chuck holding the work piece diameter was only limited to 120 mm and the maximum work piece length was limited to about 250 mm length. Standardized material were selected to ensure consistency of the alloy, which was a common wrought alloy used in industry 6061 Aluminum HINDALCO made in the form of bars with the size of diameter 22 mm 120mm length so as to fit under the chuck.

Table: 1. Chemical Composition of Aluminum Alloy

Element	Weight%
Cu	0.15-0.4
Mg	0.7-1.2
Si	0.4-0.8
Fe	0.7 max
Mn	0.2-0.8
Other	0.4

The aluminum we have chosen for turning is actually a Heat Treatable Alloy manufactured in the form of bars by HINDALCO. The inputs which were fed in the form of part program include dimensions of the work piece, cutting parameters depth of cut in mm, Speed available was 50-3500 rpm and feed in mm/min.This standard structural alloy, one of the most versatile of the heat-treatable alloys, is popular for medium to high strength requirements and has good toughness characteristics. Applications range from transportation components to machinery and equipment applications to recreation products and consumer durables.

Alloy 6061 has excellent corrosion resistance to atmospheric conditions and good corrosion resistance to sea water. This alloy also offers good finishing characteristics and responds well to anodizing. Alloy 6061 is easily welded and joined by various commercial methods. (Caution: direct contact by dissimilar metals can cause galvanic corrosion). For screw machine applications, alloy 6061 has adequate machinability characteristics in the heat-treated condition.

The different alloying elements present in a work piece are shown in the Table 1.The control factors and their levels are illustrated in Table 1. The cutting parameters ranges were selected based on machining guidelines provided by manufacturer of cutting tools

Table: 2. Cutting parameters and levels

Code	Cutting Parameter	Level 1	Level 2	Level 3
A	Speed 's' (rpm)	1700	1900	2100
B	Feed 'f ' (mm/rev)	0.1	0.125	0.15
C	Depth of cut 'd' (mm)	0.2	0.3	0.4

The surface roughness of machined surface has been measured by a Surface Roughness Measuring instrument, the Surtronic 3+, is a portable, self-contained instrument for the measurement of surface texture and is suitable for use in both the workshop and laboratory. Parameters available for surface texture evaluation are: Ra, Rq, Rz (DIN), Ry and Sm.The parameters evaluations and other functions of the instrument are microprocessor based. The measurements results are displaced on an LCD screen and can be output to an optional printer or another computer for further results.

The dependent variable is surface roughness. Table 3 shows standard L27 (33) orthogonal array designed by Taguchi with experimental results. The left side of the Table 3 includes coding values of control factors and real values of cutting parameters. The right side of the Table 3 includes the results of the measured values of the surface roughness and calculated values. The left side of the Table 3 includes coding values of control factors and real values of cutting parameters. The right side of the Table 3 includes the results of the measured values of the surface roughness and calculated S/N ratio and Residuals. The different units used here are: speed – rpm, feed mm/ rev, depth of cut – mm and surface roughness Ra - μm. Design – MINTAB software was used for Taguchi's method and for analysis of variance (ANOVA).

Table: 3. Machine readings and calculations of Roughness

Experiment.No	Control Factors			Speeds (s)	Feed (f)	Depth of cut (d)	Surface Roughness (μ)	Predicted Ra	Values got from Minitab	
	A	B	C							
	(s)	(f)	(d)	(Rev/min.)	(mm per rev.)	(mm)			S/N Ratio	RESI1
1	1	1	1	1700	0.1	0.2	0.82	0.822465	1.71067	0.02963
2	1	1	2	1700	0.1	0.3	0.94	0.923216	0.61498	0.000741
3	1	1	3	1700	0.1	0.4	0.96	1.002099	0.16418	-0.04593
4	1	2	1	1700	0.125	0.2	1.12	1.044266	-0.69093	0.105185
5	1	2	2	1700	0.125	0.3	1.06	1.172187	-0.96497	-0.1037
6	1	2	3	1700	0.125	0.4	1.1	1.272344	-1.50581	-0.13037
7	1	3	1	1700	0.15	0.2	1.44	1.269214	-2.65349	0.116296

8	1	3	2	1700	0.15	0.3	1.54	1.424692	-3.42556	0.067407
9	1	3	3	1700	0.15	0.4	1.5	1.546424	-3.65622	-0.03926
10	2	1	1	1900	0.1	0.2	0.86	0.7976	1.62485	0.076296
11	2	1	2	1900	0.1	0.3	0.92	0.895305	0.84080	-0.01259
12	2	1	3	1900	0.1	0.4	0.76	0.971804	1.18614	-0.23926
13	2	2	1	1900	0.125	0.2	1.04	1.012696	-0.22666	0.031852
14	2	2	2	1900	0.125	0.3	1.2	1.13675	-1.35483	0.042963
15	2	2	3	1900	0.125	0.4	1.1	1.233879	-1.35523	-0.1237
16	2	3	1	1900	0.15	0.2	1.44	1.230843	-2.53892	0.122963
17	2	3	2	1900	0.15	0.3	1.6	1.381621	-3.49168	0.134074
18	2	3	3	1900	0.15	0.4	1.5	1.499672	-3.52088	-0.03259
19	3	1	1	2100	0.1	0.2	0.88	0.775869	1.62294	0.125185
20	3	1	2	2100	0.1	0.3	0.78	0.870913	1.65297	-0.1237
21	3	1	3	2100	0.1	0.4	1.16	0.945327	-0.49071	0.18963
22	3	2	1	2100	0.125	0.2	1.08	0.985105	-0.28740	0.100741
23	3	2	2	2100	0.125	0.3	1.14	1.105779	-1.00775	0.011852
24	3	2	3	2100	0.125	0.4	1.26	1.200262	-1.80159	0.065185
25	3	3	1	2100	0.15	0.2	0.58	1.197309	0.53069	-0.70815
26	3	3	2	2100	0.15	0.3	1.42	1.343978	-2.81338	-0.01704
27	3	3	3	2100	0.15	0.4	1.86	1.458814	-4.46206	0.356296

Surface roughness

Surface properties such as roughness are critical to the function ability of machine components. Increased understanding of the surface generation mechanisms can be used to optimize machining process and to improve component function ability.

The present study has shown two purposes. The first was to demonstrate the use of Taguchi parameter design in order to identify the optimum surface roughness with particular combination of cutting parameters and a systematic procedure using Taguchi design in process design of turning operations. The second was to determine the optimum combination of process parameters more accurately by investigating the relative importance of process parameters using ANOVA. The obtained results are analyzed using Minitab software and all the values are shown in the Table 4.

Table: 4. ANOVA table for Surface roughness

Source	**Speed(s)**	**Feed (f)**	**Depth of cut**	**Error**
			(s)	
DOF	2	2	2	20
S.S	0.00643	1.29070	0.21923	0.88714
M.S	0.00321	0.64535	0.10961	0.04436
F Value	0.07	14.55	2.47	2.47
P Value	0.930	0.000	0.110	0.110

It can be seen from ANOVA table 4 that feed is the maximum contributing factor and other details of DOF - Degrees of freedom, S.S - Sum of Squares, M.S - Mean of Squares and Error are mentioned. Hence as a result the individual ranking of cutting parameters on the average value of mean on surface roughness are shown in Table 5:

Table: 5. Ranking of cutting parameters

Level	1	2	3	Rank
Speed	2.786	2.236	2.855	3

Feed	2.066	2.266	3.544	1
Depth of cut	2.552	2.635	2.689	2

5. Mathematical Modeling

A regression model was developed for surface roughness using Minitab software. The predictions are speed, feed and depth of cut. Regression equation for surface roughness is

$Ra = 1.564\ s^{-0.276}\ f^{1.07}\ d^{0.285}$

Main effect plots analysis

The analysis is made with the help of software package MINITAB. The main effect of plot is shown in Fig. 1 .They show the variation of individual response with three parameters i.e. speed, feed and depth of cut separately. In the plot x-axis represents the value of each process parameter and y-axis is response value. Horizontal line indicates the mean of the response.

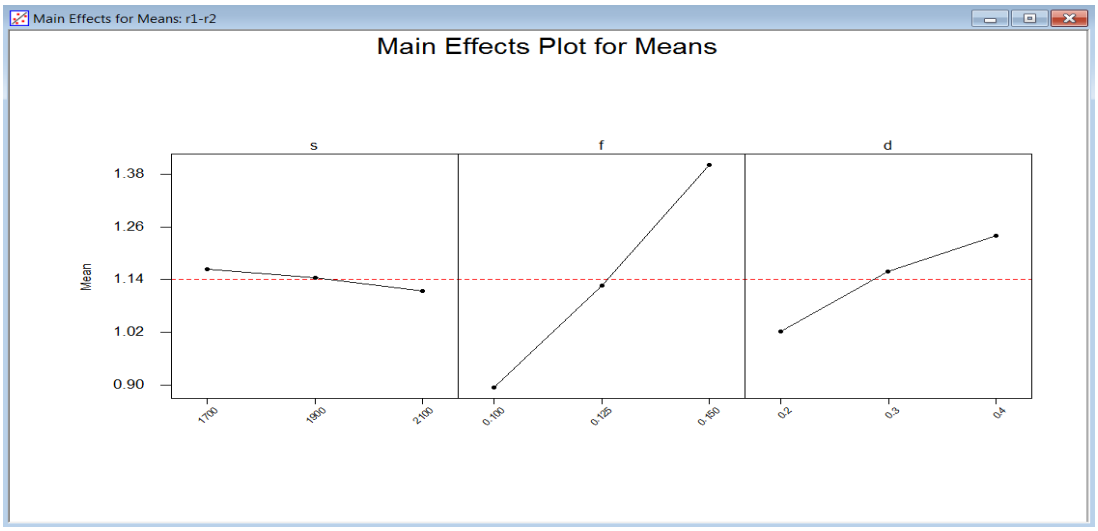

Fig: 1. Effect of turning parameters on Surface Roughness

The main effect plots are used to determine the optimal design conditions to obtain the optimal surface finish. According to this main effect plot, the optimal conditions for minimum surface roughness are speed at level (2100 RPM), feed rate at level 1 (0.1 mm/rev) and depth of cut at level 1 (0.2mm). Interaction plot for S/N ratios of the Surface roughness for data means is shown in Fig .3 Signal-to-Noise ratio of common interest for optimization for surface roughness is smaller the better.

The diagnostic checking has been performed through residual analysis for the developed model. The residual plots for surface roughness are shown in Fig. 4. These are generally fall on a straight line implying that errors are distributed normally.

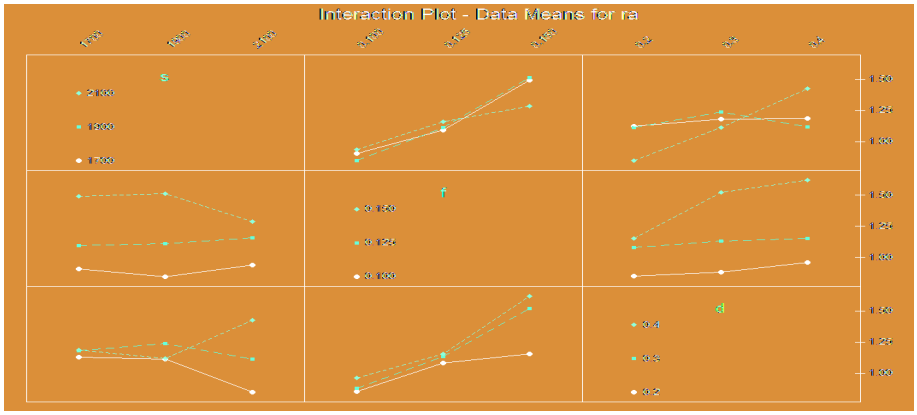

Fig: 2. Effect of turning parameters on Surface Roughness

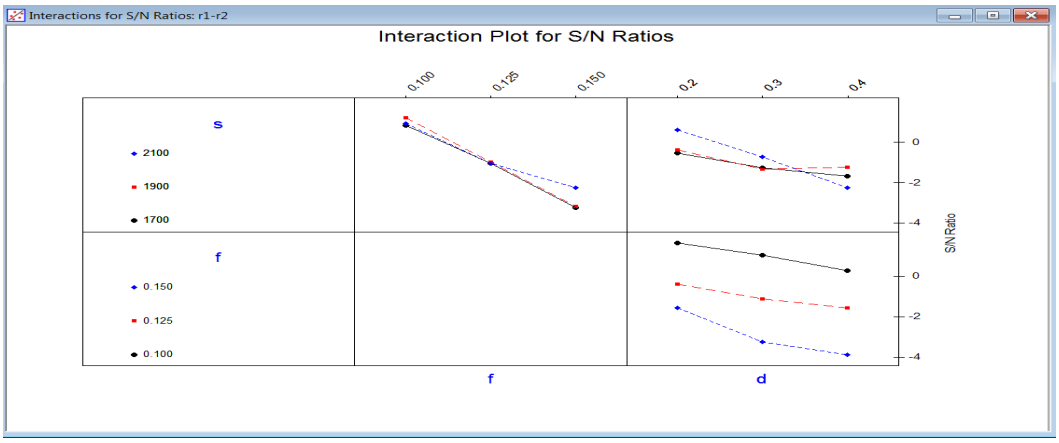

Fig: 3. Interaction plot for S/N Ratios of the Surface Roughness

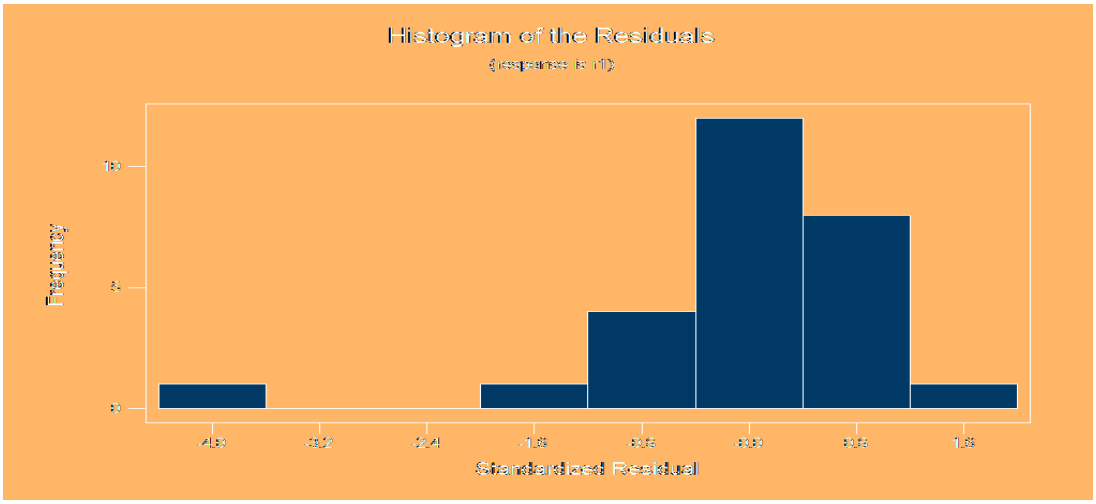

Fig: 4. Residual plot -Histogram

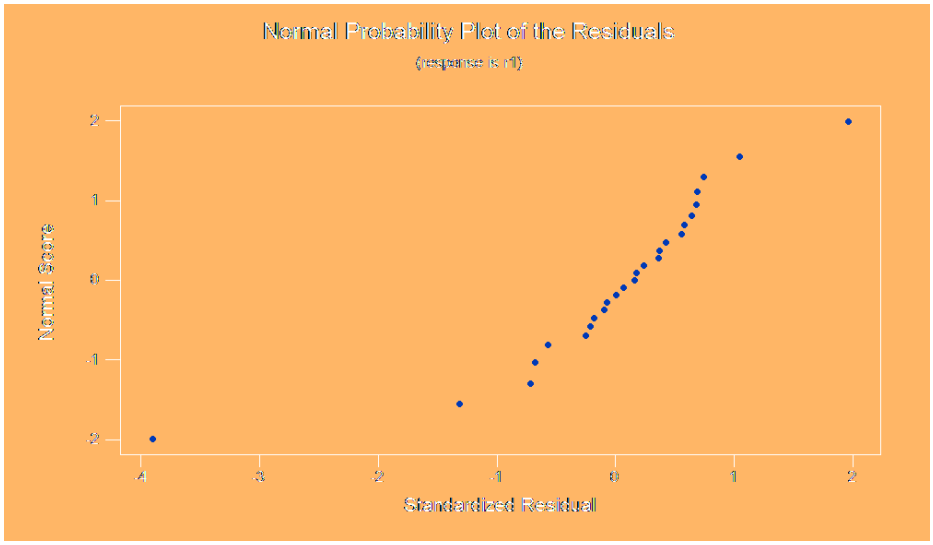

Fig: 5. Residual plot –Normal probability

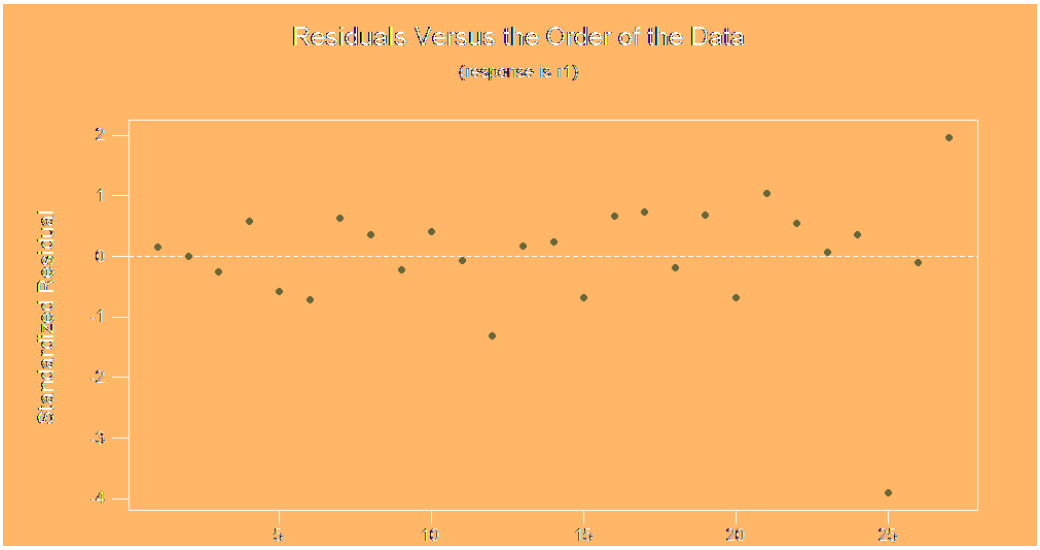

Fig: 6. Residual versus order of data

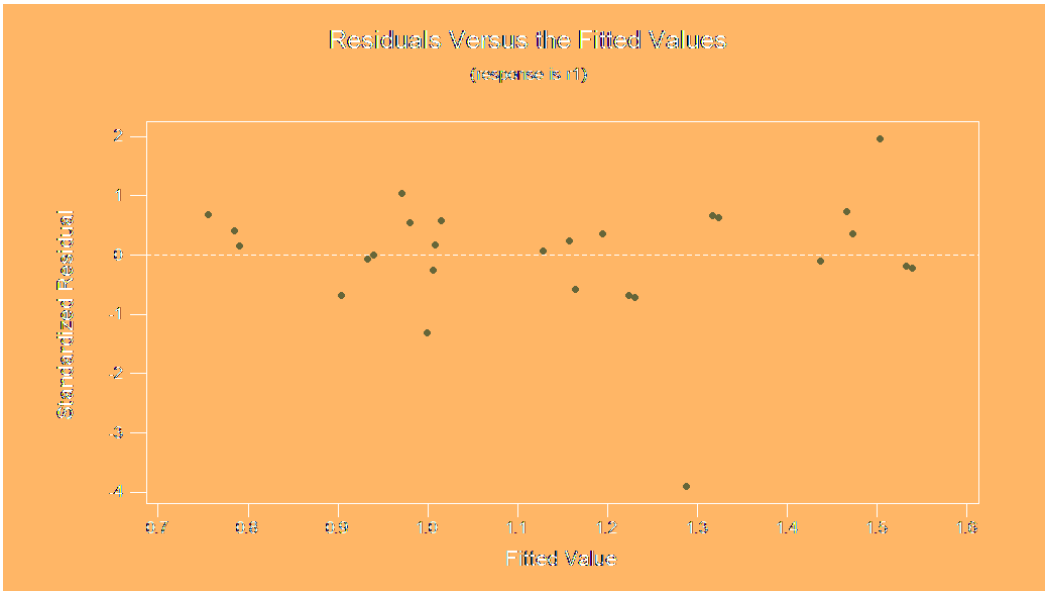

Fig: 7. Residual versus the fitted values

From Fig .4, 5, 6, 7, it can be concluded that all the values are within the control range, indicating that there is no obvious pattern and unusual structure and also the residual analysis does not indicate any model inadequacy. Hence these values yield better results in future predictions.

6. Conclusions

This work presented an experimentation approach to study the impact of machining parameters on surface roughness. Strong interactions were observed among the turning parameters. Most significant interactions were found between work materials, feed and cutting speeds. A Systematic approach was provided to design and analyze the experiments, and to utilize the data obtained to the maximum extend.

The following are conclusions drawn based on the experimental investigation conducted at three levels by employing Taguchi technique to determine the optimal level of process parameters.

- From the data collection it has been observed that the increase in cutting speed tends to improve the finish, thus the average surface roughness value decreases.

- The increase in depth of cut influences the finish slightly, but greater depth of cut marks the finish poor.
- Feed rate is the most critical parameter when finish is the criterion.
- Finish gets poor as the feed increases, thus the average surface roughness value increases with increase in feed.
- The ANOVA and F-test revealed that the feed is dominant parameter followed by depth of cut and speed for surface roughness.
- The optimal combination process parameter for minimum surface roughness is obtained at 2100 rpm, 0.1 mm/rev and 0.2mm.
- A regression model is developed for surface roughness. The developed model is reasonably accurate and can be used of prediction within limits.
- Taguchi gives systematic simple approach and efficient method for the optimum operating conditions.

References

[1] A.V.N.L.Sharma.et.al.,"Parametric Analysis And Multi Objective Optimization Of Cutting Parameters In Turning Operation Of EN353 – With CVD Cutting Tool Using Taguchi Method" Journal Of Engineering And Innovative Technology (IJEIT) 2, ISSN: 2277-3754 ISO 9001:2008, 2013

[2] Alexandru STANIMIR.et.al., "Regressions Modeling Of Surface Roughness In FinishTurning Of Hardened 205cr115 Steel Using Factorial Design Methodology" Fiabilitate Si Durabilitate - Fiability & Durability No 1(7)/ 2011,Editura "Academica Brâncuşi" , Târgu Jiu, ISSN 1844 – 640X

[3] Ananthakumar.P et.al., "Optimization Of Turning Process Parameters Using Multivariate Statistical Method-PCA Coupled With Taguchi Method International Journal of Scientific Engineering And Technology (ISSN : 2277-1581), 2(4), PP : 263-267 1 April 2013 IJSET@2013 Page 263

[4] B. Erginc, Z. Kampus, B. Sustarsic, The use of the Taguchi approach to determine the influence of injection –molding parameters on the properties of green parts, Journal of achievement in Materials and Manufacturing Engineering, 15, 2006.

[5] D.C. Montgometry, Design and analysis of experiments, 4th edition, New York: Wiley; 1997.

[6] E. Daniel Kirby [2006]" A Parameter Design Study In A Turning Operation Using The Taguchi Method" The Technology Interface/Kirby,Edkirby@Iastate.Edu

[7] Ersan Aslan, Necip Camuscu Burak Bingoren, Design of optimization of cutting parameters when turning hardened AISI 4140 steel (63 HRC) with Al 2 O3 + TiCN mixed ceramic tool, Materials and Design, date received 21.07.2005 and date accepted 06.01.2006.

[8] Puertas Arbizu, C.J. Luis Perez, Surface roughness prediction by factorial design of experiments in turning processes, Journal of Materials Processing Technology, 143- 144, 2003, 390-396.

[9] Choudhury, M.A. El-Baradie, "Surface roughness prediction in the turning of high strength steel by factorial design of experiments", Journal of Materials Processing technology, 67 (1997) 55-67

[10] Ilhan Asiltürk.et.al., "Determining the Effect Of Cutting Parameters On Surface Roughness In Hard Turning Using The Taguchi Method" Measurement 44, 2011 1697–1704, Journal Homepage:Www.Elsevier.Com/Locate/Measure ment

[11] Jitendra Verma.et.al., "Turning Parameter Optimization For Surface Roughness Of Astm A242 Type-1 Alloys Steel By Taguchi Method"International Journal Of Advances In Engineering & Technology, March. 2012 ©IJAET ISSN: 2231-1963, 255, 3(1), Pp. 255-261

[12] K. Mani Lavanya1.et.al.,"Optimization Of Process Parameters In Turning Operation Of AISI-1016 Alloy Steels With CBN Using Taguchi Method And Anova" IOSR Journal Of Mechanical And Civil Engineering (IOSR-JMCE) E-ISSN: 2278-1684,P-ISSN: 2320-334X, 7(2) (May. - Jun.) 2013, PP 24-27 Www.Iosrjournals.Org

[13] Karin Kandananond, "The Determination Of Empirical Model For Surface Roughness In Turning Process Using Design Of Experiment"ISSN: 1109-2777 1135, 8 (10), 2009

[14] M Kaladhara .et.al, "Determination of Optimum Process Parameters during Turning of AISI 304 Austenitic Stainless Steels Using Taguchi Method ANOVA"

[15] M. Kaladhar.et.al., "Application Of Taguchi Approach And Utility Concept In Solving The Multi-Objective Problem When Turning AISI 202 Austenitic Stainless Steel" Journal Of

Engineering Science And Technology Review 4 (1) 55-61, 2011
[16] M. A. Davis, Y. Chou, C.J. Evans, Ann. CIRP 45(1996) 77-82
[17] Manish Kumar Yadav.et.al.," Paper On A Comparative Study Of Surface Roughness In Multi Tool Turning With Single Tool Turning Through Factorial Design Of Experiments" International Journal Of Scientific & Engineering Research 3(8), August-2012 1 ISSN 2229-5518 IJSER © 2012 Http://Www.Ijser.Org
[18] Marinković Velibor et.al, "Optimization of Surface Roughness in Turning Alloy Steel by Using Taguchi Method" Scientific Research and Essays, 6(16), Pp. 3474-3484, 19 August, 2011, ISSN 1992-2248 ©2011 Academic Journals
[19] Muhammad Munawar.et.al., "Optimization Of Surface Finish In Turning Operation ByConsidering The Machine Tool Vibration Using Taguchi Method", 2009
[20] N. Nalbant, H. Gokkaya, G. Sur, "Application of Taguchi method in the optimization of cutting parameters for surface roughness in turning", Materials and Design, 06.01.2006
[21] Naveen, A. Sait, S, Aravindan, and Noorul Haq., A., "Influence of machining parameters on surface roughness of GFRP pipes", Journal of Advances on Production Engineering and Management, 4 (1-2), p. 47-58, 2009
[22] Onkar N. Panday "Total Quality Management
[23] Palanikumar, L. Karunamoorthy, R. Krathikeyan, Assessment of factors influencing surface roughness on the machining of glass– reinforced polymer composites, Journal of Materials and Design, 27, 2006, 862-871.
[24] Philip Selvaraj.et.al., " Optimization Of Surface Roughness Of Aisi 304 Austenitic Stainless Steel In Dry Turning Operation Using Taguchi Design Method "Journal Of Engineering Science And Technology Vol. 5, No. 3 (2010) 293 – 301
[25] Rahul Davis, Jitendra Singh Madhukar, Vikash Singh Rana, and Prince Singh, Optimization of Cutting Parameters in Dry Turning Operation of EN24 Steel . International Journal of Emerging Technology and Advanced Engineering Website: www.ijetae.com, ISSN 2250-2459, 2(10), October 2012
[26] Rodrigues L.L.R et.al, "Effect of Cutting Parameters on Surface Roughness and Cutting Force in Turning Mild Steel" Research Journal Of Recent Sciences International Science Congress Association Vol. 1(10), 19-26, October, 2012 Res.J.Recent Sci ISSN 2277-2502
[27] S. Thamizhmanii, S. Hasan, "Analyses of roughness, forces and wear in turning gray cast iron", Journal of achievement in Materials and Manufacturing Engineering, 17, 2006
[28] T. Tamizharasan, T. Selvaraj, A. Noorul Hag, "Analysis of tool wear and surface finish in hard turning", International Journal of Advanced Manufacturing Technology, 2005, DOI 10/1007 /s 00170-004-2411-1
[29] Vipin.et.al., "Surface Roughness Prediction Model by Design of Experiments For Turning Leaded Gun Metal" International Journal Of Applied Engineering Research ISSN 0973-4562, 4(12), 2009, Pp. 2621–2628
[30] W. Konigi, M. Klinger, R. Link, Ann. CIRP 39 (1990) 61-64.
[31] W. H. Yang, Y.S. Tang, "Design optimization of cutting parameters for turning operations based on Taguchi method", Journal of Materials Processing Technology, 84,1998, 122-129
[32] X. L. Liu, D.H. Wen, Z.J. Li, Xiao, .G. Yan, Experimental study on hard turning of hardened GCr15 steel with PCBN tool, Journal of Materials Processing Technology, 129, 2002, 217-221
[33] Xue Ping, C. Richard Liu, Zhenqiang Yao, "Experimental study and evaluation methodology on hard surface integrity", International Journal Advanced Manufacturing Technology, ODI 10.1007/s00170-006-0576-6.
[34] Yigit Kazancoglu1.et.al.,"Multi-Objective Optimization of the Cutting Forces In Turning Operations Using The Grey-Based Taguchi Method, Original Scientific Article/Izvirni Znanstveni ~Lanek MTAEC9, 45(2)105(), 2011, ISSN 1580-2949
[35] K. Yusuf, Y. Nukman, T. M. Yusof, S. Z. Dawal, H. Qin Yang, T. M. I. Mahlia, K. F. Tamrin, Effect of cutting parameters on the surface roughness of titanium alloys using end milling process. Journal of Scientific Research and Essays 5(11), p. 1284-1293, 2010

OTRA based Voltage mode third order Quadrature Oscillator

Rajeshwari Pandey[1] , Neeta Pandey[2] ,K.GuruMurthy[3], Rashika Anurag[4]
[1,] rajeshwaripandey@gmail.com, [2] n66pandey@rediffmail.com ,[3] murthykgm@gmail.com, [4]raashika@rediffmail.com
[1,2,3] *Department of Electronics and Communication Engineering,Delhi Technological University, Delhi-42, India*
[4]*Department of Electronics and Communication Engineering, JSS Academy of Technical Education, C-20/1 Sector 62, NOI DA, Uttar Pradesh, 201301.India*

Abstract— In this paper two topologies of operational transresistance (OTRA) based third order quadrature oscillators (QO) are proposed. The proposed oscillators are designed using combination of lossy and lossless integrators. The proposed topologies can be made fully integrated by implementing the resistors using matched transistors operating in linear region, which also facilitates electronic tuning of oscillation frequency. The non-ideality analysis of the circuit is also given and for high frequency applications self compensation can be used. Workability of the proposed QOs is verified through PSPICE simulations using 0.5μm AGILENT CMOS process parameters. The total harmonic distortion (THD) for both the QO designs is found to be less than 1%.

Keywords—*Quadrature oscillator,OTRA*

I. INTRODUCTION

Quadrature oscillators (QO) produce outputs having a phase difference of 90°. The phase-locked sine-cosine relationship of QO has useful applications in the field of telecommunications where the modulation scheme utilizes both in-phase and quadrature components, such as in single-sideband generators, and quadrature mixers [1]. The QOs are also used extensively in the field of instrumentation and power electronics [2]. For these applications low value of total harmonic distortion (THD) is an essential requirement as higher harmonics have detrimental effects on electrical equipment. These higher order harmonics can also interfere with communication transmission lines since they oscillate at the same frequencies as the transmit frequency. If left unchecked, increased temperature and interference can greatly shorten the life of electronic equipment and cause damage to power systems.

It is well known that a higher order networks as compared to lower order circuits, provide better accuracy, frequency response and distortion performance [3,4]. However, it has been observed that higher order QO designs have not been explored much, as only a few third order QOs [1, 3 – 16] have appeared in literature in recent years. A carefull observation suggests that the reported QO designs are based on forming closed loop using (i) two lossy and one lossless integrators [3 – 5], (ii) one lossy and two lossless integrators [8], (iii) a second order low pass filter followed by an integrator [1, 6,7, 10 – 16] (iv) three low pass filters and gained feedback around the loop [9]. These topologies are designed using second generation current conveyor (CCII) [1, 6], second generation current controlled conveyor (CCCII) [7– 9], differential voltage current conveyor (DVCC) [10] opamp [5], operational transconductance amplifier (OTA) [3], current difference transconductance amplifier (CDTA) [4, 11], operational transresistance amplifier (OTRA) [12] and current-controlled current difference transconductance amplifier (CCCDTA) [13]. The structure proposed in [15] uses Differential difference current conveyor (DDCC) and OTA whereas design of [16] is based on CCCDTA and OTA.

The OTRA is a current input voltage output device [17]. Being a current processing block, it inherits all the advantages of current mode techniques [12] and provides voltage output at low impedance which can readily be used to drive voltage input circuits without increasing component count. An extensive literature review suggests though a large number of OTRA based second order QOs [17-21] are available in literature, yet only a single third order QO topology using OTRA [12] is reported. This QO design and is based on forming a closed loop using a second order low pass filter followed by an integrator.

In this paper two topologies of third order QO based on OTRA have been presented which use the scheme of lossy and lossless integrators. One of the proposed circuits makes use of one inverting lossy and two lossless integrators connected in a feedback forming closed loop whereas the other configuration uses one lossless and two lossy integrators to form closed loop. The proposed structures can be made fully integrated by implementing the resistors using matched transistors operating in linear region and can be tuned electronically.

II. CIRCUIT DESCRIPTION

The OTRA is a high gain current input voltage output analog building block [17]. The input terminals of OTRA are internally grounded, thereby eliminating response limitations due to parasitic capacitances and resistances and hence is a suiatable choice for high frequency applications. The circuit symbol of OTRA is shown in Fig. 1 and the port characteristics are given by (1), where R_m is transresistance gain of OTRA.

$$\begin{bmatrix} V_p \\ V_n \\ V_O \end{bmatrix} = \begin{bmatrix} 0 & 0 & 0 \\ 0 & 0 & 0 \\ R_m & -R_m & 0 \end{bmatrix} \begin{bmatrix} I_p \\ I_n \\ I_O \end{bmatrix} \quad (1)$$

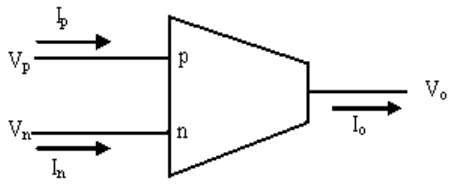

Fig.1. OTRA circuit Symbol

For ideal operations the R_m of OTRA approaches infinity and forces the input currents to be equal. Thus OTRA must be used in a negative feedback configuration [22].

CIRCUIT I

The first QO topology is shown in Fig.2. It uses two losless integrators and a lossy inverting integrator in the feddback forming a closed loop resulting in loop gain of the system as A(s)β(s) where A(s) is forward path gain involving OTRA2, OTRA3 and β(s) is feedback gain involving OTRA1.

The criterion for oscillations [23] to occur, is given by

1- A(s) β(s) =0 (2)

If this criterion is satisfied the closed loop system will result in two quadrature phase oscillations, available at nodes 1 and 2. Routine analysis of the circuit of Fig. 2 results in following characteristic equation as

$$s^3 c_1 c_2 c_3 R_2 R_3 + \frac{s^2 C_2 C_3 R_2 R_3}{R_4} + sc_3 \frac{R_3}{R_5} + \frac{1}{R_1} = 0 \quad (3)$$

From this characteristic equation the condition of oscillation (CO) and frequency of oscillation (FO) can befound to be

FO: $$f = \frac{1}{2\pi}\sqrt{\frac{1}{C_1 C_2 R_2 R_5}} \quad (4)$$

CO: $$R_4 R_5 = R_1 R_3 \quad (5)$$

The FO can be adjusted to desired value through R_2 and proper selection of resistor R_1, R_3 and R_4 would satisfy the CO**.**

CIRCUIT II

The second proposed QO configuration is shown in Fig.3 which makes use of two lossy and one lossless integrator, all in inverting mode.

The characteristic equation of the Circuit II can be deduced as

$$s^3 C_1 C_2 C_3 R_3 + s^2\left(\frac{C_2 C_3 R_3}{R_4} + \frac{C_1 C_3 R_3}{R_5}\right) + \frac{sC_3 R_3}{R_4 R_5} + \frac{1}{R_1 R_2} = 0 \quad (6)$$

FO: $$f = \frac{1}{2\pi}\sqrt{\frac{1}{C_1 C_2 R_4 R_5}} \quad (7)$$

CO: $R_1R_2R_3C_3\,[R_4C_1 + R_5C_2] \;= R_4^2R_5^2C_1C_2$ (8)

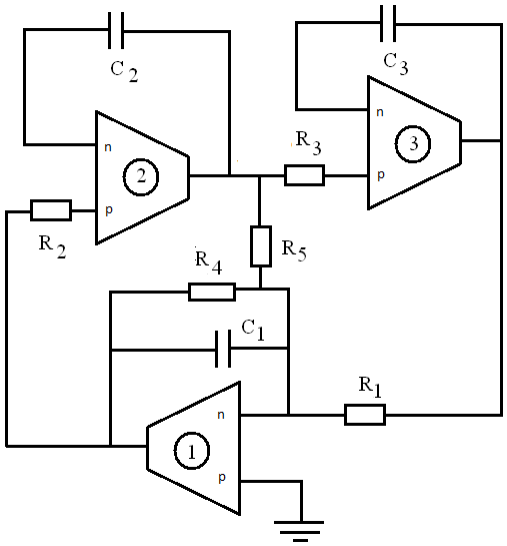

Fig.2. Proposed circuit I

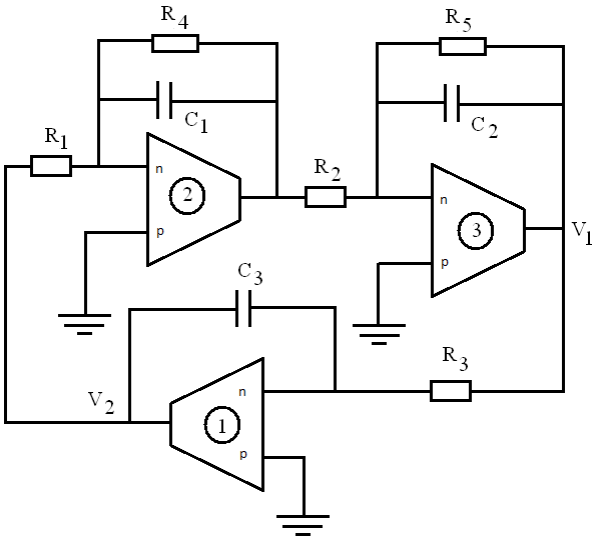

Fig.3 Proposed circuit II

By suitable selection of R_4 and R_5 the FO can be adjusted to desired value and proper selection of resistors R_1, R_2, and R_3 results in desired CO.

The current differencing property of the OTRA makes it possible to implement the resistors connected to the input terminals of OTRA, using MOS transistors with complete non linearity cancellation [17]. Each resistor requires two matched n-MOSFETs connected in a manner as shown in Fig 4 which represents a typical MOS implementation of resistance connected at negative input of OTRA.

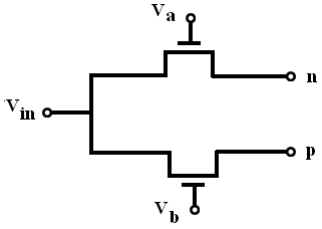

Fig.4. The MOS based resistor [17]

Symbols ‘p’ and ‘n’ represent the non-inverting and the inverting terminals of the OTRA. As can be seen from the figure, the voltages at the drain and the source terminals for both MOSFETs are equal. On taking the difference of the currents flowing in the two transistors, the non linearity gets cancelled out. The resistor value realized can be expresssed as

$$R = \frac{1}{K_N(V_a - V_b)} \tag{9}$$

where

$$K_N = \mu\, C_{OX}\, \frac{W}{L} \tag{10}$$

K_N needs to be determined for the transistors being used to implement the resistors and μ, C_{OX} and W/L represent standard transistor parameters. The MOS based implementation of Circuit I and Circuit II are shown in Fig.5 and Fig. 6 respectively.

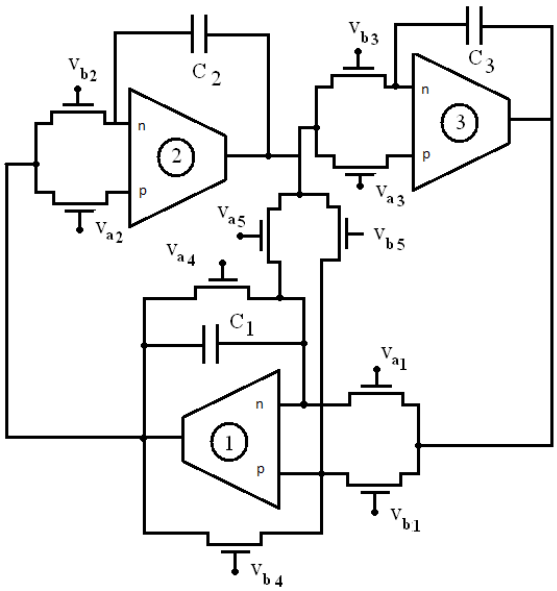

Fig.5. The MOS based implementation of QO Circuit I

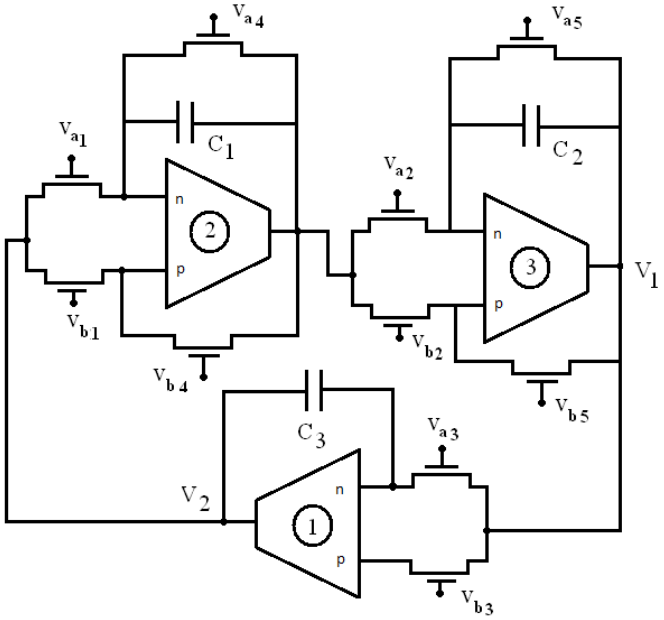

Fig.6. The MOS based implementation of QO Circuit II

III. NON-IDEAL ANALYSIS

The output of the QO may deviate due to non ideality of OTRA in practice. Ideally the transresistance gain R_m is assumed to approach infinity. However, practically R_m is a frequency dependent finite value. Considering a single pole model for the trans-resistance gain, R_m can be expressed as

$$R_m(s) = \left(\frac{R_0}{1+\frac{s}{\omega_0}}\right) \tag{11}$$

where R_0 is dc transresistance gain. For high frequency applications the transresistance gain R_m (s) reduces to

$$R_m(s) = \left(\frac{1}{sC_p}\right) \tag{12}$$

Where $C_p = \frac{1}{R_0\ \omega_0}$

Taking this effect into account (3) modifies to

$$s^3(c_1+c_p)(c_2+c_p)(c_3+c_p)R_2R_3 + s^2(c_2+c_p)(c_3+c_p)\frac{R_2R_3}{R_4} + s(c_3+c_p)\frac{R_3}{R_5} + \frac{1}{R_1} = 0 \tag{13}$$

From (13) it is found that FO for circuit I changes to

$$f = \frac{1}{2\pi}\sqrt{\frac{1}{(C_1+C_p)(C_2+C_p)R_2R_5}} \tag{14}$$

Due to nonideality effect of OTRA (6) changes to

$$s^3(c_1+c_p)(c_2+c_p)(c_3+c_p)R_3 + s^2\left((c_2+c_p)(c_3+c_p)\frac{R_3}{R_4} + (c_1+c_p)(c_3+c_p)\frac{R_3}{R_5}\right) + s(c_3+c_p)\frac{R_3}{R_4R_5} + \frac{1}{R_1R_2} = 0 \tag{15}$$

The characteristic equation represented by (15) results in modified FO for circuit II and is expressed as

$$f = \frac{1}{2\pi}\sqrt{\frac{1}{(C_1+C_p)(C_2+C_p)R_4R_5}} \tag{16}$$

The effect of C_p can be eliminated by pre-adjusting the values of capacitors C_1, C_2 and C_3 thus achieving self compensation.

IV. SIMULATION RESULTS

The proposed QO is verified through simulations using the CMOS implementation of the OTRA [22] which is shown in Fig.7. The SPICE simulations are performed using 0.5 μm CMOS process parameters provided by MOSIS (AGILENT). Supply voltages taken are ±1.5V. Both the QO topologies are designed for an FO of 159 KHz and the simulated value was observed to be 161 KHz and for Circuit I and II rspectively. The simulated transient output and corresponding frequency spectrum for Circuit I are shown in Fig.8 and Fig.9 respectively and those for Circuit II are depicted in Fig.10 and Fig.11. The percentage total harmonic distortion (THD) is 0.57% for QO Circuit I and that for Circuit II is observed to be 0.7%. These values are considerably low as compared to 6.3 % THD of QO circuit of [8].

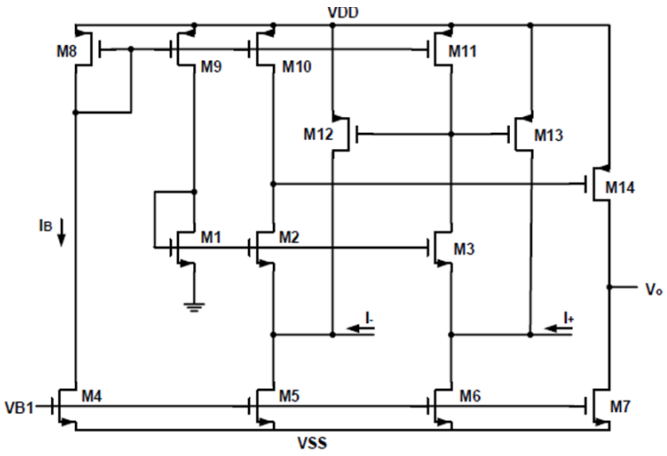

Fig.7 CMOS OTRA [22]

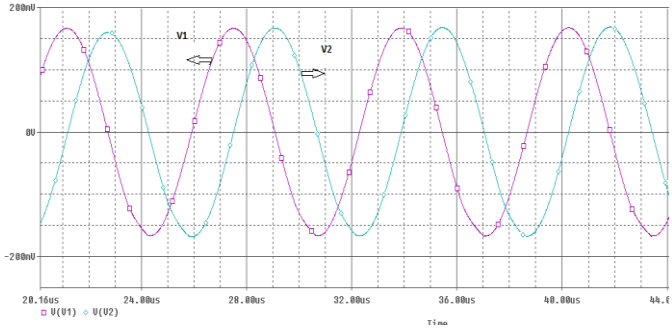

Fig.8 Transient Output of proposed QO Circuit I

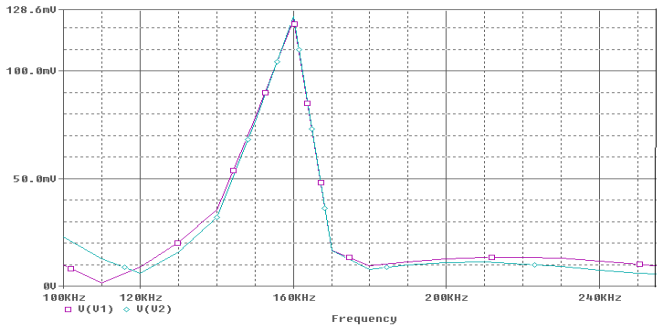

Fig.9 Frequency spectrum of output of QO Circuit I

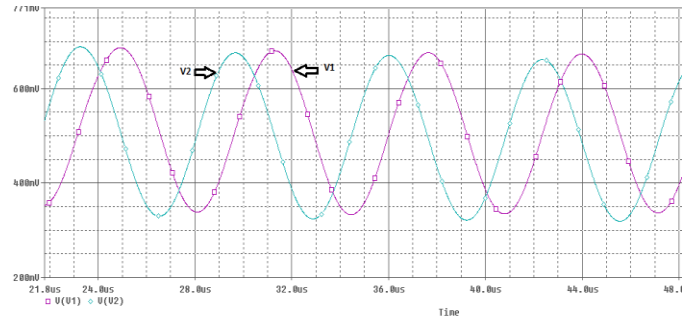

Fig.10 Transient output of proposed QO Circuit II

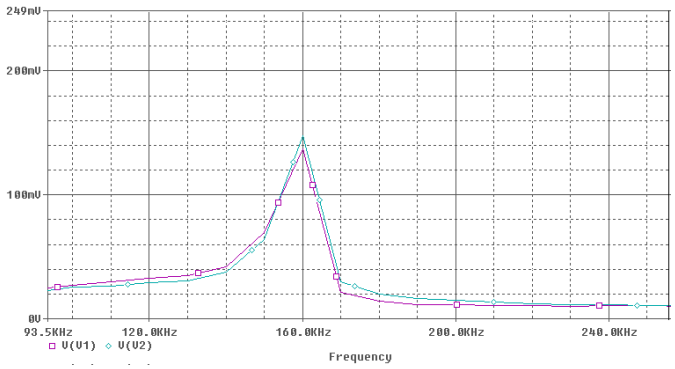

Fig.11 Frequency spectrum of output of QO Circuit II

V. CONCLUSION

Two topologies of third order OTRA based quadrature oscillator are presented in this paper using lossy and lossless integrators. The simulations are performed using PSPICE and it is observed that the results are in close agreement with theoretical propositiond. The simulated value of % THD in both the ciruits is quite low as compared to other third order structures available in literature. The effect of non ideal behavior of OTRA and high frequency compensation scheme has also been included in the proposed theory.

REFERENCES

[1] J.W. Horng, C.L. Hou, C.M. Chang, W.-Y. Chung, H.-W. Tang and Y-H. Wen "Quadrature oscillators using CCIIs," Int. J. Electron, vol. 92, pp. 21–31,2005.

[2] J.W. Horng, C.L. Hou, C.M. Chang, H.P. Chou, C.T. Tin and Y.H. Wen. "Quadrature oscillators with grounded capacitors and resistors using FDCCIIs," ETRI Journal, vol.28,pp. 486 – 94,2006.

[3] P. Promme and K. Dejhan, "An integrable electronic controlled sinusoidal oscillator using CMOS operational transconductance amplifier," Int. J. Electron., vol.89, pp. 365–379, 2002.

[4] J. W. Horng, "Current-mode third-order quadrature oscillator using CDTAs," Active and Passive Electronic Components, 2009, Article ID 789171, p. 1-5.

[5] J. W. Horng, "Quadrature Oscillators using Operational Amplifiers," Active and Passive Electronic Components 2011, Article ID 320367, DOI:10.1155/2011/32036.

[6] J. W. Horng "Current/ Voltage mode third order quadrature oscillator employing two multiple outputs CCIIs and grounded capacitor," Indian Journal of Pure and Applied Physics vol.49, pp.494-498, 2011.

[7] S Maheshwari, and I. A. Khan, "Current controlled third order quadrature oscillator," IEE Proc.-Circuits, Devices and Systems, vol. 152, pp. 605-607, 2005.

[8] S. Maheshwari and I.A. Khan, "Current controlled third order quadrature oscillator," IET Circuits Devices Systems, vol. 4, pp. 188–195,2010.

[9] S.Maheshwari and R. Verma, "Electronically Tunable Sinusoidal Oscillator Circuit," Active and Passive Electronic Components Volume 2012, Article ID 719376, 6 pages DOIi:10.1155/2012/719376

[10] S. Maheshwari, "Analogue signal processing applications using a new circuit topology," IET Circuits Devices Systems vol. 3, pp.106–115. 2009.

[11] J. W. Horng, H Lee and J.Y. Wu, "Electronically tunable third order Quadrature oscillators using CDTAs," RadioEngineering vol. 19, pp. 326-330, 2010.

[12] [12] R. Pandey, N. Pandey and S.K. Paul, "MOS-C Third Order Quadrature Oscillator using OTRA,". Third International Conference on Communication and Computer Technology, ICCCT-12, pp.77 -80, 2012.

[13] S. Lawanwisut and M. Siripruchyanun, "High Output-impedance Current-mode Third-Order Quadrature Oscillator Based on CCCCTAs," TENCON 2009 – 2009 IEEE Region 10 Conference, pp.1-4, 2009.

[14] A. Kwawsibsam, B.Sreewirote, and W. Jaikla, "Third-Order Voltage-Mode Quadratrue Oscillator Using DDCC and OTAs," 2011 International Conference on Circuits, System and Simulation, pp.317-21, 2011

[15] M. Kumngern and S. Junnapiya, "Current-Mode Third-Order Quadrature Oscillator Using Minimum Elements," 2011 International Conference on Electrical Engineering and Informatics, pp. 1 – 4, 2011.

[16] D. Duangmalai W. Jaikla, "Realization of Current-mode Quadrature Oscillator Based on Third Order Technique," ACEEE International Journal on Electrical and Power Engineering, vol.2, pp.46 – 49, 2011.

[17] K. N. Salama and A. M. Soliman, "CMOS Operational Transresistance Amplifier for analog signal processing applications." Microelectron. J.,vol. 30, pp. 235–245, 1999.

[18] K.N. Salama and A.M. Soliman, "Universal filters using the operational transresistance amplifiers," AE U—International Journal of Electronics and Communications, vol. 53, pp. 49–52, 1999.
[19] S. Kilinc and U. Cam , "Operational Transresistance Amplifier Based First-Order Allpass Filter with an Application Example," The 47th IEEE International Midwest Symposium on Circuits and System, pp. I65-I68, 2004.
[20] S. Kilinc and U. Cam, "Cascadable allpass and notch filters employing single operational transresistance amplifier," Computers and electrical Engineering vol.31, pp 391-401, 2005.
[21] C Cakir, U. Cam, and O. Cicekoglu, "Novel All pass Filter Configuration Employing Single OTRA," IEEE Transactions on circuits and systems—ii: express briefs., vol.52, pp.122-125, 2005
[22] H. Mostafa and A. M. Soliman, "A modified realization of the OTRA," Frequenz, vol.60, pp.70-76, 2006.
[23] A. S. Sedra, and K. C. Smith, Microelectronic Circuits. Oxford University Press, New York, 2004.

Accepted Manuscript

Phase transformation and two-mode phonon behavior of (1-x) [Ba $Zr_{0.025}Ti_{0.975}O_3$] – (x) [$BiFeO_3$] solid solutions

Priyanka A. Jha, Pardeep K. Jha, A.K. Jha, R. K. Kotnala, R.K. Dwivedi

PII: S0925-8388(14)00488-5
DOI: http://dx.doi.org/10.1016/j.jallcom.2014.02.118
Reference: JALCOM 30703

To appear in:

Received Date: 20 January 2014
Revised Date: 20 February 2014
Accepted Date: 20 February 2014

Please cite this article as: P.A. Jha, P.K. Jha, A.K. Jha, R. K. Kotnala, R.K. Dwivedi, Phase transformation and two-mode phonon behavior of (1-x) [Ba $Zr_{0.025}Ti_{0.975}O_3$] – (x) [$BiFeO_3$] solid solutions, (2014), doi: http://dx.doi.org/10.1016/j.jallcom.2014.02.118

This is a PDF file of an unedited manuscript that has been accepted for publication. As a service to our customers we are providing this early version of the manuscript. The manuscript will undergo copyediting, typesetting, and review of the resulting proof before it is published in its final form. Please note that during the production process errors may be discovered which could affect the content, and all legal disclaimers that apply to the journal pertain.

ACCEPTED MANUSCRIPT

Phase transformation and two-mode phonon behavior of (1-x) [Ba $Zr_{0.025}Ti_{0.975}O_3$] – (x) [$BiFeO_3$] solid solutions

Priyanka A. Jha[1, 2], Pardeep K. Jha[1], A.K.Jha[2, 3], R. K. Kotnala[4] and R.K. Dwivedi[*1]

[1] Department of Physics and Material Science &Engineering

Jaypee Institute of Information Technology

Noida, U. P., India.

[2]Thin Film & Material Science Laboratory

Department of Applied Physics

Delhi Technological University (Formerly Delhi College of Engineering)

Bawana Road, Delhi- 110042, India.

[3]Department of Applied Science

A. I. A. C. T. R. (GGSIPU), Geeta Colony

Delhi- 110031, India.

[4]National Physical Laboratory

Dr. K.S. Krishanan Marg, New Delhi-110012

Ph. No. : +91 120 2 59 43 66, Fax No. : +91 120 2 40 09 86

Abstract

In the present work the compounds with $x \leq 1.0$ in the system (1-x) [Ba $Zr_{0.025}Ti_{0.975}O_3$] – (x) [$BiFeO_3$] have been synthesized using solid state reaction method. X-ray diffractograms and Raman spectra reveal the formation of single phase solid solution. The wave number shift and intensity ratio of A-O and B-O bonds in Raman spectra reveals structural changes with the concentration of bismuth ferrite. The linear dependence of the intensity ratio at B-sites i.e. $I_{(Fe-O)}$ / $I_{(Ti-O)}$ on the concentration of substituent suggests solid solution formation with two phonon mode

ACCEPTED MANUSCRIPT

behavior. A broad minima in the plot of Intensity ratio at A-sites ($I_{(Ba-O)}/I_{(Bi-O)}$) with x has been observed for the compositions range 60% ≤ x ≤ 70%. A correlation between the variation of the intensity ratio at A-sites and B-sites with x has been established to explain multiferroicity in these samples. P-E and M-H measurements indicate that the sample with 60% BFO has exhibited prominent multiferroic properties.

Keywords: Multiferroics, X-ray diffraction, Raman spectroscopy.

1. Introduction

$BaTiO_3$ (BT) is one of the most important ferroelectric materials of the perovskite family. It is well known that a solid solution of ferroelectric $BaTiO_3$ and anti-ferroelectric $BaZrO_3$ provides a very interesting stable system for many applications [1]. Whereas, barium zirconate titanate ($BaZr_{0.025}Ti_{0.975}O_3$) [2] shows a very large dielectric constant because of the pinching effect which occurs when the phase transitions are concentrated [3].

The term multiferroics is used for those multifunctional materials in which two or more kinds of fundamental ferroic properties coexist. In the recent years, these materials have become one of the hottest topics of research in condensed matter physics and materials science. Various strategies have been followed to combine the two types of ferroic properties in a single phase system [4]. Among these, $BiFeO_3$ (BFO) is known to be the only multiferroic material at room temperature with a rhombohedrally distorted perovskite structure [4] but it suffers from weak ferroelectricity in bulk sample, which is believed to be due to bismuth volatilization [5]. The weak ferroelectricity in BFO is because of the following reasons. Firstly, it is due to the leakage problems caused by Bi-evaporation and secondly due to existence of R3c symmetry leading to the development of spontaneous polarization along the

ACCEPTED MANUSCRIPT

pseudocubic [111] direction where lone pair of electrons of Bi^{3+} in BFO lattice are displaced from their centro-symmetric positions along the three-fold rotation axis [6].

There are so many inherent problems in the single phase ME materials such as (i) high leakage current, (ii) structural distortion and instability, (iii) low ME coefficient and (iv) Magnetoelectric or Ferromagnetic ordering at low temperature. Thus combination of BFO and BT with traces of $BaZrO_3$ i.e. (BFO-BT-BZ) may be worthful to reduce the leakage and hence improved ferroelectricity and found to be the most suitable FE/FM/AFE in three component systems to get the stable structure. X-ray diffractograms confirm the stable structure with a phase change in these novel compositions. Raman spectroscopy is a very valuable technique to obtain local information of the lattice deformation due to the substitutions in multiferroic materials and hence to study the phase change if any. It is well known that there is a very close relationship between ferroelectricity and lattice dynamics. A correlation between the phase change and lattice dynamics has been justified analytically. Further through vibrational spectroscopy, ferroelectric and ferromagnetic properties have been predicted. To the best of our knowledge, there is hardly any report on the phase change over the complete composition range ($x \leq 1.0$) in the system $BiFeO_3$ - $BaTiO_3$ – $BaZrO_3$ according to the compositional formula $Bi_{1-x}\ Ba_x\ (Fe_{1-x}Zr_{0.025x}Ti_{0.975x})\ O_3$ (abbreviated as BBFZT) [7, 8] through Raman spectroscopy. The significant changes in Raman spectra and XRD profile with x in the system prompted the authors to study the phase change in these compositions because interaction between phonon modes play key role in deciding the phase in these materials. In addition to this, the detailed study of Raman spectra has been correlated with multiferroic properties in these materials. It is found that BBFZT in the composition range $0.6 \leq x \leq 0.7$ is found to

ACCEPTED MANUSCRIPT

be promising multifunctional material that has been predicted analytically and justified experimentally.

2. Experimental

Polycrystalline samples of composition (1-x) [Ba $Zr_{0.025}Ti_{0.975}O_3$] – (x) [$BiFeO_3$] [$x \leq 1.0$] were prepared using solid state reaction method as described in the previous report [8]. X- Ray diffractograms of the sintered samples were recorded using a Bruker X-ray Diffractometer with CuKα (λ=1.5406 A^o) radiations in the 2θ range $10^o \leq 2\theta \leq 70^o$ at a scanning rate of 1^o/ minute. FT-Raman spectra were recorded in backscattering geometry by means of a Varian (Digilab) dedicated FT-Raman spectrometer (Nd-YAG laser, 1064 nm, 500 mW laser power) and corrected to white light background. 1024 spectra were averaged in order to improve the signal to noise ratio. Magnetic measurements at room temperature (M-H loop) have been carried out using Vibrating Sample Magnetometer (VSM 7305, Lake Shore).

3. Results and Discussions

3.1 XRD Analysis

Fig.1 shows the X-ray diffractograms of specimens with $0 \leq x \leq 1.0$ in the system (1-x) [Ba $Zr_{0.025}Ti_{0.975}O_3$] – (x) [$BiFeO_3$] i.e. BZT-BFO system. All the samples have shown single phase formation. The detailed structural and dielectric analysis of BZT with the variation of BFO content up to x = 0.4 has already been reported [8]. A splitting is observed at $2\theta \approx 37^o$ for the compositions $x \leq 0.20$ which corresponds to (111) peak while no splitting is observed for $0.3 \leq x \leq 0.6$. There is clear splitting of (111) reflection at $2\theta \approx 37^o$ into two peaks (113) and (202) for $x \geq 0.7$ (shown in Fig. 1(a) right column). Further a reflection (110) at $2\theta \approx 32^o$ has also been observed to split into (110) and (104) peaks with the increasing concentration of BFO (see Fig. 1(a) left column). The X-ray diffractograms have been refined with Rietveld refinement using FULLPROF software package and the refined parameters are mentioned in Fig.1 (b, c, d). In the refinements, the peak shapes were described by

ACCEPTED MANUSCRIPT

pseudo-Voigt functions. Fig.1(b, c, d) depicts the calculated, observed and difference profiles of the studied specimens obtained after Reitveld refinements. The samples with $x \leq 0.2$ have been fitted with P4mm structural symmetry and a good agreement has been observed between the experimental and refined data. The agreement parameters (χ^2) obtained after refinement are 2.15 for x = 0.1 and 2.457 for x = 0.2, which lies within the acceptable limit of such structural symmetries. The diffraction data of samples within the range $0.3 \leq x \leq 0.6$ has been fitted with pseudocubic symmetry Pseudocubic does not belong to any of the crystal systems. The structure is basically referred as pseudocubic in correlation with the splitting of (100) peak. If the peak splits, the indexing has to be done according to the rhombohederal symmetry. In the present case, the samples within the range $0.3 \leq x \leq 0.6$ has been fitted according to tetragonal (P4mm) symmetry where lattice parameters are approaching equal to each other [9]. From Fig.1 (b) the fitting parameters (χ^2) are 1.862 for x = 0.3, 1.91 for x = 0.4, 2.38 for x = 0.5 and 2.34 for x = 0.6. For the compositions $x \geq 0.70$, the diffraction data is fitted with Rhombohederal (R3c symmetry) where fitting parameters (χ^2) are 2.32 for x = 0.7, 2.69 for x = 0.8 and 2.42 for x = 0.9. The refined results reveals the structural transformation from tetragonal (P4mm) structure for $x \leq 0.2$ to pseudocubic in the range $0.3 \leq x \leq 0.6$ and then to rhombohederal for $x \geq 0.7$ [9]. It has also been observed that the diffraction peaks shift towards higher angle with increasing concentration of bismuth ferrite which can be attributed to the smaller size of substituent ions like the ionic radius of Bi^{3+} (1.03Å) is less than that of Ba^{2+} (1.49Å) and ionic radii of Fe^{3+} (0.69Å) is less than that of Ti^{4+} (0.745Å) [10].

The above structural transformations due to off-valent substitutions are mainly caused by the displacement of atoms from their regular lattice positions leading to structural and microstructural transformations and change in crystal size. Microstrain,

ACCEPTED MANUSCRIPT

short range lattice strains caused by crystalline defects has been calculated from XRD results by using Williamson-Hall model. The Williamson - Hall model [11] is given by:

$\beta\cos\theta = 0.9\ \lambda /t + 4\varepsilon \sin\theta$ (1)

where t is average crystallite size and ε is microstrain, β is the full width at half maxima (FWHM) at Bragg's angle (2θ) and λ being the X-ray wavelength of CuKα (λ = 1.54098 Å). The slope of $\beta\cos\theta$ vs 4 $\sin\theta$ curve (plot not shown here) gives the value of microstrain and intercept of the graph gives the value of crystallite size. Inset of Fig.1 (e) shows the variation of microstrain and crystallite size with x. It is observed that the value of microstrain as well as crystallite size shows three different regions resembling the phase transition behavior.

Alternatively, microstrain can also be calculated using the expression, $\varepsilon = \Delta d/d_0$ (where, Δd is displacement in lattice spacing from its ideal crystal value d_0) which measures the relative mean variation of displacement. The strain broadening (β d(θ)) of diffraction reflection at scattering angle θ (half of the diffraction angle), is proportional to deformation in the crystal (tanθ) and dislocation (ε); and mathematically equal to 4 ε tanθ [12]. This expression for microstrain is in agreement with the Williamson- Hall model. An attempt has been made to find the microstrain (ε) for three planes i.e., 100, 110 and 111 at $2\theta \approx 22^o, 32^o, 37^o$ respectively. Fig.1 (e) shows the microstrain for the above mentioned planes with the change in x. Microstrain (ε) at $2\theta \approx 22^o$ has been found to change with change in crystal symmetry while at $2\theta \approx 32^o$ and $2\theta \approx 37^o$ this change is appearing only when structure shifts to low symmetric (R3c). The value of microstrain indicates the splitting of peaks revealing the phase transition. It can be attributed to the stress generated in the TiO_6

ACCEPTED MANUSCRIPT

and FeO_6 octahedra. This leads to the changes in the phase from P4mm to R3c with increasing x.

3.2 Raman Spectroscopy

In order to confirm the observations of structural transformations made from XRD data, Raman spectroscopy has been used as an additional tool to elucidate the phase change in BBFZT system. Raman spectroscopy, a potentially valuable technique has been extensively used for the study of multiferroic materials in recent years [13, 14].

Fig. 2 (a) shows the Raman spectra of the studied specimens in the wave number range from 100 cm^{-1} to 700 cm^{-1}. It is well known that the bonds in the lattice of crystal structure of these materials specimens correspond to a particular wave number or a frequency i.e. phonon modes. In the solid solutions, there is one or two-modes behavior for the different types of ionic bonds present in the same crystallographic positions e.g. (A′A″) at A-site or (B′ B″) at B-site. In the case of one-mode behavior, there is one peak corresponding to the mixed B′-O/B″-O phonon mode and nearly linear dependence of the peak position with the concentration (x) whereas in the two-mode behavior, there are two peaks corresponding to the pure B′-O and B″- O phonon modes separately and intensity ratio I (B′-O)/ I (B″-O) depends on x [15]. The basic reason behind the observation of one-mode behavior is the ionic nature of the bond leading to the long correlation length whereas two-mode behavior is due to the covalent nature leading to short correlation length [16].

It is observed from Fig. 2(a) that there is a significant change in the intensity of phonon modes around $\Delta\nu$ = 100-200 cm^{-1}within the range from x = 0.0 to 1.0 indicating diffusion of Bi^{3+} and Fe^{3+} in BZT lattice which confirm the solid solution

ACCEPTED MANUSCRIPT

formation. The formation of solid solution can be understood from the following equation:

$$xBiFeO_3 \xrightarrow{In(1-x)BaZr_{0.025}Ti_{0.975}O_3 matrix} xBi^{\bullet}_{Ba} + x(0.025Fe'_{Zr} + 0.975Fe'_{Ti}) + 3xO^{\times}_{O} \ldots\ldots\ldots (2)$$

In order to re-confirm the structural change observed in X-ray diffractograms, the analysis of Raman spectra via fitting of spectral modes into individual Gaussian components has been carried out for all the samples ($x \leq 1.0$). The number of peaks has been compared with the Raman selection rules (Bilbao crystallographic server) to know the space groups [17]. The number of peaks (obtained after fitting) is 7 for $x \leq 0.2$, 8 for $0.3 \leq x \leq 0.6$ and 12 for $0.7 \leq x \leq 1.0$. It reveals that the structure is tetragonal with space group P4mm for $x \leq 0.2$, pseudocubic (tetragonal) with space group P4mm [9] for $0.3 \leq x \leq 0.6$ and finally rhombohederal with space group R3c for $0.7 \leq x \leq 1.0$. For instance, Fig. 2(b) shows the fitting of Raman spectra and decomposed fitting curves into individual Gaussian components separately for end members of BZT-BFO system.

Fig. 3(a) shows the variation in the position of Ba-O and Bi-O bond. It is observed that the wave number shift, corresponding to Bi-O bond, first increases up to $x \leq 0.4$ and then followed by a decrease with the further increasing BFO content. Fig. 3(b) shows the variation in position of Fe-$O_{(oct)}$ and Ti-$O_{(oct)}$ with the increase in $BiFeO_3$ content. It is observed that the wave number corresponding to the stretching mode of Ti-O bond increases with increasing x. Whereas, the wave number corresponding to the Fe-O bond first decreases for $x \leq 0.4$ and then it remains nearly constant for $0.4 \leq x \leq 0.9$. The wave number shift can be explained in terms of the

ACCEPTED MANUSCRIPT

stress field originated from the clamping of each grain while crossing the transition from tetragonal to rhombohederal [18]. The difference in the nature of stress originated can originate from the difference in lattice parameters and different lattice structures with the increasing content of bismuth ferrite.

Fig.3(c) shows the dependence of intensity ratio $I_{(Ba-O)}/I_{(Bi-O)}$ on x. It is observed that the intensity ratio of Ba-O bond decreases up to $x \leq 0.6$ and thereafter increases with further increasing x. This variation of intensity with x can be attributed to the bismuth volatilisation. In spite of this, a broad minimum is also observed in the composition range $0.6 \leq x \leq 0.7$ indicates the higher intensity corresponding to Bi-O bond. Fig.3 (d) shows the linear dependence of intensity ratio $I_{(Ti-O,\ oct)}/\ I_{(Fe-O,\ oct)}$ on x. It is observed that the intensity of Ti-O bond decreases and intensity of Fe-O bond increases with the increasing x. It is well known that multiferroic nature of BFO is induced by the lone pair of electrons of Bi^{3+} [3] whereas in BZT ferroelectricity is induced by the off-centring of Ti^{4+} ion [19]. Hence the multiferroic nature of these samples is expected for the optimum value of x. Moreover, the linear behaviour in Fig. 3(d) suggests the two phonon mode behaviour in these specimens. Therefore, the wave number shift and relative change in the intensity of the peaks clearly determine the structure and multiferroic behaviour of the solid solutions.

Based on the XRD, the lattice parameters have been plotted as a function of x as shown in Fig. 4. Inset of Fig.4 shows the nature of structural compression and elongation of TiO_6 and FeO_6 octahedra with x. It is observed in fig.4 that lattice parameters change with the increasing x. The lattice parameters change can be explained in terms of the stress field originated with the different lattice structures. The stress field has been originated between the TiO_6 octahedra and FeO_6 octahedra as shown in Fig. 4 (see inset). For the low BFO content i.e. for $x \leq 0.5$, the TiO_6

ACCEPTED MANUSCRIPT

clusters are larger in number than FeO_6 clusters and in BFO c/a ratio is larger than the c/a ratio in BZT. This will lead to the contraction of FeO_6 octahedra and a slight expansion in TiO_6 octahedra. Whereas, for higher BFO content i.e. for $x \geq 0.5$, the Feo_6 clusters are larger in number than TiO_6 clusters, this will lead to the expansion of TiO_6 octahedra rather than the contraction of FeO_6 octahedra. According to Home-Ruthery rules [20], solid solution formation is expected between BZT-BFO compounds which have also been discussed earlier. The above analysis conclude that in the present compositions, Bi^{3+} ions substitute Ba^{2+} ions and Fe^{3+} ions substitute Zr^{4+} or Ti^{4+} ions as illustrated in the Eq. (1). Hence, in the present compositions solid solutions with two-mode behaviour have been formed.

3.3 Ferroelectric studies

In order to study the multiferroic nature of the studied specimens ferroelectric and ferromagnetic characterizations have been done. It is well known that the scattered intensity of a given Raman mode observed in Raman spectra is directly proportional to polarizability. As mentioned earlier in Fig.3(c), the minima of the I_{Ba-O}/I_{Bi-O} lies in between $0.6 \leq x \leq 0.7$ indicating that intensity corresponding to Bi-O bond would be higher at the minima. Further, as known that ferroelectricity in BZT and BFO is due to the off centring of Ti^{4+} ion in TiO_6 octahedra and lone pair of Bi^{3+} ion in BO_6 octahedra respectively. Thus, the maximum ferroelectricity is expected in the composition range of $0.6 \leq x \leq 0.7$. P-E hysteresis loops for (1-x) BZT- (x) BFO ($0.1 \leq x \leq 0.4$) have already been reported [8]. P-E and M-H of pure BFO has already been reported by the authors in Ref 21. Fig. 5 (inset) shows the P-E loops for (1-x) BZT- (x) BFO ($0.1 \leq x \leq 0.9$). With the substitution of BFO, the P-E hysteresis loops become unsaturated and elliptic in shape. The maximum remanent polarization ($2P_r$) is observed near $x = 0.60$ as shown in Fig.5. The reason behind increasing

ACCEPTED MANUSCRIPT

unsaturation in P-E loop may be explained as follows. There is evidence of "imprint" phenomena indicating that the ceramics present defects as oxygen vacancies which pinned the domain walls leading to the difficulty in the saturation of hysteresis loops [1]. It is also observed that the orientation and shape of loops change with the change in BFO content. This change can be associated with the phase change observed in the XRD patterns. The samples in the range $0.1 \leq x \leq 0.2$ show non relaxor behavior and in the composition range $0.3 \leq x \leq 0.4$, it is relaxor. As the phase change occurs from tetragonal to pseudocubic, the shape of P-E curve changes from loop to straight line which is indicative of paraelectric nature. With the further increase in BFO content, the phase changes from pseudocubic to rhombohederal and the shape of ferroelectric loop changes from straight line to elliptic.

3.4 Ferromagnetic studies

Fig.6 (inset) shows the M-H measurements for compositions ($0.1 \leq x \leq 0.9$) in the system (x) BZT- (1-x) BFO. As mentioned earlier in Fig.3 (d), $I_{(Ti\text{-}O,\ oct)}/ I_{(Fe\text{-}O,\ oct)}$ depends linearly on the BFO content, x. It is observed that the intensity of Ti-O bond decreases and intensity of Fe-O bond increases with increasing x. Fig.6 shows the variation of remanent magnetization ($2M_r$) with x. It is observed that the magnetization increases with the increase in BFO content. The ferroelectricity in principle should be decreased due to decrease in Ti content. Hence for the optimum Fe and Ti combination, the specimen would be better multiferroic i.e. in the range $0.6 \leq x \leq 0.7$.

4. Conclusions

In summary, series of compositions with $x \leq 1.0$ in the system $Bi_{1-x}\ Ba_x(Fe_{1-x}Zr_{0.025x}Ti_{0.975x})\ O_3$) (BBFZT) have been synthesized by solid state route. X-ray

ACCEPTED MANUSCRIPT

diffractograms reveal the formation of single phase for all the compositions. Rietveld refinement of diffraction data has shown tetragonal (P4mm) symmetry for $x \leq 0.2$, pseudocubic with P4mm space group symmetry for $0.3 \leq x \leq 0.6$ and finally rhombohederal (R3c) for $0.7 \leq x \leq 1.0$. The linear dependence of $I_{(Ti\text{-}O,\ oct)}/ I_{(Fe\text{-}O,\ oct)}$ on the BFO content (x), suggests the two-mode behaviour in the specimens. These studies suggest that the structural transformation is attributed to the B-site substituents. It is concluding from Raman spectra that the specimen with 60 mol% of bismuth ferrite possesses better multiferroic properties which have been evidenced from P-E and M-H behaviour.

Acknowledgement

Financial support from DST for this research work is acknowledged (SR/S3/ME/0048/2009-SERC). One of the authors P.A. Jha is also thankful to DST for the fellowship.

References:

1. F. Moura, A. Z. Simoes, B. D. Stojanovic, M. A. Zaghete, E. Longo, J. A. Varela, Dielectric and ferroelectric characteristics of barium zirconate titanate ceramics prepared from mixed oxide method, J. Alloys and Comp. 462 (2008) 129-134.
2. P.A. Jha, A.K. Jha, J. Alloys Compd. 513 (2012) 580–585.
3. Ph. D. Thesis by S. K. Rout, Phase formation and dielectric studies of some BaO- ZrO – TiO Perovskite Systems NIT, Rourkela, (2006).
4. K. F. Wang, J. M. Liu and Z. F. Ren, Multiferroicity: the coupling between magnetic and polarization orders , Adv. Phys. 58 (4) (2009) 321-448.
5. S. T. Zhang, M. H. Lu, D. Wu, Y. F. Chen and N. B. Ming, Larger polarization and weak ferromagnetism in quenched $BiFeO_3$ ceramics with a distorted rhombohedral crystal structure, Appl. Phys. Lett. 87, (2005), 262907.

ACCEPTED MANUSCRIPT

6. Alessandro Alan Porporati, Keisuke Tsuji, Matjaz Valant, Anna-Karin Axelssonand Giuseppe Pezzotti J Raman Spectrosc. 41, (2010), 84.

7. R.N.P. Choudhary, K. Perez, P. Bhattacharya, R.S. Katiyar, Mater. Chem. Phys. Structural and dielectric properties of mechanochemically synthesized $BiFeO_3$–$Ba(Zr_{0.6}Ti_{0.4})O_3$ solid solutions105 (2007) 286–292.

8. Priyanka A. Jha, Pardeep K. Jha, A.K.Jha and R.K. Dwivedi, Dielectric behavior of (1- x) Ba $Zr_{0.025}$ $Ti_{0.975}$ O_3–(x) $BiFeO_3$ solid solutions, Mater. Res. Bull. 48 (2013) 101-105.

9. F Sanchez Bajo, Isidro Cachadina, Juan de Dios Solier, Fernando Guiberteau and Francisco L Cumbrera, Differentiation between Pseudocubic and Cubic Phases in Y–ZrO_2 Using Rietveld Analysis, J. Am. Ceram. Soc. 80 (1) (1997) 232-236.

10. L.M. Feng, L.Q. Jiang, M. Zhu, H.B. Liu, X. Zhou, C.H. Li, Formability of ABO3 cubic perovskites, J. Phys. Chem. of Solids 69 (2008) 967-974.

11. G K Williamson, W H Hall, X-ray line broadening from filed aluminium and wolfram, Acta Metall. 1 (1953) 22-31.

12. C. O. Paiva-Santos, H. Gouveia, W. C. Las, J. A. Varela, Materials Structure, 6 (1999) 111-114.

13. R. Pirc, R. Blinc, Off-center Ti model of barium titanate, Phys. Rev. B, 70, (2004) 134107-1-8.

14. R. Blinc, J. Seligar, B. Zalar, Disorder in $BaTiO_3$ and Ti EFG Tensors, Integr. Ferroelectr. 61 [1] (2004) 255-260.

15. R. Comes, M. Lambert and A. Guinier, The chain structure of $BaTiO_3$ and $KNbO_3$ Solid State Comm. 6, (1968) 715.

16. S. Prakash, H. C. Gupta and B. B. Tripathi, Two mode behaviour of mixed crystals, Phy. Rev. B 28, 12, (1983) 7390-7392; Kunio Tochi, Nozomu Takeuchi,

ACCEPTED MANUSCRIPT

Shuichi Emura, Two mode beahavior in complex perovskite materials, J. Am. Ceram. Soc. 72 (1) (1989) 158-160.

17. E. Kroumova, M.I. Aroyo, J.M. Perez-Mato, A. Kirov, C. Capillas, S. Ivantchev and H. Wondratschek, Bilbao Crystallographic server: useful databases and tools for Phase-transition studies, Phase Transitions 76, 1-2, (2003) 155-170.
18. P. S. Dobal and R. S. Katiyar, Studies on ferroelectric perovskites and Bi-layered compounds using micro-Raman spectroscopy J. Raman Spectr. 33, (2002) 405-423.
19. S. K. Rout, P. K. Barhai, S. Panigrahi and I. W. Kim, Synthesis of ($Ba_{0.5}Sr_{0.5}$)($Ti_{1-x}Zr_x$)O_3 ceramics: Effect of Zr content on room temperature electrical Properties, J. Electroceram. 23, (2009), 37-42.
20. William Hume-Rothery, Atomic Theory for Students of Metallurgy,The Institute of Metals, London, 1969 (fifth reprint).
21. P. K. Jha, P. A. Jha, Geetika Srivastava, A. K. Jha, R. K. Kotnala and R. K. Dwivedi, Analytical comparison of magnetic and electrical properties using modified Landau theory in bismuth ferrite: Effect of milling, J. Magnetism and Magnetic Mater., Doi: 10.1016/j.jmmm.2013.08.048.

ACCEPTED MANUSCRIPT

ACCEPTED MANUSCRIPT

Figure Captions

Fig.1(a) X-ray diffractograms of (1-x) [Ba $Zr_{0.025}Ti_{0.975}O_3$] – (x) [$BiFeO_3$] [x = 0.0-1.0] specimens.

Fig. 1(b) Reitveld refinement of XRD pattern for composition x= 0.1, 0.2 and 0.3.

Fig. 1(c) Reitveld refinement of XRD pattern for composition x= 0.4, 0.5 and 0.6.

Fig. 1(d) Reitveld refinement of XRD pattern for composition x= 0.7, 0.8 and 0.9.

Fig.1 (e) Variation of microstrain for (100), (110) and (111) at respective diffraction angles with x. ε_{100}, ε_{110}, ε_{111} have been calculated from the XRD peak profiles using the expression ($\Delta d/d_0$).

Inset shows the variation of microstrain and crystallite size with x. (The lines are just to glide the eye.)

Fig. 2(a) FT-Raman spectra of the studied specimens in the wave number range from 100 cm^{-1} to 700 cm^{-1}.

Fig. 2(b) shows the fitting of FT-Raman spectra with decomposed fitting curves into individual Gaussian components of pure BZT and BFO compounds.

Fig. 3(a) Variation in the position ($\Delta\nu_{\text{stretching}}$) of Ba-O and Bi-O bond at A-sites in BBFZT system with x.

Fig. 3(b) shows the variation in position ($\Delta\nu_{\text{stretching}}$) of Fe-$O_{(oct)}$ and Ti-$O_{(oct)}$ at B-sites in BBFZT system with x.

Fig. 3(c) Variation of intensity ratio $I_{(Ba\text{-}O)}/I_{(Bi\text{-}O)}$ in BBFZT system with x

Fig.3 (d) Variation of intensity ratio $I_{(Ti\text{-}O,\ oct)}/ I_{(Fe\text{-}O,\ oct)}$ in BBFZT system with x

Fig.4 Variation of lattice parameters as a function of BFO content.

Fig.5 Variation of remanent polarization as a function of BFO content and Fig. 5 (inset) shows the variation of P-E hysteresis loops as a function of BFO content.

ACCEPTED MANUSCRIPT

Fig.6 Variation of remanent magnetization as a function of BFO content and Fig. 6 (inset) shows the variation of M-H hysteresis loops as a function of BFO content.

ACCEPTED MANUSCRIPT

ACCEPTED MANUSCRIPT

The compositions (1-x) BZT- x BFO ($x \leq 1.0$) are synthesised by SSR technique. The phase transitions from tetragonal to pseudocubic to rhombohederal are observed. The solid solution formation has been explained with two-mode phonon behaviour. A correlation between Raman analysis and ferroic properties has been established. P-E and M-H loops are studied.

.

ACCEPTED MANUSCRIPT

ACCEPTED MANUSCRIPT

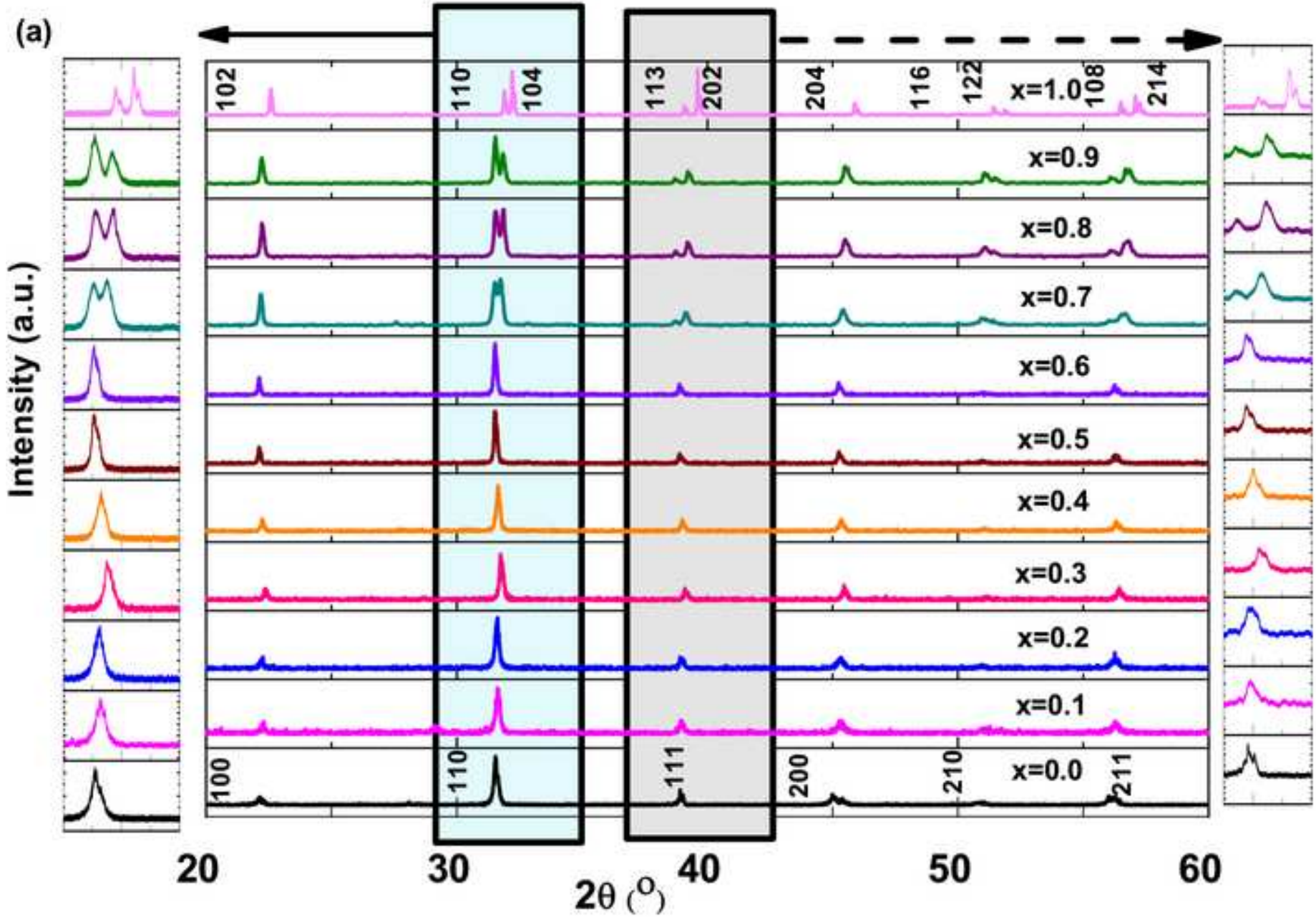

ACCEPTED MANUSCRIPT

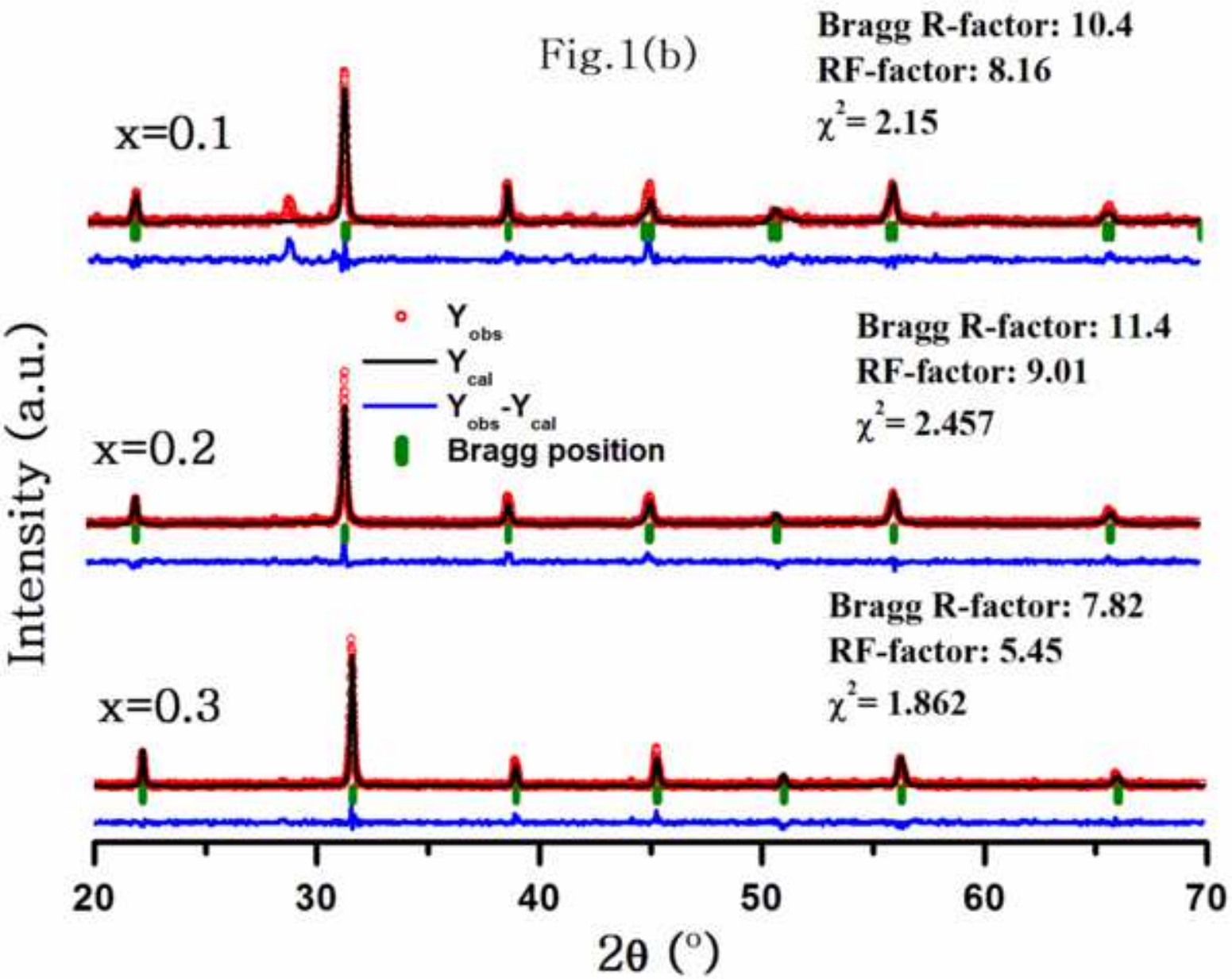

ACCEPTED MANUSCRIPT

Fig.1(c)

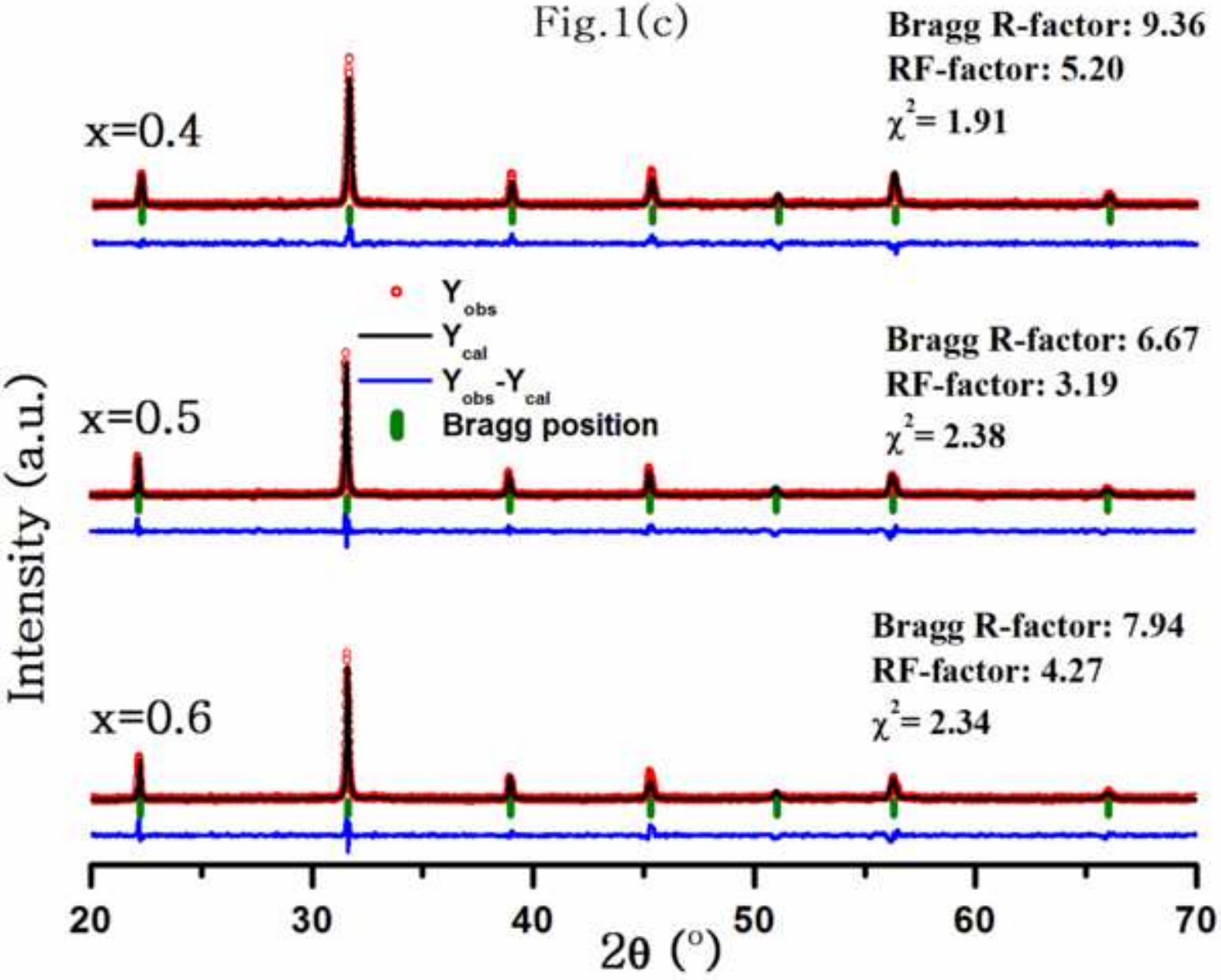

ACCEPTED MANUSCRIPT

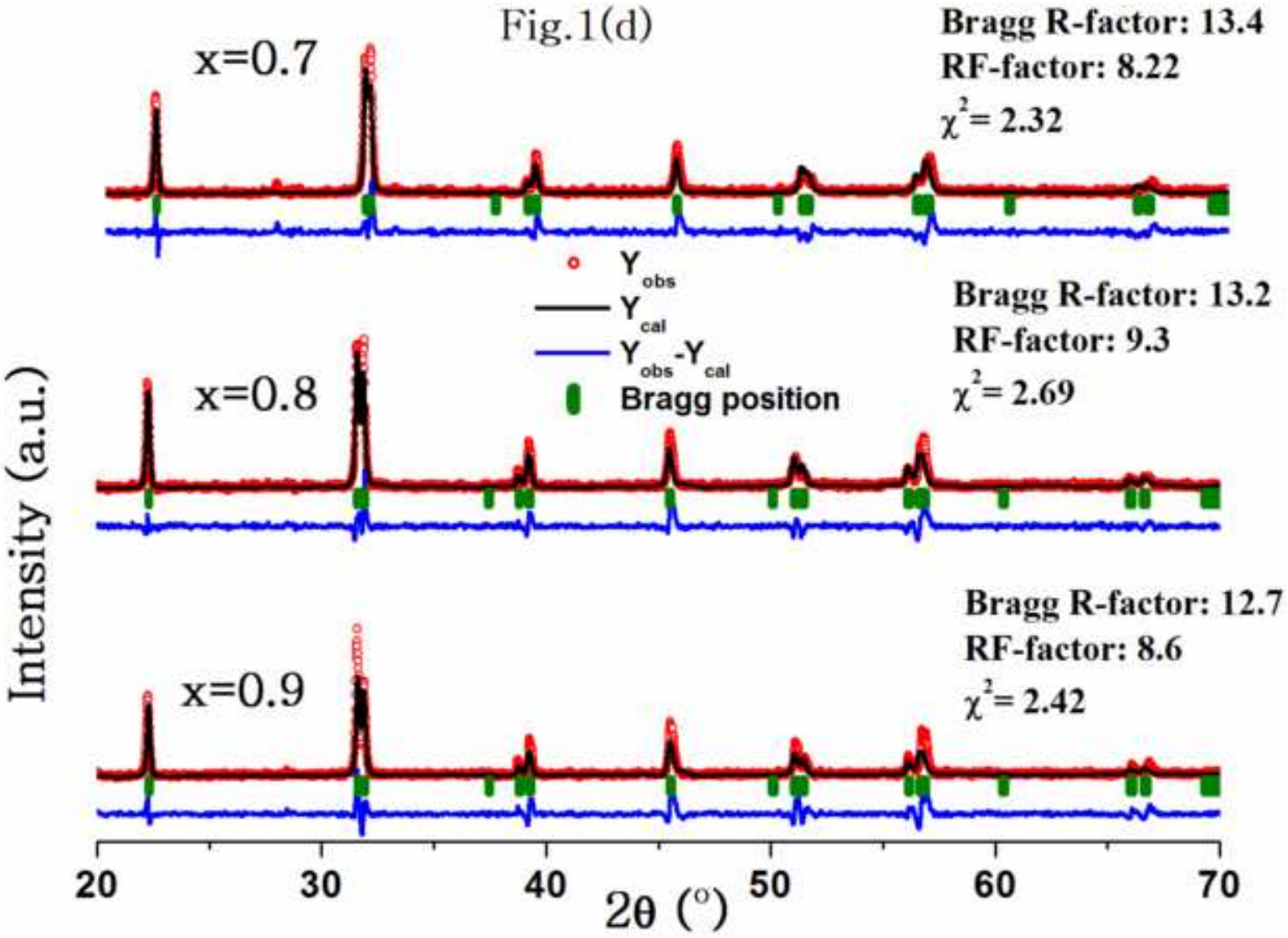

ACCEPTED MANUSCRIPT

Fig.1(e)

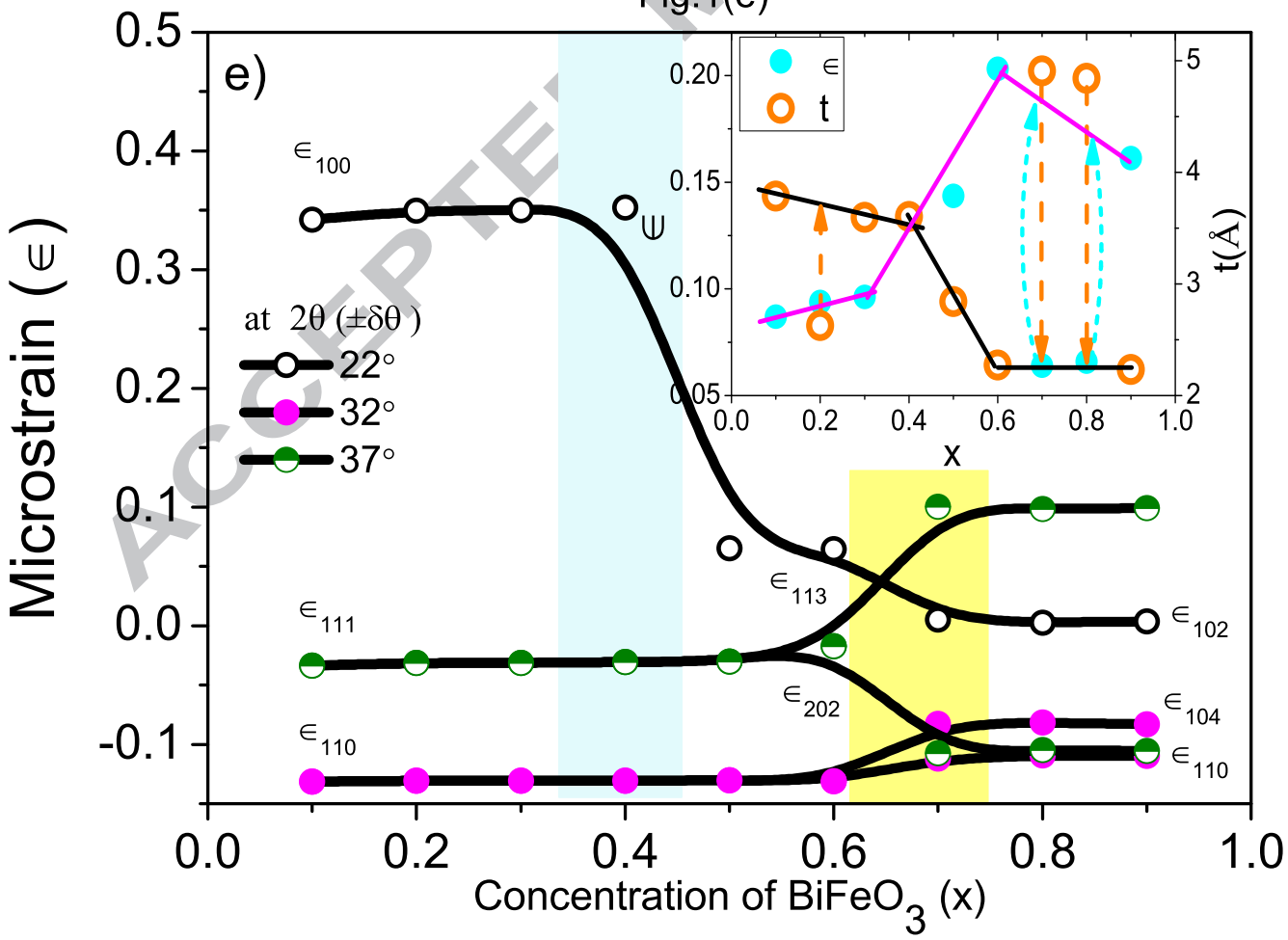

ACCEPTED MANUSCRIPT

Fig. 2(a)

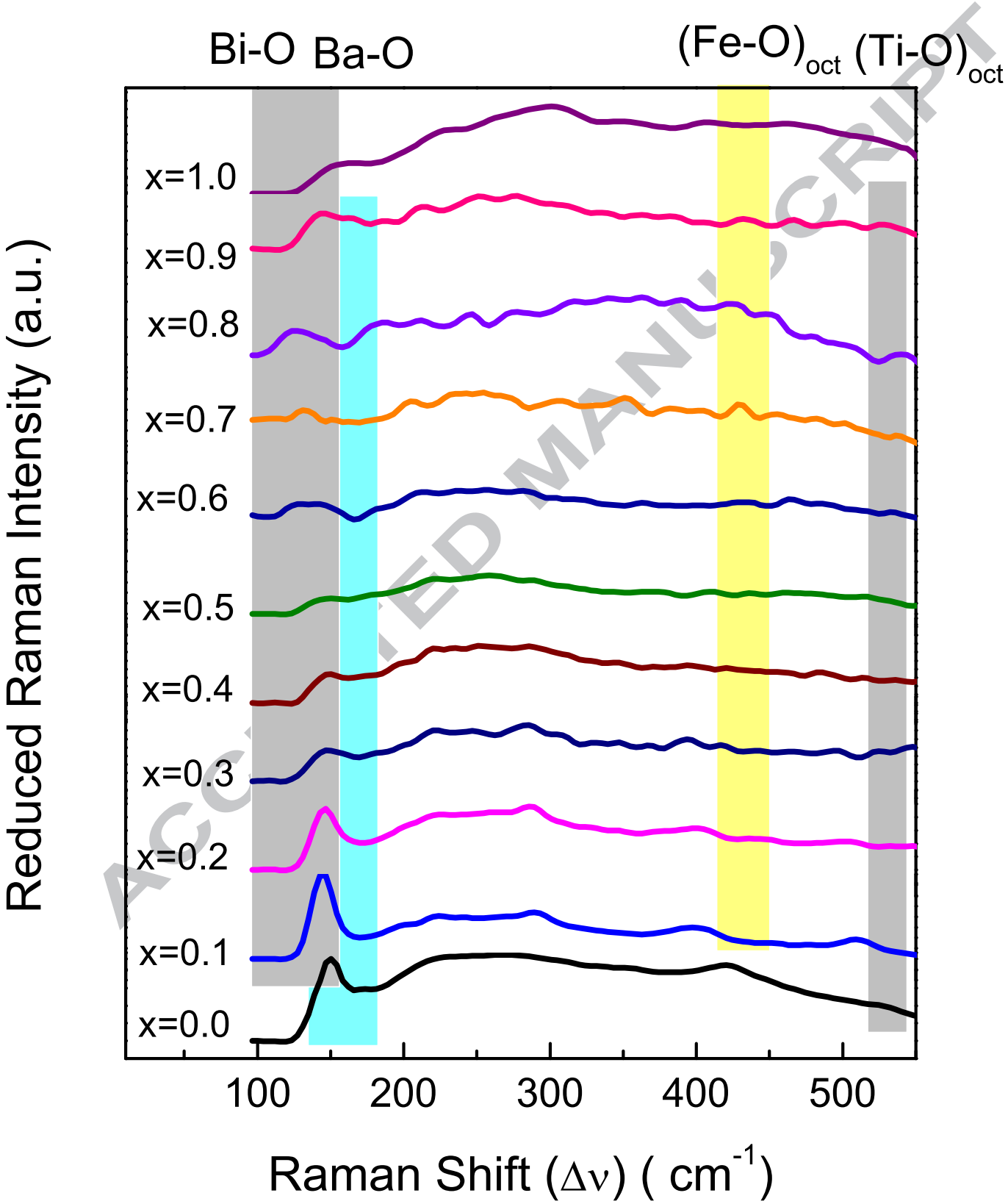

ACCEPTED MANUSCRIPT

ACCEPTED MANUSCRIPT

Fig. 2(b)

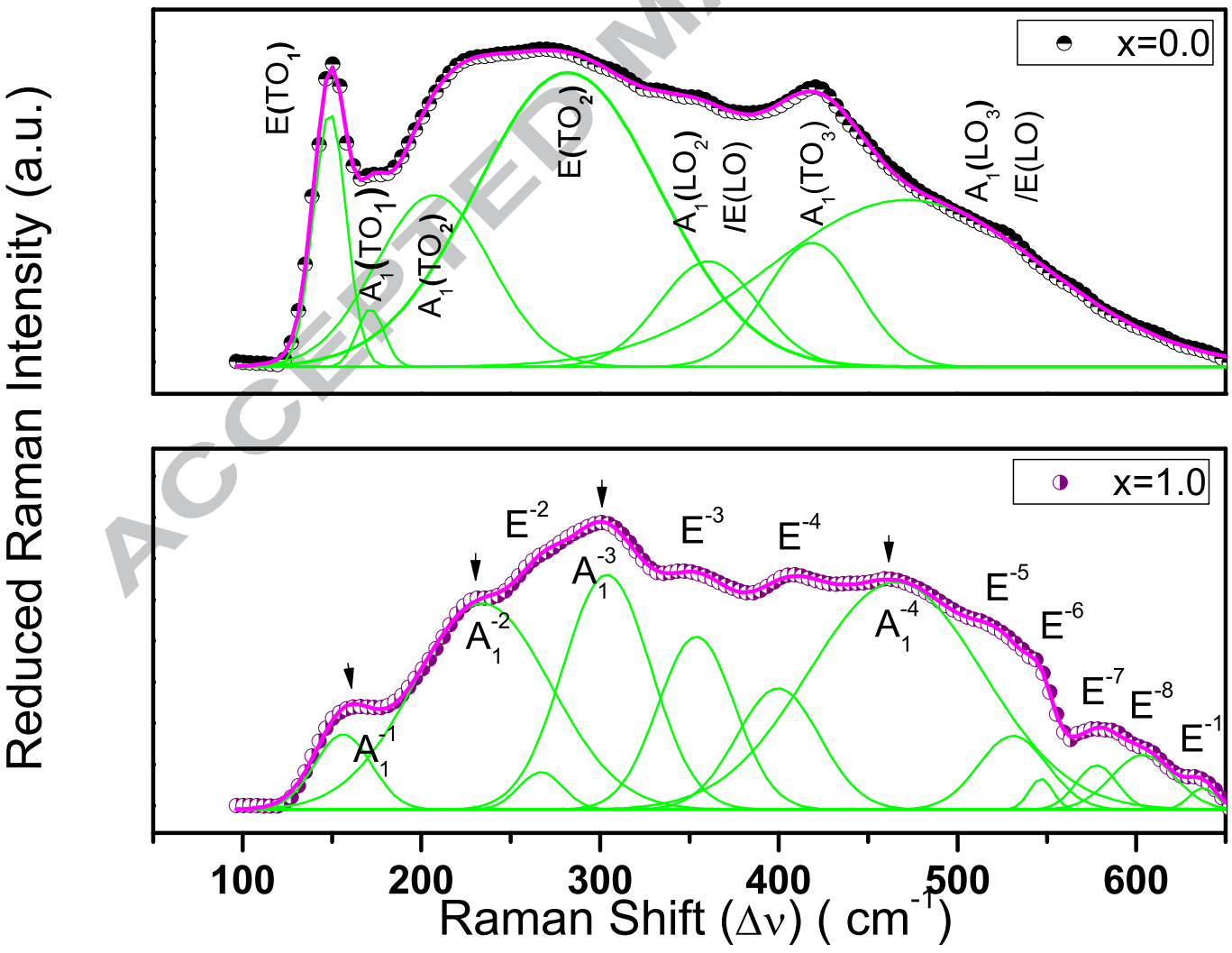

ACCEPTED MANUSCRIPT

ACCEPTED MANUSCRIPT

Fig.3

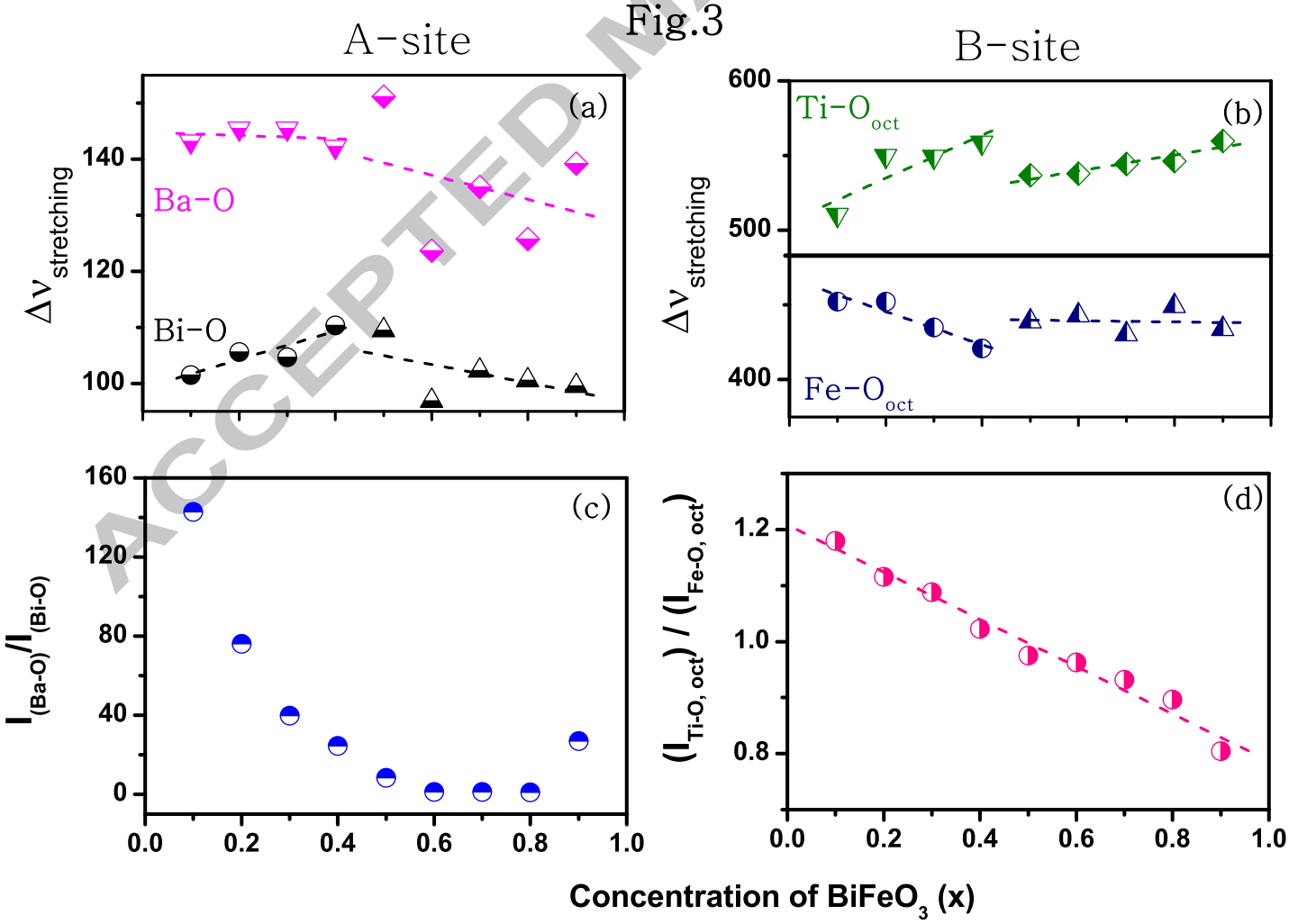

ACCEPTED MANUSCRIPT

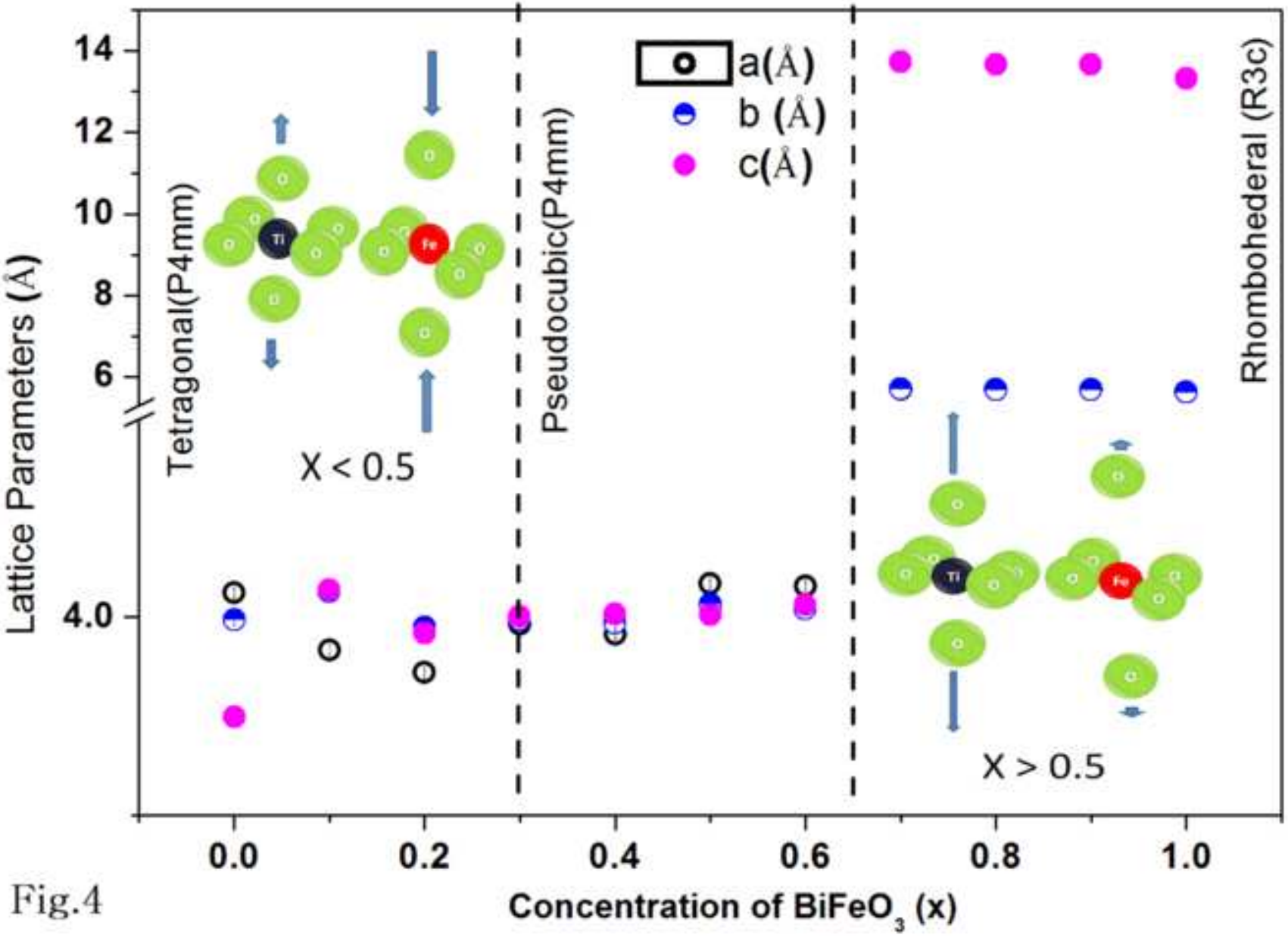
Lattice Parameters (Å)
14
12
10
8
6
4.0
a(Å)
b (Å)
c(Å)
Tetragonal(P4mm)
Pseudocubic(P4mm)
Rhombohederal (R3c)
X < 0.5
X > 0.5
Ti
Fe
0.0
0.2
0.4
0.6
0.8
1.0
Concentration of BiFeO3 (x)

Fig.4

ACCEPTED MANUSCRIPT

Fig.5

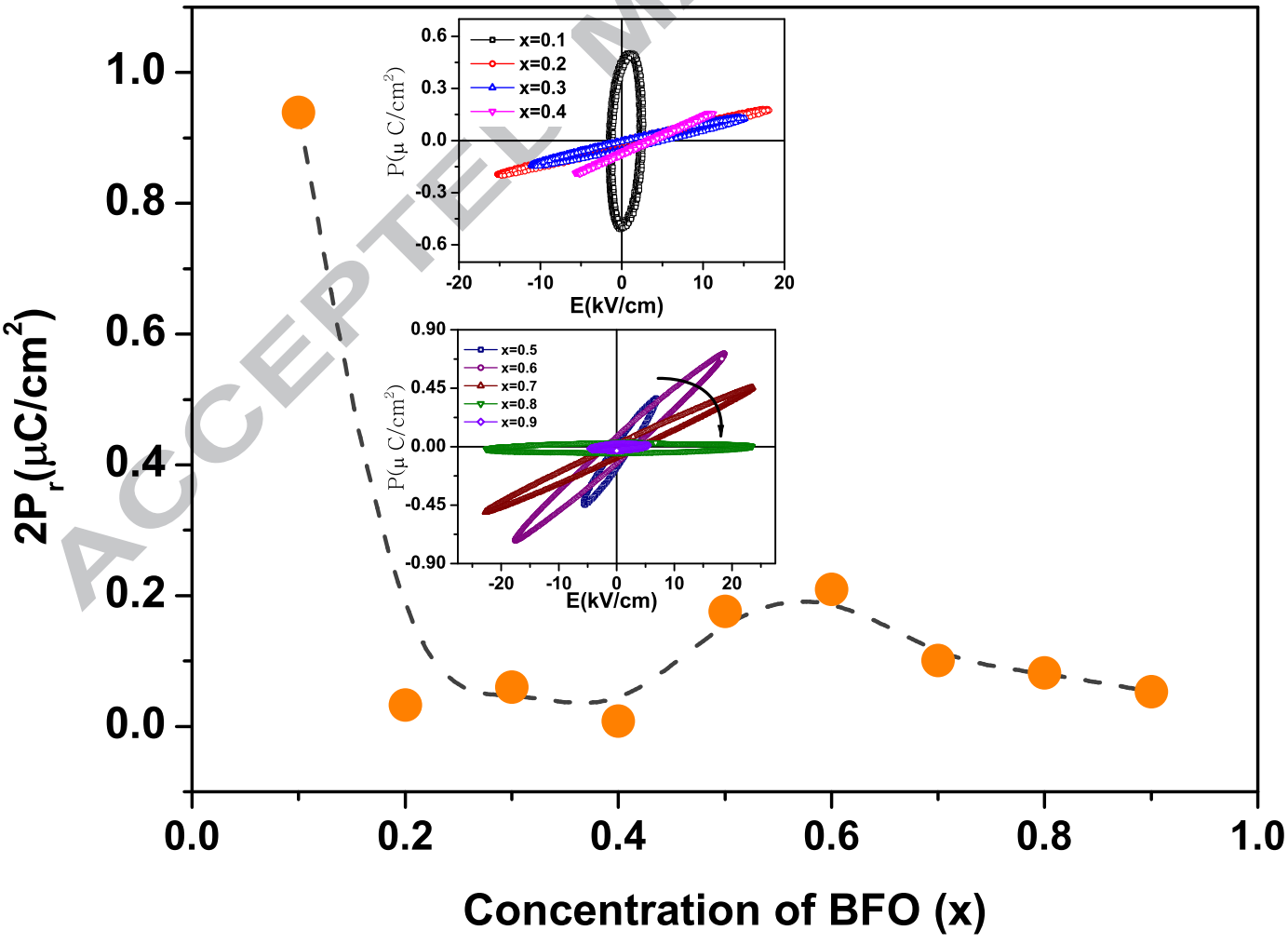

ACCEPTED MANUSCRIPT

ACCEPTED MANUSCRIPT

Fig.6

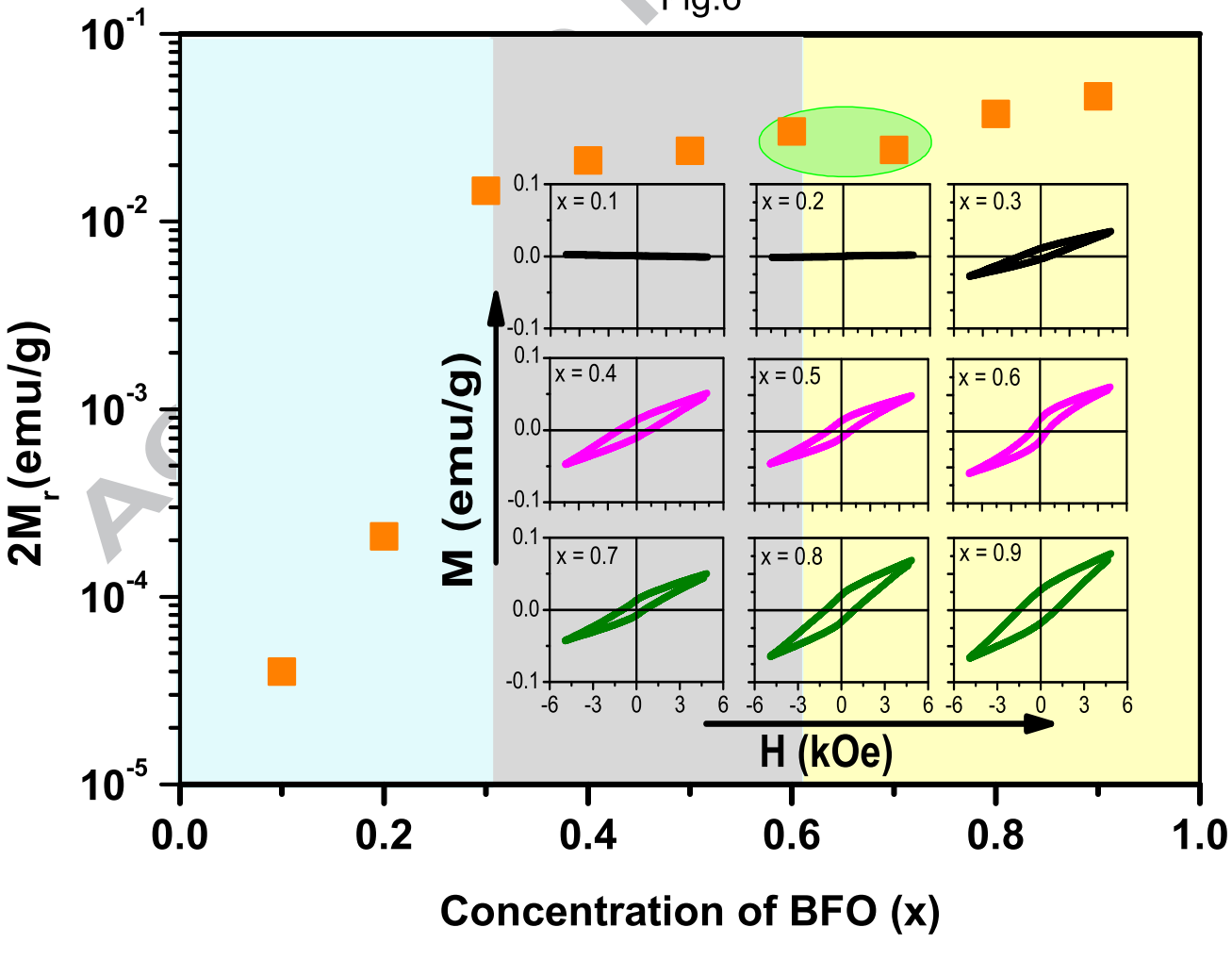

ISBN 978-93-5156-328-0
International Conference of Advance Research and Innovation (ICARI-2014)

Potential Application of Particle Image Velocimetry To Sub-Sonic Open Circuit Wind Tunnel

Vishvendra SinghTomar [a,*], Sahib Chawla[a], Shanu Sinha [a], Raj Kumar Singh[a], Arun Dhyani [b]

[a]Department of Mechanical Engineering, Delhi Technological University,New Delhi, India
[b] Department of Electronics and Communication Engineering , Delhi Technological University, New Delhi, India

Article Info

Article history:
Received 29December 2013
Received in revised form
10 January 2014
Accepted 20 January 2014
Available online 1 February 2014

Keywords

Particle Image Velocimetry
Sub-Sonic Open Circuit Wind Tunnel
Mach Number
Correlation Technique
Flow Measurement

Abstract

In this present work, Particle Image Velocimetry(PIV) as a flow visualization technique with vast potential is applied to determine the Flow Velocity Distribution around an object placed in the Test Chamber of a Sub-Sonic Open Circuit Wind Tunnel (SOWT) [Mach Number (M) = 0.15]. The two challenging tasks to accomplish during the development of instrumental set up are: 1. Electronic System Development for reducing the flash time so as to have a sharp image of the particle flow. 2. Seeding System Development by incorporating the air bubbles generators. Some details of PIV hardware, programmable PIV processor and software architecture are also discussed, emphasizing the practical benefits of various features. Further, to relax the PIV, filtered motion blurring technique has been utilized using Auto-Correlation.

1. Introduction

Particle Image Velocimetry (PIV) is the most recent entrant to the field of non-intrusive fluid flow measurement which provides instantaneous velocity fields and flow particles displacement pattern over global (2D or 3D) domains. It records the position over time of small tracer particles introduced into the flow to determine the local fluid velocity. Basically, It consists of an optically transparent test-section containing the flow seeded with tracer particles, an illuminating light source (laser), a recording medium (CCD camera) and a computer with suitable software to process the recorded images and extract the velocity information based on certain algorithms [1, 2], as shown in Fig. 1.

Hinsch [3] described, a measurement system to be labeled as (α, β, γ), where α= 1, 2, 3 indicating the number of velocity components measured, ß =0,1, 2, 3 indicating the number of spatial dimensions of the measurement domain and γ=0,1 indicating instantaneous or continuous time recording, respectively. For 2D analysis, system can be referred (2, 2, 0) and also, the majority of PIV systems in use today belong to this category. For 3D analysis, systems are described as (3, 2, 1) which provide 3D velocity data on planar domains and arebecoming increasingly popular. Thus, PIV provides too much flexibility in measurements of a wide range of systems.

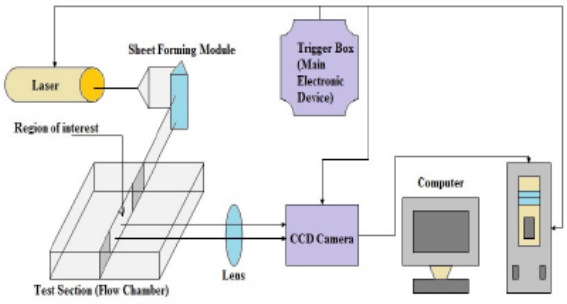

Fig: 1. A basic instrumental set up for PIV System

In today's world, Everyone's main focus is to save time, material and money which have compelled us to opt for the experimental testing on scale models, before the final product is to be shaped. The Wind Tunnel is one such platform, which provides us the appropriate desired environment conditions around

Corresponding Author,
E-mail address:vst.dtu@gmail.com
All rights reserved: http://www.ijari.org

The model scaled to the compatible dimensions. The Sub-Sonic Open Circuit Wind Tunnel can be described as the tunnel having flow velocity less than that of sound with both ends open to the ambient conditions, usually comes into role when the model is to be tested around flow velocity of 50m/s or 150 Km/hr (Fig. 2.) [4, 5]. The tunnel is supplied with a Test Chamber for flow visualization and proper monitoring but it has its own limitations ranging from accuracy to Macro-Level Measurements. Especially when flow visualization around a very small orifice or some Micro-Level portion is required, it is quite unsuitable. Thus, to enhance the flexibility of the tunnel, PIV can be used to visualize the flow in place of the Test Chamber, without any modification to rest of the tunnel.

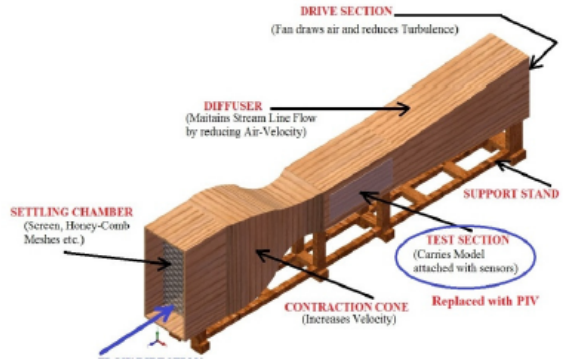

Fig. 2: A basic Isometric View of the complete model of SOWT developed using 3D Solid Modeling Program

Although the idea of application of PIV to the tunnel is quite alluring, but the real difficulty lies at: 1] As the lamps or the lasers have a flash time of the order of milliseconds, it is quite complicated to process the image and correlate the outcomes, Even more difficult at high turbulence flow. Ideal processing requires a time delay of at least some ten microseconds (μs) for a fluid speed of the order of some ten meter per second which is very smaller than the flash light decay. 2] In the tunnel, as there is flow of gases (which is not the usual case, like liquids), it is desirable to have a particle image of the same order of a pixel size, maybe of the order of 1 mm. So, the choice of the seeding particles restricts PIV's direct application to the tunnel. However with the latest technology embedded in various Electronics Circuits and Mechanical Devices, It has become possible to curb down the above limitations [6, 7]. The possible solutions are discussed in the next two sections.

2. Electronic Switch Circuit Using IGBT and SCR

There are two choices for practical implementation of switch used to turn off the lamp namely power MOSFET or IGBT, in this work IGBT is chosen to minimize the decay period. In this, the switching time is not too small but the current value is of the value of few hundred amperes which is to be turned off. IGBT has its own disadvantages too due to its large gate charge which provides it two main difficulties. The first difficulty is related to the beginning of the switch-off of the drain current directly depending on the gate-to-drain charge thus causing a delay in the shut off of the lamp with respect to trigger pulse. In fact the first part of the switch off process is the decrease of the gate voltage from its "HIGH" value to the "TRANSITION" one (Fig. 3.), by discharging the drain-to-gate charge. For reducing this time the gate current must be large, but also the "high" to "transition". It is usually good practice to have a large voltage difference to avoid staying in the intermediate stages and to dissipate power on the device. The solution to this problem is found using a powerful SCR as final driving device for the final IGBT. If C is the gate capacitance then a large resistor R is used in order to have a large value of RC so that gate voltage can be kept "HIGH". But it must be short enough to be able to relight the lamp for the next flash, while the gate is discharged via a small resistor by the SCR which is kept "FIRED" for such a time, to be sure that the deionization process of the lamp is finished and an "ON" transition of the IGBT will not restart the lamp. Therefore the trigger pulse that excites the lamp will also trigger a two stages mono-stable multi-vibrator ,the first one generating the time delay for the flash duration, the second one the time for keeping "ON" the SCR. Of course, the power supply must be able to fully recharge the main capacitor before the next flash (Fig. 4 & 5).

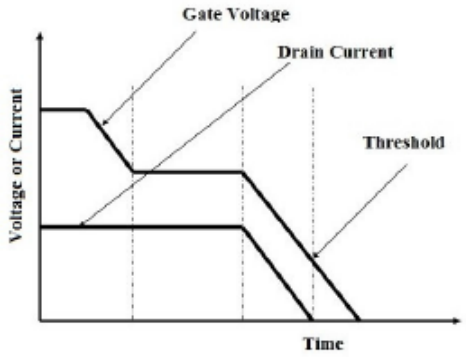

Fig: 3. Qualitative discharge process and different timing of the IGBT.

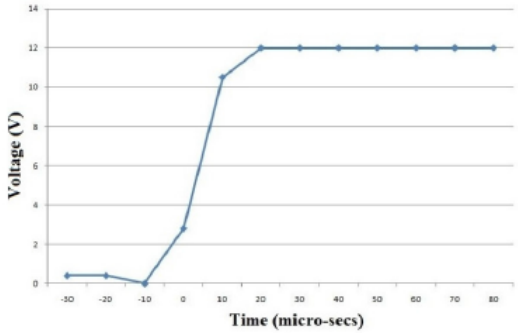

Fig: 4. Variation of IGBT collector voltage versus time.

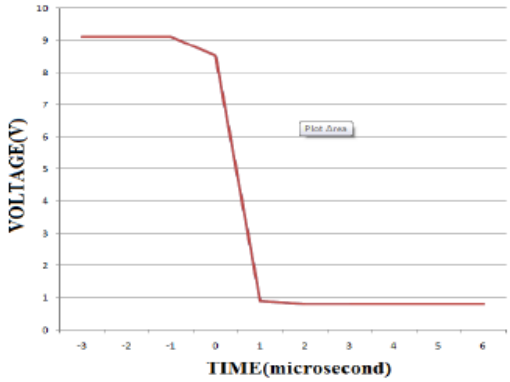

Fig: 5. Variation of IGBT gate voltage versus time.

3. Bubblesas Seeding Particles

In flow measurements where air is used as fluid, the application of soap bubbles were faced with many problems, mainly due to the difficulty of having a RAKE of bubble generators working simultaneously and due to the bubble inflation when subjected to increase the bubbles emission rate. A bubble generator consists of three concentric tubes: a] The inner one injects the filling gas, b] The medium one having high surface t tension liquid (water and soap) form the liquid film o of the bubble, c] The third one detaches the bubbles.

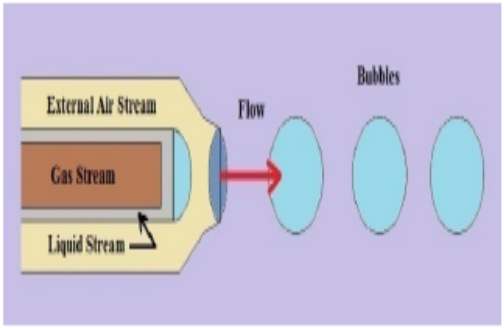

Fig. 6: Bubble generator ejecting bubbles, during air flow.

With the bubble generator described above (Fig. 6.), bubbles of a diameter almost equal to the liquid tube can be obtained, as first at a small rate.To have a much more uniform stream and a better bubble behavior a converging outer tube is added to the generator with addition of some percent of glycerin to the water-soap-mixture, providing the bubbles a lifetime of some ten seconds. Also, the liquid film of the bubbles is slightly fluorescent which causes the color dispersed by the bubbles to shift slightly toward the red increasing again the "noise" in the digitized image and requiring a further software improvement.

4. CCD Sensors as Recording Hardware and other Processing Hardware

PIV images may be recorded on a film or on CCD (Charge Coupled Device) cameras. The commonly available 8-bit 1 k × 1 k CCD sensors can store only 1 M-byte per frame. These sensors allow the set-up processes to be e accomplished in a few seconds. Digital PIV results can be viewed in almost real-time with high-speed on-board computational hardware dedicated towards computing correlations. These CCD sensors are far more light-sensitive than the film which allows them to perform the same experiment with a far less powerful laser, producing cost benefits and a safer working environment. They also provide a linear response to light intensity in contrast to the film which responds logarithmically and allow interrogation with smaller spots (in terms of pixels). Several vendors provide frame-grabbers to interface the CCD camera to the computer. The processing of PIV frames can also be performed efficiently on the PC, especially using dedicated array processing hardware. The basic requirement is that the FFT operation be performed extremely rapidly and the hardware must also support high-speed graphics to enable the visualization of the particle field, and the plotting of vector fields in almost real time [8-10].

5. PIV Relaxation Using Filtered Motion Blurring Technique

In this the start and end positions of the blurring image are filtered and the filtered image data is Auto-Correlated, which usually shows a peak similar to that of `cross-correlation of PIV revealing the direction and value of displacement (Fig. 7.). The approach used in this paper applies simple kernel filters but compensates for the impact of the particle size on the measured velocity. This is achieved measuring its size based on the highlighted width of the particle.

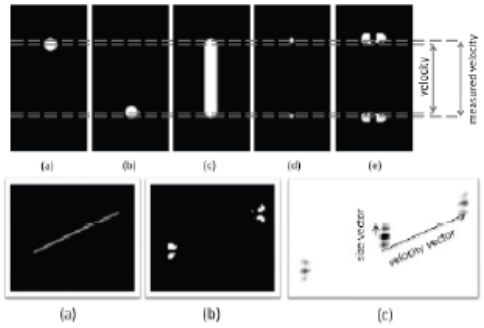

Fig: 7. Filtered Motion Technique, Using Particle Image's Intensity.

The filter results are achieved by applying Sobel filter kernels that are supplemented by a suppression factor *s*. The effect of the parameter *s* is to suppress the motion blur while maintaining the start and end position of the blurring (Fig. 8.).

$$F_{x^+} = \begin{pmatrix} 1 & 2 & -s & -2 & -1 \\ 4 & 8 & -s & -8 & -4 \\ 6 & 12 & 0 & -12 & -6 \\ 4 & 8 & -s & -8 & -4 \\ 1 & 2 & -s & -2 & -1 \end{pmatrix} \quad F_{x^+} = \begin{pmatrix} -1 & -2 & -s & 2 & 1 \\ -4 & -8 & -s & 8 & 4 \\ -6 & -12 & 0 & 12 & 6 \\ -4 & -8 & -s & 8 & 4 \\ -1 & -2 & -s & 2 & 1 \end{pmatrix}$$

$$F_{y^+} = \begin{pmatrix} -1 & -4 & -6 & -4 & -1 \\ -2 & -8 & -12 & -8 & -2 \\ -s & -s & 0 & -s & -s \\ 2 & 8 & 12 & 8 & 2 \\ 1 & 4 & 6 & 4 & 1 \end{pmatrix} \quad F_{y^+} = \begin{pmatrix} 1 & 4 & 6 & 4 & 1 \\ 2 & 8 & 12 & 8 & 2 \\ -s & -s & 0 & -s & -s \\ -2 & -8 & -12 & -8 & -2 \\ -1 & -4 & -6 & -4 & -1 \end{pmatrix}$$

Input: I Image (N,M)
Output: $\overrightarrow{v}$: Velocity Vector ; $\overrightarrow{s}$: Size Vector
Data: : I_x, I_y, I_{yx}, I_{xy} : Grayscale Image (N,M)
B_{yx}, B_{xy}, R : Binary Image (N,M)
C : Autocorrelation Matrix (M+N-1,M+N-1)
P_1, P_2, P_3 : Point

```
1  begin
2      I_x = (F_x^+ * I) + (F_x^- * I)
3      I_yx = (F_y^+ * I_x) + (F_y^- * I_x)
4      B_yx = Binarize(I_yx, 255 → 1, 0...254 → 0)
5
6      I_y = (F_y^+ * I) + (F_y^- * I)
7      I_xy = (F_x^+ * I_y) + (F_x^- * I_y)
8      B_xy = Binarize(I_xy, 255 → 1, 0...254 → 0)
9
10     R = B_yx ∘ B_xy      % Hadamard multiplication
11     C = Autocorrelation(R)
12     P_1 = argMax_1(C)
13     P_2 = argMax_2(C)
14     P_3 = argMax_3(C)
15
16     if |P_1 P_2| > |P_1 P_3| then
17         v = P_1 P_2 ; s = P_1 P_3
18     else
19         v = P_1 P_3 ; s = P_1 P_2
20     end
21 end
```

Fig: 8. Algorithm followed to calculate the velocity.

The results are invariant to the angle of the motion blurring. The vector with the highest norm is assumed to represent the velocity, the other is considered as size vector. For very thin motion blurring, a size vector may not be detected. In those particular cases, only the velocity vector is calculated and the width of the blurring is set to 1 pixel. Thus, the filtered motion technique can be applied to relax the PIV instrumentation [11-13].

6. Conclusion

The prospective appliance of PIV as a non-intrusive flow measurement technique with high degree of accuracy can be utilized to evaluate Velocity Distribution and Flow visualization in Wind tunnel. With optimum design of electronic &mechanical devices, the desired results can be obtained. Further, with inclusion of Latest Hardware and Software Techniques, It provides too much flexibility.

References

[1] "Particle image velocimetry: a review", Fluid Loading and Instrumentation Centre, Heriot-Watt University, Edinburgh, Scotland
[2] M Jahanmiri, "Particle Image Velocimetry: Fundamentals and its Applications," Division of Fluid Dynamics, Department of Applied Mechanics, Chalmers University of Technology, Goteborg, Sweden, 2011
[3] K. D. Hinsch, Meas. Sci. Technol., 1995, 742–753
[4] Types of Wind Tunnels, NASA Aeronautics and SpaceAdministration,http://www.grc.nasa.gov/ W W W/k-12/airplane/tuntype.html
[5] "Science Buddies: How to Build a Subsonic Wind Tunnel" http://www.sciencebuddies.org/science-fairprojects/wind-tunnel toc.shtml.
[6] S. Deponle, S. Frmzctti, G. Cilbertini, S. MalaVaSi, "Tow-Colour Flash P.I.V. Technique for Relatively large Flow Fields". 8th International Conference on Laser Anemometry Advances 2nd Application, Rome, 6-8 September 1999
[7] C. E. Towers, P. J. Bryanston-Cross, T. R. Judge, "Application of particle image velocimetry to large-scale transonic wind tunnels, "Optics dr Laser Technology, Vol. 23. No 5, pp. 289-295, 1991

[8] L. Rockstroh, S. Wahl, S. Simon, R. Gadow, "Accuracy of 2d particle image velocimetry measurements in thermal spraying processes," in International Thermal Spray Conference, 2011
[8] A. K. Prasad, R. J. Adrian, C. C. Landreth, P. W. Offutt, Exp. Fluids, 1992, 13, 105–116
[9] A. Boillot, A. K. Prasad, Exp. Fluids, 1996, 21, 87–93
[10] J. Westerweel, D. Dabiri, M. Gharib, Exp. Fluids, 1997, 23, 20– 28
[11] Tinne Tuytelaars, Krystian Mikolajczyk, "Local invariant feature detectors: a survey," Foundations and Trends in Computer Graphics and Vision, 3(3), pp. 177–280, 2008
[12] L. Rockstroh, S. Wahl, Z. Wang, P. Werner, R. Gadow, S. Simon, "A technique to relax particle image velocimetry based on linear spatial filters," in European Signal Processing Conference, 2011
[13] A. M. Lopez, F. Lumbreras, J. Serrat, J. J. Villanueva, "Evaluation of methods for ridge and valley detection," in Pattern Analysis and Machine Intelligence, 1999, 21, pp. 327–335

Security Requirements Engineering: Analysis and Prioritization

A. Daya Gupta[1], **B. Shruti Jaiswal**[2], **and C. Anupriya Tewari**[3]
[1,2,3]Computer Engineering Department, Delhi Technological University, Delhi, India

Abstract - *with the increase in the use of software system, security requirement engineering becomes an emergent area of study. Security requirements are constraints to a system which must be satisfied for consistent system. Most of the software engineering processes deals with security constraints during the design or implementation phases which may result into unnecessary constrained system. So the need for a new process arises which deals with security issues in requirement engineering phase and then take appropriate design decisions so that security mechanism used are optimal to some extent resulting in efficient secure system. Therefore the requirement engineers must discover security requirement along with functional and non functional requirement, so that security requirement can be dealt effectively. In this paper, we present a method for security requirement analysis and prioritization along with the other activities of security requirement engineering. Analysis is based on the technique of ontology that will automate the process and prioritization is based on risk analysis. The resultant system will be a cost effective in nature as well as it lay a foundation for further activities so that designer will adopt the most efficient technique for the implementation of security requirements*.

Keywords: Security Engineering, Security Requirements Analysis, Security Requirements Prioritization, Ontology, Risk Analysis

1 Introduction

Security engineering is a field of engineering which focuses on the security aspect of a system here we are talking about software systems. The security goals are traditionally classified into confidentiality, integrity and availability of information in an organization [24]. In early approaches, the security measures are taken during design phase, which could result in unseen constraints which can affect the cost and availability of the system and sometime failure of system. In response to this Software engineering community has proposed different methodology to elicit security requirements and then enforce measures to meet these requirements. Some of the proposals for eliciting security requirements are abuse case [4], misuse case [1, 2, 10, 11], common criteria [3, 14] and attack trees [5]. Also, methodologies like secure tropos extension of tropos methodology [19], intentional anti model extension of KAOS methodology with security requirement oriented construct [22] are also discussed. Also, there are proposals for security engineering which takes the risk and threats into consideration and then apply measures to enforce security on threats like OCTAVE [17], CORAS [16], and CRAMM [18]. Firesmith [6, 7] has given proposal to classify security requirements and identify them to mitigate threats that causes risk for a system. Methods like EBIOS [20], MEHARI [21], etc. are proposed for risk assessment and management.

In our previous work, we have proposed software engineering framework that integrates security engineering activities [15, 26] in SDLC. The process starts with the process of elicitation of security requirements along with functional and non functional requirements. These elicited requirements must be analyzed and prioritized so that proper design decisions can be taken [26]. This paper will focus on techniques for analysis and prioritization of security requirement. Process of analysis is based on Ontology and prioritization will be done using risk analysis.

Ontology is a formal, explicit specification of a shared conceptualization. Ontology consists of various domain specific concepts, their properties and relationships between them. Ontology is a hierarchical arrangement of knowledge related to a domain which can be used as a centralized dictionary. The domain relevant to our discussion is security. The advantage of using ontology as a tool for requirements analysis is that it allows the requirements engineers to analyze the requirements with respect to the semantics of the domain. The requirements are generally discovered and documented in natural language. Natural language statements may have different interpretations by different human engineers trying to analyze them, hence making the analysis difficult. Our approach of using ontology will overcome this problem as it helps in semantic analysis of the requirements. Our approach will also provide automation of the analysis process and will save human effort.

Risk analysis is important as it would tell what could possibly go wrong? What is the likelihood of it happening? How will it affect the project? So risk analysis is considered as an important factor. Further paper is organized as follows section 2 provides activities of security requirements

engineering. Section 3 provides proposed framework for analysis and prioritization of security requirements; next section will provide a case study for illustration of proposed technique; and finally section 5 concludes the paper and provides the future scope for research.

2 Activities of Security Requirement Engineering

Security engineering framework proposed in our previous work consists of four main phase that are security requirements engineering, security design engineering, security implementation and security testing. Framework representing the overall procedure for Security Requirement Engineering is shown in Fig 1. Different activities in security requirement engineering are:

2.1 Requirements Discovery and Definition

Here our aim is to discover first the functional, non functional requirements and then security requirements which mitigates threats that affects the assets used by functional requirements. We have considered twelve types of security requirements as defined by Firesmith [6] and extended view point oriented method of Sommerville [12, 13] to define security requirements which are associated with functional requirements.

Different steps in this activity are:

- Identify various stakeholders of the system using view-point analysis [12, 13]. We have identified the various abstract classes of actors as direct and indirect actors. Direct actors are those who directly interact with the system such as human, software system and hardware devices. Indirect actors refer to Engineering personals who develop software and people who regulate application domain. For this paper our interest is in direct actor.

- Identify the functionality of each actor conceptualized in above step and also determine associated non – functional requirements, with assets on which the functional requirements are based.

- Identify the threats associated with each of the functional requirements or data which is used by the functionality. Threats are identified corresponding to functionality based on common criteria approach [3, 14] by filling the stakeholders profile which contains seven fields that define the whole function and actor relationship.

- Identify the security requirements to mitigate these threats using the threat database accessed by actor profile. For details refer [15].

2.2 Analysis and Validation of the Requirements

Analysis is not an easy task it comes with lot of problems as said by sommerville [13] due to change of requirements, stakeholder don't know what they really want, etc. If requirements will change, it will in turn affect everything. So analysis and validation needs special attention in security requirement engineering.

Analyze the identified security requirements for consistency and completeness. If any conflict occurs it must be resolved and must reach to an agreement to avoid any further conflicts.

Completeness Checking ensures inclusion of all necessary security requirements identified to protect the assets of an organization that are affected by threats. Here we check whether all the identified threats are mitigated by security requirements or not.

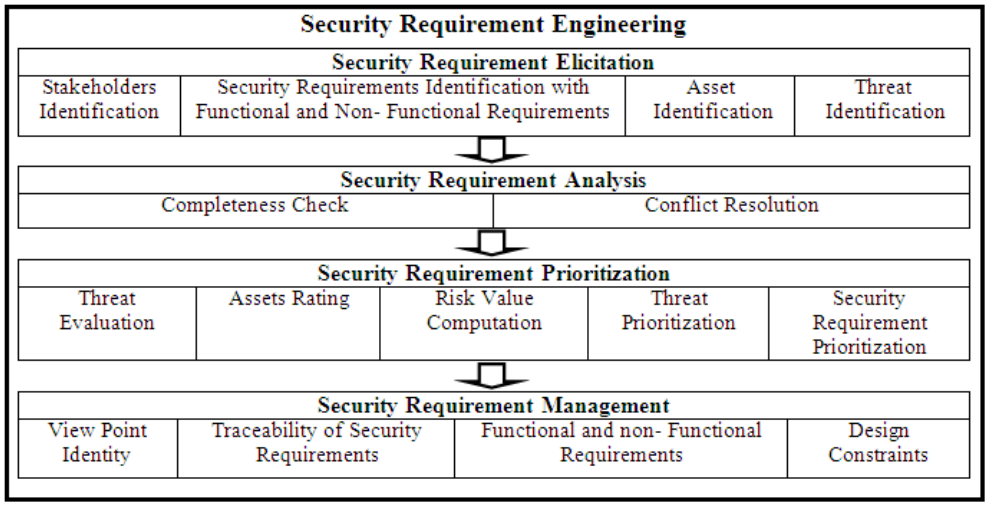

Fig 1. Framework for Security Requirements Engineering

Consistency Checking ensures that there are no contradictory security requirements. The two security requirements should not conflict. It ensures that two security requirements never conflict. Example, customer wants to authorize more number of customers to access the confidential data but want the cost incurred in providing privacy for individual and organizational data will get decreased. So, both of the requirements can't be satisfied simultaneously.

The steps involved in analysis of security requirements are discussed in the next section.

2.3 Prioritization of Security Requirements

Prioritize the security requirements so that it help the designers and other members involved in later phases to take design decisions. It tells about which security requiurement is more critical and need to be dealt first over other. The proposal devised for prioritization of security requirements is given in the next section

2.4 Management of the Requirements

Keep trace of each security requirements and its associated attributes such as requirement identity, view point identity, functional requirement, nonfunctional requirements, threats design constraint, other security requirement, design constraints. The techniques for requirement management presented in [12, 13] can be used for this activity. Details of this work will be dealt in the future.

3 Proposed Techniques for analysis and Prioritization

This section will be divided into two sub sections. The first part will cover the approach for security requirements analysis using ontology. And the next part deals with the steps involved in prioritization of security requirements using the concept of risk analysis.

3.1 Security Requirements Analysis Framework

We propose a framework for the analysis of security requirements that are discovered during security requirements elicitation. The framework is represented in Fig 2. Now various steps involved in the framework will be discussed.

Steps Involved in Analysis:

- *Creation of the Domain Ontology:* This is a major task, as it will serve as the main knowledge base for analysis. Ontology can be created using any of the various approaches available at present such as Methontology [26], OTK (On-To-Knowledge) [27], etc. Ontology will be constructed in hybrid fashion out of top down, bottom up and hybrid approaches because in the hybrid fashion, initially the ontology is constructed by a domain expert and further modifications can be made in it when needed. Protégé [30] is used for ontology development. Reason for using Protégé as a tool is that it is intuitive, easy to use, interactive, easily scalable and extensible due to plug-ins. And OWL (Web Ontology Language) is used for creation of our ontology.

- *Creation of the Application Ontology:* Application ontology will represent the elicited security requirements and their relationships. From the given set of elicited security requirements, application ontology can be created through following steps :

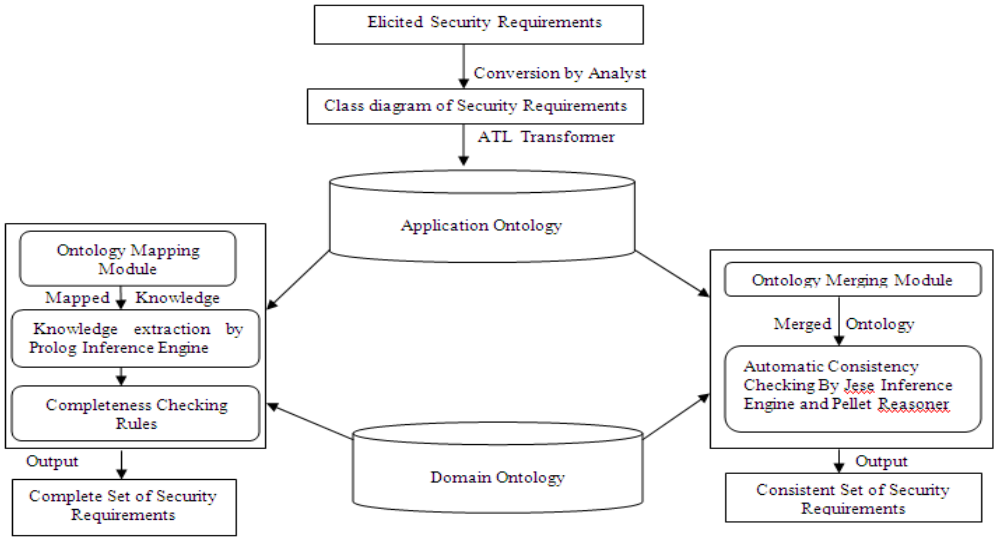

Fig 2: Ontology Based Security Requirements Analysis Freamework

i. Now classes will be converted into concepts of the ontology. As class consists of a class name, properties and relationships to other classes.

ii. Next properties of a class will become properties of corresponding concepts in ontology.

iii. The Subclass and Superclass inheritance relation will be maintained in the ontology, using Subclass and Superclass concepts.

iv. Other relations in the class diagram will be converted into properties in the ontology. For example: aggregation relation becomes PartOf property.

Various tools are available to automate the above task such as AToM3 [31], ATL [32], etc. tools can be used.

- *Mapping Application Ontology with Domain Ontology:* Ontology mapping module maps the classes and relationships in the application ontology with the corresponding classes and relationships of the domain ontology. The knowledge obtained through this mapping will serve as a knowledge base for the inference engine. The mapping process can be performed using existing ontology mapping algorithms [33]. The above tasks can be automated by tools such as OMEN [34], CROSI [35], etc.

- *Knowledge Extraction by the Inference Engine:* We can select any inference engine for querying and drawing out useful conclusions from the security requirements analysis process. In our proposal we are using the Prolog inference engine. Prolog Queries will be used to extract useful knowledge from the knowledge base. Here the knowledge base is the mapping result of the above step. For example, a Prolog query can be generated to obtain from the knowledge base, all the threats that can be mitigated by a particular security requirement.

- *Application of Completeness Checking Rules:* The following rules can be applied on the knowledge extracted by the inference engine for checking completeness of the security requirements:

i. If a concept c1 is related to concept c2 by relation R and the same concept c1 is related to concept c3 by the same relationship R in the domain ontology, then add the concept c3 to the given set of defined requirements and relate it to c1 by relation R (if it is not already in application ontology.)

ii. If c3 is already in the application ontology then just relate c3 and c1 with relation R.

iii. Repeat the above check for all the concepts of the application ontology.

For example, if we have *identification* and *privacy* as security requirements and *snooping* as threat concept in the application ontology and *snooping* is related to *authentication* in the domain ontology with relation "is mitigated by". Then *authentication* is added to our security requirements and it is related with *snooping* by "is mitigated by" relation.

- *Merging Application Ontology and Domain Ontology:* To merge the Application ontology with the Domain ontology we can use any existing ontology merging algorithm. The description of the algorithm is not given here because of the space constraints. Interested users can refer to [36].Various tools such as Chimaera [37] and PROMPT [29] are available for automated merging of ontologies.

- *Consistency Checking :* The above merging process makes consistency checking very easy for the analyst. To check consistency of the security requirements we run the merged ontology on the Protégé plateform. The recent versions of Protégé include *Jese Inference Engine* and *Pellet reasoner*[38]. The Jese Inference Engine automatically checks all the concepts for consistency and the Pellet reasoner automatically checks all the rules for consistency. The output of this step is the result phrase "consistent security requirements" or "inconsistent security requirements".

3.2 Security Requirements Prioritization Framework

As we have the list of security requirements, it's better to prioritize them. As prioritized list of security requirement would be helpful for designers and other members involved in later phases to take decisions. As it tells us about which security requirement is more critical and need to be dealt first over other.

The steps followed in security requirement prioritization are discussed in this section. Prioritization of security requirements will be done with the help of risk analysis. Risk is normally defined as the chance or likelihood of damage or loss [25, 39]. That is, it is a function of two separate components, the **likelihood** that an unwanted incident will occur and the **impact** that could result from the incident.

So risk can be calculated as :

Risk = (Probability of Occurrence of Threat * Impact of Threat Occurrence on Assets) (1)

Probability of Occurrence of Threat = Threat Rating and is represented by **TR**

Impact of Threat Occurrence on Assets = Summation of importance level of assets affected by threat, as one threat may affect more than one asset.

Represented by $\sum_{k=1}^{n} \mathbf{IL}$ where n is the maximum number of assets affected. Hence (1) will become

$$\text{Risk} = \text{TR} * \sum_{k=1}^{n} \mathbf{IL} \quad (2)$$

Steps involved in Security Requirement Prioritization

- Assign threat rating to each threats identified. Threat rating is the number which represent occurrence frequency of a threat in a system. The scale for threat rating is 1- 10. Assign lower value to threat whose occurrence frequency is low and higher to higher frequency threat.

- Assign assets a value in range of 1- 10, representing its importance to the organization. This importance level will show how much cost and resources are required to protect a praticular asset.

- List various assets affected by each threat.

- Calculate the risk value using (2).

- Now the threats will be prioritized based on risk value calculated in step4. Higher the risk value higher will be the priority of threat.

- Finally prioritize security requirements based on threats priority. For prioritization of security requirement following rules will be used:

  i. If the security requirement is mitigating single threat then in that case threat priority is simply assigned to security requirement and it acts as its priority.

  ii. If the security requirement is mitigating more than one threat in that case we add up all the corresponding threat priorities and assign the calculated value to the security requirement as its priority.

4 Case Study

The whole process of security requirement engineering is explained here with the help of a case study of "Railway Reservation System". It covers the full detail of the whole procedure that is from the identification of stakeholders to the final prioritization of security requirements.

- Various direct stakeholders or viewpoints involved are:
  i. Traveler
  ii. Railway Management
  iii. Database

- List of functional and non functional requirements is listed in Table1. And, various assets involved are:
  i. Traveler Information
  ii. Ticket Information
  iii. Credit Card/ Bank Details
  iv. IT Infrastructure (Communication Channel, System Information, etc)
  v. Employee and its Details

Various threats involved are identified using the concept of common criteria [3, 14]. We will be developing the repository of the threats. For extraction of threats from repository, one need to fill Actor Profiles that contains the seven fields as defined in [15]. All the threats identified are listed in Table1.

Various security requirements to mitigate threats are shown in Table 1.

Assigned asset importance level on the scale of 1- 10 are shown in Table 2.

Table 2 Asset Importance Level

ASSET	IMPORTANCE LEVEL (1- 10)
Traveller Information	7
Ticket Information	5
Credit Card	9
IT Infrastructure	4
Employee Details	6

Table 1. An Example "Railway Reservation System" Explaining our Process

Viewpoints	Services	Non Functional Requirements	Threats	Security Requirements
Traveler	1. Registration of Customer 2. Make Enquiry 3. Book Ticket 4. Cancel Ticket 5. Make Payment	1. Reliability 2. Response Time 3. Execution Time	1. Spoofing 2. Insider 3. Disclose Data 4. Privacy Violated 5. Change Data 6. Repudiate Receive	1. Authorization 2. Privacy 3. Non Repudiation
Railway Management	1. Update Data 2. Serve to Customer Request 3. Maintenance	1. Correctness 2. Response Time 3. Robustness 4. Scalable	1. Change Data 2. Privacy Violated 3. Social Engineer 4. Outsider	1. Integrity 2. Identification 3. Authentication
Database	1. Report Maintenance for Transaction	1. Reliability 2. Response Time 3. Integrity	1. Outsider 2. Impersonate	1. Security Auditing 2. Intrusion Detection

• Assigned threat rating values on the scale of 1 – 10 to various threats is given in Table 3.

Table 3 Threats with Threat Rating

THREAT	THREAT RATING (1 – 10)
Change Data	9
Repudiate Receive	5
Spoofing	5
Insider	3
Privacy Violated	7
Outsider	6
Disclose Data	4
Social Engineer	6
Impersonate	8

• Identify the assets affected by each threat. The identified assets corresponding to each threat is given in Table 4.

Table 4 Assets Affected by Threat

THREAT	ASSET THAT CAN BE AFFECTED
Change Data	Traveler Information, Ticket Information, Employee Details
Repudiate Receive	Credit Card Information
Spoofing	Credit Card Information
Insider	IT Infrastructure
Privacy Violated	Ticket Information, Credit Card Information, Traveler Information
Outsider	IT Infrastructure, Traveler Information, Employee Details
Disclose Data	Traveler Information, Ticket Information, Employee Details
Social Engineer	Traveler Information, Employee Details
Impersonate	Traveler Information, Employee Details

Once threats and assets affected are identified and valuated, risk valuation will be done and for above case study and computation of risk value is shown in Table 5.

Various security requirements to mitigate threats are already identified. Now the main part of our work comes into picture that is to prioritize these security requirements.

Table 5 Threat Priority

Threat	TR * $\sum_{k=1}^{n}$ IL	Risk	Threat Priority
Change Data	9 * ∑ (7 + 5 + 6)	162	8
Repudiate Receive	5 * 9	45	2
Spoofing	5 * 9	45	2
Insider	3 * 4	12	1
Privacy Violated	7 * ∑ (5 + 9 + 7)	147	7
Outsider	6 * ∑ (4 + 7 + 6)	102	6
Disclose Data	4* ∑ (7 + 5 + 6)	72	3
Social Engineer	6 * ∑ (7 + 6)	78	4
Impersonate	8 * ∑ (5 + 6)	88	5

Final computation of priorities is given in Table 6. As Security Requirement Authorization is mitigating three threats so for its priority we add the priority value of corresponding threats. And, in case of Privacy Security Requirement it is mitigating only one threat so whatever will be the priority value of threat it is directly assigned to security requirement.

Table 6 Priority of Security Requirements

Security Requirement	Threats Mitigated	Threat Priority	Security Requirement Priority
Authorization	Change Data Disclose Data Insider	8 3 1	12
Privacy	Privacy Violated	7	7
Non repudiation	Repudiate Receive Spoofing	2 2	4
Integrity	Social Engineer	4	4
Identification	Change Data Outsider	8 6	14
Authentication	Privacy Violated Outsider	7 6	13
Security Auditing	Impersonate	5	5
Intrusion Detection	Outsider	6	6

If in case two Security Requirements has same priority in that case designer will have to take decision which one to deal first. Throughout the computation higher number represent higher priority or higher value.

5 Conclusions and Future Work

In this paper we have presented techniques for analysis and prioritization of security requirement based on ontology and threat analysis respectively. This method is improvement over the method presented in [23], as it tries to quantify the value of risk value so that will get correct and consistent result. Further complexities in risk analysis are under processing which covers other factors then threat rating. Here analysis is done using the manual method of our previous paper [23] and will provide a detailed framework for it with proper example in our next paper. We are also developing a computer based tool to incorporate these techniques. Method block presented in [9] will be extended to incorporate the security characteristics also the CAME tool MERU [8] will be initiated in the construction of method which includes the security engineering.

6 References

[1] Alexander IF, "Modelling the interplay of conflicting goals with use and misuse cases". In: Proceedings of the 8th international workshop on requirements engineering: foundation for software quality (REFSQ'02), Essen, Germany, 2002.

[2] Alexander IF, "Misuse cases, use cases with hostile intent". IEEE Software, 2003, pp. 58– 66

[3] Common criteria for information technology security evaluation. Technical report CCIMB 99–031, Common Criteria Implementation Board, 1999.

[4] John Mc Dermott, Chris Fox, "Using abuse case models for security requirements analysis." Department of Computer Science, James Madison University, 1999.

[5] Robert J. Ellison, "Attack Trees", Software Engineering Institute, Carnegie Mellon University, 2005.

[6] Donald G. Firesmith, "Engineering Security Requirements", Journal of object technology, 2003, vol 2, no.1, pp.53-68.

[7] Donald G. Firesmith, "Security Use cases", Journal of object technology, 2003, vol 2, no.3, pp.53-64.

[8] Gupta D. and Prakash N., "Engineering Methods from their Requirements Specification", Requirements Engineering Journal 2006, 3, pp.133 – 160.

[9] Prakash N., "On generic Method Models", Requirements Engineering Journal 2006, pp. 221 – 237.

[10] Sindre G, Opdahl AL, "Eliciting security requirements by misuse cases". In proceeding 37th Conference Techniques of Object-Oriented Languages and Systems, TOOLS Pacific 2000, pp 120-131.

[11] Sindre G, Opdahl AL, "Eliciting security requirements with misuse cases". Requirements Engineering 10, Springer-Verlag London Ltd, January 2005, pp. 34-44.

[12] Kotonya G., Sommerville I., "Requirement Engineering with viewpoints", 1995.

[13] Sommerville, I., "Software Engineering". Seventh edition 2003. ISBN - 8129708671. Pearson Education.

[14] M. Ware, J. Bowles, C. Eastman, "Using the common criteria to Elicit security Requirements with use cases", IEEE Computer Society, 2006.

[15] Agarwal A, Gupta D, "Security Requirement Elicitation Using View Points for online System", IEEE Computer Society, 2008.

[16] CORAS - http://www2.nr.no/coras.

[17] Alberts, Christopher and Dorofee, Audrey. *OCTAVE* Method Implementation Guide v2.0. Pittsburgh, PA: Software Engineering Institute, Carnegie Mellon University, 2001. http://www.cert.org/octave.

[18] The Logic behind CRAMM's Assessment of Measures of Risk and Determination of Appropriate Countermeasures available at www.cramm.com

[19] a) Paolo Giorgini, G.Manson, Haralambos Mouratidis. I.Philip, "A Natural Extension of Tropos Methodology for Modelling Security". In the workshop on Agent-oriented methodologies, at OOPSLA 2002.

b) Paolo Giorgini, G.Manson, Haralambos Mouratidis. I.Philip, "Modelling Secure Multi agent System". AAMAS - 2003.

[20] EBIOS- Expression of need and identification of security objectives, DCSSI, France, February, 2004.

[21] MEHARI- "Information Risk Analysis and management Methodology", V-3, Concepts and Mechanism, CLUSIF, October, 2004.

[22] A. van Lamsweerde, "Elaborating security requirements by construction of intentional anti-models", Proceedings of the 26th International Conference on software engineering (ICSE'04), IEEE Computer Society, Washington DC USA, 2004, pp. 148-157.

[23] Jaiswal S., Gupta D., "Security Requirement Prioritization", in the proceeding of SERP'09, pp. 673- 679.

[24] F. Benjamin, G. Seda, H. Maritta, S. Holger, "A comparision of security requirements engineering methods", in requirement engineering, 2010.

[25] Yogesh Singh, "Software Testing", Cambridge University Press, 2011, ISBN 1107012961, 9781107012967.

[26] Chatterjee K., Gupta D., De A., "A Framework for Security Design Engineering Process", in ICIP 2011, CCIS 157, pp. 287- 293.

[27] Fernandez M., Gomez-Perez A., Juristo N., "METHONTOLOGY: From Ontological Art Towards Ontological Engineering", *AAAI Spring Symposium on Ontological Engineering*, Stanford University, March 24-26th, 1997, pp 33-40.

[28] Sure Y., Tempich C., Vrandecic D., 2006. "Ontology Engineering Methodologies," in *Semantic Web Technologies: Trends and Research in Ontology-based Systems*, Wiley, 2006, pp. 171-187.

[29] Fridman N., Musen M., " PROMPT: Algorithm and Tool for Automated Ontology Merging and Alignment ", Stanford Medical Informatics, Stanford University, Stanford,2000.

[30]Protégé: http://www.protege.stanford.edu

[31] AToM3 tool Home page: http://atom3.cs.mcgill.ca.2002.

[32] Frédéric J., Allilaire F., Bézivin J., Kurtev I., "*ATL: a model transformation tool", in* Science of Computer Programming, 72, 2008. pp. 31-39.

[33] Falconer S.,Noy N.,Storey1 M., "Ontology Mapping - A User Survey", Stanford University, 2007..

[34] Mitra P., Noy N., Jaiswal A., **"**OMEN: A Probabilistic Ontology Mapping Tool", Workshop on Meaning coordination and negotiation at the Third International Conference on the Semantic Web (ISWC-2004), Hisroshima, Japan,2004.

[35]CROSI tool: http://www.aktors.org/crosi/

[36] Noy N., Musen M., "An Algorithm for Merging and Aligning Ontologies: Automation and Tool Support" , Sixteenth National Conference on Artificial Intelligence , 1999.

[37] McGuinness D., Fikes R., Rice J., Wilder S., "The Chimaera Ontology Environment", American Association for Artificial Intelligence, 2000.

[38] Evren Sirin a , Bijan Parsia a , Bernardo Cuenca Grau a,b ,Aditya Kalyanpur a , Yarden Katz Pellet: A Practical OWL-DL Reasoner.

[39] Aven, T.," Risk analysis and risk management. Basic concepts and principles" Reliability & Risk Analysis: Theory & Applications, 2009, vol 2, pp. 57-73.

ISBN 978-93-5156-328-0
International Conference of Advance Research and Innovation (ICARI-2014)

Selection of Candidate by Political Parties Using Fuzzy Logic

Kiran Pal [a], Surendra Tyagi [b,*]
[a] Department of Mathematics, Delhi Institute of Tool Engineering, Delhi
[b] Department of Computer Science, Delhi Technological University, Delhi

Article Info

Article history:
Received 29December 2013
Received in revised form
10 January 2014
Accepted 20 January 2014
Available online 1 February 2014

Keywords
Fuzzy Logic
Election
Candidate
Selection

Abstract

Party leaders in list systems must select candidates to best accomplish their electoral, organizational, and policy goals. In particular, leaders must balance nominees' policy making skills against other aspects of candidate quality, such as electoral viability. In present scenario this is very tough to decide wining ability of candidate. Party leaders shall be with an opportunity to behave strategically. Party leaders pursue a variety of goals in determining where to rank candidates on the ballot: maximizing electoral competitiveness, rewarding party stalwarts, grooming young talent, and ensuring legislative policy making ability.
There are lots of factors which decide wining of candidate, for example publicity, credibility etc. I have made this paper keeping these all issues in my mind which affect candidature of candidate. There are no hard and fast rules or mathematical equation which can show exact result. So Fuzzy logic is best and suitable tool to used in this work.

1. Introduction

Candidate selection is the process by which political parties decide who will be on the ballot paper as their recommended candidate(s). The way in which they make that choice is mainly determined by their own internal rules and procedures. Nomination is the legal process by which election authorities screen the candidates recommended by the party, approve their candidacy, and print their names on the ballot paper. In each election, thousands of persons could potentially stand for election, but it would be impossible for voters to make an informed choice among them. Political parties therefore act as useful and necessary gate-keepers narrowing down the list of candidates to a small enough pool.

2. Introduction to concept of fuzzy logic

Fuzzy logic has rapidly become one of the most successful of today's technologies for developing sophisticated control systems. The reason for whichis very simple. Fuzzy logic addresses such perfectly as it resembles human decision making with an ability to generate precise solutions from certain or approximate information. While other approaches require accurate equations to model real-world behaviors, fuzzy design can accommodate the ambiguities of real-world in human language and logic. Although genetic algorithms and neural networks can perform just as well as fuzzy logic in many cases, fuzzy logic has the advantage that the solution to the problem can be cast in terms that human operators can understand, so that their experience can be used in the design of the controller. This makes it easier to mechanize tasks that are already successfully performed by humans.[1]

In a broad sense, fuzzy logic refers to fuzzy sets - a set with unclear boundaries. Examples of fuzzy sets are “hot,” “tall,” “medium,” etc. In a narrow sense, fuzzy logic is a logical system that aims to formalize approximate reasoning .In fuzzy logic a fuzzy symbol can take any truth values from the closed set [0, 1] of real numbers thus generalizing the Boolean truth values. As the technology was further embraced, fuzzy logic was used in more useful applications.

2.1 Fuzzy sets Background

The precision of mathematics owes its success in large part to the efforts of Aristotle and the philosophers who preceded him. In their efforts to devise a concise theory of logic, and later mathematics, the so-called "Laws of Thought" were

Corresponding Author,
E-mail address:surendratyagi2000@gmail.com
All rights reserved: http://www.ijari.org

posited. One of these, the "Law of the Excluded Middle," states that every proposition must either be True or False. Even when Parminedes proposed the first version of this law around 400 B.C.E.There were strong and immediate objections: for example, Heraclitus proposed that things could be simultaneously True and not True. It was Plato who laid the foundation for what would become fuzzy logic, indicating that there was a third region (beyond True and False) where these opposites "tumbled about." Other, more modern philosophers echoed his sentiments, notably Hegel, Marx, and Engels. But it was Lukasiewicz who first proposed a systematic alternative to the bi-valued logic of Aristotle.

In the early 1900's, Lukasiewicz described a three-valued logic, along with the mathematics to accompany it. The third value he proposed can best be translated as the term "possible" and he assigned it a numeric value between True and False. Eventually, he proposed an entire notation and axiomatic system from which he hoped to derive modern mathematics. Later, he explored four-valued logics, five-valued logics, and then declared that in principle there was nothing to prevent the derivation of an infinite-valued logic.

Lukasiewicz felt that three- and infinite-valued logics were the most intriguing, but he ultimately settled on a four-valued logic because it seemed to be the most easily adaptable to Aristotelian logic.

Knuth proposed a three-valued logic similar to Lukasiewicz's, from which he speculated that mathematics would become even more elegant than in traditional bi-valued logic.[2] His insight, apparently missed by Lukasiewicz, was to use the integral range [-1, 0 +1] rather than [0, 1, 2]. Nonetheless, this alternative failed to gain acceptance, and has passed into relative obscurity. It was not until relatively recently that the notion of an infinite-valued logic took hold. In 1965 Lotfi A. Zadeh published his seminal work "Fuzzy Sets" which described the mathematics of fuzzy set theory, and by extension fuzzy logic [3] This theory proposed making the membership function (or the values False and True) operate over the range of real numbers [0.0, 1.0]. New operations for the calculus of logic were proposed, and showed to be in principle at least a generalization of classic logic. It is this theory which we will now discuss.

2.2 Fuzzy explanation

Before illustrating the mechanisms which make fuzzy logic machines work, it is important to realize what fuzzy logic actually is. Fuzzy logic is a superset of conventional (Boolean) logic that has been extended to handle the concept of partial truth- truth values between "completely true" and "completely false". As its name suggests, it is the logic underlying modes of reasoning which are approximate rather than exact. The importance of fuzzy logic derives from the fact that most modes of human reasoning and especially common sense reasoning are approximate in nature.

The essential characteristics of fuzzy logic as founded by ZaderLotfi are as follows.

- In fuzzy logic, exact reasoning is viewed as a limiting case of approximate reasoning.
- In fuzzy logic everything is a matter of degree.
- Any logical system can be fuzzified
- In fuzzy logic, knowledge is interpreted as a collection of elastic or, equivalently, fuzzy constraint on a collection of variables .
- Inference is viewed as a process of propagation of elastic constraints.

The third statement hence, defines Boolean logic as a subset of Fuzzy logic.

2.3 Fuzzy Sets

Fuzzy Set Theory was formalised by Professor LoftiZadeh at the University of California in 1965. [4] What Zadeh proposed is very much a paradigm shift that first gained acceptance in the Far East and its successful application has ensured its adoption around the world. A paradigm is a set of rules and regulations which defines boundaries and tells us what to do to be successful in solving problems within these boundaries. For example the use of transistors instead of vacuum tubes is a paradigm shift - likewise the development of Fuzzy Set Theory from conventional bivalent set theory is a paradigm shift. Bivalent Set Theory can be somewhat limiting if we wish to describe a 'humanistic' problem mathematically.

3. Candidate selection process

Parties can select their candidates in many different ways. In numerous cases, the existing legal framework establishes that political parties should “democratically” elect their candidates, but this concept is very vague, and there are few if any applicable legal provisions. Only in a few cases does legislation lay down the process by which candidates should be selected, and the selection process can have a direct impact on the depth and breadth of the democratic process—particularly if a given party’s candidate selection process is non-transparent[5]

4. Candidate selection process Factors

Factors such as electoral system, party ideology, political culture, and the organization of government have been thought to have an influence on the centralization and participation in the candidate selection process. However, there is no evidence that any of them is decisive. It would be natural for national party agencies to be more influential in multi-member district systems (where more than one person is elected to the legislature from each constituency), while single-member constituencies would give more power to local branches.[6]

In the same logic, federal systems would tend to favor decentralized candidate selection, parties with an inclusive political ideology would favor participatory selection procedures, and parties in countries with a hierarchical political culture would foster non-participatory processes. However, all these (and more) criteria are mixed in all political parties, and conclusions are therefore hard to draw. Not even in cases where legislation stipulates a particular selection process is it always possible to say if the law has determined the processes, or if they simply reflect practice.

Following factors are considered in this project:

1. Behavior
2. Age
3. Character
4. Publicity
5. Education

4.1 Primary Elections for deciding publicity among party people

Primary elections are internal party processes that choose a political party's candidate(s) for the next general election by holding an internal election. Exactly how this is done depends on the legal framework, internal party rules, and informal practices.[7]

Primary elections are an example of a selection process with a high level of participation, meaning that ordinary members (or in some cases all voters in the electoral district) control the process.

4.2 Age

Age of person decide to work ability and experience of person. If person is less than 25 years is not suitable for fighting election, if he is between 25 and 40 years has less experience but good working capacity, if he is between 40 and 65 has good experience and good working capacity. This is most suitable age for fighting election; if he is between 60 and 75 has good experience but less working power so he should have been given less chance than of 60 years person. If person is greater than 75 in present era should leave politics or given very rare chances.

4.3 Behavior

It is most powerful tool of candidature which decides future of candidate. It is categorically divided as:

1. Bad
2. Good
3. Better
4. Best

4.4 Education

An Educated candidate can provide good governance, so education factors as:

1. Education till 8th
2. Education till 10th
3. Education till 12th
4. Education after 12th

Table: 1. System Requirements

S.No	*System Hardware/Software*	*Configurations*
1	RAM	512MB
2	Operating System	Windows 7
3	Processor (with Speed)	Core to duo (1.6 GHz) and Upwards
4	Hard Disk Size	40 GB and above
5	Front End	C++

5. Conclusions

There are two concepts that are central to the issue of party selection of candidates. One is centralization, that is, what level in the party – local, regional or national –controls the candidate selection. The second is participation, meaning who – ordinary members or top leadership – controls the process at the level where the decision is taken. Leaders determine the list rankings of a limited number of

available candidates. Obviously, candidates at the top of the list have a higher chance of winning a seat. Party leaders, therefore, choose candidates for top list positions depending on the party's goals. Experienced candidates may generally be considered of better quality; they are known to be loyal, hold promise for future elections, have more experience making policy, and are better able to attract votes in order to win elections.

In present scenario selection process has been changed by new political parties like AamAadmi party and Loksattta party in india, The proposed program may prove to be very helpful for selecting the best candidate among the large number of candidates. This will also reduce time taken for the tedious process of conventional candidate selection process. Further it may result in minimization of other resources such as papers office expenditures etc.

References

[1] http://www.doc.ic.ac.uk/~nd/surprise_96/journal/vol4/sbaa/report.fuzrules.html
[2] S. Fukumi, M. Mizurnoto, Tanaka K., Some considerations of fuzzy conditional inference,Fuzzy Sets and Systems, 4 (1980), pp. 243–273
[3] L. A. Zadeh, “Similarity relations and fuzzy ordering”, Information Sciences, 3, 177—200, 1971
[4] L. A. Zadeh, “Fuzzy sets”, Information and control, 8, 338—353, 1965
[5] http://aceproject.org/ace-en/topics/pc/pcb/pcb02/pcb02a
[6] G. Rahat, R. Y. Hazan, \Candidate Selection Methods: An Analytical Framework."Party Politics 7(3):297-322.URL: http://ppq.sagepub.com /cgi/doi/10.1177/1354068801007003003
[7] http://www.danpemstein.com/files/MPB-experience.pdf

CONTENTS

In Memoriam Mefodie Teodor Rațiu i-xx
Mitrofan Ciobanu, Ilie Burdujan, Petru Soltan, Vladimir Izbaş, Olga Izbaș, Anca Veronica Ion

Introduction to Neutrosophic Hypergroups 1-10
A.A.A. Agboola, B. Davvaz

Stiffness of the linear diffusion and wave-type Partial Differential Equations 11-25
Elisabete Alberdi Celaya, Juan José Anza Aguirrezabala

The cocartesian product and pairs of conjugate subcategories 27-33
Botnaru Dumitru, Baes Elena

On thermal stresses in anisotropic inhomogeneous microstretch cylinders 35-50
Emilian Bulgariu

On a higher order fractional differential inclusion with multi-strip fractional integral boundary conditions 51-60
Aurelian Cernea

On dense subspaces of the spaces of continuous pseudometrics 61-74
Mitrofan M. Choban, Dorin I. Pavel

On the impact of explicit or semi-implicit integration methods over the stability of real-time numerical simulations 75-88
Teodor Cioacă, Horea Cărămizaru

The implicit reducibility in the chain super-intutionistic logics 89-94
Ion Cucu, Mefodie Rațiu

Some properties of finite order solutions of a class of linear differential equations with entire coefficients 95-106
Saada Hamouda, Benharrat Belaïdi

Some sandwich results associated with a generalized linear operator 107-118
S. Sivaprasad Kumar, Virendra Kumar

On the lifetime as the maximum or minimum of the sample with power series distributed size 119-128
Alexei Leahu, Bogdan Gheorghe Munteanu, Sergiu Cataranciuc

On spectral problem for Laplace operator in domain with perturbed boundaries 129-141
Boris V. Loginov, Davran G. Rakhimov

An optimal design of the wind turbine blade geometry adapted to a specific site Using Algerian wind data 143-154
Zine Labidine Mahri, Said Zid, Rouabah Mohamed Salah

Parameters estimation for the bivariate Sarmanov distribution with normal-type marginals 155-165
Elena Pelican, Raluca Vernic

Some remarks on eigenvalue problems for the Laplace operator 167-172
Valentina Proytcheva, Snezhana Hristova

The Interval Lattice Boltzmann Method for transient heat transfer in a silicon thin film 173-179
Alicja Piasecka-Belkhayat, Anna Korczak

About the maximal number of algebraically independent Lyapunov quantities for the differential system s(1,4) 181-195
Victor Pricop

Common fixed points for Banach-Caristi contractive pairs 197-203
Mihai Turinici

RAŢIU (RAŢĂ) MEFODIE TEODOR

Corresponding Member of the Academy of Sciences of Moldova,
Corresponding Member of the
American Romanian Academy of Arts and Sciences,
Doctor Habilitatus on Physical and Mathematical Sciences, Professor

01 octombrie 1935 - 12 august 2013

„L'histoire géologique nous montre que la vie n'est qu'un court épisode entre deux etérnités de mort, et que, dans cet épisode même, la pensée consciente n'a duré et ne duréra qu'un moment. La pensée n'est qu'un éclair au milieu d'une longue nuit, mais c'est cet eclair qui est tout."

Henri Poincaré

„C'est avec la logique que nous prouvons et avec l'intuition que nous trouvons."

Henri Poincaré

The distinguished mathematician Mefodie Raţiu would have been be 78 years old at 01 October 2013. He leaved for posterity a durable scientific creation and the image of a remarkable scientist. The ideas and methods created in his scientific works represent an important moment in the development and confirmation of the Moldavian mathematics and science in the scientific world.

Professor Mefodie Raţiu was an irrefutable leader of the Moldavian school of mathematical logic, which have had an important contribution to the mathematical logic, to the organization of mathematical research in the Republic of Moldova and to the education of new generations of highly-qualified specialists.

A short life chronology of Professor Mefodie Raţiu:

- October 01, 1935 – born in village Şipoteni, Romania (now Călăraşi district, Republic of Moldova);
- 1943 - 1954, pupil of secondary school, Republic of Moldova;
- 1954-1955, school-teacher in village Volcineţ, Călăraşi district, Republic of Moldova;
- 1955 - 1959, student at "I.Creangă" State Pedagogical University, Chişinău;
- 1959 - 1962, school-teacher in village Bravicea, Călăraşi district;
- 1960 - graduated at "I.Creangă" University, Chişinău;
- 1962 - August 12, 2013, research worker at the Academy of Sciences of Republic of Moldova, holding several positions;
- 1964 – 1967 – PhD student of the Institute of Mathematics of the Academy of Sciences of R. Moldova;
- 1968 – gained the PhD Degree, at Institute of Mathematics of the Siberian Branch of the Academy of Sciences of USSR, Novosibirsk, Russian Federation;
- 1984 - 2013, leader of the Scientific Seminary on Mathematical logic and Algorithmic theory, member of the Scientific Council of the Institute of Mathematics and Computer Science;
- 1985 - 2013, scientific coordinator for doctoral theses;
- 1986 – habilitatus doctor in sciences, Moscow M.V. Lomonosov State University, Russian Federation;
- 1991 - academic rank of professor, Superior Certifying Commission of the USSR, Moscow, USSR;
- 1994 – laureat of the State Prise of R.Moldova in the fields of science, technique and production;
- 1999 - decorated with State order "Gloria Muncii" of Republic of Moldova;

- 2000 - elected at academic rank of corresponding member of the Academy of Science of Republic of Moldova;
- 2001 - laureat of prize „Academician Constantin Sibirschi";
- 2010 - elected Corresponding Member of the American Romanian Academy of Arts and Science;
- August 12, 2013 – died, after painful non-long illness.

Mefodie Raţiu (Raţă, Ratsa) was born at October 01, 1935 in village Şipoteni, Romania (now Călăraşi district, Republic of Moldova). Şipoteni is one of the old Romanian localities and is composed of two villages: Podul Lung and Şipoteni. It is now a commune in Călăraşi district, Republic of Moldova.

In 1954 he successfully finished the local secondary (ten-year) school. Mefodie's teachers at the school were so impressed with his abilities that persuaded him to attend to a university. The mathematical formulas and logical deduction charmed him, and without any doubt he decided to continue the mathematical studies. But his financial status (that of a Moldavian peasant) did not permit him to continue the studies. One year he worked as a teacher in the school of village Volcineţ, Călăraşi district, Republic of Moldova. That was not a pleasant year. He felt the absence of mathematical and special psycho-pedagogical knowledge. In 1955 he started his universitary education at the Faculty of Physics and Mathematics of "Ion Creangă" Pedagogical State Institute Chişinău (now Chişinău "Ion Creangă" Pedagogical State University). He was fascinated by the abstract algebraic construction. But the program of the algebra in the pedagogical institutions was scarce. Mefodie Raţiu began independently to explore additional facts about rings, algebraic operations, algebraic equations, algebraic identities. In 1959 he was appointed as a teacher in the school of village Bravicea, Călăraşi district, Republic of Moldova. After graduating the university in 1960, he continued exploring of additional algebraic facts.

In 1962 he heard that the Academy of Science of Moldova was founded in Chişinău. In that year he was appointed as a scientific worker of the Institute of Mathematics and Computer Sciences (named at that time Institute of Mathematics and Physics) of the Academy of Science of Moldova. Thus in 1962 Professor M.Raţiu, steady and full of energy, began the scholar activity and didactic carrier in university. His whole future life was associated with the Academy of Science of Moldova, occupying successively the positions of lower researcher, researcher, senior researcher, coordinator scientific researcher, scientific secretary of the Institute of Mathematics and Computer Sciences, founder and head of the Section of mathematical logic, principal scientific researcher, scientific consultant.

In the mathematical logic and the theoretical informatics it is well known the problem of the determination of the functions (operations) of a given logic, which can be, in a sense or other, expressible through other beforehand given functions. The expressibility relation of the functions (functional expressibility) is interpreted as the possibility to obtain some functions from certain initial functions, through the method of superposition. In the semantic construction of the classical propositional logic, the fundamental objects of the analysis are the Boolean functions, understood as functions of the Boolean bivalent algebra (the propositional algebra). The study of expressibility in the classical logic was initiated in the papers of the American mathematician E. Post, which refers to the description of all closed (relative to expressibility) classes of Boolean functions. These classes, named subsequently Post classes, constitute, relative to the inclusion, a countable lattice, illustrated by a not very complicated diagram. Any Post class can be considered as a finite-generated algebra by

means of superpositions. On the base of the general consideration of these classes, it is not difficult to build a recognition algorithm of the expressibility in the classical logic, which, for any Boolean functions $\{f, f_1, f_2, \ldots, f_m\}$ given by formulas or tables, allows to recognize if the function f can be expressed in terms of the system $\{f_1, f_2, \ldots, f_m\}$. It can also be obtained an algorithm for recognition the completeness in this logic, allowing to recognize, for any finite Boolean functions system, if the system is included in a finite number of Post classes.

A new interest, linked to the problem of the expressibility of the functions, appeared in the 50es of the past century, in connection with the applications of the mathematical logic in Informatics (Computer Sciences). The investigation of the expressibility, both in the classical logic and in its multi-valued generalizations, i.e. the general k–valued ($k = 2, 3, \ldots$) logics was stimulated by prof. P.S. Novikov's lectures at the Moscow "M.V. Lomonosov" University. The general k-valued logic is considered mostly from a functional point of view, being interpreted as the class of all operations on the set of truth values of cardinal k. In more detail it was expressed the problem of completeness (relative to expressibility), which requires to be clarified the necessary and sufficient conditions (preferably uncomplicated and algorithmically) to express all the operations of the researched logic. The existence of the completeness criterion of the functions systems in the general k-valued logic was obtained by A.V. Kuznetzov. S.V. Jablonskii has established the completeness criteria in the 2-and 3-valued logics in terms of pre-complete classes and described some similar families in the k-valued logic, for $k> 3$. I. Rosenberg has established the completeness criterion in the k-valued logic, for any $k > 3$, based on six families of pre-complete classes. The connection of these problems with the algebra and their algebraic treatment were investigated by A.V. Kuznetzov and especially by A.I.Maltzev, which proposed in 1966 to research the iterative Post algebras. Such an algebra has as a support a closed class of k-valued logic functions, and the superposition in its various variations played the role of signature. In this way, we can ascertain that the iterative algebras possess a finite signature. Consequently, we will see that, from a functional point of view, the research of the iterative algebras, in most cases, is equivalent to the investigation of their supports, that are the closed classes of functions of the k-valued logic. The general problem of description of closed classes in the k-valued logic for $k> 3$, which are exactly the iterative algebras supports, become more complicated in essence through the presence in this logic of closed classes with infinite countable basis, as well as of closed classes, which generally do not have a basis. Consequently, the set of these classes forms, relatively to inclusion, a lattice of continuum cardinality. For the case of the general k-valued logic ($k> 3$) these properties have been rendered by I.I. Ivanov and A.A. Mucinik. One should remark as well the efforts of many authors for the descriptions of some separate classes of functions from the k-valued logic, or of the families of such classes. But the problem of the complete description of these closed classes, even the problem of recognition of the completeness in the k-valued logic for $k> 3$ remains open.

Beginning with the papers of L. Brouwer, V.I. Glivenko, A. Heyting, A.N. Kolmogorov, C. Lewis, Gr. Moisil and others, the investigation of logical calculus and of non-classical logics defined through them, were initiated. These investigations appear in the context of the mathematical study of constructive notions, in the formalization of the natural language, in the demonstration theory, in the programming theory, and so on. In 1930 the intuitionistic logic was formalized and recognized as being the most important among the propositional logics used in the foundations of mathematics. We should remember that this logic, as it was demonstrated in 1932 by K. Gödel, cannot be adequately defined through a finite truth matrix, but as S. Jaskowski has shown in 1936, it can be approximated through an infinite series of such matrices.

By suitable specifications, A.V. Kuznetzov has generalized the notion of expressibility for the formulas of the so-called super-intuitionistic logics and he has initiated the research of these logics from expressibility point of view. Professor Mefodie Raţiu succeeded to solve the completeness problem relative to the expressibility in the intuitionistic logic and, in general, in any super-intuitionistic logic. In this sense, the approach consisted in the research of similar problems for certain intermediary logics between the intuitionistic and classical logics. The simplest among these intermediary logics is Jaskowski's First Matrix Logic. It coincides also with the logic of 3-valued pseudo-Boolean algebra, denoted by Mefodie Raţiu with the symbol L*T*. The L*T* logic functions are interpreted as functions of the mentioned pseudo-Boolean algebra, termed as pseudo-Boolean functions. Professor Mefodie Raţiu has proved that the class L*T* of all 3-valued pseudo-Boolean functions includes families of closed sub-classes of continuous cardinality, with bases functionally independent of countable cardinality, as well as families of continuum cardinality of closed sub-classes, which generally do not accept independent bases. He initiated and developed the theory of chain iterative classes of pseudo-Boolean functions. Professor Mefodie Raţiu built and described all those chains in *T* closed classes of pseudo-Boolean functions, each of which comprises the constant function 0. In the last 60-70 years an increasing interest was paid for modal logics, that characterizes not only logic operations, but also modalities, as would be "necessity", "possibility", "distinguishes", etc. C. Lewis and K. Gödel formulated the modal calculus, which successfully formalizes these logics. Moreover, K. Gödel, A. Tarski, P.S. Novikov, S Kripke developed the interpretation of modal logics, showing their connections with algebra, topology and foundations of mathematics. The logic *S5* and the logic *S4*, which is closely related with intuitionistic logic and its interpretations, are the most known among the various modal logics. Logics *S4* and *S5* are defined by known logical calculus and are non tabular.

In 1981 Professor Mefodie Raţiu establishied algorithmical undecidability of the expressibility problem in modal logic *S4* and in any its non-locally tabular extension, that is succeeded to demonstrate that neither for the logic *S4* nor for its extensions of the mentioned type expressibility recognition algorithms exist. A few years later he demonstrated the algorithmical undecidability of the expressibility problem in the Gödel-Lob provability logic and in some of its extensions. For this end Professor Mefodie Raţiu created the modeling method of relationship derivation of words in Post's productions systems by the syntactical expressibility relationship in modal logics and provability logics. He, for the first time, launched the concept of non-existence of recognition algorithms of syntactical expressibility in propositional logic calculus and demonstrated the non-existence of such algorithms.

Hence, the new mathematical theories proposed by Professor Mefodie Raţiu from the logical and philosophical points of view are based on fundamental concepts of mathematical logic, theory of algorithms, discrete mathematics, modern algebra, applied mathematics. Therefore, the mathematical theories of Professor Mefodie Raţiu correspond to the modern spirit of Mathematics and Computer Science, embrace both classical branches of mathematical logic and new arose conceptions and problems, as well as offer the richest arsenal of well-elaborated methods of investigations.

Professor Mefodie Raţiu published more than 140 research papers and 4 monographs. Having a good prestige in the world of mathematics, Professor Mefodie Raţiu has been invited at more them 40 prestigious international conferences in Algebra and Mathematical Logic (Russia, Belarus, Ukraine, Poland, Romania, etc). For example, he actively participated in the International Congress of Mathematicians held in Warsaw (1983), at the Eighth International Congress of Logic, Methodology and Philosophy of Science in Moscow (1988), the IV Congress with the same name held in Bucharest (1971), at the 5th Congress of

Romanian Mathematicians held in Piteşti, Romania (2003), the 6th Congress of the same name in Bucharest (2007), International Congress of ARA in Chişinau (1993), Braşov (2007), Sibiu (2009), Bari (2012) and Chişinău (2013). He passionately and skillfully organized in collaboration with his colleagues several national and international conferences on Algebra and Mathematical Logic.

The contribution of Professor Mefodie Raţiu to the education of new generations of highly-qualified mathematicians is enormous. He has trained 8 doctors of sciences and Ph.D's. He had a good influence on his colleagues and former students not only as a mathematician, but as a human being. He was simultaneous a professor of the State University of Moldova.

Professor Mefodie Raţiu was an active member of many state communities and commissions. He was a member of the Chairman Commission of Experts and of the Scientific Council of the Higher Certifying Committee of USSR for the academic degree and rank of the Republic of Moldova (1995-2006), vice-President of ROMAI (1992-2005), Head of the Seminar on Algebra, Mathematical Logic and Theory of Numbers of the Republic of Moldova (2012-2013), President of the Trade Union of AŞM (1999-2005), member of the Trade Union of Education and Science of Moldova and member of the Confederation of Trade Unions of Moldova (2000-2005) etc.

Professor Mefodie Raţiu was awarded the State Prize of the Moldova, the prize "Academician Constantin Sibirschi" (2001), the "Honour Diploma of the AŞM, medal "Distinction in Labour", medal "Dimitrie Cantemir" and order "Glory of Labour".

Professor Mefodie Raţiu was a member of the Moldavian Mathematics Society, American Mathematical Society, of the Editorial Board of the Bulletin of the Academy of Science of Moldova - Mathematics, and of ROMAI Journal.

In 2000 Professor Mefodie Raţiu was elected Corresponding Member of the Academy of Sciences of Republic of Moldova, the highest scientific forum of the Republic of Moldova and the highest recognition which a scholar may receive in the native country. In 2010 Professor Mefodie Raţiu was elected Corresponding Member of the American Romanian Academy of Arts and Sciences.

As a message to the succeeding generations we mention following words of the Academician Octav Mayer "*It is possible to bring for the great disappeared scientists varied homages. Sometimes, the strong wind of progress erases the trace of their steps. To not forget them means to continue their works, connecting them to the living present*", translated in English by Academician Radu Miron in his book "*The Geometry of Mylller Configurations. Applications to Theory of Surfaces and Nonholonomic Manifoldfs*", Ed. Academiei Române, Bucureşti, 2010.

Mitrofan Ciobanu, Ilie Burdujan, Petru Soltan, Vladimir Izbaş, Olga Izbaş, Anca Veronica Ion.

Scientific Publications of Professor Mefodie Raţiu

1. M.T. Ratsa, *About the class of functions of the logic, corresponding to Jaskowski's First matrix*, In: Issled. po Ob. Algebre, Kishinev, 1965, p. 99-110 (in Russian).

2. M.T. Ratsa, *Equivalence criterion of universal algebra to three-element pseudo-Boolean algebra,* VII Vses. Kolloq. po Ob. Algebre, Abs., Kishinev, 1965, p.89-90 (in Russian).

3. M.T. Ratsa, *A criterion for functional completeness in the logic, corresponding to Jaskowski's First matrix*, DAN SSSR 168, nr.3, 1966, p.524-527 (in Russian).

4. M.F. Ratsa, *A test for functional completeness in the logic corresponding to First Jaskowskis matrix*, Soviet Math.Dokl. 7 (1966), p.683-687.

5. M.T. Ratsa, *Questions of functional completeness in the logic, corresponding to Jaskowski's First matrix*, (PhD thesis). Kishinev: AS MSSR, IM, 1967, 120 p. (in Russian).

6. M.T. Ratsa, *Questions of functional completeness in the logic, corresponding to Jaskowski's First matrix*, (PhD thesis's synopsis). RIO AS MSSR, Kishinev, 1967, 11 p. (in Russian).

7. M.T. Ratsa, *About a class of functions of three-valued logic, corresponding to Jaskowski's First matrix*, Problemy Kibernetiki 21, Moscow: Nauka, 1969, p.185-214 (in Russian).

8. M.T. Ratsa, *On functional completeness in some logics, intermediate between classical and intuitionistic*, Mat. Issledovania, v. 5, is. 4, Kishinev, 1970, p.171-176 (in Russian).

9. M.T. Ratsa, *A criterion for functional completeness in a free pseudo-Boolean algebra*, XI Vses, Alg. Koll., Abstracts, Kishinev, 1971, p.267-268 (in Russian).

10. M.T. Ratsa, *A criterion for functional completeness in the intuitionistic propositional logic*, DAN SSSR 201, nr. 4, 1971, p.794-797 (in Russian).

11. M.F. Ratsa, *A criterion for functional completeness in the intuitionistic propositional logic,* Soviet Math. Dokl. 12 (1971), Nr.6, p.1732-1737.

12. A.V. Kuznetsov, M.T. Ratsa, V.I. Gherciu, *An investigation of superintuitionistic logics (functional completeness, finitary approximability and hiperindependence)*, IV-th Intern. Congress for Logic, Methodology and Philosophy of Science, Abs., Bucharest, 1971, p. 32.

13. M.T. Ratsa, *On functional completeness in a family of universal algebras*, XII Vses. Alg. Koll., Abstracts of reports, Notebook , Sverdlovsk, 1973, p. 302 (in Russian).

14. M.T. Ratsa, *On the criterion for functional completeness in the intuitionistic logic*, Tret. Vses. Conf. po Mat. Logike, Abstracts, 2, Novosibirsk, 1974, p.183-185 (in Russian).

15. M.T. Ratsa, *The criterion for functional completeness in S5*, IV Vses. Conf. po Mat. Logike, Abstracts, Kishinev, 1976, p.124 (in Russian).

16. M.T. Ratsa, *About the operations, expressed through pseudo-boolean terms*, XIV Vses. Alg. Conf., Abstracts, 2, Novosibirsk, 1977, p.117-118 (in Russian).

17. M.T. Ratsa, *About some subalgebras of iterative Post algebra of rank 3*, XV Vses. Alg. Conf., Abstracts, 2, Krasnoiarsk, 1979, p. 125 (in Russian).

18. A.V. Kuznetsov, M.T. Ratsa, *The criterion for functional completeness in classical first-order predicate logic*, DAN SSSR 249, nr. 3, 1979, p.540-544 (in Russian).

19. A.V. Kuznetsov, M.T. Ratsa, *The algorithm for recognition of the functional completeness in classical predicate logic*, 5-ia Vses. Conf. po Mat. Logike, Abstracts, Novosibirsk, 1979, p.78 (in Russian).

20. M.T. Ratsa, *The lack of free topo-Boolean algebra the finitary approximability on the functional completeness*, XVI Vses. Alg. Conf., Abstracts, 2, Leningrad, 1981, p.110-111 (in Russian).

21. M.T. Ratsa, *About functional completeness in the intuitionistic propositional logic*, Problemy Kibernetiki, 39, 1982, Moscow: Nauka, p.107-150 (in Russian).

22. M.T. Ratsa, *Non-table of the logic S4 on the functional completeness}, Algebra i logika* 21, nr. 3, 1982, p.283-320 (in Russian).

23. M.T. Ratsa, *The functional completeness in modal logics*, GDR, Rostock. Math. Kolloq., 19, 1982, p .19-28.

24. M.T. Ratsa, *Algorithmic questions about functional constructions in modal logics*, Int. Congress of Mathematician, Abs., v.1, Warsaw, 1982, p.19.

25. M.T. Ratsa, *Unsolvability of the logic S4 on Expressibility*, 6-ia Vses. Conf. po Mat. Logike, Abstracts, Tbilisi, 1982, p.153 (in Russian).

26. M.T. Ratsa, *On functional completeness in modal logics,* Bull. AS MSSR, Ser. Phys. Tecn. and Math. Sci., 2, Kishinev: Ştiinţa, 1983, p.37-39 (in Russian).

27. M.T. Ratsa, *On functional completeness in modal logic S5*, Issled. Po Neclas. Logikam I Formalinym systemam, Moscow: Nauka, 1983, p.222-280 (in Russian).

28. M.T. Ratsa, *Undecidability of the problem of functional expressibility in the modal logic S4*, DAN SSSR 268, nr. 4, 1983, p.814-817 (in Russian).

29. M.F. Ratsa, *Undecidability of the problem of functional expressibility in the modal logic S4*, Soviet Math. Dokl. 27, 1983, nr. 1, p. 182-186.

30. M.T. Ratsa, *The main problems of expressibility of formulas of propositional logics*, (doctoral dissertation), Kishinev: AS MSSR, Inst. of Math., 1983, 273 p. (in Russian).

31. M.T. Ratsa, *The main problems of expressibility of formulas of propositional logics*, (doctoral dissertation's synopsis), Moscow: Moscow State University, Fac. Mech.-Math., 1985, 28 p. (in Russian).

32. V.P. Malai, M.T. Ratsa, *On chain pre-completive sets of pseudo-Boolean algebra operations*, XVIII Vses. Alg. Conf., Abstracts, 2, Kishinev, 1985, p.8 (in Russian).

33. I.V. Cucu, M.T. Ratsa, *The criterion for completeness to implicit reducibility in the Jaskowski's First matrix logic*, 8-ia Vses. Conf. po Mat. Logike, Abstracts, Moscow, 1986, p.96 (in Russian).

34. M.T. Ratsa, *On the completeness of systems of formulas in dual chain logics*, Mat. Issled. 98, Kishinev: Ştiinţa, 1987, p.71-93 (in Russian).

35. M.T. Ratsa, *The main problems of expressibility of formulas in non-classical logics*, Mat. Issled. 98, Kishinev: Ştiinţa, 1987, p.94-120 (in Russian).

36. M.T. Ratsa, *On chain weak completivity in 3-element pseudo-Boolean algebra*, XIX Vses. Alg. Conf., Abstracts, 1, Lvov, 1987, p.235 (in Russian).

37. V.P. Malai, M.T. Ratsa, *About two pre-completive classes of functions of Jaskowski's First matrix logic,* V.I.N.I.T.I., Dep. manuscript nr. 6052-Â87, Ì., 1987, 34 p. (in Russian).

38. M.F. Ratsa, *The problems of expressibility of modal and predicate formulae*, 8 Intern. Congress of Logic, Methodology and Phil. of Sci., Abs., Vol. 1, Moscow, 1987, p. 317-320.

39. I.V. Cucu, M.T. Ratsa, *On the completeness to implicit reducibility in Jaskowski's First matrix logic*, Bull. AS MSSR, Ser. Phys. Tecn. and Math. Sci. 1, Kishinev Ştiinţa, 1988, p.23-28 (in Russian).

40. M.T. Ratsa, *Iterative chain classes of pseudo-boolean functions*, I, V.I.N.I.T.I., Dep. manuscript nr. 4323-88, Ì., 1988, 277 p. (in Russian).

41. A.V. Kuznetsov, M.T. Ratsa, *On sheffer criterion in the intuitionistic logic*, Bull. AS MSSR, Ser. Phys. Tecn. and Math. Sci., nr. 3, Kishinev: Ştiinţa, 1988, p.3-9 (in Russian).

42. M.T. Ratsa, *The criterion of completivity of chain systems pseudo-Boolean functions, containing the constant 0*, 2-ia Vses. Conf. po Prikl. Logike, Abstracts, Novosibirsk, 1988, p.198-199 (in Russian).

43. M.A. Coban, M.T. Ratsa, *The criterion for formulaic completeness in a extension of the logic S4*, 9-ia Vses. Conf. po Mat. Logike, Abstracts, Leningrad, 1988, p.76 (in Russian).

44. M.T. Ratsa, *Iterative chain classes of pseudo-Boolean functions, containing the constant 0,* 9-ia Vses. Conf. po Mat. Logike, Abstracts, Leningrad, 1988, p.138 (in Russian).

45. M.F. Ratsa, *Concerning description of iterative systems of pseudo-Boolean functions*, Intern. Conf. in Computer logic. Papers, Part 1, Tallin, 1988, p. 85-87.

46. M.T. Ratsa, *Questions of the expressibility formulas in logical calculi*, Proceedings of the Workshop on Discrete Math. and Its Applications, Moscow: Publ. Moscow State University, 1989, p.38-44 (in Russian).

47. M.T. Ratsa, *The algorithmic undecidability of the problem of expressibility in modal logics,* Matem. Voprosy kibernetiki 2, Moscow: Nauka, 1989, p. 71-99 (in Russian).

48. M.A. Coban, M.T. Ratsa, *The conditions of completeness of formulas in the logic of 4-element topological Boolean algebra with three open elements*, V.I.N.I.T.I., Dep. manuscript nr. 4299-89, Moscow, 1989, p.1-35 (in Russian).

49. V.P. Malai, M.T. Ratsa, *About one chain class of sectorial functions of Jaskowski's First matrix logic*, Bull. AS MSSR, Ser. Phys. Tech. and Math. Sci. 2, Kishinev, Ştiinţa, 1989, p.9-14 (in Russian).

50. M.A. Coban, M.T. Ratsa, *About formulaic completeness in 4-valued extension of pre-tabular modal logic EM4*, Bull. AS MSSR, Ser. Phys. Tecn. and Math. Sci. 3, Kishinev, Ştiinţa, 1989, p.13-16 (in Russian).

51. M.T. Ratsa, *About chain sub-algebras of Post iterative algebra of pseudo-Boolean functions*, Intern. Conf. on Algebra , Abstracts of talks on the model theory and algebraic systems, Novosibirsk, 1989, p.112 (in Russian).

52. M.T. Ratsa, *Iterative chain classes of pseudo-Boolean functions*, Chişinău, Ştiinţa, 1990, 238 p.

53. M.T. Ratsa, *On the impossibility of an algorithm for the recognition of the expressibility of modal formulae*, Bull. AS MSSR. Mathematics, 1, Chişinău, Ştiinţa, 1990, p. 69-71 (in Russian).

54. V.P. Malai, M.T. Ratsa, *On the bases of the chain classes of pseudo-Boolean functions*, 10-ia Vses. Conf. po Mat. Logike, Abstracts, Alma-Ata, 1990, p.106 (in Russian).

55. M.A. Coban, M.T. Ratsa, *About weak completeness in the logic of 8-element topological Boolean algebra with one open atom*, 10-ia Vses. Conf. po Mat. Logike, Abstracts, Alma-Ata, 1990, p.83 (in Russian).

56. M.T. Ratsa, *Expressibility in the propositional calculi*, Chişinău, Ştiinţa, 1991, 204 p. (in Russian).

57. I.V. Cucu, M.T. Ratsa, *Conditions of parametrical completeness in the logic of 5-element pseudo-Boolean algebra with two incomparable elements,* V.I.N.I.T.I., Dep. manuscript nr. 1887-A91, 1991, 41 p. (in Russian).

58. M.A. Coban, M.T. Ratsa, *About expressibility terms in Post iterative algebras of topological Boolean functions*, Intern. conf. on algebra , Abstracts of talks on the logic and univ. algebra, Novosibirsk, 1991, p.65 (in Russian).

59. M.A. Coban, M.T. Ratsa, *About expressibility terms in topological Boolean algebras*, VI-th Tiraspol Symposium on general topology and its applications, Chişinău, 1991, p. 61-62 (in Romanian).

60. V.P. Malai, M.T. Ratsa, *Two descriptions of classical complete chain systems of pseudo-Boolean functions*, VI-th Tiraspol Symposium on General Topology and its Applications, Chişinău, 1991, p. 132-133 (in Romanian).

61. I.V. Cucu, M.T. Ratsa, *Parametrical completeness in the logic of the simplest pseudo-Boolean algebra with two incomparable elements,* Bull. A.S. R.M. Mathematics, 1 (7), Chişinău, Ştiinţa, 1992, p. 46-51 (in Russian).

62. M.T. Ratsa, *The criterion for completeness with respect to expressibility in the three-valued extension of provability-intuitionistic logic*, V.I.N.I.T.I., Dep. manuscript nr. 1782-A92, Moscow, 1992, 22 p. (in Russian).

63. V.P. Malai, M.T. Ratsa, *Description of chain classically complete systems of pseudo-Boolean functions*, Bull. A.S. R.M. Mathematics, 2 (8), Chişinău, Ştiinţa, 1992, p.15-21 (in Russian).

64. Ya.N. Gkhaliekh, M.T. Ratsa, *The conditions for completeness with respect to expressibility in the simplest non-chain extension of dual-intuitionistic logic*, XI Inter. Conf. on Math. Logic, Abstracts, Kazan, 1992, p. 45 (in Russian).

65. M.A. Coban, M.T. Ratsa, *The criterion for completeness with respect to expressibility in the pretabular modal logic EM4*, XI Inter. Conf. on Math. Logic, Abstracts, Kazan, 1992, p. 76 (in Russian).

66. I.V. Cucu, M.T. Ratsa, *The criterion for parametrical completeness in the logics of pseudo-Boolean chain algebras with a lower thickening*, XI Inter. Conf. on Math. Logic, Abstracts, Kazan, 1992, p. 85 (in Russian).

67. M.T. Ratsa, A.G. Russu, *An example of a countable family of pre-complete classes of formulas in the provability logic*, XI Inter. conf. on math. logic, Abstracts, Kazan, 1992, p. 120 (in Russian).

68. I.V. Cucu, M.T. Ratsa, *The parametrical completeness in 5-valued pseudo-Boolean algebra with two incomparable elements*, Proc. of the Conf. on Algebra, Preprint 1, Babeş-Bolyai Univ., Cluj-Napoca, Romania, 1992, p.23-24.

69. M.T. Ratsa, *Chain systems of pseudo-boolean functions with autodual or linear boolean images,* Proc. of the Conf. on Algebra, Preprint 1, Babeş- Bolyai Univ., Cluj-Napoca, Romania, 1992, p. 107-108.

70. M.A. Coban, M.T. Ratsa, *On functional completeness in 8-element topological Boolean algebra with one open atom*, Proc. of the Conf. on Algebra, Preprint nr. 1, Babeş-Bolyai Univ., Cluj-Napoca, Romania, 1992, p. 51-54.

71. Ya.N. Gkhaliekh, M.T. Ratsa, *On completeness of systems of formulas in the simplest non-chain extension of dual-intuitionistic logic*, V.I.N.I.T.I., Dep. manuscript nr. 2951-A92, Moscow, 1992, 72 p. (in Russian).

72. Ya.N. Gkhaliekh, M.T. Ratsa, *Solution of the problem of completeness with respect to expressibility in a 5-valued non-chain extension of duaity intuitionistic logic*, Bull. A.S. R.M. Mathematics, 4, Conf. on Math. Logic, 1992, p. 43-51 (in Russian).

73. M.A. Coban, M.T. Ratsa, *On weak completeness in Post iterative algebras of topological Boolean functions*, 3-th Intern. Conf. on algebra memory M.I. Kargapolov, Abstracts, Krasnoyarsk, 1993, p. 154-155 (in Russian).

74. M.T. Ratsa, *The analogue of Slupecki's theorem for a family of lattices with two incomparable elements*, 3-th Intern. Conf. on algebra memory M.I. Kargapolov, Abstracts, Krasnoyarsk, 1993, p. 280-281, (in Russian).

75. M.T. Ratsa, A.G. Russu. *The construction of an infinite family of maximal subalgebras of the Post's iterative algebra of diagonalizable algebra functions*, 3-th Intern. Conf. on Algebra, Memory M.I. Kargapolov, Abstracts, Krasnoyarsk, 1993, p. 282-283 (in Russian).

76. O. Covalgiu, M.T. Ratsa, *Modeling of self-dual and commuting with 1 Boolean functions in a 3-valued extension of provability-intuitionistic logic*, Bul. A.S. R.M. Mathematics, Chişinău: Ştiinţa, 2, Conf. on Math. Logic, 1993, p. 72-78, (in Russian).

77. M.A. Coban, M.T. Ratsa, *Criterion of weak completeness in a 8-valued extension of pretabular modal logic EM4*, V.I.N.I.T.I., Dep. manuscript nr. 276-93, Moscow, 1993, 39 p. (in Russian).

78. O. Covalgiu, M.T. Ratsa, *Conditions of modeling of self-dual and commuting with 1 Boolean functions in a 3-valued extension of provability-intuitionistic logic*, V.I.N.I.T.I., Dep. manuscript nr. 2417-93, Moscow, 1993, 45 p. (in Russian).

79. V.P. Malai, M.T.Ratsa, *The bases of the pre-completive chain-systems of pseudo-Boolean functions*, The 18-th Congr. of the American-Romanian Academy of Arts and Sciences, Abs.,vol.2, Chişinău, 1993, p.27.

80. M.A. Coban, M.T. Ratsa, *On completeness concerning expressibility in the logics of topological Boolean algebras with one open element*, The 18-th Congr. of the American-Romanian Academy of Arts and Sciences, Abs., vol. 2, Chişinău,, 1993, p. 12.

81. M.T. Ratsa, *On expressibility in the logical calculus of Hilbert's type*, The 18th Congr. of the American-Romanian Academy of Arts and Sciences, Abs., vol. 2, Chişinău, 1993, p. 34.

82. O. Covalgiu, M.T. Ratsa, *The Modeling of boolean functions in the 3-valued extension of provability-intuitionistic logic*, The 18-th Congr. of the American-Romanian Academy of Arts and Sciences, Abs.,vol. 2, Chişinău, 1993, p. 15.

83. M.A. Coban, M.T. Ratsa, *On the problem of expressibility in propositional modal logics*, Prepar. Conf. for the Congr. of Romanian Mathematicians Everywhere, vol. 1, Bucharest, 1993, p. 63-65 (in Romanian).

84. M.T. Ratsa, A.G. Russu, *Construction of an example of the infinite set of classes of formulas, pre-complete in provability logic*, Prepar. Conf. for the Congr. of Romanian Mathematicians everywhere, vol 2, Bucharest, 1993, p. 56-57 (in Romanian).

85. M.A. Coban, M.T. Rata, *The analogue of Slupecki's theorem in the logic of 8-valued topological Boolean algebras with one open element*, Prepar. Conf. for the Congr. of Romanian Mathematicians everywhere, vol 2, Bucharest, 1993, p. 47-49 (in Romanian).

86. I.V. Cucu, M.T. Ratsa, *Parametrical completeness for the logics of linear ordered algebras with a lower thickening*, Prepar. Conf. for the Congr. of Romanian Mathematicians everywhere, vol 2, Bucharest, 1993, p. 53-54 (in Romanian).

87. M.T. Ratsa, A.G. Russu, *The constructions of a numerable collections of pre-complete classes of formulae in the provability logic*, Bull. A.S. a R.M. Mathematics, 1 (14), Chişinău Ştiinţa, 1994, p. 66-74.

88. M.A. Coban, M.T. Ratsa, *On functional expressibility in topological Boolean algebras with one open element*, Proc. of X-th Nation.Conf. on algebra, Univ. Timişoara, Romania, 1994, p. 67-68.

89. M.T. Ratsa, A.G. Russu, *One infinite consequence of maximal subalgebras of free diagonalizable algebra*, Proc. of the X-th Nation. Conf. on algebra, Univ. Timişoara, Romania, 1994, p. 93-94.

90. I.V. Cucu, M.T. Ratsa, *On completeness relative to implicit reducibility in pseudo-boolean linear ordered algebras*, Proc. of the X-th Nation. Conf. on algebra, Univ. Timişoara, Romania, 1994, p. 45-46.

91. O. Covalgiu, M.T. Ratsa*, On model completeness for the classes of the functions of 3-valued σ-pseudo-Boolean algebra*, Anal. St. ale Univ. "Ovidius", Seria Mat., vol. 2, Constanţa, Romania, 1994, p. 76-79.

92. M.A. Coban, M.T. Ratsa, *About maximal subalgebras of Post's iterative algebras of topological Boolean functions*, National Conf. on Algebra, Abs., Constanţa, Romania, 1994, p. 18 (in Romanian).

93. O. Covalgiu, M.T. Ratsa, *About model completeness in classes of functions of 3-valued σ-pseudo-Boolean algebra*, National Conf. on Algebra, Abs., Constanţa, Romania, 1994, p.20 (in Romanian).

94. M.A. Coban, M.T. Ratsa, *Weak completeness in logics of 4-valued and 8-valued Boolean algebras with one open atom*, Jub. Scien.-Techn. Conf., Tehn. Univ. of Moldova, Chişinău, 1994, p. 151-152. (in Romanian).

95. V.P. Malai, M.T.Ratsa, *On the bases of chain pre-completive classes of pseudo-Boolean functions*, Jub. scien.-techn. conf., Tehn. Univ. of Moldova, Chişinău, 1994, p. 148-149 (in Romanian).

96. M.A. Coban, M.T. Ratsa, *The propositional logic EM4 and its 32-valued extension*, Scien. Simp.: Forming efficient economy by market forces, Publ. of Academy of Economic Studies of Moldova, Chişinău, 1995, p. 153-156 (in Romanian).

97. O. Covalgiu, M.T. Ratsa, *The criterion of Model completeness in the closed classes of 3-valued functions*, Applied and Industrial Math., Abs., Oradea- Chişinău, 1995, p. 13.

98. M.T.Ratsa, *Results of functional completeness in logical calculi*, Bull. A.S. R.M., Mathematics, Chişinău: Ştiinţa, 1996, p. 73-104 (in Romanian).

99. M.A. Coban, M.T. Ratsa, *About derivative operations of 8-element topological Boolean algebra with one open atom*, Symposium Septimum Tiraspolense generalis topologiae et suae applicationum, Publ. „Tehnica", Tehn. Univ. of Moldova, Chişinău, 1996, p. 73 (in Romanian).

100. O. Covalgiu, M.T. Ratsa, *The conditions of model completeness in closed classes of many-valued logic*, Intern. Conf. on Math. And Informatics, Abs., Chişinău, 1996, p. 18 (in Romanian).

101. O. Covalgiu, M.T. Ratsa, *On the existence of a criterion of Model completeness for the closed classes of 3-valued functions*, Bull. A.S. R.M. Mathematics, 3, Chişinău: Ştiinţa, 1997, p. 101-104.

102. I.V. Cucu, M.T. Ratsa, *A criterion for parametrical completeness in logic of the simplest pseudo-Boolean algebra with incomparable elements*, Proceedings of the Workshop on Discrete Math. And Its Applications, Moscow: Publ. House of the Faculty of Mechanics and Mathematics, Moscow State University, 1997, p. 52-53 (in Russian).

103. V.P. Malai, M.T.Ratsa, *On the bases of chain classical complete classes of pseudo-Boolean functions*, Proceedings of the Workshop on Discrete Math. and Its Applications, Moscow: Publ. House of the Faculty of Mechanics and Mathematics, Moscow State University, 1997, p. 55-56 (in Russian).

104. O. Covalgiu, M.T. Ratsa, *A criterion of model completeness for the closed classes of 3-valued logic*, Bul. Sci. of Univ. "Politehnica", Timişoara, Romania, t. 43, nr. 1, 1998, p. 31-34.

105. M.T. Ratsa, *Undecidability of the problem of functional expressibility in the provability logic*, Proceedings of the Intern. Conf. on Math. Logic, dedicated to the 90-th anniversary of A.I. Maltsev, Novosibirsk, 1999, pgs.107-108.

106. M.T. Ratsa, *Undecidable of the expressibility problem in a free diagonalizable algebra*, The second Intern. Conf. on Algebra Ukraine, dedicated to the memory of prof. L.A. Kaluzhnin (1914-1990), Kiev-Vinitza, 1999, p.40-41.

107. M.T. Ratsa, *Undecidability of the expressibility problem in the provability logic of Gödel-Lob*, Bull. Sci., Ser. Math. and Computer Science 3, Univ. of Piteşti, Romania, 1999, p. 399.

108. M.T. Ratsa, *Algoritmical undecidability of the expressibility problem in free diagonalizable algebra*, Bull. of the Polytechnic Inst. of Iaşi, t. XLVI (L), fasc. 1 – 2, Mathematics, Theoretical mechanics, Physics, Romania, 2000, p. 18-22.

109. M.T. Ratsa, A.G. Russu, *Some properties of complete with respect to expressibility systems of formulas in Gödel -Lob provability logic*, Discretnaya Matematica 12, is.4, Moscow, 2000, p.63-82 (in Russian).

110. I.V. Cucu, M.T. Ratsa, *The reduction of parametrical completeness in pseudo-boolean algebras defined on the linear ordered sets completed with 2 atoms*, First Conf. of the Math. Society of the R. Moldova, Abs., Chişinău, 2001, p. 42-43.

111. M.T. Ratsa, *Formal reduction of the general problem of expressibility of formulas in Godel-Lob provability logic*, Discretnaya matematica, v.14, is.2, Moscow: Nauka, 2002, p.95-106 (in Russian).

112. M.T. Ratsa, *Conditions for functional completeness in the simplest extensions of Dual Intuitionistic Logic*, 5th Congress of Romanian Mathematicians, Abs., Piteşti, Romania, 2003, p. 120-121.

113. M.T. Ratsa, *Functional completeness in the simplest extensions of Dual Intuitionistic Logic*, 11th Conf. of Applied and Industrial math., Proc., Oradea, Romania, 2003, p. 190.

114. M. Ciobanu, Anca-Veronica Ion, M. Ratsa, *Professor Adelina Georgescu – profile at the age of 60*, Bull. Sci., Ser. Math. and Computer Science, nr. 9, Univ. of Piteşti, Romania, 2003, p. V – VIII.

115. V. Cebotari, M. Ratsa, *A criterion for implicit reductibility of all the formulas in the 4-valued extension of modal logic S5* , Bull. Sci., Ser. Math. and Computer Science, nr. 9, Univ. of Piteşti, Romania, 2003, p. 73-89 (in Romanian).

116. M.T. Ratsa, *Inexistence of the algorithms for the recognition of syntactical expressibility in the logical calculi*, Publ. The Flower Power, Piteşti, Romania, 2004, 106 p. (in Romanian).

117. V. Cebotari, M. Ratsa, *A completeness to implicit reductibility in the 4-valued extension of modal logic S5*, Second Conf. of Math. Soc. of R.Moldova, Comm., Chişinău, 2004, p. 92-95.

118. M.A. Coban, M.T. Ratsa, *A criterion for functional completeness in some free topological Boolean algebra*, Second Conf. of Math. Soc. of R. Moldova, Comm., Chişinău, 2004, p. 114-115.

119. I. Cucu, M. Ratsa, *On cardinality of the implicit bases in chain super-intuitionistic logics*, Second Conf. of Math. Soc. of R.Moldova, Comm., Chişinău, 2004, p. 121-123.

120. V. Cebotari, M. Ratsa, *Criterion for completeness to implicit reducibility in the logic of 4-elemente boolean topological algebra with two open elements*, 5th Intern. Algebraic Conference in Ukraine, Abs., Odessa, 2005, p. 44.

121. I. Cucu, M. Ratsa, *The lengths of implicit bases on chain pseudo-boolean algebras*, 5th Intern. Algebraic Conference in Ukraine, Abs., Odessa, 2005, p. 54.

122. M.A. Coban, M.T. Ratsa, *Conditions for functional completeness in one pre-tabular extension of Lewis logic S4*, 5th Intern. Algebraic Conference in Ukraine, Abs., Odessa, 2005, p. 53.

123. M.A. Coban, M.T. Ratsa, *Existence of an algorithm for recognition of the completeness with respect to expressibility in modal pre-tabular logic EM4*, Proc. of the 4th Annual Symposium on Mathematics Applied in Biology & Biophysics, Sci. Annals of USAMU, t. XLVIII, vol. 2, Iasi, 2005, p. 389-402.

124. M.T. Ratsa, *Loss of the property to be maximal formula centralizer attached to transition from the logic of first Jaskowsk's matrix to the Intuitionistic logic*, Proc. of the 5th Annual Symposium on Mathematics Applied in Biology & Biophysics, Scientific papers of Univ. of Agricultural Sciences and Veterinary Medicine, t. XLIX, vol. 2, Iaşi, 2006, p. 269-273.

125. M.T. Ratsa, *Disappearence of some parametrical pre-complete systems attached to transition from First Jaskowsk's matrix Logic to the Intuitionistic Logic*, The XIVth Conf. on Applied and Industrial Math., Comm., CAIM 2006, Chişinău, 2006, p. 300-301.

126. M.T. Ratsa, *Research on mathematical logic. Elements of the history of mathematics and mathematics in Moldova*, Tiraspol State Univ., State Univ. of Moldova, Chişinau, 2006, p. 252 – 291 (in Romanian).

127. M.T. Ratsa, *Recursive unsolvability of a problem of expressibility in the Logic of Provability*, ROMAI Journal, vol. 3, Romanian Soc. of Applied and Industrial Math., nr. 1, 2007, p. 185-188.

128. M.T. Ratsa, *Unsolvability of a problem of expressibility in the logic of provability*, The 31st Annual Congress of the American Romanian Academy of Arts and Sciences, Presses Internationals Polytechnique, Transilvania University of Braşov, 2007, p. 487-488.

129. M.T. Ratsa, *Algorithmic Unsovability of a problem of expressibility in the Godel-Lob Logic of Provability*, 6th Congress of Romanian Matematicians, Abs., Bucharest, Romania, 2007, p. 133-134.

130. M.T. Ratsa, *Iterative chain algebras of 3-valued pseudo-Boolean functions*, The 33 rd Annual Congress of the American Romanian Academy of Arts and Sciences (ARA), Alma Mater University of Sibiu, Romania, Proceedings, vol. 2, Polytechnique Intern. Press, Montreal, Quebec, 2009, p. 321-323 (in Romanian).

131. M. T. Raţiu, *Iterative chain algebras of trivalent pseudo-Boolean functions*, Iaşi : Editura Alexandru Myller, 2010. 276 p. ISBN 978-973-88565-3-0. (in Romanian).

132. M. Raţiu, *A maximal iterative algebra of functions of topological Boolean algebra of order 16 with an open atom*, In: The 34th Annual Congress, American Ramanian Academy of Arts and Sciences (ARA), May 18th-23rd, Bucharest, Romania, 2010, Proceedings. Sci. Ed.: FRUNZETI T.; HANGANU M. –Presses
Internationales Polytechnique, Montreal, Quebec, 2010, p. 579-581 (in Romanian).

133. M. Raţiu, I. Cucu, *A criterion for parametrical completeness in the 5-valued non-linear algebraic model of intuitionistic logic*, ROMAI Journal **6**, nr. 1, Bucharest, 2010. p. 153-154.

134. M. Raţiu, An example of maximal iterative algebra of order 16 with 3 open elements, Abstracts of the 18th Conference on Applied and Industrial mathematics, CAIM, 2010, Iaşi, Romania, 2010, p.77.

135. M. Raţiu, *On functional completeness in the Gr. Moisil dual intuitionistic logic*, In: The 35th Annual Congress, American Romanian Academy of Arts and Sciences (ARA), July 6th-11rd, Timişoara, Romania, 2010, Proceedings. Sci. Ed.: IONEL, I.; FLESER, T.; VETRES, I. Presses Internationales Polytechnique, Montreal, Quebec, 2011, p. 301-303.

136. M. Raţiu, *Criterion for functional completeness in the 16 elements algebraic model of pre-tabular EM4 logic*, The 19-th conference on applied and industrial mathematics, CAIM, September 22-25, 2011, Abstracts, Iaşi, Romania, 2011, p. 26-27.

137. M. Raţiu, A. Caşu, Gh. Ciocanu, V. Izbaş, P.Sârbu, Doctoral examen program on specialty 01.01.06- *Mathematical Logic, Algebra and Number Theory* (joint program with St.Univ. of Moldova and Tiraspol St. Univ.), Chişinău, 2011 (in Romanian).

138. M. Raţiu, *Method of the formula realization of algebras and its application in mathematical logic*, Proceedings of The 36th Anual Congress of the American Romanian Academy of Arts and Sciences (ARA). Learing Without Frontiers. Giola del Colle - Bari, Italia, May 30th - June 2nd, 2012. Presses Iternationales Polytechnique, Montréal, Quebec, Canada, 2012, pp. 137-140.

139. M. Raţiu, Expressibility of implication in intuitionistic logic with the method of the formula realization of algebras, In: The 20th Conference on Applied and Industrial Mathematics, CAIM- 2012 (dedicated to academician Mitrofan M. Ciobanu), Chişinău, Republic of Moldova, August 22-25, 2012, Communications, p. 195-196.

140. M. Raţiu, *Applying of the method of the series of matrixes to establish the cardinal of the set of iterative pseudo-boolean algebras*, Proceedings of The 37th Anual Congress of the American Romanian Academy of Arts and Sciences (ARA). The university of European Political and Economic Studies "Constantin Stere",
June 04-09, 2013: Presses Internationales Polytechnique, Montreal, Quebec, Canada, Proceedings.-Chişinau, 2013, pp. 460-462.

141. I. Cucu, M. Raţiu, *The implicit bases for chain pseudo-Boolean algebras*, MITRE-2013, Abstracts, Chişinau, p.36-37.

142. I. Cucu, M. Raţiu, *Criterion for completeness relative to implicit reductibility in the chain super-intuitionistic logics,* In the 21-th Conf. on Applied and Industrial Mathematics, CAIM-2013, Book of Abstracts, Bucharest, Romania, p. 81-82, ISSN 1841-5512.

ROMAI J., v.9, no.2(2013), 1–10

INTRODUCTION TO NEUTROSOPHIC HYPERGROUPS

Adesina Abdul Akeem Agboola[1], Bijan Davvaz[2]
[1] *Department of Mathematics, Federal University of Agriculture, Abeokuta, Nigeria*
[2] *Department of Mathematics, Yazd University, Yazd, Iran*
aaaola2003@yahoo.com, davvaz@yazd.ac.ir

Abstract The objective of this paper is to introduce the concept of *neutrosophic* hypergroup and present some of its elementary properties.

Keywords: neutrosophic group, neutrosophic sub-group, hypergroup, sub-hypergroup, neutrosophic hypergroup, neutrosophic sub-hypergroup.
2010 MSC: 03B60, 20A05, 20N20, 97H40.

1. INTRODUCTION

In 1995, Florentin Smarandache introduced the notion of Neutrosophy as a new branch of philosophy. Neutrosophy is the base of neutrosophic logic which is an extension of the fuzzy logic in which indeterminancy is included. In the neutrosophic logic, each proposition is estimated to have the percentage of truth in a subset T, the percentage of indeterminancy in a subset I, and the percentage of falsity in a subset F. Since the world is full of indeterminancy, several real world problems involving indeterminancy arising from law, medicine, sociology, psychology, politics, engineering, industry, economics, management and decision making, finance, stocks and share, meteorology, artificial intelligence, IT, communication etc can be solved by neutrosophic logic.

2. NEUTROSOPHIC ALGEBRAIC STRUCTURES

Using Neutrosophic theory, Vasantha Kandasamy and Florentin Smarandache introduced the concept of neutrosophic algebraic structures in [12]. Some of the neutrosophic algebraic structures introduced and studied included neutrosophic fields, neutrosophic vector spaces, neutrosophic groups, neutrosophic bigroups, neutrosophic N-groups, neutrosophic semigroups, neutrosophic bisemigroups, neutrosophic N-semigroup, neutrosophic loops, neutrosophic biloops, neutrosophic N-loop, neutrosophic groupoids, neutrosophic bigroupoids and so on. In [13], Vasantha Kandasamy introduced and studied *neutrosophic* rings. In [1], Agboola et al. studied the structure of neutrosophic polynomial rings and in [2], Agboola et al. studied neutrosophic ideals and *neutrosophic* quotient rings. In [3], Agboola et al. studied neutrosophic groups and subgroups.

3. NEUTROSOPHIC GROUPS

Definition 3.1. [12] *Let $(G, \star)$ be any group and let $N(G) = \langle G \cup I \rangle$. The couple $(N(G), \star)$ is called a neutrosophic group generated by G and I under the binary operation $\star$.*

I is called the neutrosophic element with the property $I \star I = I$. I^{-1}, the inverse of I is not defined and hence does not exist.

$N(G)$ is said to be commutative if $a \star b = b \star a$ for all $a, b \in N(G)$.

Theorem 3.1. [12] *Let $N(G)$ be a neutrosophic group. Then,*

(1) $N(G)$ in general is not a group;

(2) $N(G)$ always contain a group.

Definition 3.2. *Let $N(G)$ be a neutrosophic group. Then,*

(1) A proper subset $N(H)$ of $N(G)$, where $H \subset G$, is said to be a neutrosophic subgroup of $N(G)$ if $N(H)$ is a neutrosophic group, that is, $N(H)$ contains a proper subset which is a group;

(2) $N(H)$ is said to be a pseudo neutrosophic subgroup if it does not contain a proper subset which is a group.

Example 3.1. *(1) $(N(\mathbb{Z}), +)$, $(N(\mathbb{Q}), +)$ $(N(\mathbb{R}), +)$ and $(N(\mathbb{C}), +)$ are neutrosophic groups of integer, rational, real and complex numbers, respectively.*

(2) $(\langle\{\mathbb{Q} - \{0\}\} \cup I\rangle, \cdot)$, $(\langle\{\mathbb{R} - \{0\}\} \cup I\rangle, \cdot)$ and $(\langle\{\mathbb{C} - \{0\}\} \cup I\rangle, \cdot)$ are neutrosophic groups of rational, real and complex numbers, respectively.

Example 3.2. [3] *Let $N(G) = \{e, a, b, c, I, aI, bI, cI\}$ be a set, where $a^2 = b^2 = c^2 = e$, $bc = cb = a, ac = ca = b, ab = ba = c$, then $N(G)$ is a commutative neutrosophic group under multiplication since $\{e, a, b, c\}$ is the Klein 4-group. $N(H) = \{e, a, I, aI\}$, $N(K) = \{e, b, I, bI\}$ and $N(P) = \{e, c, I, cI\}$ are neutrosophic subgroups of $N(G)$.*

Theorem 3.2. [3] *Let N(H) be a non-empty proper subset of a neutrosophic group $(N(G), \star)$. Then, N(H) is a neutrosophic subgroup of N(G) if and only if the following conditions hold:*

(1) $a, b \in N(H)$ implies that $a \star b \in N(H)$;

(2) there exists a proper subset A of N(H) such that $(A, \star)$ is a group.

Theorem 3.3. [3] *Let N(H) be a non-empty proper subset of a neutrosophic group $(N(G), \star)$. Then, N(H) is a pseudo neutrosophic subgroup of N(G) if and only if the following conditions hold:*

(1) $a, b \in N(H)$ implies that $a \star b \in N(H)$;

(2) $N(H)$ does not contain a proper subset A such that $(A, \star)$ is a group.

4. HYPERGROUPS

The theory of hyperstructures was introduced in 1934 by Marty [9] at the 8th Congress of Scandinavian Mathematicians. In a classical algebraic structure, the composition of two elements is an element, while in an algebraic hyperstructure, the composition of two elements is a set. Several books have been written on this topic, see [4, 5, 5, 8, 10]. Hyperstructure theory both extends some well-known group results and introduce new topics leading us to a wide variety of applications, as well as to a broadening of the investigation fields. In this part, we present the notion of hypergroup and some well-known related concepts. These concepts will be used in the building of neutrosophic hypergroups, for more details we refer the readers to see [4, 5, 5, 8, 9, 10].

Let H be a non-empty set and $\circ : H \times H \to \mathcal{P}^{\star}(H)$ be a hyperoperation. The couple $(H, \circ)$ is called a *hypergroupoid*. For any two non-empty subsets A and B of H and $x \in H$, we define

$$A \circ B = \bigcup_{a \in A, b \in B} a \circ b, \; A \circ x = A \circ \{x\} \text{ and } x \circ B = \{x\} \circ B.$$

Definition 4.1. *A hypergroupoid $(H, \circ)$ is called a semihypergroup if for all a, b, c of H we have $(a \circ b) \circ c = a \circ (b \circ c)$, which means that*

$$\bigcup_{u \in a \circ b} u \circ c = \bigcup_{v \in b \circ c} a \circ v.$$

A hypergroupoid $(H, \circ)$ is called a quasihypergroup if for all a of H we have $a \circ H = H \circ a = H$. This condition is also called the reproduction axiom.

Definition 4.2. *A hypergroupoid $(H, \circ)$ which is both a semihypergroup and a quasihypergroup is called a hypergroup.*

Definition 4.3. *Let $(H, \circ)$ and $(H', \circ')$ be two hypergroupoids. A map $\phi : H \to H'$, is called*

(1) an inclusion homomorphism if for all x, y of H, we have $\phi(x \circ y) \subseteq \phi(x) \circ' \phi(y)$;

(2) a good homomorphism if for all x, y of H, we have $\phi(x \circ y) = \phi(x) \circ' \phi(y)$.

Let $(H, \circ)$ be a semihypergroup and R be an equivalence relation on H. If A and B are non-empty subsets of H, then

$$\begin{aligned} A\overline{R}B \text{ means that } &\forall a \in A, \exists b \in B \text{ such that } aRb \text{ and} \\ &\forall b' \in B, \exists a' \in A \text{ such that } a'Rb'; \\ A\overline{\overline{R}}B \text{ means that } &\forall a \in A, \forall b \in B, \text{ we have } aRb. \end{aligned}$$

Definition 4.4. *The equivalence relation ρ is called*

(1) regular on the right (on the left) if for all x of H, from $a\rho b$, it follows that $(a \circ x)\overline{\rho}(b \circ x)$ ($(x \circ a)\overline{\rho}(x \circ b)$ respectively);

(2) strongly regular on the right (on the left) if for all x of H, from aρb, it follows that $(a \circ x)\overline{\overline{\rho}}(b \circ x)$ *(*$(x \circ a)\overline{\overline{\rho}}(x \circ b)$ *respectively);*

(3) ρ *is called regular (strongly regular) if it is regular (strongly regular) on the right and on the left.*

Theorem 4.1. . *Let* $(H, \circ)$ *be a semihypergroup and* ρ *be an equivalence relation on H.*

(1) *If* ρ *is regular, then* H/ρ *is a semihypergroup, with respect to the following hyperoperation:* $\overline{x} \otimes \overline{y} = \{\overline{z} \mid z \in x \circ y\}$*;*

(2) *If the above hyperoperation is well defined on* H/ρ*, then* ρ *is regular.*

Corollary 4.1. *If* $(H, \circ)$ *is a hypergroup and* ρ *is an equivalence relation on H, then R is regular if and only if* $(H/\rho, \otimes)$ *is a hypergroup.*

Theorem 4.2. *Let* $(H, \circ)$ *be a semihypergroup and* ρ *be an equivalence relation on H.*

(1) *If* ρ *is strongly regular, then* H/ρ *is a semigroup, with respect to the following operation:* $\overline{x} \otimes \overline{y} = \{\overline{z} \mid z \in x \circ y\}$*;*

(2) *If the above operation is well defined on* H/ρ*, then* ρ *is strongly regular.*

Corollary 4.2. *If* $(H, \circ)$ *is a hypergroup and* ρ *is an equivalence relation on H, then* ρ *is strongly regular if and only if* $(H/\rho, \otimes)$ *is a group.*

Definition 4.5. *Let* $(H, \circ)$ *is a semihypergroup and A be a non-empty subset of H. We say that A is a complete part of H if for any nonzero natural number n and for all* $a_1, \ldots, a_n$ *of H, the following implication holds:*

$$A \cap \prod_{i=1}^{n} a_i \neq \emptyset \implies \prod_{i=1}^{n} a_i \subseteq A.$$

Theorem 4.3. *If* $(H, \circ)$ *is a semihypergroup and R is a strongly regular relation on H, then for all z of H, the equivalence class of z is a complete part of H.*

5. NEUTROSOPHIC HYPERGROUPS

Definition 5.1. *Let* $(H, \star)$ *be any hypergroup and let* $< H \cup I >= \{x = (a, bI) : a, b \in H\}$*. The couple* $N(H) = (< H \cup I >, \star)$ *is called a neutrosophic hypergroup generated by H and I under the hyperoperation* $\star$*. The part a is called the non-neutrosophic part of x and the part b is called the neutrosophic part of x.*

If $x = (a, bI)$ *and* $y = (c, dI)$ *are any two elements of* $N(H)$*, where* $a, b, c, d \in H$*, we define* $x \star y = (a, bI) \star (c, dI) = \{(u, vI) \mid u \in a \star c,\ v \in a \star d \cup b \star c \cup b \star d\} = (a \star c, (a \star d \cup b \star c \cup b \star d)I)$*. Note that* $a \star c \subseteq H$ *and* $(a \star d \cup b \star c \cup b \star d) \subseteq H$*.*

Definition 5.2. *Let $N(H)$ be a neutrosophic hypergroup and let $N(K)$ be a proper subset of $N(H)$. Then,*

(1) $N(K)$ is said to be a neutrosophic sub-hypergroup of $N(H)$ if $N(K)$ is a neutrosophic hypergroup, that is, $N(K)$ must contain a proper subset which is a hypergroup;

(2) $N(K)$ is said to be a pseudo neutrosophic sub-hypergroup of $N(H)$ if $N(K)$ is a neutrosophic hypergroup which contains no proper subset which is a hypergroup.

Theorem 5.1. *Let $N(H)$ be a neutrosophic hypergroup. Then, $N(H)$ is a semihypergroup.*

Proof. Let $x = (a, bI),\ y = (c, dI),\ z = (e, fI)$ be arbitrary elements of $N(H)$, where $a, b, c, d, e, f \in H$. Then,

$$\begin{aligned} x \star y &= (a, bI) \star (c, dI) \\ &= \{(u, vI) \mid u \in a \star c,\ v \in a \star d \cup b \star c \cup b \star d\} \\ &= (a \star c, (a \star d \cup b \star c \cup b \star d)I) \\ &\subseteq N(H). \end{aligned}$$

Hence, $(N(H), \star)$ is a hypergroupoid.

Next,

$$\begin{aligned} x \star (y \star z) &= (a, bI) \star ((c, dI) \star (e, fI)) \\ &= (a, bI) \star (c \star e, (c \star f \cup d \star e \cup d \star f)I)) \\ &= (a \star (c \star e), ((a \star (c \star f)) \cup (a \star (d \star e)) \cup (a \star (d \star f)) \cup (b \star (c \star e)) \\ &\quad \cup (b \star (c \star f)) \cup (b \star (d \star e)) \cup (b \star (d \star f)))I) \\ &= ((a \star c) \star e, (((a \star c) \star f) \cup ((a \star d) \star e) \cup ((a \star d) \star f) \cup ((b \star c) \star e) \\ &\quad \cup ((b \star c) \star f) \cup ((b \star d) \star e) \cup ((b \star d) \star f))I) \\ &= ((a, bI) \star (c, dI)) \star (e, fI) \\ &= (x \star y) \star z. \end{aligned}$$

Accordingly, $(N(H), \star)$ is a semihypergroup. ∎

Lemma 5.1. *Let $N(H)$ be a neutrosophic hypergroup. Then, $x \star N(H) = N(H) \star x \subset N(H)$ for all $x = (a, bI) \in N(H)$.*

Proof. We have

$$\begin{aligned} x \star N(H) &= (a, bI) \star N(H) \\ &= (a, bI) \star \{(h_1, h_2 I) : h_1, h_2 \in H\} \\ &= \{(a \star h_1, (a \star h_2 \cup b \star h_1 \cup b \star h_2)I) : a, b, h_1, h_2 \in H\} \\ &= \{(u, vI) : u \in a \star h_1, v \in (a \star h_2 \cup b \star h_1 \cup b \star h_2)\} \\ &\subset N(H) \end{aligned}$$

Similarly, $N(H) \star x \subset N(H)$ and therefore, $x \star N(H) = N(H) \star x \subset N(H)$. ∎

Theorem 5.2. *If $N(H)$ is a neutrosophic hypergroup, then*

(1) $N(H)$ in general is not a hypergroup;

(2) $N(H)$ always contain a hypergroup.

Proof. (1) Follows directly from Theorem 5.3 and Lemma 5.4.
(2) Follows from the definition of a *neutrosophic* hypergroup. ∎

Example 5.1. *Let $H = \{a, b, (a, aI), (a, bI), (b, aI), (b, bI)\}$ be a set and let $\star$ be a hyperoperation on H defined in the table below.*

$\star$	a	b	(a, aI)	(a, bI)	(b, aI)	(b, bI)
a	a	b	(a, aI)	(a, bI)	(b, aI)	(b, bI)
b	b	a b	(b, bI)	(b, aI) (b, bI)	(a, bI) (b, bI)	(a, aI) (a, bI) (b, aI) (b, bI)
(a, aI)	(a, aI)	(b, bI)	(a, aI)	(a, aI) (a, bI)	(b, aI) (b, bI)	(b, bI)
(a, bI)	(a, bI)	(b, aI) (b, bI)	(a, aI) (a, bI)	(a, aI) (a, bI)	(b, aI) (b, bI)	(b, aI) (b, bI)
(b, aI)	(b, aI)	(b, bI) (a, bI)	(b, aI) (b, bI)	(b, aI) (b, bI)	(a, aI) (a, bI) (b, aI) (b, bI)	(a, aI) (a, bI) (b, aI) (b, bI)
(b, bI)	(b, bI)	(a, aI) (a, bI) (b, aI) (b, bI)	(b, bI)	(b, aI) (b, bI)	(a, aI) (a, bI) (b, aI) (b, bI)	(a, aI) (a, bI) (b, aI) (b, bI)

It is clear from the table that $(H, \star)$ is a neutrosophic hypergroup since it contains a proper subset $\{a, b\}$ which is a hypergroup under $\star$.

Theorem 5.3. *Let $(N(H), \star_1)$ and $(N(K), \star_2)$ be any two neutrosophic hypergroups. Then, $(N(H) \times N(K), \star)$ is a neutrosophic hypergroup, where*

$$(x_1, x_2)\star(y_1, y_2) = \{(x, y) : x \in x_1\star_1 y_1, y \in x_2\star_2 y_2, \ \forall\, (x_1, x_2), (y_1, y_2) \in N(H)\times N(K)\}.$$

Theorem 5.4. *Let $(N(H), \star)$ be a neutrosophic hypergroup and let $(K, \circ)$ be a hypergroup. Then, $(N(H) \times K, \star')$ is a neutrosophic hypergroup, where*

$$(h_1, k_1) \star' (h_2, k_2) = \{(h, k) : h \in h_1 \star h_2, k \in k_1 \circ k_2, \ \forall\ (h_1, k_1), (h_2, k_2) \in N(H) \times K\}.$$

Definition 5.3. *Let $(N(H_1), \star_1)$ and $(N(H_2), \star_2)$ be any two neutrosophic hypergroups and let $f : N(H_1) \to N(H_2)$ be a map. Then,*

(a) f is called a homomorphism if:
(1) for all x, y of $N(H_1)$, $f(x \star_1 y) \subseteq f(x) \star_2 f(y)$,
(2) $f(I) = I$.

(b) f is called a good homomorphism if:
(1) for all x, y of $N(H_1)$, $f(x \star_1 y) = f(x) \star_2 f(y)$,
(2) $f(I) = I$.

(c) f is called an isomorphism if f is a homomorphism and f^{-1} is also a homomorphism.

(d) f is called a 2-homomorphism if for all x, y of $N(H_1)$,

$$f^{-1}(f(x) \star_2 f(y)) = f^{-1}(f(x \star_1 y)).$$

(e) f is called an almost strong homomorphism if for all x, y of $N(H_1)$,

$$f^{-1}(f(x) \star_2 f(y)) = f^{-1}(f(x)) \star_1 f^{-1}(f(y)).$$

Definition 5.4. *Let $N(K)$ be a neutrosophic sub-hypergroup of a neutrosophic hypergroup $(N(H), \star)$. Then,*

(1) $N(K)$ is said to be closed on the left (right) if for all $k_1, k_2 \in N(K)$, $x \in N(H)$ we have $k_2 \in x \star k_1$ ($k_2 \in k_1 \star x$) implies that $x \in N(K)$;

(2) $N(K)$ is said to be ultraclosed on the left (right) if for all $x \in N(H)$ we have $x \star N(K) \cap x \star (N(H) \backslash N(K)) = \emptyset (N(K) \star x \cap (N(H) \backslash N(K)) \star x = \emptyset)$;

(3) $N(K)$ is said to be left (right) conjugable if $N(K)$ is left (right) closed and if for all $x \in N(H)$, there exists $h \in N(H)$ such that $x \star h \subseteq N(K)$ ($h \star x \subseteq N(K)$);

(4) $N(K)$ is said to be (closed, ultraclosed, conjugable) if it is left and right (closed, ultraclosed, conjugable).

Lemma 5.2. *Let $N(K)$ be a neutrosophic sub-hypergroup of a neutrosophic hypergroup $(N(H), \star)$. For all $x \in N(H)$, we have*

(1) $x \star N(K) \subset N(H)$;

(2) $x \star (N(H) \backslash N(K)) \subset N(H)$;

(3) $x \star N(K) \cup x \star (N(H) \backslash N(K)) \subset N(H)$.

Lemma 5.3. *Let $N(K)$ be a neutrosophic sub-hypergroup of a neutrosophic hypergroup $(N(H), \star)$. For all $x \in N(K)$, we have*

(1) $x \star N(K) \subset N(K)$,

(2) $x \star (N(H) \backslash N(K)) \subset N(K)$;

(3) $x \star N(K) \cup x \star (N(H) \backslash N(K)) \subset N(H)$.

Theorem 5.5. *Let $N(K)$ be a neutrosophic sub-hypergroup of a neutrosophic hypergroup $(N(H), \star)$. Then,*

(1) $N(K) \star N(K) \subset N(K)$;

(2) $N(K) \star (N(H) \backslash N(K)) \subset N(K)$.

Theorem 5.6. *Let $N(K)$ be a neutrosophic sub-hypergroup of a neutrosophic hypergroup $(N(H), \star)$. If $N(K)$ is conjugable then it is not ultraclosed.*

Proof. Suppose that $N(K)$ is conjugable. Then, $N(K)$ is closed and for all $x \in N(H)$, there exists $y \in N(H)$ such that $x \star y \subseteq N(K)$ and $y \star x \subseteq N(K)$. Let $B = N(K) \cap (N(H) \backslash N(K))$ so that

$$\begin{aligned} x \star B &= x \star N(K) \cap x \star (N(H) \backslash N(K)) \\ &\subset N(H) \cap N(H) \\ &= N(H). \end{aligned}$$

This shows that $B \neq \emptyset$ and thus, $N(K)$ is not left ultraclosed. Similarly, it can be shown that $N(K)$ is not right ultraclosed. Hence, $N(K)$ is not ultraclosed. ∎

Theorem 5.7. *Let $(N(H_1), \star_1)$ and $(N(H_2), \star_2)$ be any two neutrosophic hypergroups and let $f : N(H_1) \to N(H_2)$ be a map.*

(1) If f is a bijective homomorphism, then f is an isomorphism if and only if it is good.

(2) If f is a strong homomorphism, then it is almost strong.

(3) If f is a good homomorphism and $N(K)$ is a neutrosophic(pseudo neutrosophic) sub-hypergroup of $N(H_1)$, then $f(N(K))$ is a neutrosophic(pseudo neutrosophic) sub-hypergroup of $N(H_2)$.

Theorem 5.8. *Let $(N(H), \star)$ be a neutrosophic hypergroup and let ρ be an equivalence relation on $N(H)$.*

(1) If ρ is regular, then $N(H)/\rho$ is a neutrosophic hypergroup.

(2) If ρ is strongly regular, then $N(H)/\rho$ is a neutrosophic group.

Proof. The proof follows from Theorem 4.7 and Corollary 4.8. ∎

Theorem 5.9. *Let $(N(H), \star)$ be a neutrosophic hypergroup and let ρ be a regular equivalence relation on $N(H)$. Then, the map $\phi : N(H) \to N(H)/\rho$ defined by $\phi(x) = \overline{x}$ is not a homomorphism (good homomorphism).*

Proof. It is clear since $I \in N(H)$ but $\phi(I) \neq I$. ∎

Theorem 5.10. *Let $(N(H), \star)$ be a neutrosophic hypergroup and let ρ be a strongly regular equivalence relation on $N(H)$. Then, for all $x \in N(H)$, $\overline{x}$ is a complete part of $N(H)$.*

6. CONCLUSION

In this paper, we have extended *neutrosophic* theory to hypergroup theory. Basic properties of *neutrosophic* hypergroups were presented and it was shown that every hypergroup is contained in a *neutrosophic* hypergroup but generally, a *neutrosophic* hypergroup is not a hypergroup.

Acknowledgement: The authors are grateful to the anonymous referee for valuable suggestions.

References

[1] A.A.A. Agboola, A.D. Akinola, O.Y. Oyebola, *Neutrosophic Rings I*, Int. J. of Math. Comb., **4**(2011), 1-14.

[2] A.A.A. Agboola, E.O. Adeleke, S.A. Akinleye, *Neutrosophic Rings II*, Int. J. of Math. Comb., **2**(2012), 1-8.

[3] A.A.A. Agboola, A.O. Akwu, Y.T. Oyebo, *Neutrosophic Groups and Neutrosophic Subgroups*, Int. J. of Math. Comb., **3**(2012), 1-9.

[4] P. Corsini, *Prolegomena of Hypergroup Theory*, Second edition, Aviain editore, 1993.

[5] P. Corsini, V. Leoreanu, *Applications of Hyperstructure Theory, Advances in Mathematics*, Kluwer Academic Publishers, Dordrecht, 2003.

[6] B. Davvaz, *Polygroup Theory and Related Systems*, World Sci. Publ., 2013.

[7] B. Davvaz, A. Dehghan Nezad, M.M. Heidari, *Inheritance examples of algebraic hyperstructures*, Information Sciences, **224**(2013), 180-187.

[8] B. Davvaz, V. Leoreanu-Fotea, *Hyperring Theory and Applications*, International Academic Press, USA, 2007.

[9] F. Marty, *Sur une Generalization de la Notion de Groupe*, 8th Congress Math. Scandinaves, Stockholm, Sweden,1934, 45-49.

[10] Vougiouklis, T., *Hyperstructures and Their Rrepresentations*, Hadronic Press, Inc, 115, Palm Harber, USA, 1994.

[11] F. Smarandache, *A Unifying Field in Logics: Neutrosophic Logic, Neutrosophy, Neutrosophic Set, Neutrosophic Probability*, (3rd edition), American Research Press, Rehoboth,2003, http://fs.gallup.unm.edu/eBook-Neutrosophic4.pdf.

[12] W.B. Vasantha Kandasamy, F. Smarandache, *Some Neutrosophic Algebraic Structures and Neutrosophic N-Algebraic Structures*, Hexis, Phoenix, Arizona, 2006, http://fs.gallup.unm.edu/NeutrosophicN-AlgebraicStructures.pdf.

[13] W.B. Vasantha Kandasamy, F. Smarandache, Neutrosophic Rings, Hexis, Phoenix, Arizona, 2006, http://fs.gallup.unm.edu/NeutrosophicRings.pdf.

ROMAI J., v.9, no.2(2013), 11–25

STIFFNESS OF THE LINEAR DIFFUSION AND WAVE-TYPE PARTIAL DIFFERENTIAL EQUATIONS

Elisabete Alberdi Celaya[1], Juan José Anza Aguirrezabala[2]
[1,2] *Department of Applied Mathematics,*
[1] *EUIT de Minas y Obras Públicas,* [2] *ETS de Ingeniería de Bilbao,*
[1,2] *Universidad del País Vasco UPV/EHU, Bilbao (Spain),*
elisabete.alberdi@ehu.es, juanjose.anza@ehu.es

Abstract After applying the Finite Element Method (FEM) to the one-dimensional diffusion-type and wave-type Partial Differential Equations (PDEs) with boundary conditions and initial conditions, a first order and a second order ODE systems are obtained respectively. The latter can be reduced to a first order ODE system. These first order ODE systems usually present high stiffness, so numerical methods with good stability properties are required in their resolution. In this paper, we have studied the stiffness of the resulting first order ODE systems as function of the number of elements considered in the discretization, the length of the domain in which the PDE is applied and the thermal diffusivity (in the case of the diffusion-type PDE) and the wave speed propagation (in the case of the wave-type PDE).

Keywords: Diffusion and wave equations, ODEs, stiffness, FEM.
2010 MSC: 65L05, 65N30.

1. INTRODUCTION

We will consider the diffusion equation (or heat equation) and the wave equation given in terms of Partial Differential Equations (PDEs). In the case of the diffusion equation, we will consider a thin rod of length L. We will assume that the ends of the rod are kept at the same fixed temperature. Let $u(x,t)$ represent the temperature at the point x along the rod at time t, and assume that an initial temperature distribution $u(x,0) = f(x)$ is given. The following PDE is used to model the one-dimensional linear temperature evolution:

- Diffusion equation:
$$\begin{cases} u_t = \alpha^2 u_{xx}, & 0 < x < L,\ t > 0 \\ BC : u(0,t) = 0 = u(L,t), & t > 0 \\ IC : u(x,0) = f(x), & 0 \le x \le L \end{cases} \tag{1}$$

where $\alpha^2 = \frac{k}{c\rho}$ is the thermal diffusivity, k the thermal conductivity, c the thermal capacity and ρ the density, u_t is the rate of change in temperature with respect to time, u_{xx} is the concavity of the temperature profile which compares the temperature of one point to the temperature at neighbouring points. BC and IC are the boundary conditions and the initial conditions respectively.

In the case of the wave equation, a string of length L will be considered, where its two ends held fixed at height zero. Assume that its initial position and speed are given, $f(x)$ and $g(x)$ respectively. Let $u(x,t)$ denote the vertical displacement of the string from the x axis in time t. It is assumed that the string is undergoing small amplitude transverse vibrations so that $u(x,t)$ obeys the wave equation. The one-dimensional linear wave equation with boundary conditions (BC) and initial conditions (IC) is given by:

$$\text{▪ Wave equation: } \begin{cases} u_{tt} = \alpha^2 u_{xx}, & 0 < x < L,\ t > 0 \\ BC : u(0,t) = 0 = u(L,t), & t > 0 \\ IC : u(x,0) = f(x), u_t(x,0) = g(x), & 0 \le x \le L \end{cases} \tag{2}$$

where $\alpha = \sqrt{\frac{T}{\rho}}$ is the speed propagation of the wave, T is the applied tension in the string and ρ the linear mass density.

The continuous solution of both equations, (1) and (2), can be found using the method of separation of variables [6]. The solution of the diffusion equation (1) is given by:

$$u(x,t) = \sum_{k=1}^{\infty} A_k \sin\left(\frac{k\pi x}{L}\right) e^{-(k\pi\alpha)^2 t} \tag{3}$$

where $A_k = \frac{2}{L}\int_0^L f(x)\sin\left(\frac{k\pi x}{L}\right)dx$.

And the solution of the wave equation (2) is given by:

$$u(x,t) = \sum_{k=1}^{\infty} \sin\left(\frac{k\pi x}{L}\right)\left[A_k \sin\left(\frac{k\pi\alpha t}{L}\right) + B_k \cos\left(\frac{k\pi\alpha t}{L}\right)\right] \tag{4}$$

where A_k and B_k are given by: $\begin{cases} A_k = \frac{2}{k\pi\alpha}\int_0^L g(x)\sin\left(\frac{k\pi x}{L}\right)dx \\ B_k = \frac{2}{L}\int_0^L f(x)\sin\left(\frac{k\pi x}{L}\right)dx \end{cases}$

It is also possible to find the approximate solutions of equations (1) and (2) numerically using the Finite Element Method (FEM), in which the process of finding the solution $u(x,t)$ consists of discretizing the domain L in elements and nodes. The solution approach is based on the elimination of the spatial derivatives of the PDE and this leads to a system of Ordinary Differential Equations (ODEs). The resulting system of ODEs can be solved using standard numerical methods [2], such as Runge-Kutta methods [3], Backward Differentiation Formulae [8], or using the ode solvers implemented in MATLAB [1]. The *ode45*, based on an embedded Runge-Kutta method DOPRI(5,4) [5], and the *ode15s*, based on BDFs [8], are two of the ode solvers offered by MATLAB.

The ODE system that results after the FEM discretization presents high stiffness usually. Stiffness is a delicate as well as important concept when solving ODEs. Various authors [12, 14, 15] agree saying that there is no a rigorous definition of stiffness.

It depends on the ODE, on its initial conditions, on the numerical method used for its resolution and on the time interval in which the ODE is solved. In this article we will use the definition of stiffness given in [10, 13], which says that stiffness occurs when different magnitude eigenvalues exist in the solution, where this difference in the magnitude could happen in the real part or in the imaginary part of the eigenvalues. The aim of this article is to study the stiffness of the ODE system which results after the FEM discretization of the one-dimensional diffusion and wave PDEs.

The article is organized as follows: in Section (2) the formulation of the Finite Element Method is given which enables us to obtain an ODE system from a PDE; in Sections (3) and (4) the study of the stiffness of the resulting ODE system is done and in Section (5) some conclusions are given.

2. THE FINITE ELEMENT METHOD

The Finite Element Method consists of finding solutions in a finite dimensional space. Having chosen a basis of functions and having defined finite dimensional subspaces, the PDE solution is written as linear combination of the functions of the basis. To do this it is necessary to check that the scalar product of the differential operator with all the functions of the subspace is zero. This requires a variational formulation of the problem, which is obtained by integrating by parts.

2.1. APPLICATION OF THE FEM METHOD TO THE DIFFUSION EQUATION

We will show the application of the Finite Element Method to the diffusion PDE (1). A step size $h > 0$ of the spatial mesh will be considered, being $h = L/(n+1)$ where $n \in \mathbb{N}$. In this way the partition defined by the nodes:

$$x_j = jh,\ j = 0, 1, ..., (n+1) \tag{5}$$

breaks up the spatial interval $[0, L]$ in $(n+1)$ subintervals of length h: $I_j = \left[x_j, x_{j+1}\right]$, $j = 0, ..., n$. Observe that the first and the last nodes correspond to the end of the interval $[0, L]$: $x_0 = 0$, $x_{n+1} = L$.

Each internal node x_j, $j = 1, ..., n$, is associated a piecewise continuous and linear basis function $N_j(x)$, that verifies $N_j(x_i) = \delta_{ji}$ for $j = 1, ..., n$ and $i = 0, ..., (n+1)$, being δ the Kronecker delta. Next, we introduce the vectorial subspace of dimension n spanned by the functions $\left\{N_j\right\}_{j=1,...,n}$:

$$V_h = span\left\{N_j : j = 1, ..., n\right\} \tag{6}$$

Approximate solutions of the diffusion PDE (1) in the subspace $C([0, \infty), V_h)$ are found so that:

$$u(x,t) \approx u_h(x,t) = \sum_{j=1}^{n} d_j(t) N_j(x) \tag{7}$$

Observe that function (7) depends on the spatial variable x as well as on the temporary variable t. The function (7) will be univocally defined if its coefficients $d_j(t)$ are defined precisely. It has to be taken into account that because of the election of the basis functions $\left\{N_j\right\}_{j=1,\ldots,n}$, $d_j(t)$ is the value of the function $u_h(x,t)$ in the point $x = x_j$.

The weak formulation to calculate the approximate solution u_h is given by [11]:

find $u_h \in C^1([0,\infty); V_h)$ *that verifies:*

$$\int_0^L u_{h,t}(x,t) w_h(x) dx = -\int_0^L \alpha^2 u_{h,x}(x,t) w_h'(x) dx,\ t > 0,\ \forall w_h \in V_h \tag{8}$$

and the initial condition:

$$u_h(x,0) = f_h(x),\ 0 \le x \le L. \tag{9}$$

In (9) an initial value $u_{h,0}$ has been taken. This value can be taken in different ways in order to approximate the initial value u_0 of the diffusion equation. One of the simplest ways to chose f_h is as the orthogonal projection of u_0 in V_h.

By substituting the expression (7) of $u_h(x,t)$ and its derivative $u_h'(x,t)$ in (8), and applying this equality for all the functions N_i of the basis, the following system of n first order Ordinary Differential Equations is obtained:

$$\sum_{j=1}^{n} \left(\underbrace{\int_0^L N_i(x) N_j(x) dx}_{m_{ij}} \right) d_j'(t) = -\sum_{j=1}^{n} \left(\underbrace{\int_0^L \alpha^2 N_i'(x) N_j'(x) dx}_{k_{ij}} \right) d_j(t),$$

$$i = 1, 2, ..., n \tag{10}$$

which in matricial form can be written as:

$$\begin{cases} M\mathbf{d}'(t) = -K\mathbf{d}(t) \\ \mathbf{d}(0) = (f(x_1), ..., f(x_n))^T \end{cases} \tag{11}$$

where $M = (m_{ij})$ and $K = (k_{ij})$ are the mass and stiffness matrices of the FEM discretization, and $d_j(t)$, $j = 1, ..., n$, are the unknowns.

2.2. APPLICATION OF THE FEM METHOD TO THE WAVE EQUATION

The same partition $\left\{x_j\right\}_{j=1,\ldots,n}$ as in the previous section, being $x_j = jh$ the nodes of the interval $[0, L]$ will be considered, where $h = L/(n+1)$, and $I_j = [x_j, x_{j+1}]$, $j = 0, ..., n$, the elements in which the whole interval $[0, L]$ has been partitioned. In

this case the variational formulation to calculate the approximate solution u_h is given by:

find $u_h \in C^2([0,\infty); V_h)$ *that verifies:*

$$\int_0^L u_{h,tt}(x,t)w_h(x)dx = -\int_0^L \alpha^2 u_{h,x}(x,t)w_h'(x)dx,\ t>0,\ \forall w_h \in V_h \tag{12}$$

and the initial conditions:

$$u_h(x,0) = f_h(x),\ \ u_h'(x,0) = g_h(x),\ 0 \le x \le L \tag{13}$$

where f_h and g_h *are approximations of the initial conditions* (f,g) *in* V_h.

Proceeding as before, a second order ODE system is obtained:

$$\sum_{j=1}^{n}\left(\underbrace{\int_0^L N_i(x)N_j(x)dx}_{m_{ij}}\right)d_j''(t) = -\sum_{j=1}^{n}\left(\underbrace{\int_0^L \alpha^2 N_i'(x)N_j'(x)dx}_{k_{ij}}\right)d_j(t),$$

$$i = 1,2,...,n \tag{14}$$

which in matricial form can be written using the mass $M = (m_{ij})$ and stiffness matrices $K = (k_{ij})$ of the FEM:

$$\begin{cases} M\mathbf{d}''(t) = -K\mathbf{d}(t) \\ \mathbf{d}(0) = (f(x_1),...,f(x_n))^T,\ \mathbf{d}'(0) = (g(x_1),...,g(x_n))^T \end{cases} \tag{15}$$

and $d_j(t)$, $j = 1,...,n$ are the unknowns. Equation (15) can be reduced to a first order ODE system with the form $y' = f(t,y)$:

$$\begin{pmatrix} \mathbf{y}_1'(t) \\ \mathbf{y}_2'(t) \end{pmatrix} = \begin{pmatrix} 0 & I \\ -M^{-1}K & 0 \end{pmatrix}\begin{pmatrix} \mathbf{y}_1(t) \\ \mathbf{y}_2(t) \end{pmatrix}, \tag{16}$$

where: $\begin{cases} \mathbf{y}_1(t) = \mathbf{d}(t),\ \mathbf{y}_2(t) = \mathbf{d}'(t) \\ \mathbf{y}_1(0) = \mathbf{d}(0),\ \mathbf{y}_2(0) = \mathbf{d}'(0) \end{cases}$.

3. STIFFNESS OF THE DIFFUSION PDE

We will consider the one-dimensional heat equation given by (1). In the previous section we have seen that the FEM discretization of this equation with $(n+2)$ nodes and $(n+1)$ elements leads to a system of ODEs which in the form $y' = f(t,y)$ is given by (11):

$$\mathbf{d}'(t) = -M^{-1}K\mathbf{d}(t),\ \ \mathbf{d}(0) = \mathbf{d}_0 = (f(x_1),...,f(x_n))^T$$

In this section the stiffness of the system (11) is studied, which means that the eigenvalues of the jacobian matrix $\frac{\partial \mathbf{f}}{\partial \mathbf{d}} = -M^{-1}K$ are studied depending on three variables: the number of elements of the discretization, the length of the rod L and the thermal diffusivity α^2.

3.1. STIFFNESS AS FUNCTION OF THE ELEMENTS OF THE DISCRETIZATION

Two different materials have been considered: an epoxy called Araldite and an epoxy/alumina (100/188), being their experimental thermal diffusivities $\alpha^2 = 0.129 \cdot 10^{-2}\ cm^2/s$ and $\alpha^2 = 0.449 \cdot 10^{-2}\ cm^2/s$ respectively; they coincide with the theoretical values given in [9] and [16] respectively. Having fixed α^2 and the length of the rod ($L = 20$ cm), we change the number of elements of the FEM discretization and we analyse the values of the greatest and smallest eigenvalues in module, see Table (1). The greatest eigenvalues in module of each case are represented in Figure (1).

Number of elements	$\lvert\lambda_{max}\rvert$ epoxy	$\lvert\lambda_{min}\rvert$ epoxy	$\lvert\lambda_{max}\rvert$ epoxy/alum.	$\lvert\lambda_{min}\rvert$ epoxy/alum.
5	$7.3478 \cdot 10^{-4}$	$3.2890 \cdot 10^{-5}$	$2.5575 \cdot 10^{-3}$	$1.1448 \cdot 10^{-4}$
10	$3.5991 \cdot 10^{-3}$	$3.2092 \cdot 10^{-5}$	$1.2527 \cdot 10^{-2}$	$1.1170 \cdot 10^{-4}$
20	$1.5198 \cdot 10^{-2}$	$3.1895 \cdot 10^{-5}$	$5.2897 \cdot 10^{-2}$	$1.1101 \cdot 10^{-4}$
40	$6.1635 \cdot 10^{-2}$	$3.1846 \cdot 10^{-5}$	$2.1453 \cdot 10^{-1}$	$1.1084 \cdot 10^{-4}$
80	$2.4739 \cdot 10^{-1}$	$3.1834 \cdot 10^{-5}$	$8.6108 \cdot 10^{-1}$	$1.1080 \cdot 10^{-4}$
160	$9.9043 \cdot 10^{-1}$	$3.1830 \cdot 10^{-5}$	$3.4473 \cdot 10^{0}$	$1.1079 \cdot 10^{-4}$
320	$3.9626 \cdot 10^{0}$	$3.1830 \cdot 10^{-5}$	$1.3792 \cdot 10^{1}$	$1.1079 \cdot 10^{-4}$
640	$1.5851 \cdot 10^{1}$	$3.1830 \cdot 10^{-5}$	$5.5172 \cdot 10^{1}$	$1.1079 \cdot 10^{-4}$
1280	$6.3406 \cdot 10^{1}$	$3.1829 \cdot 10^{-5}$	$2.2069 \cdot 10^{2}$	$1.1079 \cdot 10^{-4}$

Table 1: Eigenvalues of the ODE system (11) vs. number of elements.

Conclusions:

- When the number of elements of the discretization is increased, the greatest eigenvalue of the ODE system (11) grows and the smallest one does not change.

- If an initial discretization of m elements is multiplied by n, obtaining a new discretization of $n \cdot m$ elements, the greatest eigenvalue of the ODE system (11) which corresponds to the second discretization is equal to the greatest eigenvalue of the first discretization's ODE system multiplied by the coefficient n^2. For instance, in the material epoxy with 10 elements, the greatest eigenvalue is given by $|\lambda_{max}| = 3.5991 \cdot 10^{-3}$. If the number of elements is multiplied by 2, having in this way a discretization of 20 elements, the greatest eigenvalue is multiplied by 2^2: $|\lambda_{max}| = 4 \cdot 3.5991 \cdot 10^{-3} = 1.4396 \cdot 10^{-2} \approx 1.5198 \cdot 10^{-2}$.

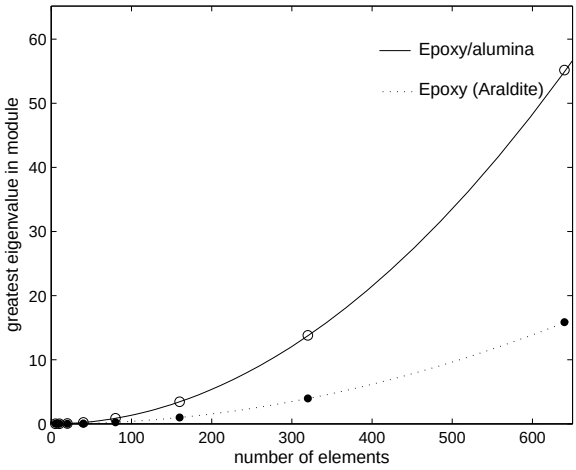

Fig. 1.: The greatest eigenvalue in module of the ODE system (11) vs. number of elements.

3.2. STIFFNESS AS FUNCTION OF THE LENGTH OF THE ROD

Having fixed α^2 and the number of elements of the discretization, the length of the rod has been changed and the values of the greatest and smallest eigenvalues in module have been analysed. A discretization of 20 elements and the materials epoxy (Araldite) and epoxy/alumina have been considered in this analysis. The greatest and smallest eigenvalues of each case have been computed in Table (2).

Length of the rod (cm)	$\lvert\lambda_{max}\rvert$ epoxy	$\lvert\lambda_{min}\rvert$ epoxy	$\lvert\lambda_{max}\rvert$ epoxy/alum.	$\lvert\lambda_{min}\rvert$ epoxy/alum.
2	$1.5198 \cdot 10^{0}$	$3.1895 \cdot 10^{-3}$	$5.2897 \cdot 10^{0}$	$1.1101 \cdot 10^{-2}$
20	$1.5198 \cdot 10^{-2}$	$3.1895 \cdot 10^{-5}$	$5.2897 \cdot 10^{-2}$	$1.1101 \cdot 10^{-4}$
200	$1.5198 \cdot 10^{-4}$	$3.1895 \cdot 10^{-7}$	$5.2897 \cdot 10^{-4}$	$1.1101 \cdot 10^{-6}$
2000	$1.5198 \cdot 10^{-6}$	$3.1895 \cdot 10^{-9}$	$5.2897 \cdot 10^{-6}$	$1.1101 \cdot 10^{-8}$
20000	$1.5198 \cdot 10^{-8}$	$3.1895 \cdot 10^{-11}$	$5.2897 \cdot 10^{-8}$	$1.1101 \cdot 10^{-10}$

Table 2: Eigenvalues of the ODE system (11) vs. length of the rod.

Conclusions:

- The shorter the length of the rod, the greater all the eigenvalues of the ODE system (11).
- Given a rod of length l, if this is multiplied by x obtaining a new rod of length $l \cdot x$, the eigenvalues of the resulting new ODE system are multiplied by $\frac{1}{x^2}$.

3.3. STIFFNESS AS FUNCTION OF THE THERMAL DIFFUSIVITY

The number of elements of the discretization and the length of the rod are fixed, and two materials with thermal diffusivities α_1^2 and α_2^2 are considered, which verify $\alpha_1^2 = k \cdot \alpha_2^2$. Making use of (10) it is easy to verify that the resulting matrices $-M_1^{-1}K_1$ and $-M_2^{-1}K_2$ of the system (11) verify the same relation as the thermal diffusivities

$$-M_1^{-1}K_1 = k \cdot \left(-M_2^{-1}K_2\right). \tag{17}$$

Given two proportional matrices A and B, we will see which is the connection of their characteristic polynomials. Given a matrix A, the notation that we will use to denote its characteristic polynomial will be $\chi_A(\lambda) = det(\lambda I - A)$.

Theorem 3.1. *Given A a square matrix of dimension n and the matrix $B = k \cdot A$, which is obtained by multiplying A by an scalar $k \neq 0$, the characteristic polynomials of both matrices verify:*

$$\chi_B(\lambda) = k^n \chi_A\left(\frac{\lambda}{k}\right) \tag{18}$$

As a consequence, the eigenvalues of B are the eigenvalues of A multiplied by the scalar k.

Proof. Taking into account the definition of the characteristic polynomial:

$$\chi_B(\lambda) = det(\lambda I - B) = \begin{vmatrix} \lambda - b_{11} & -b_{12} & \cdots & -b_{1n} \\ -b_{21} & \lambda - b_{22} & \cdots & -b_{2n} \\ \vdots & \vdots & \ddots & \vdots \\ -b_{n1} & -b_{n2} & \cdots & \lambda - b_{nn} \end{vmatrix} \tag{19}$$

where: $b_{ij} = k \cdot a_{ij}$.

Dividing each of the rows of the determinant (19) by the constant k, the value of the determinant is divided by k^n:

$$\chi_B(\lambda) = k^n \begin{vmatrix} \frac{\lambda - b_{11}}{k} & \frac{-b_{12}}{k} & \cdots & \frac{-b_{1n}}{k} \\ \frac{-b_{21}}{k} & \frac{\lambda - b_{22}}{k} & \cdots & \frac{-b_{2n}}{k} \\ \vdots & \vdots & \vdots & \vdots \\ \frac{-b_{n1}}{k} & \frac{-b_{n2}}{k} & \cdots & \frac{\lambda - b_{nn}}{k} \end{vmatrix} = k^n \begin{vmatrix} \frac{\lambda}{k} - a_{11} & -a_{12} & \cdots & -a_{1n} \\ -a_{21} & \frac{\lambda}{k} - a_{22} & \cdots & -a_{2n} \\ \vdots & \vdots & \ddots & \vdots \\ -a_{n1} & -a_{n2} & \cdots & \frac{\lambda}{k} - a_{nn} \end{vmatrix} \tag{20}$$

From (20) we have that:

$$\chi_B(\lambda) = k^n det\left(\frac{\lambda}{k}I - A\right) = k^n \chi_A\left(\frac{\lambda}{k}\right) \Rightarrow \chi_B(\lambda) = k^n \chi_A\left(\frac{\lambda}{k}\right) \tag{21}$$

So the relation (18) has been proved. Once proved (18), the next chain of equivalences is obtained:

$$\lambda \text{ eigenvalue of } B \Leftrightarrow \ \chi_B(\lambda) = 0 \Leftrightarrow \chi_A\left(\frac{\lambda}{k}\right) = 0 \Leftrightarrow \ \frac{\lambda}{k} \text{ eigenvalue of } A \tag{22}$$

Thus, if λ_j is eigenvalue of A with multiplicity p, $\lambda_j \cdot k$ is eigenvalue of B with multiplicity p. ∎

We have experimentally proved that the equality (18) is verified. The analysis has been done using a rod of copper of length $L = 20cm$ and another rod of the same length but made of epoxy/alumina (100/188). The thermal diffusivities of both rods are $\alpha^2_{ep.al.} = 0.449 \cdot 10^{-2}\ cm^2/s$ and $\alpha^2_{copper} = 1.0745\ cm^2/s$. Both values are experimental but they agree with the values given in [16] and [4]. The relation between these diffusivities is given by:

$$k = \alpha^2_{copper}/\alpha^2_{ep.al.} = 2.39 \cdot 10^2 \tag{23}$$

The eigenvalues of the resulting ODE systems have been obtained, see Table (3). When the eigenvalues obtained for the material epoxy/alumina are multiplied by the constant k (23), the eigenvalues of the copper are obtained.

Number of elements	$\lvert\lambda_{max}\rvert$ epoxy/alum.	$\lvert\lambda_{min}\rvert$ epoxy/alum.	$\lvert\lambda_{max}\rvert$ copper	$\lvert\lambda_{min}\rvert$ copper
5	$2.5575 \cdot 10^{-3}$	$1.1448 \cdot 10^{-4}$	$6.1203 \cdot 10^{-1}$	$2.7395 \cdot 10^{-2}$
10	$1.2527 \cdot 10^{-2}$	$1.1170 \cdot 10^{-4}$	$2.9979 \cdot 10^{0}$	$2.6731 \cdot 10^{-2}$
20	$5.2897 \cdot 10^{-2}$	$1.1101 \cdot 10^{-4}$	$1.2659 \cdot 10$	$2.6567 \cdot 10^{-2}$
40	$2.1453 \cdot 10^{-1}$	$1.1084 \cdot 10^{-4}$	$5.1338 \cdot 10$	$2.6526 \cdot 10^{-2}$
80	$8.6108 \cdot 10^{-1}$	$1.1080 \cdot 10^{-4}$	$2.0607 \cdot 10^{2}$	$2.6516 \cdot 10^{-2}$
160	$3.4473 \cdot 10^{0}$	$1.1079 \cdot 10^{-4}$	$8.2498 \cdot 10^{2}$	$2.6513 \cdot 10^{-2}$
320	$1.3792 \cdot 10^{1}$	$1.1079 \cdot 10^{-4}$	$3.3006 \cdot 10^{3}$	$2.6512 \cdot 10^{-2}$
640	$5.5172 \cdot 10^{1}$	$1.1079 \cdot 10^{-4}$	$1.3203 \cdot 10^{4}$	$2.6512 \cdot 10^{-2}$
1280	$2.2069 \cdot 10^{2}$	$1.1079 \cdot 10^{-4}$	$5.2814 \cdot 10^{4}$	$2.6512 \cdot 10^{-2}$

Table 3: Eigenvalues of the ODE system (11) vs. number of elements.

Conclusions:

- The greater the thermal diffusivity, the greater the eigenvalues of the resulting ODE system (11).
- Given a value of a thermal diffusivity α^2, if this value is multiplied by a constant k, all the eigenvalues of the new ODE system are multiplied by the same constant k. As the relation between the thermal diffusivities of the materials epoxy/alumina and copper is given by (23), the connection that exists among the eigenvalues of the jacobian matrices is exactly the same:

$$\begin{cases} \left|\lambda_{max,copper}\right| = 2.3931 \cdot 10^2 \cdot \left|\lambda_{max,ep.al.}\right| \\ \left|\lambda_{min,copper}\right| = 2.3931 \cdot 10^2 \cdot \left|\lambda_{min,ep.al.}\right| \end{cases} \tag{24}$$

4. STIFFNESS OF THE WAVE PDE

In Section (2) we have already seen that the FEM discretization of the wave PDE (2) with $(n + 2)$ nodes and $(n + 1)$ elements leads to the ODE system (16). In this section the eigenvalues of the jacobian matrix of the ODE system (16) have been studied.

First of all, the relation between the eigenvalues of the ODE systems derived by the diffusion and wave-type PDEs is proved. The previous relation between the eigenvalues of the jacobian matrices of these problems and the conclusions achieved in the case of the diffusion PDE have been used in order to conclude the stiffness of the problem (16) as function of the number of elements of the discretization, the length of the string and the speed of propagation of the wave.

4.1. RELATION BETWEEN THE EIGENVALUES OF THE ODE SYSTEMS DERIVED FROM THE DIFFUSION AND WAVE-TYPE PDES

The jacobian matrices of the diffusion and wave-type PDEs are given by:

$$\frac{\partial \mathbf{f}}{\partial \mathbf{d}} = A, \qquad \frac{\partial \mathbf{f}}{\partial \mathbf{d}} = \begin{pmatrix} 0 & I \\ A & 0 \end{pmatrix} \tag{25}$$

where $A = -M^{-1}K$. In the following theorem the relation between the eigenvalues of the matrices that verify (25) is proved.

Theorem 4.1. *Let be A a square matrix of dimension n and* $B = \begin{pmatrix} 0 & I \\ A & 0 \end{pmatrix}$. *Then, the characteristic polynomials of both matrices verify:*

$$\chi_B(\lambda) = \chi_A(\lambda^2) \tag{26}$$

As a consequence of this result, the eigenvalues of the matrix B are the square root of the eigenvalues of the matrix A.

Proof. The characteristic polynomial of B is given by:

$$\chi_B(\lambda) = det\begin{pmatrix} \lambda I & -I \\ -A & \lambda I \end{pmatrix} \tag{27}$$

As A is a square matrix of dimension n, the matrix B has dimension $2n \times 2n$. If in the determinant (27) the $(n+i)$ column multiplied by λ is added to column i, and this operation is repeated for the indexes $i = 1, 2, 3, ..., n$, obtaining the following determinant:

$$\chi_B(\lambda) = det\begin{pmatrix} 0 & -I \\ C & \lambda I \end{pmatrix} \tag{28}$$

where:

$$C = \begin{pmatrix} -a_{11} + \lambda^2 & -a_{12} & \cdots & -a_{1n} \\ -a_{21} & -a_{22} + \lambda^2 & \cdots & -a_{2n} \\ \vdots & \vdots & \ddots & \vdots \\ -a_{n1} & -a_{n2} & \cdots & -a_{nn} + \lambda^2 \end{pmatrix} = \lambda^2 I - A \tag{29}$$

Taking into account (29), expression (28) results:

$$\chi_B(\lambda) = det\begin{pmatrix} 0 & -I \\ \lambda^2 I - A & \lambda I \end{pmatrix} \tag{30}$$

We will develope the determinant (30) starting from the first row. All the elements of this row except from the element of position $(n+1)$ are zero. Observe that the element of this position is -1. Then, we will continue developing the resulting determinant from row 2, until we reach the row n and we develope from this row. After these developments we obtain:

$$\begin{aligned} \chi_B(\lambda) &= (-1)^{1+(n+1)}(-1)(-1)^{2+(n+2)}(-1)...(-1)^{n+2n}(-1)det(\lambda^2 I - A) \\ &= (-1)^n(-1)(-1)^n(-1)...(-1)^n(-1)det(\lambda^2 I - A) \\ &= (-1)^{n^2+n}det(\lambda^2 I - A) = det(\lambda^2 I - A) = \chi_A(\lambda^2) \end{aligned} \tag{31}$$

During the proof (31), it has to be taken into account that $n^2 + n = n(n+1)$ is even. Once the equality (26) is proved, the following chain of equivalences is obtained:

$$\lambda \text{ eigenvalue of B} \Leftrightarrow \chi_B(\lambda) = 0 \Leftrightarrow \chi_A(\lambda^2) = 0 \Leftrightarrow \lambda^2 \text{ eigenvalue of A} \tag{32}$$

Thus, if λ_j is eigenvalue of A with multiplicity p, then, $\pm\sqrt{\lambda_j}$ is eigenvalue of B with multiplicity p. ∎

In the Table (4) the greatest and smallest eigenvalues of the ODE systems derived from the diffusion and the wave-type PDEs when $\alpha^2 = 1$ and $L = 8$, are tabulated. We hereby confirm that the eigenvalues of the ODE system (16) resulted from the wave-type PDE are the square root of the eigenvalues of the ODE system obtained from the diffusion PDE (11).

Number of elements	λ_{max} diffusion	λ_{min} diffusion	λ_{max} wave	λ_{min} wave
50	$-4.6737 \cdot 10^{2}$	$-1.5426 \cdot 10^{-1}$	$\pm 2.1619 \cdot 10^{1} i$	$\pm 3.9270 \cdot 10^{-1} i$
200	$-7.4986 \cdot 10^{3}$	$-1.5422 \cdot 10^{-1}$	$\pm 8.6595 \cdot 10^{1} i$	$\pm 3.9270 \cdot 10^{-1} i$
800	$-1.2000 \cdot 10^{5}$	$-1.5421 \cdot 10^{-1}$	$\pm 3.4641 \cdot 10^{2} i$	$\pm 3.9270 \cdot 10^{-1} i$

Table 4: Eigenvalues of the ODE systems derived from the diffusion and wave-type PDEs, being $\alpha^2 = 1$ and $L = 8$.

4.2. STIFFNESS AS FUNCTION OF THE NUMBER OF ELEMENTS OF THE DISCRETIZATION

Having fixed α^2 and the length of the string, we change the number of elements of the discretization. We are interested in analysing the greatest and the smallest eigenvalues in module. Real data of a string of a guitar made of carbon fiber wire is considered [7]: length $L = 0.648m$, diameter $d = 0.254 \cdot 10^{-3}m$, area of the section $S = 0,25 \cdot \pi \cdot d^2$, frequency $f = 329.60Hz$ and tension $T = 4 \cdot \rho \cdot L^2 \cdot f^2$, being $\rho = 1750 \cdot S$ the mass per unit length and $1750kg/m^3$ the mass per unit volume of the carbon fiber. It is considered as if the string movement was linear.

Number of elements	$\lvert\lambda_{max}\rvert$	$\lvert\lambda_{min}\rvert$
50	$1.1366 \cdot 10^{5}$	$2.0649 \cdot 10^{3}$
100	$2.2757 \cdot 10^{5}$	$2.0647 \cdot 10^{3}$
200	$4.5526 \cdot 10^{5}$	$2.0646 \cdot 10^{3}$
400	$9.1062 \cdot 10^{5}$	$2.0646 \cdot 10^{3}$
800	$1.8212 \cdot 10^{6}$	$2.0646 \cdot 10^{3}$

Table 5: Eigenvalues of the problem (16) for the cited string of a guitar.

The eigenvalues of the resulting first ODE system have been computed in Table (5), and these are the conclusions:

- The greatest eigenvalue of the ODE system (16) increases as the number of elements of the discretization increases.
- Given a discretization of m elements, if this quantity is multiplied by n obtaining in this way a discretization of $n \cdot m$ elements, the greatest eigenvalue of the ODE system (16) is multiplied by n.

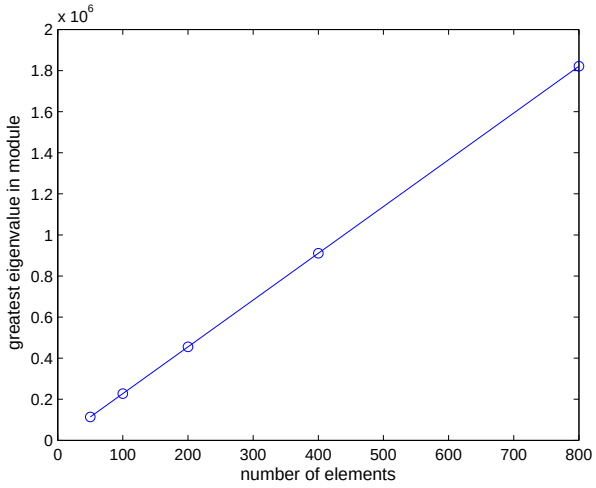

Fig. 2.: The greatest eigenvalue of the problem (16) for a string of a guitar.

4.3. STIFFNESS AS FUNCTION OF THE LENGTH OF THE STRING

Having fixed α^2 and the number of elements of the discretization, strings of different lengths are considered and the greatest and smallest eigenvalues in module are analysed. Taking into account the relation between the jacobian matrices of the ODE systems (11) and (16) obtained after having discretized the corresponding PDEs, and considering the conclusions achieved in Section (3.2), it can be concluded that:

- The smaller the length of the string, the greater the eigenvalues of the ODE system (16).
- Given a string of length l, if this length is multiplied by x obtaining in this way a new string of length $l \cdot x$, the eigenvalues of the ODE system (16) are multiplied by $\frac{1}{x}$.

4.4. STIFFNESS AS FUNCTION OF THE WAVE SPEED OF PROPAGATION

Having fixed the length of the string and the number of elements of the discretization, the parameter α^2 is changed. Taking into account the relation (26) and the conclusions achieved in Section (3.3), we have:

- The greater α^2, the greater the eigenvalues of the ODE system (16).
- Given a value of α^2, if this value is multiplied by k, all the eigenvalues of the ODE system (16) are multiplied by $\sqrt{k}$.

5. CONCLUSIONS

In this paper the one-dimensional diffusion-type and wave-type linear Partial Differential Equations (PDEs) with boundary conditions and initial conditions have been considered. After applying the FEM discretization to these equations, in the case of the diffusion-type PDE a first order ODE system is obtained and a second order ODE system in the case of the wave-type PDE, which can be reduced to a first order ODE system doubling the number of unknowns and equations.

The stiffness of the resulting ODE systems has been studied. It has been numerically proved that the ODE system that results after having discretized the diffusion-type PDE presents more stiffness when the number of elements of the discretization is increased or when the length of the rod is shortened. For the same system, it has been proved analytically that the stiffness of the ODE system increases with the increase of the thermal diffusivity.

It has also been proved the relation between the eigenvalues of the ODE systems obtained from the diffusion-type and the wave-type PDEs, the eigenvalues of the latter ODE system being the square root of the eigenvalues of the first one. Taking into account this result and the conclusions achieved for the ODE system that results from the diffusion PDE, it is concluded that the ODE system that results after discretizing the wave-type PDE presents more stiffness as the number of elements or the speed of propagation are increased, or when the length of the string is shortened.

Acknowledgements. The first author was partially funded by the Basque Government Consolidated Research Group Grant IT649-13 on "Mathematical Modeling, Simulation, and Industrial Applications (M2SI)".

References

[1] http://www.mathworks.com
[2] J. C. Butcher, *Numerical methods for Ordinary Differential Equations in the 20th century*, J. Comput. Appl. Math., **125** (2000), 1-29.
[3] J. C. Butcher, *Numerical Methods for Ordinary Differential Equations*, John Wiley& Sons, Chichester, 2008.
[4] V. Casalegno, P. Vavassori, M. Valle, M. Ferraris, M. Salvo, G. Pintsuk, *Measurement of thermal properties of a ceramic/metal joint by laser flash method*, J. Nucl. Mater., **407** (2010), 83-87.
[5] J.R. Dormand, P. J. Prince, *A family of embedded Runge-Kutta formulae*, J. Comput. Appl. Math., **6**:1 (1980), 19-26.
[6] S.J. Farlow, *Partial differential equations for Scientists & Engineers*, Dover, New York, 1993.
[7] R.M. French, *Engineering the guitar. Theory and Practice*, Springer, New York, 2009.
[8] C.W. Gear, *Numerical Initial Value Problems in Ordinary Differential Equations*, Prentice-Hall, New Jersey, 1971.
[9] S.E. Gustafsson, E. Karawacki, M.N. Khan, *Transient hot-strip method for simultaneously measuring thermal conductivity and thermal diffusivity of solids and fluids*, J. Phys. D-Appl. Phys., **12** (1979), 1411-1421.
[10] M.T. Heath, *Scientific Computing. An introductory survey*, Mc Graw Hill, New York, 1997.
[11] T.J.R. Hughes, *The finite element method. Linear Static and dynamic finite element analysis*, Prentice-Hall International Editions, Englewood Cliffs, New Jersey, 1987.

[12] E.J. Kostelich, D. Armbruster, *Introductory differential equations: From linearity to chaos*, Addison Wesley, Massachusetts, 1996.

[13] J. D. Lambert, *Computational Methods in Ordinary Differential Equations*, John Wiley, Chichester, 1973.

[14] J.D. Lambert, *Numerical methods for ordinary differential systems: the initial value problem*, John Wiley & Sons, New York, 1991.

[15] M.N. Spijker, *Stiffness in numerical initial-value problems*, J. Comput. Appl. Math., **72** (1996), 393-406.

[16] H. Yu, L. Li, L. Qi, *Viscosity and thermal conductivity of Alumina Microball/Epoxy composites*, International Conference on Electronic Packaging Technology & High Density Packaging (2011), 387-390.

ROMAI J., v.9, no.2(2013), 27–33

THE COCARTESIAN PRODUCT AND PAIRS OF CONJUGATE SUBCATEGORIES

Botnaru Dumitru[1], Baes Elena[2]
[1] *Tiraspol State University, Chişinău, Republic of Moldova*
[2] *Technical University of Moldova, Chişinău, Republic of Moldova*
dumitru.botnaru@gmail.com, baeselena@yahoo.it

Abstract A construction that allows to obtain new reflective subcategories is examined.

Keywords: bicategory structure, conjugate subcategories.
2010 MSC: 18B30, 46M15.

We use below the notions and notation of [1].

Let $\mathcal{K}$ be a coreflective subcategory, and $\mathcal{R}$ be a reflective subcategory of the category $\mathcal{C}_2\mathcal{V}$ of the locally convex topological vector Hausdorff spaces, with their corresponding functors $r : \mathcal{C}_2\mathcal{V} \longrightarrow \mathcal{R}$ and $k : \mathcal{C}_2\mathcal{V} \longrightarrow \mathcal{K}$. For any object X of category $\mathcal{C}_2\mathcal{V}$ examine the following construction: let $k^X : kX \to X$ is $\mathcal{K}$-coreplica, and $r^{kX} : kX \to rkX$ is $\mathcal{R}$-replica of respective objects. We construct the pushout square

$$\overline{v}^X \cdot k^X = u^X \cdot r^{kX} \tag{1}$$

Definition 1. 1. *The full subcategory of all isomorphic objects to objects of type $\overline{v}X$ is called the pushout right product of subcategories $\mathcal{K}$ and $\mathcal{R}$ and is denoted by $\overline{\mathcal{V}} = \mathcal{K} *_{dc} \mathcal{R}$.*

2. The pushout square diagram (1) is called the pushout right product diagram of the pair of subcategories $(\mathcal{K}, \mathcal{R})$ (diagram (PRP)).

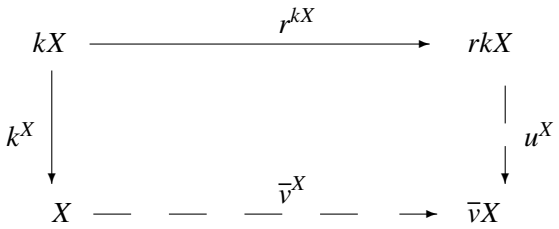

Let $\mathcal{R}$ a be reflective subcategory, and $\mathcal{K}$- a coreflective subcategory of category $\mathcal{C}_2\mathcal{V}$. Let X be an object of category $\mathcal{C}_2\mathcal{V}$, $r^X : X \to rX$ - its $\mathcal{R}$-replica, and $k^{rX} : krX \to rX$ its $\mathcal{K}$-coreplica. Then we can construct the pullback square

$$r^X \cdot \overline{w}^X = k^{rX} \cdot t^X. \tag{2}$$

Definition 2. *1. The full subcategory of all isomorphic objects to objects of type $\overline{w}X$ is called the pullback left product of subcategories $\mathcal{K}$ and $\mathcal{R}$ and it is denoted by $\overline{\mathcal{W}} = \mathcal{K} *_{sc} \mathcal{R}$.*

2. The pullback square diagram (2) is called the pullback left product diagram of pair of subcategories $(\mathcal{K}, \mathcal{R})$ (diagram (PLP)).

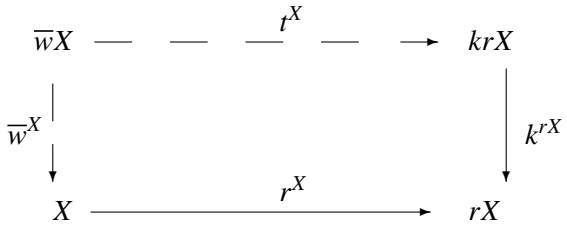

Lemma 1. $\mathcal{R} \subset \mathcal{K} *_{dc} \mathcal{R}$.

Proof. Let $|A| \in |\mathcal{R}|$, let $k^A : kA \to A$ be the $\mathcal{K}$-coreplica and $r^{kA} : kA \to rkA$ be the $\mathcal{R}$-replica of respective objects. Then $k^A = f \cdot r^{kA}$ for a morphism f. It is evident that $f \cdot r^{kA} = 1 \cdot k^A$ is the pushout square built on morphisms k^A and r^{kA}. So $\overline{v}^A = 1$. ∎

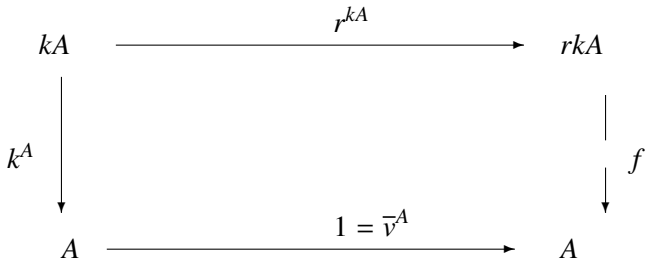

Theorem 1. *The $X \mapsto \overline{v}X$ defines a functor*

$$\overline{v} : \mathcal{C}_2\mathcal{V} \to \mathcal{K} *_{dc} \mathcal{R}.$$

Proof. Let us define the functor $\overline{v}$. Consider $f : X \to Y \in \mathcal{C}_2\mathcal{V}$. Examine the diagrams (PRP) constructed for objects X and Y (next page).

For morphism $f \cdot k^X$ there exists a unique morphism $f_1 : kX \to kY$ such that

$$f \cdot k^X = k^Y \cdot f_1 \tag{3}$$

Also, for morphism $r^{kY} \cdot f_1$ there exists a morphism $f_2 : rkX \to rkY$ such that

$$r^{kY} \cdot f_1 = f_2 \cdot r^{kX}. \tag{4}$$

We have

$$\overline{v}^Y \cdot f \cdot k^{X(3)} = \overline{v}^Y \cdot k^Y \cdot f_1 \overset{(1)}{=} u^Y \cdot r^{kY} \cdot f_1 \overset{(4)}{=} u^Y \cdot f_2 \cdot r^{kX}$$

or

$$(\overline{v}^Y \cdot f) \cdot k^X = (u^Y \cdot f_2) \cdot r^{kX}. \tag{5}$$

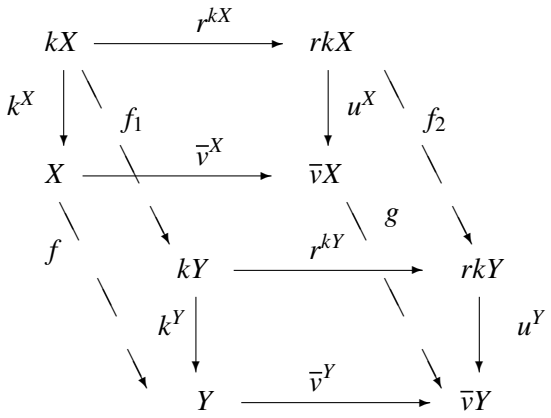

Given that (3) is an pushout square, the equality (5) implies the existence of a single morphism g, such that

$$\overline{v}^Y \cdot f = g \cdot \overline{v}^X \tag{6}$$

$$u^Y \cdot f_2 = g \cdot u^X. \tag{7}$$

We define $g = t(f)$. In equality (6) $\overline{v}^Y$ is an epimorphism. So, we deduce that morphism g verifying equality (6), is unique. It follows that $\overline{v}(1) = 1$ and $\overline{v}(f \cdot h) = \overline{v}(f) \cdot \overline{v}(h)$. ∎

Concerning the functor $\overline{v} : \mathcal{C}_2\mathcal{V} \to \mathcal{K} *_{dc} \mathcal{R}$ the next problem occurs: *When $\overline{v}$ is a reflector functor ?*

We examine the next condition:
(PRP) For any object X of category $\mathcal{C}_2\mathcal{V}$ in diagram (PRP) the morphism u^X belongs to the class $\mu\mathcal{K}$.

Theorem 2. *If the pair of subcategories $(\mathcal{K}, \mathcal{R})$ satisfies the condition (PRP), then $\overline{v}$ is a reflector functor.*

Proof. We examine the diagram (PRP) constructed for objects X and Y of category $\mathcal{C}_2\mathcal{V}$. Let $f : X \to \overline{v}Y$. Because $u^Y \in \mu\mathcal{K}$, it follows that

$$f \cdot k^X = u^Y \cdot g \tag{8}$$

for a morphism g. Further, r^{kX} is $\mathcal{R}$-replica of object kX and

$$g = h \cdot r^{kX} \tag{9}$$

for a morphism h. We have

$$f \cdot k^X \overset{(8)}{=\!=} u^Y \cdot g \overset{(9)}{=\!=} u^Y \cdot h \cdot r^{kX}$$

or

$$f \cdot k^X = (u^Y \cdot h) \cdot r^{kX} \tag{10}$$

Considering that the square (1) is pushout, we deduce that:

$$f = w \cdot \overline{v}^X \tag{11}$$

$$u^Y \cdot h = w \cdot u^X \tag{12}$$

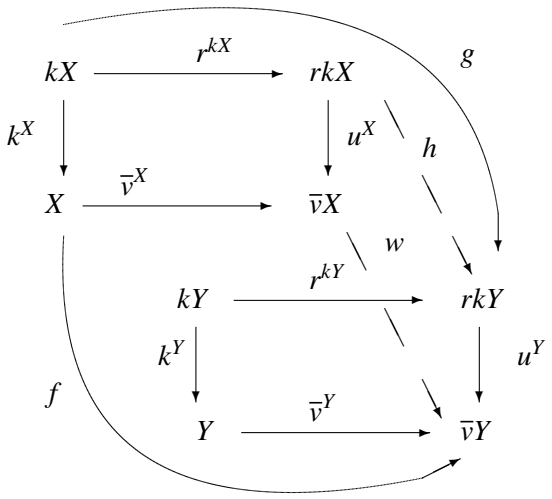

So the morphism f is extended through morphism $\overline{v}^X$. The uniqueness of this extension results from the fact that $\overline{v}^X$ is, like r^{kX}, an epimorphism. ∎

Theorem 3. *Assume that $\mathcal{K}$ is a coreflective subcategory, $\mathcal{R}$ is a reflective subcategory of the category $\mathcal{C}_2\mathcal{V}$, $\widetilde{\mathcal{M}}$ is subcategory of the spaces with Mackey topology, and $\mathcal{S}$ is subcategory of the spaces with weak topology. If $\mathcal{K} \subset \widetilde{\mathcal{M}}$, and $\mathcal{S} \subset \mathcal{R}$, then the pair of subcategories $(\mathcal{K}, \mathcal{R})$ verifies the condition (PRP).*

Proof. Because $\mathcal{S} \subset \mathcal{R}$, it follows that $\varepsilon\mathcal{R} \subset \varepsilon\mathcal{S} = \mathcal{E}_u \cap \mathcal{M}_u = \mu\widetilde{\mathcal{M}} \subset \mu\mathcal{K}$. We examine the diagram (PRP) for an arbitrary object X of category $\mathcal{C}_2\mathcal{V}$. We have $r^{kX} \in \varepsilon\mathcal{R}$. So $\overline{v}^X \in \varepsilon\mathcal{R}$. So $\overline{v}^X,\ k^X \in \mu\mathcal{K}$. But $\overline{v}^X \cdot k^X \in \mu\mathcal{K}$ and from equality

$$\overline{v}^X \cdot k^X = u^X \cdot r^{kX}$$

it follows that $u^X \cdot r^{kX} \in \mu\mathcal{K}$. Hence $u^X \in \mu\mathcal{K}$, because r^{kX} is an epimorphism. ∎

Example 1. *For any coreflective subcategory $\mathcal{K}$ we have $\mathcal{K} *_{dc} \Pi = \Pi$, where Π is a reflective subcategory of complete spaces with weak topology.*

Example 2. *For any coreflective subcategory $\mathcal{K}$ we have $\mathcal{K} *_{dc} \mathcal{S} = \mathcal{S}$, where $\mathcal{S}$ is a reflective subcategory of spaces with weak topology.*

Proof. We construct the diagram (PRP) for an arbitrary object X of the category $\mathcal{C}_2\mathcal{V}$ relative with the pair of subcategory $(\mathcal{K}, \Pi)$. We present the reflector functor $\pi : \mathcal{C}_2\mathcal{V} \to \Pi$ as composition

$$\pi = g_0 \cdot s.$$

So, assume $s^{kX} : kX \to skX$ is $\mathcal{S}$-replica of object kX, and $g_0^{skX} : skX \to g_0 skX$ is Γ_0-replica of object skX, where Γ_0 is subcategory of complete spaces. Hence $g_0^{skX} \cdot s^{kX}$ is Π-replica of object kX. We construct the pushout squares by morphisms k^X and s^{kX}:

$$u_1^X \cdot s^{kX} = \overline{v}_1^X \cdot k^X,$$

by morphisms u_1^X and g_0^{skX}:

$$\overline{v}_2^X \cdot u_1^X = u_2^X \cdot g_0^{skX}.$$

Then $(\overline{v}_2^X \cdot \overline{v}_1^X) \cdot k^X = u_2^X \cdot (g_0^{skX} \cdot s^{kX})$ is a pushout square constructed by morphisms k^X and $g_0^{skX} \cdot s^{kX}$, or by morphisms k^X and π^{kX}.

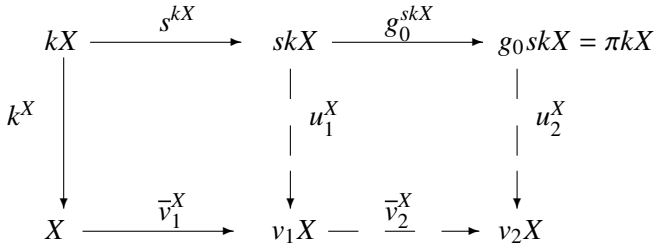

Because k^X is an epimorphism, it results that the u_1^X and u_2^X are epimorphisms. So u_2^X is retractable, and $\overline{v}_2 X \in |\Pi|$. Further $g_0^{skX} \in \mathcal{E}pi \cap \mathcal{M}_p$. So $\overline{v}_2^X \in \mathcal{E}pi \cap \mathcal{M}_p$, and $\overline{v}_1 X \in |\mathcal{S}|$. So we proved that $\mathcal{K} *_{dc} \Pi = \Pi$, and $\mathcal{K} *_{dc} \mathcal{S} = \mathcal{S}$. ∎

Return to the previous diagram. If for any object $X \in |\mathcal{C}_2\mathcal{V}|$ we have $u_2^X \in \mu\mathcal{K}$, then u_2^X is an isomorphism, and from equality

$$g_0^{skX} \cdot s^{kX} = (u_2^X)^{-1} \cdot \overline{v}_2^X \cdot \overline{v}_1^X \cdot k^X$$

it results that $k^X \in \mathcal{M}_u$, and $\widetilde{\mathcal{M}} \subset \mathcal{K}$.

Remark 1. Consider $\widetilde{\mathcal{M}}$ that does not belong to $\mathcal{K}$. Then the pair $(\mathcal{K}, \Pi)$ does not satisfy the condition (PRP), but $\mathcal{K} *_{dc} \Pi = \Pi$. So, the condition (PRP) is sufficient but not necessary as the respective product to be a reflective subcategory.

Remark 2. Lemma 1 indicates inclusion $\mathcal{R} \subset \mathcal{K} *_{dc} \mathcal{R}$, while the previous examples indicate that equality of these subcategories sometimes takes place.

Definition 3. *(see* [1]*). Consider $\mathcal{K}$ a coreflective subcategory and $\mathcal{L}$ a reflective subcategory of category $\mathcal{C}_2\mathcal{V}$ with respective functors $k : \mathcal{C}_2\mathcal{V} \longrightarrow \mathcal{K}$ and $l : \mathcal{C}_2\mathcal{V} \longrightarrow \mathcal{L}$. The pair $(\mathcal{K}, \mathcal{L})$ is called a pair of conjugate subcategories if*

$$\mu\mathcal{K} = \varepsilon\mathcal{L}.$$

Theorem 4. *Consider $(\mathcal{K}, \mathcal{L})$ a pair of conjugate subcategories, and $\mathcal{R}$-a reflective subcategory of category $\mathcal{C}_2\mathcal{V}$. Then:*

1. $\mathcal{K} *_{dc} \mathcal{R} = Q_{\varepsilon\mathcal{L}}(\mathcal{R})$*, where $Q_{\varepsilon\mathcal{L}}(\mathcal{R})$ is the full subcategory of all $(\varepsilon\mathcal{L})$-factorobjects of objects of subcategory $\mathcal{R}$,*
2. *$\mathcal{K} *_{dc} \mathcal{R}$ is a reflective subcategory of category $\mathcal{C}_2\mathcal{V}$,*
3. *the subcategory $\mathcal{K} *_{dc} \mathcal{R}$ is closed with respect to $(\varepsilon\mathcal{L})$-factorobject,*
4. $\overline{v} \cdot k = r \cdot k$,
5. *If $r(\mathcal{K}) \subset \mathcal{K}$, then the coreflector functor $k : \mathcal{C}_2\mathcal{V} \to \mathcal{K}$ and reflector functor $\overline{v} : \mathcal{C}_2\mathcal{V} \to \mathcal{K} *_{dc} \mathcal{R}$ commute: $k \cdot \overline{v} = \overline{v} \cdot k$.*

Proof. 1. In diagram (PRP) $k^X \in \mu\mathcal{K} = \varepsilon\mathcal{L}$. Hence $u^X \in \varepsilon\mathcal{L} = \mu\mathcal{K}$. So $\mathcal{K} *_{dc} \mathcal{R} \subset Q_{\varepsilon\mathcal{L}}(\mathcal{R})$.
Conversely: consider $b : A \to X \in \varepsilon\mathcal{L}$ and $A \in |\mathcal{R}|$. Then $b \cdot k^A : kA \to X$ is the $\mathcal{K}$-coreplica of object X, and

$$k^A = f \cdot r^{kA} \tag{13}$$

is the pushout square constructed by morphisms k^X and r^{kX}. So $X \in |\mathcal{K} *_{dc} \mathcal{R}|$.

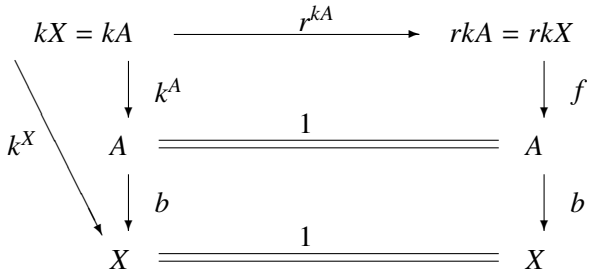

2. It results from 1 and Theorem 3.
3. It results from 1.
4. For an object of the form kX, the diagram (PRP) looks like the following

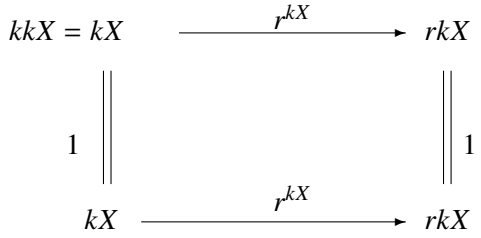

So $\overline{v}kX = rkX$.

5. We examine the diagram (PRP) constructed for an arbitrary object X of category $\mathcal{C}_2\mathcal{V}$. Then r^{kX} is $\overline{\mathcal{V}}$-replica of object kX. Further, $u^X \in \mu\mathcal{K}$ and $rkX \in |\mathcal{K}|$, in accordance with hypothesis $r(\mathcal{K}) \subset \mathcal{K}$.

So $k\overline{v}X = rkX = \overline{v}kX$, or $k \cdot \overline{v} = \overline{v} \cdot k$. ∎

References

[1] Botnaru D., *Structures bicatégorielles complémentaires*, ROMAI J., **5**, 2(2009), 5-27.

ROMAI J., v.9, no.2(2013), 35–50

ON THERMAL STRESSES IN ANISOTROPIC INHOMOGENEOUS MICROSTRETCH CYLINDERS

Emilian Bulgariu

Faculty of Horticulture, "Ion Ionescu de la Brad" University of Agricultural Sciences and Veterinary Medicine, Iaşi, Romania

"Al.I. Cuza" University of Iaşi, Department of Mathematics, Iaşi, Romania

bulgariu.emilian@gmail.com

Abstract In this paper we study the deformation of right cylinders filled with an anisotropic, inhomogeneous, microstretch elastic material. We assume it is subjected to a prescribed thermal field which is linear in the axial coordinate. In order to construct the solution, we study first the problem of extension–bending–torsion, when the thermal field does not depend of the axial coordinate. Then, we study the problem of extension–bending–torsion–flexure for a the thermal field which is linear in the axial coordinate. We reduce the three-dimensional problem to the study of four plane problems. The influence of thermal field on the deformation of the microstretch cylinder is outlined.

Keywords: microstretch solids, elastic cylinder, thermal stresses, Saint-Venant problem, anisotropic material.

2010 MSC: 74A10, 74B99, 74E05, 74E10.

1. INTRODUCTION

The theory of thermo-microstretch was introduced by Eringen [11,12]. The particles of the solid with microstretch can expand and contract independent of translations and the rotations which they execute. This theory can adequately describe the behavior of materials that have internal structure, such as: composite materials reinforced with elastic fibers or porous bodies with pores filled with gas etc.

In the classical theory of thermoelasticity the problem of thermal stresses was studied by Ieşan [18]) and Chiriţă [5] (see also Boley and Weiner [1], Hetnarski and Eslami [16]). Recently, the problem of thermal stresses was studied by Nappa [25] for the case of microstretch elasticity, by Ieşan [24] in the context of the linear theory of Cosserat thermoelasticity for Chiral elastic beams and by Bulgariu and Ghiba [4] and Se Cicco and Ieşan [9] for the theory of thermoelastic materials with voids.

The Saint-Venant problem, in the context of the theory of microstretch elastic materials, was studied by Ieşan and Nappa [21,22], De Cicco and Nappa [10] and Scalia [26].

We study the problem of equilibrium of a right cylinders filled with an anisotropic, inhomogeneous, microstretch elastic material subjected to a temperature variation which is linear in the axial coordinate. We reduce the three-dimensional problem to

the study of four plane problems using the method of semi-inverse solutions introduced by Ieşan [19,20] and Chiriţă [6,8] and used further by Galeş [13] and Ghiba [14,15]. We have introduced mechanical loads on the ends in order to compare the effects of the thermal field with those produced by the resultant of the forces which act on the bases.

2. FORMULATION OF THE PROBLEM

Consider B the interior of a cylinder of length L filled with microstretch elastic material. We choose a rectangular Cartesian system $Ox_1x_2x_3$ so that the generator of the cylinder is parallel with the Ox_3 axis and one ends lies in the x_1Ox_2 plane. We denote by ∂B the boundary of B and by $D(x_3) \subset \mathbb{R}^2$ the interior of the bounded cross-section situated at distance x_3 from the x_1Ox_2 plane.

In this paper, the Latin subscripts and superscripts are understood to range over the integers $1, 2, 3$, unless we specify else, whereas Greek subscripts and superscripts are confined to the range $1, 2$; summation over repeated subscripts is implied and comma followed by a subscript to denote partial derivative with respect to the corresponding Cartesian coordinate; where no confusion may occur, we suppress the dependence upon the spatial variables.

We consider the seven-dimensional vector $\mathbf{U} = (u_i, \varphi_i, \psi)$ at which we attach θ, the temperature variation from the reference moment, where u_i be the components of the displacement vector, φ_i the components of the microrotation vector and ψ the microstretch function.

In the absence of body loads, the problem of thermal stresses consists in determining the solution of the system of partial differential equations given by equilibrium equations [11]

$$t_{ji,j}(\mathbf{U}) = 0, \qquad m_{ji,j}(\mathbf{U}) + \varepsilon_{irs}t_{rs}(\mathbf{U}) = 0, \qquad \pi_{i,i}(\mathbf{U}) - \sigma(\mathbf{U}) = 0, \tag{1}$$

the constitutive equations

$$\begin{aligned} t_{ij} &= A_{ijrs}e_{rs} + B_{ijrs}\kappa_{rs} + D_{ijr}\gamma_r + A_{ij}\psi - \beta_{ij}\theta, \\ m_{ij} &= B_{rsij}e_{rs} + C_{ijrs}\kappa_{rs} + E_{ijr}\gamma_r + B_{ij}\psi - C_{ij}\theta, \\ 3\pi_i &= D_{rsi}e_{rs} + E_{rsi}\kappa_{rs} + D_{ij}\gamma_j + d_i\psi - \xi_i\theta, \\ 3\sigma &= A_{rs}e_{rs} + B_{rs}\kappa_{rs} + d_i\gamma_i + m\psi - \zeta\theta \end{aligned} \tag{2}$$

where the linear strain measures are given by

$$e_{ij} = u_{j,i} + \varepsilon_{jik}\varphi_k, \quad \kappa_{ij} = \varphi_{j,i}, \quad \gamma_i = \psi_{,i}. \tag{3}$$

In the above relations t_{ij} is the stress tensor, m_{ij} is the couple stress tensor, π_i is the microstress vector, σ is the scalar microstress function, ε_{ijk} is the alternating symbol and $A_{ijrs}, B_{ijrs}, C_{ijrs}, D_{ijr}, E_{ijr}, A_{ij}, B_{ij}, C_{ij}, \beta_{ij}, d_i, \xi_i, m$ and ζ are constitutive

coefficients, and $A_{ijrs}, C_{ijrs}, D_{ij}$ satisfy the symmetry conditions

$$A_{ijrs} = A_{rsij}, \quad C_{ijrs} = C_{rsij}, \quad D_{ij} = D_{ji}. \tag{4}$$

In this paper we assume that the microstretch materials are inhomogeneous cross-section. Thus, we have

$$\begin{aligned}
&A_{ijrs} = A_{ijrs}(x_1, x_2), \quad B_{ijrs} = B_{ijrs}(x_1, x_2),\\
&C_{ijrs} = C_{ijrs}(x_1, x_2), \quad D_{ijr} = D_{ijr}(x_1, x_2), \quad E_{ijr} = E_{ijr}(x_1, x_2),\\
&A_{ij} = A_{ij}(x_1, x_2), \quad B_{ij} = B_{ij}(x_1, x_2), \quad D_{ij} = D_{ij}(x_1, x_2),\\
&d_i = d_i(x_1, x_2), \quad m = m(x_1, x_2), \quad \beta_{ij} = \beta_{ij}(x_1, x_2),\\
&C_{ij} = C_{ij}(x_1, x_2), \quad \xi_i = \xi_i(x_1, x_2), \quad \zeta = \zeta(x_1, x_2).
\end{aligned} \tag{5}$$

The surface loadings at a regular point $\mathbf{x}$ of the boundary ∂B, are given by

$$t_i(\mathbf{U}) = t_{ji}(\mathbf{U})n_j, \qquad m_i(\mathbf{U}) = m_{ji}(\mathbf{U})n_j, \qquad \pi(\mathbf{U}) = \pi_i(\mathbf{U})n_i, \tag{6}$$

where n_i are the components of the unit outward normal vector at ∂B, at point $\mathbf{x}$.

The cylinder is considered free of surface loadings, i.e.

$$\begin{aligned}
\mathcal{A}_i(\mathbf{U}) &\equiv t_{\alpha i}(\mathbf{U})n_\alpha = 0,\\
\mathcal{B}_i(\mathbf{U}) &\equiv m_{\alpha i}(\mathbf{U})n_\alpha = 0,\\
\mathcal{C}(\mathbf{U}) &\equiv \pi_\alpha(\mathbf{U})n_\alpha = 0 \quad \text{on } \partial B.
\end{aligned} \tag{7}$$

Let $\mathcal{R}(\mathbf{U}) = (R_1, R_2, R_3)$ and $\mathcal{M}(\mathbf{U}) = (M_1, M_2, M_3)$ be two prescribed vectors representing the resultant force and the resultant moment about the origin of the coordinate system $Ox_1x_2x_3$ of the tractions acting on $D(0)$. On the end $D(L)$ there are tractions applied so that the equilibrium conditions for the considered cylinder to be satisfied. We have introduced mechanical loads $\mathcal{R}(\mathbf{U})$ and $\mathcal{M}(\mathbf{U})$ in order to compare the effects of temperature field with those produced by the resultants acting on the ends. Then, for $x_3 = 0$ we have the conditions

$$\begin{gathered}
\int_{D(0)} t_{3i}(\mathbf{U})da = -R_i, \ \int_{D(0)} (\varepsilon_{3\alpha\beta}x_\beta t_{33}(\mathbf{U}) + m_{3\alpha}(\mathbf{U}))da = -M_\alpha,\\
\int_{D(0)} [\varepsilon_{\alpha\beta3}x_\alpha t_{3\beta}(\mathbf{U}) + m_{33}(\mathbf{U})]da = -M_3.
\end{gathered} \tag{8}$$

The problem $(\mathcal{P})$ of thermal stresses consists in determine the solution u_i, φ_i and ψ that satisfy the equations (1), $(2)_{1,2,3,4}$ and (3) on B, the lateral surface conditions (8) and conditions (9) on the base $D(0)$, when θ and the constitutive coefficients are known, and R_i, M_i, are prescribed. The internal energy density

$$\begin{aligned}
2\mathcal{W}(\mathbf{U}) = {} & A_{ijrs}e_{ij}(\mathbf{U})e_{rs}(\mathbf{U}) + C_{ijrs}\kappa_{ij}(\mathbf{U})\kappa_{rs}(\mathbf{U}) + c_{ij}\gamma_i(\mathbf{U})\gamma_j(\mathbf{U})\\
&+\xi\psi^2(\mathbf{U}) + 2B_{ijrs}e_{ij}(\mathbf{U})\kappa_{rs}(\mathbf{U}) + 2D_{ijr}e_{ij}(\mathbf{U})\gamma_r(\mathbf{U})\\
&+2E_{ijr}\kappa_{ij}(\mathbf{U})\gamma_r(\mathbf{U}) + 2a_{ij}e_{ij}(\mathbf{U})\psi(\mathbf{U}) + 2b_{ij}\kappa_{ij}(\mathbf{U})\psi(\mathbf{U})\\
&+2d_i\gamma_i(\mathbf{U})\psi(\mathbf{U})
\end{aligned} \tag{9}$$

is assumed to be a positive defined quadratic form in terms of the quantities $e_{ij}, \kappa_{ij}, \gamma_i$ and ψ.

Following Ieşan [20] Chiriţă [5] and Bulgariu [3] we define the state of generalized thermoelastic plane strain for the interior of the cross section $D \subset \mathbb{R}^2$, to be the state in which

$$\begin{aligned} w_i = w_i(x_1, x_2), \quad \nu_i = \nu_i(x_1, x_2), \\ \omega = \omega(x_1, x_2), \quad \tau = \tau(x_1, x_2), \qquad (x_1, x_2) \in D. \end{aligned} \tag{10}$$

For every state of generalized thermoelastic plain strain $\mathbf{W} = (w_i(x_1, x_2), \nu_i(x_1, x_2), \omega(x_1, x_2))$ and temperature variation field $\tau(x_1, x_2)$ with $(x_1, x_2) \in D$, we define the operators

$$\begin{aligned} \mathfrak{T}_i(\mathbf{W}) \equiv & [A_{\alpha i\beta s}(w_{s,\beta} + \varepsilon_{s\beta k}\nu_k) + B_{\alpha i\beta s}\nu_{s,\beta} + D_{\alpha i\beta}\omega_{,\beta} + A_{\alpha i}\omega \\ & -\beta_{\alpha i}\tau - \varepsilon_{3\beta\rho}A_{\alpha i3\beta}\nu_\rho]_{,\alpha}, \\ \mathfrak{S}_i(\mathbf{W}) \equiv & [B_{\beta s\alpha i}(w_{s,\beta} + \varepsilon_{s\beta k}\nu_k) + C_{\alpha i\beta s}\nu_{s,\beta} + E_{\alpha i\beta}\omega_{,\beta} + B_{\alpha i}\omega \\ & -C_{\alpha i}\tau - \varepsilon_{3\beta\rho}B_{3\beta\alpha i}\nu_\rho]_{,\alpha} + \varepsilon_{irs}[A_{rs\beta q}(w_{q,\beta} + \varepsilon_{s\beta k}\nu_k) \\ & +B_{rs\beta q}\nu_{q,\beta} + D_{rs\beta}\omega_{,\beta} + A_{rs}\omega - \beta_{rs}\tau - \varepsilon_{3\beta\rho}A_{rs3\beta}\nu_\rho], \\ \mathfrak{P}(\mathbf{W}) \equiv & [D_{\beta s\alpha}(w_{s,\beta} + \varepsilon_{s\beta k}\nu_k) + E_{\beta s\alpha}\nu_{s,\beta} + D_{\alpha\beta}\omega_{,\beta} + d_\alpha\omega \\ & -\xi_\alpha\tau - \varepsilon_{3\beta\rho}D_{3\beta\alpha}\nu_\rho]_{,\alpha} - [A_{\beta j}(w_{j,\beta} + \varepsilon_{j\beta k}\nu_k) + B_{\beta j}\nu_{j,\beta} \\ & +d_\beta\omega_{,\beta} + m\omega - \zeta\tau - \varepsilon_{3\beta\rho}A_{3\beta}\nu_\rho] \text{ in } D, \\ \mathfrak{A}_i(\mathbf{W}) \equiv & [A_{\alpha i\beta s}(w_{s,\beta} + \varepsilon_{s\beta k}\nu_k) + B_{\alpha i\beta s}\nu_{s,\beta} + D_{\alpha i\beta}\omega_{,\beta} + A_{\alpha i}\omega \\ & -\beta_{\alpha i}\tau - \varepsilon_{3\beta\rho}A_{\alpha i3\beta}\nu_\rho]n_\alpha, \\ \mathfrak{B}_i(\mathbf{W}) \equiv & [B_{\beta s\alpha i}(w_{s,\beta} + \varepsilon_{s\beta k}\nu_k) + C_{\alpha i\beta s}\nu_{s,\beta} + E_{\alpha i\beta}\omega_{,\beta} + B_{\alpha i}\omega \\ & -C_{\alpha i}\tau - \varepsilon_{3\beta\rho}B_{3\beta\alpha i}\nu_\rho]n_\alpha, \\ \mathfrak{C}(\mathbf{W}) \equiv & [D_{\beta s\alpha}(w_{s,\beta} + \varepsilon_{s\beta k}\nu_k) + E_{\beta s\alpha}\nu_{s,\beta} + D_{\alpha\beta}\omega_{,\beta} + d_\alpha\omega - \xi_\alpha\tau \\ & -\varepsilon_{3\beta\rho}D_{3\beta\alpha}\nu_\rho]n_\alpha \text{ on } \partial D. \end{aligned} \tag{11}$$

The aim of the first part of this paper is to find the solution of the following two problems:
($\mathcal{P}_0$): extension–bending–torsion ($R_\alpha = 0$), when the temperature distribution do not depends of the axial coordinate;
($\mathcal{P}_1$): extension–bending–torsion–flexure, when the temperature distribution is linear in the axial coordinate.

3. THE SOLUTION OF THE PROBLEM ($\mathcal{P}_0$)

In the following two sections, using the method of semi-inverse solutions introduced by Ieşan [19,20] and Chiriţă [6,8], we construct the solution of the problems ($\mathcal{P}_0$) and ($\mathcal{P}_1$) defined above. The method of semi-inverse solution consists in analysing the thermal stresses problem using some generalized plane strain problems.

The problem $(\mathcal{P}_0)$ consists in finding a solution $U^0 = (u^0, \varphi^0, \psi^0)$ of the problem defined by the equations (1), boundary conditions (8) and (9) and the temperature variation θ independent of the axial coordinate, i.e.

$$\theta = T_0(x_1, x_2) \tag{12}$$

with T_0 prescribed and $R_\alpha = 0$.

Using the above method for Saint-Venant's problem, Bulgariu [3] introduced the following class C_I of semi-inverse solutions:

$$C_I = \{(u_i^0, \varphi_i^0, \psi^0) \,|\, \left[\begin{array}{ll} u^0_{i,3} = \alpha_i + \varepsilon_{ijk}\beta_j x_k, & \\ \varphi^0_{i,3} = \beta_i, & \text{cu } \alpha_i, \beta_i \in \mathbb{R}\}, \\ \psi^0_{,3} = 0, & \end{array}\right. \tag{13}$$

which after integration becomes

$$\begin{aligned} &u^0_\alpha = -\frac{1}{2}a_\alpha x_3^2 - \varepsilon_{3\alpha\beta}a_4 x_\beta x_3 + w_\alpha(x_1, x_2)\,,\ \varphi^0_3 = a_4 x_3 + \nu_3(x_1, x_2), \\ &u^0_3 = (a_1 x_1 + a_2 x_2 + a_3)x_3 + w_3(x_1, x_2), \qquad \psi^0 = \omega(x_1, x_2), \\ &\varphi^0_\alpha = \varepsilon_{3\alpha\beta}a_\beta x_3 + \nu_\alpha(x_1, x_2)\,, \end{aligned} \tag{14}$$

excepting a rigid displacement and a_s, $s = 1, 2, 3, 4$, are constants to be found. The state of generalized thermoelastic plain strain W is defined by

$$\mathbf{W} = \sum_{s=1}^{4} a_s \mathbf{W}^{(s)}. \tag{15}$$

where $\mathbf{W^{(s)}} = (w_i^{(s)}, \nu_i^{(s)}, \omega^{(s)})$, $s = 1, 2, 3, 4$, are solutions of the problems, denoted by (Δ_s) and characterized by the equations

$$\mathfrak{T}_i(\mathbf{W}^{(s)}) + f_i^{(s)} = 0\,, \quad \mathfrak{S}_i(\mathbf{W}^{(s)}) + g_i^{(s)} = 0\,, \quad \mathfrak{P}(\mathbf{W}^{(s)}) + 3h^{(s)} = 0\,, \tag{16}$$

in D with lateral boundary conditions

$$\mathfrak{A}_i(\mathbf{W}^{(s)}) = \widetilde{T}_i^{(s)} \quad \mathfrak{B}_i(\mathbf{W}^{(s)}) = \widetilde{M}_i^{(s)}\,, \quad \mathfrak{C}(\mathbf{W}^{(s)}) = 3\widetilde{\Pi}^{(s)}\,, \tag{17}$$

on ∂D, with

$$\begin{aligned} &f_i^{(\gamma)} = (A_{\alpha i 33}x_\gamma + \varepsilon_{3\rho\gamma}B_{\alpha i 3\rho})_{,\alpha}, \quad f_i^{(3)} = (A_{\alpha i 33})_{,\alpha}, \\ &f_i^{(4)} = (\varepsilon_{3\beta\rho}A_{\alpha i 3\rho}x_\beta + B_{\alpha i 33})_{,\alpha}, \\ &g_i^{(\gamma)} = (B_{33\alpha i}x_\gamma + \varepsilon_{3\rho\gamma}C_{\alpha i 3\rho})_{,\alpha} + \varepsilon_{irs}(A_{rs33}x_\gamma + \varepsilon_{3\alpha\gamma}B_{rs3\alpha}), \\ &g_i^{(3)} = (B_{33\alpha i})_{,\alpha} + \varepsilon_{irs}A_{rs33}, \\ &g_i^{(4)} = (\varepsilon_{3\beta\rho}B_{3\rho\alpha i}x_\beta + C_{\alpha i 33})_{,\alpha} + \varepsilon_{irs}(\varepsilon_{3\beta\alpha}A_{rs3\alpha}x_\beta + B_{rs33}), \\ &3h^{(\gamma)} = (D_{33\alpha}x_\gamma + \varepsilon_{3\rho\gamma}E_{3\rho\alpha})_{,\alpha} - (A_{33}x_\gamma + \varepsilon_{3\alpha\gamma}B_{3\alpha}), \\ &3h^{(3)} = (D_{33\alpha})_{,\alpha} - A_{33}, \end{aligned} \tag{18}$$

$$
\begin{aligned}
&3h^{(4)} = (\varepsilon_{3\beta\rho}D_{3\rho\alpha}x_\beta + E_{33\alpha})_{,\alpha} - (\varepsilon_{3\beta\alpha}A_{3\alpha}x_\beta + B_{33}),\\
&\widetilde{T}_i^{(\gamma)} = -(A_{\alpha i33}x_\gamma + \varepsilon_{3\rho\gamma}B_{\alpha i3\rho})n_\alpha, \quad \widetilde{T}_i^{(3)} = -A_{\alpha i33}n_\alpha,\\
&\widetilde{T}_i^{(4)} = -(\varepsilon_{3\beta\rho}A_{\alpha i3\rho}x_\beta + B_{\alpha i33})n_\alpha,\\
&\widetilde{M}_i^{(\gamma)} = -(B_{33\alpha i}x_\gamma + \varepsilon_{3\rho\gamma}C_{\alpha i3\rho})n_\alpha,\\
&\widetilde{M}_i^{(3)} = -B_{33\alpha i}n_\alpha, \quad \widetilde{M}_i^{(4)} = -(\varepsilon_{3\beta\rho}B_{3\rho\alpha i}x_\beta + C_{\alpha i33})n_\alpha,\\
&3\widetilde{\Pi}^{(\gamma)} = -(D_{33\alpha}x_\gamma + \varepsilon_{3\rho\gamma}E_{3\rho\alpha})n_\alpha, \quad 3\widetilde{\Pi}^{(3)} = -D_{33\alpha}n_\alpha,\\
&3\widetilde{\Pi}^{(4)} = -(\varepsilon_{3\beta\rho}D_{3\rho\alpha}x_\beta + E_{33\alpha})n_\alpha.
\end{aligned}
\tag{19}
$$

The solutions of the generalized plane strain isothermal problems (Δ_s) are considered known. It is easy to see that the solution $\mathbf{U}^0 \in C_I$ can be written in the form

$$
\mathbf{U}^0 = \sum_{s=1}^{4} a_s \mathbf{U}^{(s)} \tag{20}
$$

where

$$
\begin{aligned}
&u_\alpha^{(\gamma)} = -\tfrac{1}{2}x_3^2\delta_{\alpha\gamma} + w_\alpha^{(\gamma)}, \quad u_\alpha^{(3)} = w_\alpha^{(3)}, \quad u_\alpha^{(4)} = -\varepsilon_{3\alpha\beta}x_\beta x_3 + w_\alpha^{(4)},\\
&u_3^{(\gamma)} = x_\gamma x_3 + w_3^{(\gamma)}, \quad u_3^{(3)} = x_3 + w_3^{(3)}, \quad u_3^{(4)} = w_3^{(4)},\\
&\varphi_\alpha^{(\gamma)} = \varepsilon_{3\alpha\gamma}x_3 + \nu_\alpha^{(\gamma)}, \quad \varphi_\alpha^{(3)} = \nu_\alpha^{(3)}, \quad \varphi_\alpha^{(4)} = \nu_\alpha^{(4)}\\
&\varphi_3^{(\gamma)} = \nu_3^{(\gamma)}, \quad \varphi_3^{(3)} = \nu_3^{(3)}, \quad \varphi_3^{(4)} = x_3 + \nu_3^{(4)}.
\end{aligned}
\tag{21}
$$

Also Bulgariu [3] demonstrates that R_3 and M_i are such that

$$
\begin{gathered}
-R_3(\mathbf{U}^0) = \sum_{s=1}^{4} a_s\mathcal{D}_{3s}, \quad -M_\alpha(\mathbf{U}^0) = \sum_{s=1}^{4} \varepsilon_{3\alpha\beta}a_s\mathcal{D}_{\beta s},\\
-M_3(\mathbf{U}^0) = \textstyle\sum_{s=1}^{4} a_s\mathcal{D}_{4s},
\end{gathered}
\tag{22}
$$

where

$$
\begin{aligned}
\mathcal{D}_{\beta\lambda} = \int_{D(0)} &[x_\beta(t_{33}^{(\lambda)} + \varepsilon_{3\rho\lambda}B_{333\rho} + A_{3333}x_\lambda)\\
&+\varepsilon_{3\alpha\beta}(m_{3\alpha}^{(\lambda)} + \varepsilon_{3\rho\lambda}C_{3\alpha3\rho} + B_{333\alpha}x_\lambda)]da,\\
\mathcal{D}_{\beta3} = \int_{D(0)} &[x_\beta(t_{33}^{(3)} + A_{3333}) + \varepsilon_{3\alpha\beta}(m_{3\alpha}^{(3)} + B_{333\alpha})]da,\\
\mathcal{D}_{\beta4} = \int_{D(0)} &[x_\beta(t_{33}^{(4)} - \varepsilon_{3\rho\lambda}A_{333\rho}x_\lambda + B_{3333})\\
&+\varepsilon_{3\alpha\beta}(m_{3\alpha}^{(4)} - \varepsilon_{3\rho\lambda}B_{3\rho3\alpha}x_\lambda + C_{3\alpha33})]da,
\end{aligned}
\tag{23}
$$

$$\mathcal{D}_{3\alpha} = \int_{D(0)} [t_{33}^{(\alpha)} + \varepsilon_{3\beta\alpha} B_{333\beta} + A_{3333} x_\alpha] da,$$

$$\mathcal{D}_{33} = \int_{D(0)} [t_{33}^{(3)} + A_{3333}] da,$$

$$\mathcal{D}_{34} = \int_{D(0)} [t_{33}^{(4)} - \varepsilon_{3\alpha\beta} A_{333\alpha} x_\beta + B_{3333}] da,$$

$$\mathcal{D}_{4\lambda} = \int_{D(0)} [\varepsilon_{3\alpha\beta} x_\alpha (t_{3\beta}^{(\lambda)} + \varepsilon_{3\rho\lambda} B_{3\beta3\rho} + A_{3\beta33} x_\lambda) + m_{33}^{(\lambda)} + \varepsilon_{3\rho\lambda} C_{333\rho} + B_{3333} x_\lambda] da,$$

$$\mathcal{D}_{43} = \int_{D(0)} [\varepsilon_{3\alpha\beta} x_\alpha (t_{3\beta}^{(3)} + A_{3\beta33}) + m_{33}^{(3)} + B_{3333}] da,$$

$$\mathcal{D}_{44} = \int_{D(0)} [\varepsilon_{3\alpha\beta} x_\alpha (t_{3\beta}^{(4)} - \varepsilon_{3\rho\lambda} A_{3\beta3\rho} x_\lambda + B_{3\beta33}) + m_{33}^{(4)} - \varepsilon_{3\rho\lambda} B_{3\rho33} x_\lambda + C_{3333}] da.$$

and $t_{ij}^{(s)}, m_{ij}^{(s)}, \pi_i^{(s)}, \sigma^{(s)}$ are the stress tensor, the couple stress tensor, the microstress vector and respectively the scalar microstress function for the state of generalized thermoelastic plain strain in the isothermal case.

Scalia [26] proved that the system (22) has a unique solution, i.e.

$$\det(\mathcal{D}_{rs}) \neq 0 \tag{24}$$

thus, we can determine the constants the constants a_s, $s = 1, 2, 3, 4$. One can verify that the solution given in this section corresponds to $R_\alpha = 0$.

The values on the ends of the couple stress tensor and the microstress vector for the constructed solution $\mathbf{U}^0$ of the problem $(\mathcal{P}_0)$ are given by

$$\begin{aligned} m_i = m_i^{(L)} \equiv\ & B_{333i}(a_1 x_1 + a_2 x_2 + a_3) + B_{\alpha s3i}(w_{s,\alpha} + \varepsilon_{s\alpha k} \nu_k) \\ & - \varepsilon_{3\alpha\gamma} B_{3\alpha3i}(\nu_\gamma + a_4 x_\beta) + C_{3i33} a_4 + \varepsilon_{3\alpha\gamma} C_{3i3\alpha} a_\gamma \\ & + C_{3i\alpha s} \nu_{s,\alpha} + E_{3i\alpha} \omega_{,\alpha} + B_{3i} \omega - \beta_{3i} \tau \text{ on } D(L), \end{aligned} \tag{25}$$

$$\begin{aligned} & m_i = -m_i^{(L)} \text{ on } D(0), \\ & 3\pi = 3\pi^{(L)} \equiv D_{333}(a_1 x_1 + a_2 x_2 + a_3) + D_{\alpha s3}(w_{s,\alpha} + \varepsilon_{s\alpha k} \nu_k) \\ & \qquad - \varepsilon_{3\alpha\gamma} D_{3\alpha3}(\nu_\gamma + a_4 x_\beta) + E_{333} a_4 + \varepsilon_{3\alpha\gamma} E_{3\alpha3} a_\gamma \\ & \qquad + E_{\alpha s3} \nu_{s,\alpha} + D_{3\alpha} \omega_{,\alpha} + d_3 \omega - \xi_3 \tau \text{ on } D(L), \\ & 3\pi = -3\pi^{(L)} \text{ on } D(0), \end{aligned}$$

where $W = (w_i, \nu_i, \omega)$ are defined by relation (15).

4. THE SOLUTION OF THE PROBLEM ($\mathcal{P}_1$)

The problem ($\mathcal{P}_1$) consists in the study of the deformation of the microstretch cylinder similar to the problem ($\mathcal{P}_0$) but subject to the prescribed thermal field

$$\theta = T_0(x_1, x_2) + x_3 T_1(x_1, x_2), \quad (x_1, x_2) \in D. \tag{26}$$

The class C_{II} of semi-inverse solutions for the problem ($\mathcal{P}_1$) introduced by Bulgariu [3] is defined by the vectors $\mathbf{U}^* = (u_i^*, \varphi_i^*, \psi^*)$ satisfying

$$\int_D t_{3i}(\mathbf{U}^*_{,3})da = 0, \quad \int_D [\varepsilon_{3\alpha\beta} x_\alpha t_{3\beta}(\mathbf{U}^*_{,3}) + m_{33}(\mathbf{U}^*_{,3})]da = 0, \tag{27}$$

and moreover $u^*_{,33}$ has the expression of a rigid displacement. Written extensively, the solution $\mathbf{U}^*$ has the following expression

$$\begin{aligned}
u^*_\alpha &= -\frac{1}{6}b_\alpha x_3^3 - \frac{1}{2}c_\alpha x_3^2 - \frac{1}{2}\varepsilon_{3\alpha\beta}b_4 x_\beta x_3^2 - \varepsilon_{3\alpha\beta}c_4 x_\beta x_3 \\
&\quad + \sum_{s=1}^{4}(c_s + b_s x_3)w_\alpha^{(s)} + \widetilde{w}_\alpha(x_1, x_2) + x_3\widehat{w}_\alpha(x_1, x_2), \\
u^*_3 &= \frac{1}{2}(b_1 x_1 + b_2 x_2 + b_3)x_3^2 + (c_1 x_1 + c_2 x_2 + c_3)x_3 \\
&\quad + \sum_{s=1}^{4}(c_s + b_s x_3)w_3^{(s)} + \widetilde{w}_3(x_1, x_2) + x_3\widehat{w}_3(x_1, x_2), \\
\varphi^*_\alpha &= \frac{1}{2}\varepsilon_{3\alpha\beta}b_\beta x_3^2 + \varepsilon_{3\alpha\beta}c_\beta x_3 + \sum_{s=1}^{4}(c_s + b_s x_3)\nu_\alpha^{(s)} + \widetilde{\nu}_\alpha(x_1, x_2) \\
&\quad + x_3\widehat{\nu}_\alpha(x_1, x_2), \\
\varphi^*_3 &= \frac{1}{2}b_4 x_3^2 + c_4 x_3 + \sum_{s=1}^{4}(c_s + b_s x_3)\nu_3^{(s)} + \widetilde{\nu}_3(x_1, x_2) + x_3\widehat{\nu}_3(x_1, x_2), \\
\psi^* &= \sum_{s=1}^{4}(c_s + b_s x_3)\omega^{(s)} + \widetilde{\omega}(x_1, x_2) + x_3\widehat{\omega}(x_1, x_2),
\end{aligned} \tag{28}$$

where $\mathbf{W}^{(s)} = (w_i^{(s)}, \nu_i^{(s)}, \omega^{(s)})$ are the solutions of the problems (Δ_s), $\widetilde{w}_i, \widehat{w}_i$, $\widetilde{\nu}_i, \widehat{\nu}_i, \widetilde{\omega}$ and $\widehat{\omega}$ are unknown functions, independent of x_3 and b_s, c_s, $(s = 1, 2, 3, 4)$, are unknown constants which will be further determined.

We denote by $\widetilde{e}_{ij}, \widetilde{\kappa}_{ij}$ and $\widetilde{\gamma}_i$ the strain measure of the generalized strain problem characterized by $\widetilde{w}_i$ the components of displacement vector, $\widetilde{\nu}_i$ the components of microrotation vector and with $\widetilde{\omega}$ the microstretch function. In this way

$$\begin{aligned}
&\widetilde{e}_{\alpha j} = \widetilde{w}_{j,\alpha} + \varepsilon_{j\alpha k}\widetilde{\nu}_k\,, \quad \widetilde{e}_{3\alpha} = -\varepsilon_{3\alpha\beta}\widetilde{\nu}_\beta\,, \quad \widetilde{e}_{33} = 0\,, \\
&\widetilde{\kappa}_{\alpha j} = \widetilde{\nu}_{j,\alpha}\,, \quad \widetilde{\kappa}_{3j} = 0\,, \quad \widetilde{\gamma}_\alpha = \widetilde{\omega}_{,\alpha}\,, \quad \widetilde{\gamma}_3 = 0\,.
\end{aligned} \tag{29}$$

Let us use the notations

$$\begin{aligned}
\widetilde{t}_{ij} &= A_{ij\alpha s}\widetilde{e}_{\alpha s} + A_{ij3\alpha}\widetilde{e}_{3\alpha} + B_{ij\alpha s}\widetilde{\kappa}_{\alpha s} + D_{ij\alpha}\widetilde{\gamma}_{\alpha} + A_{ij}\widetilde{\omega} - \beta_{ij}T_0,\\
\widetilde{m}_{ij} &= B_{\alpha sij}\widetilde{e}_{\alpha s} + B_{3\alpha ij}\widetilde{e}_{3\alpha} + C_{ij\alpha s}\widetilde{\kappa}_{\alpha s} + E_{ij\alpha}\widetilde{\gamma}_{\alpha} + B_{ij}\widetilde{\omega} - C_{ij}T_0,\\
3\widetilde{\pi}_i &= D_{\alpha si}\widetilde{e}_{\alpha s} + D_{3\alpha i}\widetilde{e}_{3\alpha} + E_{\alpha si}\widetilde{\kappa}_{\alpha s} + D_{i\alpha}\widetilde{\gamma}_{\alpha} + d_i\widetilde{\omega} - \xi T_0,\\
3\widetilde{\sigma} &= A_{\alpha j}\widetilde{e}_{\alpha j} + A_{3\alpha}\widetilde{e}_{3\alpha} + B_{\alpha j}\widetilde{\kappa}_{\alpha j} + d_{\alpha}\widetilde{\gamma}_{\alpha} + m\widetilde{\omega} - \zeta T_0.
\end{aligned} \tag{30}$$

It is easy to observe that $\widetilde{t}_{ij}, \widetilde{m}_{ij}, \widetilde{\pi}_i$ and $\widetilde{\sigma}$ are the components of stress tensor, the couple stress tensor, microstress vector and respectively the scalar microstress function that coresponds to the generalized plane strain state given by $\widetilde{w}_i, \widetilde{\nu}_i, \widetilde{\omega}$ and T_0.

Similarly, the strain measures corresponding to the state of generalized thermoelastic plane strain defined by the field $\widehat{W} = (\widehat{w}_i, \widehat{\varphi}_i, \widehat{\psi})$ and T_1 are

$$\begin{aligned}
&\widehat{e}_{\alpha j} = \widehat{w}_{j,\alpha} + \varepsilon_{j\alpha k}\widehat{\nu}_k, \quad \widehat{e}_{3\alpha} = -\varepsilon_{3\alpha\beta}\widehat{\nu}_{\beta}, \quad \widehat{e}_{33} = 0,\\
&\widehat{\kappa}_{\alpha j} = \widehat{\nu}_{j,\alpha}, \quad \widehat{\kappa}_{3j} = 0, \quad \widehat{\gamma}_{\alpha} = \widehat{\omega}_{,\alpha}, \quad \widehat{\gamma}_3 = 0,
\end{aligned} \tag{31}$$

and

$$\begin{aligned}
\widehat{t}_{ij} &= A_{ij\alpha s}\widehat{e}_{\alpha s} + A_{ij3\alpha}\widehat{e}_{3\alpha} + B_{ij\alpha s}\widehat{\kappa}_{\alpha s} + D_{ij\alpha}\widehat{\gamma}_{\alpha} + A_{ij}\widehat{\omega} - \beta_{ij}T_1,\\
\widehat{m}_{ij} &= B_{\alpha sij}\widehat{e}_{\alpha s} + B_{3\alpha ij}\widehat{e}_{3\alpha} + C_{ij\alpha s}\widehat{\kappa}_{\alpha s} + E_{ij\alpha}\widehat{\gamma}_{\alpha} + B_{ij}\widehat{\omega} - C_{ij}T_1,\\
3\widehat{\pi}_i &= D_{\alpha si}\widehat{e}_{\alpha s} + D_{3\alpha i}\widehat{e}_{3\alpha} + E_{\alpha si}\widehat{\kappa}_{\alpha s} + D_{i\alpha}\widehat{\gamma}_{\alpha} + d_i\widehat{\omega} - \xi_i T_1,\\
3\widehat{\sigma} &= A_{\alpha j}\widehat{e}_{\alpha j} + A_{3\alpha}\widehat{e}_{3\alpha} + B_{\alpha j}\widehat{\kappa}_{\alpha j} + d_{\alpha}\widehat{\gamma}_{\alpha} + m\widehat{\omega} - \zeta T_1.
\end{aligned} \tag{32}$$

Using the relations (3), (28), (29) and (31), we obtain that

$$\begin{aligned}
e_{\alpha i} &= \sum_{s=1}^{4}(c_s + b_s x_3)e_{\alpha i}^{(s)} + \widetilde{e}_{\alpha i} + x_3\widehat{e}_{\alpha i},\\
e_{3\alpha} &= \sum_{s=1}^{4}(c_s + b_s x_3)e_{3\alpha}^{(s)} + \widetilde{e}_{3\alpha} + x_3\widehat{e}_{3\alpha} - \varepsilon_{3\alpha\beta}(c_4 + b_4 x_3)x_{\beta} + \widehat{w}_{\alpha}\\
&\quad + \sum_{s=1}^{4} b_s w_{\alpha}^{(s)},\\
e_{33} &= c_1 x_1 + c_2 x_2 + c_3 + (b_1 x_1 + b_2 x_2 + b_3)x_3 + \widehat{w}_3 + \sum_{s=1}^{4} b_s w_3^{(s)},
\end{aligned}$$

$$
\begin{aligned}
\kappa_{\alpha i} &= \sum_{s=1}^{4}(c_s + b_s x_3)\kappa_{\alpha i}^{(s)} + \widetilde{\kappa}_{\alpha i} + x_3\widehat{\kappa}_{\alpha i},\\
\kappa_{3\alpha} &= \varepsilon_{3\alpha\beta}(c_\beta + b_\beta x_3) + \widehat{\nu}_\alpha + \sum_{s=1}^{4} b_s \nu_\alpha^{(s)},\\
\kappa_{33} &= c_4 + b_4 x_3 + \widehat{\nu}_3 + \sum_{s=1}^{4} b_s \nu_3^{(s)},\\
\gamma_\alpha &= \sum_{s=1}^{4}(c_s + b_s x_3)\gamma_\alpha^{(s)} + \widetilde{\gamma}_\alpha + x_3\widehat{\gamma}_\alpha,\\
\gamma_3 &= \sum_{s=1}^{4} b_s \omega^{(s)} + \widehat{\omega},
\end{aligned}
\tag{33}
$$

where $e_{ij}^{(s)}, \kappa_{ij}^{(s)}$ and $\gamma_i^{(s)}, (s = 1, 2, 3, 4)$ are the strain measures corresponding to the functions $w_i^{(s)}, \varphi_i^{(s)}$ and $\psi^{(s)}$ and hence

$$
\begin{aligned}
&e_{\alpha j}^{(s)} = w_{j,\alpha}^{(s)} + \varepsilon_{j\alpha k}\nu_k^{(s)}\,, \quad e_{3\alpha}^{(s)} = -\varepsilon_{3\alpha\beta}\nu_\beta^{(s)}\,, \quad e_{33}^{(s)} = 0\,,\\
&\kappa_{\alpha j}^{(s)} = \nu_{j,\alpha}^{(s)}\,, \quad \kappa_{3j}^{(s)} = 0\,, \quad \gamma_\alpha^{(s)} = \omega_{,\alpha}^{(s)}\,, \quad \gamma_3^{(s)} = 0\,.
\end{aligned}
\tag{34}
$$

The constitutive equations (2), in the light of relations (33), become

$$
\begin{aligned}
t_{ij} = &\sum_{s=1}^{4}(c_s + b_s x_3)t_{ij}^{(s)} + \widetilde{t}_{ij} + x_3\widehat{t}_{ij} + \sum_{s=1}^{4} b_s(A_{ij3r}w_r^{(s)} + B_{ij3r}\nu_r^{(s)}\\
&+D_{ij3}\omega^{(s)}) + A_{ij3r}\widehat{w}_r + B_{ij3r}\widehat{\nu}_r + D_{ij3}\widehat{\omega} - \varepsilon_{3\alpha\beta}[A_{ij3\alpha}(c_4\\
&+b_4 x_3)x_\beta - B_{ij3\alpha}(c_\beta + b_\beta x_3)] + A_{ij33}(c_1 x_1 + c_2 x_2 + c_3)\\
&+A_{ij33}(b_1 x_1 + b_2 x_2 + b_3)x_3 + B_{ij33}c_4 + B_{ij33}b_4 x_3,
\end{aligned}
\tag{35}
$$

$$
\begin{aligned}
m_{ij} = &\sum_{s=1}^{4}(c_s + b_s x_3)m_{ij}^{(s)} + \widetilde{m}_{ij} + x_3\widehat{m}_{ij} + \sum_{s=1}^{4} b_s(B_{3rij}w_r^{(s)}\\
&+C_{ij3r}\nu_r^{(s)} + E_{ij3}\omega^{(s)}) + B_{3rij}\widehat{w}_r + C_{ij3r}\widehat{\nu}_r + E_{ij3}\widehat{\omega}\\
&-\varepsilon_{3\alpha\beta}[B_{3\alpha ij}(c_4 + b_4 x_3)x_\beta - C_{ij3\alpha}(c_\beta + b_\beta x_3)] + B_{33ij}(c_1 x_1\\
&+c_2 x_2 + c_3) + B_{33ij}(b_1 x_1 + b_2 x_2 + b_3)x_3 + C_{ij33}c_4 + C_{ij33}b_4 x_3,
\end{aligned}
$$

$$
\begin{aligned}
3\pi_i &= 3\sum_{s=1}^{4}(c_s + b_s x_3)\pi_i^{(s)} + 3\widetilde{\pi}_i + 3x_3\widehat{\pi}_i + \sum_{s=1}^{4} b_s(D_{3ri}w_r^{(s)} \\
&\quad + E_{3ri}\nu_r^{(s)} + D_{i3}\omega^{(s)}) + D_{3ri}\widehat{w}_r + E_{3ri}\widehat{\nu}_r + D_{i3}\widehat{\omega} - \varepsilon_{3\alpha\beta}[D_{3\alpha i}(c_4 \\
&\quad + b_4 x_3)x_\beta - E_{3\alpha i}(c_\beta + b_\beta x_3)] + D_{33i}(c_1 x_1 + c_2 x_2 + c_3) \\
&\quad + D_{33i}(b_1 x_1 + b_2 x_2 + b_3)x_3 + E_{33i}c_4 + E_{33i}b_4 x_3, \\
3\sigma &= 3\sum_{s=1}^{4}(c_s + b_s x_3)\sigma^{(s)} + 3\widetilde{\sigma} + 3x_3\widehat{\sigma} + \sum_{s=1}^{4} b_s(A_{3r}w_r^{(s)} + B_{3r}\nu_r^{(s)} \\
&\quad + d_3\omega^{(s)}) + A_{3r}\widehat{w}_r + B_{3r}\widehat{\nu}_r + d_3\widehat{\omega} - \varepsilon_{3\alpha\beta}[A_{3\alpha}(c_4 + b_4 x_3)x_\beta \\
&\quad - B_{3\alpha}(c_\beta + b_\beta x_3)] + A_{33}(c_1 x_1 + c_2 x_2 + c_3) \\
&\quad + A_{33}(b_1 x_1 + b_2 x_2 + b_3)x_3 + B_{33}c_4 + B_{33}b_4 x_3,
\end{aligned}
$$

where $t_{ij}^{(s)}, m_{ij}^{(s)}, \pi^{(s)}$ and $\sigma^{(s)}$ are given by

$$
\begin{aligned}
t_{ij}^{(s)} &= A_{ij\alpha r}e_{\alpha r}^{(s)} + A_{ij3\alpha}e_{3\alpha}^{(s)} + B_{ij\alpha r}\kappa_{\alpha r}^{(s)} + D_{ij\alpha}\gamma_\alpha^{(s)} + A_{ij}\omega^{(s)}, \\
m_{ij}^{(s)} &= B_{\alpha rij}e_{\alpha r}^{(s)} + B_{3\alpha ij}e_{3\alpha}^{(s)} + C_{ij\alpha r}\kappa_{\alpha r}^{(s)} + E_{ij\alpha}\gamma_\alpha^{(s)} + B_{ij}\omega^{(s)}, \\
3\pi_i^{(s)} &= D_{\alpha ri}e_{\alpha r}^{(s)} + D_{3\alpha i}e_{3\alpha}^{(s)} + E_{\alpha ri}\kappa_{\alpha r}^{(s)} + D_{i\alpha}\gamma_\alpha^{(s)} + d_i\omega^{(s)}, \\
3\sigma^{(s)} &= A_{\alpha r}e_{\alpha r}^{(s)} + A_{3\alpha}e_{3\alpha}^{(s)} + B_{\alpha r}\kappa_{\alpha r}^{(s)} + d_\alpha\gamma_\alpha^{(s)} + m\omega^{(s)}.
\end{aligned}
\tag{36}
$$

Now, we are able to say that the unknown functions $\widetilde{w}_i, \widehat{w}_i, \widetilde{\nu}_i, \widehat{\nu}_i, \widetilde{\omega}$ and $\widehat{\omega}$ are solutions of the following equations

$$
\widetilde{t}_{\beta i,\beta} + \widetilde{f}_i = 0, \quad \widetilde{m}_{\beta i,\beta} + \varepsilon_{ipq}\widetilde{t}_{pq} + \widetilde{g}_i = 0, \quad \widetilde{\pi}_{\alpha,\alpha} - \widetilde{\sigma} + \widetilde{h} = 0 \text{ in } D(0) \tag{37}
$$

and

$$
\widehat{t}_{\beta i,\beta} = 0, \quad \widehat{m}_{\beta i,\beta} + \varepsilon_{ipq}\widehat{t}_{pq} = 0, \quad \widehat{\pi}_{\alpha,\alpha} - \widehat{\sigma} = 0 \text{ in } D(0). \tag{38}
$$

Also, the solutions of the problems characterized by the above equations must verify the boundary conditions

$$
\widetilde{t}_{\beta i}n_\beta = \widetilde{T}_i, \quad \widetilde{m}_{\beta i}n_\beta = \widetilde{M}_i, \quad \widetilde{\pi}_\alpha n_\alpha = \widetilde{P} \text{ on } \partial D(0) \tag{39}
$$

and

$$
\widehat{t}_{\beta i}n_\beta = 0, \quad \widehat{m}_{\beta i}n_\beta = 0, \quad \widehat{\pi}_\alpha n_\alpha = 0 \text{ on } \partial D(0), \tag{40}
$$

where

$$
\begin{aligned}
\widetilde{f}_i &= \widehat{t}_{3i} + \sum_{s=1}^{4} b_s[t_{3i}^{(s)} + (A_{\alpha i3r}w_r^{(s)} + B_{\alpha i3r}\nu_r^{(s)} + D_{\alpha i3}\omega^{(s)})_{,\alpha}] \\
&\quad + (A_{\alpha i3r}\widehat{w}_r + B_{\alpha i3r}\widehat{\nu}_r + D_{\alpha i3}\widehat{\omega})_{,\alpha} - \varepsilon_{3\alpha\beta}[A_{3i3\alpha}b_4 x_\beta - B_{3i3\alpha}b_\beta] \\
&\quad + A_{3i33}(b_1 x_1 + b_2 x_2 + b_3) + B_{3i33}b_4,
\end{aligned}
\tag{41}
$$

$$
\begin{aligned}
\widetilde{g}_i &= \widehat{m}_{3i} + \sum_{s=1}^{4} b_s[m_{3i}^{(s)} + (B_{3r\alpha i}w_r^{(s)} + C_{\alpha i3r}\nu_r^{(s)} + E_{\alpha i3}\omega^{(s)})_{,\alpha} \\
&+\varepsilon_{ipq}(A_{pq3r}w_r^{(s)} + B_{pq3r}\nu_r^{(s)} + D_{pq3}\omega^{(s)})] + (B_{3r\alpha i}\widehat{w}_r + C_{\alpha i3r}\widehat{\nu}_r \\
&+E_{\alpha i3}\widehat{\omega})_{,\alpha} + \varepsilon_{ipq}(A_{pq3r}\widehat{w}_r + B_{pq3r}\widehat{\nu}_r + D_{pq3}\widehat{\omega}) \\
&-\varepsilon_{3\alpha\beta}(B_{3\alpha 3i}b_4x_\beta - C_{3i3\alpha}b_\beta) + B_{333i}(b_1x_1 + b_2x_2 + b_3) \\
&+C_{3i33}b_4, \\
3\widetilde{h} &= 3\widehat{\pi}_3 + \sum_{s=1}^{4} b_s[3\pi_3^{(s)} + (D_{3r\alpha}w_r^{(s)} + E_{3r\alpha}\nu_r^{(s)} + D_{\alpha 3}\omega^{(s)})_{,\alpha} \\
&-A_{3r}w_r^{(s)} - B_{3r}\nu_r^{(s)} - d_3\omega^{(s)}] + (D_{3r\alpha}\widehat{w}_r + E_{3r\alpha}\widehat{\nu}_r + D_{\alpha 3}\widehat{\omega})_{,\alpha} \\
&-A_{3r}\widehat{w}_r - B_{3r}\widehat{\nu}_r - d_3\widehat{\omega} - \varepsilon_{3\alpha\beta}(D_{3\alpha 3}b_4x_\beta - E_{3\alpha 3}b_\beta) \\
&+D_{333}(b_1x_1 + b_2x_2 + b_3) + E_{333}b_4, \\
\widetilde{T}_i &= -\Big[\sum_{s=1}^{4} b_s(A_{\alpha i3r}w_r^{(s)} + B_{\alpha i3r}\nu_r^{(s)} + D_{\alpha i3}\omega^{(s)}) \\
&\qquad +A_{\alpha i3r}\widehat{w}_r + B_{\alpha i3r}\widehat{\nu}_r + D_{\alpha i3}\widehat{\omega}\Big]n_\alpha, \\
\widetilde{M}_i &= -\Big[\sum_{s=1}^{4} b_s(B_{3r\alpha i}w_r^{(s)} + C_{\alpha i3r}\nu_r^{(s)} + E_{\alpha i3}\omega^{(s)}) \\
&\qquad +B_{3r\alpha i}\widehat{w}_r + C_{\alpha i3r}\widehat{\nu}_r + E_{\alpha i3}\widehat{\omega}\Big]n_\alpha, \\
3\widetilde{P} &= -\Big[\sum_{s=1}^{4} b_s(D_{3r\alpha}w_r^{(s)} + E_{3r\alpha}\nu_r^{(s)} + D_{\alpha 3}\omega^{(s)}) \\
&\qquad +D_{3r\alpha}\widehat{w}_r + E_{3r\alpha}\widehat{\nu}_r + D_{\alpha 3}\widehat{\omega}\Big]n_\alpha.
\end{aligned}
\tag{42}
$$

We denote by (Π_0) the thermoelastic generalized plane strain problem characterized by the equations (29), (30), (37) and the boundary conditions (39), while with (Π_1) we denote the thermoelastic generalized plane strain problem characterized by the equations (31), (32), (38) and the boundary conditions (40).

The necessary and sufficient conditions for the existence of the solution of the problem (Π_1) are satisfied, while the problem (Π_0) has a solution if and only if the following conditions are satisfied

$$
\begin{gathered}
\int_{D(0)} \widetilde{f}_i da + \int_{\partial D(0)} \widetilde{T}_i ds = 0, \\
\int_{D(0)} (\varepsilon_{3\alpha\beta}x_\alpha\widetilde{f}_\beta + \widetilde{g}_3)da + \int_{\partial D(0)} (\varepsilon_{3\alpha\beta}x_\alpha\widetilde{T}_\beta + \widetilde{M}_3)ds = 0.
\end{gathered}
\tag{43}
$$

In the view of relations (23), (35), (41), (42) and the divergence theorem, we find that

$$\int_{D(0)} \widetilde{f_\alpha} da + \int_{\partial D(0)} \widetilde{T}_\alpha ds = \int_{D(0)} t_{3\alpha,3} da \tag{44}$$

and moreover

$$\int_{D(0)} \widetilde{f_3} da + \int_{\partial D(0)} \widetilde{T}_3 ds = \sum_{s=1}^{4} b_s \mathcal{D}_{3s} + \int_{D(0)} \widehat{t_{33}} da, \tag{45}$$

$$\int_{D(0)} (\varepsilon_{3\alpha\beta} x_\alpha \widetilde{f_\beta} + \widetilde{g}_3) da + \int_{\partial D(0)} (\varepsilon_{3\alpha\beta} x_\alpha \widetilde{T}_\beta + \widetilde{M}_3) ds$$

$$= \sum_{s=1}^{4} b_s \mathcal{D}_{4s} + \int_{D(0)} (\varepsilon_{3\alpha\beta} x_\alpha \widehat{t_{3\beta}} + \widehat{m}_{33}) da.$$

As in [24], we have

$$\begin{aligned} t_{3\alpha} &= (x_\alpha t_{\rho 3})_{,\rho} + x_\alpha t_{33,3} + \varepsilon_{3\beta\alpha} m_{\rho\beta,\rho} + \varepsilon_{3\beta\alpha} m_{3\beta,3}, \\ t_{3\alpha,3} &= (x_\alpha t_{\rho 3})_{,\rho 3} + x_\alpha t_{33,33} + \varepsilon_{3\beta\alpha} m_{\rho\beta,\rho 3} + \varepsilon_{3\beta\alpha} m_{3\beta,33}. \end{aligned} \tag{46}$$

Using the divergence theorem and the constitutive equations (35), we find

$$\begin{aligned} &\int_{D(0)} t_{3\alpha} da = \sum_{s=1}^{4} b_s \mathcal{D}_{\alpha s} + \int_{D(0)} (x_\alpha \widehat{t_{33}} + \varepsilon_{3\beta\alpha} \widehat{m}_{3\beta}) da, \\ &\int_{D(0)} t_{3\alpha,3} da = 0. \end{aligned} \tag{47}$$

In the same way as in Ieşan [24], we obtain that the systems to determine the constants b_s and $c_s, (s = 1, 2, 3, 4)$ are

$$\sum_{s=1}^{4} b_s \mathcal{D}_{\alpha s} = -R_\alpha - R^*_\alpha, \quad \sum_{s=1}^{4} b_s \mathcal{D}_{3s} = K_1, \quad \sum_{s=1}^{4} b_s \mathcal{D}_{4s} = K_2, \tag{48}$$

and

$$\begin{aligned} &\sum_{s=1}^{4} c_s \varepsilon_{3\alpha\beta} \mathcal{D}_{\beta s} = -M_\alpha - M^*_\alpha, \quad \sum_{s=1}^{4} c_s \mathcal{D}_{3s} = -R_3 - R^*_3, \\ &\sum_{s=1}^{4} c_s \mathcal{D}_{4s} = -M_3 - M^*_3, \end{aligned} \tag{49}$$

where

$$\begin{aligned} &R^*_\alpha = \int_{D(0)} (x_\alpha \widehat{t_{33}} + \varepsilon_{3\beta\alpha} \widehat{m}_{3\beta}) da, \quad K_1 = -\int_{D(0)} \widehat{t_{33}} da, \\ &K_2 = -\int_{D(0)} (\varepsilon_{3\alpha\beta} x_\alpha \widehat{t_{3\beta}} + \widehat{m}_{33}) da, \end{aligned} \tag{50}$$

$$
\begin{aligned}
M_\alpha^* = \int_{D(0)} \Big\{ & \varepsilon_{3\alpha\beta} x_\beta \Big[\widetilde{t}_{33} + \sum_{s=1}^{4} b_s (A_{333r} w_r^{(s)} + B_{333r} \nu_r^{(s)} \\
& + D_{333} \omega^{(s)}) + A_{333r} \widehat{w}_r + B_{333r} \widehat{\nu}_r + D_{333} \widehat{\omega} \Big] + \sum_{s=1}^{4} b_s (B_{3r3\alpha} w_r^{(s)} \\
& + C_{3\alpha 3r} \nu_r^{(s)} + E_{3\alpha 3} \omega^{(s)}) + \widetilde{m}_{3\alpha} + B_{3r3\alpha} \widehat{w}_r + C_{3\alpha 3r} \widehat{\nu}_r \\
& + E_{3\alpha 3} \widehat{\omega} \Big\} da,
\end{aligned}
\tag{51}
$$

$$
\begin{aligned}
R_3^* = \int_{D(0)} & \Big[\widetilde{t}_{33} + \sum_{s=1}^{4} b_s (A_{333r} w_r^{(s)} + B_{333r} \nu_r^{(s)} + D_{333} \omega^{(s)}) \\
& + A_{333r} \widehat{w}_r + B_{333r} \widehat{\nu}_r + D_{333} \widehat{\omega} \Big] da, \\
M_3^* = \int_{D(0)} & \Big\{ \varepsilon_{3\alpha\beta} x_\alpha \Big[\widetilde{t}_{3\beta} + \sum_{s=1}^{4} b_s (A_{3\beta 3r} w_r^{(s)} + B_{3\beta 3r} \nu_r^{(s)} + D_{3\beta 3} \omega^{(s)}) \\
& + A_{3\beta 3r} \widehat{w}_r + B_{3\beta 3r} \widehat{\nu}_r + D_{3\beta 3} \widehat{\omega} \Big] + \sum_{s=1}^{4} b_s (B_{3r33} w_r^{(s)} + C_{333r} \nu_r^{(s)} \\
& + E_{333} \omega^{(s)}) + \widetilde{m}_{33} + B_{3r33} \widehat{w}_r + C_{333r} \widehat{\nu}_r + E_{333} \widehat{\omega} \Big\} da.
\end{aligned}
$$

Hence, the solution of the problem $(\mathcal{P}_2)$ is completely determined.

The values on the ends of the couple stress tensor and the microstress vector for the constructed solution $\mathbf{U}^*$ of the problem $(\mathcal{P}_1)$ are given by

$$
\begin{aligned}
m_i = -\Big\{ & \sum_{s=1}^{4} c_s m_{3i}^{(s)} + \widetilde{m}_{3i} + \sum_{s=1}^{4} b_s (B_{3r3i} w_r^{(s)} + C_{3i3r} \nu_r^{(s)} \\
& + E_{3i3} \omega^{(s)}) + B_{3r3i} \widehat{w}_r + C_{3i3r} \widehat{\nu}_r + E_{3i3} \widehat{\omega} - \varepsilon_{3\alpha\beta} [B_{3\alpha 3i} c_4 x_\beta \\
& - C_{3i3\alpha} c_\beta] + B_{333i} (c_1 x_1 + c_2 x_2 + c_3) + C_{3i33} c_4 \Big\} \text{ on } D(0),
\end{aligned}
\tag{52}
$$

$$
\begin{aligned}
m_i = & \sum_{s=1}^{4} (c_s + L b_s) m_{3i}^{(s)} + \widetilde{m}_{3i} + L \widehat{m}_{3i} + \sum_{s=1}^{4} b_s (B_{3r3i} w_r^{(s)} \\
& + C_{3i3r} \nu_r^{(s)} + E_{3i3} \omega^{(s)}) + B_{3r3i} \widehat{w}_r + C_{3i3r} \widehat{\nu}_r + E_{3i3} \widehat{\omega} \\
& - \varepsilon_{3\alpha\beta} [B_{3\alpha 3i} (c_4 + L b_4) x_\beta - C_{3i3\alpha} (c_\beta + L b_\beta)] \\
& + B_{333i} (c_1 x_1 + c_2 x_2 + c_3) + B_{333i} (b_1 x_1 + b_2 x_2 + b_3) L \\
& + C_{3i33} c_4 + C_{3i33} L b_4 \text{ on } D(L),
\end{aligned}
$$

$$3\pi = -\Big\{3\sum_{s=1}^{4} c_s\pi_3^{(s)} + 3\widetilde{\pi}_3 + \sum_{s=1}^{4} b_s(D_{3r3}w_r^{(s)} + E_{3r3}\nu_r^{(s)} + D_{33}\omega^{(s)}) + D_{3r3}\widehat{w}_r + E_{3r3}\widehat{\nu}_r + D_{33}\widehat{\omega} - \varepsilon_{3\alpha\beta}[D_{3\alpha3}c_4x_\beta - E_{3\alpha3}c_\beta] + D_{333}(c_1x_1 + c_2x_2 + c_3) + E_{333}c_4\Big\} \text{ on } D(0),$$

$$3\pi = 3\sum_{s=1}^{4}(c_s + Lb_s)\pi_3^{(s)} + 3\widetilde{\pi}_3 + 3L\widehat{\pi}_3 + \sum_{s=1}^{4} b_s(D_{3r3}w_r^{(s)} + E_{3r3}\nu_r^{(s)} + D_{33}\omega^{(s)}) + D_{3r3}\widehat{w}_r + E_{3r3}\widehat{\nu}_r + D_{33}\widehat{\omega} - \varepsilon_{3\alpha\beta}[D_{3\alpha3}(c_4 + Lb_4)x_\beta - E_{3\alpha3}(c_\beta + Lb_\beta)] + D_{333}(c_1x_1 + c_2x_2 + c_3) + D_{333}(b_1x_1 + b_2x_2 + b_3)L + E_{333}c_4 + E_{333}Lb_4 \text{ on } D(L).$$

From (28), (48) and (49) we can see how being linear in the axial coordinate, the thermal field produces an extension characterized by the force R_3^*, a bending by the moments M_α^*, a torsion generated by the moment M_3^*, a flexure associated with the forces R_α^* and a plane deformation parallel to the end $D(0)$. If $T_1 = 0$, then from (31), (32), (38) and (40) we find that $\widehat{t}_{ij}, \widehat{m}_{ij}, \widehat{\pi}_i$ and $\widehat{\sigma}$ are zero and hence from (48), we have that $R_\alpha^* = 0$ and $K_\alpha = 0, \alpha = 1, 2$.

A thermal field independent of x_3 produces extension, bending and torsion of the cylinder.

Acknowledgments The author acknowledges support from the Romanian Ministry of Education and Research through CNCSIS -UEFISCSU, project PN II-RU TE code 184, no. 86/30.07.2010.

References

[1] B.A. Boley and J.H. Weiner, *Theory of thermal stresses*, Wiley, New York, (1960).

[2] C.I. Borş, *On the general problem of orthotropic beams loaded on the lateral surface and on the ends*, An. Şt. Univ. Iaşi, Mat., **19** (1973), 427–436.

[3] E. Bulgariu, *On the Saint-Venant's problem in microstretch elasticity*, Libertas Mathematica, **31** (2011), 147–162.

[4] E. Bulgariu and I.D. Ghiba, *On the thermal stresses in anisotropic porous cylinders*, DCDS - Series S, **6**: 6 (2013), 1539–1550.

[5] S. Chiriţă, *Thermal stresses in anisotropic cylinders*, Acta. Mech., **23** (1975), 301–306.

[6] S. Chiriţă, *Saint-Venant's problem for anisotropic circular cylinder*, Acta. Mech., **34** (1979), 243–250.

[7] S. Chiriţă, *Semi-inverse solutions and Almansi's problem for viscoelastic cylinder*, Arch. Mech., **44** (1992), 247–260.

[8] S. Chiriţă, *Saint-Venant's problem and semi-inverse solutions in linear viscoelasticity*, Acta Mech., **94** (1992), 221–232.

[9] S. De Cicco and D. Ieşan, *Thermal effects in anisotropic porous elastic rods*, J. Therm. Stresses, **36**: 4 (2013), 364–377.

[10] S. De Cicco and L. Nappa, *Torsion and flexure of microstretch elastic circular cylinder*, Int. J. Engng. Sci., **35** (1997), 573–583.

[11] A.C. Eringen, *Theory of thermo-microstretch elastic solids*, Int. J. Eng. Sci., **28** (1990), 1291–1301.

[12] Eringen, A.C., *Microcontinuum field theories I: Foundations and solids*, Springer-Verlag, New York, Berlin, Heidelberg, (1999);

[13] C. Galeş, *On Saint-Venant's problem in micropolar viscoelasticity*, An. Şt. Univ. Iaşi, Mat., **46** (2000), 131–148.

[14] I.D. Ghiba, *Semi-inverse solution for Saint-Venant's problem in the theory of porous elastic materials*, Eur. J. of Mech. A/Solids, **27** (2008), 1060–1074.

[15] I.D. Ghiba, *On the deformation of transversely isotropic porous elastic circular cylinder*, Arch. Mech., **61** (2009), 407–421.

[16] R.B. Hetnarski and M.R. Eslami, *Thermal stresses - Advanced theory and applications*, Springer Verlag, Berlin, New York, (2010).

[17] D. Ieşan, *Almansi's problem in micropolar elasticity*, Int. J. Eng. Sci. **12** (1974), 361–374.

[18] D. Ieşan, *Thermal stresses in composite cylinder*, J. Therm. Stresses, **3** (1980), 495–508.

[19] D. Ieşan, *On Saint-Venant's problem*, Arch. Rat. Mech. Anal., **91** (1986), 363–373.

[20] D. Ieşan, *Saint-Venant's problem*, în Lecture Notes in Mathematics, ed. A. Dold and B. Eckmann, Springer, Berlin (1987).

[21] D. Ieşan and L. Nappa, *Saint-Venant's problem for microstretch elastic solids*, Int. J. Engng. Sci., **32** (1994), 229–236.

[22] D. Ieşan and L. Nappa, *Extension and bending of microstretch elastic circular cylinders*, Int. J. Engng. Sci., **33** (1995), 1139–1151.

[23] D. Ieşan, *Deformation of porous Cosserat elastic bars*, Int. J. Solids Struct., **48** (2010), 573–583.

[24] D. Ieşan, *Thermal stresses in chiral elastic beams*, J. Therm. Stresses, **34**: 5 (2011), 458–487.

[25] L. Nappa, *Thermal stresses in microstretch elastic cylinders*, J. Therm. Stresses, **18**: 5 (1995), 537–550.

[26] A. Scalia, *Extension, bending and torsion of anisotropic microstretch elastic cylinders*, Math. Mech. Solids, **5** (2000), 31–40.

ROMAI J., v.9, no.2(2013), 51–60

ON A HIGHER ORDER FRACTIONAL DIFFERENTIAL INCLUSION WITH MULTI-STRIP FRACTIONAL INTEGRAL BOUNDARY CONDITIONS

Aurelian Cernea

Faculty of Mathematics and Informatics, University of Bucharest, Bucharest, Romania

acernea@fmi.unibuc.ro

Abstract We study the existence of solutions for a fractional differential inclusion with multi-strip fractional integral boundary conditions. We establish Filippov type existence results in the case of nonconvex set-valued maps.

Keywords: fractional differential inclusion, Caputo fractional derivative, boundary value problem, multi-strip fractional integral boundary conditions.

2010 MSC: 34A60, 34A08.

1. INTRODUCTION

In this paper we study the following boundary value problem

$$\begin{aligned} &D_c^q x(t) \in F(t, x(t)) \quad a.e.\ ([0,T]),\\ &x(0) = 0, \quad x'(0) = 0, \quad ... \quad , x^{(m-2)}(0) = 0\\ &x(T) = \sum_{i=1}^{n} \gamma_i [I^{\beta_i} x(\eta_i) - I^{\beta_i} x(\xi_i)], \end{aligned} \tag{1.1}$$

where $m \in \mathbf{N}$, $m \geq 2$, $q \in (m-1, m]$, D_c^q is the Caputo fractional derivative, I^β is the fractional integral of order β, $F : [0,T] \times \mathbf{R} \to \mathcal{P}(\mathbf{R})$ is a set-valued map, $\gamma_i \in \mathbf{R}$, $\beta_i > 0$, $i = 1, 2, ..., n$ and $0 < \xi_1 < \eta_1 < ... < \xi_n < \eta_n < 1$.

Differential equations with fractional order have recently proved to be strong tools in the modelling of many physical phenomena. As a consequence there was an intensive development of the theory of differential equations of fractional order ([15, 17] etc.). The study of fractional differential inclusions was initiated by El-Sayed and Ibrahim ([12]).

The present paper is motivated by a recent paper of Ahmad and Ntouyas ([1]) where existence results for problem (1.1) are established for convex as well as nonconvex set-valued maps. The existence results in [1] are based on a nonlinear alternative of Leray-Schauder type and Covitz-Nadler contraction principle for set-valued maps. The situation when F is a single-valued map was studied in [2]. For the motivation, discussion on multi-strip boundary conditions, examples and a consistent bibliography on these problems we refer to [1] and the references therein.

As it is pointed out in [1] the boundary condition in (1.1) can be interpreted in the sense that a controller at the right-end of the considered interval is influenced by a discrete distribution of finite many nonintersecting strips of arbitrary length expressed in terms of fractional integral boundary conditions.

The aim of our paper is to consider the situation when $F(.,.)$ has nonconvex values and to present two new existence results for problem (1.1) which are Filippov type existence results for this problem.

In our first approach we obtain an existence result by the application of the set-valued contraction principle in the space of derivatives of solutions instead of the space of solutions as in [1]. We note that the idea of applying the set-valued contraction principle due to Covitz and Nadler ([11]) in the space of derivatives of the trajectories belongs to Tallos ([14, 18]) and it was already used for similar results obtained for other classes of differential inclusions ([5-8]).

In our second approach we show that Filippov's ideas ([13]) can be suitably adapted in order to obtain the existence of solutions for problem (1.1). Recall that for a differential inclusion defined by a lipschitzian set-valued map with nonconvex values, Filippov's theorem ([13]) consists in proving the existence of a solution starting from a given "quasi" or "almost" solution. Moreover, the result provides an estimate between the "quasi" solution and the solution obtained.

The paper is organized as follows: in Section 2 we recall some preliminary results that we need in the sequel and in Section 3 we prove our main results.

2. PRELIMINARIES

In this short section we sum up some basic facts that we are going to use later.

Let (X, d) be a metric space and consider a set valued map T on X with nonempty values in X. T is said to be a λ-contraction if there exists $0 < \lambda < 1$ such that:

$$d_H(T(x), T(y)) \leq \lambda d(x, y) \quad \forall x, y \in X,$$

where $d_H(.,.)$ denotes the Pompeiu-Hausdorff distance. Recall that the Pompeiu-Hausdorff distance of the closed subsets $A, B \subset X$ is defined by

$$d_H(A, B) = \max\{d^*(A, B), d^*(B, A)\},\ d^*(A, B) = \sup\{d(a, B); a \in A\},$$

where $d(x, B) = \inf_{y \in B} d(x, y)$.

The set-valued contraction principle ([11]) states that if X is complete, and $T : X \to \mathcal{P}(X)$ is a set valued contraction with nonempty closed values, then $T(.)$ has a fixed point, i.e. a point $z \in X$ such that $z \in T(z)$.

We denote by $Fix(T)$ the set of all fixed points of the set-valued map T. Obviously, $Fix(T)$ is closed.

Lemma 2.1. ([16]) *Let X be a complete metric space and suppose that T_1, T_2 are λ-contractions with closed values in X. Then*

$$d_H(Fix(T_1), Fix(T_2)) \leq \frac{1}{1-\lambda} \sup_{z\in X} d(T_1(z), T_2(z)).$$

Let $I = [0, T]$, we denote by $C(I, \mathbf{R})$ the Banach space of all continuous functions from I to $\mathbf{R}$ with the norm $\|x(.)\|_C = \sup_{t\in I} |x(t)|$ and $L^1(I, \mathbf{R})$ is the Banach space of integrable functions $u(.) : I \to \mathbf{R}$ endowed with the norm $\|u(.)\|_1 = \int_0^T |u(t)|dt$.

Definition 2.2. ([15]) a) *The fractional integral of order $q > 0$* of a Lebesgue integrable function $f(.) : (0, \infty) \to \mathbf{R}$ is defined by

$$I^q f(t) = \int_0^t \frac{(t-s)^{q-1}}{\Gamma(q)} f(s)ds,$$

provided the right-hand side is pointwise defined on $(0, \infty)$ and $\Gamma(.)$ is the (Euler's) Gamma function defined by $\Gamma(q) = \int_0^\infty t^{q-1}e^{-t}dt$.

b) *The Caputo fractional derivative of order $q > 0$* of a function $f(.) : [0, \infty) \to \mathbf{R}$ is defined by

$$D_c^q f(t) = \frac{1}{\Gamma(n-q)} \int_0^t (t-s)^{-q+n-1} f^{(n)}(s)ds,$$

where $n = [q] + 1$. It is assumed implicitly that $f(.)$ is n times differentiable whose n-th derivative is absolutely continuous.

We recall (e.g., [15]) that if $q > 0$ and $f(.) \in C(I, \mathbf{R})$ or $f(.) \in L^\infty(I, \mathbf{R})$ then $(D_c^q I^q f)(t) \equiv f(t)$.

Lemma 2.3. ([1]) *For a given function $f(.) \in C(I, \mathbf{R})$ the unique solution of the boundary value problem*

$$\begin{aligned} &D_c^q x(t) = f(t), \\ &x(0) = 0, \quad x'(0) = 0, \quad \ldots \quad , x^{(m-2)}(0) = 0 \\ &x(T) = \textstyle\sum_{i=1}^n \gamma_i [I^{\beta_i} x(\eta_i) - I^{\beta_i} x(\xi_i)], \end{aligned}$$

is given by

$$\begin{aligned} x(t) &= \tfrac{1}{\Gamma(q)} \textstyle\int_0^t (t-s)^{q-1} f(s)ds - \tfrac{t^{m-1}}{\lambda\Gamma(q)} \int_0^T (T-s)^{q-1} f(s)ds \\ &+ \tfrac{t^{m-1}}{\lambda\Gamma(q)} \textstyle\sum_{i=1}^n \tfrac{\gamma_i}{\Gamma(\beta_i)} [\int_0^{\eta_i} \int_0^s (\eta_i - s)^{\beta_i - 1} (s-u)^{q-1} f(u)duds \\ &- \textstyle\int_0^{\xi_i} \int_0^s (\eta_i - s)^{\beta_i - 1} (s-u)^{q-1} f(u)duds], \end{aligned} \tag{2.1}$$

where

$$\lambda = (T^{m-1} - \sum_{i=1}^n \gamma_i \frac{(\eta_i^{\beta_i+m-1} - \xi_i^{\beta_i+m-1})\Gamma(m)}{\Gamma(\beta_i + m)}) \neq 0$$

Remark 2.4. We denote $A(t,s) = \frac{(t-s)^{q-1}}{\Gamma(q)}\chi_{[0,t]}(s)$, $B(t,s) = -\frac{t^{m-1}}{\lambda\Gamma(q)}(T-s)^{q-1}$, $C(t,s) = \frac{t^{m-1}}{\lambda\Gamma(q)}\sum_{i=1}^{n}\frac{\gamma_i}{\Gamma(\beta_i)}[(\int_s^{\eta_i}(\eta_i-u)^{\beta_i-1}(u-s)^{q-1}du)\chi_{[0,\eta_i]}(s) - (\int_s^{\xi_i}(\xi_i-u)^{\beta_i-1}(u-s)^{q-1}du)\chi_{[0,\xi_i]}(s)]$, where $\chi_S(.)$ is the characteristic function of the set S.

Using the fact that $\frac{\Gamma(\alpha)\Gamma(\beta)}{\Gamma(\alpha+\beta)} = \frac{1}{t^{\alpha+\beta-1}}\int_0^t(t-s)^{\beta-1}s^{\alpha-1}ds$, $C(.,.)$ can be written as

$$C(t,s) = \frac{t^{m-1}}{\lambda}\sum_{i=1}^{n}\frac{\gamma_i}{\Gamma(\beta_i+q)}[(\eta_i-s)^{\beta_i+q-1}\chi_{[0,\eta_i]}(s) - (\xi_i-s)^{\beta_i+q-1}\chi_{[0,\xi_i]}(s)].$$

We define $G(t,s) = A(t,s) + B(t,s) + C(t,s)$. Then the solution $x(.)$ in Lemma 2.3 may be written as

$$x(t) = \int_0^T G(t,s)f(s)ds, \tag{2.2}$$

Moreover, for any $t, s \in I$ we have

$$|G(t,s)| \le \frac{T^{q-1}}{\Gamma(q)} + \frac{T^{m+q-2}}{|\lambda|\Gamma(q)} + \frac{T^{m-1}}{|\lambda|}\sum_{i=1}^{n}\frac{|\gamma_i|}{\Gamma(\beta_i+q)}(\eta_i^{\beta_i+q-1} + \xi_i^{\beta_i+q-1}) =: M$$

At the same time, if we put

$$M_1 := \frac{T^q}{\Gamma(q+1)} + \frac{T^{m+q-1}}{|\lambda|\Gamma(q+1)} + \frac{T^{m-1}}{|\lambda|}\sum_{i=1}^{n}\frac{|\gamma_i|}{\Gamma(\beta_i+q+1)}(\eta_i^{\beta_i+q} + \xi_i^{\beta_i+q})$$

and using the fact that $\Gamma(a+1) = a\Gamma(a)$, $a > 0$ we obtain that if $q \ge T$ then $M_1 \le M$.

Definition 2.5. A function $x(.) \in C(I,\mathbf{R})$ with its Caputo derivative of order q existing on $[0,T]$ is a solution of problem (1.1) if there exists a function $f(.) \in L^1(I,\mathbf{R})$ such that $f(t) \in F(t,x(t))$ *a.e.* (I) and (2.1) is satisfied.

3. THE MAIN RESULTS

We study first problem (1.1) with fixed point techniques. In order to do this we introduce the following hypothesis.

Hypothesis 3.1. (i) $F(.,.) : I \times \mathbf{R} \to \mathcal{P}(\mathbf{R})$ *has nonempty closed values and for every* $x \in \mathbf{R}$, $F(.,x)$ *is measurable.*

(ii) *There exists* $L(.) \in L^1(I,\mathbf{R}_+)$ *such that for almost all* $t \in I, F(t,.)$ *is* $L(t)$*-Lipschitz in the sense that*

$$d_H(F(t,x),F(t,y)) \le L(t)|x-y| \quad \forall\ x,y \in \mathbf{R}.$$

(iii) $d(0,F(t,0)) \le L(t)$ *a.e.* (I)

Denote $L_0 := \int_0^T L(s)ds$.

Theorem 3.2. *Assume that Hypothesis 3.1 is satisfied and* $ML_0 < 1$. *Let* $y(.) \in C(I, \mathbf{R})$ *be such that* $y(0) = 0, y'(0) = 0, ..., y^{(m-2)}(0) = 0$, $y(T) = \sum_{i=1}^{n} \gamma_i [I^{\beta_i} y(\eta_i) - I^{\beta_i} y(\xi_i)]$ *and there exists* $p(.) \in L^1(I, \mathbf{R}_+)$ *with* $d(D_c^q y(t), F(t, y(t))) \leq p(t)$ *a.e.* (I).

Then for every $\varepsilon > 0$ *there exists* $x(.) \in C(I, \mathbf{R})$ *a solution of problem (1.1) satisfying for all* $t \in I$

$$|x(t) - y(t)| \leq \frac{M}{1 - ML_0} \int_0^T p(t)dt + \varepsilon.$$

Proof. For $u(.) \in L^1(I, \mathbf{R})$ define the following set-valued maps

$$M_u(t) = F(t, \int_0^T G(t, s)u(s)ds), \quad t \in I,$$

$$T(u) = \{\phi(.) \in L^1(I, \mathbf{R}); \quad \phi(t) \in M_u(t) \quad a.e.\ (I)\}.$$

It follows from Lemma 2.3 that $x(.)$ is a solution of problem (1.1) if and only if $D_c^q x(.)$ is a fixed point of $T(.)$.

We shall prove first that $T(u)$ is nonempty and closed for every $u \in L^1(I, \mathbf{R})$. The fact that the set valued map $M_u(.)$ is measurable is well known. For example the map $t \to \int_0^T G(t, s)u(s)ds$ can be approximated by step functions and we can apply Theorem III. 40 in [4]. Since the values of F are closed with the measurable selection theorem (Theorem III.6 in [4]) we infer that $M_u(.)$ admits a measurable selection ϕ. One has

$$|\phi(t)| \leq d(0, F(t, 0)) + d_H(F(t, 0), F(t, \int_0^T G(t, s)u(s)ds)) \leq$$

$$\leq L(t)(1 + M \int_0^T |u(s)|ds),$$

which shows that $\phi \in L^1(I, \mathbf{R})$ and $T(u)$ is nonempty.

On the other hand, the set $T(u)$ is also closed. Indeed, if $\phi_n \in T(u)$ and $\|\phi_n - \phi\|_1 \to 0$ then we can pass to a subsequence ϕ_{n_k} such that $\phi_{n_k}(t) \to \phi(t)$ for a.e. $t \in I$, and we find that $\phi \in T(u)$.

We show next that $T(.)$ is a contraction on $L^1(I, \mathbf{R})$.

Let $u, v \in L^1(I, \mathbf{R})$ be given and $\phi \in T(u)$. Consider the following set-valued map

$$H(t) = M_v(t) \cap \{x \in \mathbf{R}; \quad |\phi(t) - x| \leq L(t)| \int_0^T G(t, s)(u(s) - v(s))ds|\}.$$

From Proposition III.4 in [4], $H(.)$ is measurable and from Hypothesis 3.1 ii) $H(.)$ has nonempty closed values. Therefore, there exists $\psi(.)$ a measurable selection of $H(.)$. It follows that $\psi \in T(v)$ and according with the definition of the norm we have

$$\|\phi - \psi\|_1 = \int_0^T |\phi(t) - \psi(t)|dt \leq \int_0^T L(t)(\int_0^T |G(t, s)|.|u(s) - v(s)|ds)dt$$

$$= \int_0^T \Big(\int_0^T L(t)|G(t,s)|dt \Big) |u(s) - v(s)|ds \leq ML_0 \|u - v\|_1.$$

We deduce that

$$d(\phi, T(v)) \leq ML_0 \|u - v\|_1.$$

Replacing u by v we obtain

$$d_H(T(u), T(v)) \leq ML_0 \|u - v\|_1,$$

thus $T(.)$ is a contraction on $L^1(I, \mathbf{R})$.

We consider next the following set-valued maps

$$F_1(t,x) = F(t,x) + p(t)[-1,1], \quad (t,x) \in I \times \mathbf{R},$$

$$M_u^1(t) = F_1(t, \int_0^T G(t,s)u(s)ds),$$

$$T_1(u) = \{\psi(.) \in L^1(I, \mathbf{R}); \quad \psi(t) \in M_u^1(t) \quad a.e.\ (I)\}, \quad u(.) \in L^1(I, \mathbf{R}).$$

Obviously, $F_1(.,.)$ satisfies Hypothesis 3.1.

Repeating the previous step of the proof we obtain that T_1 is also a ML_0-contraction on $L^1(I, \mathbf{R})$ with closed nonempty values.

We prove next the following estimate

$$d_H(T(u), T_1(u)) \leq \int_0^T p(t)dt. \tag{3.1}$$

Let $\phi \in T(u)$ and define

$$H_1(t) = M_u^1(t) \cap \{z \in \mathbf{R}; \quad |\phi(t) - z| \leq p(t)\}.$$

With the same arguments used for the set valued map $H(.)$, we deduce that $H_1(.)$ is measurable with nonempty closed values. Hence let $\psi(.)$ be a measurable selection of $H_1(.)$. It follows that $\psi \in T_1(u)$ and one has

$$\|\phi - \psi\|_1 = \int_0^T |\phi(t) - \psi(t)|dt \leq \int_0^T p(t).$$

As above we obtain (3.1).

We apply Lemma 2.1 and we infer that

$$d_H(Fix(T), Fix(T_1)) \leq \frac{1}{1 - ML_0} \int_0^T p(t)dt.$$

Since $v(.) = D_c^q y(.) \in Fix(T_1)$ it follows that for any $\varepsilon > 0$ there exists $u(.) \in Fix(T)$ such that

$$\|v - u\|_1 \leq \frac{1}{1 - ML_0} \int_0^T p(t)dt + \frac{\varepsilon}{M}.$$

We define $x(t) = \int_0^T G(t,s)u(s)ds$, $t \in I$ and we have

$$|x(t) - y(t)| \leq \int_0^T |G(t,s)|.|u(s) - v(s)|ds \leq \frac{M}{1 - ML_0} \int_0^T p(t)dt + \varepsilon$$

which completes the proof. ∎

The assumption in Theorem 3.2 is satisfied, in particular, for $y(.) = 0$ and therefore, via Hypothesis 3.1 (iii), with $p(.) = L(.)$. We obtain the following consequence of Theorem 3.2.

Corollary 3.3. *Assume that Hypothesis 3.1 is satisfied and $ML_0 < 1$. Then for every $\varepsilon > 0$ there exists $x(.)$ a solution of problem (1.1) satisfying for all $t \in I$*

$$|x(t)| \leq \frac{ML_0}{1 - ML_0} + \varepsilon. \tag{3.2}$$

Remark 3.4. A similar result to the one in Corollary 3.3 is Theorem 3.4 in [1]. More exactly, if in addition to Hypothesis 3.1 $F(.,.)$ has compact values and $L(.) \in C(I, \mathbf{R})$, then there exists a solution of problem (1.1) provided that $M_1 L_0 < 1$.

Taking into account Remark 2.4, if $q \geq T$ then Corrolary 3.3. improves Theorem 3.4 in [1].

Moreover, the approach in [1], does not provides a priori bounds as in (3.2).

We present next the main result of this paper.

Theorem 3.5. *Assume that Hypothesis 3.1 (i), (ii) is satisfied and $ML_0 < 1$. Let $y(.) \in C(I, \mathbf{R})$ be such that $y(0) = 0, y'(0) = 0, ..., y^{(m-2)}(0) = 0$, $y(T) = \sum_{i=1}^n \gamma_i [I^{\beta_i} y(\eta_i) - I^{\beta_i} y(\xi_i)]$ and there exists $p(.) \in L^1(I, \mathbf{R}_+)$ with $d(D_c^q y(t), F(t, y(t))) \leq p(t)$ a.e. (I).*

Then there exists $x(.) \in C(I, \mathbf{R})$ a solution of problem (1.1) satisfying for all $t \in I$

$$|x(t) - y(t)| \leq \frac{M}{1 - ML_0} \int_0^T p(t)dt. \tag{3.3}$$

Proof. The set-valued map $t \to F(t, y(t))$ is measurable with closed values and

$$F(t, y(t)) \cap \{D_c^q y(t) + p(t)[-1, 1]\} \neq \emptyset \quad a.e.\ (I).$$

It follows (e.g., Theorem 1.14.1 in [3]) that there exists a measurable selection $f_1(t) \in F(t, y(t))$ $a.e.$ (I) such that

$$|f_1(t) - D_c^q y(t)| \leq p(t) \quad a.e.\ (I) \tag{3.4}$$

Define $x_1(t) = \int_0^T G(t,s) f_1(s)ds$ and one has

$$|x_1(t) - y(t)| \leq M \int_0^T p(t)dt.$$

We claim that it is enough to construct the sequences $x_n(.) \in C(I, \mathbf{R})$, $f_n(.) \in L^1(I, \mathbf{R})$, $n \geq 1$ with the following properties

$$x_n(t) = \int_0^T G(t,s) f_n(s) ds, \quad t \in I, \tag{3.5}$$

$$f_n(t) \in F(t, x_{n-1}(t)) \quad a.e.\,(I),\ n \geq 1, \tag{3.6}$$

$$|f_{n+1}(t) - f_n(t)| \leq L(t)|x_n(t) - x_{n-1}(t)| \quad a.e.\,(I), n \geq 1. \tag{3.7}$$

If this construction is realized then from (3.4)-(3.7) we have for almost all $t \in I$

$$|x_{n+1}(t) - x_n(t)| \leq \int_0^T |G(t,t_1)|.|f_{n+1}(t_1) - f_n(t_1)| dt_1 \leq$$

$$M \int_0^T L(t_1)|x_n(t_1) - x_{n-1}(t_1)| dt_1 \leq M \int_0^T L(t_1) \int_0^T |G(t_1,t_2)|.$$

$$|f_n(t_2) - f_{n-1}(t_2)| dt_2 \leq M^2 \int_0^T L(t_1) \int_0^T L(t_2)|x_{n-1}(t_2) - x_{n-2}(t_2)| dt_2 dt_1$$

$$\leq (M)^n \int_0^T L(t_1) \int_0^T L(t_2) ... \int_0^T L(t_n)|x_1(t_n) - y(t_n)| dt_n ... dt_1 \leq$$

$$\leq (ML_0)^n M \int_0^T p(t) dt.$$

Therefore $\{x_n(.)\}$ is a Cauchy sequence in the Banach space $C(I, \mathbf{R})$, hence converging uniformly to some $x(.) \in C(I, \mathbf{R})$. Therefore, by (3.7), for almost all $t \in I$, the sequence $\{f_n(t)\}$ is Cauchy in $\mathbf{R}$. Let $f(.)$ be the pointwise limit of $f_n(.)$.

Moreover, one has

$$\begin{array}{l} |x_n(t) - y(t)| \leq |x_1(t) - y(t)| + \sum_{i=1}^{n-1} |x_{i+1}(t) - x_i(t)| \leq \\ M \int_0^T p(t) dt + \sum_{i=1}^{n-1} (M \int_0^T p(t) dt)(ML_0)^i = \frac{M \int_0^T p(t) dt}{1 - ML_0}. \end{array} \tag{3.8}$$

On the other hand, from (3.4), (3.7) and (3.8) we obtain for almost all $t \in I$

$$\begin{array}{l} |f_n(t) - D_c^q y(t)| \leq \sum_{i=1}^{n-1} |f_{i+1}(t) - f_i(t)| + \\ +|f_1(t) - D_c^q y(t)| \leq L(t) \frac{M \int_0^T p(t) dt}{1 - ML_0} + p(t). \end{array}$$

Hence the sequence $f_n(.)$ is integrably bounded and therefore $f(.) \in L^1(I, \mathbf{R})$.

Using Lebesgue's dominated convergence theorem and taking the limit in (3.5), (3.6) we deduce that $x(.)$ is a solution of (1.1). Finally, passing to the limit in (3.8) we obtained the desired estimate on $x(.)$.

It remains to construct the sequences $x_n(.)$, $f_n(.)$ with the properties in (3.5)-(3.7). The construction will be done by induction.

Since the first step is already realized, assume that for some $N \geq 1$ we already constructed $x_n(.) \in C(I, \mathbf{R})$ and $f_n(.) \in L^1(I, \mathbf{R})$, $n = 1, 2, ...N$ satisfying (3.5), (3.7) for $n = 1, 2, ...N$ and (3.6) for $n = 1, 2, ...N - 1$. The set-valued map $t \to F(t, x_N(t))$ is measurable. Moreover, the map $t \to L(t)|x_N(t) - x_{N-1}(t)|$ is measurable. By the lipschitzianity of $F(t, .)$ we have that for almost all $t \in I$

$$F(t, x_N(t)) \cap \{f_N(t) + L(t)|x_N(t) - x_{N-1}(t)|[-1, 1]\} \neq \emptyset.$$

Theorem 1.14.1 in [3] yields that there exist a measurable selection $f_{N+1}(.)$ of $F(., x_N(.))$ such that

$$|f_{N+1}(t) - f_N(t)| \leq L(t)|x_N(t) - x_{N-1}(t)| \quad a.e.\ (I).$$

We define $x_{N+1}(.)$ as in (3.5) with $n = N + 1$. Thus $f_{N+1}(.)$ satisfies (3.6) and (3.7) and the proof is complete. ∎

Remark 3.6. Obviously, Theorem 3.5 extends Theorem 3.2. We do not suppose that $d(0, F(t, 0)) \leq L(t) \quad a.e.\ (I)$ and the estimate in (3.3) is better than the one in Theorem 3.2.

Even if Theorem 3.5 improves Theorem 3.2, we chosen to present both results; on one hand because the methods used in their proofs are different and on the other hand to show that there exists situations when the fixed point approaches are less powerful.

References

[1] B. Ahmad, S. K. Ntouyas, *Existence results for higher order fractional differential inclusion with multi-strip fractional integral boundary conditions*, Electron. J. Qual. Theory Differ. Equations, **2013**(2013), No. 20, 1-19.

[2] B. Ahmad, S. K. Ntouyas, A. Alsaedi, *A study of nonlinear fractional differential equations of arbitrary order with Riemann-Liouville type multi-strip boundary conditions*, Math. Prob. Engin., ID 320415 (2013), 1-9.

[3] J. P. Aubin, A. Cellina, *Differential Inclusions*, Springer, Berlin, (1984).

[4] C. Castaing, M. Valadier, *Convex Analysis and Measurable Multifunctions*, Springer, Berlin (1977).

[5] A. Cernea, *On the existence of solutions for a higher order differential inclusion without convexity*, Electron. J. Qual. Theory Differ. Equations, **8** (2007), 1-8.

[6] A. Cernea, *An existence result for a Fredholm-type integral inclusion*, Fixed Point Theory, **9** (2008), 441-447.

[7] A. Cernea, *On the existence of solutions for fractional differential inclusions with boundary conditions*, Fract. Calc. Appl. Anal., **12** (2009), 433-442.

[8] A. Cernea, *A note on the existence of solutions for some boundary value problems of fractional differential inclusions*, Fract. Calc. Appl. Anal., **15** (2012), 183-194.

[9] A. Cernea, *Continuous version of Filippov's theorem for fractional differential inclusions*, Nonlinear Anal., **72** (2010), 204-208.

[10] Y.K. Chang, J.J. Nieto, *Some new existence results for fractional differential inclusions with boundary conditions*, Mathematical and Computer Modelling, **49**(2009), 605-609.

[11] H. Covitz, S.B. Nadler jr., *Multivalued contraction mapping in generalized metric spaces*, Israel J. Math., **8**(1970), 5-11.

[12] A.M.A. El-Sayed, A.G. Ibrahim, *Multivalued fractional differential equations of arbitrary orders*, Appl. Math. Comput., **68**(1995), 15-25.

[13] A.F. Filippov, *Classical solutions of differential equations with multivalued right hand side*, SIAM J. Control, **5**(1967), 609-621.

[14] Z. Kannai, P. Tallos, *Stability of solution sets of differential inclusions*, Acta Sci. Math. (Szeged), **61**(1995), 197-207.

[15] A.A. Kilbas, H.M. Srivastava, J.J. Trujillo, *Theory and Applications of Fractional Differential Equations*, Elsevier, Amsterdam (2006).

[16] T.C. Lim, *On fixed point stability for set-valued contractive mappings with applications to generalized differential equations*, J. Math. Anal. Appl., **110**(1985), 436-441.

[17] I. Podlubny, *Fractional Differential Equations*, Academic Press, San Diego (1999).

[18] P. Tallos, *A Filippov-Gronwall type inequality in infinite dimensional space*, Pure Math. Appl., **5**(1994), 355-362.

ROMAI J., v.9, no.2(2013), 61–73

ON DENSE SUBSPACES OF THE SPACES OF CONTINUOUS PSEUDOMETRICS

Mitrofan M. Choban[1], Dorin I. Pavel[2]
[1] *Academy of Sciences of Moldova, Chişinău, Republic of Moldova*
[1,2] *Department of Mathematics, Tiraspol State University, Chişinău, Republic of Moldova*
mmchoban@gmail.com, paveldorin@gmail.com

Abstract In this article, the distinct classes of continuous pseudometrics and metrics (perfect, pseudo-perfect, quasi-perfect, complete pseudometrics and metrics) are defined and studied in depth. The conditions under which the given class of pseudometrics is dense in the space of all continuous pseudometrics are determined. Distinct examples which show that the above mentioned notions are distinct are proposed.

Keywords: paracompact p-space, M-space, pseudocompact space, pseudo-perfect mapping, dense subspace.
2010 MSC:54E18, 54E35.

1. INTRODUCTION

By a space we understand a completely regular Hausdorff space. We use the terminology from [6]. Let $\mathbb{R}$ be the space of reals, $\mathbb{R}^\infty = \mathbb{R} \cup \{+\infty\}$ and the sets $I = [0, 1]$, $\mathbb{N} = \{1, 2, ...\}$ are subspaces of the space $\mathbb{R}$. We assume that $x \leq +\infty$ and $x + (+\infty) = (+\infty) + x = +\infty$ for each $x \in \mathbb{R}^\infty$. The space $\mathbb{R}$ is an open subspace of the space $\mathbb{R}^\infty$ and the family $\{V_n\infty = \{x \in \mathbb{R}^\infty : n < x\} : n \in \mathbb{N}\}$ is a base of the space $\mathbb{R}^\infty$ at the point $+\infty$.

In the present article we study the properties of some concrete subspaces of the space $F(X \times X)$ of all real functions on a space $X \times X$ endowed with the distinct topologies. We continue the investigations started in [5, 11, 12, 14, 15]. On the space $F(X \times X)$ the topology of uniform convergence is generated by distance of uniform convergence $d(f, g) = sup\{|f(x, y) - g(x, y)| : x, y \in X\}$.

We also, investigate some subspaces of functions with distinct properties of space $F(X \times X)$. For instance, we study the subspaces:

• $F_s(X \times X) = \{g \in F(X \times X) : g(x, y) = g(y, x)$ *for all* $x, y \in X\}$ of all symmetrical functions;

• $F_d(X \times X) = \{g \in F(X \times X) : g(x, x) \leq g(x, y)$ *for all* $x, y \in X\}$ of all pseudo-distance functions;

• $F_t(X \times X) = \{g \in F(X \times X) : g(x, z) \leq g(x, y) + g(y, z)$ *for all* $x, y, z \in X\}$ of all triangular functions.

• $F_z(X \times X) = \{g \in F(X \times X) : g(x,x) = 0, g(x,y) \geq 0$ *for all* $x, y \in X\}$ of all non-negative functions.

A pseudo-quasimetric on a set X is a function $\rho : X \times X \to \mathbb{R}^{\infty}$ with the properties $\rho(x,x) = 0$, $\rho(x,y) \geq 0$ and $\rho(x,z) \leq \rho(x,y) + \rho(y,z)$ for all $x, y, z \in X$. The pseudo-quasimetric ρ is a quasimetric when $\rho(x,y) + \rho(y,x) = 0$ holds if and only if $x = y$. If ρ is a pseudo-quasimetric and $\rho(y,x) = \rho(x,y)$ for all $x, y \in X$, then ρ is called a pseudometric. If ρ is a pseudometric and a quasimetric, then ρ is called a metric.

For any pseudo-distance function d on X, any point $x \in X$ and any $\varepsilon > 0$ we put $B(x,d,\varepsilon) = \{y \in X : d(x,y) < d(x,x) + \varepsilon\}$. The set $U \subseteq X$ is called d-open if for each point $x \in U$ there exists $\varepsilon > 0$ such that $B(x,d,\varepsilon) \subseteq U$. The family $T(d)$ of all d-open sets is the topology generated by the pseudo-distance function d on X.

If X is a topological space, then the pseudo-distance function d is continuous if the sets $B(x,d,\varepsilon)$ are open in X. We say that the pseudo-distance function d is weak continuous if the d-open sets are open.

Any continuous pseudo-distance function is weak continuous.

Example 1.1. Let $S = \{(0,0)\} \cup \{(n,0) : n \in \mathbb{N}\} \cup \{(n,m) : n, m \in \mathbb{N}\}$, $d(x,x) = 0$ for each $x \in S$, $d((0,0),(n,0)) = d((n,0),(0,0) = n^{-1}$ for each $n \in \mathbb{N}$, $d((n,0),(n,m)) = d((n,m),(n,0) = m^{-1}$ for each $n, m \in \mathbb{N}$ and $d(x,y) = 1$ for other distinct $x, y \in S$. The distance function d is symmetric and non-negative. The topology $T(d)$ is completely regular. If $\epsilon \leq 1$, $U \subseteq B((0,0),d,\epsilon)$ and the set U is open, then $U = \emptyset$. Thus the pseudo-distance function d is weak continuous and not continuous.

Remark 1.2. *For a pseudo-quasimetric ρ on a space X the following assertions are equivalent:*

• *ρ is continuous;*

• *ρ is weak continuous;*

• *for every $a \in X$ the function $f_a(x) = \rho(a,x)$ is continuous.*

Denote by $Pq(X)$ the space of all continuous pseudo-quasimetrics on a space X and by $P(X)$ the space of all continuous pseudometric on a space X.

For any continuous pseudometric ρ on a space X there exist a unique metric space $(X/\rho, \hat{\rho})$ and a continuous mapping $p_\rho : X \to X/\rho$ of X onto X/ρ such that $\rho(x,y) = \hat{\rho}(p_\rho(x), p_\rho(y))$ for all $x, y \in X$.

The pseudometric $\rho \in P(X)$ is complete if the metric space $(X/\rho, \hat{\rho})$ is complete. Denote by $CP(X)$ the space of all complete pseudometrics on a space X.

For any continuous pseudo-quasimetric ρ on a space X there exist a unique metric space $(X/\rho, \hat{\rho})$ and a continuous mapping $p_\rho : X \to X/\rho$ of X onto X/ρ such that $\rho(x,y) = \hat{\rho}(p_\rho(x), p_\rho(y))$ for all $x, y \in X$.

Let ρ be a pseudo-quasimetric on X. The sequence $\{x_n : n \in \mathbb{N}\}$ is a ρ-Cauchy sequence if for each $\varepsilon > 0$ there exists $k \in \mathbb{N}$ such that $\rho(x_n, x_m) < \varepsilon$ for all $n, m \geq k$.

We say that the pseudo-quasimetric ρ is complete if on X/ρ any $\hat{\rho}$-Cauchy sequence is convergent.

If X is a discrete space, then $P(X)$ is the space of all pseudometrics on X. Therefore it is sufficient to study only the continuous pseudometrics and the weak continuous distance function.

2. THE TOPOLOGY OF UNIFORM CONVERGENCE

Denote by $C(X)$ the space of all continuous real-valued functions of a space X. If $d(f,g) = \sup\{|f(x) - g(x)| : x \in X\}$ for all $f, g \in C(X)$, then $(C(X), d)$ is a complete metric space. The topology generated by the metric d is called the topology of uniform convergence on $C(X)$.

Obviously, $P(X)$ and $Pq(X)$ are subsets of the space $C(X \times X)$. The topology of uniform convergence on $F(X\times X)$ is generated by the metric $d(\rho_1, \rho_2) = \sup\{|\rho_1(x,y) - \rho_2(x,y)| : x, y \in X\}$ for all $\rho_1, \rho_2 \in F(X \times X)$.

Proposition 2.1. *For any space X the following assertions are true:*

1. The set $F_s(X \times X)$ of all symmetrical functions is closed in the space $(F(X \times X), d)$.

2. The set $F_d(X\times X)$ of all pseudo-distance functions is closed in the space $(F(X\times X), d)$.

3. The set $F_t(X\times X)$ of all triangular functions is closed in the space $(F(X\times X), d)$.

4. The set $F_z(X \times X)$ of all non-negative functions is closed in the space $(F(X \times X), d)$.

Proof. Let $\rho \in F(X \times X) \setminus F_s(X \times X)$. Then there exist two distinct points $a, b \in X$ such that $\rho(a,b) \neq \rho(b,a)$. Assume that $2r = \rho(a,b) - \rho(b,a) > 0$. If $\psi \in F(X \times X)$ and $d(\rho, \psi) < r$, then $\psi(a,b) - \psi(b,a) \geq r - d(\rho,\psi) > 0$. Hence the set $U = \{\psi \in F(X\times X) : d(\rho,\psi) < r\}$ is open in the space $(F(X\times X), d)$, $\rho \in U$ and $U \cap F_s(X\times X) = \emptyset$. Assertion 1 is proved.

Let $\rho \in F(X \times X) \setminus F_d(X \times X)$. Then there exist two distinct points $a, b \in X$ such that $\rho(a,b) < \rho(a,a)$. Assume that $2r = \rho(a,a) - \rho(a,b) > 0$. If $\psi \in F(X \times X)$ and $d(\rho,\psi) < r$, then $\psi(a,a) - \psi(a,b) \geq r - d(\rho,\psi) > 0$. Hence the set $U = \{\psi \in F(X\times X) : d(\rho,\psi) < r\}$ is open in the space $(F(X \times X), d)$, $\rho \in U$ and $U \cap F_d(X \times X) = \emptyset$. We prove that the set $F_d(X \times X)$ of all pseudo-distance functions is closed in the space $(F(X \times X), d)$. Assertion 2 is proved.

Let $\rho \in F(X \times X) \setminus F_t(X \times X)$. Then there exist three distinct points $a, b, c \in X$ such that $\rho(a,c) > \rho(a,b) + \rho(b,c)$. Assume that $2r = \rho(a,c) - \rho(a,b) - \rho(b,c) > 0$. If $\psi \in F(X \times X)$ and $d(\rho,\psi) < r$, then $\psi(a,c) - \psi(a,b) - \psi(b,c) \geq r - d(\rho,\psi) > 0$. Hence the set $U = \{\psi \in F(X \times X) : d(\rho,\psi) < r\}$ is open in the space $(F(X \times X), d)$, $\rho \in U$ and $U \cap F_t(X \times X) = \emptyset$. Assertion 3 is proved.

Let $\rho \in F(X \times X) \setminus F_z(X \times X)$. It is possible one of the following two cases.

Case 1. $\psi(a,b) < 0$ for some $a, b \in X$. If $0 < 2\varepsilon < |\psi(a,b)|$, then $B(\psi, d, \varepsilon) \cap F_t(X \times X) = \emptyset$.

Case 2. $\psi(a,a) > 0$ for some $a \in X$. If $0 < 2\varepsilon < \psi(a,a)$, then $B(\psi, d, \varepsilon) \cap F_t(X \times X) = \emptyset$.

Assertion 4 is proved. The proof is complete. ∎

Since the subspace $C(X \times X)$ of all continuous functions on $X \times X$ is closed in the space $(F(X \times X), d)$ and for the set $Pq(X)$ of all continuous pseudo-quasimetrics on X we have $Pq(X) = C(X \times X \cap F_d(X \times X) \cap F_t(X \times X) \cap F_z(X \times X)$, then from Proposition 2.1 it follows:

Corollary 2.2. *The set $Pq(X)$ of all continuous pseudo-quasimetrics on X is closed in the spaces $(C(X \times X), d)$ and $(F(X \times X), d)$.*

Since for the set $P(X)$ of all continuous pseudometrics on X we have $P(X) = Pq(X) \cap F_s(X \times X)$, then from Proposition 2.1 and Corollary 2.2 it follows:

Corollary 2.2. *The set $P(X)$ of all continuous pseudoimetrics on X is closed in the spaces $(C(X \times X), d)$ and $(F(X \times X), d)$.*

Corollary 2.3. *$(P(X), d)$ and $(Pq(X), d)$ are the complete metric spaces.*

Let $CPq(X)$ be the set of all complete continuous pseudo-quasimetrics on X and $CP(X)$ be the set of all complete continuous pseudometrics on X

A space X is pseudocompact if any continuous function on X is bounded.

Proposition 2.4. *For a space X the following assertions are equivalent:*
1. X is pseudocompact.
2. The set $CP(X)$ of complete pseudometrics on a space X is closed in $(P(X), d)$.
3. $CP(X) = P(X)$.

Proof. Assume that X is not a pseudocompact space. Then there we have two cases.

Case 1. There exists a continuous function $f \in C(X)$ such that:
• $f(x) \geq 1$ for any $x \in X$;
• the set $f(X) \cap (n, +\infty)$ is not connected for any $n \in \mathbb{N}\}$.

Then there exists a sequence $\{t_n \in \mathbb{R} \setminus f(X) : n \in \mathbb{N}\}$ such that $t_{n+1} > 1 + t_n$ and $f(X) \cap (t_n, t_{n+1}) \neq \emptyset$ for any $n \in \mathbb{N}$. We put $U_1 = f^{-1}(-\infty, t_1)$ and $U_{n+1} = f^{-1}(t_n, t_{n+1})$ for any $n \in \mathbb{N}$. By construction, $\{U_n : n \in \mathbb{N}$ is an infinite discrete cover of the space X. For any $n \in \mathbb{N}$ there exists a point $b_n \in U_n$.

We construct the function $g : X \to [0,1]$ such that $g^{-1}(2^{-1}(2^{-n}) = U_n$ for any $n \in \mathbb{N}$. Let $g_n(x) = sup\{g(x), 2^{-n}\}$ for any $n \in \mathbb{N}$ and for each $x \in X$. The functions g, g_n are continuous.

Now we put $\rho_n(x,y) = |g_n(x) - g_n(y)|$, $\rho(x,y) = |g(x) - g(y)|$ for all $x, y \in X$ and $n \in \mathbb{N}$. The pseudometrics ρ_n are complete, since X/ρ_n are finite spaces. Since $\{b_n : n \in \mathbb{N}\}$ is a non-convergent Cauchy sequence of the metric space $(X/\rho, \hat{\rho})$, the

pseudometrics ρ is not complete and $d(\rho, \rho_n) = 2^{-n-1}$ for any $n \in \mathbb{N}$. Thus the set $CP(X)$ is not closed in $P(X)$.

Case 2. For any non-negative continuous function $f \in C(X)$ there exists $t(f) \in \mathbb{R}$ such that the set $f(X) \cap (t(f), +\infty)$ is connected.

Since the space X is not pseudocompact, then there exists a non-negative unbounded continuous function $f : X \to \mathbb{R}$. We put $g(x) = (1 + sup\{t(f), f(x)\} - t(f))^{-1}$ for any $x \in X$. Then g is a continuous function on X and $g(X) = (0, 1]$. For any $n \in \mathbb{N}$ we fix a point $b_n \in g^{-1}(2^n)$. Let $g_n(x) = sup\{g(x), 2^{-n}\}$ for any $n \in \mathbb{N}$ and for each $x \in X$. The functions g_n are continuous.

As in the case 1, now we put $\rho_n(x, y) = |g_n(x) - g_n(y)|$, $\rho(x, y) = |g(x) - g(y)|$ for all $x, y \in X$ and $n \in \mathbb{N}$. The pseudometrics ρ_n are complete, since X/ρ_n are compact spaces. Since $\{b_n : n \in \mathbb{N}\}$ is a non-convergent Cauchy sequence of the metric space $(X/\rho, \hat{\rho})$, the pseudometrics ρ is not complete and $d(\rho, \rho_n) = 2^{-n-1}$ for any $n \in \mathbb{N}$. Thus the set $CP(X)$ is not closed in $P(X)$.

Let X be a pseudocompact space. If $\rho \in P(X)$, then the $(X/\rho, \hat{\rho})$ is a compact space. Thus $\hat{\rho} \in CP(X)$. The proof is complete. ∎

3. THE SPACE OF PERFECT PSEUDOMETRICS

A pseudometric $\rho \in P(X)$ is called a perfect pseudometric on a space X if the mapping $p_\rho : X \to X/\rho$ is perfect, i.e. is continuous, closed and the fibers $p_\rho^{-1}(z)$ are compact subsets of the space X.

Fix $\rho \in P(X)$. We put $H(x, \rho) = \{y \in X : \rho(x, y) = 0\}$. The pseudometric ρ is perfect if and only if:

– $H(x, \rho)$ ia a compact set for any $x \in X$;

– for any $x \in X$ and any open set $U \supseteq H(x, \rho)$ there exists $\varepsilon > 0$ such that $B(x, \rho, \varepsilon) \subseteq U$.

Let $PK(X)$ be the set of all perfect pseudometrics on a space X. The space $PK(X)$ is non-empty if and only if X is a paracompact p-space. A space X is called a paracompact p-space if X admits a perfect mapping onto some metric space [2].

We put $CPK(X) = CP(X) \cap PK(X)$. The space $CPK(X)$ is non-empty if and only if X is a paracompact Čech-complete space [2, 7].

Proposition 3.1. *For a space X the following assertions are equivalent:*

1. X is a paracompact p-space.

2. $PK(X) \neq \emptyset$.

3. The set $PK(X)$ *is dense in the space* $P_n(X)$.

Proof. Implication $1 \to 2 \to 1$ follows from the Arhangel'skii's caracterization theorem of the paracompact p-spaces [2].

Implication $3 \to 1$ is obvious.

Let $\rho_0 \in PK(X), \rho \in P(X)$ and $\varepsilon > 0$. We can assume that $\rho_0(x, y) \leq 1$ for any $x, y \in X$. We put $\rho_\varepsilon = \rho(x, y) + \varepsilon\rho_0(x, y)$ for any $x, y \in X$. Then $\rho_\varepsilon \in PK(X)$ and $d(\rho, \rho_\varepsilon) \leq \varepsilon$. The proof is complete. ∎

If $\rho_0 \in CPK(X)$, then $\varepsilon\rho_0 + \rho \in CPK(X)$ for any $\rho \in P(X)$ and $\varepsilon > 0$. Hence we proved the next proposition.

Proposition 3.2. *For a space X the following assertions are equivalent:*
1. X is a paracompact Čech-complete space.
2. $CPK(X) \neq \emptyset$.
3. The set $CPK(X)$ is dense in the space $(P(X), d)$.

Corollary 3.3. *For a space X the next assertions are equivalent:*
1. X is a compact space.
2. $CPK(X) = PK(X) = P(X)$.
3. $PK(X)$ is a non-empty closed subset of the space $(P(X), d)$.

Let $M(X)$ be the set of all continuous metrics on a space X. Then the metrics from $MK(X) = M(X) \cap PK(X)$ generalized the topology of the space X.

Corollary 3.4. *For a space X the next assertions are equivalent:*
1. $M(X) \neq \emptyset$.
2. The set $M(X)$ is dense in $P_n(X)$.

Corollary 3.5. *For a space X the next assertions are equivalent:*
1. $MK(X) \neq \emptyset$.
2. The set $MK(X)$ is dense in $P_n(X)$.

Denote by $CM(X)$ the set of all complete continuous metrics on a space X and $CMK(X) = CM(X) \cap PK(X)$ the space of all complete metrics which generate the topology of the space X. The space X is called complete submetrizable if $CM(X) \neq \emptyset$.

Corollary 3.6. *For a space X the next assertions are equivalent:*
1. The set $CM(X) \neq \emptyset$.
2. The set $CM(X)$ is dense in $P_n(X)$.
3. The space X is complete submetrizable.

Corollary 3.7. *For a space X the next assertions are equivalent:*
1. The set $CMK(X) \neq \emptyset$.
2. The set $CMK(X)$ is dense in $P_n(X)$.
3. The space X is complete metrizable.

Remark 3.8. *If the space X is not compact, then on X there exists a continuous pseudometric which is not a perfect pseudometric.*

4. THE SPACE OF QUASI-PERFECT PSEUDOMETRICS

A mapping $f : X \longrightarrow Y$ of a space X onto a space Y is called quasi-perfect if it is continuous, closed and the fibers $f^{-1}(y)$, $y \in Y$, are countably compact. Any perfect mapping is quasi-perfect.

One of the most important results of the theory of p-spaces is the following Arhangel'skii's characteristic of the perfect pre-images of the metric space: a space X is a paracompact p-space if and only if X admits a perfect mapping onto some metric space (see [2]). In this context it is interesting the next Morita's concept: a space X is called *an M-space* if X admits a quasi-perfect mapping onto some metric space (see [10]). If Y is a complete metric space, then we say that X is a complete M-space [4].

A pseudometric $\rho \in P(X)$ is called a quasi-perfect pseudometric on a space X if the mapping $p_\rho : X \to X/\rho$ is quasi-perfect.

Fix $\rho \in P(X)$. The pseudometric ρ is quasi-perfect if and only if:

– $H(x, \rho)$ ia a countably compact set for any $x \in X$;

– for any $x \in X$ and any open set $U \supseteq H(x, \rho)$ there exists $\varepsilon > 0$ such that $B(x, \rho, \varepsilon) \subseteq U$.

Let $PQ(X)$ be the set of all quasi-perfect pseudometrics on a space X. The space $PQ(X)$ is non-empty if and only if X is an M-space.

We put $CPQ(X) = CP(X) \cap PQ(X)$. The space $CPQ(X)$ is non empty if and only if X is a complete M-space.

Proposition 4.1. *For a space X the following assertions are equivalent:*
1. X is an M-space.
2. $PQ(X) \neq \emptyset$.
3. The set $PQ(X)$ is dense in the space $P_n(X)$.

The proof is similar to the proof of Proposition 3.1.

Proposition 4.2. *For a space X the following assertions are equivalent:*
1. X is a complete M-space.
2. $CPQ(X) \neq \emptyset$.
3. The set $CPQ(X)$ is dense in the space $(P(X), d)$.

The proof is similar to the proof of Proposition 3.2.

Corollary 4.3. *For a space X the next assertions are equivalent:*
1. X is a countably compact space.
2. $CPQ(X) = PQ(X) = P(X)$.
3. $PQ(X)$ is a non-empty closed subset of the space $(P(X), d)$.

Remark 4.4. *If the space X is not countably compact, then on X there exists a continuous pseudometric which is not a quasi-perfect pseudometric.*

Remark 4.5. *If the space X is countably compact and not compact, then on X there exists a quasi-perfect pseudometric which is not a perfect pseudometric.*

5. THE SPACE OF PSEUDO-PERFECT PSEUDOMETRICS

A subset L of a space X is called *bounded* if for every locally finite family γ of open subsets in X the set $\{U \in \gamma : U \cap L \neq \emptyset\}$ is finite.

A subset L of a Tychonoff space X is bounded if and only if every continuous function on X is bounded on L (see [6]).

A space X is called a μ-complete space if the closure $cl_X F$ of any bounded subset F of X is a compact subset of X.

A subset F of a space X is called a functionally closed subset of X if $F = g^{-1}(0)$ for some continuous functions [6].

A mapping $f : X \longrightarrow Y$ is called *z-closed* if the set $f(H)$ is closed in Y for any functionally closed subset H of the space X.

A mapping $f : X \longrightarrow Y$ is called *pseudo-perfect* if it is z-closed and the fibers $f^{-1}(y)$, $y \in Y$, are bounded subsets of X.

Any quasi-perfect mapping is pseudo-perfect.

We say that a space X is *an $a\Pi$-space* (respectively, a complete $a\Pi$-space) if X admits a pseudo-perfect mapping onto some (respectively, complete) metric space [4].

Let $PB(X)$ be the set of all quasi-perfect pseudometrics on a space X. The space $PB(X)$ is non-empty if and only if X is an $a\Pi$-space.

We put $CPB(X) = CP(X) \cap PB(X)$. The space $CPB(X)$ is non empty if and only if X is a complete $a\Pi$-space.

Proposition 5.1. *For a space X the following assertions are equivalent:*
1. X is an $a\Pi$-space.
2. $PB(X) \neq \emptyset$.
3. The set $PB(X)$ is dense in the space $P_n(X)$.

The proof is similar to the proof of Proposition 3.1.

Proposition 5.2. *For a space X the following assertions are equivalent:*
1. X is a complete $a\Pi$-space.
2. $CPB(X) \neq \emptyset$.
3. The set $CPB(X)$ is dense in the space $(P(X), d)$.

The proof is similar to the proof of Proposition 3.2.

Corollary 5.3. *For a space X the next assertions are equivalent:*
1. X is a pseudocompact space.
2. $CPB(X) = PB(X) = P(X)$.
3. $PB(X)$ is a non-empty closed subset of the space $(P(X), d)$.

Remark 5.4. *We mention that for each space X the next assertions are true:*
1. $PK(X) \subseteq PQ(X) \subseteq PB(X)$ and $MK(X) = M(X) \cap PB(X)$.

2. If $PK(X) \neq \emptyset$, then $PK(X) = PQ(X) = PB(X)$.
3. If $PQ(X) \neq \emptyset$, then $PQ(X) = PB(X)$.

Remark 5.5. *If the space X is not pseudocompact, then on X there exists a continuous pseudometric which is not a pseudo-perfect pseudometric.*

Remark 5.6. *If the space X is pseudocompact and not countably compact, then on X there exists a pseudo-perfect pseudometric which is not a quasi-perfect pseudometric.*

6. THE SPACE OF PERFECT PSEUDO-QUASIMETRICS

A pseudo-quasimetric $\rho \in P(X)$ is called a perfect pseudometric on a space X if the mapping $p_\rho : X \to X/\rho$ is perfect.

Fix $\rho \in P(qX)$. We put $H(x,\rho) = \{y \in X : \rho(x,y) + \rho(y,x) = 0\}$. The pseudometric ρ is perfect if and only if:

– $H(x,\rho)$ ia a compact set for any $x \in X$;

– for any $x \in X$ and any open set $U \supseteq H(x,\rho)$ there exists $\varepsilon > 0$ such that $B(x,\rho,\varepsilon) \subseteq U$.

Let $PKq(X)$ be the set of all perfect pseudo-quasimetrics on a space X.

We put $CPKq(X) = CPq(X) \cap PKq(X)$.

Proposition 6.1. *For a space X the following assertions are equivalent:*
1. $PKq(X) \neq \emptyset$.
2. The set $PKq(X)$ is dense in the space $Pq(X)$.

Proof. Implication $2 \to 1$ is obvious.

Let $\rho_0 \in PKq(X), \rho \in Pq(X)$ and $\varepsilon > 0$. We can assume that $\rho_0(x,y) \leq 1$ for any $x, y \in X$. We put $\rho_\varepsilon = \rho(x,y) + \varepsilon\rho_0(x,y)$ for any $x, y \in X$. Then $\rho_\varepsilon \in PKq(X)$ and $d(\rho,\rho_\varepsilon) \leq \varepsilon$. The proof is complete. ∎

If $\rho_0 \in CPKq(X)$, then $\varepsilon\rho_0 + \rho \in CPK(X)$ for any $\rho \in P(X)$ and $\varepsilon > 0$. Hence we proved the next proposition.

Proposition 6.2. *Let $CPKq(X)$ be the set of all complete quasimetrics on a space X If the set $CPKq(X)$ is non-empty, then the set $CPKq(X)$ is dense in the space $(Pq(X), d)$.*

7. THE COMPACT-OPEN TOPOLOGY

Let $C_{co}(X,Y)$ be the set of all continuous mappings of a space X into a space Y in the compact-open topology with the open base $S(F_1, F_2, ..., F_n; V_1, V_2, ..., V_n) = \{f \in C(X,Y) : f(F_i) \subseteq V_i\}$ for any $i \leq n\}$, where $F_1, F_2, ..., F_n$ are compact subsets of X and $V_1, V_2, ..., V_n$ are open subsets of Y.

Any compact subset F of X and any pseudometric $\rho \in P(Y)$ generated the pseudometric $d_{(\rho,F)}(f,g) = \sup\{\rho(f(x), g(x)) : x \in F\}$ on $C(X,Y)$. The topology of the space $C_{co}(X,Y)$ is generated by the pseudometrics $d_{(\rho,F)}$. The compact-open topology is called the compact convergence topology too.

For any space X the identical mapping $C_n(X) \to C_{co}(X)$ is continuous.

Denote by $P_{co}(X)$ the space $P(X)$ in the compact-open topology.

Fix on X a family ξ of subsets with the properties:

• $X = \cup\xi$;

• if $L, H \in \xi$ then $L \cup H \in \xi$.

We say that ξ is an additive cover of X.

Then any $L \in \xi$ generated the pseudometric $d_L(\rho_1, \rho_2) = \sup\{|\rho_1(x,y) - \rho_2(x,y)| : x, y \in L\}$. The pseudometrics $\{d_L : L \in \xi\}$ generated the topology $\mathcal{T}(\xi)$. If $X \in \xi$, then $\mathcal{T}(\xi)$ is the uniform topology. If ξ is the family of all compact subsets of X, then $\mathcal{T}(\xi)$ is the compact open topology on $P(X)$. If ξ is the family of finite subsets, then $\mathcal{T}(\xi)$ is the topology of pointwise convergence. We say that $\mathcal{T}(\xi)$ is the topology of uniform convergence on the sets $L \in \xi$.

The identical mapping $P_U(X) \to P_\xi(X)$ is continuous.

If some set $L \subseteq P(X)$ is dense in $P_n(X)$, then the set L is dense in $P_\xi(X)$ for any additive cover ξ on X.

Thus from the results of the above Sections we obtain the next sentences.

Corollary 7.1. *For a space X the following assertions are equivalent:*
1. $MK(X) \neq \emptyset$.
2. The set $MK(X)$ is dense in $P_\xi(X)$ for some additive cover ξ on X.
3. The set $MK(X)$ is dense in $P_\xi(X)$ for every additive cover ξ on X.
4. The set $MK(X)$ is dense in $P_{co}(X)$.

Corollary 7.2. *For a space X the following assertions are equivalent:*
1. $PK(X) \neq \emptyset$.
2. The set $PK(X)$ is dense in $P_\xi(X)$ for some additive cover ξ on X.
3. The set $PK(X)$ is dense in $P_\xi(X)$ for every additive cover ξ on X.
4. The set $PK(X)$ is dense in $P_{co}(X)$.

Corollary 7.3. *For a space X the following assertions are equivalent:*
1. $CPK(X) \neq \emptyset$.
2. The set $CPK(X)$ is dense in $P_\xi(X)$ for some additive cover ξ on X.
3. The set $CPK(X)$ is dense in $P_\xi(X)$ for every additive cover ξ on X.
4. The set $CPK(X)$ is dense in $P_{co}(X)$.

Corollary 7.4. *For a space X the following assertions are equivalent:*
1. X is a compact space.
2. $PK(X)$ is a non-empty closed subset of $P_\xi(X)$ for some additive cover ξ on X.
3. $CPK(X)$ is a non-empty closed subset of $P_\xi(X)$ for some additive cover ξ on X.

4. $P(X) = PK(X) = CPK(X)$.

Corollary 7.5. *For a space X the following assertions are equivalent:*

1. X is a complete metrizable space.

2. The set of complete perfect metrics $CPK(X)$ *is dense in the space* $P_\xi(X)$ *for some additive cover* ξ *on X.*

3. The set $CPK(X)$ *is dense in the space* $P_\xi(X)$ *for any additive cover* ξ *on X.*

4. The set $CPK(X)$ *is dense in* $P_{co}(X)$.

Implication $1 \to 4$ for separable locally compact spaces was prowed by C.Varga and G.Farcas in [15]. Problems of structure of the set of all complete metrics were arised in [8, 9, 11, 12, 13, 14].

8. ON HEMICOMPACT SPACES

A space X is hemicompact if there exists a comutable family ξ_0 of compact subsets of X such that for any compact subset F of X there exists $\Phi \in \xi_0$ such that $F \subseteq \Phi$.

Proposition 8.1. *Let* ξ *be an additive cover of a space X. The following assertions are equivalent:*

1. The space $P_\xi(X)$ *is metrizable.*

2. The space $P_\xi(X)$ *is first countable.*

3. There exists a countable subfamily $\xi_0 \subseteq \xi$ *such that for any* $F \in \xi$ *there exists* $\Phi \in \xi_0$ *such that* $F \subseteq cl_X\Phi$.

Proof. Implication $1 \to 2$ is obvious.

Fix an additive countable cover ξ_0 of the space X. Then the topology of the space $P_{\xi_0}(X)$ is generated by a countably family of pseudometrics. Thus the space $P_\xi(X)$ is metrizable. Let $\bar{\xi} = \{cl_X F : F \in \xi\}$. Then the spaces $P_\xi(X)$ and $P_{\bar{\xi}}(X)$ are homeomorphic, i.e. $\mathcal{T}(\xi) = \mathcal{T}(\bar{\xi})$. If $\xi_0 \subseteq \xi$ and for any $F \in \xi$ we have $F \subseteq cl_X\Phi$ for some $\Phi \in \xi_0$, then $\mathcal{T}(\xi) = \mathcal{T}(\xi_0)$. This fact proves the implication $3 \to 1$.

Assume that $P_\xi(X)$ is a first countable space and $\{U_n : n \in \mathbb{N}\}$ is a base of the space $P_\xi(X)$ at the pseudometric 0, where $0(x, y) = 0$ for all $x, y \in X$. For any n there exist $\varepsilon_n > 0$ and $\Phi_n \in \xi$ such that $V_n = \{\rho \in P(X) : d_{\Phi_n}(0, \rho) < \varepsilon_n\} \subseteq U_n$ and $\varepsilon_n \leq 2^{-n}$. By construction, $\{V_n : n \in \mathbb{N}\}$ is a base of the space $P_\xi(X)$ at 0. Fix $F \in \xi$. There exists n such that $0 \in V_n \subseteq \{\rho \in P(X) : d_F(0, \rho) < 1\}$. We affirm that $F \subseteq cl_X\Phi_n$. Assume that $b \in U \in cl_X\Phi_n \backslash F$. There exists a continuous function $f : X \to [0, 1]$ such that $f(b) = 1$ and $F \subseteq f^{-1}(0)$. Then $\rho_f(x, y) = |f(x) - f(y)|$ is a continuous pseudometric on $X, d_F(0, \rho_F) = 0$, $d_{\Phi_n}(0, \rho) = 1$ and $\rho_f \notin V_n$, a contradiction. Implication $2 \to 3$ is proved. The proof is complete. ∎

Corollary 8.2. *For a space X the following assertions are equivalent:*

1. The space $P_{co}(X)$ *is metrizable.*

2. The space $P_{co}(X)$ *is first countable.*

3. The space X is hemicompact.

9. ON SPACES OF ADMISSIBLE PSEUDOMETRICS

In special cases we have dealings with pseudometrics or metrics with concrete properties. In this case it is necessary to have special constructions of "small" pseudometrics.

A family $p = \{f_\alpha \in C(X) : \alpha \in A\}$ of continuous functions on a space X is called locally finite if for each point $x \in X$ there exists an open set U such that $x \in U$ and the set $\{\alpha \in A : U \cap f_\alpha^{-1}(\mathbb{R} \setminus \{0\}) \neq \emptyset\}$ is finite.

If $p = \{f_\alpha) : \alpha \in A\}$ is a locally finite family of continuous functions on a space X, then $d_p(x, y) = \Sigma\{|f_\alpha(x) - f_\alpha(y)| : \alpha \in A\}$ is a continuous pseudometric on X.

A family $p = \{f_\alpha : \alpha \in A\}$ of continuous functions on a space X is called a partition of unity of the space X if:

- $\Sigma\{f_\alpha(x) : \alpha \in A\} = 1$ for each $x \in X$;
- $f_\alpha(x) \geq 0$ for all $x \in X$ and $\alpha \in A$;
- the family p is locally finite.

The partition of unity can be used to show the existence of Riemannian metrics and of complete smooth metrics on manifolds. If X is a smooth manifold and d is a pseudometric on X, then me say that the pseudometric d is smooth of the class C^n if for each $a \in X$ the function $d_a(x) = d(a, x)$ is continuous on X and of the class C^n on the domain $X \setminus \{a\}$.

A class $aP(X)$ of continuous pseudometrics on a space X is called additive if it has the following properties:

- if $c > 0$ and $\rho \in aP(X)$, then $c\rho \in aP(X)$;
- if $\rho_1, \rho_2 \in aP(X)$, then $\rho_1 + \rho_2 \in aP(X)$.

Proposition 9.1. *Assume that ξ is an additive cover of a space X, $aP(X)$ is an additive class of continuous pseudometrics on a space X and for each $Y \in \xi$ there exists $\rho \in aP(X) \cap CM(X)$ such that $\rho(x, y) \leq 1$ for each $x, y \in Y$. Then the set $aP(X) \cap CM(X)$ is dense in the space $(aP(X), \mathcal{T}(\xi))$.*

Proof. In this case the set $\{d + c\rho : d \in aP(X), \rho \in aP(X) \cap CM(X), c > 0\}$ is dense in the space $(aP(X), \mathcal{T}(\xi))$. ∎

Corollary 9.2. *Assume that ξ is an additive cover of compact subsets of a space X, $aP(X)$ is an additive class of continuous pseudometrics on a space X and $aP(X) \cap CM(X) \neq \emptyset$. Then the set $aP(X) \cap CM(X)$ is dense in the space $(aP(X), \mathcal{T}(\xi))$.*

Corollary 9.3. *Assume that ξ is an additive cover of compact subsets of a space X, $aP(X)$ is an additive class of continuous pseudometrics on a space X and $aP(X) \cap CMK(X) \neq \emptyset$. Then the set $aP(X) \cap CMK(X)$ is dense in the space $(aP(X), \mathcal{T}(\xi))$.*

References

[1] R. Arens. *A topology for spaces of transformations.* Ann of Math, **47**(1946), 480-495.

[2] A. V. Arhangeliskii. *A class of spaces which contains all metric and all locally compact spaces*,Matem.Sb.**67**(1965),33-60(English translation: Amer Math. Soc. Transl. **92**(1970),1-39).

[3] A. V. Arhangel'skii, M.M. Choban, P. S. Kenderov, *Topological games and continuity of group operations*, Topol. Appl. 157(2010) 2542-2552.

[4] M. M. Choban, *Spaces and mappings with conditions related to paracompactness*, Proceedings ICTA2011, Islamabad, Pakistan, July 4-10, 2011, Cambridge Scientific Publishers (2012), 105-132.

[5] M. M. Choban, D. I. Pavel, *On a space of pseudometrics*, International Conference "Mathematics and Information Technologies: Research and Education (MITRE-2011)", August 22-25, 2011, Abstracts, Moldova State University, Chisinau, 2011, p. 36-37.

[6] R. Engelking, *General Topology*. Warsawa: PWN, 1977.

[7] Z. Frolik, *On the topological product of paracompact spaces*, Bull.Acad.Polon.Sci. Ser.Math. **8**(1960), 747-750.

[8] W. B. Gordon. *An analytical criterion for the completeness of Riemannian manifolds*, Proceed. Amer. Math. Soc. **37**(1973), 221-225.

[9] Ju. Jost, *Riemannian Geometry and Geometric Analysis*, Berlin, New York: Springer-Verlag, 2008.

[10] K. Morita, *A survey of the theory of M-spaces*, General Topol. Appl. 1 (1971) 49-55.

[11] K.Nomizu, H.Oseki. *The existence of complete Riemannian metrics*, Proceed. Amer. Math. Soc. **12**(1961), 889-891.

[12] R. Palais, *Homotopy theory of infinite dimensional manifolds*, Topology **5**(1966), 1-16.

[13] L. Băileanu, *Varietaţi topologice şi diferenţiale*, Iaşi, 1984.

[14] C. Udrişte, *Completness of Finsler manifolds*, Publicationas Math. **42**, Fasc. 1-2(1993), 45-51.

[15] C. Varga, G. Farcas, *On the completeness of metric spaces*, Colloquium on topology. J.Bolyai Math. Society. August 23-27, 1993, Szekszard, Hungary, 1993, p.19.

ROMAI J., v.9, no.2(2013), 75–87

ON THE IMPACT OF EXPLICIT OR SEMI-IMPLICIT INTEGRATION METHODS OVER THE STABILITY OF REAL-TIME NUMERICAL SIMULATIONS

Teodor Cioacă[1], Horea Cărămizaru[2]
[1,2] *"Politehnica" University Bucharest*
t.cioaca@gmail.com

Abstract Physics-based animation of soft or rigid bodies for real-time applications often suffers from numerical instabilities. We analyse one of the most common sources of unwanted behaviour: the numerical integration strategy. To assess the impact of popular integration methods, we consider a scenario where soft and hard constraints are added to a custom designed deformable linear object. Since the goal for this class of simulation methods is to attain interactive frame-rates, we present the drawbacks of using explicit integration methods over inherently stable, implicit integrators. To help numerical solver designers better understand the impact of an integrator on a certain simulated world, we have conceived a method of benchmarking the efficiency of an integrator with respect to its speed, stability and symplecticity.

Keywords: numerical simulation, computer graphics, computer animation, numerical modeling.
2010 MSC: 65L07, 65L20, 62P35, 37M15, 68U20.

1. INTRODUCTION

Intricate physical and mathematical models for simulating soft or rigid bodies are the centre of intensive research efforts. Computer animation, laparoscopic haptic surgery simulations, graphical special effects or robotic manipulation are just a few of the fields where such models play a key role. The focus of our research is to address the issue of carrying out stable, physics-based simulations at interactive update rates. For this purpose, we have conceived an elementary framework for building deformable objects with soft or stiff constraints. Using this framework, we can test the efficiency and impact of several, well-known numerical integrators. To address our goal, we look find an equilibrium between an integrator's computational overhead, its precision, symplecticity and, most importantly, its inherent stability.

Following the aforementioned goals, we present a short literature survey on the numerical simulation of soft or semi-rigid bodies in section 2. The mathematical apparatus for creating and simulating constrained objects is explained in section 3, and our own, deformable linear object model case study is presented in section 4. We present a general update strategy that supports any type of explicit or semi-implicit

integration method in section 5. Finally, the efficiency of several popular integrators is analysed and discussed in section 6, and we conclude this research in section 7.

2. RELATED WORK

Stability as a central attribute to Physics-based object simulation within the Computer Graphics world was addressed by directly consider inherently stable integrators. The most popular method employed is the first order, implicit Euler scheme. Servin et al. [15] treated infinitely stiff springs as kinematic constraints and developed a system capable of simulating elastic behaviour at the cost of solving a large sparse linear system for each iteration. The hybrid method of Schroeder et al. [14] uses explicit updates for the elastic forces and implicit strategies for other components. This complex idea tries to reduce the effect of suppressing material vibrations due to the use of pure implicit integrators. By alternating between implicit, semi-implicit and explicit methods, Volino et al. [20] demonstrated how different cloth materials can be modeled to overcome the inabilities of one integrator to support a certain material property. Some object models allow using for computing an analytical force approximation for an implicit solver as demonstrated by Mesit et al. [12]. Their method of simulating gas filled soft bodies can thus easily support any integrator, but it relies on the topological structure for all analytical derivations. Finally, structured mass-spring models using pure implicit integrators were popularized by Baraf and Witkin [2] in their seminal paper on stable cloth simulation and by Desbrun et al. [5] where inverse dynamics were used to tackle outstretching artefacts. For a discussion of the performance of some popular implicit solvers we direct the user to the paper of Hauth et al. [9].

Explicit methods are more popular due to their reduced complexity. Finite element simulations using explicit integrators were performed by Fierz et al. [8]. To stabilize the numerical process, the authors proposed modifying the stiffness matrices of ill-conditioned tetrahedral elements. This allowed their simulation to use higher time steps in spite of the explicit updates. Although less computationally demanding and stable than their implicit counterparts, explicit integrators can share a fair amount of stability, energy conserving capabilities and time reversibility. In this respect, Tsai et al. [18] present a comprehensive survey on symplectic integrators used in molecular dynamics.

In a different class of their own, position-based dynamics (see Bender et al. [1] for a survey) offer a workaround for any force or impulse based system, avoiding the intricacies of using integrators. This family of methods is, however, inaccurate for scenarios where velocities and forces need to be measured, hence we mention it as an alternative for special effects applications.

For a comprehensive list of simulation methods involving deformable objects, we invite the reader to consult the work of Nealen et al. [13] or that of Jimenez [11].

3. CONSTRAINED OBJECT ANIMATION

To better understand the elements involved in most physics-based animation scenarios, we will briefly introduce a simple constraint enforcing system. Supporting this kind of simulation mechanism requires a discrete geometrical sampling of the initial shape of the object. For exemplification purposes, we consider a deformable linear object, embedded in a 3D space, whose cross-section is considerably smaller than its length. Its elastic properties that determine how its discrete structure changes are implemented by adding geometric constraints enforced by potentials (see the work of Teschner et al. [17] for a more detailed and generalized application). These potentials provide a direct measure of how the structure of points differs from its initial configuration.

Generally, if $\mathbf{p}_1, \ldots, \mathbf{p}_N$ are the vertices of a constrained group, then a constraint function is defined as follows:

$$C(\mathbf{p}_1, \ldots, \mathbf{p}_N) : \mathbb{R}^{3N} \to \mathbb{R}. \tag{1}$$

This function incorporates additional information relating the current vertex configuration of the group to the initial geometrical image through specific scalar measures of length, area, angle, volume, etc. For example, a length based constraint incorporates the initial or rest lengths of directly connected vertices as a reference for the measure of deviation. Generally, an energy function produces only positive amounts and can be written as:

$$E(\mathbf{p}_1, \ldots, \mathbf{p}_N) = \frac{1}{2} C(\mathbf{p}_1, \ldots, \mathbf{p}_N)^2. \tag{2}$$

For a $\{\mathbf{p}_1, \ldots, \mathbf{p}_N\}$ configuration, we now consider the restriction of the energy function at a node $\mathbf{p}_i$. This function is written as:

$$E_{\mathbf{p}_i}(\mathbf{x}) : \mathbf{x} \in \mathbb{R}^3 \to \mathbb{R}_+. \tag{3}$$

Since the gradient vector coincides with the direction of maximum potential increase, it is natural to consider a penalty function that points in the opposite direction:

$$F_{\mathbf{p}_i}(\mathbf{x}) = -\nabla E_{\mathbf{p}_i}(\mathbf{x}). \tag{4}$$

This last equation can be written in an equivalent form:

$$F_{\mathbf{p}_i}(\mathbf{x}) = -C_{\mathbf{p}_i}(\mathbf{x}) \nabla C_{\mathbf{p}_i}(\mathbf{x}). \tag{5}$$

The simplest example of such a behaviour is the case of a linear spring connecting two points $\mathbf{p}_i$ and $\mathbf{p}_j$. The natural constraint function is defined as:

$$C(\mathbf{p}_i, \mathbf{p}_j) = \sqrt{K_l} \left(\|\mathbf{p}_i - \mathbf{p}_j\| - L_0 \right), \tag{6}$$

where L_0 denotes the spring's rest length. From this constraint function, a corresponding elastic deformation potential energy can be expressed as:

$$E(\mathbf{p}_i, \mathbf{p}_j) = \frac{K_l}{2}\left(|\|\mathbf{p}_i - \mathbf{p}_j\|| - L_0\right)^2. \tag{7}$$

We define the following operator:

$$\frac{\partial}{\partial \mathbf{p}_i} E = \nabla E_{\mathbf{p}_i}, \tag{8}$$

also known in some works as the variational or functional derivative operator.

An elastic spring force at node $\mathbf{p}_i$ can be derived using equation (7):

$$F_{\mathbf{p}_i}^{spring}(\mathbf{p}_i, \mathbf{p}_j) = -\frac{\partial}{\partial \mathbf{p}_i}\left(\frac{K_l}{2}\left(|\|\mathbf{p}_i - \mathbf{p}_j\|| - L_0\right)^2\right).$$

After applying several derivative computation rules (chain rule and the derivative of a product of two functions), we find the general elastic force expression:

$$F_{\mathbf{p}_i}^{spring}(\mathbf{p}_i, \mathbf{p}_j) = -\mathrm{K_l}\left(|\|\mathbf{p}_i - \mathbf{p}_j\|| - L_0\right)\frac{(\mathbf{p}_i - \mathbf{p}_j)}{\|\mathbf{p}_i - \mathbf{p}_j\|}, \tag{9}$$

where $\mathrm{K_l}$ is the linear spring's stiffness coefficient.

A deformable object defined as a closed surface can be discretized by dividing its interior volume into tetrahedral cells. Apart from linear springs, it is desirable to enforce local constraints aimed at preserving the volumes under deformation. Such forces are easy to introduce by deriving them from a volume preserving constraint function involving tetrahedral cells:

$$C_V(\mathbf{p}_i, \mathbf{p}_j, \mathbf{p}_k, \mathbf{p}_l) = \frac{\frac{\sqrt{K_V}}{6}\left\langle \mathbf{p}_j - \mathbf{p}_i, (\mathbf{p}_k - \mathbf{p}_i) \times (\mathbf{p}_l - \mathbf{p}_i)\right\rangle - V_0}{V_0}, \tag{10}$$

where V_0 is the volume of the tetrahedron in its rest configuration. Subsequently, the volume preserving potential is:

$$E_V(\mathbf{p}_i, \mathbf{p}_j, \mathbf{p}_k, \mathbf{p}_l) = \frac{K_V}{2} C_v(\mathbf{p}_i, \mathbf{p}_j, \mathbf{p}_k, \mathbf{p}_l)^2. \tag{11}$$

Using the same method as for linear springs, we compute the force at the $\mathbf{p}_i$ vertex by using the $\frac{\partial}{\partial \mathbf{p}_i}$ operator:

$$F_{V_{\mathbf{p}_i}}(\mathbf{p}_i, \mathbf{p}_j, \mathbf{p}_k, \mathbf{p}_l) = -\frac{\partial}{\partial \mathbf{p}_i} E_V(\mathbf{p}_i, \mathbf{p}_j, \mathbf{p}_k, \mathbf{p}_l). \tag{12}$$

After conveniently arranging the results from the derivation of equation (12), we can write down the expanded formula of this force:

$$\begin{aligned} F_{V_{\mathbf{p}_i}}(\mathbf{p}_i, \mathbf{p}_j, \mathbf{p}_k, \mathbf{p}_l) = &\frac{K_V}{6V_0^2}\left[\frac{1}{6}(\mathbf{p}_j - \mathbf{p}_i) \cdot (\mathbf{p}_k - \mathbf{p}_i) \times (\mathbf{p}_l - \mathbf{p}_i) - V_0\right] \cdot \\ &\cdot (\mathbf{p}_j - \mathbf{p}_l) \times (\mathbf{p}_k - \mathbf{p}_l), \end{aligned} \tag{13}$$

where K_V is an added-in stiffness coefficient. Examining figure 1, we can see how the

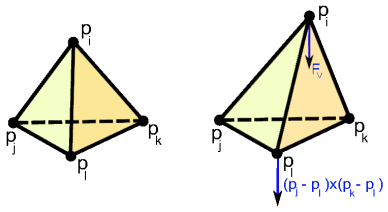

Fig. 1.: Volumetric force on a tetrahedral cell.

volumetric force acts to prevent volume changes. For example, if point $\mathbf{p}_i$ is shifted and the volume increases as a consequence, the direction of the volumetric force is given by the cross product vector $(\mathbf{p}_j - \mathbf{p}_l) \times (\mathbf{p}_k - \mathbf{p}_l)$. Inconsistent or "flipped" cell configurations, as well as degenerate tetrahedra can and are likely to be encountered during a simulation. Compressible bodies prevent themselves from being completely flattened by acting as non-linear spring elements. When their state is close to a collapse, the elastic forces should increase asymptotically towards infinity. Since the volumetric force component acts like a vertex to face spring in our system, we add a non-linear spring component, as suggested in [3]. Hence, if V is the current volume of a $(\mathbf{p}_i, \mathbf{p}_j, \mathbf{p}_k, \mathbf{p}_l)$ tetrahedron, then we can write the expression of the improved volumetric force as:

$$F_{V_{\mathbf{p}_i}}(\mathbf{p}_i, \mathbf{p}_j, \mathbf{p}_k, \mathbf{p}_l) = \\ K_V \left[\frac{V - V_0}{6V_0^2} - \sigma(V_0)\frac{V_0^2}{|V|} + V \right] \cdot (\mathbf{p}_j - \mathbf{p}_l) \times (\mathbf{p}_k - \mathbf{p}_l), \tag{14}$$

where $\sigma(x)$ is the sign function defined on the set of real values.

Another scenario that can prevent the simulation from recovering its initial rest shape in the absence of perturbing forces is the inversion phenomenon. The authors of [16] present an improved mechanism, capable of handling the inversion of a tetrahedral structure for finite element simulations. This process relies on finding a rotation that best aligns the deformed cell with its undeformed counterpart and then deriving penalty forces. While we could have used a similar approach, the above modification works for cases where negative volumes are reported. The elastic penalty forces described by equation (14) are capable of acting against the inversion. Additionally, other constraint-based forces can be derived (e.g. area preserving forces for the triangular faces of a tetrahedron or angle preserving forces).

4. DEFORMABLE LINEAR OBJECT MODEL

Using constrained mass point configuration, we can now describe the steps required to build a tetrahedral cell-based deformable object along the geometric image of a support curve:

1 *A curve discretization:* $\{\mathbf{r}_0, \ldots, \mathbf{r}_{N-1}\}$ where $\mathbf{r}_i$ is a sample 3D point.

2 *A set of frames:* define the orientation vectors $\mathbf{q}_k = \frac{\overrightarrow{\mathbf{r}_k\mathbf{r}_{k-1}} \times \overrightarrow{\mathbf{r}_k\mathbf{r}_{k+1}}}{\|\overrightarrow{\mathbf{r}_k\mathbf{r}_{k-1}} \times \overrightarrow{\mathbf{r}_k\mathbf{r}_{k+1}}\|}$, and $\mathbf{p}_k = \frac{1}{\|\overrightarrow{\mathbf{r}_k\mathbf{r}_{k-1}}\|}\mathbf{q}_k \times \overrightarrow{\mathbf{r}_k\mathbf{r}_{k-1}}$. At each point $\mathbf{r}_k$, a coordinate frame $\{\overrightarrow{\mathbf{r}_k\mathbf{r}_{k+1}}, \overrightarrow{\mathbf{r}_k\mathbf{q}_k}, \overrightarrow{\mathbf{r}_k\mathbf{p}_k}\}$ is attached.

3 *Volumetric cells:* for each pair of neighbouring vertices, $\mathbf{r}_k\mathbf{r}_{k+1}$, three tetrahedra are constructed: $(R_{k+1}P_kQ_kR_k)$, $(R_{k+1}Q_{k+1}Q_kP_k)$, and $(R_{k+1}P_kP_{k+1}Q_{k+1})$ (as depicted in figure 2).

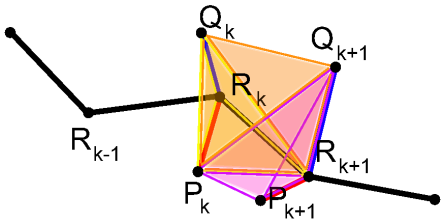

Fig. 2.: Tetrahedral cell division of a DLO segment.

The tetrahedral cells allow retrieving consistent information about local torsion and curvature changes from one link to another adjacent segment. A direct reference for how the object twists around the R_kR_{k+1} line is given by the relative orientation of $\overrightarrow{R_kQ_k}$ to $\overrightarrow{R_{k+1}Q_{k+1}}$. Structural resistance is added by substituting the edges of the tetrahedra with linear springs. These constraints tend to act like curvature springs since they oppose the bending of the object around the R_kQ_k line.

To account for plausible twisting behaviour, we introduce a quaternion based constraint system that acts like a torsional spring at each R_k node of the object. Considering there are three connected nodes, R_i, R_j and R_k, in this order, the torsional spring tends to reposition the Q_j point such that the resulting configuration is closer to the initial, rest configuration. Such a process requires finding a suitable axis and computing the relative orientation of the $\overrightarrow{R_jQ_j}$ vector with respect to the $\overrightarrow{R_iQ_i}$ and $\overrightarrow{R_kQ_k}$ vectors. We achieve this behaviour by computing a torsion compensating quaternion:

$$\tilde{\mathfrak{q}}_j = \texttt{SLERP}(\check{\mathfrak{q}}_{ij}, \check{\mathfrak{q}}^*_{jk}, \lambda), \tag{15}$$

where $\check{\mathfrak{q}}_{ij} = \texttt{Quat}(\widehat{R_iR_j}, \frac{1}{2}(u_ij^{(0)} - u_{ij}))$, $\check{\mathfrak{q}}_{jk} = \texttt{Quat}(\widehat{R_jR_k}, \frac{1}{2}(u^{(0)}_{jk} - u_{jk}))$. Further, $\texttt{Quat}(\hat{\mathbf{w}}, u)$ is the axis-angle representation of a quaternion and $\texttt{SLERP}(\mathfrak{q}_1, \mathfrak{q}_2, \lambda)$ is the

spherical linear interpolation result of the two unit quaternions with a ratio of λ, thus a minimum torque path generator on the 3-sphere. The spherical interpolation scalar is given by a linear blending based on the segment lengths $\lambda = \frac{\|\overrightarrow{R_iR_j}\|}{\|\overrightarrow{R_iR_j}\|+\|\overrightarrow{R_jR_k}\|}$. The angle expression $u_{ab} = \texttt{angle}_{\widehat{R_aR_b}}(\overrightarrow{R_aQ_a}, \overrightarrow{R_bQ_b})$ represents the angle between the $\overrightarrow{R_aQ_a}$ and $\overrightarrow{R_bQ_b}$ vectors with respect to the $\widehat{R_aR_b}$ axis , and the $^{(0)}$ superscript designates values for the initial, undeformed state of the object. The torsion quaternion, $\breve{\mathfrak{q}}_j$ can then be used to rotate the $\overrightarrow{R_jQ_j}$ vector to minimize the torsion offset. Instead of directly rotating this vector, a force will be applied to the Q_j node, thus mimicking the effects of an angular spring. Figure 3 depicts how the torsion quaternions are derived with respect to local geometry.

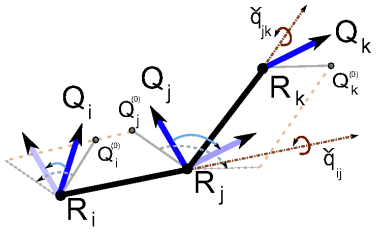

Fig. 3.: Torsion compensation using quaternions.

5. SIMULATION UPDATE LOGIC

In general, the steps required for a complete update of the object's state can be assembled as follows:

- *Numerical integration:* compute the current acceleration $\mathbf{a}^{(n)}$ from the current state $(\mathbf{x}, \mathbf{v})^{(n)}$. This is achieved by summing all force contributions acting at the $^{(n)}$ instance. Any force contributions from the collision solver stage are also added. Using an explicit integration method, the new $(\mathbf{x}, \mathbf{v})^{(n+1)}$ state is computed.

- *Approximate forces:* $\mathbf{f}^{(n+1)} = \frac{\mathbf{v}^{(n+1)}-\mathbf{v}^{(n)}}{\Delta t}$. These values are to be used in the collision response stage.

- *Collision resolution:* pairwise link collisions are detected and response forces and impulses are derived. These quantities are computed such that any colliding links are driven out of the interpenetrating configuration. To correct the positions and velocities, velocity ($\Delta\mathbf{v}$) and force ($\Delta\mathbf{f}$) residues are accumulated by using the response impulses and reaction and friction forces. These residues are fed back to the numerical integration scheme and are included in the acceleration component the next iteration will use. Since the design of collision

solvers for rigid and soft bodies is a vast field, beyond the scope of this paper, we direct the interested readers in more general models to consult the work of Ericson [6].

These steps must then be performed in this order, leading to a plausible update effect at interactive frame-rates.

6. RESULTS

We have used our model to simulate a simple laparoscopic suturing task. Given a physical substrate, a thread was driven through a tissue-like structure (see figure 4). The wire model we used is ideal for testing the behaviour of an integrator where both stiff and soft constraints drive the simulation. A simple methodology was employed to compute a score sheet for each integration scheme. We tracked the speed and stability of several methods while varying the time-step. The results were quantized by considering the explicit Euler method as a reference. The order of accuracy is not particularly important as it is orthogonal to our stability goals. Due to their energy-conserving properties, symplectic integrators are favoured when competing with other methods that achieve similar scores.

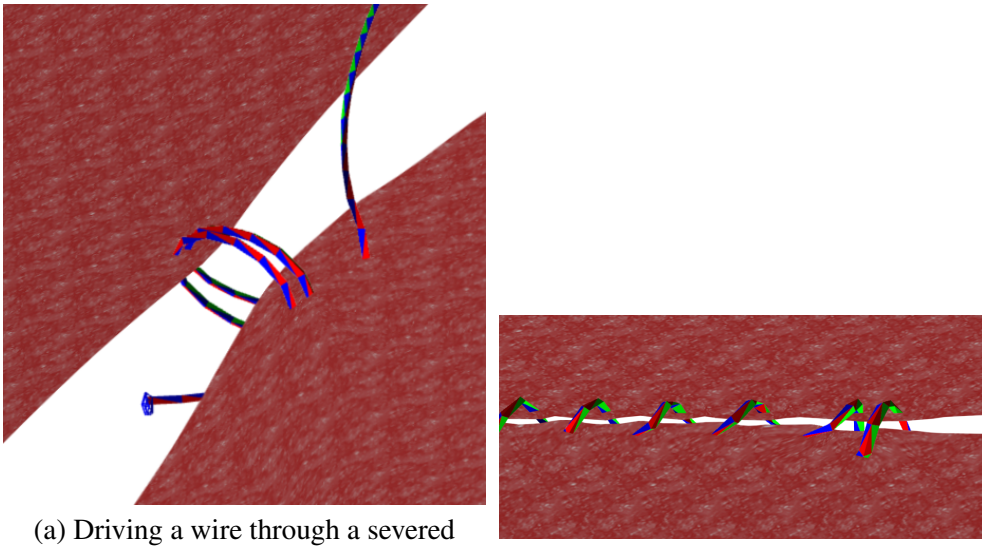

(a) Driving a wire through a severed tissue layer

(b) Tightening the suturing wire

Fig. 4.: Suturing simulation using our custom C++ implementation

Analyzing table 1, the symplectic Euler method (discussed by Cromer [4]) is the most stable for the total iteration time it needs (the score is obtained as the ratio between the maximum time step and the time needed to execute one simulation it-

	Criteria				
Method	Max Δt	Time	Symplectic	Order	Score
Explicit Euler	0.0098s	8ms	NO	$O(h)$	1.225
Symplectic Euler	0.0294s	8ms	YES	$O(h)$	3.675
Midpoint	0.0153s	8ms	NO	$O(h^2)$	1.9125
Half-Step	0.0168s	10ms	NO	$O(h^2)$	1.68
Verlet	0.023s	10ms	YES	$O(h^2)$	2.3
Forest-Ruth	0.021s	12ms	YES	$O(h^3)$	1.75
Symplectic Midpoint	0.028s	8ms	YES	$O(h^2)$	3.5
Runge-Kutta 4	0.027s	14ms	NO	$O(h^4)$	1.928
Moified Half-Step	0.0216s	10ms	NO	$O(h^2)$	2.16

Table 1: Integrator benchmark results

eration). We modified the Midpoint method to achieve symplecticity, obtaining the second highest score. Given the fact that the Midpoint family of methods is accurate to the second order for the position terms (while being a first order method for the velocity terms), we recommend it for applications where accuracy is of some importance. The Verlet method ([19]), popular for molecular dynamics simulations, also benefits from its relatively high stability, symplecticity and second order accuracy. A third order method, the Forest-Ruth integration scheme [7], represents the best alternative for applications where accuracy is a key element. The Runge-Kutta fourth order method, although supporting relatively high time steps, is the most time consuming and probably not a good choice for real time applications.

Although symplectic integrators excel in scenarios where their energy preserving features are central (e.g. where only conservative forces are involved), we have found this family of integrators to outperform their explicit integrator counterparts. As a last remark, we have also modified the Half Step method ([10]) to support a semi-implicit update for the middle estimation ($\mathbf{x}_{n+\frac{1}{2}}, \mathbf{v}_{n+\frac{1}{2}}$). This modification significantly increases the method's stability, as seen in table 1.

As an additional benchmark study, we have used the pendulum equation, $\ddot{\theta} = -\sin(\theta)$. The explicit Euler is clearly the most unstable, introducing ghost energies as seen in the phase space diagram comparison with respect to the midpoint method in figure 5a. On the other hand, in figure 5b, the symplectic Euler and Midpoint methods have a much higher stability range, with the latter yielding slightly lower energy variations. As second order explicit integrators, the modified half step method is also more stable than the original version (as depicted in figure 6a). Nevertheless, both methods tend to add ghost energies, but are much more stable than the first order explicit Euler. As the order of accuracy increases, larger time steps can be used (as it is the case with Runge-Kutta methods), but the performance impact does not justify

such a trade-off. Finally, for models where no damping or non-conservative forces are involved, the Forest-Ruth and Verlet methods are the natural choices (comparative phase space plots in figure 6b). Nevertheless, in case accuracy can be sacrificed, we still recommend using the first order symplectic Euler method as it has the highest stability versus complexity score.

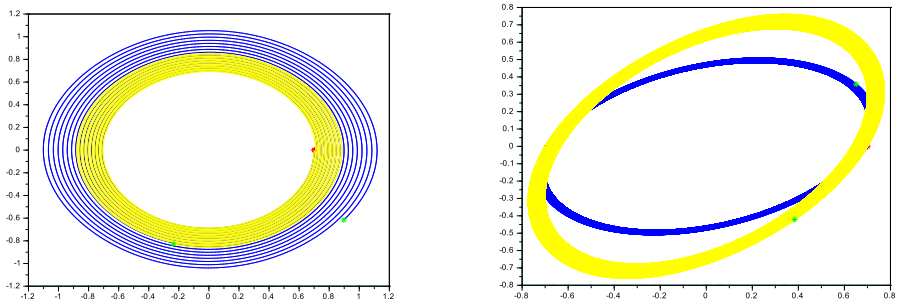

(a) Explicit Euler (blue) and Midpoint (yellow), $\Delta t = 0.03$

(b) Symplectic Midpoint (blue) and Symplectic Euler (yellow), $\Delta t = 0.9$

Fig. 5.: First order integrators (phase space diagrams generated using `SciLab`)

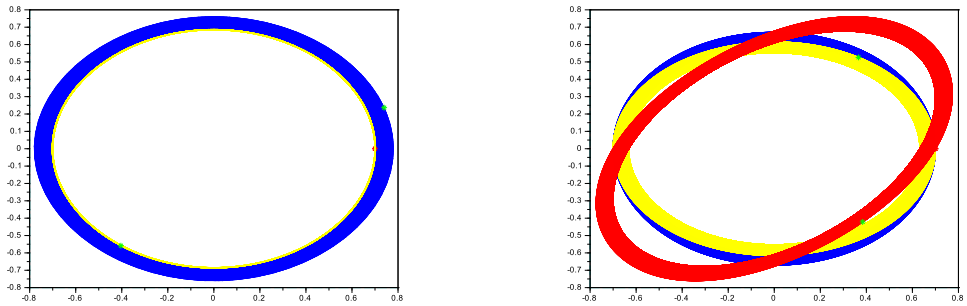

(a) Half Step (blue) and Modified Half Step (yellow), $\Delta t = 0.3$

(b) Symplectic Euler (red), Verlet (yellow), Forest-Ruth (blue), $\Delta t = 0.9$

Fig. 6.: Higher order integrators (phase space diagrams generated using `SciLab`)

7. CONCLUSION

In this work we have discussed the implications of employing an explicit integration method for updating a soft or semi-rigid body simulation. For real time applica-

tions where accuracy is not a goal, we recommend using a symplectic integrator as it has the best performance and stability score. Even when non-conservative forces are involved, this class of integrators is able to cope with stiff constraints. However, for applications where accuracy cannot be sacrificed, both the Runge-Kutta or the Forest-Ruth integrators can be used. The latter choice is accurate up to the third order and conserves energy, while the Runge-Kutta progressively loses small amounts of energy, counting for a slight increase in stability.

(a) Creating complex knots: tight knots tend correspond to very high elastic potentials. The numerical stability is crucial for plausible knot behaviour.

(b) Highly elastic cable unknotting itself under the action of strong constraint forces

Fig. 7.: Hose object knot tying - screenshots from our custom C++ implementation

On a final note, implicit integrators, mentioned in the related work section 2, are not the usual choice for real time applications, thus motivating our investigation towards an explicit integrator alternative.

APPENDIX. EXPLICIT INTEGRATION METHODS

In this appendix, we present the minor modifications of the explicit integration methods that were tested in our simulation application.

Symplectic Midpoint	Modified Half Step
$\mathbf{v}_{n+1} = \mathbf{v}_n + \frac{h}{2} f(\mathbf{x}_n, \mathbf{v}_n)$	$\mathbf{v}_{n+\frac{1}{2}} = \mathbf{v}_n + \frac{h}{2} f(\mathbf{x}_n, \mathbf{v}_n)$
$\mathbf{x}_{n+1} = \mathbf{x}_n + h\mathbf{v}_{n+1}$	$\mathbf{x}_{n+\frac{1}{2}} = \mathbf{x}_n + \frac{h}{2}\mathbf{v}_{n+\frac{1}{2}}$
	$\mathbf{v}_{n+1} = \mathbf{v}_n + hf(\mathbf{x}_{n+\frac{1}{2}}, \mathbf{v}_{n+\frac{1}{2}})$
	$\mathbf{x}_{n+1} = \mathbf{x}_n + h\mathbf{v}_{n+\frac{1}{2}}$

Table 2: Slightly modified integrators for improved stability and accuracy

These numerical methods make use of an acceleration function, f, a fixed time-step, h, and compute new positions and velocities, given the previous state $(\mathbf{x}_n, \mathbf{v}_n)$.

References

[1] Jan Bender, Matthias Müller, Miguel A. Otaduy, Matthias Teschner, *Position-based methods for the simulation of solid objects in computer graphics*, EUROGRAPHICS 2013 State of the Art Reports, Eurographics Association, 2013.

[2] David Baraff, Andrew Witkin, *Large steps in cloth simulation*, Proceedings of the 25th annual conference on Computer graphics and interactive techniques, SIGGRAPH '98, pgs 43–54, New York, NY, USA, 1998. ACM.

[3] Lee Cooper Cooper, Steve Maddock, *Preventing collapse within mass-spring-damper models of deformable objects*, In The Fifth Internation Conference in Central Europe on Computer Graphics and Visualization, pgs 70–78, 1997.

[4] Alan Cromer, *Stable solutions using the euler approximation*, American Journal of Physics, 49(5):455-459, 1981.

[5] Mathieu Desbrun, Peter Schröder, Alan Barr, *Interactive animation of structured deformable objects*, Proceedings of the 1999 conference on Graphics interface '99, pages 1-8, San Francisco, CA, USA, 1999. Morgan Kaufmann Publishers Inc.

[6] C. Ericson, *Real-Time Collision Detection*, The Morgan Kaufmann Series in Interactive 3D Technology, Morgan Kaufmann Publishers Inc., San Francisco, 2004.

[7] E. Forest, R. D. Ruth, *Fourth-order symplectic integration*, Phys. D, 43(1):105–117, April 1990.

[8] Basil Fierz, Jonas Spillmann, Matthias Harders, *Stable explicit integration of deformable objects by filtering high modal frequencies*, Journal of WSCG, 18(1-3):81–88, February 2010.

[9] Michael Hauth, Olaf Etzmuβ, *A high performance solver for the animation of deformable objects using advanced numerical methods*, Comput. Graph. Forum, 20(3):319–328, 2001.

[10] E. Hairer, S. P. Nørsett, G. Wanner, *Solving ordinary differential equations I (2nd revised. ed.): nonstiff problems*, Springer-Verlag New York, Inc., New York, NY, USA, 1993.

[11] P. Jiménez. *Survey on model-based manipulation planning of deformable objects*, Robot. Comput.-Integr. Manuf., 28(2):154–163, April 2012.

[12] Jaruwan Mesit, Ratan K. Guha, Shafaq Chaudhry, *3d soft body simulation using mass-spring system with internal pressure force and simplified implicit integration*, JCP, 2(8):34-43, 2007.

[13] Andrew Nealen, Matthias Müller, Richard Keiser, Eddy Boxerman, Mark Carlson, *Physically based deformable models in computer graphics*, Computer Graphics Forum, 25(4):809–836, 2006.

[14] Craig A. Schroeder, Nipun Kwatra, Wen Zheng, Ronald Fedkiw, *Asynchronous evolution for fully-implicit and semi-implicit time integration*, Comput. Graph. Forum, 30(7):1983–1992, 2011.

[15] Martin Servin, C. Lacoursiére, N. Melin, *Interactive simulation of elastic deformable materials*, SIGRAD 2006 Conference Proceedings, pgs 22–32, 2006.

[16] Ruediger Schmedding, Matthias Teschner, *Inversion handling for stable deformable modeling*, Vis. Comput., 24(7):625–633, July 2008.

[17] Matthias Teschner, Bruno Heidelberger, Matthias Muller, Markus Gross, *A versatile and robust model for geometrically complex deformable solids*, Proceedings of the Computer Graphics International, CGI '04, pgs 312–319, Washington, DC, USA, 2004. IEEE Computer Society.

[18] Shan-Ho Tsai, M. Krech, D.P. Landau. Symplectic integration methods in molecular and spin dynamics simulations. *Brazilian Journal of Physics*, 34:384 - 391, 06 2004.

[19] Loup Verlet, *Computer "experiments" on classical fluids. i. thermodynamical properties of Lennard-Jones molecules*, Phys. Rev., 159:98-103, Jul 1967.

[20] P. Volino, N. Magnenat-Thalmann, *Accurate garment prototyping and simulation*, Computer-Aided Design & Applications, 2(5):645–654, 2005.

ROMAI J., v.9, no.2(2013), 89–94

THE IMPLICIT REDUCIBILITY IN THE CHAIN SUPER-INTUTIONISTIC LOGICS

Ion Cucu[1], Mefodie Raţiu[2]

[1] *State University of Moldova, Chişinău, Republic of Moldova*

[2] *Academy of Sciences of Moldova, Chişinău, Republic of Moldova*

cucuion2012@gmail.com

Abstract One examines the chain logics $C_2, C_3, \ldots$, which are intermediary between classical and intuitionistic logics. The formula F is said to be implicitly expressible in logic L by the system Σ of formulas if the relation $L \vdash (F \sim q) \sim ((G_1 \sim H_1) \,\&\, \ldots \,\&\, (G_k \sim H_k))$ is true, where q do not appear in F, and formulas G_i and H_i, for $i = 1, \ldots, k$, are explicitly expressible in L via Σ. The formula F is said to be implicitly reducible in logic L to formulas of Σ if there exists a finite sequence of formulas $G_1, G_2, \ldots, G_l$ where G_l coincides with F and for $j = 1, \ldots, l$ the formula G_j is implicitly expressible in L by $\Sigma \cup \{G_1, \ldots, G_{j-1}\}$. The paper contains researches of completeness with respect to implicit reducibility in the logic C_m, for any $m = 2, 3, \ldots$.

Keywords: Chain intermediate logic, pseudo-Boolean algebra, expressibility, implicit reducibility, centralizer.

2010 MSC: 03B55.

1. INTRODUCTION

The criterion of functional completeness in classical logic [1, 2] gives an algorithm which permits, for each finite system of Boolean functions given by formulas or tables, to recognise whether it is possible or not to obtain any Boolean function via this system using superpositions. Analogous criteria of completeness have been obtained in general k-valued logic, $k > 2$ [2, 3], in propositional intuitionistic logic [4], etc. Each of these criteria is based on a finite number of closed (relative to expressibility in corresponding logic) classes of functions or formulas that are pre-complete (i. e. maximal and non-complete).

A.V. Kuznethov [5] introduced the concepts of implicit expressibility, implicit reducibility and parametrical expressibility, which are natural generalizations of usual expressibility. He found a criterion for parametrical expressibility in any general k-valued logic for $k \geq 2$.

Formulas (of propositional logic) are constructed from variables p, q, r by means of logical operations: $\&$ (conjunction), $\vee$ (disjunction), $\supset$ (implication), $\neg$ (negation). In this paper the formulas are designated with capital letters of the Latin alphabet. Using the mark $\rightleftharpoons$, and reading it as "means" we introduce designations for seven formulas: $1 \rightleftharpoons (p \supset p)$, $0 \rightleftharpoons (p \,\&\, \neg p)$, $\perp\ F \rightleftharpoons (F \vee \neg F)$ (ternondation), $(F \sim$

$G) \rightleftharpoons ((F \supset G)\,\&\,(G \supset F))$ (equivalence), $(F \cdot G) \rightleftharpoons ((F \sim G)\,\&\,\neg\neg G)$, $(F\,\&'\,G) \rightleftharpoons ((F\,\&\,G) \sim \perp (F \sim G)$ and $(F, G, H) \rightleftharpoons ((F\,\&\,G) \vee (F\,\&\,H) \vee (G\,\&\,H))$ (median). In the interpretation of formulas, the symbol $F[\alpha_1, \ldots, \alpha_n]$ designates the result of substitution in the formula F of the values $\alpha_1, \ldots, \alpha_n$ for variables $p_1, \ldots, p_n$, respectively.

2. MAIN RESULT

We examine logics that are intermediary between classical logic and intuitionistic one. They are constructed on finite or infinite chains (i.e. linear ordered sets) of true values. It is known that the logic is called a chain if the formula $((p \supset q) \vee (q \supset p))$ is true in it. In the considered m-valued logic ($m = 2, 3, \ldots$) the variables will take values from the set E_m, where $E_m = \{0, 1, \tau_1, \tau_2, \ldots, \tau_{m-2}\}$ if m is finite and $E_m = \{0, 1, \tau_1, \tau_2, \ldots\}$ if m is infinite. We remind that the set of all functions as mappings from E_m into E_m is usually called general m-valued logic P_m. Further we consider the linear ordering on the set E_m by the relation $0 < \tau_1 < \tau_2 < \ldots\ldots < \tau_{m-2} < 1$. We define the operations $\&, \vee, \supset$, and $\neg$ on E_m as follows:

$$p\,\&\,q = \min(p, q), \qquad p \vee q = \max(p, q), \qquad p \supset q = \begin{cases} 1 & \text{if } p \le q, \\ q & \text{if } p > q, \end{cases} \qquad \neg p = p \supset 0.$$

In the considered interpretation of symbols $\&, \vee, \supset$ and $\neg$ each formula expresses some function of general m-valued logic. Let us observe that the function $\lrcorner p$ of P_3 defined by the equalities $\lrcorner 0 = \lrcorner \tau_1 = 1$ and $\lrcorner 1 = 0$ is not expressed by any formula. We remind that the pseudo-Boolean algebra is the system $\mathfrak{A} =< M; \&, \vee, \supset, \neg >$ that is a lattice by $\&$ and $\vee$, where $\supset$ is relative pseudo-complement and $\neg$ is pseudo-complement. The logic of this algebra is defined as the set of all formulas that are true on $\mathfrak{A}$, i.e. formulas identically equal to the greatest element 1 of this algebra. We will denote the algebra $< E_m; \&, \vee, \supset, \neg >$ ($m = 2, 3, \ldots$) by Z_m. The logic of this algebra LZ_m is denoted by C_m.

The formula F is called implicitly expressible in logic L [5] via the system of formulas Σ if there exist the formulas G_i and H_i ($i = 1, \ldots, k$) explicitly expressible in L by Σ such that the predicate $L \vdash (F \sim q)$, where q is a variable not contained in F, is equivalent to the predicate $L \vdash ((G_1 \sim H_1)\,\&\,\ldots\,\&\,(G_k \sim H_k))$.

Since the relation of implicit expressibility, generally speaking, is not transitive, we are going to introduce a new concept. The formula F is called implicitly reducible in logic L via formulas of Σ if there exists a finite sequence of formulas $G_1, G_2, \ldots, G_l$, where G_l coincides with F and each term of this sequence can be implicitly expressible in L by Σ and terms of the sequence placed before it. We will say that the system Σ' of formulas is implicitly reducible in L to the system Σ if each formula of Σ' is implicitly reducible in L to Σ. It is clear that the relation of implicit reducibility is transitive. The system Σ of formulas is called complete with respect to implicit reducibility in logic L if each formula (in language of this logic) is implicitly reducible in L to Σ. The system Σ of formulas is said to be pre-complete with respect to implicit

reducibility in L if Σ is not complete by this reducibility in L, but the system $\Sigma \cup \{F\}$ is complete relative to implicit reducibility in L, for any formula F.

Two functions $f(x_1, x_2, \ldots, x_n)$ and $g(x_1, x_2, \ldots, x_k)$ of P_m are called permutable if the identity

$$f(g(x_{11}, \ldots, x_{1k}), \ldots, g(x_{n1}, \ldots, x_{nk})) = g(f(x_{11}, \ldots, x_{n1}), \ldots, f(x_{1k}, \ldots, x_{nk}))$$

is true. The set of all functions of P_m, permutable with the given function f, is called the centralizer of function f (denoted $\prec f \succ$). The set of all formulas which in the interpretation on Z_m are permutable with the function f (from P_m) is called the formula centralizer on the algebra Z_m of function f. We say the function $f(x_1, \ldots, x_n)$ of P_m preserves the predicate (relation) $R(x_1, \ldots, x_w)$ if for any possible values of variables $x_{ij} \in E_m$ $(i = 1, \ldots, w;\ j = 1, ..n)$, from the truth of

$$R(x_{11}, x_{21}, \ldots, x_{w1}), \ldots, R(x_{12}, x_{22}, \ldots, x_{w2}), \ldots, R(x_{1n}, x_{2n}, \ldots, x_{wn})$$

follows the truth of

$$R(f(x_{11}, x_{12}, \ldots, x_{1n}), \ldots, f(x_{21}, x_{22}, \ldots, x_{2n}), \ldots, f(x_{w1}, x_{w2}, \ldots, x_{wn})).$$

The centralizer $\prec f(x_1, \ldots, x_n) \succ$ coincides with the set of all functions of P_m which preserve the predicate $f(x_1, \ldots, x_n) = x_{n+1}$, where the variable x_{n+1} differs from $x_1, \ldots, x_n$ [5]. We say that the formula F preserves, on the algebra Z_m, the predicate R if the function of logic C_m, expressed by formula F, preserves R. The predicate could be replaced by the corresponding to it matrix (α_{ij}) $(i = 1, \ldots, w;\ j = 1, \ldots, t)$ of elements of algebra Z_m such that the predicate R is true on all those and only those sets of elements that are columns in this matrix.

We present the next affirmation without any proof.

Proposition. *If the function f belongs to the class C_m $(m = 2, 3, \ldots)$ then the following identity:*

$$f(\neg\neg x_1, \ldots, \neg\neg x_n) = \neg\neg f(x_1, \ldots, x_n)$$

is true.

Theorem 1 (A.V. Kuznetsov [5]). *The system Σ of formulas is complete by the implicit reducibility in logic C_2 iff Σ is not included in any of classes* of formulas preserving the predicates $x = 0,\ x = 1,\ \neg x = y,\ x \,\&\, y = z,\ x \vee y = z,\ (x \sim (y \sim z)) = u$ on Z_2.

According to [6] the next criterion of completeness relative to the implicit reducibility in logic of First Iaśkowski's Matrix is true:

Theorem 2. *The system Σ of formulas is complete with respect to the implicit reducibility in logic C_3 iff Σ is complete in logic C_2 and is not included in any of classes of formulas preserving the predicates* $\neg\neg x = y,\ \bot x = \bot y,\ (x \,\&\, y = z) \,\&\, (\neg x = \neg y), ((x \sim y) \,\&\, \neg\neg y = z) \,\&\, (\neg x = \neg y),\ ((x \,\&\, y) \sim ((x \sim y) \vee \neg(x \sim y)) = z) \,\&\, (\neg x = \neg y)$ *on* Z_3.

The next criteria of completeness with respect to the implicit reducibility in any chain logic included in C_4 are true:

Theorem 3. *For any $m = 4, 5, \ldots$ the system Σ of formulas is complete by the implicit reducibility in logic C_m iff Σ is complete by implicit reducibility in logic C_3 and is not included in the following two classes of formulas preserving the predicates $f_1(x) = y$ and $f_2(x) = y$ on Z_4.*

Proof. Necessity. Let the system Σ be complete with respect to the implicit reducibility in logic C_m ($m \geq 4$). Then, since the implicit reducibility in logic C_m ($m \geq 2$) implies the implicit reducibility in C_{m-1}, it results that Σ is complete by the implicit reducibility in C_3. Because formula centralizers are closed relative to the implicit reducibility in logic C_4, then they are closed relative to the implicit reducibility in C_m where $m > 4$. Moreover, they are not complete in C_m, because they do not contain for example the formula $((x \supset y) \,\&\, \neg\neg y)$. So no one of them could contain Σ.

Sufficiency. Let Σ be complete by the implicit reducibility in logic C_3 and be not included in any of two formula centralizers $\prec f_1(p)\succ$, $\prec f_2(p)\succ$. Let us suppose that these formulas do not contain other variables except $p_1, \ldots, p_n$. It is sufficient to prove that every formula of system $\{p \,\&\, q,\ p \vee q,\ p \supset q,\ \neg p\}$ is implicitly reducible to the system Σ of formulas in C_m ($m = 4, 5, \ldots$). It is known that in any chain logic C_m the relation

$$C_m \vdash (p \vee q) \sim (((p \supset q) \supset q) \,\&\, ((q \supset p) \supset p))$$

is true. The conjunction is implicitly expressible via the implication in any chain logic C_m, because the relation

$$C_m \vdash ((p \,\&\, q) \sim r) \sim (((p \supset (q \supset r)) \sim 1) \& ((r \supset p) \supset 1) \& ((r \supset q) \sim 1))$$

is true. It remains to prove that the formulas $\neg p$ and $p \supset q$ are implicit reducible to the system Σ in any chain logic included in C_4.

This fact results from the next lemmas.

Lemma 1. *If the formula $\neg\, p$ is implicitly reducible to the system Σ of formulas in logic C_3 then this formula is implicitly reducible to Σ in logic C_m, for any $m = 3, 4, \ldots$*

Lemma 2. *If the formula 0 is implicitly reducible to the system Σ of formulas in logic C_2 then this formula is implicitly reducible to Σ in logic C_m, for any $m = 3, 4, \ldots$*

Lemma 3. *The formula 1 is explicitly expressible through 0 and $\neg p$ in C_m, for any $m = 3, 4, \ldots$*

Lemma 4. *If the formula $\bot p$ is implicitly reducible to the system Σ of formulas in logic C_3 then this formula is implicitly reducible to Σ in logic C_m, for any $m = 3, 4, \ldots$*

Lemma 5. *If the formula $p \,\&\, q$ is implicitly reducible to the system Σ of formulas in logic C_2 then the formula $\neg\neg(p \,\&\, q)$ is explicitly expressible through 0, 1, $\neg p$ and Σ in logic C_m, for any $m = 3, 4, \ldots$*

Lemma 6. *If the formula $\neg p \,\&\, q$ is implicitly reducible to the system Σ of formulas in logic C_3 then the formulas $\neg p \,\&\, q$ and $\neg p \vee q$ are implicitly expressible through $0,\ 1,\ \neg p,\ \bot p,\ \neg\neg(p \,\&\, q)$ and Σ in the logic C_m, for any $m = 3, 4, \ldots$*

In order to obtain the implication we further present 5 lemmas without proofs.

Lemma 7. *For any $m = 3, 4, \ldots$ at least one of 4 following formulas:*

$$p \supset q,\ p \sim q,\ \bot p \vee \bot q,\ (p \,\&\, q) \sim ((p \sim q)\ \vee\ \neg(p \sim q))$$

is explicitly expressible in C_m through formulas of the system

$$\{0,\ 1,\ \neg p,\ \bot p,\ \neg p \,\&\, q,\ \neg p \vee q\} \tag{1}$$

and F, which don't preserve the predicate $(x \,\&\, y = z) \,\&\, (\neg x = \neg y)$ on Z_3.

Lemma 8. *For any $m = 3, 4, \ldots$ at least one of 3 formulas:*

$$p \supset q,\ \bot p \vee \bot q,\ (p \,\&\, q) \sim ((p \sim q)\ \vee\ \neg(p \sim q))$$

is explicitly expressible through formulas of the system (1) and F, G which do not preserve the predicate $((x \sim y) \,\&\, \neg\neg y = z) \,\&\, (\neg x = \neg y)$ on Z_3.

Lemma 9. *For any $m = 3, 4, \ldots$ at least one of following 4 systems:*

$$\{p \supset q\},\ \ \{(p \sim q) \vee q\},\ \ \{(p \,\&\, q) \sim ((p \sim q)\ \vee\ \neg(p \sim q)), T'\}, \{\bot p \vee \bot q, T'\}, \tag{2}$$

is explicitly expressible through formulas of the system (1) and $F, G,\ M$ which do not preserve the predicate $((x \,\&\, y) \sim ((x \sim y)\ \vee\ \neg(x \sim y)) = z) \,\&\, (\neg x = \neg y)$ on Z_3 where

$$T'[\tau, \tau, 1] = T'[\tau, 1, \tau] = \tau,\ \ T'[\tau, 1, 1] = 1. \tag{3}$$

Lemma 10. *The implication $(p \supset q)$ is implicitly expressible in C_m, for any $m = 4, 5, \ldots$, through formulas of system (1), formula N, which do not preserve the predicate $f_1(x) = y$ on Z_4 and any of two systems $\{(p \sim q) \vee q\}$ or $\{(p \,\&\, q) \sim ((p \sim q)\ \vee\ \neg(p \sim q)), T'\}$, where T' is 3-ary formula, which satisfies (3) conditions.*

Lemma 11. *The formula $p \supset q$ is implicitly expressible in C_m, for any $m = 4, 5, \ldots$, through formulas of (1), formulas N, P, which do not preserve the predicate $f_2(x) = y$ on Z_4 and the system $\{\bot\ p \vee\ \bot\ q, T'\}$, where T' is the 3- ary formula satisfying conditions (3).*

From the formulated above lemmas it results that conditions of theorem are sufficient, namely the formula $\neg p$ is implicitly reducible to the system Σ of formulas in logic C_m, for any $m = 3, 4, \ldots$. Lemmas 1 – 11 allow us to deduce that the implication $p \supset q$ is implicitly reducible to Σ in any chain logic C_m included in C_4. So, according to lemmas 1 – 6 the formulas of the system (1) are implicitly reducible to Σ. Lemmas 7 – 9 permit to conclude that at least one of 4 systems of formulas (2) is explicitly expressible in logic C_m through formulas (1) and F, G, M. Therefore it remains to observe that one of these systems consists of $p \supset q$, but the implication is implicitly expressible in C_m through any other of 3 systems and formulas N, P and (1), in accordance with Lemmas 10 and 11. ∎

References

[1] Post E.L., *Two-valued iterative systems of mathematical logic,* Princeton, 1941.

[2] Iablonski S.V., *Functional constructions in k-valued logic,* Trudy MIAN SSSR, **T. 51**, Moscow, 1958, 5–142. (in Russian)

[3] Rosenberg I, *Structure des fonctions de plusieurs variables sur un ensemble fini*, C.R. Acad. Sci. Groupe 1, Paris, 1965, **260**, 3817–3819.

[4] Raţa M.F., *On functional completeness in the intuitionistic logic,* Probl. Kibern., 1982, **N 39**, 107–150. (in Russian)

[5] Kuznetsov A.V., *On tools for the discovery of nondeducibility or nonexpressibility,* Logical Deduction, Moscow, Nauka, 1979, 5–33. (in Russian)

[6] Raţa M.F., Cucu I.V., *On completeness with respect to implicit reducibility in the logic of First Iaśkowski's Matrix,* Bul. Acad. of Sci. of Moldova, 1988, **N 1**, 23–29. (in Russian)

ROMAI J., v.9, no.2(2013), 95–106

SOME PROPERTIES OF FINITE ORDER SOLUTIONS OF A CLASS OF LINEAR DIFFERENTIAL EQUATIONS WITH ENTIRE COEFFICIENTS

Saada Hamouda, Benharrat Belaïdi
Department of Mathematics, Laboratory of Pure and Applied Mathematics,
University of Mostaganem (UMAB), Algeria
hamoudasaada@univ-mosta.dz, belaidi@univ-mosta.dz

Abstract In this paper, we investigate the growth of solutions of some higher order linear differential equations. We find conditions on the coefficients which will guarantee the existence of an asymptotic value for a transcendental entire solution of finite order and its derivatives.

Keywords: linear differential equations, entire solutions, order of growth.
2010 MSC: 4M10, 30D35.

1. INTRODUCTION

Throughout this paper, we assume that the reader is familiar with the fundamental results and the standard notations of the Nevanlinna value distribution theory [9], [10], [15]. In addition, we will use the notation $\sigma(f)$ to denote the order of an entire function $f(z)$, $\tau(f)$ to denote the type of $f(z)$ with $0 < \sigma(f) = \sigma < +\infty$, which is defined to be

$$\tau(f) = \limsup_{r\to+\infty} \frac{\log M(r,f)}{r^{\sigma}},$$

where $M(r,f) = \max_{|z|=r} |f(z)|$. The hyper-order $\sigma_2(f)$ of f is defined by ([15])

$$\sigma_2(f) = \limsup_{r\to+\infty} \frac{\log\log T(r,f)}{\log r} = \limsup_{r\to+\infty} \frac{\log\log\log M(r,f)}{\log r},$$

where $T(r,f)$ is the Nevanlinna characteristic function of f.

For $k \geqslant 2$, we consider the linear differential equation

$$f^{(k)} + A_{k-1}(z) f^{(k-1)} + \cdots + A_1(z) f' + A_0(z) f = 0, \tag{1}$$

where $A_0(z), \cdots, A_{k-1}(z)$ are entire functions with $A_0(z) \not\equiv 0$. It is well known that all solutions of (1) are entire functions. A classical result, due to Wittich [14], tells that all solutions of (1) are of finite order of growth if and only if all coefficients are

polynomials. For a complete analysis of possible orders in the polynomial case, see [8]. If some (or all) of the coefficients are transcendental, a natural question is to ask when and how many solutions of finite order may appear. Partial results have been available since a paper of Frei [4]. In its generality, however, the problem remains open.

Throughout this paper, we will use the following notations: Given $\varepsilon > 0$ small enough and $0 \leqslant \theta_1 < \theta_2 < 2\pi$, let $S(\varepsilon)$ denote the sector $S(\varepsilon) = \{z \in \mathbb{C} : \theta_1 + \varepsilon \leqslant \arg z \leqslant \theta_2 - \varepsilon\}$. We also denote $S(0) = \{z \in \mathbb{C} : \theta_1 \leqslant \arg z \leqslant \theta_2\}$.

In [5], Gundersen proved the following results.

Theorem 1.1. *[5] Let $A_0(z) \not\equiv 0$ and $A_1(z)$ be entire functions such that for real constants $\alpha, \beta, \theta_1, \theta_2$ with $\alpha > 0, \beta > 0$ and $\theta_1 < \theta_2$, we have*

$$|A_0(z)| \geqslant \exp\left\{(1 + o(1))\,\alpha |z|^{\beta}\right\}$$

and

$$|A_1(z)| \leqslant \exp\left\{o(1)\,|z|^{\beta}\right\}$$

as $z \to \infty$ with $\theta_1 \leqslant \arg z \leqslant \theta_2$. Then every solution $f \not\equiv 0$ of the differential equation

$$f'' + A_1(z) f' + A_0(z) f = 0 \tag{2}$$

has infinite order.

Theorem 1.2. *[5] Let $A_0(z) \not\equiv 0$ and $A_1(z)$ be entire functions such that for real constants $\alpha, \beta, \theta_1, \theta_2$ with $\alpha > 0, \beta > 0$ and $\theta_1 < \theta_2$, we have*

$$|A_1(z)| \geqslant \exp\left\{(1 + o(1))\,\alpha |z|^{\beta}\right\}$$

and

$$|A_0(z)| \leqslant \exp\left\{o(1)\,|z|^{\beta}\right\}$$

as $z \to \infty$ with $\theta_1 \leqslant \arg z \leqslant \theta_2$. If f is a nontrivial solution of (2) of finite order, then the following conclusions hold:
(i) There exists a constant $b \neq 0$ such that $f(z) \to b$ as $z \to \infty$ in $S(\varepsilon)$. Indeed,

$$|f(z) - b| \leqslant \exp\left\{-(1 + o(1))\,\alpha |z|^{\beta}\right\}.$$

(ii) For each integer $k \geqslant 1$

$$\left|f^{(k)}(z)\right| \leqslant \exp\left\{-(1 + o(1))\,\alpha |z|^{\beta}\right\}$$

as $z \to \infty$ in $S(\varepsilon)$.

Theorem 1.1 has been generalized to the higher order case by Belaïdi and Hamouda as follows.

Theorem 1.3. *[1] Let $A_0(z) \not\equiv 0, A_1(z), \cdots, A_{k-1}(z)$ be entire functions such that for real constants $\alpha, \beta, \mu, \theta_1, \theta_2$ with $0 \leqslant \beta < \alpha, \mu > 0$ and $\theta_1 < \theta_2$, we have*

$$|A_0(z)| \geqslant e^{\alpha|z|^\mu}$$

and

$$\left|A_j(z)\right| \leqslant e^{\beta|z|^\mu} \ (j = 1, \cdots, k-1)$$

as $z \to \infty$ with $\theta_1 \leqslant \arg z \leqslant \theta_2$. Then every solution $f \not\equiv 0$ of (1) has infinite order.

Theorem 1.2 has been generalized to the higher order case by Belaïdi and Hamani as follows.

Theorem 1.4. *[2] Let $A_0(z) \not\equiv 0, A_1(z), \cdots, A_{k-1}(z)$ be entire functions such that for real constants $\alpha, \beta, \theta_1, \theta_2$ with $\alpha > 0, \beta > 0$ and $\theta_1 < \theta_2$, we have*

$$|A_1(z)| \geqslant \exp\left\{(1 + o(1))\,\alpha|z|^\beta\right\},$$

$$\left|A_j(z)\right| \leqslant \exp\left\{(o(1))\,|z|^\beta\right\}, \quad j = 0, 2, 3, \cdots, k-1$$

as $z \to \infty$ with $\theta_1 \leqslant \arg z \leqslant \theta_2$. If f is a nontrivial solution of (1) of finite order, then the following conclusions hold:
(i) There exists a constant $b \neq 0$ such that $f(z) \to b$ as $z \to \infty$ in $S(\varepsilon)$. Indeed,

$$|f(z) - b| \leqslant \exp\left\{-(1 + o(1))\,\alpha|z|^\beta\right\}.$$

(ii) For each integer $m \geqslant 1$

$$\left|f^{(m)}(z)\right| \leqslant \exp\left\{-(1 + o(1))\,\alpha|z|^\beta\right\}$$

as $z \to \infty$ in $S(\varepsilon)$.

This result has been generalized by Laine and Yang by taking $A_s(z)$ instead of $A_1(z)$.

Theorem 1.5. *[11] Let $\theta_1 < \theta_2$ be given to fix a sector $S(0) = \{z \in \mathbb{C} : \theta_1 \leqslant \arg z \leqslant \theta_2\}$, let $k \geqslant 2$ be a natural number, and let $\delta > 0$ be any real number such that $k\delta < 1$. Suppose that $A_0(z), A_1(z), \cdots, A_{k-1}(z)$ with $A_0(z) \not\equiv 0$ are entire functions such that for real constants $\alpha > 0, \beta > 0$, we have, for some $s = 1, \cdots, k-1$,*

$$|A_s(z)| \geqslant \exp\left\{(1 + \delta)\,\alpha|z|^\beta\right\}, \tag{3}$$

$$\left|A_j(z)\right| \leqslant \exp\left\{\delta\alpha|z|^\beta\right\} \tag{4}$$

for all $j = 0, \cdots, s-1, s+1, \cdots, k-1$ *whenever* $|z| = r \geqslant r_\delta$ *in the sector* $S(0)$. *Given* $\varepsilon > 0$ *small enough, if* f *is a transcendental solution of* (1) *of finite order* $\rho < \infty$, *then the following conclusions hold:*
(i) There exists $j \in \{0, \cdots, s-1\}$ *and a complex constant* $b_j \neq 0$ *such that* $f^{(j)}(z) \to b_j$ *as* $z \to \infty$ *in* $S(\varepsilon)$. *More precisely,*

$$\left|f^{(j)}(z) - b_j\right| \leqslant \exp\left\{-(1 - k\delta)\alpha |z|^\beta\right\}$$

in $S(\varepsilon)$, *provided* $|z|$ *is large enough.*
(ii) For each integer $m \geqslant j+1$,

$$\left|f^{(m)}(z)\right| \leqslant \exp\left\{-(1 - k\delta)\alpha |z|^\beta\right\}$$

in $S(3\varepsilon)$ *for all* $|z|$ *large enough.*

Recently in [13], Tu and Yi investigated the case when most coefficients in (1) have the same order with each other and obtained the following result.

Theorem 1.6. [13] *Let* $A_j(z)$ $(j = 0, \cdots, k-1)$ *be entire functions satisfying* $\sigma(A_0) = \sigma$, $\tau(A_0) = \tau$, $0 < \sigma < \infty$, $0 < \tau < \infty$, *and let* $\sigma\left(A_j\right) \leqslant \sigma$, $\tau\left(A_j\right) < \tau$ *if* $\sigma\left(A_j\right) = \sigma$ $(j = 1, \cdots, k-1)$, *then every solution* $f \not\equiv 0$ *of* (1) *satisfies* $\sigma_2(f) = \sigma(A_0)$.

The remainder of the paper is organized as follows. In Section 2, we shall show our main results which improve and extend many results in the above-mentioned papers. Section 3 is for some lemmas and basic theorems. The other sections are for the proofs of our main results.

2. RESULTS

In this paper, we extend the above results by proving the following two theorems.

Theorem 2.1. *Let* $A_0(z) \not\equiv 0, A_1(z), \cdots, A_{k-1}(z)$ *be entire functions such that for real constants* $\alpha, \beta, \mu, \theta_1, \theta_2$ *with* $0 \leqslant \beta < \alpha$, $\mu > 0$ *and* $(\theta_1, \theta_2) \subset \left[0, \frac{\pi}{2n}\right) \cup \left(\frac{3\pi}{2n}, \frac{2\pi}{n}\right)$, *we have*

$$|A_0(z)| \geqslant \exp\{\alpha |z|^\mu\} \tag{5}$$

and

$$\left|A_j(z)\right| \leqslant \exp\{\beta |z|^\mu\} \quad (j = 1, \cdots, k-1) \tag{6}$$

for $\arg z \in (\theta_1, \theta_2)$, *with* $|z|$ *large enough. Then every solution* $f \not\equiv 0$ *of the differential equation*

$$f^{(k)} + A_{k-1}(z) e^{z^n} f^{(k-1)} + \cdots + A_1(z) e^{z^n} f' + A_0(z) e^{z^n} f = 0 \tag{7}$$

has infinite order.

Theorem 2.2. *Let $A_0(z) \not\equiv 0, A_1(z), \cdots, A_{k-1}(z)$ be entire functions such that for real constants $\alpha, \beta, \mu, \theta_1, \theta_2$ with $0 \leqslant \beta < \alpha$, $\mu > 0$ and $(\theta_1, \theta_2) \subset \left[0, \frac{\pi}{2n}\right) \cup \left(\frac{3\pi}{2n}, \frac{2\pi}{n}\right)$, we have for some $s = 1, \cdots, k-1$,*

$$|A_s(z)| \geqslant \exp\{\alpha |z|^\mu\} \tag{8}$$

and

$$\left|A_j(z)\right| \leqslant \exp\{\beta |z|^\mu\} \tag{9}$$

for all $j = 0, \cdots, s-1, s+1, \cdots, k-1$ for $\arg z \in (\theta_1, \theta_2)$, with $|z|$ large enough. Given $\varepsilon > 0$ small enough, if f is a transcendental solution of (7) of finite order $\sigma < \infty$, then the following conclusions hold:
(i) There exists $j \in \{0, \cdots, s-1\}$ and a complex constant $b_j \neq 0$ such that $f^{(j)}(z) \to b_j$ as $z \to \infty$ in $S(\varepsilon)$. More precisely,

$$\left|f^{(j)}(z) - b_j\right| \leqslant \exp\{(\beta + \tau - \alpha)|z|^\mu\}$$

in $S(\varepsilon)$, provided $|z|$ is large enough, where $0 < \tau < \frac{\alpha-\beta}{k}$.
(ii) For each integer $m \geqslant j+1$,

$$\left|f^{(m)}(z)\right| \leqslant \exp\{(\beta + \tau - \alpha)|z|^\mu\}$$

in $S(3\varepsilon)$, provided $|z|$ is large enough, where $0 < \tau < \frac{\alpha-\beta}{k}$.

3. PRELIMINARY LEMMAS

Lemma 3.1. [6] *Let f be a transcendental entire function of finite order σ, let $\Gamma = \{(k_1, j_1), (k_2, j_2), \cdots, (k_m, j_m)\}$ denote a finite set of distinct pairs of integers that satisfy $k_i > j_i \geqslant 0$ $(i = 1, \cdots, m)$, and let $\varepsilon > 0$ be a given constant. Then there exists a set $E \subset [0, 2\pi)$ that has linear measure zero, such that if $\psi_0 \in [0, 2\pi) - E$, then there is a constant $R_0 = R_0(\psi_0) > 1$ with the property that for all z satisfying $\arg z = \psi_0$ and $|z| \geqslant R_0$, and for all $(k, j) \in \Gamma$, we have*

$$\left|\frac{f^{(k)}(z)}{f^{(j)}(z)}\right| \leqslant |z|^{(k-j)(\sigma-1+\varepsilon)}.$$

Remark 3.1. *In this paper, we use Lemma 3.1 several times and the resulting exceptional sets E are not the same each time, although they are denoted by the same letter.*

Lemma 3.2. [11] *Let $f(z)$ be an entire function and suppose that $\left|f^{(k)}(z)\right|$ is unbounded on some ray $\arg z = \theta$. Then there exists an infinite sequence of points $z_j = r_j e^{i\theta}$ $(j = 1, 2, \cdots)$, where $r_j \to +\infty$, such that $f^{(k)}\left(z_j\right) \to \infty$ and*

$$\left|\frac{f^{(q)}\left(z_j\right)}{f^{(k)}\left(z_j\right)}\right| \leqslant \frac{1}{(k-q)!}(1 + o(1))\left|z_j\right|^{k-q} \quad (q = 0, \cdots, k-1).$$

Lemma 3.3. *Given $\mu > 0$ and $h > 0$, the integral $I(r) = \int_r^{+\infty} \exp(-ht^\mu)\, dt$ converges. More precisely we have*

$$I(r) \leqslant \exp\{(-h+\varepsilon) r^\mu\}$$

for r large enough and $\varepsilon > 0$.

Proof. It is easy to prove that $\int_r^{+\infty} \exp(-ht^\mu)\, dt$ converges. For r large enough, we have

$$I(r) = \int_r^{+\infty} \exp(-ht^\mu)\, dt = \int_r^{+\infty} \frac{t^2}{t^2} \exp(-ht^\mu)\, dt$$

$$\leqslant r^2 \exp(-hr^\mu) \int_r^{+\infty} \frac{1}{t^2} dt = r \exp(-hr^\mu) \leqslant \exp\{(-h+\varepsilon) r^\mu\} \quad (\varepsilon > 0).$$

∎

Lemma 3.4. *(Phragmén-Lindelöf Theorem, see [12], p. 214). Let $f(z)$ be analytic in the sector $D = \{z : \alpha < \arg z < \beta,\ r_0 < |z| < \infty\}$ and continuous on $\overline{D} = D \cup \Gamma$, where Γ is the boundary of D. If for any given small $\varepsilon > 0$, there exists $r_1(\varepsilon) > 0$ such that for $|z| \geqslant r_1(\varepsilon)$, $z \in D$, we have*

$$|f(z)| < \exp\left\{\varepsilon |z|^{\frac{\pi}{\beta-\alpha}}\right\},$$

and for $z \in \Gamma$, we have $|f(z)| \leqslant M$ ($M > 0$ is a constant), then $|f(z)| \leqslant M$ for all $z \in D$. $|f(z)| = M$ if and only if f is a constant.

Remark 3.2. *(see [3]). Now suppose that $g(z)$ is analytic in the sector $D = \{z : \alpha < \arg z < \beta,\ r_0 \leqslant |z| < \infty\}$ and satisfies $|g(z)| \leqslant \exp\{|z|^\sigma\}$ for some constant $0 \leqslant \sigma < \infty$. If a subset $E \subset (\alpha, \beta)$ has linear measure zero and for any $\psi_0 \in (\alpha, \beta) - E$, $|g(z)|$ is bounded for all z satisfying $\arg z = \psi_0$ and $|z| \geqslant r_0$, then for any given small $\varepsilon > 0$, there exists $r_1(\varepsilon) > r_0$ such that $|g(z)| \leqslant \exp\left\{\varepsilon |z|^{\sigma+1}\right\}$ for $|z| = r > r_1$. We may choose points $\theta_j \in (\alpha, \beta) - E$ $(j = 1, \cdots, n)$ such that $\theta_1 < \theta_2 < \cdots < \theta_n$ $(\alpha < \theta_1 \leqslant \alpha + \varepsilon,\ \beta - \varepsilon \leqslant \theta_n < \beta)$ and $\max\{\theta_{j+1} - \theta_j : 1 \leqslant j \leqslant n-1\} < \frac{\pi}{\sigma+1}$. Now from Lemma 3.4, $|g(z)| \leqslant M$ holds in the sectors $\{z : \theta_j \leqslant \arg z \leqslant \theta_{j+1}, |z| \geqslant r_0\}$ $(j = 1, \cdots, n-1)$. Hence $|g(z)| \leqslant M$ holds in the sector $\{z : \alpha + \varepsilon \leqslant \arg z \leqslant \beta - \varepsilon, |z| \geqslant r_0\}$.*

Here, we give a special case of the result due to G. G. Gundersen and E. Steinbart in [7]:

Lemma 3.5. *Let $k \geqslant 2$ be an integer. Suppose that $w(z)$ is an entire function, where $\sigma(w) < +\infty$. Let $\lambda, \mu, \eta, \theta_1$ and θ_2 be real constants satisfying $\lambda > 0, \mu > 0, 0 < \eta < \frac{\lambda}{k}$*

and $\theta_1 < \theta_2$. *Suppose that there exists a set* $E \subset \mathbb{R}$ *that has linear measure zero such that for any* $\theta \in (\theta_1, \theta_2) - E$, *we have*

$$|w(z)| \leqslant \exp\{(-\lambda + \eta)|z|^{\mu}\} \tag{10}$$

as $z \longrightarrow \infty$ *along* $\arg z = \theta$. *Then for any* $\theta \in (\theta_1, \theta_2)$, (10) *holds as* $z \longrightarrow \infty$ *along* $\arg z = \theta$.

4. PROOF OF THEOREM 2.1

Suppose that $f \not\equiv 0$ is a solution of (7) with $\sigma(f) = \sigma < \infty$. From Lemma 3.1, there exists a set $E \subset [0, 2\pi)$ that has linear measure zero, such that if $\psi_0 \in (\theta_1, \theta_2) - E$, then

$$\left|\frac{f^{(j)}(z)}{f(z)}\right| \leqslant |z|^{k\sigma}, \quad j = 1, \cdots, k \tag{11}$$

as $z \to \infty$ with $\arg z = \psi_0 \in (\theta_1, \theta_2) \subset \left[0, \frac{\pi}{2n}\right) \cup \left(\frac{3\pi}{2n}, \frac{2\pi}{n}\right)$. From (7), we obtain

$$1 \leqslant \left|\frac{1}{A_0(z)\, e^{z^n}}\right| \left|\frac{f^{(k)}}{f}\right| + \sum_{j=1}^{k-1} \frac{|A_j(z)|}{|A_0(z)|} \left|\frac{f^{(j)}}{f}\right|. \tag{12}$$

By using (5), (6) and (11), we get

$$\left|\frac{A_j(z)}{A_0(z)}\right| \left|\frac{f^{(j)}(z)}{f(z)}\right| \leqslant \frac{1}{e^{(\alpha-\beta)|z|^{\mu}}} |z|^{k\sigma} \quad (j = 1, \cdots, k-1).$$

So

$$\lim_{z\to\infty} \left|\frac{A_j(z)}{A_0(z)}\right| \left|\frac{f^{(j)}(z)}{f(z)}\right| = 0 \quad (j = 1, \cdots, k-1). \tag{13}$$

Also from (5) and (11), we have

$$\left|\frac{1}{A_0(z)\, e^{z^n}}\right| \left|\frac{f^{(k)}(z)}{f(z)}\right| \leqslant \frac{1}{e^{\alpha|z|^{\mu} + |z|^n \cos(n \arg z)}} |z|^{k\sigma}$$

and by taking $z \to \infty$ with $\arg z \in (\theta_1, \theta_2) \subset \left[0, \frac{\pi}{2n}\right) \cup \left(\frac{3\pi}{2n}, \frac{2\pi}{n}\right)$, we obtain

$$\lim_{z\to\infty} \left|\frac{1}{A_0(z)\, e^{z^n}}\right| \left|\frac{f^{(k)}(z)}{f(z)}\right| = 0. \tag{14}$$

Using (13) and (14) in (12) we get a contradiction. So, every solution $f \not\equiv 0$ of (7) has infinite order.

5. PROOF OF THEOREM 2.2

First we prove that $f^{(s)}(z)$ is bounded in $S(\varepsilon)$. From Lemma 3.1, there exists a set $E \subset [0, 2\pi)$ that has linear measure zero, such that for all $j = s+1, \cdots, k$

$$\left|\frac{f^{(j)}(z)}{f^{(s)}(z)}\right| \leqslant |z|^{(j-s)(\sigma-1+\varepsilon)} \leqslant |z|^{k\sigma} \tag{15}$$

along any ray $\arg z = \varphi \in (\theta_1, \theta_2) - E$ with $|z| \geqslant r_1$ large enough, provided $0 < \varepsilon < 1$. If we suppose that $f^{(s)}(z)$ is unbounded on some ray $\arg z = \phi \in S(0) \setminus E$, then by Lemma 3.2 there exists an infinite sequence of points $z_q = r_q e^{i\phi}$ $(q = 1, 2, \cdots)$, where $r_q \to +\infty$, such that $f^{(s)}\left(z_q\right) \to \infty$ and

$$\left|\frac{f^{(j)}\left(z_q\right)}{f^{(s)}\left(z_q\right)}\right| \leqslant \frac{1}{(s-j)!}(1 + o(1))\left|z_q\right|^{s-j} \leqslant 2\left|z_q\right|^{k} \tag{16}$$

for all $j = 0, \cdots, s-1$ when $\left|z_q\right| \geqslant r_2$ large enough. From (7), we can write

$$\begin{aligned} 1 \leqslant \frac{1}{|A_s(z)|}\left|\frac{1}{e^{z^n}}\right|\left|\frac{f^{(k)}(z)}{f^{(s)}(z)}\right| + \frac{|A_{k-1}(z)|}{|A_s(z)|}\left|\frac{f^{(k-1)}(z)}{f^{(s)}(z)}\right| \\ + \cdots + \frac{|A_{s+1}(z)|}{|A_s(z)|}\left|\frac{f^{(s+1)}(z)}{f^{(s)}(z)}\right| + \frac{|A_{s-1}(z)|}{|A_s(z)|}\left|\frac{f^{(s-1)}(z)}{f^{(s)}(z)}\right| \\ + \cdots + \frac{|A_0(z)|}{|A_s(z)|}\left|\frac{f(z)}{f^{(s)}(z)}\right|. \end{aligned} \tag{17}$$

Combining (8), (9), (15) and (16) with (17) we obtain a contradiction as $r_q \to +\infty$. Therefore, $f^{(s)}(z)$ remains bounded on all rays $\arg z = \phi \in S(0) \setminus E$. By Remark 3.2, we conclude that $f^{(s)}(z)$ is bounded, say $\left|f^{(s)}(z)\right| \leqslant M$, in the whole sector $S(\varepsilon)$. By s-fold iterated integration along the line segment $[0, z]$, we have

$$\begin{aligned} f(z) = f(0) + f'(0)z + \cdots + \frac{1}{(s-1)!}f^{(s-1)}(0)z^{s-1} \\ + \int_0^z \cdots \int_0^{\zeta} \int_0^{\xi} f^{(s)}(t)\, dt d\xi \cdots du. \end{aligned}$$

So, we get

$$|f(z)| \leqslant M'|z|^s. \tag{18}$$

Now, from (7), we can write

$$\left|f^{(s)}(z)\right| \leqslant \frac{|f(z)|}{|A_s(z)|}\left(\left|\frac{1}{e^{z^n}}\right|\left|\frac{f^{(k)}(z)}{f(z)}\right| + |A_{k-1}(z)|\left|\frac{f^{(k-1)}(z)}{f(z)}\right|\right.$$

$$+\cdots+|A_1(z)|\left|\frac{f'(z)}{f(z)}\right|+|A_0(z)|\Bigg) \tag{19}$$

and recalling Lemma 3.1, (18) and the assumptions (8) and (9), we conclude

$$\left|f^{(s)}(z)\right| \leqslant \frac{C|z|^{s+k\sigma}\exp\left(\beta|z|^{\mu}\right)}{\exp\left(\alpha|z|^{\mu}\right)} = C|z|^{s+k\sigma}\exp\left\{(\beta-\alpha)|z|^{\mu}\right\},$$

where $C>0$ is a constant, so

$$\left|f^{(s)}(z)\right| \leqslant \exp\left\{(\beta+\tau-\alpha)|z|^{\mu}\right\}, \tag{20}$$

where $0<\tau<\dfrac{\alpha-\beta}{k}$, along any ray $\arg z=\phi\in(\theta_1+\varepsilon,\theta_2-\varepsilon)\setminus E$, provided $|z|\geqslant r_3$ large enough. By combining $\rho\left(f^{(s)}\right)<+\infty$ and Lemma 3.5, we obtain that (20) remains valid in the sector $S(2\varepsilon)$. For $m>s$, we take $z=re^{i\theta}\in S(3\varepsilon)$ such that the disk $\Gamma(z)$ centered at z and of radius at most $\rho=((m-s)!)^{1/(m-s)}$ is contained in $S(2\varepsilon)$, i.e., we must take $r\geqslant\rho/\sin\varepsilon$. By the Cauchy formula

$$f^{(m)}(z)=\frac{(m-s)!}{2\pi i}\int\limits_{\Gamma(z)}\frac{f^{(s)}(w)}{(w-z)^{m-s+1}}dw$$

and using (20), we get

$$\left|f^{(m)}(z)\right| \leqslant \exp\left\{(\beta+\tau-\alpha)|z|^{\mu}\right\} \tag{21}$$

as $|z|$ is large enough along any ray $\arg z=\phi\in S(2\varepsilon)$. Until now, we have proved the second assertion for $m\geqslant s$. We start to prove the first assertion for $j=s-1$. Set

$$a_{s-1}=\int\limits_0^{+\infty}f^{(s)}\left(te^{i\theta}\right)e^{i\theta}dt.$$

By (20), it is easy to see that $\int\limits_0^{+\infty}f^{(s)}\left(te^{i\theta}\right)e^{i\theta}dt$ converges for $\theta\in S(2\varepsilon)$. Moreover, a_{s-1} is independent of θ, because by using (20), the integral of $f^{(s)}(z)$ over the arc $Re^{i\theta}$, $\theta\in(\phi,\varphi)$ in $S(2\varepsilon)$ tends to zero as $R\to+\infty$. Define now $b_{s-1}=f^{(s-1)}(0)+a_{s-1}$, and suppose that $b_{s-1}\neq 0$. Let $z=re^{i\theta}$ (r large enough) be an arbitrary point in $S(2\varepsilon)$. Then by applying (20), and Lemma 3.3, we get

$$\left|f^{(s-1)}(z)-b_{s-1}\right|=\left|f^{(s-1)}(z)-f^{(s-1)}(0)-a_{s-1}\right|$$

$$=\left|\int\limits_0^{z}f^{(s)}(u)\,du-\int\limits_0^{+\infty}f^{(s)}\left(te^{i\theta}\right)e^{i\theta}dt\right|$$

$$= \left| \int_0^{|z|} f^{(s)}\left(te^{i\theta}\right) e^{i\theta} dt - \left(\int_0^{|z|} f^{(s)}\left(te^{i\theta}\right) e^{i\theta} dt + \int_{|z|}^{+\infty} f^{(s)}\left(te^{i\theta}\right) e^{i\theta} dt \right) \right|$$

$$= \left| -\int_{|z|}^{+\infty} f^{(s)}\left(te^{i\theta}\right) e^{i\theta} dt \right| \leqslant \int_{|z|}^{+\infty} \left| f^{(s)}\left(te^{i\theta}\right) \right| dt \leqslant \exp\left\{ (\beta + 2\tau - \alpha) |z|^{\mu} \right\} \tag{22}$$

as $|z|$ large enough along any ray $\arg z = \theta \in S(2\varepsilon)$. Thus, we have completed the proof in the case $b_{s-1} \neq 0$. Now if $b_{s-1} = 0$, we define $a_{s-2} = \int_0^{+\infty} f^{(s-1)}\left(te^{i\theta}\right) e^{i\theta} dt$ and $b_{s-2} = f^{(s-2)}(0) + a_{s-2}$. To estimate $f^{(s-2)}(z) - b_{s-2}$, we apply Lemma 3.3 and

$$\left| f^{(s-1)}(z) \right| \leqslant \exp\left\{ (\beta + 2\tau - \alpha) |z|^{\mu} \right\}$$

in place of (20) exactly as in (22) to obtain

$$\left| f^{(s-2)}(z) - b_{s-2} \right| \leqslant \exp\left\{ (\beta + 3\tau - \alpha) |z|^{\mu} \right\}$$

as $|z|$ is large enough in $S(2\varepsilon)$. By the same method, if $b_{s-1} = b_{s-2} = \cdots = b_{j+1} = 0$ and $b_j \neq 0$ $(j \in \{0, \cdots, s-1\})$, then

$$\left| f^{(j)}(z) - b_j \right| \leqslant \exp\left\{ (\beta + (s - j + 1)\tau - \alpha) |z|^{\mu} \right\}. \tag{23}$$

Now it remains to show that the case $b_{s-1} = b_{s-2} = \cdots = b_0 = 0$ is not possible. In this case we have

$$\left| f^{(m)}(z) \right| \leqslant \exp\left\{ (\beta + (s - m + 1)\tau - \alpha) |z|^{\mu} \right\} \quad (\text{ for all } 0 \leqslant m \leqslant s) \tag{24}$$

and for $m \geqslant s$ we have formula (21). From (7), we can write

$$\left| \frac{f^{(s)}(z)}{f(z)} \right| \leqslant \frac{1}{|A_s(z)|} \left| \frac{1}{e^{z^n}} \right| \frac{\left| f^{(k)}(z) \right|}{|f(z)|} + \frac{|A_{k-1}(z)|}{|A_s(z)|} \frac{\left| f^{(k-1)}(z) \right|}{|f(z)|}$$

$$+ \cdots + \frac{|A_1(z)|}{|A_s(z)|} \frac{|f'(z)|}{|f(z)|} + \frac{|A_0(z)|}{|A_s(z)|}. \tag{25}$$

By using (8), (9) and Lemma 3.1 in (25), we obtain

$$\left| \frac{f^{(s)}(z)}{f(z)} \right| \leqslant \exp\left\{ (\beta + \tau - \alpha) |z|^{\mu} \right\}. \tag{26}$$

Also by using (24) for $m = 0$ in (26), we get

$$\left| f^{(s)}(z) \right| \leqslant \exp\left\{ [2(\beta - \alpha) + (s + 2)\tau] |z|^{\mu} \right\} \tag{27}$$

in $S(2\varepsilon)\setminus E$, hence in $S\left(2\varepsilon+\frac{\varepsilon}{2}\right)$ by Lemma 3.5. If we repeat the steps (22) and (23) until $j=0$ by using (27), we will get

$$|f(z)|\leqslant \exp\left\{\left[2(\beta-\alpha)+(2s+2)\tau\right]|z|^{\mu}\right\}. \tag{28}$$

Then (28) with (26) give

$$\left|f^{(s)}(z)\right|\leqslant \exp\left\{\left[3(\beta-\alpha)+(2s+3)\tau\right]|z|^{\mu}\right\}$$

in $S\left(2\varepsilon+\frac{\varepsilon}{2}\right)\setminus E$, hence in $S\left(2\varepsilon+\frac{\varepsilon}{2}+\frac{\varepsilon}{2^2}\right)$ by Lemma 3.5. Now inductively, suppose that we have

$$\left|f^{(s)}(z)\right|\leqslant \exp\left\{\left[T(\beta-\alpha)+((T-1)s+T)\tau\right]|z|^{\mu}\right\} \tag{29}$$

holds in the sector $S\left(2\varepsilon+\sum_{j=1}^{T-1}\frac{\varepsilon}{2^j}\right)$. Repeating the steps (22), (23) until $j=0$ with (26), we get

$$\left|f^{(s)}(z)\right|\leqslant \exp\left\{\left[(T+1)(\beta-\alpha)+(Ts+T+1)\tau\right]|z|^{\mu}\right\}$$

in $S\left(2\varepsilon+\sum_{j=1}^{T-1}\frac{\varepsilon}{2^j}\right)\setminus E$ provided $|z|$ large enough. By Lemma 3.5, this inequality remains valid in the whole sector $S\left(2\varepsilon+\sum_{j=1}^{T}\frac{\varepsilon}{2^j}\right)$. Thus we have proved in this special case of $b_{s-1}=b_{s-2}=\cdots=b_0=0$, that (29) is valid in $S\left(2\varepsilon+\sum_{j=1}^{+\infty}\frac{\varepsilon}{2^j}\right)=S(3\varepsilon)$ for all $T\in\mathbb{N}^*$, provided $|z|$ large enough. Fix now a finite line segment in $S(3\varepsilon)$ with $|z|$ large enough. Since $(s+1)\tau\leqslant k\tau<\alpha-\beta$, it follows that

$$T(\beta-\alpha)+((T-1)s+T)\tau=-\left[(\alpha-\beta)-(s+1)\tau\right]T-s\tau\to-\infty$$

as $T\to+\infty$. By (29), we will obtain that $f^{(s)}(z)$ vanishes identically on such line segment. Therefore, by the standard uniqueness theorem of entire functions, f has to be a polynomial, a contradiction. So, the case $b_{s-1}=b_{s-2}=\cdots=b_0=0$ is not possible, which completes the proof.

Acknowledgments. The authors would like to thank the referee for his helpful remarks and suggestions to improve the paper.

References

[1] B. Belaïdi, S. Hamouda, *Orders of solutions of an n-th order linear differential equations with entire coefficients*, Electronic J. Diff. Equations, **2001**, 61(2001), 1-5.

[2] B. Belaïdi, K. Hamani, *Order and hyper-order of entire solutions of linear differential equations with entire coefficients,* Electronic J. Diff. Equations, **2003**, No 17(2003), 1-12.

[3] Z. X. Chen, *The zero and order of some second order linear differential equations with transcendental meromorphic coefficients*, Appl. Math.-JCU, **9B** (1994), 365-374.

[4] M. Frei, *Sur l'ordre des solutions entières d'une équation différentielle linéaire*, C. R. Acad. Sci. Paris 23(1953), 38-40.

[5] G. G. Gundersen, *Finite order solutions of second order linear differential equations*, Trans. Amer. Math. Soc., 305(1988), 1, 415–429.

[6] G. G. Gundersen, *Estimates for the logarithmic derivative of a meromorphic function, plus similar estimates*, J. London Math. Soc., (2)37, 1(1988), 88–104.

[7] G. G. Gundersen, E. Steinbart, *Finite order solutions of nonhomogeneous linear differential equations*, Ann. Acad. Sci. Fenn. Ser. A I Math., 17(1992), 2, 327–341.

[8] G. G. Gundersen, E. Steinbart, S. Wang, *The possible orders of solutions of linear differential equations with polynomial coefficients,* Trans. Amer. Math. Soc., 350(1998), 1225-1247.

[9] W. K. Hayman, *Meromorphic functions*, Oxford Mathematical Monographs Clarendon Press, Oxford, 1964.

[10] I. Laine, *Nevanlinna theory and complex differential equations*, de Gruyter Studies in Mathematics, 15. Walter de Gruyter & Co., Berlin, 1993.

[11] I. Laine, R. Yang, *Finite order solutions of complex linear differential equations,* Electronic J. Diff. Equations, **2004** , 65(2004), 1-8.

[12] A. I. Markushevich, *Theory of functions of a complex variable,* Vol. II, Prentice-Hall, Englewood Cliffs, New Jersey, 1965.

[13] J. Tu, C. F. Yi, *On the growth of solutions of a class of higher order linear differential equations with coefficients having the same order*, J. Math. Anal. Appl., **340**, 1(2008), 487–497.

[14] H. Wittich, *Zur Theorie linearer Differentialgleichungen im Komplexen,* Ann. Acad. Sci. Fenn. Ser. A I Math. **379** (1966), 1-18.

[15] C. C. Yang, H. X. Yi, *Uniqueness theory of meromorphic functions*, Mathematics and its Applications, 557, Kluwer Academic Publishers Group, Dordrecht, 2003.

ROMAI J., v.9, no.2(2013), 107–118

SOME SANDWICH RESULTS ASSOCIATED WITH A GENERALIZED LINEAR OPERATOR

S. Sivaprasad Kumar, Virendra Kumar

Department of Applied Mathematics, Delhi Technological University, Delhi, India

vktmaths@yahoo.in

Abstract A generalized linear operator $\mathcal{O}_{g,h}(\alpha)$ is defined on the space of normalized analytic functions for each pair (g, h) of normalized analytic functions. In the present investigation differential subordination, differential superordination and corresponding sandwich results are obtained for this generalized linear operator $\mathcal{O}_{g,h}(\alpha)$ as well as some relevant connections with earlier results are pointed out.

Keywords: analytic function, subordination, starlike function, convex function.

2010 MSC: 30C45, 30C80.

1. INTRODUCTION

Let $\mathcal{H}(\mathbb{D})$ be the set of analytic functions defined on unit disk $\mathbb{D} := \{z \in \mathbb{C} : |z| < 1\}$. For any $a \in \mathbb{C}$ and $n \in \mathbb{N}^*$, we shall denote $\mathcal{H}[a, n] = \{f \in \mathcal{H}(\mathbb{D}) : f(z) = z+a_n z^n+\cdots\}$ and the class of normalized analytic functions $\mathcal{A}_n = \{f \in \mathcal{H}(\mathbb{D}) : f(z) = z+a_{n+1}z^{n+1} + \cdots\}$. Indeed the class $\mathcal{A} = \mathcal{A}_1$ consists of normalized analytic functions of the form

$$f(z) = z + a_2 z^2 + a_3 z^3 + \cdots . \tag{1}$$

The subclass of $\mathcal{A}$ consisting of univalent functions is denoted by $\mathcal{S}$. Among all the geometrically defined classes in the Geometric Function Theory (GFT) the classes of starlike and convex functions are the most prominent topics. A domain $D \subset \mathbb{C}$ is starlike with respect to a point $w_0 \in D$ if the line segment joining any point in D to w_0 lies entirely inside D, while a domain is convex if it is starlike with respect to all its points. A function $f \in \mathcal{A}$ is starlike if and only if $f(\mathbb{D})$ is starlike with respect to origin, and convex if $f(\mathbb{D})$ is convex. A function which maps $\mathbb{D}$ onto starlike domain is called the starlike function and the one which maps $\mathbb{D}$ onto a convex domain is called the convex functions. Analytically, a function $f \in \mathcal{A}$ is starlike if and only if $\mathrm{Re}(zf'(z))/(f(z)) > 0$, whereas $f \in \mathcal{A}$ is convex if and only if $\mathrm{Re}(1 + (zf''(z))/(f'(z))) > 0$. The classes consisting of starlike and convex functions are denoted by $\mathcal{S}^*$ and $\mathcal{K}$ respectively.

For two analytic functions f and g, we say that f is *subordinate* to g or g is *superordinate* to f, if there is a Schwarz function w with $|w(z)| \leq |z|$ such that $f(z) = g(w(z))$. If g is univalent, then $f \prec g$ if and only if $f(0) = g(0)$ and $f(\mathbb{D}) \subseteq g(\mathbb{D})$.

Let $\psi : \mathbb{C}^3 \times \mathbb{D} \to \mathbb{C}$ and ϕ be an univalent function in the unit disk $\mathbb{D}$. Let p be an analytic function in $\mathbb{D}$ and satisfies the second order differential subordination

$$\psi(p(z), zp'(z), z^2p''(z); z) \prec \phi(z), \tag{2}$$

then p is called a solution of the differential subordination. The univalent function q is called a dominant of p, if $p \prec q$ for all p satisfying (2). A dominant $\tilde{q}$ such that $\tilde{q} \prec q$ for all dominants q of p is called the best dominant. The best dominant is unique up to the rotation of the unit disk $\mathbb{D}$.

Let $\psi : \mathbb{C}^3 \times \mathbb{D} \to \mathbb{C}$ and ϕ be a univalent function in the open unit disk $\mathbb{D}$. Assume p is analytic and $\psi(p(z), zp'(z), z^2p''(z); z)$ analytic univalent function in $\mathbb{D}$ that satisfies the second order differential subordination

$$\phi(z) \prec \psi(p(z), zp'(z), z^2p''(z); z). \tag{3}$$

Then p is called a solution of the differential superordination. The analytic function q is called a subordinant of p, if $q \prec p$ for all p satisfying (3). A subordinant $\tilde{q}$ such that $q \prec \tilde{q}$ for all subordinants q of p is called the best subordinant. The best subordinant is unique up to the rotation of the unit disk $\mathbb{D}$.

In the recent past, differential subordination and differential superordination results involving various linear operators were studied by many authors [1, 2, 4, 5, 7, 16, 17, 18, 19] (see also the references cited therein).

Lupaş in two sperate papers [3] and [4] introduced a new operator $RI^{\alpha}(n, \lambda, l)$ for functions $f \in \mathcal{A}$ and $f \in \mathcal{A}_n$ respectively as follows:

$$RI^{\alpha}(n, \lambda, l)f(z) = (1 - \alpha)R^n f(z) + \alpha I(n, \lambda, l)f(z) \quad (\alpha \geq 0),$$

where $R^n f(z)$ and $I(n, \lambda, l)f(z)$ are respectively the Ruscheweyh derivative operator [14] and the generalized multiplier transform [2].

Lupaş also introduced [1] another operator using the generalized Sălăgean operator [5] D^n_{λ} and Ruscheweyh derivative operator for $f \in \mathcal{A}$ as follows:

$$RD^n_{\lambda,\alpha}f(z) = (1 - \alpha)R^n f(z) + \alpha D^n_{\lambda}f(z) \quad (\alpha \geq 0, n \in \mathbb{N}).$$

In the present investigation an attempt has been made to unify these above mentioned operators of Lupaş using the Hadamard product and derive the differential sandwich results associated with this operator introduced here for functions in $\mathcal{A}$. Recall that the Hadamard product of two functions f given by (1) and $g(z) = z + g_2z^2 + g_3z^3 + \cdots$ is defined by

$$(f * g)(z) = z + a_2g_2z^2 + a_3g_3z^3 + \cdots .$$

Definition 1.1. *For $f \in A$ and $\alpha \in C$, let us define the operator $\mho_{g,h}(\alpha)$ by*

$$\mho_{g,h}(\alpha)f(z) = (1 - \alpha)(f * g)(z) + \alpha(f * h)(z),$$

where $g(z) = z + \sum_{k=2}^{\infty} g_k z^k$ *and* $h(z) = z + \sum_{k=2}^{\infty} h_k z^k$.

Remark 1.1. *By taking suitable values to* α *and appropriate functions* g, h*, the operator* $\mho_{g,h}(\alpha)$ *reduces to the several known operator introduced in [1, 2, 3, 4, 5, 12, 13, 15, 17]. For instance, if we set* $\alpha \geq 0$*,*

$$g(z) = z + \sum_{k=2}^{\infty} C_{n+k-1}^{n} z^k \quad \text{and} \quad h(z) = z + \sum_{k=2}^{\infty} \left(\frac{1 + \lambda(k-1) + l}{l+1} \right)^m z^k,$$

then the operator $\mho_{g,h}(\alpha)$ *reduces to the operator* $RI^{\alpha}(m, \lambda, l)$ *introduced by Lupas [4]. Further if we take* $g(z) = z + \sum_{k=2}^{\infty} C_{n+k-1}^{n} z^k$ *and* $h(z) = z + \sum_{k=2}^{\infty} [1 + (k-1)\lambda]^n z^k$*, then* $\mho_{g,h}(\alpha) = RD_{\lambda,\alpha}^{n}$*, the operator introduced by Lupas [1].*

The following notation and lemmas are required in sequel: let us denote by $\mathcal{Q}$, the set of all functions $f(z)$ that are analytic and injective on $\overline{\mathbb{D}} \setminus E(f)$, where

$$E(f) = \{\zeta \in \partial\mathbb{D} : \lim_{z \to \zeta} f(z) = \infty\},$$

and are such that $f'(\zeta) \neq 0$ for $\zeta \in \partial\mathbb{D} \setminus E(f)$.

Lemma 1.1. [6, 8] *Let* ϕ *be a convex function in* $\mathbb{D}$*, with* $\phi(0) = a, \gamma \neq 0$ *and* $\operatorname{Re} \gamma \geq 0$*. If* $p \in \mathcal{H}[a, n]$ *satisfies the subordination*

$$p(z) + \frac{zp'(z)}{\gamma} \prec \phi(z),$$

then

$$p(z) \prec q(z) \prec \phi(z),$$

where

$$q(z) = \frac{\gamma}{n z^{\gamma/n}} \int_0^z \phi(t) t^{\gamma/n - 1} dt.$$

The function q is the convex and is the best (a,n)-dominant.

Lemma 1.2. *[9] Let* ϕ *be a convex function in* $\mathbb{D}$*, with* $\phi(0) = a, \gamma \neq 0$ *and* $\operatorname{Re} \gamma \geq 0$*. Let* $p \in \mathcal{H}[a, n] \cap \mathcal{Q}$ *be such that* $p(z) + (zp'(z))/\gamma$ *is univalent in* $\mathbb{D}$ *and satisfies the subordination*

$$\phi(z) \prec p(z) + \frac{zp'(z)}{\gamma}.$$

Then

$$q(z) = \frac{\gamma}{n z^{\gamma/n}} \int_0^z \phi(t) t^{\gamma/n - 1} dt \prec p(z).$$

The function q is the convex and is the best (a,n)-subordinant.

Lemma 1.3. [7] *Let w be a convex function in $\mathbb{D}$ and let $\phi(z) = w(z) + n\delta z w'(z)$, where $\delta > 0$ and n is a positive integer. If*

$$p(z) = w(0) + p_n z^n + p_{n+1} z^{n+1} + \cdots,$$

is analytic in $\mathbb{D}$ and $p(z) + \delta z p'(z) \prec \phi(z)$, then $p(z) \prec w(z)$ and this result is sharp.

For real or complex numbers a, b and c $(c \neq 0, -1, -2, -3, \cdots)$, the Gauss hypergeometric function [20] is defined by

$${}_2F_1(a, b; c; z) = 1 + \frac{ab}{c}\frac{z}{1!} + \frac{a(a+1)b(b+1)}{c(c+1)}\frac{z^2}{2!} + \cdots.$$

Lemma 1.4. [20] *For real or complex parameters a, b and c $(c \neq 0, -1, -2, -3, \cdots)$,*

$$\int_0^1 t^{b-1}(1-t)^{c-b-1}(1-tz)^{-a}dt = \frac{\Gamma(b)\Gamma(c-b)}{\Gamma(c)}\,{}_2F_1(a, b; c; z) \quad (\mathrm{Re}(c) > \mathrm{Re}(b) > 0); \tag{4}$$

$$(b+1)\,{}_2F_1(1, b; b+1; z) = (b+1) + bz\,{}_2F_1(1, b+1; b+2; z). \tag{5}$$

2. SANDWICH RESULTS

Let us denote $B_\alpha^\delta(g, h) := \{f \in \mathcal{A} : \mathrm{Re}(\mathcal{O}_{g,h}(\alpha)f(z))' > \delta, 0 \leq \delta < 1\}$.

Theorem 2.1. *The set $B_\alpha^\delta(g, h)$ is convex.*

Proof. Let

$$f_j(z) = z + \sum_{k=2}^{\infty} a_{kj} z^k \in B_\alpha^\delta(g, h) \quad (j = 1, 2).$$

Define the function H by

$$H(z) = \gamma_1 f_1(z) + \gamma_2 f_2(z),$$

where γ_1 and γ_2 are non-negative real number such that $\gamma_1 + \gamma_2 = 1$. Now it suffices to show that the function $H \in B_\alpha^\delta(g, h)$ or $\mathrm{Re}(\mathcal{O}_{g,h}(\alpha)H(z))' > \delta$. We have

$$H(z) = z + \sum_{k=2}^{\infty} [\gamma_1 a_{k1} + \gamma_2 a_{k2}] z^k.$$

Therefore

$$\mathcal{O}_{g,h}(\alpha)H(z) = z + \sum_{k=2}^{\infty} (\alpha h_k + (1-\alpha)g_k)[\gamma_1 a_{k1} + \gamma_2 a_{k2}] z^k$$

and

$$\mathrm{Re}(\mathcal{O}_{g,h}(\alpha)H(z))' = 1 + \mathrm{Re}\sum_{k=2}^{\infty} (\alpha h_k + (1-\alpha)g_k)[\gamma_1 a_{k1} + \gamma_2 a_{k2}] k z^{k-1}. \tag{6}$$

Since $f_j \in B_\alpha^\delta(g,h)$, we have

$$\mathrm{Re}\{\sum_{k=2}^{\infty}(\alpha h_k + (1-\alpha)g_k)ka_{kj}z^{k-1}\} > \delta - 1 \quad (j = 1,2). \tag{7}$$

Thus, it is clear from (6) and (7) that $\mathrm{Re}(\mathcal{O}_{g,h}(\alpha)H(z))' > \delta$ and hence $B_\alpha^\delta(g,h)$ is convex. ∎

Remark 2.1. *The above Theorem 2.1 can be extended as follows: If $f_j \in B_\alpha^\delta(g,h)$ $(j = 1,2,3...n)$, then $\sum_{j=1}^n \gamma_j f_j \in B_\alpha^\delta(g,h)$, where γ_i are non-negative real numbers such that $\sum_{j=1}^n \gamma_j = 1$. Note that Theorem 2.1 generalizes the result [4, Theorem 2.1] of Lupaş.*

Theorem 2.2. *Let ϕ be a convex function in $\mathbb{D}$ with $\phi(0) = 1$. Let $\mathrm{Re}(c) > -1$, $f \in \mathcal{A}$ and the function F is defined by*

$$F(z) = \frac{c+1}{z^c}\int_0^z t^{c-1}f(t)dt. \tag{8}$$

1 *If $(\mathcal{O}_{g,h}(\alpha)f(z))' \prec \phi(z)$, then $((\mathcal{O}_{g,h}(\alpha))F(z))' \prec q(z)$, where q is a convex function and is the best dominant given by*

$$q(z) = \frac{c+1}{z^{c+1}}\int_0^z \phi(t)t^c dt. \tag{9}$$

2 *Let $(\mathcal{O}_{g,h}(\alpha)f(z))'$ be analytic univalent in $\mathbb{D}$. If $\phi(z) \prec (\mathcal{O}_{g,h}(\alpha)f(z))'$ and $(\mathcal{O}_{g,h}(\alpha)F(z))' \in \mathcal{H}[1,1] \cap \mathcal{Q}$, then $q(z) \prec ((\mathcal{O}_{g,h}(\alpha))F(z))'$, where q, given by (9), is a convex function and is the best subordinant.*

Proof. It can be easily seen from (8) that

$$cF(z) + zF'(z) = (c+1)f(z). \tag{10}$$

Now convoluting on both sides of (10) with $\phi(z) = z + \sum_{k=2}^{\infty}(\alpha h_k + (1-\alpha)g_k)z^k$ and then differentiating, we get

$$(\mathcal{O}_{g,h}(\alpha)F(z))' + \frac{z(\mathcal{O}_{g,h}(\alpha)F(z))''}{c+1} = (\mathcal{O}_{g,h}(\alpha)f(z))'. \tag{11}$$

In view of the first assumption of Theorem 2.2 namely $(\mathcal{O}_{g,h}(\alpha)f(z))' \prec \phi(z)$, (11) reduces to

$$(\mathcal{O}_{g,h}(\alpha)F(z))' + \frac{z(\mathcal{O}_{g,h}(\alpha)F(z))''}{c+1} \prec \phi(z). \tag{12}$$

If we assume $p(z) = (\mathcal{O}_{g,h}(\alpha)F(z))'$, then (12) becomes

$$p(z) + \frac{zp'(z)}{c+1} \prec \phi(z). \tag{13}$$

Now an application of Lemma 1.1 with $n = 1$, $\gamma = c + 1$ implies $p(z) \prec q(z)$ or equivalently $(\mathcal{O}_{g,h}(\alpha)F(z))' \prec q(z)$, where q given by (9), is convex and is the best dominant. The second half of the proof follows in a similar way by using Lemma 1.2. ∎

The above Theorem 2.2 leads to the following sandwich result:

Corollary 2.1. *Let ϕ_i $(i = 1, 2)$ be convex function in $\mathbb{D}$, with $\phi_i(0) = 1$. Let $\operatorname{Re} c > -1$, $f \in \mathcal{A}$, $(\mathcal{O}_{g,h}(\alpha)f(z))'$ is analytic univalent in $\mathbb{D}$ and $(\mathcal{O}_{g,h}(\alpha)F(z))' \in \mathcal{H}[1, 1] \cap \mathcal{Q}$. If*

$$\phi_1(z) \prec (\mathcal{O}_{g,h}(\alpha)f(z))' \prec \phi_2(z),$$

then

$$q_1(z) \prec (\mathcal{O}_{g,h}(\alpha)F(z))' \prec q_2(z),$$

where q_i be given by

$$q_i(z) = \frac{c+1}{z^{c+1}} \int_0^z \phi_i(t)t^c dt, \tag{14}$$

and F is given by (8).

Corollary 2.2. *Let $f \in \mathcal{A}$ and F be defined by (8). If $\operatorname{Re} c > -1$ and*

$$f'(z) + (1 - \alpha)zf''(z) \prec \frac{1 + (1 - 2\beta)z}{1 + z} \quad (\beta < 1), \tag{15}$$

then

$$F'(z) + (1 - \alpha)zF''(z) \prec 2(1 - \beta)\, {}_2F_1(1, c + 1; c + 2; -z) + 2\beta - 1. \tag{16}$$

The function on the right hand side of (16) is convex and is the best dominant.

Proof. If we take $g(z) = z/(1 - z)$ and $h(z) = z/(1 - z)^2$, then it is easy to see that $(f * g)(z) = f(z)$ and $(f * h)(z) = zf'(z)$. Therefore, we have $\mathcal{O}_{g,h}(\alpha)f(z) = (1 - \alpha)(f * g)(z) + \alpha(f * h)(z) = (1 - \alpha)f(z) + \alpha zf'(z)$ and thus, $(\mathcal{O}_{g,h}(\alpha)f(z))' = f'(z) + \alpha zf''(z)$. Similarly $(\mathcal{O}_{g,h}(\alpha)F(z))' = F'(z)+\alpha zF''(z)$. By taking $\phi(z) = (1+(1-2\beta)z)/(1+z)$, $\beta < 1$ in the first part of Theorem 2.2 yields (25). Further we have

$$q(z) = \frac{c+1}{z^{c+1}} \int_0^z \frac{1 + (1 - 2\beta)t}{1 + t} t^c dt.$$

Now a computation using Lemma 1.4, yields

$$q(z) = 2(1 - \beta)\, {}_2F_1(1, c + 1; c + 2; -z) + 2\beta - 1.$$

This completes the proof. ∎

Remark 2.2. *When $c = 0$ and $\alpha = 1$ Corollary 2.2 reduces to the result [8, Lemma 5.5k] of Miller and Mocanu.*

Theorem 2.3. *Let q be a convex function in $\mathbb{D}$ with $\phi(0) = 1$. Further assume that $f \in \mathcal{A}$ and F is defined by (8). If*

$$(\mathcal{O}_{g,h}(\alpha)f(z))' \prec q(z) + \frac{zq'(z)}{c+1} \quad (c > -1),$$

then $(\mathcal{O}_{g,h}(\alpha)F(z))' \prec q(z)$.

Proof. Let $p(z) = (\mathcal{O}_{g,h}(\alpha)F(z))'$. Proceeding as described in the proof of Theorem 2.2, we arrive at

$$p(z) + \frac{zp'(z)}{c+1} \prec q(z) + \frac{zq'(z)}{c+1}.$$

Now the result follows at once by an application of Lemma 1.3. ∎

If we set $q(z) = (1 + (1 - 2\beta)z)/(1 - z)$ $(0 \leq \beta < 1)$ in Theorem 2.3, we obtain the following result:

Corollary 2.3. *Let $f \in \mathcal{A}$ and the function F be as defined in (8). If*

$$\mathrm{Re}(\mathcal{O}_{g,h}(\alpha)f(z))' > \beta + \frac{\beta - 1}{2(c+1)} \quad (0 \leq \beta < 1, c > -1), \tag{17}$$

then $\mathrm{Re}(\mathcal{O}_{g,h}(\alpha)F(z))' > \beta$. The result is best possible.

Proof. Let

$$q(z) = \frac{1 + (1 - 2\beta)z}{1 - z} \quad (0 \leq \beta < 1).$$

Clearly q is convex in $\mathbb{D}$ with $q(0) = 1$. A calculation shows that

$$q(z) + \frac{zq'(z)}{c+1} = \frac{1 + (1 - 2\beta)z}{1 - z} - \frac{2(1 - \beta)z}{(c+1)(1 - z)^2}.$$

Now an application of Theorem 2.3 yields

$$(\mathcal{O}_{g,h}(\alpha)f(z))' \prec \frac{1 + (1 - 2\beta)z}{1 - z} - \frac{2(1 - \beta)z}{(c+1)(1 - z)^2}.$$

This implies (26) and hence the result follows at once. ∎

Remark 2.3. *By setting $\beta = 0$ in the above Corollary 2.3, we have*

$$\mathrm{Re}(\mathcal{O}_{g,h}(\alpha)f(z))' > \frac{-1}{2(c+1)}, \quad c > -1$$

implies $\mathrm{Re}(\mathcal{O}_{g,h}(\alpha)F(z))' > 0$. This shows that $\mathcal{O}_{g,h}(\alpha)F(z)$ is univalent even though $\mathcal{O}_{g,h}(\alpha)f(z)$ is not.

Theorem 2.4. *Let ϕ be a convex function in $\mathbb{D}$, with $\phi(0) = 1$ and $f \in \mathcal{A}$.*

1 *If* $(\mathcal{O}_{g,h}(\alpha)f(z))' \prec \phi(z)$, *then* $((\mathcal{O}_{g,h}(\alpha))f(z))/z \prec q(z)$, *where* q *is a convex function and is the best dominant given by*

$$q(z) = \frac{1}{z}\int_0^z \phi(t)dt. \tag{18}$$

2 *Let* $(\mathcal{O}_{g,h}(\alpha)f(z))'$ *be analytic univalent in* $\mathbb{D}$. *If* $\phi(z) \prec (\mathcal{O}_{g,h}(\alpha)f(z))'$ *and* $((\mathcal{O}_{g,h}(\alpha))f(z))/z \in \mathcal{H}[1,1] \cap \mathcal{Q}$, *then* $q(z) \prec ((\mathcal{O}_{g,h}(\alpha))f(z))/z$, *where* q, *given by (9), is a convex function and it is the best subordinant.*

Proof. Let us prove the first part of the theorem by assuming

$$p(z) = \frac{\mathcal{O}_{g,h}(\alpha)f(z)}{z}. \tag{19}$$

It is clear that $p(0) = 1$ and $p \in \mathcal{H}[1,1]$. From (19), we have

$$p(z) + zp'(z) = (\mathcal{O}_{g,h}(\alpha)f(z))'. \tag{20}$$

Since $(\mathcal{O}_{g,h}(\alpha)f(z))' \prec \phi(z)$, (20) implies $p(z) + zp'(z) \prec \phi(z)$. Now an application of Lemma 1.1 with $n = 1$ and $\gamma = 1$ leads to $p(z) \prec q(z)$ or

$$\frac{\mathcal{O}_{g,h}(\alpha)f(z)}{z} \prec q(z),$$

where q, given by (1), is a convex function and it is the best dominant. The second half of the proof follows in a similar way by using Lemma 1.2. ∎

Corollary 2.4. *Let* ϕ_i $(i = 1, 2)$ *be convex in* $\mathbb{D}$ *with* $\phi_i(0) = 1$ *and* $f \in \mathcal{A}$. *Assume that* $((\mathcal{O}_{g,h}(\alpha))f(z))/z \in \mathcal{H}[1,1] \cap \mathcal{Q}$ *and* $(\mathcal{O}_{g,h}(\alpha)f(z))'$ *is analytic univalent in* $\mathbb{D}$. *If*

$$\phi_1(z) \prec (\mathcal{O}_{g,h}(\alpha)f(z))' \prec \phi_2(z),$$

then

$$q_1(z) \prec (\mathcal{O}_{g,h}(\alpha)F(z))' \prec q_2(z),$$

where q_i *is given by*

$$q_i(z) = \frac{1}{z}\int_0^z \phi_i(t)dt. \tag{21}$$

By taking $g(z) = z/(1-z)$, $h(z) = z/(1-z)^2$ and $\phi(z) = (1 + (1-2\beta)z)/(1-z)$ with $(0 \le \beta < 1)$ in Theorem 2.4, we obtain the following result:

Corollary 2.5. *Let* $f \in \mathcal{A}$. *If*

$$\mathrm{Re}(f'(z) + (1-\alpha)zf''(z)) > \beta,$$

then

$$\operatorname{Re}\left(\frac{\alpha f(z)+(1-\alpha)zf'(z)}{z}\right) > 2(\beta-1)\ln 2 + 2\beta - 1.$$

Remark 2.4. *The above result generalizes the result of Owa* et al. *[11, Corollary 1] and, for $\alpha = 0$, the result reduces to the result [6, Theorem 6] of Hallenbeck.*

Theorem 2.5. *Let q be a convex function in $\mathbb{D}$ with $q(0) = 1$. If $f \in \mathcal{A}$ satisfies the subordination $(\mathcal{O}_{g,h}(\alpha)f(z))' \prec q(z) + zq'(z)$, then*

$$((\mathcal{O}_{g,h}(\alpha))f(z))/z \prec q(z).$$

The function q is convex and is the best dominant.

Proof. Proceeding as in the proof of Theorem 2.4, we have (20). Now (20) and the assumption $\phi(z) = q(z) + zq'(z)$ lead to

$$p(z) + zp'(z) \prec q(z) + zq'(z).$$

An application of Lemma 1.3 completes the proof. ∎

Remark 2.5. *Let us consider*

$$q(z) = \frac{1+(1-2\beta)z}{1-z} \qquad (0 \le \beta < 1).$$

Then q is convex in $\mathbb{D}$ and $q(0) = 1$. Further taking $g(z) = z/(1-z)$ and $h(z) = z/(1-z)^2$ in Theorem 2.5 we conclude that

$$\frac{\alpha f(z)+(1-\alpha)zf'(z)}{z} \prec \frac{1+(1-2\beta)z}{1-z}$$

whenever

$$f'(z) + (1-\alpha)zf''(z) \prec \frac{1+(1-2\beta)z}{1-z} + \frac{2(1-\beta)z}{(1-z)^2}.$$

Thus we have the following result:

Corollary 2.6. *Let $f \in \mathcal{A}$. If*

$$\operatorname{Re}(f'(z) + (1-\alpha)zf''(z)) > \frac{3\beta-1}{2} \quad (0 \le \beta < 1),$$

then

$$\operatorname{Re}\left(\frac{\alpha f(z)+(1-\alpha)zf'(z)}{z}\right) > \beta.$$

Remark 2.6. *The Corollary 2.6 coincide with the results [16, Example 3.5] of Kumar* et al. *and [10, Theorem 2] of Obradović, for $\alpha = 0$ and 1 respectively.*

Theorem 2.6. *Let ϕ be a convex function in $\mathbb{D}$, with $\phi(0) = 0$ and $f \in \mathcal{A}$.*

1 *If $\mathcal{O}_{g,h}(\alpha)f(z) + z(\mathcal{O}_{g,h}(\alpha)f(z))' \prec \phi(z)$, then $\mathcal{O}_{g,h}(\alpha)f(z) \prec q(z)$, where the function q, given by (1), is convex and is the best dominant.*

2 *Let $\mathcal{O}_{g,h}(\alpha)f(z)+z(\mathcal{O}_{g,h}(\alpha)f(z))'$ be analytic univalent in $\mathbb{D}$. If $\phi(z) \prec \mathcal{O}_{g,h}(\alpha)f(z)+ z(\mathcal{O}_{g,h}(\alpha)f(z))'$ and $\mathcal{O}_{g,h}(\alpha)f(z) \in \mathcal{H}[0,1] \cap \mathcal{Q}$, then $q(z) \prec \mathcal{O}_{g,h}(\alpha)f(z)$, where the function q, given by (1), is convex and is the best subordinant.*

Proof. Let

$$p(z) = \mathcal{O}_{g,h}(\alpha)f(z). \tag{22}$$

Then clearly $p(0) = 0$ and $p \in \mathcal{H}[0,1]$. A computation using (22) yields

$$p(z) + zp'(z) = \mathcal{O}_{g,h}(\alpha)f(z) + z(\mathcal{O}_{g,h}(\alpha)f(z))'. \tag{23}$$

Since $\mathcal{O}_{g,h}(\alpha)f(z) + z(\mathcal{O}_{g,h}(\alpha)f(z))' \prec \phi(z)$, (23) reduces to $p(z) + zp'(z) \prec \phi(z)$. Now an application of Lemma 1.1 with $\gamma = n = 1$ completes the proof of first part of the theorem. The second half of the proof follows similarly by using Lemma 1.2. ∎

From Theorem 2.6, we have the following sandwich result:

Corollary 2.7. *Let ϕ_i $(i = 1, 2)$ be convex functions in $\mathbb{D}$, with $\phi_i(0) = 0$ and $f \in \mathcal{A}$. Assume that $\mathcal{O}_{g,h}(\alpha)f(z)+z(\mathcal{O}_{g,h}(\alpha)f(z))'$ is analytic univalent in $\mathbb{D}$ and $\mathcal{O}_{g,h}(\alpha)f(z) \in \mathcal{H}[0,1] \cap \mathcal{Q}$. If*

$$\phi_1(z) \prec \mathcal{O}_{g,h}(\alpha)f(z) + z(\mathcal{O}_{g,h}(\alpha)f(z))' \prec \phi_2(z),$$

then

$$q_1(z) \prec \mathcal{O}_{g,h}(\alpha)f(z) \prec q_2(z),$$

where q_i $(i = 1, 2)$ is given by (21).

By taking $g(z) = h(z) = \phi(z) = z/(1-z)^2$ in the first part of Theorem 2.6, we obtain the following result:

Example 2.1. *Let $f \in \mathcal{A}$. If*

$$\mathrm{Re}(\alpha f(z) + (2-\alpha)zf'(z) + (1-\alpha)z^2 f''(z)) > -\frac{1}{2},$$

then $\mathrm{Re}(\alpha f(z) + (1-\alpha)zf'(z)) > \ln 2 - 1$.

Theorem 2.7. *Let q be a convex function in $\mathbb{D}$ and $\phi(z) = q(z) + zq'(z)$. Assume that $f \in \mathcal{A}$. If*

$$\mathcal{O}_{g,h}(\alpha)f(z) + z(\mathcal{O}_{g,h}(\alpha)f(z))' \prec \phi(z),$$

then

$$\mathcal{O}_{g,h}(\alpha)f(z) \prec q(z).$$

The proof is much akin to the proof of Theorem 2.5 and hence it is skipped here.

Theorem 2.8. *Let ϕ be a convex function in $\mathbb{D}$, with $\phi(0) = 1$ and $f \in \mathcal{A}$.*

1 *If $(\mathcal{O}_{g,h}(\alpha)f(z))' + z(\mathcal{O}_{g,h}(\alpha)f(z))'' \prec \phi(z)$, then $(\mathcal{O}_{g,h}(\alpha)f(z))' \prec q(z)$, where the function q, given by (1) is convex and is the best dominant.*

2 *Let $(\mathcal{O}_{g,h}(\alpha)f(z))'+z(\mathcal{O}_{g,h}(\alpha)f(z))''$ is analytic univalent in $\mathbb{D}$. If $\phi(z) \prec (\mathcal{O}_{g,h}(\alpha)f(z))'$ $+z(\mathcal{O}_{g,h}(\alpha)f(z))''$, and $\mathcal{O}_{g,h}(\alpha)f(z) \in \mathcal{H}[1,1] \cap \mathcal{Q}$, then $q(z) \prec (\mathcal{O}_{g,h}(\alpha)f(z))'$, where the function q, given by (1), is convex and is the best subordinant.*

The proof is similar to that of Theorem 2.6 and hence it is skipped here.

We have the following sandwich result from Theorem 2.8:

Corollary 2.8. *Let ϕ_i $(i = 1, 2)$ be convex functions in $\mathbb{D}$, with $\phi_i(0) = 1$ and $f \in \mathcal{A}$. Assume that $(\mathcal{O}_{g,h}(\alpha)f(z))' + z(\mathcal{O}_{g,h}(\alpha)f(z))''$ is analytic univalent in $\mathbb{D}$ and $\mathcal{O}_{g,h}(\alpha)f(z) \in \mathcal{H}[1,1] \cap \mathcal{Q}$. If*

$$\phi_1(z) \prec (\mathcal{O}_{g,h}(\alpha)f(z))' + z(\mathcal{O}_{g,h}(\alpha)f(z))'' \prec \phi_2(z),$$

then

$$q_1(z) \prec (\mathcal{O}_{g,h}(\alpha)f(z))' \prec q_2(z),$$

where q_i $(i = 1, 2)$ be given by (21).

By taking $g(z) = h(z) = z/(1-z)$ and $\phi(z) = (1 + (1-2\beta)z)/(1-z)$ with $0 \le \beta < 1$ in the first part of Theorem 2.8, we deduce the following result:

Example 2.2. *Let $f \in \mathcal{A}$. If*

$$\mathrm{Re}(f(z) + zf'(z)) > \beta \quad (0 \le \beta < 1),$$

then $\mathrm{Re}(f(z)) > 2(1-\beta)\ln 2 + 2\beta - 1$.

Theorem 2.9. *Let q be a convex function in $\mathbb{D}$ and $\phi(z) := q(z) + zq'(z)$. Assume that $f \in \mathcal{A}$. If*

$$(\mathcal{O}_{g,h}(\alpha)f(z))' + z(\mathcal{O}_{g,h}(\alpha)f(z))'' \prec \phi(z),$$

then

$$(\mathcal{O}_{g,h}(\alpha)f(z))' \prec q(z).$$

The proof of theorem is similar to that of Theorem 2.5 and hence we skip it here.

By setting $g(z) = h(z) = z/(1-z)$ and $q(z) = (1 + (1-2\beta)z)/(1-z)$, $0 \le \beta < 1$ in Theorem 2.9, we deduce the following result:

Example 2.3. *Let $f \in \mathcal{A}$. If* $\mathrm{Re}(f'(z) + zf''(z)) > 2(1-\beta)\ln 2 + 2\beta - 1$ $(0 \le \beta < 1)$, *then* $\mathrm{Re}f'(z) > \beta$.

Acknowledgement The work presented here is supported by a Senior Research Fellowship from Delhi Technological University, New Delhi, INDIA. The authors are thankful to the referee for the several suggestions that improved the clarity of this manuscript.

References

[1] A. Alb Lupaş, *On special differential superordinations using a generalized Sălăgean operator and Ruscheweyh derivative*, Comput. Math. Appl. **61** (2011), no. 4, 1048–1058.

[2] A. Alb Lupaş, *A special comprehensive class of analytic functions defined by multiplier transformation*, J. Comput. Anal. Appl. **12** (2010), no. 2, 387–395.

[3] A. Alb Lupaş, *A note on a subclass of analytic functions Defined by Ruscheweyh derivative and multiplier transformations*, Int. J. Open Problems Complex Analysis, **2**,(2010) no. 2, 60-66.

[4] A. Alb Lupaş, *On special differential subordinations using multiplier transformation and Ruscheweyh derivative*, ROMAI J. **6** (2010), no. 2, 1–14.

[5] F. M. Al-Oboudi, *On univalent functions defined by a generalized Sălăgean operator*, Int. J. Math. Math. Sci. **2004**, no. 25-28, 1429–1436.

[6] D. J. Hallenbeck, *Convex hulls and extreme points of some families of univalent functions*, Trans. Amer. Math. Soc. **192** (1974), 285–292.

[7] S. S. Miller, P. T. Mocanu, *On some classes of first-order differential subordinations*, Michigan Math. J. **32** (1985), no. 2, 185–195.

[8] S. S. Miller, P. T. Mocanu, *Differential subordinations*, Monographs and Textbooks in Pure and Applied Mathematics, 225, Dekker, New York, 2000.

[9] S. S. Miller, P. T. Mocanu, *Subordinants of differential superordinations*, Complex Var. Theory Appl. **48** (2003), no. 10, 815–826.

[10] M. Obradović, *Estimates of the real part of $f(z)/z$ for some classes of univalent functions*, *Mat. Vesnik* **36** (1984), no. 4, 266–270.

[11] S. Owa, M. Obradović, M. Nunokawa, *On certain analytic functions and subordinations*, Appl. Math. Lett. **3** (1990), no. 1, 41–45.

[12] S. F. Ramadan, M. Darus, *Univalence of an integral operator defined by generalized operators*, Int. J. Comput. Math. Sci. **4** (2010), no. 8, 392–394.

[13] S. F. Ramadan, M. Darus, *A multiplier transform defined by convolution involving a differential operator*, Int. J. open problems complex analysis, **2** (2010), no. 2, , 127–139.

[14] S. Ruscheweyh, *New criteria for univalent functions*, Proc. Amer. Math. Soc. **49** (1975), 109–115.

[15] G. Ş. Sălăgean, *Subclasses of univalent functions*, in *Complex analysis—fifth Romanian-Finnish seminar, Part 1 (Bucharest, 1981)*, 362–372, Lecture Notes in Math., 1013 Springer, Berlin.

[16] S. S. Kumar, V. Kumar and V. Ravichandran, *Subordination and superordination for multivalent functions defined by linear operators*, Tamsui Oxf. J. Inf. Math. Sci., **29**(3) (2013) 361-387.

[17] V. Ravichandran, S. S. Kumar, *On a class of analytic functions involving Carlson-Shaffer linear operator*, Riv. Mat. Univ. Parma (7) **3** (2004), 35–48 (2005).

[18] S. S. Kumar, V. Ravichandran, H. C. Taneja, *Differential sandwich theorems for linear operators*, Int. J. Math. Model. Simul. Appl. **2** (2009), no. 4, 490–507.

[19] S. S. Kumar, H. C. Taneja, V. Ravichandran, *Classes of multivalent functions defined by Dziok-Srivastava linear operator and multiplier transformation*, *Kyungpook Math. J.* **46** (2006), no. 1, 97–109.

[20] E. T. Whittaker, G. N. Watson, *A course of modern analysis. An introduction to the general theory of infinite processes and of analytic functions: with an account of the principal transcendental functions*, Fourth edition. Reprinted Cambridge Univ. Press, New York, 1962.

ROMAI J., v.9, no.2(2013), 119–128

ON THE LIFETIME AS THE MAXIMUM OR MINIMUM OF THE SAMPLE WITH POWER SERIES DISTRIBUTED SIZE

Alexei Leahu[1], Bogdan Gheorghe Munteanu[2], Sergiu Cataranciuc[3]

[1] *Technical University of Moldova, Chişinău, Republic of Moldova*

[2] *Henri Coandă Air Forces Academy, Braşov, Romania*

[3] *Moldova State University, Chişinău, Republic of Moldova*

alexe.leahu@gmail.com, munteanu.b@afahc.ro, s.cataranciuc@gmail.com

Abstract The present paper treats the topic of the distribution of the maximum and minimum of a sequence of an independent identically distributed random variables (i.i.d.r.v.) in a random number in a unitary manner and from the perspective of the power series distribution class. The general formulas are obtained, and by using concrete examples, they lead to some of the distributions obtained by Adamidis and Loukas (1998), Kus (2007), Tahmasbi and Rezaei (2008), Leahu and Lupu (2010), Baretto-Souza, Morais and Cordeiro (2011), Morais and Baretto-Souza (2011), Cancho, Louzada and Barriga (2011), Louzada, Roman and Cancho (2011), Flores, Borges, Cancho and Louzada (2013). Examples of new distributions are also presented.

Keywords: power series distribution, distribution of the maximum, distribution of the minimum.
2010 MSC: Primary 60K10, Secondary 62N05.

1. INTRODUCTION

The introduction of this new (generalized) distribution is connected with reliability problems when lifetime can be expressed as the maximum or minimum of a sequence of i.i.d.r.v., which represents the risk times of the system components. In recent years, some researchers have proposed a series of new distributions for the maximum and minimum of a sequence of i.i.d.r.v.. For example, Adamidis and Loukas [1], Kus [6], Tahmasbi and Rezaei [12], Leahu and Lupu [7], Louzada, Roman and Cancho [9], as well as the Cancho, Louzada and Barriga [3], have been concerned with determining the maximum or minimum distribution when the components in a sequence of i.i.d.r.v. are exponentially distributed, and the number of the components are of a discrete type. Next, Flores, Borges, Cancho and Louzada [4] treat the distribution of a vector's maximum with components that are exponentially distributed in an random number of a power series distribution type. This type of distribution is called complementary exponential power series (CEPS) distribution. Also, Morais and Baretto-Souza [11] considered the analysed Weibull distribution class by means of the power series distribution class (WPS). Recently, Louzada, Bereta and Franco [10] have formulated a mathematical model that unifies the procedure for obtaining a

distribution of the maximum and minimum of a sequence of i.i.d.r.v. of the absolutely continuous type in a random number N characterized by the generating function. But the problem of determining the general formula when the r.v. N forms part of a power series distributions remains unsolved.

2. THE POWER SERIES DISTRIBUTION OF THE MAXIMUM AND MINIMUM

Let us consider r.v. Z such that $\mathbb{P}(Z \in \{1, 2, \ldots\}) = 1$.

Definition 2.1. ([5]) *We say that r.v. Z has a power series distribution if:*

$$\mathbb{P}(Z = z) = \frac{a_z \Theta^z}{A(\Theta)},\ z = 1, 2, \ldots;\ \Theta \in (0, \tau); \tag{1}$$

where $a_1, a_2, \ldots$ are nonnegative real numbers, τ is a positive number bounded by the convergence radius of power series (series function) $A(\Theta) = \sum\limits_{z \geq 1} a_z \Theta^z,\ \forall\ \Theta \in (0, \tau)$, and Θ is power parameter of the distribution (Table 1).

PSD denotes the power series distribution functions class. If the r.v. Z has the distribution from relationship (1), then we write that $Z \in PSD$.

Table 1: The representative elements of the PSD class for various truncated distributions

Distribution	a_z	Θ	$A(\Theta)$	τ
$Binom^*(n, p)$	$\binom{n}{z}$	$\frac{p}{1-p}$	$(1+\Theta)^n - 1$	∞
$Poisson^*(\alpha)$	$\frac{1}{z!}$	α	$e^{\Theta} - 1$	∞
$Log(p)$	$\frac{1}{z}$	p	$-ln(1-\Theta)$	1
$Geom^*(p)$	1	$1-p$	$\frac{\Theta}{1-\Theta}$	1
$Pascal(k, p)$	$\binom{z-1}{k-1}$	$1-p$	$\left(\frac{\Theta}{1-\Theta}\right)^k$	1
$Bineg^*(k, p)$	$\binom{z+k-1}{z}$	p	$(1-\Theta)^{-k} - 1$	1

On the other hand, as Z is a r.v. discrete type for which $\mathbb{P}(Z \in \{1, 2, \ldots\}) = 1$, then we can write its distribution function:

$$F_Z(x) = \mathbb{P}(Z \leq x) = \begin{cases} 0 & \text{if} \quad x < 1 \\ \sum\limits_{z=1}^{[x]} \mathbb{P}(Z = z) & \text{if} \quad x \geq 1. \end{cases} .$$

Therefore we can formulate the following proposition which characterizes the power series distribution class.

Proposition 2.1. *The necessary and sufficient condition for the r.v. Z to have a power series distribution is that the distribution function be characterized by:*

$$F_Z(x) = \sum_{z=1}^{[x]} \frac{a_z \Theta^z}{A(\Theta)}, \ x \geq 1, \tag{2}$$

where the entities $(a_z)_{z\geq 1}$, Θ, $A(\Theta)$ are characterized by the Definition 2.1.

Proof. Necessity: assume that r.v. $Z \in PSD$. Then in accordance with Definition 2.1, this has the distribution

$$Z : \begin{pmatrix} 1 & 2 & 3 \dots & n \dots \\ \frac{a_1\Theta}{A(\Theta)} & \frac{a_2\Theta^2}{A(\Theta)} & \frac{a_3\Theta^3}{A(\Theta)} \cdots & \frac{a_n\Theta^n}{A(\Theta)} \cdots \end{pmatrix}.$$

Then the distribution function $F_Z(x) = \mathbb{P}(Z \leq x) = \sum\limits_{z\leq x} \mathbb{P}(Z = z) = \sum\limits_{z=1}^{[x]} \frac{a_z\Theta^z}{A(\Theta)}$.

Sufficiency: assume that r.v. Z has the distribution function characterized by the relationship (2). With this we can restore the values of the r.v., namely $\mathbb{P}(Z \in \{1, 2, \dots\} = 1)$, as well as the probabilities. We have that: $\mathbb{P}(Z = i) = F(i) - F(i-0) = \sum\limits_{z=1}^{i} \frac{a_z\Theta^z}{A(\Theta)} - \sum\limits_{z=1}^{i-1} \frac{a_z\Theta^z}{A(\Theta)} = \frac{a_z\Theta^z}{A(\Theta)}$, therefore $Z \in PSD$. ∎

The next result defines the distribution function for the maximum and minimum of a sequence of i.i.d.r.v. in random number.

Proposition 2.2. *If r.v. $U = \max\{X_1, X_2, \dots, X_Z\}$ and $V = \min\{X_1, X_2, \dots, X_Z\}$, where $(X_i)_{i\geq 1}$ are nonnegative i.i.d.r.v., with the known distribution function $F_{X_i}(x) = F(x)$, $\forall x > 0$ and $Z \in PSD$ with $\mathbb{P}(Z = z) = \frac{a_z\Theta^z}{A(\Theta)}$, $z = 1, 2, \dots$; $\Theta \in (0, \tau)$, $\tau > 0$, r.v. $(X_i)_{i\geq 1}$ and Z being independent, then the distribution function of the r.v. U, respectively V are the following:*

$$U(x) = \frac{A[\Theta F(x)]}{A(\Theta)}, \ x > 0, \tag{3}$$

$$V(x) = 1 - \frac{A[\Theta(1 - F(x))]}{A(\Theta)}, \ x > 0. \tag{4}$$

Proof. For $Z = z$, the distribution function of the maximum of a sample of size z with the distribution function F, is $U_z(x) = [F(x)]^z$. Using the total probability formula, then the distribution function of the maximum of a sequence of i.i.d.r.v. in random number Z has the expression $U(x) = \sum\limits_{z\geq 1} U_z(x) \cdot \mathbb{P}(Z = z) = \sum\limits_{z\geq 1} [F(x)]^z \cdot \mathbb{P}(Z = z)$. Since $Z \in PSD$ (the relationship (1)), the result is relationship (3).

In the case of the minimum, we have $V(x) = \sum\limits_{z\geq 1} V_z(x) \cdot \mathbb{P}(Z = z)$, where the distribution function of the minimum of a sample of size z, is characterized by the relationship $V_z(x) = 1 - [1 - F(x)]^z$.

Therefore,

$$\begin{aligned} V(x) &= \sum_{z\geq 1} \left[1 - [1 - F(x)]^z\right] \cdot \mathbb{P}(Z = z) \\ &= 1 - \sum_{z\geq 1} \frac{a_z \left[\Theta(1 - F(x))\right]^z}{A(\Theta)}. \end{aligned}$$

Taking into account the definition of $A(\Theta)$, relation (4) is obtained. ∎

The following results characterize the survival functions and the probability density functions (pdf) for the maximum, respectively minimum of a sequence of i.i.d.r.v. in random number.

Consequence 2.1. *If r.v.* $U = \max\{X_1, X_2, \ldots, X_Z\}$ *and* $V = \min\{X_1, X_2, \ldots, X_Z\}$, *where* $(X_i)_{i\geq 1}$ *are nonnegative i.i.d.r.v., with the known distribution function* $F_{X_i}(x) = F(x)$, $\forall x > 0$ *and* $Z \in PSD$ *with* $\mathbb{P}(Z = z) = \frac{a_z \Theta^z}{A(\Theta)}$, $z = 1, 2, \ldots$; $\Theta \in (0, \tau)$, $\tau > 0$, *r.v.* $(X_i)_{i\geq 1}$ *and* Z *being independent, then the survival function of the r.v.* U, *respectively* V *are the following:*

$$S_U(x) = 1 - \frac{A\left[\Theta F(x)\right]}{A(\Theta)}, \ x > 0, \tag{5}$$

$$S_V(x) = \frac{A\left[\Theta(1 - F(x))\right]}{A(\Theta)}, \ x > 0. \tag{6}$$

Consequence 2.2. *If r.v.* $U = \max\{X_1, X_2, \ldots, X_Z\}$, *where* $(X_i)_{i\geq 1}$ *are nonnegative i.i.d.r.v., absolutely continuous type, with the known pdf* $f_{X_i}(x) = f(x)$, $\forall x > 0$ *and* $Z \in PSD$ *with* $\mathbb{P}(Z = z) = \frac{a_z \Theta^z}{A(\Theta)}$, $z = 1, 2, \ldots$; $\Theta \in (0, \tau)$, $\tau > 0$, *r.v.* $(X_i)_{i\geq 1}$ *and* Z *being independent, then the pdf of the r.v.* U *is the following:*

$$u(x) = \frac{\Theta f(x) A'\left[\Theta F(x)\right]}{A(\Theta)}, \ x > 0. \tag{7}$$

Proof. The pdf of the r.v. U is obtained by determining the derivative of the relationship (3) with respect to variable x. ∎

Consequence 2.3. *If r.v.* $V = \min\{X_1,\ X_2, \ldots, X_Z\}$, *where* $(X_i)_{i\geq 1}$ *are nonnegative i.i.d.r.v., absolutely continuous type, with the known pdf* $f_{X_i}(x) = f(x),\ \forall x > 0$ *and* $Z \in PSD$ *with* $\mathbb{P}(Z = z) = \frac{a_z\Theta^z}{A(\Theta)},\ z = 1, 2, \ldots;\ \Theta \in (0, \tau),\ \tau > 0$, *r.v.* $(X_i)_{i\geq 1}$ *and* Z *being independent, then the pdf of the r.v.* V *is the following:*

$$v(x) = \frac{\Theta f(x)A'\left[\Theta(1 - F(x))\right]}{A(\Theta)},\ x > 0. \tag{8}$$

Proof. By determining the derivative of the relationship (4) with respect to variable x, (8) is obtained. ∎

In the above conditions, the hazard rate under definition, we can formulate the following proposition:

Proposition 2.3. *The hazard rate for the r.v. U, respectively V are characterized by the following relations:*

$$h_U(x) = \frac{u(x)}{1 - U(x)} = \frac{\Theta f(x)A'\left[\Theta F(x)\right]}{A(\Theta) - A\left[\Theta F(x)\right]},$$

and

$$h_V(x) = \frac{v(x)}{1 - V(x)} = \frac{\Theta f(x)A'\left[\Theta(1 - F(x))\right]}{A\left[\Theta(1 - F(x))\right]}.$$

The next result shows a characteristic of the distribution of the maximum of a random number of i.i.d.r.v. with the distribution function $F_{X_i}(x) \equiv F(x),\ x > 0$.

Proposition 2.4. *If* $(X_i)_{i\geq 1}$ *is a sequence of i.i.d.r.v., nonnegative, absolutely continuous type, with the distribution function* $F_{X_i}(x) \equiv F(x),\ x > 0$ *and* $Z \in PSD$ *with* $\mathbb{P}(Z = z) = \frac{a_z\Theta^z}{A(\Theta)}$, $(a_z)_{z\geq 1}$ *a sequence of nonnegative real numbers;* $A(\Theta) = \sum\limits_{z\geq 1} a_z\Theta^z,\ \forall\ \Theta \in (0, \tau)$, *then r.v.* $U = \max\{X_1,\ X_2, \ldots, X_Z\}$ *has the limited distribution* F *if* $\Theta \to 0^+$. *In other words,*

$$\lim_{\Theta\to 0^+} U(x) = [F(x)]^k,\ x > 0$$

where $k = \min\{n \in \mathbb{N}^*,\ a_n > 0\}$.

Proof. By using the power series in (3) and by passing to the limit when $\Theta \to 0^+$, we obtain:

$$\lim_{\Theta\to 0^+} U(x) = \lim_{\Theta\to 0^+} \frac{A\left[\Theta F(x)\right]}{A(\Theta)} = \frac{0}{0}.$$

By applying the l′ Hospital rule k-time, we have:

$$\begin{aligned}\lim_{\Theta\to 0^+} U(x) &= \lim_{\Theta\to 0^+} \frac{A^{(k)}\left[\Theta F(x)\right]\cdot[F(x)]^k}{A^{(k)}(\Theta)} \\ &= \frac{k!a_k[F(x)]^k}{k!a_k} = [F(x)]^k,\ x > 0\end{aligned}$$

and $k = \min\{n \in \mathbb{N}^*,\ a_n > 0\}$. ∎

Similarly, we can formulate a result regarding the distribution of the minimum of a sequence of i.i.d.r.v. in a random number.

Proposition 2.5. *Given the conditions the hypothesis of Proposition 2.4, r.v.* $V = \min\{X_1,\ X_2, \ldots, X_Z\}$ *has the limited distribution* F *if* $\Theta \to 0^+$, *or*

$$\lim_{\Theta \to 0^+} V(x) = 1 - [1 - F(x)]^l,\ x > 0$$

where $l = \min\{n \in \mathbb{N}^*,\ a_n > 0\}$.

The expressions of the r^{th} moments of the two distributions (maximum and minimum) can be derived as follows.

Proposition 2.6. *The* r^{th} *moment,* $r \in \mathbb{N},\ r \geq 1$ *of the r.v.* $U = \max\{X_1,\ X_2, \ldots, X_Z\}$, *where* $Z \in PSD$, *is given by:*

$$\mathbb{E}U^r = \sum_{z \geq 1} \frac{a_z \Theta^z}{A(\Theta)} \mathbb{E}\left[\max\{X_1,\ X_2, \ldots, X_z\}\right]^r. \tag{9}$$

Proof. By using the total probability formula with the help of the conditional mean, we obtain:

$$\begin{aligned} \mathbb{E}U^r &= \mathbb{E}\left(\mathbb{E}U^r | Z = z\right) = \sum_{z \geq 1} \mathbb{E}\left[\max\{X_1,\ X_2, \ldots, X_z\}\right]^r \cdot \mathbb{P}(Z = z) \\ &= \sum_{z \geq 1} \frac{a_z \Theta^z}{A(\Theta)} \cdot \mathbb{E}\left[\max\{X_1,\ X_2, \ldots, X_z\}\right]^r \end{aligned}$$

and this ends the proof. ∎

Similarly, we obtain the s^{th} moment, $s \in \mathbb{N},\ s \geq 1$ of the r.v. V:

$$\mathbb{E}V^s = \sum_{z \geq 1} \frac{a_z \Theta^z}{A(\Theta)} \mathbb{E}\left[\min\{X_1,\ X_2, \ldots, X_z\}\right]^s. \tag{10}$$

Consequence 2.4. *If* $(X_i)_{i \geq 1}$ *is a sequence of i.i.d.r.v., nonnegative, absolutely continuous type, with the distribution function* $F_{X_i}(x) \equiv F(x),\ x > 0$ *and pdf* $f_{X_i}(x) \equiv f(x),\ x > 0$, *then the* r^{th} *and* s^{th} *moments,* $r, s \in \mathbb{N},\ r, s \geq 1$ *of the r.v. U, respectively V are given by (9) and (10) where pdf' s* $f_{\max\{X_1,\ X_2, \ldots, X_z\}}(x) = z f(x) [F(x)]^{z-1}$ *and* $f_{\min\{X_1,\ X_2, \ldots, X_z\}}(x) = z f(x) [1 - F(x)]^{z-1}$.

3. SPECIAL CASES

This section presents examples of the distribution class of the maximum (U) and minimum (V) of a sequence $(X_i)_{i\geq 1}$ of i.i.d.r.v., nonnegative, of the absolutely continuous type. Briefly, let us call them the *Max-Poisson distribution* and the *Min-Poisson distribution*. The special cases are accompanied by expressions of the distribution function, the pdf, the hazard rate, the survival function, the mean and the variance.

3.1. THE MAX-POISSON DISTRIBUTION

In this subsection we present general distributions , which, when using concrete examples, can lead us to the complementary exponential Poisson distribution introduced by Cancho and others [3]. How $Z \sim Poisson^{\star}(\alpha) \in PSD,\ \alpha > 0$, and $A(\Theta) = e^{\Theta} - 1,\ \Theta = \alpha$, then the distribution function of the r.v. $U_{Poisson}$ is:

$$U_{Poisson}(x) = \frac{e^{\Theta F(x)} - 1}{e^{\Theta} - 1},\ x > 0, \tag{11}$$

and the pdf., hazard rate and survival function are given by:

$$u_{Poisson}(x) = \frac{\Theta f(x) e^{\Theta F(x)}}{e^{\Theta} - 1}, \tag{12}$$

$$h_{U_{Poisson}}(x) = \frac{\Theta f(x) e^{\Theta F(x)}}{e^{\Theta} - e^{\Theta F(x)}}$$

and

$$S_{U_{Poisson}}(x) = \frac{e^{\Theta} - e^{\Theta F(x)}}{e^{\Theta} - 1}.$$

The mean and variance of the Max-Poisson distribution are given by:

$$\mathbb{E}\ U_{Poisson} = \frac{1}{e^{\Theta} - 1} \sum_{z\geq 1} a_z \Theta^z \mathbb{E}\left[\max\{X_1,\ X_2, \ldots, X_z\}\right],$$

and

$$\begin{aligned} \mathbb{V}ar\ U_{Poisson} &= \frac{1}{e^{\Theta} - 1}\left[\sum_{z\geq 1} a_z \Theta^z \mathbb{E}\left[\max\{X_1,\ X_2, \ldots, X_z\}\right]^2 - \right. \\ &- \left. \frac{1}{e^{\Theta} - 1}\left(\sum_{z\geq 1} a_z \Theta^z \mathbb{E}\left[\max\{X_1,\ X_2, \ldots, X_z\}\right]\right)^2\right]. \end{aligned}$$

Particular case: if $X_i \sim Exp(\lambda),\ \lambda > 0$, then the relationships (11) and (12) lead to the distribution function introduced by Cancho and others [3]:

$$U_{Exp-Poisson}(x) = \frac{e^{-\alpha e^{-\lambda x}} - e^{-\alpha}}{1 - e^{-\alpha}}$$

and

$$u_{Exp-Poisson}(x) = \frac{\alpha\lambda e^{-\lambda x - \alpha e^{-\lambda x}}}{1 - e^{-\alpha}}.$$

3.2. THE MIN-POISSON DISTRIBUTION

A new general distribution is illustrated in this section given the fact that $V = \min\{X_1,\ X_2, \ldots, X_Z\}$, $Z \sim Poisson^{\star}(\alpha) \in PSD,\ \alpha > 0$, $A(\Theta) = e^{\Theta} - 1,\ \Theta = \alpha$, while $(X_i)_{i\geq 1}$ are i.i.d.r.v. absolutely continuous and nonnegative type.

Taking into account the relations (4) and (8) we obtain the distribution function, the pdf, the hazard rate and the survival function

$$V_{Poisson}(x) = \frac{e^{\Theta} - e^{\Theta(1-F(x))}}{e^{\Theta} - 1}, \tag{13}$$

$$v_{Poisson}(x) = \frac{\Theta f(x) e^{\Theta(1-F(x))}}{e^{\Theta} - 1}, \tag{14}$$

while

$$h_{V_{Poisson}}(x) = \frac{\Theta f(x) e^{\Theta(1-F(x))}}{e^{\Theta} - e^{\Theta(1-F(x))}}$$

and

$$S_{V_{Poisson}}(x) = \frac{e^{\Theta(1-F(x))} - 1}{e^{\Theta} - 1}.$$

The mean and variance of the Min-Poisson distribution are:

$$\mathbb{E}\ V_{Poisson} = \frac{1}{e^{\Theta} - 1} \sum_{z\geq 1} a_z \Theta^z \mathbb{E}\left[\min\{X_1,\ X_2, \ldots, X_z\}\right],$$

while

$$\begin{aligned} \mathbb{V}ar\ V_{Poisson} &= \frac{1}{e^{\Theta} - 1}\left[\sum_{z\geq 1} a_z \Theta^z \mathbb{E}\left[\min\{X_1,\ X_2, \ldots, X_z\}\right]^2 - \right. \\ &- \left. \frac{1}{e^{\Theta} - 1}\left(\sum_{z\geq 1} a_z \Theta^z \mathbb{E}\left[\min\{X_1,\ X_2, \ldots, X_z\}\right]\right)^2\right]. \end{aligned}$$

Particular case: if $X_i \sim Exp(\lambda),\ \lambda > 0$, then through the relationships (13) and (14), the distribution function and the pdf, obtained by Kus [6] are the following:

$$V_{Exp-Poisson}(x) = \frac{1 - e^{-\Theta F(x)}}{1 - e^{-\Theta}} = \frac{1 - e^{-\alpha\left(1-e^{-\lambda x}\right)}}{1 - e^{-\alpha}},$$

and:

$$v_{Exp-Poisson}(x) = \frac{\Theta f(x) e^{-\Theta F(x)}}{1 - e^{-\Theta}} = \frac{\alpha\lambda e^{-\alpha-\lambda x+\alpha e^{-\lambda x}}}{1 - e^{-\alpha}}.$$

4. ON SOME DISTRIBUTIONS IN PROGRESS

We present in tabular form the different distributions that have been discussed and analyzed by some researchers in works [6] and [11], as well as an example of the new Gamma-Poisson distribution for the minimum and the Weibull-Poisson distribution for the maximum. The distribution function and the pdf are determined for each case.

Table 2: Distribution function and pdf of the r.v. $V_{Poisson}$ for different combinations

Authors	**Distribution**		**Distribution function**	**Probability density**
	Z	X_i		
Kus(2007)	$Poisson^{\star}(\alpha)$	$Exp(\lambda)$	$\frac{1-e^{\alpha\left(e^{-\lambda x}-1\right)}}{1-e^{-\alpha}}$	$\frac{\alpha\lambda e^{-\alpha-\lambda x+\alpha e^{-\lambda x}}}{1-e^{-\alpha}}$
Morais and Bareto-Souza (2011)		$Weibull(\lambda, \nu)$	$\frac{e^{\alpha}-e^{\alpha e^{-\left(\frac{x}{\lambda}\right)^{\nu}}}}{e^{\alpha}-1}$	$\frac{\alpha\frac{\nu}{\lambda}\left(\frac{x}{\lambda}\right)^{\nu-1}e^{-\left(\frac{x}{\lambda}\right)^{\nu}}e^{\alpha e^{-\left(\frac{x}{\lambda}\right)^{\nu}}}}{e^{\alpha}-1}$
New		$Gamma(a, b)$	$\frac{e^{\alpha e^{-bx}\sum_{i=0}^{a-1}\frac{(bx)^i}{i!}}}{e^{\alpha}-1}$	$\frac{\alpha b^a x^{a-1} e^{-bx+\alpha e^{-bx}\sum_{i=0}^{a-1}\frac{(bx)^i}{i!}}}{(a-1)!(e^{\alpha}-1)}$

Table 3: Distribution function and pdf of the r.v. $U_{Poisson}$ for different combinations

Authors	**Distribution**		**Distribution function**	**Probability density**
	Z	X_i		
Cancho and al (2011)	$Poisson^{\star}(\alpha)$	$Exp(\lambda)$	$\frac{e^{-\alpha e^{-\lambda x}}-e^{-\alpha}}{1-e^{-\alpha}}$	$\frac{\alpha\lambda e^{-\lambda x-\alpha e^{-\lambda x}}}{1-e^{-\alpha}}$
New		$Weibull(\lambda, \nu)$	$\frac{e^{-\alpha e^{-\left(\frac{x}{\lambda}\right)^{\nu}}}-e^{-\alpha}}{1-e^{-\alpha}}$	$\frac{\alpha\frac{\nu}{\lambda}\left(\frac{x}{\lambda}\right)^{\nu-1}e^{\alpha\frac{\nu}{\lambda}\left(\frac{x}{\lambda}\right)^{\nu-1}e^{-\left(\frac{x}{\lambda}\right)^{\nu}}-\left(\frac{x}{\lambda}\right)^{\nu}}}{e^{\alpha}-1}$

References

[1] K. Adamidis, S. Loukas, *A Lifetime Distribution with Decreasing Failure Rate*, Statistics and Probability Letters, **39**, 1(1998), 35-42.

[2] W. Barreto-Souza, A. L. Morais, G. M. Cordeiro, *The Weibull-geometric distribution*, Journal of Statistical Computation and Simulation , **81**, 5(2011), 645-657.

[3] V. Cancho, F. Louzada, G. Barriga, *The Poisson-Exponential Lifetime Distribution*, Computational Statistics and Data Analysis , **55**, 8(2011), 677-686.

[4] J. Flores, P. Borges, V.G. Cancho, *The complementary exponential power series distribution*, Braz. J. Probab. Stat. **27**, 4(2013), 565-584.

[5] N.L. Johnson, A.W. Kemp, S. Kotz, *Univariate Discrete Distribution*, New Jersey, 2005.

[6] C. Kus, *A New Lifetime Distribution Distributions*, Computational Statistics and Data Analysis , **11**, 9(2007), 4497-4509.

[7] A. Leahu, C.E. Lupu *On the Binomially Mixed Exponential Lifetime Distributions*, Proceedings of the Seventh Workshop on Mathematical Modelling of Environmental and Life Sciences Problems, Bucharest, 2010, 191-196.

[8] E.L. Lehmann, *Testing Statistical Hypotheses* (second edition), New York: Wiley, 1986.

[9] F. Louzada, M. Roman, V. Cancho, *The Complementary Exponential Geometric Distribution: Model, Properties and a Comparison with Its Counterpart*, Computational Statistics and Data Analysis , **55**, 8(2011), 2516-2524.

[10] F. Louzada, M. P.E. Bereta, M. A. P. Franco *On the Distribution of the Minimum or Maximum of a Random Number of i.i.d. Lifetime Random Variables*, Applied Mathematics, **3**, 4(2012), 350-353.

[11] A. L. Morais, W. Barreto-Souza, *A Compound Class of Weibull and Power Series Distributions*, Computational Statistics and Data Analysis , **55**, 3(2011), 1410-1425.

[12] R. Tahmasbi, S. Rezaei, *A Two-Parameter Life-Time Distribution with Decreasing Failure Rate*, Computational Statistics and Data Analysis , **52**, 8(2008), 3889-3901.

ROMAI J., v.9, no.2(2013), 129–141

ON SPECTRAL PROBLEM FOR LAPLACE OPERATOR IN DOMAINS WITH PERTURBED BOUNDARIES

Boris V. Loginov[1], Davran G. Rakhimov[2]
[1] *Ulyanovsk State Technical University, Ulyanovsk, Russia*
[2] *National University of Uzbekistan, Tashkent, Uzbekistan*
loginov@ulstu.ru, Davranaka@yandex.ru

Abstract Boundary eigenvalue problems for Laplace operator are solved by regularized perturbation theory methods in domains with perturbed boundaries.

Keywords: domains with perturbed boundaries; Laplace operator; boundary eigenvalue problems; perturbation and pseudoperturbediteration methods, regularization.
2010 MSC: 47A55, 35B20.

1. INTRODUCTION

Taking its origins within the works of F.Rellich [1], T.Kato [2] and B.Sz-Nagy, the perturbation theory extends and attracts more and more the mathematical community. To the comparatively new subjects of this theory, spectral problems for differential operators in domains with perturbed boundaries are related [3]-[5]. The most powerful approach to solve spectral problems in the perturbation theory of Fredholm operators, based on Newton diagram method of bifurcation theory was developed by V.A.Trenogin [6, 7]. M.K.Gavurin has suggested [8] the pseudoperturbediteration method, developed later by the authors [9]-[11], based on the special perturbation construction such that the known approximations of the eigenvalues, eigenvectors and generalized Jordan chains become exact for the perturbed operator.

In this work, the perturbation and pseudoperturbation methods are applied to spectral problems for Laplace operator in domains with perturbed boundaries.

When applying perturbation processes, at every step, it is required to solve nonhomogeneous equations. For the application of classical results, it is needed to assume that the right-hand sides of these equations also would satisfy the boundary conditions, that significantly restricts the classical Fourier method application possibilities. The relevant particular cases of its application are indicated in n.3 and 4. Such difficulties can be avoided by considering the investigated problems in the space $L_2(\Omega_0)$ or some Sobolev spaces.

To solve the problems investigated in sections 3.2, 4.2 the pseudoperturbation method is applied. Since the multiplicities of sought for eigenvalues are in advance unknown, here the regularization methods suggested in the work [11] are used.

Everywhere below the terminology and notations of the monograph [7] are used.

Acknowledgements - The obtained results are supported for the first author by Federal Program "Sci.&Sci.-Pedagogical Personnel of Innovation Russia" (agreement no.14.B37.21.0373).
- The authors thank to Prof. A. V. Ion for the idea from which the basic results of the article developed.

2. REGULARIZATION IN THE PERTURBATION OF DISCRETE SPECTRUM

Let E_1, E_2 be Banach spaces, $A(\lambda;\varepsilon)$ be a family of operators, depending on spectral parameter λ and on small complex parameter ε and λ_0 be Fredholm point of $A(\lambda;0)$, i.e. $B = A(\lambda_0;0)$ is densely defined operator with relevant zero- and defect-subspaces $N(B) = span\{\varphi_{i0}\}_1^n, N^*(B) = span\{\psi_{i0}\}_1^n, \{\gamma_{i0}\}_1^n \in E_1^*$ and $\{z_{i0}\}_1^n \in E_2$ are biorthogonal systems $\langle\varphi_{i0},\gamma_{j0}\rangle = \delta_{ij}, \langle z_{i0},\psi_{j0}\rangle = \delta_{ij}$.

For $\lambda = \lambda_0 + \mu$ we assume the analytical dependence of $A(\lambda;\varepsilon) - A(\lambda_0;0)$ on μ and ε, that is $A(\lambda;\varepsilon) - A(\lambda_0;0) = \sum\limits_{k+l\geq 1} A_{kl}\mu^k\varepsilon^l$. It is required to find the eigenvalues $\lambda_0+\mu(\varepsilon)$ of the operator $A(\lambda;\varepsilon)$ such that $\mu(\varepsilon)\to 0$, $\varepsilon\to 0$ and the corresponding to them eigenelements. According to F. Rellich theorem [1] the operator $A(\lambda;\varepsilon)$ has exactly n eigenvalues $\lambda_i(\varepsilon)$, taking into account their multiplicities with relevant eigenelements $\varphi_i(\varepsilon)$, $\psi_i(\varepsilon)$, where the multiplicity of $\lambda_i(\varepsilon)$ is beforehand unknown.

Everywhere below the following assumption is assumed to be fulfilled.

Condition 2.1. (degeneration removal). The unperturbed operator and perturbation haven't common zero-elements.

For every $i = \overline{1,n}$ and λ close to λ_0 we introduce the operators

$$\overline{A_i}(\lambda;\varepsilon) \equiv A(\lambda;\varepsilon) + \sum_{j\neq i}\left\langle\cdot,\gamma_{j0}\right\rangle z_{j0}. \tag{1}$$

Theorem 2.1. *For every $i = \overline{1,n}$ and sufficiently small ε there exist constants $c_{is}(\varepsilon)$, $d_{is}(\varepsilon), s\neq i$, such that $\lambda_i(\varepsilon)$ are simple eigenvalues of the operator* (1) *with the relevant eigenelement $\tilde{\varphi}_i(\varepsilon) = \varphi_i(\varepsilon) + \sum\limits_{s\neq i} c_{is}(\varepsilon)\varphi_s(\varepsilon)$ and defect-functional $\tilde{\psi}_i(\varepsilon) = \psi_i(\varepsilon) + \sum\limits_{s\neq i} d_{is}(\varepsilon)\psi_s(\varepsilon)$.*

Proof. From the equality $0 = \overline{A_i}(\lambda_i;\varepsilon)\tilde{\varphi}_i(\varepsilon) =$

$$= A(\lambda_i;\varepsilon)\varphi_i + \sum_{j\neq i} c_{ij}A(\lambda_i;\varepsilon)\varphi_j + \sum_{j\neq i}\left\langle\varphi_i,\gamma_{j0}\right\rangle z_{j0} + \sum_{j\neq i}\sum_{s\neq i} c_{is}\left\langle\varphi_s,\gamma_{j0}\right\rangle z_{j0}$$

we obtain

$$0 = \sum_{j\neq i} c_{ij}A(\lambda_i;\varepsilon)\varphi_j + \sum_{j\neq i}\left\langle\varphi_i,\gamma_{j0}\right\rangle z_{j0} + \sum_{j\neq i}\sum_{s\neq i} c_{is}\left\langle\varphi_s,\gamma_{j0}\right\rangle z_{j0}.$$

After the functionals $\psi_{k0}, k \neq i$ application one has

$$\sum_{s\neq i} c_{is}\left[\langle\varphi_s,\gamma_{k0}\rangle + \langle A(\lambda_i;\varepsilon)\varphi_s,\psi_{k0}\rangle\right] = -\langle\varphi_i,\gamma_{k0}\rangle,\ k\neq i. \tag{2}$$

Here is $A(\lambda_i;\varepsilon)\varphi_s = A(\lambda_i;\varepsilon)\varphi_i + A(\lambda_i;\varepsilon)(\varphi_s-\varphi_i) = A(\lambda_i;\varepsilon)(\varphi_s-\varphi_i)$. Then according to the expansions [1] $\varphi_s(\varepsilon) = \varphi_{s0} + \varepsilon\varphi_{s1} + \varepsilon^2\varphi_{s2} + \cdots$ and $A(\lambda_i;\varepsilon) = A(\lambda_0;0) + O(\varepsilon)$, one can find

$$A(\lambda_i;\varepsilon)(\varphi_s-\varphi_i) = (A(\lambda_0;0)+O(\varepsilon))(\varphi_{s0}-\varphi_{i0}+O(\varepsilon)) = O(\varepsilon).$$

Since $\langle\varphi_i,\gamma_{k0}\rangle = 1 + O(\varepsilon)$, the determinant of the system (2) is nonzero and it has unique solution. The uniqueness of $\tilde{\psi}_i(\varepsilon)$ can be proved analogously. ∎

Let $\tilde{\varphi}_i(\varepsilon)$ be eigenelement of the operator $\overline{A_i}(\lambda_i;\varepsilon)$ corresponding to the eigenvalue $\lambda_i(\varepsilon)$. Then $\overline{A}_i(\lambda_i;\varepsilon)\tilde{\varphi}_i(\varepsilon) = 0$, that can be rewritten in the form

$$A(\lambda_0)\tilde{\varphi}_i(\varepsilon) = \overline{A}(\mu_i(\varepsilon))\tilde{\varphi}_i(\varepsilon) + H_i(\lambda_i(\varepsilon);\varepsilon)\tilde{\varphi}_i(\varepsilon) - \sum_{j\neq i}\left\langle\tilde{\varphi}_i(\varepsilon),\gamma_{j0}\right\rangle z_{j0}, \tag{3}$$

where $\overline{A}(\mu_i(\varepsilon)) = \overline{A}(\mu_i(\varepsilon),0) = [A(\lambda_0;0) - A(\lambda_i(\varepsilon);0) - \sum\limits_{j\neq i}\left\langle\cdot,\gamma_{j0}\right\rangle z_{j0}]$,

$$H_i(\lambda_i(\varepsilon);\varepsilon) = A(\lambda_i(\varepsilon),0) - A(\lambda_i(\varepsilon);\varepsilon).$$

By using the E. Schmidt regularizer $\tilde{A}(\lambda_0)$, $\Gamma = \tilde{A}^{-1}(\lambda_0)$ [7], we change the equation (3) by the equivalent system

$$\begin{cases} \tilde{A}(\lambda_0)\tilde{\varphi}_i(\varepsilon) = \overline{A}(\mu_i(\varepsilon))\tilde{\varphi}_i(\varepsilon) + H_i(\lambda_i(\varepsilon);\varepsilon)\tilde{\varphi}_i(\varepsilon) + \xi_i z_{i0}, \\ \xi_i = \langle\tilde{\varphi}_i(\varepsilon),\gamma_{i0}\rangle. \end{cases} \tag{4}$$

The substitution of the solution

$$\tilde{\varphi}_i(\varepsilon) = \xi_i\left[I - \Gamma\overline{A}(\mu_i(\varepsilon)) - \Gamma H_i(\lambda_i(\varepsilon);\varepsilon)\right]^{-1}\varphi_{i0} \tag{5}$$

of the first equation (4) into the second one gives the branching equation (BEq) separetely for every $\lambda_i(\varepsilon)$:

$$\langle\left[\overline{A}(\mu_i(\varepsilon)) + H_i(\lambda_i(\varepsilon);\varepsilon)\right]\left[I - \Gamma\overline{A}(\mu_i(\varepsilon)) - \Gamma H_i(\lambda_i(\varepsilon);\varepsilon)\right]^{-1}\varphi_{i0},\psi_{i0}\rangle = 0. \tag{6}$$

Since $L_{10} = \langle A_1\varphi_{i0},\psi_{i0}\rangle \neq 0$, $\mu_i(\varepsilon)$ for every $i = \overline{1,n}$ are determined from the equations (6) in the form of the series on integer degrees of ε. Determination of $\mu_i(\varepsilon)$ according to (5) allows to find the relevant eigenelement $\tilde{\varphi}_i(\varepsilon)$ also in the form of series on integer degrees of ε. By this the following statement is proved

Theorem 2.2. *If* $dimN(A(\lambda_0)) = dimN^*(A(\lambda_0)) = n$ *and* $\langle A_1\varphi_{i0},\psi_{i0}\rangle \neq 0$ *for all* $i = \overline{1,n}$, *then for sufficiently small* ε *there exict exactly* n *simple eigenvalues* $\lambda_i(\varepsilon)$ $(\lambda_i(0) = \lambda_0)$ *of the operator* $\overline{A_i}(\lambda,\varepsilon)$ *with corresponding eigenelements* $\tilde{\varphi}_i(\varepsilon)$ *and defect-functionals* $\tilde{\varphi}_i(\varepsilon)$, *which are analytic by* ε.

3. BOUNDARY EIGENVALUE PROBLEM FOR LAPLACE OPERATOR IN PERTURBED RECTANGULAR DOMAIN

In planar membranes oscillation theory the following problem arises

$$A(u,\lambda) \equiv \Delta u + \lambda u = 0 \text{ in } \Omega = \Omega_\varepsilon;\ u = 0 \text{ on } \partial\Omega_\varepsilon, \tag{7}$$

where $\Omega_\varepsilon = \{(x,y)|\, 0 \le x \le \pi,\ -\varepsilon f(x) \le y \le \pi + \varepsilon f(x)\}$, $f(0) = f(\pi) = 0$, and $f(x)$ is 2π- periodic function, continuous together with their derivatives up to second order, ε is a small real parameter, $|\varepsilon| < \frac{\pi}{2M}$, $M = \max\limits_{x\in[0,\pi]} |f(x)|$. Thus Ω_ε is the perturbed square with symmetrically perturbed lower and upper boundaries.

3.1. USUAL PERTURBATION THEORY TECHNIQUES APPLICATION.

For this techniques application introduce the change of variables

$$\xi = x,\ \eta = \eta(x,y) = \frac{\pi(y+\varepsilon f(x))}{\pi + 2\varepsilon f(x)},\ \eta(x,-\varepsilon f(x)) = 0,\ \eta(x,\pi+\varepsilon f(x)) = \pi, \tag{8}$$

which realizes the mapping of the domain Ω_ε on the square with side of the length π. Then taking into account the relations $x = \xi$, $y = \left(1 + \frac{2}{\pi}\varepsilon f(\xi)\right)\eta - \varepsilon f(\xi)$ one has the boundary eigenvalue problem (1),(2) in variables ξ, η

$$\begin{gathered} w''_{\xi\xi} + w''_{\eta\eta}\left[\left(1-\frac{2}{\pi}\eta\right)\frac{\varepsilon^2 f'2(\xi)}{\left(1+\frac{2}{\pi}\varepsilon f(\xi)\right)^2} + \frac{1}{\left(1+\frac{2}{\pi}\varepsilon f(\xi)\right)^2}\right] + \\ +2w''_{\xi\eta} f'(\xi)\left(1-\frac{2}{\pi}\eta\right)\frac{\varepsilon}{\left(1+\frac{2}{\pi}\varepsilon f(\xi)\right)} + \\ +w'_\eta\left(1-\frac{2}{\pi}\eta\right)\left[\varepsilon\frac{f''(\xi)}{1+\frac{2}{\pi}\varepsilon f(\xi)} - \frac{4}{\pi}f'2(\xi)\frac{\varepsilon^2}{\left(1+\frac{2}{\pi}\varepsilon f(\xi)\right)^2}\right] + \lambda w = 0, \\ w = 0 \text{ on } \partial\Omega_0. \end{gathered} \tag{9}$$

Remark 1. If the unknown function w together with its derivatives on η up to second order and mixed second derivative satisfies the boundary conditions then to arised further inhomogeneous equations can be applied Fourier method in the space $C^2(\Omega_0)$.

This gives the following perturbed boundary eigenvalue problem equivalent to the original one (1),(2)

$$A(\mu,\varepsilon)w \equiv A_0 w + \sum_{n=1}^{\infty} \varepsilon^n A_{0n} w + \mu A_{10} w = 0, \tag{10}$$

$$w|_{\partial\Omega_0} = 0,$$

where $\mu = \lambda - \lambda_0$, $\lambda_0 = k_{mn}^2 = m^2 + n^2$ (m, n are integers) are the eigenvalues of unperturbed operator A_0 with relevant eigenfunctions $\varphi_{mn} = \frac{2}{\pi} sinm\xi sinn\eta$ corresponding to the problem (1) in the square domain Ω_0. Simple computations at the usage of power series give

$$A_{01}w = 2f'\left(1 - \frac{2}{\pi}\eta\right)w''_{\xi\eta} - \frac{4f}{\pi}w''_{\eta\eta} + \frac{4f}{\pi}\left(1 - \frac{2}{\pi}\eta\right)f''w'_\eta,$$

$$A_{02}w = -f'\left(1 - \frac{2}{\pi}\eta\right)\frac{4f}{\pi}w''_{\xi\eta} + \left[f'^2\left(1 - \frac{2}{\pi}\eta\right)^2 + 3\left(\frac{2f}{\pi}\right)^2\right]w''_{\eta\eta} +$$

$$+\left(1 - \frac{2}{\pi}\eta\right)\left[f''\left(\frac{2f}{\pi}\right)^2 - \frac{4}{\pi}f'^2\right]w'_\eta,$$

.....

$$A_{0n}w = (-1)^{n-1}2\left(\frac{2f}{\pi}\right)^{n-1}\left(1 - \frac{2}{\pi}\eta\right)f'w''_{\xi\eta} +$$

$$+(-1)^n\left(\frac{2f}{\pi}\right)^{n-2}\left[f'^2\left(1 - \frac{2}{\pi}\eta\right)(n-1) + (n+1)\left(\frac{2f}{\pi}\right)^2\right]w''_{\eta\eta} +$$

$$+(-1)^{n-1}\left(1 - \frac{2}{\pi}\eta\right)\left(\frac{2f}{\pi}\right)^{n-2}\left[-f''\left(\frac{2f}{\pi}\right)^2 + \frac{4}{\pi}(n-1)f'^2\right]w'_\eta,$$

Consider the partial case of two-multiple eigenvalue λ_0, s.t. $m_i^2 + n_i^2 = k^2 = \lambda_0$, $i = 1, 2$. Then the Schmidt regularizator $\Gamma_0 = \tilde{A_0}^{-1}$ for

$$\tilde{A_0}w = \Delta w + \lambda_0 w + \sum_{j=1}^{2}\langle w, \varphi_{j0}\rangle\varphi_{j0}$$

is presented by the integral operator $w = \Gamma_0 h = \int\limits_0^\pi\int\limits_0^\pi K(t; s; \xi; \eta)h(t; s)dtds$, where $K(t, s, \xi, \eta) = \sum\limits_{m=1}^{\infty}\sum\limits_{n=1}^{\infty}\omega_{mn}\sin mt\sin ns\sin m\xi\sin n\eta$, $\omega_{m_in_i} = \frac{\pi^2}{4}$, $\omega_{mn} = \frac{\pi^2}{4}\cdot\frac{1}{\lambda_0 - m^2 - n^2}$. Obviously that $\Gamma\varphi_{i0} = \varphi_{i0}$, for $i = \overline{1, 2}$.

Applying to the equation (10) the Schmidt regularization write it as the system:

$$\tilde{A_0}w + \mu A_{10} + \sum_{n=1}^{\infty}\varepsilon^n A_{0n}w = \sum_{i=1}^{2}\xi_i\varphi_{i0},\ \ \xi_k = \langle w, \varphi_{k0}\rangle.$$

Determination of $w = \sum\limits_{i=1}^{2} \xi_i \left[I + \mu\Gamma A_{10} + \sum\limits_{n=1}^{\infty} \varepsilon^n A_{0n} \right]^{-1} \varphi_{i0}$ from the first equation with subsequent its substitution in the second one gives the branching equation (BEq):

$$L(\mu;\varepsilon) \equiv \sum_{k+s\geq 2} L_{ks}\mu^k\varepsilon^s = 0 \tag{11}$$

where $L_{20} = det\|\langle A_{10}\varphi_{i0}, \varphi_{j0}\rangle\| = 1, A_{10} = I$. Then Newton diagram method leads to the following result

Theorem 3.1. *If the function* $f(\xi)$ *is such that* $L_{oj} = 0$ *for* $j = \overline{2, q-1}$ *and* $L_{0q} \neq 0$, *then* $\mu_i(\varepsilon), \varphi_i(\varepsilon), i = 1, 2$, *are represented by the convergent series on the degrees of* ε^q. *In particular when* $L_{02} = det\|\langle A_{01}\varphi_{i0}, \varphi_{j0}\rangle\| \neq 0$, $q = 2$ *and* $\mu_i(\varepsilon), \varphi_i(\varepsilon)$ *are analytic functions of small parameter* ε.

Example 3.1. *Let* $f(x) = \frac{1}{4} sinx$, *and* $\lambda_0 = 5$.

Here $\varphi_{10} = \frac{2}{\pi}\sin 2\xi \cdot \sin\eta, \varphi_{20} = \frac{2}{\pi}\sin\xi \cdot \sin 2\eta$ and BEq (11) coefficients are the following:

$$L_{20} = 1,\ L_{11} = \left(\frac{2}{\pi}\right)^2 \cdot \frac{281}{48} \approx 2,375,\ L_{02} = \frac{1105}{96\pi^2} \approx 0,474.$$

Branching equation (11) has the following solutions $\mu_\sigma = \lambda_2^{(\sigma)} \cdot \varepsilon^2 + o(\varepsilon^2), \sigma = 1, 2$, where $\lambda_2^{(\sigma)}$ are the roots of the equation $L_{02} + L_{11}\lambda_2 + L_{20}\lambda_2^2 = 0$, i.ĂĽ. $\lambda_2^{(1)} = -0,695,\ \lambda_2^{(1)} = -1,68$. Consequently,

$$\mu_1 = -0,695 \cdot \varepsilon^2 + o(\varepsilon^2),\ \mu_2 = -1,68 \cdot \varepsilon^2 + o(\varepsilon^2).$$

3.2. PSEUDOPERTURBITERATION METHOD APPLICATION.

Here it is more conveniently to represent the problem (9), i.e. the problem (7), after the change of variables, without small parameter ε, considering $f(x)$ as the small magnitude

$$A(\lambda)w = w''_{\xi\xi} + w''_{\eta\eta}\left[\frac{1}{\left(1+\frac{2}{\pi}f(\xi)\right)^2} + \frac{f'^2(\xi)\left(1-\frac{2}{\pi}\eta\right)^2}{\left(1+\frac{2}{\pi}f(\xi)\right)^2}\right] + 2w''_{\xi\eta}\cdot\frac{f'(\xi)\left(1-\frac{2}{\pi}\eta\right)}{1+\frac{2}{\pi}f(\xi)} +$$

$$+w'_\eta\left(1-\frac{2}{\pi}\eta\right)\left[\frac{f''(\xi)}{1+\frac{2}{\pi}f(\xi)} - \frac{4}{\pi}\cdot\frac{f'^2(\xi)}{\left(1+\frac{2}{\pi}f(\xi)\right)^2}\right] + \lambda w = 0 \tag{12}$$

$$w(0,\eta) = 0,\ w(\pi,\eta) = 0,\ w(\xi,0) = 0,\ w(\xi,\pi) = 0.$$

In a neighborhood of the eigenvalue $\lambda_0 = m_i^2 + n_i^2$ of the unperturbed problem (12) there are two eigenvalues $\lambda^{(1)}$ and $\lambda^{(2)}$, to the finding of which further the pseudoperturbation method is applied.

Approximate eigenvalue λ_0 to the following perturbed boundary eigen-value problem is λ_0 with relevant eigenvectors $\varphi_{10}, \varphi_{20}$. Choosing them as initial approximations, compute the discrepancies $\sigma_{i0}, \tau_{i0}, i = 1, 2$, $\sigma_{i0} = A(\lambda_0)\varphi_{i0}$, $\tau_{i0} = A^*(\lambda_0)\psi_{i0}$ (here $\psi_{i0} = \varphi_{i0}$, $\gamma_{i0} = z_{i0} = \varphi_{i0}$). It is required to construct the conjugate operator $A^*(\lambda_0)$ applying standard methods [12]. Conjugate equation has the form

$$A^*(\lambda)v = v''_{\xi\xi} + v''_{\eta\eta}\left[\frac{1}{\left(1+\frac{2}{\pi}f(\xi)\right)^2} + \frac{f'^2(\xi)\left(1-\frac{2}{\pi}\eta\right)^2}{\left(1+\frac{2}{\pi}f(\xi)\right)^2}\right] + 2v''_{\xi\eta}\cdot\frac{f'(\xi)\left(1-\frac{2}{\pi}\eta\right)}{1+\frac{2}{\pi}f(\xi)} -$$

$$-\frac{4}{\pi}\cdot\frac{f'(\xi)}{1+\frac{2}{\pi}f(\xi)}v'_\xi + v'_\eta\cdot\frac{\left(1-\frac{2}{\pi}\eta\right)^2}{\left(1+\frac{2}{\pi}f(\xi)\right)^2}\left[-\frac{8}{\pi}f'^2 + f''\left(1+\frac{2}{\pi}f(\xi)\right)\right] +$$

$$+v\cdot\left[-\frac{2}{\pi}\frac{f''(\xi)}{1+\frac{2}{\pi}f(\xi)} + \frac{8}{\pi^2}\frac{f'^2}{\left(1+\frac{2}{\pi}f(\xi)\right)^2}\right] + \lambda v = 0$$

The regularization is made

$$\overline{A}_i(\lambda) = A(\lambda) + \sum_{j\neq i}\langle\cdot, \varphi_{j0}\rangle\varphi_{j0},\ i = 1, 2.$$

$$\overline{A^*}_i(\lambda) = A^*(\lambda) + \sum_{j\neq i}\langle\varphi_{j0}, \cdot\rangle\varphi_{j0},\ i = 1, 2.$$

Computing the discrepancies $\sigma_{i0} = \overline{A}_i(\lambda_0)\varphi_{i0}, \tau_{i0} = \overline{A^*}_i(\lambda_0)\varphi_{i0}$ introduce the pseudoperturbation operator $D_{i0}w = \langle w, \gamma_{i0}\rangle\sigma_{i0} + \langle w, \tau_{i0}\rangle z_{i0}$ posessing by the properties $D_{i0}\varphi_{i0} = \sigma_{i0}$, $D^*_{i0}\psi_{i0} = \tau_{i0}$, $i = \overline{1,2}$. Then $N(\overline{A}_i(\lambda_0) - D_{i0}) = \{\varphi_{i0}\}, N(\overline{A^*}_i(\lambda_0) - D^*_{i0}) = \{\varphi_{i0}\}$.

According to theorem 2.1 there are two simple eigenvalues $\lambda^{(1)}$ and $\lambda^{(2)}$ of the operators $\overline{A}_i(\lambda), i = 1, 2$, correspondingly.

Writing the regularized problem in the form

$$\overline{A}_i(\lambda)w \equiv \left(\overline{A}_i(\lambda_0) - D_{i0} + \langle\cdot, \varphi_{i0}\rangle\varphi_{i0}\right)w + (\lambda - \lambda_0)A_{10}w + D_{i0}w = \xi\varphi_{i0},$$

and applying to them Schimdt's regularization, obtain nonlinear algebraic equations, as simple roots of which are $\lambda^{(1)}$ and $\lambda^{(2)}$:

$$F_i(t) \equiv \left\langle\{I - [I - \Gamma_{i0}((t-\lambda_0)A_{10} + D_{i0})]^{-1}\}\varphi_{i0}, \gamma_{i0}\right\rangle = 0,\ i = 1, 2, \qquad (13)$$

where $\Gamma_{i0} = \Gamma_0 = \left[A(\lambda_0) - D_{i0} + \sum\limits_{i=1}^{2}\langle\cdot, \gamma_{i0}\rangle z_{i0}\right]^{-1}$ [7].

Our further actions more detaily are described in sec. 4.2.

For the determination $\lambda^{(1)}$ and $\lambda^{(2)}$ the modified Newton-Kantorovich method is applied $\lambda_{\nu+1}^{(i)} = \lambda_\nu^{(i)} - \left[F_i'(\lambda_0\right]^{-1} F_i(\lambda_\nu^{(i)})$, $\nu = 1, 2, \ldots$. Since $F_i(\lambda_\nu^{(i)}) = \langle X_i^{(\nu)}, \varphi_{i0}\rangle - 1$, where $X_i^{(\nu)} = \left[I - (\lambda_\nu^{(i)} - \lambda_0)\Gamma_0 A_{10} + \Gamma_0 D_0\right]^{-1}\varphi_{i0}$, then for the iteration process realization it is needed to solve on every step one equation of the form

$$\Delta X_i^{(\nu)} + \lambda_\nu X_i^{(\nu)} + \sum_{j=1}^{2}\langle X_i^{(\nu)}, \gamma_{i0}\rangle z_{i0} = g(X_i^{(\nu)}, \xi, \eta),\ i = 1, 2. \tag{14}$$

For the solving of the equation (14) the successive approximations method is applied

$$\Delta X_{in}^{(\nu)} + \lambda_\nu X_{in}^{(\nu)} + \sum_{j=1}^{2}\langle X_{in}^{(\nu)}, \gamma_{j0}\rangle z_{j0} = g(X_{i,n-1}^{(\nu)}, \xi, \eta),\ i = 1, 2, \tag{15}$$

setting $X_{i0}^{(\nu)} = \varphi_{i0}$. The solution to (15) is sought in the form $X_{i,n}^{(\nu)} = \sum\limits_{k=1}^{\infty}\sum\limits_{l=1}^{\infty} B_{inkl}^{(\nu)} sink\xi sinl\eta$. Note that on the first step for the computation of the magnitude $F_i'(\lambda_0)$, it is needed to solve one more equation

$$\Delta Y_i^{(0)} + \lambda_0 Y_i^{(0)} + \sum_{j=1}^{2}\langle Y_i^{(0)}, \gamma_{i0}\rangle z_{i0} = A_{10} X_i^{(0)} + g(Y_i^{(0)}, \xi, \eta),\ i = 1, 2.$$

4. BOUNDARY EIGENVALUE PROBLEM FOR LAPLACE OPERATOR IN THE ELLIPSE DOMAIN

4.1. SOLVING OF A PROBLEM BY METHODS OF THE PERTURBATION THEORY

Now consider the problem (7) for the ellipse domain $\Omega = \left\{(x, y)|\frac{x^2}{a^2} + \frac{y^2}{b^2} \le 1\right\}$, after the following linear transform $\xi = \frac{b}{a}x$, $\eta = y$ application Ω is transformed in the circle $D = \left\{(\xi, \eta)|\frac{\xi^2}{b^2} + \frac{\eta^2}{b^2} \le 1\right\}$ and the equation (7) takes the form

$$\frac{b^2}{a^2}\cdot\frac{\partial^2 v}{\partial\xi^2} + \frac{\partial^2 v}{\partial\eta^2} + \lambda v = 0,\ v|_{\partial D} = 0. \tag{16}$$

Let the ellipse eccentricity will be small $\varepsilon = \sqrt{1 - \frac{b^2}{a^2}}$. Then the following perturbed eigenvalue problem arises

$$\left(A_0 - \varepsilon^2 B + \lambda I\right) v \equiv \Delta v - \varepsilon^2 \frac{\partial^2 v}{\partial \xi^2} + \lambda v = 0, \ v|_{\partial D} = 0. \tag{17}$$

or in polar coordinates

$$A(\rho,\theta)w + \lambda w = \varepsilon^2 B(\rho,\theta)w, \ w(b,\theta) = 0, \tag{18}$$

where $B(\rho,\theta)w = \cos^2\theta \cdot \dfrac{\partial^2 w}{\partial \rho^2} - \dfrac{\sin 2\theta}{\rho}\dfrac{\partial^2 w}{\partial \rho \partial \theta} + \dfrac{\sin^2\theta}{\rho^2}\dfrac{\partial^2 w}{\partial \theta^2} + \dfrac{\sin 2\theta}{\rho}\cdot\dfrac{\partial w}{\partial \theta} + \dfrac{\sin^2\theta}{\rho}\dfrac{\partial w}{\partial \rho}$,
$A(\rho,\theta)w = \dfrac{1}{\rho}\cdot\dfrac{\partial}{\partial \rho}\left(\rho\dfrac{\partial w}{\partial \rho}\right) + \dfrac{1}{\rho^2}\cdot\dfrac{\partial^2 w}{\partial \theta^2}$.

The eigenvalues of the operator $A(\rho,\theta)$ for the circle are $\lambda_{mn} = \left(\frac{\mu_m^{(n)}}{b}\right)^2$ with relevant eigenelements $\varphi_{1mn}(\rho,\theta) = J_n\left(\frac{\mu_m^{(n)}}{b}\rho\right) cosn\theta$,
$\varphi_{2mn}(\rho,\theta) = J_n\left(\frac{\mu_m^{(n)}}{b}\rho\right) sinn\theta$, where $\mu_m^{(n)}$ - is the m-th root of the Bessel function $J_n(\mu)$. Since the unperturbed problem (4) is selfadjoint, then $\varphi_{jmn}(\rho,\theta) = \psi_{jmn}(\rho,\theta)$, $z_{jmn} = \gamma_{jmn} = \frac{2}{b^2\varepsilon_n\pi\left[J_n'(\mu^{(n)})\right]^2}\varphi_{jmn}$, $\varepsilon_n = \begin{cases} 2, \ n = 0, \\ 1, \ n \neq 0. \end{cases}$

Let $\lambda_0 = \left(\frac{\mu_{m_0}^{(n_0)}}{b}\right)^2$ be some its 2-multiple eigenvalue with the relevant eigenelements $\varphi_{1m_0n_0}(\rho,\theta) = J_{n_0}\left(\frac{\mu_{m_0}^{(n_0)}}{b}\rho\right)\cos n_0\theta$, $\varphi_{2m_0n_0}(\rho,\theta) = J_{n_0}\left(\frac{\mu_{m_0}^{(n_0)}}{b}\rho\right)\sin n_0\theta$.

The inverse operator to $\tilde{A_0}(\rho,\theta)w = A_0(\rho,\theta)w + \sum\limits_{s=1}^{2}\langle w, \varphi_{sm_0n_0}\rangle\varphi_{sm_0n_0}$, where $A_0(\rho,\theta)w = \Delta w + \lambda_0 w$ is the integral operator

$$w = \Gamma h = \int\limits_0^{2\pi}\int\limits_0^{b} K(\rho,\theta,r,\varphi)h(r,\varphi)rdrd\varphi.$$

Here $K(\rho,\theta,r,\varphi) = \sum\limits_{n=0}^{\infty}\sum\limits_{m=1}^{\infty}\omega_{mn}J_n\left(\frac{\mu_m^{(n)}}{b}\rho\right)J_n\left(\frac{\mu_m^{(n)}}{b}r\right)\cos n(\theta-\varphi)$ and

$$\omega_{mn} = \frac{2}{(\lambda_{m_0n_0} - \lambda_{mn})\pi b^2\left[J_n'(\mu_m^{(n)})\right]^2}, \ \omega_{m_0n_0} = \frac{2}{\pi b^2\left[J_n'(\mu_m^{(n)})\right]^2}.$$

The BEq for two-multiple λ_0 takes the form:

$$\sum_{k+l\geq 2} L_{kl}\mu^k\varepsilon^l \equiv$$

$$\equiv det \left\| \left\langle \left[I + \mu\Gamma - \varepsilon^2 \Gamma B(\rho,\theta) \right]^{-1} \varphi_{im_0n_0}, \varphi_{jm_0n_0} \right\rangle - \delta_{ij} \right\| = 0 \tag{19}$$

where

$$L_{20} = \left[b^2 \cdot \varepsilon_n \cdot \frac{\pi^2}{2} \cdot \left[J'_{n_0}(\mu_{m_0}^{(n_0)}) \right]^2 \right]^2,$$

$$L_{12} = b^2 \cdot \varepsilon_n \cdot \frac{\pi^2}{2} \cdot \left[J'_{n_0}(\mu_{m_0}^{(n_0)}) \right]^2 \cdot \left[\left(\frac{\mu_{m_0}^{(n_0)}}{b} \right)^2 \cdot a_1 - n_0^2 \cdot a_2 + \frac{\mu_{m_0}^{(n_0)}}{b} \cdot a_3 \right],$$

$$L_{04} = \frac{\pi^2}{4} \left(\frac{\mu_{m_0}^{(n_0)}}{b} \right)^4 \cdot a_1^2 + \frac{\pi^2}{4} \cdot \left(-n_0^2 \cdot a_2 + \frac{\mu_{m_0}^{(n_0)}}{b} \cdot a_3 \right) \left(n_0^2 \cdot a_2 + \frac{\mu_{m_0}^{(n_0)}}{b} \cdot a_1 \right).$$

$$a_1 = \int_0^b J_{n_0} \left(\tfrac{\mu_{m_0}^{(n_0)}}{b} \rho \right) J''_{n_0} \left(\tfrac{\mu_{m_0}^{(n_0)}}{b} \rho \right) \rho d\rho =$$

$$= -\tfrac{b^2}{2} \cdot \left[J'_{n_0} \left(\mu_{m_0}^{(n_0)} \right) \right]^2 + \tfrac{n_0 b^2}{\left(\mu_{m_0}^{(n_0)} \right)^2} \cdot \left[1 - J_0^2 \left(\mu_{m_0}^{(n_0)} \right) - \sum_{k=1}^{n_0-1} J_k^2 \left(\mu_{m_0}^{(n_0)} \right) \right],$$

$$a_2 = \int_0^b \tfrac{1}{\rho} \left[J_{n_0} \left(\tfrac{\mu_{m_0}^{(n_0)}}{b} \rho \right) \right]^2 d\rho = \tfrac{b}{2n_0 \mu_{m_0}^{(n_0)}} \cdot \left[1 - J_0^2 \left(\mu_{m_0}^{(n_0)} \right) - \sum_{k=1}^{n_0-1} J_k^2 \left(\mu_{m_0}^{(n_0)} \right) \right],$$

$$a_3 = \int_0^b \left[J_{n_0} \left(\tfrac{\mu_{m_0}^{(n_0)}}{b} \rho \right) \right]^2 d\rho = (-1)^{n_0} \cdot \mu_{m_0}^{(n_0)} \cdot b \cdot J_0^2 \left(\mu_{m_0}^{(n_0)} \right).$$

According to Newton diagram method this branching equation has the solutions of the form $\mu^{(\sigma)} = \lambda_2^{(\sigma)} \varepsilon^2 + o(\varepsilon^2)$, where $\lambda_2^{(\sigma)}$ are the roots of quadratic equation $L_{04} + L_{12}\lambda_2 + L_{20}\lambda_2^2 = 0$, i.e.

$$\lambda_2^{(\sigma)} = \left(-L_{12} \pm \sqrt{L_{12}^2 - 4L_{04}L_{20}} \right) \cdot \frac{1}{2L_{20}}.$$

Since $\Delta = L_{12}^2 - 4L_{04}L_{20} \neq 0$, then the BEq (19) has two small solutions

$$\mu^{(\sigma)} = \lambda_2^{(\sigma)} \varepsilon^2 + \sum_{i=1}^{\infty} a_{\sigma i} \varepsilon^{2+i}, \ \sigma = 1, 2.$$

4.2. APPROXIMATE SOLVING OF PROBLEM BY PSEUDOPERTURBATION METHOD

The considered problem is selfadjoint, therefore

$$\varphi_{i0} = \psi_{i0}, \ z_{i0} = \gamma_{i0} = \frac{2}{b^2 \pi \varepsilon_n \left[J'_{n_0}(\mu_{m_0}^{(n_0)}) \right]^2} \varphi_{i0}, i = 1, 2, \ \varepsilon_n = \begin{cases} 2, \ n = 0, \\ 1, \ n \neq 0. \end{cases}$$

According to theorem 2.2 the eigenvalue problem (18) has two eigenvalues which are simple for the regularized operator $\tilde{A}_i(\lambda) = A(\lambda) + \sum\limits_{j\neq i}\langle\cdot, \varphi_{j0}\rangle\varphi_{j0}$, $i = 1, 2$, where $A(\lambda)w = A(\rho, \theta)w - \frac{a^2-b^2}{a^2}B(\rho, \theta)w + \lambda w$. Computing the discrepancies $\tau_{i0} = \sigma_{i0} = A(\lambda_0)\varphi_{i0}$, $i = 1, 2$, construct the pseudoperturbation operators in the form $D_{i0}w = \langle w, \gamma_{i0}\rangle\sigma_{i0} + \langle w, \sigma_{i0}\rangle z_{i0}$. Then the sought for eigenvalues $\lambda^{(i)}$ turn out to be simple of the equation

$$F_i(t) \equiv \left\langle \{I - [I - \Gamma_{i0}((t - \lambda_0)A_{10} + D_{i0})]^{-1}\}\varphi_{i0}, \gamma_{i0}\right\rangle = 0,\ i = 1, 2, \tag{20}$$

At the application Newton-Kantorovich method to the equation (20) on every step of the iteration it is needed to solve the equation

$$\Delta X_i^{(\nu)} + \lambda_\nu \cdot X_i^{(\nu)} + \sum_{k=1}^{2}\langle X_i^{(\nu)}, \varphi_{k0}\rangle z_{k0} = z_{i0} + B(\rho, \theta)X_i^{(\nu)},\ i = 1, 2. \tag{21}$$

For the solving of (21) the successive approximations method is applied

$$\Delta X_{in}^{(\nu)} + \lambda_\nu X_{in}^{(\nu)} + \sum_{j=1}^{2}\langle X_i^{(\nu)}, \gamma_{i0}\rangle z_{i0} = z_{i0} + B(\rho, \theta)X_{i,n-1}^{(\nu)},\ i = 1, 2, \tag{22}$$

setting $X_{i0}^{(\nu)} = \varphi_{i0}$, the solution of which is sought for the form

$$X_{i,n}^{(\nu)} = \sum_{m=1}^{\infty}\sum_{l=0}^{\infty}\left[B_{inml}^{(\nu)}J_l\left(\frac{\mu_m^{(l)}}{b}\rho\right)\cos l\theta + C_{inml}^{(\nu)}J_l\left(\frac{\mu_m^{(l)}}{b}\rho\right)\sin l\theta\right].$$

On the first step for the computation of $F_i'(\lambda_0)$, it is needed to solve two more equations

$$\Delta Y_i^{(0)} + \lambda_0 Y_i^{(0)} + \sum_{j=1}^{2}\langle Y_i^{(0)}, \gamma_{i0}\rangle z_{i0} = X_i^{(0)} + B(\rho, \theta)Y_i^{(0)},\ i = 1, 2.$$

For the proof of the convergence of soccessive approximations method consider the differences

$$X_{i,s+1}^{(\nu)} - X_{i,s}^{(\nu)} =$$

$$= \sum_{m,l} J_l\left(\frac{\mu_m^{(l)}}{b}\rho\right)\left[(B_{i,s+1,ml} - B_{isml})^2\cos l\theta + (C_{i,s+1,ml} - C_{isml})^2\, sinl\theta\right],$$

for which by virtue at Parseval-Steklov equality the relation

$$\left\|X_{i,s+1}^{(\nu)} - X_{i,s}^{(\nu)}\right\|^2 =$$

$$= \sum_{m,l} \left[(B_{i,s+1,ml} - B_{isml})^2 + (C_{i,s+1,ml} - C_{isml})^2 \right] \cdot \left[b^2 \pi \varepsilon_n \left[J'_{n_0}(\mu_{m_0}^{(n_0)}) \right]^2 \right]^2 \qquad (23)$$

is true. Since

$$B_{i,s+1,ml} - B_{isml} =$$

$$= \frac{1}{(\lambda_0 - \lambda_{ml})\|\varphi_{1m_0n_0}\|} \int_0^{2\pi} \int_0^b B(r,\varphi) \left(X_{i,s}^{(\nu)} - X_{i,s-1}^{(\nu)} \right) J_l \left(\frac{\mu_m^{(l)}}{b} \rho \right) \cos l\varphi r dr d\varphi,$$

$$C_{i,s+1,ml} - C_{isml} =$$

$$= \frac{1}{(\lambda_0 - \lambda_{ml})\|\varphi_{2m_0n_0}\|} \int_0^{2\pi} \int_0^b B(r,\varphi) \left(X_{i,s}^{(\nu)} - X_{i,s-1}^{(\nu)} \right) J_l \left(\frac{\mu_m^{(l)}}{b} \rho \right) \sin l\varphi r dr d\varphi,$$

then according to absolute convergence of the series (23) there exist the numbers $M_{is} < 1$ such that

$$\left\| X_{i,s+1}^{(\nu)} - X_{i,s}^{(\nu)} \right\| \le M_{is} \left\| X_{i,s}^{(\nu)} - X_{i,s-1}^{(\nu)} \right\|.$$

The introduction of the designations $N = \max\limits_{i,m,l} \{\|\varphi_{iml}\|\}$, $K^2 = \sum\limits_{m,l} \frac{1}{|\lambda_0 - \lambda_{ml}|^2}$, gives

$$|B_{i,s+1,m,l} - B_{isml}| \le \frac{1}{|\lambda_0 - \lambda_{ml}| \cdot \|\varphi_{1m_0n_0}\|} \cdot M \cdot \|\varphi_{1mn}\| \cdot \left\| X_{i,s}^{(\nu)} - X_{i,s-1}^{(\nu)} \right\|$$

and

$$|C_{i,s+1,m,l} - C_{isml}| \le \frac{1}{|\lambda_0 - \lambda_{ml}| \cdot \|\varphi_{2m_0n_0}\|} \cdot M \cdot \|\varphi_{2mn}\| \cdot \left\| X_{i,s}^{(\nu)} - X_{i,s-1}^{(\nu)} \right\|.$$

Then $M_{is} = MNK$ and if to suppose $MNK < 1$, the operator wuold be contractive, i.e. the iterations are convergent.

Remark. Note that the last proof takes place when the problem is investigated in Sobolev's space W_2^2.

References

[1] F. Rellich, *Stőrungstheory der Spektalzerlegung.* I, Math. Ann., **113**, (1936), 600–619.

[2] T. Kato, *Perturbation theory for linear operators*, Springer-Verlag Berlin · Heidelberg · New York, 1966.

[3] O. P. Bruno, F. Reitich, *Boundary-Variation Solution of Eigenvalue Problems for elliptic operators.* The Journal of Fourier Analysis and Applications, **7**, 2(2001), 169-187.

[4] B. Simon, *Fifty years of eigenvalue perturbation theory.* Bulletin of the American Mathematical Society, 24(1991), 303-319.

[5] M. R. Dostanic, *The properties of the Cauchy transform on a bounded domain.* J. Operator Theory, 36(1996), 233-247.

[6] V. A. Trenogin, *Perturbation of eigenvalues and eigenelements of linear operators.* USSR Acad. Sci. Doklady. Mathematics,**167**, 3(1966),519–522.

[7] M. M. Vainberg, V. A. Trenogin, *Branching Theory of Solutions to Nonlinear Equations.* Nauka, Moscow, 1969, Engl. Transl. Wolters-Noordorf Int. Publ., Leyden, 1974.

[8] M.K. Gavurin, *On pseudoperturbation method for eigenvalues determination.* J. Comput. Math. Math. Phys., **1**, 5(1961), 751-770, Russian.

[9] B. V. Loginov, O. V. Makeeva, *Pseudoperturbed iteration method in generalized eigenvalue problems.* ROMAI Journal, **1**, 1(2008), 149-168.

[10] B. V. Loginov, O. V. Makeeva, *The pseudoperturbation method in generalized eigenvalue problems.* Doklady Mathematics, 2009, **77**, 2(2009), 194-197.

[11] D.G. Rakhimov, *On computation of multiple Fredholm points of discrete spectra of the linear operator-functions by pseudoperturbation methods.* Trudy Srednevolzskogo Matematicheskogo Obshchestva, 2010, **12**, 3(2010), 106-112, Russian.

[12] M. A. Naimark, *Ordinary differential operators.* Nauka, Moscow, 1969, (Russian).

ROMAI J., v.9, no.2(2013), 143–154

AN OPTIMAL DESIGN OF THE WIND TURBINE BLADE GEOMETRY ADAPTED TO A SPECIFIC SITE USING ALGERIAN WIND DATA

Zine Labidine Mahri, Said Zid, Rouabah Mohamed Salah
University Constantine1, Constantine, Algeria
zlmahri@hotmail.com

Abstract The aerodynamic modeling of the wind turbine blades constitutes one of the most important processes in the design of the turbine. The aim of this modeling is to calculate the aerodynamic loads, to determine the optimal parameters of the blades and estimate the wind extracted power. The design of the blade geometry must provide the optimal shape of the rotor blade capable to produces the maximum extracted power. This design must be done for a specific aerodynamic profile and a specific site, since this modeling must be based on statistical analysis of meteorological data of this given site.
In this work aerodynamic loads for small wind turbine blades are calculated as well as the total power extracted by the turbine. This design has a great impact on the turbine efficiency and consequently on its economical feasibility.

Keywords: Wind Energy, Aerodynamics, Numerical Methods, fluid mechanics.
2010 MSC:97U99.

1. INTRODUCTION

Small wind turbine technology can be a meaningful contributor to long-term economic growth by assuring independence in energy supplies and providing benefits to local economy. Moreover wind is a clean non-polluting energy source and the electricity generated by this mean is becoming economically efficient compared to other sources. The aerodynamic modeling of the wind turbine blades constitutes one of the most important processes in the design of the turbine. The rotor blades are the most important part of this turbine because of their aerodynamic shape and profiles that play the main role in extracting the wind energy.
The aerodynamic modeling is used in order to estimate the aerodynamic loads and the wind extracted power. This modeling must be done for a given wind speed and a given rotor blades. The design of the blade geometry must provide the optimal shape of the rotor blade capable to produce the maximum extracted power. In order to determine the optimal shape of the blades, one must compute the optimal parameters of the blade geometry such as the chord length distribution, the thickness and the twist angle distribution along the blade span.
In the aerodynamic modeling two aerodynamic theories are used, the first one is the axial momentum theory and the second is the blade element theory [1]. In the first

theory, the flow is considered to be completely axial, while in the second theory the effect of wake rotation is included, assuming that the flow downstream rotates.
The momentum theory that employs simply the mass and momentum conservation principles cannot provide alone the necessary information for the rotor design. However, the blade element theory that uses the angular momentum conservation principal, gives complementary information about the blade geometry such as airfoil shape and twist distribution. When both theories are combined the aerodynamic loads and the produced power can be obtained.
In order to compute the optimal parameters of the blade geometry that give the maximum power, an iterative algorithm is used until the maximum value of extracted power is reached. This design must be done for a specific aerodynamic profile and a specific site, since we must use the characteristic wind speed that gives the maximum available power in a given site. This characteristic wind speed is determined by statistical modeling of meteorological data. The design can be repeated for different sites and profiles.
The estimation of aerodynamic loads can be useful as well in strength calculation of the blades in order to predict the structural problems such as fatigue failure, which is the major cause of wind turbine breakdown.
This design has a great impact on the turbine efficiency and consequently on its economical feasibility.

2. AERODYNAMIC MODELING

In this aerodynamic modeling two aerodynamic theories are used.

2.1. AERODYNAMIC MODELING

In this simple one-dimensional model, airflow is assumed to be incompressible, completely axial and rotationally symmetric [2]. This model applies the principles of mass and momentum conservation on the annular control volumes surrounding the flow as shown in figure 1. In this figure, the symbol Ai represents the section area at the station i, and the symbol A is the section area at the rotor plane, while V represents the wind speed.

The thrust force T at the rotor disc can be found, by applying the conservation of linear momentum to the control volume in the axial direction:

$$T = \dot{m}(V_0 - V_1) = \rho A V(V_0 - V_1) \tag{1}$$

where ρ is the density of the air.
Bernoulli's equation can be applied to obtain the thrust as:

$$(p - p')A = T = \frac{1}{2}\mathrm{A}\rho(V_0^2 - V_1^2) \tag{2}$$

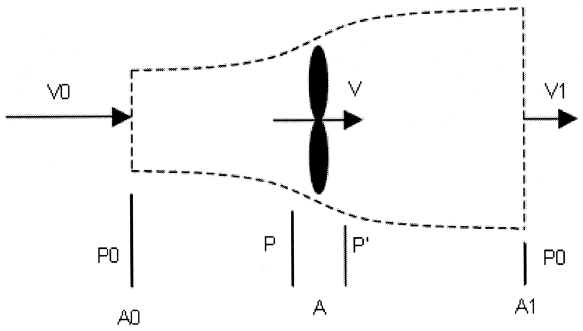

Fig. 1.: Annular control volume

The power extracted from the wind by the rotor is:

$$P = \frac{1}{2}\dot{m}(V_0^2 - V_1^2) = \frac{1}{2}\rho VA(V_0^2 - V_1^2) \tag{3}$$

Introducing the axial interference factor,***a***, which is defined as the fractional decrease in wind velocity between the free stream and the rotor plane:

$$V = (1 - a)V_0 \tag{4}$$

The thrust expression of equation (2) becomes:

$$T = \frac{1}{2}\rho AV_0^2 4a(1 - a) \tag{5}$$

The power extracted by the rotor is:

$$P = \frac{1}{2}\rho AV_0^3 4a(1 - a)^2 \tag{6}$$

2.2. THE BLADE ELEMENT THEORY

This analysis uses the angular momentum conservation principle, taking into account the blade geometry characteristics, in order to determine the forces and the torque exerted on a wind turbine. This method is known as blade element theory [3]. The control volume used in the previous one-dimensional model can be divided into several annular stream tube control volumes, which split the blade into a number of

distinct elements, each of length dr (figure 2).In this figure, the symbol wi represents the wake angular velocity at the station i, and w is the wake angular velocity at the rotor plane.

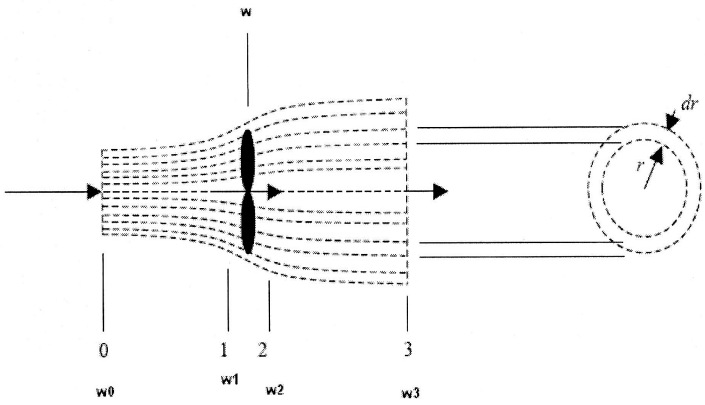

Fig. 2.: Annular stream tube control volumes

In this theory it is assumed that there is no interference between these blade elements and these elements behave as airfoils.
The differential rotor thrust, dT, at a given span location on the rotor (at a specified radius r) can be derived from the previous theory using equation (5):

$$dT = 4a(1-a)\rho V_0^2 \pi r dr \tag{7}$$

In the previous model, it was assumed that airflow doesn't rotate. However, the conservation of angular momentum implies the rotation of the wake, if the rotor is to extract useful torque. Moreover, the flow behind the rotor will rotate in the opposite direction [3], as shown in figure 3.
The effect of wake rotation will be now included. In describing this effect, the assumption is made that upstream of the rotor, the flow is entirely axial and that the flow downstream rotates with an angular velocity ω.
The conservation of angular momentum can be applied to obtain the differential torque at the rotor disc, dQ, resulting in:

$$dQ = 2\pi\rho V \omega r^3 dr \tag{8}$$

The total torque is:

$$\mathrm{Q} = 2\pi\rho \int_0^R V\omega r^3 dr \tag{9}$$

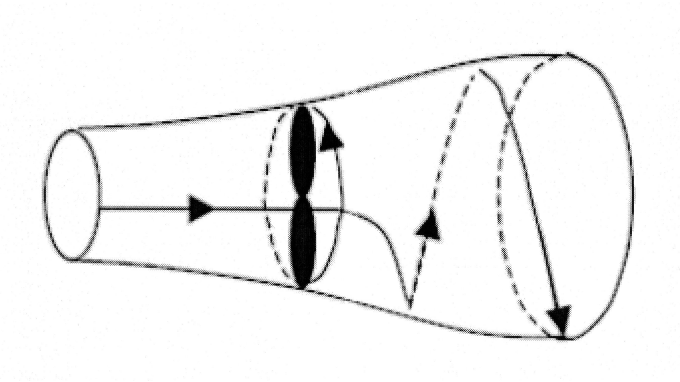

Fig. 3.: Wake rotation

The differential extracted power is given by the expression:

$$\mathrm{d}P{=}2\pi\rho\Omega V\omega r^3 dr \tag{10}$$

The total extracted power is:

$$P{=}2\pi\rho\Omega\int_0^R V\omega r^3 dr \tag{11}$$

In order to calculate P and Q, the wake angular velocity ω has to be known. Introducing, for this purpose, the tangential interference factor a' defined as:

$$\omega = a'\Omega \tag{12}$$

The differential lift and drag forces are:

$$dL = C_L.dq \tag{13}$$

$$dD = C_D.dq \tag{14}$$

with:

$$dq = \frac{1}{2}\rho W^2 dA = \frac{1}{2}\rho W^2 cdr \tag{15}$$

where C_L and C_D are lift and drag coefficients.
The components of the resulting force are (see figure 4.):

$$dF_x = C_x.dq \tag{16}$$

$$dF_y = C_y.dq \tag{17}$$

where:

$$C_x = C_L \sin\phi - C_D \cos\phi \tag{18}$$

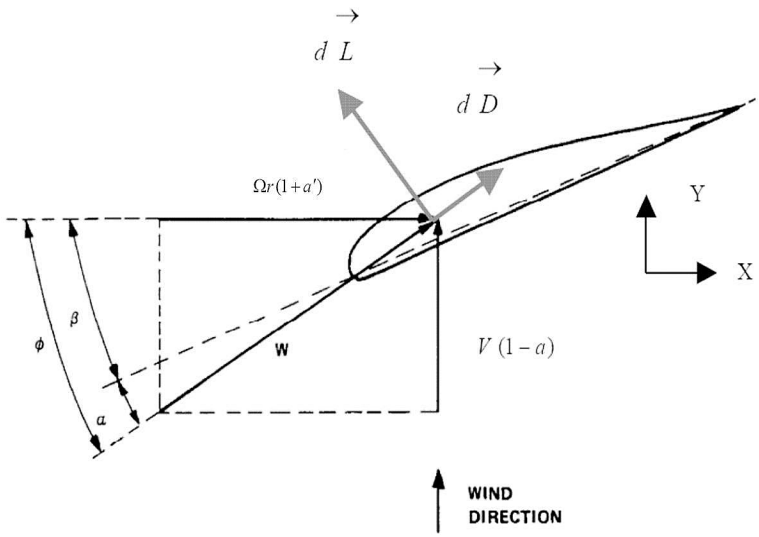

Fig. 4.: Blade element section at radius r

$$C_y = C_L \cos\phi + C_D \sin\phi \tag{19}$$

The following relation can be derived from figure 4:

$$\tan\phi = \frac{(1-a)V_0}{(1+a')\Omega r} \tag{20}$$

where:

$$\alpha = \phi - \beta \tag{21}$$

The differential thrust and torque can now be derived as follows:

$$dT = BC_y dq = BC_y \frac{1}{2}\rho W^2 c dr \tag{22}$$

$$dQ = BC_x dqr = BC_x \frac{1}{2}\rho W^2 c r dr \tag{23}$$

where:
Ω: is the rotation speed of the rotor
W: is the wind relative speed
c: is the chord length
Equating the thrust in equations (7) and (22) as well as the torque in equations (8) and (23), will yield to the expressions of the both interference factors:

$$a = \frac{1}{\frac{4\sin^2\phi}{\sigma C_y} + 1} \tag{24}$$

$$a' = \frac{1}{\frac{4\sin\phi\cos\phi}{\sigma C_x} - 1} \tag{25}$$

The local solidity σ is defined by the following formula:

$$\sigma = \frac{cB}{2\pi r} \tag{26}$$

where: B is the number of blades.
In order to carry out this calculation:
• The wind speed must be determined from the graph of the power probability density (figure 9).
• This calculation procedure is repeated iteratively till the values of the interference factors are corrected.
• In order the get the optimal blade geometry that can extract the maximum power, one must use the optimal incidence angle α_{opt} that gives $\left(\frac{C_L}{C_D}\right)_{Max}$

The distributions of aerodynamic loads (at different blade stations) due to a wind speed of 15 m/s for a blade having a NACA 63-421 profile, are given by table 1.

Table 1: Distribution of aerodynamic loads wind speed 15 m/s

Station (r/R)	Axial force(N)	Tangential force (N)	Torque (N.m)
0.16	86.02	221.24	206.30
0.25	81.92	351.16	305.56
0.34	73.37	466.19	372.82
0.43	57.87	586.57	467.49
0.51	35.67	764.83	724.62
0.60	39.33	908.37	1120.22
0.69	83.60	998.27	1686.21
0.78	221.50	1012.80	2591.9
0.87	211.31	1109.45	2746.15
0.96	169.79	1181.84	2434.31
1.00	140.04	1206.90	2100.65

The local (differential) loads obtained are integrated numerically, over the length of the blade, to determine the overall aerodynamic loads as well as the total output power. Their values are given as follows:
Total axial force on one blade = 553.24 N
Total tangential force on one blade = 4729.56 N
Total axial force on the rotor= 1659.72N
Total torque = 8218.81 N.m

3. OPTIMIZATION OF THE BLADE GEOMETRY

In this part the blade optimal form (chord length and twist angle) is determined. It has been established, that the extracted power of the turbine is given by the following expression [2]:

$$P=\frac{1}{2}\rho\pi R^2 {V_0}^3.\frac{4\lambda^2}{R^4}\int_0^R (1-a)a' r^3 dr \tag{27}$$

The power coefficient is defined as follows:

$$C_p = \frac{P}{\frac{1}{2}\rho V_0^3 A} = \frac{Extracted.power}{Available.Power} \tag{28}$$

The extracted Power reaches its maximum value when C_p is maximum.
It has been demonstrated that C_p is maximum when:

$$a' = \frac{(1-3a)}{(4a-1)} \tag{29}$$

Thorough calculation will yield that the optimal chord length is given by the expression:

$$C = \frac{8\pi r}{BC_L}(1-\cos\theta) \tag{30}$$

and the optimal twist is expressed as follows:

$$\beta = \phi - \alpha_{opt} \tag{31}$$

where: $\theta = \frac{2}{3}\tan^{-1}\left(\frac{V_0}{\Omega r}\right)$ and the optimal incidence angle α_{opt} is obtained when the ratio of the lift coefficient to the drag coefficient is maximum, that means: $\alpha = \alpha_{opt} \Rightarrow \left(\frac{c_l}{c_d}\right)_{\max}$.
The optimal distribution of the twist angle and the chord length are given by figure 5. and 6.

4. STATISTICAL ANALYSIS OF WIND DATA

In this part a statistical analysis is carried out in order to estimate wind characteristics in different regions of Algeria and accordingly determine the most efficient sites. The statistical distribution of wind speed (the frequency of occurrence of each speed) is also valuable in making an optimal design of wind turbine such as in fatigue failure prediction as well as in the adaptation of a machine to a site [4].

4.1. EXPERIMENTAL WIND DATA STATISTICAL DISTRIBUTION

The estimation of the wind resources presents a particular difficulty because of the variability of wind speed characteristics which varies with the season and the hour of

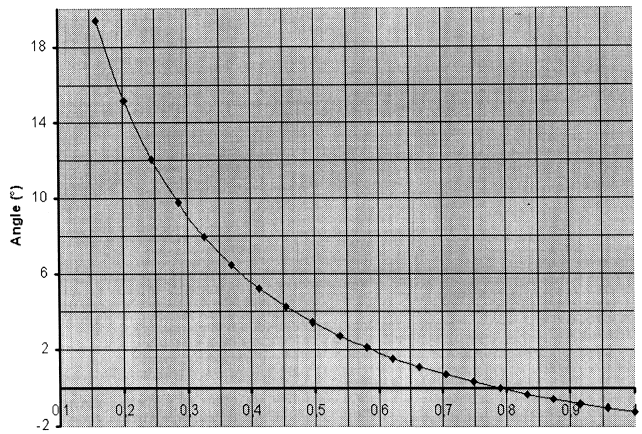

Fig. 5.: optimal distribution of twist angle

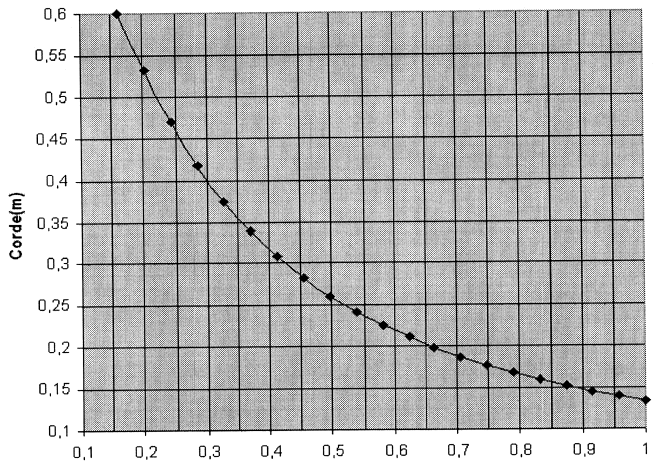

Fig. 6.: optimal distribution of chord length

the day [5].
The statistical distribution of wind speed characteristics varies also from one place to another, since it depends on the local climatic conditions and the landscape of the site.
Wind characteristics such as: average speed, speed frequency and directions facilitate

the estimation of the total energy extracted by wind turbine. These parameters have a direct influence on the operation of turbine (starting, stopping, orientation etc.)
This information is also required to optimize the design of the wind turbine in order to maximize the extracted energy and therefore to minimize the electricity production cost [6].
In order to determine the wind properties of a site, wind data must be available over a long period of time (one to ten years).

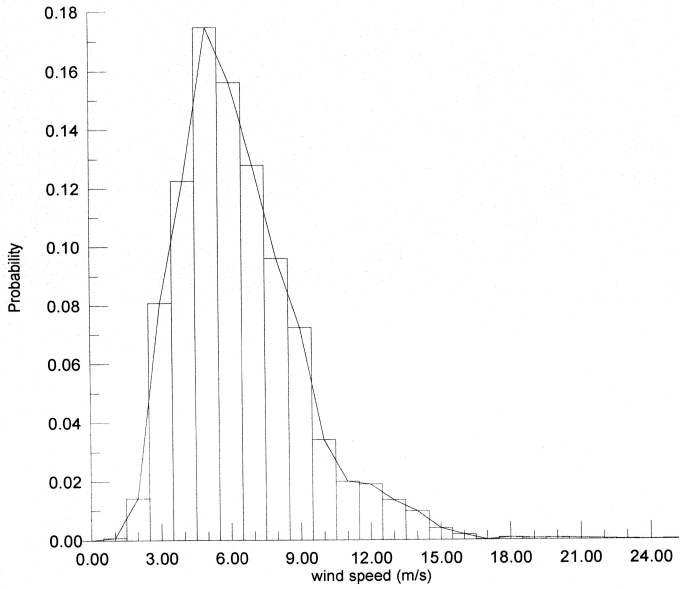

Fig. 7.: Probability Density of wind speed (Town of Adrar)

4.2. ESTIMATION OF THE AVERAGE AVAILABLE POWER (POWER DISTRIBUTION)

The available wind power per unit area varies proportionally with the cube of the wind speed, as follows:

$$P = \frac{1}{2}\rho V^3 \tag{32}$$

where ρ is the density of the air, P is the available power of the wind per unit of area. By multiplying the available power (at each wind speed) by the probability of occurrence of this speed, one obtains the distribution of the wind power at various speeds

of wind. This last distribution is also called the power density [7]. It is important

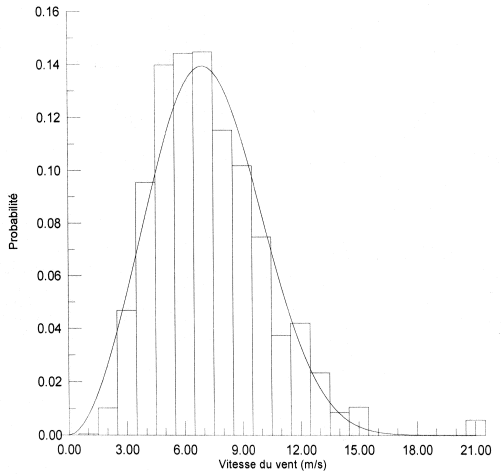

Fig. 8.: probability Density of the average power (Town of Setif))

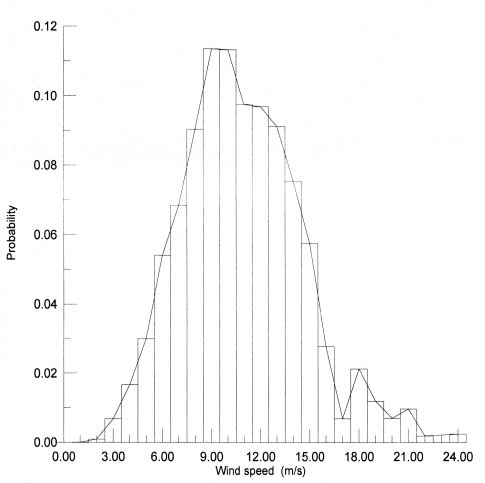

Fig. 9.: Probability Density of the average power (Town of Tindouf))

to note that at speeds higher than the mean velocity, in a given site, where the major part of power is produced.
The optimal design of the wind rotor, for a given site, must be based on the speed of

wind that gives the maximum available energy. For the town of Setif (Figure 8) this speed is 7 m/s.

5. CONCLUSION

In this work the blade element theory was used to calculate aerodynamic loads for small wind turbine blades. This method can also estimate the power extracted by the turbine. This design must is done for a specific aerodynamic profile and a specific site, since we must use the characteristic wind speed that gives the maximum available power in a given site. The value of this characteristic wind speed is determined from the wind data statistical analysis of this site. The design can be repeated for different sites and profiles until we determine the right blade profile the suits each site.

According to results of the wind statistical analysis Tindouf has the highest average power (figure 9). This average power is the most determinant parameter to use in the selection of the wind site.

Actually the criterion of maximum annual energy production used to optimize blade geometry is not sufficient. Whereas the optimization of wind turbine must be based on minimum cost of energy which requires a multidisciplinary method that includes aerodynamic and structural models for blades along with a cost model for the whole turbine [8]. This work can be a part of a global optimization study aiming to minimize cost and structural problems of wind turbine while maximizing its energetic performance.

References

[1] J.M. Jonkman, *Modeling of the UAE Wind Turbine for Refinement of Fast Ad*, National Renewable Energy Laboratory Technical reportTask No. WER32010 NREL, (2003).

[2] E. Lysen, *Introduction to Wind Energy*, Amersfort 2nd ed, Netherlands, 1983.

[3] C. Masson, A. Smaili, C. Leclerc, *Aerodynamic Analysis of HAWT Operating in Unsteady Conditions*, Wind Energy, **4**, 4(2001), 1-22.

[4] J.L. Tangler, *The Evolution of Rotor and blade Design*, Palm springs, California, 2000.

[5] D.A. Stewart, O. M. Essenwagner, *Distribution of wind speed near surface*, J. Applied Meteorology, **17**, (1978), 1633-1642.

[6] P.S. Veers, T.D. Ashwill, *Trends in Design, Manufacture and Evaluation of Wind Turbine Blades*, Wind Energy, **6**, 3(2003), 245-259.

[7] E.L. Petersen, I. Troen, S. Frandsen, K. Hedegaard, *Wind Atlas for Denmark*, Riso National Laboratory, Denmark, 1981.

[8] D. Wood, *Design and Analysis of Small Wind Turbine*, University of New Castle, Australia, 2002.

ROMAI J., v.9, no.2(2013), 155–165

PARAMETERS ESTIMATION FOR THE BIVARIATE SARMANOV DISTRIBUTION WITH NORMAL-TYPE MARGINALS

Elena Pelican[1], Raluca Vernic[1,2,*]

[1] *Faculty of Mathematics and Computer Science, Ovidius University of Constanţa, Romania*

[2] *"Gh. Mihoc - C. Iacob" Institute of Mathematical Statistics and Applied Mathematics of the Romanian Academy, Bucharest, Romania*

[*] *Corresponding author*

epelican@univ-ovidius.ro, rvernic@univ-ovidius.ro

Abstract Recently, Sarmanov's family of bivariate distributions gained interest due to its flexible structure that easily joins given marginals. In this paper, we focus on the parameters estimation for the bivariate Sarmanov distribution with normal-type marginals. The maximum likelihood method is discussed and illustrated on both real and simulated data.

Keywords: Sarmanov distribution, maximum likelihood method, normal-type marginals.
2010 MSC: 62G05, 62H12, 65C10.

1. INTRODUCTION

Sarmanov's bivariate distribution was originally introduced in the literature by Sarmanov (1966), and, later on, it was also proposed in physics by Cohen (1984) under a more general form. Lee (1996) suggested a multivariate version and discussed several applications in medicine. Recently, due to its flexible structure, Sarmanov's bivariate distribution became of interest in different applied studies. For example, Schweidel et al. (2008) used a bivariate Sarmanov model to capture the relationship between a prospective customer's time until acquisition of a particular service and the subsequent duration for which he retains it. Miravete (2009) presented two models based on Sarmanov distribution and used them to compare the number of tariff plans offered by two competing cellular telephone companies. Danaher and Smith (2011) discussed applications to marketing (see also the references therein). In the insurance field, Hernández-Bastida et al. (2009) and Hernández-Bastida and Fernández-Sánchez (2012) used the bivariate Sarmanov distribution for premiums evaluation.

The flexible structure and, hence, the applicability of Sarmanov's distribution results from the way this distribution is built: the marginal distributions are guaranteed to take a desired form and joint into a dependence structure that can model a vast range of data dependencies. However, performing statistical inference for this dis-

tribution raises some difficulties, due also to its high number of parameters. This is why, in this paper, we focus on the parameters estimation for the bivariate Sarmanov distribution with some normal-type marginals that could be of interest in different applications. Therefore, the structure of the paper is as follows: we start by recalling in Section 2 the univariate distributions that we shall use as marginal distributions (i.e., the normal, lognormal and skew-normal distributions). In Section 3, we present the general bivariate Sarmanov distribution and the corresponding maximum likelihood method, followed by the particular cases of interest and the related likelihood systems. We end with some numerical studies in Section 4, both on real and simulated data.

2. NOTATION AND USEFUL FORMULAS

We shall now introduce some notation and present some formulas on the univariate normal distribution and two related distributions that will be useful in next section.

2.1. NORMAL DISTRIBUTION

Let $\varphi(\cdot)$ and $\Phi(\cdot)$ denote the probability density function (pdf) and, respectively, the cumulative distribution function (cdf) of the standard normal $N(0,1)$ distribution. To denote the pdf of the general normal $N\left(\mu,\sigma^2\right)$ distribution, we use the same symbol φ emphasizing the parameters, i.e.,

$$\varphi\left(x;\mu,\sigma^2\right)=\frac{1}{\sigma\sqrt{2\pi}}e^{-\frac{(x-\mu)^2}{2\sigma^2}},\ x,\mu\in\mathbb{R},\sigma>0.$$

We also recall the Laplace transform of the normal distribution

$$\mathcal{L}_{N(\mu,\sigma^2)}(\alpha)=\int_{-\infty}^{\infty}e^{-\alpha x}\varphi\left(x;\mu,\sigma^2\right)dx=e^{-\alpha\mu+\alpha^2\sigma^2/2}. \tag{1}$$

Also, some calculation gives

$$\begin{aligned}\frac{1}{\sigma\sqrt{2\pi}}\int_{-\infty}^{\infty}xe^{-\alpha x}e^{-\frac{(x-\mu)^2}{2\sigma^2}}dx &= e^{\alpha^2\sigma^2/2-\alpha\mu}\frac{1}{\sigma\sqrt{2\pi}}\int_{-\infty}^{\infty}xe^{-\frac{\left(x-\mu+\alpha\sigma^2\right)^2}{2\sigma^2}}dx\\ &= e^{\alpha^2\sigma^2/2-\alpha\mu}\left(\mu-\alpha\sigma^2\right),\end{aligned} \tag{2}$$

from where

$$\begin{aligned}\nu_{N(\mu,\sigma^2)}(\alpha) &= \int_{-\infty}^{\infty}x\left(e^{-\alpha x}-\mathcal{L}_{N(\mu,\sigma^2)}(\alpha)\right)\varphi\left(x;\mu,\sigma^2\right)dx\\ &= e^{-\alpha\mu+\alpha^2\sigma^2/2}\left(\mu-\alpha\sigma^2\right)-\mu e^{-\alpha\mu+\alpha^2\sigma^2/2}\\ &= -\alpha\sigma^2e^{-\alpha\mu+\alpha^2\sigma^2/2}.\end{aligned}$$

2.2. LOGNORMAL DISTRIBUTION

As it is well-known, a random variable (rv) X follows a lognormal $LN\left(\mu,\sigma^2\right)$ distribution if $\ln X \sim N\left(\mu,\sigma^2\right), \sigma > 0$, hence having the pdf

$$f_{LN(\mu,\sigma^2)}(x) = \frac{1}{x\sigma\sqrt{2\pi}} e^{-\frac{(\ln x-\mu)^2}{2\sigma^2}}, x > 0.$$

The first two moments of this distribution are

$$\mathbb{E}X = e^{\mu+\sigma^2/2},\ VarX = e^{2\mu+\sigma^2}\left(e^{\sigma^2}-1\right).$$

2.3. SKEW-NORMAL DISTRIBUTION

To allow for asymmetry, Azzalini (1985) introduced an additional parameter into the normal distribution leading to the so called skew-normal distribution. We say that the rv X follows a skew-normal distribution $SN\left(\mu,\sigma^2,\lambda\right), \sigma > 0$, if its pdf is given by

$$f_{SN(\mu,\sigma^2,\lambda)}(x) = 2\varphi\left(x;\mu,\sigma^2\right)\Phi\left(\lambda\left(x-\mu\right)/\sigma\right), x \in \mathbb{R}. \tag{3}$$

Later on, more general forms and extensions to the multivariate setting were derived, see e.g., the survey of Arnold and Beaver (2002).

The first moments of the above skew-normal distribution are

$$\mathbb{E}X = \mu + \sqrt{\frac{2}{\pi}}\gamma,\ VarX = \sigma^2 - \frac{2}{\pi}\gamma^2,\ \mathbb{E}\left(X-\mathbb{E}X\right)^3 = \frac{\sqrt{2}\left(4-\pi\right)}{\pi^{3/2}}\gamma^3, \tag{4}$$

where $\gamma = \lambda\sigma/\sqrt{1+\lambda^2}$.

3. BIVARIATE SARMANOV DISTRIBUTION

3.1. THE GENERAL DISTRIBUTION

The bivariate random vector $\mathbf{X} = (X_1, X_2)'$ follows a bivariate Sarmanov distribution if its joint pdf is given by (see, e.g., Kotz et al., 2000)

$$f_{\mathbf{X}}(x_1,x_2) = f_1(x_1) f_2(x_2)\left(1+\omega\phi_1(x_1)\phi_2(x_2)\right), \tag{5}$$

where $(f_i)_{i=1,2}$ are the corresponding marginal pdf's, $(\phi_i)_{i=1,2}$ are bounded non-constant kernel functions, and ω is a real number such that

$$\int_{-\infty}^{\infty}\phi_i(x) f_i(x)\,dx = 0,\ i = 1,2, \text{ and} \tag{6}$$

$$1+\omega\phi_1(x_1)\phi_2(x_2) \geq 0, \text{ for all } (x_1,x_2) \in \mathbb{R}^2. \tag{7}$$

If we denote $\nu_i = \int_{-\infty}^{\infty} x\phi_i(x) f_i(x)\,dx,\ i = 1,2$, then

$$cov(X_1,X_2) = \omega\nu_1\nu_2. \tag{8}$$

Note that when ω=0, from (5), X_1 and X_2 are independent. As to the choice of the kernel functions ϕ_i, the following particular cases satisfying (6) have already been discussed in the literature (see, e.g., Lee, 1996):

1 $\phi_i = 1 - 2F_i$, where F_i is the cdf of X_i. In this case, Sarmanov's distribution is called Farlie-Gumbel-Morgenstern and verifies the restrictive condition that the correlation coefficient $corr(X_1, X_2)$ cannot exceed 1/3 in absolute value. However, in general, Sarmanov's distribution is not restricted by such a condition.

2 $\phi_i(x) = x^\alpha - \mathbb{E}\left[X_i^\alpha\right]$, assuming that $\mathbb{E}\left[X_i^\alpha\right] < \infty$. In this case, $\nu_i = \mathbb{E}\left[X_i^{\alpha+1}\right] - \mathbb{E}\left[X_i^\alpha\right]\mathbb{E}X_i$, if it is finite. If, moreover, $\alpha = 1$, then the marginal correlation is $corr(X_1, X_2) = \omega\sqrt{Var[X_1]\,Var[X_2]}$.

3 $\phi_i(x) = e^{-\alpha x} - \mathbb{E}\left[e^{-\alpha X_i}\right]$, where $\mathbb{E}\left[e^{-\alpha X_i}\right]$ is the Laplace transform of X_i.

4 $\phi_i(x) = f_i(x) - \int_{-\infty}^{\infty} f_i^2(y)\,dy$.

3.2. PARAMETERS ESTIMATION

3.2.1 General case. We shall estimate the parameters using the maximum likelihood method (MLM) based on the random data sample $\left\{\left(x_{1j}, x_{2j}\right)\right\}_{j=1}^{n}$ consisting of n successive couples of observations. If Θ denotes the parameters set of Sarmanov's distribution, then the loglikelihood function to be maximized results from (5) as

$$\ln L\left(\left\{\left(x_{1j}, x_{2j}\right)\right\}_{j=1}^{n}; \Theta\right) = \sum_{j=1}^{n}\left(\ln f_1\left(x_{1j}\right) + \ln f_2\left(x_{2j}\right) + \ln\left(1 + \omega\phi_1\left(x_{1j}\right)\phi_2\left(x_{2j}\right)\right)\right).$$

The parameters to be estimated are ω, the parameters of f_i, and, eventually, the parameters of ϕ_i. Letting θ denote a generic parameter of f_i, the corresponding maximum likelihood (ML) system is

$$\begin{cases} 0 = \dfrac{\partial \ln L}{\partial\theta} = \displaystyle\sum_{j=1}^{n}\left(\frac{\partial \ln f_1\left(x_{1j}\right)}{\partial\theta} + \frac{\partial \ln f_2\left(x_{2j}\right)}{\partial\theta}\right) + \omega\sum_{j=1}^{n}\frac{1}{1 + \omega\phi_1\left(x_{1j}\right)\phi_2\left(x_{2j}\right)} \\ \qquad\qquad \times\left(\phi_1\left(x_{1j}\right)\dfrac{\partial\phi_2\left(x_{2j}\right)}{\partial\theta} + \phi_2\left(x_{2j}\right)\dfrac{\partial\phi_1\left(x_{1j}\right)}{\partial\theta}\right), \quad \theta \in \Theta \\ \\ 0 = \dfrac{\partial \ln L}{\partial\omega} = \displaystyle\sum_{j=1}^{n}\frac{\phi_1\left(x_{1j}\right)\phi_2\left(x_{2j}\right)}{1 + \omega\phi_1\left(x_{1j}\right)\phi_2\left(x_{2j}\right)} \end{cases} . \tag{9}$$

This system can become quite complex and, therefore, it must be solved by numerical methods that require starting values for the unknown parameters. Such starting values easily result by the method of moments (MM). Moreover, since the last equation of the system raised numerical problems as noticed by Pelican and Vernic (2013), a value for ω can be obtained from the empirical correlation coefficient, ρ.

Alternatively, instead of solving the ML system, one can use numerical methods to directly find the maximum of the loglikelihood function. The corresponding maximization problem

$$\max_{\Theta} \ln L\left(\left\{\left(x_{1j}, x_{2j}\right)\right\}_{j=1}^{n}; \Theta\right),$$

can be completed with some constraints (see in the following the formulas of σ_i^2), and can be solved using, e.g., a Variable Neighborhood Search (VNS) algorithm as presented by Mladenovic and Hansen (1997).

3.2.2 Normal marginals. We start by considering normally distributed marginals, i.e., $X_i \sim N\left(\mu_i, \sigma_i^2\right), \mu_i \in \mathbb{R}, \sigma_i > 0$. In this case, the loglikelihood function is

$$\ln L\left(\left\{\left(x_{1j}, x_{2j}\right)\right\}_{j=1}^{n}; \Theta\right) = -n\left(\ln \sigma_1 + \ln \sigma_2 + \ln (2\pi)\right)$$

$$-\sum_{j=1}^{n}\left(\frac{\left(x_{1j}-\mu_1\right)^2}{2\sigma_1^2} + \frac{\left(x_{2j}-\mu_2\right)^2}{2\sigma_2^2}\right) + \sum_{j=1}^{n} \ln\left(1 + \omega\phi_1\left(x_{1j}\right)\phi_2\left(x_{2j}\right)\right),$$

with $\Theta = (\mu_1, \mu_2, \sigma_1, \sigma_2, \omega)$. Then the ML system (9) becomes for $i = 1, 2$

$$\begin{cases} 0 = \dfrac{\partial \ln L}{\partial \mu_i} = \dfrac{1}{\sigma_i^2}\left(\sum\limits_{j=1}^{n} x_{ij} - n\mu_i\right) + \omega \sum\limits_{j=1}^{n} \dfrac{\phi_{3-i}\left(x_{3-i;j}\right)}{1 + \omega\phi_1\left(x_{1j}\right)\phi_2\left(x_{2j}\right)} \dfrac{\partial \phi_i\left(x_{ij}\right)}{\partial \mu_i} \\ 0 = \dfrac{\partial \ln L}{\partial \sigma_i} = -\dfrac{n}{\sigma_i} + \sum\limits_{j=1}^{n} \dfrac{\left(x_{ij}-\mu_i\right)^2}{\sigma_i^3} + \omega \sum\limits_{j=1}^{n} \dfrac{\phi_{3-i}\left(x_{3-i;j}\right)}{1 + \omega\phi_1\left(x_{1j}\right)\phi_2\left(x_{2j}\right)} \dfrac{\partial \phi_i\left(x_{ij}\right)}{\partial \sigma_i} \\ 0 = \dfrac{\partial \ln L}{\partial \omega} = \sum\limits_{j=1}^{n} \dfrac{\phi_1\left(x_{1j}\right)\phi_2\left(x_{2j}\right)}{1 + \omega\phi_1\left(x_{1j}\right)\phi_2\left(x_{2j}\right)} \end{cases} . \tag{10}$$

Particular case I: $\phi_i(x) = x - \mathbb{E}[X_i]$**..** This particular case has also been studied in Pelican and Vernic (2013). Since $\phi_i(x) = x - \mu_i$, the second equation of system (10) yields

$$-\frac{n}{\sigma_i} + \sum_{j=1}^{n} \frac{\left(x_{ij}-\mu_i\right)^2}{\sigma_i^3} = 0,$$

and therefore the ML system reduces to

$$\begin{cases} \sigma_i^2 = \dfrac{1}{n}\sum\limits_{j=1}^{n}\left(x_{ij}-\mu_i\right)^2 \\ \dfrac{n\left(\sum_{j=1}^{n} x_{ij}-n\mu_i\right)}{\sum_{j=1}^{n}\left(x_{ij}-\mu_i\right)^2} - \omega\sum\limits_{j=1}^{n}\dfrac{x_{3-i;j}-\mu_{3-i}}{1+\omega\left(x_{1j}-\mu_1\right)\left(x_{2j}-\mu_2\right)} = 0 \\ \sum\limits_{j=1}^{n}\dfrac{\left(x_{1j}-\mu_1\right)\left(x_{2j}-\mu_2\right)}{1+\omega\left(x_{1j}-\mu_1\right)\left(x_{2j}-\mu_2\right)} = 0 \end{cases},$$

$i = 1, 2$.
Moreover, we have the correlation coefficient

$$corr\left(X_1, X_2\right) = \omega\sqrt{Var\left[X_1\right]Var\left[X_2\right]} = \omega\sigma_1\sigma_2,$$

from which we can obtain an estimated/starting value for ω.

Particular case II: $\phi_i(x) = e^{-\alpha_i x} - \mathbb{E}\left[e^{-\alpha_i X_i}\right]$.. Recalling the Laplace transform of a normal distribution from (1), we have in this case $\phi_i(x) = e^{-\alpha_i x} - e^{-\alpha_i\mu_i+\alpha_i^2\sigma_i^2/2}$, $i = 1, 2$. Inserting this into the first two equations of system (10) yields

$$\begin{cases} \omega\alpha_i e^{-\alpha_i\mu_i+\alpha_i^2\sigma_i^2/2}\sum\limits_{j=1}^{n}\dfrac{e^{-\alpha_{3-i}x_{3-i;j}} - e^{-\alpha_{3-i}\mu_{3-i}+\alpha_{3-i}^2\sigma_{3-i}^2/2}}{1+\omega\left(e^{-\alpha_1 x_{1j}} - e^{-\alpha_1\mu_1+\alpha_1^2\sigma_1^2/2}\right)\left(e^{-\alpha_2 x_{2j}} - e^{-\alpha_2\mu_2+\alpha_2^2\sigma_2^2/2}\right)} \\ \qquad +\dfrac{1}{\sigma_i^2}\left(\sum\limits_{j=1}^{n} x_{ij} - n\mu_i\right) = 0 \\ -\omega\alpha_i^2\sigma_i e^{-\alpha_i\mu_i+\alpha_i^2\sigma_i^2/2}\sum\limits_{j=1}^{n}\dfrac{e^{-\alpha_{3-i}x_{3-i;j}} - e^{-\alpha_{3-i}\mu_{3-i}+\alpha_{3-i}^2\sigma_{3-i}^2/2}}{1+\omega\left(e^{-\alpha_1 x_{1j}} - e^{-\alpha_1\mu_1+\alpha_1^2\sigma_1^2/2}\right)\left(e^{-\alpha_2 x_{2j}} - e^{-\alpha_2\mu_2+\alpha_2^2\sigma_2^2/2}\right)} \\ \qquad -\dfrac{n}{\sigma_i} + \sum\limits_{j=1}^{n}\dfrac{\left(x_{ij}-\mu_i\right)^2}{\sigma_i^3} = 0 \end{cases},$$

$i = 1, 2$.
Therefore, the ML system becomes

$$\begin{cases} \sigma_i^2 = \dfrac{\sum_{j=1}^{n}\left(x_{ij}-\mu_i\right)^2}{n-\alpha_i\left(\sum_{j=1}^{n} x_{ij}-n\mu_i\right)} \\ \omega\alpha_i e^{-\alpha_i\mu_i+\alpha_i^2\sigma_i^2/2}\sum\limits_{j=1}^{n}\dfrac{e^{-\alpha_{3-i}x_{3-i;j}} - e^{-\alpha_{3-i}\mu_{3-i}+\alpha_{3-i}^2\sigma_{3-i}^2/2}}{1+\omega\left(e^{-\alpha_1 x_{1j}} - e^{-\alpha_1\mu_1+\alpha_1^2\sigma_1^2/2}\right)\left(e^{-\alpha_2 x_{2j}} - e^{-\alpha_2\mu_2+\alpha_2^2\sigma_2^2/2}\right)} \\ \qquad +\dfrac{1}{\sigma_i^2}\left(\sum\limits_{j=1}^{n} x_{ij} - n\mu_i\right) = 0 \\ \sum\limits_{j=1}^{n}\dfrac{\left(e^{-\alpha_1 x_{1j}} - e^{-\alpha_1\mu_1+\alpha_1^2\sigma_1^2/2}\right)\left(e^{-\alpha_2 x_{2j}} - e^{-\alpha_2\mu_2+\alpha_2^2\sigma_2^2/2}\right)}{1+\omega\left(e^{-\alpha_1 x_{1j}} - e^{-\alpha_1\mu_1+\alpha_1^2\sigma_1^2/2}\right)\left(e^{-\alpha_2 x_{2j}} - e^{-\alpha_2\mu_2+\alpha_2^2\sigma_2^2/2}\right)} = 0 \end{cases},$$

$i = 1, 2$.
Note that since this system has five equations, it is useful for estimating μ_i and σ_i, $i = 1, 2$, when the values of the parameters α_1 and α_2 are known. If we also want to estimate the α_is, we need two more equations that can be obtained from $\dfrac{\partial \ln L}{\partial \alpha_i} = 0$, yielding

$$\sum_{j=1}^{n} \frac{\left(\left(\mu_i - \alpha_i \sigma_i^2\right) e^{-\alpha_i \mu_i + \alpha_i^2 \sigma_i^2/2} - x_{ij} e^{-\alpha_i x_{ij}}\right)\left(e^{-\alpha_{3-i} x_{3-i;j}} - e^{-\alpha_{3-i}\mu_{3-i} + \alpha_{3-i}^2 \sigma_{3-i}^2/2}\right)}{1 + \omega\left(e^{-\alpha_1 x_{1j}} - e^{-\alpha_1 \mu_1 + \alpha_1^2 \sigma_1^2/2}\right)\left(e^{-\alpha_2 x_{2j}} - e^{-\alpha_2 \mu_2 + \alpha_2^2 \sigma_2^2/2}\right)} = 0,$$

$i = 1, 2$.
Also, using formula (3), we obtain $\nu_i = -\alpha_i \sigma_i^2 e^{-\alpha_i \mu_i + \alpha_i^2 \sigma_i^2/2}$, and hence (8) yields

$$corr\,(X_1, X_2) = \frac{\omega \nu_1 \nu_2}{\sigma_1 \sigma_2} = \omega \alpha_1 \alpha_2 \sigma_1 \sigma_2 e^{-\alpha_1 \mu_1 - \alpha_2 \mu_2 + \left(\alpha_1^2 \sigma_1^2 + \alpha_2^2 \sigma_2^2\right)/2}.$$

We can use this relation to estimate ω by MM.

3.2.3 Lognormal marginals and $\phi_i(x) = x - \mathbb{E}[X_i]$. We shall now assume that each marginal is lognormally distributed, i.e., $X_i \sim LN\left(\mu_i, \sigma_i^2\right), \mu_i \in \mathbb{R}, \sigma_i > 0$. Taking $\phi_i(x) = x - \mathbb{E}[X_i]$ yields the corresponding Sarmanov pdf

$$f_{\mathbf{X}}(x_1, x_2) = \prod_{i=1}^{2} \frac{1}{x_i \sigma_i \sqrt{2\pi}} e^{-\frac{(\ln x_i - \mu_i)^2}{2\sigma_i^2}} \left(1 + \omega\left(x_1 - e^{\mu_1 + \sigma_1^2/2}\right)\left(x_2 - e^{\mu_2 + \sigma_2^2/2}\right)\right),$$

$x_1, x_2 > 0$.
Denoting $y_i = \ln x_i$, this pdf can be rewritten as

$$f_{\mathbf{X}}(y_1, y_2) = \prod_{i=1}^{2} \frac{1}{e^{y_i} \sigma_i \sqrt{2\pi}} e^{-\frac{(y_i - \mu_i)^2}{2\sigma_i^2}} \left(1 + \omega\left(e^{y_1} - e^{\mu_1 + \sigma_1^2/2}\right)\left(e^{y_2} - e^{\mu_2 + \sigma_2^2/2}\right)\right),$$

from where we note that $f_{\mathbf{X}}(y_1, y_2) = \dfrac{g(y_1, y_2)}{e^{y_1 + y_2}}$, with g a Sarmanov pdf having normal marginals and kernel functions $\phi_i'(x) = e^{-\alpha_i x} - \mathbb{E}\left[e^{-\alpha_i X_i}\right]$ with $\alpha_1 = \alpha_2 = -1$. Moreover, the loglikelihood functions are related by $\ln f_{\mathbf{X}}(y_1, y_2) = \ln g(y_1, y_2) - (y_1 + y_2)$, hence we can estimate the parameters of $f_{\mathbf{X}}$ by estimating the parameters of g. In other words, we can estimate the parameters of a Sarmanov distribution with lognormal marginals $X_i \sim LN\left(\mu_i, \sigma_i^2\right)$ and kernel functions $x - \mathbb{E}[X_i]$ by simply estimating the parameters of a Sarmanov distribution having the normal marginals $Y_i = \ln X_i$ and the kernel functions $e^x - \mathbb{E}\left[e^{Y_i}\right]$. Therefore, we reduced the estimation problem to the above particular case II.

3.2.4 Different marginals: one normal and one skew-normal. We shall now take advantage of Sarmanov's distribution characteristic to easily join distinct marginals. Therefore, we consider that $X_2 \sim N\left(\mu_2, \sigma_2^2\right)$, while this time $X_1 \sim SN\left(\mu_1, \sigma_1^2, \lambda\right)$. Sarmanov's pdf (5) becomes in this case

$$\begin{aligned} f_{\mathbf{X}}(x_1, x_2) &= 2\varphi\left(x_1; \mu_1, \sigma_1^2\right)\varphi\left(x_2; \mu_2, \sigma_2^2\right)\Phi\left(\lambda\left(x_1 - \mu_1\right)/\sigma_1\right) \\ &\quad \times\left(1 + \omega\phi_1(x_1)\,\phi_2(x_2)\right). \end{aligned}$$

For simplicity, we shall consider only the case $\phi_i(x) = x - \mathbb{E}[X_i], i = 1, 2$, where $\xi_1 = \mathbb{E}[X_1]$ results from (4).

4. NUMERICAL STUDY

4.1. REAL DATA STUDY

We used the distributions presented in Section 3.2 to model a bivariate data sample from motor insurance consisting of estimated and approved costs from a Romanian insurer during 2002-2004. All the claims included in our sample had been settled. The sample size is n=101, and for each claim we observed X_1 the estimated cost of the total damage and X_2 the approved (and paid) cost in ROL. Since the data values are quite large (e.g., their empirical means are 21312871 and, respectively, 19453147), we logaritmized the entire data set and obtained the following empirical characteristics

	Min	Max	Mean	Variance
X_1	13.9978	19.3369	16.3211	1.0397
X_2	13.4970	18.6349	16.2666	1.0805

and correlation coefficient $\rho = 0.831$.

These empirical characteristics were used as starting values when estimating the parameters by the methods described above. To compare the fitted distributions, we calculated the corresponding loglikelihood and AIC values, where AIC (Akaike's information criterion, see e.g., Akaike, 1974) is defined as

$$AIC = 2(s - \ln L);$$

here s is the number of estimated parameters and L the likelihood function. The preferred model is the one with the lowest AIC value.

We assumed that both log-marginals are normally distributed and considered both cases for ϕ_i. For $\phi_i(x) = e^{-\alpha_i x} - \mathbb{E}\left[e^{-\alpha_i X_i}\right]$, we also considered the case $\alpha_1 = \alpha_2 = -1$, i.e., the distribution we fitted to the not transformed data has lognormal marginals (as in Section 3.2.3). The results are presented in Table 1, columns 2 and 3. According to

$\ln L$ and AIC, the best fit is given by the second log-Sarmanov distribution with normal marginals (bold values), followed by the Sarmanov distribution with lognormal marginals.

Table 1. Estimations and ranking results for the real data set

	$\phi_i(x) = x - \mu_i$	$\phi_i(x) = e^{-\alpha x} - \mathbb{E}\left[e^{-\alpha X_i}\right]$ $\alpha_1 = -1.3946$ $\alpha_2 = -1.2914$	$\alpha_1 = -1$ $\alpha_2 = -1$	$\phi_i(x) = x - \mu_i$ $\lambda_1 = 0.7805$ $\lambda_2 = 0.2644$
μ_1	16.3920	16.2758	16.3334	16.2288
σ_1^2	1.0345	1.0856	1.0424	1.2127
μ_2	16.2760	16.3017	16.2645	16.2507
σ_2^2	1.0699	1.0781	1.0675	0.9889
ω	0.454	7.55×10^{-20}	7×10^{-15}	0.9776
$\ln L$	-3558.01	**-3456.92**	-3504.40	-3548.27
AIC	7126.02	**6927.84**	7018.80	7110.54

Moreover, hoping to improve the fitting, we also assumed that both log-marginals are skew-normal distributed. Unfortunately, the results presented in the last column of Table 1 are not as good as expected, and the AIC penalizes this model.

4.2. SIMULATION STUDY

To illustrate the estimation methods for the bivariate Sarmanov distribution with different marginals, we used generated samples from a bivariate Sarmanov distribution having one skew-normal marginal and one normal marginal, i.e., we considered $X_1 \sim SN\left(\mu_1, \sigma_1^2, \lambda\right)$ and $X_2 \sim N\left(\mu_2, \sigma_2^2\right), \sigma_1, \sigma_2 > 0$. As in Pelican and Vernic (2013), we used the inversion method as generating method, based on the conditional cdf

$$\begin{aligned} F_{X_2|X_1=x_1}(x) &= \int_{-\infty}^{x} \frac{f_{\mathbf{X}}(x_1, x_2)}{f_1(x_1)} dx_2 \\ &= F_2(x) + \omega(x_1 - \xi_1) \int_{-\infty}^{x} f_2(x_2)(x_2 - \mu_2)\, dx_2 \\ &= \Phi\left(\frac{x - \mu_2}{\sigma_2}\right) - \omega(x_1 - \xi_1) \frac{\sigma_2}{\sqrt{2\pi}} e^{-\frac{1}{2}\left(\frac{x-\mu_2}{\sigma_2}\right)^2}, \end{aligned}$$

with $\xi_1 = \mathbb{E}X_1$. Moreover, we applied MM and MLM to estimate the parameters, the values obtained by MM being used as starting values for MLM. The moments used in MM for the skew-normal distribution are the ones from (4).

We started by generating samples of different sizes, while the parameters values were set at $\mu_1 = \mu_2 = \sigma_1 = \sigma_2 = \lambda = 1$ and $\omega = 0.5$. The results are presented in Table 2 and we note that the sample size strongly affects the results (of course, this

is also related to the generating errors). Also, based on the loglikelihoods values, the MLM outperforms the MM as expected.

Table 2. Estimations results for MM and MLM when varying the sample size (real values $\mu_1 = \mu_2 = \sigma_1 = \sigma_2 = \lambda = 1, \omega = 0.5$)

	$n = 1000$		$n = 2000$		$n = 5000$		$n = 10000$	
	MM	MLM	MM	MLM	MM	MLM	MM	MLM
μ_1	0.8402	0.9045	1.1449	1.0848	1.0213	0.9990	1.0736	1.0049
μ_2	1.0521	1.0596	0.9957	0.9916	1.0030	1.0091	0.9967	0.9923
σ_1	1.1139	1.0671	0.9285	0.9606	0.9808	0.9898	1.0277	0.9966
σ_2	1.0365	1.0176	1.0016	1.0014	1.0101	1.0100	0.9632	1.0277
λ	3.4200	1.4710	0.8019	0.8000	1.2707	0.9700	1.0277	0.9631
ω	0.4627	0.6940	0.4909	0.6846	0.4690	0.6179	0.4760	0.6097
$\ln L$	-2656.39	-2521.18	-5110.88	-5076.90	-12862.89	-12728.24	-25893.48	-25672.22

We also varied the value of the parameter λ that controls the asymmetry of the skew-normal distribution, while keeping the other parameters and the sample size fixed at $\mu_1 = \mu_2 = \sigma_1 = \sigma_2 = 1, \omega = 0.5$ and $n = 10000$. From Table 3, it seems that the results are better for a larger λ (meaning a more asymmetric distribution).

Also, when looking at the estimated values of λ in both tables, the MM clearly gives biased results.

Table 3. Estimations results for MM and MLM when varying λ (real values $\mu_1 = \mu_2 = \sigma_1 = \sigma_2 = 1, \omega = 0.5$)

	Real $\lambda = 0.5$		Real $\lambda = 1$		Real $\lambda = 1.5$	
$n = 10000$	MM	MLM	MM	MLM	MM	MLM
μ_1	1.2423	0.9861	1.0736	1.0049	1.0384	1.0025
μ_2	0.9955	0.9828	0.9967	0.9923	0.9925	1.0002
σ_1	0.9445	0.9993	1.0277	0.9966	0.9746	1.0066
σ_2	1.0103	1.0104	0.9632	1.0277	0.9998	0.9997
λ	0.1487	0.4801	1.0277	0.9631	2.2501	1.4970
ω	0.4457	0.6089	0.4760	0.6097	0.4690	0.5704
$\ln L$	-26703.97	-26538.18	-25893.48	-25672.22	-25228.33	-24626.06

References

[1] Akaike, H., *A new look at the statistical model identification*, IEEE Transactions on Automatic Control, (1974)19, 716-723.

[2] Arnold, B.C., Beaver, R.J., *Skewed multivariate models related to hidden truncation and/or selective reporting*, Sociedad de Estadistica e Investigacion Operativa Test 11, no.1(2002), 7-54.

[3] Azzalini, A., *A class of distributions which includes the normal ones*, Scandinavian Journal of Statistics 12(1985), 171-178.

[4] Cohen, L., *Probability distributions with given multivariate marginals*, Journal of Mathematical Physics 25(1984), 2402-2403.

[5] Danaher, P., Smith, M., *Modeling multivariate distributions using copulas: applications in marketing*, Marketing Science, 30 (1)(2011), 4-21.

[6] Hernández-Bastida, A., Fernández-Sánchez, M.P., Gómez-Déniz, E., *The net Bayes premium with dependence between the risk profiles*, Insurance: Mathematics and Economics, 45, (2)(2009), 247-254.

[7] Hernández-Bastida, A., Fernández-Sánchez, M.P., *A Sarmanov family with beta and gamma marginal distributions: an application to the Bayes premium in a collective risk model*, Statistical Methods & Applications, 21 (4)(2012), 391-409.

[8] Kotz, S., Balakrishnan, N., Johnson, N.L., *Continuous Multivariate Distributions. Vol.1: Models and Applications*, Wiley, 2000.

[9] Lee, M.L., *Properties and applications of the Sarmanov family of bivariate distributions*, Communications in Statistics- Theory and Methods, 25 (6)(1996), 1207-1222.

[10] Miravete, E.J., *Multivariate Sarmanov count data models*, CEPR DP No. 7463(2009) (http://www.cepr.org/pubs/dps/DP7463.asp).

[11] Mladenovic, N., Hansen, P., *Variable neighborhood search*, Computers and Operations Research 24(1997), 1097-1100.

[12] Sarmanov, O.V., *Generalized normal correlation and two-dimensional Frechet classes*, Doklady (Soviet Mathematics), 168(1966), 596-599.

[13] Schweidel, D., Fader, P., Bradlow, E., *A Bivariate Timing Model of Customer Acquisition and Retention*, Marketing Science 27(2008) (5), 829-843.

[14] Pelican E., Vernic R., *An estimation procedure for the multivariate Sarmanov distribution. Numerical study*, To appear in International Journal of Computer Mathematics (2013).

ROMAI J., v.9, no.2(2013), 167–172

SOME REMARKS ON EIGENVALUE PROBLEMS FOR THE LAPLACE OPERATOR

Valentina Proytcheva[1], Snezhana Hristova[2]
[1] *Technical University of Sofia, branch Plovdiv, Bulgaria*
[2] *Plovdiv University, Plovdiv, Bulgaria*
vproicheva@abv.bg, snehri@uni-plovdiv.bg

Abstract This paper deals with the eigenvalue problems in some bounded convex domain $\Omega \subset \mathbb{R}^N$, $N \geq 2$, under Dirichlet and Neumann conditions. In particular another proof of Payne - Weinberger's inequality $\mu_1 \geq \left(\frac{\pi}{D}\right)^2$ will be provided, where μ_1 is the first nontrivial eigenvalue of the free membrane problem, and D is the diameter of Ω.

Keywords: eigenvalue problems for Laplace operator, maximum principle, inequalities.
2010 MSC: 35P05, 35P15.

1. INTRODUCTION

This paper deals with the following basic eigenvalue problems

$$\Delta u + \lambda u = 0, \quad x \in \Omega, \qquad u = 0, \quad x \in \partial\Omega, \tag{1}$$

and

$$\Delta v + \mu v = 0, \quad x \in \Omega, \qquad \frac{\partial v}{\partial n} = 0, \quad x \in \partial\Omega, \tag{2}$$

where Ω is a bounded convex domain in $\mathbb{R}^N$, $N \geq 2$. In (2) $\frac{\partial v}{\partial n}$ is the outward normal derivative of v on the boundary $\partial\Omega$.

It is well known that these problems have nontrivial solutions only for specific values λ and μ called eigenvalues satisfying

$$0 < \lambda_1 < \lambda_2 \leq \lambda_3 \leq \rightarrow \infty, \tag{3}$$

$$0 = \mu_0 < \mu_1 \leq \mu_2 \leq \rightarrow \infty, \tag{4}$$

The corresponding eigenfunctions are denoted by u_k (associated to λ_k) and v_k (associated to μ_k). These eigenvalues and eigenfunctions depend on the geometry and the size of Ω.

These quantities are known only for particular domains including parallelepipeds and balls. The goal of this paper is to derive the following result:

Let Ω be a bounded convex domain in $\mathbb{R}^N$, $N \geq 2$. Then we have

$$|u|_{\max}^{-2} \int_\Omega u^2 dx \le \frac{1}{2}|\Omega|, \tag{5}$$

$$|v|_{\max}^{-2} \int_\Omega v^2 dx \le \frac{1}{2}|\Omega|, \tag{6}$$

where $|\Omega| := \int_\Omega dx$ is the volume of Ω. Assuming that Ω is bounded strictly convex in $\mathbb{R}^2$, we have the inequalities

$$u^2(P) \le \frac{1}{2}|u|_{\max}^2, \quad \text{with } |\nabla u(P)| = \max_\Omega |\nabla u|, \tag{7}$$

$$v^2(P) \le \frac{1}{2}|v|_{\max}^2, \quad \text{with } |\nabla v(P)| = \max_\Omega |\nabla v|, \tag{8}$$

Inequalities (5), (7) are valid for all eigenfunctions $u_k(x)$ and (6), (8) are valid for all nontrivial eigenfunctions $v_k(x)$. Finally, a new proof of Payne-Weinberger's inequality [5]

$$\mu_1 \ge \left(\frac{\pi}{D}\right)^2 \tag{9}$$

will be provided. Inequality (9) holds for a bounded convex domain $\Omega \subset \mathbb{R}^N$, $n \ge 2$, D is the diameter of Ω. Section 2 of this paper reviews Payne-Stakgold's maximum principle ([4]) which is the main tool of this investigation. The proofs of (5)-(9) are presented in Section 3.

2. PAYNE-STAKGOLD'S MAXIMUM PRINCIPLE

Payne and Stakgold have established the following maximum principle ([4]):

Theorem 2.1. *Let $u(x)$ be an arbitrary eigenfunction of the problem (1) associated to the eigenvalue λ. Assuming Ω bounded convex with a smooth boundary $\partial\Omega$, the auxiliary function*

$$\Psi(x) := |\nabla u|^2 + \lambda u^2 \tag{10}$$

takes its maximum value at a critical point of $u(x)$, i.e. we have

$$|\nabla u|^2 \le \lambda\left\{|u|_{\max}^2 - u^2\right\}, \quad x \in \Omega. \tag{11}$$

Payne and Stakgold have formulated Theorem 2.1 only for the first eigenvalue and eigenfunction, but the result and the proof extends to all (λ_k, u_k). A similar maximum principle holds for all eigenfunctions v_k of the problem (2).

Theorem 2.2. *Let $v(x)$ be an arbitrary eigenfunction of the problem (2) associated to the nontrivial eigenvalue μ. Assuming Ω is bounded and convex with a smooth boundary $\partial\Omega$, the auxiliary function*

$$\Phi(x) := |\nabla v|^2 + \mu v^2, \qquad x \in \Omega, \tag{12}$$

takes its maximum value at a critical point of $v(x)$, i.e. we have

$$|\nabla v|^2 \leq \mu\left\{|v|^2_{\max} - v^2\right\}, \quad x \in \Omega. \tag{13}$$

Proof. : The proof of Theorem 2.2 is similar to that of Theorem 2.1. We have to show that the auxiliary function Φ satisfies the following two conditions

$$\frac{\partial \Phi}{\partial n} \leq 0, \quad x \in \partial\Omega, \tag{14}$$

and

$$\Delta\Phi + |\nabla v|^{-2}\vec{W}\cdot\nabla\Phi \geq 0, \quad x \in \Omega - \omega, \tag{15}$$

where $\bar{W}$ is some regular vector field defined on Ω, and $\omega := \{x \in \Omega |\ \nabla v(x) = 0\}$ is the set of critical points of $v(x)$. The conclusion of Theorem 2.2 is a straightforward consequence of (14), (15), together with Hopf's first ([1], [6]) and second ([2], [6]) principles. The differential inequality (15) is established in [4]. It remains to justify (14). Let $\vec{n} = (n_1, \ldots, n_N)$ be the outward unit normal vector on $\partial\Omega$. Making use of the notation $v_{,k} = \frac{\partial v}{\partial x_k}$, $k = 1, \ldots, N$ and adopting the summation convention on repeated subscripts we compute

$$\frac{\partial \Phi}{\partial n} = \frac{1}{2}\frac{\partial}{\partial n}\left(|\nabla v|^2\right) = v_{,k}v_{,ki}n_i = v_{,k}\left(v_{,i}n_i\right)_{,k} - v_{,k}v_{,i}n_{i,k} \tag{16}$$

with $\frac{\partial v}{\partial n} = v_{,i}n_i$ we have for $x \in \partial\Omega$

$$v_{,k}\left(v_{,i}n_i\right)_{,k} = v_{,k}\left\{n_l\left(n_l\frac{\partial}{\partial x_k} - n_k\frac{\partial}{\partial x_l}\right)\left(\frac{\partial v}{\partial n}\right) + n_l n_k\left(\frac{\partial v}{\partial n}\right)_{,l}\right\} = 0 \tag{17}$$

Note that the first term on the right side of (17) vanishes since it is a linear combination of tangential derivatives of $\frac{\partial v}{\partial n}$. Moreover, we have

$$v_{,i}v_{,k}n_{i,k} = v_{,i}v_{,k}\left\{n_{i,k} - n_{i,j}n_j n_k\right\} = v_{,i}v_{,k}B_{ik}, \tag{18}$$

where

$$B_{ik} := n_{i,k} - n_{i,j}n_j n_k \tag{19}$$

is the curvature matrix associated to $\partial\Omega$. This matrix depends only on the geometry of Ω. If $\partial\Omega$ is represented locally by the equation $\varphi(x) = 0$, then B_{ik} has the form

$$B_{ik} = \frac{\varphi_{,ik}}{|\nabla\varphi|} - \frac{1}{|\nabla\varphi|^3}\{\varphi_{,lk}\varphi_{,l}\varphi_{,i} + \varphi_{,li}\varphi_{,l}\varphi_{,k}\} + \frac{\varphi_{,lj}\varphi_{,l}\varphi_{,j}}{|\nabla\varphi|^5}\varphi_{,i}\varphi_{,k}. \tag{20}$$

This shows that B_{ik} is symmetric. The eigenvalues of B_{ik} are therefore real. Moreover we have $B_{ik}n_i n_k = 0$ so that $\vec{n}$ is an eigenvector associated to the eigenvalue zero. The $N-1$ other eigenvalues $k_1, \ldots, k_{N-1}$ are the principal curvatures of $\partial\Omega$. By the

convexity of Ω we have $k_i \geq 0$ on $\partial\Omega$, $i = 1, \ldots, N-1$. The matrix B_{ik} is therefore positive semi-definite. From this fact together with (16), (17), (18) we obtain

$$\frac{\partial \Phi}{\partial n} = -B_{ik} v_{,i} v_{,k} \leq 0, \quad x \in \partial\Omega. \tag{21}$$

This achieves the proof of Theorem 2.2. ∎

3. APPLICATIONS

1. Integrating (13) over Ω we obtain

$$\int_\Omega |\nabla v|^2 dx + \mu \int_\Omega v^2 dx \leq \mu |\Omega| \, |v|^2_{\max}, \tag{22}$$

where $|\Omega| := \int_\Omega dx$ is the volume of Ω. Dividing (22) by $\int_\Omega v^2 dx$ and noting that $\frac{\int_\Omega |\nabla v|^2 dx}{\int_\Omega v^2 dx} = \mu$, we get

$$|v|^{-2}_{\max} \int_\Omega v^2 dx \leq \frac{1}{2} |\Omega|, \tag{23}$$

in agreement with (6). The proof of (5) is similar.

2. For the proof of (7), (8) we need the following two results of Payne (see [3]).

Theorem 3.1. *Let $u(x)$ be an arbitrary function in $C^2(\Omega)$ with $u = \Delta u = 0$ on a portion γ of $\partial\Omega$ on which the average curvature is positive. Then $|\nabla u|$ takes its maximum value at $P \in \gamma$ if and only if $u \equiv 0$ in Ω.*

Theorem 3.2. *Let $v(x)$ be an arbitrary function in $C^2(\Omega)$ with $\frac{\partial v}{\partial n} = 0$ on a portion γ of $\partial\Omega$ on which the $(N-1)$ principal curvatures k_i are positive.*

Then $|\nabla v|$ takes its maximum value at $P \in \gamma$ if and only if $v \equiv const$ in Ω.

It follows from Theorem 3.1 that each point P at which an eigenfunction $u(x)$ of (1) satisfies $|\nabla u(P)| = |\nabla u|_{\max}$ is an interior point of Ω assumed bounded and convex, so that we must have at P

$$\frac{1}{2}\Big(|\nabla u|^2\Big)_{,k} = u_{,ik} u_{,i} = 0, \quad k = 1, \ldots, N \tag{24}$$

and

$$\frac{1}{2}\Delta\Big(|\nabla u|^2\Big) = u_{,ik} u_{,ik} + 2(\Delta u)_{,k} u_{,k} = u_{,ik} u_{,ik} - \lambda |\nabla u|^2 \leq 0, \tag{25}$$

where λ is the corresponding eigenvalue. With $|\nabla u| \neq 0$ at P, (24) implies

$$\det |u_{,ik}| = 0 \quad \text{at } P \tag{26}$$

In the particular case of a plane domain Ω, (26) leads to

$$u_{,ik} u_{,ik} = (\Delta u)^2 = \lambda^2 u^2 \quad \text{at } P. \tag{27}$$

From (25) and (27) we obtain

$$|\nabla u|^2 \geq \lambda u^2 \ \text{ at } P. \tag{28}$$

Inequalities (11) and (28) lead to

$$2\lambda u^2 \leq |\nabla u|^2 + \lambda u^2 \leq \lambda |u|^2_{\max} \quad \text{at } P, \tag{29}$$

in agreement with (7). The proof of (8) is similar except that we make use of Theorem 3.2 instead of Theorem 3.1.

3. To conclude this section we want to produce another proof of Payne-Weinberger's inequality (9), based on the maximum principle (13). We note that the first nonconstant eigenfunction $v(x)$ of (2) changes sign in Ω. Its nodal set $\Gamma := \{x \in \Omega : v(x) = 0\}$ separates Ω in two subdomains $\Omega_\pm$ with $v > 0$ in Ω_+ and $v < 0$ in Ω_-. Γ has no self intersection and extends up to the boundary $\partial\Omega$. In $\mathbb{R}^2$, Γ is a curve inside Ω joining two distinct boundary points. From Hopf's second principle ([2]. [6]), $|\nabla v|$ does not vanish on Γ, so that the auxiliary function Φ defined by (12) cannot take its maximum value on Γ. Theorem 2.2 is therefore separately applicable on both subdomains $\Omega_\pm$. This lead to the somewhat sharper version of (13)

$$|\nabla v|^2 \leq \begin{cases} \mu\{v^2_{\max} - v^2\}, & x \in \Omega_+, \\ \mu\{v^2_{\min} - v^2\}, & x \in \Omega_-. \end{cases} \tag{30}$$

Let P_+ be a point in $\bar{\Omega}_+$ at which $v(x)$ takes its maximum value , and Q_+ be a point of Γ nearest to P_+. Integrating (30) along the segment $|P_+Q_+|$ located in Ω_+ we obtain

$$\sqrt{\mu}\int_{Q_+}^{P_+} dx = \sqrt{\mu}d_+ \geq \int_0^{v_{\max}} \frac{dv}{\sqrt{v^2_{\max} - v^2}} = \frac{\pi}{2}, \tag{31}$$

where d_+ is the length of $|P_+Q_+| \in \Omega_+$. In the same way we obtain

$$\sqrt{\mu}d_- \geq \frac{\pi}{2}, \tag{32}$$

where d_- is the length of $|P_-Q_-| \in \Omega_-$ joining P_- where $v(x)$ takes its minimum value to the nearest point Q_- of Γ. Adding the inequalities (31) and (32) we obtain

$$\pi \leq \sqrt{\mu}(d_- + d_+) \leq \sqrt{\mu}D \tag{33}$$

where D is the diameter of Ω. This achieves the proof of (9).

Acknowledgments. We would like to thank G. A. Philippin for his encouragement to write this paper.

Research was partially supported by Fund Scientific Research MU13FMI002, Plovdiv University.

References

[1] E. Hopf, *Bemerkung über die Lösung partieller Differentialgleichung zweiter Ordnung von elliptischen Typus*, Sitzungsberichte der preussichen Akademic der Wissenschaften, Berlin, **19**, (1927), 147-152.

[2] E. Hopf, *A remark on elliptic differential equations of the second order*, Proceeding of the AMS, **3**, (1952), 791-793.

[3] L. E. Payne, *Some remarks on maximum principles*, Journal d'Analyse Mathématique, **30**, (1976), 421-433.

[4] L. E. Payne, I. Stakgold, *On the mean value of the fundamental mode in the fixed membrane problem*, Applicable Analysis, **3**, (1973), 295-303.

[5] L. E. Payne , H. F. Weinberger, *An optimal Poincaré inequality for convex domains*, Arch. Rat. Mech. Anal., **5**, (1960), 286-292.

[6] M. H. Protter, H. F. Weinberger, *Maximum principles in differential equations*, Springer Verlag, 1984.

ROMAI J., v.9, no.2(2013), 173–179

THE INTERVAL LATTICE BOLTZMANN METHOD FOR TRANSIENT HEAT TRANSFER IN A SILICON THIN FILM

Alicja Piasecka-Belkhayat, Anna Korczak

Institute of Computational Mechanics and Engineering, Silesian University of Technology, Gliwice, Poland

alicja.piasecka-belkhayat@polsl.pl, anna.korczak@polsl.pl

Abstract In this paper the numerical modelling of heat transfer in a two-dimensional crystalline solid is considered. It is assumed that some parameters (the relaxation time and the boundary conditions) appearing in the mathematical model of the problem analyzed are given as interval numbers. The problem discussed has been solved using the interval form of the lattice Boltzmann method using the rules of the directed interval arithmetic [2].

Keywords: interval lattice Boltzmann method, directed interval arithmetic, heat transport.
2010 MSC: 97U99.

1. INTRODUCTION

Microscale heat transfer is a new field of study which arises from the need to understand the mechanisms of the energy transport in thin films. Microscale heat transfer can be defined as the study of thermal energy transfer with taking into account individual carriers. The classical diffusion-based model for transient heat transfer cannot be used for analyzing small length scale. In semiconductors and dielectric materials, the heat transfer is carried mainly by vibrations in the crystal lattice called phonons. The more common method to analyze this kind of phenomena is the application of the Boltzmann transport equation.

In the mathematical model describing this process some parameters as the relaxation time are estimated experimentally, so it seems natural to take the values of these parameters as interval numbers [5]. This assumption is closer to the real physical conditions of the problem analyzed. In the paper the interval lattice Boltzmann method for solving non-steady transient heat transfer with interval thermophysical parameters has been presented.

2. DIRECTED INTERVAL ARITHMETIC

Let us consider a directed interval $\bar{a}$ which can be defined as a set D of all directed pairs of real numbers defined as

$$\bar{a} = [a^-,\ a^+] := \left\{\bar{a} \in\ D \middle| a^-,\ a^+ \in R\right\}$$

where a^- and a^+ denote the beginning and the end of the interval, respectively. The left or the right endpoint of the interval $\bar{a}$ can be denoted as $a^s,\ \ s \in \{+,\ -\}$, where s is a binary variable. This variable can be expressed as a product of two binary variables and is defined as follows

$$\begin{array}{c} + + = - - = + \\ + - = - + = - \end{array}$$

An interval is called proper if $a^- \leq a^+$, improper if $a^- \geq a^+$ and degenerate if $a^- = a^+$. The set of all directed interval numbers can be written as $D = P \cup I$, where P denotes a set of all directed proper intervals and I denotes a set of all improper intervals. Additionally a subset $Z = Z_P \cup Z_I \in D$ should be defined, where

$$\begin{array}{c} Z_P = \{\bar{a} \in P | a^- \leq 0 \leq a^+\} \\ Z_I = \{\bar{a} \in I | a^+ \leq 0 \leq a^-\} \end{array}$$

For directed interval numbers two binary variables are defined. The first of them is the direction variable

$$\tau(\bar{a}) = \begin{cases} +, & if\ \ a^- \leq a^+ \\ -, & if\ \ a^- > a^+ \end{cases}$$

and the other is the sign variable

$$\sigma(\bar{a}) = \begin{cases} +, & if\ \ a^- > 0,\ a^+ > 0 \\ -, & if\ \ a^- < 0,\ a^+ < 0 \end{cases}, \qquad \bar{a} \in D\backslash Z$$

For zero argument $\sigma([0,\ 0]) = \sigma(0) = +$, for all intervals including the zero element $\bar{a} \in Z$, $\sigma(\bar{a})$ is not defined.

The sum of two directed intervals $\bar{a} = [a^-,\ a^+]$ and $\bar{b} = [b^-,\ b^+]$ can be written as

$$\bar{a} + \bar{b} = [a^- + b^-,\ a^+ + b^+], \quad \bar{a},\ \bar{b} \in D$$

The difference is of the form

$$\bar{a} - \bar{b} = [a^- - b^+,\ a^+ - b^-], \quad \bar{a},\ \bar{b} \in D$$

The product of the directed intervals is described by the formula

$$\bar{a} \cdot \bar{b} = \begin{cases} \left[a^{-\sigma(\bar{b})} \cdot b^{-\sigma(\bar{a})},\ a^{\sigma(\bar{b})} \cdot b^{\sigma(\bar{a})}\right] & \bar{a},\ \bar{b} \in D\backslash Z \\ \left[a^{\sigma(\bar{a})\tau(\bar{b})} \cdot b^{-\sigma(\bar{a})},\ a^{\sigma(\bar{a})\tau(\bar{b})} \cdot b^{\sigma(\bar{a})}\right], & \bar{a} \in D\backslash Z,\ \bar{b} \in Z \\ \left[a^{-\sigma(\bar{b})} \cdot b^{\sigma(\bar{b})\tau(\bar{a})},\ a^{\sigma(\bar{b})} \cdot b^{\sigma(\bar{b})\tau(\bar{a})}\right], & \bar{a} \in Z,\ \bar{b} \in D\backslash Z \\ \left[\min\left(a^- \cdot b^+,\ a^+ \cdot b^-\right),\ \max\left(a^- \cdot b^-,\ a^+ \cdot b^+\right)\right], & \bar{a},\ \bar{b} \in Z_P \\ \left[\max\left(a^- \cdot b^-,\ a^+ \cdot b^+\right),\ \min\left(a^- \cdot b^+,\ a^+ \cdot b^-\right)\right], & \bar{a},\ \bar{b} \in Z_I \\ 0, & \left(\bar{a} \in Z_P,\ \bar{b} \in Z_I\right) \cup \left(\bar{a} \in Z_I,\ \bar{b} \in Z_P\right) \end{cases}$$

The quotient of two directed intervals can be written using the formula

$$\bar{a}/\bar{b} = \begin{cases} \left[a^{-\sigma(\bar{b})}/b^{\sigma(\bar{a})},\ a^{\sigma(\bar{b})}/b^{-\sigma(\bar{a})}\right], & \bar{a},\ \bar{b} \in D\backslash Z \\ \left[a^{-\sigma(\bar{b})}/b^{-\sigma(\bar{b})\tau(\bar{a})},\ a^{\sigma(\bar{b})}/b^{-\sigma(\bar{b})\tau(\bar{a})}\right], & \bar{a} \in Z,\ \bar{b} \in D\backslash Z \end{cases}$$

In the directed interval arithmetic are defined two extra operators, inversion of summation

$$-_D\bar{a} = \left[-a^-,\ -a^+\right], \quad \bar{a} \in D$$

and inversion of multiplication

$$1/_D\bar{a} = \left[1/a^-,\ 1/a^+\right], \quad \bar{a} \in D\backslash Z$$

So, two additional mathematical operations can be defined as follows

$$\bar{a} -_D \bar{b} = \left[a^- - b^-,\ a^+ - b^+\right], \quad \bar{a},\ \bar{b} \in D$$

and

$$\bar{a}/_D\bar{b} = \begin{cases} \left[a^{-\sigma(\bar{b})}/b^{-\sigma(\bar{a})},\ a^{\sigma(\bar{b})}/b^{\sigma(\bar{a})}\right], & \bar{a},\ \bar{b} \in D\backslash Z \\ \left[a^{-\sigma(\bar{b})}/b^{\sigma(\bar{b})},\ a^{\sigma(\bar{b})}/b^{\sigma(\bar{b})}\right], & \bar{a} \in Z,\ \bar{b} \in D\backslash Z \end{cases}$$

Now, it is possible to obtain the number zero by subtraction of two identical intervals $\bar{a} -_D \bar{a} = 0$ and the number one as the result of the division $\bar{a}/_D\bar{a} = 1$, which was impossible when applying classical interval arithmetic [2].

3. THE INTERVAL LATTICE BOLTZMANN METHOD

In dielectric materials and semiconductors the heat transport is mainly realized by quanta of lattice vibrations called phonons. Phonons always ”move” from the part with the higher temperature to the part with the lower temperature. During this process phonons carry energy. This process can be described by the Boltzmann transport equation (BTE)

$$\frac{\partial f}{\partial t} + v \cdot \nabla f = \frac{f^0 - f}{\tau_r} + g_{ef}$$

where f is the phonon distribution function, f^0 is the equilibrium distribution function given by the Bose-Einstein statistic, **v** is the frequency-dependent phonon propagation speed, τ_r is the frequency-dependent phonon relaxation time and g_{ef} is the phonon generation rate due to electron-phonon scattering.

The BTE is one of the fundamental equations of solid state physics. In order to take advantage of the simplifying assumption of the Debye model, the Boltzmann

transport equation can be transformed to an equivalent phonon energy density equation [1]

$$\frac{\partial e}{\partial t} + v \cdot \nabla e = -\frac{e - e^0}{\tau_r} + q_v$$

where e is the phonon energy density, e^0 is the equilibrium phonon energy density and q_v is the internal heat generation rate related to an unit of volume. This equation must be supplemented by the adequate boundary-initial conditions.

The dependence between phonon energy and lattice temperature can be calculated from the following formula using the Debye model

$$e(T) = \left(\frac{9\eta\, k_b}{\Theta_D^3} \int_0^{\Theta_D/T} \frac{z^3}{\exp(z) - 1}\, \mathrm{d}z \right) T^4$$

where Θ_D is the Debye temperature of the solid, k_b is the Boltzmann constant, T is the lattice temperature while η is the number density of oscillators.

The interval lattice Boltzmann method (ILBM) is a discrete representation of the interval Boltzmann transport equation [6]. The ILBM discretizes the space domain considered by defining lattice sites where the phonon energy density is calculated. The lattice is a network of discrete points arranged in a regular mesh with phonons located in lattice sites.

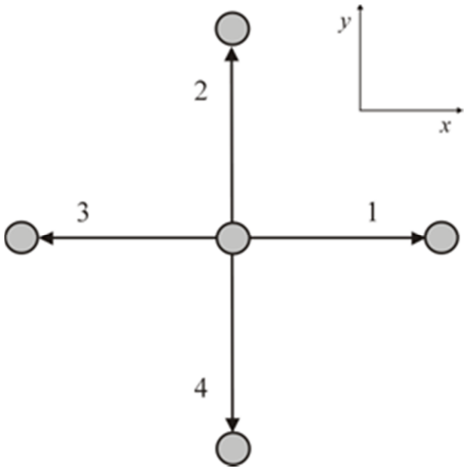

Fig. 1. Two dimensional 4-speed (D2Q4) lattice Boltzmann model

There are a few possibilities for spatial position of the particles. In the paper the D2Q4 lattice, which has two dimensions and four velocities, has been applied. Phonons can travel only to neighboring lattice sites by ballistically travelling with a certain velocity and collide with other phonons residing at these sites (see Fig. 1).

The discrete set of propagation velocities in the main lattice directions can be defined as

$$c_1 = (c, 0) \quad c_2 = (0, c) \quad c_3 = (-c,\ 0) \quad c_4 = (0, -c)$$

In the ILBM it is needed to solve four interval equations supplemented by the boundary and initial conditions allowing to compute interval phonon energy in different lattice nodes. The interval Boltzmann transport equations for a two-dimensional problem take the following form [1, 3, 4]

$$\begin{aligned}
\frac{\partial \bar{e}_1}{\partial t} + c\frac{\partial \bar{e}_1}{\partial x} &= -\frac{\bar{e}_1 - \bar{e}_1^0}{[\tau_r^-,\ \tau_r^+]} + q_v \\
\frac{\partial \bar{e}_2}{\partial t} + c\frac{\partial \bar{e}_2}{\partial y} &= -\frac{\bar{e}_2 - \bar{e}_2^0}{[\tau_r^-,\ \tau_r^+]} + q_v \\
\frac{\partial \bar{e}_3}{\partial t} - c\frac{\partial \bar{e}_3}{\partial x} &= -\frac{\bar{e}_3 - \bar{e}_3^0}{[\tau_r^-,\ \tau_r^+]} + q_v \\
\frac{\partial \bar{e}_4}{\partial t} - c\frac{\partial \bar{e}_4}{\partial y} &= -\frac{\bar{e}_4 - \bar{e}_4^0}{[\tau_r^-,\ \tau_r^+]} + q_v
\end{aligned}$$

This set of equations must be supplemented by the boundary conditions

$$\begin{cases}
x = 0, \quad 0 \le y \le L: & \overline{e}(0, y, t) = \overline{e}(\overline{T}_{b1}) \\
x = L, \quad 0 \le y \le L: & \overline{e}(L, y, t) = \overline{e}(\overline{T}_{b2}) \\
y = 0, \quad 0 \le x \le L: & \overline{e}(x, 0, t) = \overline{e}(\overline{T}_{b3}) \\
y = L, \quad 0 \le x \le L: & \overline{e}(x, L, t) = \overline{e}(\overline{T}_{b4})
\end{cases}$$

and the initial condition of the following form

$$t = 0: \qquad \bar{e}\,(x,\ y,\ 0) = \bar{e}\,(T_0)$$

where $\bar{T}_{b1} = [T_{b1}^-,\ T_{b1}^+]$, $\bar{T}_{b2} = [T_{b2}^-,\ T_{b2}^+]$, $\bar{T}_{b3} = [T_{b3}^-,\ T_{b3}^+]$ and $\bar{T}_{b4} = [T_{b4}^-,\ T_{b4}^+]$ are the interval boundary temperatures, T_0 is the initial temperature.

The total interval energy density is defined as the sum of discrete interval phonon energy densities in all the lattice directions

$$\bar{e} = \sum_{d=1}^{4} \bar{e}_d$$

After subsequent computations the interval lattice temperature is determined using the formula describing the relation between interval phonon energy and interval lattice temperature

$$\bar{T}^{f+1} = \sqrt[4]{\bar{e}(\bar{T}^f)\,\Theta_D^3 \Big/ \left(9\eta\, k_b \int_0^{\Theta_D/\bar{T}^f} \frac{z^3}{\exp(z) - 1}\, \mathrm{d}z \right)}$$

4. RESULTS OF COMPUTATIONS

As a numerical example the heat transport in a silicon thin film of the dimensions 200 nm × 200 nm has been analyzed. The following input data have been introduced: the relaxation time $\bar{\tau}_r = [6.36675,\ 6.69325]$ ps, the Debye temperature $\Theta_D = 640$ K, the boundary conditions $\bar{T}_{b1} = [780,\ 820]$ K and $\bar{T}_{b2} = \bar{T}_{b3} = \bar{T}_{b4} = [292.5,\ 307.5]$ K, the initial temperature $T_0 = 300$ K. The lattice step $\Delta x = \Delta y = 20$ nm and the time step $\Delta t = 5$ ps have been assumed.
Calculations were carry out at the three internal nodes (40, 20) - 1, (160, 40) - 2 and (100, 100) - 3 (see fig. 2).

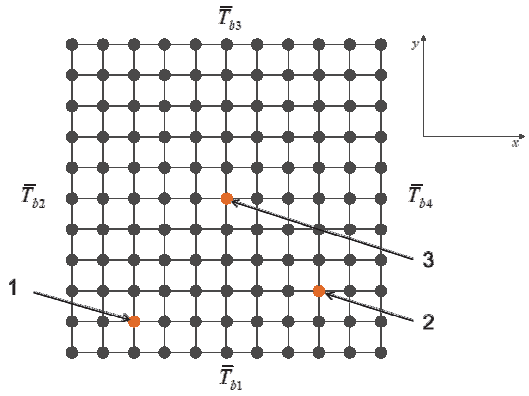

Fig. 2. Discretized domain

Figures 3 and 4 present the courses of the temperature function at chosen internal nodes for the heat source $q_v = 0$ and $q_v = 10^{18}$ W/m^3 respectively.

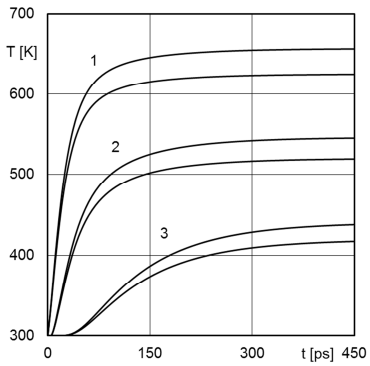

Fig. 3. The interval heating curves for $q_v = 0$

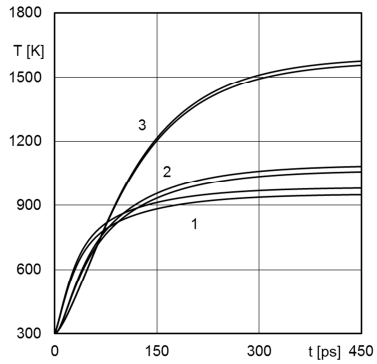

Fig. 4. The interval heating curves for $q_v = 10^{18}\ W/m^3$

5. CONCLUSIONS

The interval lattice Boltzmann method is an effective tool to numerical simulation of the heat transfer in crystalline solids. The generalization of LBM allows one to find the numerical solution in the interval form and such an information may be important especially for the parameters which are estimated experimentally, for example the relaxation time. In the paper the Boltzmann transport equation with the interval values of the relaxation time and the boundary conditions has been considered.

References

[1] R. A. Escobar, S. S. Ghai, M. S. Jhon, C. H. Amon, *Multi-length and time scale thermal transport using the lattice Boltzmann method with application to electronics cooling*, Journal of Heat and Mass Transfer, 49, 2006, 97-107.

[2] S. M. Markov, *On Directed Interval Arithmetic and its Applications*, Journal of Universal Computer Science, Vol. 1, 1995, 514-526.

[3] A. Piasecka Belkhayat, *The interval lattice Boltzmann method for transient heat transport*, Scientific Research of the Institute of Mathematics and Computer Science, 1(8), Czestochowa, 2009, 155-160.

[4] A. Piasecka Belkhayat, A. Korczak, *Modelling of transient heat transport in one-dimensional crystalline solids using the interval lattice Boltzmann method*, 20th International Conference on Computer Methods in Mechanics CMM-2013, Poznan, 2013, MS11-3.

[5] S. Narumanchi, J. Y. Murthy, C. H. Amon, *Simulation of unsteady small heat source effects in sub-micron heat conduction*, Journal of Heat Transfer, 123, 2003, 896-903.

[6] M. Kaviany, A. J. H. McGaughey, *Integration of molecular dynamics simulations and Boltzmann transport equation in phonon thermal conductivity analysis*, IMECE 2003-41899.

ROMAI J., v.9, no.2(2013), 181–195

ABOUT THE MAXIMAL NUMBER OF ALGEBRAICALLY INDEPENDENT LYAPUNOV QUANTITIES FOR THE DIFFERENTIAL SYSTEM $S(1,4)$

Victor Pricop

Institute of Mathematics and Computer Sciences, Academy of Sciences of Moldova

"Ion Creangă" State Pedagogical University, Chişinău, Republica Moldova

pricopvv@gmail.com

Abstract The nonlinear differential system $s(1,4)$ $\dot{x} = P_1(x,y) + P_4(x,y)$, $\dot{y} = Q_1(x,y) + Q_4(x,y)$, is considered, where P_i and Q_i are homogeneous polynomials of degree i ($i \in \{1,4\}$) in x and y. From the paper M. N. Popa, V. V. Pricop *Applications of algebraic methods in solving the center-focus problem*, BASM n.1 (71), 2013 (http://arxiv.org/abs/1310.4343), it is known that the number of algebraically independent Lyapunov quantities in Sibirsky algebra on the Sibirsky invariant variety, which take part in solving the center-focus problem for the differential system $s(1,4)$, does not exceed 13. Using Hilbert series and Sibirsky graded algebras of invariants we obtain that the number of algebraically independent Lyapunov quantities, which take part in solving the center-focus problem for the differential system $s(1,4)$, may not exceed 11.

Keywords: differential systems, the center-focus problem, Lyapunov quantities, Sibirsky graded algebras, Hilbert series, Krull dimension, Lie algebras of operators.

1. INTRODUCTION

Let the differential system $s(1,4)$

$$\begin{aligned} \dot{x} &= cx + dy + gx^4 + 4hx^3y + 6ix^2y^2 + 4jxy^3 + ky^4 \equiv P(x,y), \\ \dot{y} &= ex + fy + lx^4 + 4mx^3y + 6nx^2y^2 + 4oxy^3 + py^4 \equiv Q(x,y), \end{aligned} \tag{1}$$

is given, where variables and coefficients of the right-hand side of the analyzed system take values from the field $\mathbb{R}$ of real numbers.

It is known that if the roots of the characteristic equation of the singular point $O(0,0)$ of the system (1) are imaginary, then the singular point O is either a center (surrounded by closed trajectories) or a focus (surrounded by spirals) [1]. In this case the origin of coordinates is said to be a singular point of the second type.

The center-focus problem for the differential system (1) was examined in [2]-[4] when this system has some special properties.

In the abstact of [5] (CAIM, 2011) there are given some estimations of the number of algebraically independent Lyapunov quantities in Sibirsky algebra on the Sibirsky invariant variety (Remark 1.1), which take part in solving the center-focus problem for the differential system (1), without any restrictions. Further, using the methods of generating functions and Hilbert series for Sibirsky graded algebras of comitants and invariants [6], the results announced in [5] are argued.

It is known from [1] that for the singular point $O(0,0)$ of the system (1) to be a center it is necessary and sufficient that the infinite sequence of polynomials (called Lyapunov quantities)

$$L_1, L_2, ..., L_k, ... \tag{2}$$

that depend on the coefficients of the right-hand side of the system (1) to be equal to zero. Otherwise this point is a focus.

From [6], using Sibirsky graded algebra of comitants and invariants on Sibirsky invariant variety (Remark 1.1), we conclude that the number of algebraically independent Lyapunov quantities from (2), which take part in distinguishing center from focus for the system (1), does not exceed 13.

In what follows we improve this estimation.

Let us examine the Lyapunov function U for the system (1) having the form [6]

$$U(x,y) = k_2 + \sum_{k=3}^{\infty} f_k(x,y), \tag{3}$$

where

$$k_2 = -ex^2 + (c-f)xy + dy^2, \tag{4}$$

is the center-affine (unimodular) comitant [7]–[8] of the system (1), and $f_k(x,y)$ is a homogeneous function of degree k in the phase variables x, y.

Using the comitant (4) and invariants [7] $i_1 = c + f$, $i_2 = c^2 + 2de + f^2$ of the system (1) in [6] is given the next Remark

Remark 1.1. *Note that the set*

$$\mathcal{V} = \{i_1 = c + f = 0,\ Discr(k_2) = 2i_2 - i_1^2 < 0\} \tag{5}$$

is a Sibirsky invariant variety for center and focus for the system (1)*, because the comitant* $k_2 \not\equiv 0$ *from* (4) *through a real center-affine transformation of the plane xOy can be brought to the form*

$$x^2 + y^2, \tag{6}$$

and the system (1) *can be brought to the corresponding form* [5]*, for which the roots of the characteristic equation are imaginary, i. e. the origin of coordinates for this system is a singular point of the second type* (*center or focus*)*.*

Considering the Remark 1.1 we get

Remark 1.2. *Taking into account the comitant k_2 from* (4) *and the fact that its expression through a real center-affine transformation on the invariant variety $\mathcal{V}$ can be brought to the form* (6)*, then formally this variety for the system* (1) *can be written as*

$$\mathcal{V} = \{f = -c\} \cup \{c = 0,\ d = -e = 1\}. \tag{7}$$

Let us consider for the system (1) the identity

$$P(x,y)\frac{\partial U}{\partial x} + Q(x,y)\frac{\partial U}{\partial y} = \sum_{k=1}^{\infty} G_k k_2^{k+1}, \tag{8}$$

where $U(x,y)$ has the form (3).

According to the Remark 1.1 or Remark 1.2 and formulation of the center-focus problem [6] for any polynomial differential system, in particular case for the system (1), we conclude that between L_k from (2) and G_k from (8) the following equalities take place:

$$L_k = G_k|_{\mathcal{V}}\ (k = 1, 2, ...), \tag{9}$$

where $\mathcal{V}$ is from (5).

From the above mentioned follows

Remark 1.3. *The identity* (8) *with the function* (3) *on the variety $\mathcal{V}$ from* (5) *guarantees that the system* (1) *has at the origin of coordinates a singular point of the second type* (*center or focus*)*.*

We write the function (3) as

$$\begin{gathered} U = k_2 + [a_0x^3 + 3a_1x^2y + 3a_2xy^2 + a_3y^3] + [b_0x^4 + 4b_1x^3y + \\ +6b_2x^2y^2 + 4b_3xy^3 + b_4y^4] + [c_0x^5 + 5c_1x^4y + 10c_2x^3y^2 + \\ +10c_3x^2y^3 + 5c_4xy^4 + c_5y^5] + [d_0x^6 + 6d_1x^5y + 15d_2x^4y^2 + \\ +20d_3x^3y^3 + 15d_4x^2y^4 + 6d_5xy^5 + d_6y^6] + [e_0x^7 + 7e_1x^6y + \\ +21e_2x^5y^2 + 35e_3x^4y^3 + 21e_5x^2y^5 + 7e_6xy^6 + e_7y^7] + [f_0x^8 + \\ +8f_1x^7y + 28f_2x^6y^2 + 56f_3x^5y^3 + 70f_4y^4 + 56f_5x^3y^5 + \\ +28f_6x^2y^6 + 8f_7xy^7 + f_8y^8] + ..., \end{gathered} \tag{10}$$

where $k_2 \not\equiv 0$ is from (4) and $a_0, a_1, ..., f_7, f_8, ...$ are unknown constants. Then, taking into account the identity (8) along the trajectories of the system (1) with the function (10), we observe that it splits into a linear system of equations in powers of $x^3, x^2y, xy^2, y^3, ...$ with respect to unknowns $a_0, a_1, ..., f_7, f_8, ..., G_1, G_2, ...$ Note that from the obtained equalities besides x^2, xy, y^2 according to $k_2 \not\equiv 0$ we obtain $i_1 = c + f = 0 \in \mathcal{V}$, which we will call *the null Lyapunov pseudo-quantity*. To determine the quantities G_k we use the matrix form of the system, in which the identity (8) splits in case of the system (1) without taking into account $i_1 = 0 \in \mathcal{V}$. From

this system we obtain that the quantities G_1, G_2 are null. In order to determine the quantity G_3 we use the matrix equation

$$A_3 B_3 = C_3, \tag{11}$$

where $A_3 = [A_3'|A_3''|A_3''']$ and

$$A_3' = \begin{pmatrix} 5c & 5e & 0 & 0 & 0 & 0 & 0 \\ 5d & 20c+5f & 20e & 0 & 0 & 0 & 0 \\ 0 & 20d & 30c+20f & 30e & 0 & 0 & 0 \\ 0 & 0 & 30d & 20c+30f & 20e & 0 & 0 \\ 0 & 0 & 0 & 20d & 5c+20f & 5e & 0 \\ 0 & 0 & 0 & 0 & 5d & 5f & 0 \\ 5g & 5l & 0 & 0 & 0 & 0 & 8c \\ 20h & 20g+20m & 20l & 0 & 0 & 0 & 8d \\ 30i & 80h+30n & 30g+80m & 30l & 0 & 0 & 0 \\ 20j & 120i+20o & 120h+120n & 20g+120m & 20l & 0 & 0 \\ 5k & 80j+5p & 180i+80o & 80h+180n & 5g+80m & 5l & 0 \\ 0 & 20k & 120j+20p & 120i+120o & 20h+120n & 20m & 0 \\ 0 & 0 & 30k & 80j+30p & 30i+80o & 30n & 0 \\ 0 & 0 & 0 & 20k & 20j+20p & 20o & 0 \\ 0 & 0 & 0 & 0 & 5k & 5p & 0 \end{pmatrix}$$

$$A_3'' = \begin{pmatrix} 0 & 0 & 0 & 0 & 0 & 0 \\ 0 & 0 & 0 & 0 & 0 & 0 \\ 0 & 0 & 0 & 0 & 0 & 0 \\ 0 & 0 & 0 & 0 & 0 & 0 \\ 0 & 0 & 0 & 0 & 0 & 0 \\ 0 & 0 & 0 & 0 & 0 & 0 \\ 8e & 0 & 0 & 0 & 0 & 0 \\ 56c+8f & 56e & 0 & 0 & 0 & 0 \\ 56d & 168c+56f & 168e & 0 & 0 & 0 \\ 0 & 168d & 280c+168f & 280e & 0 & 0 \\ 0 & 0 & 280d & 280c+280f & 280e & 0 \\ 0 & 0 & 0 & 280d & 168c+280f & 168e \\ 0 & 0 & 0 & 0 & 168d & 56c+168f \\ 0 & 0 & 0 & 0 & 0 & 56d \\ 0 & 0 & 0 & 0 & 0 & 0 \end{pmatrix}$$

$$A_3''' = \begin{pmatrix} 0 & 0 & 0 \\ 0 & 0 & 0 \\ 0 & 0 & 0 \\ 0 & 0 & 0 \\ 0 & 0 & 0 \\ 0 & 0 & 0 \\ 0 & 0 & -e^4 \\ 0 & 0 & 4ce^3 - 4e^3 f \\ 0 & 0 & -6c^2e^2 + 4de^3 + 12ce^2 f - 6e^2 f^2 \\ 0 & 0 & 4c^3 e - 12cde^2 - 12c^2 ef + 12de^2 f + 12cef^2 - 4ef^3 \\ 0 & 0 & -c^4 + 12c^2 de - 6d^2 e^2 + 4c^3 f - 24cdef - 6c^2 f^2 + 12def^2 + 4cf^3 - f^4 \\ 0 & 0 & -4c^3 d + 12cd^2 e + 12c^2 df - 12d^2 ef - 12cdf^2 + 4df^3 \\ 56e & 0 & -6c^2 d^2 + 4d^3 e + 12cd^2 f - 6d^2 f^2 \\ 8c+56f & 8e & -4cd^3 + 4d^3 f \\ 8d & 8f & -d^4 \end{pmatrix}$$

and

$$B_3 = \begin{pmatrix} c_0 \\ c_1 \\ c_2 \\ c_3 \\ c_4 \\ c_5 \\ f_0 \\ f_1 \\ f_2 \\ f_3 \\ f_4 \\ f_5 \\ f_6 \\ f_7 \\ f_8 \\ G_3 \end{pmatrix}, \quad C_3 = \begin{pmatrix} 2eg - cl + fl \\ -cg + fg + 8eh - 2dl - 4cm + 4fm \\ -4ch + 4fh + 12ei - 8dm - 6cn + 6fn \\ -6ci + 6fi + 8ej - 12dn - 4co + 4fo \\ -4cj + 4fj + 2ek - 8do - cp + fp \\ -ck + fk - 2dp \\ 0 \\ 0 \\ 0 \\ 0 \\ 0 \\ 0 \\ 0 \\ 0 \end{pmatrix} \tag{12}$$

Because the dimension of the matrix A_3 is 15×16, it is obvious we have at least one free parameter. Therefore, choosing f_i ($i \in \{0, 1, ..., 8\}$) as a free parameter with the help of Cramer's rule, from the system (11) for each fixed i we obtain

$$G_3 = \frac{G_{3,i} + F_{3,i} f_i}{\sigma_{3,i}}, \tag{13}$$

where $G_{3,i}, F_{3,i}, \sigma_{3,i}$ are polynomials in the coefficients of the system (1), and f_i are undetermined coefficients of the function $U(x, y)$ from (10).

Studying the matrices (12) of the system (11) we conclude that $G_{3,i}$ from (13) are homogeneous polynomials of degree 14 with respect to the coefficients of linear part, and of degree 2 with respect to the coefficients of nonhomogeneities of degree 4 of the system (1).

Since $G_{3,i}$ from (13) are homogeneous polynomials with respect to the coefficients of the system (1), then according to [10],[11] for $i = \overline{0,8}$ we can determine the corresponding isobarities

$$(7, -1),\ (6, 0),\ (5, 1),\ (4, 2),\ (3, 3),\ (2, 4),\ (1, 5),\ (0, 6),\ (-1, 7)$$

For the system (1), using the formula of comitant's weight from the theory of invariants of differential systems [8],[10], we obtain that the numerators of the fractions (13) can be coefficients in comitants of weight -1 of the type $(4, 14, 2)$. Using the Lie differential operator D_3 from (17) for the system (1), taking into account [6],[10] and the numerator of the fraction (13), we obtain the system of 8 linear homogeneous differential equations equations

$$\begin{aligned} &D_3(G_{3,0} + F_{3,0} f_0) = G_{3,1} + F_{3,1} f_1,\ D_3(G_{3,1} + F_{3,1} f_1) = -G_{3,2} - F_{3,2} f_2, \\ &-D_3(G_{3,2} + F_{3,2} f_2) = G_{3,3} + F_{3,3} f_3,\ D_3(G_{3,3} + F_{3,3} f_3) = -G_{3,4} - F_{3,4} f_4 \\ &-D_3(G_{3,4} + F_{3,4} f_4) = G_{3,5} + F_{3,5} f_5,\ D_3(G_{3,5} + F_{3,5} f_5) = -G_{3,6} - F_{3,6} f_6 \\ &-D_3(G_{3,6} + F_{3,6} f_6) = G_{3,7} + F_{3,7} f_7,\ D_3(G_{3,7} + F_{3,7} f_7) = -G_{3,8} - F_{3,8} f_8 \end{aligned} \tag{14}$$

with respect to nine unknowns $f_0, f_1, ..., f_8$. Note that a particular solution of this system is $f_0 = f_1 = ... = f_8 = 0$, for which the polynomial

$$f_8'(x,y) = G_{3,0}x^8 - 8G_{3,1}x^7y - 4G_{3,2}x^6y^2 + 8G_{3,3}x^5y^3 + 2G_{3,4}x^4y^4 - \\ -8G_{3,5}x^3y^5 - 4G_{3,6}x^2y^6 + 8G_{3,7}xy^7 + G_{3,8}y^8 \tag{15}$$

is a center-affine comitant of the system (9). This fact is confirmed by the Theorem 1 [6] using the operators

$$X_1 = x\frac{\partial}{\partial x} + D_1,\ X_2 = y\frac{\partial}{\partial x} + D_2,\ X_3 = x\frac{\partial}{\partial y} + D_3,\ X_4 = y\frac{\partial}{\partial y} + D_4, \tag{16}$$

where

$$\begin{aligned}
D_1 &= d\frac{\partial}{\partial d} - e\frac{\partial}{\partial e} - 3g\frac{\partial}{\partial g} - 2h\frac{\partial}{\partial h} - i\frac{\partial}{\partial i} + k\frac{\partial}{\partial k} - 4l\frac{\partial}{\partial l} - 3m\frac{\partial}{\partial m} - \\
&\quad -2n\frac{\partial}{\partial n} - o\frac{\partial}{\partial o}, \\
D_2 &= e\frac{\partial}{\partial c} + (f-c)\frac{\partial}{\partial d} - e\frac{\partial}{\partial f} + l\frac{\partial}{\partial g} + (m-g)\frac{\partial}{\partial h} + (n-2h)\frac{\partial}{\partial i} + \\
&\quad +(o-3i)\frac{\partial}{\partial j} + (p-4j)\frac{\partial}{\partial k} - l\frac{\partial}{\partial m} - 2m\frac{\partial}{\partial n} - 3n\frac{\partial}{\partial o} - 4o\frac{\partial}{\partial p}, \\
D_3 &= -d\frac{\partial}{\partial c} + (c-f)\frac{\partial}{\partial e} + d\frac{\partial}{\partial f} - 4h\frac{\partial}{\partial g} - 3i\frac{\partial}{\partial h} - 2j\frac{\partial}{\partial i} - k\frac{\partial}{\partial j} + \\
&\quad +(g-4m)\frac{\partial}{\partial l} + (h-3n)\frac{\partial}{\partial m} + (i-2o)\frac{\partial}{\partial n} + (j-p)\frac{\partial}{\partial o} + k\frac{\partial}{\partial p}, \\
D_4 &= -d\frac{\partial}{\partial d} + e\frac{\partial}{\partial e} - h\frac{\partial}{\partial h} - 2i\frac{\partial}{\partial i} - 3j\frac{\partial}{\partial j} - 4k\frac{\partial}{\partial k} + l\frac{\partial}{\partial l} - n\frac{\partial}{\partial n} - \\
&\quad -2o\frac{\partial}{\partial o} - 3p\frac{\partial}{\partial p},
\end{aligned} \tag{17}$$

which in case of the system (1) can be written as

$$X_1(f_8') = X_4(f_8') = f_8',\ X_2(f_8') = X_3(f_8') = 0.$$

It is obvious that the differential system (14) has an infinity of solutions $f_0, f_1, ..., f_8$ that define a center-affine comitants of the type (15).

According to the above mentioned and following [6] we obtain that these comitants, and in particular case (15), belongs to the linear space $S_{1,4}^{(4,14,2)}$.

Note that the comitant (15) on the variety $\mathcal{V}$ from (5) for the system (1) has the following form:

$$f_8'(x,y)|_{\mathcal{V}} = 648L_1(x^2+y^2)^4, \tag{18}$$

where

$$L_1 = 7gh + 18hi + 3gj + 18ij + 3hk + 7jk - 7gl - 3il - 8hm - 7lm -$$
$$-3gn + 3kn - 18mn + 8jo - 3lo - 18no + 3ip + 7kp - 3mp - 7op,$$

is the first non-zero Lyapunov quantity of the system (1) on the invariant variety $\mathcal{V}$.

Similarly to the previous case, for the non-zero quantities G_n ($n = 3k$) of the differential system $s(1,4)$ we obtain

$$G_{3k} = \frac{G_{3k,i_1,i_2,\ldots,i_k} + B_{3k,i_1,i_2,\ldots,i_k} b_{i_1} + \cdots + Z_{3k,i_1,i_2,\ldots,i_k} z_{i_k}}{\sigma_{3k,i_1,i_2,\ldots,i_k}}. \tag{19}$$

Now it is important to determine degree of the polynomial $G_{3k,i_1,i_2,\ldots,i_k}$ in coefficients of the system (1). It has been found that a comitant of weight -1 of the system $s(1,4)$ from (1), containing as a semi-invariant (the coefficient of the highest degree of x) the expression $G_{3k,i_1,i_2,\ldots,i_k}$, which corresponds to the quantity G_{3k}($G_n = 0$ if $n \neq 3k$), has the type

$$\left(2(k+1), \frac{1}{2}(15k^2 + 11k + 2), 2k\right), \tag{20}$$

where $2(k+1)$ is degree of homogeneity of the comitant in the phase variables x, y, $\frac{1}{2}(15k^2 + 11k + 2)$ is degree of homogeneity of the comitant in coefficients of the linear part, $2k$ is degree of homogeneity of the comitant in coefficients of nonhomogeneities of degree 4 of the system $s(1,4)$ from (1).

Hereafter the expressions $G_{3k,i_1,i_2,\ldots,i_k}$, which determine the types of comitants (20) corresponding to the quantity G_{3k} ($k = 1, 2, 3, \ldots$) will be called *generalized Lyapunov pseudo-quantities*. The comitants of the type (20) for $k = 1, 2, 3, \ldots$, which contain as coefficients expressions with the generalized Lyapunov pseudo-quantities

$$G_{3k,i_1,i_2,\ldots,i_k} + B_{3k,i_1,i_2,\ldots,i_k} b_{i_1} + \cdots + Z_{3k,i_1,i_2,\ldots,i_k} z_{i_k}.$$

will be called *comitants associated to the generalized Lyapunov pseudo-quantities*.

2. GRADED ALGEBRAS OF COMITANTS WHOSE SPACES CONTAIN COMITANTS ASSOCIATED TO THE GENERALIZED LYAPUNOV PSEUDO-QUANTITIES OF THE SYSTEM (1)

Thus for the system (1) we obtain the set of spaces of center-affine (unimodular) comitants

$$\mathbb{R} = S_{1,4}^{(0,0,0)},\ S_{1,4}^{(0,1,0)},\ S_{1,4}^{(4,14,2)},\ S_{1,4}^{(6,42,4)}, \ldots, S_{1,4}^{(2(k+1),\frac{1}{2}(15k^2+11k+2),2k)}, \ldots \subset S_{1,4}, \tag{21}$$

where $S_{1,4}$ is a Sibirsky graded algebra of comitants and invariants of the system (1).

Let consider the graded algebra $S'_{1,4}$, generated by the spaces $S_{1,4}^{(\delta',d'_1,d'_2)}$ from (21), which can be written as

$$S'_{1,4} = \bigoplus_{(d')} S_{1,4}^{(d')}. \tag{22}$$

Denote by $S_{1,4}^{(d')}$ the linear spaces, contained in $S_{1,4}^{(\delta',d'_1,d'_2)}$ for all (d'), as well as the spaces from $S_{1,4}$ which contain all possible products of the spaces (21).

Since the algebra $S'_{1,4}$ is a graded subalgebra of the algebra $S_{1,4}$ for the system (1) we obtain that for the Krull dimensions of these algebras the following inequality takes place:

$$\varrho(S'_{1,4}) \leq \varrho(S_{1,4}). \tag{23}$$

Taking into account this inequality, and that $\varrho(S_{1,4}) = 13$, we have

Lemma 2.1. *The maximal number of algebraically independent generalized Lyapunov pseudo-quantities in the center-focus problem for the system* (1) *does not exceed* 13.

Following [6], according to the equality (9) and the conclusion that the number of algebraically independent Lyapunov quantities L_k ($k = \overline{0,\infty}$) in Sibirsky algebra on the variety $\mathcal{V}$ can not exceed the maximal number of algebraically independent generalized Lyapunov in this algebra, using Lemma 2.1, we obtain

Theorem 2.1. *The maximal number of algebraically independent Lyapunov quantities of the system* (1) *in Sibirsky algebra on the variety* $\mathcal{V}$ *from* (5) *or, equivalently, from* (7)*, which take part in solving the center-focus problem does not exceed* 13.

Noting the argument from [6] can be formulated

Hypothesis. *The number of essential conditions for center, which solve the center-focus problem for the system* (1)*, having at the origin of coordinates a singular point of the second type, does not exceed* 13.

3. HILBERT SERIES AND KRULL DIMENSION FOR THE ALGEBRAS $S_{1,4}$ AND $SI_{1,4}$

Let V is a vector space, which can be represented in the form of direct sum of finite dimensional subspaces

$$V = \bigoplus_{n=0}^{\infty} V_n,\ V_n \bigcap_{(n\neq m)} V_m = \{0\}.$$

Such a decomposition we call *graduation*. The formal series

$$\Phi_V(t) = \sum_{n=0}^{\infty} (dim_{\mathbb{R}} V_n) t^n \tag{24}$$

will be called *generating function* for V or of sequence $dim_{\mathbb{R}} V_n$ $(n = 0, 1, 2, 3, ...)$.

In case when $V = A$ is a graded algebra, (24) is called Hilbert series of this algebra denoted by $H_A(t)$, which contains a consistent information about the asymptotic character of the algebra A.

In studying of the space V or the algebra A, in some cases can be introduced generating functions or Hilbert series, which depend on several variables. This reflects a more detailed graduation of these objects. In consequence these functions are called *generalized* generating function or generalized Hilbert series, but those of type (24) are called *common*.

According to [8] $S_{1,4}$ ($SI_{1,4}$) is a Sibirsky graded algebra of comitants (invariants) of the system (1), where $SI_{1,4} \subset S_{1,4}$.

The graded algebra $S_{1,4}$ will be written as

$$S_{1,4} = \bigoplus_{(d)} S_{1,4}^{(d)} \ (d \geq 0),$$

where $(d) = (\delta, d_1, d_2)$ is the type of comitants which belong to the space $S_{1,4}^{(d)}$ and have degree δ with respect to the phase variables, degree d_1 with respect to coefficients of the linear part, and degree d_2 with respect to coefficients of nonhomogeneities of degree 4 of the system (1), and $S_{1,4}^{(0)} = \mathbb{R}$.

It is known [8] that $dim_{\mathbb{R}} S_{1,4}^{(d)} < \infty$ for all (d).

The sequence that appears here $\{dim_{\mathbb{R}} S_{1,4}^{(d)}\}$ and the corresponding generalized Hilbert series [8] is

$$H(S_{1,4}, u, b, e) = \sum_{(d)} dim_{\mathbb{R}} S_{1,4}^{(d)} u^{\delta} b^{d_1} e^{d_2}, \tag{25}$$

where $dim_{\mathbb{R}} S_{1,4}^{(0)} = 1$.

The common Hilbert series is obtained from the generalized Hilbert series as follows

$$H_{S_{1,4}}(u) = H(S_{1,4}, u, u, u). \tag{26}$$

Remark 3.1. *The generalized* (*respectively common*) *Hilbert series for the algebra of invariants* $SI_{1,4} \subset S_{1,4}$ *of the system* (1) *is obtained formally from* (25) *for* $u = 0$ (*respectively* $b = e = t$).

Remark 3.2. *Note that the Krull dimension* $\varrho(S_{1,4})$ (*respectively* $\varrho(SI_{1,4})$) *is equal to the maximal number of algebraically independent elements in* $S_{1,4}$ (*respectively* $SI_{1,4}$), *and also is equal to the multiplicity of the pole of the common Hilbert series at the unit.*

Hereafter we need the generalized Hilbert series of the algebras $S_{1,4}$ and $SI_{1,4}$, and the common Hilbert series of the algebra $SI_{1,4}$.

In [9] there is demonstrated

Theorem 3.1. *The generalized Hilbert series of the Sibirsky graded algebra $S_{1,4}$ for the system* (1) *is a rational function of $u,\ b,\ e$, having the following form*

$$H(S_{1,4}, u, b, e) = \frac{N_{1,4}(u, b, e)}{D_{1,4}(u, b, e)}, \tag{27}$$

where

$$\begin{aligned} D_{1,4}(u, b, e) = (1-b)(1-b^2)(1-bu^2)(1-be^2)^2(1-b^3e^2)^2(1-b^5e^2)(1-e^4)^2\cdot \\ \cdot(1-e^2)(1-e^6)^2(1-e^8)^2(1-eu)^2(1-eu^3)^2(1-eu^5), \end{aligned} \tag{28}$$

$$N_{1,4}(u, b, e) = \sum_{k=0}^{13} R_k(b, e)u^k, \tag{29}$$

$R_i(b, e)$ $(i = \overline{0, 13})$ *are from* [9].

From the equalities (25)–(29) and Remark 3.1 we obtain

Corollary 3.1. *The common Hilbert series for the Sibirsky graded algebra of invariants $SI_{1,4}$ for the system* (1) *has the following form*

$$H_{SI_{1,4}}(t) = \frac{N_{1,4}(t)}{D_{1,4}(t)}, \tag{30}$$

where

$$\begin{aligned} D_{1,4}(t) = (1-t^3)(1-t^4)^3(1-t^5)^2(1-t^6)^2(1-t^7)(1-t^8)^2, \\ N_{1,4}(t) = 1 + t + t^2 + 3t^3 + 8t^4 + 15t^5 + 32t^6 + 67t^7 + 129t^8 + 217t^9 + \\ +355t^{10} + 546t^{11} + 812t^{12} + 1122t^{13} + 1511t^{14} + 1948t^{15} + 2447t^{16} + \\ +2923t^{17} + 3410t^{18} + 3827t^{19} + 4183t^{20} + 4375t^{21} + 4461t^{22} + 4375t^{23} + \\ +4183t^{24} + 3827t^{25} + 3410t^{26} + 2923t^{27} + 2447t^{28} + 1948t^{29} + 1511t^{30} + \\ +1122t^{31} + 812t^{32} + 546t^{33} + 355t^{34} + 217t^{35} + 129t^{36} + 67t^{37} + 32t^{38} + \\ +15t^{39} + 8t^{40} + 3t^{41} + t^{42} + t^{43} + t^{44}. \end{aligned} \tag{31}$$

Theorem 3.2. *The Krull dimension $\varrho(SI_{1,4})$ of the Sibirsky graded algebra of invariants $SI_{1,4}$ is equal to* 11*, i. e. $\varrho(SI_{1,4}) = 11$.*

Write the graded decomposition of the space $V_{1,4}$, which consists of the spaces (21)

$$V_{1,4} = S_{1,4}^{(0,0,0)} \bigoplus S_{1,4}^{(0,1,0)} \bigoplus_{k=1}^{\infty} S_{1,4}^{(2(k+1),\frac{1}{2}(15k^2+11k+2),2k)}. \tag{32}$$

The generalized generating function of the space (32) can be written in the following form:

$$\Phi(S_{1,4},u,b,e)=dim_{\mathbb{R}}S_{1,4}^{(0,0,0)}+dim_{\mathbb{R}}S_{1,4}^{(0,1,0)}b+ \\ +\sum_{k=1}^{\infty}dim_{\mathbb{R}}S_{1,4}^{(2(k+1),\frac{1}{2}(15k^2+11k+2),2k)}u^{2(k+1)}b^{\frac{1}{2}(15k^2+11k+2)}e^{2k}. \tag{33}$$

Using the computer, expand the Hilbert series $H(S_{1,4},u,b,e)$ [9] in a power series and have for (33)

$$\Phi(V_{1,4},u,b,e)=1+b+153u^4b^{14}e^2+4589u^6b^{42}e^4+ \\ +49632u^8b^{85}e^6+...+ \\ +C_{2(k+1),\frac{1}{2}(15k^2+11k+2),2k}u^{2(k+1)}b^{\frac{1}{2}(15k^2+11k+2)}e^{2k}+..., \tag{34}$$

where $C_{2(k+1),\frac{1}{2}(15k^2+11k+2),2k}$ is undetermined coefficient.

Using this generalized generating function and Hilbert series $H(S_{1,4},u,b,e)$ from Theorem 3.1, the first terms until $u^8b^{85}e^6$ of the Hilbert series $H(S'_{1,4},u,b,e)$ were built

$$H(S'_{1,4},u,b,e)=1+b+2b^2+2b^3+3b^4+3b^5+4b^6+4b^7+5b^8+ \\ +5b^9+6b^{10}+6b^{11}+7b^{12}+7b^{13}+8b^{14}+8b^{15}+9b^{16}+9b^{17}+ \\ +10b^{18}+10b^{19}+11b^{20}+11b^{21}+12b^{22}+12b^{23}+13b^{24}+13b^{25}+ \\ +14b^{26}+14b^{27}+15b^{28}+15b^{29}+16b^{30}+16b^{31}+17b^{32}+17b^{33}+ \\ +18b^{34}+18b^{35}+19b^{36}+19b^{37}+20b^{38}+20b^{39}+21b^{40}+21b^{41}+ \\ +22b^{42}+22b^{43}+23b^{44}+23b^{45}+24b^{46}+24b^{47}+25b^{48}+25b^{49}+ \\ +26b^{50}+26b^{51}+27b^{52}+27b^{53}+28b^{54}+28b^{55}+29b^{56}+29b^{57}+ \\ +30b^{58}+30b^{59}+31b^{60}+31b^{61}+32b^{62}+32b^{63}+33b^{64}+33b^{65}+ \\ +34b^{66}+34b^{67}+35b^{68}+35b^{69}+36b^{70}+36b^{71}+37b^{72}+37b^{73}+ \\ +38b^{74}+38b^{75}+39b^{76}+39b^{77}+40b^{78}+40b^{79}+41b^{80}+41b^{81}+ \\ +42b^{82}+42b^{83}+43b^{84}+43b^{85}+242b^{14}e^2u^4+264b^{15}e^2u^4+ \\ +281b^{16}e^2u^4+303b^{17}e^2u^4+320b^{18}e^2u^4+342b^{19}e^2u^4+359b^{20}e^2u^4+ \\ +381b^{21}e^2u^4+398b^{22}e^2u^4+420b^{23}e^2u^4+437b^{24}e^2u^4+459b^{25}e^2u^4+ \\ +476b^{26}e^2u^4+498b^{27}e^2u^4+515b^{28}e^2u^4+537b^{29}e^2u^4+554b^{30}e^2u^4+$$

$$+576b^{31}e^2u^4 + 593b^{32}e^2u^4 + 615b^{33}e^2u^4 + 632b^{34}e^2u^4 + 654b^{35}e^2u^4+$$
$$+671b^{36}e^2u^4 + 693b^{37}e^2u^4 + 710b^{38}e^2u^4 + 732b^{39}e^2u^4 + 749b^{40}e^2u^4+$$
$$+771b^{41}e^2u^4 + 788b^{42}e^2u^4 + 810b^{43}e^2u^4 + 827b^{44}e^2u^4 + 849b^{45}e^2u^4+$$
$$+866b^{46}e^2u^4 + 888b^{47}e^2u^4 + 905b^{48}e^2u^4 + 927b^{49}e^2u^4 + 944b^{50}e^2u^4+$$
$$+966b^{51}e^2u^4 + 983b^{52}e^2u^4 + 1005b^{53}e^2u^4 + 1022b^{54}e^2u^4+$$
$$+1044b^{55}e^2u^4 + 1061b^{56}e^2u^4 + 1083b^{57}e^2u^4 + 1100b^{58}e^2u^4+$$
$$+1122b^{59}e^2u^4 + 1139b^{60}e^2u^4 + 1161b^{61}e^2u^4 + 1178b^{62}e^2u^4+$$
$$+1200b^{63}e^2u^4 + 1217b^{64}e^2u^4 + 1239b^{65}e^2u^4 + 1256b^{66}e^2u^4+$$
$$+1278b^{67}e^2u^4 + 1295b^{68}e^2u^4 + 1317b^{69}e^2u^4 + 1334b^{70}e^2u^4+$$
$$+1356b^{71}e^2u^4 + 1373b^{72}e^2u^4 + 1395b^{73}e^2u^4 + 1412b^{74}e^2u^4+$$
$$+1434b^{75}e^2u^4 + 1451b^{76}e^2u^4 + 1473b^{77}e^2u^4 + 1490b^{78}e^2u^4+$$
$$+1512b^{79}e^2u^4 + 1529b^{80}e^2u^4 + 1551b^{81}e^2u^4 + 1568b^{82}e^2u^4+$$
$$+1590b^{83}e^2u^4 + 1607b^{84}e^2u^4 + 1629b^{85}e^2u^4 + 9591b^{42}e^4u^6+$$
$$+9845b^{43}e^4u^6 + 10084b^{44}e^4u^6 + 10338b^{45}e^4u^6 + 10577b^{46}e^4u^6+$$
$$+10831b^{47}e^4u^6 + 11070b^{48}e^4u^6 + 11324b^{49}e^4u^6 + 11563b^{50}e^4u^6+$$
$$+11817b^{51}e^4u^6 + 12056b^{52}e^4u^6 + 12310b^{53}e^4u^6 + 12549b^{54}e^4u^6+$$
$$+12803b^{55}e^4u^6 + 13042b^{56}e^4u^6 + 13296b^{57}e^4u^6 + 13535b^{58}e^4u^6+$$
$$+13789b^{59}e^4u^6 + 14028b^{60}e^4u^6 + 14282b^{61}e^4u^6 + 14521b^{62}e^4u^6+$$
$$+14775b^{63}e^4u^6 + 15014b^{64}e^4u^6 + 15268b^{65}e^4u^6 + 15507b^{66}e^4u^6+$$
$$+15761b^{67}e^4u^6 + 16000b^{68}e^4u^6 + 16254b^{69}e^4u^6 + 16493b^{70}e^4u^6+$$
$$+16747b^{71}e^4u^6 + 16986b^{72}e^4u^6 + 17240b^{73}e^4u^6 + 17479b^{74}e^4u^6+$$
$$+17733b^{75}e^4u^6 + 17972b^{76}e^4u^6 + 18226b^{77}e^4u^6 + 18465b^{78}e^4u^6+$$
$$+18719b^{79}e^4u^6 + 18958b^{80}e^4u^6 + 19212b^{81}e^4u^6 + 19451b^{82}e^4u^6+$$
$$+19705b^{83}e^4u^6 + 19944b^{84}e^4u^6 + 20198b^{85}e^4u^6 + 7110b^{28}e^4u^8+$$
$$+7393b^{29}e^4u^8 + 7691b^{30}e^4u^8 + 7974b^{31}e^4u^8 + 8272b^{32}e^4u^8+$$
$$+8555b^{33}e^4u^8 + 8853b^{34}e^4u^8 + 9136b^{35}e^4u^8 + 9434b^{36}e^4u^8+$$
$$+9717b^{37}e^4u^8 + 10015b^{38}e^4u^8 + 10298b^{39}e^4u^8 + 10596b^{40}e^4u^8+$$
$$+10879b^{41}e^4u^8 + 11177b^{42}e^4u^8 + 11460b^{43}e^4u^8 + 11758b^{44}e^4u^8+$$
$$+12041b^{45}e^4u^8 + 12339b^{46}e^4u^8 + 12622b^{47}e^4u^8 + 12920b^{48}e^4u^8+$$
$$+13203b^{49}e^4u^8 + 13501b^{50}e^4u^8 + 13784b^{51}e^4u^8 + 14082b^{52}e^4u^8+$$
$$+14365b^{53}e^4u^8 + 14663b^{54}e^4u^8 + 14946b^{55}e^4u^8 + 15244b^{56}e^4u^8+$$
$$+15527b^{57}e^4u^8 + 15825b^{58}e^4u^8 + 16108b^{59}e^4u^8 + 16406b^{60}e^4u^8+$$
$$+16689b^{61}e^4u^8 + 16987b^{62}e^4u^8 + 17270b^{63}e^4u^8 + 17568b^{64}e^4u^8+$$
$$+17851b^{65}e^4u^8 + 18149b^{66}e^4u^8 + 18432b^{67}e^4u^8 + 18730b^{68}e^4u^8+$$

$$+19013b^{69}e^4u^8 + 19311b^{70}e^4u^8 + 19594b^{71}e^4u^8 + 19892b^{72}e^4u^8+$$
$$20175b^{73}e^4u^8 + 20473b^{74}e^4u^8 + 20756b^{75}e^4u^8 + 21054b^{76}e^4u^8+$$
$$+21337b^{77}e^4u^8 + 21635b^{78}e^4u^8 + 21918b^{79}e^4u^8 + 22216b^{80}e^4u^8+$$
$$+22499b^{81}e^4u^8 + 22797b^{82}e^4u^8 + 23080b^{83}e^4u^8 + 23378b^{84}e^4u^8+$$
$$+23661b^{85}e^4u^8 + 137561b^{85}e^6u^8 + ...$$

From here we obtain that the first 100 terms of the common Hilbert series $H_{S'_{1,4}}(t)$ will be written as

$$H_{S'_{1,4}}(t) = 1 + t + 2t^2 + 2t^3 + 3t^4 + 3t^5 + 4t^6 + 4t^7 + 5t^8 + 5t^9+$$
$$+6t^{10} + 6t^{11} + 7t^{12} + 7t^{13} + 8t^{14} + 8t^{15} + 9t^{16} + 9t^{17} + 10t^{18}+$$
$$+10t^{19} + 253t^{20} + 275t^{21} + 293t^{22} + 315t^{23} + 333t^{24} + 355t^{25}+$$
$$+373t^{26} + 395t^{27} + 413t^{28} + 435t^{29} + 453t^{30} + 475t^{31} + 493t^{32}+$$
$$+515t^{33} + 533t^{34} + 555t^{35} + 573t^{36} + 595t^{37} + 613t^{38} + 635t^{39}+$$
$$+7763t^{40} + 8068t^{41} + 8384t^{42} + 8689t^{43} + 9005t^{44} + 9310t^{45}+$$
$$+9626t^{46} + 9931t^{47} + 10247t^{48} + 10552t^{49} + 10868t^{50} + 11173t^{51}+$$
$$+21080t^{52} + 21639t^{53} + 22194t^{54} + 22753t^{55} + 23308t^{56}+$$
$$+23867t^{57} + 24422t^{58} + 24981t^{59} + 25536t^{60} + 26095t^{61}+ \qquad (35)$$
$$+26650t^{62} + 27209t^{63} + 27764t^{64} + 28323t^{65} + 28878t^{66}+$$
$$+29437t^{67} + 29992t^{68} + 30551t^{69} + 31106t^{70} + 31665t^{71}+$$
$$+32220t^{72} + 32779t^{73} + 33334t^{74} + 33893t^{75} + 34448t^{76}+$$
$$+35007t^{77} + 35562t^{78} + 36121t^{79} + 36676t^{80} + 37235t^{81}+$$
$$+37790t^{82} + 38349t^{83} + 38904t^{84} + 39463t^{85} + 39974t^{86}+$$
$$+40533t^{87} + 41087t^{88} + 41646t^{89} + 42200t^{90} + 42759t^{91}+$$
$$+41667t^{92} + 42204t^{93} + 42741t^{94} + 43278t^{95} + 23378t^{96}+$$
$$+23661t^{97} + 137561t^{99} + ...$$

Analogically we expand the common Hilbert series $H_{SI_{1,4}}(t)$ from (30)-(31) and have

$$H_{SI_{1,4}}(t) = 1 + t + 2t^2 + 5t^3 + 14t^4 + 26t^5 + 57t^6 + 119t^7 + 248t^8 + 461t^9+$$
$$+864t^{10} + 1547t^{11} + 2737t^{12} + 4601t^{13} + 7662t^{14} + 12383t^{15} + 19768t^{16}+$$
$$+30664t^{17} + 47066t^{18} + 70770t^{19} + 105300t^{20} + 153783t^{21} + 222506t^{22}+$$
$$+317223t^{23} + 448337t^{24} + 625302t^{25} + 865296t^{26} + 1184226t^{27} + 1609007t^{28}+$$

$$+2164498t^{29} + 2892657t^{30} + 3832653t^{31} + 5047384t^{32} + 6595561t^{33}+$$
$$+8570829t^{34} + 11061230t^{35} + 14202137t^{36} + 18120878t^{37} + 23011677t^{38}+$$
$$+29058179t^{39} + 36532673t^{40} + 45692819t^{41} + 56917559t^{42} + 70566839t^{43}+$$
$$+87158250t^{44} + 107183955t^{45} + 131345992t^{46} + 160313871t^{47}+$$
$$+195025339t^{48} + 236375592t^{49} + 285608968t^{50} + 343916178t^{51}+$$
$$+412927382t^{52} + 494204023t^{53} + 589868721t^{54} + 701958526t^{55}+$$
$$+833207339t^{56} + 986241378t^{57} + 1164562071t^{58} + 1371538331t^{59}+$$
$$+1611612886t^{60} + 1889064095t^{61} + 2209499727t^{62} + 2578327522t^{63}+$$
$$+3002568564t^{64} + 3488999055t^{65} + 4046367551t^{66} + 4683127424t^{67}+$$
$$+5410102263t^{68} + 6237758509t^{69} + 7179427892t^{70} + 8248015477t^{71}+$$
$$+9459839180t^{72} + 10830705810t^{73} + 12380506870t^{74} + 14128528398t^{75}+$$
$$+16098882290t^{76} + 18314961754t^{77} + 20805884383t^{78} + 23599922669t^{79}+$$
$$+26732062272t^{80} + 30236294034t^{81} + 34154507484t^{82} + 38527430455t^{83}+$$
$$+43404991223t^{84} + 48835760568t^{85} + 54879055119t^{86} + 61592616546t^{87}+$$
$$+69046625211t^{88} + 77309433488t^{89} + 86463824763t^{90} + 96590473934t^{91}+$$
$$+107786664234t^{92} + 120147246938t^{93} + 133786223574t^{94} + 148814805866t^{95}+$$
$$+165366127962t^{96} + 183570124286t^{97} + 203581864473t^{98} + 225552766408t^{99} + ... \tag{36}$$

Comparing term by term the series (35) and (36) we have

$$H_{S'_{1,4}}(t) \leq H_{SI_{1,4}}(t).$$

Assuming that this inequality is true for the remaining terms of these series, we obtain the inequality (Remark A, [11])

$$\varrho(S'_{1,4}) \leq \varrho(SI_{1,4}).$$

Note that $S'_{1,4}$ is not a subalgebra in $SI_{1,4}$.
Therefore, according to the above mentioned and Theorem 3.2 we obtain

Theorem 3.3. *The maximal number of algebraically independent Lyapunov quantities of the system* (1) *on the variety* $\mathcal{V}$ *from* (5)*, which take part in solving the center-focus problem may not exceed* 11.

Remark 3.3. *The number indicated in Theorem* 3.3 *is smaller by two units than the number indicated in Theorem* 2.1.

References

[1] Mathematical Encyclopedia *Center and focus problem.* http://www.encyclopediaofmath.org/index.php/Centre_and_focus_problem.

[2] J. Chavarriga, J. Giné, M. Grau, *Integrable systems via polynomial inverse integrating factors*, Bull. Sci. math. 126 (2002), pp. 315-331.

[3] J. Chavarriga, J. Giné, *Integrability of a linear center perturbed by a fourth degree homogeneous polynomial*, Publicacions Matemàtiques, Vol 40 (1996), pp. 21-39.

[4] Iurie Calin, Stanislav Ciubotaru, *The center conditions for the bidimensional polynomial systems of differential equations with nonlinearities of the fourth degree*, International Conference Mathematics and Information Technologies: Research and Education, MITRE-2013, Abstracts, August 18–22, 2013, Chişinău, Republic of Moldova, pp. 22-23.

[5] Pricop V. V., *The differential system* $s(1,4)$ *and algebraically independent focal pseudo-quantities*. The 19th Conference on Applied and Industrial Mathematics, CAIM 2011, Abstracts, September 22-25, 2011, Iaşi, Romania, pp. 15-16.

[6] M. N. Popa, V. V. Pricop, *Applications of algebraic methods in solving the center-focus problem*, Buletinul AŞM, Matematica, **1(71)**, (2013), pp. 45-71. (http://arxiv.org/abs/1310.4343)

[7] Sibirsky K. S., *Introduction to the algebraic theory of invariants of differential equations*, Translated from Russian. Nonlinear Science: Theory and applications, Manchester University Press, Manchester, (1988).

[8] Popa M. N., *Algebraic methods for differential systems*, Editura the Flower Power, Universitatea din Piteşti, Seria Matematică Aplicată şi Industrială, 2004, (15) (in Romanian).

[9] N. Gherştega, M. Popa, V. Pricop, *About characteristics of graded algebras* $S_{1,4}$ *and* $SI_{1,4}$, Buletinul AŞM, Matematica, **1(62)**, (2010), pp. 23-32.

[10] Vulpe N. I., *Polynomial bases of comitants of differential systems and their application in qualitative theory*, Kishinev, Shtiintsa, 1986 (in Russian).

[11] Popa M. N., Pricop V. V., *Applications of algebras to the center-focus problem*, Preprint, Chişinău, AŞM, Institute of Mathematics and Computer Science, No. 0007, 2011, 59 p. http://www.math.md/files/download/epublications/PreprintPopaMPricopV.pdf

ROMAI J., v.9, no.2(2013), 197–203

COMMON FIXED POINTS FOR BANACH-CARISTI CONTRACTIVE PAIRS

Mihai Turinici

"A. Myller" Mathematical Seminary; "A. I. Cuza" University; Iaşi, Romania

mturi@uaic.ro

Abstract Further extensions are given for the common fixed point statement in Dien [J. Math. Anal. Appl., 187 (1994), 76-90], involving Banach-Caristi contractive pairs.

Keywords: metric space, Banach-Caristi contractive pair, common fixed point.
2010 MSC:54H25 (Primary), 06A06 (Secondary).

1. INTRODUCTION

Let (X, d) be a complete metric space; and $T \in \mathcal{F}(\mathcal{X})$ be a selfmap of X. [Here, for each couple of sets $\{A, B\}$, $\mathcal{F}(\mathcal{A}, \mathcal{B})$ stands for the class of all functions from A to B; if $A = B$, one writes $\mathcal{F}(\mathcal{A}, \mathcal{A})$ as $\mathcal{F}(\mathcal{A})$]. The following fixed point statement in Caristi and Kirk [6] (referred to as: Caristi-Kirk theorem) is our starting point.

Theorem 1.1. *Assume that there exists a function $\alpha : X \to R_+ := [0, \infty[$ with*

(a01) $d(x, Tx) \leq \alpha(x) - \alpha(Tx)$, for each $x \in X$

(a02) $\alpha(.)$ is lsc on X ($\liminf_n \alpha(x_n) \geq \alpha(x)$, whenever $x_n \longrightarrow x$).

Then, T has at least one fixed point in X.

Note that, in terms of the [associated to $\alpha(.)$] order

(a03) $(x, y \in X)$: $x \leq y$ iff $d(x, y) \leq \alpha(x) - \alpha(y)$

the contractive condition (a01) becomes

(a04) $x \leq Tx$, for each $x \in X$ (i.e.: T is *progressive* on X).

So, Theorem 1.1 is deductible from the arguments in Ekeland's variational principle [8]. Further aspects may be found in Brezis and Browder [4]; see also Turinici [12].

Now, the Caristi-Kirk theorem found (especially via Ekeland's approach) some basic applications to control and optimization, generalized differential calculus, critical point theory and normal solvability; see the above references for details. As a consequence, many extensions of this result were proposed. Here, we shall concentrate on the 1981 statement in this area due to Bhakta and Basu [3]. Let $\{S, T\}$ be a couple of selfmaps in $\mathcal{F}(\mathcal{X})$. We say that $z \in X$ is a *common fixed point* of $\{S, T\}$ if $Sz = Tz = z$.

Sufficient conditions guaranteeing such a property are obtainable as below. Call the selfmap U in $\mathcal{F}(\mathcal{X})$, *orbitally continuous* (on X), if

(a05) $z = \lim_n U^{i(n)}x$ implies $Uz = \lim_n U^{i(n)+1}x$;

here, $(i(n); n \geq 0)$ is a rank sequence with $i(n) \to \infty$ as $n \to \infty$.

Theorem 1.2. *Suppose that*

(a06) both S and T are orbitally continuous;

and let the functions $\alpha, \beta : X \to R_+$ be such that

(a07) $d(Sx, Ty) \leq \alpha(x) - \alpha(Sx) + \beta(y) - \beta(Ty)$, for all $x, y \in X$.

Then,
i) *S and T have a unique common fixed point $z \in X$,*
ii) *$S^n x \longrightarrow z$ and $T^n x \longrightarrow z$ as $n \to \infty$, for each $x \in X$.*

A partial extension of this result was given in the 1994 paper by Dien [7]:

Theorem 1.3. *Suppose that (a06) holds. In addition, let the number $q \in [0, 1[$ and the function $\alpha : X \to R_+$ be such that*

(a08) $d(Sx, Ty) \leq qd(x, y) + \alpha(x) - \alpha(Sx) + \alpha(y) - \alpha(Ty)$, $\forall x, y \in X$.

Then, conclusions of Theorem 1.2 are retainable.

[As a matter of fact, the original result is with $\alpha = \alpha_1 + ... + \alpha_k$, where $\{\alpha_i; 1 \leq i \leq k\}$ is a finite system in $\mathcal{F}(\mathcal{X}, \mathcal{R}_+)$. But it gives, practically, the same amount of information as the result in question].

Note that, when $\alpha(.)$ is a constant function and $S = T$, then Theorem 1.3 implies the Banach contraction principle [2]. In addition, (a01) follows from (a08) when $S = I$ (=the *identity map* of $\mathcal{F}(\mathcal{X})$) and $x = y$; for this reason, the couple $\{S, T\}$ above will be referred to as *Banach-Caristi contractive*. It is to be stressed that Theorem 1.1 does not follow from Theorem 1.3; because, the (essential for Theorem 1.1) condition (a02) is not obtainable from the conditions of Theorem 1.3. However, the underlying relationship between these results holds whenever (a06) is accepted, in place of (a02). (This clarifies an assertion made in Ume and Yi [13]; we do not give details). On the other hand, Dien's result cannot be deduced from Caristi-Kirk's; because (a06) cannot be deduced from the conditions of Theorem 1.1. Finally, Theorem 1.2 cannot be viewed as a particular case of Theorem 1.3 (when $q = 0$); because the functions $\alpha(.)$ and $\beta(.)$ may be distinct.

Having this precise, it is our aim in the following to establish (cf. Section 2) a common extension of these statements; as well as (in Section 3) a sum approach of it. Some other aspects will be delineated elsewhere.

2. MAIN RESULT

Let $\varphi \in \mathcal{F}(\mathcal{R}_+)$ be a function; call it *regressive* provided $\varphi(0) = 0$ and $\varphi(t) < t$, $\forall t \in R_+^0 :=]0, \infty[$; the class of all these will be denoted as $\mathcal{F}()(\mathcal{R}_+)$. For example, any function $\varphi = qJ$ where $q \in [0, 1[$, is regressive; here, J is the *identity function* of $\mathcal{F}(\mathcal{R}_+)$ ($J(t) = t, t \in R_+$).

Now, fix some $\varphi \in \mathcal{F}()(\mathcal{R}_+)$. Denote $\psi := J - \varphi$; and call it, the *complement* of φ. Clearly, $\psi \in \mathcal{F}(\mathcal{R}_+)$; precisely,

$$\psi(0) = 0;\ 0 < \psi(t) \leq t,\ \forall t \in R_+^0. \tag{1}$$

For an easy reference, we list our basic hypotheses. The former of these is

(b01) φ is super-additive: $\varphi(t + s) \geq \varphi(t) + \varphi(s)$, for all $t, s \geq 0$;

clearly, φ must be increasing in such a case. And the latter condition writes:

(b02) $\psi := J - \varphi$ is coercive: $\psi(t) \to \infty$ as $t \to \infty$;

referred to as: φ is *complementary coercive*. Note that (by this very definition)

$$g(r) := \sup\{t \geq 0; \psi(t) \leq r\} < \infty, \quad \text{for each } r \in R_+; \tag{2}$$

whence, $g(.)$ is an element of $\mathcal{F}(\mathcal{R}_+)$. Moreover (from (1) above)

$$g(0) = 0;\ g(r) \geq r,\ \forall r \in R_+. \tag{3}$$

The following auxiliary fact will be useful for us.

Lemma 2.1. *Let $\varphi \in \mathcal{F}()(\mathcal{R}_+)$ be super-additive and complementary coercive. Further, let the sequence $(\theta_n; n \geq 0)$ in R_+ be such that*

(b03) $\theta_{m+1} \leq \varphi(\theta_m) + \delta_m - \delta_{m+1}$, *for all* $m \geq 0$;

where $(\delta_n; n \geq 0)$ is a sequence in R_+. Then, the series $\sum_n \theta_n$ converges.

Proof. Let $(\sigma_i := \theta_0 + ... + \theta_i; i \geq 0)$ be the partial sum sequence attached to $(\theta_n; n \geq 0)$. For each $j \geq 0$, we have (summing in (b03) from $m = 0$ to $m = j$)

$$\theta_1 + ... + \theta_{j+1} \leq \varphi(\theta_0) + ... + \varphi(\theta_j) + \delta_0 - \delta_{j+1}.$$

This, along with the super-additivity of φ, gives $\sigma_j \leq \varphi(\sigma_j) + \theta_0 + \delta_0$. But then, (2) yields $[\sigma_n \leq g(\theta_0 + \delta_0) < \infty, \forall n]$; wherefrom, all is clear. ∎

We now state the promised result. Let (X, d) be a complete metric space; and $\{S, T\}$ be a pair in $\mathcal{F}(\mathcal{X})$.

Theorem 2.1. *Suppose that (a06) holds. In addition, let the function $\varphi \in \mathcal{F}()(\mathcal{R}_+)$ as in (b01)+(b02), and the map $\gamma : X \times X \to R_+$, be taken so as*

(b04) $d(Sx, Ty) \le \varphi(d(x,y)) + \gamma(x,y) - \gamma(Sx, Ty)$, *for all* $x, y \in X$.

Then, conclusions of Theorem 1.2 are retainable.

Proof. Given $x_0, y_0 \in X$, put $(x_n = S^n x_0; n \ge 0)$, $(y_n = T^n y_0; n \ge 0)$. From (b04), one has (by a finite induction argument), the iterative type relations

$$d(x_{m+1}, y_{m+1}) \le \varphi(d(x_m, y_m)) + \gamma(x_m, y_m) - \gamma(x_{m+1}, y_{m+1}), \text{ for all } m \ge 0.$$

Combining with Lemma 2.1 (and the adopted notations), one derives that the series $\sum_n d(S^n x_0, T^n y_0)$ converges.

Further, let us develop the same reasoning by starting from the points $u_0 = Sx_0$ and y_0; one derives that the series $\sum_n d(S^n u_0, T^n y_0)$ converges; or, equivalently: the series $\sum_n d(S^{n+1} x_0, T^n y_0)$ converges. This, along with

$$d(S^n x_0, S^{n+1} x_0) \le d(S^n x_0, T^n x_0) + d(S^{n+1} x_0, T^n y_0), \quad \forall n \ge 0$$

tells us that the series $\sum_n d(S^n x_0, S^{n+1} x_0)$ converges; wherefrom, $(S^n x_0; n \ge 0)$ is a d-Cauchy sequence. In a similar way (starting from the points x_0 and $v_0 = Ty_0$) one proves that the series $\sum_n d(T^n y_0, T^{n+1} y_0)$ converges; whence, $(T^n y_0; n \ge 0)$ is a d-Cauchy sequence. As (X, d) is complete, we have that $S^n x_0 \to z$ and $T^n y_0 \to w$, for some $z, w \in X$. Combining with the orbital continuity of both S and T, gives $S(S^n x_0) \to Sz$, $T(T^n y_0) \to Tw$. But, $S(S^n x_0) = S^{n+1} x_0 \to z$, $T(T^n y_0) = T^{n+1} y_0 \to w$; and this yields $z = Sz$, $w = Tw$. Finally, from (b04) again, we have $d(z, w) \le \varphi(d(z, w))$; so that, $z = w$. Hence, z is a common fixed point of $\{S, T\}$. Its uniqueness is obtainable by the argument we just developed for (z, w); and, from this, we are done. ∎

In particular, when $\varphi \in \mathcal{F}()(\mathcal{R}_+)$ is taken as

(b05) $\varphi(t) = qt$, $t \ge 0$, for some $q \in [0, 1[$,

conditions (b01)+(b02) hold; and then, under the choice

(b06) $\gamma(x, y) = \alpha(x) + \alpha(y)$, $x, y \in X$ (where $\alpha \in \mathcal{F}(\mathcal{X}, \mathcal{R}_+)$)

the corresponding version of Theorem 2.1 is just Theorem 1.3. Note that, under the same framework, a more general choice for γ is

(b07) $\gamma(x, y) = \alpha(x) + \beta(y)$, $x, y \in X$ (where $\alpha, \beta \in \mathcal{F}(\mathcal{X}, \mathcal{R}_+)$).

This version of Theorem 2.1 is (under $\varphi = 0$) just Theorem 1.2 above. Further aspects may be found in Alimohammady et al [1]; see also Kadelburg et al [10].

3. FURTHER EXTENSIONS

A simple inspection of the argument we just developed shows that it depends (via Lemma 2.1) on the super-additivity of the function $\varphi \in \mathcal{F}()(\mathcal{R}_+)$; so, we may ask

whether this cannot be removed. An appropriate answer is available, if we arrange for the sums given by the argument of Theorem 2.1 being obtainable in a direct way from the contractive conditions.

Let (X, d) be a complete metric space; and $\{S, T\}$ be a pair of selfmaps in $\mathcal{F}(\mathcal{X})$.

Theorem 3.1. *Suppose that (a06) holds. In addition, let the function $\varphi \in \mathcal{F}()(\mathcal{R}_+)$ as in (b02) and the map $\gamma : X \times X \to R_+$ be taken so as*

$$(c01)\ \sum_{j=1}^{n} d(S^j x, T^j y) \leq \varphi(\sum_{j=0}^{n-1} d(S^j x, T^j y)) + \gamma(x, y) - \gamma(S^n x, T^n y),$$

for all $x, y \in X$ and all $n \geq 1$. Then, conclusions of Theorem 1.3 are retainable.

Proof. Given $x_0, y_0 \in X$, put $(x_n = S^n x_0; n \geq 0)$, $(y_n = T^n y_0; n \geq 0)$. Further, denote $(\theta_i = d(x_i, y_i); i \geq 0)$. By (c01) one has, for each $n \geq 1$,

$$\theta_1 + ... + \theta_n \leq \varphi(\theta_0 + ... + \theta_{n-1}) + \gamma(x_0, y_0) - \gamma(x_n, y_n);$$

wherefrom (after some transformations)

$$\theta_0 + ... + \theta_{n-1} \leq \varphi(\theta_0 + ... + \theta_{n-1}) + \theta_0 + \gamma(x_0, y_0),\ \forall n \geq 1.$$

This, from (b02) (and the notations in Section 2), gives

$$\theta_0 + ... + \theta_{n-1} \leq g[\theta_0 + \gamma(x_0, y_0)] < \infty,\ \text{for all } n \geq 1;$$

so that (by the adopted notations) the series $\sum_n d(S^n x_0, T^n y_0)$ converges. Further, let us develop the same reasoning by starting from the points $u_0 = S x_0$ and y_0; one derives that the series $\sum_n d(S^n u_0, T^n y_0)$ converges; or, equivalently: the series $\sum_n d(S^{n+1} x_0, T^n y_0)$ converges. This, along with

$$d(S^n x_0, S^{n+1} x_0) \leq d(S^n x_0, T^n x_0) + d(S^{n+1} x_0, T^n y_0),\ \ \forall n \geq 0$$

tells us that the series $\sum_n d(S^n x_0, S^{n+1} x_0)$ converges; wherefrom $(S^n x_0; n \geq 0)$ is a d-Cauchy sequence. In a similar way (starting from the points x_0 and $v_0 = T y_0$), one proves that the series $\sum_n d(T^n y_0, T^{n+1} y_0)$ converges; whence, $(T^n y_0; n \geq 0)$ is a d-Cauchy sequence. As (X, d) is complete, $S^n x_0 \to z$ and $T^n y_0 \to w$, for some $z, w \in X$. The remaining part of the argument runs as in Theorem 2.1, because (c01) $\Longrightarrow$ (b04); and, from this, all is clear. ∎

Now, concrete examples of complementary coercive functions $\varphi \in \mathcal{F}()(\mathcal{R}_+)$ are obtainable by starting from the choice

$$(c02)\ \ \varphi(t) = t\chi(t),\ t \geq 0,$$

where $\chi \in \mathcal{F}(\mathcal{R}_+)$ fulfills the regularity conditions

(c03) χ is increasing on R_+^0 and $\chi(t) < 1, \forall t \in R_+^0$.

The standard case is $[\chi(t) = q,\ t \geq 0]$, for some $q \in [0, 1[$; when Theorem 3.1 includes, in a direct way, Theorem 1.3; due, as above said, to Dien [7]. A technical extension of this one may be constructed according to

(c04) $\chi(t) = r_{n+1}$, when $t \in [t_n, t_{n+1}[$, for each $n \geq 0$;

where the sequence $(r_n; n \geq 1)$ in $]0, 1[$ and the strictly ascending sequence $(t_n; n \geq 0)$ in R_+ with $t_0 = 0$ and $t_n \to \infty$ are to be determined. To this end, we have

$$t - \varphi(t) = t(1 - r_{n+1}),\ t \in [t_n, t_{n+1}[,\ n \geq 0.$$

Assume that $(t_n; n \geq 1)$ is a strictly ascending sequence in $]1, \infty[$ with

(c05) $t_n / \sqrt{t_{n+1}} \to \infty$ (hence $t_n \to \infty$).

Then, choose the sequence $(r_n; n \geq 1)$ in $]0, 1[$ according to

(c06) $1 - r_n = 1 / \sqrt{t_n}$, for each $n \geq 1$.

Note that, as a consequence of this, $(r_n; n \geq 1)$ is strictly ascending in $]0, 1[$ (hence, (c03) holds) and $r_n \to 1$ as $n \to \infty$. Replacing in a preceding formula, yields

$$t - \varphi(t) = t / \sqrt{t_{n+1}},\ \text{ when } t \in [t_n, t_{n+1}[,\ n \geq 0.$$

This gives an evaluation like

$$t - \varphi(t) \geq t_n / \sqrt{t_{n+1}},\ \text{ for } t \in [t_n, t_{n+1}[, n \geq 0;$$

wherefrom (by (c05)), $\psi := J - \varphi$ is coercive. On the other hand, some useful superadditivity tests for the functions $\varphi \in \mathcal{F}()(\mathcal{R}_+)$ like before are obtainable from the methods developed by Bruckner [5]. Some other aspects may be found in Liu, Xu and Cho [11]; see also Fisher [9].

References

[1] M. Alimohammady, J. Balooee, S. Radojević, V. Rakočević, M. Roohi, *Conditions of regularity in cone metric spaces,* Appl. Math. Comput., 217 (2011), 6259-6263.

[2] S. Banach, *Sur les opérations dans les ensembles abstraits et leur application aux équations intégrales.* Fund. Math., 3 (1922), 133-181.

[3] P. C. Bhakta, T. Basu, *Some fixed point theorems on metric spaces,* J. Indian Math. Soc., 45 (1981), 399-404.

[4] H. Brezis, F. E. Browder, *A general principle on ordered sets in nonlinear functional analysis,* Advances Math., 21 (1976), 355-364.

[5] A. M. Bruckner, *Tests for the superadditivity of functions,* Proc. Amer. Math. Soc., 13 (1962), 126-130.

[6] J. Caristi, W. A. Kirk, *Geometric fixed point theory and inwardness conditions,* in "The Geometry of Metric and Linear Spaces" (Michigan State Univ., 1974), pp. 74-83, Lecture Notes Math., vol. 490, Springer, Berlin, 1975.

[7] N. H. Dien, *Some remarks on common fixed point theorems,* J. Math. Anal. Appl., 187 (1994), 76-90.

[8] I. Ekeland, *Nonconvex minimization problems,* Bull. Amer. Math. Soc. (New Series), 1 (1979), 443-474.

[9] B. Fisher, *Four mappings with a common fixed point,* J. Univ. Kuwait Sci., 8 (1981), 131-139.

[10] Z. Kadelburg, S. Radenović, S. Simić, *Abstract metric spaces and Caristi-Nguyen-type theorems,* Filomat, 25 (2011), 111-124.

[11] Z. Liu, Y. Xu, Y. J. Cho, *On characterizations of fixed and common fixed points,* J. Math. Anal. Appl., 222 (1998), 494-504.

[12] M. Turinici, *Functional versions of the Caristi-Kirk theorem,* Revista Union Mat. Argentina, 50 (2009), 89-97.

[13] J. S. Ume, S. Yi, *Common fixed point theorems for a weak distance in complete metric spaces,* Internat. J. Math. Mathemat. Sci., 30 (2002), 605-611.

ISBN 978-93-5156-328-0
International Conference of Advance Research and Innovation (ICARI-2014)

Sort Range Optical Wireless Communication

Sanjeev Mishra
Department of Technical Instructor, Delhi Technological University, Delhi, India

Article Info

Article history:
Received 29December 2013
Received in revised form
10 January 2014
Accepted 20 January 2014
Available online 1 February 2014

Keywords

Abstract

It is commonly accepted that the next generation of wireless communication systems, usually referred to as 4G systems, will not be based on a single access technique but it will encompass a number of different complementary access technologies. The ultimate goal is to provide ubiquitous connectivity, integrating seamlessly operations in most common scenarios, ranging from fixed and low-mobility indoor environments in one extreme to high-mobility cellular systems in the other extreme. Surprisingly, perhaps the largest installed base of short-range wireless communications links are optical, rather than RF, however. Indeed, 'point and shoot' links corresponding to the Infra-Red Data Association (IRDA) standard are installed in 100 million devices a year, mainly digital cameras and telephones. In this paper we argue that optical wireless communications (OW) has a part to play in the wider 4G vision.

1. Introduction and Motivation

As the third generation mobile communication system (3G) is being deployed, manufacturers and scientific community are increasingly turning their research interests toward future wireless communication systems. It is commonly agreed that the next generation of wireless communication systems, usually referred to as 4G systems, will not be based on a single access technique but it will encompass a number of different complementary access technologies. Future systems will not only connect users and their personal equipment but also access to independent (stand-alone) equipment will be provided. Ultimately one would expect that everybody and everything will be wirelessly connected. This vision places short-range communications in a position of preponderance, as one could argue that most of the wireless links in future wireless communication networks will be established over relatively short distances. In addition, a significant part of these links will be characterized by high data throughputs. Probably the largest portion of practical applications of short-range communications take the form of WLAN, WPAN and WBAN (Wireless Local, Personal and Body Area Networks), covering ranges from a few tens of meters down to sub-meter communications. In the context of short-range communications, two techniques have received increasingly attention in the last years, namely multicarrier (MC) and Ultra Wideband (UWB). These fundamental technologies for the physical layer have been extensively studied in the literature, for a comprehensive introduction and initial pointers[1, 2] [3, 4]. Application of these techniques in short-range environments will be considered in detail within the framework of WWRF [5]. In this paper we argue that optical wireless communications (OW) has a part to play in the wider 4G vision. The optical wireless channel has THz of unregulated bandwidth, and characteristics that are distinct from that of radio. Together these media might provide a broad spectrum of channel characteristics and capabilities that radio alone would find it difficult to meet. The aims of this paper are to; (i) Introduce OW and the components and systems used (ii) Summarize the state of the art, and rich research community that exists (iv) Identify particular areas where OW can contribute to the vision and areas of future research Optical Wireless Communications as an Alternative Technology for Short-Range Communications In this section an overview of Optical Wireless Communication systems is presented. The main emphasis in this paper is put on OW for indoor environments. Another important approach to OW, freespace optics (FSO), a point-to-point optical connection supporting very high rates in outdoor environments, will not be considered in this paper.

Corresponding Author,
E-mail address:
All rights reserved: http://www.ijari.org

ISBN 978-93-5156-328-0

We start with a brief introduction and classification of OW systems and then continue with different engineering aspects, including transmitters, receivers, the optical channel and other related issues. This introduction is based on the studies and reviews presented by [6],[7-9]. Comparisons to conventional radio systems are presented to give the reader a broader perspective of the possible baseband technologies. An up to- date account of different techniques, practical systems and standards related to OW as well as future research issues complete the paper. Basic system configuration. In a diffuse system an undirected source (usually Lambertian) illuminates the coverage space, much as it would be illuminated with artificial lighting. The high reflectivity of normal building surfaces then scatters the light to create optical 'ether'. A receiver within the coverage space can detect this radiation, which is modulated in order to provide data transmission. Diffuse systems are robust to blocking and do not require that transmitter and receiver are aligned, as many paths exist from transmitter to receiver. However, multipath interference at the receiver can cause Inter Symbol Interference (ISI) and the path loss for most systems is high. The alternative approach is to use directed Line of Sight paths between transmitter and receiver. Variants of this use structured illumination (perhaps using arrays of spots) [10, 11]. There is a large amount of simulation and more limited amount of measurement data that describes these channels in some detail. In contrast with radio frequencies simulation of indoor coverage spaces generally gives a good estimate of the channel characteristics System components.

1.1 Transmitter

The transmitter consists of a single, or a number of sources, and an optical element to shape the beam and also render it eyesafe if required. The main element of the transmitter is the optical source. Light Emitting Diodes (LED) and laser diodes are employed as the optical radiating element, and their transmission power is limited by eye safety regulation. In the near IR region (between the visible and 1400nm) the limit for point sources is less than 1mW. Beyond 1400nm this limit increases by a factor of 20 or so. However in both cases much higher powers are available by diffusing the sources, thus increasing their apparent emitted areas. Several types of engineered diffuser have been developed, including holographic [12] and reflective [13]. This latter device has been incorporated in a commercial optical link [14]. Most systems use laser diodes, due to their higher modulation bandwidth and efficiency. IR LEDs are also important optical sources being considered for establishing optical links. In addition, there is a small and growing interest in using visible LEDs that would be installed in a building to provide solid-state lighting for optical communications [15]. In such cases multiplexing of the low bandwidth devices might be used to increase amplification data rate.

1.2 Receiver

A typical OW receiver consists of an optical system to collect and concentrate incoming radiation, an optical filter to reject ambient illumination, and a photo detector to convert radiation to photocurrent.

1.3 Optical Systems

Receiver optical systems can be characterized in terms of their angular Field of View (FOV) and their collection area. These are linked to the detection area by the constant radiance theorem.

1.4 Optical Channel

LOS optical channels are subject to path loss, and this can be modeled using either ray-tracing or analytical techniques. Thediffuse channel has both high path loss (>40dB typically) and is subject to multipath dispersion. Both of these characteristics are dependent on the orientation of the source and receiver within the space. There has been extensive work on predicting the characteristics of the diffuse channel, including [25, 36] [37] as well as analytical models of the channel impulse results. Most building materials are found to have a high reflectivity (0.4-0.9) and they can be approximately modeled as Lambertian reflectors. Ray tracing techniques therefore allow generally good predictions of the channel response, even in the presence of chairs and other objects. Depending on the balance of LOS and diffuse paths within a space channels can be modeled as Rician [38] or Rayleigh, with exponential impulse responses. Various measurements have also been made [39, 40]. Recent high-resolution data indicate that transparent 'unlimited' bandwidth diffuse channels are available in particular directions for most diffuse environments [41].

2. Modulation schemes

Unlike in conventional RF systems, the optical channel uses intensity modulation and direct detection. The optical power output of the transmitting source is controlled according to some

ISBN 978-93-5156-328-0

characteristics of the information bearing signal. The transmitted signal is thus always positive and its average amplitude is limited [42]. Analog and digital optical modulation is possible but, due to the intensity modulation, common modulation schemes employed in the radio frequency domain will perform differently when applied to optical systems. The changes in optical power produced by intensity modulation are detected by direct detection, that is, a current proportional to the incident optical power is induced in the photo detector. As pointed out in [7] two criteria should be used to evaluate the feasibility of an optical modulation system; the average optical received power required to achieve a given target BER performance and the required receiver electrical bandwidth. Three basic modulation schemes are usually used in OW systems, namely On-Off Keying (OOK), Pulse-Position Modulation (PPM) and Sub carrier Modulation (SCM). An extensive account of these and other techniques can be found in [42]. Other issues to take into account when considering optical modulation schemes are their robustness to multipath propagation and, in networks, their suitability to multiple access environments. PPM is very well suited to work in low signal to- noise ratio scenarios, quite typical in optical channels due to blocking effects (shadowing) and ambient noise. However, multipath propagation induces inter symbol interference and PPM is particularly sensitive to these dispersive effects of the optical channel [42]. Many techniques have been considered in order to combat the deleterious effects of dispersive optical channels, among them the use of equalizers, angle-diversity and spread spectrum techniques. Different equalization approaches at chip or symbol rate have been studied for PPM based systems, including linear and decision-feedback equalizers [42].

Spread-spectrum modulation techniques can also be used to combat multipath distortion as well as to reduce the effects of interference, in a similar fashion as they are exploited with radio systems. Direct sequence techniques are usually used in conjunction with optical links. Since bipolar spreading sequences cannot be used to modulate an always positive optical signal, a unipolar sequence is formed by biasing to the bipolar sequence with a fixed DC offset. This unipolar sequence preserves the correlation properties of the original sequence and it can be correlated with a bipolar sequence at the receiver. Several direct sequence spread spectrum approaches specially designed for optical systems have been proposed and studied, including sequence inversion keying modulation (SIK), complementary SIK (CSIK) and M-ary bi-orthogonal keying modulation (MBOK) [43, 44]. Sequences with low auto and cross-correlation side lobes are preferred in order to minimize the degrading effects of inter symbol interference.

3. Optical wireless vs. radio communications

Over the past decade the capacity of an optical fiber link has increased by several orders of magnitude, showing almost ‘Moore’s Law’ growth, largely due to the availability of optical spectrum. At the same time regulation of the RF spectrum limitavailable bandwidth to several orders of magnitude below this. The vision of a highly connected world is likely to require unaffordable amounts of the already scarce radio frequency spectrum. OW occupies fully unlicensed spectrum bands, and the possibility of using unregulated and unlicensed bandwidth is one of the most attractive characteristics of OW. Unlike radio communications, the nature of the optical radiation is such that the transmitted signal is obstructed by opaque objects, and the radiation can have high directivity using sub-millimeter scale beam shaping elements. This combination of high directivity and spatial confinement gives optical channels an unmatched advantage in terms of security. Furthermore, these characteristics allow exploiting wavelength reuse at room level, without taking special provisions for interference from and to neighboring rooms. Since the optical radiation produces no interference to electrical equipment, OW can be used in sensitive environments where conventional radio wave transmission is not allowed. Another unique characteristic of wireless optical links is in the channel itself, and it is the fact that these links are not affected by multipath fading. This is because the dimensions of the receiver’s photo detector are many orders of magnitude larger that the wavelength of the optical radiation and thus, the spatial fluctuations in signal strength due to multipath are averaged over the large detector area, which acts as an integrator. For most of the cases, and as an essential advantage, optical components are small in size, low-cost and they have low power consumption. Furthermore, transceivers are relatively simple compared with their radio frequency counterparts. There are several drawbacks, however; since IR radiation can reach the retina and eventually cause thermal damage, the maximum power that can be transmitted is limited by eye safety regulations and extra optical elements are required to render high power sources safe. In diffuse optical communication systems, multipath propagation caused by the

ISBN 978-93-5156-328-0

dispersive optical channel will introduce pulse spreading and intersymbol interference (ISI), much as would be experienced by a radiochannel, although the process is due to incoherent, rather than coherent fading. Systems above 50Mb/s or so might typically require some form of equalization. Perhaps the major difference for the optical wireless channel is the detection process is usually incoherent, so that the detector responds linearly with power, rather than amplitude as is the case with a radio receiver. Receiver sensitivity is therefore substantially lower than for radio channels, and therefore systems are more susceptible to path loss, especially in the case of diffuse systems. More complex receiver and transmitter structures can be used to reduce this, and the effect of noise from ambient illumination. As the detection process is incoherent there is no inherent rejection in the detection process, so filtering mechanisms must be introduced, as mentioned earlier. The wavelength of optical radiation makes directive channels easy to implement, and system design often leads to asymmetric channels [45]. Such directive channels are necessarily subject to blocking, which is again distinct from radio applications [9, 45] and [46].

4. Applications areas for optical Wireless

There is little doubt that radio solutions will remain dominant for most applications, but there are several areas where OW is attractive.

4.1 Telemetric Applications

There is also a growing interest in optical communications between moving vehicles, and between vehicles and roadside hubs. These are being considered for telemetric applications, such as road pricing and navigation, as indicated by the development of an ISO standard (ISO CALM 204) for such systems. The German government has adopted an optical communications system for its tolling system for freight vehicles [47]. Several train-operating companies are investigating FSO for communications with trains, to provide broadband 'to the seat'.

4.2 Secure Wireless Applications

There are a number of applications where OW can provide secure communications. The IRDA is promoting 'Financial Messaging', where a secure transaction takes place between a handheld and a retail terminal, albeit at low data rates [48]. Such a concept might be extended to retailing of high bandwidth content such as DVDs and CDs to portable players. In the future this might require several Gb/s in order to achieve reasonable download times. Theft of content would be limited by the confined nature of the optical signal, and extremely high spatial bandwidth could be achieved within the retail environment. This is relatively straightforward to achieve with a directed OW link used in a 'point and shoot' manner, or in a booth in which the link environment can be controlled. There may also be other environments such as dealing rooms where secure wireless networks are required, and OW can easily provide this.

4.3 Ultra-high bandwidth wireless

Applications such as virtual reality suites and wireless TV studios require multi Gb/s wireless communications with very high spatial bandwidth density. The directivity available with optical links, combined with tracking makes this feasible.

5. RF Hazardous environments

One of the major growth sectors in avionics is data and speech communications to aircraft. Satellite broadband is being added to aircraft, and many aircraft are equipped with telephone to the seat. The wireless link from the passenger to the data infrastructure is currently not possible, and OW represents perhaps the only allowable alternative. A mobile phone or PDA containing a radio and optical terminal could allow seamless communications with a local optical base station part of the aircraft infrastructure. Hospitals offer similar opportunities, both in wireless instrumentation and transmission of data. In sensitive environments, the access point or network could automatically disable the radio interface, enabling communications through the optical link.

5.1 Hybrid Wireless Systems

In broad terms optical wireless provides high bandwidth, and providing coverage is problematic, whilst for RF approaches the opposite is the case. Perhaps the key advantage of OW (in a general environment where security is unimportant) is the ease with which high bandwidth LOS channels can be provided, and the potential these have to decrease the load on the infrastructure. Hybrid systems that can allow this are therefore attractive, and fit well within the 4G vision of heterogeneous wireless systems working together to provide a seamless infrastructure. Very simple hybrid approaches combining optical and radio frequency links have been proposed recently for short-range (indoor) communications [49, 50]. Reference [51] describes protocols that use RF

ISBN 978-93-5156-328-0

signaling and reallocate the optical sources under blocking conditions. Future research in this area is discussed in later sections.

The IrDA (Infrared Data Association) is a worldwide organization that develops standards for point-to-point very short-range optical communications, with a sub-meter range. This optical wireless interfaces can be found nowadays in a variety of portable equipment, like mobile phones, laptop computers and personal digital assistants, among others. In its basic version this standard defines a very low-cost, low-power with a maximum operating range of 1 m and data rates of up to 4 Mb/s. High speed IrDA versions providing up to 16 Mb/s are also available. Various interest groups are working on financial messaging (IrFm), transport (IrTM), and higher data rates (IrBurst) and (UFIR). It is noted that the IrdA optical air interface supports no mobility as it usually requires manual alignment between transmitter and receiver. The standard defines the physical layer as well as different protocols used by upper layers. An overview of IrDA can be found in [52]

6. Traffic management

As mentioned previously there is both standards and commercial activity in this area. IRDA has formed The Travel Mobility Special Interest Group (IrTM) in order to develop a specification for toll payment. A standard also exists for longer-range communications (ISO TC 204 CALM). A major commercial amount of activity is by Efkon, who have won large contracts for payment systems worldwide, notably a German project for truck traffic tolling.

6.1 Ultra-high bandwidth wireless

JVC have recently introduced a tracking 1.5 Gb/s link between a HDTV source and Flat screen TV [14]. This uses mechanically tracked terminals and a novel diffuser to achieve eye safety.

6.2 Secure applications

IrFM is a ratified standard and a number of point and shoot products designed for electronic funds transfer. The high speed Special Interest Groups (SIGs) (IrBurst and UFIR) are working on data transmission at 100Mb/s and greater, and a major applications area is secure downloading of multimedia files.

7. Networks

5.2 State of the art Standards IrDA

There are few low speed IR networks that are commercially available, and several in developments. A LOS network was available from JVC [54] and diffuse LANs from spectrix [55]. The low cost and complexity of OW components also makes the attractive for relatively low speed home networks, and such networks are being developed by Infracom [56]. In the research area diffuse networks that operate up to 50Mb/s have been demonstrated [57]. A solid-state tracked link that operates at 155Mb/s has been fabricated [30] that uses components optimized for OW applications. This includes custom CMOS transmitter and receiver devices, and detectors optimized for this application. Recent advances in LED technology has led to the fabrication of high efficiency white light devices. Even though the primary function of white LEDs was for illuminating and signaling purposes, some recent studies suggested and even demonstrated that such a LED can be used for establishing simultaneously a communication link [58, 59]. Achievable data rates depend on the angle of irradiance and field of view, and also on the use or not of tracking systems. In [59]data rates of few hundred Mb/s and even much higher are reported based on numerical results. This is a new emerging area for research and it has generated considerable interest, in especial in Asia. Recently the Visible Light Communication Consortium was created with the aim of investigating and promoting these techniques [60]

8. Future Perspectives and Areas of Research in Optical Wireless Communications

The part that OW might play in the 4G vision will be driven by different reasons in different applications areas. Where directive links are required, for instance for reasons of security, power efficiency or a requirement for very high spatial bandwidth density OW has clear benefits over RF approaches. Low cost optical and electrical components can be used to provide high capacity links over a wide variety of distances, with data rates from Mb/s to greater than Gb/s. Providing full coverage using LOS links is possible with some sort of tracking mechanism, and in cases where user density is low, and the environmental geometry is controlled to manage blocking. These systems might find application where ultrahigh bandwidth is required, together with mobility. The most common use of LOS

ISBN 978-93-5156-328-0

links might be to augment the capacity and capability of an RF network. Such links might offer

- Point to- point capacity within a hybrid network
- High bandwidth between RF base stations
- Optical hotspots with low latency data links
- Wireless access when RF systems are not desirable, such as medical or avionic environments.

Diffuse and quasi-diffuse channels can provide complete coverage without the need for RF channels, with varying degrees of complexity depending on the bit-rate desired. At low bit rates (~10Mb/s) diffuse OW can offer wireless connectivity with simple and therefore low cost components. This might find application in cost sensitive environments, such as the home, or in RF sensitive areas, such as hospitals, where wireless medical sensing is of interest. At much higher bit-rates (10-100s Mb/s) the increased path loss of the optical channel makes achieving coverage challenging, and relatively complex systems are required to achieve this. In this regime, some of the signal processing techniques used for radio systems may be valuable, using different front-ends and a common electronic system. RF is likely to be dominant particularly in this regime (as similar bit-rates may be available and allowed path losses are higher), with OW used in special situations, such as secure or RF sensitive environments.

9. Research Directions

The distinct properties of the OW channel can add to the 4G vision, with the possibility of a future terminal having a number of interfaces, both radio and optical. In order to achieve this work in the following areas is proposed, although this is not an exhaustive list.

10. Comprehensive Performance

10.1 Comparisons

Short-range optical systems and their counterpart based on conventional RF approaches; there is a need to understand the properties of both channels between the same points, so that alternative data paths can be modeled, and the performance of a network that chooses the optimum path be determined.

10.2 Network modeling

Understanding how optical and radio communications might coexist

10.3 Signal processing

Examination of radio processing techniques such as Multisensor (MIMO) optical systems exploiting space and angular diversity. Space-time coding for optical wireless channels. Some work in this field has already been recently introduced by [61], where space-time codes are designed specifically for optical channels, specifically in the context of free-space optics communications. A MIMO channel model applied to diffuse WOC has been recently presented by [62].

10.4 Hybrid optical-RF systems

Determination of the optimum method of using the alternative resources under different conditions, and the resulting performance improvement

11. Visible light communications

Fundamental capabilities and limitations of communication systems based on visible light (combined with illumination). The bandwidth and directivity of the optical wireless channel, together with the security and safety of the optical wireless channel in RF sensitive environments are useful and distinct properties that have a part to play in the wireless world. Together RF and optical approaches might significantly add to the capabilities of terminals, and there is a significant body of research effort that is working towards this.

References

[1] Van Nee, R. and R. Prasad, “OFDM for Wireless Multimedia Communications”, 2000: Artech House.

[2] J. Foerster, et al., “Ultra-Wideband technology for short or medium-range wireless communications”, Intel Technology Journal, 2001 (2),

[3] Dr. Bhupendra singh chauhan, Assistant professor, DTU, Delhi, India

[4] http://www.efkon.com. 2004.

[5] www.irda.org.

[6] S. Miyamoto, Y. Hirayama, and N. Morinaga, “Indoor wireless local area network system using infrared and radio communications in Proceedings of APCC/OECC'99 5th Asia Pacific Conference on Communications/4th

Optoelectronics and Communications, Conference”. 18(22) Oct. 1999 Beijing, China, 1999: Beijing Univ. Posts & Telecommun,

ISBN 978-93-5156-328-0

Beijing, China.
[7] http://www.jvc.com/ds2/f_prod.htm.
[8] www.spectrixcorp.com.
[9] www.infracom.com.
[10] M. Kavehrad and S. Jivkova, "Indoor broadband optical wireless communications: optical subsystems designs and their impact on channel characteristics", 2003: Pennsylvania State Univ. University Park PA USA.
[11] Khoo, S.H., et al. Eyesafe optical link using a holographic diffuser. in IEE Colloquium on Optical Wireless Communications. 1999: IEE.
[12] Benitez, P., et al. Eye-safe collimated laser emitter for optical wireless communications. 2002: ETSI Telecomunicacion Univ. Politecnica de Madrid Spain.
[13] JVC, www.jvc.com .luciole link. 2003.
[14] Y. Tanaka, S. Haruyama, and M. Nakagawa, "Wireless optical transmissions with white colored LED for wireless home links Proceedings of 11th International Symposium on Personal", Indoor and Mobile Radio Communication. 2000. London, UK: Dept. of Electr. Eng. Keio Univ. Kanagawa Japan 11th IEEE International Symposium on Personal Indoor and Mobile Radio Communications, PIMRC 2000, Proceedings, IEEE Piscataway NJ USA
[15] Welford, W.T., The optics of no imaging concentrators, light and solar energy. 1978, New York: Academic Press.
[16] www.opticalantennasolutions.com.
[17] S. Jivkova, and M. Kavehrad, "Holographic optical receiver front end for wireless infrared indoor communications", Applied Optics, 2001. 40(17): p. 2828-35
[18] K. Samaras, et al., BER performance of NRZ-OOK and Manchester modulation in indoor wireless infrared links. International Journal of Wireless Information Networks, 1998, 5(3): p. 219-33.
[19] O'Brien, D.C., et al., "Solid state tracking integrated optical wireless transceivers for line-of-sight optical links. in Free space laser communication and active laser illumination III", 2003. San Diego: SPIE
[20] McCullagh, M.J. and D.R. Wisely, "155mbit/S Optical Wireless Link Using a Bootstrapped Silicon Apd Receiver. Electronics Letters", 1994, 30(5): p. 430-432
[21] G. W. Marsh, and J.M. Kahn, "Performance evaluation of experimental 50-Mb/s diffuse infrared wireless link using on-off keying with decision-feedback equalization", IEEE Transactions on Communications, 1996. 44(11): p. 1496-1504
[22] D. C. O'Brien, et al. "Solid state tracking integrated optical wireless transceivers for line-of-sight optical links. in Free space laser communication and active laser illumination II". 2003. San Diego: SPIE
[23] Lalithambika, V.A., et al., "Development of a CMOS 310 Mb/s receiver for free-space optical wireless links. In Proceedings of the SPIE, the International Society for Optical Engineering", 2001: SPIE.

ISBN 978-93-5156-328-0
International Conference of Advance Research and Innovation (ICARI-2014)

Study of 4 Wheel Steering Systems to Reduce Turning Radius and Increase Stability

Arun Singh *, Abhishek Kumar, Rajiv Chaudhary, R. C. Singh
Department of Mechanical Engineering, Delhi Technological University, Delhi, India

Article Info

Article history:
Received 2 January 2014
Received in revised form
10 January 2014
Accepted 20 January 2014
Available online 1 February 2014

Keywords
Four-Wheel Steering,
4WS,
Rear Wheels Control

Abstract

Nowadays, the every vehicle existed mostly still using the two wheel steering system to control the movement of the vehicle whether it is front wheel drive, rear wheel drive or all wheel drive. But due to the awareness of safety, four wheel steering vehicles are being used increasingly due to high performance and stability that they bring to the vehicles. In this report, the performance of four wheels steered vehicle model is considered which is optimally controlled during a lane change maneuver in three type of condition which is low speed maneuver, medium speed maneuver and high speed maneuver. Four-Wheel Steering – Rear Wheels Control. For parking and low-speed maneuvers, the rear Wheel steer in the opposite direction of the front wheels, allowing much sharper turns. At higher speeds, the rest wheels steer in the same direction as the front wheels. The result is more stability and less body lean during fast lane changes and turns because the front wheels don't have to drag non-steering rear wheels onto the path.

1. Introduction

1.1 What is Steering?

Steering is the term applied to the collection of components, linkages, etc. which will allow a vessel (ship, boat) or vehicle (car, motorcycle, and bicycle) to follow the desired course. An exception is the case of rail transport by which rail tracks combined together with railroad switches provide the steering function. The most conventional steering arrangement is to turn the front wheels using a hand–operated steering wheel which is positioned in front of the driver, via the steering column, which may contain universal joints, to allow it to deviate somewhat from a straight line. Other arrangements are sometimes found on different types of vehicles, for example, a tiller or rear–wheel steering. Tracked vehicles such as bulldozers and tanks usually employ differential steering that is, the tracks are made to move at different speeds or even in opposite directions, using clutches and brakes, to bring about a change of course or direction.

1.2 Basic Geometry

Corresponding Author
E-mail address: arun_singh011@yahoo.com
All rights reserved: http://www.ijari.org

The basic aim of steering is to ensure that the wheels are pointing in the desired directions. This is typically achieved by a series of linkages, rods, pivots and gears. One of the fundamental concepts is that of caster angle - each wheel is steered with a pivot point ahead of the wheel; this makes the steering tend to be self-centering towards the direction of travel.

The steering linkages connecting the steering box and the wheels usually conforms to a variation of Ackermann steering geometry, to account for the fact that in a turn, the inner wheel is actually travelling a path of smaller radius than the outer wheel, so that the degree of toe suitable for driving in a straight path is not suitable for turns. The angle the wheels make with the vertical plane also influences steering dynamics (see camber angle) as do the tires.

Many modern cars use rack and pinion steering mechanisms, where the steering wheel turns the pinion gear; the pinion moves the rack, which is a linear gear that meshes with the pinion, converting circular motion into linear motion along the transverse axis of the car (side to side motion). This motion applies steering torque to the swivel pin ball joints that replaced previously used kingpins of the stub axle of the steered wheels via tie rods and a short lever arm called the steering arm.

The rack and pinion design has the advantages of a large degree of feedback and direct steering "feel". A disadvantage is that it is not adjustable, so that when it does wear and develop lash, the only cure is replacement.

Older designs often use the recirculating ball mechanism, which is still found on trucks and utility vehicles. This is a variation on the older worm and sector design; the steering column turns a large screw (the "worm gear") which meshes with a sector of a gear, causing it to rotate about its axis as the worm gear is turned; an arm attached to the axis of the sector moves the Pitman arm, which is connected to the steering linkage and thus steers the wheels. The recirculating ball version of this apparatus reduces the considerable friction by placing large ball bearings between the teeth of the worm and those of the screw; at either end of the apparatus the balls exit from between the two pieces into a channel internal to the box which connects them with the other end of the apparatus, thus they are "recirculated".

The recirculating ball mechanism has the advantage of a much greater mechanical advantage, so that it was found on larger, heavier vehicles while the rack and pinion was originally limited to smaller and lighter ones; due to the almost universal adoption of power steering, however, this is no longer an important advantage, leading to the increasing use of rack and pinion on newer cars. The recirculating ball design also has a perceptible lash, or "dead spot" on centre, where a minute turn of the steering wheel in either direction does not move the steering apparatus; this is easily adjustable via a screw on the end of the steering box to account for wear, but it cannot be entirely eliminated because it will create excessive internal forces at other positions and the mechanism will wear very rapidly. This design is still in use in trucks and other large vehicles, where rapidity of steering and direct feel are less important than robustness, maintainability, and mechanical advantage.

The worm and sector was an older design, used for example in Willys and Chrysler vehicles, and the Ford Falcon (1960s).

Other systems for steering exist, but are uncommon on road vehicles. Children's toys and go-karts often use a very direct linkage in the form of a bell crank (also commonly known as a Pitman arm) attached directly between the steering column and the steering arms, and the use of cable-operated steering linkages (e.g. the Capstan and Bowstring mechanism) is also found on some home-built vehicles such as soapbox cars and recumbent tricycles.

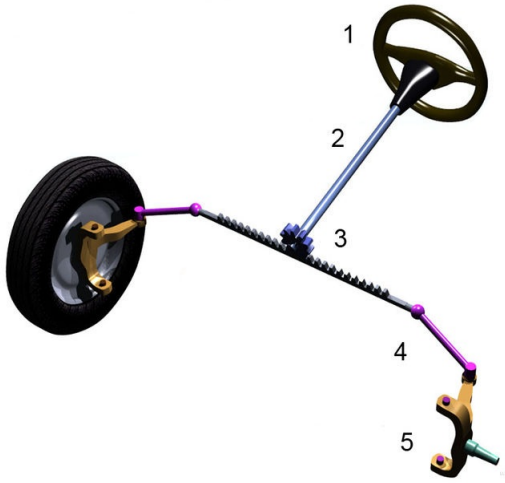

Fig: 1. Rack and pinion steering mechanism
1 Steering wheel; 2 Steering column; 3 Rack and pinion; 4 Tie rod; 5 Kingpin.

2. Four Wheel Steering

2.1 4 Wheel Steering

Four-wheel steering, 4WS, also called rear-wheel steering or all-wheel steering, provides a means to actively steer the rear wheels during turning maneuvers. It should not be confused with four-wheel drive in which all four wheels of a vehicle are powered. It improves handling and helps the vehicle make tighter turns. Production-built cars tend to under steer or, in few instances, over steer. If a car could automatically compensate for an under steer /over steer problem, the driver would enjoy nearly neutral steering under varying conditions.

4WS is a serious effort on the part of automotive design engineers to provide near-neutral steering. The front wheels do most of the steering. Rear wheel turning is generally limited to half during an opposite direction turn. When both the front and rear wheels steer toward the same direction, they are said to be in-phase and this produces a kind of sideways movement of the car at low speeds. When the front and rear wheels are steered in opposite direction, this is called anti-phase, counter-phase or opposite-phase and it produces a sharper, tighter turn.

This project aims at developing a 4 Wheel Steering System which would cater to the needs of people. This system is employed to improve steering response, increase vehicle stability while maneuvering at high speed, or to decrease turning radius at low speed.

The concept is simple. Rather than controlling a car solely by the angle at which the front tires meet the road the method used by wheeled vehicles since

the horse-drawn carriage, four-wheel steering turns the wheels simultaneously at both ends of the car. The idea is intuitively appealing to any city driver who has ever pulled up to a too-short parking space and wished he could point all four tires toward the curb and crab right in.

Not so easy. For starters, the rear wheels of a four-wheel-steer car do not always turn in tandem with the front wheels. Depending on the speed of the car, the rear wheels may turn in the same direction (same-side steering) as the front wheels, or in the opposite direction (counter steering). Most of the new four-wheel-steer autos are capable of both counter steering and same-side steering. In sharp, slow-speed turns, counter steering can shave a full yard off a standard sedan's turning radius. At high speeds, however, counter steering can make a car dangerously unstable, while same-side steering actually improves the ride.

The difference comes from the dynamics of high-speed motoring. When a driver traveling at highway speeds turns the wheel of a conventional, two-wheel steering car, the front tires immediately begin to pivot and the car's forward momentum generates a powerful sideways or cornering force at the front axle. The rear tires, however, have to wait until the car has actually started its turn before they begin to generate a corresponding force at the rear axle. That is why a car with two-wheel steering fishtails during lane changes; the back end is trying to catch up to the front. In extreme cases, or under slippery conditions, the rear of the car may fishtail out of control.

In a four-wheel-steer car, this high-speed sway can be damped or even eliminated through the use of same-side steering. When the rear wheels are turned at the same time and in the same direction as the front wheels, the back end turns with the front, and the cornering forces occur at both axles simultaneously. The car slides smoothly to the side without sway or fishtail.

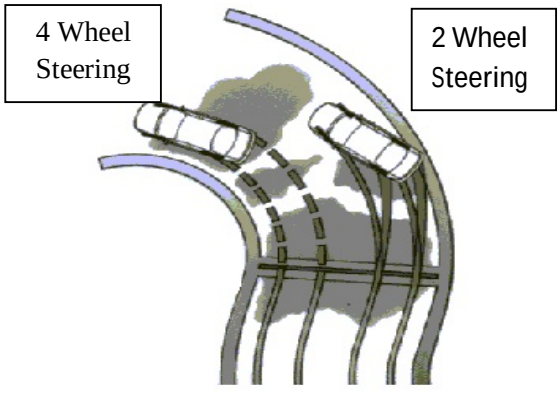

Fig 2: Comparison between two drives

2.2 Technical Details

In four-wheel steering systems, the rear wheels are steered by a computer and actuators. The rear wheels generally cannot turn as far as the front wheels. Some systems allow the rear wheels to be steered in the opposite direction as the front wheels during low speeds. This allows the vehicle to turn in a significantly smaller radius—sometimes critical for large trucks or tractors and vehicles with trailers.

Many modern vehicles offer a form of passive rear steering to counteract normal vehicle tendencies. On many vehicles, when cornering, the rear wheels tend to steer slightly to the outside of a turn, which can reduce stability. The passive steering system uses the lateral forces generated in a turn (through suspension geometry) and the bushings to correct this tendency and steer the wheels slightly to the inside of the corner. This improves the stability of the car, through the turn. This effect is called compliance under steer and it, or its opposite, is present on all suspensions.

Typical methods of achieving compliance under steer are to use a Watt's Link on a live rear axle, or the use of toe control bushings on a twist beam suspension. On an independent rear suspension it is normally achieved by changing the rates of the rubber bushings in the suspension. Some suspensions will always have compliance over steer due to geometry.

Four-wheel steering found its most widespread use in monster trucks, where manoeuvrability in small arenas is critical, and it is also popular in large farm vehicles and trucks. Some of the modern European Intercity buses also utilize four-wheel steering to assist manoeuvrability in bus terminals, and also to improve road stability.

Previously, Honda had four-wheel steering as an option in their 1987–2000 Prelude and Honda Ascot Innova models (1992–1996). Mazda also offered four-wheel steering on the 626 and MX6 in 1988. General Motors offered Delphi's Quadra steer in their consumer Silverado/Sierra and Suburban/Yukon. However, only 16,500 vehicles have been sold with this system since its introduction in 2002 through 2004. Due to this low demand, GM discontinued the technology at the end of the 2005 model year.[2] Nissan/Infiniti offer several versions of their HICAS system as standard or as an option in much of their line-up. A new "Active Drive" system is introduced on the 2008 version of the Renault Laguna line. It was designed as one of several measures to increase security and stability. The Active Drive should lower the effects of under steer and decrease the chances of spinning by diverting part of the G-forces generated in a turn from the front to the rear tires. At low speeds

the turning circle can be tightened so parking and manoeuvring is easier.

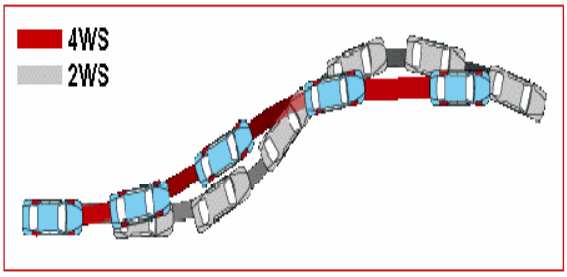

Fig: 3. Comparing turning radius for a 4WS and a 2WS

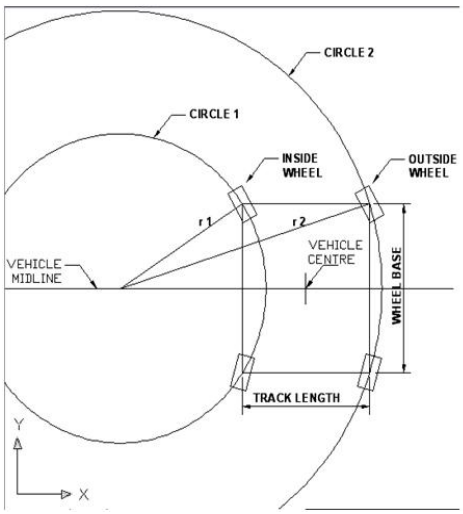

Fig: 4. Turning radius for inner and outer wheel

2.3 Modes in 4WS system

2.3.1 Four Wheel Steer

In Four Wheel Steer mode the rear wheels will always follow the front ones and will give the tightest turning circle. You may switch to and from this position at any time in the field and the rear wheels will re-align automatically regardless of the front wheel position.

2.3.2 Crab Steer

Crab steering is a special type of active four-wheel steering. It operates by steering all wheels in the same direction and at the same angle. Crab steering is used when the vehicle needs to proceed in a straight line but under an angle (i.e. when moving loads with a reach truck, or during filming with a camera dolly), or when the rear wheels may not follow the front wheel tracks (i.e. to reduce soil compaction when using rolling farm equipment).

2.3.3 Rear Wheel Steering

A few types of vehicle use only rear wheel steering, notably fork lift trucks, camera dollies, early pay loaders, Buckminster Fuller's Dymaxion car, and the Thrusts SC.

Rear wheel steering tends to be unstable because in turns the steering geometry changes hence decreasing the turn radius (oversteer), rather than increase it (Understeer). A rear wheel steered automobile exhibits non-minimum phase behavior. It turns in the direction opposite of how it is initially steered. A rapid steering input will cause two accelerations, first in the direction that the wheel is steered, and then in the opposite direction: a "reverse response." This makes it harder to steer a rear wheel steered vehicle at high speed than a front wheel steered vehicle.

2.3.4 Passive Rear Wheel Steering

Many modern vehicles offer a form of passive rear steering to counteract normal vehicle tendencies. For example, Subaru used a passive steering system to correct for the rear wheel's tendency to toe-out. On many vehicles, when cornering, the rear wheels tend to steer slightly to the outside of a turn, which can reduce stability. The passive steering system uses the lateral forces generated in a turn (through suspension geometry) and the bushings to correct this tendency and steer the wheels slightly to the inside of the corner. This improves the stability of the car, through the turn. This effect is called compliance Understeer and it, or its opposite, is present on all suspensions. Typical methods of achieving compliance Understeer are to use a Watt's Link on a live rear axle, or the use of toe control bushings on a twist beam suspension. On an independent rear suspension it is normally achieved by changing the rates of the rubber bushings in the suspension. Some suspensions will always have compliance oversteer due to geometry, such as Hotchkiss live axles or a semi-trailing arm IRS.

3. Components And Working

3.1 Components

3.1.1 Primary Components

- Vehicle speed sensors Interpret speedometer shelf revolutions and send signal to the electronic computer unit. Two sensors, one within the speedometer and the other at the transmission output, are used to crosscheck the other for accuracy and failsafe measures.
- Steering phase control unit conveys to the power steering cylinder booster valve the direction and

stroke of rear wheel steering by the combined movement of the control yoke angle and bevel gear revolutions.

- Electric stepper motor Performs altering of the yoke angle and bevel gear phasing
- Rear steering shaft Transmits front wheel steering angle by turning the small bevel gear in the steering phase control unit, which rotates the main bevel gear in the assembly.
- Control valve Feeds hydraulic pressure to the steering actuator, according to the phase and stroke required for appropriate rear wheel steering.
- Hydraulic power cylinder operates the output rod by hydraulic pressure and steers the rear wheels. It locks the rear wheels in a "neutral"(straightforward) position with the centering lock spring, which is activated by a solenoid valve in case of failure to ensure a normal 2WS
- Function for the vehicle hydraulic pump provides hydraulic pressure to both the front and rear steering systems.

3.1.2 Steering Phase Control Unit

The steering phase control unit alters the direction and degree of rear wheel steering. It consists of a stepper motor that controls the rear steering ratio, a control yoke, a swing arm, a main bevel gear engaged to the rear steering shaft via a small bevel gear, and a control rod connected to the control valve. It operates:

- Opposite phase (direction) steering under 35km/h (22mph)
- Control Yoke is at an angle activated by the stepper motor
- Front wheels are steered to the right. The small bevel gear is rotated in direction X by the rotation of the rear steering shaft. The small bevel gear, in turn, rotates the main bevel gear.
- Rotation of the main bevel gear causes movement of the control rod toward the control valve.
- Input rod of the control valve is pushed to the right, according to the degree of the control rod's movement (determined by the disposition of the swing arm), which is positioned to move in an upward direction, to the right. The rear wheels are thus steered to the left, in an opposite direction to the front wheels.
- As the angle of the control yoke is increased in direction A as vehicle speed decreases, the rear-to-front steering ratio proportionately increases and the vehicle's steering lock tightens.
- Same phase (direction) over 35km/h (22mph). The operation of this phase is the reverse of the opposite phase one, because the control yoke is angled toward "positive" in this vehicle speed range, as illustrated. The phasing of the swing arm, yoke rod and bevel gear steers the rear wheels toward the right-the same direction as the front wheels.
- Neutral phase, at 35km/h (22mph) the control yoke's angle is horizontal (neutral). Thus, the input rod is not affected, even if the control rod is moved with the rotation of the bevel gear unit. As a result, the rear wheels are not steered in this mode.

3.2 Working Mechanism

- Consists of a rack-and-pinion front steering system that is hydraulically assisted by a twin-tandem pump main power source.
- The rear wheel steering mechanism is also hydraulically assisted by the main pump and electronically controlled - according to the front steering angle and vehicle speed.
- The rear steering shaft extends from the rack bar of the front steering gear assembly to the rear steering-phase control unit.
- The rear steering system is comprised of the input end of the rear steering shaft, vehicle speed sensors, a steering-phase control unit (determining direction and degree), a power cylinder and an output rod
- A centering lock spring is incorporated, which locks the rear system in a neutral (straightforward) position in the event of hydraulic failure. Additionally, a solenoid valve that disengages hydraulic assist (thereby activating the centering lock spring) in case of an electrical failure is included.
- The 4WS system varies the phase and ratio of the rear-wheel steering to the front wheels, according to the vehicle speed.
- It steers the rear wheels toward the opposite phase (direction) of the front wheel during speeds less than 35km/h (22mph) for a tighter turn and "neutralizes" them (to a straightforward direction, as in a conventional two-wheel steering principle) at 35km/h (22mph).
- Above the speed of 35 km/h, the system steers toward the same phase-direction as the front

wheels, thereby generating an increased cornering force for stability.

- The maximum steering angle of the rear wheels extends 10 degrees.

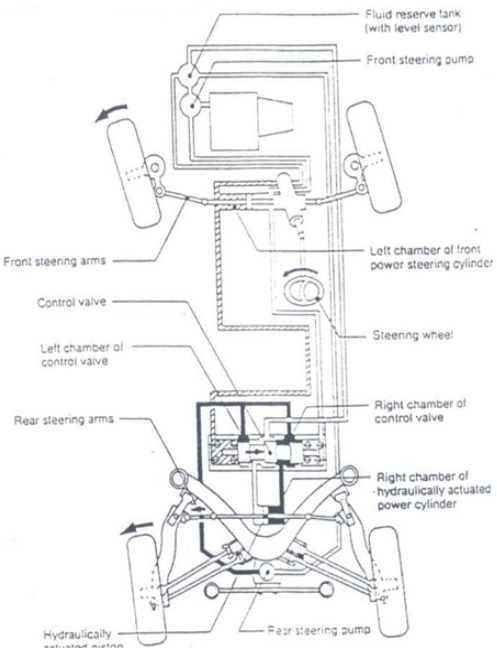

Fig: 5. 4 Wheel Steering mechanisms

3.3 Fail-Safe Measures

- The system automatically counteracts possible causes of failure, both electronic and hydraulic. In either case, the centering lock spring housed in the steering system unit returns the output rods in the "neutral" straightforward position, essentially alternating the entire steering system to a conventional 2WS principle.
- Specifically, if a hydraulic defect should render a reduction in pressure level (by a movement malfunction or a broken driving belt), the rear wheel steering mechanism is automatically locked in a neutral position, activating a low-level warning light.
- In the event of an electrical failure, such would be detected by a self-diagnostic circuit integrated within the 4WS control unit, which stimulates a solenoid valve and then neutralizes hydraulic pressure and return lines, thereby alternating the system again to that of a 2WS principle. Henceforth, the warning light referencing the 4WS system within the main instrument display is activated, indicating a system failure.

4. Advantages & Disadvantages

4.1 Advantages

- **Superior cornering stability:** The vehicle cornering behavior becomes more stable and controllable at high speed as well as on wet slippering road surfaces.
- **Improved steering response and precision:** The vehicle response to steering input becomes quicker and more precise throughout the vehicle enter speed range.
- **High speed straight line stability:** The vehicle's straight –line stability at high speed is improved. Negative effects of road irregularities and crosswinds on the vehicles stability are minimized.
- **Improved rapid lane-changing maneuvers:** This is stability in lane changing at high speed is improved. In high speed type operation become easier. The vehicle is less likely to go into a spin even in situations in which the driver must make a sudden and relatively large change of direction.
- **Smaller turning radius:** By steering the rear wheels in the duration opposite the front wheels at low speed, the vehicle's turning circle is greatly reduced. Therefore, vehicle maneuvering on narrow roads and during parking become easier.
- **Controlling:** Computer-controlled Quadrasteer can be switched on and off and has an effective trailer towing mode.

4.2 Disadvantages

- The 4ws, due to construction of many new components, the system becomes more expensive.
- The system includes as many components (especially electronically) there is always a chance to get any of the part inactive, thus the system become in operative.

5. Application

- **Parking:** During a parking a vehicles driver typically turns the steering wheels through a large angle to achieve a small tuning radius. By counter phase steering of the rear wheels, 4ws system realizes a smaller turning radius then is possible with 2ws system. As a result vehicle is turned in small radius at parking.
- **Junctions:** On a cross roads or other junction where roads intersect at 900 degrees or tighter angles, counter phase steering of the rear wheels

- causes the front and rear wheels to follow more-or-less path. As a result the vehicle can be turned easily at a junction.
- **Slippery road surfaces:** During steering operation on low friction surfaces, steering of the rear wheels suppress sideways drift of the vehicle's rear end. As a result the vehicles direction is easier to control.
- **High speed straight line operation:** When traveling in a straight line at high speed, a vehicle's driver frequently needs to make small steering correction to maintain the desired direction, in phase steering of the rear wheels minimizes these corrective steering inputs.
- **Narrow roads:** On narrow roads with tight bends, counter-phase steering of the rear wheels minimizes the vehicle's turning radius, thereby reducing side-to –side rotation of the steering wheels and making the vehicle easier to turn.
- **U-Turns:** By minimizing the vehicle's turning radius, counter –phase steering of the rear wheels enables U-turns to be performed easily on narrow roads.

6. Conclusion

Four wheel steering is a relatively new technology, that imposes maneuverability in cars, trucks and trailers .in standard two wheels steering vehicles, the rear set of wheels are always directed forward therefore and do not play an active role in controlling the steering in four wheel steering system the rear wheel can turn left and right . To keep the driving controls as simple as possible.

The aim of 4WS system is a better stability during overtaking manoeuvres, reduction of vehicle oscillation around its vertical axis, reduced sensibility to lateral wind, neutral behaviour during cornering, etc., i.e. improvement of active safety.

References

[1] F. Vlk, "Dynamika motorových vozidel", Nakladatelství a zasilatelství VLK, Brno, 2001
[2] S. C. Chang, "Synchronization in a steer-by-wire vehicle dynamic system", International journal of engineering science, 45(2-8), 628-643, 2007
[3] C. D. Gadda, P. Yih, J. C. Gerdes, "Incorporating a model of vehicle dynamics in a diagnostic system for steer-by-wire vehicles", 2004
[4] T. Hiraoka, O. Nishihara, H. Kumamoto, Automatic path-tracking controller of a four-wheel steering vehicle, Vehicle System Dynamics, 47(10), 1205-1227, 2009
[5] H. S. Kim, S. S. You, "Estimation of Vehicle Sideslip Angle for Four-Wheel Steering Passenger Cars", Transactions on Control, Automation and Systems Engineering, 3, 71-76, 2001
[6] M. Kreutz, M. Horn, J. Zehetner, "Improving vehicle dynamics by active rear wheel steering systems", Vehicle System Dynamics, 47(12), 1551-1564, 2009
[7] R. B. Gupta, "Automobile Engineering, Satya Prakashan", New Delhi, pp 3-8 and 571-579, 2007
[8] K. Singh, "Automobile Engineering Vol. 1, Standard Publishers Distributors, New Delhi, pp 448-453, 463-471, 2008
[9] Y. G. Cho, "Vehicle steering returnability with maximum steering wheel angle at low speeds", International Journal of Automotive Technology, 10(4), pp 431−439, 2009
[10] http://www.parker hire.co.uk/cy/large_excavators.html
[11] http://auto.howstuffworks.com/jeep-hurricane2.html
[12] R. S. Khurmi, J. K. Gupta, "A text book of Machine Design. Eurasia Publishing house (PVT.) Ltd", First multi color edition, pp 576-586 658-679, 1037-1040, 2005

.

Indian Journal of Chemistry
Vol. 53B, March 2014, pp. 325-331

Synthesis and antimicrobial activity of some new 1,2,4-triazine and benzimidazole derivatives

Abha Bishnoi*[a], Suruchi Singh[a], Anil K Tiwari[a], Archna Rani[b], Sapna Jain[b] & C K M Tripathi[c]

[a]Department of Chemistry, Lucknow University, Lucknow 226 007, India

[b]Department of Applied Chemistry, Delhi College of Engineering, New Delhi 110 042, India

[c]Fermentation Division, CSIR-Central Drug Research Institute, Lucknow 226 001, India

E-mail: dr.abhabishnoi@gmail.com

Received 14 August 2012; accepted (revised) 7 November 2013

1-(4-Substituted phenyl)-3-(substituted)propan-1-(1*H*-benzo[*d*]imidazol-2-yl)hydrazines and 1-(4-substituted phenyl)-3-(substituted)propan-1-(5*H*-[1,2,4]triazino[5,6-*b*]indol-3-yl) hydrazines have been synthesized by the fusion of triazine and benzimidazole derivatives with Mannich bases. The synthesized compounds have been characterized and screened against ITCC 5226 *Sclerotium rolfsii* and ITCC 0482 *Macrophomina phaseolina* and MTCC739 *Escherichia coli*, ATCC6533 *Bacillus subtilis*, ATCC9144 *Staphylococcus aureus*, ATCC25619 *Pseudomonas aeruginosa* and ATCC24433 *Candida albicans.*

Keywords: Antimicrobial, animal pathogens, plant pathogens, benzimidazole, Mannich bases, triazine

Recent years have seen increased problem of microbial infection on human beings as well as on plants. In order to combat these infections, a wide range of antimicrobial agents are available but their continuous use has lead to development of resistance and resurgence of dangerous microbes. This has necessitated synthetic diversification through a new approach. In this regard development of broad spectrum antimicrobial agents can overcome the ever growing burden of newer and newer chemicals entering in the environment, designed against very specific microbes. Approaches to address this problem comprises the design of compounds, including more than one kind of active chemical moiety in a single molecule, to enhance antimicrobial activity and minimize the prevalence of resistance in microbes.

Mannich bases have been reported as potent biological agents finding application in pharmaceutical chemistry as antibacterial, antimalarial, vasorelaxant, anticancer and analgesics as well as in agricultural chemistry as pesticides against various plant pathogens[1-4]. Similarly, literature revealed that benzimidazole or triazine exhibit broad spectrum of biological activity[4-6] *viz.*, fungicidal like benomyl (Benlate), carbendazim, propiconazole which have well known commercial value in protecting desirable plants from the development of fungal diseases. These are benzimidazole or triazine derivatives, containing nitrogen bearing side chain (**Figure 1**). Imazalil, an imidazole fungicide (**Figure 1d**) used to control powdery mildews in cucumbers, marrows and ornamentals and *Fusarium* in sweet potatoes, also inhibits the growth of several other fungi[7,8]. Similarly, a series of 1,2,4-triazines has been discovered with potent antifungal activity[9-11]. These observations have prompted the design and synthesis of new series of Mannich bases containing 1,2,4-triazine or benzimidazole moieties in single molecular structure to explore their potency as agrochemicals and chemotherapeutics. Based on these findings and in continuation of the work on heterocycles[12-15], 1-(4-substituted phenyl)-3-(substituted) propan-1-(1*H*-benzo[*d*]imidazol-2-yl)-hydrazines **7a-d** and 1-(4-substituted phenyl)-3-substituted propan-1-(5*H*-[1,2,4]triazino[5,6-*b*]indol-3-yl)hydrazines **8a-c** were synthesized and screened against multi host plant pathogenic fungi ITCC 5226 *Sclerotium rolfsii*, ITCC 0482 *Macrophomina phaseolina*, and animal fungi ATCC24433 *Cadida albicans*, along with some gram positive as well as gram negative bacterial strains, *viz.* MTCC739 *Escherichia coli*, ATCC6533 *Bacillus subtilis*, ATCC9144 *Staphylococcus aureus* and ATCC25619 *Pseudomonas aeruginosa.*

Results and Discussion

The preparation of new 1-(4-substituted phenyl)-3-substituted propane-1-(1*H* benzo[*d*]imidazol-2-yl)hydrazines **7a-d** and 1-(4substituted phenyl)-3-

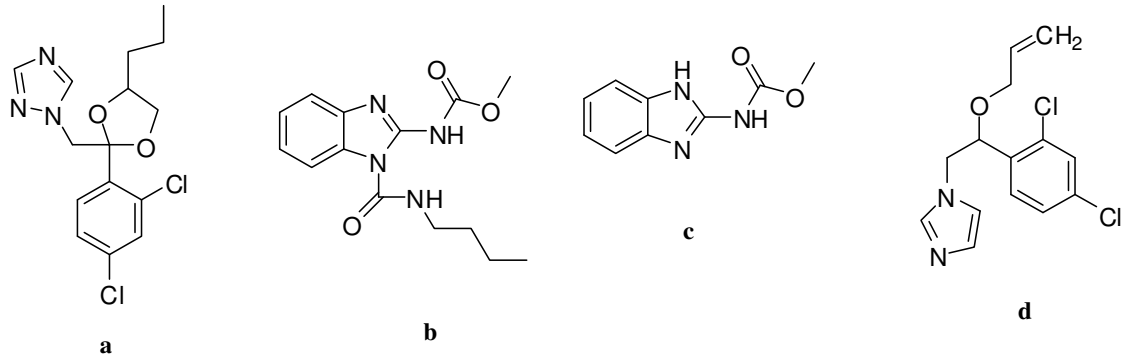

Figure 1 — **a**: Propiconazole, **b**: Benomyl, **c**: Carbendazim, **d**: Imazalil

substitutedpropane-1-(5*H*-[1,2,4]-triazino[5,6-*b*]indol-3-yl)hydrazines **8a-c** involves three steps: (i) Mannich reaction of different acetophenones and secondary amines, (ii) reduction of the keto compounds by sodium borohydride to the corresponding 3-*N*-substituted amino-1-phenyl-propanols **4a-e** and (iii) the reaction of alcohol derivatives with thionyl chloride followed by addition of 2-hydrazinyl-1-*H*-benzo[*d*]imidazoles 5/3-hydrazinyl-1-5*H*-[1,2,4]triazino[5,6-*b*]indole **6** in alcohol to produce compounds **7a-d** and **8a-c** (**Scheme I**). The structures of all products were in good agreement with the spectral data and elemental analysis.

Biological Activity

Seven compounds were examined for their antifungal activity at a concentration of 500 ppm (**Table I**). Biological data against *Macrophomina phaseolina* indicate that benzimidazole derivatives of Mannich bases **7a-c** exihibit slightly better inhibition than triazine derivatives of these bases **8a-c**. It is very interesting to observe that two compounds **7b** and **8c** with substituents R (=OH) and R_1R_2 (=morpholine group) inhibited the growth of fungus to a considerable extent. It appears that these two groups, present together in a single molecular structure, play a greater role in conferring the antifungal activity to the compound than other groups studied in the current piece of work. Maximum inhibition of compound **7b** against *Macrophomina phaseolina* suggests benzimidazole derivatives of Mannich base derived from *p*-hydroxy acetophenone and morpholine finds comparatively a better fit at the receptor site than the compounds bearing other group at these positions.

Antifungal efficacy of **7b** is also correlated with its energetically favoured conformation. It seems that the caged geometry of the compound **7b** allows it to interact in a more favorable way with the receptor site of the organism. On the other hand, all the seven compounds were found to show random activity towards *Sclerotium rolfsii*.

Most of the synthesized compounds have shown promising activity against *S. aureus* while very mild activity against *P. aeruginosa* was observed (**Table I**). Compounds **7c** and **8a** exhibited moderate activity against *C. albicans*, *E. coli* and *B. subtilis*. It may therefore be inferred that in order to elucidate a structure activity relationship, synthesis and antimicrobial evaluation of more such compounds with larger number of substituents is required and this work is in progress.

Materials and Methods

In vitro antifungal assay: Determination of percentage of inhibition

Potato dextrose agar of HI MEDIA, MUO96 was used as culture medium. The compounds were dissolved in DMSO. Food poisoning method was followed to determine antifungal activity in terms of percentage of inhibition as described below[16].

Mother cultures of fungal species, grown and maintained on potato dextrose agar media at 28±1°C were used for the experiments. The compounds were mixed aseptically with PDA media and were sterilized. The medium with acetone was served as control. The Petri plates having 9 cm inner diameter were taken, and 25 mL of the sterilized PDA containing test samples were plated in the centre. After solidification, 0.5 cm diameter agar discs taken from a 48 hr old fungal mother culture was placed with the fungal side downward in the centre of each plate with the help of sterile cork borer and glass rod. The plates were incubated in dark at 28±1°C. Radial growths were determined by measuring the colony size along two diameters at right angles after complete growth in the control. Three replicates for

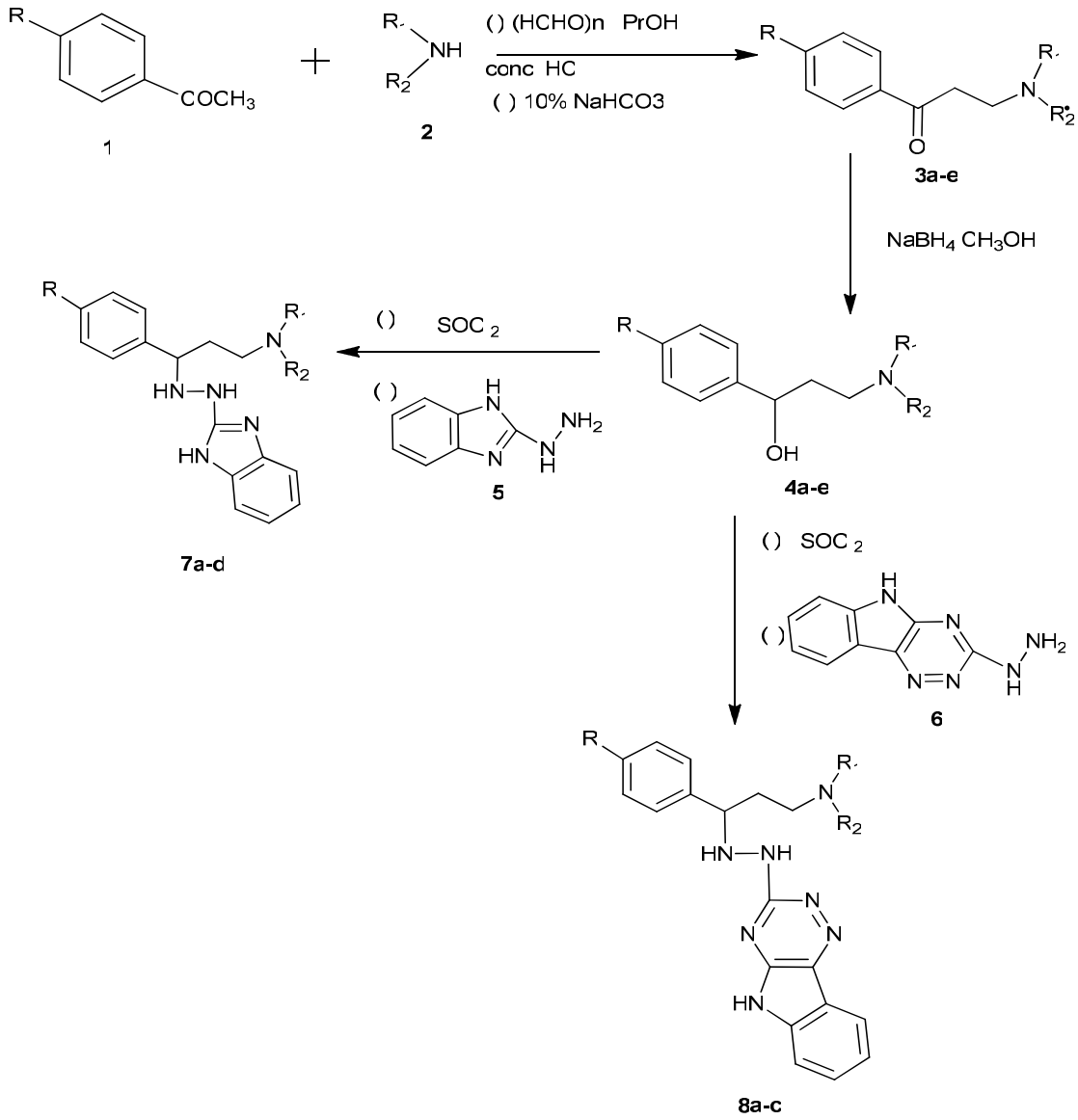

3 and **4**; a: R=H, R_1=Morpholine, b: R=H, R_1=N-benzyl methylamine, c: R=OH, R_1= Morpholine, d: R=OH, R_1=Pyrrolidine, e: R=NH_2, R_1= Pyrrolidine, **7**; a: R=H, R_1=Morpholine, b: R=OH, R_1= Morpholine, c: R=OH, R_1=Pyrrolidine, d: R=NH_2, R_1= Pyrrolidine, **8**; a: R=H, R_1=Morpholine, b: R=H, R_1=N-benzyl methylamine, c: R=OH, R_1= Morpholine.

Scheme I

each treatment were prepared. The experiments were repeated three times. The zone of inhibition was then calculated[17].

In vitro antibacterial assay

A loopful of culture was taken from the slants of individual bacterial strain and inoculated in 25 mL of sterile nutrient broth. Inoculation was carried out by dipping a sterile cotton-wool swab into the suspension and spread evenly over the entire surface of the petriplate by swabbing in three directions. The plates were allowed to dry for some time before applying discs. Cultures were incubated at 37°C and 120 rpm in an orbital shaker for 10 hr. A volume of 100 µL of actively growing culture was evenly spread onto the surface of the nutrient agar plate. Impregnated discs were placed on the agar surface with sterile forceps and gently pressed down to ensure contact. A concentration of 1000 µg/µL of the compounds in ethyl alcohol was added to each disc (20 µL/disc)

Table I — Antimicrobial activity of the synthesized compounds

	Antifungal activity (Zone of Inhibition in mm) (conc. 500 ppm)					Antibacterial activity (Zone of Inhibition in mm) (conc. 2 mg/disc)	
Compd	ITCC 0482 *M. phaseolina*	ITCC5226 *S. rolfsii*	ATCC24433 *C. albicans*	MTCC739 *E. coli*	ATCC6533 *B. subtilis*	ATCC9144 *S. aureus*	ATCC25619 *P. aeruginosa*
7a	11	14	6	6	6	17	6
7b	22	6	6	6	6	20	7
7c	15	6	6	9	8	11	6
7d	6	14	8	6	6	6	6
8a	6	6	7	10	8	14	7
8b	10	13	9	6	6	12	6
8c	15	11	10	8	6	10	6

placed on a sterile Petri plate. The impregnated discs were dried for 3-5 min and placed on pre-inoculated agar surface. A control was also established by using just the solvent in which each compound was dissolved. The plates were incubated at 37°C for 24 hr. The degree of inhibition of the test compounds was observed by the formation of zones around the impregnated discs. It was measured in mm[18].

Experimental Section

Melting points were determined in open capillaries in an electrically heated block and are uncorrected. The progress of the reaction was monitored by TLC, using TLC grade silica gel (G) and was developed by exposure to an atmosphere of iodine vapours. IR spectra were recorded on Perkin-Elmer 1430 spectrophotometer using KBr pellets and ^{1}H and ^{13}C NMR spectra were obtained on Bruker F 400 MHz NMR spectrometer in $CDCl_3$, CD_3OD and DMSO-d_6 using TMS as an internal standard (chemical shifts in δ, ppm). Mass spectra were recorded on a Va 70-70H spectrometer at 70 eV. Elemental analyses were carried out on Carlo Erba EA-1108 elemental analyzer.

Synthesis: Compounds **5** and **6** were prepared by known procedures[19,20].

Synthesis of 3-*N*-substituted aminopropiophenones, 3a-e: Compound **3b** was prepared by known procedure[21].

3-Morpholino-1-phenylpropan-1-one, 3a. m.p. 172°C. Yield 78%; R_f value: 0.411 (9:1, Hexane:EtOAc); IR: 2808(C-H), 1719(C=O), 1360(C-N), 1050 cm^{-1} (C-O). Anal. Calcd for $C_{13}H_{17}NO_2$: C, 71.23; H, 7.76; N, 6.39. Found: C, 71.33; H, 7.52; N, 6.19%.

1-(4-Hydroxyphenyl)-3-morpholinopropan-1-one, 3c. m.p.196°C. Yield 72%; R_f value: 0.393 (9:1, Hexane:EtOAc); IR: 3225 (O-H), 2810 (C-H), 1720 (C=O), 1357 (C-N), 1078 (C-O), 760 cm^{-1} (Ar monosubs.); ^{1}H NMR (400 MHz, $CDCl_3$): δ 9.40 (4-OH), 8.31 (d, 2H, 2,6CH in ArH), 8.11 (d, 2H, 3,5CH in ArH), 4.33 (t, 2H, 2-CH_2), 3.60 (t, 4H, CH_2-N-CH_2), 3.56 (t, 2H, 3-CH_2N), 1.32 (t, 4H, CH_2-N-CH_2); ^{13}C NMR ($CDCl_3$): δ 198.0 (C-1), 67.5 (C-O-C), 53.3 (C-N-C), 49.3 (C-3), 29.6 (C-2); MS: *m/z* 235(M^+). Anal. Calcd for $C_{13}H_{17}NO_3$: C, 66.38; H, 7.23; N, 5.95. Found: C, 66.21; H, 7.11; N, 5.52%.

1-(4-Hydroxyphenyl)-3-(pyrrolidin-1-yl) propan-1-one, 3d. m.p. 116°C. Yield 70%; R_f value: 0.224 (9:1, Hexane:EtOAc); IR: 3312 (O-H), 2886 (C-H), 1739 (C=O), 1357 (C-N), 776 cm^{-1} (Ar monosubs.). Anal. Calcd for $C_{13}H_{17}NO_2$: C, 71.23; H, 7.76; N, 6.39. Found: C, 71.53; H, 7.63; N, 6.02%.

1-(4-Aminophenyl)-3-(pyrrolidin-1-yl) propan-1-one, 3e. m.p. 51-62°C, Yield 83%; R_f value: 0.143 (8:2, Hexane:EtOAc); IR: 3584 (N-H), 2985 (C-H), 1747 (C=O), 1640 (N-H bend), 1351 (C-N), 765 cm^{-1} (Ar monosubs.). Anal. Calcd for $C_{13}H_{18}N_2O$: C, 71.55; H, 8.25; N, 12.84. Found: C, 71.22; H, 8.14; N, 11.97%.

Synthesis of 3-*N*-substituted amino-1-phenylpropanol, 4a-e: Free base of keto compound (**3a-e**; 0.026 mol) in methanol (50 mL) was cooled in ice-bath for 30 min and powdered $NaBH_4$ (0.074 mol) was added in equal portions in 1 h. The reaction mixture was further stirred in an ice-bath for 30 min. It was then concentrated under reduced pressure and the residue was treated with water (10 mL) and ethyl acetate (60 mL). The ethyl acetate layer was separated, washed with water till neutral washings, dried (over anhyd. Na_2SO_4) and concentrated. The crude product **4a, 4c** were purified by recrystallization

from ethanol, **4b** from chloroform and **4d, 4e** from absolute ethanol as solvents. The TLCs were obtained using hexane:ethyl acetate (8.5:1.5 and 8.2:1.8 v/v) as mobile phase.

3-Morpholino-1-phenylpropan-1-ol, 4a. The copmpound **4a** was obtained as an oil. Yield 75%; R_f value: 0.47 (8.5:1.5, Hexane:EtOAc); IR: 3300 (O-H), 3010 (C-H str. Ar), 2889 (C-H), 1343 (C-N), 1047 cm^{-1} (C-O). Anal. Calcd for $C_{13}H_{19}NO_2$: C, 70.58; H, 8.59; N, 6.33. Found: C, 70.42; H, 8.69; N, 6.1%.

3-(*N*-Benzyl-*N*-methyl amino)-1-phenylpropan-1-ol, 4b. m.p.164°C. Yield 66%; R_f value: 0.332 (8.2:1.8, Hexane:EtOAc); IR: 3250 (O-H), 3078 (C-H str. Ar), 2927 (C-H), 1458 cm^{-1} (Ar stretch); ^{1}H NMR (400 MHz, $CDCl_3$): δ 7.38-7.21 (m, 10H, ArH), 4.94-4.90 (m, 1H, 1-CH), 3.68-3.46 (q, 2H, CH_2-Benzyl J_A=12.9Hz, J_B=12.6Hz), 2.87-2.57 (m, 2H, 3-CH_2), 2.27 (s, 3H, N-CH_3), 2.05-1.86 (m. 2H, 2-CH_2); MS: *m/z* 255(M^+), 134, 120, 91. Anal. Calcd for $C_{17}H_{21}NO$: C, 77.92; H, 9.09; N, 6.06. Found: C, 77.36; H, 9.14; N, 5.72%.

4-(1-Hydroxy-3-morpholinopropyl) phenol, 4c. m.p. 169.5°C. Yield 76%; R_f value: 0.513(8.5:1.5, Hexane:EtOAc); IR: 3323 (O-H), 3046 (C-H str. Ar), 2911 (C-H), 1334 (C-N), 1053 cm^{-1} (C-O). Anal. Calcd for $C_{13}H_{19}NO_3$: C, 65.82; H, 8.01; N, 5.90. Found: C, 65.21; H, 8.25; N, 4.33%.

4-(1-Hydroxy-3-(pyrrolidin-1-yl) propyl) phenol, 4d. The compound **4d** was obtained as an oil. Yield 41.12%; R_f value: 0.4 (8.5:1.5, Hexane:EtOAc); IR: 3411 (O-H), 3033 (C-H str. Ar), 2885 (C-H), 1372 cm^{-1} (C-N). Anal. Calcd for $C_{13}H_{19}NO_2$: C, 70; H, 8.59; N, 6.33. Found: C, 70.24; H, 8.63; N, 5.96%.

1-(4-Aminophenyl)-3-(pyrrolidin-1-yl) propan-1-ol, 4e. The compound **4e** was obtained as an oil. Yield 80%; R_f value: 0.28 (8.2:1.8, Hexane:EtOAc); IR: 3396 (O-H), 3028 (C-H str. Ar), 2812 (C-H), 1348 cm^{-1} (C-N). Anal. Calcd for $C_{13}H_{20}N_2O$: C, 70.90; H, 9.09; N, 12.72. Found: C, 70.42; H, 9.04; N, 11.97%.

Synthesis of 1-(4-substituted phenyl)-3-(substituted)propan-1-(1*H*-benzo[*d*]imidazol-2-yl) hydrazines, 7a-d, and 1-(4-substituted phenyl)-3-substituted propan-1-(5*H*-[1,2,4]triazino[5,6-*b*]indol-3-yl)hydrazines, 8a-c: $SOCl_2$ (0.04 mol) in benzene (10 mL) was added to 3-N-substituted amino-1-phenyl-propanol **4a-e** (0.0015 mol) and the reaction mixture was heated on a water-bath for about 6 hr. Excess of $SOCl_2$ was removed by azeotropic distillation with dry benzene. The chloride derivative of **4a, 4c, 4d, 4e** without purification were mixed with 2-hydrazinyl-1-*H*-benzo[*d*]imidazole **5** (0.01 mol) and that of **4a, 4b, 4c** with 3-hydrazinyl-1-5*H*-[1,2,4]triazino[5,6-*b*]indole **6** (0.01 mol) in absolute ethanol and refluxed for 10-15 hr on water bath. The reaction mixture was concentrated under reduced pressure and the crude product was purified by recrystallization from absolute ethanol. Thus seven new compounds were synthesized and characterized. The TLCs were checked using Hexane:EtOAc (8:2 and 7.5:2.5 v/v) as mobile phase.

2-(1*H*-Benzo[*d*]imidazol-2-yl)-1-(3- morpholino-1-phenylpropyl) hydrazine, 7a. m.p. 110-120°C. Yield 65%; R_f value: 0.66 (8:2, Hexane:EtOAc); IR: 3010 (C-H str. Ar), 2874 (C-H), 1671 (N-H bend), 1351 (C-N), 1154 (C-O), 810 cm^{-1} (Ar monosubs.); ^{1}H NMR (400 MHz, DMSO-d_6): δ 7.70-7.51 (m, 4H, ArH imidazole), 7.12-7.08 (m, 5H, ArH), 5.48 (s, 1H,-NH imidazole), 3.82-3.78 (s, 1H, 1-NH hydrazine), 3.60 (m, 2H, 2-CH_2; J_A= 8.32Hz, J_B= 12.86 Hz), 3.37 (t, 4H,-CH_2-O-CH_2), 3.20-3.11 (s, 1H, 2-NH hydrazine), 2.73 (m, 2H, 3-CH_2N), 2.73-2.66 (m, 2H, 3-CH_2N), 2.57 (t, 4H,-CH_2-N-CH_2); ^{13}C NMR (400 MHz, DMSO-d_6): δ 141.0, 136.6 (C-3,4 imidazole), 65.6 (C-O-C), 60.4 (C-N-C), 57.1 (C-1), 36.1 (C-2), 48.9 (C-3), 36.1 (C-2); MS: 351(M^+). Anal. Calcd for $C_{20}H_{25}N_5O$: C, 68.37; H, 7.12; N, 19.94. Found: C, 68.42; H, 7.23; N, 18.26%.

2-(1*H*-Benzo[*d*]imidazol-2-yl)-1-(3-morpholino-1-*p*-hydroxy-phenylpropyl)hydrazine, 7b. m.p. 148°C. Yield 74%; R_f value: 0.43 (8:2, Hexane:EtOAc); IR: 3330 (O-H), 3210 (C-H str. Ar), 2990 (C-H), 1690 (N-H bend), 1390 (C-N), 1084 (C-O), 792 cm^{-1} (Ar monosubs.); ^{1}H NMR (400 MHz, DMSO-d_6): δ 8.00-7.86 (m, 4H, ArH imidazole), 6.95-6.78 (m, 4H, ArH), 4.50-4.32 (s, 1H, OH), 4.12-3.95 (s, 1H,-NH imidazole), 3.89 (s, 1H, 1-NH hydrazine), 3.20-3.18 (m, 1H, 1-CH), 2.62 (s, 1H, 2-NH hydrazine), 2.57 (m, 4H,-CH_2-O-CH_2), 2.43 (m, 4H,-CH_2-N-CH_2), 2.40 (m, 2H, 3-CH_2N), 1.49 (m, 2H, 2-CH_2; J_A= 8.68Hz, J_B= 12.53Hz); ^{13}C NMR (400 MHz, DMSO-d_6): δ 141.0, 133.8 (C-3,4 imidazole), 67.5 (C-O-C), 63.3 (C-N-C), 56.6 (C-1), 49.3 (C-3), 34.9 C-2); MS: 367(M^+). Anal. Calcd for $C_{20}H_{25}N_5O_2$: C, 65.39; H, 6.81; N, 19.07. Found: C, 64.99; H, 7.00; N, 18.39%.

2-(1*H*-Benzo[*d*]imidazol-2-yl)-1-(1-*p*-hydroxy-phenyl-3-(pyrrolidin-1-yl)propyl)hydrazine, 7c. m.p. 90-110°C. Yield 70%; R_f value: 0.55 (8:2, Hexane:EtOAc); IR: 3552 (N-H, str.), 3274 (O-H), 3027 (C-H str. Ar), 2789 (C-H), 2720 (C-H), 1550 (N-H bend), 729 cm^{-1} (Ar monosubs.); ^{1}H NMR (400 MHz, DMSO-d_6): δ 7.86-7.60 (m, 4H, ArH imidazole), 7.00-6.21 (m, 4H, ArH), 4.35 (s, 1H, OH;

exchangeable with D_2O), 3.41 (s, 1H, 2-NH hydrazine), 3.90 (s, 1H, NH imidazole), 2.69-2.62 (s, 1H, 1-NH hydrazine), 2.67 (m,1H, 1-CH), 2.36 (t, 2H, 3-CH_2), 2.32-2.25 (m, 4H, 2,5-CH_2 pyrollidine), 2.20 (m, 2H, 2-CH_2; J_A= 8.92Hz, J_B= 12.64Hz), 1.59 (m, 4H, 3,4-CH_2 pyrollidine); ^{13}C NMR (400 MHz, DMSO-d_6): δ 140.6, 136.2 (C-3,4 imidazole), 59.1 (C-1), 54 (2,5 in pyrollidine), 48.2 (C-3), 28.5(3,4 in pyrollidine); MS: *m/z* 351(M^+). Anal. Calcd for $C_{20}H_{25}N_5O$: C, 68.37; H, 7.12; N, 19.94. Found: C, 68.42; H, 7.09; N, 19.06%.

2-(1*H*-Benzo[*d*]imidazol-2-yl)-1-(1-*p*-aminophenyl-3-(pyrrolidin-1-yl)propyl)hydrazine, 7d. The compound **7d** was obtained as an oil. R_f value: 0.50 (8:2, Hexane:EtOAc); IR: 3429 (N-H str.), 2981 (C-H str. Ar), 2981 (C-H str. Ar), 2749 (C-H), 1450 (N-H bend), 735 cm^{-1} (Ar monosubs); ^{1}H NMR (400 MHz, DMSO-d_6): δ 7.70-7.26 (m, 4H, ArH imidazole), 6.95-6.68 (m, 4H, ArH), 5.36 (s, 1H, OH, D_2O exchangeable), 4.98 (s, 1H, NH imidazole), 4.20 (s, 1H, 2-NH hydrazine), 3.92 (m, 1H, 1-CH), 2.36 (t, 2H, 3-CH_2), 2.11 (m, 4H, 2,5CH_2 pyrollidine), 1.99 (s, 1H, 1-NH hydrazine), 1.94 (m, 2H, 2-CH_2; J_A= 8.15Hz, J_B=11.93Hz), 1.42 (m, 4H, 3,4 CH_2 pyrollidine); ^{13}C NMR (400 MHz, DMSO-d_6): δ 142.2, 136.2 (C-3,4 imidazole), 56.1 (C-1), 54.3 (2,5 in pyrollidine), 46.2 (C-3), 38.5 (3,4 in pyrollidine), 33.5 (C-2); MS: *m/z* 350(M^+). Anal. Calcd for $C_{20}H_{26}N_6$: C, 68.57; H, 7.28; N, 24.00. Found: C, 68.12; H, 7.38; N, 23.63%.

2-(5*H*-[1,2,4]Triazino[5,6-*b*]indol-3-yl)-1-(3-morpholino-1-phenylpropyl)hydrazine, 8a. m.p. 216-220°C. Yield 67%; R_f value:0.34 (7.5:2.5, Hexane:EtOAc); IR: 3520 (N-H str.), 2760 (C-H), 1680 (N-H bend), 770 cm^{-1} (Ar monosubs.); ^{1}H NMR (400 MHz, CD_3OD): δ 8.92 (s, 1H,-NH indole), 7.55-7.30 (m, 4H, ArH indole), 7.21-7.08 (m, 5H, ArH), 3.90-3.84 (m, 1H, 1-CH), 3.89 (s, 1H, 1-NH hydrazine), 3.71-3.67 (t, 4H,-CH_2-O-CH_2), 2.59 (t, 4H,-CH_2-N-CH_2), 2.59-2.37 (t, 4H,-CH_2-N-CH_2), 2.31-2.26 (t, 2H, 3-CH_2), 1.97-1.941 (m, 2H, 2-CH_2; J_A= 8.76Hz, J_B= 11.73Hz), 1.92 (s, 1H, 2-NH hydrazine); ^{13}C NMR (400 MHz, DMSO-d_6): δ199.9 (C-4, 5 indole), 144.2, 142.6, 102.1 (C-2, 3 indole); MS: *m/z* 403(M^+). Anal. Calcd for $C_{22}H_{25}N_7O$: C, 65.50; H, 6.20; N, 24.31. Found: C, 65.30; H, 6.12; N, 23.63%.

3-(2-(5*H*-[1,2,4]Triazino[5,6-*b*]indol-3-yl)hydrazinyl)-N-benzyl-N-methyl-3-phenylpropan-1-amine, 8b. m.p. 93-100°C. Yield 70.5%; R_f value:0.45 (8:2, Hexane:EtOAc); IR: 2962 (C-H str. Ar), 2740 (C-H), 1625 (C-N, N-benzyl), 798 cm^{-1} (Ar monosubs.); ^{1}H NMR (400 MHz, CD_3OD): δ 9.42 (S, 1H,-NH indole), 8.00-7.92 (m, 4H, ArH indole), 7.82-7.76 (m, 10H, ArH), 4.20-4.10 (s, 1H, 1-NH hydrazine). 3.82 (m, 1H, 1-CH), 2.52(t, 2H, CH_2-N), 2.41 (s, 3H, N-CH_3), 1.98 (s, 1H, 2-NH hydrazine), 1.30-1.22 (m, 2H, 2-CH_2; J_A= 8.71Hz, J_B= 12.38Hz); ^{13}C NMR (400 MHz, DMSO-d_6): δ 210.3, 143 (C-4, 5 indole), 140.1, 100.6 (C-2, 3 indole), 62.7 (N-CH_2), 43.3 (N-CH_3); MS: *m/z* 437(M^+). Anal. Calcd for $C_{26}H_{27}N_7$: C, 71.39; H, 6.17; N, 22.42. Found: C, 71.52; H, 6.23; N, 20.86%.

2-(5*H*-[1,2,4]Triazino[5,6-*b*]indol-3-yl)-1-(3-morpholino-1-*p*-hydroxy-phenylpropyl) hydrazine, 8c. m.p. 204°C. Yield 65%; R_f value: 0.421 (7.5:2.5, Hexane:EtOAc); IR: 3300 (O-H), 2950 (C-H str. Ar), 2768 (C-H) 1640 (C-N, indole), 1392 (C-O), 786 cm^{-1} (Ar monosubs.); ^{1}H NMR (400 MHz, CD_3OD): δ 9.86 (s, 1H,-NH indole), 8.15-8.08 (m, 4H, ArH), 7.82-7.35 (m, 4H, ArH indole), 3.90 (m, 1H, 1-CH), 3.89-3.87 (s, 1H, OH), 3.49 (s, 1H, 1-NH hydrazine), 3.30-3.31 (t, 4H,-CH_2-O-CH_2), 3.20-3.23 (t, 4H,-CH_2-N-CH_2), 2.82-2.80 (t, 2H, 3-CH_2-N), 2.39 (s, 1H, 2-NH hydrazine), 1.25-1.27 (m, 2H, 2-CH_2; J_A= 8.37Hz, J_B= 12.63Hz); ^{13}C NMR (400 MHz, DMSO-d_6): δ 196.5, 143.2 (C-4, 5 indole), 98.8 (C-2, 3 indole); MS: 419(M^+), 333, 169, 86. Anal. Calcd for $C_{22}H_{25}N_7O$: C, 65.39; H, 6.81; N, 23.50. Found: C, 65.40; H, 6.91; N, 22.62%.

Acknowledgement

The authors express their sincere thanks to the Head, Department of Chemistry, Lucknow University, Lucknow, for providing laboratory facilities. They are also thankful to the Director, CDRI, Lucknow for elemental analysis and spectral data. Authors are also grateful to Head, Division of Agrochemicals, Indian Agricultural Research Institute, Pusa Road, New Delhi, for biological screening.

References

1 Gul H I, Ojanen T & Hanninen O, *Biol Pharm Bull*, 25, **2002**,1307.
2 Gul H I, Sahin F, Gul M, Ozturk S & Yerdelen K O, *Arch Pharm (Weinheim)*, 338(7), **2005**, 335.
3 Sharma B K, Srivastava J S, Prithviraj B, Singh U P & Pandeya S N, *Folia Microbiol*, 43(4), **1998**, 393.
4 Sridhar S K, Pandeya S N, Stables J P & Ramesh A, *Eur J Pharm Science*, 26, **2002**, 129.
5 Dimmock J R & Kumar P, *Curr Med Chem*, 4, **1997**, 1.
6 Cremlyn R J, "Chiral imidazole fungicide composition and their use", in *Agrochemicals* (John Wiley and Sons, New York), **1991**, pp.157-216.

7 Ansari K F & Lal C, *J Chem Sci*, 121(6), **2009**, 1017.

8 Helmick R A, Fletcher A E, Gardner A M, Gessner C R, Hvitved A N, Gustin M C & Gardner P R, 2005, *Antimicrob Agents Chemother*, 49(5), **2005**, 1837.

9 Christova D & Schuster G, *J Phytopathol*, 32, **1991**, 168.

10 Hund J C A, Briggs E & Clarke E D, *Bioorg Med Chem Lett*, 17, **2007**, 5222.

11 Salzmann D, Handley R J & Muller-Scharer H, *Basic Appl Ecol*, 9(5), **2008**, 577.

12 Bishnoi A, Srivastava K, Joshi M N & Bajpai S K, *Indian J Heterocycl Chem*, 15, **2006**, 307.

13 Bishnoi A, Srivastava K & Tripathi C K M, *Indian J Chem*, 45B, **2006**, 2136.

14 Bishnoi A, Srivastava K & Joshi M N, *Indian J Chem*, 45B, **2006**, 1961.

15 Bishnoi A, Saxena R, Singh S, Rani A, Joshi M N & Bajpai S K, *Lett Drug Des Disc*, 6 (4), **2009**, 252.

16 Damayanti M, Susheela K H & Sharma G J, *Ceratocystis Paradoxa Cytobio*, 86, **1966**, 155.

17 Vincent J M, *Nature*, 159, **1947**, 850.

18 *Performance standards for antimicrobial disk susceptibility tests. Approved standard M2-A6*. CLSI, Clinical and Laboratory Standards Institute Wayne, PA USA, **1997**.

19 Joshi K C & Chand P, *J Heterocycl Chem*, 17, **1980**, 1783.

20 Marvel C S & Hiers G S, *Org Synth*, 5, **1925**, 71.

21 Sharma V L, Bhandari K, Shankar G, Singh H K, Srivastava P & Panday V C, *Indian J Chem*, 43B, **2004**, 207.

ISBN 978-93-5156-328-0
International Conference of Advance Research and Innovation (ICARI-2014)

Theoretical Investigation and Flow Simulation of a Sub-Sonic Open Circuit Wind Tunnel Model

Vishvendra Singh Tomar *,Vasu Kumar, Raj Kumar Singh ,Sahib Chawla
Department of Mechanical Engineering, Delhi Technological University, Delhi-110042, India

Article Info

Article history:
Received 29December 2013
Received in revised form
10 January 2014
Accepted 20 January 2014
Available online 1 February 2014

Keywords

Sonic Open Circuit Wind Tunnel
Simulation
Solid-Works Flow Express
Mach Number

Abstract

The Wind Tunnel has become an integral part of the design process in many industries, typically used to verify and tune the aerodynamic properties of solid objects with origin to Civil, Environmental, Automobile or Aeronautical Engineering. It provides the appropriate desired environment conditions (Pressure Distribution, Flow Velocity, Turbulent Kinetic Energy etc.) at the Test Chamber. Hence, it should have optimum design to generate the required conditions. In this present work, a suction type Sub-Sonic Open Circuit Wind Tunnel (SOWT) was designed and simulated in computer environment. The Mach Number (M) taken for the model is 0.15 (Maximum Operating Speed = 50m/s). The guiding dimensions taken for the Test Chamber are: L_T = 45cm, H_T = 18cm and W_T = 24cm. The design and development of the wind tunnel model was performed using the 3D solid modeling program, Solid-Works. The computer aided simulation was done using the Solid-Works Flow Express program. For the flow simulation through the tunnel, the theoretical ideal experimental conditions have been created on this model. The Pressure Distribution and Flow velocity curves are plotted against the tunnel length.

1. Introduction

The Wind Tunnel plays a very vital role during the design and development of modern aircraft, automobile, building structures etc as it accounts for the desired environment conditions around the scale model. With the help of this, various measurements including Drag and Lift Forces are done which helps in the rectification of the earlier design having certain shortcomings and as such in finalizing the optimum design. The Open Circuit Wind Tunnels (OCWTs) Models are generally constructed in order to study drag forces acting on different automotive designs as it measures aerodynamic forces acting on scale models of cars, trucks etc [1-3]. Wind tunnels are designed for a specific purpose and speed range. To make an accurate measurement in wind tunnel, the test chamber conditions should be as close as possible to the actual atmospheric conditions. Moreover, the Pressure Distribution and Flow velocity are two important factors affecting the design of the scale model directly. Therefore, these two factors along with the Test Chamber dimensions are taken as the guiding factors, directing the appropriate designing of the Tunnel [4].

Till today, a lot of research work has been accomplished to optimize the Wind Tunnel Design and still to make it better at various levels depending upon the situations, research work is still in progress. Peter et al. in their work, focused on the wind tunnel test section flow quality and its application to a numerical CCWT by studying the effects of various variables for its evaluation [5]. Batill et al. [6] validated the vacuum effect created by fan in the three dimensional Sub-Sonic suction type Wind Tunnel and calculated the energy losses in the boundary layer flows due to this effect emerged. Lohan [7] in his article on Design and Applications of Low Speed Wind Tunnels (LSWTs), focused on the design and application of LSWTs having well-defined, controllable, uniform flow of air for experimental and design validation purposes. Cogotti [8] described the evolution of the automotive wind tunnels in parallel with developments in measurement techniques and

Corresponding Author,
E-mail address: vst.dtu@gmail.com
All rights reserved: http://www.ijari.org

ISBN 978-93-5156-328-0

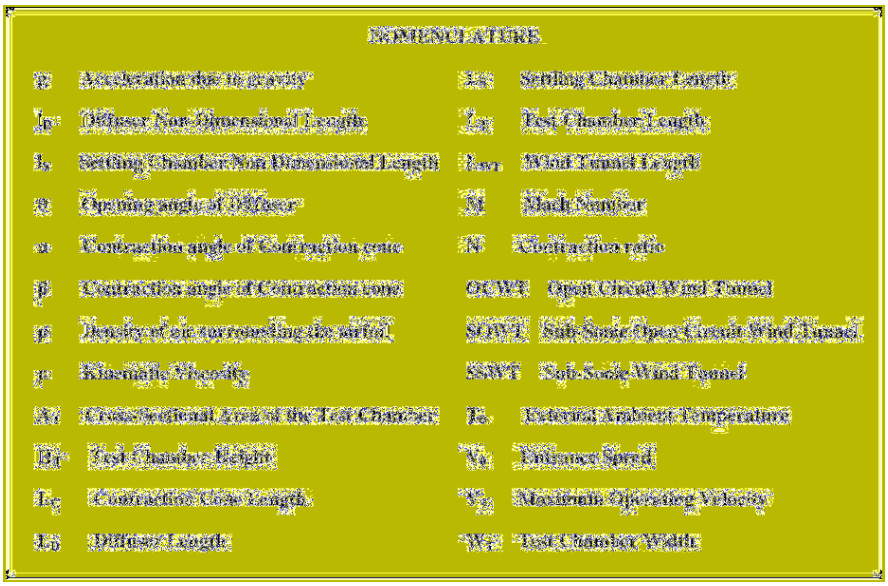

performedaerodynamics and aerostatics measurements in new cars. Inan [9] designed and manufactured a multi-purpose low-speed open-loop wind tunnel and subsequently measured turbulence, flow rate and pressure in the test section of it.Eckert et al. in his technical note discussed someAerodynamic design guidelines and computerprogram for estimation of SSWT performance [10]. In this paper, following the previous research worksand developed guidelines, a model design of SOWT Model is developed having a test chamberwith 24 cm x 18 cm cross sectional area. Theairflow in this tunnel is modeled using computer-aided simulation software Solid-Works FlowExpress. Flow velocity and Pressure Distributionchanges within the windtunnel are investigated.

2. SOWT Model Design

The OCWT consists of five basic parts, which are (From front to back)the Settling Chamber, theContraction Cone, the Test Section, the Diffuserand the Drive Section. The Settling Chamber is atthe very

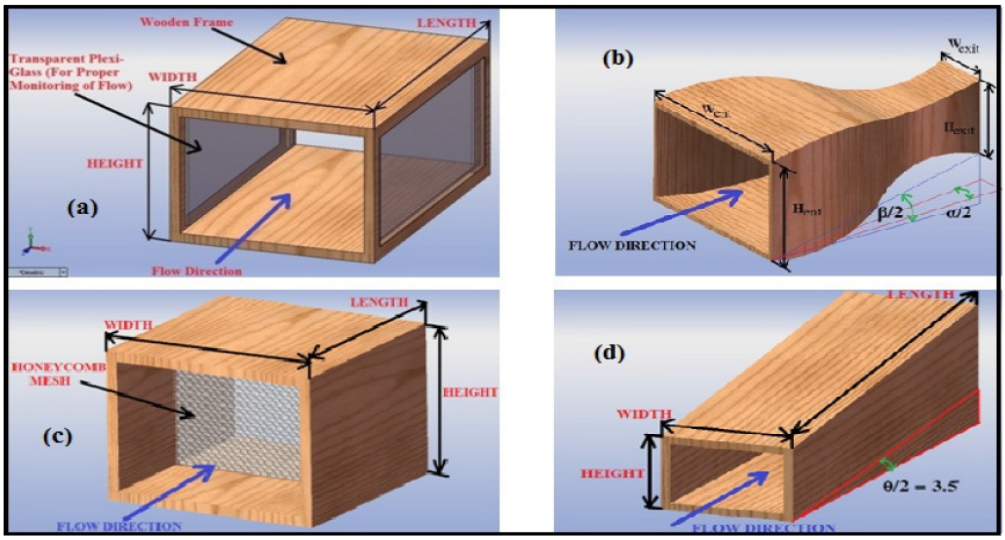

Fig: 1. The four basic parts of a Sub-Sonic Open Circuit Wind Tunnel: (a) Test Chamber, (b) Contraction Cone, (c) Settling Chamber and (d) Diffuser.

front of the wind tunnel and is made up ofscreens and honeycomb-shaped mesh, which straighten out the air and reduce turbulence. The Contraction Cone forces a large volume of airthrough a small opening in order to increase thewind velocity in the tunnel, as there is gradualdecrease in area. The Test Section is the placewhere a model is mounted on sensors. The Diffuser is at the end of the Test Section and keeps the air running smoothly as it goes toward the back. It also increases in volume in order to slow the air down as it exits the tunnel (Fig. 1.). The Drive Section is at the very back of the wind tunnel, and it is where the fan is housed and draws air into the wind tunnel by blowing air out of it and hence reduces turbulence along with greater control of the airflow through the tunnel [2].

The decisive characteristic of wind tunnels lies in the flow quality inside the test chamber and the overall performances. Three main criteria that are commonly used to define them are: maximum achievable speed, flow uniformity and turbulence level. Hence in general, the design aim of a wind tunnel is to get a controlled flow in the test chamber, achieving the necessary flow performance and quality parameters. Also, it is crucial to avoid flow separation close to the walls of the contraction zone.

During the design, some guidelines are followed: The equivalent frontal area of the model should not be higher than 10% of the test chamber cross-sectional area. The width to height ratio adopted for 3-D (Three-Dimensional) Tests is 4:3. The flow acceleration and non-uniformity attenuations mainly depend on the ratio of cross-section area of inlet to that of exit, termed as contraction ratio (N). For this current model, value of N is taken to be 5.The Primary Design Parameters for the overall design of the Wind Tunnel include Test chamber dimensions i.e. Width (W_T), Height (H_T) and length (L_T). With the help of these parameters cross-sectional area of the Test Chamber can be calculated as $A_T = W_T.H_T$. The Contraction ratio (N) is taken 5 for the Wind Tunnel with Mach number (M= 0.15), having Maximum operating speed (VT) to be 50 m/s.These Design variables are summarized in the Table. 1

Table: 1. The primary and secondary design parameters required for designing of SOWT Model.

PRIMARY DESIGN PARAMETERS	SECONDARY DESIGN PARAMETERS
Test Chamber Width (W_T)	Semi Angle In Contraction Cone ($\alpha/2$)
Test Chamber Height (H_T)	Semi Angle in Diffuser ($\theta/2$)
Test Chamber Length (H_T)	Settling Chamber Non Dimensional Length (l_S)
Contraction Ratio (N)	Diffuser Non Dimensional Length (l_D)
Maximum Operating Speed (V_T)	Settling Chamber Length (L_S)
Mach Number (M)	Contraction Cone Length (L_C)
	Diffuser Length (L_D)

The dimensions for the Test Section are W_T = 24cm, H_T = 18cm, L_T = 45cm and the V_T is taken to be 50m/s which gives us the Mach Number to be 0.15. So, The Designing of all other parts is done based on these dimensions with N=5. The semi angle in the Contraction Cone ($\alpha/2$) is taken as 12° and the semi angle in the Diffuser ($\theta/2$) is taken as 3.5°. The non-dimensional lengths for the Settling Chamber (I_S) and Diffuser (I_D), for Sub-Sonic Open Circuit Flow, are taken as 0.5 and 3.2 respectively [11-15]. The calculated parameters are displayed in Table. 2. And the final design for this analytical analysis is represented by (Fig. 2).

Table 2: The values calculated for the Secondary design Parameters

Cross-Sectional Area of the Test Chamber (A_T)	$A_T = W_T H_T$	432 cm^2
Hydraulic Diameter of the Test Chamber (D_T)	$D_T = \frac{2W_T H_T}{W_T + H_T}$	20.57 cm
Length of The Contraction Cone (L_C)	$L_C = \frac{(\sqrt{N} - 1) W_T}{2\tan(\alpha/2)}$	69.78 cm
Length of The Settling Chamber (L_S)	$L_S = \sqrt{N}\ W_T I_S$	26.83 cm
Length of The Diffuser (L_D)	$L_D = W_T I_D$	76.80 cm

ISBN 978-93-5156-328-0

As the length of each segment is calculated, therefore the total length of the tunnel is nothing but the sum of all section.The total length of the SOWT can be calculated as:

$L_{WT} = L_S + L_C + LT + L_D$
$L_{WT} = 26.83 + 45 + 69.78 + 76.80 = 218cm$
Hence, L_{WT} is equal to 218cm or 7.15 ft.

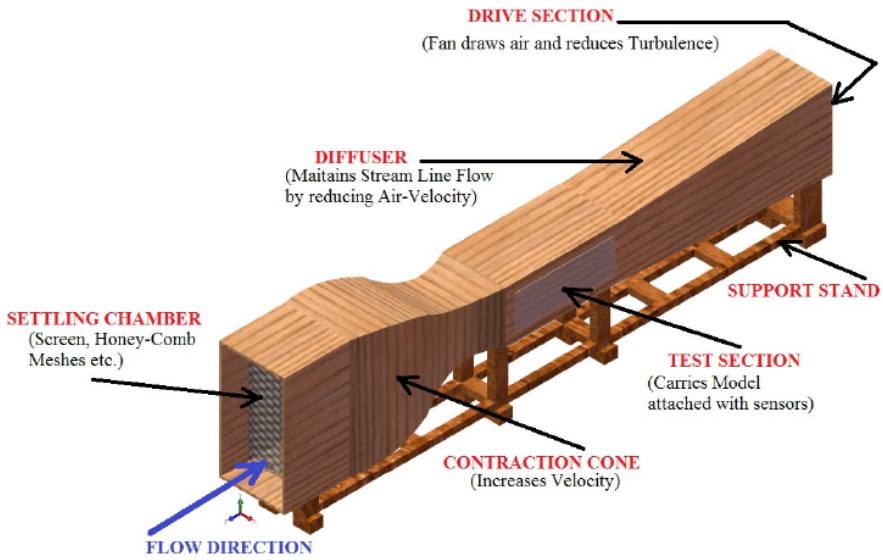

Fig: 2. Isometric View of the complete model of the SOWT developed using 3D Solid Modeling Program.

3. SOWT Model Simulation

Solid-Works Flow-Express is a first pass qualitative flow analysis tool which gives insight into water or air flow inside the Solid-Works model. Using this, the simulation is carried out. The constants and assumptions used in the simulation study are tabulated as (Table. 3.):

Table: 3. The constants and various parameters determining the environment conditions for the simulation of SOWT Model.

CONSTANTS AND VARIOUS PARAMETERS	VALUES
Inlet Pressure	100890 Pa
Outlet Pressure	100000 Pa
External Ambient Temperature	293.20 ℃
Gas Constant	287 J/kg-℃
Kinematic Viscosity	1.714×10^{-5} Kg/m-s
Acceleration due to gravity	9.81 m/s^{-2}
Air Density	1.2251 kg/m^3
Entrance Speed	11.335 m/s

The flow velocity simulation of the designed Wind Tunnel have been performed (using pipe line flow visualization and particle flow visualization) under the above mentioned environment conditions (Fig. 3, Fig. 4.). Also, the variation of flow velocity against the length of the tunnel is obtained. Fig. 5 shows the flow speed changes within the wind tunnel. The lowest flow speed is occurred at the surfaces of the entrance section, at the corners joining the settling chamber and the contraction cone, and the diffuser exit. Flow speed accelerates while passing through the contraction and it reaches the highest required value

(49.118 m/s. 50 m/s) in the test chamber. Also the flow rate increases throughout the contraction and chamber and enters into the diffuser. Further, at the diffuser exit, it reaches the same value with the wind tunnel entrance.

remains constant throughout the test chamber. Flow rate gradually decreases as air exits from the

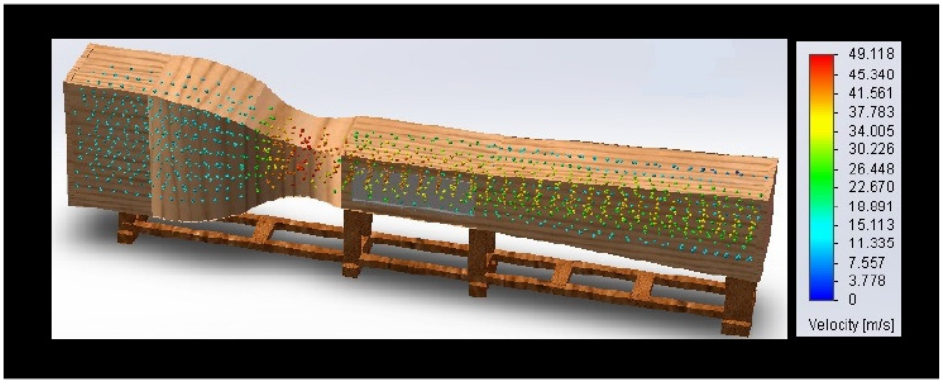

Fig: 3. Particle Flow Visualization of Air as fluid inside the SOWT, illustrating Velocity variation along the length of the Tunnel.

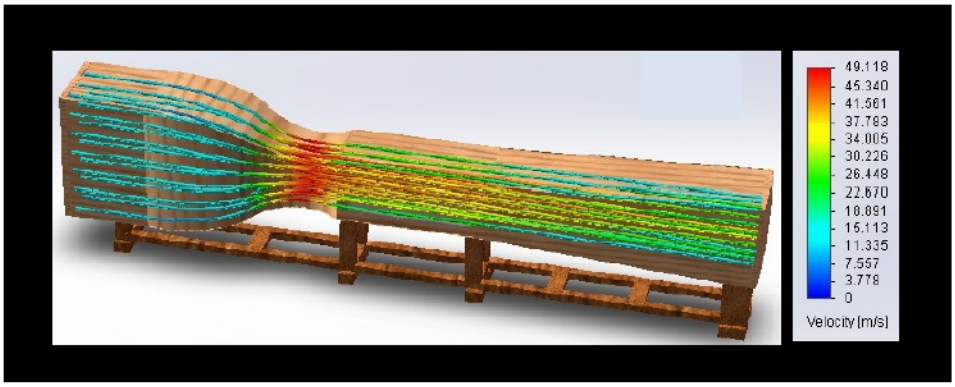

Fig: 4. Pipe-Line Flow Visualization of Air as fluid inside the SOWT, illustrating Velocity variation along the length of the Tunnel

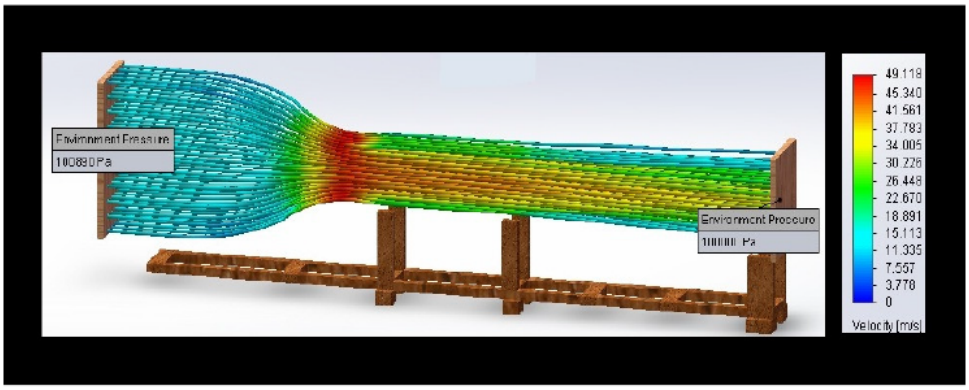

Fig: 5. Flow Velocity Variation of Air as fluid inside the SOWT along the length of the Tunnel.

The graphic of static pressure distribution and velocity changes throughout the wind tunnel is shown in Fig. 6. and Fig. 7.

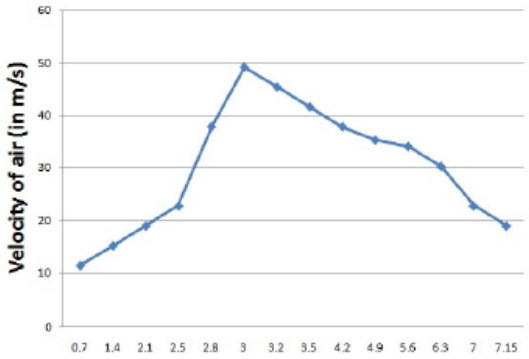

Fig: 6. Flow Velocity Variation (Quantitatively) of Air as fluid inside the SOWT along the length of the Tunnel.

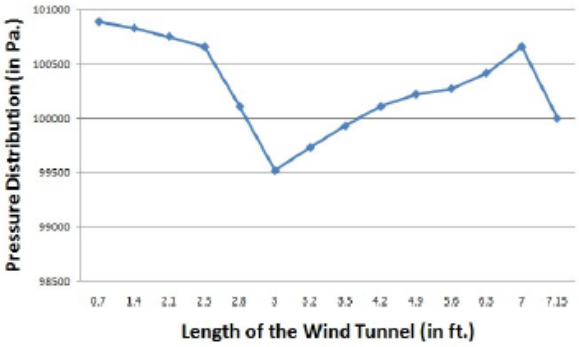

Fig: 7. Pressure Distribution (Quantitatively) of Air as fluid inside the SOWT along the length of the Tunnel.

The static pressure on the edges of the entrance section is the maximum value (100890 Pa.). It can be said that a major turbulence and counter pressure zone are created at these points. Static pressure values are closed to the each other's at the settling chamber (x=2.5 ft.) and the diffuser exit (x=7 ft.). A bit of static pressure drop is occurred in the middle zone of the contraction cone. The pressure is reached to the lowest value at the test chamber exit. Since the static pressure changes are very small throughout the test chamber, it can be said that there is not any boundary layer thickening along the test chamber walls and the air flow quality is good.

4. Conclusion

The main considerations like Boundary Layer Separation, Controlled Air Flow Quality, Turbulence Intensity, Stream Line Flow, Cost-Effectiveness, Design Ease and Mach Number (M = 0.15) etc were taken into the account and accordingly the design was finalized. Both Pipe-Line and Particle flow visualizations are adopted to describe the results efficiently. The Velocity Variations and Static Pressure changes throughout this model were simulated. Moreover, the quantitative variation of Velocity and Pressure is plotted against the tunnel's length. With the final design, the maximum operating speed obtained at the test chamber is 49.12 m/s, quite close to desired value 50 m/s. The air flow obtained is of smooth quality with no boundary layer thickening process at the Test Chamber. Thus, the final SOWT Model design obtained can be used wherever the maximum operating velocity required is 50 m/s or 180 km/h, which generally is the case with the automobiles at high speeds.

References

[1] Types of Wind Tunnels, NASA Aeronautics and Space Administration, http://www.grc.nasa.gov /WWW/k12/airplane/tuntype.html.

[2] Science Buddies: How to Build a Subsonic Wind Tunnel http://www.sciencebuddies.org/science-fairprojects/wind-tunnel-toc.shtml.

[3] A Textbook of Fluid Mechanics and Hydraulic Machines, Dr. R. K. Bansal, Laxmi Publications Pvt. Ltd., New Delhi, Forces on Submerged Bodies, Page No. 657-659.

[4] Barlow, J. B, Rae, W. H, & Pope, A. Low-speed wind tunnel testing, John Wiley & Sons New York, 1999

[5] Peter Moonen, Bert Blocken, Jan Carmelieta, Indicators for the evaluation of wind tunnel test section flow quality and application to a numerical closed-circuit wind tunnel, Journal of Wind Engineering and Industrial Aerodynamics 95, 2007, 1289–1314.

[6] S. M. Batill, J. J. Hoffmann, "The Aerodynamic Design of Three Dimensional Subsonic Wind Tunnel Inlets", AIAA Journal, 24(2), 1986, pp. 268-269

[7] John Lohan, PhD, Article on Design and Applications of Low Speed Wind Tunnels, Department of Mechanical and Industrial Engineering, Galway-Mayo Institute of Technology (GMIT), Dublin Road, Galway, Ireland.

[8] A. Cogotti, “Evolution of Performance of an Automotive Wind Tunnel”, J. Wind Engineering and Industrial Aerodynamics, V. 96, 2008, pp. 667700

[9] A. T. Inan, "Design of Multi-Purpose Low Speed Subsonic Air Tunnel and Turbulence Measurements", Ph.D. Thesis, Marmara University, Science Institute, Istanbul, 2003

[10] W. T. Eckert, K. W. Mort, J. Jope, “Aerodynamic design guidelines and computer program for estimation of subsonic wind tunnel Performance”, NASA technical note / D-8243, NASA Washington, 1976

[11] E. C. Maskell, “A theory of the blockage effects on bluff bodies and stalled wings in a closed wind tunnel, R. & M. 3400, November, 1963

[12] The Royal Aeronautical Society. Wind tunnels and wind tunnel test techniques, Royal Aeronautical Society London, (1992).

[13] R. D. Mehta, P. Bradshaw, “Design Rules for Small Low-Speed Wind Tunnels”, Aero. Journal, (Royal Aeronautical Society), (1979), 73, 443

[14] G. G. Borger, The optimization of wind tunnel contractions for the subsonic range, NASA Technical Translation / F-16899, NASA Washington, 1976

[15] J. Scheiman, “Considerations for the installation of honeycomb and screens to reduce wind-tunnel turbulence, NASA Technical Memorandum/ 81868, NASA Washington, (1981)

Volume 1 (2013) 59-64 ISSN 2347 - 3258
International Journal of Advance Research and Innovation

Thermal analysis of a Claude system for Liquefaction of Various Gases

Devender Kumar *, R. S. Mishra
Department of Mechanical Engineering, Delhi Technological University, New Delhi, India

Article Info

Article history:
Received 1 July 2013
Received in revised form
15 July 2013
Accepted 22 July 2013
Available online 1 August 2013

Keywords

Thermodynamics Analysis
Lindesystem
COP
Exergy Efficiency
Exergy Destruction

Abstract

From various Cryogenics systems a detailed thermo analysis of Claude cryogenic system for various gases is done. A comprehensive Second law analysis of Claude system is carried out by using various properties variables in system to find out the more efficient statics of system included exergy efficiency of system After a applying numerical computational technique to Claude system it find out the Methane gas is more suitable than any other observed gas and 350 and 500 bar is best compressor pressure per kg of gas, other han this it is noticed from analysis that the inlet pressure is kept between in range of 3 to 5 bar and inlet temperature is kept below for high second law efficiency.

Nomenclature

m_2=mass of air compressed I compressor
m_8=mass of air in expander
m_4=mass of air in second heat exchanger
m_8=mass of air liquefied in the separator
h=Enthalpy
s=Entropy
X=Dryness fraction
T=temperature
P=Pressure
η_{comp}=Efficiency of compressor (approx. 80%)
$\eta_{expander}$=Efficiency of expander (approx. 80%)
$\eta_{2nd\ law}$=Second law efficiency
Ɛ=Effectiveness of heat exchanger (approx. 80%)
C=Specific heat capacity fluid or gas
W_t=Work of reversible isothermal compression
W_{comp}=Shaft work supplied to compressor per unit mass
R=Universal gas constant

1. Introduction

From the introduction of refrigeration in human world, curiosity of find out the least temperature that any material can attain is increases and with effect of time and by human theoretical effort in science field

Absolute Zero is find out and considered as the least Temperature, but in practical point of view this absolute temperature (0 Kelvin) seem impossible and it taken as ideal reference, With effect of attaining least temperature a new field is introduce called cryogenics. Cryogenics is defined as process for producing very low temperature (Below -150 or 123 K) but temperature below from -180 (93.15 K) consider as the dividing line of refrigeration and cryogenics, its coming out from fact that boiling point of various permanent gases like helium, hydrogen, oxygen, nitrogen and air etc. Number of process is design and practically lays to achieve cryo temperature. As per place requirements of cryogenics is called from different name like cryobiology, cryonics, cryo- electronics, cryotrons, cryosurgery etc. The liquefy gases are store in special containers called Dewar flask. To transfer the liquid from carrier to tank the pump which used are called cryogenics transfer pumps.

Claude system is design to liquefy various particular gases like air, oxygen, nitrogen, feron etc. To achieve high performance of a cyclic process, various analyses is done to identify the inefficient parts of process and upgrade them to their upper level.

2. Literature review

Exergy is defined as the useful part of energy and anergy defined as the unused part or wasted part of energy. In other words Exergy is defining as the

Corresponding Author,
E-mail address: devenderdahiya@in.com
All rights reserved: http://www.ijari.org

availability of maximum useful work that can be obtained from a system. A good exergetic design of a heat exchanger would allow for an increase in the global efficiency of the process, by defining a thermodynamic cycle in which the exergetic losses would be limited [1]. From past few years exergy analysis has used as a power tool to upgrade a system by analyzing there inefficient part or energy destruction parts and with the help of all this optimization of a process is possible. Exergy and anergy defined the economically feasibility of a procession a given environment conditions. Exergy analysis provides useful information with respect to the theoretical upper limit of the system performance, which cannot be obtained from an energy analysis alone. The analysis allows the determination of the sites with the losses of exergy, and therefore showing the direction for the minimization of exergy losses to approach the reversible COP [2].

In exergy analysis exergy and anergy are noted in various terms for each component. The Bejan [3] work is bseof allexergetic analysis of heat exchangers. Various problems are studied related to exergy analysis which a are mentioning or summarized in [4], From the vast study it noticed that most new methods differ only in the way that entropy generation is non-dimensional [5]. Irreversibility that is just another form of exergy destroyed waste potential. So irreversibility is a factor which try to keep low as possible as an optimizer can do without affecting other properties.

Various components are taken under studied and ASU (air separation unit) using distillation columns are one of the main methods used for separating air components. Exergy analysis, inefficiencies were identified in the distillation system for an efficient cryogenic air separation plant producing large-tonnage quantities of nitrogen [6]. Exergy efficiency of a double diabatic column, with heat transfer all through the length of the column, is 23% higher than that of the conventional adiabatic double columns. In a simple adiabatic distillation column, most of the exergy losses occur in the column itself (57%) [7].Now as advancement goes on technology switching toward more efficient method of separation; polymeric membrane and membrane on ceramic technology are used for separating oxygen [8].

Number of parameters for optimization are analyzed but still compressor are the main element which determining the energy parameters of low cryogenic technology. So, we have to first eliminate not only compressor part but use of all these type of machines which are not only efficient but also eco friendly too. In other word : the problem of making a transiting to new cooling principle's is critical and for this one of the most promising alternatives may be electro caloric cooling [9].Claude cycle is a very is a very useful process in cryo industries but its less exergy efficiency still a major drawback in advancement of Claude cycle. With help of Claude cycle number of gases can be liquefy. It is noticed by experiment that more than half of the exergy loss takes place in the liquefaction part and one-third in the air compression unit. Minor but prominent exergy losses are taking place in the distillation unit and the main heat exchanger. The major cause of exergy loss is the use of compressors and to a lesser extent the use of turbines [10].Bye various experimental data It is noticed that the evaporating and condensing temperatures put a strong effects on the exergy losses in the evaporator, condenser, second law of efficiency and COP of the cycle but little effects on the exergy losses in the compressor and the expansion valve. The second law efficiency and the COP increases, and the total exergy loss decreases with decreasing temperature difference between the evaporator and refrigerated space and between the condenser and outside air [11] and if advance technology like nano fluid include it noticed that Nano fluid and Nano lubricant cause to reduce the exergy losses in the compressor indirectly [12].

3. Thermo analysis of Claude system for liquefication of gases

Compressor work:

$$\eta_{comp} = \frac{W_t}{W_{comp}} \quad (1)$$

$$W_t = mRTln\frac{P_2}{P_1} \quad (2)$$

$$W_{comp} = h_2 - h_1 - T_1(s_2 - s_1) \quad (3)$$

$$W_{reversible} = W_{actual} - T_0 s_{gen} \quad (4)$$

$$W_{Total} = W_{comp} + W_{Expander} \quad (5)$$

First heat exchanger:

$$m_2(h_2 - h_3) = (m_2 - m_6)(h_1 - h_{10}) \quad (7)$$

Expander:

$$\frac{T_8}{T_3} = \left(\frac{P_8}{P_3}\right)^{\left(\frac{\gamma-1}{\gamma}\right)\eta_{expander}} \quad (8)$$

$$W_{Expander} = h_8 - h_3 \quad (9)$$

$$(m_4 - m_6 + m_8)h_9 = m_8 h_8 + (m_4 - m_6)(h_7) \quad (10)$$

Second Heat exchanger:

$$m_4(h_3 - h_4) = (m_2 - m_6)(h_{10} - h_9) \quad (10)$$

Throttle valve:

$$h_4 = h_5 \quad (11)$$

Heat Balance of the separator

$$m_4 h_5 = m_6 h_6 + (m_4 - m_6)(h_7) \quad (12)$$

Second law analysis:

$$\eta_{2nd}(\%) = m_6\left(\frac{h_7 - h_6 - T_0(s_7 - s_6)}{W_c}\right)_{*100} \quad (13)$$

COP (coefficient of performance):

$$COP = \frac{h_1 - h_7}{h_2 - h_1 - T_1 (s_2 - s_1)} \quad (14)$$

Claude Cycle

A complete analysis of Claude cycle is performing with the help of Engineer equation solver for various gases. Claude cycle as shown in Fig1 is taken for analysis. Claude system consist a compressor, expander, two heat exchangers with throttle valve and separator. The fluid which have to liquefy first fed to compressor in its gaseous form at atmospheric pressure, it is compress isothermally in compressor after that the high pressure gas is partially cooled by passing through the first heat exchanger, at the exits of first heat exchanger a portion if air is bled and called by expansion in expander ,the remaining portion of air passes through the second heat exchanger ,the gas from second heat exchanger is throttled irreversibly at atmospheric pressure. The liquid gas is collect in separator after throttling. The low temp gas from expander is mixed with the un-liquefied gas from the separator, producing an effect of increased mass flow rate at feed system.

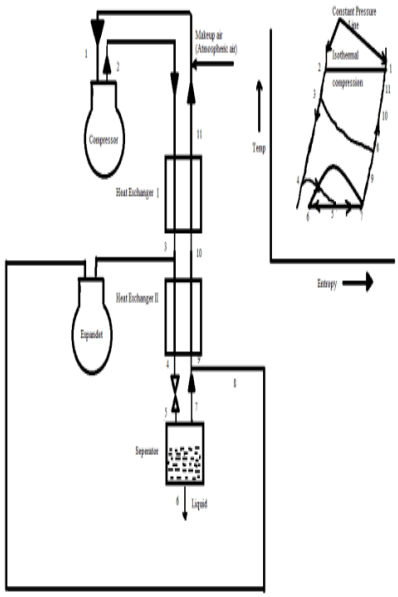

Fig: 1. Claude System

Various results are drawn for particular inlet temperature, pressure and compressor outlet pressure for different gases

4. Results and Discussion

Fig: 2. show the variation of Second law efficiency with compressor pressure and from the graph analysis it concluded that after a specific pressure the efficiency start decreasing, for all considered gases ,the pressure ranging from 250 to 450 show highest second law efficiency.

The variation in liquefaction mass with compressor pressure is not always directly proportional to each other, Fig: 3. show that the liquefaction mass after exceeding some range of compressor reverse the directly proportional behavior and pressure become inversely proportional to compressor pressure the pressure at which change of behavior observed is 300 to 400 for gases considered here COP is inversely proportional to the compressor pressure as it increases COP of system decreasing. In Fig: 4. COP vs. compressor pressure show that from 100 to 200 ranger the rate of decreasing COP with comp. pressure is high but as further increase of pressure the rate of decreasing in COP of system is suppress. Fig: 5. show that the rate of increase of liquefaction mass with inlet pressure is very slow and it is almost linear, because increase in mass only infractions. Fig: 6. Show that rate of increase in COP with inlet pressure is in fraction. COP is directly proportional to the inlet pressure and COP behavior with inlet pressure is same for all considered gases. Fig: 7. Show that increase in inlet pressure also reduces the requirement of very low liquefaction temperature. The Inlet pressure increase also increases the liquefaction temperature of gas. Rate of increase of second law efficiency with inlet pressure is very low and it almost linear due increment show only in fraction. Fig: 8. show variation in Second law efficiency with inlet pressure Fig: 9. show variation in Compressor work with respect to Inlet pressure and from graph it observed that inlet pressure have high impact on the compressor pressure as seen from graph I bar increase in inlet pressure decreases approx. 11% compressor pressure. Fig: 10. show decrease in second law efficiency with increase in inlet temperature, natural gas (methane composition 98%) Claude setup show large drop with inlet temperature. Liquefaction mass decreases as the inlet temperature increases, Fig: 11. show decrease in mass rate with respect to inlet temperature. Fig: 12. Show that gas other than methane and fluorine present very marginal increases in COP with increase in inlet temperature whereas fluorine and methane gas inlet temperature is directly proportional to the COP. Fig: 13. show there is increase in work done by compressor with inlet temperature.

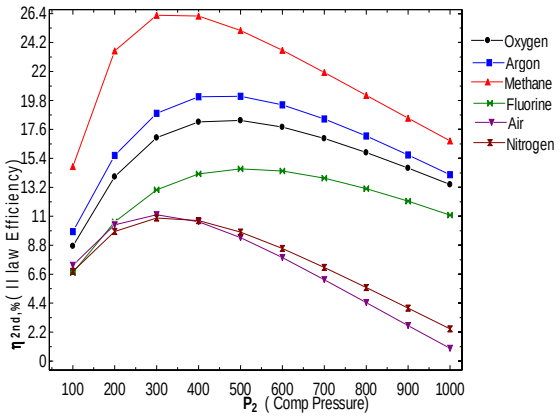

Fig: 2. Variation of Second law Efficiency with Compressor Pressure.

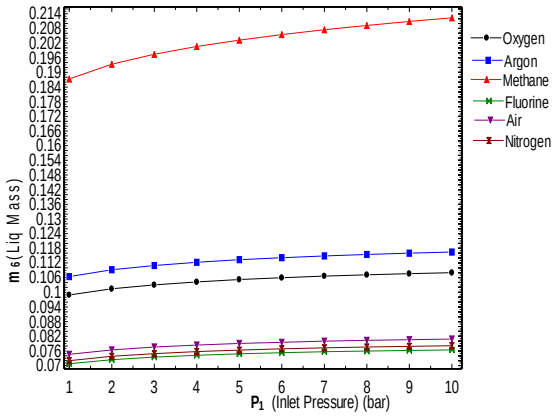

Fig: 5. Variation of liqufecation mass with inlet Pressure.

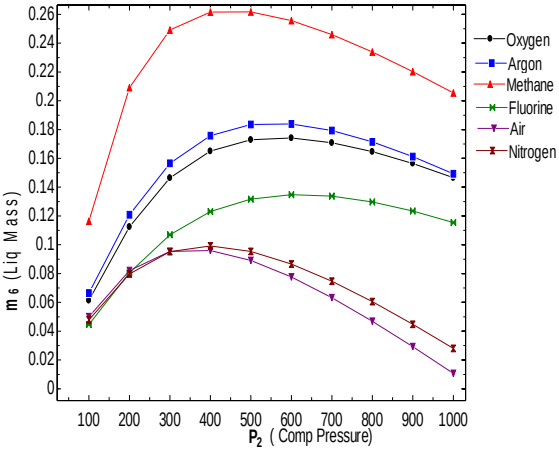

Fig: 3. Variation of liqufecation mass with compressor pressure.

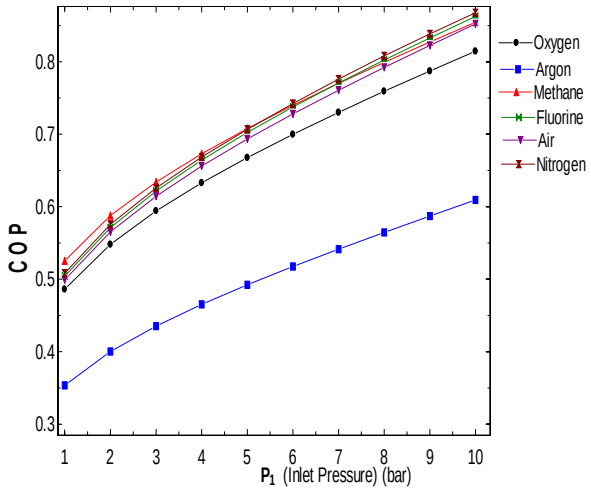

Fig: 6. Variation of COP with inlet pressure.

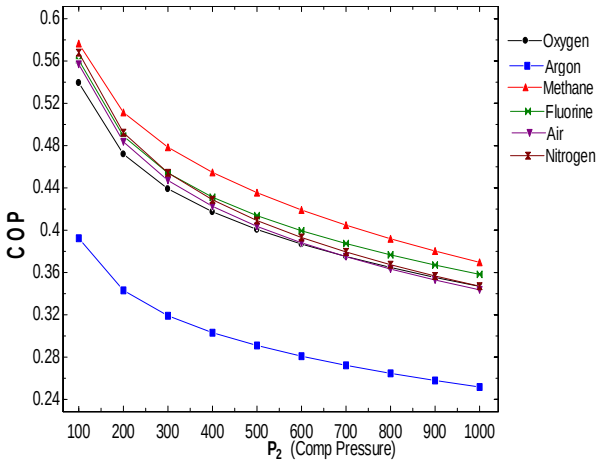

Fig: 4. Variation of COP with compressor pressure.

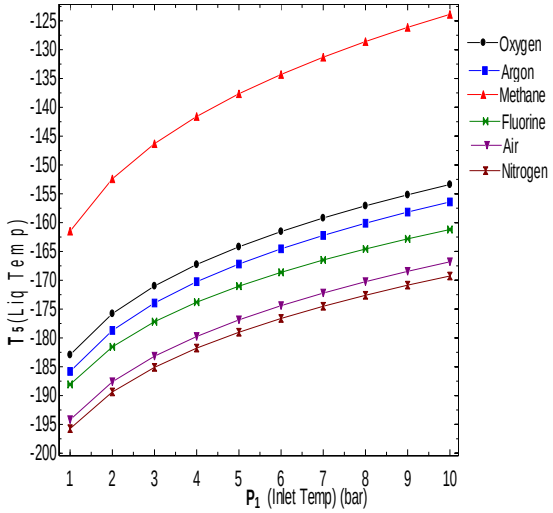

Fig: 7. Variation of liquefication Temperature with inlet pressure.

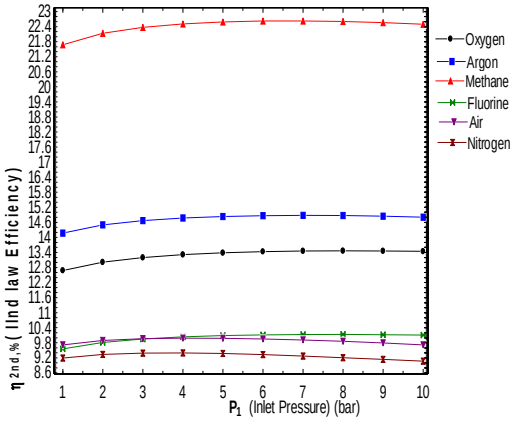

Fig: 8. Variation of 2nd law efficiency with inlet Pressure

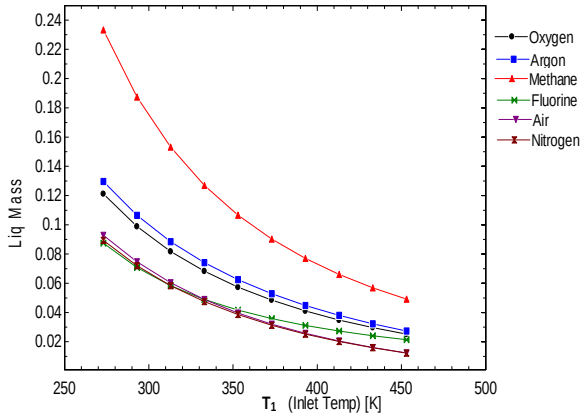

Fig: 11. Variation of liquefaction mass with inlet Temperature

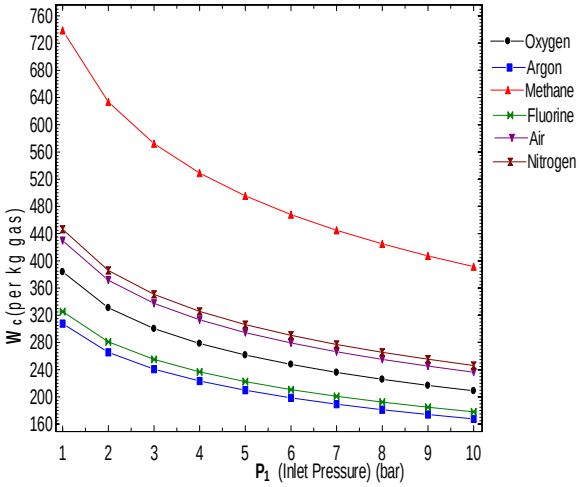

Fig: 9. Variation in W_{comp} with inlet pressure.

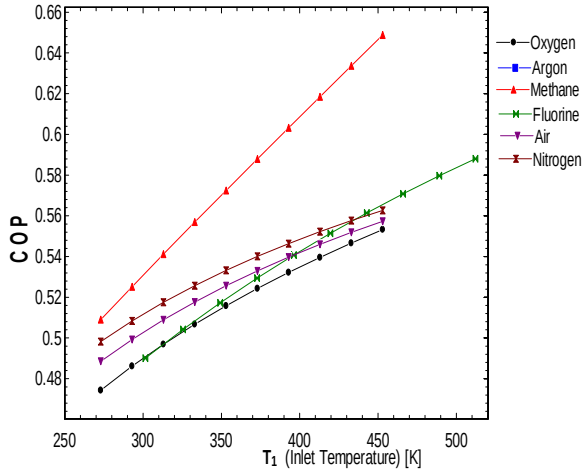

Fig: 12. Variation of COP with inlet Temperature

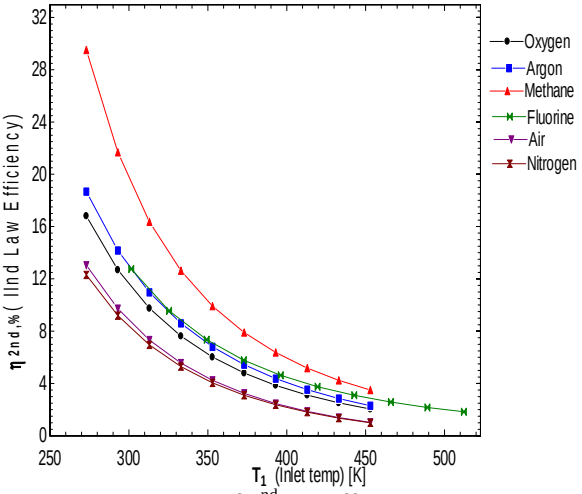

Fig: 10. Variation of 2nd law efficiency with inlet Temperature

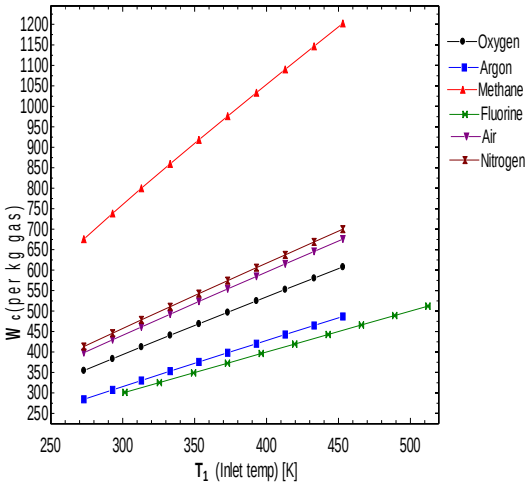

Fig: 13. Variation in W_{comp} with inlet temperature

5. Conclusions

1. Working with methane gas as compare to other gases are more efficient.
2. COP is directly proportional to inlet temperature but show slight slop after some inlet pressure increases
3. Compressor pressure for most of gases in Claude system suite the range of 300 to 500 bars.
4. At low inlet temperature the second law efficiency is more and start decreasing as temperature increases but after a 400 the decrement in second law efficiency ids very low
5. The inlet pressure between 3 to 5 bar is good exergy point of view.

References

[1] T. J. Kotas, "The Exergy Method of Thermal Plant Analysis", 1995 Ed.; Krieger Publishing Company: London, UK, 1985.
[2] M. Kanoglu, MeldaOzdinc, Carpınlıoglu and MurtazaYıldırım, "Energy and exergy analyses of an experimental open-cycle desiccant cooling system", Applied Thermal Engineering 24, 2004, 919–932
[3] A. Bejan, "General criterion for rating heat-exchanger performance", Int. J. Heat Mass Transf, 1978, 21, 655–658
[4] M. Yilmaz, O. N. Sara, S. Karsli, "Performance evaluation criteria for heat exchangers based on Second law analysis", Exergy Int. J. 2001, 4, 278–294
[5] S. T. Wu, X. F. Yuan, Y. R. Li, L. Xiao, "Exergy transfer effectiveness on heat exchanger for finite pressure drop", Energy 2006, 32, 2110–2120
[6] R. Agrawal, D. W. Woodward, "Efficient cryogenic nitrogen generators: An exergy analysis, Gas Separation & Purification", 5 (3), September 1991, Pages 139-150, ISSN 0950-4214.
[7] J. Rizk, M. Nemer, D. Clodic, "A real column design exergy optimization of a cryogenic air separation unit", Energy, 37(1), January 2012, Pages 417-429, ISSN 0360-5442
[8] GaëlleGosselin, "Thermodynamic study of oxygen-enhanced combustion: analysis of different techniques of oxidant production", KTH industrial engineering and management, Master of Science Thesis EGI 2012: HT.
[9] Yu. V. Sinyavskii, "Electrocaloric refrigerators: A promising alternative to current low-temperature apparatus", Chemical and Petroleum Engineering, June 1995, 31(6), pp 295-306, ISSN 1573-8329.
[10] R. L. Cornelissen, G. G. Hirs, "Exergy analysis of cryogenic air separation, Energy Conversion and Management", 39(16–18), November–December 1998, Pages 1821-1826, ISSN 0196-8904
[11] RecepYumrutaş, Mehmet Kunduz, Mehmet Kanoğlu, "Exergy analysis of vapor compression refrigeration systems", Exergy, An International Journal, 2(4), 2002, Pages 266-272, ISSN 1164-0235
[12] J. U. Ahamed, R. Saidur, H. H. Masjuki, "A review on exergy analysis of vapor compression refrigeration system", Renewable and Sustainable Energy Reviews, 15(3), April 2011, Pages 1593-1600, ISSN 1364-0321

International Journal of Applied Engineering Research.
ISSN 0973-4562, Volume 8, Number 17 (2013) pp. 2017-2022
© Research India Publications
http://www.ripublication.com/ijaer.htm

Thermodynamic Analysis of a Absorption Refrigeration Cycle Using Flat Plate Collector

Rohit Goyal[*1], D K Gupta[2], Rajesh Kumar[3] and Md. Nadim Shams[4]

[1,2,3,4] *Department of Mechanical Engineering, Delhi Technological University (Government of NCT of Delhi), Bawana Road, Delhi-110042, India.*

Abstract

The thermodynamic analysis shows the first law and second law efficiencies of the various components and the overall system of the single effect absorption refrigeration cycle. In this cycle, the generator is taking desired heat by solar radiations collected through flat plate collector using water as the heat transfer fluid. The heated up water exits the flat plate collector 10^oC above the generator temperature and gives up the heat to it at constant temperature. The proposed single effect absorption refrigeration cycle used $LiBrH_2O$ solution as the working fluid. The analysis shows that the Flat plate collector gives highest energy as well as exergy losses. The first law efficiency of the proposed cycle is about 38% while second law efficiency of the same is about 3%. The effects of some influenced parameters like; generator temperature and the evaporator temperature have been observed on first and second law performance.

Keywords: Solar energy, absorption cycle, first law efficiency, second law efficiency.

1. Introduction

Presently the solar powered absorption refrigeration system is one of the most attractive applications of solar energy due to it requires very low or no electrical input, the physical dimensions of an absorption refrigeration system are usually smaller than that of conventional refrigeration system . The absorption cooling systems are also important due to its usage of natural refrigerants such as ammonia–water and lithium bromide–water solutions.

Fan et al. [1] shows that solar power ejector absorption technologies are attractive alternatives that not only can serve the needs of air-conditioning and refrigeration purposes, but also can meet demand for energy conservation and environmental

protection. Dincer et al [2] proposed a system which consists of four flat plate collectors, an evaporator, an absorber, a generator, a condenser, a solution pump and two heat exchangers. In this system, a mixture of R22 and DMETEG (DiMethyl Ether Tetra Ethylene Glycol) is used as the working fluid and the thermodynamic results of the experimental system were compared with theoretical calculations. Joudi & Lafta et al [3] developed a simulation model to predict the performance of an absorption refrigeration system using LiBr–H_2O as a working pair. They developed a computer program to simulate the effect of various operating conditions on the performance of the individual components of the simulated system.

The analysis of single effect absorption refrigeration cycle by using flat plate collector, second law of thermodynamics along with the traditional first law approach is highly desirable in order to make the theoretical treatment of the proposed cycle in general and to identify and quantify the sources of losses for evaluating its true efficiency in particular. The effect of most influenced parameters has been observed on the first law and second law efficiency of the proposed cycle along with the exergy destruction in its various components.

2. Description of the Proposed Cycle

The proposed system consists of single effect absorption refrigeration cycle (SEARC) by using flat plate collector as shown Figure 1. The solar radiations which fall onto the flat plate collector results increase in temperature of the absorber plate of the collector. The heat absorbed raised the temperature of heat transfer fluid (Water) in collector.

Table 1: Main parameters considered for the analysis.

Environment Temperature(0C)	27
Generator temperature(0C)	80-70
Solar radiation received per unit area(Wm-2)	800
Apparent Sun temperature(K)	4500
Flat plate collector area(m2)	20
Evaporator temperature (0C)	4 –11
Condenser temperature (0C)	35
Absorber temperature (0C)	35

The water is flowing through the pipes which transfer the thermal energy from collector to the generator (a-b) and gives heat to the generator at constant temperature to the absorption refrigeration cycle which uses this heat to raise the temperature of the $LiBrH_2O$ solution so that only water vapors comes out from the generator makes it weak solution and the water vapors coming out from generator (1) is cooled in condenser (C). The saturated liquid (2) coming out of the condenser passed through the throttle valve (TV1) where the pressure and temperature is reduced (3) at constant enthalpy. The cool fluid coming out from the TV1 passed through the evaporator (E) and gives the refrigeration output. The out coming refrigerant (4) sent to the absorber (A) where it mixes with the $LiBrH_2O$ makes the solution rich. The rich solution is pumped to heat exchanger (HX) to take some heat from out coming weak solution

from generator so the less heat is required to vaporize the water within the rich solution and increases efficiency of cycle. For the analysis, the specifications of the SEARC and solar cycle are given in Table 1

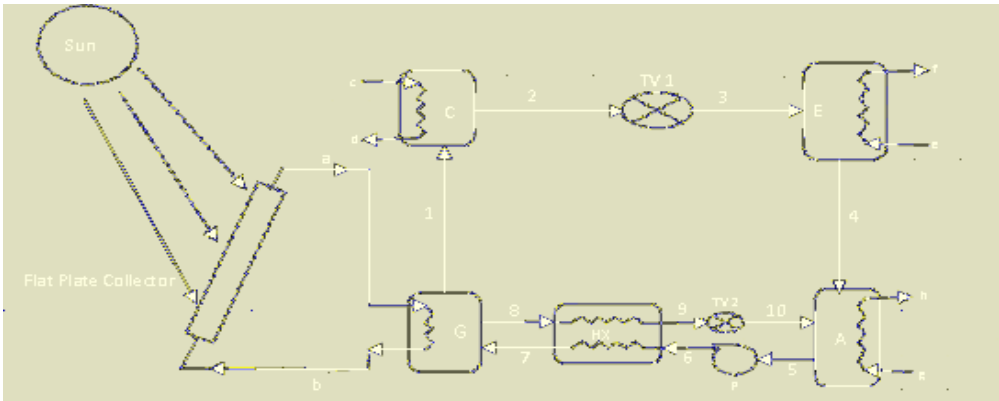

Figure 1: Schematic diagram of single effect absorption refrigeration cycle by using flat plate collector.

3. Thermodynamic Analysis

In the absence of magnetic, surface tension effect, nuclear, electrical, and considering the system is at rest relative to the environment, the total exergy associated with the work obtainable by bringing a stream of matter from its initial state to a state that is in thermal and mechanical equilibrium with the environment. Mathematically,

$$\dot{E} = \dot{m}[(h - h_0) - T_0(s - s_0)] \tag{1}$$

According to the Bejan [4] entropy generation over a control volume is given by

$$\dot{S}_{gen} = \frac{dS}{dt} - \sum_{i=o}^{n} \frac{\dot{Q}_i}{T_i} - \sum_{in} \dot{m}\, s + \sum_{out} \dot{m}\, s \geq 0 \tag{2}$$

According to Gouy-Stodola theorem, the exergy destruction and entropy generation are related as

$$\dot{E}_D = T_0\, \dot{S}_{gen}$$

3.1 Analysis of Flat Plate Collector

According to Hottel -Whillier-Bliss equation the total energy absorbed by the Flat plate collector is given as:-

$$Q_{abs} = A\left[F_R(\tau\alpha)_e - F_R U_L(T_i - T_a)\right] \tag{3}$$

Where factors $F_R(\tau\alpha)$ and $F_R U_L$ for double-glazed flat-plate solar collector are taken as 0.8 and 3.5 respectively.

The exergy of the solar heat input of a Flat plate collector is given as:-

$$E_{abs} = Q_{abs}\left[1-\left(\frac{T_{atm}}{T_i}\right)\right] \tag{4}$$

3.2 First Law Efficiency (η_I)

The first law efficiency can be defined as the ratio of the desired effect to the thermal energy of solar input $\dot{Q}_{solar}$.

$$\eta_I = \frac{\dot{Q}_E}{\dot{Q}_{Solar}} \tag{5}$$

3.3 Second Law Efficiency (η_{II})

Second law efficiency is defined as the ratio of exergy contained in the product to the exergy associated with the solar energy input and the second law efficiency of cycle may be reported as

$$\eta_{II} = \frac{\Delta \dot{E}_E}{\dot{E}_{Solar}} \tag{6}$$

Where, $\dot{E}_{Solar}$ is incoming exergy associate with solar radiation falling on heliostat, $\Delta\dot{E}_{E1}$ is the change in exergy at evaporator of SEARC.

4. Results and Discussion

A thermodynamic investigation has been persuaded to identify the effect of some influenced parameters on the performance of the single effect absorption refrigeration cycle by using flat plate collector. The parameters have been chosen in the typical range of its operation; generator temperature (70^0C-80^0C) and evaporator temperature (4^0C-11^0C).

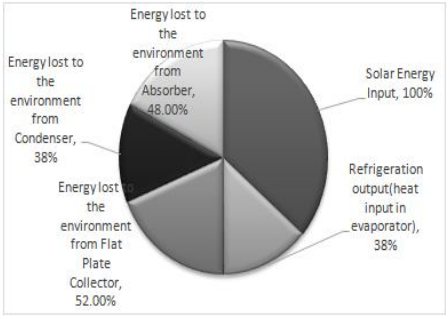

Figure 2. Energy lost from various components of the cycle

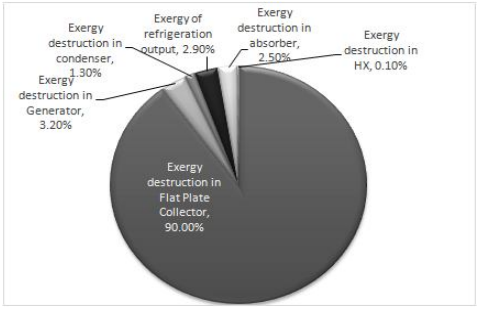

Figure 3. Exergy distructed from various components of the cycle

The first law efficiency and energy distribution of solar heat source is obtained by energy balance approach or first law analysis of the cycle. The exergy destruction in each component of the cycle as a whole is non dimensional by expressing it as a

percentage of the solar heat source exergy. Thermodynamic properties of LiBr/H_2O mixture for the operation of absorption refrigeration are taken from Chua et al. [10]. In order to clarify, the energy and exergy distribution of solar heat driven cycle is shown in Figs. 2 -3.

Fig. 2 indicates that out of 100% solar energy supplied to the system, around 38% is available as useful energy output (refrigeration capacity), 138% is lost to the environment via thermal energy exhaust from the system. Application of second law analysis to the proposed cycle leads to the exergy distribution in the system. It is found that around 2.9% of the total input exergy is available as an exergy output and 97.1% of the input (solar heat) exergy is destructed and lost due to irreversibilities occurred in various components of the proposed cycle are as shown in Fig.3.

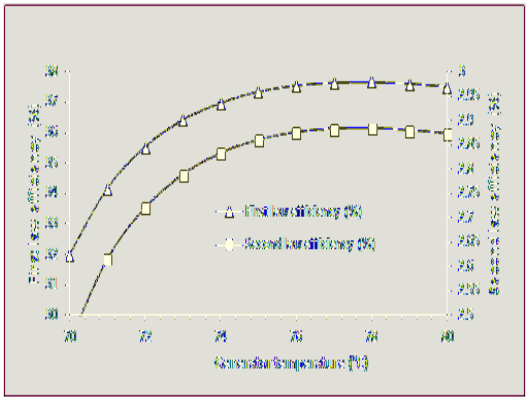

Figure 4. Variation of the generator temperature on the first law and second law efficiency

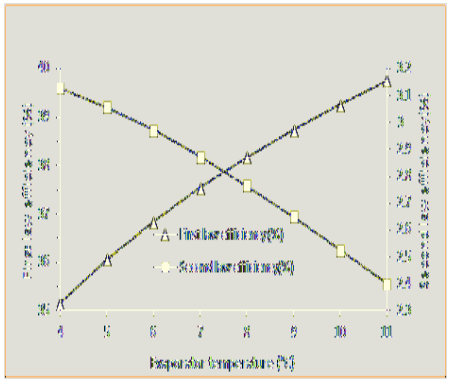

Figure 5. Variation of the Evaporator temperature on the first law and second law efficiency

Fig. 4 shows the variation of the generator temperature on the first law and second law efficiency refrigeration cycle. It is observed that both first law and second law efficiencies are increase with generator temperature. This is due to the fact that the quantity of vaporized refrigerant will be improved with the increase in generator temperature.

The effect of change in evaporator temperature on first and second law efficiency of the system is shown in Fig.5 and it is found that first law efficiency increases significantly with the increase in ejector evaporator temperature while the second law efficiency of the system decreases due to higher losses.

5. Conclusion

The conclusions of the present analysis can be summarized as follows:

- Out of 100% energy (solar heat source) supplied to the system around 38% is produced as refrigeration capacity and 138% is lost to the environment.

- About 2.9% of the input exergy is available as exergetic refrigeration output and 97.1% is lost due to irreversibilities in the components and via thermal lost to the ambient.
- The largest contribution to cycle irreversibility comes from flat plate collector and solely destructed 90% of the input exergy.

References

[1] Fan Y, Luo L, Souyri B (2007). Review of solar sorption refrigeration technologies: development and applications. *Renewable and Sustainable Energy Reviews.***11,**1758-1775.

[2] Joudi, K.A., Lafta, A.H.(2001). Simulation of a simple absorption refrigeration system. Energy Conversion and Management 42, 1575–1605.

[3] Dincer I, Edin M, Ture IE (1996). Investigation of thermal performance of a solar powered absorption refrigeration system. *Energy Conversion & Management* .**37,** 51-58.

[4] Bejan A (2002). Fundamentals of exergy analysis, entropy generation minimization, and the generation of flow architecture. *International Journal of Energy Research.* **26**, 545-565

[5] Chua HT, Toh HK, Malek A, Ng KC, Srinivasan K (2000). Improved thermodynamic property fields of LiBr-H_2O solutions. *International Journal of Refrigeration.* **23**,412-429.